Talanta

The International Journal of Pure and Applied Analytical Chemistry

Publication information: *Talanta* (ISSN 0039-9140). For 2007, volumes 71–73 are scheduled for publication. Subscription prices are available upon request from the Publisher or from the Regional Sales Office nearest you or from this journal's website (http://www.elsevier.com/locate/talanta). Further information is available on this journal and other Elsevier products through Elsevier's website: (http://www.elsevier.com). Subscriptions are accepted on a prepaid basis only and are entered on a calendar year basis. Issues are sent by standard mail (surface within Europe, air delivery outside Europe). Priority rates are available upon request. Claims for missing issues should be made within six months of the date of dispatch.

Orders, claims, and journal enquiries: please contact the Customer Service Department at the Regional Sales Office nearest you:
Orlando: Elsevier, Customer Service Department, 6277 Sea Harbor Drive, Orlando, FL 32887-4800, USA; phone: (+1) (877) 8397126 [toll free number for US customers], or (+1) (407) 3454020 [customers outside US]; fax: (+1) (407) 3631354; e-mail: usjcs@elsevier.com
Amsterdam: Elsevier, Customer Service Department, PO Box 211, 1000 AE Amsterdam, The Netherlands; phone: (+31) (20) 4853757; fax: (+31) (20) 4853432; e-mail: nlinfo-f@elsevier.com
Tokyo: Elsevier, Customer Service Department, 4F Higashi-Azabu, 1-Chome Bldg, 1-9-15 Higashi-Azabu, Minato-ku, Tokyo 106-0044, Japan; phone: (+81) (3) 5561 5037; fax: (+81) (3) 5561 5047; e-mail: jp.info@elsevier.com
Singapore: Elsevier, Customer Service Department, 3 Killiney Road, #08-01 Winsland House I, Singapore 239519; phone: (+65) 63490222; fax: (+65) 67331510; e-mail: asiainfo@elsevier.com

USA mailing notice: *Talanta* (ISSN 0039-9140) is published monthly by Elsevier B.V. (P.O. Box 211, 1000 AE Amsterdam, The Netherlands). Annual subscription price in the USA US$ 3,818 (valid in North, Central and South America), including air speed delivery. Application to mail at periodical postage rate is paid at Rathway, NJ and additional mailing offices.
USA POSTMASTER: Send address changes to *Talanta*, Publications Expediting Inc., 200 Meacham Avenue, Elmont, NY 11003.
AIRFREIGHT AND MAILING in the USA by Publications Expediting Inc., 200 Meacham Avenue, Elmont, NY 11003.

Available online at www.sciencedirect.com
ScienceDirect
Talanta 72 (2007) 1540–1545
Talanta
www.elsevier.com/locate/talanta

Chemical analysis of acidic silicon etch solutions II. Determination of HNO_3, HF, and H_2SiF_6 by ion chromatography

Jörg Acker [a,c,*], Antje Henßge [b,c]

[a] Department of Biological, Chemical, and Process Engineering, Fachhochschule Lausitz, University of Applied Sciences, Großenhainer Straße 57, D-01968 Senftenberg, Germany
[b] Department of Chemical Engineering, Hochschule für Technik und Wirtschaft Dresden, University of Applied Science, Friedrich-List-Platz 1, D-01069, Germany
[c] Leibniz-Institute for Solid State and Materials Research Dresden (IFW Dresden), P.O. Box 270016, D-01171 Dresden, Germany

Received 24 July 2006; received in revised form 30 January 2007; accepted 5 February 2007
Available online 15 February 2007

Abstract

The processing of silicon in microelectronics and photovoltaics involves the isotropic chemical etching using HF–HNO_3 mixtures to clean the surface from contaminations, to remove the saw damage, as well as to polish or to texture the wafer surface. Key element of an effective etch process control is the knowledge of the actual etch bath composition in order to maintain a certain etch rate by replenishment of the consumed acids. The present paper describes a methods for the total analysis of the etch bath constituents HF, HNO_3, and H_2SiF_6 by ion chromatography. First step is the measurement of the total fluoride and nitrate content in the analyte. In a second step, H_2SiF_6 is precipitated as K_2SiF_6. After careful filtration of the precipitate, the fluoride concentration in the filtrate is measured and the content of free HF is calculated therefrom. The K_2SiF_6 is dissolved again and the fluoride content measured and recalculated as H_2SiF_6. The results obtained with the presented method are discussed with respect to the results from two other, previously published methods, based on a titration using methanolic cyclohexylamine solution as titrant and based on a method using a fluoride ion selective electrode (F-ISE). An evaluation with respect to the needs for an industrial application is given.

Keywords: HF–HNO_3 etch solution; Ion chromatography; Silicon; H_2SiF_6

1. Introduction

The processing of silicon wafers for microelectronic or photovoltaic applications involves the isotropic chemical etching of silicon using HF–HNO_3 mixtures. Depending on the technological requirements, e.g. the removal of mechanically damaged surface layers after crystal slicing (saw damage), surface cleaning, and texturing or polishing, different acid compositions have to be used. It is common sense, that any etch bath should be utilized up to its maximum in order to minimize the amount of hazardous and environmental harmful waste and to reduce the costs of silicon processing. As consequence, used etch solutions have to be replenished by concentrated acids to increase their utilization [1–3]. The essential precondition for that is a robust analytical procedure to determine the concentration of the individual etch bath constituents HNO_3, HF, and H_2SiF_6.

H_2SiF_6 is a reaction product that is formed in a formalized two-step-process in the dissolution of silicon in a HF–HNO_3 mixture. In the first step silicon is formally oxidized by HNO_3 to SiO_2. In the second step, the oxide reacts with HF to SiF_4 that is complexed in excess of HF as SiF_6^{2-}. The total reaction is written as follows (Eq. (1)) [4]:

$$3Si + 4HNO_3 + 18HF \rightarrow 3H_2SiF_6 + 4NO + 8H_2O \quad (1)$$

Recent investigations have shown that the reaction mechanism of silicon etching is much more complex and therefore only insufficiently represented by Eq. (1) [5,6].

The total acid concentration and the amount of H_2SiF_6 can be determined by potentiometric aqueous acid–base titration [7]. The first observed equivalence point consists mainly of the sum of the protons of HNO_3, HF, and H_2SiF_6. The difference between

* Corresponding author at: Department of Biological, Chemical, and Process Engineering, Fachhochschule Lausitz, University of Applied Sciences, Großenhainer Straße 57, D-01968 Senftenberg, Germany. Tel.: +49 35 73 85 839; fax: +49 35 73 85 809.
E-mail address: jacker@fh-lausitz.de (J. Acker).

0039-9140/$ – see front matter © 2007 Elsevier B.V. All rights reserved.
doi:10.1016/j.talanta.2007.02.005

the second and the first equivalence point is equal to the amount of H_2SiF_6. The previous publication [8] describes two methods to determine the individual acid concentrations. The base for both methods is the aqueous acid–base titration mentioned above. In method 1, a defined aliquot of the analyte solution is mixed with ethanol and a certain amount of KCl is given to the solution to precipitate H_2SiF_6 as K_2SiF_6. As consequence, two equivalents of HCl are formed with respect to the present amount of H_2SiF_6. The titration of this solution with methanolic cyclohexylamine solution (CHA) yields to the total amount of HNO_3 and HCl at the first equivalence point. The amount of HNO_3 is calculated with the knowledge of the H_2SiF_6 content from the acid–base titration. Finally, the amount of HF is the difference from of the total acid and HNO_3 and H_2SiF_6. In method 2, the total fluoride concentration is measured using a fluoride ion-selective electrode (F-ISE). The difference between that value and the amount of H_2SiF_6 from the aqueous acid–base titration gives the quantity of HF. The amount of HNO_3 is finally calculated from the total amount of acid minus that of HF and H_2SiF_6. The present paper describes a third method (method 3) to analyze the etch solution constituents by ion chromatography (IC). The three methods are compared to each other and their specific advantages and disadvantages are discussed.

2. Experimental

2.1. Sample preparation

The sample preparation was described in detail in the previous part [8]. In short, two series were prepared by dissolution of either SiO_2 (series 1) or silicon (series 2) in HF–HNO_3 mixtures in vessels of polyethylene (PE).

2.2. Ion chromatography

All measurements were performed by a 761 Compact IC with suppressor system and conductivity detector (Metrohm AG, Herisau, Switzerland). An ASupp4/5 Guard (length 5 mm, diameter 4.0 mm) was used as precolumn and a METROSEP ASupp5 (Metrohm AG, Herisau, Switzerland; length 250 mm, diameter 4.0 mm) as separation column. The carbonate eluent consisting of 3.2 mmol L^{-1} Na_2CO_3 and 1.0 mmol L^{-1} $NaHCO_3$ was prepared by dissolution of the appropriate weighed solid compounds (p.a., Merck, Darmstadt, Germany). The eluent flow was constant at 0.7 mL min^{-1}. The suppressor module was regenerated with 0.05 mol L^{-1} H_2SO_4 (Titrisol, Merck, Darmstadt, Germany) and subsequently washed with water (18 MΩ, Seral, Ransbach-Baumbach, Germany). Sample and standard solutions were purified from silicon by using of SPE-H^+-cartridge (Alltech Grom GmbH, Rottenberg-Hailfingen, Germany). The analysis was carried out at 20 °C, a sensitivity of 250 μS cm^{-1} and an injection volume of 20 μL.

For nitrate analysis, the calibration of the ion chromatograph was performed by standards prepared from a 0.1 mol L^{-1} HNO_3 solution (Titrisol, Merck, Darmstadt, Germany) with nitrate contents between 3.1 and 12.4 mg L^{-1} nitrate. The titer of the used HNO_3 solution was steadily determined by titration with NaOH solution (prepared from ampoules, Titrisol, Merck, Darmstadt, Germany). The linear range of nitrite determination ranges up to 14.8 mg L^{-1} and a detection limit of 0.17 mg L^{-1} was calculated for the given conditions. Total fluoride analysis is performed from neutral sample solutions. Calibration standards with fluoride contents between 3.0 and 11.5 mg L^{-1} were prepared from a fluoride standard solution (1 g L^{-1} fluoride (NaF), Merck, Darmstadt, Germany). For the method results a detection limit of 0.08 mg L^{-1} and a linear range up to 13.4 mg L^{-1}.

In preliminary examinations, the methods of nitrate and fluoride determination were validated with respect to stability, linearity, and recovery by the defined addition of diluted HNO_3 (for nitrate validation) and HF as well as NaF (for fluoride validation) and alternatively by standard solutions of nitrate and fluoride, respectively, to the synthetic etch bath mixtures. Different amounts of the added standards were chosen in order to cover the maximum range of the linear region of the calibration curves. The mean recovery of the added standards for both ions amounts to (100.8 ± 1.2)%. Major error source is the tolerance of the used automatic pipette (volume of 100–1000 μL) used to prepare the second dilution by factor 200. Including the tolerance a real dilution factor of 200 ± 6 results. This can be avoided by weighing the samples for dissolution, however, this effort in handling is unrealistic for a practical application in industry.

2.3. Methods

2.3.1. Determination of the total fluoride and the nitrate concentration

Sample analysis starts by weighing of 0.5 mL etch solution and filling up to 200 mL in a volumetric flask. Thereafter, the sample was diluted by a factor of 200 and injected into the ion chromatograph.

2.3.2. H_2SiF_6 and HF contents

The etch solution was diluted to a final silicon concentration close to 3 mg mL^{-1}. A 410 mg KCl (p.a., Merck, Darmstadt, Germany) were weighed in a polyethylene beaker and 5 mL of the diluted sample solution were added followed by the addition of 40 mL ethanol after the completed dissolution of KCl. The beaker was covered with parafilm "M" (Laboratory film, Pechiney plastic packaging, Chicago, USA) and cooled to 4–8 °C for at least 2 h.

2.3.2.1. Determination of the H_2SiF_6 content from the K_2SiF_6 precipitate. The filtrate was separated from the precipitate by vacuum filtration using a hard filtering paper. For a complete separation the filtrate was collected and passed again into the filtration procedure for three to four times. Finally, the precipitate was washed with 10–15 mL ethanol for three times and the wash solution was added to the filtrate.

The K_2SiF_6 precipitate and the filtering paper were transferred into an Erlenmeyer flask, 100–150 mL water, and three drops of phenolphthalein were added. The solution was heated until boiling and titrated with 0.1 mol L^{-1} NaOH (Titrisol, Merck, Darmstadt, Germany) until the turn of color around a pH of 9. Then, the solution was transferred into a 250 mL

Table 1
HNO_3 content in series 1 and 2 obtained by ion chromatography (method 3) (*m* denotes the number of analyses)

Series 1					Series 2		
Sample	$w(HNO_3)$ initial (mg g^{-1})	$w(HNO_3)$ analyzed (mg g^{-1})	*m*	Recovery (%)	Sample	$w(HNO_3)$ analyzed (mg g^{-1})	*m*
S1-A	212.7	208.2 ± 0.1	2	97.9	S2-A	197.6 ± 0.2	2
S1-B	214.5	209.4 ± 0.3	2	97.6	S2-B	179.1 ± 0.1	2
S1-C	210.1	208.0 ± 0.1	2	99.0	S2-C	170.2 ± 0.1	2
S1-D	206.1	203.7 ± 0.1	2	98.9	S2-D	139.0 ± 0.2	2
S1-E	203.9	200.6 ± 0.3	2	98.4	S2-E	131.4 ± 0.1	2
S1-F	201.4	196.0 ± 0.1	2	97.3	S2-F	133.3 ± 0.4	2
S1-G	197.2	196.3 ± 0.1	2	99.6	S2-G	122.4 ± 0.1	2

volumetric flask and filled up. Particles were separated by membrane filtration (single-filter-Chromafil PET-45/25; pore diameter 0.45 μm, Macherey-Nagel GmbH & Co. KG, Düren, Germany). For analysis, an aliquot of this solution was diluted by factor 50.

2.3.2.2. Determination of the HF content in the filtrate. The filtrate was adjusted to an alkaline pH of approx. 8.9 by titration with NaOH in presence of phenolphthalein and filled up to 250 mL. The factor for the second dilution, from which an aliquot is injected into the ion chromatograph, depends on the fluoride content of the sample and on the calibrated fluoride concentration range of the ion chromatograph. A factor of 200 is the most common value.

2.3.2.3. Total fluoride content. A volume of 0.5 mL concentrated sample solution was weighed into a polyethylene beaker, filled up to 150 mL water and titrated with NaOH solution in presence of phenolphthalein until the turn of color. The titrated sample solution was transferred into a 250 mL volumetric flask and filled up. Following, an aliquot of this solution was diluted by factor of 50 for the injection into the chromatograph.

3. Results and discussion

3.1. Determination of HNO_3 content

The calculation of the HNO_3 content from the nitrate ion concentration is only possible if the etch solution is free of any dissolved metals. The results for series 1, prepared by the dissolution of SiO_2 in a HF–HNO_3 mixture, are given in Table 1. The recovery is calculated with respect to the initial HNO_3 since it is not consumed by the dissolution of SiO_2. Fig. 1 compares these results with those obtained by the titration in non-aqueous media using cyclohexylamine in methanol as titrant (method 1) and by a combined method based on the measurement of the total fluoride content using a F-ISE (method 2) [8]. The procedure of method 2 gives values that are significantly below the ones of the two other methods due to the propagation of uncertainty using different experimental values to calculate the final content. Best recoveries to the initial HNO_3 contents are found for the CHA titration and the ion chromatography method. Apart from the samples S1-C and S1-D, the results of both methods agree within 3.5%.

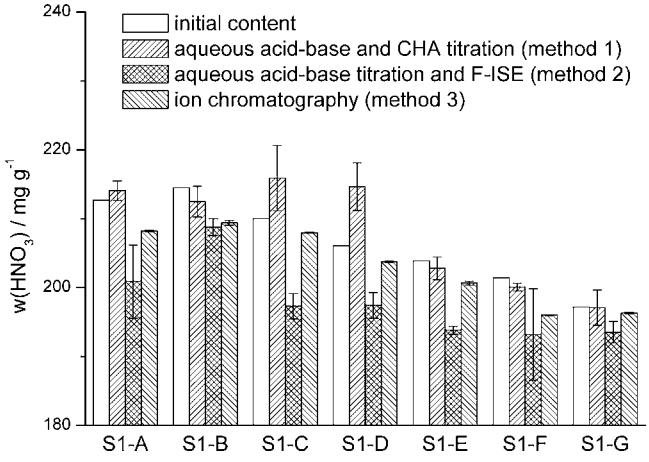

Fig. 1. Summary of all developed methods to determine the HNO_3 content in sample series 1.

The right hand side of Table 1 displays the analytical results of series 2, in which HNO_3 is consumed by the dissolution of silicon. The comparison with the other methods in Fig. 2 follows the same trend as found for series 1. In contradiction to series 1, method 2 gives values with a much better agreement to the ones of the both other methods. The reason for this is yet unknown. Ion chromatography and the CHA titration based method agree within 3% by neglecting the unexplained high value in sample S2-F, In general, the relative uncertainty of method 3 is much smaller than those of the two other methods.

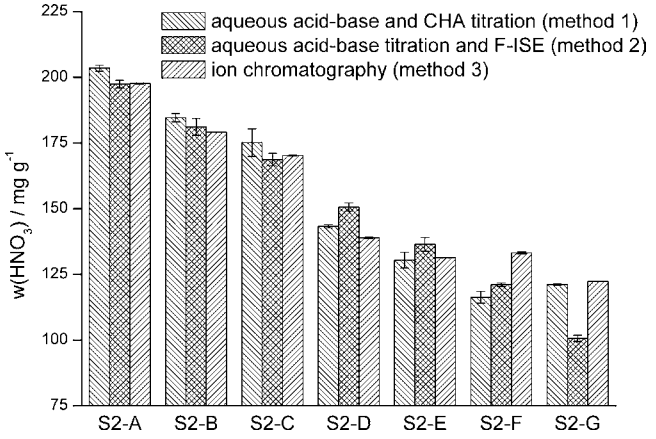

Fig. 2. Summary of all developed methods to determine the HNO_3 content in sample series 2.

Table 2
H_2SiF_6 content in series 1 obtained by ion chromatography from the K_2SiF_6 precipitate (m denotes the number of analyses)

Sample	w(Si) initial (mg g^{-1})	w(Si) analyzed (mg g^{-1})	m	Recovery (%)	w(H_2SiF_6) (mg g^{-1})
S1-A	10.2	10.5 ± 0.3	7	102.1	53.7 ± 1.1
S1-B	17.6	17.5 ± 0.1	3	99.4	89.7 ± 0.4
S1-C	23.8	23.6 ± 0.1	3	99.2	121.2 ± 0.1
S1-D	29.9	29.1 ± 0.1	3	97.1	149.0 ± 0.7
S1-E	36.3	35.3 ± 0.1	3	97.3	181.1 ± 0.5
S1-F	42.0	40.4 ± 0.1	3	96.2	207.2 ± 0.7
S1-G	47.8	45.3 ± 0.9	5	94.7	232.4 ± 4.5

This is simply achieved by a direct measurement of the nitrate ion concentrations in the sample solutions instead of their calculations involving different analytical values and the unavoidable propagation of uncertainty.

3.2. Determination of H_2SiF_6 content by precipitation as K_2SiF_6

Due to strong interferences between H_2SiF_6 and the other present acids, H_2SiF_6 needs to be completely removed from the sample solution in order to obtain reliable analytical results. This interference is attributed to the complex and yet not fully understood speciation of H_2SiF_6 in the presence of HF and/or HNO_3 yielding to silicon–fluorine solution species with a molar composition that significantly differs from H:Si:F = 2:1:6 [9–11].

The removal of H_2SiF_6 is carried out according to Eq. (2) by precipitation of K_2SiF_6 from the sample in ethanolic solution and in the cold using KCl as precipitant.

$$2KCl(s) + H_2SiF_6(aq) \rightarrow K_2SiF_6(s) + 2HCl(aq) \quad (2)$$

KCl has to be added in a high excess to facilitate a complete precipitation according to the law of mass action. Due to its low solubility in ethanol excessive KCl precipitates during the addition of ethanol and promotes the crystallization of K_2SiF_6. After filtering, washing, and dissolution in water NaOH is added until a pH of around 9 (phenolphthalein indicator). The reaction of the SiF_6^{2-} anion, simplified described by Eq. (3), delivers free fluoride ions which are measured by ion chromatography. Finally, the measured fluoride content is converted into the content of H_2SiF_6.

$$K_2SiF_6(s) + 4OH^-(aq) \rightarrow Si(OH)_4(aq) + 2K^+(aq) + 6F^-(aq) \quad (3)$$

The analytical results for series 1 are shown in Table 2. Reliability and validity of the developed procedure are underlined in Fig. 3 by the comparison with the results obtained by methods 1 and 2 [8].

Table 3 and Fig. 4 summarize the results for sample series 2 and show again the validity of the developed precipitation method. However, samples S2-F and S2-G are of special interest. Both samples are supersaturated with respect to silicon resulting in a molar Si:F ratio of less than 1:6 (the lowest reported ratio is 1:4.5 [9]). Precipitation from such solutions gives only K_2SiF_6 regardless the degree of supersaturation.

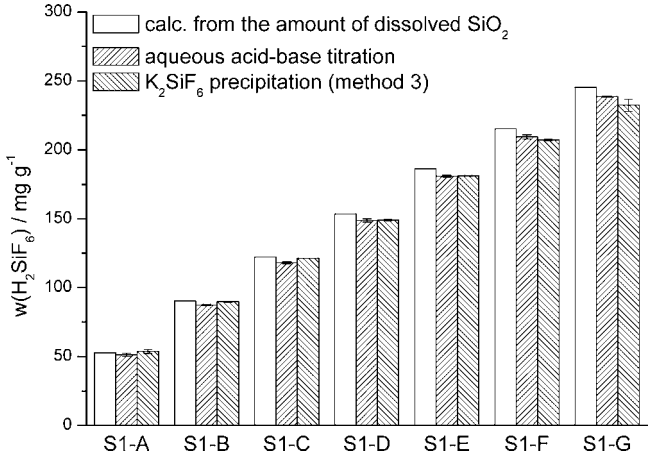

Fig. 3. Summary of all developed methods to determine the H_2SiF_6 content in sample series 1.

The silicon contents determined by ion chromatography after K_2SiF_6 precipitation are in reasonable agreement of less than 2.5% to the results of the aqueous acid–base titration. Exceptions of larger deviation are found only for the samples S1-A (4.5%) and S2-A (3.2%). The relative uncertainties from the aqueous acid–base titration and ion chromatography after K_2SiF_6 precipitation are comparable so that both methods are considered to be equivalent in their performance to analyze the silicon content in etch bath solutions. Furthermore, these series show that losses of silicon during the dissolution cannot be avoided neither by

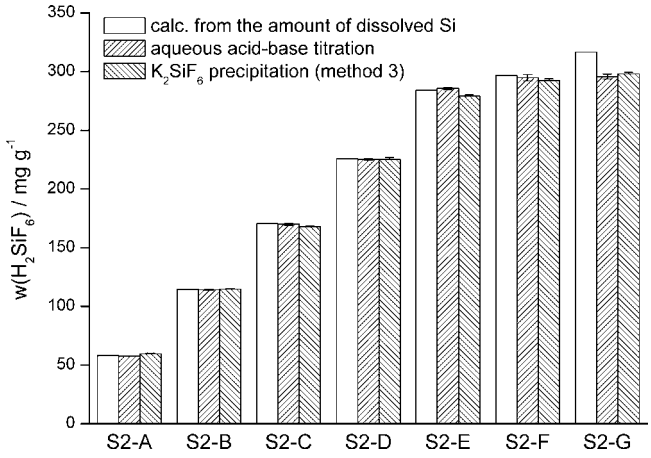

Fig. 4. Summary of all developed methods to determine the H_2SiF_6 content in sample series 2.

Table 3
H_2SiF_6 content in series 2 obtained by ion chromatography from the K_2SiF_6 precipitate (*m* denotes the number of analyses)

Sample	w(Si) initial (mg g^{-1})	w(Si) analyzed (mg g^{-1})	*m*	Recovery (%)	$w(H_2SiF_6)$ (mg g^{-1})
S2-A	11.3	11.6 ± 0.1	4	102.7	59.6 ± 0.5
S2-B	22.3	22.4 ± 0.1	3	100.2	114.8 ± 0.4
S2-C	33.3	32.7 ± 0.1	3	98.4	167.9 ± 0.6
S2-D	44.0	43.9 ± 0.3	3	99.8	225.3 ± 1.6
S2-E	55.4	54.4 ± 0.2	2	98.2	279.1 ± 1.2
S2-F	57.8	57.0 ± 0.3	3	98.5	292.4 ± 1.4
S2-G	61.7	58.1 ± 0.3	3	94.1	298.1 ± 1.3

Table 4
Total fluoride content in sample series 1 and 2 measured by ion chromatography (*m* denotes the number of analyses)

Series 1					Series 2				
Sample	$w(F^-)$ initial (mg g^{-1})	$w(F^-)$ analyzed (mg g^{-1})	*m*	Recovery (%)	Sample	$w(F^-)$ initial (mg g^{-1})	$w(F^-)$ analyzed (mg g^{-1})	*m*	Recovery (%)
S1-A	249.6	242.7 ± 0.1	2	97.3	S2-A	253.1	241.4 ± 1.8	8	95.4
S1-B	242.9	236.0 ± 0.4	2	97.1	S2-B	250.2	247.2 ± 0.1	2	98.8
S1-C	240.0	236.2 ± 0.5	2	98.4	S2-C	248.3	236.0 ± 0.3	4	95.0
S1-D	236.18	229.8 ± 0.4	2	97.3	S2-D	247.0	245.7 ± 0.4	2	99.5
S1-E	232.6	227.8 ± 0.1	2	97.9	S2-E	242.5	229.9 ± 4.3	8	94.8
S1-F	229.0	222.8 ± 0.6	2	97.3	S2-F	240.9	232.9 ± 1.9	10	96.7
S1-G	225.5	221.5 ± 0.4	2	98.2	S2-G	240.4	237.3 ± 0.3	2	98.7

the use of silicon nor by SiO_2 nor by the choice of mild reaction conditions.

3.3. Determination of total fluoride content

The total fluoride content needs to be measured to calculate the content of HF. Table 4 summarizes the analytical results for series 1 and 2. In both cases, a significant loss due to sample preparation had occurred, even if the dissolution processes were carried out very slowly. Particularly, the dissolution of silicon in HF–HNO_3 mixtures seems to be very arbitrarily affected.

3.4. Determination of HF content

Finally, the HF content in etch solutions is determined by two different ways:

- *Route a*: by chromatographic determination of the fluoride ion concentration in the filtrate of the K_2SiF_6 precipitation or
- *Route b*: as the difference between the total fluoride content and the fluoride content bound in the K_2SiF_6 precipitate.

Table 5 shows a remarkable agreement between the HF contents directly measured in the filtrate of the K_2SiF_6 precipitation (route a) and the calculated values according to route b. The etch mixture analysis based on ion chromatography and precipitation gives the most uniform results compared to the other methods.

The results of series 2 in Table 5 shows clearly that the dissolution of silicon in HF–HNO_3 mixtures is affected from arbitrary influences as mentioned already in Sections 3.2 and 3.3. Even if silicon is dissolved in small portions and at 1 °C to slow down the reaction rate, considerable losses of SiF_4 are inevitable. Furthermore, it becomes obviously that Eq. (1) is not applicable to calculate the theoretical amount of remaining free HF after the

Table 5
HF content in sample series 1 and 2 measured in the filtrate of the K_2SiF_6 by ion chromatography and calculated from the difference between the total fluoride content and the fluoride content bound as K_2SiF_6 (*m* denotes the number of analyses)

Series 1				Series 2			
Sample	Filtrate (route a)		Calculated (route b)	Sample	Filtrate (route a)		Calculated (route b)
	w(HF) (mg g^{-1})	*m*	w(HF) (mg g^{-1})		w(HF) (mg g^{-1})	*m*	w(HF) (mg g^{-1})
S1-A	209.8 ± 4.4	3	210.9 ± 1.1	S2-A	199.8 ± 2.4	7	204.5 ± 2.0
S1-B	173.1 ± 1.3	3	173.8 ± 0.6	S2-B	167.1 ± 5.8	3	164.7 ± 0.3
S1-C	145.0 ± 0.6	3	147.7 ± 0.6	S2-C	107.5 ± 0.7	3	108.6 ± 0.6
S1-D	120.1 ± 2.3	2	117.9 ± 0.7	S2-D	66.7 ± 0.6	3	71.0 ± 1.4
S1-E	90.5 ± 1.3	3	89.0 ± 0.4	S2-E	15.7 ± 0.4	4	9.6 ± 4.6
S1-F	62.1 ± 0.8	5	62.0 ± 0.8	S2-F	8.5 ± 0.1	3	1.7 ± 2.4
S1-G	39.7 ± 1.0	5	39.6 ± 3.8	S2-G	1.5 ± 0.1	3	1.5 ± 1.2

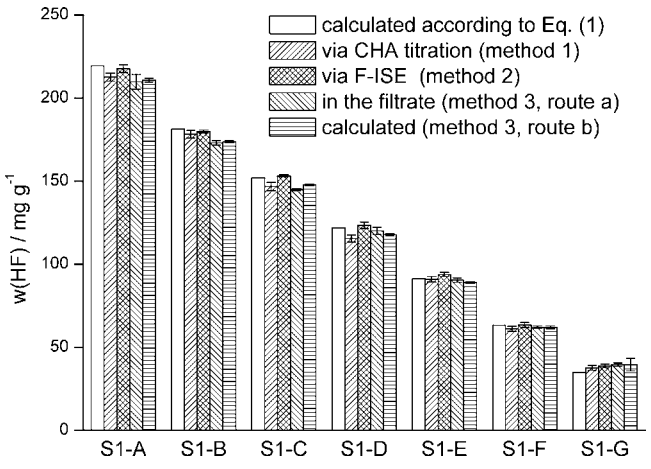

Fig. 5. Summary of all developed methods to determine the HF content in sample series 1.

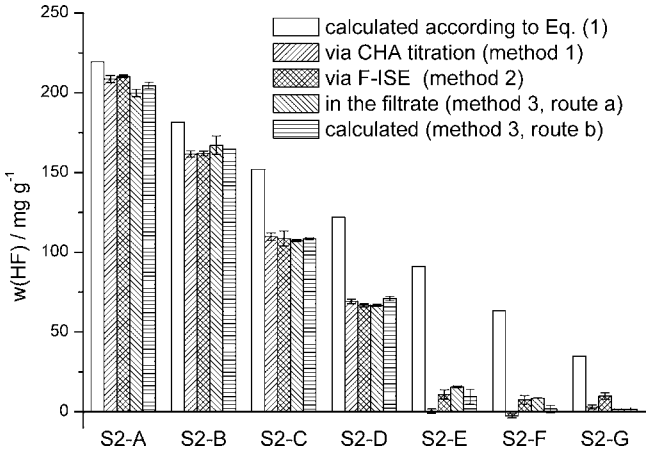

Fig. 6. Summary of all developed methods to determine the HF content in sample series 2.

dissolution of HF. The difference between the theoretical and the measured values becomes as larger as more silicon is dissolved.

Figs. 5 and 6, comparing the results of the HF content analysis by the applied methods, show a satisfying agreement in the determination of the total HF concentration, as long as the content is not too low (S2-E) or the solutions are not over-saturated with silicon (S2-F and S2-G). The samples S2-E to S2-G mark the limits of the developed methods. They are characterized by a very low content of HF, furthermore, the samples S2-F and S2-G are supersaturated with silicon. The CHA titration method fully fails to analyze the HF content in these samples. It seems, that method 2 and the ion chromatographic method are more suitable to analyze such solutions. However, any statement about accuracy and precision have to be omitted, since these solution are lying outside the capabilities of the applied methods.

4. Conclusions

The present study compared three different methods for the chemical analysis of the etch bath constituents HF, HNO_3, and H_2SiF_6 by a non-aqueous titration-based method (method 1), by a combination of a titration in a non-aqueous media and F-ISE (method 2), and an ion chromatography method (method 3). Related to the both other methods, the ion chromatography procedure allows a direct determination of the ion concentrations with lesser efforts and, hence, much lesser costs. Furthermore, the analytical results show lower uncertainties because they arise from the method and the sample preparation only. In contrast, the individual etch bath constituents in the two other methods are not directly measured and obtained only from calculations involving at least two other experimentally obtained values. The propagation of uncertainty leads then to quite high-observed uncertainties. The results show clearly that the analysis by ion chromatography should be preferred for the analysis of etch bath solutions. However, the decision which of the developed method is applicable in practice depends on various other factors like available manpower, the demanded precision of the analytical results, the investment costs, and finally, whether a manual analysis should be replaced by an automated procedure.

Both, the present and the previous studies describe three complex procedures to analyze HF–HNO_3–H_2SiF_6 mixtures. The major challenge is the not fully understood speciation of H_2SiF_6 in presence of the two other acids [11]. As consequence, the developed methods are focused either to the prevailing stabilization of the SiF_6^{2-} anion or to its full cleavage. However, both studies show clearly that the precision of the results and the obtained recoveries are sufficiently only for technical application but not for a deep scientific understanding of the H_2SiF_6 speciation.

Acknowledgements

The authors gratefully acknowledge the European Regional Development Fund 2000–2006 and the Free State of Saxony for funding within the project "SILCYCLE" under contract number 8323/1293 at the Sächsische Aufbaubank (SAB). The authors thank Ms Anja Rietig and Ms Romy Keller for technical assistance.

References

[1] S. DeWolf, P. Choulat, E. Vazsonyi, R. Einhaus, E. van Kerschaver, K. DeClercq, J. Szlufcik, Proceedings of the 16th EC PVSEC, Glasgow, 2000, pp. 1521–1523.
[2] I. Röver, K. Wambach, W. Weinreich, G. Roewer, K. Bohmhammel, Proceedings of the 20th EU-PVSEC, Barcelona, 2005, pp. 899–902.
[3] W. Weinreich, Diploma Thesis, Freiberg University of Mining and Technology, Freiberg, Germany, 2005.
[4] H. Robbins, B. Schwartz, J. Electrochem. Soc. 106 (1959) 505–508.
[5] M. Steinert, J. Acker, A. Henßge, K. Wetzig, J. Electrochem. Soc. 152 (2005) C843–C850.
[6] M. Steinert, J. Acker, M. Krause, S. Oswald, K. Wetzig, J. Phys. Chem. B 110 (2006) 11377–11382.
[7] A. Henßge, J. Acker, C. Müller, Talanta 68 (2006) 581–585.
[8] A. Henßge, J. Acker, Talanta, submitted for publication.
[9] K. Kleboth, Monatsh. Chem. 99 (1968) 1177–1185.
[10] C.E. Shuchart, D.C. Buster, Proceedings of the International Symposium on Oilfield Chemistry, San Antonio, Society of Petroleum Engineers, vols. 14–17, Richardson, TX, 1995, pp. 305–316.
[11] E.T. Urbansky, Chem. Rev. 102 (2002) 2837–2854.

Available online at www.sciencedirect.com
ScienceDirect
Talanta 72 (2007) 1239–1247
Talanta
www.elsevier.com/locate/talanta

Novel reactions for simple and sensitive spectrophotometric determination of nitrite

Riyad Ahmed Al-Okab, Akheel Ahmed Syed *

Department of Studies in Chemistry, University of Mysore, Manasagangothri, Mysore 570006, India

Received 2 October 2006; received in revised form 8 January 2007; accepted 8 January 2007
Available online 17 January 2007

Abstract

Nine spectrophotometric methods based on new reactions for the determination of tracer amounts of nitrite in environmental samples were developed. Replacement of toxic reagents was explored to attain the standards of clean chemistry. These methods utilize two classes of compounds namely; phenoxazines and sulphonamides, the well established drugs in the presence of limited amounts of hydrochloric acid. The methods were based on the oxidation of sulfanilamide (SAA), sulfadoxine (SDX) or sulfamethoxazole (SMX) by nitrite in hydrochloric acid medium and coupling with phenoxazine (PNZ), 2-chlorophenoxazine (CPN) or 2-trifluoromethylphenoxazine (TPN) which yielded red colored derivatives having an absorbance maximum in the range 530–540 nm and were stable for about 4 h. Beer's law was obeyed for nitrite in the concentration range 0.13–1.60 $\mu g\,mL^{-1}$. The reaction conditions and other important analytical parameters were optimized to enhance the sensitivity of the methods. Interference if any, by non-target ions was also investigated. The methods were applied determining nitrite in environmental samples. The performance of these methods were evaluated in terms of Student's *t*-test and variance ratio *F*-test to find out the significance of proposed methods over the reference spectrophotometric method.

Keywords: Spectrophotometry; Nitrite; Sulphonamides; Phenoxazines; Environmental samples

1. Introduction

The monitoring of nitrite in environmental samples is being practiced by most health authorities' world wide, with legislation being levied on its permissible levels in drinking water; at present the maximum contamination level in drinking water is 1 $\mu g\,mL^{-1}$ [1]. Excessive concentration of nitrite in drinking water could be hazardous to health, especially for infants and pregnant women. Nitrite oxidizes iron in hemoglobin of the red blood cells to form methemoglobin, which loses its oxygen carrying ability. This creates the condition known as methemoglobinemia [2]. Nitrite has also direct impact on the health because of its reaction with amines or amides in human body to produce different types of nitrosamines, which are very powerful carcinogens [3]. Therefore, elucidation of nitrite concentration is desirable from the stand point of environmental analytical chemistry.

Environmental analytical chemistry contributes significantly to the growth of environmental responsibility for sustainable development through environmental monitoring. This has been possible due to the advances in analytical techniques which enable the study of toxicants and their role in environmental pollution. Nowadays, analytical methodologies are well established for environmental monitoring. However, a paradoxical situation has emerged as majority of the analytical methods employed to investigate environmental problems generate chemical wastes, which contribute to environmental pollution [4]. In some situations, the chemicals employed are more toxic than the species being monitored. As a consequence, some environmental analytical chemists are focusing this work on the development of methodologies less harmful to human and to the environment. Nowadays, in the development of a new analytical method or a procedure the amount and toxicity of the reagents used and of the wastes produced are as important as any other analytical feature. For example, the analytical method based on Griess *diazo-coupling reaction* with sulfanilamide and *N*-(1-napthyl)ethylenediamine hydrochloride (NEDA) yielding an azo dye is a well established procedure for environmental

* Corresponding author. Tel.: + 91 821 2419660.
E-mail address: akheelahmed54@rediffmail.com (A.A. Syed).

0039-9140/$ – see front matter © 2007 Published by Elsevier B.V.
doi:10.1016/j.talanta.2007.01.027

Table 1
Analytical features of some spectrophotometric (Griess *diazo-coupling reaction*) methods used for the determination of nitrite

Reagent	λ_{max} nm	Beers law range (μg/mL)	Molar absorptivity ($L\,mol^{-1}\,cm^{-1}$)	Reaction time (min)	Remarks	Ref.
p-Nitroaniline+2-methyl-8-quinolinol	585	0.002–0.400	4.72×10^4	3	Most cations and anions interfered	[18]
P-Aminophenylmercaptoacetic acid + NEDA[a]	565	0.02–0.80	4.65×10^4	15	Time consuming	[19]
4-(1-Metyl-1- mesitylcyclobutan-3-yl)-2-aminothiazole + *n*,*n* dimethyl aniline	482	0.05–2.00	2.03×10^4	15	pH-dependent, time consuming and extractive	[20]
p-Nitroaniline + 8-quinolinol	550	0.01–0.06	5.85×10^4	10	pH-dependent and extractive	[21]
Sulfanilic acid + 1-naphthol	418	0.02–0.87	1.70×10^4	20	pH-dependent and time consuming	22
Sulfanilamide + ethyl acetoacetate	356	0.20–3.00	1.22×10^4	7	Fe^{3+} interferes and less sensitive	[23]
p-Nitroaniline + diphenylamine	500	0.05–0.80	1.43×10^4	11	Time consuming and less sensitive	[24]
p-Aminobenzioc acid + NEDA	550	0.05–1.20	2.74×10^4	5	Fe^{2+}, Fe^{3+} interfere and less sensitive	[25]
Acetyl acetone + *p*-nitroaniline	490	0.05–1.40	3.20×10^4	9	Fe^{3+}, Cu^{2+} and Co^{2+} interfere	[26]
Proposed methods	540	0.13–1.00	3.48×10^4	2		

[a] *N*-(1-naphthyl)ethylenediamine dihydrochloride.

monitoring of nitrite. Paradoxically, this analytical methodology uses reagent(s) or generates chemical wastes, which are more toxic than the species being monitored [5]. As a consequence, the analytical methods with high performance but which are not environmentally friendly are not acceptable. Hence, there is a great need to develop methods which are less harmful to human and to the environment—1 of the 12 basic principles of Green Chemistry [6].

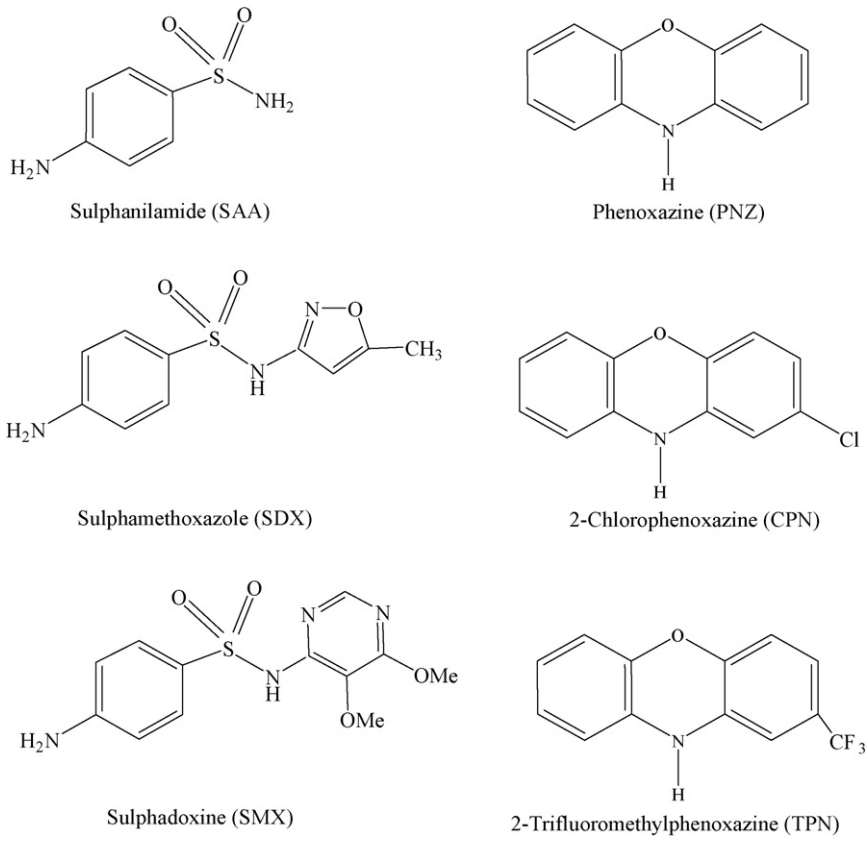

Fig. 1. Structures of sulfonamides and phenoxazines.

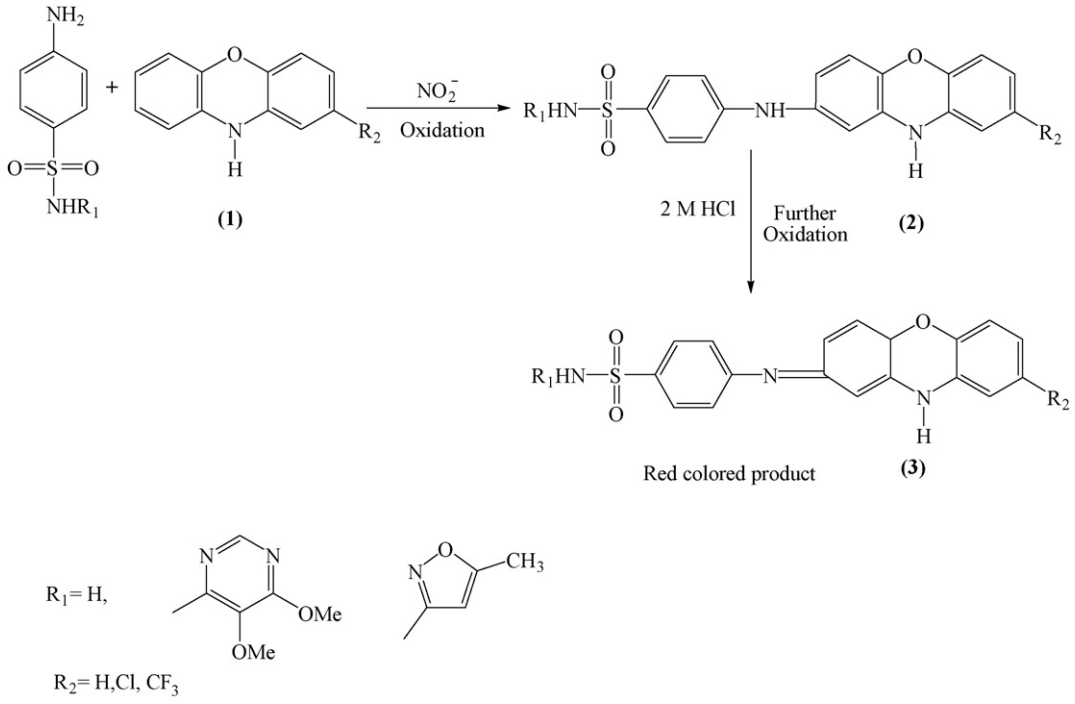

Fig. 2. General reaction mechanism proposed for spectrophotometric determination of nitrite using phenoxazines and sulphonamides.

Various techniques developed so far for the determination of nitrite in environmental samples include: chromatography [7–10], electroanalytical [11–13] and optical techniques [14–16]. Among the optical techniques, simple methods based on UV–vis spectrophotometry have become an accepted analytical tool for the determination of nitrite in environmental samples.

Visible spectrophotometric methods are convenient, sensitive and are relatively inexpensive. These methods employ different routes for determination of chromogen produced [17–29]. Most of the spectrophotometric procedures for nitrite determination are based on diazo-coupling reaction resulting in dye formation and these are characterized by high sensitivity, but often have drawbacks of pH dependence, diazotization temperature and coupling time. Besides, these procedures often use large sample volumes of carcinogenic reagent(s), which makes it outside of the standards of clean chemistry [30]. A comparison of a few selected procedures; their spectral characteristics and drawbacks are enumerated in Table 1.

With the objective of utilizing the non-toxic chemicals which is a 'control exercise' for the formation of hazardous substances, nine novel oxidative coupling reactions using phenoxazines as new class of spectrophotometric chromogens and sulphonamides as new class of electrophilic coupling reagents (Fig. 1) for the determination of nitrite to yield red color derivatives have been developed and these have been shown in Fig. 2. Based on this, highly sensitive, selective and rapid methods were developed and applied for the determination of nitrite in environmental samples. Besides, the reagents offer clear advantages over the chromogenic reagents currently used for the purpose and the procedures show positive feature over the reference method, which necessary involve multiple steps and have drawback of pH dependence, diazotization temperature and coupling time.

2. Experimental

2.1. Reagents

Sulfanilamide (SAA), sulfadoxine (SDX) and sulfamethoxazole (SMX) are gift samples from SmithKline Beecham, India were used as received. Sodium nitrite (Ranbaxy, India) PNZ (Aldrich) were used without further purification. CPN and TPN were synthesized as per the procedures [31,32]. All reagents used were of analytical grade chemicals unless specified otherwise.

Stock sodium nitrite solution, 2.176×10^{-2} M (1000 μg nitrite mL^{-1}) in 1000 mL volumetric flask was prepared by dissolving 1.50 g sodium nitrite (predried at 110°C for 4 h) in water. A small amount of sodium hydroxide to prevent nitrite decomposition and a few drops of chloroform to prevent bacterial growth were also added. Required standard solution of (10 μg nitrite/mL) was prepared by diluting 10 mL of standard sodium nitrite solution to 1000 mL with water.

Stock solutions (0.025%, w/v) of PNZ, CPN and TPN were prepared by dissolving 25 mg of each in distilled ethyl alcohol and diluting quantitatively to 100 mL with distilled ethyl alcohol. Solutions (0.25%, w/v) of SAA, SDX and SMX were prepared by dissolving 250 mg each of them and diluting quantitatively to 100 mL with water. One molar hydrochloric acid (20 mL) was added during the preparation of sulfadoxine and sulfamethoxazole to increase its solubility. Two molar hydrochloric acid solution was prepared by diluting quantitatively 176.99 mL of 35% HCl (Merck, Germany) to 1 L with distilled water.

Table 2
Spectral data for determination of nitrite using sulphonamides as electrophilic coupling agents and phenoxazines as chromogens

Parameters	PNZ			CPN			TPN		
	SAA	SDX	SMX	SAA	SDX	SMX	SAA	SDX	SMX
Color	Red	Red	Red	Red	Red	Red	Red	Red	Red
λ_{max} (nm)	540	540	540	530	530	530	530	530	530
Stability (h)	4	4	4	4	4	4	4	4	4
Beer's law ($\mu g\,mL^{-1}$)	0.13–1.00	0.15–1.10	0.20–1.30	0.20–1.10	0.23–1.20	0.19–1.10	0.30–1.60	0.40–1.60	0.31–1.00
Recommended ion concentration[a] ($\mu g\,mL^{-1}$)	0.50	0.50	0.50	0.50	0.50	0.50	0.50	0.50	0.50
Molar absorptivity ($L\,mol^{-1}\,cm^{-1}$) × 104	3.48	3.30	2.86	2.67	2.38	2.57	1.60	1.30	1.40
Sandell's sensitivity ($\mu g\,cm^{-2}$)	0.0013	0.0014	0.0016	0.0017	0.0019	0.0018	0.0029	0.0035	0.0031
Detection limit ($\mu g\,mL^{-1}$)	0.08	0.08	0.17	0.09	0.10	0.09	0.12	0.20	0.06
Regression equation[b]									
Slope (a)	0.772	0.219	0.046	0.045	0.045	0.128	0.496	0.381	0.772
Intercept (b)	−0.012	−0.006	−0.005	0.007	−0.017	−0.006	−0.107	−0.070	−0.012
Correlation coefficient	0.9920	0.9985	0.9990	0.9890	0.9980	0.9964	0.9890	0.9880	0.9920
Reaction time (min)	2	2	2	2	2	2	2	2	2
RSD[c]% ($n = 7$)	0.37	0.22	0.25	0.25	0.42	0.62	0.56	0.32	0.73

[a] Almost middle of the Beer's law range.
[b] $y = ax + b$ where x is the concentration of nitrite in $\mu g\,mL^{-1}$.
[c] Relative standard deviation.

2.2. Apparatus

Specord 50 UV–vis spectrophotometer with 1.0-cm silica quartz matched cell was used for measuring the absorbance.

2.3. General procedure

To a series of 25 mL calibrated flasks; 2 mL of SAA, SDX or SMX (0.25%, w/v) reagent, nitrite solution, 1 mL of PNZ, CPN or TPN (0.025%, w/v) and 1 mL of 2M HCl were added and the mixture shaken thoroughly and allowed to stand for 5 min and the volume was made up with water. Absorbance at 540 nm for PNZ–SAA/SDX/SMX and at 530 nm for CPN/TPN–SAA/SDX/SMX methods were measured in 1.0-cm quartz cell against reagent blank which was prepared without nitrite.

2.4. Interference

The selectivity of the proposed methods was studied by the effect of various chemical species on the determination of nitrite. The tolerance limit was defined as the concentration of added ion causing less than ±3% relative error for the nitrite determination.

3. Results and discussion

The optical characteristics for the determination of nitrite with PNZ, CPN and TPN using SAA, SDX and SMX are detailed in Table 2. Phenoxazine is an isolog of phenothiazine and is known since 1887. It is a part of the chemical structure of actinomycin D, which is known to exert intensive anticancer activity on malignant tumors in children [33] and is reported to be more potent and less toxic chemosensitizer [34]. Phenoxazine derivatives exist in neutral form, as monocations, as dications and even as trications depending on the environment [35]. Their molecular structure and luminescent properties have been studied to a great extent [36]. Besides, they have impressive applications as biological stains [37], as laser dyes [38] and as redox indicators [39]. Phenoxazine derivatives are nervous system depressants particularly with sedative, antiepileptic, tranquillizing activity [40] spasmalytic activity [41] antitubercular activity [42] and anthelmentic activity [43]. In recent years phenoxazine derivatives are reported to be potential chromophoric compounds in host–guest artificial photonic antenna systems [44].

The sulphonamides are analogues of *p*-aminobenzoic acid and are known since 1932. Though a large number of sulphonamides are synthesized and reported in the literature, only about two dozens of them have been used in clinical practice [45]. They differ only slightly in their antimicrobial activity but vary greatly in their pharmacokinetic properties, or rate of excretion. Accordingly, they are classified as short-, medium-, long- and ultra-long acting drugs [46]. Sulfanilamide (SAA) belongs to short-acting, sulfamethoxazole (SMX) medium-acting and sulfadoxine (SDX) ultra-long acting sulphanomides.

Electrophilic coupling reaction has attracted considerable attention for quantitave analysis of many environmental active compounds [47,48]. In the present investigations SSA, SDX or SMX is oxidized quantitatively by nitrite ions and coupled with PNZ, CPN or TPN to form red color. A general reaction mechanism proposed is prescribed in Fig. 2.

The standard method for the determination of nitrite in water samples uses the reddish purple azo dye produced at pH 2.0–2.5 by coupling diazotized sulfanilamide with NEDA. The aim of this study was to avoid diazotisation reaction to make the method greener. Consequently, we have exploited the quantitative prop-

Table 3
Tolerance limits of some diverse ions on the reaction of nitrite (0.5 μg mL^{-1}) with sulfanilamide using phenoxazine[a]

Foreign ions	Tolerance limit (μg mL^{-1})
Na^+, Mg^{2+}, Al^{3+}, Zn^{2+}, Pb^{2+}, Bi^{2+}, K^+	100
EDTA, F^-, Br^-, Bi^{3+}, Ba^{2+}, Ti^{4+}	200
NO_3^-, Cl^-, Br^-, SO_4^{2-}, NH_4^+, CO_3^{2-}, Cu^{2+}	50
Fe^{3+}	0.5
Chloramine T, Chloramine B	1.0
Cl_2	0.2
S^{2-}	50
IO_3^-, IO_4^-, BrO_3^-	0.4

[a] Similar results were found with other proposed methods.

erty of nitrite to oxidize sulfanilamide and subsequently couple with phenoxazines to yield red color which forms the basis for spectrophotometric determination.

The following experiments were carried out to prove this point: the diazotized sulfanilamide was made to react with phenoxazine instead of NEDA which did not develop any color. Alternatively, instead of nitrite, chloramine-T was used to oxidize sulfanilamide and subsequently coupled with phenoxazine, which developed red color. These experiments confirmed that the proposed reactions were not based on conventional diazotization reaction; instead, they followed an alternate route to produce color based on oxidative electrophilic coupling reactions.

Key parameters that influenced the performance of the method were studied to arrive at the optimum working configurations. All the data given and %RSD in the optimization steps for both physical and chemical parameters are the mean values from successive determinations. All the optimization steps were carried out with a chosen nitrite concentration as mentioned in Table 2. The effects of possible interference and the maximum tolerable concentration are given in Table 3.

3.1. Wavelength determination

In order to have minimum interferences, it was necessary to identify optimum wavelength for nitrite determination in the method. This wavelength must be specific for the quantitative and specific monitoring of the nitrite SAA, SDX or SMX-PNZ, CPN or TPN. The wavelength of maximum absorbance was identified by scanning the product of nitrite–PNZ–SAA, SDX or SMX, nitrite–CPN–SAA, SDX or SMX and TPN–SAA, SDX or SMX over the range 300–800 nm with a specord 50 UV–vis spectrophotometer. A wavelength of 530, 540 and 540 nm, respectively, was found optimum for getting best results (Figs. 3 and 4).

3.2. Effect of reagents and acid concentration

The effect of PNZ, CPN and TPN reagents was studied in the range 0.10–10.00 mL (0.025%, w/v) solution of each to achieve the maximum color intensity; volume of 0.50–3.00 mL of the solution gave good result. Hence, 1 mL (0.025%, w/v) PNZ,

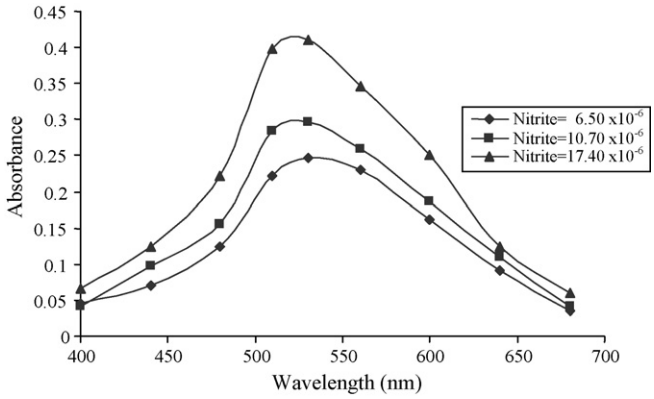

Fig. 3. Absorption spectra of phenoxazine–sulfanilamide complex at different concentrations of nitrite.

CPN and TPN solution in 25 mL standard flask was selected for further studies, under optimized conditions. The maximum intensity of the red color was achieved in hydrochloric acid medium.

Preliminary investigations showed that hydrochloric acid was better than sulphuric, phosphoric or acetic acid. Maximum intensity of the red color was achieved in the range of 1–6 mL of 2 M HCl. Therefore, 1 mL of 2 M HCl in 25 mL was used for getting the best results.

Similarly, the same procedure was adopted to ascertain the amount of SAA, SDX and SMX required for getting constant and maximum color intensity. It was found that 0.50–3.00 mL of the solution were needed to get good result. Hence, 1 mL of (0.25%, w/v) SAA, SDX or SMX solutions is sufficient to get reproducible results.

Experiments were carried out to optimize temperature and time of the reaction. It was found that the maximum color developed within 2 min at room temperature and remained almost stable for about 4 h. Increase in the temperature decreased the intensity of the red color. Hence, 2 min reaction at room temperature was sufficient for the routine analysis.

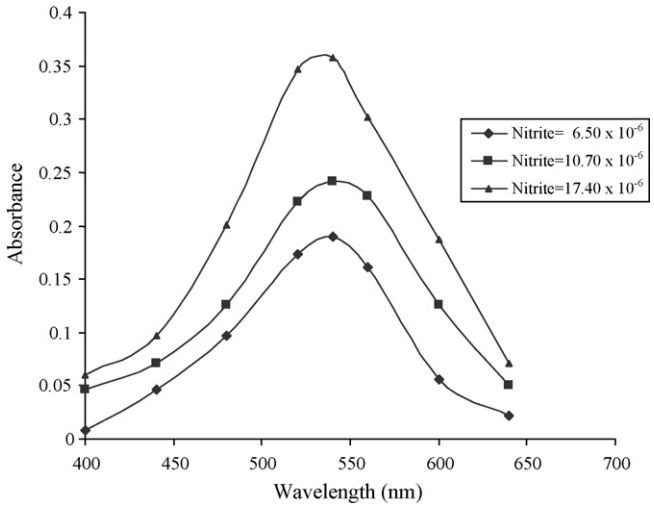

Fig. 4. Absorption spectra of phenoxazine–sulfadoxine complex at different concentrations of nitrite.

Table 4
Determination of nitrite in different environmental samples using SAA and PNZ

Sample	Nitrite added (μg/mL)	Proposed method		Reported method [29]			
		Nitrite recovered (μg/mL)	Recovery% ± RSD[a]	Nitrite recovered (μg/mL)	Recovery% ± RSD[a]	*t*-Value[b]	*F*-value[c]
Lake water	0.300	0.290	97.00 ± 0.59	0.229	99.70 ± 0.51	1.68	2.30
	0.500	0.490	98.00 ± 0.25	0.502	100.4 ± 0.31	1.09	1.90
Tap water	0.300	0.310	97.00 ± 0.50	0.301	100.3 ± 0.62	2.10	3.10
	0.500	0.501	100.2 ± 1.20	0.499	99.40 ± 0.91	1.54	2.90
Mineral water	0.300	0.305	102.0 ± 0.54	0.298	99.30 ± 0.37	1.88	4.10
	0.500	0.498	99.60 ± 0.75	0.497	99.40 ± 0.57	1.21	2.80
Well water	0.300	0.303	101.0 ± 0.34	0.302	100.7 ± 0.61	1.47	3.90
	0.500	0.508	101.8 ± 0.83	0.501	100.2 ± 0.78	2.10	1.70
Manured garden soil	0.300	0.310	97.00 ± 0.40	0.290	97.00 ± 0.56	2.41	3.41
	0.500	0.498	99.00 ± 0.31	0.501	100.2 ± 0.72	1.40	2.56
Farmland soil	0.300	0.303	101.0 ± 0.65	0.299	99.70 ± 0.57	1.23	4.10
	0.500	0.507	101.0 ± 0.53	0.508	101.0 ± 0.21	1.21	3.70
Roadside soil	0.300	0.301	101.0 ± 0.68	0.309	103.0 ± 0.38	0.38	3.90
	0.500	0.504	100.8 ± 0.52	0.498	99.60 ± 0.31	1.60	3.40

[a] Average of five determinations ± relative standard deviation.
[b] Tabulated *t*-value at 95% confidence level is 2.78.
[c] Tabulated *F*-value at 95% confidence level is 6.39.

3.3. Order of addition of reactants

During the course of the investigation it was observed that the sequence of addition of reactants was also important as it influence the intensity and the stability of the color of the product to great extent. The sequence (i) PNZ, CPN or TPN–HCl–nitrite–SAA, SDX or SDX and (ii) nitrite–HCl–PNZ, CPN or TPN-SAA, SDX or SDX gave less intense and unstable color. While, (iii) nitrite–SAA, SDX or SDX–HCl–PNZ, CPN and TPN gave more intense and stable red color. This is expected as the reaction (i) and (ii) produced radical cation, while, in (iii) electrophilic reaction was evident.

4. Analytical figures of merit

The spectrophotometric methods were evaluated under the optimum conditions with respect to linearity, accuracy, precision, molar absorptivity and Sandell's sensitivity.

Table 5
Determination of nitrite in different environmental samples using SDX and PNZ

Sample	Nitrite added (μg/mL)	Proposed method		Reported method [29]			
		Nitrite recovered (μg/mL)	Recovery% ± RSD[a]	Nitrite recovered (μg/mL)	Recovery% ± RSD[a]	*t*-Value[b]	*F*-value[c]
Lake water	0.300	0.301	101.0 ± 0.81	0.309	103.0 ± 0.50	2.10	3.40
	0.500	0.503	100.6 ± 0.85	0.501	100.2 ± 0.67	1.90	5.60
Tap water	0.300	0.299	99.70 ± 0.73	0.305	102.0 ± 0.74	1.10	5.70
	0.500	0.504	100.8 ± 0.52	0.498	99.60 ± 0.31	1.70	4.80
Mineral water	0.300	0.297	99.00 ± 0.41	0.290	97.00 ± 0.59	2.20	1.90
	0.500	0.498	99.60 ± 0.75	0.507	101.4 ± 0.53	2.50	2.70
Well water	0.300	0.303	101.0 ± 0.76	0.310	97.00 ± 0.41	1.60	3.10
	0.500	0.502	100.4 ± 0.32	0.498	99.60 ± 0.75	1.80	4.90
Manured garden soil	0.300	0.303	101.0 ± 0.34	0.290	100.7 ± 0.52	2.10	2.60
	0.500	0.501	100.2 ± 1.20	0.501	99.40 ± 0.82	1.10	3.70
Farmland soil	0.300	0.309	103.0 ± 0.48	0.299	101.0 ± 0.90	0.98	2.60
	0.500	0.502	100.4 ± 0.39	0.508	100.2 ± 0.81	1.70	4.20
Roadside soil	0.300	0.290	97.00 ± 0.57	0.309	99.70 ± 0.61	1.30	3.40
	0.500	0.501	100.2 ± 0.80	0.498	100.0 ± 0.52	1.10	2.41

[a] Average of five determinations ± relative standard deviation.
[b] Tabulated *t*-value at 95% confidence level is 2.78.
[c] Tabulated *F*-value at 95% confidence level is 6.39.

Table 6
Determination of nitrite in different environmental samples using SMX and PNZ

Sample	Nitrite added (μg/mL)	Proposed method		Reported method [29]			
		Nitrite recovered (μg/mL)	Recovery% ± RSD[a]	Nitrite recovered (μg/Ml)	Recovery% ± RSD[a]	*t*-Value[b]	*F*-Value[c]
Lake water	0.300	0.310	97.00 ± 0.41	0.290	97.00 ± 0.56	2.43	3.41
	0.500	0.507	101.0 ± 0.53	0.508	101.0 ± 0.21	1.90	5.62
Tap water	0.300	0.290	97.00 ± 0.57	0.303	101.0 ± 0.41	2.10	1.77
	0.500	0.498	99.00 ± 0.31	0.501	100.2 ± 0.72	2.60	2.31
Mineral water	0.300	0.309	103.0 ± 0.48	0.298	99.30 ± 0.78	1.40	2.56
	0.500	0.507	101.4 ± 0.82	0.498	99.50 ± 0.89	0.98	2.80
Well water	0.300	0.303	101.0 ± 0.65	0.299	99.70 ± 0.57	1.50	4.10
	0.500	0.501	100.2 ± 0.62	0.502	100.4 ± 0.39	1.70	5.20
Manured garden soil	0.300	0.310	97.00 ± 0.41	0.290	102.0 ± 0.74	1.30	3.40
	0.500	0.501	100.2 ± 0.68	0.501	100.6 ± 0.34	1.70	3.10
Farmland soil	0.300	0.298	99.30 ± 0.71	0.299	100.2 ± 0.70	1.30	4.60
	0.500	0.508	101.8 ± 0.36	0.508	99.30 ± 0.23	1.90	3.30
Roadside soil	0.300	0.290	97.00 ± 0.56	0.309	101.0 ± 0.41	0.98	1.50
	0.500	0.501	100.2 ± 0.39	0.498	101.4 ± 0.28	1.30	2.68

[a] Average of five determinations ± relative standard deviation.
[b] Tabulated *t*-value at 95% confidence level is 2.78.
[c] Tabulated *F*-value at 95% confidence level is 6.39.

The linearity of the spectrophotometric method for the determination of nitrite was evaluated under optimum conditions. The regression calibration equation obtained under optimum conditions for nitrite, PNZ and SSA was: $Y = -0.0119 + 0.7722X$; $r = 0.9992$ and $n = 7$, where Y is the absorbance and X is the nitrite concentration as mg/L. The calibration curve was linear over the range 0.13–1.00 mg/L.

The detection limit (D_l) gives an indication of the lowest concentration of nitrite that can be distinguished from the blank absorbance with 99% certainty. The D_l was calculated as: $D_l = 3.3\delta/m$. Where δ is the standard deviation of the blank absorbance $n = 10$, m is the slope of the graph. The calculated D_l for keeping PNZ as an example was 0.048 mg/L of nitrite. The molar absorptivity was 3.48×10^4 L mol^{-1} cm^{-1} for PNZ-SAA complex and Sandell's sensitivity 0.0013 μg cm^{-2}.

Sandell's sensitivity (S) represents the number of micrograms of the determinant per milliliter of a solution having an absorbance (A) of 0.001 for a path length (l) of 1-cm. Thus, $S = 10^{-3}/a = \mu g\ cm^{-2}$ where a is the specific absorptivity and its value (in mL g^{-1} cm^{-1}) corresponds to the determinant in a cuvette with an optical length of 1-cm. Also, $a = (b/\text{molecular weight of nitrite ion}) \times 1000$, where b = molar absorptivity = A/Cl, where C is the molar concentration of the determinant and l = 1-cm path length.

The accuracy of the method was evaluated by comparing the results obtained for real environmental samples (obtained from lake, well and tap water and soil) with the proposed spectrophotometric methods and with the result of standard spectrophotometric method. The results obtained in the proposed spectrophotometric methods compared very well with those from the standard method. The %RSD was found to be <0.8 ($n = 5$). The proposed method was found as accurate and precise as that of the official method (Tables 4–6).

To further confirm the validity and accuracy of the proposed method recovery tests were performed by standard addition method. Each test was repeated five times. The results presented in Tables 4–6 indicate very good recoveries and non-interference from commonly encountered constituents normally present in the real sample.

4.1. Method validation

To validate the proposed spectrophotometric method, Student's *t*-test was performed on the results of five real samples (Tables 4–6). Comparison was made between the proposed spectrophotometric method and the standard method to find out whether the two methods give the same results at the 95% confidence level. The *t*-test with multiple samples was applied to examine whether the two methods for nitrite determination differ significantly at the 95% confidence level.

The calculated Student's *t*-value and *F*-value did not exceed the tabulated value indicating that the proposed method is as accurate and precise as the official method [29].

5. Application to polluted water and soil

Samples of potable water were collected in wide-mouthed plastic vessels from different taps and different packaged water bottles. The samples were frozen at 0 °C within 1 h of collection. Samples were filtered through Whatman No. 41 paper before analysis.

Samples of manured garden soil, farmland soil and roadside soil were collected. Each sample was broken into lumps, and 5-g portion was dried at 55 °C in an oven for 12–16 h. The dried sample was ground, passed through a 2-mm mesh sieve and transferred to Whatman No. 50 filter paper on a Buchner funnel.

Sufficient water (containing one or two drops of concentrated sulphuric acid) was poured on to soak the soil completely. After a few minutes, gentle suction was applied and the soil was washed with double distilled water until about 250 mL of filtrate was collected. The filtrate was made up to a standard volume and aliquots were analyzed [49].

6. Conclusion

Phenoxazines are attractive as a new class of spectrophotometric reagents for the determination of nitrite—an environmental toxicant. Phenoxazines as reagents exhibit better sensitivity and higher reproducibility. While, using these compounds as spectrophotometric reagents it is essential to use SAA, SDX or SMX as electrophilic coupling reagent. The use of aqueous mild acidic medium and choice available with the reagents make the procedure cost-effective and versatile. The proposed methods have distinct advantages of simplicity, sensitivity, reproducibility and generate lesser amounts of toxic waste. Besides, they are superior to the NEDA method [29] for the determination of nitrite which necessary involves multiple steps and have drawback of pH dependence, diazotization temperature and coupling time. Furthermore, the use of sulpha drugs as electrophilic reagents in the determination of environmental toxicants will open up new areas of research. A value-addition to these methods can be achieved, if the procedure is combined with on-line or at-line system and this is under investigation.

In brief, environmental analytical methods showing high performance but which are not environmentally friendly tend to be unacceptable and this will stimulate the development of cleaner methods. Simplicity of the procedures and less cost of the instrument are the hallmark of spectrophotometry. The progress of selective methodologies has contributed much to the technique, but there is a long road to go and the potentialities have not been fully exploited. The replacement of old procedures by attractive methods exploiting available myriad molecules in the field of pharmaceutical chemistry will result in the phenomenal increase in the utilization of less or non-toxic reagents, which consequently will result in the reduction of toxic waste. This will develop an essential environmental conscience for the future. This paper is a step in this direction.

Acknowledgements

The authors thank Prof. M. Afzal Pasha, Department of Chemistry, Central College, Bangalore University, Bangalore 560 009, India for providing the facilities to synthesize the phenoxazine derivatives. One of the authors (RAA) thanks Taiz University, Republic of Yemen for the grant of Research Fellowship and University of Mysore for granting permission to carryout the research work.

References

[1] U.S. Environmental Protection Agency, Drinking Water Standards and Health Advisories, Washington, DC, 2004 (EPA 822-R-04-005).
[2] A.D. Eaton, L.S. Clesceri, A.E. Greenberg, Standard Methods for the Environmental of Water and waste Water, 19th ed., American Public Health Association, Washington, DC, 1995, pp. 475–484.
[3] W. Lijinsky, Chemistry and Biology of *N*-Nitroso Compounds, Cambridge Monographs on Cancer Research, Cambridge, 1992.
[4] P.T. Anastas, Crit. Rev. Anal. Chem. 29 (1999) 167.
[5] F.R.P. Rocha, J.A. Nóbrega, O.F. Filho, Green Chem. 3 (2001) 216.
[6] P.T. Anastas, M.M. Kirchhoff, Acc. Chem. Res. 35 (2002) 686.
[7] D. Tsikas, R.H. Böger, S.M. B-Boger, F.-M. Gutzki, J.C. Frölich, J. Chromatogr. B 661 (1994) 185.
[8] M.I.H. Helaleh, T. Korenaga, J. Chromatogr. B 744 (2000) 433.
[9] S.B. Butt, M. Riaz, M.Z. Iqbal, Talanta 55 (2001) 789.
[10] B.S. Yu, P. Chen, L.-H. Nie, S.-Z. Yao, Anal. Sci. 17 (2001) 495.
[11] J. Davis, R.G. Compton, Anal. Chim. Acta 404 (2000) 241.
[12] M. Badea, A. Amine, G. Palleschi, D. Moscone, G. Volpe, A. Curulli, J. Electroanal. Chem. 509 (2001) 66.
[13] A.A. Ensafi, A. Kazemzadeh, Anal. Chim. Acta 382 (1999) 15.
[14] Z. Huang, T. Korenaga, M.I.H. Helaleh, Microchim. Acta 134 (2000) 179.
[15] T. Odake, M. Tabuchi, T. Sato, H. Susaki, T. Korenaga, Anal. Sci. 17 (2001) 535.
[16] A. Afkhami, M. Bahram, S. Gholami, Z. Zand, Anal. Biochem. 336 (2005) 295.
[17] H.D. Revanasiddappa, T.N.K. Kumar, Chem. Anal. (Warsaw) 48 (2003) 759.
[18] J. Nair, V.K. Gupta, Anal. Chim. Acta 111 (1979) 311.
[19] P.K. Tarafder, D.P.S. Rathore, Analyst 113 (1988) 1073.
[20] H. Ozmen, F. Polat, A. Cukurovali, Anal. Lett. 39 (2006) 823.
[21] A. Chaube, A.K. Baveja, V.K. Gupta, Anal. Chim. Acta 143 (1982) 273.
[22] M. Satake, G.-F. Wang, Fresenius J. Anal. Chem. 357 (1997) 433.
[23] N.V. Sreekumar, B. Narayana, P. Hegde, B.R. Manjunatha, B.K. Sarojini, Microchem. J. 74 (2003) 27.
[24] A. Afkhami, S. Masahi, M. Bahram, Bull. Kor. Chem. Soc. 25 (2004) 1009.
[25] P. Nagaraja, M.S.H. Kumar, K.S. Rangappa, A.S. Suresh, Asian J. Chem. 40 (1999) 509.
[26] Revanasiddappa, K. Kumar, M. Bilwa, Mikrochim. Acta 137 (2001) 249.
[27] X.-F. Yue, Z.-Q. Zhang, H.-T. Yan, Talanta 62 (2004) 97.
[28] K. Horita, M. Satake, Analyst 122 (1997) 1569.
[29] AOAC, Official Methods of Analysis of the Association of Official Analytical chemists, 16 th ed., AOAC, Gaithersburg, 1997 (Method 36.1.21).
[30] S.E. Allen, Chemical Analysis of Ecological Materials, second ed., Blackwell, Oxford, 1989, pp. 132–134.
[31] M.P. Olmsted, P.N. Craig, J.J. Lafferty, A.M. Pavloff, C.L. Zirkle, J. Org. Chem. 26 (1961) 1901.
[32] G.E. Bonvicino, L.H. Yogoazinste, R.A. Harves, J. Org. Chem. 26 (1961) 2797.
[33] R. Ishida, S. Yamanaka, H. Kawai, H. Ito, M. Iwai, M. Nishizawa, M. Hamatake, A. Tomoda, Anti-Cancer Drugs 7 (1996) 591.
[34] K.N. Thimmaiah, J.K. Horton, X.D. Qian., W.T. Beck, J.A. Houghton, P.J. Houghton, Cancer Commun. 2 (1990) 249.
[35] R. Gvishi, R. Reisfeld, M. Eisen, Chem. Phys. Lett. 161 (1989) 455.
[36] A. Grofcsik, M. Kubinyi, A. Ruzsinszky, T. Veszprémi, W.J. Jones, J. Mol. Struct. 555 (2000) 15.
[37] B.C. Channu, H.N. Kalpana, G.B. Eregowda, C. Dass, P.J. Houghton, K.N. Thimmaiah, J. Pharm. Biomed. Anal. 21 (1999) 775.
[38] F.P. Schäfer (Ed.), Dye Lasers, Springer-Verlag, Berlin, 1973.
[39] Z. Stránsky, J. Grúz, Chem. Zvesti. 26 (1972) 507.
[40] A. Ribbentrop, W. Schaumann, Arch. Int. Pharmacodyn. Ther. 149 (1964) 374.
[41] A.E. Gel, S. Avakian, J. Med. Chem. 6 (1963) 809.
[42] A. Girard, US Patent 3,048,586, 1962.;
A. Girard, Chem. Abstr., 58 (1963) 1471g.
[43] W.P. Rogers, J.C. Craig, G.P. Warwick, Br. J. Pharmacol. 10 (1955) 340.

[44] G. Calzaferri, M. Pauchard, H. Maas, S. Huber, A. Khatyr, T. Schaafsma, J. Mater. Chem. 12 (2002) 1.
[45] E.H. Northey, The Sulfonamides and Allied Compounds, ACS Monogr. Ser. American Chemical Society, Washington, DC, 1948.
[46] J.E.F. Reynolds, The Extra Pharmacopoeia, 30th ed., The Pharmaceutical Press, London, 1993, p. 112.
[47] S. Suresha, M.F. Silwadi, A.A. Syed, Int. J. Environ. Anal. Chem. 82 (2002) 275.
[48] D. Rekha, K. Suvardhan, K.S. Kumar P. Subrahmanyam, B. Jayaraj, G.R. Naidu, P. Chiranjeevi, J. Hazard. Mater., in press.
[49] A. Chaube, A.K. Baveja, V.K. Gupta, Talanta 31 (1984) 391.

Available online at www.sciencedirect.com
ScienceDirect
Talanta 72 (2007) 1255–1260
Talanta
www.elsevier.com/locate/talanta

Exploiting sequential injection analysis with lab-on-valve and miniaturized potentiometric detection Epinephrine determination in pharmaceutical products

C.G. Amorim, A.N. Araujo, M.C.B.S.M. Montenegro *

REQUIMTE, Departamento de Química-Física, Faculdade de Farmácia da Universidade do Porto, Rua Aníbal Cunha 164, 4099-030 Porto, Portugal

Received 31 July 2006; received in revised form 28 December 2006; accepted 9 January 2007
Available online 15 February 2007

Abstract

Miniaturized potentiometric units were constructed, evaluated and incorporated in a SIA-LOV manifold in order to the control of pharmaceutical analysis. The method validation was done with ephinefrine determinations in commercial pharmaceutical products. The optimization procedures were directed at potential versus epinephrine concentration. This approach was achieved by selecting 60 cm of reactor and a flow rate of 11 $\mu L\,s^{-1}$ and injecting 78 μL of epinephrine standard solutions in a 1.0×10^{-3} mol L^{-1} IO_4^- solution. A linear range was found for epinephrine concentrations between 2.0×10^{-4} and 2.5×10^{-3} mol L^{-1} with a slope of 35528 mV L mol^{-1} and $r^2 = 0.997$. Under these conditions the analytical results for the commercial pharmaceutical formulations of 0.908 and 0.454 mg mL^{-1}, respectively, with a R.S.D. of 0.34 for both, was obtained. Through down scaling periodate-selective electrode it was possible to benefit from the recognized advantages of the lab-on-valve sequential-injection based systems, namely regarding equipment portability, reduced consumption of the sample and the reagents and the reduction of effluent waste. Furthermore, the new periodate electrode configuration is easy to achieve in common laboratories and enables the implementation of low volume detection cell where the electrical noise, that is frequently presented in potentiometric based procedures, is significantly reduced.

Keywords: Electrode miniaturized; LOV-potentiometry; Epinephrine

1. Introduction

Traditionally, pharmaceutical analysis relies heavily on chromatography. However, automation and miniaturization requirements simple solution-based assays to make them fast and efficient which are essential for many routine and research tasks in pharmaceutical laboratories. Ideally, the setups should be open for the accommodation of a wide variety of determinations without the need for system reconfiguration, and should be compatible with both optical and electrochemical detectors. The sequential injection analysis (SIA) [1], based on programmable flow to fulfil those requisites, has been recently enhanced by the miniaturization implemented in lab-on-valve (LOV) format [2]. A LOV manifold comprises a monolithic structure of flow channels incorporated in a multi-position valve that can perform a variety of sample manipulation operations. In the SI-LOV system, the volume of the sample path from the injector to the detector can be minimized and a smaller volume of waste solution is generated when compared with common SI system. The SI-LOV technique has been explored directly by coupling spectrophotometric [2,3,4], fluorescence [2], electrothermal atomic absorption spectrometry and inductively coupled plasma mass spectrometry [5,6] detection.

The advantages of using ion-selective electrodes (ISE) for determining organic species in pharmaceutical preparations are well known as they may be an expedient alternative to the time consuming and tedious procedures suggested in the pharmacopoeias [7]. When compared to many other analytical techniques, ion-selective electrodes are relatively inexpensive and simple to use and have an extremely wide range of applications and wide concentration range. Potentiometric methods are also adequate for flow analysis due to their favourable characteristics of sensitivity, controllable selectivity and easy of signal handling through automation. From this coupling, enhanced precision and accuracy are usually achieved. However, one cannot find any published work concerning to the association of ISE

* Corresponding author.
E-mail address: mcbranco@ff.up.pt (M.C.B.S.M. Montenegro).

0039-9140/$ – see front matter © 2007 Elsevier B.V. All rights reserved.
doi:10.1016/j.talanta.2007.01.070

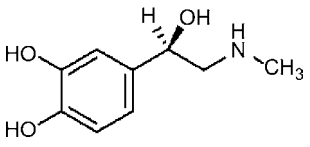

Fig. 1. Chemical structure of epinephrine.

with SI-LOV. Smaller sample injection and waste volumes are reduced once compared with conventional flow systems where these volumes are usually in the range of 0.5 and 4 mL per assay, respectively. In this paper, attempts were made to explore SIA with the LOV and potentiometric detection. For this purpose miniaturized potentiometric units were constructed, evaluated and incorporated in a SIA-LOV manifold in order to control the pharmaceutical analysis. The method validation was done with ephinefrine determinations in commercial pharmaceutical products.

Catecholamines (CAs) are compounds containing an *o*-catechol nucleus and amine group on a chain of two-carbon *m* or *p* atoms to the phenolic hydroxyl groups. Several CAs are dopamine, levedopa, metyldopa and adrenaline. Epinephrine is a sympathomimetic drug, acting on both alpha- and beta-receptors. Chemically, epinephrine or 4-(1-hydroxy-2-[methylamino]ethyl)-1,2-benzenediol hydrochloride as the structure depicted in Fig. 1.

It is the drug of choice for emergencies treatment of severe allergic reactions (type I) to insect stings or bites, food, drugs, and other allergens. It can also be used in the treatment of idiopathic or exercise-induced anaphylaxis. The strong vasoconstrictor action of epinephrine through its effect on alpha adrenergic receptors acts quickly to counter vasodilatation and increased vascular permeability which can lead to loss of intravascular fluid volume and hypotension during anaphylactic reactions. Until now, epinephrine determinations has been done by liquid chromatography [8], spectrophotometry [9–11], capillary electrophoresis [12], fluorescence spectroscopy [13] and chemiluminescence[14,15] detection. In this work, an indirect oxidative reaction with periodate (IO_4^-) was observed, measuring the decrease of the periodate concentration after the reaction with epinephrine. Periodate is widely used as reagent in quantitative analytical chemistry [16] because of its strong oxidizing characteristics.

Although the proposed method presents a detection limit slightly higher then those previously reported [8–15], which is a characteristic of potentiometry, the linear range is almost the same as previously referred [8–15]. However, the most important advantages of the developed method is it accuracy, simplicity, low cost and specially the reduced sample and waste volumes spended.

2. Experimental

2.1. Reagents and solutions

Distilled, deionised water (conductivity <0.1 $\mu S\,cm^{-1}$) and analytical grade chemicals were used without further purification unless otherwise stated.

A stock solution of sodium periodate ($NaIO_4$) (Riedel-de-Haën) was daily prepared by using 0.214 g of reagent (Riedel-de-Haën), carefully weighed, into a 100 mL volumetric flask and subsequent dilution to the mark with sodium sulphate solution with a ionic strength of 0.1 mol L^{-1}. Periodate calibrating solutions, in the range between 1×10^{-6} and 1×10^{-2} mol L^{-1} was done using as carrier in the flow set-up sodium sulphate solution with an ionic strength of 0.1 mol L^{-1}.

A stock solution of epinephrine hydrochloride was daily prepared of 0.219 g of reagent (Sigma), carefully weighed, into a 100 mL volumetric flask and subsequent dilution to the mark with deionised water. Epinephrine calibrating solutions, in the range between 2.20×10^{-2} and 5.49×10^{-1} mg mL^{-1} were prepared adding $Na_2S_2O_5$ at a final concentration of 3.6 mg mL^{-1}, as preservative. A 1×10^{-3} mol L^{-1} $NaIO_4$ solution in a buffer solution (CH_3COONa/CH_3COOH (Riedel-de-Haën/Merck)), with pH of 5 and a ionic strength adjusted to 0.1 mol L^{-1} was prepared and used as carrier in the flow set-up.

Two hospitalar samples for intramuscular injection were obtained for this study. As the samples contained high levels of sodium metabisulphite, $Na_2S_2O_5$, as preservative, this was removed before analysis by adding 100 μL of concentrated HCl to 15 mL of each solution. Afterwards, the solutions were bubbled with N_2 and finally with pressed air to quantitatively release the dissolved SO_2.

2.2. Apparatus

The schematic representation of the computer-controlled SI-LOV system used is depicted in Fig. 2. It comprises a Minipuls 3 Gilson (Viliers-le-Bell, France) peristaltic pump with a PVC pumping tube ($\emptyset_{int}$ = 0.90 mm) of the same brand, a VICI C25-3118.E, eight-port stream selecting valve (Valco Instruments, Houston, TX), a 161T031 NResearch three-way solenoid valve (Stow, MA), and a Crison MicropH-2002 potentiometer to which a Metrohm electrode of Ag/AgCl (KCl 3 mol L^{-1}), model 6.0727.000 was connected. A homemade lab-on-valve on a single acrylic block with 20 mm thick were four channels ($\emptyset_{int}$ = 0.5 mm) were drilled in order to respectively accesses the central and three lateral ports of the selecting valve. In one

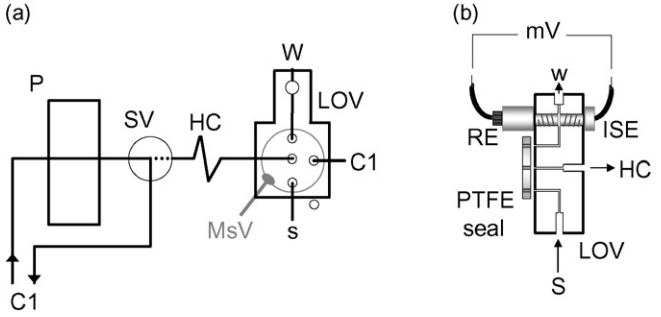

Fig. 2. Schematic view of the proposed set-up. (a) The system comprises a peristaltic pump (P) synchronized with a solenoid valve (SV), a holding coil (HC), an acrylic lab-on-valve manifold (LOV) screwed over the rotor of a stream selecting valve (MsV). W, waste; C_1, carrier solution; S, sample. (b) Side view of the reference and periodate electrode screwed on LOV; RE, reference electrode; ISE, periodate-selective electrode.

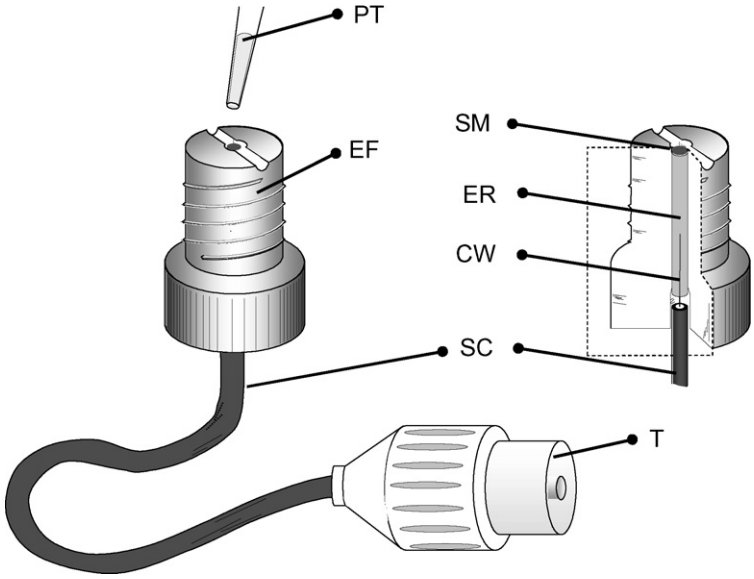

Fig. 3. Schematic view of the miniaturized periodate-selective electrode obtained by drop wising 20 μL of the sensor solution from a 100 μL pipette tip (PT) over the central hole of a commercial end fitting (EF), previously filled with an conductive epoxi resin (ER) in contact with the central wire (CW) of a shielded cable (SC). SM, sensing membrane; T, terminal connector to decimilivoltemer.

of these channels a transverse hole with 0.5 mm diameter was drilled in order to screw from top to top the reference and the periodate-selective electrodes (Fig. 3). A PTFE coil with 60 cm (HC) and flow lines were made with $\emptyset_{int}$ = 0.5 mm PTFE tubing. The rotation speed of the peristaltic pump (P), the rotor position of the eight-port valve (MsV) and the solenoid valve (SV) on/off switching were controlled through a PCL-711 Advanced interface card coupled to a microcomputer running a software written in Quick Basic 4.5.

2.3. Periodate-selective electrode construction

As detector a periodate ion selective electrode, was constructed using the central hole with an internal diameter of 1.5 mm of a commercial end-fitting (Fig. 2b). The ionic sensor was prepared as described by Montenegro [17] by adding 0.36 g tetraoctylamonium bromide (Fluka) plus 9.75 g dibutyl phthalate (Sigma) into 5 mL chloroform (Sigma). The final mixture was mixed in with six 15 mL aliquots of a 0.1 mol L^{-1} sodium periodate (Riedel-de-Haën) solution. The aqueous phase was discarded and the chloroform was evaporated slowly in order to obtain the liquid ionophore. For the membrane preparations, 0.18 g polyvinyl chloride (PVC-Fluka), 6 mL tetrahydrofuran (Riedel-de-Haën) and 0.4 mL of ionophore solution was mixed. The membrane was dropped directly on the conductive surface of the electrode. Drying was accomplished by leaving the electrodes at room temperature for 1 day. Thereafter, the electrodes were placed in contact with 0.01 mol $L^{-1}NaIO_4$ for at least 30 min, in order to achieve equilibrium of the inner reference system.

2.4. Procedures

In a previous publication several drawbacks were identified of the use of a peristaltic pump to drive precise and accurate small volumes of solutions, mainly related with the inertial startup of the rotating head and with the initial position of its rollers [18]. To overcome those problems a three-way solenoid valve was coupled and activated in a synchronized way relative to a preset position of the head of the peristaltic pump. In this way, for a pumping tube with 1.60 mm internal diameter, it was possible to drive volumes of solutions higher than 8 μL with a precision better than 4%. Thus, in this work, a similar study was carried out, in order to evaluate if the detector performance under flow conditions was impaired by the precision of the driving device. Sodium periodate solutions at different concentrations were aspirated at 13 μL s^{-1} by the port 6 (sample port in Fig. 2) and sent towards the flow-through detection cell at the same flow rate. This procedure was repeated ten times for each calibrating solution. A solution with 1.0×10^{-1} mol L^{-1} ionic strength of Na_2SO_4 was chosen as carrier solution.

To extend the application of the mounting to periodate-epinephrine reaction, an analytical cycle comprising three steps was established. In the first two steps epinephrine solution and a 1.0×10^{-3} mol L^{-1} IO_4^- with ionic strength 0.1 mol L^{-1} of Na_2SO_4 solution were sequentially aspirated into the holding coil HC and then propelled towards the detector. A 1×10^{-3} mol L^{-1} $NaIO_4$ solution prepared in a buffer solution (CH_3COONa/CH_3COOH), with pH of 5 and with ionic strength adjusted to 0.1 mol L^{-1} was used as carrier. Afterwards, the downhill simplex method in this work modified to be feed with the experimental results was applied to optimize the flow conditions of the calibration, such as time and flow rate of the different solutions to be aspirated or pumped in the system to find the best relationship between sensibility, resolution and reproducibility.

Finally, to accomplish the epinephrine determination in real samples and taking in consideration the presence of high levels of sodium metabisulphite, $Na_2S_2O_5$, a previous treatment was done. As at pH 1.84 the $Na_2S_2O_5$ can be destroyed going through SO_2, 100 μL of concentrated HCl was added to 15 mL

of each solution, after that, N_2 and air streams were bubbled to quantitatively remove the SO_2.

3. Results and discussion

3.1. Optimization of chemical and hydrodynamic variables

The general working characteristics of periodate electrode were evaluated after coupling it to a homemade LOV SI-system (Fig. 2). Considering the distance of 0.5 mm between the periodate membrane and the reference electrode frit contact as well as the circular diameter exposed to the flow a theoretical 1.4 μL volume was calculated for the flow-through detection cell. For this low volume it was necessary to evaluate if the driving device was capable of aspirating reproducible small volumes, and at the same time evaluate the minimum volume of calibrating solutions, that guarantees similar electrode calibrations to those obtained under conventional flow injection set-ups. For the assay of two calibration solutions with periodate concentrations of 2×10^{-6} and 1×10^{-2} mol L^{-1}, volume independent signals were obtained above aspirated volumes of 85 μL. Even for the lowest injection volume R.S.D. is always lower than 1.2%. In both cases, the volume is relatively high and could be explained by the dead volume of the detection cell, by the response time of the electrodes which is of about 2 s and to some degree of dilution of the injected sample in the detection cell. An important finding was the detector robustness regarding electrical noise, which was almost non existent in the herein proposed system and which demands for an additional ground electrode in the conventional flow tubular electrode configuration where the proximity between the reference and indicator electrodes are difficult to achieve. An optimized periodate calibration curve in LOV-SI system was thus found for an aspiration of 85 μL of periodate solutions with a flow rate of 13 μL s^{-1}. The carrier, a sodium sulfate solution ($I = 0.1$ mol L^{-1}) was pumped to the detector with a flow rate of 12 μL s^{-1} for a 105.47 s period, thus enabling a maximum throughput determination rate of 32 h^{-1}. A linear correlation was found for a concentration interval 1×10^{-5} to 1×10^{-2} mol L^{-1}, with a slope of 61.7 mV per decade and a practical detection limit of 5.4×10^{-6} mol L^{-1} (Fig. 4).

Relative standard deviation of 2.11 and 0.43% were obtained after 8 consecutive injections of two standard solutions of

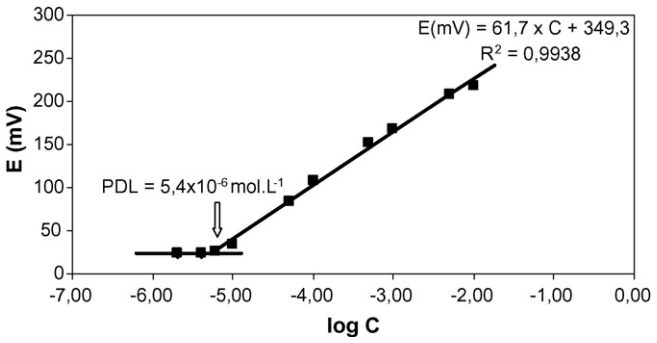

Fig. 4. Potential (E) of the periodate-selective electrode vs. log of IO_4^- concentration. The ionic strength of all solutions was adjusted to 0.1 mol L^{-1} with Na_2SO_4.

Table 1
General working characteristics for the IO_4^- selective electrode

Characteristics	Miniaturized	Tubular
LIRL (mol L^{-1})	1×10^{-5}	8×10^{-6}
Slope (mV/decade)	-61.7 ± 1.0	-58.7 ± 0.1
Reproducibility (mV/decade)	±0.5	±0.3
Response time (s)	<2	<3

sodium periodate 5.0×10^{-5} and 5.0×10^{-3} mol L^{-1}, respectively. The influence of the pH in the electrode behaviour was evaluated, by the addition of NaOH and H_2SO_4 concentrated solutions to 200 mL of a 1.0×10^{-3} mol L^{-1} IO_4^- solution with the ionic strength adjusted to 1.0×10^{-1} mol L^{-1}. Between 2.0 and 6.8 pH the potential readings stayed within ±5 mV, which is consistent to the periodate-selective electrode specifications previously reported [17]. However, the slope of calibrations started to decrease significantly after 10 days of continuous use for 8 h periods. The lower lifetime obtained for this unit compared with the 2 years reported for tubular electrode [17], is probably due to the lower sensor volume used in the membrane preparation and to the continuous sensor exposition to the oxidation reaction (Table 1).

3.2. Optimization of epinephrine determinations

The use of LOV potentiometric system was extended to epinephrine determinations. Knowing that IO_4^- promptly oxidizes vicinal alcohols or amine-alcohol groups through a pseudo first order mechanism [16] epinephrine concentrations could be assessed by the potentiometric monitoring the decrease of circulating periodate in the flow system after sample injection. All epinephrine solutions were aspirated by the sample lateral port of MsV. To improve the signal height, a periodate solution of 1.0×10^{-3} mol L^{-1} IO_4^- with ionic strength 0.1 mol L^{-1} of Na_2SO_4, was sequentially aspirated into the holding coil through an extra lateral port of MsV (Fig. 2). After the carrier, a solution of 1.0×10^{-3} mol L^{-1} IO_4^- with ionic strength 0.1 mol L^{-1} of Na_2SO_4 impelled both injected solutions to the detector. The simplex optimization algorithm was applied to optimize the flow conditions of the periodate/epinephrine reaction, as well as volume and flow rate of the different solutions to be aspirated or pumped in the system. Under these conditions, the injection volume of epinephrine solution was investigated in the range 23–131 μL and the volume of carrier to be aspirated in the second lateral port was also evaluated in the range 9–63 μL. The flow rate of the carrier was studied in the range of 2–51 μL s^{-1}. Once more both the slope of calibration curve as well as the sample throughput rate were considered for maximization in the response function. For the best signals, a detailed evaluation was done to find a good relation between sensibility, resolution and reproducibility. To perform an optimum periodate/epinephrine calibration curve about 78 μL of a solution that contains an accurate epinephrine concentration was aspirated into the holding coil at the flow rate of 13 μL s^{-1}. After this, 43 μL of sodium periodate was aspirated at the flow rate of 12 μL s^{-1} either to increase the epinephrine dispersion and the

reaction extent. Finally, 643 μL of the content volume of holding coil was pumped to the detector during one minute. Due to the mechanism reaction involved a linear dependence between the analytical signal and the analyte concentration was found, as already explained before. Different periodate concentrations of the carrier (1.0×10^{-4} to 1.0×10^{-2} mol L^{-1}) were studied to evaluate sensibility and linearity of the periodate/epinephrine reaction. A higher linearity range and sensibility was found for 1.0×10^{-3} mol L^{-1} of periodate as carrier. This concentration is also in agreement with the one reported by Efstathiou et al. [9], which argued for its use for a better preservation of the selective membrane. Epinephrine is not stable in a neutral or alkaline solution, which rapidly becomes red from oxidation to adrenochrome and brown from the formation of melanin on exposure to air. Aqueous solutions of epinephrine have their optimum stability at about pH 3.6 [7]. Taking this in consideration, a pH study was done to evaluate the optimum pH for the periodate/epinephrine reaction. The studied range was between 3 and 6. A maximum signal was found for solutions at pH 5. A linear range was found for epinephrine concentrations between 2.0×10^{-4} and 2.5×10^{-3} mol L^{-1} with a slope of 35528 mV L mol^{-1} with $r^2 = 0.997$ and a practical detection limit of 1.8×10^{-4} mol L^{-1}. Based on the studied preformed by Montenegro et al., where an oxidation reaction of periodate and dopamine was monitoring by a periodate selective electrode, a 2nd order reaction is expected. Accordingly, the overall IO_4^- consumption determined by the selective electrode gives a linear relationship between potential measure and epinephrine concentration.

The extent of the interference of some organic and inorganic anions was evaluated at the interferent/epinephrine concentration ratios of 1:1, 1:10, 1:100. Sodium chloride, sodium metabisulfite, sodium sulphite and chlorobutanol were selected for this evaluation due to their presence in the pharmaceutical formulations tested. This study was based on performing recovery trials of epinephrine solutions (2.0×10^{-4} and 1.0×10^{-3} mol L^{-1}). Recoveries between 99 and 101% were obtained in all trials except for sodium metabisulphite. This is oxidized by periodate and for the epinephrine concentrations of 2.0×10^{-4} and 1.0×10^{-3} mol L^{-1}, 218 and 168% in the recovery trials were respectively obtained, for the interferent/epinephrine ratio of 1:1. At this level, in both cases, sodium metabisulphite has a concentration lower than in the real samples. For the ratio1:100, it was impossible to measure the height of the peak, because they were wide and irreproducible. For this reason, samples were acidified before injection, to allow the quantitative conversion to sulphur dioxide promptly removed in order to avoid the formation of bubbles inside the system during the aspiration step.

3.3. Real sample analysis

The epinephrine concentrations in two hospital common used formulations (Table 2) were determined using the previously optimized procedure.

Therefore, the content of six injections from the same package were mixed and five times diluted with deionised water. The concentration of the samples 1 and 2 was 0.908 and 0.454 mg mL^{-1}, respectively, with a R.S.D. of 0.34% for both. For comparison purposes, the same samples were also processed using the official USP method [7], based on HPLC and the result was 0.905 and 0.451 mg/mL, with a R.S.D. of 0.50 and 0.79%, respectively.

Table 2
Sample composition of the two hospital formulations

Sample composition	Sample 1	Sample 2
Epinephrine chlorohydrate (mg)	1	0.5
NaCl (mg)	8	8
$Na_2S_2O_5$ (mg)	3.6	3.6
Chlorobutanol (mg)	40	40
Na_2SO_3 (mg)	0.8	0.8
Water (mL)	1	1

This results obtained, revealed a good statistical agreement between both procedures used once t values of 1.64 ($p > 0.05$) and 1.86 ($p > 0.05$) were obtained for samples 1 and 2, respectively. As they are smaller then the critical value ($t_8 = 1.89$), both methods do not give significantly difference results for the epinephrine concentration.

4. Conclusions

Through down scaling periodate-selective electrode, it was possible to benefit from the advantages recognized to lab-on-valve sequential-injection based systems, namely regarding equipment portability, reduced consumption of sample and reagents and reduction of effluent waste. Furthermore, the new periodate electrode configuration is easy to achieve in common laboratories and enables the implementation of low volume detection cell, where the electrical noise, that is frequently present in potentiometric-based procedures, is significantly reduced. Albeit the reduction of lifetime of the electrode, the volume of prepared sensor cocktail enables to prepare an increased number of electrodes, which the response characteristics are similar to previously described conventional units or tubular configured electrodes.

Acknowledgments

C.M.P.G. Amorim gratefully acknowledge FCT and FSE (III Quadro Comunitário de Apoio) for a PhD Grant (SFRH/BD/19461/2004).

References

[1] J. Ruzicka, G.D. Marshdl, Anal. Chim. Acta 237 (1990) 329.
[2] J. Ruzicka, Analyst 125 (2000) 1053.
[3] C.H. Wu, L. Scampavia, J. Ruzicka, B. Zamost, Analyst 126 (2001) 291.
[4] C.H. Wu, J. Ruzicka, B. Zamost, Analyst 126 (2001) 1947.
[5] H. Wang, E.H. Hansen, M. Miro, Anal. Chim. Acta 499 (2003) 139.
[6] P. Ampan, J. Ruzicka, R. Atallah, G.D. Christian, J. Jakmunee, K. Grudpa, Anal. Chim. Acta 499 (2003) 167.
[7] United States Pharmacopoeia 24; NF19, 2000, p. 646.
[8] Y. Yui, T. Fujita, T. Yamamotto, Y. Itokawa, C. Kawai, Clin. Chem. 26 (1980) 194.
[9] C.E. Efstathiou, J. Pharm. Biomed. Anal. 22 (5) (2000) 781.

[10] A. Afkhami, H.A. Khatami, J. Anal. Chem. 58 (2) (2003) 135.
[11] T. Madrakian, A. Afkhami, L. Khalafi, M. Mohammadnejad, J. Braz. Chem. Soc. 17 (7) (2006) 1259.
[12] P. Britz-Mckibbin, A.R. Kranack, A. Paprica, D.D.Y. Chen, Analyst 123 (1998) 1461.
[13] M. Valcarcel, A. Gomez-Hens, S. Rubio, Clin. Chem. 31 (1985) 1790.
[14] A. Kojlo, E. Nalewajko, Chem. Anal. (Warsaw) 49 (2004) 653.
[15] J. Michalowski, A. Kojlo, A. Estrela, Chem. Anal. (Warsaw) 47 (2002) 267.
[16] J.R. Clamp, L. Hough, Biochem. J. 101 (1966) 120.
[17] M.C.B.S.M. Montenegro, M. Goreti, F. Sales, J. Pharm. Sci. 89 (2000) 7.
[18] A.N. Araújo, R.C.C. Costa, J.L.F.C. Lima, B.F. Reis, Anal. Chim. Acta 358 (1998) 111.

Available online at www.sciencedirect.com
ScienceDirect
Talanta 72 (2007) 1438–1445
Talanta
www.elsevier.com/locate/talanta

Effect of surfactants on the voltammetric response and determination of an antihypertensive drug

Nada F. Atta *, Soher A. Darwish, Sayed E. Khalil, A. Galal *

Department of Chemistry, College of Science, University of Cairo, Postal Code 12613, Giza, Egypt

Received 13 November 2006; received in revised form 22 January 2007; accepted 23 January 2007
Available online 1 February 2007

Abstract

The effect of adding surface-active agents to electrolytes containing terazosin, an antihypertensive drug, on the voltammetric response of glassy carbon electrode was studied. The current signal due to the oxidation process was a function of the amount of terazosin, pH of the medium, type of surfactant, and accumulation time at the electrode surface. Two surfactants were used, an anionic type, sodium dodecyl sulfate (SDS) and a cationic type, cetyl trimethyl ammonium bromide (CTAB). Addition of SDS to the terazosin-containing electrolyte was found to enhance the oxidation current signal while CTAB showed an opposite effect. Beside the interfacial interaction of the surfactant with the electrode surface in reference to the bias applied potential and the charge of surfactant, terazosin-surfactant interaction in the electrolytic solution was found to be critical to the magnitude of current signal. Addition of SDS to terazosin-containing buffer solution resulted in a decrease in the drug absorption spectrum both in the ultra-violet and visible (UV–vis) regions. Moreover, NMR measurements showed considerable chemical shifts for the aromatic protons of the quinazolinyl moiety of the terazosin in presence of SDS. The affected aromatic protons are positioned next to the interacting protonated amino-group of the terazosin with the charged sulfonate-group of SDS. On the other hand, addition of CTAB did not cause noticeable changes both to the UV–vis and NMR spectra of the drug. The use of SDS in the electrochemical determination of terazosin using linear sweep voltammetry and differential pulse voltammetry at solid glassy carbon electrode enhanced the detection limit from 6.00×10^{-7} mol L^{-1} in absence of surfactant to 4.58×10^{-9} mol L^{-1} when present. The validity of using this method in the determination of drug active ingredient in urine samples and tablet formulations was also demonstrated.

Keywords: Surfactants; Modified electrodes; Voltammetry; UV–vis; NMR; Drug interaction; Terazosin

1. Introduction

Surfactants have been widely used in chemistry and in particular affecting several electrochemical processes [1]. Several applications of surfactants in electrochemistry are in electroplating [2], corrosion [3], fuel cells [4], electrocatalysis [5], and electroanalysis [6]. The area of surface modified electrodes is of particular interest because of its application in sensors. Rusling [7] indicated the influence of surfactant aggregates at the electrode/electrolyte interface in micelle solutions. In his study [7], it was shown that the entry of an electrochemical reactant into this dynamic surface film is a key preceding electron transfer step.

On the other hand, surfactants have proven effective in the electroanalysis of biological compounds and drugs. For example, it was recently shown that surfactants are highly effective in stabilizing the voltammetric response of serotonin by protecting the electrode surface from fouling [8]. In another study [9], it was shown that anionic surfactants could also be used to improve the accumulation of some electroactive organic molecules such as ethopropazine at gold electrodes. Recently, the influence of micelles in the simultaneous determination of two components was also demonstrated, as in the case of ascorbic acid and dopamine [10] and catechol and hydroquinone [11]. It was not clear whether the micelle interaction with the analyte in the solution phase contributes to the selective response. It is well established that interaction between aggregates and solutes in the solution phase is controlled by diffusion and takes place in the microsecond time scale [12]. Electrode surfaces with hydrophobic characters such as carbon paste electrodes interact

* Corresponding authors. Tel.: +20 2 567 6561; fax: +20 2 572 7556.
E-mail address: galalah1@yahoo.com (A. Galal).

0039-9140/$ – see front matter © 2007 Elsevier B.V. All rights reserved.
doi:10.1016/j.talanta.2007.01.053

with surfactants, namely through surface adsorption. Thus, carbon paste electrode modified with surfactants proved to be useful for the determination of both inorganic species [13] and biological compounds [14].

Terazosin hydrochloride is an α_1-adrenoceptor blocker with a long lasting action. It is used in the management of hypertension [14], and in benign prostate hyperplasia to relieve symptoms of urinary obstruction [15]. Terazosin is rapidly and almost completely absorbed from the gastrointestinal tract after oral administration; the bioavailability is reported to be about 90%. Peak plasma concentrations are achieved in about 1 h. It is metabolized in the liver; one of the metabolites is reported to possess antihypertensive activity and the half-life in plasma is approximately 12 h. It is excreted in phases via the bile, and in the urine, as unchanged drug and metabolites. Terazosin is 90–94% protein bound when administered orally as the hydrochloride, but doses are usually expressed in terms of the base. Following oral administration its hypotensive effects are seen within 15 min and may last for up to 24 h, permitting once daily dose.

It is therefore essential to study the effect of changing the charge of the surfactant used, namely SDS and CTAB, its connection with the solution pH, and concentration of analyte on the voltammetric response of this drug. The electrochemical behavior of this drug in aqueous solutions at solid electrodes was not studied. Moreover, in this work we relate the observed UV–vis and NMR measurements of terazosin in the absence and presence of each surfactant type to the electrochemical data obtained.

2. Experimental

2.1. Materials and reagents

2.1.1. Metal substrates and electrochemical cell

A glassy carbon (GC) electrode (3.0 mm diameter) from BAS (USA) was used as the working electrode, a platinum wire (2.0 mm diameter, 10 cm long) as auxiliary electrode, and an Ag/AgCl (3 mol L^{-1} NaCl) as the reference electrode. A one-compartment glass cell (30 mL) fitted with gas bubbler was used for electrochemical measurements. Solutions were degassed using pure nitrogen prior to and throughout the electrochemical measurements.

2.1.2. Reagents and solution preparations

Terazosin hydrochloride (TH) and Itrin® tablets (5.0 mg TH per tablet) were supplied by Kahira Pharmaceutical and Chemical Industries Co. (Egypt). A stock solution of TH (1.0×10^{-3} mol L^{-1}) was prepared with deionized water. Diluted working standard solutions were then prepared daily with deionized water freshly just prior to use. Britton–Robinson (B–R) (4.0×10^{-2} mol L^{-1}) buffer of pH 2–11 was used as the supporting electrolyte. All solutions were prepared from analytical grade chemicals and sterilized Milli-Q deionized water. The surfactants, SDS from Aldrich (USA), and CTAB from Prolabo (France) were prepared as a stock solution of 1.0×10^{-2} mol L^{-1}/deionized water.

2.2. Electrochemical and spectroscopy instrumentation

The voltammetric measurements were performed using a PC-controlled AEW2 electrochemistry workstation and data were analyzed with EC_{prog3} electrochemistry software (Sycopel, UK). The one-compartment cell with the three electrodes was connected to the electrochemical workstation through a C_3-stand from BAS (USA). A JENWAY 3510 pH meter (England) with a glass combination electrode was used for pH measurements. All UV measurements were performed using a Shimadzu 1601 spectrophotometer (Kyoto, Japan). NMR measurements were performed using a 300 MHz Varian NMR instrument in D_2O and with TEMAC as internal standard.

3. Results and discussion

3.1. Cyclic voltammetry of terazosin in presence and absence of surfactant

The drug under investigation, terazosin ((RS)-1-(4-amino-6,7-dimethoxy-2-quinazolinyl)-4-((tetrahydro-2-furanyl) carbonyl) piperazine monohydochloride dihydrate), has a structure in which the central element is a piperazine ring and contains a quinazoline moiety. The mechanism of anodic oxidation of terazosin is expected to be complicated at the glassy carbon electrode in aqueous media [16]. The first step is the removal of an electron to form a radical–cation. However, in this particular structure with the presence of an amino-group, the electron will also be removed from the heteroatom and oxidation takes place around 1.0 V or less [17]. The ease of oxidation at this relatively lower positive potential is attributed to the resonance stabilization of the radical–cation. Fig. 1 shows the cyclic voltammograms (CVs) of 4.76×10^{-5} mol L^{-1} terazosin (in B–R buffer, pH 2) at GC electrode (curve I), in presence of 1.1×10^{-4} mol L^{-1} SDS anionic surfactant without stirring (curve II), and after stirring for 5 min (curve III). The

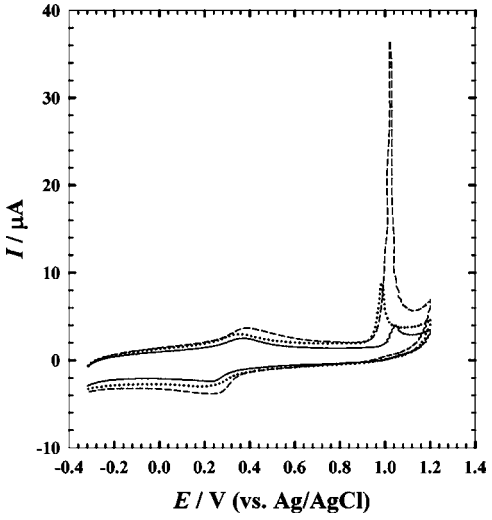

Fig. 1. CVs of 4.76×10^{-5} mol L^{-1} terazosin (in B–R buffer, pH 2) at GC electrode (—), in presence of 2.5×10^{-5} mol L^{-1} SDS without stirring (●●●●), and after stirring for 5 min (—-). Scan rate 100 mV s^{-1}.

CVs are characterized by the appearance of distinct anodic peaks at +1.05 V, +0.98 V, and +1.02 V for the three curves, respectively. The reverse scan in the negative direction did not show any indication of a reduction peak in the potential window studied. It was indicated that a reduction peak would be expected at relatively lower potentials, ca. −1.60 V at mercury surfaces [18]. It is interesting to notice the large difference in the oxidation peak current, i_{pa}, in the three cases: 0.9 μA, 1.9 μA, and 25 μA, respectively. A pair of ill-defined peaks can be distinguished in the potential range +0.2 V to +0.4 V that could be related to the redox behavior of C=O group in tetrahydro-2-furanyl piperazine moiety. The reversibility and current signal of this pair of peaks is a function of the pH and type of buffer used.

The suggested mechanisms for the aggregation of surfactants on the electrode surface in the form of bilayers, cylinders, or surface micelles (in the case of relatively higher concentrations added of SDS) could explain the increase in current in the presence of surfactants [7]. The electron transfer process will take place when the electroactive species approaches the vicinity of the electrode surface. Two main possibilities allow the transfer of charge; first is the displacement of the adsorbed surfactant by the analyte, and second is the approach of the analyte to the surface of the electrode within the space of one to two head groups of adsorbed surfactant moieties. We believe that the second mechanism is more plausible, as will be indicated later from the data obtained when using the cationic surfactant CTAB. Furthermore, a possible mechanism suggests the formation of ion-pair that anchor onto the surface of the electrode that should posses some hydrophobic character [19]. Thus, the resulting ion-pair of the charged surfactant and drug tend to adhere to the surface through the lipophilic parts in both moieties.

3.2. Effect of pH on the electrochemical response of terazosin

The reported pK_a value of terazosin is 7.1 [20]. The effect of changing the pH on the electrochemical response of terazosin was examined in the absence and presence of the surfactant. Fig. 2a and b shows the effect of changing pH of B–R buffer on the voltammetric response of 4.76×10^{-5} mol L^{-1} terazosin in the absence and presence of 2.5×10^{-5} mol L^{-1} SDS, respectively. In general, the oxidation peak potential shifts to more positive values as the pH decreases in the absence and presence of SDS. Maximum oxidation current signal was obtained in pH 5.0 and the minimum in pH 9.0 in the SDS-containing and free solution. Therefore, all subsequent electrochemical measurements will be conducted in either pH 2.0 or 5.0. The pH dependency of the oxidation peak potential indicates that protonation/deprotonation is taking part in the charge transfer process. The pair of peaks appearing in the potential range of +0.2 V to +0.4 V was greatly affected by the pH change that proves the involvement of carbonyl group in the charge exchange.

3.3. Comparison of the cyclic voltammetry of terazosin in presence of anionic and cationic surfactants

The use of different surfactants with varying charges and lengths of hydrocarbon chain affects the redox behavior of electroactive species and complicates the corresponding voltammetric response [21]. Terazosin could be considered lipophilic in nature with amphiphilic molecules that are capable of adsorbing on the surface of the electrode. This leads to the formation of self-micelle aggregates and mixed aggregates with the surfactant. The adsorption of amphiphilic species on electrode surface may result in changing the overpotential of the electrochemical

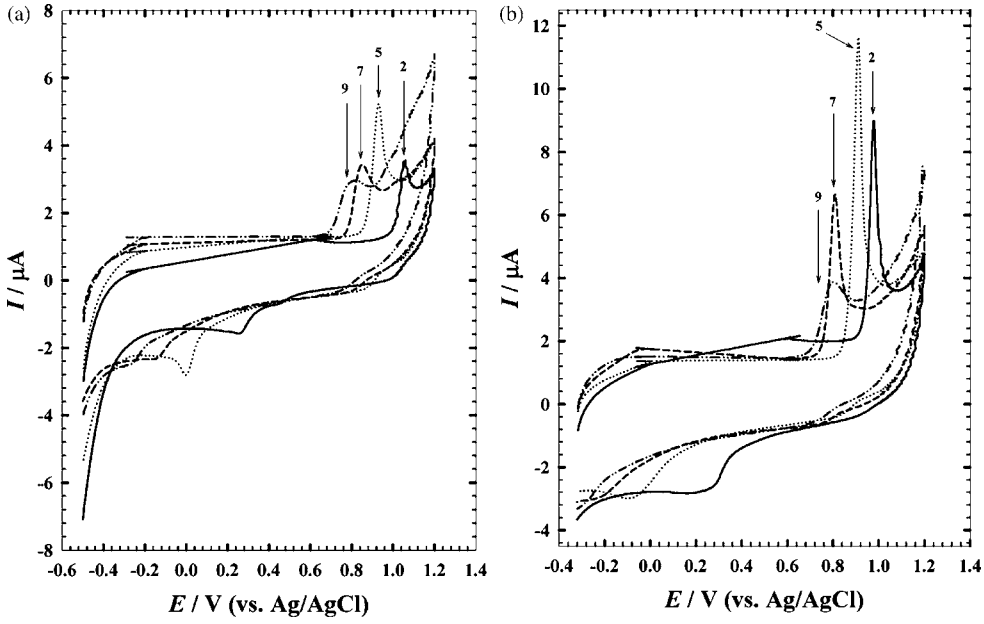

Fig. 2. (a) Effect of pH on the response of 4.76×10^{-5} mol L^{-1} terazosin at GC electrode. pH 2(—), pH 5(●●●●), pH 7(—·—), pH 9(●●-●●-). Scan rate 100 mV s^{-1}. (b) Effect of pH on the response of 4.76×10^{-5} mol L^{-1} terazosin at GC electrode in presence of 2.5×10^{-5} mol L^{-1} SDS. Scan rate 100 mV s^{-1}. pH 2(—), pH 5(●●●●), pH 7(—·—), pH 9(●●-●●-). Scan rate 100 mV s^{-1}.

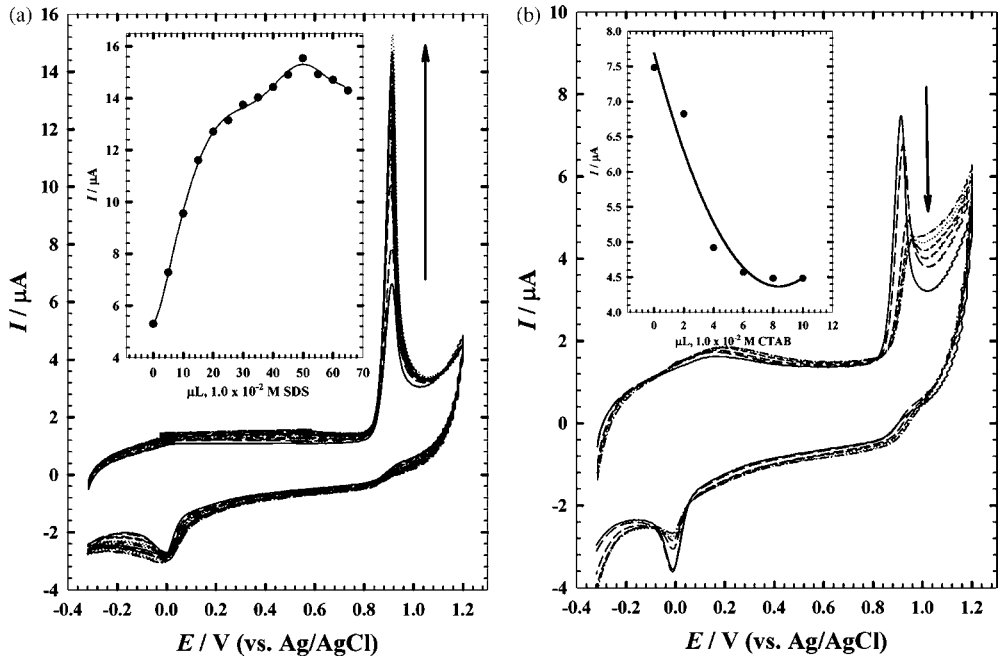

Fig. 3. (a) Effect of successive addition of SDS (increments add 1.0×10^{-5} mol L^{-1} SDS of each addition) on the voltammetric response of terazosin in universal buffer, pH at GC electrode. Scan rate 100 mV s^{-1}. (b) Effect of successive addition of CTAB (increments add 4.0×10^{-6} mol L^{-1} CTAB of each addition) on the voltammetric response of terazosin in universal buffer, pH 5 at GC electrode. Scan rate 100 mV s^{-1}.

process and the rate of its corresponding charge transfer [22]. Alternatively, in the solution phase the premicellar aggregate formation will affect the mass transport of the electroactive species [23]. The data in Fig. 3a and b show the cyclic voltammetry response of a GC electrode for 4.76×10^{-5} mol L^{-1} terazosin in B–R buffer (pH 5.0) upon incremental addition of 5 μL 0.01 mol L^{-1} SDS and 2 μL 0.01 M CTAB, respectively.

Upon closer examination of the data in Fig. 3a and b, one observes the anodic oxidation peak potential, E_{pa}, and current, i_{pa}, of terazosin are concentration-dependent upon the addition of CTAB. On the other hand, only the oxidation peak current, i_{pa}, showed the concentration-dependent behavior upon the addition of SDS. The value of i_{pa} plateaus as the concentration of surfactant reaches a definite concentration, namely 1.1×10^{-4} mol L^{-1} SDS and 2.0×10^{-5} mol L^{-1} CTAB, respectively. This is attributed to the adsorption of the surfactant molecules on the electrode surface that could be followed by the formation of micelle aggregates as the distance from the electrode surface increases [7,21]. The presence of positive charge on the amino-group of terazosin, at this pH, and its hydrophobic character enhances the aggregation of the latter with SDS, which possesses negatively charged polar groups. The possibility of aggregation of terazosin with CTAB can only be attributed to hydrophobic interactions and lead to reduced aggregation as compared to the SDS case. The strength of interaction and binding between the drug and the surfactant should result in the observed distinct behavior and should also partially affect the transport of their corresponding aggregates in solution [24]. It was previously mentioned that the saturation adsorption over the electrode surface is reached with the critical micelle concentration of the surfactant (CMC) [25] and should coincide with the concentration of added surfactant that resulted in the plateau indicated in Fig. 3a and b. However, the values we obtained are different from those reported earlier for the CMC of SDS and CTAB [21,25]. One might suggest that other factors such as the type of buffer used (supporting electrolyte) and the nature of analyte studied should affect greatly the estimate of CMC from the cyclic voltammetric results. It is important to mention that no visual turbidity formation was observed in the solution as the final addition of surfactant was reached. Additionally, the oxidation peak potential, E_{pa}, shifted to lower positive values of ca. 100–25 mV in presence of SDS for all pHs studied except for solutions with pH ≥ 5 in which the potential shifted by the relatively small value of 2 mV.

3.4. Effect of scan rate on the voltammetric response of terazosin

The relation between anodic oxidation peak current, i_{pa} (mA), diffusion coefficient of the electroactive species, D_0 (cm^2 s^{-1}), and scan rate, ν (V s^{-1}), is given by [26]:

$$i_{pa} = (2.99 \times 10^5) n\alpha^{1/2} A C_0^* D_0^{1/2} \nu^{1/2} \quad (1)$$

where n is the number of electrons exchanged in oxidation, α is the transfer coefficient, A is the apparent surface area of the electrode (cm^2), C_0^* is the concentration of the electroactive species (mmol dm^{-3}). The transfer coefficientα, for an irreversible process can be calculated from [26]:

$$|E_{pa} - E_{pa/2}| = \frac{47.7}{\alpha} \quad (2)$$

where $E_{pa/2}$ is the potential at which the current equals one half of the peak current. A plot of i_{pa} versus $\nu^{1/2}$ (ranging from 10 to 250 mV s^{-1}) gave a straight line according to Eq. (1). Careful

Table 1
Electrochemical parameters of terazosin determined at GC electrode in different electrolyte solutions

Electrolyte (B–R buffer pH 5)	[a]E_{pa}/mV (vs. Ag/AgCl)	[a]I_{pa}/μA	α	D/cm^2 s^{-1}
4.76×10^{-5} mol L^{-1} terazosin	0.91	1.696	0.3	1.61×10^{-7}
4.76×10^{-5} mol L^{-1} terazosin + 2.5×10^{-5} mol L^{-1} SDS	0.89	3.075	0.2	4.19×10^{-6}
4.76×10^{-5} mol L^{-1} terazosin + 3.0×10^{-6} mol L^{-1} CTAB	0.96	1.384	0.6	9.61×10^{-8}

[a] Oxidation peak potential E_{pa}, and current i_{pa}, were determined at scan rate $\nu = 50$ mV s^{-1}.

inspection of data on the effect of scan rate reveals that the linearity of the relationship is realized up to a scan rate of 150 mV s^{-1} that is followed by a deviation from linearity at higher scan rates. This indicates that the charge transfer is under a partially diffusion control process and that adsorption of aggregates at the electrode surface is also possible. The relation between the oxidation peak potential E_{pa}, and the scan rate ν, shows that deviation also begins at a scan rate of 150 mV s^{-1}. The apparent diffusion coefficients (D_0) can be calculated and are listed in Table 1. D_0 can be considered as an average value of the diffusion process in the bulk, within the surfactant aggregates in solution and the surfactant layer adsorbed at the surface of the electrode.

The size of the diffusion layer at the electrode surface proximity changes with the voltage scan used. At relatively slow voltage scans the diffusion layer grows much further towards the solution side and further from the electrode surface. Therefore, as the scan rate increases the flux to the electrode surface increases considerably. At relatively higher scan rates and in presence of SDS that mainly aggregates at the electrode surface and forms a pair with the drug in electrolyte, the diffusion layer grows less further from the vicinity of the electrode. This results in the observed two slopes in the i_{pa} versus $\nu^{1/2}$ and E_{pa} versus ν relations.

The values indicated in Table 1 for D_0 show that the diffusion is enhanced in presence of SDS compared to GC and that the lowest value was in presence of CTAB. The values reported are relative and cannot be considered as absolute, and therefore, further studies can be conducted using chronoamperometry measurements.

3.5. UV–vis studies

Interaction of anionic surfactant (SDS) or cationic surfactant (CTAB) and terazosin in aqueous B–R buffer solutions were followed by UV–vis spectroscopy. Fig. 4a shows the effect of different concentrations of SDS surfactant on the absorption spectrum of terazosin. Basically, the anionic surfactant SDS showed no absorption background. The anionic character of SDS favors coulombic forces with the drug and should lead to the formation of aggregates in the solution phase. Successive aliquots of 15 μL of 0.01 mol L^{-1} SDS were added to the UV–vis cuvette containing 4.0 mL of 1.96×10^{-5} mol L^{-1} terazosin (pH 2.0). All the bands in the UV and visible regions at ca. 210 nm, 240 nm, and 330–340 nm (broad), decreased with each SDS addition. It was mentioned previously that aggregation in aromatic systems could be also attributed to the formation of larger units (possibly due to the formation of longer repeat unit chains) [27]. This "oligomerization" was due to the London–Margenau attractive forces between the π-electrons that is counterbalanced

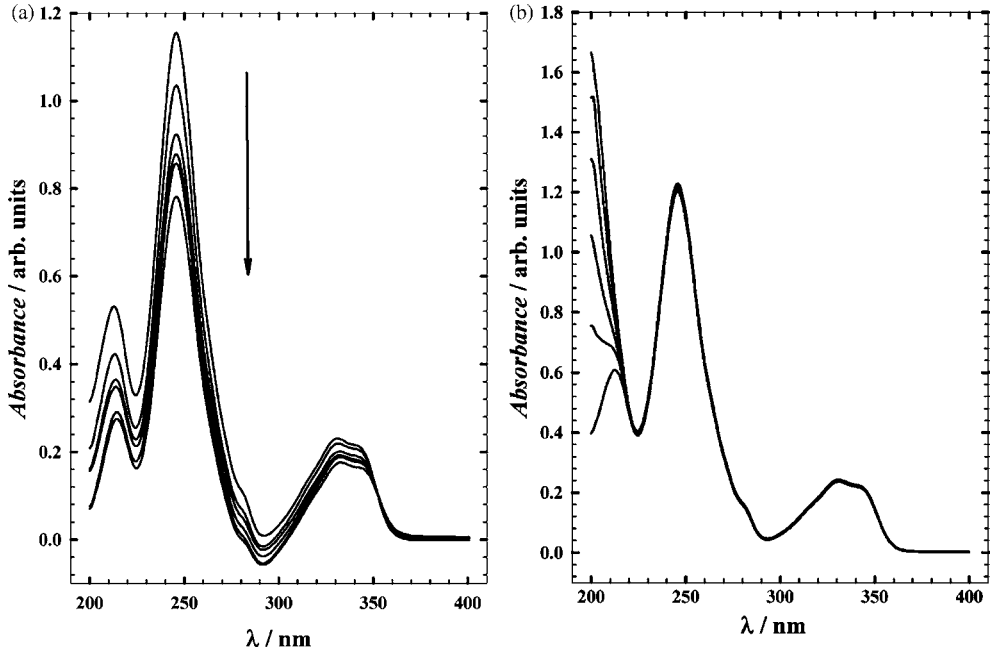

Fig. 4. (a) The effect of different concentrations of SDS surfactant on the absorption spectrum of 4.76×10^{-5} mol L^{-1} terazosin dye in aqueous universal buffer, pH 2.0. (b) The effect of different concentrations of CTAB surfactant on the absorption spectrum of 4.76×10^{-5} M terazosin dye in aqueous universal buffer, pH 2.0.

by the coulombic and Lenard–Jones repulsive forces. This should be accompanied with a blue-shift [27] or a red-shift [28] in the corresponding spectra that was not observed in the present case for terazosin. This indicates that the charge interaction of the drug with SDS is the main contribution to the association that resulted in the decrease in the absorption spectra. It is important to mention that a total of 0.09 mL SDS was added, and therefore no dilution effect is expected to be observed on the absorption spectra. Moreover, as the pH of solution increases the effect of addition of SDS on the change of the terazosin spectra decrease.

CTAB is a cationic surfactant, therefore coulombic repulsion are expected to be significant and should result in the exclusion of terazosin. Thus, as shown in Fig. 4b the successive addition of small aliquots, ca. 15 μL, of 0.01 mol L^{-1} CTAB (pH 2.0) showed no significant effect on the absorption intensity bands at ca. 210 nm, 240 nm, and 330–340 nm (broad). We would expect that the repulsive coulombic forces between the positively charged amino-group of terazosin and the positively charged ammonium group of CTAB prevent the aggregation of the drug molecules in solution. Therefore, the only existing attractive forces competing with the repulsive ones are the hydrophobic interactions.

The foregoing data showed that aggregation in the solution phase takes place between the drug and the surfactant molecules and is mainly based on the type of charge on the drug that is dictated by the pH of the buffer used and the corresponding charge of the polar group of the surfactant. Secondary interactions from the hydrophobic character of these species are also possible; however they are apparently weaker than the coulombic forces. The spectrophotometry data are in good agreement with what we obtained in the voltammetry experiments. One important conclusion is that the aggregation of an electroactive species is still possible at submicellar concentrations depending on the strength of binding with the corresponding surfactant.

3.6. NMR studies

NMR measurements led us to similar conclusions, and ascertain to a great extent the involvement of direct interaction between the drug and the SDS. The proton NMR spectra of terazosin are given in Fig. 5a. As noticed, NMR spectra of terazosin show characteristic signals for the aromatic quinazolinyl moiety at 6.561 ppm and 6.829 ppm, respectively. The multiplets between 2.0 and 2.6 ppm are attributed to the protons of the tetrahydrofuranyl, while those between 3.6 and 4.2 ppm are attributed to the protons of the piperazine moieties, respectively. The proton peaks at approximately 4.8 ppm (of D_2O) are attributed to the dimethoxy protons.

Therefore, the three regions of interest in which the chemical shift and interactions are observed upon the addition of surfactants are for quinazolinyl, tetrahydrofuranyl, and piperazine moieties, respectively. We believe that the most clearly influenced environment of terazosin protons is that of the quinazolinyl portion of the molecule as shown in Fig. 5b. The protons are expected to be in close proximity to the interacting $-NH_3^+$ group with the incoming polar end, in the particular case of

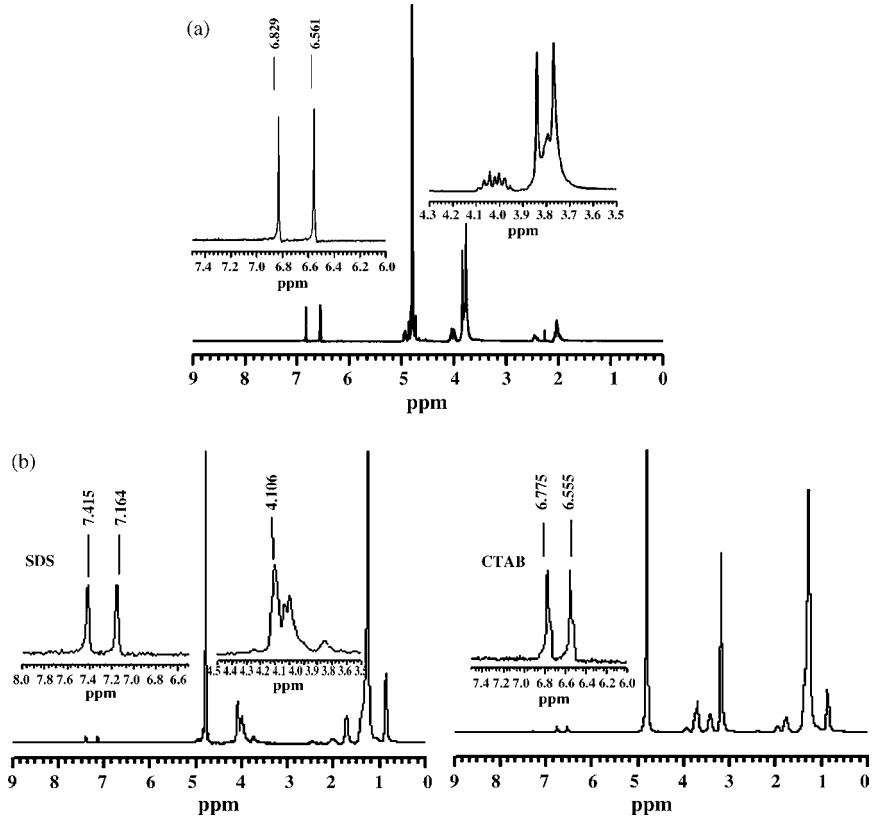

Fig. 5. (a) NMR spectra of terazosin in absence of surfactants. (b) Effect of addition of SDS and CTAB on the NMR spectra of terazosin.

SDS. On the other hand, both protons of the tetrahydrofuranyl and piperazine moieties are equally affected by the hydrophobic interaction of the surfactant's hydrocarbon chains for SDS and CTAB. In this respect, and as depicted in Fig. 5b, the shielding and deshielding effects experienced by the quinazolinyl protons upon the addition of SDS and CTAB show a change in chemical shift of $+\Delta\delta = 0.59, 0.58$ ppm and $-\Delta\delta = 0.10, 0.17$ ppm, respectively. It is important to notice that the change in chemical shift is opposite in direction upon addition of SDS and CTAB and is substantially higher in magnitude in the case of SDS. Moreover, the intensity of the signal decreased relatively in the case of SDS when compared to that of CTAB. As previously mentioned in the electrochemical and UV–vis section, the hydrophobic interaction between the surfactant and drug molecule affects the solution composition as is made clear from the noticeable change in the chemical shifts of protons of the tetrahydrofuranyl and piperazine moieties upon the addition of SDS or CTAB (cf. Fig. 5b).

3.7. Applications on commercial tablets and urine

The effect of changing the concentration of terazosin, in the presence of 1.1×10^{-4} mol L^{-1} SDS in pH 2.0, on the differential pulse voltammograms, DPV, measured with a GC working electrode and an accumulation time of 300 s is given in Fig. 6a. The following are the parameters for the DPV experiments: $E_i = 0.45$ V, $E_f = 1.35$ V, scan rate = 10 mV s^{-1}, pulse width = 25 ms, pulse period = 200 ms, and pulse amplitude = 10 mV. The oxidation peak current for terazosin is linearly proportional to the concentration of the drug in the range of 4.0×10^{-8} mol L^{-1} to 2.4×10^{-6} mol L^{-1}. A linear regression relation results from the fitting with the following equation:

$$I = (4.65 \times 10^6)C + 0.0708 \quad (3)$$

The correlation coefficient, $r = 0.998$, and the detection limit, DL, is 4.58×10^{-9} mol L^{-1} and were calculated from the equation

$$\mathrm{DL} = \frac{3s}{m} \quad (4)$$

where s is the standard deviation ($s = 7.10 \times 10^{-3}$) and m is the slope.

The above procedure was used for the determination of terazosin in commercial tablets both for buffered solutions and urine samples. The commercial tablets containing terazosin, Itrin® (5 mg/tablet terazosin) were analyzed without pre-measurement treatment. Fig. 6b shows the data generated by standard addition method for the analysis of Itrin® in buffered solutions of pH 2. The Itrin® was dissolved in buffer solution with a "start concentration" of 3.78×10^{-7} mol L^{-1}. This was calculated per mass of a 5 mg containing tablet. The standard terazosin provided by the National Organization for Drug Control and Research of Egypt was then injected by a micro-syringe with concentrations of 4.0×10^{-7} mol L^{-1}, 8.0×10^{-7} mol L^{-1}, 12×10^{-7} mol L^{-1}, 16×10^{-7} mol L^{-1}, and 20×10^{-7} mol L^{-1}. Data represented are calculated from five replicates and the assay data are reported in Table 2. A linear relationship was obtained from fitting with the following equation:

$$I = (5.93 \times 10^6)C + 0.234 \quad (5)$$

The same measurements were conducted successfully on urine samples. In this set of experiments, terazosin was dissolved

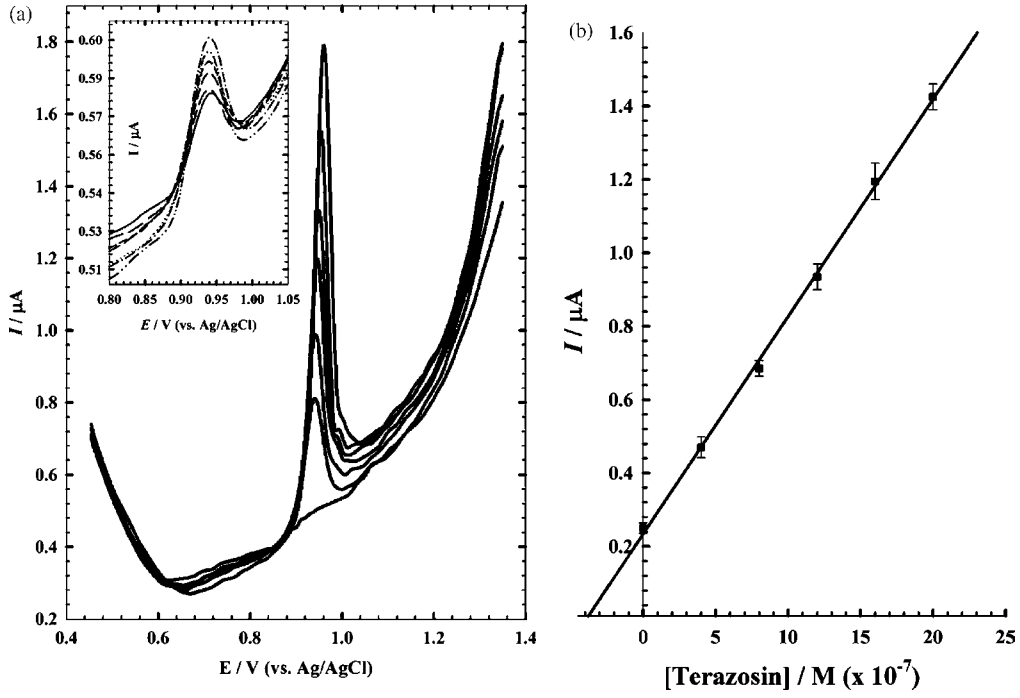

Fig. 6. (a) DPV of different concentrations of terazosin, insert (4.0×10^{-8} mol L^{-1} to 2.4×10^{-7} mol L^{-1}), main (4.0×10^{-7} mol L^{-1} to 2.4×10^{-6} mol L^{-1}) in presence of 2.5×10^{-5} mol L^{-1} SDS, universal buffer (pH 2.0). (b) Standard addition plot of Itrin® in buffer pH = 2.

Table 2
Assay data of terazosin in Itrin® in buffer pH = 2 (data from Fig. 6b)

Analyte concentration in sample solution ($g\,L^{-1}$) × 10^{-4}	Spike solution		Total found ($g\,L^{-1}$) × 10^{-4}	R.S.D. (%)	Recovery (%)
	Volume added (μL)	Concentration ($g\,L^{-1}$)			
1.837	4.0	0.4593	3.673	1.04	100.01
3.672			5.510	0.851	100.19
5.505			7.308	0.730	98.37
7.338			9.122	1.31	97.43
11.01			12.81	1.01	99.94

in urine to make a stock solution with 1.0×10^{-3} mol L^{-1} concentration. A 4 μL of this urine stock containing terazosin was injected in a 10 mL buffer (pH 2). Standard addition of 4 μL of 1.0×10^{-3} mol L^{-1} terazosin (in buffer pH 2) was made and the corresponding DPV was measured. The calibration curve gave a straight line with correlation coefficient, $r^2 = 0.999$, R.S.D. (%) = 1.04, recovery (%) = 100.02.

4. Conclusions

In conclusion, we were able to examine the voltammetric behavior of terazosin in different pH buffer solutions. The oxidation peak potential and current values were function of pH of electrolyte. The use of surfactants affects the oxidation peak current according to the nature of charge of the surfactant's polar group. Spectrophotometric measurements showed that solution aggregate formation affects the surface interaction of the adsorbed species at the electrode surface and consequently the rate of charge transfer. NMR studies showed that predominant interactions between the drug molecule and the surfactant are coulombic in nature and that the secondary forces are less predominant on the electrochemical behavior. The use of surfactants can be applied for the analysis of drug with a direct analytical procedure in aqueous, drug formulations, and urine samples.

Acknowledgments

The authors are grateful to the University of Cairo (Office of Vice President for Graduate Studies and Research) for providing partial financial support through "The Young Researchers' Program." We would like to thank the National Organization for Drug Control and Research (NODCAR, Egypt) for providing the standard materials.

References

[1] R. Vittal, H. Gomathi, K.-J. Kim, Adv. Colloid Interface Sci. 119 (2006) 55.
[2] S. Guan, B.J. Nelson, J. Microelectromech. Syst. 15 (2006) 330.
[3] R. Fuchs-Godec, Colloids Surf. A: Physicochem. Eng. Aspects 280 (2006) 130.
[4] M. Mamak, N. Coombs, G. Ozin, J. Am. Chem. Soc. 122 (2000) 8932.
[5] J. Jiang, A. Kucernak, J. Electroanal. Chem. 520 (2002) 64.
[6] C. Gouveia-Caridade, R. Pauliukaite, C.M.A. Brett, Electroanalysis 18 (2006) 854.
[7] J.F. Rusling, Colloids Surf. 123–124 (1997) 81.
[8] B. Hoyer, N. Jensen, Electrochem. Comm. 8 (2006) 323.
[9] L. Huang, L. Bu, F. Zhao, B. Zeng, J. Solid State Electrochem. 8 (2004) 976.
[10] A.P. dos Reis, C.R.T. Tarley, N. Maniasso, L.T. Kubota, Talanta 67 (2005) 829.
[11] J. Peng, Z.-N. Gao, Anal. Bioanal. Chem. 384 (2006) 1525.
[12] A. Diaz, A.E. Kaifer, J. Electroanal. Chem. 249 (1988) 333.
[13] M. Galík, M. Cholota, I. Švancara, A. Bobrowski, K. Vytřas, Electroanalysis 22 (2006) 2218.
[14] C. Hu, Q. He, Q. Li, S. Hu, Anal. Sci. 20 (2004) 1049.
[15] T. Lytle, S. Coles, M.A. Waite, J. Hum. Hypertens. 5 (1991) 35.
[16] Y. Tanaka, N. Masumori, N. Itoh, Y. Sato, A. Takahashi, H. Ogura, S. Furuya, T. Tsukamoto, J. Urol. 167 (2002) 2492.
[17] N.L. Weinberg, H.R. Weinberg, Chem. Rev. 68 (1968) 449.
[18] I. Jane, A. McKinnon, R.J. Flanagan, J. Chromatogr. 323 (1985) 191.
[19] M. Galik, M. Cholota, I. Scancara, A. Bobrowski, K. Vytras, Electroanalysis 18 (2006) 2218.
[20] M.M. Ghoneim, M.A. El Ries, E. Hammam, A.M. Beltagi, Talanta 64 (2004) 703.
[21] United Kingdom Poisoning Information Database (UKPID), ABPI Compdendium of Data Sheets and Summaries of Products, Characteristics Datapharm Publications Ltd. (1996–1997).
[22] J. Kostela, M. Elmgren, P. Hansson, M. Almgren, J. Electroanal. Chem. 536 (2002) 97.
[23] D.E. Ormonde, R.D. O'Neill, J. Electroanal. Chem. 279 (1990) 109.
[24] A.E. Kaifer, A.J. Bard, J. Phys. Chem. 91 (1987) 2006.
[25] Z.L. Liu, Z.X. Han, K.C. Yu, Y.L. Zhang, Y.C. Liu, J. Phys. Org. Chem. 5 (1992) 33.
[26] A.B. Mandal, B.U. Nair, J. Phys. Chem. 95 (1991) 9008.
[27] A.J. Bard, L.R. Faulkner, Electrochemical Methods "Fundamentals and Applications, second ed., John Wiley & Sons, New York, 2001, 236.
[28] N. Leventis, M. Chen, Chem. Mater. 9 (1997) 2621.

Available online at www.sciencedirect.com
ScienceDirect
Talanta 72 (2007) 1362–1369
Talanta
www.elsevier.com/locate/talanta

Supported liquid membrane-modified piezoelectric flow sensor with molecularly imprinted polymer for the determination of vanillin in food samples

Mónica Ávila [a], Mohammed Zougagh [a], Alberto Escarpa [b], Ángel Ríos [a,*]

[a] Department of Analytical Chemistry and Food Technology, University of Castilla-La Mancha, Campus de Ciudad Real, E-13004 Ciudad Real, Spain
[b] Department of Analytical Chemistry and Chemical Engineering, University of Alcalá, E-28871 Alcalá de Henares, Madrid, Spain

Received 27 September 2006; received in revised form 16 January 2007; accepted 19 January 2007
Available online 30 January 2007

Abstract

An on-line supported liquid membrane-piezoelectric detection system, based on a molecularly imprinted polymer (SLM-QCM-MIP) manifold, has been developed and applied to the quantitative determination of vanillin in food samples. The analyte is extracted from a donor phase into the hydrophobic membrane, and then back extracted into a second aqueous phase used as the acceptor solution. The quantification of vanillin was performed using a quartz crystal microbalance modified with a molecularly imprinted polymer (MIP). The method shows a linear range between 5 and 65 μM, with a relative standard deviation of ±4.8% (at 5 μM). The method was validated by analysing food samples and comparing the results with an SLM based on spectrophotometric quantification.

Keywords: Supported liquid membrane; Molecularly imprinted polymer; Piezoelectric sensor; Vanillin; Food samples

1. Introduction

Sensor technology has attracted considerable attention in the last two decades [1]. In particular, molecular recognition phenomena, which have similarities to bio-recognition systems, have been intensively studied for the development of chemically robust sensors with long-term stability and highly selective capabilities. The selective enrichment of an analyte in the sensitive layer alters the coating in a physico-chemical manner. Various detectable properties may be used to follow this process of incorporation into the polymer and these include mass, fluorescence, electrical resistance and capacitance. The most favourable sensors, however, are composed of microelectronic transducers, such as the quartz crystal microbalance (QCM) [2], surface acoustic wave (SAW) [3], field-effect transistor (FET) [4] and optical devices [5].

For QCM, however, there is no specific selectivity. As a result, various chemicals and biomaterials have been used to modify (physically or chemically) the QCM surface in an effort to obtain selectivity for a bulk acoustic wave (BAW) sensor. Pre-coated piezoelectric crystals have been successfully applied to biological, environmental and chemical fields [6–10]. Unfortunately, many systems are either not as specific as expected for chemicals, or are not stable for biomaterials. One technique uses molecularly imprinted polymers (MIPs) and is based on the development of either non-covalent or reversible covalent interactions between a compound (print molecule) and suitable functional monomers during the prepolymerization step [11,12]. Imprinting polymers are prepared in situ by copolymerization of cross-linkers and functional monomers that form complexes during the polymerization process, producing recognition sites with polymeric functionality positioned to complement those of the template molecule. MIPs have been used for the preparation of stationary phases for chromatographic and electrophoretic techniques, with many systems having the ability to separate efficiently the enantiomeric forms of peptides and drugs [13–16]. Such polymers have also been used for the quantification of drugs in real samples using competitive binding assays [17,18]. Another area of interest concerns the use of imprinted materials as the recognition elements in biomimetic sensors [19,20].

* Corresponding author. Tel.: +34 926295232; fax: +34 926295232.
E-mail address: angel.rios@uclm.es (Á. Ríos).

0039-9140/$ – see front matter © 2007 Elsevier B.V. All rights reserved.
doi:10.1016/j.talanta.2007.01.045

Finally, a variety of approaches have been followed in order to prepare polymers with catalytic properties [21,22].

In particular, the application of MIPs in a QCM sensor is a potentially attractive area [11,12,23,24]. Unfortunately, in some cases this technique suffers from the drawback that other structurally similar molecules can be held within the cavities and sites present in the MIP that have a selective affinity for the original print molecules.

The use of a hydrophobic membrane offers a way to overcome these problems. The most important of these techniques – supported liquid membrane (SLM) extraction [25,26] – is based on a three-phase system with an organic phase sandwiched between two aqueous phases. The organic phase is immobilized in a porous hydrophobic membrane. The SLM technique can be seen as a combination of a two-step LLE with dialysis. This approach offers a number of advantages in comparison to other extraction methods traditionally used for sample pre-treatment in trace analysis. The most important characteristic is that a high selectivity and very clean extracts can be obtained along with a high degree of concentration enrichment. This fact facilitates analysis by removing interference and increasing the concentration of analytes to measurable levels. Other advantages are the convenient connection to analytical instruments and the near total avoidance of organic solvents.

Vanilla is one of the world's popular flavour extracts and is obtained primarily from "*Vanilla planifolia*", a species of tropical climbing orchid native to Mexico. It is one of the most widely used flavour resources in confectionery, food and beverages. A wide variety of chemical techniques have been applied to the analysis of vanilla in an attempt to identify the primary components responsible for its delicate and unique flavour and to protect the integrity, and therefore the quality, of this product from unscrupulous manufacturers and suppliers, who are willing to adulterate vanilla or even pass off a completely synthetic imitation product as natural [27]. The quantification method most often used by the flavour industry is the AOAC 964.10 method [28], which determines vanillin through a time-consuming and laborious technique. Quantification involves absorbance measurements on an alkaline solution of the extract at 348 nm, with the vanillin absorbance depending on the final pH of the sample. If by simple error the measurement sample of vanillin extract has a pH below 11.0, the quantification result will be significantly lower than expected. It is also known that some compounds are present in the vanilla extract (e.g. 4-hydroxybenzaldehyde) that interfere in this method and lead to greater (10–20%) vanillin values than one would expect.

Several methods for determining vanillin and ethylvanillin from several food samples or vanilla extracts have been described and involve the use of gas chromatography/mass spectrometry (GC–MS) [29,30], high-performance liquid chromatography (HPLC) [31–35], capillary electrophoresis (CE) [36–39] and amperometric detections [40–43]. GC–MS methods employ the solid-phase microextraction (SPME) technique. The analytes are extracted from various matrixes by transferring them from a liquid sample into SPME fibre. The SPME fibre must be exposed to the headspace for a prolonged time period. Therefore, the GC–MS methods have advantages in terms of sensitivity and specificity, but also suffer from disadvantages in terms of time. High-performance liquid chromatography methods also have inherent disadvantages because HPLC requires a great deal of time for column equilibration. On the other hand, although CE is a powerful separation technique that can provide high resolution efficiency, it has a major drawback in terms of cost. Different amperometric biosensing configurations have been used and examples include peroxidase enzyme-modified solid graphite and carbon-paste biosensors [41], stabilized polymerized lipid film based biosensors [42] and chemically modified electrodes containing immobilized bacteria [43].

In the work reported here, a new method for the determination of vanillin in food samples is proposed and involves the use of SLM with a piezoelectric detector based on a molecularly imprinted polymer (SLM-PZ-MIP). To the best of our knowledge, an application based on piezoelectric sensing for the determination of vanillin has not been reported to date. In the present work, an MIP was used as the sensing component and was coated onto a QCM sensor. A highly sensitive QCM-MIP sensor was fabricated in this way. The use of SLM coupled on-line to QCM-MIP enhances selectivity by avoiding interference from matrix constituents, such as 4-hydroxybenzaldehyde, 4-hydroxy-3-methoxybenzyl alcohol and 4-hydroxybenzyl alcohol.

2. Experimental

2.1. Apparatus

The crystals used were AT-cut 10 MHz specimens with gold-plated electrodes (0.17 mm thick and 14 mm in diameter). Prior to use, the crystals were washed with 0.5 ml of "piranha" solution for about 5 min. This treatment was followed by rinsing with distilled water, ultrasonic cleaning in distilled water for 5 min, rinsing several times with distilled water and absolute ethanol, and drying in a nitrogen stream. The clean, dry crystals were coated with MIP, placed in a flow-through PTFE^{TM} cell and clamped between two O-rings recessed into the housing; a coated crystal was exposed to the sample in a 70 μl cell. The piezoelectric crystal and flow-through PTFE^{TM} cell were supplied by Universal Sensors, Inc. A laboratory-made oscillator circuit was connected to the electrode via platinum foil. A galvanic insulation filter was incorporated into the oscillator circuit to attenuate electronic noise and improve the system baseline. The resonant frequency was monitored with a Hewlett Packard HP-53131A/225 MHz frequency counter that was connected to a PC through an HP-IB interface (Hewlett Packard). HP-34812A Bench Link software (HP BenchLink/Meter) was used to acquire and store data.

The SLM unit (see Fig. 1) was similar to that used to house the crystal. This unit was machined from two rectangular Teflon blocks (length 5 cm, height 4 cm and width 1 cm). A fluoropore PTFE membrane with an average effective pore size of 0.5 μm, an average thickness of 175 mm and porosity of 85% was used as a support for the organic solvent, di-*n*-hexyl ether. The membrane was impregnated with the solvent mixture by soaking for at least 15 min before being placed in the unit. Finally, the mem-

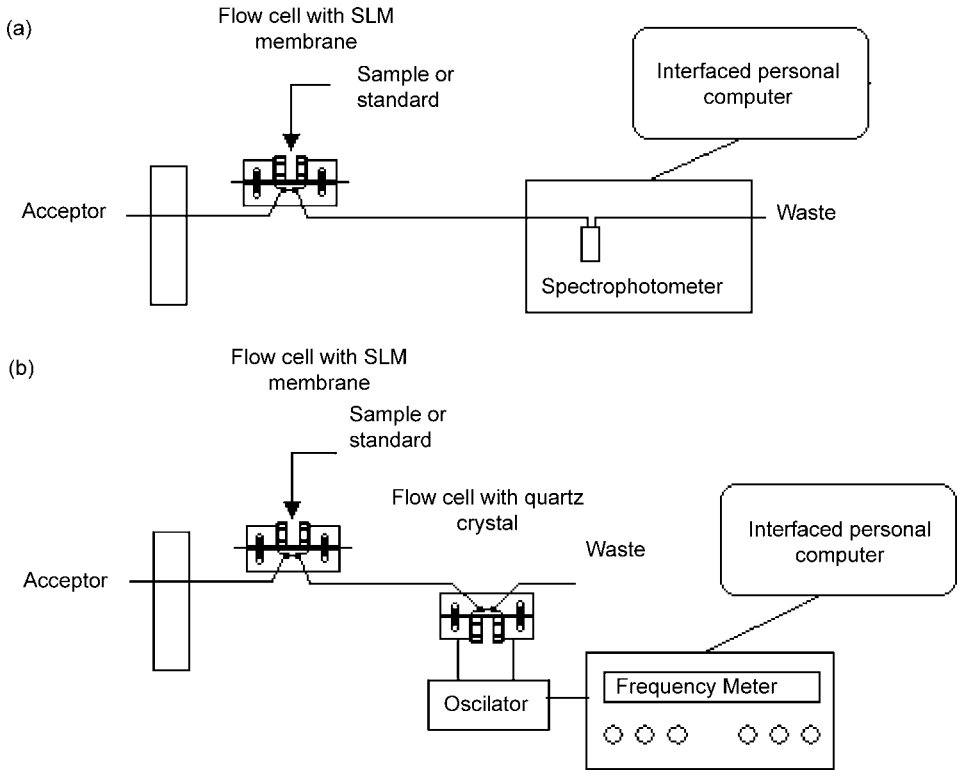

Fig. 1. Schematic diagram of the manifold used for the determination of vanillin with (a) spectrophotometric detection and (b) piezoelectric detection.

brane was placed in a unit and clamped between two O-rings recessed into the housing.

A Beckman Du-70 diode array spectrophotometer equipped with Hellma QS flow cell (18 μl inner volume, 10 mm light path) and a Gilson Minipuls-3 peristaltic pump were also used.

2.2. Reagents and samples

All reagents were prepared from analytical reagent grade chemicals. Methacrylic acid (MAA), ethylene glycol dimethacrylate (EDMA), vanillin, 4-hydroxybenzaldehyde, 4-hydroxy-3-methoxybenzyl alcohol and 4-hydroxybenzyl alcohol were purchased from Sigma. α,α′-Azoisobutyronitrile (AIBN) and low molecular weight poly(vinyl chloride) (PVC) were purchased from Fluka. Tetrahydrofuran (THF) was used as received to dissolve PVC.

A standard stock solution of 10 g l^{-1} vanillin was prepared by dissolving vanillin in ethanol. The acceptor solution was prepared by mixing the same volume of 0.2 M boric acid and 0.2 M potassium chloride and sufficient 0.2 M sodium hydroxide to give pH 9. Standard working solutions were prepared by appropriate dilution of the stock with 0.2 M H_2SO_4. Various vanilla sugar samples purchased in local supermarkets were analysed. These samples were dissolved in 0.2 M H_2SO_4.

2.3. Synthesis of the polymer

The procedure for synthesizing MIP involves the following four steps (see Fig. 2): (i) choosing a template molecule; (ii) allowing functional monomers to form complexes with the template; (iii) polymerizing the monomers with cross-linker while maintaining the complexes; (iv) subsequent washing of polymers reveals recognition sites that can specifically bind the template. After polymerization and removal of the print molecule by extraction, the resulting polymer shows selectivity towards the imprinted molecule due to both the three-dimensional structure and to the arrangement of the functional groups of the monomer units around the template molecule.

For the preparation of the polymer, 1 mmol of vanillin (template), 4 mmol of MAA (functional monomer), 20 mmol of EDMA (cross-linker) and 0.31 mmol of AIBN (initiator) were weighed into a 25-ml volumetric flask and dissolved in 10 ml of chloroform. The mixture was degassed in a sonicating bath and flushed with nitrogen for 5 min. Polymerization began within 30 min at 65 °C inside a thermostatted water bath and was continued for 24 h. The resultant polymer was ground with a mortar and pestle to produce a fine powder and passed through a sieve (mesh size 44 μm). To produce anti-vanillin polymer, the print molecule (vanillin) was removed from the polymer powder (0.5 g) by Soxhlet extraction using 150 ml of methanol/acetic acid (9:1, v/v) over 24 h.

2.4. Modification of the QCM sensor

Surface modification of the QCM was carried out as follows: 30 mg of fine polymer powder was suspended in 5 ml of THF containing 10 mg of polyvinyl chloride (PVC) powder. A small amount (5 μl) of this mixture was dropped onto the centre of the Au electrode on one side of a quartz crystal (10 MHz, 14 mm diameter). The THF was evaporated at room temperature in air to

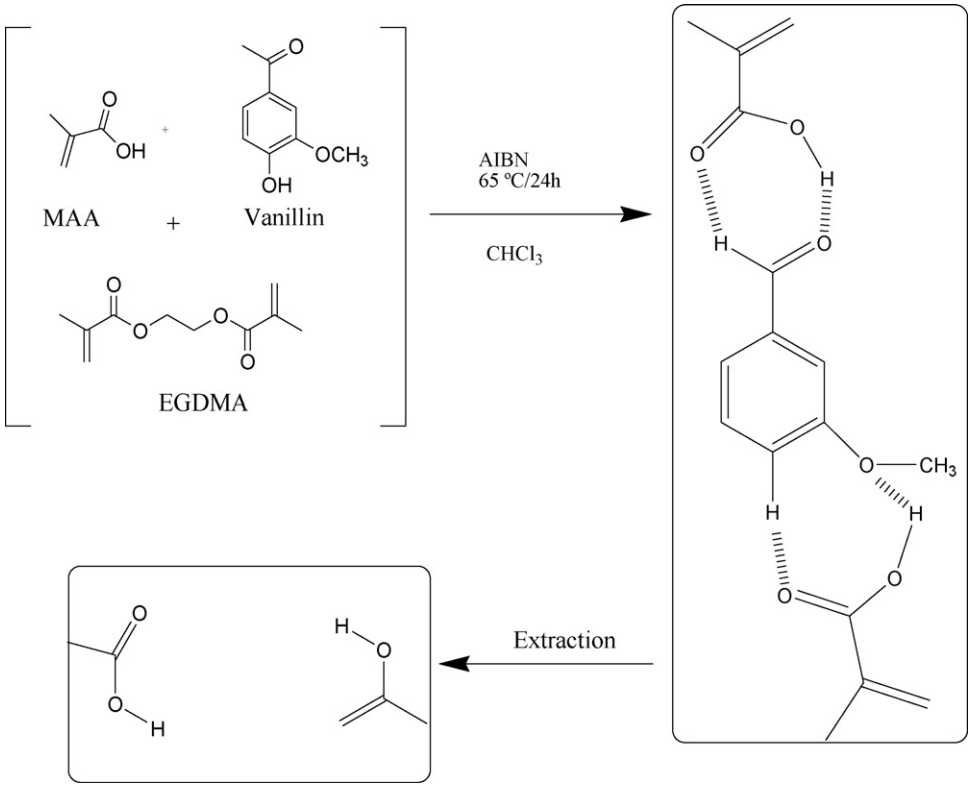

Fig. 2. Schematic illustration of the molecular imprinting procedure.

give an MIP coating on the Au electrode. The sensor was stored in double-distilled water when not in use. The sensor experiments were performed using a flow system with an optimized flow rate of 1 ml min^{-1}. Prior to analytical use, the sensor was stabilised for 5 h by running a receptor solution at pH 9. Before and after the application of MIP as a coating material, the resonant frequency of the sensor was measured with a Hewlett Packard HP-53131A/225 MHz frequency counter. The average frequency for the MIP sensors (viz. those assumed to have been coated by MIP) was 9,976,365 Hz, whereas that for the uncoated sensors was 9,985,501 Hz. This allowed the average amount of MIP deposited on the crystals to be determined.

2.5. Vanillin extraction and spectrophotometric detection

The flow injection (FI) manifold, which is depicted in Fig. 1a, comprised a single channel (the acceptor) flowing through the bottom part of the membrane unit. The porous membrane used was cut to fit in the holder and soaked for least 15 min in the selected solvent and placed between the two blocks. The blocks were screwed together and the channels connected. After mounting, the excess solvent was washed away from the membrane surface with water. The acceptor solution, a pH 13 NaOH/KCl solution, was pumped through the system in order to establish the baseline. A volume of 0.2 ml of sample prepared in 0.2 M H_2SO_4 was placed on the top of the membrane, allowing direct contact between the sample and the membrane. After 15 min, in which the analytes were extracted into the membrane, the pump was switched on and the analyte was re-extracted into the acceptor solution. When this reached the detector, the vanillin in the acceptor stream gave rise to an absorbance signal that was registered by the computer.

2.6. Vanillin extraction and piezoelectric detection

The flow manifold used for on-line separation and detection of vanillin is shown in Fig. 1b, and this is based on the coupling of the piezoelectric sensor. The first experiment involved the use of the manifold as represented in Fig. 1a, whereas the second experiment employed a single detector. The acceptor solution, flow rate, sample volume and stopped time were H_3BO_4/KCl at pH 9, 1 ml min^{-1}, 0.5 ml and 15 min, respectively. The separated vanillin was transferred into the piezoelectric flow-cell (FC-PZ), where the signal was detected, transmitted to the frequency counter (F) and then recorded (PC). The desorption time after vanillin uptake never exceeded 10 min, which is acceptable for a sensor. Once the measurement was made, the upper cavity was washed with copious amounts of water. Between successive determinations, 0.5 ml of di-*n*-hexyl ether was placed in the top of the membrane for 5 min to regenerate it. The excess organic reagent was removed by washing with copious amounts of water and occasionally using a piece of paper tissue. Meanwhile, the acceptor cavity was emptied by pumping air through the acceptor tubing, in order to avoid carry-over effects, and then refilled with acceptor solution. Samples and calibration standards were injected into the flow once the base resonant frequency (F_b) levelled off and measurements were found to be $\Delta F = F_p - F_b$, where F_p is the maximum frequency during each run. After five

detections, the rest of the vanillin was removed from the coating with methanol/acetic acid (1:1, v/v) and distilled water during 15 min.

3. Results and discussion

3.1. Optimisation of the method

The selection of the liquid membrane and its regeneration process was based on the results of a previous study by Luque et al. [40]. A fluoropore PTFE membrane with an average effective pore size of 0.5 μm and di-*n*-hexyl ether were the optimum membrane and organic phase, respectively. The membrane was regenerated between analyses by adding 0.5 ml of the organic component onto the top membrane during 5 min.

3.1.1. Effect of pH on the extraction and adsorption of vanillin in the PZ-MIP

A study of the influence of pH on the transport of the analyte through the membrane was carried out using a spectrophotometric configuration (Fig. 1a). The pH values of the donor and acceptor solutions are important parameters for the optimisation of the membrane system. The donor pH should be sufficiently low to ensure that the analytes are protonated – and therefore uncharged – so that they can be extracted into the organic membrane liquid. For this reason, all standard solutions were prepared in 0.2 M H_2SO_4. In order to assess the influence of the pH of the acceptor phase on the extraction, pH was varied over a wide a range by changing the buffer solution. The effect of the pH of the acceptor solution is shown in Fig. 3a. Increases in the pH led to increases in the signal, with a sharp maximum attained at pH 13.

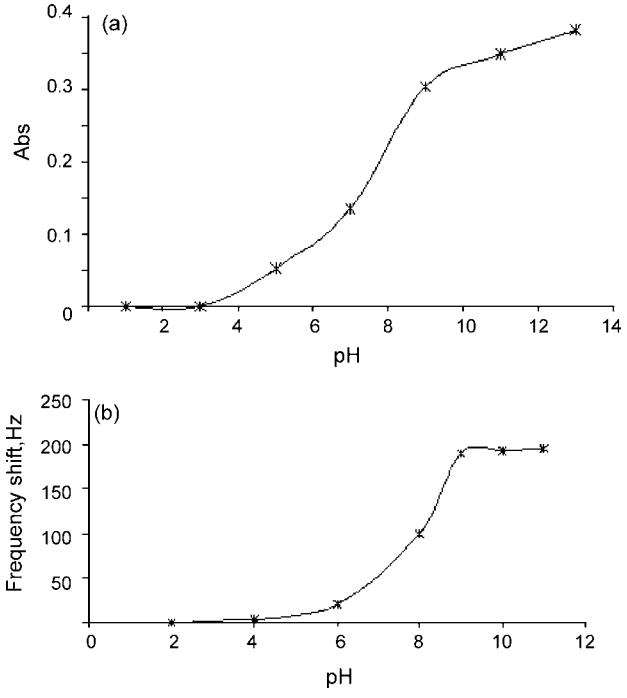

Fig. 3. (a) Study of pH acceptor phase using a spectrophotometric configuration. Donor phase: 0.2 M H_2SO_4. (b) Influence of pH on the response of the QCM-MIP sensors.

The binding sites of the MIP coating the QCM sensor are synthesized in situ by copolymerization of functional monomers and cross-linkers around the template molecules. In this work, MMA was employed as the functional monomer and this has carboxyl functional groups. The binding of the template onto imprinted polymers is due to hydrogen bonding as well as electrostatic forces and charge transfer between the carboxyl groups and the imprinted molecules. As a result, the pH will greatly influence the interactions between the analyte and the coating, and will consequently influence the stabilization of the sensor. Solutions of 0.2 M H_3BO_3 and 0.2 M KCl adjusted with 0.2 M NaOH or HCl were used to control the pH in the range 1.0–11.0 for the determination of a 5 μM of vanillin standard solution using the QCM sensor coated with a MIP (QCM-MIP) (without a separation with SLM). It can be seen from Fig. 3b that the frequency shift is relatively stable when the pH value is at the range 9–11. For pH values below 9, however, ionic and covalent adsorption will be enhanced and the frequency shift will increase, but the frequency of the QCM is unstable. In order to ensure good extraction and detection in the PZ-MIP, a value of pH 9 was selected as the optimum pH for the acceptor phase and this was used throughout the study.

3.1.2. Effect of flow rate and the stopped-flow time

The flow-rate of the acceptor solution was optimised. Flow rate values between 0.2 and 3 ml min^{-1} were tested using 5 μM vanillin standard solutions. The increasing acceptor flow rate in the range 0.5–1 ml min^{-1} increased the frequency shift. When the flow rate of the accepting solution was above 1 ml min^{-1}, the frequency shift decreased, probably due to the fact that the analyte quickly passes through the piezoelectric flow-cell and the vanillin is hardly absorbed. A flow rate of 1 ml min^{-1} was finally selected.

The effect of stopped-flow time on the frequency shift was studied in the range 1–30 min. Sensitivity enhancements were achieved by increasing the stopped-flow time; however, a stopped-flow time of 15 min was selected in order to achieve a reasonable degree of sensitivity. A longer stopped-flow time can be employed for samples with low concentrations of vanillin.

3.2. Features of the determination of vanillin

The important values for the proposed SLM- PZ-MIP method and SLM-spectrophotometric method, namely linear dynamic range, relative standard deviation and limit of detection, are shown in Table 1. Standard solutions of vanillin were added onto the top of the membrane at variable concentrations and determined under the optimum conditions.

A calibration graph was obtained using standard solutions of vanillin over the range 1.3–65 μM. Each solution was injected in triplicate. The linear range, intercept and slope of the curve are given in Table 1 along with the regression coefficient for vanillin. The precision of the method for aqueous standards (evaluated as the relative standard deviation obtained after analysing 10 series' of 10 replicates) was 4.8% at the 5 μM level of vanillin. The theoretical limit of detection, defined as the concentration of the analyte giving a signal equivalent to the blank signal plus

Table 1
Analytical characteristics of the proposed method

Parameter	SLM-QCM-MIP	SLM-UV-VIS
Working concentration range (μM)	1.3–65	33–657
Calibration function ($\log(\Delta F) = a \log(C_{vanillin}) + b$), ($n = 3$)	$\log(\Delta F) = 0.6601 \log(C_{vanillin}) + 1.079$	$Abs = 0.0006 (C_{vanillin}) + 0.0221$
Standard deviation of residuals (S_y/x)	0.0127	0.0036
Regression coefficient (R^2)	0.9993	0.9995
Precision, R.S.D. (%) ($n = 10$)	4.8	2.5
Detection limit (μM)	1.14	17.51

three times its standard deviation, was 1.14. This method shows clear advantages in terms of sensitivity with respect to the spectrophotometric method described in this work and other existing alternatives that involve the use of an electrochemical detector [40] (see Table 2).

3.3. Selectivity

Molecular imprinting is a technique for the design of biomimetic receptors. After removal of the template molecules by extraction, MIP shows a high selectivity to the imprinted molecules due to both the 3-D structure and the arrangement of the functional groups of the monomer units around the print molecules. When the MIP sensor is applied to determine vanillin in real samples, all other substances hardly interfere with the determination. Structurally similar compounds that are commonly present in these samples, such as 4-hydroxybenzaldehyde, 4-hydroxy-3-methoxybenzyl alcohol and 4-hydroxybenzyl alcohol, were studied for selectivity purposes. The molecular structures of these compounds are shown in Fig. 4. These compounds were selected because they are present in the analysed samples and they have similar structures to the imprinted molecule (vanillin).

The sensor responses to these molecules when they were adsorbed directly in the PZ-MIP without SLM sample pretreatment are shown in Fig. 5a. The results indicate that the interference caused by 4-hydroxybenzaldehyde, 4-hydroxy-3-methoxybenzyl alcohol and 4-hydroxybenzyl alcohol is very high. When the membrane was coupled to a PZ-MIP, such interference can be dramatically reduced (Fig. 5b) because the compounds do not pass through the membrane under the experimental conditions. The results obtained using SLM show that this interference can be easily avoided with this methodology.

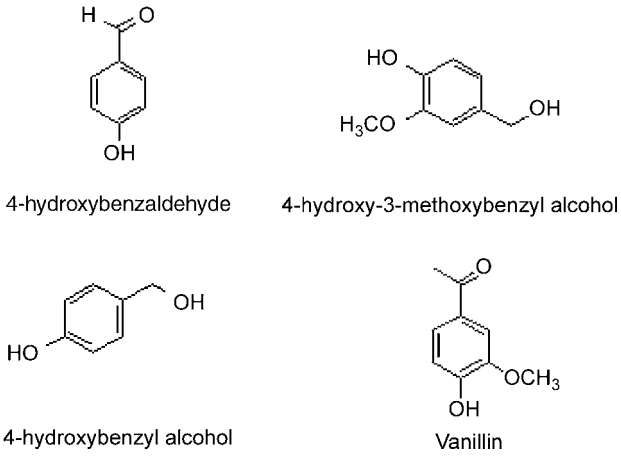

Fig. 4. Molecular structures of compounds used to study the selectivity of PZ-MIP.

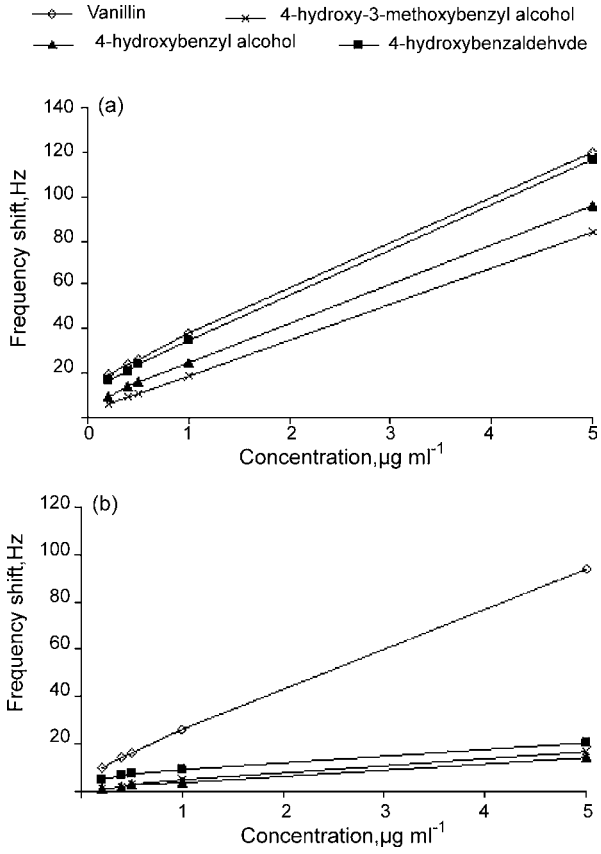

Fig. 5. (a) Study of vanillin selectivity for the developed sensor using analytes with similar chemical structures to vanillin, e.g. 4-hydroxybenzaldehyde, 4-hydroxy-3-methoxybenzyl alcohol and 4-hydroxybenzyl alcohol. (a) Without SLM step, (b) with SLM step.

Table 2
Comparison of the proposed method with other methods for the determination of vanillin

Method	Calibration range (μM)	Detection limit (μM)	Recovery (%)	R.S.D. (%)	Reference
SLM-UV-Vis	33–657	17.51	103–115	2.5	This work
SLM-Amperometric	657–9201	291	83–120	6	[20]
SLM-QCM-MIP	1.3–65	1.14	85–115	4.8	This work

Table 3
Analysis of synthetic solutions of vanillin ($n = 3$)

Concentration added (μM)	SLM-QCM-MIP		SLM-UV-Vis	
	Found (μM)	Recovery (%)	Found (μM)	Recovery (%)
2.0	1.7	85	–	–
5.0	4.5	90	–	–
7.5	8.0	107	–	–
20.0	23.0	115	–	–
50.0	50.5	101	49	97
100	–	–	111	111
260	–	–	287	110
400	–	–	412	103
500	–	–	574	115

Table 4
Analysis of real samples for vanillin

Samples	SLM-QCM-MIP ($\mu g\,g^{-1}$)	SLM-UV-Vis ($\mu g\,g^{-1}$)	Recovery (%)
Vanilla sugar 1	113 ± 4	123 ± 4	92
Vanilla sugar 2	102 ± 3	114 ± 3	89
Vanilla sugar 3	135 ± 6	141 ± 2	96
Vanilla sugar 4	80 ± 3	81 ± 4	99
Vanilla sugar 5	71 ± 2	73 ± 1	97

3.4. Analytical applications

The applicability of the proposed method was assessed by determining vanillin in synthetic solutions in the range 2–500 μM (Table 1). The concentrations added and found (Table 3) were generally in good agreement, with a recovery between 85 and 115%. The proposed method was then applied to the determination of vanillin in real samples. Food samples were purchased in local markets. All the samples were found to contain vanillin. The determination was made without any treatment of the samples. The results obtained are shown in Table 4. As in the case of the synthetic samples, the results showed a good agreement with those provided by the spectrophotometric method described in Section 2.5.

4. Conclusion

Although imprinted polymers used as biomimetic sensors are reported to have substantially lower sensitivity than related biosensors [44,45], the applicability of these systems in the analysis of real samples has not been well demonstrated. The main problem arises from the interference produced by other compounds present in the sample matrix that have similar structures to the print molecule. Such compounds can be held within the cavities and sites present in the MIP that have a selective affinity for the original print molecules. This methodology combines the advantages of the SLM technique, such as analyte enrichment and efficient removal of interfering matrix constituents, with rapidity, low cost, simplicity and sensitivity. The use of SLM greatly enhances the selectivity compared to the MIP-QCM methods, thus avoiding interfering matrix constituents, such as 4-hydroxybenzaldehyde, 4-hydroxy-3-methoxybenzyl alcohol and 4-hydroxybenzyl alcohol.

Acknowledgements

The Spanish Ministerio de Ciencia y Tecnología (MCyT) and JJCC Castilla-La Mancha are gratefully acknowledged for funding this work with Grants CTQ2004-02362 and PAC05-001-1. The support given through a "Juan de la Cierva" research contract for M. Zougagh is also acknowledged.

References

[1] K. Cammann, U. Lemke, A. Rohen, J. Sander, H. Wikken, B. Winter, Agrew. Chem. 103 (1991) 512.
[2] L. Manganiello, A. Ríos, M. Valcárcel, Anal. Chem. 74 (2002) 921.
[3] F.L. Dickert, P. Forth, P. Lieberzeit, M. Tortschanoff, Fresenieus J. Anal. Chem. 360 (1998) 759.
[4] E. Hedberg, F. Winquist, I. Lindström, L.I. Anderson, K. Mosbach, Sens. Actuators A 37 (1999) 796.
[5] F.L. Dickers, S. Thierer, Adv. Mater. 8 (1996) 987.
[6] R.C. Ebersole, J.A. Miller, J.R. Moran, M.D. Ward, J. Am. Chem. Soc. 12 (1999) 173.
[7] L. Deng, F.J. He, T.J. Jiang, L.H. Nie, S.Z. Yao, J. Microbiol. Methods 23 (1995) 229.
[8] M. Zougagh, A. Ríos, M. Valcárcel, Talanta 65 (2005) 29.
[9] C. Steegborn, P. Skladal, Biosens. Bioelectron. 12 (1997) 19.
[10] T. Bein, K. Brown, G.C. Frye, C.J. Brinder, J. Am. Chem. Soc. 111 (1989) 7640.
[11] Y. Tan, Z. Zhou, P. Wang, L. Nie, S. Yao, Talanta 55 (2001) 337.
[12] M. Zougagh, A. Ríos, M. Valcárcel, Anal. Chim. Acta 539 (2005) 117.
[13] O. Ramström, R.J. Ansell, Chirality 10 (1998) 195.
[14] L.I. Andersson, K. Mosbach, J. Chromatogr. 516 (1990) 313.
[15] D.W. Armstrong, J.M. Schneiderheinze, Y.S. Hwang, B. Sellergren, Anal. Chem. 70 (1998) 3717.
[16] J.M. Lin, T. Nakagama, K. Uchiyama, T. Hobo, Chromatographia 43 (1996) 585.
[17] O. Vlatakis, L.I. Andersson, R. Muller, K. Mosbach, Nature 361 (1993) 645.
[18] L.I. Anderson, Anal. Chem. 68 (1996) 111.
[19] D. Kriz, K. Mosbach, Anal. Chim. Acta 300 (1994) 71.
[20] T. Petra, W. Barbara, D.D. Graham, S.P. William, Anal. Chem. 70 (1998) 2025.
[21] W.R. Ahmad, M.B. Davig, Catal. Lett. 40 (1996) 109.
[22] M.B. Davis, A. Katz, W.R. Ahmad, Chem. Mater. 8 (1996) 1820.
[23] Y. Tan, J. Yin, C. Liang, H. Peng, L. Nie, S. Yao, Bioelectrochemistry 53 (2001) 141.
[24] H. Liao, Z. Zhang, L. Nie, S. Yao, J. Biochem. Biophys. Methods 59 (2004) 75.
[25] J.A. Joensson, L. Mathiasson, Trends Anal. Chem. 11 (1992) 106.
[26] D. Barcelo, M.-C. Hennion, Trace Determination of Pesticides and their Degradation Products in Water. Techniques and Instrumentation in Analytical Chemistry, vol. 19, Elsevier, Amsterdam, 1997.
[27] Code of Federal Regulations, Title 21, part 169.175, US Government Printing Office, Washington, DC, USA, 1987.
[28] Official Methods of Analysis, fifteenth ed., vol. 2, Association of Official Analytical Chemists (AOAC), Arlington, VA, 1990, pp. 890–896.
[29] T. Sostaric, M.C. Boyce, E.E. Spickett, J. Agric. Food Chem. 48 (2000) 5802.
[30] N. Jensen, P. Varelis, F.B. Whitfield, Lett. Appl. Microbiol. 33 (2001) 339.
[31] E. Jagerdeo, E. Passetti, S.M. Dugar, J. AOAC Int. 83 (2000) 237.
[32] A. Ranadive, J. Agric. Food Chem. 40 (1992) 1922.
[33] G. Lamprecht, F. Pichlmayer, E. Schmid, J. Agric. Food Chem. 42 (1994) 1722.

[34] B.K. Lavine, S. Hendayana, J. Tetreault, Anal. Chem. 66 (1994) 3458.
[35] S. Kahan, D.A. Krueger, J. AOAC Int. 80 (1997) 564.
[36] U. Bütehorn, U. Pyell, J. Chromatogr. A 736 (1996) 321.
[37] T. Watanabe, A. Yamamoto, S. Nagai, S. Terabe, J. Chromatogr. A 793 (1998) 409.
[38] M.C. Boyce, P.R. Haddad, T. Sostaric, Anal. Chem. Acta 485 (2003) 179.
[39] M. Ohashi, H. Omae, M. Hashida, Y. Sowa, S. Imai, J. Chromatogr. A 1138 (2007) 262.
[40] M. Luque, E. Luque, A. Ríos, M. Valcárcel, Anal. Chim. Acta 410 (2000) 127.
[41] T. Ruzgas, J. Emneus, L. Gorton, G. Marko-Varga, Anal. Chim. Acta 311 (1995) 245.
[42] D.P. Nikolelis, G. Theoharis, Electroanalysis 14 (2002) 1661.
[43] P. Kladal, O. Natalya, A.N. Reshetilov, Biosens. Bioelectron. 17 (2002) 867.
[44] B.S. Ebarvia, C.A. Binag, F. Sevilla III, Anal. Bioanal. Chem. 378 (2004) 1331.
[45] B.S. Ebarvia, C.A. Binag, F. Sevilla III, Sens. Actuators B 107 (2005) 782.

Available online at www.sciencedirect.com
ScienceDirect
Talanta 72 (2007) 1552–1563
Talanta
www.elsevier.com/locate/talanta

Characterization of the aromatic profile for the authentication and differentiation of typical Italian dry-sausages

F. Bianchi [a], C. Cantoni [b], M. Careri [a], L. Chiesa [b], M. Musci [a,*], A. Pinna [a]

[a] *Dipartimento di Chimica Generale ed Inorganica, Chimica Analitica, Chimica Fisica, Università di Parma, Parco Area delle Scienze 17/A, 43100 Parma, Italy*
[b] *Dipartimento di Scienze e Tecnologie Veterinarie per la Sicurezza Alimentare, Università degli Studi di Milano, Via Celoria 10, 20133 Milano, Italy*

Received 4 September 2006; received in revised form 21 January 2007; accepted 5 February 2007
Available online 25 February 2007

Abstract

In order to chacterize two kinds of typical Italian dry-sausages, namely "Salame Mantovano" and "Salame Cremonese", the volatile composition was determined for seven samples of "Salame Mantovano" and for five samples of "Salame Cremonese". The study was performed by the dynamic headspace extraction technique (DHS) coupled with gas chromatography–mass spectrometry (GC–MS). Among the 104 volatiles identified, terpenes, aldehydes, ketones and alcohols represented the most abundant compounds. Peak area data for all the substances from the above mentioned group was used for statistical purposes. Firstly, principal component analysis (PCA) was carried out in order to visualize data trends and to detect possible clusters within samples. Then, linear discriminant analysis (LDA) was performed in order to detect the volatile compounds able to differentiate the two kinds of sausages investigated. The data obtained by GC–MS shows that the most important contributions to the differentiation of the two kinds of typical Italian salami were seven volatile compounds, i.e. 3-methylbutanal, 6-camphenol, dimethyl disulfide, 1-propene-3,3′-thiobis, ethyl propanoate, 1,4-*p*-menthadiene and 2,6-dimethyl-1,3,5,7-octatetraene. Prediction ability of the calculated model was estimated to be 100% by the "leave-one-out" cross-validation.

Keywords: Dry-sausages; Volatile compounds; Dynamic headspace technique; Gas chromatography–mass spectrometry; Linear discriminant analysis; Principal component analysis

1. Introduction

A wide variety of typical dry-sausages is produced in several countries of Italy. These meat-based foods, that represent a large part of the Italian market, are greatly appreciated by the consumers due to their characteristic sensory properties and their image of traditional products.

Among them, "Salame Mantovano" and "Salame Cremonese" are produced in the Lombardia region, in the northern of Italy, by rural families as well as by small and medium factories. Despite similarity in the raw matter and spices used, some differences in production techniques, such as manufacturing and ripening time, can be pointed out. "Salame Mantovano" is produced in the Mantova country following a traditional recipe; the pork meat and fat are coarsely minced, according to the original ancient custom, and mixed with salt (maximum 2.5%), black pepper (maximum 0.3%), and spices (maximum 0.3%) as clove and nutmeg. Sugars, starters and nitrate could be used. "Salame Mantovano" is mainly characterized by a rather high content of garlic. Average weight is approximately 1 kg, but smaller sizes are also available. A drying stage at 12–23 °C for 9 days is followed by the ripening stage at 11–16 °C. Ripening time varies from 2 to 6 months, depending on size and ripening conditions.

Also "Salame Cremonese", produced in Cremona country, is made of pure medium-fine ground pork meat and fat and contains spices and garlic; sugars, starters and nitrate could also be added. However, with respect to the "Salame Mantovano", the flavor is distinctive and less intense. The drying stage is carried out at 15–25 °C for a maximum of 10 days, then the ripening

* Corresponding author at: Dipartimento di Chimica Generale ed Inorganica, Chimica Analitica, Chimica Fisica, Università degli Studi di Parma, Parco Area delle Scienze 17/A, 43100 Parma, Italy. Tel.: +39 0521 906023; fax: +39 0521 905557.
E-mail address: marilena.musci@unipr.it (M. Musci).

0039-9140/$ – see front matter © 2007 Elsevier B.V. All rights reserved.
doi:10.1016/j.talanta.2007.02.019

step occurs for at least 5 weeks at 11–16 °C. The "Salame Cremonese" weight is about 500 g, the diameter 7–10 cm and the length 20 cm. It is characterized by cylindrical shape, slightly irregular, and by a creamy texture at the end of the ripening.

Since 2000 "Salame Mantovano" and "Salame Cremonese" are included in the "List of traditional foods of Lombardia country" [1]. In order to protect the peculiar characteristics of both these products in the European market, some small and medium size production factories gathered in two Safeguarding Consortia. For each kind of salami, production rules have been proposed and the Protected Geographical Indication (PGI) has been required. Since the PGI labeled foods must be produced in a well defined geographical area, possessing unique human and natural characteristic and following well defined production rules [2], the preservation of the authenticity of these traditional products is becoming a concern of great interest. Of course, the acquisition of the PGI label provides a large economical added-value to the products, so economical frauds and/or adulteration are possible.

Since the aroma is one of the most typical features of a food, the characterization of the aromatic profile can represent a useful tool to evaluate the organoleptic quality and it could be used to guarantee its authenticity [3–5]. Really, the aromatic profile represents a chemical "fingerprint" of the product, since the nature and the relative amount of the compounds present in the volatile fraction are distinctive features of the product.

Different techniques have been proposed for the extraction of the volatile compounds of dry-sausages, e.g. the simultaneous distillation-extraction (SDE) [6–8], dynamic headspace (DHS) and purge-and-trap techniques [9–12], and more recently, solid phase microextraction (SPME) [13]. High resolution gas chromatography–mass spectrometry (HRGC–MS) analysis is usually carried out for identification and quantification purposes [3,6,7,10–13].

On the basis of these remarks, our study was firstly aimed at the characterization of the volatile fraction of "Salame Mantovano" and "Salame Cremonese" with the objective of authenticating these traditional foods. For this purpose, the DHS technique coupled to HRGC–MS was used. Secondly, a supervised chemometric procedure, the linear discriminant analysis [14,15], was applied in order to detect the volatile compounds able to differentiate the two kinds of sausages investigated. This chemometric approach has been widely reported in literature to classification problems involving the authentication of foodstuffs [16–19].

2. Materials and methods

2.1. Reagents

C6–C16 normal alkanes and boric acid (99.5% purity) were from Sigma–Aldrich (Milan, Italy). Diethyl ether (99.8% purity) and ammonium hydroxide solution were from Fluka (Buchs SG, Germany). Phosphosulfuric acid, sulfuric acid 96%, sodium hydroxide and sodium sulfate were from Carlo Erba (Milan, Italy). Hydrochloric acid 36–38% was from J.T. Baker (Deventer, The Netherlands).

2.2. Samples

Seven samples of "Salame Mantovano" (indicated as MN1–MN7) and five samples of "Salame Cremonese" (indicated as CR1–CR5) were purchased from different producers following the production rule described in the respective regulations. The number of samples analyzed, although rather small, has to be considered representative of the reduced industrial production, limited to about 15 producers for each type of salami. For each sample, ripening time was about 70 days, corresponding to the end of the ripening stage, being the sausages analyzed of similar size and weight.

Samples were frozen under liquid nitrogen and ground in a domestic blender, then stored in screw-cap glass vials at −20 °C until analysis.

2.3. Chemical composition

Water content was determined by drying samples at 100–102 °C [20]. Nitrogen content was determined by the Kjeldahl method by using the DK6 Heating Digester and the mineralizer UDK 130A (VELP Scientifica, Milan, Italy); protein content was estimated by multiplying the nitrogen content by 6.25 [21]. Total fat was extracted by Soxhlet extractor SRE 148 Solvent Extraction (VELP Scientifica) using diethyl ether [22]. Each determination was performed in triplicate.

2.4. Dynamic headspace extraction

2.5 g of frozen sample were placed in a 200 ml Erlenmayer flask at 40 °C. Purified helium (40 ml min^{-1}) was passed through the system for 30 min and the entrained volatiles were adsorbed on a glass tubes (16 cm × 0.4 cm i.d.) trap filled with Tenax TA (90 mg, 20–35 mesh) (Chrompack, Middelburg, The Netherlands), previously conditioned at 300 °C for 8 h. The volatile compounds were subsequently thermally desorbed and transferred to the GC system by using a TCT thermal desorption cold trap (TD800, Fisons Instruments, Milan, Italy). Desorption was performed at 280 °C for 10 min under a helium flow (10 ml min^{-1}) and the substances were cryofocused in a glass lined tube at −120 °C with liquid nitrogen. The volatile components were injected into the GC capillary column by heating the cold trap to 220 °C.

Three independent DHS extractions were performed for each sample.

To assess possible environmental contamination, blank analyses were carried out using an empty 200 ml Erlenmayer flask following the same procedure as for the samples. In addition, in order to assess the presence of carry-over effects, the adsorbent trap was desorbed before and after each entire sampling procedure.

2.5. Gas chromatography–mass spectrometry

Gas chromatography–mass spectrometry analysis of the salami headspace was carried out using a system consisting of a TRACE GC 2000 gas chromatograph and of a TRACE

MS quadrupole mass spectrometer (Thermo Electron Corporation, Milan, Italy). The interface and the source temperatures were kept at 230 and 200 °C, respectively. Electron impact mass spectra were recorded at 70 eV ionization energy (scan time, 0.5 s; electron multiplier voltage, 350 V) scanning the mass spectrometer from *m/z* 35 to 350. The carrier gas was helium (pressure, 70 kPa). Chromatographic separation was performed on a fused-silica bonded-phase capillary column Supelcowax 10 (30 m × 0.25 mm; d.f. = 0.25 μm) (Supelco, Palo Alto, CA, USA). The temperature program was isothermal at 35 °C for 8 min, ramped to 60 °C at 4 °C min^{-1}, then to 160 °C at 6 °C min^{-1} and to 220 °C at 20 °C min^{-1}, holding this temperature for 1 min.

2.6. Data analysis

The mass spectrometer data acquisition was performed using the release 1.2 Xcalibur™ software (Thermo Electron Corporation).

The identification of the volatile compounds was achieved by comparing their mass spectra with those stored in the National Institute of Standards and Technology (NIST) US Government library. In addition, retention indices were calculated for each peak with reference to the normal alkanes C6–C16 series according to the following equation [23]:

$$RI = 100z + 100\frac{(RT_i - RT_z)}{(RT_{z+1} - RT_z)}$$

where RI is the retention index of the unknown peak, RT_i is the retention time for the unknown peak, RT_z and RT_{z+1} are the retention times for the *n*-alkanes that bracket the unknown peak, *z* is the number of carbon atoms in the *n*-alkane standard that elute just before the unknown peak.

Calculated retention indices were then compared with those stored in a proprietary database obtained by injecting 250 volatile compounds usually found in a variety of food samples [24].

In order to evaluate quantitative differences in the aromatic profile of the samples investigated, GC peak areas were calculated for the identified compounds.

2.7. Statistical analysis

Principal component analysis (PCA) and linear discriminant analysis (LDA) were performed on the areas of the chromatographic peaks detected in at least four samples of "Salame Mantovano" and in at least three samples of "Salame Cremonese", representing, for each kind of salami, more than the half of the samples analyzed. Peak area data were corrected taking into account different amount of water in the samples, in order to consider the content of volatile compound referred to the same amount of dry-matter. Then, data were autoscaled to mean zero and unit variance.

Firstly, principal component analysis (PCA) was carried out in order to visualize data trends and to detect possible clusters within samples, thus providing a first evaluation of the discriminant efficiency of the considered variables.

Then, forward stepwise linear discriminant analysis (LDA) (*F*-to-enter = 0.05) was performed in order to detect the variables (i.e. volatile compounds) more contributing to differentiate the aromatic profile of the two kinds of sausages.

The predictive ability of the calculated model was then evaluated by the "leave-one-out" cross-validation: each sample is removed one-at-time from the initial matrix of data, then the classification model is rebuilt and the case removed is classified in the new model.

Statistical analysis was performed by using the SPSS package version 9.0 (SPSS Italia, Bologna, Italy).

3. Results and discussion

3.1. Chemical composition

Results of chemical composition analysis are reported in Tables 1 and 2.

The water content in the "Salame Mantovano" samples under investigation ranged from 33.4 to 49.9%; this variability can be attributed to different sample size and ripening conditions. Fat content ranged from 25.1 to 32.1% and protein content from 21.7 to 31.7%. Production rules included in the proposed PGI state water content has to be lower than 50%, fat amount lower than 35% and protein content at least 18%. For all the analyzed samples of "Salame Mantovano" the obtained values of these parameters are in accordance with reference values.

As for "Salame Cremonese", the water content ranged from 31.3 to 40.1%; the fat content from 18.8 to 36.5% and the protein content from 20.2 to 27.8%.

The ratios water/protein and fat/protein both have to be lower then 2%, according to the production rules included in the

Table 1
Results of chemical composition analysis for "Salame Mantovano" samples

Sample	Water %	Fat %	Protein %	Water/protein	Fat/protein
MN1	33.6 ± 0.3	30.0 ± 1.1	28.8 ± 0.8	1.17 ± 0.03	1.04 ± 0.05
MN2	44.6 ± 0.3	27.9 ± 0.5	21.7 ± 0.4	2.05 ± 0.04	1.28 ± 0.03
MN3	39.6 ± 0.5	29.3 ± 1.3	26.7 ± 0.4	1.48 ± 0.03	1.09 ± 0.05
MN4	40.7 ± 0.3	32.1 ± 0.5	21.7 ± 0.1	1.87 ± 0.02	1.47 ± 0.02
MN5	39.0 ± 0.1	25.1 ± 0.4	31.7 ± 0.5	1.23 ± 0.02	0.79 ± 0.02
MN6	49.9 ± 0.2	25.7 ± 0.3	21.9 ± 0.1	2.27 ± 0.01	1.17 ± 0.01
MN7	33.4 ± 0.1	28.2 ± 0.2	30.8 ± 0.1	1.084 ± 0.005	0.91 ± 0.01

Table 2
Results of chemical composition analysis for "Salame Cremonese" samples

Sample	Water %	Fat %	Protein %	Water/protein	Fat/protein
CR1	36.6 ± 0.3	29.2 ± 0.1	24.1 ± 0.3	1.51 ± 0.02	1.21 ± 0.01
CR2	31.3 ± 0.3	36.5 ± 0.1	27.8 ± 0.8	1.12 ± 0.03	1.31 ± 0.04
CR3	36.5 ± 0.3	18.8 ± 0.2	20.2 ± 0.1	1.81 ± 0.02	0.93 ± 0.01
CR4	40.1 ± 0.3	28.1 ± 0.2	25.1 ± 0.4	1.59 ± 0.03	1.12 ± 0.02
CR5	39.9 ± 0.3	30.4 ± 0.2	23.3 ± 0.2	1.71 ± 0.02	1.30 ± 0.01

proposed PGI for "Salame Cremonese". For all the samples of "Salame Cremonese" the obtained values of these parameters are in accordance with reference values.

A statistical *t*-test ($\alpha = 0.05$) was performed in order to compare mean values of all these analytical parameters between the two kinds of salami.

No significant differences were detected with respect to the chemical composition of the two classes of salami, except than for the fat/protein ratio, being significant lower for the "Salame Mantovano".

These findings allowed us to conclude that compositional analysis is not useful to distinguish between the types of salami analyzed.

3.2. Volatile compounds analysis

Fig. 1 shows typical gas chromatograms of the DHS extracts obtained respectively for a sample of "Salame Mantovano" and a sample of "Salame Cremonese".

Table 3 lists the compounds detected in at least four samples of "Salame Mantovano" and/or in at least three samples of "Salame Cremonese". Tables 4 and 5 list chromatographic peak areas respectively for "Salame Mantovano" and "Salame Cremonese" referred to the compounds reported in Table 3. Owing to the high variability in water content, raw areas were corrected by dividing them for the dry-matter amount.

Identification of the volatile compounds was performed by comparing their mass spectra with those reported in the NIST library. In addition, retention indices were calculated for each chromatographic peak and compared with those stored in a proprietary database including about 250 volatile compounds usually found in food matrices.

Since it is very expensive and time-consuming to inject many pure compounds, as in the case of complex chromatograms, retention indices can offer an effective alternative thus allowing to distinguish among compounds producing similar spectra, as for examples terpenes.

Compounds were considered positively identified when both mass spectra and retention indices led to the same identification, taking into account that a difference of 10 KI units can be considered acceptable, since different commercial stationary phases and temperature programs were used.

In total, 90 volatile substances were identified in at least four samples of "Salame Mantovano", belonging to different chemical classes. In particular, a total of 32 terpenes, 13 aldehydes, 11 ketones, 9 alcohols, 8 aromatic hydrocarbons, 6 esters, 5 sulfur compounds, 4 linear hydrocarbons and 2 furans were detected in "Salame Mantovano".

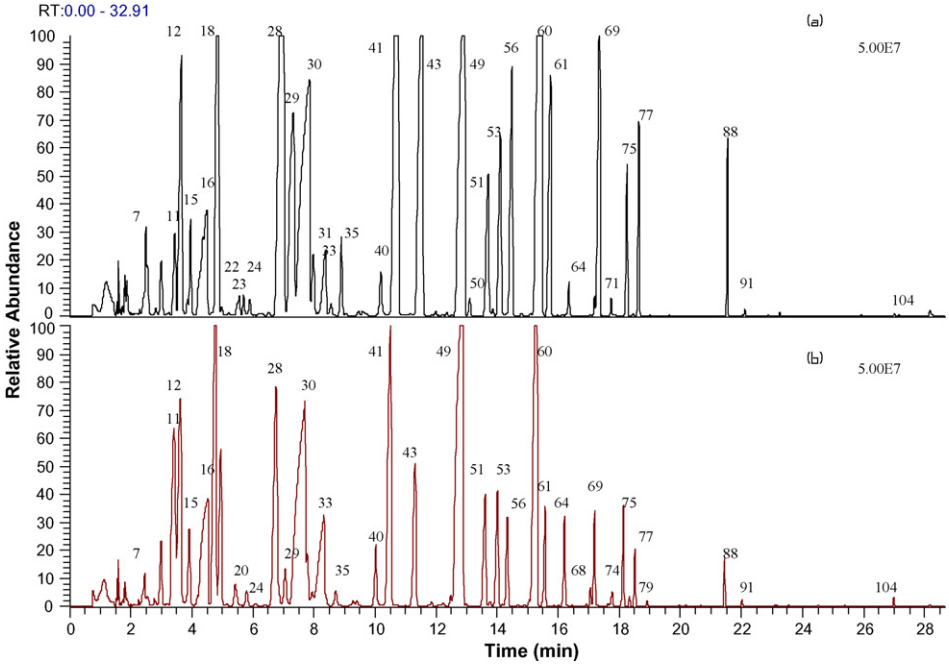

Fig. 1. DHS-GC–MS total ion chromatograms of (a) a "Salame Mantovano" sample (MN7) (b) a "Salame Cremonese" (CR5). For peak identification see Table 3.

Table 3
Volatile compounds detected in "Salame Mantovano" and "Salame Cremonese"

Peak number[a]	Compound	RI_{calc}[b]	RI_{tab}[c]	Identification[d]	Previous identifications
Terpenes (35)					
25	Tricyclene	998		MS	
28	α-Pinene	1012	1010	MS, RI	[6–10,12]
29	α-Thujene	1015	1013	MS, RI	[6,8–10]
34	Terpene (not identified)	1056		MS	
35	Camphene	1057	1053	MS, RI	[6,8–10]
36	Terpene (not identified)	1070		MS	
41	β-Pinene	1096	1095	MS, RI	[6,8–10,12]
42	Terpene (not identified)	1105		MS	
43	1,4-*p*-Menthadiene	1121		MS	
49	3-Carene	1149	1144	MS, RI	[10,12]
51	α-Phellandrene	1164	1160	MS, RI	[10,12]
52	Terpene (not identified)	1168		MS	
53	β-Myrcene	1169	1167	MS, RI	[6,10,12]
56	α-Terpinene	1179	1175	MS, RI	[6,8–10]
60	Limonene	1197	1194	MS, RI	[6,8–10,12]
61	β-Phellandrene	1198	1202	MS, RI	[8,10]
63	2,6-Dimethyl-1,3,5,7-octatetraene	1204		MS	
68	β-(Z)-Ocimene	1240		MS	
69	γ-Terpinene	1244	1240	MS, RI	[6,9,10]
70	Terpene (not identified)	1248		MS	
71	β-(E)-Ocimene	1250		MS	[8,10]
75	*p*-Cymene	1269	1266	MS, RI	[7–10,12]
76	α-Terpinolene	1278	1276	MS, RI	[6]
77	Terpene (not identified)	1283		MS	
81	Terpene (not identified)	1314		MS	
82	Terpene (not identified)	1320		MS	
88	Terpene (not identified)	1378		MS	
90	Terpene (not identified)	1396		MS	
91	Terpene (not identified)	1398		MS	
92	Terpene (not identified)	1429		MS	
96	2-Caren-4-ol	1457		MS	
99	6-Camphenol	1468		MS	
100	Copaene	1470		MS	[6]
102	Linalool	1554	1554	MS, RI	[6]
104	β-Caryophyllene	1592	1598	MS, RI	[6,8]
Aldehydes (15)					
6	Propanal	801	801	MS, RI	
9	2-Propenal	840		MS	
11	Butanal	883	878	MS, RI	[13]
14	2-Methylbutanal	915	914	MS, RI	[7,9,10,13]
15	3-Methylbutanal	920	917	MS, RI	[7,9,10,12,13]
22	Pentanal	983	977	MS, RI	[10,12,13]
40	Hexanal	1085	1080	MS, RI	[6,7,9,10,12,13]
48	(E)-2-Pentenal	1140	1135	MS, RI	
59	Heptanal	1188	1186	MS, RI	[6,9,10,13]
65	(E)-2-Hexenal	1224	1225	MS, RI	
79	Octanal	1292	1286	MS, RI	[6,10,13]
83	(Z)-2-Heptenal	1331		MS	[6,9,12,13]
93	(E)-2-Octenal	1432	1432	MS, RI	[6,10,13]
98	(Z)-2-Octenal	1460		MS	
101	Benzaldehyde	1529	1528	MS, RI	[6,7,12,13]
Ketones (14)					
7	Acetone	813	814	MS, RI	[9,13]
13	2-Butanone	905	901	MS, RI	[9,13]
17	3-Buten-2-one	947	953	MS, RI	
21	2-Pentanone	980	980	MS, RI	[9,10,13]
23	2,3-Butanedione	989	986	MS, RI	[7,9,12]
27	4-Methyl-2-pentanone	1010	1008	MS, RI	[12]
37	2,3-Pentanedione	1071	1071	MS, RI	[9,12]
58	2-Heptanone	1187	1185	MS, RI	[6,9,10,12,13]
72	3-Octanone	1255	1251	MS, RI	[9,12]
78	2-Octanone	1285	1280	MS, RI	[12,13]

Table 3 (*Continued*)

Peak number[a]	Compound	RI_{calc}[b]	RI_{tab}[c]	Identification[d]	Previous identifications
80	1-Octen-3-one	1300	1299	MS, RI	
84	2,3-Octanedione	1335		MS	
85	6-Methyl-5-hepten-2-one	1345	1340	MS, RI	[9,12]
89	2-Nonanone	1394	1394	MS, RI	[12,13]
Alcohols (10)					
16	Ethanol	934	932	MS, RI	[9,13]
30	2-Butanol	1031	1035	MS, RI	[7,12]
33	1-Propanol	1052	1052	MS, RI	[7,13]
47	2-Pentanol	1139	1142	MS, RI	[7]
55	1-Penten-3-ol	1175	1176	MS, RI	[10]
64	3-Methyl-1-butanol	1221	1215	MS, RI	[7,10,12,13]
73	1-Pentanol	1262	1256	MS, RI	[9,10,12,13]
87	1-Hexanol	1362	1355	MS, RI	[6,9,10,12,13]
97	1-Octen-3-ol	1458	1456	MS, RI	[9,10]
103	1-Octanol	1565	1561	MS, RI	[12]
Aromatic hydrocarbons (9)					
31	Toluene	1035	1040	MS, RI	[6,7,9,10,13]
44	Ethylbenzene	1125	1125	MS, RI	[6]
46	*p*-Xylene	1130	1127	MS, RI	[6,7,9,10,13]
54	Hydrocarbon (not identified)	1176		MS	
57	*o*-Xylene	1186	1182	MS, RI	[7,9]
62	Propylbenzene	1200	1207	MS, RI	[7]
66	1,2,4-Trimethylbenzene	1230		MS	[6]
74	Styrene	1263	1261	MS, RI	[6,7,9,10,13]
95	Dimethyl-*p*-styrene	1456		MS	
Esters (8)					
8	Methyl acetate	825	828	MS, RI	[13]
12	Ethyl acetate	899	893	MS, RI	[7,12,13]
19	Ethyl propanoate	960	957	MS, RI	[7,9,10,12,13]
20	Ethyl isobutanoate	962	960	MS, RI	
32	Ethyl butanoate	1040	1040	MS, RI	[6,7,9,10,12,13]
39	Ethyl isopentanoate	1073	1068	MS, RI	[7,12,13]
45	Isopentyl acetate	1127	1125	MS, RI	
94	Ethyl octanoate	1440	1438	MS, RI	[6,12,13]
Linear hydrocarbons (5)					
1	Heptane	700	700	MS, RI	[9,10,13]
3	1,2-Dimethyl cyclopentane	726		MS	
4	Methyl cyclohexane	762		MS	
5	Octane	800	800	MS, RI	[6,9,10,13]
26	Decane	1000	1000	MS, RI	[6,13]
Sulfur compounds (5)					
2	Carbon disulfide	701		MS	[13]
18	Allyl methyl sulfide	956		MS	[6,7]
24	1-Propene-1-methylthio	997		MS	[9,10]
38	Dimethyl disulfide	1072	1075	MS, RI	[7,9,10,13]
50	1-Propene-3,3′-thiobis	1150		MS	[6,9,12]
Furans (2)					
10	2-Methyl tetrahydrofuran	876		MS	
67	2-Pentyl furan	1239	1240	MS, RI	[8,13]
Ethers (1)					
86	Anisole	1355		MS, RI	

[a] Peak number according to retention time.
[b] Calculated RI.
[c] Tabulated RI (proprietary database) [24].
[d] Identification method: MS, identification by comparison with mass spectra stored in NIST library; RI, identification by comparison with tabulated RI.

In the aromatic profile of "Salame Cremonese" 94 compounds were identified in at least 3 samples. Among these compounds, 30 terpenes, 15 aldehydes, 14 ketones, 9 alcohols, 7 esters, 8 aromatic hydrocarbons, 4 sulfur compounds, 5 linear hydrocarbons, 2 furans and 1 ether were detected.

In the last years, many studies have been performed on characterization of the aromatic profile of European dry-sausages

Table 4
Chromatographic peak areas (arbitrary units) of volatile compounds identified in "Salame Mantovano"

Peak	Compound	Occurrence	MN1	MN2	MN3	MN4	MN5	MN6	MN7
Terpenes									
25	Tricyclene	5	n.d.	28 ± 6	55 ± 9	4 ± 0.4	1.6 ± 0	n.d.	49 ± 5
28	α-Pinene	7	8900 ± 700	6700 ± 1400	6300 ± 1400	930 ± 80	250 ± 40	1620 ± 240	11500 ± 1700
29	α-Thujene	7	1350 ± 173	1002 ± 133	2357 ± 433	225 ± 26	74 ± 14	385 ± 65	4293 ± 713
34	Terpene (not identified)	7	327 ± 68	113 ± 20	352 ± 54	11 ± 1.1	3 ± 0	164 ± 23	132 ± 15
35	Camphene	4	n.d.	335 ± 51	n.d.	45 ± 4	12 ± 0	n.d.	615 ± 100
41	β-Pinene	7	5423 ± 555	7217 ± 1212	7878 ± 807	912 ± 56	278 ± 29	4177 ± 453	9186 ± 1926
42	Terpene (not identified)	7	1857 ± 231	2529 ± 562	4464 ± 607	384 ± 38	128 ± 17	1082 ± 88	7870 ± 1590
43	1,4-*p*-Menthadiene	5	17.7 ± 0.8	33 ± 8	91 ± 25	n.d.	122 ± 15	n.d.	14 ± 2
49	Terpene (not identified)	7	7159 ± 290	10855 ± 1993	6463 ± 1485	852 ± 103	493 ± 41	3508 ± 943	7456 ± 1338
51	α-Phellandrene	7	1183 ± 172	377 ± 66	428 ± 129	87 ± 17	536 ± 48	86.7 ± 15.3	1687 ± 201
52	Terpene (not identified)	7	37 ± 9	39 ± 9	87 ± 46	4.4 ± 0.8	2.4 ± 0	34 ± 8	57 ± 4
53	Myrcene	7	1033 ± 156	1356 ± 323	873 ± 55	131 ± 20	71 ± 6	464 ± 94	2147 ± 323
56	α-Terpinene	6	n.d.	418 ± 70	822 ± 232	136 ± 19	60 ± 11	212 ± 49	2651 ± 363
60	Limonene	7	4832 ± 267	6595 ± 1291	1052 ± 131	917 ± 102	554 ± 36	3117 ± 838	10118 ± 1115
61	β-Phellandrene	7	772 ± 22	643 ± 128	51 ± 13	140 ± 21	81 ± 13	255 ± 55	2550 ± 242
63	2,6-Dimethyl-1,3,5,7-octatetraene	6	n.d.	15 ± 10	19.2 ± 1.2	1.9 ± 0.3	1.4 ± 0.3	22 ± 3	12 ± 2
68	β-(Z)-Ocimene	5	26 ± 8	48 ± 12	78 ± 14	3.1 ± 0.7	n.d.	n.d.	134 ± 24
69	γ-Terpinene	7	639 ± 138	644 ± 174	1024 ± 269	127 ± 14	49 ± 5	247 ± 54	3045 ± 213
70	Terpene (not identified)	5	12 ± 5	3.3 ± 0.4	33 ± 7	0.4 ± 0.1	n.d.	14 ± 2	n.d.
71	β-(E)-Ocimene	6	n.d.	2.5 ± 0.6	22 ± 2	0.7 ± 0.2	1.1 ± 0.4	3.4 ± 1.9	101 ± 5
75	*p*-Cymene	7	320 ± 109	1103 ± 201	1911 ± 482	90 ± 9	59 ± 13	697 ± 163	16 ± 4
76	α-Terpinolene	6	13 ± 5	6.1 ± 1.4	13.7 ± 0.1	0.8 ± 0.3	1 ± 0	3.2 ± 1.8	n.d.
77	Terpene (not identified)	7	154 ± 54	119 ± 25	355 ± 84	28 ± 6	12 ± 1	119 ± 32	1185 ± 34
81	Terpene (not identified)	4	n.d.	n.d.	14 ± 4	0.2 ± 0.1	n.d.	6.4 ± 1	5.6 ± 0.4
82	Terpene (not identified)	4	n.d.	n.d.	27 ± 5	0.3 ± 0.1	0.2 ± 0.1	5.3 ± 0.6	n.d.
88	Terpene (not identified)	6	n.d.	230 ± 72	388 ± 125	23 ± 5	3.1 ± 0.4	154 ± 27	1024 ± 37
90	Terpene (not identified)	7	3.2 ± 0.8	2.5 ± 0.3	6 ± 0.6	0.4 ± 0	0.3 ± 0.2	179.6 ± 191	8.1 ± 0.6
91	Terpene (not identified)	7	23 ± 3	20 ± 2	82 ± 9	2.7 ± 0.4	2.1 ± 1.4	86 ± 7	41 ± 5
92	Terpene (not identified)	6	n.d.	3.1 ± 1	5.2 ± 1.2	0.3 ± 0.1	0.3 ± 0.3	5.2 ± 1.7	5.5 ± 1.1
100	Copaene	4	n.d.	n.d.	7.3 ± 1.5	0.3 ± 0.2	n.d.	19 ± 3	4.9 ± 2.3
102	Linalool	5	n.d.	n.d.	9.9 ± 1	0.2 ± 0.1	0.3 ± 0.1	18 ± 5	5.5 ± 2.5
104	β-Caryophyllene	7	5.5 ± 1.5	1.8 ± 0.4	8 ± 3.3	0.4 ± 0.3	0.4 ± 0.2	23 ± 7	24 ± 14
Aldehydes									
6	Propanal	7	32 ± 9	644 ± 253	1750 ± 123	40 ± 7	16 ± 1	2194 ± 142	44 ± 5
9	2-Propenal	6	48 ± 8	99 ± 33	235 ± 21	13 ± 2	n.d.	91 ± 13	103 ± 10
11	Butanal	6	n.d.	260 ± 86	1000 ± 198	22 ± 2	9 ± 1	1093 ± 105	57 ± 5
14	2-Methylbutanal	7	105 ± 23	132 ± 41	3979 ± 756	11 ± 1	7.6 ± 1	89 ± 15	143 ± 25
15	3-Methylbutanal	6	481 ± 96	758 ± 201	n.d.	136 ± 12	38 ± 11	431 ± 65	934 ± 71
22	Pentanal	6	n.d.	1903 ± 391	5224 ± 740	238 ± 22	64 ± 18	3545 ± 286	294 ± 92
40	Hexanal	7	1267 ± 301	11255 ± 2713	27331 ± 5019	848 ± 143	355 ± 95	18653 ± 2414	584 ± 69
59	Heptanal	6	28 ± 7	86 ± 48	7454 ± 1354	13 ± 2.1	4.3 ± 2.5	778 ± 99	n.d.
65	(E)-2-Hexenal	4	n.d.	7.2 ± 0.9	79 ± 21	4.4 ± 1.5	n.d.	7.9 ± 0.6	n.d.
79	Octanal	6	3.5 ± 0.3	6.8 ± 2	149 ± 17	0.8 ± 0.1	0.7 ± 0.2	105 ± 16	n.d.
83	(Z)-2-Heptenal	6	n.d.	13 ± 6	104 ± 14	1.2 ± 0.2	0.9 ± 0.1	160 ± 23	6 ± 0.4
93	(E)-2-Octenal	4	n.d.	n.d.	20 ± 2.7	0.3 ± 0.1	0.2 ± 0.7	80 ± 11	n.d.
101	Benzaldehyde	7	4.4 ± 0.6	6.8 ± 2.4	139 ± 36	0.6 ± 0.1	0.3 ± 0.3	29 ± 5	5.2 ± 0.6
Ketones									
7	Acetone	7	642 ± 36	596 ± 186	1486 ± 424	82 ± 4	155 ± 29	344 ± 14	586 ± 36
13	2-Butanone	7	3268 ± 328	6297 ± 1053	6445 ± 1458	259 ± 9	16 ± 0.7	167 ± 36	4537 ± 250
17	3-Buten-2-one	4	27 ± 5	53 ± 15	126 ± 21	5.2 ± 0.5	n.d.	n.d.	n.d.
21	2-Pentanone	5	n.d.	165 ± 71	428 ± 114	24 ± 4	5.5 ± 0.4	197 ± 93	102 ± 60
27	4-Methyl-2-pentanone	6	33 ± 11	12 ± 2	38 ± 9	1.9 ± 0.2	1.2 ± 0.8	n.d.	44 ± 7
37	2,3-Pentanedione	7	11 ± 2	520 ± 106	1381 ± 238	77 ± 9	26 ± 8	87 ± 14	55 ± 8
58	2-Heptanone	7	24 ± 3	27 ± 6	120 ± 7	2.2 ± 0.5	2.5 ± 2	140 ± 21	23.3 ± 0.5
78	2-Octanone	4	n.d.	13 ± 18	17 ± 4	n.d.	0.3 ± 0.2	14 ± 2	n.d.
80	1-Octen-3-one	5	n.d.	4.2 ± 0.7	38 ± 6	0.5 ± 0.2	0.3 ± 0.1	34 ± 4	n.d.
84	2,3-Octanedione	5	n.d.	8.5 ± 5.2	178 ± 21	1.1 ± 0.2	2.4 ± 1	62 ± 13	n.d.
89	2-Nonanone	6	1.7 ± 0.1	n.d.	2.3 ± 0.2	0.1 ± 0.1	0.2 ± 0.4	7.8 ± 1.8	2.1 ± 0.1

Table 4 (*Continued*)

Peak	Compound	Occurrence	MN1	MN2	MN3	MN4	MN5	MN6	MN7
Alcohols									
16	Ethanol	7	2532 ± 171	3263 ± 522	2196 ± 682	420 ± 48	481 ± 54	6108 ± 711	3687 ± 129
30	2-Butanol	7	5717 ± 243	924 ± 154	4847 ± 1261	229 ± 30	4.1 ± 1	63 ± 3	10960 ± 1558
33	1-Propanol	7	607 ± 60	187 ± 34	578 ± 238	19 ± 2	6.8 ± 1	285 ± 51	1270 ± 108
47	2-Pentanol	5	33 ± 2	14 ± 13	n.d.	3.6 ± 1	3.5 ± 1	n.d.	12.9 ± 1.2
55	1-Penten-3-olo	6	819 ± 164	160 ± 58	666 ± 107	8.3 ± 2.1	5.8 ± 4	777 ± 91	n.d.
64	3-Methyl-1-butanol	6	86 ± 23	873 ± 553	n.d.	89 ± 12	244 ± 67	2796 ± 586	315 ± 27
73	1-Pentanol	5	n.d.	103 ± 97	1273 ± 297	54 ± 3	45 ± 30	2462 ± 498	n.d.
87	1-Hexanol	6	n.d.	14 ± 8	88 ± 28	0.6 ± 0.1	1.4 ± 0.1	465 ± 41	3.5 ± 0.6
97	1-Octen-3-ol	7	2 ± 0.3	20 ± 10	185 ± 50	1.4 ± 0.3	1.5 ± 0.7	472 ± 47	2.8 ± 0.3
Aromatic hydrocarbons									
31	Toluene	7	1205 ± 146	364 ± 60	765 ± 176	146 ± 13	36 ± 6	263 ± 72	840 ± 70
44	Ethylbenzene	7	135 ± 5	37 ± 15	196 ± 82	3.9 ± 0.6	4.9 ± 1	74 ± 3	44 ± 2
46	*p*-Xylene	6	82 ± 13	n.d.	94 ± 59	2.8 ± 0.9	3.6 ± 1	32 ± 4	32 ± 2
54	Hydrocarbon (not identified)	6	17 ± 4	67 ± 11	72 ± 2	5.8 ± 4.5	n.d.	99 ± 24	22 ± 3
57	*o*-Xylene	7	40 ± 13	26 ± 8	61 ± 13	3.1 ± 0.3	3 ± 1	42 ± 4	32 ± 2
66	Trimethyl benzene	5	5.9 ± 1.7	2.8 ± 0.5	169 ± 31	n.d.	0.7 ± 0.1	n.d.	6.4 ± 0.5
74	Styrene	4	7 ± 0.7	n.d.	n.d.	0.7 ± 0.2	1.2 ± 0.2	n.d.	1114 ± 81
95	Dimethyl-*p*-styrene	6	n.d.	7.4 ± 0.5	19 ± 7	1 ± 0.1	0.6 ± 0.3	34 ± 7	25 ± 6
Esters									
12	Ethyl acetate	7	913 ± 133	3037 ± 587	505 ± 77	183 ± 5	285 ± 40	4341 ± 469	1148 ± 34
19	Ethyl propanoate	6	316 ± 54	279 ± 92	n.d.	5.1 ± 1.4	13 ± 3	355 ± 104	95 ± 5.2
20	Ethyl isobutanaoate	7	32 ± 7	29 ± 9	16 ± 2	44 ± 32	101 ± 36	65 ± 23	37 ± 2.4
32	Ethyl butanoate	4	n.d.	93 ± 21	n.d.	6.6 ± 0.4	30 ± 6	487 ± 31	n.d.
45	Isopentyl acetate	5	33 ± 8	36 ± 8	n.d.	2.5 ± 0.4	3.5 ± 1	90 ± 1	n.d.
94	Ethyl octanoate	4	n.d.	n.d.	n.d.	0.2 ± 0.1	1.2 ± 1	29 ± 6	1.4 ± 0.1
Linear hydrocarbons									
1	Heptane	7	98 ± 7	367 ± 162	496 ± 154	30 ± 3	214 ± 29	1641 ± 264	161 ± 19
3	1,2-Dimethyl-ciclopentane	6	19 ± 4	13 ± 8	n.d.	3.7 ± 0.7	6.6 ± 1	117 ± 21	20 ± 2
4	Methyl cyclohexane	5	22 ± 4	20 ± 15	n.d.	5.7 ± 1.5	7.4 ± 4	35 ± 10	n.d.
5	Octane	7	144 ± 29	701 ± 221	767 ± 75	22 ± 2	190 ± 33	1100 ± 269	169 ± 9
Sulfur compounds									
2	Carbon disulfide	5	258 ± 22	380 ± 138	25 ± 4	13 ± 0.2	n.d.	n.d.	313 ± 26
18	Allyl methyl sulfide	6	6519 ± 459	110 ± 36	194 ± 35	431 ± 42	300 ± 50	n.d.	7879 ± 236
24	1-Propene-1-methylthio	5	781 ± 161	33 ± 5	n.d.	60 ± 9	20 ± 1	n.d.	218 ± 17
37	Dimethyl disulfide	6	75 ± 10	179 ± 43	n.d.	12 ± 2	19 ± 5	95 ± 56	121 ± 21
50	1-Propene-3,3′-thiobis	5	94 ± 26	53 ± 14	n.d.	10 ± 2	18 ± 6	n.d.	161 ± 19
Furans									
10	2-Methyl tetrahydrofuran	5	n.d.	208 ± 73	2132 ± 500	42 ± 6	24 ± 6	325 ± 145	n.d.
67	2-Pentyl-furan	7	2.9 ± 0.2	3.9 ± 1.1	45 ± 3	0.4 ± 0.2	0.6 ± 0.1	50 ± 31	16 ± 0.3

n.d.: not detected.

[6,7,9,12,25,26], including typical Italian salami [8,10,11]. As known, the typical aroma of meat products can not be ascribed to a few compounds, but it depends on a large number of volatiles the nature and relative amount of which can be related to the raw matter composition, to seasoning ingredients, as spices, and to the processing conditions including fermentation and ripening, thus determining a "fingerprint" of the product. Meat products aroma compounds can arise from a complex pattern of chemical reactions involving the components of the matrix, like oxidation of unsaturated fatty acids and microbiological metabolism of lipids, proteins and carbohydrates [9,10,12,27].

Terpenes were the most abundant class of aroma compounds detected in both the kinds of salami. A total of 35 terpenes were detected; the most abundant were α-pinene, β-pinene, 3-carene and limonene. Terpenes can result from animal feedstuffs, but they mainly come from spices used in salami production, as black pepper (α-pinene, β-caryophyllene, 3-carene, limonene, and β-pinene), nutmeg (α-pinene, β-pinene and limonene) and clove (β-caryophyllene). The variability observed in the content of terpenes can be ascribed to the different amount and kind of spices added during the salami production.

A total of 15 aldehydes were identified in the analyzed samples. Linear aliphatic aldehydes, both saturated (propanal, butanal, pentanal, hexanal, heptanal and octanal) and unsaturated ((E)-2-pentenal, (E)-2-hexenal, (E)-2-heptenal, (E)-2-octenal and (Z)-2-octenal), are produced during the lipid

Table 5
Chromatographic peak areas (arbitrary units) of volatile compounds identified in "Salame Cremonese"

Peak	Compound	Occurrence	CR1	CR2	CR3	CR4	CR5
Terpenes							
28	α-Pinene	5	9961 ± 2855	404 ± 1	5605 ± 825	8742 ± 141	6100 ± 970
29	α-Thujene	4	2518 ± 1979	n.d.	418 ± 86	2694 ± 26	877 ± 219
34	Terpene (not identified)	3	154 ± 31	n.d.	90 ± 17	57 ± 18	n.d.
35	Camphene	5	583 ± 243	38 ± 4	249 ± 68	429 ± 21	285 ± 102
36	Terpene (not identified)	3	11 ± 3	n.d.	8.6 ± 1.8	n.d.	19 ± 6
41	β-Pinene	5	9495 ± 2856	1011 ± 253	5063 ± 778	5687 ± 111	6220 ± 477
42	Terpene (not identified)	4	5631 ± 1869	n.d.	539 ± 111	1483 ± 132	2365 ± 266
49	3-Carene	4	8733 ± 2533	1183 ± 244	69 ± 14	n.d.	11874 ± 1579
51	α-Phellandrene	4	654 ± 182	n.d.	258 ± 87	534 ± 27	1780 ± 351
52	Terpene (not identified)	4	46 ± 9	n.d.	43 ± 7	50 ± 6	63 ± 16
53	Myrcene	5	1438 ± 426	98 ± 35	1205 ± 14	963 ± 21	1723 ± 299
56	α-Terpinene	4	689 ± 914	n.d.	178 ± 8	828 ± 43	1137 ± 298
60	Limonene	5	7803 ± 849	669 ± 207	4907 ± 1156	4278 ± 77	7880 ± 894
61	β-Phellandrene	5	1575 ± 453	43 ± 5	248 ± 58	1700 ± 24	1290 ± 316
63	2,6-Dimethyl-1,3,5,7-octatetraene	3	24 ± 2	n.d.	32.4 ± 0.2	n.d.	14 ± 7
68	β-(Z)-Ocimene	3	138 ± 23	n.d.	92 ± 15	65 ± 4	n.d.
69	γ-Terpinene	5	1873 ± 674	12 ± 2	125 ± 43	870 ± 206	1073 ± 304
70	Terpene (not identified)	5	25 ± 2	11 ± 1	18 ± 5	8.1 ± 0.8	22 ± 4
71	β-(E)-Ocimene	4	28 ± 8	n.d.	15.6 ± 0.2	6.6 ± 1.5	31 ± 24
75	*p*-Cymene	5	1533 ± 474	169 ± 60	771 ± 214	450 ± 134	1021 ± 370
76	α-Terpinolene	4	26 ± 7	n.d.	33 ± 11	2 ± 0.1	75 ± 48
77	Terpene (not identified)	4	717 ± 288	n.d.	106 ± 44	113 ± 7	474 ± 253
81	Terpene (not identified)	4	6.4 ± 1.5	n.d.	10 ± 9	6.1 ± 0.2	12 ± 15
88	Terpene (not identified)	5	659 ± 293	7.5 ± 0.3	416 ± 168	655 ± 46	479 ± 349
90	Terpene (not identified)	4	7.4 ± 2.7	n.d.	6.2 ± 0.9	2.7 ± 0.2	6.7 ± 3.6
91	Terpene (not identified)	4	75 ± 21	n.d.	39 ± 6	37 ± 1	52 ± 6
92	Terpene (not identified)	3	5.3 ± 1.1	n.d.	n.d.	1.3 ± 0.3	5.1 ± 4.4
96	2-Caren-4-ol	3	3 ± 0.3	0.7 ± 1	n.d.	1 ± 0.1	n.d.
99	6-Camphenol	3	n.d.	5.6 ± 0.4	1.1 ± 1	n.d.	3.2 ± 2.7
104	β-Caryophyllene	3	11 ± 4	1.5 ± 2.1	n.d.	2.4 ± 1.7	n.d.
Aldehydes							
6	Propanal	5	945 ± 63	2119 ± 33	621 ± 12	12 ± 2	72 ± 32
9	2-Propenal	3	199 ± 9	275 ± 2	n.d.	43 ± 4	n.d.
11	Butanal	5	566 ± 34	1139 ± 76	564 ± 0	31 ± 3	4960 ± 527
14	2-Methylbutanal	5	224 ± 19	319 ± 30	510 ± 20	190 ± 12	111 ± 17
15	3-Methylbutanal	5	2198 ± 221	1046 ± 41	2110 ± 65	2099 ± 26	1519 ± 273
22	Pentanal	5	3465 ± 381	3688 ± 41	3314 ± 95	93 ± 8	217 ± 325
40	Hexanal	5	14326 ± 2504	11829 ± 316	15312 ± 1391	686 ± 23	2131 ± 1065
48	(E)-2-Pentanal	4	24 ± 21	47 ± 15	8127 ± 2007	1802 ± 43	n.d.
59	Heptanal	5	264 ± 28	330 ± 72	199 ± 17	43.5 ± 0.7	71 ± 14
65	(E)-2-Hexenal	3	39 ± 36	84 ± 15	51 ± 7	n.d.	n.d.
79	Octanal	5	40 ± 12	87 ± 53	42 ± 33	7.6 ± 0.9	48 ± 40
83	(Z)-2-Heptenal	4	79 ± 15	609 ± 510	21 ± 2	n.d.	27 ± 32
93	(E)-2-Octenal	3	15 ± 3	26 ± 18	6.5 ± 0.7	n.d.	n.d.
98	(Z)-2-Octenal	3	7.4 ± 2.3	11 ± 5	2.6 ± 0.2	n.d.	n.d.
101	Benzaldehyde	3	10 ± 3	7.9 ± 3	n.d.	9.1 ± 3.2	n.d.
Ketones							
7	Acetone	5	618 ± 102	1160 ± 118	349 ± 24	1079 ± 109	648 ± 498
13	2-Butanone	4	3932 ± 664	4635 ± 233	3101 ± 33	2284 ± 122	n.d.
17	3-Buten-2-one	3	39 ± 3	69 ± 6	n.d.	26 ± 1	n.d.
21	2-Pentanone	5	129 ± 5	206 ± 22	154 ± 23	150 ± 22	285 ± 266
23	2,3-Butanedione	4	189 ± 11	223 ± 9	n.d.	197 ± 24	48 ± 30
27	4-Methyl-2-pentanone	5	17 ± 2	24 ± 2	70 ± 2	65 ± 30	26 ± 12
37	2,3-Pentanedione	5	1307 ± 213	423 ± 139	795 ± 25	22 ± 8	207 ± 113
58	2-Heptanone	5	35 ± 15	66 ± 19	62 ± 5	55.6 ± 0.3	20 ± 11
72	3-Octanone	3	45 ± 6	n.d.	n.d.	38 ± 1	29 ± 6
78	2-Octanone	4	3.4 ± 1.3	11 ± 4	10 ± 10	2.8 ± 0.9	n.d.
80	1-Octen-3-one	3	25 ± 4	38 ± 24	13 ± 11	n.d.	n.d.
84	2,3-Octanedione	5	156 ± 67	47 ± 45	62 ± 12	1 ± 0.2	37 ± 42
85	6-Metil-5-epten-2-one	4	3.6 ± 1.3	4.1 ± 2.3	2.9 ± 0.2	n.d.	9.2 ± 4.5
89	2-Nonanone	5	9.7 ± 1.3	26 ± 13	2.6 ± 0.7	5.6 ± 1.2	4.6 ± 2.9

Table 5 (*Continued*)

Peak	Compound	Occurrence	CR1	CR2	CR3	CR4	CR5
Alcohols							
16	Ethanol	5	4354 ± 994	843 ± 55	2820 ± 93	3754 ± 341	4333 ± 103
30	2-Butanol	5	7633 ± 3379	4684 ± 1456	3474 ± 98	1908 ± 92	9912 ± 1014
33	1-Propanol	5	1181 ± 618	294 ± 29	496 ± 13	152 ± 34	2926 ± 497
47	1-Penten-3-ol	3	n.d.	463 ± 145	290 ± 46	n.d.	29 ± 12
64	3-Methyl-1-butanol	5	1274 ± 462	98 ± 33	312 ± 36	748 ± 29	1121 ± 302
73	1-Pentanol	4	451 ± 141	711 ± 373	407 ± 30	n.d.	21 ± 4
87	1-hexanol	5	31 ± 8	50 ± 36	13.4 ± 1.3	3.5 ± 1.2	11 ± 11
97	1-Octen-3-ol	5	74 ± 23	126 ± 114	32 ± 4	21 ± 10	13 ± 10
103	1-Octanol	3	n.d.	1.5 ± 2.1	13 ± 6	n.d.	33 ± 30
Aromatic hydrocarbons							
31	Toluene	5	1301 ± 108	327 ± 41	609 ± 107	483 ± 139	1057 ± 469
44	Ethylbenzene	4	43 ± 22	n.d.	78 ± 15	64 ± 4	82 ± 17
46	*p*-Xylene	4	26 ± 10	n.d.	63.4 ± 1.3	40 ± 11	37 ± 24
54	Hydrocarbon (not identified)	5	48 ± 6	7.5 ± 0.2	74.3 ± 8.1	37 ± 2	24 ± 4
57	*o*-Xylene	5	28 ± 13	28.5 ± 1.7	34 ± 4	46 ± 6	34 ± 13
62	Propyl benzene	3	6.2 ± 5.4	n.d.	n.d.	16 ± 5	7.8 ± 2.4
74	Styrene	3	4.6 ± 0.5	n.d.	n.d.	5 ± 1	9 ± 0
96	Dimethyl-*p*-styrene	5	16 ± 5	2.2 ± 0.4	4.1 ± 1.7	4 ± 0.1	15 ± 14
Esters							
8	Methyl acetate	3	144 ± 22	n.d.	n.d.	62 ± 2	49 ± 5
12	Ethyl acetate	5	3075 ± 408	253 ± 20	335 ± 15	1693 ± 143	4233 ± 522
19	Ethyl propanoate	5	1353 ± 249	59 ± 5	39 ± 3	36 ± 8	63 ± 22
20	Ethyl isobutanaoate	3	24 ± 6	n.d.	36 ± 1	61 ± 9	n.d.
32	Ethyl butanoate	4	109 ± 24	45 ± 3	n.d.	80 ± 1	374 ± 154
39	Ethyl isopentanoate	3	44 ± 2	n.d.	n.d.	46 ± 1	38 ± 1
45	Isopentyl acetate	4	39 ± 11	n.d.	43 ± 4	30 ± 18	35 ± 14
Linear hydrocarbons							
1	Heptane	5	240 ± 46	175 ± 21	712 ± 11	328 ± 17	64 ± 46
3	1,2-Dimethyl-cyclopentane	5	27 ± 5	90 ± 1	61 ± 1	28 ± 1	12 ± 3
4	Methyl cyclohexane	3	83 ± 11	n.d.	n.d.	58 ± 4	29 ± 5
5	Octane	5	196 ± 16	813 ± 18	636 ± 8	462 ± 11	389 ± 121
26	Decane	3	n.d.	12 ± 3	26 ± 7	n.d.	37 ± 13
Sulfur compounds							
2	Carbon disulfide	5	225 ± 6	153 ± 14	345 ± 9	169 ± 39	97 ± 5
18	Allyl methylsulfide	4	214 ± 47	n.d.	146 ± 3	3021 ± 2	8112 ± 46
24	1-Propene-1-methylthio	4	359 ± 63	n.d.	58.5 ± 0.4	64 ± 18	322 ± 106
38	Dimethyl disulfide	5	131 ± 13	112 ± 23	63.4 ± 0.5	6 ± 0.9	48 ± 7
Furans							
10	2-Methyl tetrahydrofuran	3	261 ± 54	832 ± 72	212 ± 29	n.d.	n.d.
67	2-Pentyl-furan	5	17 ± 3	35 ± 13	34 ± 8	6.5 ± 1.4	26 ± 11
Ether							
87	Anisole	3	n.d.	2 ± 1.1	8.9 ± 7.1	4.8 ± 0.7	n.d.

n.d.: not detected.

oxidation. Hexanal, that can be considered as a marker of the oxidation process, is the most abundant saturated linear aldehyde, thus confirming the results already observed in Italian salami [8,10,11,25].

Branched short-chain aldehydes as 2-methylbutanal and 3-methylbutanal, the presence of which is involved in dry-sausage aroma [25], are produced by Strecker degradation of the amino acids isoleucine and leucine. Finally an aromatic aldehyde, benzaldehyde, was found in most of the analyzed salami; it is considered to be one of substances that gives specific flavor notes in pork meat [6,28].

Fourteen ketones were identified in salami volatile fraction; they were mainly 2-methyl ketones from C4 to C9 (2-hexanone was not reported in the Table 3 since it was present only in few samples), formed by β-oxidation of fatty acids. As linear aldehydes, also 2-methyl ketones are responsible for dry-sausage aroma [25]. Other ketones were the diketones 2,3-butanedione (diacetyl), 2,3-pentanedione and 2,3-octanedione, characterized by a buttery-creamy flavor, that are produced during the Maillard reaction. 1-octen-3-one was identified for the first time in this work in dry-sausages volatile fraction.

Twelve alcohols were identified; they were mainly aliphatic linear alcohols (2-butanol, 1-propanol, 2-pentanol, 1-pentanol, 1-hexanol and 1-octanol) resulting from degradation of lipid hydroperoxides [10]. 1-octen-3-ol, an alcohol produced during lipid oxidation with a characteristic mushroom note and a very

low sensory threshold, has been previously detected in meat products [9,10].

Eight esters, mainly ethyl esters (ethyl acetate, ethyl propanoate, ethyl isobutanoate, ethyl isopentanoate and ethyl octanoate), were identified in the analyzed salami samples. Ethyl esters are usually present in fermented meat products, contributing with a fruity note to the flavor [25]. They could be produced from alcohol oxidation or from esterification of alcohols and acids [12].

Linear and aromatic hydrocarbons, formed during rearrangements of lipid oxidation products, poorly contribute to sausages aroma due to their high threshold value.

Five sulfur-containing compounds were identified, the most abundant being allyl methyl sulfide. Aliphatic sulfur compounds derived from garlic are important aroma compounds since they are characterized by very low sensory threshold. Other sulfur compounds, as 1-propene-1-methylthio and 1-propene-3,3′-thiobis, probably derive from reaction between garlic and meat components [11], since they have been previously identified in other dry-sausages [6,9–12], but they were not detected in garlic volatile fraction.

Also furans, as 2-pentyl-furan, a product of the linoleic acid oxidation, have been detected in sausages and cooked pork [8].

3.3. Statistical analysis

Statistical analysis was performed by running first PCA and after LDA. PCA is an unsupervised statistical method, allowing to describe the behavior of the data without the constraint of initial assumptions on samples. Analyzing the whole set of data, seven principal components were needed to explain about 90% of the total variance. However, PCA did not reveal useful in the discrimination of the samples investigated, since clusters of them were not clearly detected. Better results were obtained when variables were divided into groups corresponding to chemical classes. For example, considering the class of aldehydes, the first two PCs, accounting for the 68% of the variance, allowed to group the samples according to their kind (Fig. 2).

A linear discriminant analysis (LDA) [14,15] was then applied in order to calculate a discrimination function for the classification of samples in the corrected group and to find the most useful variables in the differentiation between the two classes of salami.

LDA is a supervised chemometric method widely used for classification purposes. This method minimizes the variance within categories and maximizes the variance between categories. LDA renders a number of orthogonal linear discriminant functions equal to the number of categories minus one; when two classes are considered, one linear discriminant function is obtained. The importance of each variable in discrimination was investigated by analyzing their coefficients in the discriminant functions. In addition, the calculation of the values of these functions for each sample makes it possible to allocate it to the group for which the probability of belonging is highest.

According to the standardized discriminant coefficients, seven variables were found able to discriminate between the two considered groups, the most important variables for characterizing the groups being those with the highest standardized discriminant coefficient (Table 6).

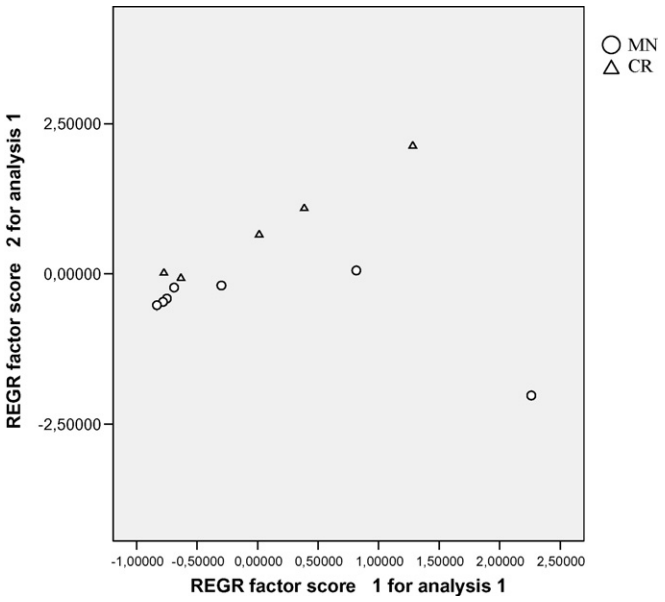

Fig. 2. PC1 vs. PC2 score plot for aldehyde peak area data.

They were in descending absolute value: 3-methylbutanal, 6-camphenol (present only in "Salame Cremonese" samples); dimethyl disulfide and 1-propene-3,3′-thiobis, both contributing with a negative sign (the latest one identified only in "Salame Mantovano" samples); ethyl propanoate; 1,4-*p*-menthadiene (present only in "Salame Mantovano" samples) and finally 2,6-dimethyl-1,3,5,7-octatetraene. Table 7 summarizes the results of the classification matrix of the LDA model, obtained for all the samples and separated for class. Fig. 3 shows the discriminant function for "Salame Mantovano" and "Salame Cremonese". The discriminant function allowed the correct classification of the 12 salami samples into their respective group with a success rate of 100%, so achieving a perfect discrimination (Table 7).

The prediction capacity of the discriminant model was evaluated by the "leave-one-out" cross-validation in order to determine the stability of the model. During the validation procedure each sample is removed one-at-time from the initial matrix of data; then the classification model is rebuilt and the

Table 6
Standardized canonical discriminant function coefficients and classification function coefficients

Peak	Compound	Coefficient	"Salame Mantovano"	"Salame Cremonese"
15	3-Methylbutanal	19.826	−1513.967	2119.554
99	6-Camphenol	17.801	−809.717	1133.604
19	Ethyl propanoate	5.608	−213.604	299.045
43	1,4-*p*-Menthadiene	2.706	−116.239	162.735
63	2,6-Dimethyl-1,3,5,7-octatetraene	−1.932	73.039	−102.255
38	Dimethyl disulfide	−9.798	364.516	−510.323
50	1-Propene-3,3′-thiobis	−5.843	248.393	−347.751
	Constant		−761.717	−1492.784

Table 7
Classification and cross-validation results

	Predicted group membership	
	"Salame Mantovano"	"Salame Cremonese"
Original model		
"Salame Mantovano"	100%	0
"Salame Cremonese"	0	100%
Cross-validated model		
"Salame Mantovano"	100%	0
"Salame Cremonese"	0	100%

100% of original cases correctly classified.
100% of cross-validated cases correctly classified.

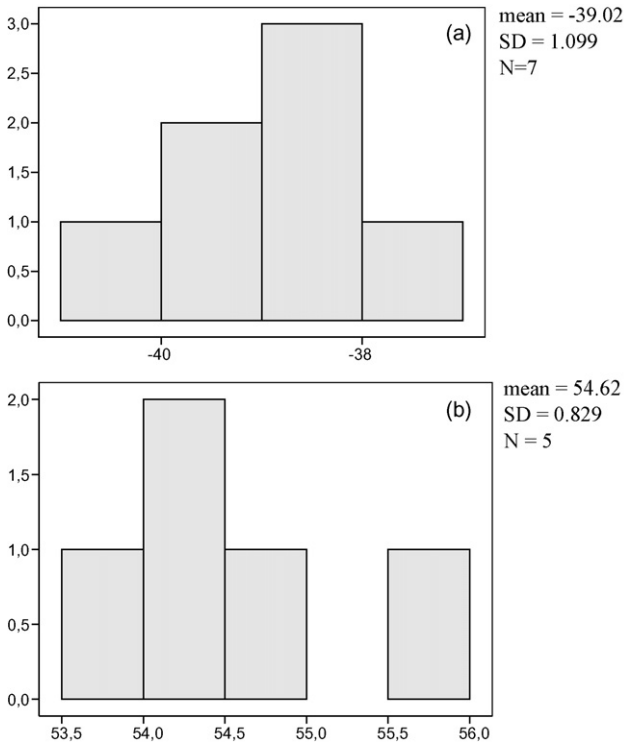

Fig. 3. Canonical discriminant function for (a) "Salame Mantovano" and (b) "Salame Cremonese".

case removed is classified in this new model. The results of cross-validation analysis are reported in Table 7.

The results obtained from LDA can be considered very satisfactory, since they allowed to select a small number of volatile compounds able to classify and differentiate, on the basis of their geographical origin, two kinds of dry-sausages produced in a limited area in Northern Italy.

In addition, these results can be useful to detect possible adulterations and falsifications.

Acknowledgments

This work was financially supported by MIUR (Ministero dell'Istruzione, dell'Università e della Ricerca, Italy), COFIN 2004 Project "Characterization of microorganism and volatile fraction in artisanal and typical meat products". The authors acknowledge funding support from Laboratorio Regionale per la Sicurezza e la Qualità degli Alimenti (SIQUAL) (Project no. 9, Programma Regionale per la Ricerca industriale, l'Innovazione e il Trasferimento tecnologico (PRRIITT)).

References

[1] D.G.R. Lombardia no. VI/49424 del 7/04/2000.
[2] EC Regulation 2081/92 – On the protection of geographical indications and designations of origin for agricultural products and foodstuffs (PDO/PGI). Off. J. Eur. Commun. L208 (1992) 1.
[3] G. Barbieri, L. Bolzoni, G. Parolari, R. Virgili, R. Buttini, M. Careri, A. Mangia, J. Agric. Food Chem. 40 (1992) 2389.
[4] B.S. Radovic, M. Careri, A. Mangia, M. Musci, M. Gerboles, E. Anklam, Food Chem. 72 (2001) 511.
[5] F. Bianchi, M. Careri, M. Musci, Food Chem. 89 (2005) 527.
[6] D. Ansorena, O. Gimeno, I. Astiasaran, J. Bello, Food Res. Int. 34 (2001) 67.
[7] J. Mateo, J.M. Zumalacarregui, Meat Sci. 44 (1996) 255.
[8] V.M. Moretti, G. Madonia, C. Diaferia, T. Mentasti, M.A. Paleari, S. Panseri, G. Pirone, G. Gandini, Meat Sci. 66 (2004) 845.
[9] C. Viallon, J.L. Berdaguè, M.C. Montel, R. Talon, J.F. Martin, N. Kondjoyan, C. Denoyer, Food Res. Int. 29 (1996) 667.
[10] A. Meynier, E. Novelli, R. Chizzolini, E. Zanardi, G. Gandemer, Meat Sci. 51 (1999) 175.
[11] L.O. Sunesen, V. Dorigoni, E. Zanardi, L.H. Stahnke, Meat Sci. 58 (2001) 93.
[12] R.A. Edwards, J.A. Ordonez, R.H. Dainty, E.M. Hierro, L. de la Hoz, Food Chem. 64 (1999) 461.
[13] A. Marco, J.L. Navarro, M. Flores, Food Chem. 84 (2004) 633.
[14] J.N. Miller, J.C. Miller, Statistics and Chemometrics for Analytical Chemistry, fourth ed., Pearson Education, London, Great Britain, 2000.
[15] D.L. Massart, B.G.M. Vandeginste, L.C.M. Buydens, S. De Jong, P.J. Lewi, J. Smeyers-Verbeke, Handbook of Chemometrics and Qualimetrics: Part A and Part B, Elsevier, Amsterdam, The Netherlands, 1997.
[16] I.S. Arvanitoyannis, M. van Houwelimgen-Koukaliaroglou, Crit. Rev. Food Sci. Nutr. 43 (2003) 173.
[17] D. Ollivier, J. Artaud, C. Pinatel, J.P. Durbec, M. Guérère, Food Chem. 97 (2006) 982.
[18] J.S. Câmara, M.A. Alves, J.C. Marques, Talanta 68 (2006) 1512.
[19] P.J. Dunlop, C.M. Bignell, J.F. Jackson, D. Brynn Hibbert, Chemom. Intell. Lab. Syst. 30 (1995) 59.
[20] AOAC Official methods of analysis. 950.46. Association of Analytical Chemists, Washington DC, USA, 1990.
[21] P.T. Slack, Analytical Methods Manual. Leather Head Food R.A. London, England, 1987.
[22] ISO standard method 1443. International Organization for Standardization. Meat and Meat products. Determination of total fat content, 1973.
[23] H. van den Dool, P.D. Kratz, J. Chromatogr. 11 (1963) 463.
[24] F. Bianchi, M. Careri, A. Mangia, M. Musci, J. Sep. Sci., 2007, in press.
[25] D. Demeyer, M. Raemaekers, A. Rizzo, A. Holck, A. De Smedt, B. ten Brink, B. Hagen, C. Montel, E. Zanardi, E. Murbrekk, F. Leroy, F. Vandendriessche, K. Lorentsen, K. Venema, L. Sunesen, L. Stahnke, L. De Vuyst, F. Talon, R. Chizzolini, S. Eerola, Food Res. Int. 33 (2000) 171.
[26] S. Schmidt, R.G. Berger, Z. Lebensm. Unters. Forsch 31 (1998) 559.
[27] H.D. Belitz, W. Grosch, P. Schieberle, Food Chemistry, third ed., Springer-Verlag, Berlin, Germany, 2004.
[28] F. Shaididi, Flavour of Meat and Meat Products, Blackie Academic and Profesional, London, United Kingdom, 1994.

Available online at www.sciencedirect.com
ScienceDirect
Talanta 72 (2007) 1423–1431
Talanta
www.elsevier.com/locate/talanta

Coal analysis by diffuse reflectance near-infrared spectroscopy: Hierarchical cluster and linear discriminant analysis

M.T. Bona, J.M. Andrés *

Instituto de Carboquímica, CSIC, Procesos Químicos, Miguel Luesma Castán, n. 4, 50018 Zaragoza, Spain

Received 22 November 2006; received in revised form 19 January 2007; accepted 22 January 2007
Available online 30 January 2007

Abstract

An extensive study was carried out in coal samples coming from several origins trying to establish a relationship between nine coal properties (moisture (%), ash (%), volatile matter (%), fixed carbon (%), heating value (kcal/kg), carbon (%), hydrogen (%), nitrogen (%) and sulphur (%)) and the corresponding near-infrared spectral data. This research was developed by applying both quantitative (partial least squares regression, PLS) and qualitative multivariate analysis techniques (hierarchical cluster analysis, HCA; linear discriminant analysis, LDA), to determine a methodology able to estimate property values for a new coal sample. For that, it was necessary to define homogeneous clusters, whose calibration equations could be obtained with accuracy and precision levels comparable to those provided by commercial online analysers and, study the discrimination level between these groups of samples attending only to the instrumental variables. These two steps were performed in three different situations depending on the variables used for the pattern recognition: property values, spectral data (principal component analysis, PCA) or a combination of both. The results indicated that it was the last situation what offered the best results in both two steps previously described, with the added benefit of outlier detection and removal.

Keywords: Near-infrared spectroscopy (NIR); Coal analysis; Partial least squares regression (PLS); Hierarchical cluster analysis (HCA); Linear discriminant analysis (LDA)

1. Introduction

The demand for electricity at the lowest possible cost has led to the development for online analysers able to provide fast and representative information about coal feed in a power plant [1–3]. Real time information on coal quality helps efficient management of coal stockpiles and improves plant performance. Thus, traditional methods consisted of laboratory analysis using standard methods are substituted by several techniques, some of them, based on nuclear, capacitance, microwave or ultrasonic energy [4–6]. These techniques are characterized for relying on the inorganic coal constituents to further extrapolate for the calculation of the other coal properties. Really useful for coal batches of the same origin, the usual practice of blending coals to fulfil environmental regulations [7] prevents its widespread use in coal burning power plants.

In order to find an alternative technique, several research works present Fourier transform diffuse reflectance infrared spectroscopy (DRIFT) as a proper technique able to characterise scattering samples with very little preparation and a high signal-to-noise ratio (SNR) in a non-destructive way. These advantages were detailed by Fuller and Griffiths [8] when they used this optical technique to the measurement of powder samples, subsequently applied in the analysis of coal blends [9,10]. Other applications for quantification of functional groups followed [11] and the full characterization of thermal coals was attempted by applying multivariate calibration techniques to the mid infrared spectra [12–16] with relative success.

Advances in data acquisition and processing computer packages allowed the use of DRIFT-near infrared spectroscopy [17,18] to characterise coal samples and, lately, modified DRIFT-near IR spectra have been correlated with coal properties such as moisture, volatile matter, oxygen content, maximum fluidity temperature and solidification temperature, by the application of multivariate calibration [19].

Once demonstrated the adequacy of the technique to the coal analysis, the object of this study is the establishment of a method

* Corresponding author. Tel.: +34 976 73 39 77; fax: +34 976 73 33 18.
E-mail address: jmandres@carbon.icb.csic.es (J.M. Andrés).

0039-9140/$ – see front matter © 2007 Elsevier B.V. All rights reserved.
doi:10.1016/j.talanta.2007.01.050

able to estimate coal property values (moisture, ash, volatile matter, fixed carbon, heating value, carbon, hydrogen, nitrogen and sulphur) for an unknown sample attending only to its DRIFT-near IR spectral data.

For that, a wide and diverse coal sample set was analysed and correlated to near-infrared spectral variables [20], obtaining relatively good precision. In the same paper, the application of this technique to a more homogeneous set of samples, referred to its origin, showed that most of the properties could be determined with better reproducibility analysis results. Nevertheless, because of the origin of the coal is sometimes unknown, coal samples were grouped into six clusters following the ASTM D388 reference norm [21] for coal classification covering from lignite B to anthracite coal samples. The improvement of the prediction error compared with the obtained for the whole set of samples was proved [22]; however, the clusters could not be differentiated in a reliable way, neither by soft independent modelling of class analogy (SIMCA) nor linear discriminant analysis.

As a consequence of that, there is a major interest in establishing other coal sample groups based on different variables leading to an adequate calibration equation accompanied by a proper differentiation between the clusters when spectral data were used.

In this way, three situations have been studied depending on the independent variables used in the hierarchical clustering process: laboratory coal analysis values, spectroscopic near-IR variables or a combination of both.

Once established the clusters and defined the calibration equations for all the coal properties, coal samples are classified attending only to its spectral data to study the capability of the system to discriminate properly among the groups. An adequate classification process would be the first stage in a feasible estimation of coal properties for a new coal sample.

2. Experimental

2.1. Coal samples

One hundred and forty-two samples of coal from different suppliers were used. Some of them are raw coal samples coming from mines and other from power stations. All of them follow the specifications for pulverized coal burners, attending to a controlled particle size [23], typically: 98% < 300 μm; 95% < 150 μm; 75% < 75 μm. They were analysed for moisture, ash, volatile matter (VM), fixed carbon (FC), heating value (HV), carbon, hydrogen, nitrogen and sulphur by the usual ISO/ASTM standard methods [24–29]. The statistical results, minimum, maximum, mean property value and standard deviation of the full set of samples analyses are presented in a previous work [20].

2.2. Data acquisition and multivariate statistical analysis

NIR spectra were acquired by using an ATI Mattson Infinity Series FTIR spectrometer equipped with a tungsten-halogen source, quartz beamsplitter and an InGaAs detector. The sample was placed in a diffuse reflectance sample cup and the instrument was controlled by the WinFIRST 3.5 software package by Mattson Instruments. Spectra obtained were the result of co-adding 32 scans over the range 1100–2500 nm performed at 1 cm^{-1} of digital resolution.

All the spectra were acquired in absorbance mode, viz. log (1/reflectance), subsequently pre-processed mathematically in order to reduce extraneous effects such as differences in surface roughness or particle size [30] and to study the correlation between the modified spectral data and the coal properties in the calibration models.

Pre-treatment spectra and multivariate techniques were performed with The Unscrambler v9.1, from CAMO, whereas hierarchical cluster analysis (HCA) and linear discriminant analysis (LDA) were implemented using SPSS v12.0 for Windows.

3. Results and discussion

A wide and varied group of samples were considered for the study, with significant differences both in analytical and spectral values [20]. These differences were the basis of the constitution of homogeneous clusters with the aim of improving the calibration and prediction errors for each coal property after the application of the appropriate calibration model.

In that way, the analysis of a new coal sample would be divided in three steps: spectrum acquisition; sample classification based on the obtained spectrum and coal property determination by applying to the spectrum the calibration method established for that group. The fully establishment of the analytical method would be achieved by studying the following stages: the definition of the groups, the determination of appropriate calibration methods for every property and group previously defined and finally, the development of a successful assignation methodology able to classify each sample with high sensitivity and specificity to its corresponding group.

In this paper, the definition of the groups examines three situations depending on the variables used in the hierarchical clustering process [31]: laboratory coal property values (Situation A), DRIFT-near spectral data (Situation B) or a combination of both (Situation C). These three situations were processed similarly by using the Ward's minimum variance algorithm [32] and the squared Euclidean distance as centroid-linkage measurement to create the clusters.

Independently, each situation presented the corresponding coal distribution dendrogram plot and, consequently, calibration models were applied by partial least squares regression (PLSR). To decide the final number of clusters the reduction of the hydrogen content prediction error [20] determined by the root mean squared error of cross-validation (RMSECV) was followed along the clustering process.

Once defined the clusters, a supervised linear discriminant analysis [33,34] was applied to evaluate the discriminating capacity of the spectral variables in the clusters differentiation. The development of this methodology requires a reduction of the dimensionality as LDA cannot deal with the high number of variables provided by the spectra. Thus, two possibilities were considered for each situation: (i) the scores obtained by apply-

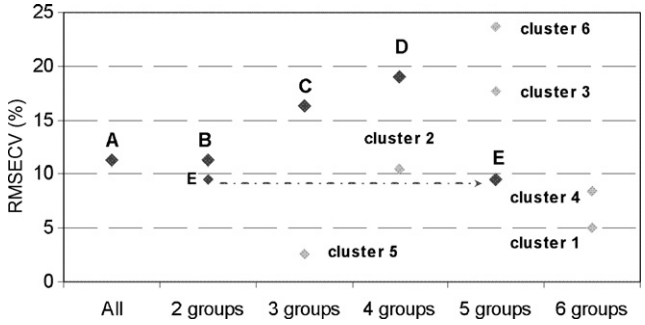

Fig. 1. Relative root mean squared error of cross-validation (RMSECV) obtained for hydrogen (%) content along the splitting process. Intermediate groups are labelled with letters whereas final groups are those in numbers.

ing a principal component analysis (PCA) [35], which needs three principal components to account for 99.86% the explained variance using log (1/*R*) data, and (ii) the scores produced by a discriminant PLS2, where it calibrates for group membership instead of a continuous variable. In this situation, a 0/1 variable is defined for each group. It has value equal to 1 when the sample belongs to the group and 0 elsewhere [36]. The results for each situation are detailed below.

3.1. Situation A: coal properties as clustering variables

3.1.1. Phase I. Grouping

According to the methodology previously indicated, a property coal matrix (142×9) as a whole was considered for the hierarchical process. All the variables included in the matrix were referred in percentage units, assigning 100% for 10,000 kcal/kg in the case of heating value (gross calorific value).

Fig. 1 shows how the prediction ability of hydrogen content (%), referred to the cluster mean property value, varies as the clusters number increases. In this plot, big black points indicate the cluster that is divided in each step whereas grey points represent the final groups. The splitting process progresses until the new clusters do not present significant differences – checked by Fisher's test – in comparison with the previous cluster or when the cluster is too small to be divided.

In this case, it has constituted four intermediate groups (B, C, D and E) that progressed to six final ones. Although the first division was characterized for separating low rank coals (group B, 101 coal samples) from high rank coals (group E, 41 coal samples) with hardly a hydrogen calibration improvement, the following splits led to more homogenous sample sets with absolute error values significantly lower than the whole sample set, except for the group 6. It is worth highlighting that the samples included in this group were considered as outliers when the full coal sample set was studied as a whole in a previous work [20]. This fact led to more precise results for the rest of the groups and to the discrimination of a potential outlier within a new coal sample set, for its subsequent rejection.

On the other side, group 2 formed by raw and blended coal samples showed similar prediction ability than the full sample set, group A, the system not being able to recognize more differences between these coal samples with regard only to their property values.

Finally, groups 1, 4 and 5 were those with better results while group 3, consisted of lignite coal samples, presented an absolute error value quite low (0.4%) increasing to 17.6% when the cluster mean property value was taken into account.

The statistical results obtained for each cluster are presented in Table 1 in order to know all the groups in-depth.

3.1.2. Phase II. Calibration methods

Once the clusters were defined, the study was extended to the rest of the coal properties at the same time as several mathematical pre-treatments were applied to spectral data in order to minimize the effect of physical features of the samples in the calibration. Among all possible pre-treatments, the most commonly used ones to correct the spectral variations were used in this work: baseline offset, range normalization, baseline offset followed by range normalization and full multiplicative scatter correction, MSC [37]. All the pre-treatments were applied to the different spectral data group corresponding to each cluster.

Even though group 6 contained the formerly determined outliers, it is noteworthy that the detection of outliers was done independently for each different cluster. Samples with high leverages or studentized residual values over ±3 were some of the criteria considered for the selection of anomalous coal samples in each group [38]. In these cases, the deletion of each outlier must be considered subjectively.

All the errors obtained after applying PLS regression are shown in Fig. 2. In this plot, the bars correspond to the prediction error, expressed in percentage error around the cluster mean, RMSECV (%) given by the different spectral data pre-treatment, whereas the line represents the error for the full set of samples. This line shows the errors obtained when baseline offset/normalization pre-treatment was applied, considered the best result for the whole set of samples [20].

Generally, properties related to inorganic coal matter, such as ash and sulphur content, show the highest prediction error values due to the low absorption coefficient this compounds present in NIR region. Moreover, sulphur and nitrogen are variables with successful absolute error values that turn into prediction abilities out of usefulness when they are expressed as relative errors.

The results obtained for moisture calibration were not suitable despite the feasibility of the technique [39]. This property presents the most important variations along the clusters in relation to the origin of the moisture content. The moisture included in coal samples is present in different states: free, physisorbed, chemisorbed and hydration water in minerals. The determination of moisture measures only water in the first three states while NIR measures the full water content. This divergence is more pronounced in coal samples with a low moisture content (groups 1 and 4) in contrast to low rank coal sample (group 3) with a higher moisture content where the main increment is due to free, physisorbed and chemisorbed water components.

Finally, properties related to organic coal matter, such as volatile matter, fixed carbon, heating value and carbon content, present the best results for all the clusters but group 3 (lignite sample coals) and 6 (outliers). Among them, it is worth high-

Table 1
Statistical results for each cluster and property value compared to the full sample set

		All (142)	Cluster 1 (25)	Cluster 2 (26)	Cluster 3 (7)	Cluster 4 (16)	Cluster 5 (63)	Cluster 6 (5)
Moisture (%)	Mean	11.20	5.92	10.22	35.30	1.36	13.96	5.59
	S.D.	7.32	3.37	1.08	1.15	0.54	1.99	2.32
Ash (%)	Media	13.46	11.57	27.23	23.33	7.36	5.75	54.15
	S.D.	12.22	3.37	7.23	5.91	2.37	1.86	12.88
Volatile matter (%)	Mean	35.07	28.49	32.68	22.31	28.91	42.96	18.66
	S.D.	8.58	3.76	3.79	2.52	8.68	1.65	5.23
Fixed carbon (%)	Mean	40.27	54.02	29.87	19.04	62.37	37.34	21.59
	S.D.	12.95	3.13	5.20	4.39	7.65	1.76	13.91
Heating value (kcal/kg)	Mean	5152.60	6478.83	4044.54	2590.57	7570.03	5007.49	1962.80
	S.D.	1423.41	301.74	576.01	578.21	368.28	204.79	503.42
Carbon (%)	Mean	54.95	67.54	43.44	27.30	78.21	54.47	22.17
	S.D.	14.16	2.59	5.30	5.82	2.61	1.67	5.42
Hydrogen (%)	Mean	4.28	3.97	3.72	2.35	4.54	4.96	2.11
	S.D.	0.95	0.53	0.50	0.36	1.09	0.27	0.62
Nitrogen (%)	Mean	0.90	1.47	0.62	0.42	1.37	0.77	0.34
	S.D.	0.41	0.24	0.16	0.06	0.34	0.14	0.11
Sulphur (%)	Mean	0.91	0.95	1.72	1.75	0.86	0.49	0.88
	S.D.	0.99	0.88	1.64	0.34	0.57	0.46	0.62

These clusters are obtained considering property values as independent variables in the hierarchical process. The number in brackets refers to the samples corresponding to each cluster.

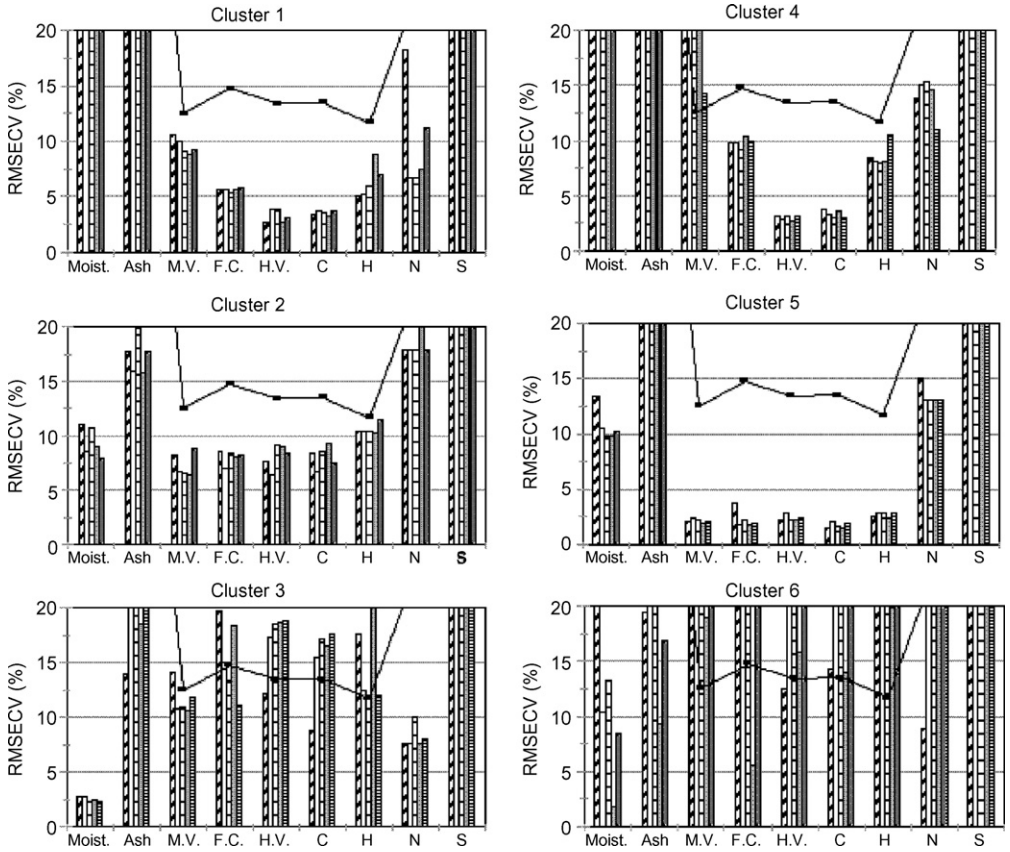

Fig. 2. RMSECV (%) obtained for each cluster (Situation A) and coal property after applying different pre-treatment: the first bar corresponds to original spectra followed by baseline correction, baseline/normalization, normalization and MSC. The line represents the error for the full sample set.

Table 2
Percentage of samples correctly classified depending on the covariance matrix

Method	PC	Covariance matrix		
		Separate-groups	Within-groups	Within-groups cross-validation
PCA	3	83.1	78.9	78.2
PLS2-0,1	4	87.3	83.8	81.7

lighting the results obtained for heating value calibration, below 3% in three clusters.

Focusing on the different spectral modifications, it can be observed different behaviour for each of the groups. It seems to be quite similar the results obtained for groups 1, 4 and 5, particularly for those properties related to organic matter compounds, whereas the rest of the clusters present a major dependence on a certain mathematical pre-treatment. The spectral homogeneity of the clusters and its relationship with the different properties may be some of the factors that lead to the use of a given pre-treatment.

3.1.3. Phase III. Classification

After calculating the discriminant functions, the samples were classified in order to check the sensitivity and specificity of the system. Table 2 shows the percentage of samples correctly classified considering separate-groups, within-groups and cross-validation leave-one-out within-groups covariance matrix computing prior probability from group sizes in each case. The results conclude that the use of principal components as independent variables, selected after a discriminant PLS2, increase the percentage of samples correctly classified regardless of the covariance matrix applied. Even so, group 6 presents a very low sensitivity, 40%, interfering with the new outliers identification. It is important the overlapping between group 1 and 4 leading to sensitivities of 84% (group 1) and 62.5% (group 4). On the contrary, group 3 is highly sensitive, 100%, useful for the calibration of moisture and finally, group 5 consisting of subbituminous sample coals is quite sensitive, 96.8% and it is interesting in the determination of properties related to organic matter coal, such as volatile matter, heating value and carbon content.

In order to improve the discrimination and classification process, another situation was studied taking into account exclusively spectral data as independent variables for the establishment of a new set of clusters in hierarchical analysis.

3.2. Situation B: spectral data as clustering variables

Since the discrimination and classification process for a new coal sample is developed according to its near spectral data, we consider the approximation of studying the influence that instrumental variables present in the hierarchical process.

For that, a PCA was used to reduce the dimensionality of the data matrix prior to the clustering process. Both spectral data in absorbance and baseline/normalization pre-treatment mode were considered. Table 3 shows the increasing explained variance corresponding to each case, wherein it is worth emphasizing that absorbance mode PCA was decomposed in a fewer number of principal components able to explain a higher percentage of information. So, three principal components were necessary to account for 99.86% explained variance when log (1/*R*) scores were studied. Nevertheless, spectral variables seemed to be insufficient for the distinction between the samples leading to unsatisfactory results. When the prediction ability for each cluster was compared to those obtained for other methods – ASTM [22] or prior Situation A – the errors turned out to be higher as it is shown in Fig. 3.

Table 3
Principal component analysis explained variance depending on the spectral data matrix

PC	Explained variance			
	No pre-treatment (absorbance)		Baseline offset/normalization	
	X-Calibration	*X*-Validation	*X*-Calibration	*X*-Validation
1	99.158	99.131	78.587	78.239
2	99.676	99.648	87.914	87.354
3	**99.882**	**99.861**	94.437	94.167
4	99.917	99.893	97.611	97.421
5	99.935	99.904	98.571	98.436
6	99.949	99.908	98.859	98.711
7	99.957	99.915	**99.023**	**98.876**
8	99.962	99.918	99.108	98.882
9	99.965	99.918	99.192	98.935
10	99.969	99.919	99.254	98.941

However, spectral data would be interesting to make more precise the establishment of coal groups in combination with coal properties, facilitating the difference between the groups in the classification step.

3.3. Situation C: coal properties and spectral data as clustering variables

3.3.1. Phase I. Grouping

A way to introduce subtle distinctions into the hierarchical clustering process was combining coal properties with spectral data as independent variables. A $142 \times (9+3)$ matrix was introduced, referring to 142 coal samples, 9 coal properties and 3 principal components from a PCA in log (1/*R*) units. As explained before, in this situation eight final clusters were estab-

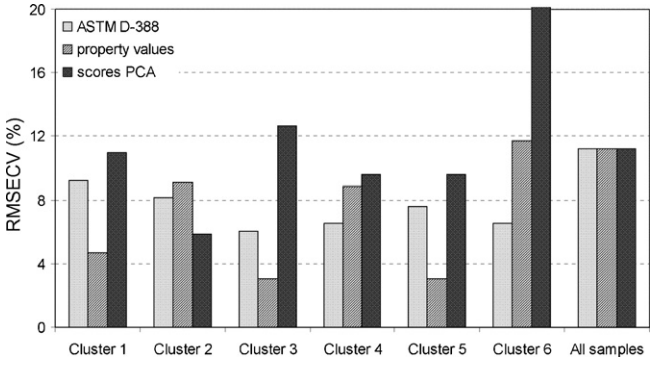

Fig. 3. Comparative between hydrogen (%) error determinations for three different situations.

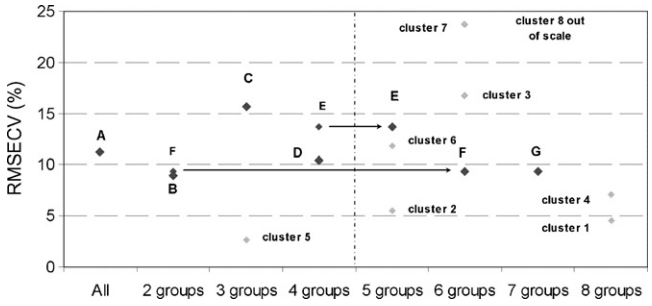

Fig. 4. Relative root mean squared error of cross-validation (RMSECV) obtained for hydrogen (%) content along the splitting process. Property coal values and spectral data are combined for hierarchical cluster analysis.

lished attending to hydrogen content calibration, as it is shown in Fig. 4. As above, big black points indicate the cluster that is divided in each step whereas grey points represent the final groups. Moreover, a discontinuous line indicates the moment when spectral data contribute in the process. These spectral variables have an effect on the clusters constitution with the exception of cluster 5, mainly defined by coal's analytical values. From that moment on, it is observed the establishment of cluster 2 (blended coal) and 6, both proceeding from the prior cluster 2 (Situation A), as well as several coal sample interchanges between clusters 1 and 4. In addition to that, few coal samples are selected to constitute cluster 8 (outliers-high rank coals) whereas cluster 7 (outliers-low rank coals) and 3 remain as in Situation A.

3.3.2. *Phase II. Calibration methods*

Once defined the clusters, PLS calibration models were developed for all the coal properties considering likewise the mathematical pre-treatments previously indicated. The RMSECV (%) corresponding to each situation is shown in Fig. 5. Generally, the system presents determination errors quite dis-

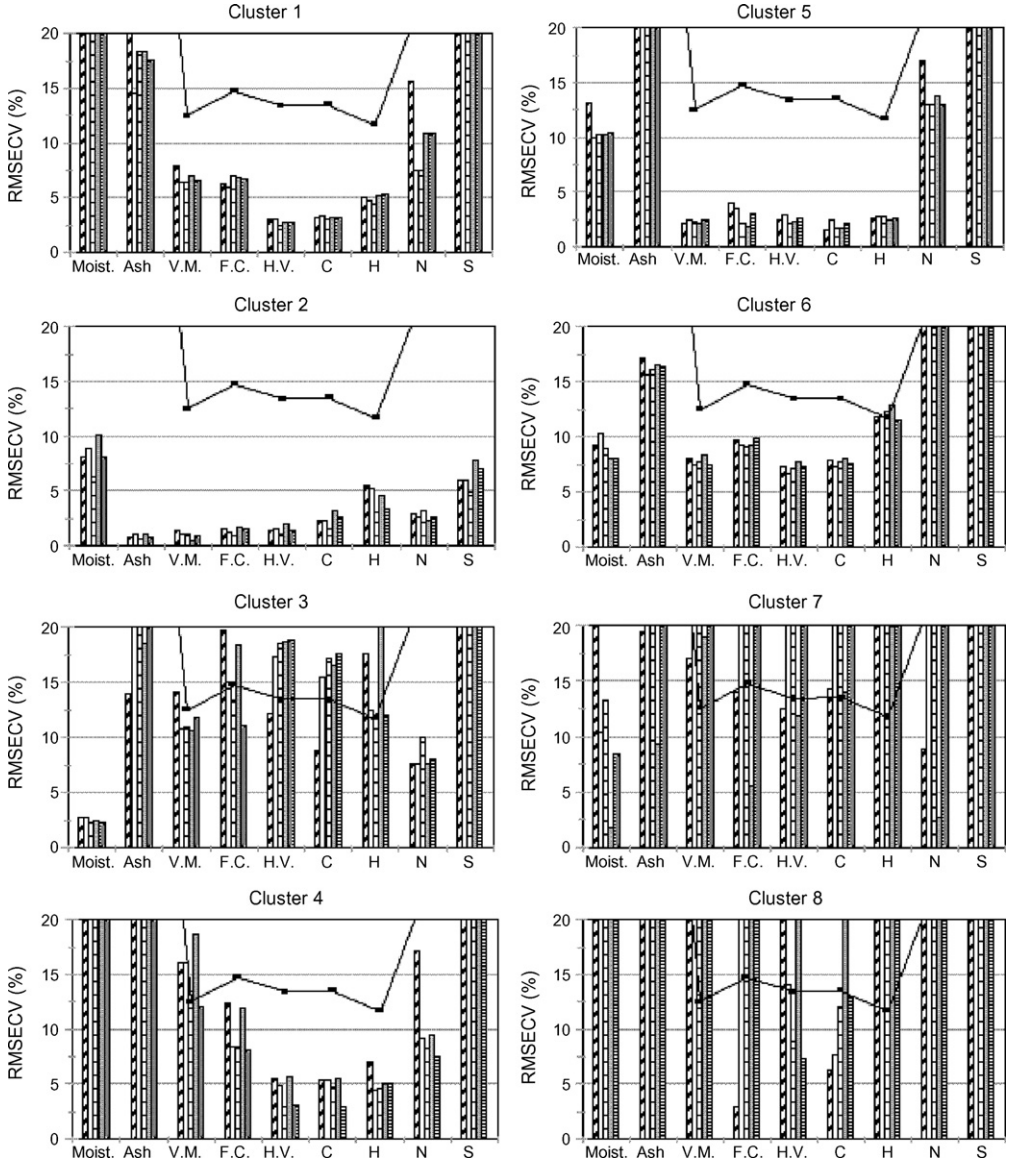

Fig. 5. RMSECV (%) obtained for each cluster (Situation C) and property after applying different pre-treatment: the first bar corresponds to original spectra followed by baseline correction, baseline/normalization, normalization and MSC. The line represents the error for the full sample set.

Table 4
Best results for calibration and prediction error obtained for each group

Cluster (samples)	Property	Pre-treatment	Mean	RMSEC	RMSEC (%)	RMSECV	RMSECV (%)	PC
1(20)	Moisture	Baseline/norm.	6.41	1.34	20.92	1.79	27.95	2
	Ash	Baseline/norm.	12.47	1.60	12.83	1.82	14.60	1
	Volatile matter	Baseline/norm.	27.18	1.27	4.67	1.74	6.40	3
	Fixed carbon	Baseline	53.95	2.22	4.12	3.26	6.04	3
	Heating value	Baseline/norm.	6387.74	120.50	1.89	156.80	2.45	2
	C	Baseline/norm.	66.82	1.33	1.99	2.07	3.10	3
	H	Baseline/norm.	3.80	0.13	3.42	0.17	4.48	3
	N	Baseline/norm.	1.47	0.10	6.82	0.11	7.50	1
	S	MSC	0.84	0.40	47.51	0.49	58.20	2
2(5)	Moisture	Baseline/norm.	10.49	0.30	2.86	0.66	6.29	0
	Ash	Baseline/norm.	22.49	0.05	0.22	0.14	0.62	0
	Volatile matter	Baseline/norm.	29.08	0.13	0.45	0.32	1.10	0
	Fixed carbon	Baseline/norm.	37.94	0.17	0.45	0.36	0.95	0
	Heating value	Baseline/norm.	4870.00	24.58	0.50	52.08	1.07	0
	C	Baseline/norm.	49.52	0.36	0.73	0.76	1.53	0
	H	Baseline/norm.	3.24	0.04	1.23	0.10	3.08	0
	N	Normalization	0.86	0.01	1.63	0.02	2.33	0
	S	Baseline/norm.	4.85	0.11	2.27	0.24	4.95	0
3(7)	Moisture	Baseline/norm.	35.30	0.32	0.91	0.73	2.07	1
	Ash	–	23.33	0.50	1.99	3.50	13.93	3
	Volatile matter	Normalization	22.31	0.99	4.44	2.25	10.08	1
	Fixed carbon	MSC	19.04	1.97	10.35	2.49	13.08	1
	Heating value	–	2590.57	66.80	2.73	296.59	12.13	2
	C	–	27.30	0.72	2.77	2.30	8.84	1
	H	Baseline/norm.	2.35	0.14	5.95	0.27	11.48	1
	N	–	0.42	0.01	2.52	0.03	7.57	2
	S	Baseline/norm.	1.75	0.27	15.45	0.34	19.46	1
4(18)	Moisture	Baseline/norm.	1.84	0.30	16.27	0.59	32.00	4
	Ash	Baseline/norm.	7.07	1.40	19.80	1.53	21.64	1
	Volatile matter	Baseline/norm.	30.89	0.14	0.45	4.16	13.47	7
	Fixed carbon	MSC	60.19	2.44	4.05	4.92	8.17	4
	Heating value	Baseline/norm.	7478.78	13.91	0.19	219.82	2.94	7
	C	MSC	76.57	0.13	0.17	2.27	2.96	7
	H	Baseline/norm.	4.77	0.19	3.98	0.22	4.61	2
	N	MSC	1.46	0.10	6.84	0.11	7.52	1
	S	MSC	0.89	0.33	37.20	0.39	43.40	1
5(64)	Moisture	Baseline/norm.	13.91	0.75	5.39	1.43	10.28	11
	Ash	Normalization	5.92	0.37	6.25	1.21	20.45	14
	Volatile matter	–	42.91	0.44	1.03	0.92	2.14	12
	Fixed carbon	Normalization	37.26	0.22	0.59	0.68	1.83	14
	Heating value	Baseline/norm.	4999.78	31.38	0.63	108.15	2.16	14
	C	–	54.39	0.27	0.50	0.80	1.47	14
	H	Normalization	4.95	0.08	1.62	0.12	2.42	10
	N	Baseline/norm.	0.76	0.06	7.85	0.10	13.09	10
	S	MSC	0.51	0.11	21.65	0.27	52.17	12
6(20)	Moisture	Normalization	10.11	0.56	5.54	0.82	8.11	4
	Ash	Baseline	28.94	3.64	12.58	4.51	15.58	3
	Volatile matter	Baseline	33.21	1.89	5.69	2.48	7.47	3
	Fixed carbon	Baseline/norm.	27.74	2.01	7.25	2.53	9.12	2
	Heating value	Baseline	3814.70	197.31	5.17	254.56	6.67	3
	C	Baseline	41.62	2.36	5.67	3.04	7.31	3
	H	MSC	3.81	0.33	8.66	0.44	11.55	3
	N	Baseline/norm.	0.55	0.09	16.23	0.11	19.84	2
	S	Normalization	0.94	0.44	46.96	0.51	54.43	2
7(5)	Moisture	Normalization	5.59	0.03	0.54	0.10	1.79	2
	Ash	Normalization	54.15	1.29	2.38	5.10	9.42	1
	Volatile matter	Normalization	18.66	2.09	11.17	3.53	18.92	1
	Fixed carbon	Normalization	21.59	0.52	2.41	1.19	5.51	1
	Heating value	Normalization	1962.80	115.13	5.87	232.70	11.86	1
	C	Normalization	22.17	1.98	8.93	3.10	13.98	1
	H	Normalization	2.11	0.26	12.30	0.42	19.87	1

Table 4 (*Continued*)

Cluster (samples)	Property	Pre-treatment	Mean	RMSEC	RMSEC (%)	RMSECV	RMSECV (%)	PC
	N	Normalization	0.34	0.01	1.76	0.01	2.65	1
	S	Baseline	0.88	0.21	23.40	0.37	42.24	1
8(3)	Moisture	Baseline	2.80	0.56	5.54	1.75	62.43	1
	Ash	MSC	10.14	0.79	7.74	2.64	26.03	1
	Volatile matter	Baseline/norm.	25.04	0.51	2.02	15.80	63.10	1
	Fixed carbon	–	62.02	2.26	3.64	1.85	2.98	1
	Heating value	MSC	6906.16	158.15	2.29	512.42	7.42	1
	C	–	75.01	1.61	2.15	4.77	6.36	1
	H	Baseline/norm.	0.15	4.47	8.66	2.27	67.58	1
	N	MSC	1.01	0.02	1.98	0.62	61.49	1
	S	Normalization	1.57	0.31	19.71	0.87	55.33	1

Property coal values and spectral data are combined for the establishment of the clusters.

tant from the reproducibility limits allowed by the ISO/ASTM norm; however, these values are comparable to those obtained by commercial equipment [2,3], especially for properties related to organic coal matter. Numerical details about absolute and relative error values for calibration and prediction models, spectral pre-treatment and number of principal components selected for the best calibration models are presented in Table 4 .

Whereas clusters 3, 5 and 7 present the same results as in Situation A (clusters 3, 5 and 6), several differences can be observed for the rest of the clusters, especially those assigned to cluster 2. The homogeneity of this new group leads to relative error values around 1% for properties related to organic coal matter (volatile matter, fixed carbon, heating value and carbon content) even ash content. Furthermore, the fact that the system requires 0 principal components for the development of the calibration models suggests the possibility to estimate the property value for a new coal sample by referring to its respective mean property value with a standard deviation corresponding to the absolute error value determined by multivariate calibration. In any case, it is necessary an appropriate classification for the new coal sample to its respective group attending only to its spectral data.

3.3.3. Phase III. Classification

As it was presented previously, two possibilities were considered for the application of a supervised LDA: a PCA or a discriminant PLS2-0,1 to select the principal components prior the calculation of the discriminant functions. In this case, cluster 8 was excluded from the study as it consists only of three coal samples, insufficient to determine the discriminant functions. Consequently, it is necessary to recalculate the corresponding scores both for the PCA and discriminant PLS2 without these coal samples. Three and four principal components were, respectively, introduced as independent variables in the LDA. The percentage of samples correctly classified revealed a similar tendency as it was observed in Situation A, with values ranging from 88.5 to 82.7% when separate-groups or LOO cross-validation within-groups covariance matrix was applied.

For studying the suitability of the process it was necessary taking into account the sensitivity and the specificity of each of the clusters. Although it would be interesting an improvement in specificity, especially in cluster 2 and 5 for further applications, the results in percentage values, detailed in Table 5, revealed a surprising increase in sensitivity for some clusters.

Table 5
Classification results in percentages for cross-validation within-groups covariance matrix (Situation C)

Clusters	Predicted group membership							Total
	1	2	3	4	5	6	7	
1	**55**	15	0	30	0	0	0	100
2	0	**100**	0	0	0	0	0	100
3	0	0	**100**	0	0	0	0	100
4	11.1	11.1	0	**77.8**	0	0	0	100
5	0	0	1.6	0	**96.9**	1.6	0	100
6	0	0	0	0	40	**60**	0	100
7	0	0	0	0	0	60	**40**	100

The combination of property coal variables and near-infrared spectral data allows the system to establish more specific clusters by means of a hierarchical clustering process than those obtained by other methods [22]. This fact joined with adequate cluster discrimination would lead to consider near spectroscopy as a feasible way to analyse coal samples in an online configuration.

4. Conclusions

A hierarchical clustering process is studied as a mean to improve the rapid analysis of coal based on its near-IR spectra. Three situations are considered depending on the variables introduced into the hierarchical process: property values, spectral data (principal component analysis) or a combination of both. Among them, only those including coal property values lead to significant improvement error calibration determination. The results indicate that properties related to organic coal matter, such as volatile matter, fixed carbon, heating value or carbon content, present absolute error values around 1–3% for some clusters, suitable to be applied in an online system.

Once established the groups, the discrimination between the clusters are studied by a linear discriminant analysis, which presents better sensitivity and specificity results if coal samples are classified into those clusters determined when property values and spectral data are considered for the establishment of the clusters. Calibration and classification methods allow the calculation of the property values of coal with accuracy similar

or even better than that obtained by commercial online analyser, pointing to near-IR spectroscopy as a valid option for this task.

Acknowledgements

The authors are grateful to the European Coal and Steel Community for funding this research within the framework of Project 7220-PR/118. We also thank to ENDESA, RWE Ag, EVN Ag and PPC for providing us coal samples.

References

[1] H. Nalbandian, IEA Clean Coal Centre, CCC/100, 2005.
[2] A. Kirchner, On-Line Analysis of Coal, IEA Coal Research, IEACR/40, 1991.
[3] A. Kirchner, C. Maude, On-Line Analysis of Coal-Symposium Review, IEA Coal Research, Perspectives, IEAPER/13, 1994.
[4] M.N. Skorupska, IEA Coal Res. 52 (1993).
[5] J.V. Thomas, Anal. Chem. 67 (12) (1995) 317R.
[6] G.R. Couch, IEA Coal Res. 22 (1996).
[7] A.M. Carpenter, IEA Coal Res. 81 (1995).
[8] M.P. Fuller, P.R. Griffiths, Anal. Chem. 50 (13) (1978) 1906.
[9] M.P. Fuller, I.M. Hamadeh, P.R. Griffiths, d.E. Lowenhaupt, Fuel 61 (1982) 529.
[10] P.M. Fredericks, R. Kobayashi, P.R. Osborn, Fuel 66 (1987) 1603.
[11] H.H. Schobert, Coal, The Energy Source of the Past and Future, American Chemical Society, 1987.
[12] S. Tesch, K.-H. Rentrop, M. Otto, Fresenius J. Anal. Chem. 344 (1992) 206.
[13] C.E. Alciaturi, M.E. Escobar, R. Vallejo, Fuel 75 (4) (1996) 491.
[14] C.E. Alciaturi, T. Montero, C. De La Cruz, M.E. Escobar, Anal. Chim. Acta 340 (1997) 233.
[15] C.E. Alciaturi, M.E. Escobar, D. De La Cruz, R. Vallejo, Anal. Chim. Acta 436 (2001) 265.
[16] E.A. Cloutis, Fuel 82 (2003) 2239.
[17] O. Ito, H. Seki, M. Iino, Fuel 67 (1988) 573.
[18] O. Ito, Energy Fuels 6 (1992) 662.
[19] M. Kaihara, T. Takahashi, T. Akazawa, T. Sato, S. Takahashi, Spectrosc. Lett. 35 (3) (2002) 369.
[20] J.M. Andrés, M.T. Bona, Anal. Chim. Acta 535 (2005) 123.
[21] ASTM D 388-92a, Standard Classification of Coals by Rank.
[22] J.M. Andrés, M.T. Bona, Talanta 70 (4) (2006) 711.
[23] R.L. Charmichael, International Symposium on Mining Technology and Science, Xuzhou, China, September 18, 1985, China Coal Industry Publishing House, China, 1987, p. 1365.
[24] ISO-589-1981 Hard coal-Determination of total moisture.
[25] ISO-1171-1976 Combustibles minéraux solides-Détermination des cendres.
[26] ISO-562-1974 Houille et coke-Détermination du taux de matières volatiles.
[27] ASTM D 3172-89 Standard Practice for Proximate Analysis of Coal and Coke (reapproved 1993).
[28] ISO-1928-95 Solid mineral fuels-Determination of gross calorific value by the bomb calorimetric method, and calculation of net calorific value.
[29] ASTM D 3177-89 Standard Test Methods for Total Sulfur in the Analysis Sample of Coal and Coke.
[30] T. Naes, T. Isaksson, T. Fearn, T. Davies, A User-Friendly Guide to Multivariate Calibration and Classification, NIR Publications, 2002, p. 105.
[31] K.R. Beebe, R.J. Pell, M.-B. Seasholtz, Chemometrics: A Practical Guide, John Wiley & Sons, Inc., 1998.
[32] J.H. Ward, J. Am. Stat. Assoc. 58 (1963) 236.
[33] W.R. Dillon, M. Goldstein, Multivariate Analysis, John Wiley & Sons Inc., 1984.
[34] M.A. Sharaf, D.L. Illman, B.R. Kowalski, Chemometrics, vol. 195, John Wiley & Sons, New York, 1986.
[35] S. Wold, K. Esbensen, P. Geladi, Chemom. Intell. Lab. Syst. 2 (1987) 37.
[36] U.G. Indhal, N.S. Sing, B. Kirkhuus, T. Naes, Chemom. Intell. Lab. Syst. 49 (1999) 19.
[37] P. Geladi, D. MacDougall, H. Martens, Appl. Spectrosc. 39 (3) (1985) 491.
[38] P.B. Coleman, Practical Sampling Techniques for Infrared Analysis, CRC Press, 1993.
[39] H.M. Siesler, Y. Ozaki, S. Kawata, H.M. Heise, Near-Infrared Spectroscopy. Principles, Instruments, Applications, Wiley-VCH, 2002.

Available online at www.sciencedirect.com
ScienceDirect
Talanta 72 (2007) 1357–1361
Talanta
www.elsevier.com/locate/talanta

Determination of polycyclic aromatic hydrocarbons (PAHs) in particulate matter collected with low volume samplers

Paolo Bruno, Maurizio Caselli, Gianluigi de Gennaro *, Maria Tutino

Dipartimento di Chimica, Università Degli Studi di Bari, via Orabona 4, 70126 Bari, Italy

Received 22 September 2006; received in revised form 15 January 2007; accepted 19 January 2007
Available online 30 January 2007

Abstract

The determination of polycyclic aromatic hydrocarbons (PAHs) contained in samples of particulate matter (PM), collected with low volume pumps, were carried out with an high sensitivity method that comes from several revisions of a previous method. The present work describes how, by using programmable temperature vaporization (PTV) and a mass selective detector with inert ionic source for the GC–MS analysis and the modifications of microwave-assisted extraction (MAE), the sensitivity of the method can be increased.

The PAHs chosen for testing the method are: benzo[a]anthracene (BaA), benzo[b]fluoranthene (BbF), benzo[k]fluoranthene (BkF), benzo[a]pyrene (BaP), indeno[1,2,3-cd]pyrene (Ip) and dibenzo[a,h]anthracene (DbA). They, in fact, belong to that group of substances that are the most harmful for human health for their carcinogenicity.

PAHs recoveries for spiked standard solutions at different concentrations were between 95 and 100% with relative standard deviation ranging from 1 to 3%. The revised method was validated using a 1649a urban dust standard reference material (SRM). The results obtained were in good agreement with certified values. The high sensitivity of the method allows to carry out analyses using only a half of the sampled filter (usually 47 mm diameter membranes). In this way, the other half can be used for the characterization of the other components of PM (heavy metals, organic carbon, ions, etc). The last step has been constituted by application of the optimized method on real samples collected in two cities located in Southern Italy (Bari and Taranto).

Keywords: PAHs; PTV; MAE; Inert ion sources; Particulate matter; PM 2.5

1. Introduction

In recent years, particulate matter has been widely studied for its potential human health impact and the subsequent need to control and regulate pollutants. Several studies indicate that the effects depend on the dimensions of particles, on their concentration and on chemical composition. In particular, finer particulate causes a greater impact on health [1–3].

Some authors stated that the exposure at PM 2.5 (fine particles with aerodynamic diameter smaller than 2.5 μm) can cause short and long-term effects for human health, such as premature death, increased respiratory symptoms and disease, decrease lung function and alterations in lung tissue and structure and respiratory tract defense mechanisms [4–6].

In the urban area, where heavy metals and PAHs are strongly associated with the fine particles, the toxicity and the carcinogenicity of the particulate matter is increased [7,8].

Therefore, the determination of particle-bound PAHs is very important, in particular, those compounds with higher number of rings have particular toxicological interest [9–10]. In literature, there are many methods for PAH determination, that depends on the conditions of aspiration flow and the instrumentations used [11–18]. Sample preparation with traditional procedures is performed by Soxhlet extraction, but this technique is time consuming and produces large amounts of solvent waste. To achieve faster extraction and reduction of solvent volume, some of modern extraction techniques, such as sonication, microwave-assisted extraction (MAE), supercritical fluid extraction (SFE), pressurized liquid extraction (PLE) and subcritical water extraction (SWE), were tested on several environmental samples [9,5,19,20]. Some of these methods require the preconcentration of the extracted solutions before the analysis. This

* Corresponding author. Tel.: +39 0805442023; fax: +39 0805442023.
E-mail address: giangi@chimica.uniba.it (G. de Gennaro).

0039-9140/$ – see front matter © 2007 Elsevier B.V. All rights reserved.
doi:10.1016/j.talanta.2007.01.043

step can cause a decrease of analytical reproducibility as there is more sample handling and anyway a higher time analysis.

The aim of this study was the implementation of an analytical procedure for PAH determination already presented in a previous work [11]. In particular, the sensitivity of the method has been increased improving the extraction step, GC inlet system and MS detection. The extraction was performed with microwaves in closed vessels with lower amount of solvent. GC analysis was carried out with an injection system characterized by a programmable temperature vaporization (PTV) and the MS detection with an inert mass ion source.

PAH analysis requires a high sensitive analytical method when it must be performed on filters collected with low volume samplers. This sampling method, unlike the high volume sampling, is often chosen because it can be automated. An automatic sampling means lower possibility of measurement errors and costs (due to daily intervention of an operator).

In this work, benzo[a]anthracene (BaA), benzo[b]fluoranthene (BbF), benzo[k]fluoranthene (BkF), benzo[a]pyrene (BaP), indeno[1,2,3-cd]pyrene (Ip) and dibenzo[a,h]anthracene (DbA) were analyzed as they represent harmful substances for human health. In fact, these PAHs are classified by the International Agency for Research on Cancer (IARC) as possible carcinogenic [4].

In this work, the analytical performances of the whole procedure (extraction recovery, extraction linearity, analytical repeatability, LOD) were verified; the revised method accuracy was tested using a standard reference material (SRM 1649a National Institute of Standards and Technology, NIST). Finally, the procedure was applied on real samples collected in the urban area of Bari (Italy).

2. Experimental

2.1. Sampling

The PAHs in airborne particulate matter were collected on QM-A Whatman (Maidstone, Kent, UK) filters of quartz fibers (i.d. 47 mm). The sampling was performed by an HYDRA (FAI Instruments s.r.l., Roma, Italy) low volume sampler that, with a volumetric flow of 1 m^3/h and a size selective inlet (SSI), allows the collection of particles with an aerodynamic diameter less than 2.5 μm. Sampling times of the measures reported in this work are of 24 h. After sampling the filters were easily cut in two parts by using a stainless steel socket punch and were stored in a refrigerator at 4 °C before the analysis.

2.2. Extraction

The extraction of PAHs was realized by a microwave-assisted solvent extraction by Milestone (Milestone s.r.l., Sorisole (BG), Italy), model Ethos D, which allows the simultaneous extraction up to 10 samples at the same conditions. MAE technique combines microwave heating, under controlled temperature conditions through a microwave transparent fiber-optic probe with magnetic stirring of extraction solvent inside multiple closed sample vessels. Agitation ensures homogeneous mixing and uniform temperature distribution throughout extraction mixtures. The procedure was optimized in order to perform a simple, fast and efficient extraction of PAHs contained in 47 mm sampled filters. Amount of solvents, microwave power and extraction time were studied. The best found conditions of extraction are listed in Table 1.

Table 1
MAE extraction parameters

Solvent	Acetone (5 ml) + hexane (5 ml)
Time	25 min
Temperature	110 °C
Power	200 W
Vent	5 min

Table 2
Operating conditions for GC–MS analysis

PTV	50 °C for 0.5 min, at a rate of 720 °C/min, to 300 °C for 2 min
Analytical column MDN-5S (Supelco)	30 m × 0.25 mm i.d., 0.25 μm stationary phase thickness
Mobile phase	He
Internal standard	Perylene D12
Column flow	1.3 ml/min
Oven temperature	50 °C for 2.5 min, at a rate of 30 °C/min, to 210 °C, then at 5 °C/min to 300 °C for 3 min
Acquisition mode	Selected ion monitoring (SIM)

2.3. Analysis

The extracted samples were analyzed using an Agilent 6890 PLUS gas chromatograph (Agilent Technologies, Wilmington DE) equipped with a programmable temperature vaporization injection system (PTV) and interfaced to a mass selective spectrometer with an inert ion source (Agilent MS-5973 N).

Significant gains in sensitivity were realized by using the PTV inlet in the "solvent vent" mode, as it is compatible with injections up to 40 μl (the maximum volume that can be used with the installed liner). Further improvements were obtained using the inert mass selective spectrometer, which is characterized by a solid ion source with an inert coating that minimizes the degradation of active compounds and produces a better spectral quality and higher reliability. Moreover, this source can operate at high temperatures (300 °C), which constitutes an advantage for the analysis of compounds with high boiling points, such as PAHs. The resulting improvements in spectra quality make possible analyses of low amounts of PAHs, as those collected with low volume samplers. The GC–MS conditions for analyses are listed in Table 2. The quantitative determination was carried out using the signals corresponding to the molecular ions of PAHs: BaA (228), BbF (252), BkF (252), BaP (252), Ip (276), DbA (278). Perylene-D12 (PrD, 264) was used as internal standard (I.S.).

3. Results and discussion

The optimization of the extraction step was performed in order to increase the recovery of each analyte and to improve the reproducibility.

Table 3
Recovery percentage and relative standard deviation (R.S.D.%) for triplicate extractions for 2, 4, 20 and 40 ng of PAHs

Compounds	R^2	Recovery% (2 ng)	Recovery% (4 ng)	Recovery% (20 ng)	Recovery% (40 ng)
BaA	0.9994	96 ± 1	100 ± 1	100 ± 1	100 ± 1
BbF	0.9991	96 ± 2	94 ± 1	100 ± 1	100 ± 1
BkF	0.9991	96 ± 3	97 ± 1	96 ± 1	97 ± 1
BaP	0.9997	95 ± 1	100 ± 1	95 ± 1	100 ± 1
Ip	0.9991	100 ± 1	99 ± 1	100 ± 1	100 ± 1
BgP	0.9993	98 ± 1	100 ± 1	98 ± 1	98 ± 1
DbA	0.9989	95 ± 2	95 ± 2	95 ± 2	95 ± 1

R^2 values for the lines obtained with extracted standards.

During a microwave-assisted solvent extraction the critical parameters are the temperature, the irradiation time and the volume of the solvent chosen for the extraction. In particular, increasing the temperature and the irradiation time, the recovery of analytes should increase, but the probability of analyte losses or their decomposition increases. The parameter values were set in order to reach a good compromise between good recovery and good reproducibility (Table 1) [21].

In particular, during the extraction step, recovery tests were carried out spiking known amounts of a PAH standard solution, diluted in hexane and acetone mixture (EPA 525 PAH Mix A, Supelco, Bellefonte, PA, USA), onto a blank filter. Each test was tripled. In Table 3 are listed: the medium value for each spiked amount, the relative standard deviations (R.S.D.%) and the R^2 of the obtained lines. The results show a good recovery for all investigated compounds apart from the amounts. High recovery values and good linearity allow to quantify real samples using no extracted standards solutions avoiding to perform every time the extraction procedure. In this way, the methodology becomes further handier and does not penalize the result quality. For example, the comparison between calibration lines obtained with extracted and non-extracted standards for BaP showed a good correlation, $R^2 = 0.997$ for the former ($y = 0.1874x + 0.0656$) and $R^2 = 0.998$ for the later ($y = 0.1936x + 0.0538$).

The large-volume injection using PTV technique was studied too. In this work the linearity of analyte response with PTV inlet in "solvent vent" mode was verified injecting growing volume of standard solutions. In particular, 10, 20, 30 and 40 μl of PAHs standard solutions at 1 μg/ml were analyzed in the same conditions (Table 1). Plotting the signal versus the injection volume a good linearity from 10 to 40 μl for all PAHs was obtained; the R^2 values were: 1.000 for BaA, 0.999 for BbF, 0.997 for BkF, 0.999 for BaP, 0.998 for Ip, 0.998 for BgP and 0.997 for DbA.

The use of the inert source allowed to increase the sensitivity of the method. For each PAH the peak height was improved ranging from three to seven times. This improved response gave better linearity across the calibration range. Moreover, the possibility of working at 300 °C, instead of the typical 250 °C, in combination with the new uncoated solid source material produced better peak shapes, above all for higher mass PAHs with long retention times.

Then the limit of detection (LOD) and the limit of quantification (LOQ) were calculated (Table 4) for all investigated compounds. Considering a sampling of 24 h with a volumetric flow of 1 m^3/h it was possible to calculate the corresponding concentrations in atmosphere. The LOD and LOQ values are much lower than the Italian legal limit of benzo[a]pyrene (1 ng/m^3) [22].

Table 4
Limit of detection (LOD) and limit of quantification (LOQ) for all investigated PAHs in solution (pg/ml) and in atmosphere (ng/m^3)

Compounds	LOD (pg/ml)	LOD (ng/m^3)	LOQ (pg/ml)	LOQ (ng/m^3)
BaA	23	0.009	77	0.032
BbF	38	0.016	127	0.052
BkF	23	0.010	77	0.032
BaP	6	0.003	20	0.008
Ip	4	0.003	13	0.006
BgP	25	0.010	83	0.035
DbA	30	0.012	100	0.042

The performances of the method were tested on a standard reference material, the urban dust SRM 1649a. Aliquots of about 0.01, 0.02 and 0.05 g of SRM were extracted and analyzed in the same conditions. The results of analysis of the repeated extractions (four extractions for each amount), the standard deviations, and the percentage differences between reference and measured concentrations are listed in Tables 5–7. The tables show a good agreement between the reference concentrations and the measured values; for all compounds the differences calculated were less than 7%.

The high sensitivity of the method allowed to carry out the analyses using an half of the sampled 47 mm filter. The homogeneity of filter was tested comparing the concentrations

Table 5
Results of repeated extractions and analyses of about 0.01 g of SRM 1649a

Compounds	Certified values (μg g^{-1})	Measured concentration (μg g^{-1})	Difference%
BaA	2.21 ± 0.073	2.05 (0.02)	7
BbF	6.45 ± 0.64	6.25 (0.23)	3
BkF	1.913 ± 0.031	1.95 (0.06)	2
BaP	2.509 ± 0.087	2.41 (0.16)	4
Ip	3.18 ± 0.72	3.01 (0.32)	2
BgP	4.01 ± 0.91	3.88 (0.34)	3
DbA	0.288 ± 0.023	0.31 (0.03)	6

Measured concentration is the mean of four repeated extractions and analyses; the standard deviations are reported between brackets.

Table 6
Results of repeated extractions and analyses of about 0.02 g of SRM 1649a

Compounds	Certified values ($\mu g\,g^{-1}$)	Measured concentration ($\mu g\,g^{-1}$)	Difference%
BaA	2.21 ± 0.073	2.19 (0.04)	1.3
BbF	6.45 ± 0.64	6.28 (0.41)	3
BkF	1.913 ± 0.031	1.90 (0.16)	0.5
BaP	2.509 ± 0.087	2.39 (0.06)	5
Ip	3.18 ± 0.72	3.01 (0.32)	2
BgP	4.01 ± 0.91	3.78 (0.34)	4
DbA	0.288 ± 0.023	0.38 (0.03)	3

Measured concentration is the mean of four repeated extractions and analyses; the standard deviations are reported between brackets.

Table 7
Results of repeated extractions and analyses of about 0.05 g of SRM 1649a

Compounds	Certified values ($\mu g\,g^{-1}$)	Measured concentration ($\mu g\,g^{-1}$)	Difference%
BaA	2.21 ± 0.073	2.22 (0.05)	-
BbF	6.45 ± 0.64	6.32 (0.31)	2
BkF	1.913 ± 0.031	1.98 (0.16)	4
BaP	2.509 ± 0.087	2.59 (0.25)	3
Ip	3.18 ± 0.72	3.10 (0.24)	1
BgP	4.01 ± 0.91	4.00 (0.17)	0.5
DbA	0.288 ± 0.023	0.36 (0.03)	2

Measured concentration is the mean of four repeated extractions and analyses; the standard deviations are reported between brackets.

obtained by each half of filter. The results of this test are shown in Table 8.

Finally, the optimized method was applied on real samples collected in Bari and Taranto, two cities located in Southern Italy. A monitoring campaign of one month was performed in February 2006. It was carried out in course Cavour, a high-density traffic street in the urban area of Bari, and in via Orsini, near to the industrial area of Taranto. Each sampling lasted 24 h. In Table 9, the monthly medium concentrations and the standard deviation over the month are listed. The data show that in Bari BaP monthly medium concentration is lower than the Italian legal limit; this limit was exceeded only twice during February 2006. In Taranto BaP monthly medium level is double than the legal limit with a high variability on the month. This trend is due to the sampling site closeness to the industrial activities [23].

Table 8
PAHs measured concentrations ($\mu g/m^3$) for each half of filter

Compounds	First half of filter	Second half of filter	Difference%
BaA	0.95 ± 0.02[a]	0.97 ± 0.02	2.1
BbF	2.43 ± 0.20	2.39 ± 0.20	1.7
BkF	0.64 ± 0.03	0.68 ± 0.03	6.0
BaP	0.24 ± 0.02	0.23 ± 0.02	4.3
Ip	1.16 ± 0.07	1.17 ± 0.07	0.6
BgP	1.24 ± 0.04	1.19 ± 0.03	4.1
DbA	0.18 ± 0.01	0.20 ± 0.01	10

[a] $(c \pm \delta c)$ where $\delta c = t_{0.95}\sqrt{\sum s_i^2}$ and s_i^2 are the variances on extraction and quantification by the calibration curves.

Table 9
Monthly medium of PAH concentrations and the standard deviation (S.D.) over the month of PM 2.5 samples collected in Bari and Taranto (Southern Italy)

Compounds	Bari concentration ($\mu g\,m^{-3}$)	S.D.	Taranto concentration ($\mu g\,m^{-3}$)	S.D.
BaA	0.47	0.30	1.90	2.84
BbF	1.33	0.82	3.91	5.26
BkF	0.41	0.22	1.34	1.82
BaP	0.56	0.41	2.05	2.90
Ip	0.79	0.56	2.41	3.28
BgP	1.07	0.75	2.30	2.74
DbA	0.13	0.08	0.55	0.79

Table 10
Percentage differences between the measured concentration in the extraction day and the detected concentrations after 3, 7, 14 days of storage, respectively, for a standard solution (1 ng/ml)

Compounds	Differences% 3rd day	Differences% 7th day	Differences% 14th day
BaA	6	8	8
BbF	4	7	8
BkF	2	8	8
BaP	4	5	6
Ip	9	8	9
BgP	2	4	4
DbA	5	7	8

Table 11
Percentage differences between the measured concentration in the extraction day and the detected concentrations after 3, 7, 14 days of storage, respectively, for a collected real sample in the urban area of Bari (Italy)

Compounds	Differences% 3rd day	Differences% 7th day	Differences% 14th day
BaA	1	1	2
BbF	2	2	3
BkF	3	2	2
BaP	3	2	3
Ip	11	8	11
BgP	3	1	2
DbA	1	1	1

Using the method proposed, the time for the analysis of all samples collected was only of 6 days. Moreover, there was the possibility of analyzing the extracts after several days as most of the PAHs resulted stable in solution. The stability of PAH solutions was tested on two extracts, a standard solution (1 ng/ml) and a real sample, which were stored in freezer at 4 °C and analyzed at different periods of storage. For each solution, the differences between the concentration measured the day of the extraction and those measured after 3, 7 and 14 days were calculated for all investigated PAHs (see Tables 10 and 11). Both extracted solutions showed a good stability with differences ranging from 1 to 14%.

4. Conclusions

The proposed method, which has improved the analytical performances of the previous method [11], allowed to analyze

with high repeatability, sensitivity and accuracy all investigated compounds. MAE technique with low solvent volume allows to get a good and reproducible recovery of standard solutions and SRM. Moreover, the possibility to extract at the same time up to 10 samples reduces time and cost of the analysis, making the method suitable for routine monitoring.

High volumes injection by PTV inlet and the inert source of the detector increase the sensitivity of the GC–MS analysis and permit to use low volume pumps for sampling.

Besides, thanks to the high sensitivity of the method it is possible to quantify the PAHs using just a half of the sampled filter. For this, it is possible to perform, on the remaining half, a more detailed characterization of the other components of PM (heavy metals, organic carbon, ions, etc.).

Using this methodology, it was possible to single out the different criticalities present in the considered cities in relation to the characteristics of each urban area.

The next step of this study will be to extend the validate method to polychlorinated biphenyls (PCBs) and other organic compounds contained in PM.

References

[1] D.W. Dockery, C.A. Pope, X. Xu, J.D. Spengler, J.H. Ware, M.E. Faye, F.E. Speizer, J. Med. 329 (1993) 1753.
[2] J.F. Gamble, Environ. Health Perspect. 106 (1998) 535.
[3] G. Oberdorster, Arch. Occup. Emviron. Health 74 (2001) 1.
[4] Polynuclear Aromatic Compound. Part 1. Chemicals, Environmental and Experimental data. Monograph vol.32, IARC, Lyon, 1984.
[5] R. Westerholm, A. Christensen, M. Törnqvist, L. Ehrenberg, U. Rannug, M. Sjögren, J. Rafter, C. Soontjens, J. Almén, K. Grägg, Environ. Sci. Technol. 35 (2001) 1748.
[6] Overall Evaluation of Carcinogenicity: An Updating of IARC Monographs, IARC, Lyon, 1987.
[7] M.E. Gutiérrez-Castillo, D.A. Roubicek, M.E. Cebrián-García, A. De Vizcaya-Ruíz, M. Sordo-Cedeño, P. Ostrosky-Wegman, Environ. Mol. Mutagen. 47 (2006) 199.
[8] L. Risom, P. Møller, S. Loft, Mutat. Res. Fundam. Mol. Mech. Mutagen. 592 (2005) 119.
[9] L. Pozzoli, S. Gilardoni, M.G. Perrone, G. de Gennaro, M. de Rienzo, D. Vione, Ann. Chim. 94 (2004) 17.
[10] K.A. Van Cauwenberghe, in: A. Bjorset, T. Ramdahl (Eds.), Handbook of Polycyclic Aromatic Hydrocarbons, Emission Sources and Recent Progress in Analytical Chemistry, vol. 2, Marcel Dekker, New York, Basel, 1985, p. 351.
[11] P. Bruno, M. Caselli, G. de Gennaro, M. de Rienzo, A. Traini, J. Environ. Monit. 2 (2000) 223.
[12] P. Bruno, M. Caselli, G. de Gennaro, M. de Rienzo, P. Ielpo, D. Manigrassi, Ann. Chim. 92 (2002) 815.
[13] S. Karthikeyan, R. Balasubramanian, S.W. See, Talanta 69 (2006) 79.
[14] M. Shimmo, P. Antiila, K. Hartonen, T. Hyotylainen, J. Paatero, M. Kulmala, M. Riekkola, J. Chromatogr. A 1002 (2004) 151.
[15] M. Zheng, M. Fang, F. Wang, K.L. To, Atmos. Environ. 34 (2000) 2691.
[16] A.M. Caricchia, S. Chiavarini, M. Pezza, Atmos. Environ. 33 (1999) 3731.
[17] J. Jacob, Method Development for the Determination of Polycyclic Aromatic Hydrocarbons (PAHs) in Environmental Matrices. Quality Assurance for Environmental Analysis, Elsevier, Amsterdam, 1995, p. 563.
[18] R. Romero, R. Sienra, P. Ritcher, Atmos. Environ. 36 (2002) 2375.
[19] M.C.H. Lim, G.A. Ayoko, L. Morawska, Atmos. Environ. 39 (2005) 463.
[20] M.G. Perrone, E. Bolzacchini, V. Gianelle, G. Mognaschini, J. Aerosol Sci. 35 (Suppl. 2) (2004) S1073.
[21] M. Tutino, Determination of atmospheric pollutants: volatile organic compounds and polycyclic aromatic hydrocarbons, Ph.D. Thesis, Department of Chemistry, University of Bari, Italy, 2005.
[22] Ministry Decree of 25 November 1994, Gazzetta Ufficiale n. 290, 13 December 1994, Aggiornamento delle norme tecniche in materia di limiti di concentrazione e di livelli di attenzione e di allarme per gli inquinamenti atmosferici nelle aree urbane e disposizioni per la misura di alcuni inquinanti di cui al decreto ministeriale 15 aprile 1994.
[23] S.O. Bae, R.A. Field, M.E. Goldstone, P.W. Kirk, J.N. Lester, R. Perry, Water, Air, Soil Pollut. 60 (1991) 279–300.

Available online at www.sciencedirect.com
ScienceDirect
Talanta 72 (2007) 1586–1592
Talanta
www.elsevier.com/locate/talanta

Glassy carbon electrodes modified with composites of starburst-PAMAM dendrimers containing metal nanoparticles for amperometric detection of dopamine in urine

Erika Bustos Bustos [a], Ma. Guadalupe García Jiménez [b], Blanca R. Díaz-Sánchez [c], Eusebio Juaristi [c], Thomas W. Chapman [a], Luis A. Godínez [a,*]

[a] *Electrochemistry Department, Centro de Investigación y Desarrollo Tecnológico en Electroquímica S.C., P.O. Box 064, C.P. 76700, Pedro Escobedo, Querétaro, Mexico*
[b] *Electrochemistry Department, Centro de Investigaciones Científicas, Universidad de Guanajuato, C.P. 36040, Guanajuato, Mexico*
[c] *Chemistry Department, Centro de Investigación y de Estudios Avanzados del I.P.N., P.O. Box 14-740, C.P. 07000, México, D.F., Mexico*

Received 16 October 2006; received in revised form 5 February 2007; accepted 6 February 2007
Available online 20 February 2007

Abstract

Composites of hydroxyl-terminated PAMAM dendrimers, generation 4.0 (64 peripheral OH groups) containing either Ir, Pt or Rh nanoparticles were synthesized and characterized in solution. Each one of these composites was then immobilized on a glassy carbon electrode (GC) and incorporated as an amperometric detector for dopamine in a high-performance liquid chromatograph (HPLC). Comparison of the analytical performance of the novel electrochemical detectors with a typical UV–vis optical detector for dopamine revealed that the sensitivity of the GC electrode modified with dendrimer-Rh composite is comparable to that of the spectroscopic detector, with a detection limit of 0.15 μM, and is linear up to at least 1.0 mM ($R^2 = 0.998$). Furthermore, it was found that the electroanalytical approach suffers minimal matrix effects that arise in the analysis of dopamine in samples of urine.

Keywords: Dopamine; HPLC; PAMAM dendrimers; Dendrimer-nanoparticle composites

1. Introduction

Dopamine (DA) is a neurotransmitter that plays an important role in the functioning of the central nervous system as well as in the cardiovascular, renal and hormonal systems [1]. Analytical methods are desired for the direct determination of this substance for the monitoring of its level in patients. High-performance liquid chromatography (HPLC) is the most important analytical technique for this purpose as it is able to resolve mixtures with a large number of similar analytes in a short time. An HPLC detector should be able to determine the presence of an eluted substance quantitatively as well as to indicate deviations from a baseline calibration [2]. Spectroscopic [3] and electrochemical [4] sensors may be used as detectors in HPLC to allow sensitive detection of dopamine in urine samples, but they each present drawbacks. With the former interferences arise from the optical absorption by other compounds in the sample matrix. With electrochemical detection one may encounter adsorption on the electrode surface that causes passivation. To eliminate such problems (matrix effects), samples generally require pretreatment by chemical or physico-chemical methods [2], thus making the analysis less efficient and more cumbersome.

One promising approach for eliminating matrix effects in an electrochemical detector consists of modifying the electrode surface with monolayers of polyamidoamine (PAMAM) dendrimers that can interact specifically with the target molecules and exclude interfering species from the surface. This approach relies on the fact that dendrimers, being structured macromolecules capable of forming thin porous films on electrode surfaces, can absorb organic target species but block undesired

* Corresponding author. Tel.: +52 442 211 6006; fax: +52 442 211 6007.
E-mail address: lgodinez@cideteq.mx (L.A. Godínez).

0039-9140/$ – see front matter © 2007 Elsevier B.V. All rights reserved.
doi:10.1016/j.talanta.2007.02.017

adsorption on the substrate surface while allowing electron-transfer processes to occur [5,6]. In addition to their interesting electrode-modification properties, PAMAM dendrimers can also be used to prepare and accommodate catalytic nanoscale metallic particles as Crooks and co-workers have readily demonstrated. These monodisperse metal-particle-dendrimer nanocomposites have been shown to catalyze specific reactions of alcohols [7] and oxygen [8] by conveniently avoiding particle aggregation and the blocking of active sites on the surface of the metallic clusters, thus increasing the catalytic efficiency [9].

In this work we compare the performance of dendrimer-nanoparticle-modified amperometric electrodes with a conventional optical detector in terms of the detection and quantification of dopamine in synthetic aqueous solution and in samples of urine by high-performance liquid chromatography (HPLC). The modified glassy carbon electrodes studied here were prepared by nucleophilic attachment of hydroxylated G4.0 PAMAM dendrimers containing metal nanoparticles of Ir, Pt, or Rh. The metal nanoparticles serve as electrocatalysts for the electro-oxidation of dopamine. By supporting the particles in the tethered dendrimer film, one can avoid passivation phenomena and related matrix effects.

2. Experimental

G4-OH PAMAM dendrimers in a 10–25% methanol solution were purchased from Dendritech, Inc. (Midland, MI), and used as received. The metal particle precursors $(NH_4)_3IrCl_6{\cdot}xH_2O$, K_2PtCl_4, $(NH_4)_3RhCl_6{\cdot}xH_2O$ were obtained from Strem Chemicals, Inc., and $NaBH_4$, NaF, KCl, $K_3Fe(CN)_6$ and H_2SO_4 were obtained from J.T. Baker. All aqueous solutions were prepared with deionized water ($\rho \geq 18\,M\Omega\,cm$). Reagent-grade dopamine (DA) was obtained from Sigma.

The HPLC equipment was a 1050 Hewlett-Packard instrument, fitted with a Supelco Inc. Hypersil C-18 BDS column (250 mm × 4.6 mm, 5 μm), operated with flowrate of 0.5 mL min^{-1} at 328 K and at a pressure of 80 psi, and controlled by ChromGraph 95/98 v2.0.01 software. The sample volume was 20 μL. The instrument was equipped with both a conventional spectroscopic detector (UV-Vis 116A) and an amperometric detector (BAS epsilon Trade Mark) mounted in series. The latter employed a glassy carbon (GC) working electrode (0.2827 cm^2, BAS MF1000 model), a stainless-steel counter electrode, and an Ag/AgCl (3 M NaCl) reference electrode in a BAS CC-5 thin-layer, laminar-flow cell. The mobile phase was prepared with 475 mL of H_2O, 4.7 mg of monochloroacetic acid, 75 mg of sodium octylsulfate, 93 mg of disodium ethylenediaminetetraacetate dihydrate (EDTA), 25 mL MeCN and 4 mL tetrahydrofuran (adjusted to pH 3.2 with 6 M NaOH), mixed in a 1:1 ratio with water. Calibration curves were obtained by standard-addition techniques [4]. At the end of each experiment with synthetic samples, the column was washed with water, then with a mixture of 30% water with 70% MeOH for at least 10 min or until no UV–vis signal was indicated. Prior to the analysis of biological samples, the column was washed with MeCN for 15 min or until the disappearance of the UV–vis signal.

Fourier transform infrared external reflection spectroscopy (FTIR-ERS) measurements of the electrode surface were performed using a Nicolet Spectrometer equipped with a reflection accessory. All spectra comprised an average of 250 individual scans with p-polarized light at an 80° angle of incidence with respect to the GC substrate.

UV–vis spectra were recorded at 298 K using an Agilent Model 8453 UV–vis spectrophotometer with diode-array detector, 2-nm resolution, and a wavelength range of 250–950 nm. Less than 0.03% stray light was standard.

Cyclic and steady-state voltammetry and electrochemical impedance spectroscopy experiments were conducted in a 10 mL glass cell with BAS glassy carbon (GC), platinum wire, and Ag/AgCl (3 M NaCl) installed as working, counter, and reference electrodes, respectively. The cyclic voltammetry (CV) and amperometric experiments were controlled using a BAS Epsilon Trade Mark potentiostat from Bioanalytical Systems, Inc. Electrochemical Impedance Spectroscopy (EIS) was carried out employing a BAS-Zahner IM6(e) impedance instrument. Before each electrochemical experiment, the electrolytic solutions were deoxygenated by bubbling ultra-pure nitrogen (PRAXAIR, grade 5.0) for at least 10 min, and during electrochemical experiments N_2 was blown gently over the solution surface.

The EIS measurements were performed on modified GC electrodes using a 10 mV amplitude wave around the equilibrium potential of the $Fe(CN)_6^{3-/4-}$ redox couple in an aqueous solution containing this electroactive probe (1 mM $K_3Fe(CN)_6$) in 0.1 M KCl. The range of frequencies applied was from 0.1 Hz to 100 kHz, and impedance values were recorded at 500 discrete frequencies per decade. The charge-transfer resistance R_{ct} and the total capacitance C_t, which is approximately equal to the capacitance of the particles in the dendrimer film (C_f) plus that of the double-layer (C_{dl}), were obtained by fitting the experimental impedance data to the Randles equivalent-circuit model included in the BAS-Zahner software. The Randles equivalent circuit, while not the only model possible, has frequently been employed to represent modified electrochemical interfaces and in the present case provided an excellent fit to the data [10,11].

Scanning electron microscopy (SEM) and emission diffraction X-ray (EDX) experiments were carried out with a JEOL scanning electron microscope, Model JSM-5400LV, using an acceleration voltage of 15 kV with 2000× augmentation.

3. Results and discussion

Fig. 1 illustrates the methodology for the modification of glassy carbon (GC) with dendrimer-encapsulated nanoparticles (DENs). Following previous reports in the literature, DENs in solution were prepared in three steps [8,12]: (1) ion-dendrimer complex preparation, (2) reduction of the ions encapsulated within the dendrimer molecules, and (3) dialysis to purify the DENs. In the first step, stock solutions were prepared containing 2.0 mM of each metal salt with 50 μM PAMAM G4-OH. These were stirred for 65 h to allow the metallic ions to complex with the internal amines of the dendrimer molecules. In the second step, zero-valent metallic nanoparticle-dendrimer composites

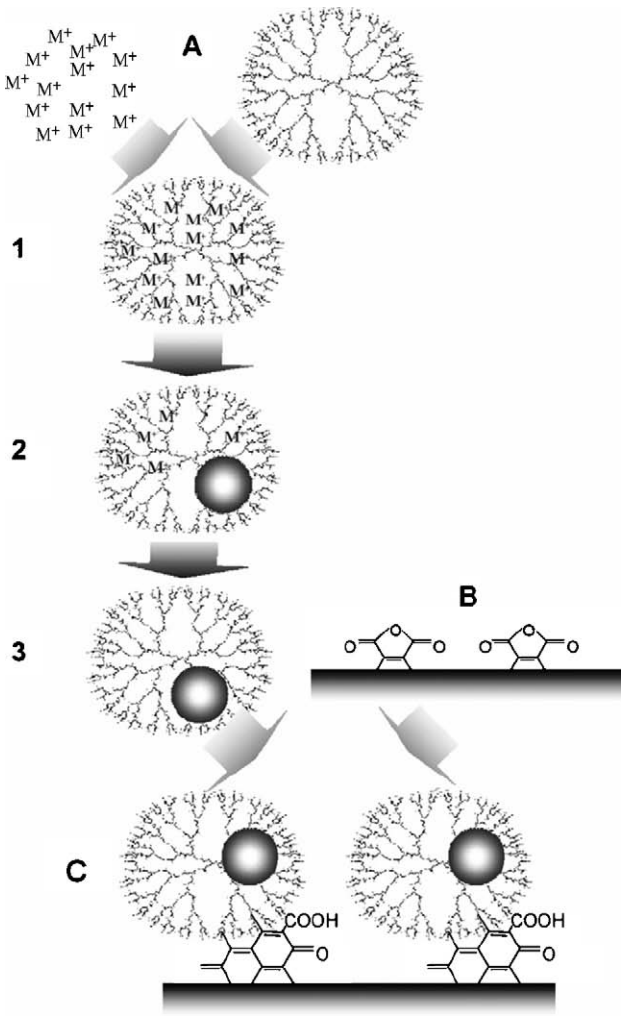

Fig. 1. Schematic representation of the methodology used to prepare the DEN-modified GC electrode (C) from (A) dendrimer-encapsulated nanoparticles (DENs) and (B) electrochemically treated glassy carbon. Numbers correspond to the following DEN preparation stages: (1) ion-dendrimer complex formation, (2) chemical reduction of the ions, and (3) dialysis to purify the DENs.

were synthesized by slow addition of 2.0 mL of aqueous 0.5 M $NaBH_4$ solution. Each of the resulting DEN solutions was allowed to stand in a closed vial for 12 h with the pH adjusted to 1.0 (with HCl) in order to ensure the dissolution of any precipitate. Finally, in the third step, the solution was dialyzed for 48 h using a cellulose dialysis sack having a molecular weight cutoff of 12,000 (Sigma Diagnostics, Inc.) in order to remove impurities. This methodology is simple and leads to robust, catalytically active DENs (Fig. 1A).

In order to follow progress of the DEN preparation process, UV–vis spectroscopy experiments were performed for each salt studied [9]. The d–d transition peaks of the metal–ligand interactions of the relevant cation in aqueous solution, which appear in the visible region, change substantially upon complexation of the metal ions with the internal amine groups of the dendrimer molecule. After chemical reduction with borohydride, a new signal appears at shorter wavelengths, around 300 nm [13], and this signal exhibits particularly strong optical extinction coefficients for Ir, Pt, and Rh, which were found to be 5863, 7868 and 10,446 $M^{-1}\,cm^{-1}$, respectively. These values in the UV spectral range, due to resonantly driven electron plasma oscillations, were similar to those reported in the literature [9]. The plasmon resonance band is known to be dependent on the size, shape, and material properties of the metal nanoparticles as well as the surrounding medium [14–16] and is characterized by a steep decrease with increasing wavelength. This pattern suggests that the reduced metallic species do not exist as isolated atoms but rather as dendrimer-encapsulated metallic clusters [13,17].

The glassy carbon (GC) electrodes were prepared for surface modification with DENs by sequentially polishing the electrode on a polishing cloth (Buehler) with 1.0, 0.3, and 0.05 μm alumina (Buehler) in deionized water followed by sonification in a glass vessel for 10 min [18]. This methodology results in relatively clean GC surfaces characterized by several functional groups on the surface [19–23]. It is desirable to improve the chemical homogeneity of the surface and to enhance its reactivity necessary for the nucleophilic substitution between the GC and the DENs in a later stage of preparation [24]. In order to investigate their electrochemical reactivity, CV experiments were performed with these electrodes in an acidic aqueous solution (0.5 M H_2SO_4 at 298 K). Voltammetric responses are observed in three different potential windows, by which one can identify the formation of hydroquinone, phthalic anhydride, and carboxylic acid surface species at their characteristic potentials (0.6 V, 1.6 and 2.2 V versus Ag/AgCl/3 M NaCl, respectively). Based on this information, the application of a potential of 1.6 V versus Ag/AgCl for 1 h was selected to promote the phthalic anhydride functionalization of the GC surface [19]. As can be seen by comparison of the IR spectra (data not shown), this electrochemical treatment of the surface increases effectively the presence of the phthalic anhydride groups (from C–O–C, C–O and C=C vibrations) [20–23]. An approximate value for the surface coverage by phthalic anhydride groups was estimated to be 5.8×10^{-8} mol cm^{-2}, obtained from the charge obtained in the CV oxidation peak at 1.6 V versus Ag/AgCl, assuming transfer of four electrons. Furthermore, in comparison with other methods, the pre-treatment of the GC at 1.6 V was found to produce the greatest anodic charge in CVs with electrodes subjected to the PAMAM G4.0-OH modification protocol, indicating the best dendrimer coverage (Fig. 1B).

Nucleophilic attachment of the various DENs considered in this study to the pre-treated GC electrode surfaces was accomplished in the following stage by polarizing the substrate for 1 h at 1.6 V (versus Ag/AgCl) in a 0.1 M NaF aqueous solution also containing 20 μM of the relevant DEN [24]. The dendrimers interact directly with the phthalic anhydride groups on the surface to bind the DENs (Fig. 1C). To estimate the effective fractional coverage of the dendrimer-nanoparticle composite on the surface, an impedance analysis was performed. The resulting Nyquist plots were fit by the Randles equivalent-circuit model using a Simulation/Complex Nonlinear Least Squares SIM/CNLS program to estimate the physical parameters of the surface. For naked GC, a 45° line characteristic of Warburg diffusion dominates almost the entire range of frequencies, and there is only a barely discernible semicircle at high frequencies. The dominance of the Warburg impedance indicates that

the $Fe(CN)_6^{3-/4-}$ redox reaction is diffusion-controlled over a broad frequency range.

Estimation of the relative fractional coverage of the surfaces by dendrimer and by metal-dendrimer composites was accomplished by comparing the charge-transfer resistances indicated by the impedance measurements. The fraction of the surface blocked by adsorbed dendrimer that contains no catalytic metal (Θ) was calculated from the equation:

$$\Theta = \frac{R_{ct} - R_{ct}^0}{R_{ct}} \quad (1)$$

where R_{ct}^0 and R_{ct} are the charge-transfer resistances for the redox-probe reaction measured on a naked GC electrode and that on the coated electrode, respectively. This equation is derived from a model that assumes a heterogeneous surface composed of a fractional area that fully blocks electron transfer (Θ) and a fractional area that is completely accessible to the redox-probe molecule ($1 - \Theta$) [10]. In this case, the model requires the assumption that the surface covered by dendrimer containing metal nanoparticles passes current as readily as the bare GC but that dendrimer without nanoparticles does not allow any current to pass. Comparison of the results obtained for the different DENs shows that the effective fractional surface coverage accessible to the redox-probe molecule ($1 - \Theta$), as estimated from these indirect measurements, increases in the order: Ir < Pt < Rh (0.03, 0.04 and 0.55, respectively). The results of this analysis are not entirely consistent in that the GC electrode coated solely with dendrimer exhibits a resistance lower than that with Ir and Pt, but it is nevertheless clear that the Rh-coated electrode provides the best electrocatalysis among the dendrimer films.

Modified GC electrodes were prepared with each one of the DENs under study, and the presence of the nanoparticles was corroborated by the appearance of aggregates in SEM microphotographs and the elemental signals of the metals from EDX microanalysis (data not shown). It is seen again that the Rh film achieved the best coverage of nanoparticles, followed by Pt and then by Ir.

The three forms of DEN-modified GC electrode were tested as amperometric detectors of DA in the BAS cell with the HPLC apparatus and compared with the performance of a standard spectroscopic detector. The DA measurement parameters for spectroscopic and electrochemical detection were obtained from UV–vis spectra and CV tests. DA can be detected optically and quantified from an absorbance signal at 281 nm. The electrochemical response of DA was examined using the bare GC electrode in CV and in a stirred BAS cell. Based on the latter results, the amperometric detector was operated at a potential of 900 mV versus Ag/AgCl to attain the mass-transfer limiting current for the dopamine oxidation reaction, $DA - 2e^- \rightarrow DOQ + 2H^+$, where DOQ is the *o*-quinone form of DA [1]. The CV response of each of the forms of GC electrode studied indicated that the rhodium DEN presents the best electrocatalysis for DA oxidation, as indicated by the greatest peak current compared with the other electrodes.

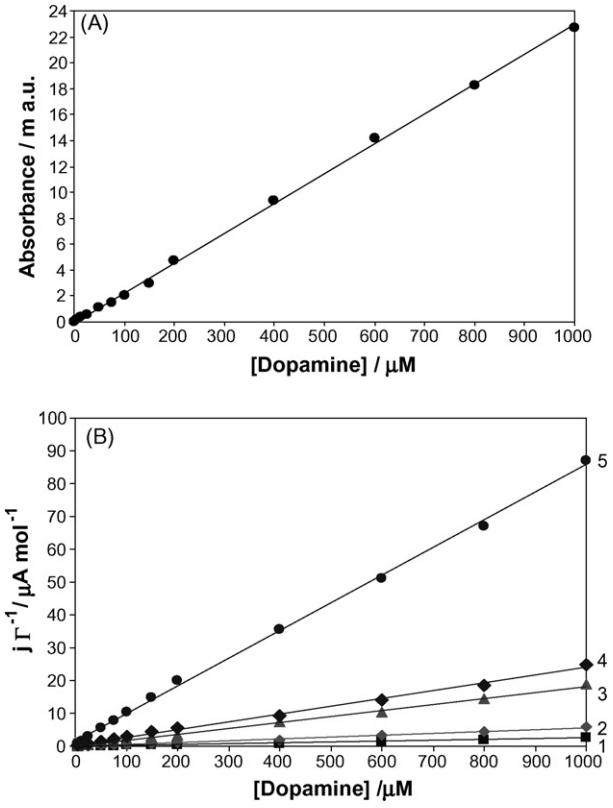

Fig. 2. Spectroscopic (A) and amperometric (B) HPLC calibration curves for synthetic aqueous solutions of DA. The electrochemical data were obtained using the various electrodes: (1) GC, (2) GC-(G4.0-OH), (3) GC-DEN-Ir, (4) GC-DEN-Pt, and (5) GC-DEN-Rh.

With the optical and amperometric detectors assembled in series, HPLC calibration curves for both were obtained with synthetic-sample solutions at an elution time for DA of 13 min. The results are shown in Fig. 2 and given in Table 1, from which it can be clearly seen that the performance of the GC-DEN-Rh-modified electrode showed the best response with greatest sensitivity according to the slopes of the curves for the electrochemical detection of DA (Fig. 2B–5). The sensitivity was

Table 1
Detection (D.L.) and quantification limits (Q.L.) for the electrochemical and spectrophotometric detection of DA in HPLC analysis of synthetic samples

Detector	Equation y (μA cm^{-2}) = mx (μM) + b	R^2	D.L. (μM)	Q.L. (μM)
UV–vis	y (m a.u.) = 0.0198x + 0.0589	0.997	0.14	0.47
GC	y = 0.0027x − 0.0576	0.994	3.01	10.02
GC-(G4-OH)	y = 0.0053x − 0.1153	0.994	1.72	5.73
GC-DENs-Ir	y = 0.0178x + 0.0308	0.998	0.29	0.97
GC-DENs-Pt	y = 0.0228x + 0.3365	0.997	0.25	0.82
GC-DENs-Rh	y = 0.0458x + 0.0995	0.998	0.15	0.51

comparable to that obtained with spectrophotometric measurement (detection limit of 0.15 μM) and greater than that with GC-DEN-Pt, GC-DEN-Ir, GC-(G4.0-OH), or the naked GC electrode, by factors of 2, 3, 9 and 17, respectively, as it can be seen in Table 1. This result is consistent with the relative values obtained for fractional surface coverage by the DENs obtained by impedance experiments (Table 1). Thus, it appears that the electrocatalysis is primarily a consequence of the quantity of electroactive material present on the surface of the GC.

To confirm the importance of the PAMAM dendrimer films in the observed electrocatalytic effect, the DEN-modified electrodes were treated thermally at 348 K for 72 h, which should promote selectively the conversion of the tetraester of the polymeric molecules to the corresponding triester via a retro-Michael reaction [25]. The idea behind these experiments was to destroy the dendrimer structure of the DEN-modified electrodes and to observe the resulting difference in the electrocatalytic activity of the film, thus verifying the importance of the dendrimer-nanoparticle matrix for a good analytical response. Fig. 3 compares the HPLC calibration curve obtained for the GC-DEN-Rh electrode after the thermal treatment with those for a clean GC, a dendrimer-coated GC electrode, and the original GC-DENs-Rh modified electrode. It is seen that the thermal treatment reduces the sensitivity of the electrode and that the linearity of the calibration curve is lost. Presumably the degradation of the dendritic structure of the electrocatalytic film allows the nanoparticles to be lost or to passivate, causing a loss of activity. EDX results, presented in Fig. 4, show that rhodium remained on the surface after the thermal treatment, but SEM images reveal a change in the distribution and size of the aggregates, indicating the passivation of the catalyst. Measurements with GC and the GC-PAMAM-G4.0-OH surface, which do not show any metal species present, are included for comparison.

Given that the GC-DEN-Rh electrode offers sensitivity for DA detection comparable to that of the optical method in synthetic DA samples, its application was tested in the HPLC with samples of urine without any pre-treatment. The standard-addition technique was used with the biological samples, which

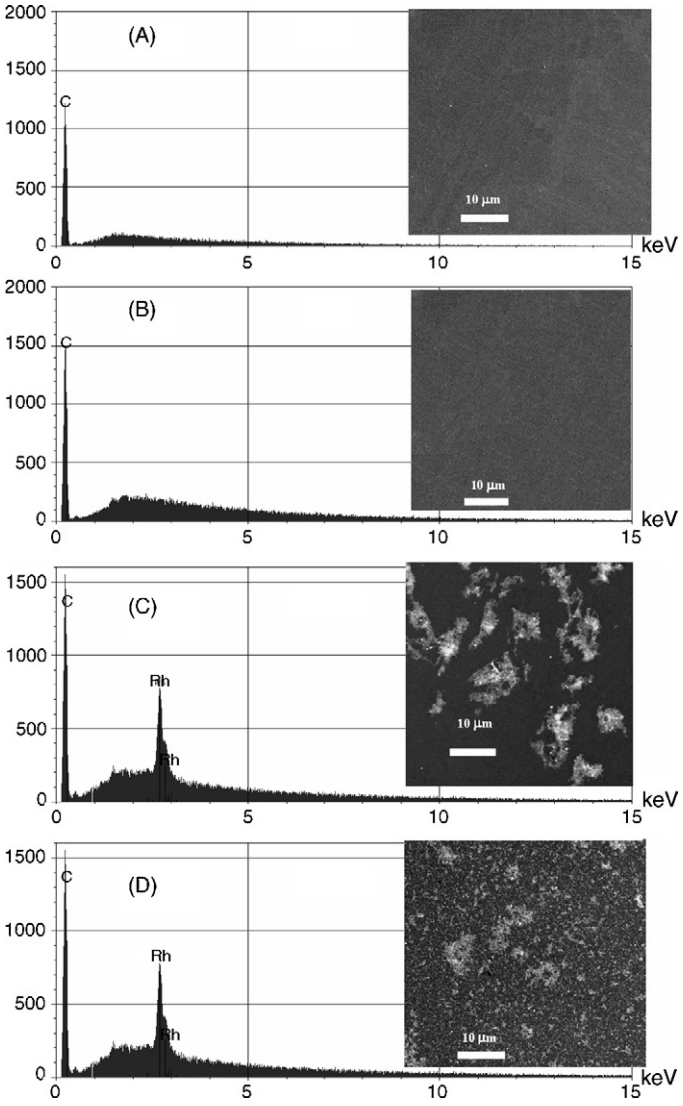

Fig. 4. EDX spectra and SEM images for the following surfaces: (A) GC, (B) GC-(G4.0-OH), (C) GC-DEN-Rh before, and (D) GC-DEN-Rh after thermal treatment at 348 K for 72 h. The experiments were made using an acceleration voltage of 15 kV and 5000× augmentation.

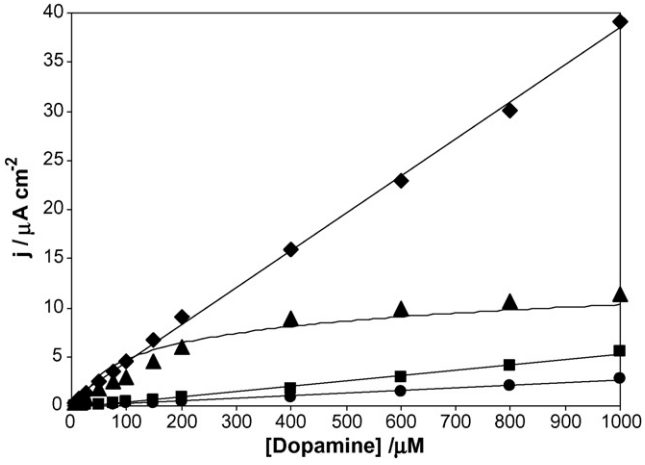

Fig. 3. HPLC calibration curves for the amperometric detection of DA with the following electrodes: (●) GC, (■) GC-(G4.0-OH), (♦) GC-DEN-Rh, and (▲) GC-DEN-Rh after thermal treatment at 348 K for 72 h.

involves measuring the HPLC response as known amounts of the target compound are added to samples of the unknown to be determined [2]. The objective was to compare the relative performance of the new amperometric detector with that of the optical method when potentially interfering species are present in the sample. In agreement with the results obtained with the synthetic DA solutions, the GC-DEN-Rh modified electrode again showed the best sensitivity among the DEN-modified electrodes surveyed.

Fig. 5A shows the HPLC standard-addition curve obtained by optical detection with the synthetic DA solutions compared with that obtained with a urine sample. It is seen that the slope of the curve changes in the former case (from 0.0198 to 0.0398), indicating a shift in sensitivity because of the solution matrix apparently introduces at the same wavelength proportional and systematic deviations caused by additional compounds in the urine sample [2]. The insert (i) in Fig. 5 shows that the response

Table 2
Detection (D.L.) and quantification limits (Q.L.) for the spectroscopic (A) and electrochemical (B) detection of DA in HPLC analysis of urine samples, using the DEN-Rh-modified GC electrode

Detector	Equation	R^2	D.L. (μM)	Q.L. (μM)
A	y (m a.u.) = 0.0398x (μM) + 1.0143	0.999	0.07	0.23
B	y (μA cm^{-2}) = 0.0431x (μM) + 1.0391	0.997	0.16	0.54

of the optical detector contains at least one extraneous peak on the shoulder of the DA signal. Whereas the synthetic-solution calibration curve would indicate from the response with the original sample, 1.0 m a.u., that the sample concentration was close to 50 μM, extrapolation of the standard-addition line to the X-axis indicates that the concentration of DA in the urine sample was only 25 μM.

Fig. 5B shows the comparable standard-addition curves obtained with the GC-DEN-Rh electrode in the amperometric detector. It is seen that the slopes are nearly the same at 0.0458 and 0.0431 for synthetic and biological samples, respectively,

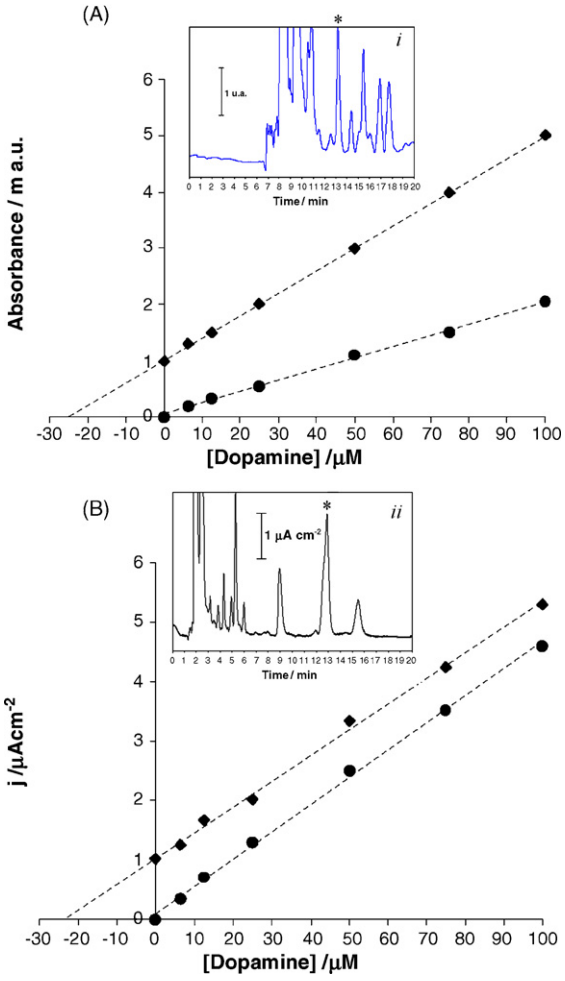

Fig. 5. Standard-addition HPLC DA calibration curves for (●) synthetic DA and (♦) urine samples by (A) optical absorption at 281 nm and by (B) amperometric measurement at 900 mV (vs. Ag/AgCl) on a GC-DEN-Rh-modified electrode. The inserts present chromatograms produced by the spectroscopic (i) and electrochemical (ii) detectors for a urine sample. The DA signal (*) appears at an elution time of 13 min.

indicating that the urine matrix has little effect on the amperometric measurement. There is little if any interference with the electrochemical signal by the additional compounds present in the urine sample, thus providing selectivity for amperometric detection of dopamine at 900 mV. Extrapolation of the upper, standard-addition line indicates a DA concentration in the sample of about 25 μM. This value is close to the concentration indicated by the synthetic-sample calibration curve obtained for an output of 1 μA cm^{-2}. Furthermore, insert (ii) shows that the electrochemical output signal is much cleaner at the DA elution time than is the optical signal.

Table 2 compares the equations fit to the two standard-addition lines of Fig. 5 obtained with the real biological specimen. In this case, the sensitivity, i.e. the slope, of the optical measurement appears to be greater than that with the synthetic samples. Furthermore, the detection limit of the optical method, derived from the scatter of experimental points around the linear fit shown in Table 2, seems to be somewhat lower than that for the amperometric technique. Nevertheless, the shift in the slope suggests that the optical method is more susceptible to interfering matrix effects.

In conclusion, GC electrodes modified with composites of dendrimer and metallic nanoparticles (DENs) show good performance in detecting DA in both synthetic and clinical urine samples. Compared with the typical spectroscopic detection in HPLC analyses, the amperometric method offers a detector that appears to be less susceptible to matrix effects. Among the three DEN-modified electrodes surveyed in this study, the best electrocatalytic nanocomposite film was found to be that based on GC-DEN-Rh. Our research group is currently working to determine optimal conditions for obtaining stability and durability of these sensors for long-term use as electroanalytical HPLC detectors for dopamine and other compounds with biological importance, preferably without the requirement for sample pretreatment.

Acknowledgements

The authors are grateful to Consejo Nacional de Ciencia y Tecnología (CONACyT, Grant 45157) for financial support of this work. EB and BD are also grateful to CONACyT for their doctoral scholarships. TWC is a CONACyT Cooperante in CIDETEQ under the sponsorship of the U.S. Peace Corps.

References

[1] S.S. Kumar, J. Mathiyarasu, K.L. Phani, J. Electroanal. Chem. 578 (2005) 95.

[2] V.R. Meyer, Practical High-Performance. Liquid Chromatography, 3rd ed., John Wiley & Sons, West Sussex, England, 1998.
[3] R. Zhu, W.T. Kok, Anal. Chem. 69 (1997) 4010.
[4] T.J. O'Shea, M.W. Telting-Díaz, S.M. Lunte, C.E. Lunte, Electroanalysis 4 (1992) 463.
[5] H. Maeda, K. Katayama, R. Matsui, Y. Yamauchi, H. Ohmori, Anal. Sci. 16 (2000) 293.
[6] E. Bustos, J. Manríquez, G. Orozco, L.A. Godínez, Langmuir 21 (2005) 3013.
[7] R.W.J. Scott, A.K. Datye, R.M. Crooks, J. Am. Chem. Soc. 125 (2003) 3709.
[8] H. Ye, R.M. Crooks, J. Am. Chem. Soc. 127 (2005) 4930.
[9] R.M. Crooks, B.I. Lemon III, L. Sun, L.K. Yeung, M. Zhang, Dendrimer-Encapsulated Metals and Semiconductors: Synthesis Characterization and Applications, Springer, New York, 2001, p. 89.
[10] H. Tokuhisa, M. Zhao, L.A. Baker, V.T. Phan, D.L. Dermody, M.E. Garcia, R.F. Peez, R.M. Crooks, Th.M. Mayer, J. Am. Chem. Soc. 120 (1998) 4492.
[11] L.V. Protsailo, W.R. Fawcett, Electrochim. Acta 45 (2000) 3497.
[12] R.M. Crooks, J. Phys. Chem. B 109 (2005) 692.
[13] M. Zhao, R.M. Crooks, Angew. Chem. Int. Ed. 38 (1999) 3.
[14] B. Lamprecht, G. Schider, R.T. Lechner, H. Ditlbacher, J.R. Krenn, A. Leitner, F.R. Aussenegg, Phys. Rev. Lett. 84 (2000) 4721.
[15] M. Barbic, J.J. Mock, D.R. Smith, S.J. Schultz, J. Appl. Phys. 91 (2002) 9341.
[16] J.D. Kottman, O.J.F. Martin, D.R. Smith, S. Schultz, Chem. Phys. Lett. 341 (2001) 1.
[17] K. Esumi, A. Suzuki, A. Llamaría, K. Torigue, Langmuir 16 (2000) 2604.
[18] G.K. Kiema, G. Fitzpatrick, M.T. McDermott, Anal. Chem. 71 (1999) 4306.
[19] K. Kinoshita, Carbon: Electrochemical and Physicochemical Properties, John Wiley & Sons, USA, 1988.
[20] Y. Yang, Z.G. Lin, J. Appl. Electrochem. 25 (1995) 259.
[21] V.M. Jovanovic, S. Terzic, A.V. Tripkovic, K.D. Popovic, J.D. Lovic, Electrochem. Commun. 6 (2004) 1254.
[22] H. Maeda, Anal. Sci. 16 (2000) 293.
[23] P. Chen, R.L. McCreery, Anal. Chem. 68 (1996) 3958.
[24] R.T. Morrison, R.N. Boyd, Química Orgánica, 2nd ed., Adisson Iberoamericana, USA, 1987, p. 811.
[25] J. Peterson, V. Allikmaa, T. Pehk, M. Lopp, Proc. Estonian Acad. Sci. Chem. 3 (2001) 167.

Available online at www.sciencedirect.com
ScienceDirect
Talanta 72 (2007) 1410–1415
Talanta
www.elsevier.com/locate/talanta

A new electrochemiluminescent sensing system for glucose based on the electrochemiluminescent reaction of bis-[3,4,6-trichloro-2-(pentyloxycarbonyl)-phenyl] oxalate

Zhihuang Chen, Jian Wang, Zhenyu Lin, Guonan Chen *

Ministry of Education Key Laboratory of Analysis and Detection Technology for Food Safety, and Department of Chemistry, Fuzhou University, Fuzhou, Fujian 350002, China

Received 29 November 2006; received in revised form 19 January 2007; accepted 19 January 2007
Available online 30 January 2007

Abstract

In this paper, the electrochemiluminescence (ECL) behavior of bis-[3,4,6-trichloro-2-(pentyloxycarbonyl)-phenyl] oxalate (BTPPO) at glassy carbon electrode (GCE) in phosphate buffer solution in the presence of hydrogen peroxide has been investigated when linear sweep voltammetry was applied. The optimum chemical conditions and electrochemical parameters for this ECL system have been investigated in detail. Under the optimum conditions, it was found that the concentration of BTPPO was linear with the ECL intensity in the range of 3.0×10^{-6} to 3.0×10^{-4} mol/L, and the detection limit (S/N = 3) for BTPPO was 1.0×10^{-7} mol/L. The possible mechanism for ECL of BTPPO at the GCE in the presence of hydrogen peroxide was also discussed. Furthermore, based on the fact that glucose oxidase can react with glucose to produce hydrogen peroxide, a new ECL sensing system of BTPPO has been developed for detection of glucose. The enhanced ECL intensity has a linear relationship with the concentration of glucose in the range of 1.0×10^{-4} to 1.0×10^{-3} mol/L, and the detection limit for glucose is found to be 5.0×10^{-5} mol/L (S/N = 3).

Keywords: Bis-[3,4,6-trichloro-2-(pentyloxycarbonyl)-phenyl] oxalate; Electrochemiluminescence; Glucose oxidase; Glucose

1. Introduction

Bis-[3,4,6-trichloro-2-(pentyloxycarbonyl)-phenyl] oxalate (BTPPO) is one of the most efficient chemiluminescent (CL) reagents among the aryl oxalate ester compounds [1]. Since the CL systems based on the reaction between various oxalic acid derivatives and hydrogen peroxide in the presence of a suitable fluorophore was first described by Chandross [1] in 1963, and the further developments of this chemistry was made by Rauhut and co-workers [2–5], more efficient reagents have become available for what is now referred to as peroxyoxalate chemiluminescence (POCL). Then there are many papers reported about the CL of peroxide oxalate [6–12]. Mechanism studies of oxalate CL systems have indicated that peroxyoxalate derivatives can be formed during the reaction, depending on the reactants and reaction conditions, and indicated that the concerted multiple bond cleavage decomposition of such intermediates is the source of the large and synchronous energy release required for electronic excitation of the emitting fluorescer [2,3]. Due to the highly efficient as a CL system, the POCL enables the excitation of various fluorophores to have emission wavelengths from the ultraviolet to near infrared, which facilitates its utilization for numerous analytical applications [13–16]. In addition, the POCL has also been used for the detection of hydrogen peroxide [17,18] and fluorescent compounds [19,20].

Electrochemiluminescence (ECL), also known as electrogenerated CL, has become an important detection method in analytical chemistry in recent years [21–26]. In comparison to CL, many of the properties of ECL are very similar to those of CL, such as the high sensitivity, but for an ECL reaction the process of CL can be controlled by adjusting the potentials, therefore, ECL method also has high selectivity.

Just like the above statement, there are many papers, which have reported the CL of the aryl oxalate. However, we do not found any papers about the ECL of aryl oxalate. Therefore, the goal of this study was to investigate the ECL behavior of BTPPO

* Corresponding author. Fax: +86 591 83713866.
E-mail address: gnchen@fzu.edu.cn (G. Chen).

0039-9140/$ – see front matter © 2007 Elsevier B.V. All rights reserved.
doi:10.1016/j.talanta.2007.01.051

in the presence of hydrogen peroxide at the glassy carbon electrode. The optimum chemical conditions and electrochemical parameters for this ECL system have been investigated in detail, and the possible mechanism of this ECL system is discussed.

It was found that in the mixture of glucose and glucose oxidase, BTPPO would also give the stronger ECL signal in the absence of hydrogen peroxide, which was attributed to the reaction between glucose and glucose oxidase to produce the hydrogen peroxide. Therefore, the ECL system of BTPPO can be used to detect the hydrogen peroxide generated by enzymatic reaction [27,28], based on which, we developed a new ECL method for detection of glucose.

2. Experimental

2.1. Chemicals and solutions

BTPPO was obtained from Fluka. A stocking solution of 1.0×10^{-3} mol/L BTPPO was prepared by dissolving the solids in ethanol and stored at 4 °C in a refrigerator, to minimize exposure to light and air. Glucose oxidase (GOD, EC, 1.1.3.4, 139 U/mg, from *Aspergillus niger*) was purchased from Sigma. A working solution of H_2O_2 was prepared fresh daily from 30% (v/v) H_2O_2 (Xinke Electrochemical Reagent Factory, Bengbu, China). Working solutions were made by dilution of these stock solutions. All other chemical reagents were of analytical grade or better, double-distilled water was used throughout the experiments.

2.2. Apparatus

ECL intensity versus potential was detected by using a BPCL Ultra-Weak Chemiluminescence Analyzer controlled by a personal computer with BPCL program (Institute of Biophysics, Chinese Academy of Science) in conjunction with a CH Instruments model 660a Electrochemical Analyzer (Shanghai Chenghua Instrument Co., China). The electrochemical analyzer was used for controlling waveforms and potentials. The detail of this ECL detection system has been given in the previous reports [25,29].

A conventional three-electrode system was used as the electrolytic system, which was composed of a glassy carbon electrode as the working electrode, a platinum wire as the counter electrode and an Ag/AgCl (sat. KCl) electrode as the reference electrode. A commercial 5 mL cylindroid's glass cell was used as an ECL cell, and it was placed directly in the front of the photomultiplier tube. The ECL cell was washed with 0.2 mol/L nitric acid and water in sequence before use. Before each measurement, the working electrode was pretreated by polishing their surfaces with aqueous slurries of alumina powders (average particle diameters: 1.0 and 0.3 μm α-Al_2O_3) on the polishing microcloth and rinsed with water to give a smooth electrode surface.

2.3. Procedures

A three electrodes electrochemical cell system was constructed in a standard quartz photocuvette (i.e. ECL cell) to perform electrochemical and ECL measurement simultaneously at room temperature. BTPPO and hydrogen peroxide were mixed just before the experiment in phosphate buffer solution. Linear sweep voltammetry with appropriate parameters (see Table 1) was performed and the ECL signal was recorded simultaneously. The emission at 0.68 V was used as the quantitative analysis.

Table 1
Linear sweep voltammetry parameters

Initial E (V)	Final E (V)	Scan rate (V/s)	Sample interval (V)
0.0	1.2	0.2	0.001

3. Results and discussion

3.1. ECL behavior of BTPPO in the presence of hydrogen peroxide

The ECL of BTPPO was primarily examined at a glassy carbon electrode (GCE) by linear sweep voltammetry (LSV) in phosphate buffer solution. The primary experiments showed that the BTPPO did not give ECL by itself at GCE in the absence of hydrogen peroxide. However, a broad ECL peak of BTPPO could be observed at the GCE in the presence of hydrogen peroxide (see Fig. 1). When the applied potential was at 0.68 V, the ECL intensity reached a maximum value. Therefore, the ECL intensity at 0.68 V was selected for quantitative analysis of BTPPO, because the maximum ECL intensity could be measured conveniently.

3.2. Selection of electrochemical parameters

The linear sweep voltammetry and square wave voltammetry (SWV) were selected to examine the ECL behavior of BTPPO/H_2O_2 system at GCE over the potential range of 0–1200 mV. The result showed that, when LSV was performed, the most stable ECL was obtained and the peak shape was better. Therefore, LSV was selected for the subsequently studies.

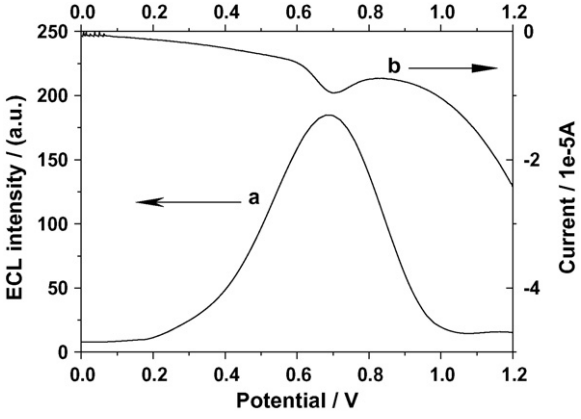

Fig. 1. LSV and ECL curves in phosphate buffer solution (pH 10.0) containing 0.15 mmol/L BTPPO at GCE: (a) ECL curve and (b) LSV; conditions of LSV were the same as in Table 1. $[H_2O_2] = 7.0 \times 10^{-3}$ mol/L.

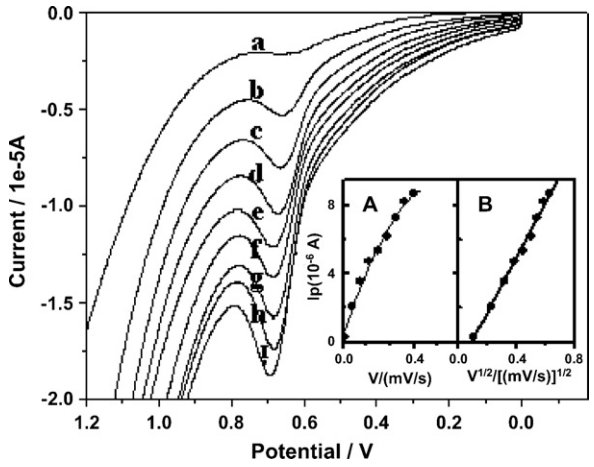

Fig. 2. Linear sweep voltammograms obtained at the GCE of 2×10^{-4} mol L^{-1} BTPPO in phosphate buffer solution (pH 10) at the different scan rate. (A) Plot of peak current (ip) vs. scan rate (υ); (B) plot of peak current (ip) vs. square root of scan rate ($\upsilon^{1/2}$). (a) 0.01 V/s; (b) 0.05 V/s; (c) 0.10 V/s; (d) 0.15 V/s; (e) 0.20 V/s; (f) 0.25 V/s; (g) 0.30 V/s; (h) 0.35 V/s; (i) 0.40 V/s; $[H_2O_2] = 7.0 \times 10^{-3}$ mol/L.

Under the mode of LSV, the effect of scanning rate on the ECL of BTPPO/H_2O_2 system has been examined and the result showed that the ECL intensity was increased with the scanning rate below 200 mV s^{-1}, and the ECL intensity reached the maximum and then kept constant at scanning rate of 200 mV s^{-1}. Therefore, 200 mV s^{-1} was selected as the scanning rate in subsequent work.

The effect of scanning rate on the peak current under LSV mode was shown in Fig. 2. It can be seen from Fig. 2 that the peak current is increased with the scan rate, but the peak current is not linear with the scan rate (see Fig. 2A). However, it can be seen from Fig. 2B that the peak current is linear with the square root of scan rate, which indicates that in the anodic process, the electrochemical oxidation of BTPPO in the presence of hydrogen peroxide at the glassy carbon electrode is diffusion-controlled, i.e., BTPPO is not adsorptive or weakly adsorptive at glassy carbon electrode.

3.3. Selection of chemical reaction conditions

3.3.1. Selection of reaction medium

Since BTPPO was difficult to dissolve in the water, so we paid more attention to the dissolution of BTPPO, and tried to use some solvents to increase the solubility of BTPPO. However, we found that the tested solvents except ethanol could enhance the CL signal of BTPPO but not the ECL signal. Therefore, we investigated the ECL behavior of BTPPO in ethanol solvent mixed with phosphate buffer solution. It was found that the signal of BTPPO was stable and reproducible. So ethanol and aqueous mixture solution with the ratio of 1:100 was used as the solvent for this ECL system.

The ECL behavior of BTPPO/H_2O_2 system in different buffer media (pH 10), such as acetate buffer, borate buffer, B.R buffer and phosphate buffer solution, was investigated in detail. The experiments showed that the maximum ECL intensity could be obtained in phosphate buffer solution.

3.3.2. Selection of pH

In phosphate buffer solution, the ECL behavior of BTPPO/H_2O_2 system has been examined under the different pH value. It was found that when pH was below pH 8.0, the BTPPO/H_2O_2 system did not give ECL signal or the ECL intensity was very week. Beyond pH 8.0, the ECL intensity was increased quickly with the increase of pH value, and in the range of pH 10.0–10.5, the ECL intensity reached the maximum and kept constant, beyond pH 10.5, the ECL intensity was decreased slightly with the increasing of pH. Therefore, pH 10 was selected as the optimum pH for subsequent experiments.

3.3.3. Effect of hydrogen peroxide concentration

The effect of concentration of hydrogen peroxide on the ECL intensity was investigated, and the results show that the ECL intensity was increased quickly with the concentration of hydrogen peroxide below 7.0×10^{-3} beyond 7.0×10^{-3} mol/L the ECL intensity was only increased slightly with the concentration of hydrogen peroxide. 7.0×10^{-3} mol/L of hydrogen peroxide was used in subsequent experiment.

3.4. Linear response range of ECL for BTPPO system

Fig. 3 shows the effect of the concentration of BTPPO on the ECL intensity. It can be seen from Fig. 3 that the ECL intensity is increased with the concentration of BTPPO (see Fig. 3A), and the peak current of the LSV is also increased with the concentration of BTPPO in the presence of H_2O_2 (see Fig. 3B).

Under the optimum conditions, the ECL intensity had a linear relationship with the concentration of BTPPO in the range of 3.0×10^{-6} to 3.0×10^{-4} mol/L. The regression equation was

$$\frac{I_{ECL}}{(a.u.)} = 1.23 + 1.25 \times 10^6 C/(mol/L) \qquad (R = 0.9986)$$

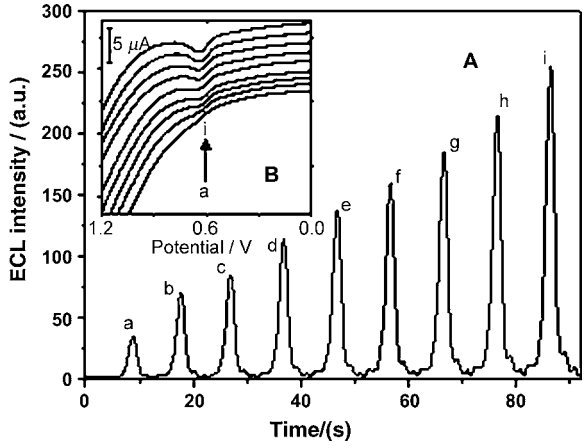

Fig. 3. LSV and ECL curves in various concentration of BTPPO in pH 10.0 phosphate buffer solution: (A) ECL curve and (B) LSV; (a) 3.0×10^{-5} mol/L; (b) 5.0×10^{-5} mol/L; (c) 7.0×10^{-5} mol/L; (d) 9.0×10^{-5} mol/L; (e) 1.1×10^{-4} mol/L; (f) 1.3×10^{-4} mol/L; (g) 1.5×10^{-4} mol/L; (h) 1.7×10^{-4} mol/L; (i) 2.0×10^{-4} mol/L; $[H_2O_2] = 7.0 \times 10^{-3}$ mol/L; conditions of LSV were the same as in Table 1.

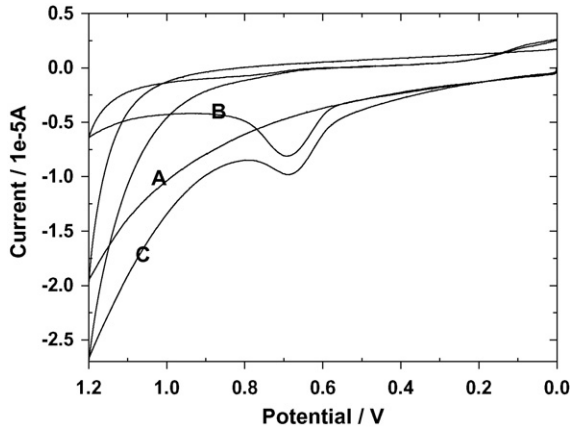

Fig. 4. Cyclic voltammograms of BTPPO/H_2O_2 solution at the GCE: (A) phosphate buffer solution (pH 10.0); (B) phosphate buffer solution (pH 10.0) with BTPPO (2.0×10^{-4} mol/L); (C) phosphate buffer solution (pH 10.0) with BTPPO (2.0×10^{-4} mol/L) and H_2O_2 (7.0×10^{-3} mol/L); conditions of LSV were the same as in Table 1.

where I_{ECL} is the intensity of ECL, C is the concentration of BTPPO. The relative standard deviation for 1.0×10^{-5} mol/L BTPPO was 2.7% ($n = 11$). The detection limit (defined as the concentration that could be detected at the signal-to-noise ratio of 3) was 1.0×10^{-7} mol/L.

3.5. Mechanism for the ECL of BTPPO in the presence of hydrogen peroxide

3.5.1. Cyclic voltammetry of BTPPO/H_2O_2 system

The cyclic voltammograms of BTPPO in phosphate buffer solution (pH 10.0) at a GC electrode was recorded. It was evident from the cyclic Voltammograms (as shown in Fig. 4) that the electrode processes for the oxidations of BTPPO were totally irreversible and the oxidation peak potential was 0.68 V. In Fig. 4B, the solution only contains BTPPO and in Fig. 4C there is the mixture of BTPPO and H_2O_2. The ECL experiment also showed that the ECL intensity in the solution of BTPPO and H_2O_2 is much stronger than that in the solution of BTPPO.

3.5.2. Determination of the number of transfer electron and proton involved in the electrode reaction of BTPPO/H_2O_2 system

The influences of scan rate on the oxidation peak current and potential have been discussed (see Fig. 2). The oxidation peak current of BTPPO is proportional to the square root of scan rate, which indicated that the oxidation of BTPPO at GCE is diffusion-controlled. The oxidation peak potential (E_p) shifts towards positive direction when increasing the scan rate (v), and the relationship between E_p (V) and v (V/s) is in accordance with the following equation:

$$E_p = 0.7009 + 0.0135 \ln(v) \quad (1)$$

For a totally irreversible electrode process, E_p and v can be defined by the following equation [30]:

$$E_p = E^{0'} + \left(\frac{RT}{\alpha n_a F}\right)\left[0.780 + \ln\left(\frac{D_R^{1/2}}{k^0}\right) + \ln\left(\frac{\alpha n_a F v}{RT}\right)^{1/2}\right] \quad (2)$$

where $E^{0'}$ is the formal potential, k^0 the standard heterogeneous rate constant, D_R the diffusion coefficient of BTPPO, A the electrode area and α is transfer coefficient of the oxidation of BTPPO. Other symbols have their usual significance. From Eqs. (1) and (2), we can obtain:

$$\frac{RT}{2\alpha n_a F} = 0.0135 \quad (3)$$

The value of αn_a, calculated from Eq. (3), is 0.95. Generally, α in the totally irreversible electrode process is assumed as 0.5. Consequently, two electrons are involved in the oxidation of BTPPO.

3.5.3. The ECL spectrum

The ECL emission spectrum for BTPPO (2.0×10^{-4} mol/L) in pH 10.0 phosphate buffer solution from 400 to 535 nm was obtained by using a series of filters. It can be seen from the spectrum that the maximum emission wavelength was 460 nm, which was similar to other peroxyoxalate background chemiluminescence [31].

3.5.4. Possible mechanism for the ECL behavior of BTPPO in the presence of H_2O_2

From the above discussion of the electrochemical characteristics of BTPPO, the oxidation of BTPPO was a two-electron irreversible process. Fig. 4 shows the cyclic voltammetric behavior of BTPPO under the optimum chemical reaction conditions at a glassy carbon electrode. With a scan rate of 200 mV/s, an oxidation peak was seen at 0.68 V. The wave was due to the oxidation of BTPPO on the electrode. However, BTPPO did not give ECL signal or gave only very weak ECL without addition of H_2O_2, which indicates that the excited species was not produced directly by the electrochemical reaction of BTPPO at the glassy carbon electrode surface, but the electrolytically oxidized species reacted with other chemicals to produce an excited intermediate which emitted light. Therefore, when the potential applied to oxidize BTPPO is between 0 and 1.2 V, BTPPO is oxidized to produce an intermediate, which would react with the hydrogen peroxide in the diffusion layer to form the 1,2-dioxetanedione. 1,2-Dioxetanedione was decomposed into a singlet excited state carbon dioxide CO_2^* and a ground state carbon dioxide CO_2, when the singlet excited state carbon dioxide returned to the ground state to emit light at 460 nm. Emission from excited CO_2 is not normally observed in the visible region. However, a singlet excited state for bent ($122^\circ \pm 2$) carbon dioxide exists about 46,700 cm^{-1} above the ground state [31]. The bent state of CO_2 has been characterized from examination of the flame emission spectrum of carbon monoxide [32]. Therefore, the ECL mechanism for BTPPO in the presence of H_2O_2 may be proposed as Fig. 5.

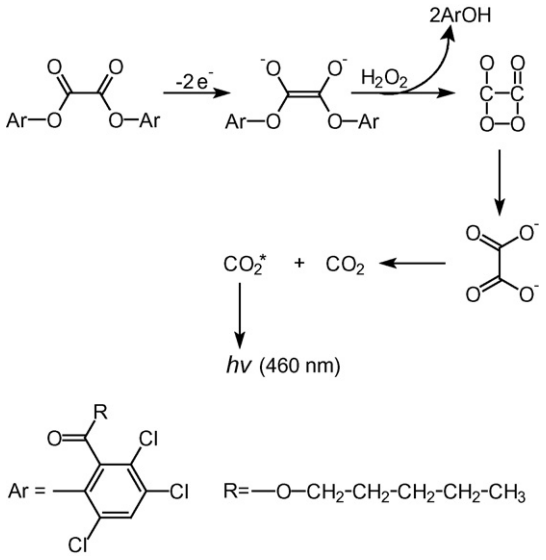

Fig. 5. ECL mechanism for BTPPO in the presence of H_2O_2.

3.6. Development of an ECL sensing system for glucose

3.6.1. Principle

From the above discussions, it has been known that the BTPPO can give the ECL signal in the presence of trace hydrogen peroxide, and we also know that glucose oxidase can react with glucose to form hydrogen peroxide, so we found that BTPPO would give the ECL signal in the presence of glucose oxidase and glucose even though without existing hydrogen peroxide. Based on which, the BTPPO/glucose oxidase/glucose ECL system can be used as the sensing system for detection of glucose. The principle of this sensing system is shown in Fig. 6 [33,34].

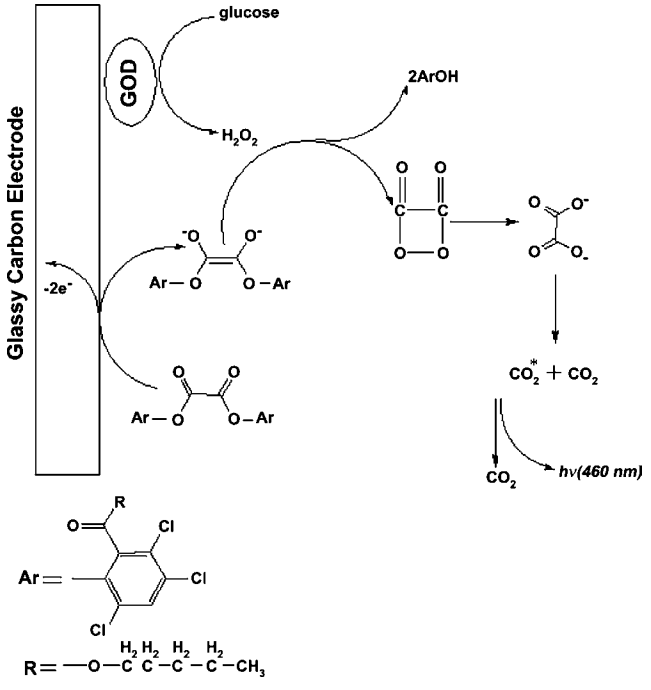

Fig. 6. Principle of this ECL sensing system.

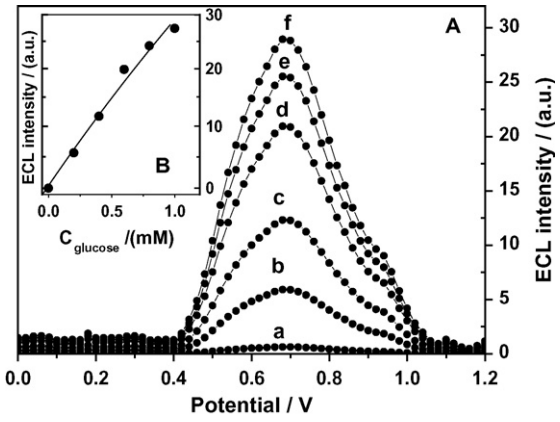

Fig. 7. ECL of BTPPO elicited by the glucose oxidase reaction: (A) ECL curves with various concentration of glucose: (a) 0.0 mol/L, (b) 2.0×10^{-4} mol/L, (c) 4.0×10^{-4} mol/L, (d) 6.0×10^{-4} mol/L, (e) 8.0×10^{-4} mol/L and (f) 1.0×10^{-3} mol/L; (B) ECL intensity with the concentration of glucose; reaction mixtures contained 0.05 mg/ml glucose oxidase, and 3.0×10^{-4} mol/L BTPPO at pH 9.0 phosphate buffer solution; conditions of LSV were the same as in Table 1.

3.6.2. Application for detection of glucose

We investigated the ECL behavior of BTPPO in the presence of glucose and glucose oxidase and found that BTPPO did not give an ECL signal in the presence of glucose oxidase. However, when glucose was added, an ECL signal would be observed. It has been indicated that the ECL signal of this system would be affected greatly by the concentration of BTPPO, and we found that when the concentration of BTPPO reached 3.0×10^{-4}, the ECL signal of this system was stronger and beyond this concentration there was no much change in the ECL signal observed. Therefore, we choose the 3.0×10^{-4} as the concentration of BTPPO for determination of glucose. It can be seen from Fig. 7 that the light emissions of BTPPO in the presence of glucose oxidase was increased with the increase of glucose. The enhanced ECL intensity had a linear relationship with the concentration of glucose in the range of 1.0×10^{-4} to 1.0×10^{-3} mol/L (see Fig. 7B). The regression equation was

$$\frac{I_{\mathrm{ECL}}}{(\mathrm{a.u.})} = 0.43 + 2.87 \times 10^4 C/(\mathrm{mol/L}) \qquad (R = 0.9924)$$

where I_{ECL} is the net intensity of ECL and C is the concentration of glucose. The relative standard deviation for 1.0×10^{-3} mol/L was 3.8% ($n = 11$). The detection limit was 5.0×10^{-5} mol/L (S/N = 3).

4. Conclusions

BTPPO has been found to be able to give an ECL signal in the presence of hydrogen peroxide at the GCE, based on which a novel ECL detector can be successfully used for the determination of hydrogen peroxide. The possible mechanism of this ECL system has been discussed, it can be concluded that the electrochemical reaction of BTPPO was a two-electron and none proton irreversible oxidation processes. The emission of light of BTPPO was resulted from the intermediate (1,2-dioxetanedione), which was produced by the oxidized reaction

of BTPPO and hydrogen peroxide. In addition, it was found that BTPPO could also give the same ECL signal with hydrogen peroxide, which was generated by the enzymatic reaction between glucose and the glucose oxidase, based on which a new ECL sensing system for glucose was possibly developed. We also assume that this ECL sensing system can be used for the other enzymatic reaction which would produce hydrogen peroxide.

Acknowledgement

This project was financially supported by the National Nature Sciences Funding of China (20575011), the Science Foundation of State Education Department (20040386002).

References

[1] E.A. Chandross, Tetrahedron Lett. 12 (1963) 761.
[2] M.M. Rauhut, L.J. Bollyky, B.G. Roberts, M. Loy, R.H. Whitman, A.V. Iannotta, A.M. Semsel, R.A. Clark, J. Am. Chem. Soc. 89 (1967) 6515.
[3] L.J. Bollyky, R.H. Whitman, B.G. Roberts, M.M. Rauhut, J. Am. Chem. Soc. 89 (1967) 6523.
[4] M.M. Rauhut, Acc. Chem. Res. 12 (1969) 80.
[5] D.R. Maulding, R.A. Clarke, B.G. Roberts, M.M. Rauhut, J. Org. Chem. 33 (1968) 250.
[6] A.C. Capomacchia, R.N. Jennings, S.M. Hemingway, P. D'Souza, W. Prapaitrakul, A. Gingle, Anal. Chim. Acta 196 (1987) 305.
[7] M. Lin, C.W. Huie, Anal. Chim. Acta 339 (1997) 131.
[8] M. Du, C.W. Huie, Anal. Chim. Acta 443 (2001) 269.
[9] D.W. Kim, C.W. Lee, S.W. Joo, M.S. Gong, J. Lumin. 99 (2002) 205.
[10] M.M. Nakamura, N. Coichev, J.M. Lin, M. Yamada, Anal. Chim. Acta 484 (2003) 101.
[11] M. Shamsipur, M.J. Chaichi, A.R. Karami, H. Sharghi, J. Photochem. Photobiol. A 174 (2005) 23.
[12] V. Stepanyana, A. Arnousa, C. Petrakisa, P. Kefalasa, A. Calokerinosb, Talanta 65 (2005) 1056.
[13] B. Mann, M.L. Grayeski, J. Chromatogr. 386 (1987) 149.
[14] N. Wu, W.J. Horvath, C.W. Huie, Anal. Chim. Acta 269 (1992) 99.
[15] M. Tsunoda, K. Takezawa, T. Santa, K. Imai, Anal. Biochem. 269 (1999) 386.
[16] J.J. Soto-Chinchilla, L. Gamiz-Gracia, A.M. Garcia-Campana, K. Imai, L.E. Garcia-Ayuso, J. Chromatogr. 1095 (2005) 60.
[17] A. Arnous, C. Petrakis, D.P. Makris, P. Kefalas, J. Pharmacol. Toxicol. Methods 48 (2002) 171.
[18] A. Mansouri, D.P. Makris, P. Kefalas, J. Pharm. Biomed. Anal. 39 (2005) 22.
[19] J.J. Soto-Chinchilla, A.M. Garcia-Campana, L. Gamiz-Gracia, L. Cuadros-Rodriguez, J.L.M. Vidal, J. Chromatogr. 524 (2004) 235.
[20] K. Hayakawa, C. Lu, S. Mizukami, A. Toriba, N. Tang, J. Chromatogr. 1107 (2006) 286.
[21] A.W. Knight, Trends Anal. Chem. 18 (1999) 47.
[22] G.N. Chen, L. Zhang, R.E. Lin, Z.C. Yang, J.P. Duan, H.Q. Chen, D.B. Hibbert, Talanta 50 (2000) 1275.
[23] Y.Y. Su, J. Wang, G.N. Chen, Talanta 68 (2006) 883.
[24] S.C. Liu, Y.J. Liu, J. Li, M.L. Guo, W. Pan, S.Z. Yao, Talanta 69 (2006) 154.
[25] Z.Y. Lin, G.N. Chen, Talanta 70 (2006) 111.
[26] S.N. Ding, J.J. Xu, H.Y. Chen, Talanta 70 (2006) 403.
[27] W.R. Seitz, Crit. Rev. Anal. Chem. 13 (1981) 1.
[28] D. Pilosof, T.A. Nieman, Anal. Chem. 54 (1982) 1698.
[29] X. Wu, F. Huang, J. Duan, G. Chen, Talanta 65 (2005) 1279.
[30] A.J. Bard, L.R. Faulkner, Electrochemical Methods Fundamentals and Applications, Wiley, New York, 1980, p. 222.
[31] B. Mann, M.L. Grayeski, Anal. Chem. 62 (1990) 1532.
[32] R.N. Dixon, Proc. R. Soc. 275a (1963) 431.
[33] J.P. Auses, S.L. Cook, J.T. Maloy, Anal. Chem. 47 (1975) 244.
[34] C.S. Ouyang, C.M. Wang, J. Electroanal. Chem. 474 (1999) 82.

Available online at www.sciencedirect.com
ScienceDirect
Talanta 72 (2007) 1322–1328
Talanta
www.elsevier.com/locate/talanta

Generic simple enzyme immunoassay approach to avert small molecule immobilization problems on solid phases Application to the determination of tobramycin in serum

Ibrahim A. Darwish *, Ashraf M. Mahmoud, Abdel-Rahman A. Al-Majed

Department of Pharmaceutical Chemistry, College of Pharmacy, King Saud University, P.O. Box 2457, Riyadh 11451, Saudi Arabia

Received 14 January 2007; received in revised form 14 January 2007; accepted 14 January 2007
Available online 20 January 2007

Abstract

Generic simple and sensitive universal enzyme immunoassay approach for the determination of small analytes has been developed to avert the problems associated with small molecule immobilization onto solid phases. The developed assay employed a heterogeneous non-competitive binding format. The assay used anti-analyte antibody coupled to polyacrylamide beads as a solid-phase and β-D-galactosidase enzyme-labeled analyte as a label. In this assay, the analyte in a sample was firstly incubated to react with an excess of the antibody-coupled beads, and then the unoccupied antibody binding sites were allowed to react with the enzyme-labeled analyte. Analyte bound to the antibody-coupled beads was separated by centrifugation, and the enzyme activity of the supernatant was measured spectrophotometrically at 420 nm, after reaction with 4-nitrophenyl-β-D-galactopyranoside as a substrate for the enzyme. The signal was directly proportional to the concentration of analyte in the sample. The optimum conditions for the developed assay were established and applied to the determination of tobramycin, as a representative example of the small analytes, in serum samples. The assay limit of detection was 10 ng mL^{-1} and the effective working range at relative standard deviation of ≤10% was 40–800 ng mL^{-1}. The assay precisions were acceptable; the relative standard deviations were 4.36–5.17 and 5.62–7.40% for intra- and inter-assay precision, respectively. Analytical recovery of tobramycin spiked in serum ranged from 95.89 ± 4.25 to 103.45 ± 4.60%. The assay results correlated well with those obtained by high-performance liquid chromatography ($r = 0.992$). The assay described herein has great practical value in determination of small analytes because it is sensitive, rapid, and easy to perform in any laboratory. Although the assay was validated for tobramycin, however, it is also anticipated that the same methodology could be used for essentially any analyte for which a selective antibody exists, and an appropriate enzyme conjugate can be made.

Keywords: Enzyme immunoassay; Non-competitive binding; Aminoglycoside antibiotics; Tobramycin; Therapeutic drug monitoring

1. Introduction

Immunoassay methods have been widely used in many important areas of pharmaceutical analysis such as diagnosis of diseases, therapeutic drug monitoring, clinical pharmacokinetic and bioequivalence studies in drug discovery and pharmaceutical industries [1,2]. The analysis in these areas usually involves measurement of very low concentrations of drugs [3–6], biomolecules of pharmaceutical interest [7], metabolites [8], and/or biomarkers which indicate disease diagnosis [9–13] and/or prognosis [14]. The importance and widespread of immunoassay methods in pharmaceutical analysis are attributed to their inherent specificity, high sensitivity, high-throughput, and applicability to the analysis of wide range of low molecular weight and macromolecular analytes in complex matrices (e.g. biological samples).

Immunoassays involving radioactive labels [15] are extremely sensitive and quite precise, however, the handling of radioactive materials and radioactive waste and high cost are inhibitory factors. Enzyme immunoassays (EIA) have become the most universal assay method in pharmaceutical analysis because of its simplicity, rapidity, sensitivity and low cost. One additional advantage of enzyme immunoassays is the possibility of utilizing the enzyme labels in the amplification of the signal, if the signal is not sufficient to give the desired assay sensitivity [16]. The use of these labels results in assay methods

* Corresponding author. Tel.: +966 14677348; fax: +966 14676220.
E-mail address: iadarwish@yahoo.com (I.A. Darwish).

0039-9140/$ – see front matter © 2007 Elsevier B.V. All rights reserved.
doi:10.1016/j.talanta.2007.01.036

with extremely high sensitivity and low limits of detection [17]. The traditional enzyme immunoassays, e.g. microplate-based enzyme-linked immunosorbent assays (ELISA) are not practical for the analysis of small molecules (e.g. drugs, metabolites, etc.) because they adsorb very poorly or not at all to the solid-phase supports. To enhance the adsorption of small molecules to solid-phase supports, different pre-treatment approaches were used. These approaches include: irradiation of the solid-phase with ultra-violet light [18], or treatment with alcian blue [19], treatment of the target with carbodiimides [20], or conjugation with protein and subsequent immobilization of the conjugate by passive adsorption [21]. The majority of these approaches are still associated with drawbacks such as long incubation periods, multiple washing and mixing steps, high non-specific binding signals, they are labour intensive and/or expensive. Considering the drawbacks of performing ELISA for small molecules, there was a growing interest in the development of new EIA devoid of these drawbacks.

In a previous study, Darwish [22] has developed a continuous-flow EIA system for determination of small analytes. The system completely resolved the adsorption problems; however, it was specifically designed for laboratories that are equipped with HPLC instrument, and it is requested to screen large number of specimens. This limited the application of this system in small pharmaceutical and clinical laboratories that are not equipped with HPLC instruments and/or requested to screen small batches of specimens (e.g. emergency rooms, urgent-care centers, physician clinics, etc.). The present study is focused on development and validation of an alternative new EIA approach for determination of small analytes. The assay is specifically designed for use in conjunction with a dedicated spectrophotometer, the common instrument in all pharmaceutical and clinical laboratories. In the study described herein, tobramycin (TOB) was used as a representative example for the small analytes. The proposed assay depended on a non-competitive binding reaction and utilized an anti-TOB monoclonal antibody coupled to polyacrylamide beads as a solid-phase, and TOB-β-galactosidase conjugate (TOB-β-GAL) as a label. In this method, an excess of the antibody-coupled beads was first incubated with TOB sample, and then separately incubated with TOB-β-GAL. After separation of the beads by centrifugation, the enzyme activity of the supernatant was measured spectrophotometrically at 420 nm, after reaction with 4-nitrophenyl-β-D-galactopyranoside as a substrate for the enzyme. The measured absorbance was directly related to the concentration of TOB in the sample.

2. Experimental

2.1. Chemicals

Tobramycin (TOB) was purchased from Eli Lilly Co. (Indianapolis, IN, USA). Monoclonal antibody against TOB was obtained from Fitzgerald Industries International Inc. (Concord, MA, USA). β-D-Galactosidase enzyme (β-GAL, EC 3.2.1.23, grade III), bovine serum albumin and Tween-20 (polyethylene sorbitan monolaurate) were purchased from Sigma Chemical Co. (St. Louis. MO, USA). *m*-Maleimidobenzoyl-*N*-hydroxysuccinimide ester (MBS) was obtained from Pierce Chemical Co. (Rokford, IL, USA). Glutraldehyde was obtained from Merck (New York, USA). 4-Nitrophenyl-β-D-galactopyranoside (NPGP) was purchased from Boehringer-Mannheim Biochemicals (Indianapolis, IN, USA). Polyacrylamide beads (Bio-Gel P) was a product of Bio-Rad Laboratories (Richmond, CA, USA), and polystyrene test tubes was a product of Walter Sarstedt (Leicester, UK). All other chemicals were of analytical grade.

2.2. Reagent solutions

Water was purified by filtration through Nanopure II water purification system (Barnsead/ThermLyne, Dubuque, IA, USA) and used for all solutions. Washing buffer; phosphate buffered saline (PBS, 137 mM NaCl, 3 mM KCl and 10 mM sodium phosphate buffer, pH 7.4) containing Tween 20 (0.05%, v/v). Assay buffer; PBS containing bovine serum albumin (0.1%, w/v). Substrate solution; PBS containing 1.5 mM of NPGP. Enzymatic reaction terminator solution; 0.1 M potassium phosphate buffer adjusted to pH 11 with NaOH.

2.3. Preparation of TOB-β-GAL conjugate and antibody-coupled beads

Tobramycin was conjugated with β-GAL enzyme using MBS reagent, and according to the method described by Darwish [22]. The unconjugated tobramycin was removed from the TOB-β-GAL conjugate by buffer exchange using a Centricon-30 filter (Amicon Inc., Beverly, MA, USA). Protein concentration of the conjugate was determined using the kit obtained from Pierce Chemical Co. (Rockford, IL, USA), and the conjugate was characterized in terms of specific activity of β-GAL. The specific activity was 242 units mg^{-1} protein; unit was defined as the amount of β-GAL enzyme that converts 1 μmol of NPGP in 1 min.

The antibody-coupled beads were prepared by activation of the polyacrylamide beads with glutraldehyde, and covalently linking the glutraldehyde-activated beads to the anti-TOB antibody [23]. The antibody-coupled beads were thoroughly washed with PBS and finally diluted into the assay buffer solution to a concentration of 50 mg mL^{-1} and stored at 4 °C.

2.4. Determination of optimum concentrations of TOB-β-GAL enzyme conjugate and antibody-coupled beads

The optimal concentrations of TOB-β-GAL and antibody-coupled beads were determined by checkerboard titration. Purified TOB-β-GAL was diluted into the assay buffer at concentrations of 0.1, 0.25, 0.5, and 1 μg mL^{-1} and mixed in polystyrene test tubes with the antibody-coupled beads at concentrations of 5, 10, 15, and 20 mg mL^{-1}. The binding was then allowed to proceed by incubation at room temperature (25 ± 2 °C) for 15 min with gentle shaking to prevent the sedimentation of the beads. The tubes were centrifuged at 3000 rpm for 2 min, and 50 μL the supernatant was dispensed into a separate test tube contained 450 μL of NPGP substrate solution. The

color-developing enzymatic reaction was allowed to proceed for 10 min, and then 2.5 mL of the enzymatic reaction terminator solution was added to each tube. The absorbances were measured by spectrophotometer (UV-1601PC, Shimadzu Co., Kyoto, Japan) at 420 nm. The concentration of TOB-β-GAL that was sufficient enough to saturate all the binding sites of the antibody, and yielded a signal between 0.8 and 1.0 absorbance units, in absence of antibody-coupled beads, was considered as optimum.

2.5. Assay procedure

All procedures were carried out at room temperature (25 ± 5 °C) in triplicate. Fifty microliters of TOB sample (serum or standard solution) was dispensed into each polystyrene test tube contained 500 μL of antibody-coupled beads suspension (20 mg mL^{-1}). The tubes were incubated for 30 min with gentle shaking to prevent the sedimentation of the beads particles, and then centrifuged at 3000 rpm for 2 min. The supernatants were aspirated to waste; care being taken to avoid the disturbance of the beads pellet at the bottom of the tubes. The beads were washed three times by shaking with 1 mL of the washing buffer for about 2 min, centrifugation, and aspiration of the supernatants. Five hundred microliters of TOB-β-GAL solution (0.25 μg mL^{-1} in assay buffer) was added and the tubes were incubated for 15 min with gentle shaking. The tubes were then centrifuged for 2 min, and 50 μL of the supernatant was dispensed into a separate test tube. The enzyme activity of the supernatants was determined as described above, and the data were transformed to a four-parameter curve using Slide Write Plus software version 5.011 (Advanced Graphics Software Inc., CA, USA).

3. Results

This study describes a simple non-competitive enzyme immunoassay for determination of TOB, as a representative example for small analytes, in serum; Fig. 1 illustrates the general procedure of this assay. The assay was carried out in two main steps; the immunchemical reaction and the color developing reaction. In the first step, TOB in samples was allowed to bind to an excess of anti-TOB monoclonal antibody linked to polyacrylamide beads, as solid phase. Then, TOB-β-GAL conjugate was allowed to bind to the remaining antibody binding sites. In the second step, the enzyme activity in the supernatant, after centrifugal sedimentation of the solid-phase beads, was determined using NPGP substrate. The absorbances, measured spectrophotometrically, were directly proportional to the concentration of TOB in the sample.

3.1. Optimum assay conditions

The optimal concentration of TOB-β-GAL conjugate was considered as the concentration that was able to saturate all the binding sites of the antibody and yielded a signal between 0.8 and 1.0 absorbance unit in the absence of antibody-coupled beads. This concentration was 0.25 μg mL^{-1} when the concentration of the antibody-coupled beads was 20 mg mL^{-1} (Fig. 2). Unless otherwise stated, these concentrations were used for further experiments. The kinetics of TOB binding to the antibody was studied at different temperatures in order to determine the optimum time and incubation temperature required for the immunological reaction. As shown in Fig. 3, the reaction proceeded faster to completion as the temperature was increased

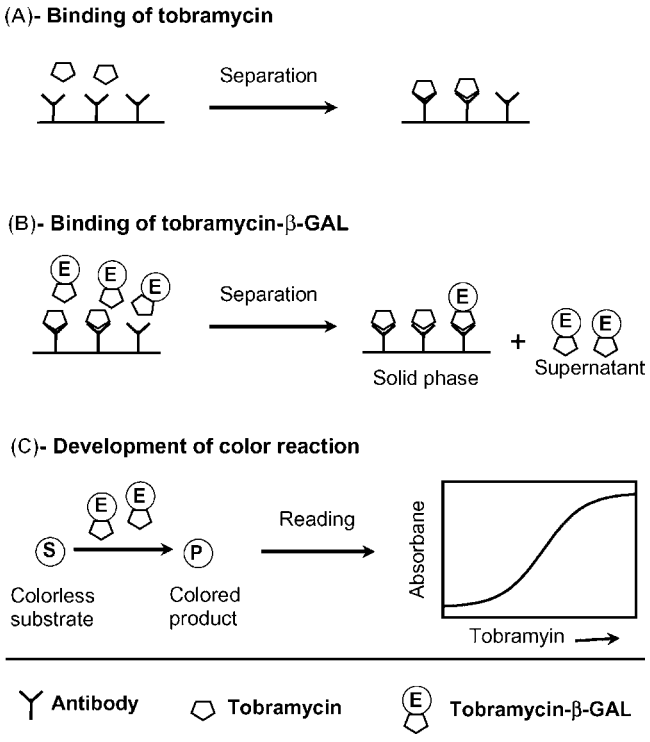

Fig. 1. Schematic diagram of the non-competitive EIA for determination of TOB in serum. (A) The serum sample-containing TOB was allowed to bind to an excess of anti-TOB antibody-coupled beads, and then the serum was removed by washing. (B) The beads were subsequently incubated with TOB-β-GAL, and then the antibody beads were separated by centrifugation. (C) The enzyme activity of the supernatant was determined by chromogenic substrate, and the color development was directly proportional to the concentration of TOB in the original sample.

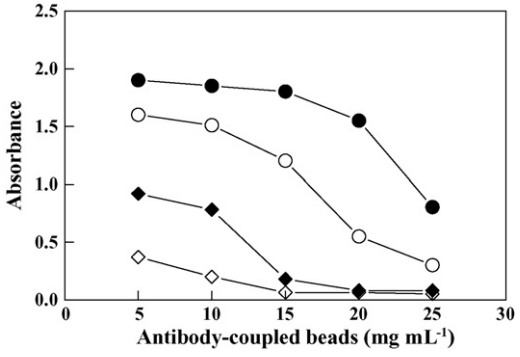

Fig. 2. Checkerboard titration of TOB-β-GAL conjugate versus anti-TOB antibody-coupled beads. The conjugate at concentrations of 0.1 μg mL^{-1} (◊), 0.25 μg mL^{-1} (♦), 0.5 μg mL^{-1} (○), and 1 μg mL^{-1} (●) were allowed to bind the antibody-coupled beads at the indicated concentrations. The signals were generated as described in Section 2.

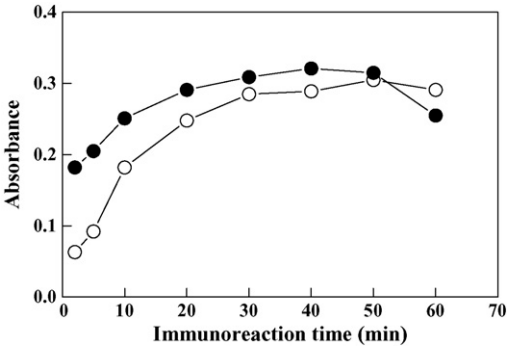

Fig. 3. Immunoreaction kinetics for binding of TOB to antibody-coupled beads. An assay buffer solution containing 50 ng mL^{-1} TOB was incubated with 20 mg mL^{-1} antibody beads suspension at 25 °C (◯) and 37 °C (●) for the indicated periods of time, and then processed as described in Section 2.

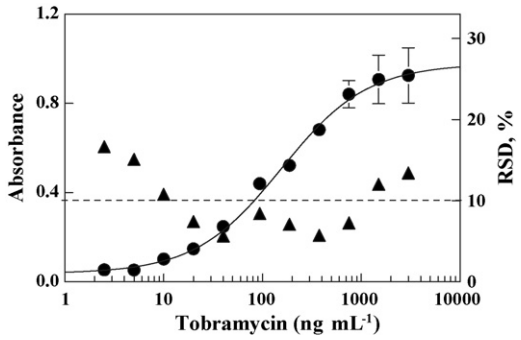

Fig. 5. Calibration curve (●) and precision profile (▲) of the non-competitive EIA for determination of TOB. Various concentrations of TOB were prepared in the assay buffer, and allowed to bind to an excess of anti-TOB antibody-coupled beads. After washing, the beads were subsequently incubated with TOB-β-GAL. The excess unbound reagent was removed by centrifugation, and the enzyme activity of the supernatant was determined by chromogenic substrate as described in Section 2. The values plotted were the mean of three determinations ± S.D.

from 25 to 37 °C. There was no significant difference between the results of the reaction at 37 °C for 30 min and that of at room temperature (25 ± 2 °C) for 40 min. For convenience, further experiments were carried out at room temperature to avoid using an additional temperature control instrument. In order to determine the color-developing time, the enzyme reaction kinetic was studied using 25, 50 or 75 μL supernatant. The results (Fig. 4) showed that 25, 50 or 75 μL could be incubated with the substrate solution for 20, 10 or 5 min, respectively. For reading precision consideration, the enzyme color reaction for the subsequent experiments was carried out using 50 μL of the supernatant and 10 min for incubation with the substrate.

3.2. Analytical performance

3.2.1. Calibration curve and sensitivity

The calibration curve of TOB using the proposed non-competitive EIA is shown in Fig. 5. The data showed good correlation coefficient ($r = 0.998$) on the four-parameter curve fit. The limit of detection of the proposed non-competitive EIA, calculated as the lowest TOB concentration significantly different from zero concentration at 95% confidence limit, i.e. mean of zero ± 4.65 S.D. [24] was 10 ng mL^{-1}, based on the basis of 5 replicate measurements of the reagent blank. The supernatant solutions that have been used for generating the calibration curve were stored overnight at 4 °C, and then were used for generating a new curve. The two curves were completely superimposed (not shown data) indicating the stability of the enzyme conjugate. This allowed the removing of the supernatants and storing them for delayed measurements of the enzyme activity. This increases the convenience of the analysis, and allows the easy handling of large batches of specimens.

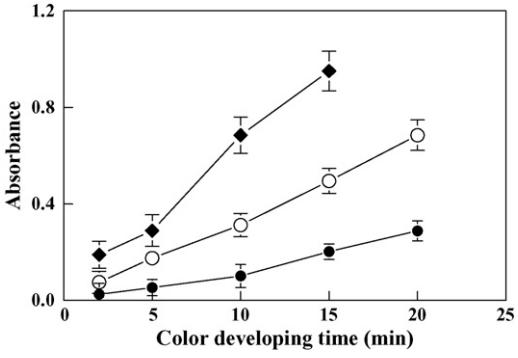

Fig. 4. Time-course of the color development reaction in the non-competitive EIA for TOB. The non-competitive assay was performed using 50 ng mL^{-1} TOB. After centrifugation of the TOB-bound antibody beads: 25 μL (●), 50 μL (◯), and 75 μL (♦) of the supernatant was incubated with 450 μL of the substrate solution for the indicated periods, and then processed as described in Section 2. Values were the mean of three determinations ± S.D.

3.2.2. Serum matrix effect and specificity

Studying the effect of serum matrix was necessary in the development of the proposed method, since the assay was designed for quantitation and therapeutic monitoring of TOB in serum. Quality control TOB-free serum sample was serially diluted into the assay buffer solution and each dilution was spiked with 200 ng mL^{-1} of TOB standard. The spiked samples were then analyzed by the proposed assay to investigate the feasibility of the assay. The measured concentrations increased with the increase in the serum dilution, and then leveled off when the serum dilution was 20-fold. Therefore, serum samples should be diluted, in assay buffer, at least 20-fold in order to reduce possible false-negative analytical results (Fig. 6). It is worth to mention that the high sensitivity of the assay (limit of detection was 10 ng mL^{-1}) allowed the dilution of a clinical specimen up to 100-fold as the TOB concentration would remain in the clinical therapeutic range (5–10 μg mL^{-1}).

Although, the assay utilized a monoclonal antibody specific to TOB, it was necessary to investigate the effect of the experimental assay conditions on this specificity. The specificity study was performed using various aminoglycoside antibiotics (kanamycin, gentamicin, amikacin, and streptomycin) at concentrations considerably higher than that may be present in patient serum [25]. No cross reactivity was detected with any of the tested compounds indicating the good specificity of the method under the experimental conditions.

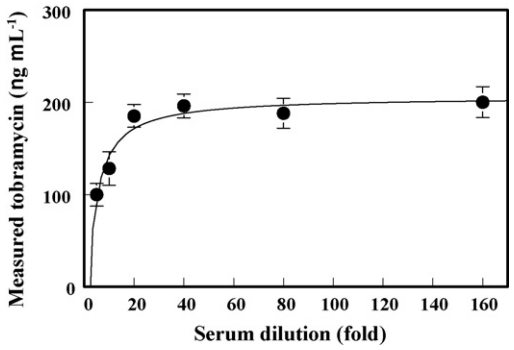

Fig. 6. Effect of serum matrix on the performance of the non-competitive EIA for TOB. TOB-free serum sample was serially diluted in the assay buffer solution, and each of the diluted samples was spiked with 200 ng mL^{-1} TOB. The spiked samples were analyzed by the EIA as described in Section 2. The plotted values were the mean of three determinations ± S.D.

3.2.3. Precision

The assay precision profile obtained from the results of calibration standard samples, assayed in triplicate, is shown in Fig. 5. From this profile, the working range of the assay (40–800 ng mL^{-1}), whereas the values of relative standard deviation (R.S.D.) were less than 10%, was derived. The R.S.D. at the detection limit of the assay (10 ng mL^{-1}) was found to be 12.02%. The intra- and inter-assay precisions were tested at three different levels (low, intermediate, and high) of TOB concentrations (40, 100, and 500 ng mL^{-1}). The intra-assay precision was assessed by analyzing 8 replicates of each sample in a single run and the inter-assay precision was assessed by analyzing the same sample, as duplicates, in four separate runs. According to the recommendation of immunoassay validation [26], the assay gave satisfactory results; the R.S.D. was 4.36–5.17 and 5.62–7.40% for intra- and inter-assay precision, respectively (Table 1).

3.2.4. Analytical recovery

Recovery of the assay was assessed by adding various known concentrations (40, 100 and 500 ng mL^{-1}) of TOB to three different individual samples of drug-free serum, and the samples were analyzed for their TOB content, as described in Section 2. The mean analytical recovery was calculated as the ratio between the TOB concentrations found and the concentrations added, expressed as percentage. As shown in Table 2, a quantitative recovery was obtained; the recovery percentages ranged from 95.89 ± 4.25 to 103.45 ± 4.60%). This indicated the accuracy of the proposed method for determination of TOB in serum samples.

Table 1
Precision data of the proposed EIA for tobramycin

Precision	Tobramycin (ng mL^{-1})		
	40	100	500
Intra-assay (n = 8)			
Mean (ng mL^{-1})	41.00	97.74	505.422
S.D. (ng mL^{-1})	2.12	4.26	2.30
R.S.D. (%)	5.17	4.36	4.41
Inter-assay (n = 8)			
Mean (ng mL^{-1})	38.92	104.24	496.25
S.D. (ng mL^{-1})	2.88	5.86	31.20
R.S.D. (%)	7.40	5.62	6.29

Table 2
Analytical recovery of tobramycin added to serum

Serum code	Tobramycin (ng mL^{-1})		Recovery (%)
	Added	Found	
A	40	41.38 ± 0.92[a]	103.45 ± 4.60
	100	100.20 ± 2.68	100.20 ± 2.68
	500	479.45 ± 21.26	95.89 ± 4.25
B	40	39.14 ± 1.02	97.58 ± 5.10
	100	100.50 ± 3.72	100.50 ± 3.72
	500	502.10 ± 20.16	100.42 ± 4.03
C	40	40.80 ± 1.08	102.13 ± 5.40
	100	96.70 ± 4.74	96.70 ± 4.74
	500	502.60 ± 30.57	100.52 ± 6.11

[a] Values are mean of three determinations ± S.D.

Table 3
Comparison of the proposed EIA with HPLC for determination of serum samples spiked with tobramycin

Spiked tobramycin (μg mL^{-1})	Found tobramycin (μg mL^{-1})	
	EIA	HPLC
2.0	1.86 ± 0.12[a]	1.65 ± 0.04
4.0	4.28 ± 0.22	4.12 ± 0.10
6.0	5.05 ± 0.19	6.05 ± 0.13
8.0	8.26 ± 0.42	7.84 ± 0.14
10.0	9.53 ± 0.61	10.75 ± 0.26

[a] Values are mean of three determinations ± S.D.

3.2.5. Comparison with HPLC

In order to compare the present EIA with HPLC, serum samples were spiked with TOB at concentrations of 2, 4, 6, 8 and 10 μg mL^{-1}, and then analyzed by HPLC [27]. These samples were then diluted 40 times with the assay buffer to get their concentrations within the working range of the proposed EIA method, and analyzed by the proposed method. The values obtained by both methods were correlated well with each other (Table 3). The regression analysis of the results showed a good agreement between the results obtained by the two methods: HPLC = 0.146 + 1.118EIA (r = 0.992).

4. Discussion

This study described the development of new sensitive assay format for determination of small analytes in serum. Two main objectives were behind this study; the first one was the elimination of the adsorption problems encountered in the microwell plate-based assays, and the second one was the applicability of the assay in any pharmaceutical and/or clinical laboratory.

Tobramycin (TOB) is widely used in the treatment of human and animal diseases caused by aerobic gram-negative bacillary infections [28]. The major concern in treatment with TOB is

its low therapeutic index whereas serum concentrations of less than 5 $\mu g\,mL^{-1}$ are generally ineffective, and the concentrations exceeding 10 $\mu g\,mL^{-1}$ are associated with oto- and nephrotoxicity [29]. For safe and effective treatment with TOB, routine monitoring of its serum concentrations followed by adjustment of the patient dose regimen is required [30].

Tobramycin levels in serum have been measured by microbiological assay [31], high-performance liquid chromatography (HPLC) [32–36], and enzyme immunoassay (EIA) [37,38]. Microbiological assays are semi-quantitative approach, time consuming, and subject to interferences by other antimicrobial drugs. HPLC is a very accurate method; however, the analysis requires derivatization of the sample to improve detectability, and long time for carrying out. The conventional EIA methods were not practical because it adsorbs very poorly or not at all to the solid-phase supports, in standard adsorption conditions, as well as after using various approaches to enhance its adsorption of TOB to solid-phase supports [18–20,39,40]. Therefore, an alternative assay formats that would be able to overcome these drawbacks was essential. For these reasons, the present study was dedicated to adopt TOB as an analyte in the development of the targeted analytical approach.

β-GAL enzyme was chosen for this work because it is absent from human blood, therefore avoid interferences from endogenous enzymes, particularly the proposed assay was designed to use serum samples in the analysis. Furthermore, the optimal enzyme-substrate reaction of β-GAL takes place at pH of 6–8 which is compatible with most antigen–antibody interaction systems. 4-Nitrophenyl-β-D-galactopyranoside was selected from the β-GAL substrates because it has high turnover rate for the generation of the product (λ_{max} at 420 nm), and consequently gives sensitive assay.

The solid-phase beads used in the assay allowed the employment of the simplest separation technique, which is the centrifugation, and only two washing steps were required. A final washing step was not necessary because the enzymatic activity was measured in the supernatant after separation of the solid-phase antibody. The assay was carried out in test tubes, thus avoided the problems of TOB adsorption to the microwell plates. Measurement of the enzyme activity in the supernatant was adapted to spectrophotometer, the common instrument in all clinical laboratories. The assay procedure was carried out at room temperature, thus no extra temperature control instrument was needed. For these reasons, the assay is applicable in most clinical laboratory.

Although the assay was specifically designed for use where small batches of specimens have to be screened (physician clinics, emergency rooms, urgent-care centers, etc.); however, the stability of the TOB-β-GAL conjugate in the supernatant solution allowed gathering the supernatants and storing them in large batches. This increased the convenience of the assay as well as made it applicable for large number of specimens.

The present assay depended on non-competitive binding reaction format. The use of excess reagents in this assay droved the immunochemical reaction to the formation of the immune complex, thus yielded rapid assay with high sensitivity and wide dynamic range. In the present approach, the sample's analyte (TOB) and enzyme conjugate (TOB-β-GAL) were sequentially added to the antibody, and never been in contact. This sequential addition procedure completely eliminated the non-specific antibody binding interferences that are encountered with competitive assay format. The assay was very sensitive; its sensitivity was higher than that achieved by other non-competitive immunoassay [19], and entire protocol of the assay described herein could be performed in less than one hour, compared to more than 5 h in the other method. The assay reproducibility was acceptable, however in order to obtain good precision, it was essential that a precise amount of the antibody-coupled beads should be used. This was achieved by keeping the beads in suspension using a magnetic stirrer during the pipetting process.

With attention to reagents preparation and technical manipulations, coupling of the antibody to the beads and conjugation of TOB to the enzyme could be easily performed using established procedures, and once prepared they were stable. All other reagents are inexpensive, could be easily obtained and had excellent shelf life.

5. Conclusion

The immunoassay approach described in this study has great practical value in the determination of small analytes as it eliminated the adsorption problems encountered in the microwell plate-based assays, and it is applicable in any pharmaceutical and/or clinical laboratory, as the approach adapted to a spectrophotometer, the common instrument in these laboratories. Furthermore, the approach showed high sensitivity, reproducibility, and simplicity to perform. Although, the approach was validated for tobramycin, however, it is anticipated that the same methodology could be essentially used for any analyte for which a selective antibody exists, and an appropriate enzyme conjugate can be made.

References

[1] I.A. Darwish, IJBS 2 (2006) 217.
[2] M.J. Wheeler, Meth. Mol. Biol. 324 (2006) 1.
[3] X. Chuanlai, P. Cifang, H. Kai, J. Zhengyu, W. Wukang, Luminescence 21 (2006) 126.
[4] Zh.V. Samsonova, O.S. Shchelokova, N.L. Ivanova, M.U. Rubtsova, A.M. Egorov, Prikl. Biokhim. Mikrobiol. 41 (2005) 668.
[5] K. lachenmeier, F. Musshoff, B. Madea, For. Sci. Intl. 159 (2006) 189.
[6] E. Benito-Pena, M.C. Moreno-Bondi, G. Orellana, A. Maquieira, A. van Amerongen, J. Agric. Food Chem. 53 (2005) 6635.
[7] T. Koszegi, J. Biochem. Biophys. Meth. 53 (2002) 157.
[8] A.D. Fraser, D. Worth, Therap. Drug Monitor. 24 (2002) 746.
[9] N. Kobayashi, K. Kubota, H. Oiwa, J. Goto, T. Niwa, K. Kobayashi, J. Immunol. Meth. 272 (2003) 1.
[10] I.V. Karakulova, A.A. Shutov, Klin. Lab. Diagn. 1 (2006) 9.
[11] S. Desruisseau, J. Palmari, C. Giusti, S. Romain, P.M. Martin, Y. Berthois, Br. J. Cancer 94 (2006) 239.
[12] L. Ball, A. Jones, P. Boogaard, W. Will, P. Aston, Biomarkers 10 (2005) 127.
[13] P. Signo, A. Barassi, R. Novario, G.V. Melzi d'Eril, Clin. Chem. Lab. Med. 43 (2005) 883.
[14] W.E. Fiets, M.A. Blankenstein, H. Struikmans, H.M. Ruitenberg, J.W. Nortier, Int. J. Biol. Markers 17 (2002) 24.
[15] C.C. Lin, J. Veals, C. Korduba, M.J. Hilbert, A. Nomeir, Therap. Drug Monitor. 19 (1997) 675.

[16] L.O. White, Therap. Drug Monitor. 20 (1998) 464.
[17] H.J. Pieniaszek, A.F. Davidson, H.L. Walton, D.J. Pinto, R.E. Olson, T.M. Reilly, Y.C. Barrett, J. Pharm. Biomed. Anal. 30 (2003) 1441.
[18] F. Boudet, J. Thèze, M. Zouali, J. Immunol. Meth. 142 (1991) 73.
[19] S. Sachetelli, C. Beaulac, J. Lagacé, Biochim. Biophys. Acta 1379 (1998) 35.
[20] J. Sondergard-Anderson, E. Lauritzen, K. Lind, A. Holm, J. Immunol. Meth. 131 (1990) 99.
[21] I.A. Darwish, D.A. Blake, Anl. Chem. 74 (2002) 52.
[22] I.A. Darwish, J. Pharm. Biomed. Anal. 30 (2003) 1539.
[23] E. Harlow, D. Lane, Antibodies: A Laboratory Manual, Cold Spring Harbor Laboratory, USA, 1988, p. 533.
[24] D.J. Anderson, Clin. Chem. 35 (1989) 2152.
[25] Y.G. Tsay, R.G. Palmer, Clin. Chim. Acta 109 (1981) 151.
[26] J.W.A. Findlay, W.C. Smith, J.W. Lee, G.D. Nordblom, I. Das, B.S. DeSilva, M.N. Khan, R.R. Bowsher, J. Pharm. Biomed. Anal. 21 (2000) 1249.
[27] C. Beaulac, S. Clément-Major, J. Hawari, J. Lagacé, Antimicrob. Agents Chemother. 40 (1996) 665.
[28] R.M. Shawar, D.L. MacLeod, R.L. Garber, J.L. Burns, J.R. Stapp, C.R. Clausen, S.K. Tanaka, Antimicrob. Agents Chemother. 43 (1999) 2877.
[29] E. Jametz, B.G. Katzung (Eds.), Basic and Clinical Pharmacology, Appleton & Lange, Connecticut, 1992, p. 645.
[30] C.A. Hammett-Stabler, T. Johns, Clin. Chem. 44 (1998) 1129.
[31] T. Koeda, K. Umemura, M. Yokota, in: H. Umezawa, I.R. Hooper (Eds.), Aminoglycoside Antibiotics, Springer-Verlag, Berlin, 1982, p. 293.
[32] V.P. Hanko, J.S. Rohrer, J. Pharm. Biomed. Anal. 40 (2006) 1006.
[33] B.G. Keevil, S.J. Lockhart, D.P. Cooper, J. Chromatogr. B: Analyt. Technol. Biomed. Life Sci. 794 (2003) 329.
[34] L. Soltes, Biomed. Chromatogr. 13 (1999) 3.
[35] R. Tawa, H. Matsunaga, T. Fujimoto, J. Chromatogr. A 812 (1998) 141.
[36] C.D.C. Salisbury, in: H. Oka, H. Nakazawa, K. Harada, J.D. MacNeil (Eds.), Chemical Analysis for Antibiotics Used in Agriculture, AOAC Inter, Arlington, VA, 1995, p. 307.
[37] J. Centofanti, in: D. Wild (Ed.), The Immunoassay Handbook, Stockton Press, New York, 1994, p. 216.
[38] D.A. Stead, J. Chromatogr. B 747 (2000) 69.
[39] M. Laakel, M. bouhard, J.J. Lagacé, J. Immunol. Meth. 190 (1996) 267.
[40] J. Lagacé, S. Arsenault, E.A. Cohen, J. Immunol. Meth. 175 (1994) 131.

Available online at www.sciencedirect.com
ScienceDirect
Talanta 72 (2007) 1546–1551
Talanta
www.elsevier.com/locate/talanta

Extraction study of algal pigments in river bed sediments by applying factorial designs

R. Devesa [a,*], A. Moldes [a,b], F. Díaz-Fierros [a], M.T. Barral [a]

[a] *Departamento de Edafología y Química Agrícola, Facultad de Farmacia, USC, 15782 Santiago de Compostela, Spain*
[b] *Departamento de Ingeniería Química, Facultad de Ciencias, Universidad de Vigo, 32004 Ourense, Spain*

Received 23 August 2006; received in revised form 30 January 2007; accepted 5 February 2007
Available online 15 February 2007

Abstract

Phytopigment content of river bed sediments changes in response to different concentrations of available nutrients and results in a useful descriptor of their trophic state and environmental quality. In this work three incomplete factorial designs of experiments were carried out for extracting algal pigments from river sediments using dimethylsulphoxide (DMSO), methanol or acetone. The independent variables used in this study and their variation limits were: extractant:sediment ratio (1–5 mL/g), temperature (40–80 °C) and duration of treatments (30–90 min). The experimental data obtained (chlorophyll-*a*, chlorophyll-*b* and total carotenoids content) allowed the development of empirical models for each phytopigment, describing the interrelationship between operational and experimental variables by equations, including linear, interaction and quadratic terms. The experimental results obtained showed that methanol and acetone were less effective extractants for phytopigments from river sediments when compared to DMSO. The model predicted that in a single extraction using 3.6 mL of DMSO/g of sediment at 38 °C during 40 min, DMSO releases the 89% of chlorophyll-*a* in the range tested, whereas the best conditions for extracting chlorophyll-*b* and total carotenoids are achieved using 3.6–3.7 mL of DMSO/g of sediment, at 64–67 °C for 50–51 min, respectively, releasing the 76% of the chlorophyll-*b* and the 100% of the total carotenoids in a single extraction.

Keywords: Phytopigments; River sediments; Methanol; Acetone; Dimethylsulphoxide; Factorial design

1. Introduction

Human activity can accelerate the development of anoxic bottom waters. The addition of algal nutrients such as phosphorus derived from agricultural runoff and from sewage discharges can led to an increase in algal growth and a consequent increase in the amount of organic matter undergoing respiration, leading to the depletion of dissolved oxygen. This process is termed eutrophication. The development of bottom water anoxia has a number of undesirable consequences. Perhaps the most obvious is the enormous amount of fish that are killed, particularly those species that need oxygen-rich water to survive. Moreover anoxia and especially eutrophication can lead to blooms of nuisance and toxic algae and the productions of water-borne toxins. Phytoplankton represents the major synthesis of organic matter in aquatic systems, even at different rates of anoxia, where phytoplankton community is capable of assimilating bicarbonate ions under low free CO_2 concentrations. Consequently, phytopigment content of river bed sediments changes in response to different sources of anthropogenic impact and results in a useful descriptor of their trophic state and environmental quality [1–4]. In the literature there are a variety of methods for extracting phytopigments from epilithic biofilms using solvents, but their relative efficiency have not been determined and there is no recognized a standard procedure for analyzing phytopigments in river sediments. In some works chlorophyll from microbial biofilms has been extracted by immersing samples in acetone [5–7], alcohol [8–11] or mixtures of solvents [12,13]. In this work, we aimed at optimizing the extraction of phytopigments from river bed sediments by testing three different solvents, dimethylsulphoxide, methanol and acetone, acting at different sediment:solution ratios and extraction times. The algal pigments analyzed were chlorophyll-*a*, chlorophyll-*b* and total carotenoids. Since a systematic study of the effects caused by the

* Corresponding author. Tel.: +34 981563100.
E-mail address: rosadrey@usc.es (R. Devesa).

0039-9140/$ – see front matter © 2007 Elsevier B.V. All rights reserved.
doi:10.1016/j.talanta.2007.02.006

Table 1
Equations proposed by Wellburn [14] to determine phytopigments by measuring the absorbances at different wavelenghs in various solvents

Solvent	Phytopigment	Equations proposed
DMSO	Chlorophyll-*a*	$C_a = 12.47A_{665.1} - 3.62A_{649.1}$
	Chlorophyll-*b*	$C_b = 25.06A_{649.1} - 6.5A_{665.1}$
	Total carotenoids	$C_{x+c} = (1000A_{480} - 1.29C_a - 53.78C_b)/220$
Methanol	Chlorophyll-*a*	$C_a = 16.72A_{665.2} - 9.16A_{652.4}$
	Chlorophyll-*b*	$C_b = 34.09A_{652.4} - 15.28A_{665.2}$
	Total carotenoids	$C_{x+c} = (1000A_{470} - 1.63C_a - 104.96C_b)/221$
80% acetone	Chlorophyll-*a*	$C_a = 12.25A_{663.2} - 2.79A_{646.8}$
	Chlorophyll-*b*	$C_b = 21.5A_{646.8} - 5.1A_{663.2}$
	Total carotenoids	$C_{x+c} = (1000A_{470} - 1.82C_a - 85 - 0.02C_b)/198$

operational variables on the extraction of phytopigments would require a great amount of experimental work, an incomplete, factorial design of experiments was carried out for each solvent, to select the best conditions, in which three dependent variables (chlorophyll-*a*, chlorophyll-*b* and total carotenoids) were assayed at three levels.

2. Materials and methods

2.1. Extraction process

Samples of river sediments were freeze-dried and sieved by 2 mm. Pigment extractions were carried out employing 5 g of surface sediment samples taken from the Anllóns River (NW, Spain). The sediment samples were mixed with variable volumes of extractant and incubated at different times under different temperatures. Algal pigments were extracted with DMSO (99.5%), methanol (99.5%) or acetone (80%), using an incomplete 3^3 factorial design in order to study the influence of volume of extractant (x_1), temperature (x_2) and extraction time (x_3) on the chlorophyll-*a* (y_1), chlorophyll-*b* (y_2) and total carotenoids (y_3) content. Moreover, in order to calculate the percentage of extraction, consecutive extractions were carried out for the different organic solvents, until negligible concentrations of phytopigments were detected in the extracts.

2.2. Determination of phytopigments

In the extracts, chlorophyll-*a*, chlorophyll-*b* and total carotenoids were determined following the methodology proposed by Wellburn [14]. The equations employed to determine the concentrations of chlorophyll-*a* and chlorophyll-*b* as well as total carotenoids, expressed in $\mu g\,mL^{-1}$, in different solvents, are shown in Table 1. C_a and C_b represent the concentration of chlorophyll-*a* and chlorophyll-*b*, respectively, $A_{665.1}$ the absorbance at 665.1 nm and $A_{649.1}$ is the absorbance at 649.1 nm (used for DMSO extractions). $A_{665.2}$ is the absorbance at 665.2 and $A_{652.4}$ is the absorbance at 652.4 nm (used for methanol extractions), and $A_{663.2}$ is the absorbance at 663.2 nm and $A_{646.8}$ is the absorbance at 646.8 nm (used for acetone extractions). C_{x+c} is the concentration of total carotenoids and A_{480} is the absorbance at 480 nm (used for DMSO), whereas A_{470} is the absorbance at 470 nm (used for methanol and acetone). Concentrations of phytopigments were given as microgram of phytopigment per gram of sediment.

2.3. Experimental design and statistical analysis

In order to optimize the extraction of phytopigments from river sediments, an incomplete 3^3 factorial design [15] was used to study the influence of volume of extractant, temperature and reaction time on the concentration of phytopigments in the organic phase.

The experimental data were analyzed by the response surface method using the software Statistica 5.0. The experimental data allowed the development of empirical models describing the interrelationship between operational and experimental variables by equations including linear, interaction and quadratic terms:

$$y = b_0 + b_1x_1 + b_2x_2 + b_3x_3 + b_{12}x_1x_2 + b_{13}x_1x_3 + b_{23}x_2x_3 + b_{11}x_1^2 + b_{22}x_2^2 + b_{33}x_3^2$$

where y is the dependent variable, b denotes the regression coefficients (calculated from experimental data by multiple regression using the least-squares method) and x denotes the independent variables.

The independent variables used in this study and their variations limits were: extractant:sediment ratio ES (1–5 mL/g sediment corresponding to 5–25 mL of extractant), temperature T (40–80 °C) and duration of treatments t (30–90) min. Table 2 lists the independent and dependent variables considered: chlorophyll-*a*, was measured by the variable y_1; chlorophyll-*b* by the variable y_2 and carotenoids by the variable y_3. The standardized (coded) dimensionless variables employed, having variations limits (−1, 1), were defined as

Table 2
Independent and dependent variables employed in this study

Variable	Nomenclature	Units	Variation range
(a) Independent variables			
Extractant:sediment ratio	ES	mL/g	1–5
Temperature	T	°C	40–80
Time	t	min	30–90

Variable	Nomenclature	Definition	Variation range
(b) Dimensionless, coded independent variables			
Dimensionless volume of extractant	x_1	(ES − 25)/5	(−1, 1)
Dimensionless temperature	x_2	(T − 80)/40	(−1, 1)
Dimensionless time	x_3	(t − 90)/30	(−1, 1)

Variable	Nomenclature
(c) Dependent variables	
Chlorophyll-*a*	y_1
Chlorophyll-*b*	y_2
Carotenoids	y_3

Table 3
Operational conditions considered in this study (expressed in terms of the coded independent variables dimensionless volume of dimethylsulphoxide (DMSO) x_1, dimensionless temperature x_2 and dimensionless time x_3) and experimental results achieved for the dependent variables y_1 (chlorophyll-*a*), y_2 (chlorophyll-*b*), and y_3 (carotenoids) as μg of phytopigments/g of sediment

Experimental	Independent variables			Dependent variables		
	x_1	x_2	x_3	y_1	y_2	y_3
1	0	−1	−1	60.0	36.4	10.9
2	0	1	−1	21.0	15.3	3.8
3	0	−1	1	46.6	32.6	10.4
4	0	1	1	27.0	21.4	5.2
5	−1	−1	0	10.0	7.2	1.6
6	−1	1	0	8.5	6.1	1.1
7	1	−1	0	30.0	21.2	6.2
8	1	1	0	30.0	20.8	6.6
9	−1	0	−1	9.5	8.5	1.3
10	−1	0	1	10.1	9.3	1.3
11	1	0	−1	40.0	27.0	8.2
12	1	0	1	45.0	30.4	10.1
13	0	0	0	48.0	32.4	10.9
14	0	0	0	48.0	32.2	10.2
15	0	0	0	48.0	31.8	10.6

Table 5
Operational conditions considered in this study (expressed in terms of the coded independent variables dimensionless volume of acetone x_1, dimensionless temperature x_2 and dimensionless time x_3) and experimental results achieved for the dependent variables y_1 (chlorophyll-*a*), y_2 (chlorophyll-*b*), and y_3 (carotenoids) as μg of phytopigments/g of sediment

Experimental	Independent variables			Dependent variables		
	x_1	x_2	x_3	y_1	y_2	y_3
1	0	−1	−1	19.6	18.3	3.5
2	0	1	−1	21.4	19.3	4.2
3	0	−1	1	21.0	19.0	3.7
4	0	1	1	19.9	18.5	3.3
5	−1	−1	0	4.8	4.3	0.7
6	−1	1	0	4.5	4.1	0.3
7	1	−1	0	24.6	23.2	4.7
8	1	1	0	21.6	19.5	3.9
9	−1	0	−1	4.9	4.6	1.0
10	−1	0	1	5.2	4.7	0.9
11	1	0	−1	24.8	23.8	4.2
12	1	0	1	22.0	21.4	3.4
13	0	0	0	19.7	18.4	3.9
14	0	0	0	20.0	18.4	4.1
15	0	0	0	19.9	19.0	4.0

x_1 (coded volume of extractant), x_2 (coded temperature) and x_3 (coded duration of treatment). The correspondence between coded and uncoded variables was established by linear equations deduced from their respective variation limits. Moreover, in order to test the reproducibility of the model, the optima conditions predicted by the model will be tested experimentally.

3. Results and discussion

Tables 3–5 show the set of experimental conditions assayed for each organic extractant (expressed in terms of coded variables), as well as the experimental data obtained for variables y_1–y_3. The sequence for the experimental work was randomly established to limit the influence of systematic errors on the interpretation of results. It can be noted that experiments 1–12 allowed the calculation of the regression coefficients, whereas experiments 13–15 were replications in the central point of the design to estimate the influence of the experimental error.

Table 6 shows the optima conditions for obtaining the maximum amount of phytopigments by using DMSO, methanol and acetone in a single extraction. The extractant:sediment ratio was the most influent parameter, followed by the temperature of extraction. The time of extraction showed the lower effect on the extraction process. The extraction of phytopigments with acetone or methanol was less effective than the

Table 4
Operational conditions considered in this study (expressed in terms of the coded independent variables dimensionless volume of methanol x_1, dimensionless temperature x_2 and dimensionless time x_3) and experimental results achieved for the dependent variables y_1 (chlorophyll-*a*), y_2 (chlorophyll-*b*), and y_3 (carotenoids) as μg of phytopigments/g of sediment

Experimental	Independent variables			Dependent variables		
	x_1	x_2	x_3	y_1	y_2	y_3
1	0	−1	−1	32.0	23.0	3.6
2	0	1	−1	29.8	21.0	4.0
3	0	−1	1	28.4	20.8	1.2
4	0	1	1	21.8	16.2	0.1
5	−1	−1	0	8.0	7.1	0.4
6	−1	1	0	7.8	6.9	0.8
7	1	−1	0	35.6	25.0	5.1
8	1	1	0	27.6	19.5	3.5
9	−1	0	−1	8.3	7.0	0.1
10	−1	0	1	8.9	7.0	0.2
11	1	0	−1	31.0	21.8	3.5
12	1	0	1	37.4	25.0	3.0
13	0	0	0	25.2	18.1	2.5
14	0	0	0	25.4	18.2	2.4
15	0	0	0	25.4	18.0	2.6

Table 6
Optima conditions predicted by the model for obtaining the maximum concentration of phytopigments through extraction with dimethylsulphoxide (DMSO), methanol and acetone

Phytopigments	Independent variables			Dependent variables
	ES ratio (mL/g)	Extraction time (min)	T (°C)	μg of phytopigment/g of sediment
DMSO				
Chlorophyll-*a*	3.6	38	40	53.4
Chlorophyll-*b*	3.7	50	67	34.4
Total carotenoids	3.7	51	64	11.4
Methanol				
Chlorophyll-*a*	5.0	30	40	36.2
Chlorophyll-*b*	4.9	30	40	25.6
Total carotenoids	5.0	30	48	5.1
Acetone				
Chlorophyll-*a*	4.8	30	40	25.0
Chlorophyll-*b*	4.9	30	40	24.0
Total carotenoids	4.3	69	40	4.7

Table 7
Regression coefficients, significance level (p) and statistical parameters (r^2 and F) measuring the correlation an significance of the models proposed for the extraction of phytopigments from river sediments with DMSO

Coefficients	y_1	p_{y_1}	y_2	p_{y_2}	y_3	p_{y_3}
b_0	−11.8915	0.000650	−11.4130	0.00136	−12.590	0.03621
b_1	7.0669	0.000002	4.5325	0.00001	1.492	0.00360
b_{11}	−0.2045	0.000001	−0.1292	0.00001	−0.045	0.00183
b_2	0.3070	0.000180	0.3184	0.00032	0.180	0.03280
b_{22}	−0.0089	0.000009	−0.0058	0.00004	−0.002	0.00772
b_3	−0.1483	0.002718	−0.1131	0.00896	0.173	0.11060
b_{33}	−0.0036	0.000275	−0.0011	0.00601	−0.002	0.05378
b_{12}	0.0012	0.003790	−0.0001	0.38160	0.001	0.32996
b_{13}	0.0055	0.000438	0.0031	0.00255	0.002	0.12931
b_{23}	0.0081	0.000022	0.0039	0.00018	0.001	0.11971

Variable	R^2	F_{exp}	Significance level (based on the F test)
y_1	0.88	79,319	99
y_2	0.91	11,997	99
y_3	0.89	54	98

extraction carried out with DMSO. The model predicted, under the optima conditions, that DMSO will extract 89% of the total chlorophyll-*a*, 76% of the total chlorophyll-*b*, and 100% of the total carotenoids. The extraction by using methanol will extract 60% of the total chlorophyll-*a*, 66% of the total chlorophyll-*b*, and 44% of the total carotenoids; whereas acetone will extract 41% of chlorophyll-*a*, 62% of chlorophyll-*b*, and 41% of carotenoids. Methanol poorly extracted phytopigments compared to the results obtained by Thompson et al. [16], which extracted phytopigments from rocks employing acetone, methanol or mixtures of solvents, and found that acetone had very poor extraction efficiency (less than 50% of phytopigments), whereas hot ethanol extracted 86%, and methanol, at room temperature, released over 96% of the total chlorophyll during a single extraction. The differences between the results obtained by Thompson et al. [16] and our data can be due to the nature of the microbial biomass. Algal biomass that grows in marine and river sediments is not the same; also, the effectiveness of the organic solvent for extracting phytopigments can be conditioned by the nature of sediments or rocks. For instance, some authors consider that acetone is satisfactory for extracting phytopigments from diatoms, whereas alcohol is more adequate for extracting phytopigments from cyanobacteria [8,17,18]. Moreover other authors have reported that hot alcohol favoured rapid phytopigment extractions [8] whereas others proposed the utilization of longer extraction periods at room temperature [12,19,20] or under refrigerated conditions [18].

Moreover, Tables 7–9 list the regression coefficients and their statistical significance. The same tables include statistical parameters (r^2 and F) measuring the correlation and the statistical significance of the models, respectively. It can be noted that all the models showed good statistical parameters for correlation and significance, allowing a close reproduction of experimental data. The significance levels (p) for some regression coefficients were higher than 0.05, but their corresponding coefficients had very low values in the equation proposed by the model. So, these parameters will not have a great influence in the values of the dependent variables. Moreover, the statistical significance of the model was satisfactory, based on the F-test. Nevertheless, in order to assess the prediction ability of the model, experimental work was carried out under the optima conditions predicted by the model and the differences observed between experimental and calculated data were lower than 15%. The prediction ability of the model was tested only for DMSO, as it is the extractant that achieves the best phytopigment extractions and, in consequence, the extractant proposed to carry out the phytopigment extractions. So, under the optima conditions, with DMSO, the model predicted the extraction of 53.4 μg of chlorophyll-*a*/g of sediment, 34.4 μg of chlorophyll-*b*/g of sediment and 11.4 μg of total carotenoids/g of sediment, which are close to the concentrations obtained under experimental conditions (Table 10).

Fig. 1 shows the model prediction for the dependence of chlorophyll-*a* (y_1), chlorophyll-*b* (y_2) and carotenoids (y_3) extracted with DMSO on the most influential operational

Table 8
Regression coefficients, significance level (p) and statistical parameters (r^2 and F) measuring the correlation an significance of the models proposed for the extraction of phytopigments from river sediments with methanol

Coefficients	y_1	p_{y_1}	y_2	p_{y_2}	y_3	p_{y_3}
b_0	14.059	0.00012	12.6451	0.0025	−5.5162	0.0201
b_1	3.018	0.00000	2.0884	0.0001	0.3922	0.0054
b_{11}	−0.061	0.00000	−0.0428	0.0001	−0.0028	0.0461
b_2	0.069	0.00092	−0.0308	0.0703	0.0206	0.1958
b_{22}	0.001	0.00050	0.0009	0.0039	0.0003	0.0586
b_3	−0.656	0.00004	−0.4311	0.0014	0.1550	0.0167
b_{33}	0.005	0.00003	0.0034	0.0013	−0.0013	0.0152
b_{12}	−0.006	0.00004	−0.0043	0.0014	−0.0016	0.0148
b_{13}	0.007	0.00007	0.0041	0.0035	−0.0007	0.1606
b_{23}	−0.002	0.00010	−0.0010	0.0059	−0.0006	0.0256

Variable	R^2	F_{exp}	Significance level (based on the F-test)
y_1	0.97	27949	99
y_2	0.98	515	99
y_3	0.88	106	99

Table 9
Regression coefficients, significance level (p) and statistical parameters (r^2 and F) measuring the correlation an significance of the models proposed for the extraction of phytopigments from river sediments with acetone

Coefficients	y_1	p_{y_1}	y_2	p_{y_2}	y_3	p_{y_3}
b_0	−11.4289	0.0096	−10.0389	0.0503	−5.9341	0.0075
b_1	3.1292	0.0002	2.9010	0.0009	0.6833	0.0008
b_{11}	−0.0615	0.0002	−0.0550	0.0011	−0.0145	0.0008
b_2	0.0830	0.0325	0.1171	0.0664	0.0485	0.0203
b_{22}	0.0001	0.3365	−0.0004	0.2018	−0.0002	0.0654
b_3	−0.0243	0.4879	−0.0771	0.3262	0.0836	0.0241
b_{33}	0.0011	0.0353	0.0012	0.1130	−0.0004	0.0496
b_{12}	−0.0023	0.0153	−0.0030	0.0368	−0.0004	0.1127
b_{13}	−0.0038	0.0125	−0.0032	0.0671	−0.0009	0.0402
b_{23}	−0.0012	0.0132	−0.0007	0.1516	−0.0004	0.0206

Variable	R^2	F_{exp}	Significance level (based on the F-test)
y_1	0.99	30	97
y_2	0.99	9	90
y_3	0.98	42	98

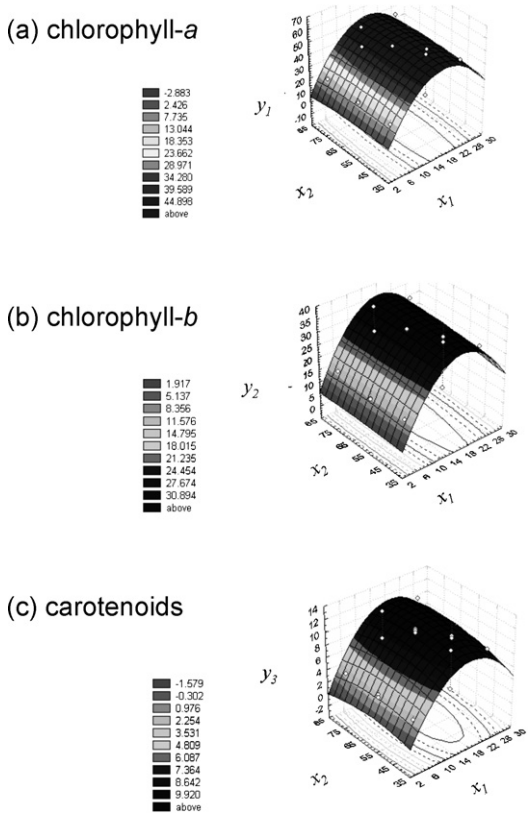

Fig. 1. (a) Dependence of chlorophyll-a (variable y_1) on extractant:sediment ratio (x_1) and temperature (x_2) predicted for samples extracted during 60 min; (b) dependence of chlorophyll-b (variable y_2) on extractant:sediment ratio (x_1) and temperature (x_2) predicted for samples extracted during 60 min; (c) dependence of carotenoids (variable y_3) on extractant:sediment ratio (x_1) and temperature (x_2) predicted for samples extracted during 60 min.

variable (extractant:sediment ratio) and on temperature, in experiments lasting 60 min (the intermediate duration of treatments). As it was said before, the parameter that mostly influence phytopigment extraction is the extractant:sediment ratio. In the range tested, temperature of extraction caused lower effects on the phytopigment extractions with DMSO. Finally, the time of extraction was the parameter with lesser influence on the phytopigment extraction. Increased severity (defined by DMSO:sediment ratios up to 3.6 mL/g) resulted in a remarkable increase in the release of phytopigments, however ratios of DMSO:sediment higher than 3.6 mL/g reduced the amount of phytopigments in the extract. This fact can be due to that, before analyzing phytopigments, the extractant has to be filtered and, in samples with higher volume of extractant, the filtration process with DMSO takes longer and the phytopigments can be unstable. Table 10 shows the optima conditions for DMSO extraction. It can be observed that the model predicts slightly different conditions for each phytopigment extraction. Consequently, a suitable approach for analyzing chlorophyll-a, chlorophyll-b and total carotenoids in the same set of experiments would be to utilize intermediate optima conditions obtained from the mean values of the optima conditions predicted by the model for each phytopigment. These intermediate optima conditions do not modify to a great extent the optima predicted by the model as they suppose negligible variations on the extractant:sediment ratio, the parameter that mostly influences the phytopigment extractability. So, the intermediate conditions for DMSO consisted in 3.6 mL of DMSO/g of sediments during 42 min at 57 °C. Using these conditions the model predicts that 52 μg g^{-1} of chlorophyll-a, 31.4 μg g^{-1} of chlorophyll-b and 11 μg g^{-1} of carotenoids would be obtained in the extracts. These values are very close to the values predicted by the model under the optima conditions (see Table 10).

In this study, we have observed that DMSO was the best extractant to analyze phytopigments from river bed sediments compared with methanol or acetone. In all the extractions the main algal phytopigments in the extract consisted in chlorophyll-a and chlorophyll-b. Among the independent variables assayed the extractant:sediment ratio was the most influential variable.

Table 10
Total concentrations of phytopigments predicted by the model after extraction of phytopigments with DMSO under the optima conditions and experimental results obtained under the same conditions

Phytopigments	ES ratio DMSO (mL/g)	t (min)	T (°C)	Predicted μg of phytopigment/g of sediment	Experimental μg of phytopigment/g of sediment
Chlorophyll-a	3.6	38	40	53.4	48.1
Chlorophyll-b	3.7	50	67	34.4	31.0
Total carotenoids	3.7	51	64	11.4	9.9

In all cases the differences between the model and the experimental data were under 15%.

4. Conclusion

The extraction of phytopigment from river bed sediments using DMSO, methanol or acetone can be described by using empirical models, through the interrelationship between operational and experimental variables by equations including linear, interaction and quadratic terms. Among the organic solvents employed, DMSO gave the best results for extracting phytopigments from river bed sediments. The optima conditions predicted by the model for extracting chlorophyll-*a* consisted in 3.6 mL of DMSO/g of sediment at 38 °C during 40 min, whereas for extracting chlorophyll-*b* and carotenoids it would be necessary to employ 3.6–3.7 mL of DMSO/g of sediment at 64–67 °C during 50–51 min, respectively.

Acknowledgements

The present study was financed by the Science and Education Ministry of Spain (MEC, REN 2003-08673/BES-2004-5894). Rosa Devesa was granted with a FPI grant.

References

[1] E. Litchman, D. Steiner, P. Bossard, Freshw. Biol. 48 (2003) 2141–2148.
[2] A. Dell'Anno, M. Mei, A. Pusceddu, R. Danovaro, Mar. Pollut. Bull. 44 (2002) 611–622.
[3] M. Bechmann, D. Berge, H. Eggestad, S. Vandsemb, J. Hydrol. 304 (2005) 238–250.
[4] P. Pagliosa, F. Rodrigues Barbosa, Biol. Conserv. 129 (2006) 408–417.
[5] A.J. Underwood, J. Exp. Mar. Biol. Ecol. 78 (1984) 199–220.
[6] K. Wiltshire, Limnologica 30 (2000) 205–214.
[7] N. Reuss, D.J. Conley, T.S. Bianchi, Mar. Chem. 95 (2005) 283–302.
[8] A.S. Hill, S.J. Hawkins, J. Mar. Biol. Assoc. U.K. 70 (1990) 77–88.
[9] R.H. Bustamante, G.M. Branch, S. Eekhout, B. Robertson, P. Zoutendyk, M. Schleyer, A. Dye, N. Hanekom, D. Keats, M. Jurd, C. McQuaid, Oecologia 102 (1995) 189–201.
[10] V. Brotas, M.R. Plante-Cuny, Acta. Oecologica Int. J. Ecol. 24 (2003) 109–115.
[11] B. Jesus, C.R. Mendes, V. Brotas, D.M. Paterson, J. Exp. Mar. Biol. Ecol. 332 (2006) 60–74.
[12] A.H. Dye, R.A. White, South Afr. J. Mar. Sci. 11 (1991) 483–489.
[13] E. Ergun, B. Demirata, G. Gumus, R. Apak, Anal. Bioanal. Chem. 379 (2004) 803–811.
[14] A. Wellburn, J. Plant Physiol. 144 (1994) 307–313.
[15] G.E.P. Box, W.G. Hunter, J.S. Hunter, Statistic for Experimenters: an Introduction to Design, Data Analysis and Model Building, John Wiley, New York, 1978.
[16] R.C. Thompson, M.L. Tobin, S.J. Hawkins, T.A. Norton, J. Mar. Biol. Assoc. U.K. 79 (1999) 551–558.
[17] A.F.H. Marker, E.A. Nusch, H. Rai, B. Riemann, Ergenbisse der Limnologie 14 (1980) 91–106.
[18] S. Nagarkar, G.A. Willians, Mar. Ecol. Prog. Ser. 154 (1997) 281–291.
[19] R.W. Castenholz, Ecology 42 (1961) 783–794.
[20] M.E. Nicotri, Ecology 58 (1977) 1020–1032.

Available online at www.sciencedirect.com
ScienceDirect
Talanta 72 (2007) 1275–1282
Talanta
www.elsevier.com/locate/talanta

Preparation and characterization of sensing membranes for the detection of glucose, lactate and tyramine in microtiter plates

Hong Dinh Duong, Jong Il Rhee *

Department of Material and Biochemical Engineering, School of Applied Chemical Engineering, Research Center for Biophotonics, Chonnam National University, YongBong-dong 300, 500-757 GwangJu, Republic of Korea

Received 13 November 2006; received in revised form 10 January 2007; accepted 10 January 2007
Available online 19 January 2007

Abstract

In this work, sensing membranes for the detection of glucose, lactate and tyramine were successfully prepared by immobilizing enzymes and fluorophore on sol–gels. The membranes were fabricated on the bottom of the wells in a microtiter plate. Glucose oxidase (GOD), lactate oxidase (LOD) and tyramine oxidase (TOD) were immobilized on individual sol–gels or a mixture of different sol–gels (3-glycidoxypropyl-trimethoxysilane (GPTMS), methyl-triethoxysilane (MTES), aminopropyl-trimethoxysilane (APTMS)). The oxidation of the analytes specifically catalyzed by the enzymes resulted in the reduction of the oxygen concentration, which changed the fluorescence intensity (FI) of the oxygen sensitive ruthenium complex acting as the transducer. The linear calibration graphs were in the ranges of 0.0–5.0 g/l for glucose, 0.0–9.0 mg/l for lactate and 0.0–100 mg/l for tyramine. The values of the detection limit were found to be 0.10–0.52 g/l for glucose, 7.77 mg/l for lactate and 6.30–8.73 mg/l for tyramine. The covalent binding between the epoxy and amine groups of the sol–gels and enzymes, respectively, prevented the enzymes from being washed out and preserved the high stability of the sensing membranes. The different ratios of silanes in the sol–gels, which were used as the supporting matrix for the immobilization of the enzymes led to different responses of the sensing membranes to various concentrations of glucose, lactate and tyramine. The kinetic parameters of the enzymatic reactions, and the stability and other parameters for the sensing membranes were also investigated.

Keywords: Enzyme immobilization; Fluorophore; Glucose oxidase; Microtiter plate; Lactate oxidase; Sol–gel; Tyramine oxidase

1. Introduction

Microtiter plates have been extensively used for high-throughput screening applications, enzyme-immunometric assay or toxicity tests, etc. [1]. They offer the advantages of a small sample volume and simultaneous screening of high numbers of samples. For the simultaneous measurements of samples, microplate readers capable of quickly detecting the absorbance or fluorescence changes in the plate have also come into wide use in many works [1–4]. Furthermore, microplate readers have been applied to other functions such as the measurement of enzyme kinetics [3,5] and respiration of cells [4,7,10,12], as well as bio- and chemi-luminescence multiplexed quantitative assays [6]. In a microtiter plate, enzymes or analytes such as metabolites and proteins can be integrated with some indicators in a liquid medium [7–9] or in a thin layer at the bottom of the wells [10–12]. Their integration over the selected target areas allows for the quantitative evaluation of the emitted light, which is related to the identity and concentration of the analytes.

Many chemical and physical methods have been employed for the integration of enzymes or analytes into supporting materials. Among them, a few chemical immobilization methods, which involve the covalent coupling of the enzymes/analytes to functionalized carriers or the intermolecular cross-linking of the biomolecules are widely applied in the preparation of sensing membranes [13]. Among the various immobilization methods, the sol–gel technique, i.e. the encapsulation of the analyte/enzyme into a supporting material, has been intensively considered, since sol–gel solutions are chemically inert, physically stable and optically transparent materials [14]. Many sol–gel systems have been developed for the immobilization of enzymes or other biomolecules [15–21] to date. However, the relationship between the properties of the sol–gel systems and the resulting activity of the immobilized enzyme or biomolecule

* Corresponding author. Tel.: +82 62 530 1847; fax: +82 62 530 0846.
E-mail address: jirhee@chonnam.ac.kr (J.I. Rhee).

0039-9140/$ – see front matter © 2007 Elsevier B.V. All rights reserved.
doi:10.1016/j.talanta.2007.01.028

is not yet well understood. Moreover, there are few general sol–gel systems which can be used in similar applications. Therefore, it is often necessary to find optimal sol–gel systems for the effective immobilization of a certain enzyme or biomolecule onto the supporting materials.

Recently, the need to analyze glucose, lactate and tyramine in fermentation processes, food preparation and medical studies has increased. Glucose is by far the most important nutrient source for microorganisms in biotechnological processes. This carbon source is used in almost 95% of all fermentation processes. Therefore, the measurement of glucose concentrations is essential for the control of various biotechnological processes [22]. Moreover, glucose monitoring plays an important role in diagnosing many metabolic disorders, especially in the diagnosis and therapy of diabetes. For the measurement of lactate, the determination of D(−)- and L(+)-lactic acid is required whenever the quality of a food product has to be assessed. Levels of L(+)-lactic acid higher than 3 g/kg are usually considered as an index of microbial contamination [23,24]. This is the same principle as that used in the determination of tyramine in fermented foods. The presence of tyramine and other biogenic amines might pose a health risk to consumers who have a deficiency or lower activity of amino acid oxidase, due to the intake of inhibitory drugs, alcohol or gastrointestinal diseases [25].

From this point of view, we designed optical planar biosensors for the detection of glucose, lactate and tyramine using a microtiter plate. The principle of the measurement is based on the oxidation of the analytes (glucose, lactate, tyramine) specifically catalyzed by enzymes:

$$\text{Analytes} + O_2 \xrightarrow{\text{Enzyme}} \text{Oxidized products} + H_2O_2$$

This reaction leads to a reduction in the concentration of oxygen, which has an effect on the fluorescence intensity (FI) of the ruthenium complex acting as the transducer. The enzymes (glucose oxidase (GOD), lactate oxidase (LOD), tyramine oxidase (TOD)) and fluorophore were immobilized on an individual sol–gel or a mixture of sol–gels consisting of 3-glycidoxypropyl-trimethoxysilane (GPTMS), methyl-triethoxysilane (MTES) and aminopropyl-trimethoxysilane (APTMS). In this work, we prepared three different sol–gel systems for the immobilization of the ruthenium complex and enzymes and investigated the performances of these sol–gel systems to detect the concentrations of glucose, lactate and tyramine.

2. Experimental

2.1. Materials

Glucose oxidase (from *Aspergilus niger*, 47.2 U/mg solid), lactate oxidase (from *Pediococcus* sp., 20 U/mg solid), tyramine oxidase (from *Arthrobacter* sp., 3.9 U/mg solid), 3-aminopropyl-trimethoxysilane, 3-glycidoxypropyl-trimethoxysilane and methyltriethoxysilane were purchased from Sigma–Aldrich Chemical Co. (Seoul, Korea). Tris(4,7-diphenyl-1,10-phenanthroline) ruthenium complex was synthesized in our laboratory.

Table 1
Mixture ratio of silanes used for the preparation of the sol–gels

Sol–gel	GPTMS (v/v, %)	APTMS (v/v, %)	MTES (v/v, %)	EtOH (v/v, %)	35% HCl (μl/ml)
GT	37.5	–	–	62.5	20
GA1	12.5	6.25	–	81.25	40
GA2	25.0	6.25	–	68.75	40
GM1	12.5	–	12.5	75.0	40
GM2	12.5	–	25.0	62.5	40

All other chemicals were of analytical grade and used without further purification.

2.2. Preparation of the sensing membrane

The sensing membrane consisted of a transducer (ruthenium complex + sol–gel) and a biological detection element (enzyme + sol–gel). The sol–gels used were prepared by the hydrolyzation and polymerization of mixtures of GPTMS and APTMS or GPTMS and MTES or GPTMS alone in 99% ethanol solvent. The mixture ratio of these silanes and the volume of 35% hydrochloric acid added to the mixture solution are shown in Table 1. After adding hydrochloric acid, the sol–gels were kept at room temperature for at least 2 h before being used in the next steps.

The preparation of the transducers was done by adding 50 μl of a 0.044 mM ruthenium complex solution to 200 μl of sol–gel GM1 or GM2. The mixtures of the ruthenium complex and the sol–gels were vortexed and stored at room temperature for 2 h. The 5 μl of these mixtures were deposited on the bottom of a well in a 96-well microtiter plate (NUNC Co., Denmark) and dried at 95 °C for 18 h. After the heat treatment, the transducers were covered by different sol–gels (GT, GA1, GA2, GM1 or GM2) on which 40 μl of enzyme solution (GOD: 100 U, or LOD: 1 U, or TOD: 0.005 U) were added to one well of a 96-well microtiter plate. The enzyme immobilization was performed at room temperature for 18 h.

2.3. Characterization of the sensing membrane

2.3.1. Immobilization efficiency

The efficiency of the enzyme immobilization in the well was calculated by dividing the amount of immobilized enzyme protein by the total amount of enzyme protein used for the immobilization. The amount of immobilized enzyme protein was determined by subtracting the amount of un-immobilized enzyme protein from the total amount of enzyme protein used. The un-immobilized enzyme was removed by washing several times with 300 μl of 0.1M phosphate buffer (pH 7), for which the protein values were determined by the Bradford method. The enzyme immobilization and protein measurements were performed in triplicate for each type of sol–gel.

2.3.2. Effect of pH and temperature

The effect of pH and temperature on the sensing membrane was investigated in the range of pH from 4.5 to pH 10, and also

from room temperature (23 °C) to 40 °C. The 1N NaOH or 1N HCl was used to adjust the pH values of the analyte solution. The 100 μl of analyte solution at pH 10 were added to a well containing the sensing membrane in a 96-well microtiter plate. The microtiter plate was then inserted into the measurement chamber of the microplate reader (Wallac Victor 2, Perkin-Elmer Co., USA) to measure the fluorescence intensity at an excitation wavelength of 485 nm and emission wavelength of 535 nm. After performing the measurement at pH 10, the sensing membrane was washed with distilled water several times, and then analyte solution at pH 9 was added to the well and its fluorescence intensity was measured. These steps were repeated for analyte solutions of lower pH. To test the effect of temperature, 35 μl of a certain concentration of analyte were added to the well holding the sensing membrane. The solution was incubated in the measurement chamber of the microplate reader for 10 min at a given temperature and its fluorescence intensity was measured.

2.3.3. Kinetic parameters

The maximum enzymatic reaction rate (V_{max}) and Michaelis–Menten constant (K_M) for each immobilized enzyme were determined from the Lineweaver-Burk plot. The 100 μl of various concentrations of analytes were added to wells containing the sensing membranes in a 96-well microtiter plate. Thereafter, the plate was immediately inserted into the measurement chamber of the microplate reader and the change in the fluorescence intensity was recorded as a function of time. The measurements of the kinetic parameters were done from low to high concentrations of analytes. After measuring the fluorescence intensity each time, the sensing membranes were washed several times with distilled water.

2.3.4. Stability

The stability of the sensing membrane was determined from the change in the fluorescence intensity of the sensing membrane at oxygen concentrations of 100 and 0% after repeating the measurements at least three times. After the measurements, the sensing membranes were stored in 0.1 M phosphate buffer (pH 7.0) under dark conditions at 4 °C. The lifetime of the sensing membranes was checked every month at all concentrations of the analytes and evaluated by measuring the change in their sensitivity (i.e. the change in the slope values of the fluorescence intensity).

2.4. Data analysis

Differences in the fluorescence intensity at different temperatures were assessed by one-way analysis of variance (ANOVA). A significant difference between the samples was accepted with a $P < 0.05$ [16]. Statistical tests are performed using the software InStat (vers.3.01, GraphPad Software Inc., San Diego, USA).

The fluorescence intensity measured was also normalized by transforming the measurement data into percentages of the maximum value. In some cases, after normalizing the measured fluorescence intensity into percentage data, the normalized data were changed again by taking the log 10 value of their normalized values.

3. Results and discussion

3.1. Choice of supporting materials

The Ruthenium complex used in this study is a strong fluorescent dye, which is highly sensitive to oxygen in the medium, due to its long unquenched lifetime ($t_0 \approx 6$ μs) [14]. Its excitation and emission wavelengths are 470 and 600 nm, respectively, which enables it to be used in many applications. As shown in our previous studies [26], GPTMS, APTMS and MTES are good materials to use as support matrices for fluorescent indicators, due to their inert chemical, physical stability and optical properties. The covalent binding between the epoxy group of the sol–gel GPTMS and amine group of the enzyme was exploited to assure the long time stability of the sensing membranes. However, the amount of GOD immobilized on GPTMS alone (sol–gel GT) in Fig. 1 is not as high as that immobilized on the mixture of silanes (sol–gel GA1 or GA2). In theory [27], the amine groups of the sol–gel play a role in maintaining the pH balance of the sol–gel medium and preventing the protonation of other functional groups of the immobilized materials on the sol–gel matrix. Therefore, the presence of the sol–gel, APTMS, provides good conditions for the immobilization of GOD.

3.2. GOD-immobilized sensing membrane

For the preparation of the sensing membranes, transducers were fabricated from the mixture of the ruthenium complex with sol–gel GM1 or GM2. In Fig. 2, the sensitivity of the GOD-immobilized sensing membranes with the transducer GM2 was

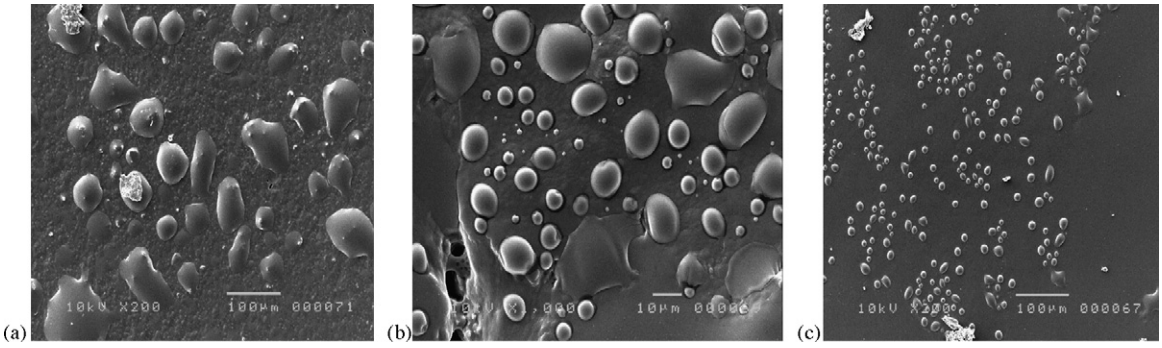

Fig. 1. SEM images of GOD immobilized on the sol–gels of (a) GA1, (b) GA2 and (c) GT.

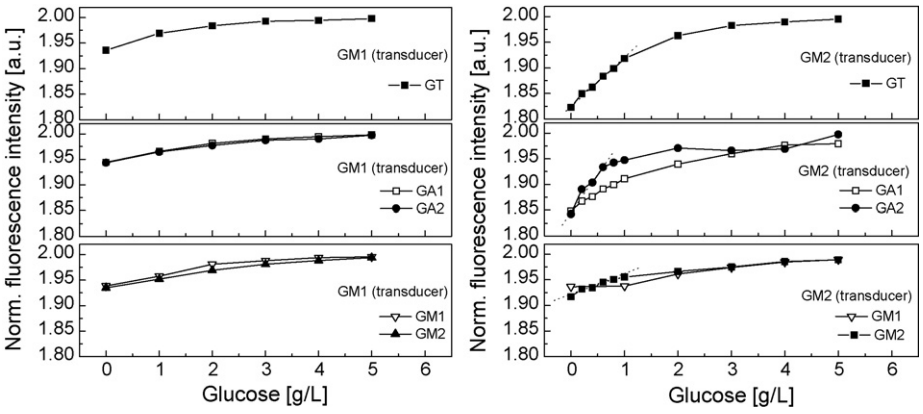

Fig. 2. Calibration curves of glucose for the GOD-immobilized sensing membranes with the transducer GM1 or GM2 and different kinds of sol–gels for GOD.

higher than that of the sensing membranes with the transducer GM1 when the same kind of sol–gel was used for the immobilization of GOD. This might result from the softer texture of the transducer GM2 as compared to that of GM1 (images not shown). The greater number of cavities in the transducer GM2 would help oxygen molecules to penetrate into the sol–gel layer and react with the ruthenium molecules more easily, leading to the faster response and higher sensitivity for the GOD-immobilized sensing membrane. The results in Fig. 2 also indicate that all of the GOD-immobilized sensing membranes were sensitive to various glucose concentrations, among which the sensing membrane GM2 (transducer)–GA2 showed the best properties. Its linear calibration range was 0.0–1.0 g/l for glucose ($R^2 = 0.9189$) and its sensitivity (slope value = 0.1015) was higher than that of the other sensing membranes throughout this range. The detection limit for the GM2–GA2 was 0.211 g/l. From the protein analysis, the immobilization efficiency of GOD on the sol–gel GA2 (40.3%) was higher than that on the sol–gels GT (36.2%), GA1 (38.5%), GM1 (37.3%) and GM2 (36%). In addition, the mixture ratio of GPTMS and APTMS had significant effects on the properties of the sol–gel GAs. These effects could be recognized in the differences in the responses between the sensing membranes GM2–GA1 and GM2–GA2. The latter is more sensitive and shows higher fluorescence intensity than the former.

The temperature of the analyte solution (sample) affects the response of the GOD-immobilized sensing membranes significantly. For the GOD-immobilized sensing membranes with the transducer GM1, the optimal temperature was 23 °C. Increasing the temperature of the analyte solution led to a decrease in the fluorescence intensity, but no significant difference ($P = 0.99$) in the change of fluorescence intensity with temperature was observed for any of the GOD-immobilized sensing membranes in the temperature range between 25 and 40 °C, whereas the fluorescence intensity of all of the GOD-immobilized sensing membranes with the transducer GM2 decreased with increasing temperature (data not shown).

The response time (T_{95}) of the GOD-immobilized sensing membranes was investigated by exposing all of the sensing membranes to 1.0 g/l glucose and the results are presented in Table 2. The repeatability of some of the sensing membranes was tested at glucose concentrations of 0.0 and 1.0 g/l and the results are shown in Fig. 3. All of the sensing membranes that were tested could recover their fluorescence intensity values after several repeated measurements with small errors. The relative standard deviations (R.S.D.) were less than 3% at glucose concentrations of both 0.0 and 1.0 g/l. The sensing membranes using the sol–gel GAs are still the best membranes, since the signals were immediately stable after sensing for less than 0.15–0.5 min, moreover the response time of all of the sensing membranes was reasonably short, with the longest response time being only 4.6 min.

The kinetic parameters (K_M, V_{max}) were calculated first by transforming the fluorescence intensity measured at different concentrations of glucose into the quenching form (fluorescence intensity in the absence of oxygen (FI_0)/fluorescence intensity at 100% oxygen (FI)) and then plotting these modified values as a function of time. The slope values which were collected from the linear range of these graphs are the reaction rates ($V = d(FI_0/FI)/dt$). They were used to draw the graph in the style of a Lineweaver-Burk plot, in which 1/V is a function of 1/glucose concentration.

According to the theory of enzyme kinetics [28], the higher the value of V_{max} and the lower the value of K_M, the greater the number of moles of substrate that will be converted to the product per second. This means that larger amounts of oxygen are consumed resulting in a higher sensitivity of the

Table 2
Characteristics of the GOD-immobilized sensing membranes

Sensing membranes		R.S.D.		T_{95} (min)	K_M (M)	V_{max} (M/s)
Transducer	GOD-immobilized	100% O_2	0% O_2			
GM1	GT	0.9669	0.9166	3.1	0.0981	0.5137
GM1	GA1	0.7131	1.0326	3.0	0.0279	0.2431
GM1	GA2	1.4597	1.1113	0.5	0.2775	1.3865
GM1	GM1	0.8423	1.0197	2.9	0.1064	0.4566
GM1	GM2	0.6326	1.2581	3.1	1.4322	7.0972
GM2	GT	0.8612	2.7168	2.9	0.0052	0.4109
GM2	GA1	1.3486	1.6852	3.7	0.0090	0.3343
GM2	GA2	1.3966	0.6923	0.15	0.0014	0.3054
GM2	GM1	2.4863	2.8300	4.6	0.4687	0.8764
GM2	GM2	0.5401	1.0230	3.5	0.0129	0.1982

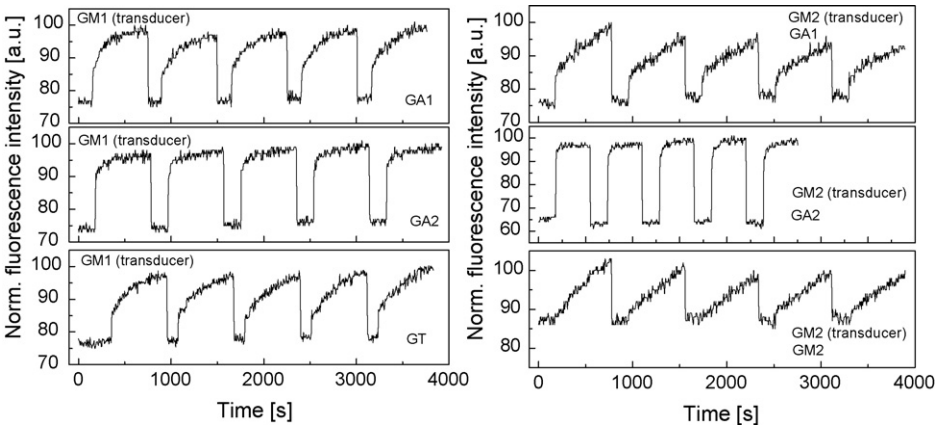

Fig. 3. Repeatability of the GOD-immobilized sensing membranes at 0.0 g/l and 1.0 g/l glucose.

sensing membrane to glucose concentrations. As shown in Fig. 2, the GOD-immobilized sensing membranes with the sol–gel GM2 in the transducer were highly sensitive to low glucose concentrations. These results were consolidated again in Table 2, since the K_M values of the sensing membrane using the sol–gel GM2 as the transducer were smaller than those of the sensing membrane using the sol–gel GM1 as the transducer. Based on these K_M and V_{max} values, the sensitivity of the GOD-immobilized sensing membranes with the transducer GM2 could be arranged in order of decreasing sensitivity, as follows: GA2 → GT → GA1 → GM2 → GM1. Among the sensing membranes with the transducer GM1, the sensing membrane GA2 showed the highest response. Thus, the sol–gels, GM2 and GA2, are the best materials for the fabrication of the transducer and for the immobilization of GOD, respectively.

The stability of the GOD-immobilized sensing membranes is expressed by the change in their sensitivity after their operation and storage for a certain period of time. Since the GOD-immobilized sensing membranes GMs–GAs exhibited excellent properties, as shown in Table 3, the importance of their lifetimes is increased, both for economic and other reasons. Fortunately, the results in Table 3 indicate that the lifetimes of the membranes are up to expectations. After 10 months of operation and storage, the sensitivity of the GOD-immobilized sensing membranes with GAs was changed very little or unchanged. The other membranes exhibited a long lifetime, but a faster decrease in their sensitivity.

Table 3
Change in the sensitivity of the GOD-immobilized sensing membranes after operation and storage for a certain period (i.e. difference in slope values of fluorescence intensity at initial and final use and storage).

Sensing membranes		Initial	Final	Decrease (%)	Time (month)
Transducer	GOD-immobilized				
GM1	GT	46,549	12,328	73.5	10
GM1	GA1	70,488	71,300	0	10
GM1	GA2	45,541	57,921	0	10
GM1	GM1	94,194	20,212	78.5	3
GM1	GM2	14,667	0	100	1
GM2	GT	73,640	28,509	61.3	3
GM2	GA1	260,351	219,651	15.6	10
GM2	GA2	150,762	188,641	0	10
GM2	GM1	62,579	53,906	13.8	5
GM2	GM2	164,169	97,369	40.7	10

3.3. LOD-immobilized sensing membranes

The procedures used for the preparation of the sol–gels, fluorescent layer and enzyme immobilization on the sol–gels were the same as those described in Section 2.2. In our pre-study, LOD was immobilized on several kinds of sol–gels which were used to immobilize GOD, and sol–gel GM2 and GA2 were found to be the best materials for the encapsulation of the ruthenium complex and for the covalent binding with LOD, respectively. Therefore, only the sensing membrane GM2–GA2 was used in the experiments involving the detection of lactate.

From Fig. 4, the linear calibration graph of the LOD-immobilized sensing membrane was in the range from 0.0 to 90 mg/l (=1 mM) ($R^2 = 0.9543$) with a detection limit of 7.77 mg/l. This shows the potential of the lactate sensing membrane for the measurement of low concentrations of lactate in blood samples, since the normal range of lactate in both the blood and food processing is 0.5–2.5 mM [11]. In addition, the kinetic parameters ($V_{max} = 3.12$ M/s, $K_M = 0.008$M) of LOD indicated

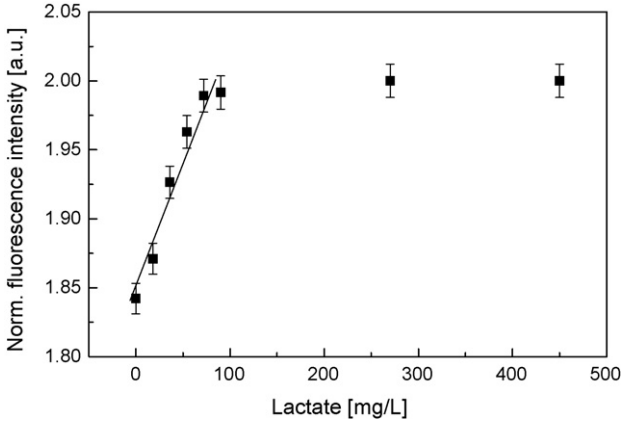

Fig. 4. Response of the LOD-immobilized sensing membrane (GM2–GA2) at various lactate concentrations.

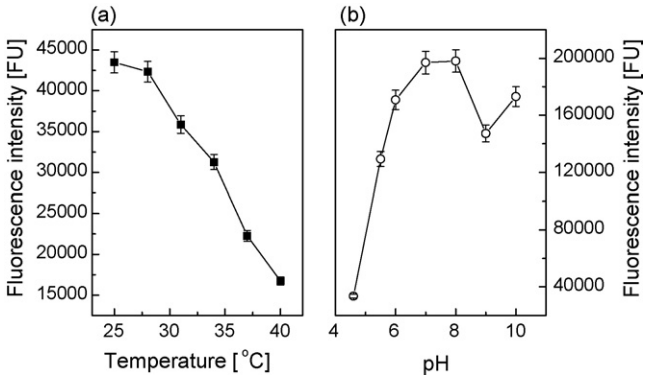

Fig. 5. Effect of the (a) temperature and (b) pH of the reaction solution on the LOD-immobilized sensing membrane (35 or 100 μl of 45 mg/l lactate were added to each well of the micro plate in the experiments designed to measure the temperature and pH dependence, respectively).

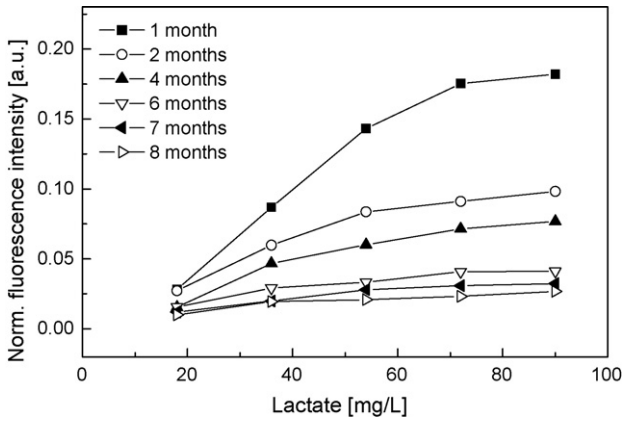

Fig. 6. Long-term stability of the LOD-immobilized sensing membrane after 8 months of operation and storage.

that the reaction rate of oxygen consumption of lactate under the catalysis of LOD was very high as compared with that of the oxygen consumption of glucose under the catalysis of GOD. The immobilization efficiency of LOD was 66.89%. Thus, the LOD-immobilized sensing membrane showed a high sensitivity to lactate in the range of concentrations tested in this work.

In general, the response and stability of enzyme-immobilized sensing membranes depend on the temperature and pH of the reaction solution surrounding them. In the case of the LOD-immobilized sensing membrane, the fluorescence intensity decreased with increasing temperature. The optimal temperature for the measurement of lactate was 25 °C, as shown in Fig. 5a. In the oxidation of lactate, the lactate was converted into pyruvate and H_2O_2 under the catalysis of the LOD immobilized on the sol–gel. The protons, H^+, generated from H_2O_2 can change the pH of the medium and, therefore, buffer solution was used to maintain a favorable pH value for enzyme activity. Fig. 5b shows that pH 7 and 8 are optimal to preserve the high level of fluorescence intensity.

The repeatability of the LOD-immobilized sensing membrane is excellent, as shown by the relative standard deviations of 0.766, 1.64 and 3.32% at lactate concentrations of 0, 36 and 90 mg/l, respectively. The good stability of the sensing membrane is due to the tightly covalent binding between the sol–gel and LOD, as well as the suitable conditions for the sensing operation. The response time of the sensing membrane to obtain 95% of the total signal value is around 5.3 min for lactate concentrations of both 0.4 and 1.0 mM.

After 8 months of operation and storage, the sensitivity (slope value) of the LOD-immobilized sensing membrane decreased to 91% of the initial slope value. However, Fig. 6 shows that the sensing membrane was still able to operate after 4–5 months. As compared with other models of lactate sensor [23–24,29–31], the lifetime of our sensor for lactate detection is similar or longer, even though the components of the sensors are totally different.

3.4. TOD-immobilized sensing membranes

For the detection of tyramine, sol–gel GM2 was used to encapsulate the fluorescence dye, and sol–gels GA1 and GA2 were employed as support materials for the immobilization of TOD. Fig. 7 indicates that the linear calibration curves of the TOD-immobilized sensing membranes employing GA1 and GA2 were in the ranges of 0–100 mg/l ($R^2_{GM2–GA1} = 0.9602$) and 0–70 mg/l ($R^2_{GM2–GA2} = 0.9489$). The values of the detection limit were found to be 8.73 mg/l for GA1 and 6.30 mg/l for GA2. When only a small amount of TOD was used for the immobilization on the detection layer, the sensors showed a high sensitivity to tyramine in the range of 0–100 mg/l (the immobilization efficiencies of TOD on sol–gels GA1 and GA2 were 64.78 and 67.13%, respectively). The change in the fluorescence intensity between the tyramine concentrations of 0.0 and 100 mg/l was significant. However, the sensitivity of the sensors was rapidly decreased at the higher concentration of tyramine of 100 mg/l, especially in the case of the sensing membrane GM2–GA1. For the sensing membrane GM2–GA1, the kinetic parameters V_{max} and K_{M1} were 6.39 M/s and 11.71 mM, respectively, whereas the corresponding values for the sensing membrane GM2–GA2 were 0.191 M/s and 0.171 mM. Thus, the oxidation of tyramine on the sensing membrane GM2–GA1 occurred more rapidly than that on the sensing membrane GM2–GA2, because K_{M1} is larger than K_{M2}. But a larger amount of tyramine were converted, because V_{max1} is larger than V_{max2}.

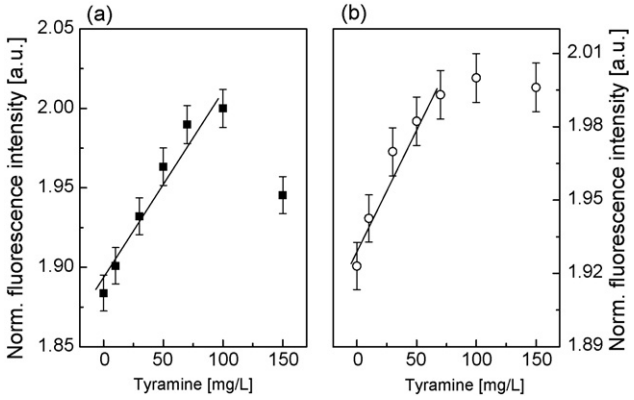

Fig. 7. Response of the TOD-immobilized sensing membranes at various concentrations of tyramine (a) sensing membrane GM2–GA1 and (b) sensing membrane GM2–GA2.

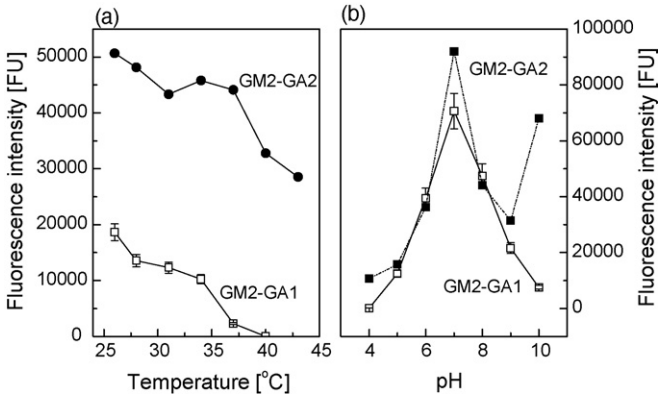

Fig. 8. Effect of (a) temperature and (b) pH on the TOD-immobilized sensing membranes, GM2–GA1 and GM2–GA2.

The signals of both sensing membranes decreased with increasing temperature. As in the case of the other enzymes, TOD could not operate or operated with decreased activity at high temperature. The temperature range of 23–25 °C is the optimal temperature range to obtain the maximal fluorescence intensity (Fig. 8a). The results in Fig. 8b show the effect of pH on the sensing membranes, and it can be seen that pH 7 is the optimal pH value to maintain high stability and sensitivity of the sensing membranes. However, we could not explain the reason why the fluorescence intensity of the sensing membrane GM2–GA2 did not change very much at pH 10.

Both sensing membranes were able to recover their original fluorescence signal values after repeated use at 0.0 and 50 mg/l of tyramine. The relative standard deviations of both sensing membranes were less than 5% (R.S.D.s of 3.21 and 2.65% for the sensing membrane GM2–GA1 and 1.06 and 1.55% for the sensing membrane GM2–GA2 at 50 and 0.0 mg/l, respectively). These results indicate that the wash-out of the enzyme in the sensing membrane was overcome, due to the tightly covalent binding between the sol–gel and the enzyme. The complexes of the sol–gel GM2 and GAs reconfirmed their excellent properties for the fabrication of the sensing membranes. The response time of the sensing membrane GM2–GA1 was around 9 s to obtain 95% of the total value of the fluorescence intensity, whereas the sensing membrane GM2–GA2 needed approximately 3 min. These results fit the calculated data for V_{max} and K_M.

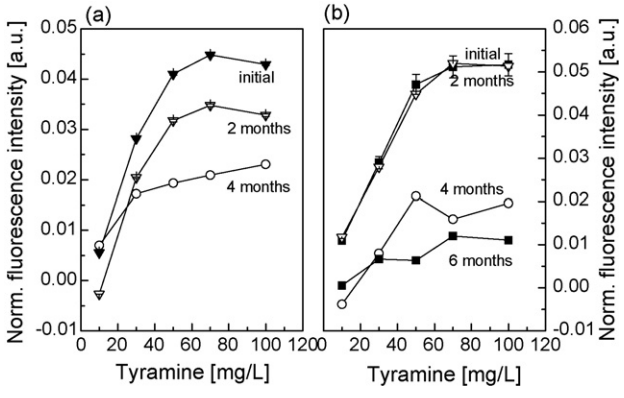

Fig. 9. Long-term stability of the TOD-immobilized sensing membranes (a) GM2–GA1 and (b) GM2–GA2.

Both sensing membranes operated for 4–6 months even though their sensitivity and stability were decreased (Fig. 9). For the sensing membrane GM2–GA2, these parameters were not changed after 2 months of operation and storage. In fact, there have not been many studies involving the analysis of tyramine, and no tyramine biosensors have been fabricated, which are similar to the one fabricated in this study. Therefore, we could not compare its properties to that of other biosensors, however, it can be considered that a life-time of 4–6 months for a biosensor indicates that its quality is good.

4. Conclusion

The typical characteristics of the sol–gels which were applied for the immobilization or encapsulation of organic or biomaterials contributed significantly to the sensitivity and stability of the sensing membranes for the detection of glucose, lactate and tyramine. Choosing the appropriate ratio of silanes in the mixture of sol–gels allowed for the optimization of the sensing membranes. Sensing membranes fabricated based on this design can be applied for some analytes which follow the principle of the oxidation reaction. Sol–gel GM2 is a feasible material for use as a support matrix of fluorescent dye, while sol–gel GA2 is suitable for enzyme immobilization. The sensing membranes fabricated herein should operate in the temperature range of 23–25 °C and at pH 7.

Acknowledgements

This work was supported by grant No. RTI04-03-03 from the Regional Technology Innovation Program of the Ministry of Commerce, Industry and Energy (MOCIE), and also in part by BK21 program from the Ministry of Education & Human Resources Development, Republic of Korea.

References

[1] H. Ukeda, M. Ohira, A.K. Sarker, M. Sawamura, Food Res. Int. 31 (4) (1998) 297.
[2] H. Ukeda, Y. Fujita, M. Ohira, M. Sawamura, J. Agric. Food Chem. 44 (1996) 3858.
[3] L. Fraisse, M.C. Bonnet, J.P. de Farcy, C. Agut, D. Dersigny, A. Bayol, Anal. Biochem. 309 (2002) 173.
[4] P. Druekes, R. Schinzel, D. Palm, Anal. Biochem. 230 (1995) 173.
[5] M.V. Zakhartsev, H.O. Portner, R. Blust, Anal. Chem. 330 (2004) 10.
[6] S. Arain, G.T. John, C. Krause, J. Gerlach, O.S. Wolfbeis, I. Klimant, Sens. Actuators B: Chem. 113 (2) (2006) 639.
[7] J. Alderman, J. Hynes, S.M. Floyd, J. Kruger, R. O'Conor, D.B. Papkovsky, Biosens. Bioelectron. 19 (2004) 1529.
[8] F. Moris-Varas, A. Shah, J. Aikens, N.P. Nadkarni, J.D. Rozzell, D.C. Demirjian, Bioorg. Med. Chem. 7 (1999) 2183.
[9] G.T. John, E. Heinzle, Biotechnol. Bioeng. 72 (2001) 620.
[10] G.T. John, I. Klimant, C. Wittmann, E. Heinzle, Biotechnol. Bioeng. 81 (2003) 829.
[11] R.D. Guarino, L.E. Dike, T.H. Haq, J.A. Rowley, J.B. Pitner, M.R. Timmins, Biotechnol. Bioeng. 86 (2004) 775.
[12] T.C. O'Riordan, D. Buckley, V. Ogurtsov, R. O'Conor, D.B. Pabkovsky, Anal. Biochem. 278 (2000) 221.

[13] B. Kuswandi, R. Andres, R. Narayanaswamy, Analyst 126 (2001) 1469.
[14] B.D. MacCraith, C.M. McDonagh, G. O'Keeffe, A.K. McEvoy, T. Butler, F.R. Sheridan, Sens. Actuators B: Chem. 29 (1995) 51.
[15] X.J. Wu, M.M.F. Choi, Anal. Chim. Acta 514 (2004) 219.
[16] S.G. Ignatov, J.A. Ferguson, D.R. Walt, Biosens. Bioelectron. 16 (2001) 109.
[17] E.A. Garcia, R.G. Fernandez, M.E. Dia-Garcia, Microporous Mesoporous Mater. 77 (2005) 235.
[18] U. Kunzelmann, H. Bottcher, Sens. Actuators B: Chem. 38–39 (1997) 222.
[19] C.M. Mcdonagh, A.M. Shields, A.K. Mcevoy, B.D. Maccraith, J.F. Gouin, J. Sol–gel Sci. Technol. 13 (1998) 207.
[20] U. Georgi, H. Graebner, G. Roewer, G. Wolf, J. Sol–gel Sci. Technol. 13 (1998) 295.
[21] K. Han, Z. Wu, J. Lee, I.S. Ahn, J.W. Park, B.R. Min, K. Lee, Biochem. Eng. J. 22 (2005) 161.
[22] M. Lepore, M. Portaccio, E. De Tommasi, P. De Luca, U. Bencivenga, P. Maiuri, D.G. Mita, J. Mol. Cat. B: Enzymatic 31 (2004) 151.
[23] F. Mazzei, A. Azzoni, B. Cavalieri, F. Botre, C. Botre, Food Chem. 55 (1996) 413.
[24] V. Casimiri, C. Burstein, Anal. Chim. Acta 361 (1998) 45.
[25] R.G. Leuschner, M. Heidel, W.P. Hammes, Int. J. Food Microbiol. 39 (1998) 1.
[26] H.D. Duong, O.J. Sohn, T.H. Lam, H.J. Kim, J.I. Rhee, Proceedings of the Regional Symposium on Chemical Engineering, 2005.
[27] M.C. Burt, B.C. Dave, Sens. Actuators B: Chem. 107 (2005) 552.
[28] K. Van't Riet, J. Tramper, Basic Bioreactor Design, Marcel Dekker, Inc., 1991.
[29] S. Suman, R. Singhal, A.L. Sharma, B.D. Malthotra, C.S. Pundir, Sens. Actuators B: Chem. 107 (2) (2005) 768.
[30] V. Casimiri, C. Burstein, Biosens. Bioelectron. 11 (8) (1996) 783.
[31] Q. Yang, P. Atanasov, E. Wilkins, Biosens. Bioelectron. 14 (1999) 203.

Available online at www.sciencedirect.com
ScienceDirect
Talanta 72 (2007) 1494–1499
Talanta
www.elsevier.com/locate/talanta

Chemical speciation and recovery of gold(I, III) from wastewater and silver by liquid–liquid extraction with the ion-pair reagent amiloride mono hydrochloride and AAS determination

M.S. El-Shahawi *, A.S. Bashammakh, S.O. Bahaffi

Department of Chemistry, Faculty of Science, King Abdulaziz University, P.O. Box 80203, Jeddah 21589, Saudi Arabia

Received 30 October 2006; received in revised form 25 January 2007; accepted 26 January 2007
Available online 9 February 2007

Abstract

A novel and low cost liquid–liquid extraction procedure for the separation of gold(III) at trace level from aqueous medium of pH 5–9 has been developed. The method has been based upon the formation of a yellow colored ternary complex ion associate of tetrachloro gold(III) complex anion, $AuCl_4^-$ with the ion-pair reagent 1-(3,5-diamino-6-chloropyrazinecarboxyl) guanidine hydrochloride monohydrate, namely amiloride, $DPG^+{\cdot}Cl^-$. The effect of various parameters, e.g. pH, organic solvent, shaking time, etc. on the preconcentration of gold(III) from the aqueous media by the $DPG^+{\cdot}Cl^-$ reagent has been investigated. The colored gold species was quantitatively extracted into 4-methyl pentan-2-one. The chemical composition of the ion associate of $DPG^+{\cdot}Cl^-$ with $AuCl_4^-$ in the organic solvent has been determined by the Job's method. The molar absorptivity (2.19×10^4 L mol^{-1} cm^{-1}) of the associate $DPG^+{\cdot}AuCl_4^-$ at 362 nm enabled a convenient application of the developed extraction procedure for the separation and AAS determination of traces of aurate ions. Mono-valence gold ions after oxidation to gold(III) with bromine water in HCl (1.0 mol L^{-1}) media have been also extracted quantitatively from the aqueous media by the developed procedure. The chemical speciation of mono- and/or tri-valence gold species spiked to fresh and industrial wastewater samples has been achieved. The method has been also applied successfully from the separation of gold(I) and gold(III) species from metallic ions and silver. The developed method has also the advantage of freedom from most diverse ions.

Keywords: Mono- and tri-valence gold species; Ion-pair reagent $DPG^+{\cdot}Cl^-$; Liquid–liquid extraction; Chemical speciation; Wastewater; Silver; Recovery and AAS

1. Introduction

Gold is widely distributed in nature and the chemistry of gold remains an active research area [1]. Some gold(I) compounds are biologically active and used as anti-inflammatory drugs in the treatment of rheumatoid arthritis [1–3]. Due to the low level of gold in the environmental samples and its great importance, many articles have been reported on the separation of traces of gold in water and other matrices containing Cd^{2+}, Zn^{2+}, Cu^{2+}, Ni^{2+}, Mn^{2+}, Co^{2+}, Pd^{2+}, Hg^{2+}, Pb^{2+}, Pt^{4+}, Fe^{3+}, alkaline and alkaline earth ions before their actual determination [3–9].The spectrometric methods, e.g. ICP-AES, FAAS, ETAAS, electrophoresis and other spectrophotometric methods involving 2-carboxyl-1-naphthalthiorhodanine (CNTR), Spheron (R) and (biphenyl) dimethanethiol, etc. are the most used techniques in the analysis of gold at low level [7,9–15]. Few of these methods have sufficient sensitivity and selectivity for the trace levels of mono-and tri-valence gold species in fresh water and industrial wastewater samples [7,11–15]. However, the low level of gold in drinking waters is not compatible with the detection limit and some of these methods are expensive, unselective and require careful experimental conditions and considerable time consuming. Thus, preconcentration and separation techniques using liquid–liquid and liquid–solid are frequently required to improve the detection capability and the selectivity of these techniques [7,12–14].

The ion-pair reagents containing bulky anions are often used to form extractable complex ion associates with charged bulky cationic complex species of neutral ligands, e.g. crown ethers, *o*-phenanthroline derivatives, and metal ions [6–10,16–18]. On the other hand, the bulky cations, e.g. rhodamine derivatives, basic dyes, 18-crown-6 (18C6) oxonium cation, tetra alkyl

* Corresponding author. Tel.: +966 551691130; fax: +966 26952292.
E-mail address: mohammad_el_shahawi@yahoo.co.uk (M.S. El-Shahawi).

0039-9140/$ – see front matter © 2007 Elsevier B.V. All rights reserved.
doi:10.1016/j.talanta.2007.01.057

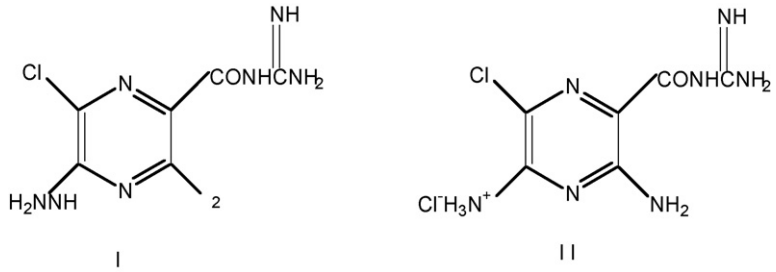

Fig. 1. Chemical structures of the amiloride (I) and amiloride hydrochloride (II).

phosphonium or arsonium halides and tetrazolium salts are also often used to form extractable ion associates with charged bulky oxoanions or bulky anionic complexes of metal [18–30] and gold(III) halides, cyanide and thiocyanate [31–33].

Burns et al. [34,35] and others [36,37] have been successfully used the compound amiloride mono hydrochloride (Fig. 1) as a selective analytical ion-pair reagent for the determination of the oxoanions perchlorate, perrhenate and periodate in different matrixes. The extraction of the produced complex ion associates of amiloride with these oxoanions proceeded rapidly with high recovery factor [27–31].

Recent years [7,10–15] have seen an upsurge of interest for rapid and sensitive analytical methods for the separation and speciation of chemical forms of precious metal ions in environmental samples. A recent literature on the analytical applications of the ion-pair reagent $DPG^+ \cdot Cl^-$ has revealed no study on the use of the reagent on the liquid–liquid separation of gold(III) from silver and other base metal ions and chemical speciation of chemical forms of mono- and tri-valent gold ions. Thus, the goals of the present article are focused on the use of the title reagent for the separation of gold(III) and speciation of chemical forms of mono- and tri-valence gold species as a ternary complex ion associate of $AuCl_4^-$ and $DPG^+ \cdot Cl^-$ in non-aqueous media. The extraction mechanism and the chemical separation of gold(I) and (III) species from silver(I) and other base metal (Fe^{3+}, Co^{2+}, Ni^{2+}, and Cu^{2+}) ions have been also included.

2. Experimental

2.1. Reagents and materials

Analytical reagent grade chemicals nickel(II) sulphate, iron(III) sulphate and copper(II) sulphate and solvents (BDH, USA) were used. Potassium aurocyanide, $KAu(CN)_2$ (Fluka AG, USA), chloroauric acid, $HAuCl_4$ (Johnson Mathey & Co., UK), silver nitrate (Fluka, USA) and amiloride mono hydrochloride (E Merck, India) were used for the preparation of stock solutions (1000 μg mL^{-1}) of gold(I), gold(III) and silver(I) ions, respectively. A stock solution (0.01 mol L^{-1}) of amiloride mono hydrochloride (E Merck, India) was prepared by dissolving an accurate weight (0.03 g) of the reagent in 100 mL H_2O–HCl (1:1, v/v). Double distilled de-ionized water was used throughout the work for the preparation of stock solutions (1000 μg mL^{-1}). A series of Britton–Robinson buffers (0.04 mol L^{-1} in each of acetic, orthophosphoric, and boric acids) adjusted to the required pH with sodium hydroxide (0.2 mol L^{-1}) was prepared [38].

2.2. Apparatus

Carbon, hydrogen and nitrogen content were determined on a Perkin-Elmer 2400C series elemental analyzer, USA. A Perkin-Elmer (model Lambda EZ-210, USA) spectrophotometer (190–1100 nm) with a 10 mm long quartz cell was used for recording the electronic spectra of the reagent and the complex ion associate of gold(III). The absorbance of the organic extract was measured with a single beam Perkin-Elmer (model Lambda EZ-150, USA) UV–vis spectrophotometer with quartz cell (10 mm). A Perkin-Elmer (Analyst TM 800, USA) furnace atomic absorption spectrometer (AAS) was used for measuring the concentration of Au, Ag, Fe, Ni, and Cu at the wavelengths 242.8, 328.1, 372.0, 232.0 and 324.7 nm, respectively at 0.5 nm slit width except for iron and nickel at 0.2 nm before and after separation step from the aqueous phase under instrument's optimum settings.

2.3. Recommended extraction procedures

2.3.1. Extraction procedures of gold(III) species

In a separating funnel (50 mL), a 2 mL aliquot of the ion-pairing reagent $DPG^+ \cdot Cl^-$ (1.0×10^{-5} mol L^{-1}) was mixed with 9.0 mL of B–R buffer (pH 6–7) containing various concentrations ($(1.0–6) \times 10^{-5}$ mol L^{-1}) of $HAuCl_4$ to adjust the pH of the final aqueous solution. The aqueous solution was then diluted to 20.0 mL with double distilled water. The aqueous solution was shaken twice, each with 2.5 mL of the solvent 4-methyl pentan-2-one for 2 min. After separation of the layers, the organic extract was then collected in a 25 mL beaker containing anhydrous sodium sulphate (1.0 g) swirled to mix the contents and transferred to a 10 mL volumetric flask. The residue was also washed with 5 mL (2×2.5) of the same organic solvent, transferred to the measuring flask and finally made up to the mark with the same solvent. The absorbance of the organic extract was then measured at 362 nm against a reagent blank. After extraction, the pH of the aqueous phase was determined as equilibrated pH and the amount of gold ions remained in the aqueous phase (C_f) was determined also by AAS. The amount of gold ions of the parallel samples containing the same amount (C_i) of gold(III) ions and the reagent $DPG^+ \cdot Cl^-$ was also measured by AAS. The amount of gold(III) ions in the organic phase was finally calculated by

the difference ($C_i - C_f$) and the distribution ratio (D_{Au}) was then calculated employing the equation:

$$D_{Au} = \frac{[DPG^+ \cdot AuCl_4^-]_{(org)}}{[AuCl_4^-]_{(aq)} + [DPG^+ \cdot AuCl_4^-]_{(aq)}} \quad (1)$$

2.3.2. Extraction procedures of gold(I) species

An accurate volume (10 mL) of the aqueous solution containing gold(I) ions at different concentrations (1.0–15 μg mL^{-1}) was transferred to the conical flask (50 mL capacity). Another 10 mL of HCl (1 mol L^{-1}) and bromine water (2 mL) were added to oxidize gold(I) solutions to gold(III) complex species. The solutions were left for 5 min and the excess Br_2 and HCl were then removed by boiling the solutions for 10–15 min and finally allowed to cool to room temperature (25 ± 1 °C). The solution mixtures were then adjusted to pH 6–7 with B–R buffer, transferred with the washing solutions to a 50 mL separating funnels. The resulting solutions were then extracted as described earlier for gold(III) extraction. The concentration of the produced gold ions was then determined with AAS using calibration curves of gold(III) and (I) ions.

2.3.3. Extraction of the binary mixtures of gold(I) and (III)

An aliquot (10 mL) of a mixture of mono- and tri-valent gold ions at a total concentration ≤25 μg mL^{-1} was transferred to a 50 mL separating funnel. The mixture was analyzed with AAS according to the described procedure for the extraction of tri-valent gold ions. Another aliquot portion (10 mL) was transferred and analyzed with AAS as described before for gold(I) determination. On the basis of these procedures, the amount of gold in the organic extract of the first aliquot (C_1) could be a measure of the gold(III) ions in the mixture, while the amount of gold in the organic extract of the second aliquot (C_2) is a measure of the sum of the mono- and tri-valent gold ions. Therefore, the difference ($C_2 - C_1$) is a measure of the gold(I) ions in the binary mixture.

2.4. Analytical applications

2.4.1. Analysis of gold(III) and total gold(I, III) in tap and wastewater samples

Tap and/or industrial wastewater samples (50 mL) of fertilizer industry were collected, filtered through a 0.45 μm membrane filter and the solutions pH were then adjusted to pH 6–7 with B–R buffer. To each of the sample solutions an accurate concentration of gold(I, III) species at a total concentration in the range 5.0–25.0 μg Au mL^{-1} and 2.0 mL of the reagent $DPG^+ \cdot Cl^-$ (8.0×10^{-5} mol L^{-1}) were added. The solution mixtures were then transferred to 50 mL separating funnels. Analyze the mixtures according to the described procedure for gold(III). Another aliquot (50 mL) portions were taken exactly and analyzed as described for gold(I) species. On the basis of these procedures, the gold concentration determined by AAS in the first organic extract will be a measure of tri-valent gold ions in the mixture, while the amount of gold in the organic extract of the second aliquot is a measure of the sum of the gold(I) and (III) ions. Therefore, the difference between the two measurements will be a measure of the mono-valent gold ions in the mixture.

2.4.2. Separation of gold(III) from silver(I) and base metal ions in tap water

An aliquot of tap water (10 mL) spiked with gold(III) ions in the concentration range 5.0–25.0 μg mL^{-1} Au was accurately transferred into a 50 mL separating funnel as described above. To the solution mixture, 2 mL containing silver(I) and/or base metal ions (Fe^{3+}, Co^{2+}, Ni^{2+}, Cu^{2+}or Zn^{2+}) at 10.0 μg mL^{-1} for each ion and few drops (0.2–0.3 mL) of KCl (1%, w/v)were added by the spiking method. The presence of KCl eliminates the possible interference of silver ions by forming AgCl precipitate. The solutions were then analyzed as described for gold(III) ions. The amount of gold(III) and base metal ions in the aqueous phase were determined with AAS from the standard curves of each ion at the optimum wavelength as described before.

3. Results and discussion

On mixing the reagent $DPG^+ \cdot Cl^-$ with tetrachloro gold anion, $AuCl_4^-$ in aqueous media and shaking with 4-methyl pentan-2-one, a yellow colored complex associate was developed in the organic phase. After equilibrium, the organic phase containing the complex ion associate of $DPG^+ \cdot Cl^-$ and $AuCl_4^-$ was separated out and its absorption electronic spectrum was then recorded. The spectrum showed one well-defined peak at 362 nm of the organic extracted while, the absorption spectrum of the reagent blank $DPG^+ \cdot Cl^-$ against pure 4-methyl pentan-2-one showed no absorption peaks in the same wavelength range. On the absence of $HAuCl_4$ or $DPG^+ \cdot Cl^-$ in the aqueous phase, no color or extraction of gold ions was detected in the organic layer as indicated from AAS measurement of gold ions in the organic or aqueous layer. Thus, each of $DPG^+ \cdot Cl^-$ or $AuCl_4^-$ separately did not extract in the organic phase. Therefore, in the subsequent work, the absorbance of the organic extract was measured at 362 nm against a reagent blank.

3.1. Investigation of the various experimental variables

Comparative tests of various organic solvents, e.g. *n*-hexane, dichloromethane, carbon tetrachloride, toluene, chloroform, diethyl ether, methyl ethyl ester, aromatic hydrocarbons and 4-methyl pentan-2-one with a wide range of functional group types was investigated for their ability to extract the produced complex associate. The data revealed that, the nature of the solvent contributes substantially to the maximum extraction of the produced complex ion associate of the $DPG^+ \cdot Cl^-$ and $AuCl_4^-$ ions. Good results were achieved with 4-methyl pentan-2-one and cyclohexanone and the absorbance of the organic phase followed the following order: 4-methyl pentan-2-one > cyclohexanone > ester > ether > dichloromethane > chloroform > toluene > carbon tetrachloride and *n*-hexane, respectively. The relatively high dielectric constant of these two solvents favors extensive ion-pairing formations [39]. Thus, the good extraction percentage (96–98%) with maximum apparent molar absorptivity, and solubility of the produced complex ion associate were

achieved. At room temperature, the extraction was complete in less than 2 min with better separation of phases in 4-methyl pentan-2-one. The reagent $DPG^+ \cdot Cl^-$ in this solvent has no extraction and the colored complex ion associate was extracted quantitatively. The ion associate was found also stable for up to 2 h in this solvent. Thus, in the subsequent work, the solvent 4-methyl pentan-2-one was selected as a proper solvent. The amount of gold(III) extracted from the aqueous solution into the organic phase versus the amount of gold(III) in the aqueous phase at equilibrium varied linearly at low and moderate tri-valent gold(III) concentration ($\leq 10\,\mu g\,mL^{-1}$) followed by a plateau at higher concentration. A solvent capacity of 5 μg gold(III) ions uptake per milliliter of organic solvent was obtained.

The optimum shaking time was ascertained by measuring the absorbance of the organic extract after 0.5–10 min shaking time. Rapid attainment of extraction equilibrium was achieved within 1.5–2 min. Thus, a 2 min shaking time was taken as the optimum time in the subsequent work to ensure complete extraction. The volume ratio of the aqueous phase (5 $\mu g\,mL^{-1}$ Au) to the organic phase ($V^-_{(aq)}/V^-_{(org)}$) was also examined for the extraction of gold (5 $\mu g\,mL^{-1}$ Au) species. For a single extraction, it was found that, quantitative extraction of gold was attainable up to 20-fold ($V^-_{(aq)}/V^-_{(org)} = 20{:}1$).

The effect of pH of the aqueous solution employing B–R buffer on the extraction of the developed colored complex ion associate was studied by measuring the absorbance of the organic extract at 362 nm against the reagent blank. Maximum absorbance of the produced ion associate was obtained at pH 5–9 (Fig. 2). In the aqueous solution of $pH \leq 5$, the ion pair $DPG^+ \cdot Cl^-$ is less dissociated and gold(III) is most likely exists as chloroauric acid ($HAuCl_4$) species, which is less dissociated at lower pH as follows:

$$HAuCl_{4(aq)} \rightleftharpoons AuCl_{4(aq)}{}^- + H^+ \quad (2)$$

Thus, in acidic pH, the equilibrium (Eq. (2)) moves to the left and the quantity of $AuCl_4{}^-{}_{(aq)}$ ions available to form complex ion associate with $DPG^+ \cdot Cl^-{}_{(aq)}$ decreased. On the other hand, in aqueous solution of $pH \geq 9$, the absorbance of the organic extract also decreased. The formation of non-extractable complex species of gold(III), e.g. hydroxo-species of gold(III) which minimizes the associate formation [40] may account for such trend. Thus, in the subsequent work the pH of the aqueous solution was adjusted at pH 6–7 and the overall reaction between $DPG^+ \cdot Cl^-{}_{(aq)}$ and $HAuCl_{4(aq)}$ is most likely be proceeded as follows:

$$HAuCl_{4(aq)} + DPG^+ \cdot Cl_{(aq)}{}^- \rightleftharpoons [AuCl_4{}^- \cdot DPG^+]_{(org)} + HCl_{(aq)} \quad (3)$$

The influence of $DPG^+ \cdot Cl^-$ concentration on the extraction of the formed ion associate at the optimum experimental conditions was studied. A 2 mL of 8.0×10^{-5} mol L^{-1} of $DPG^+ \cdot Cl^-$ was found sufficient to extract quantitatively (96–98%) up to 10 $\mu g\,mL^{-1}$ of gold(III) from the aqueous by double extraction (2× 2.5 mL) of the organic solvent. The molar absorptivity of the produced ternary complex ion associate $DPG^+ \cdot AuCl_4{}^-$ at 362 nm calculated from the absorbance measurement was found equal 2.19×10^4 L mol^{-1} cm^{-1} in 4-methyl pentan-2-one. A large excess of the reagent slightly decreased the absorbance of the organic phase possibly owing to the increased acidity of the aqueous phase which minimizes the associate formation.

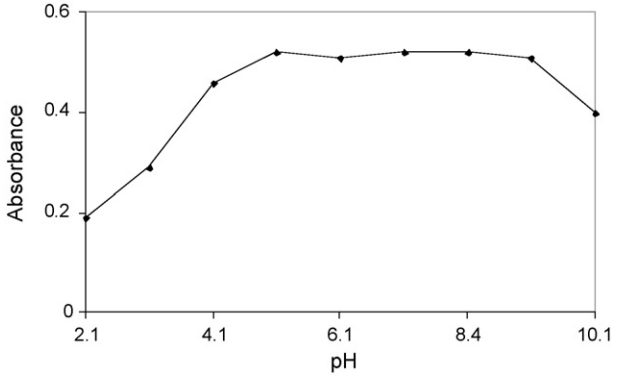

Fig. 2. Influence of pH on the uptake of the ion associate [$DPG^+ \cdot AuCl_4{}^-$] onto the solvent 4-methyl pentan-2-one (5 mL). Aqueous phase (20 mL) at pH 6–7, Au = 2 $\mu g\,mL^{-1}$ and 0.1 mL $DPG^+ \cdot Cl^-$ (0.01%, w/v).

3.2. Effect of foreign ions

The selectivity of the developed method for the extraction of 5 $\mu g\,mL^{-1}$ of tri-valent gold ions in the presence of a relatively high excess (0.05–0.1 mg mL^{-1}) of some cations and anions was investigated. The tolerance limit was defined as the concentration of the foreign ion added causing a relative error within ±2% of the recovery of gold. It was found that, in the extraction of gold(III), the ions: Li^+, Na^+, K^+, Ca^{2+}, $NH_4{}^+$, Al^{3+}, Fe^{2+}, Ni^{2+}, Co^{2+}, $Cu^{2+}$and Zn^{2+} and the anions: Cl^-, Br^-, $SO_4{}^{2-}$, $CO_3{}^{2-}$, $C_2O_4{}^{2-}$, $PO_4{}^{3-}$ and $S_2O_8{}^{2-}$ do not interfere at 1:100 tolerable concentration of gold(III) to the diverse ions, respectively. Interference due to Fe^{3+} and $VO_3{}^-$ and $MnO_4{}^-$ (1:100, w/w) was eliminated by the addition of few drops of NaF (1%, w/v) and NaN_3 (0.1%, w/v) prior to the extraction, respectively. Interference of Ag^+ ions was removed by adding few drops of KCl (0.1%, w/v) to form AgCl precipitate. In the presence of some other ions, e.g. Pd^{2+} and Pt^{2+} even at low concentrations (1:10, v/v), positive interference was noticed. The ability of these ions to form extractable stable complex ion associates with the reagent $DPG^+ \cdot Cl^-$ under the optimum experimental condition is most likely account for such behavior. These ratios do not induce limitations in the matrixes, e.g. salty effluents that could be analyzed by the developed extraction procedure.

3.3. Characterization of the gold(III) ion associates

The composition of the extracted species was determined at two different concentrations of the gold(III) ions and reagent by Job's method [41]. A plot of the absorbance of the organic extract at 362 nm versus the mole fraction of $DPG^+ \cdot Cl^-$ revealed a graph that indicated the formation of an ion-association complex having gold(III) to a reagent molar

Table 1
Analytical results for the extraction of the binary mixture of mono- and tri-valent gold ions in aqueous media by the developed procedure

Gold species ($\mu g\,mL^{-1}$)				Recovery (%)[a]	
Gold(I) and (III) added		Average gold(I) and (III) found		Au^{+}	Au^{3+}
Au^{+}	Au^{3+}	Au^{+}	Au^{3+}		
5.0	10.0	4.9	10.3	98.0 ± 2.7	103.0 ± 2.7
10.0	15.0	9.7	15.2	97.0 ± 2.2	101.3 ± 2.3
15.0	10.0	14.8	10.2	98.7 ± 2.1	102 ± 1.6

[a] Average recovery of five measurements ± relative standard deviation.

ratio of 1:1. The organic extract was also evaporated under vacuum and analyzed for C, H, N and Au. The analytical data of the produced associate was found as follows: $[AuOC_6H_9N_7Cl_5]$ required 12.62% C, 1.57% H, 17.24% N and 34.7% Au; Found 13.12% C, 1.76% H, 16.96% N and 35.23% Au. These data add further confirmation that, the extracted species are most likely represented as $AuCl_4^{-}\cdot DPG^{+}$. The stability constant of the produced complex ion associate calculated from the Job's plot from the ratio of the true absorbance (A) to the extrapolated (A_{extp}) absorbance [41] was found equal to 2.46×10^3.

A series of oxidizing agents such as H_2O_2, $K_2S_2O_8$ or bromine water has been tested for complete oxidation of mono-valence gold species to tri-valent gold species in aqueous media containing dilute acids (1 mol L^{-1}), e.g. CH_3COOH, HCl or H_2SO_4 or KCl (1 mol L^{-1}). Among these oxidizing agents, bromine water in HCl (1 mol L^{-1}) medium and boiling the aliquot aqueous solution of mono-valence gold species for 2 min was the most suitable oxidizing agent for gold(I) to gold(III) species. The oxidation performance of mono-valence gold to gold(III) species in the aqueous media followed the sequence:

bromine water > $K_2S_2O_8$ > H_2O_2

The variation of HCl concentration (0.1–2 mol L^{-1}) in the extraction media on the oxidation of gold(I) to gold(III) by bromine water and boiling was investigated following the same extraction procedure. The results revealed that optimum conditions for complete oxidation of gold(I) to gold(III) is to have an aqueous medium containg HCl (1 mol L^{-1}).

The extraction of gold(I) at concentration levels 1.0–15 $\mu g\,mL^{-1}$ after oxidation with Br_2 water in HCl (1 mol L^{-1} and following the recommended extraction procedure for gold(III) was successfully achieved with a recovery percentage of 98 ± 3.4% (n = 5)). Thus, the analysis of the binary mixtures of gold(I) and (III) ions in the aqueous media by the developed extraction procedure was attempted. The results are summarized in Table 1. Satisfactory recovery percentage of various gold(I) and gold(III) species was obtained.

3.4. Analytical applications

3.4.1. Chemical speciation and recovery of gold(I) and (III) from water samples

The validity of the developed extraction procedure was investigated by the determination of the mean percentage recoveries (n = 5) of gold(III) in distilled water ((10 $\mu g\,mL^{-1}$ Au) using both the calibration graph and standard addition methods. The average percentage recoveries were found reproducible. The limits of detection (LOD) of gold(III) estimated using the equation: LOD = $3S_{y/x}/b$ [42]; where $S_{y/x}$ is the standard deviation of y-residuals and b is the slope of the calibration plot was found equal 6.1×10^{-7}. The value of the lower limit of quantification (LOQ) calculated using the equation: LOQ = $10\,S_{y/x}/b$ [42], was found equal 9.2×10^{-7} mol L^{-1}. This level of precision is suitable for the routine analysis of the gold(III) in water.

The application of the developed extraction procedure for the chemical speciation and recovery of traces of gold(I) and (III) at a total concentration ≤25.0 $\mu g\,mL^{-1}$ in tap water was investigated as described in Section 2. A recovery percentage of 97 ± 2.9 was achieved with good reproducibility. Thus, attempts were also applied for the analysis of gold(I, III) in wastewater samples of fertilizer industry following the described experimental procedure. The data are summarized in Table 2. The accuracy of the developed procedure was evaluated by the recovery studies of the gold added. Also, on plotting the amount of gold added versus the amount recovered a regression line with a slope of 0.998 and a correlation coefficient of 0.999 was achieved. The slightly higher values of recoveries in the wastewater may be due the presence of other impurities in the wastewater (Table 2). The F-test at 95% confidence levels did not exceed the tabulated (the-

Table 2
Analytical results of the chemical speciation and recovery of mono- and tri-valent gold ions in wastewater samples by the proposed extraction procedure

Gold species ($\mu g\,mL^{-1}$)				Recovery (%)[a]	
Gold(I) and (III) added		Average gold(I) and (III) found		Au^{+}	Au^{3+}
Au^{+}	Au^{3+}	Au^{+}	Au^{3+}		
5.0	10.0	4.8	10.4	96.0 ± 2.4	104.0 ± 2.9
10.0	15.0	9.7	15.2	97.0 ± 2.8	101.3 ± 2.1
15.0	15.0	14.8	14.8	98.7 ± 3.1	98.7 ± 1.9

[a] Average of five measurements ± relative standard deviation.

Table 3
Analytical results of the recovery of Au^{3+ss} (5–15 μg mL^{-1}) from Ag^{+} and other metal ions, e.g. Fe^{3+}, Co^{2+}, Ni^{2+}I, Cu^{2+}or Zn^{2+} at 10.0 μg mL^{-1} interfering in tap water samples by the proposed procedure

Gold(III) added (μg mL^{-1})	Gold(III) found (μg mL^{-1})	Recovery (%)[a]
5.0	5.15	103 ± 2.1
10.0	10.35	103.5 ± 1.9
15.0	14.8	98.7 ± 2.1

[a] Average of three measurements ± relative standard deviation.

oretical) ones and revealed no significant differences between the averages and the variances of the developed procedure and the reported method [30].

3.4.2. Separation of gold(I) and (III) from silver(I) and other base metal ions

The developed extraction procedure was also applied successfully for the separation of gold(III) ions in the concentration range 5–15.0 μg mL^{-1} Au from silver(I) and base metal (Fe^{3+}, Co^{2+}, Ni^{2+}, $Cu^{2+}$and Zn^{2+}) ions at 10.0 μg mL^{-1} level in tap water samples. The results are summarized in Table 3. More or less complete recovery of gold ions was achieved with good precision (R.S.D. ≤ 2.1%). In terms of *F* (0.075)) and Student's *t* tests (1.91), no significant differences in the accuracy and precision [42] between the proposed and the published method [31] were observed.

4. Conclusion

The method provides an excellent alternative approach for the analytical determination of gold because of its low cost, repeatability and sufficient precision. The reaction of the reagent $DPG^{+}\cdot Cl^{-}$ with the anion $AuCl_4^{-}$ is rapid, simple, does not involve any stringent conditions and no standing time is needed. The produced ternary complex ion associate $DPG^{+}\cdot AuCl_4^{-}$ is stable before determining the ions. Thus, the developed extraction procedures was also applied for the extraction and subsequent AAS determination of inorganic gold(I) and/or (III) ions in fresh and industrial wastewater samples after oxidation of the former ion to gold(III) with bromine water. The procedures have the advantage of virtual freedom from most interfering ions and can serve as a low cost procedure for the separation of gold from silver and base metal ions. However, work is continuing for the recovery of gold species from different matrixes and application of on line procedures for the chemical speciation of inorganic and organic bound gold species in reference and real samples.

References

[1] B. Pal, P.K. Sen, K.K. Sen Gupta, Indian J. Chem. Soc. 83 (2006) 762.
[2] N. Pourreza, S. Rastegarzadeh, Chem. Anal. (Warsaw) 50 (2005) 695.
[3] T.R. Dulski, Trace Elemental Analysis of Metals, Marcel Dekker Inc., 1999, P.99.
[4] M. Behpour, A.M. Attaran, S.M. Ghoreishi, N. Soltani, Anal. Bioanal. Chem. 382 (2005) 444.
[5] H.R. Li, Q.X. Rong, X.L. Hou, X.Y. Mao, Talanta 44 (1997) 1313.
[6] A. Aworn, A. Thiravetyan, W. Nakbanpote, J. Colloid Interf. Sci. 287 (2005) 394.
[7] Y. Yang, C. Li, K.H. Lee, H.G. Craighead, Electrophoresis 26 (2005) 3622.
[8] Z. Marczenko, Spectrophotometric Determination of Elements, 3rd ed., Ellis Horwood, Chichester, UK, 1986 (and references cited in Chapter 23).
[9] Q. Hu, X. Chen, X. Yang, Z. Huang, J. Chen, G. Yang, Anal. Sci. (Jpn.) 22 (2006) 627.
[10] O. Shima, N. Hirayama, K. Kubono, H. Kokusen, T. Honjo, Anal. Chim. Acta 441 (2001) 157.
[11] J.-F. Li, Li-F. Bai, Y.-H. Wang, H.-Y. Wang, Anal. Sci. (Jpn.) 22 (2006) 841.
[12] F. Menegazzo, M. Manzoli, A. Chiorino, F. Boccuzzi, T. Tabakova, M. Signoretto, F. Pinna, N. Pernicone, J. Catal. 237 (2006) 431.
[13] Z.Y. Chen, Z.J. Huang, J. Chen, J.Y. Yin, Q.D. Su, G.Y. Yang, Anal. Lett. 39 (2006) 579.
[14] V. Balaram, R. Mathur, V.K. Banakar, J.R. Hein, C.R.M. Rao, T.G. Rao, B. Dasaram, Indian J. Mar. Sci. 35 (2006) 7.
[15] B. Dasaram, Indian J. Mar. Sci. 35 (1) (2006) 7.
[16] S. Oshima, N. Hirayama, K. Kubono, H. Kokusen, T. Honjo, Anal. Chim. Acta 441 (2001) 157.
[17] J. Rydberg, C. Musikas, G.R. Choppin, Principles and Practices of Solvent Extraction, Marcel Dekker, New York, 1992.
[18] M. Tanaka, H. Akaiwa, Solvent Extraction Chemistry, Shokabo, Tokyo, 2000.
[19] B. Saad, S.M. Sultan, Talanta 42 (1995) 1349.
[20] M.S. El-Shahawi, S.M. Al-Dhaheri, Fresen. J. Anal. Chem. 354 (1996) 200.
[21] M.H. Cordoba, P. Navarro, I.L. Garcia, Int. J. Environ. Anal. Chem. 32 (1988) 97.
[22] P. Das, H.K. Das, J. Indian Chem. Soc. 70 (1993) 90.
[23] M.S. El-Shahawi, A.M. Othman, M.A. Abdel-Fadeel, Anal. Chim. Acta 546 (2005) 221.
[24] M.S. El-Shahawi, S.S.M. Hassan, A.M. Othman, M.A. Zyada, M.A. El-Sonbati, Anal. Chim. Acta 534 (2005) 319.
[25] P. Padmaja, N. Balasubramanian, T.V. Ramakrishna, Talanta 41 (1994) 255.
[26] S.S.M. Hassan, M.S. El-Shahawi, A.M. Othman, M.A. Mosaad, Anal. Sci. 21 (2005) 673.
[27] D.T. Burns, S.A. Barakat, M. Hariott, M.S. El-Shahawi, Anal. Chim. Acta 270 (1992) 213.
[28] D.T. Burns, S.A. Barakat, M.S. El-Shahawi, M. Hariott, Fresen. J. Anal. Chem. 344 (1992) 131.
[29] M.S. El-Shahawi, F.A. Al-Hashimi, Talanta 43 (1996) 2037.
[30] C.T. Camagong, T. Honjo, Anal. Sci. (Jpn.) 17 (2001) 1725.
[31] K. Gavazov, A. Dimitrov, V. Lekova, Chem. Papers (2007), in press.
[32] S. Biswas, H.K. Mondal, S. Basu, Indian J. Chem. 35A (1996) 804.
[33] P.R. Haddad, N.E. Rochester, Anal. Chem. 60 (1998) 536.
[34] D.T. Burns, P. Hanprasopwattana, Anal. Chim. Acta 118 (1980) 185.
[35] D.T. Burns, M.S. El-Shahawi, M.J. Kerrigan, P.M.T. Smyth, Anal. Chim. Acta 322 (1996) 107.
[36] M.S. El-Shahawi, Anal. Chim. Acta 356 (1997) 85.
[37] S.M. AlDhaheri, Talanta 46 (1998) 1613.
[38] A.I. Vogel, A Text Book of Quantitative Inorganic Analysis, 3rd ed., Longman Group Ltd., England, 1966.
[39] M. Hiraoka, Crown Compounds, their Characteristics and Applications, Elsevier Science Ltd., Tokyo, 1982.
[40] S. Yamaguchi, K. Uesugi, Analyst 109 (1984) 1393.
[41] D.T. Sawyer, W.R. Heinemann, J.M. Beebe, Chemistry Experiments for Instrumental Methods, John Wiley & Sons, 1984.
[42] J.C. Miller, J.N. Miller, Statistics for Analytical Chemistry, 4th ed., Ellis-Horwood, New York, 1994, p. 115.

Available online at www.sciencedirect.com
ScienceDirect
Talanta 72 (2007) 1302–1306
Talanta
www.elsevier.com/locate/talanta

Study on electrochemical behavior of tryptophan at a glassy carbon electrode modified with multi-walled carbon nanotubes embedded cerium hexacyanoferrate

Bin Fang [a,c,*], Yan Wei [a,b,c], Maoguo Li [a,c], Guangfeng Wang [a,c], Wei Zhang [a,c]

[a] College of Chemistry and Materials Science, Anhui Normal University, Wuhu 241000, China
[b] Department of Chemistry, Wannan Medical College, Wuhu 241000, PR China
[c] Anhui Key Laboratory of Functional Molecular Solids, Wuhu 241000, China

Received 20 October 2006; received in revised form 3 January 2007; accepted 14 January 2007
Available online 20 January 2007

Abstract

Electrochemical behavior of cerium hexacyanoferrate (CeHCF) incorporated on multi-walled carbon nanotubes (MWNTs) modified GC electrode is investigated by scanning electron microscopy (SEM) and electrochemical techniques. The CeHCF/MWNT/GC electrode showed potent electrocatalytic activity toward the electrochemical oxidation of tryptophan in phosphate buffer solution (pH 7.0) with a diminution of the overpotential of 240 mV. The anodic peak currents increased linearly with the concentration of tryptophan in the range of 2.0×10^{-7} to 1.0×10^{-4} M with a detection limit of 2.0×10^{-8} M (at a S/N = 3). And the determination of tryptophan in pharmaceutical samples was satisfactory.

Keywords: Cerium hexacyanoferrate; Multi-walled carbon nanotubes; Modified electrode; Tryptophan; Electroanalysis

1. Introduction

Tryptophan (Trp) is an amino acid essential to humans. It is a vital constituent of proteins and indispensable in human nutrition for establishing and maintaining a positive nitrogen balance. These compounds are sometimes added to dietary, food products, pharmaceutical formulas due to the scarcely presence in vegetables. Therefore simple, sensitive and less expensive detection of Trp is of great interest. The methods based on electroanalysis of Trp have been many reported [1–8]. It is well known that the direct electrochemical oxidation of Trp at a bare electrode takes place at high overpotential. The reported overpotential at pH 7.0 is 0.800 V at glassy carbon (GC) electrode [3]. Many efforts have been devoted to the goal of finding the new material (mediators) for electrode modification that will reduce the overpotential of the oxidation of Trp [1–8]. Recently, Lin et al. [3] have reported the electrocatalytic oxidation of Trp at a GC electrode modified with butyrylcholine with decreasing of 131 mV in overpotential.

Cerium compound possesses many attractive properties which makes it highly promising for a wide range of applications such as solid electrolytes in solid oxide fuel cells [9], automotive three-way catalysts, ultraviolet absorbers [10,11], and oxygen sensors [12]. It is also used as a catalyst for large-scale fluid cracking in refineries and dehydrogenation of ethyl benzene to styrene [13]. Studies on metal hexacyanoferrate have been documented on transition metal compounds [14–21]. A cerium hexacyanoferrate (CeHCF) modified glassy carbon electrode was prepared by electrochemical method in this paper. However, this modified electrode is instable. As we all know, stability of modified electrode is highly desirable in order to expand its use in numerous practical applications. Electrodes based on carbon nanotubes are an attractive research area now [22–25]. Carbon nanotube is a kind of inorganic material with a nano-structure, which is promising as immobilization substance because of its significant mechanical strength, high surface area, excellent electrical conductivity and good chemical stability [26].

* Corresponding author at: College of Chemistry and Materials Science, Anhui Normal University, Wuhu 241000, China.
E-mail address: binfang_47@yahoo.com.cn (B. Fang).

0039-9140/$ – see front matter © 2007 Elsevier B.V. All rights reserved.
doi:10.1016/j.talanta.2007.01.039

In this paper, the multi-walled carbon nanotubes (MWNTs) were added so as to improve the stability of the CeHCF modified electrode. The resulting electrode exhibited good stability. Using such modified electrodes, the electrochemical behavior of Trp was investigated and a procedure for its electrochemical determination was proposed.

2. Experimental

2.1. Materials

Trp and tyrosine (Tyr) were purchased from Shanghai Medicine Company. Acid-treated MWNTs were obtained from Chengdu Institute of Organic Chemistry of the Academy of Sciences. All other regents used were of analytical grade. Solutions of Trp and Tyr were prepared in water prior to use. Phosphate-buffered solutions (PBS) of 0.1 M for different pH were prepared by mixing stock solutions of 0.1 M H_3PO_4, KH_2PO_4, K_2HPO_4 and K_3PO_4. Double distilled water was used. High purity nitrogen was used.

2.2. Measurement methods and apparatus

Scanning electron microscopy (SEM) was performed with a Hitachi X-650 microscope. Electrochemical techniques including cyclic voltammetry (CV) and amperometric experiment were performed on a CHI 660B electrochemical workstation (Chenhua Instruments Co., Shanghai, China). Three-electrode system was used with a saturated calomel electrode (SCE) as reference electrode, a platinum wire electrode as counter electrode and a bare glassy carbon (diameter = 3 mm) or modified electrode as working electrode. All potentials reported in this paper were versus SCE. The electrolyte solutions were deoxygenated with nitrogen bubbling for 10 min before each voltammetric ran, and all experiments were performed at a temperature of $25 \pm 1\,^{\circ}C$ and under nitrogen atmosphere.

3. Results and discussion

3.1. Preparation of CeHCF modified electrode

Two milliliters of 1.50×10^{-2} M $Ce(NO_3)_3$, 2 ml 1.50×10^{-2} M $K_3Fe(CN)_6$ and 2 ml 1.5 M KCl were added, respectively, to a 10 ml cell so as to obtain a mixed solution (pH 5.0) for the preparation of the CeHCF modified electrode. Then a three-electrode system was set up; the potential cycling was performed between −0.20 and 0.80 V for 40 cycles at a rate of 100 mV s^{-1} under a nitrogen atmosphere. The cyclic voltammograms for the preparation of the CeHCF on the surface of the GC electrode were shown in Fig. 1, from which we can see that the peak currents decrease gradually with the scan cycles. This phenomenon showed that the state of the electrode surface changed with increasing number of scan cycles and CeHCF was formed. In fact, this deposit was formed from crystals of CeHCF. The formation process of CeHCF on electrode surface can be

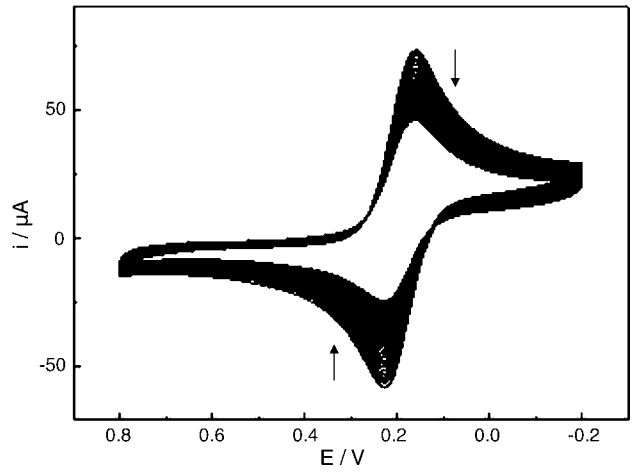

Fig. 1. Cyclic voltammograms of the CeHCF deposition process on a GC electrode surface in a solution containing 2 ml 1.50×10^{-2} M $Ce(NO_3)_3$, 2 ml 1.50×10^{-2} M $K_3Fe(CN)_6$ and 2 ml 1.5 M KCl. The scan rate is 50 mV/s.

expressed by the following EC reaction mechanism:

$$Fe(CN)_6^{3-} + e^- \rightarrow Fe(CN)_6^{4-} \quad \text{(electrochemical reaction)} \tag{1}$$

$$Fe(CN)_6^{4-} + Ce^{3+} + K^+ \rightarrow KCeFe(CN)_6 \quad \text{(chemical reaction)} \tag{2}$$

Fig. 2, curve a, exhibited a cyclic voltammogram of a CeHCF/GC electrode obtained in a solution of 0.1 M PBS at a scan rate of 100 mV/s. There was a pair of well-defined redox peaks in the potential range of −0.2 to 0.8 V, with the anodic potentials of 225 mV and cathodic peak potentials of 84 mV. The separation of the anodic and cathodic peak potentials, ΔE_p is 141 mV. There was no redox peaks in curve e, which was a cyclic voltammogram (at 100 mV/s) of a GC electrode in 0.1 M PBS after the electrode was scanned for 40 cycles in a solution

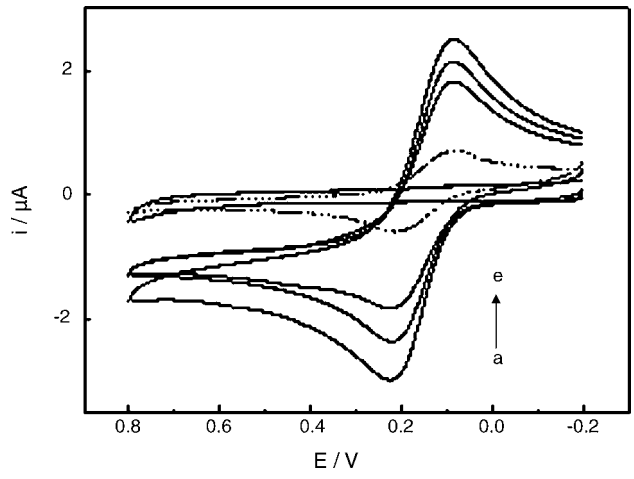

Fig. 2. Cyclic voltammograms of a CeHCF/GC electrode in 0.1 M pH 7.0 PBS at a scan rate of 100 mV/s: (a) the first cycle; (b) the second cycle; (c) the third cycle; (d) the sixth cycle; (e) cyclic voltammograms at a GC electrode (at 100 mV/s) in 0.1 M pH 7.0 PBS after the GC electrode was scanned for 40 cycles in a solution of 1.50×10^{-2} M $K_3Fe(CN)_6$ + 4 ml 1.5 M KCl in the potential range of −0.2 to 0.8 V. The scan rate is 50 mV/s.

of 4 ml 1.50×10^{-2} M $K_3Fe(CN)_6$ containing4 ml 1.5 M KCl as supporting electrolyte at a scan rate of 100 mV/s. These results indicated that the redox peaks in curve a were due to the electrochemical reaction of deposited electrochemically on the surface of GC electrode, not the $Fe(CN)_6^{3-}$, which may be adsorbed on the GC electrode surface as the electrode is cycled in the preparation solution [3].

3.2. Preparation of CeHCF/MWNT/GC electrode

However, CeHCF/GC was not absorbed strongly on the electrode surface. A continuous CV experiment was carried out and it was found from Fig. 2 (curve a → d) that the peak currents decreased gradually with the scan cycles. To improve the attachment to electrode surface, we added the multi-walled carbon nanotube (MWNT) to the electrode.

Firstly, 1.0 mg of acid-treated MWNTs was dispersed in 10 ml of acetone with the aid of ultrasonic agitation to form a black suspension. Then, 20 μl of MWNT solution was cast on the surface of a GC electrode, and the solvent acetone was evaporated in the air to form an MWNT-modified (MWNT/GC) electrode. Lastly, the MWNT/GC electrode was used as working electrode in place of a bare glassy carbon to construct, and other conditions were the same as Section 3.1.

The resulted CeHCF/MWNT/GC electrode exhibited a high stability. The following continuous CV experiment showed that only 3.1% loss of CV current was found after 15 successive scans in PBS.

In this work, the morphology of CeHCF film and CeHCF/MWNT film on electrode surface were characterized by using scanning electron microscopy (SEM). Fig. 3 illustrated the SEM photographs of CeHCF film (A) and CeHCF/MWNT film (B). As shown in photograph A, the surface of the CeHCF film on the electrode surface is very smooth and uniform. Many multi-walled carbon nanotubes were observed on the CeHCF/MWNT/GC electrode surface, as shown in Fig. 3B. The SEM pictures of CeHCF film and CeHCF/MWNT film showed significant difference in the film morphology, which suggested that the MWNTs were embedded into the CeHCF film. Carbon nanotubes, modified at the electrode, increased the surface-to-volume ratio effectively and enhanced the electron-transfer reactions so as to fasten the rate of the polymerization reaction of the CeHCF. At the same time, CeHCF was deposited on the walls of the MWNTs, and linked with each other, which enhanced the mechanical intensity and the electrical conductivity. Therefore the stability and sensitivity of the modified electrode improved.

3.3. Electrochemical behavior of Trp at the CeHCF/MWNT/GC electrode

Fig. 4 exhibited the voltammograms of Trp. The direct oxidation of Trp at an unmodified glassy carbon electrode showed a broad oxidation peak at 800 mV in pH 7.0 PBS (curve a). It could be seen from Fig. 4 curve c that at CeHCF/MWNT/GC electrode in pH 7.0 PBS the oxidation peak potential of Trp appeared at

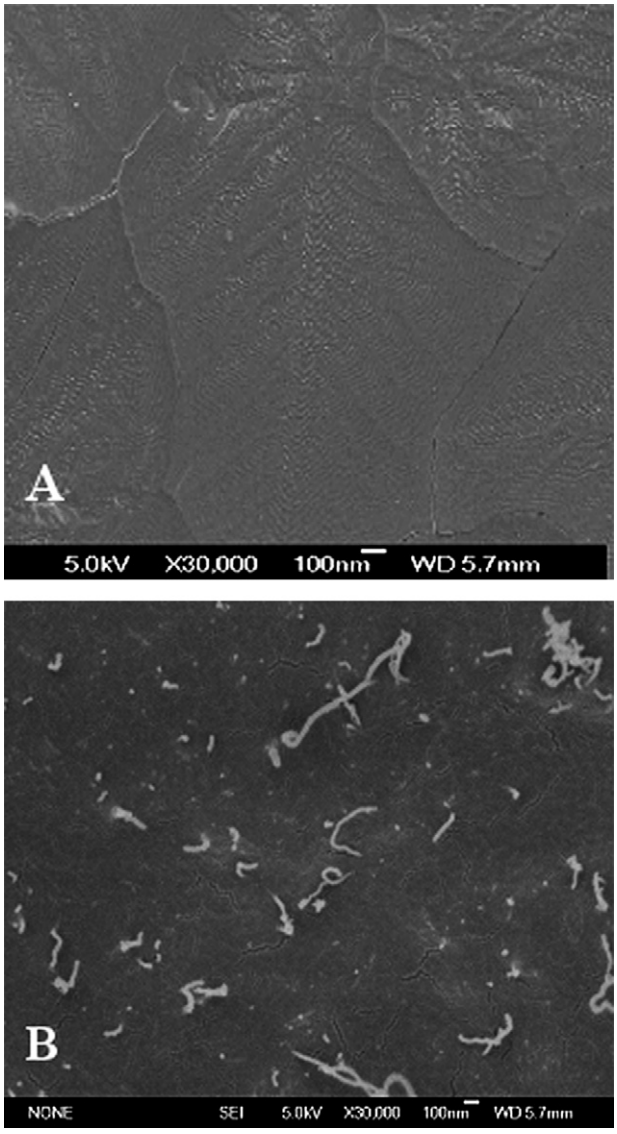

Fig. 3. SEM images of CeHCF film (A) and CeHCF/MWNT film (B) on the glassy carbon electrode surface.

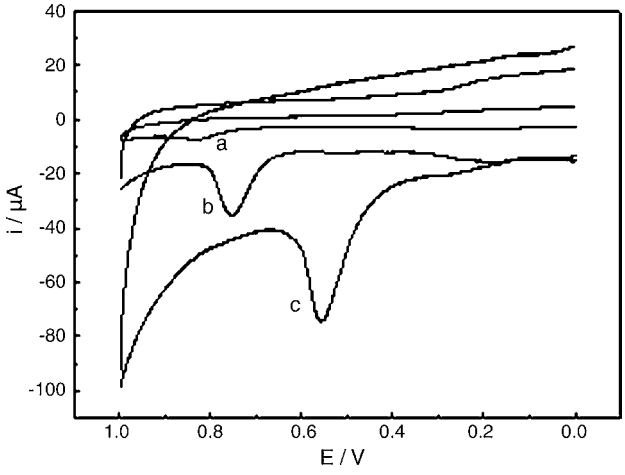

Fig. 4. Cyclic voltammograms of 50 μM Trp at bare glassy carbon electrode (a), MWNT/GC electrode (b), and CeHCF/MWNT/GC electrode (c) in 0.1 M pH 7.0 PBS at a scan rate of 50 mV/s.

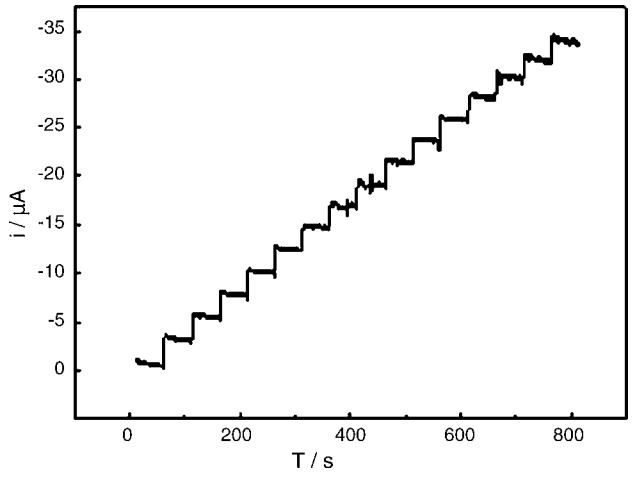

Fig. 5. Amperometric detection of Trp by CeHCF/MWNT/GC electrode in 0.1 M pH 7.0 PBS, each addition of 2 mM (alternating current was measured at constant potential of 0.20 V modulated with pulse 50 mV in time interval of 0.5 s in a stirred system).

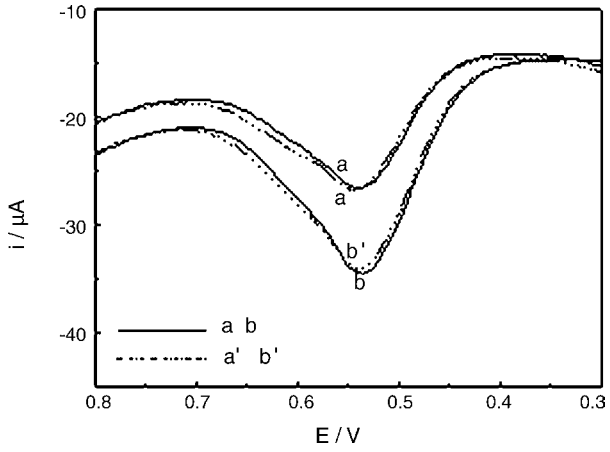

Fig. 6. Differential pulse voltammetry at the modified electrode in pH 7.0 PBS: (a) 5.0×10^{-6} M Trp; (b) 5.0×10^{-6} M Trp + 5.0×10^{-5} M Tyr; (a′) 1.0×10^{-5} M Trp; (b′) 1.0×10^{-5} M Trp + 1.0×10^{-4} M Tyr. Amplitude: 50 mV; pulse width: 50 ms; pulse period: 200 ms; sensitivity: 1.0×10^{-5} A/V.

560 mV. The oxidation potential of Trp at CeHCF/MWNT/GC electrode shifted by about 240 mV toward the negative values compared with that at a bare GC electrode. When the multi-walled carbon nanotube modified electrode was used to detect the Trp, only 60 mV negatively peak shift was received (seen in Fig. 4 curve b). This suggested that CeHF was a dominating participator in the electrocatalytic activity of Trp. In addition, the dependence of voltammetric response of CeHCF/MWNT/GC electrode on the Trp concentrations showed that with the addition of Trp, there was an enhancement in the anodic current, so the electrocatalytic activity of the modified electrode could be applied to the determination of Trp.

To optimize the electrocatalytic response of the CeHCF/MWNT/GC electrode for Trp oxidation, the pH effect was studied between pH 4.0 and 9.0. It showed that the largest oxidation peak current of Trp was obtained at pH 7.0 PBS. Hence, the solution pH of 7.0 was selected in the following experiments.

3.4. Determination of Trp

In order to test the response of CeHCF/MWNT/GC electrode for Trp, the amperometric experiments were carried out and the results were shown in Fig. 5. The current signal of the CeHCF/MWNT/GC electrode was proportional to the concentration from 2.0×10^{-7} to 1.0×10^{-4} M. The linear regression equation is I_p (μA) = 0.4948–0.4447C (μM), with a correlation coefficient $r = -0.9971$. The response time (time for the signal increase from 10 to 75%) in the amperometric mode was less than 0.95 s. The detection limit (S/N = 3) was estimated to be 2.0×10^{-8} M.

3.5. Interference study

Tyrosine (Tyr) coexists with Trp in human and herbivores bodied. Fig. 6 illustrated differential pulse voltammograms obtained at the modified electrode. While simultaneously varying the concentration of both Trp and Tyr, the anodic peak current increased, respectively. The fact that the peak current of Trp at the CeHCF/MWNT/GC electrode in the absence and presence of Tyr was about the same, showing Tyr did not influence the measurement of Trp.

We also studied the interference effects of 18 amino acids for determination of Trp. The results showed that none (100 times content) of 18 amino acids interfered with the determination of Trp.

3.6. Determination of Trp in pharmaceutical samples

In order to test the reliability of this method, the proposed method was applied to detect the concentration of tryptophan in amino acid injection. The determination was performed as follows: the amino acid injection was firstly from 1.0 to 10.0 ml with double distilled water. One hundred microliters of the diluted

Table 1
Results for determinations of trp in pharmaceutical samples

Samples	Labeled values (g l^{-1})	Found (mg l^{-1}) ($n = 10$)	R.S.D. (%) ($n = 10$)	Recovery (%)	Uncertainty budget[a]
A	0.900	0.921	3.8	102.3	±0.036
B	0.900	0.918	3.6	102.0	±0.034
C	0.900	0.896	2.6	99.55	±0.024
D	0.900	0.892	2.2	99.11	±0.020
E	0.900	0.911	3.2	101.2	±0.030

Samples were obtained form Guangzhou Green Cross Pharmaceutical Corporation.
[a] Uncertainty budget was described as $\pm ts/\sqrt{n}$ ($n = 10$, $t_{0.01,9} = 3.25$).

sample was diluted again to 10 ml with pH 7.0 PBS and then transferred to an electrolysis cell. The solution was purged with purified nitrogen for 5 min to remove oxygen, and then a three-electrode system was placed into the solution. The injection of Trp was analysed by the standard addition method. The results are given in Table 1. The results were satisfactory, suggesting that the proposed method could be used for the determination of Trp in injection.

3.7. The repeatability and stability of the CeHCF/MWNT/GC electrode

The modified electrode exhibited a high stability. The relative standard deviation (R.S.D.) of six successive scans was 3.6% for 5.0×10^{-6} M Trp. And whenever it was placed in phosphate buffer, only 3.2% loss of DPV current was found even after 1 week. The reproducibility of six independently fabricated electrodes showed a satisfactory value of 2.1% (R.S.D.).

4. Conclusion

The CeHCF and MWNTs were modified onto the glassy carbon electrode to fabricate the modified electrode. It provided a good example of applying the good catalysis of rare earth to electrochemistry. Electrocatalytic oxidation of Trp at the CeHCF/MWNT/GC electrode was studied. The CeHCF/MWNT/GC electrode could be used to detect tryptophan without interference. And it has been applied to the determination of tryptophan in pharmaceutical samples with satisfactory results. The reliability and stability of the CeHCF/MWNT/GC electrode offered a good possibility for applying the technique to routine analysis of tryptophan in clinical use.

Acknowledgements

We appreciated the support of the National Natural Science Foundation of China (No. 20675001), Science Foundation of Education Office of Anhui Province (Nos. 2006kj119B and 2006kj145B), and Scientific Research Sustentation Program of Anhui Province College Young Teacher (2005JQ1048ZD).

References

[1] G.N. Chen, Z.F. Zhao, X.L. Wang, J.P. Duan, H.Q. Chen, Anal. Chim. Acta 452 (2002) 245.
[2] A.R. Fiorucci, E.T.G. Cavalheiro, J. Pharmaceut. Biomed. Anal. 28 (2002) 909.
[3] G.P. Jin, X.Q. Lin, Electrochem. Commun. 6 (2004) 454.
[4] F.H. Wu, G.C. Zhao, X.W. Wei, Z.S. Yang, Microchim. Acta 144 (2004) 243.
[5] S.M. MacDonald, S.G. Roscoe, Electrochim. Acta 42 (1997) 1189.
[6] K. Ogura, M. Kobayashi, M. Nakayama, Y. Miho, J. Electroanal. Chem. 463 (1999) 218.
[7] J. Saurina, S. Hernandez Cassou, E. Fabregas, S. Alegret, Anal. Chim. Acta 405 (2000) 153.
[8] L. Aguy, A. Gonzalez Cortes, P. Yanez Sedeno, J.M. Pingarron, Anal. Chim. Acta 401 (1999) 145.
[9] B.C.H. Steele, Solid State Ionics 129 (2000) 95.
[10] T. Masui, K. Fujiwara, K.I. Machida, G.Y. Adachi, Chem. Mater. 9 (1997) 2197.
[11] R.X. Li, S. Yabe, M. Yamashita, S. Momose, S. Yoshida, S. Yin, T. Sato, Solid State Ionics 151 (2002) 235.
[12] P. Jasinski, T. Suzuki, H.U. Anderson, Sens. Actuators B 95 (2003) 73.
[13] J.M. Pemba-Mabiala, M. Lenzi, J. Lenzi, A. Lebugle, Surf. Interf. Anal. 15 (1990) 663.
[14] R. Vittal, H. Gomathi, J. Phys. Chem. 106 (2002) 10135.
[15] A. Abbaspour, M.A. Mehrgardi, Anal. Chem. 76 (2004) 5690.
[16] D.N. Upadhyay, V. Yegnaraman, G.P. Rao, Langmuir 12 (1996) 4249.
[17] S.Q. Liu, H.Y. Chen, J. Electroanal. Chem. 528 (2002) 190.
[18] P. Wu, S. Lu, C.X. Cai, J. Electroanal. Chem. 569 (2004) 143.
[19] G.C. Yang, Y. Shen, M.K. Wang, H.J. Chen, B.F. Liu, S.J. Dong, Talanta 68 (2006) 741.
[20] L. Qian, X.R. Yang, Talanta 69 (2006) 957.
[21] P.A. Fiorito, C.M.A. Brett, S.I.C. Torresi, Talanta 69 (2006) 403.
[22] A. Profumo, M. Fagnoni, D. Merli, et al., Anal. Chem. 78 (12) (2006) 4194.
[23] T.M. Day, N.R. Wilson, J.V. Macpherson, J. Am. Chem. Soc. 126 (2004) 16724.
[24] Z.Y. Lin, G.N. Chen, Talanta 70 (2006) 111.
[25] L. Qian, X.R. Yang, Talanta 68 (2006) 721.
[26] B.I. Yakabson, R.E. Smally, Am. Sci. 85 (1997) 324.

Available online at www.sciencedirect.com
ScienceDirect
Talanta 72 (2007) 1248–1254
Talanta
www.elsevier.com/locate/talanta

On-line preconcentration with a novel alkyl phosphinic acid extraction resin coupled with inductively coupled plasma mass spectrometry for determination of trace rare earth elements in seawater

Qiang Fu [a], Limin Yang [a], Qiuquan Wang [a,b,*]

[a] *Department of Chemistry & The MOE Key Laboratory of Modern Analytical Sciences, College of Chemistry and Chemical Engineering, Xiamen University, Xiamen 361005, China*
[b] *State Key Laboratory of Marine Environmental Science, Xiamen University, Xiamen 361005, China*

Received 7 October 2006; received in revised form 8 January 2007; accepted 8 January 2007
Available online 16 January 2007

Abstract

A newly synthesized alkyl phosphinic acid resin (APAR) was used for on-line preconcentration of trace rare earth elements (REES, lanthanides including yttrium) and then determined by inductively coupled plasma mass spectrometry. REEs in seawater could be on-line concentrated on the APAR packed column (4.6 mm i.d. × 50 mm in length), and eluted from the column with 0.5 mL 0.1 mol L^{-1} nitric acid within 30 s. An enrichment factor of nearly 400 was achieved for all REEs when the seawater sample volume was 200 mL, while the matrix and coexisting spectrally interfering ions such as barium, tin and antimony could be simultaneously separated. The detection limits of this proposed method for REEs were in the range from 1.43 pg L^{-1} of holmium to 12.7 pg L^{-1} of lanthanum. The recoveries of REEs were higher than 97.9%, and the precision of the relative standard deviation (R.S.D., $n = 6$) was less than 5%. The method has been applied to the determination of soluble REEs in seawater.

Keywords: Alkyl phosphinic acid resin; Rare earth elements; On-line preconcentration; Seawater; Inductively coupled plasma mass spectrometry

1. Introduction

Rare earth elements (REEs) have been widely used as micro-additives in functional materials, catalysts, medicines and cosmetics as well as fertilizers (especially in China) in recent years [1], resulting in a potential risk to the environment [2,3]. Information concerning REEs' concentration and their relative distribution in seawater is very important for environment science and marine geochemistry. Due to the low concentrations of REEs, normally at nanogram level in seawater, either preconcentration methods or advanced analytical techniques are required for their detection [4]. Neutron activation analysis [5,6] and isotope dilution mass spectroscopy [7–10] were early choices for determination of ultra-trace REEs in seawater. Over the last 20 years inductively coupled plasma mass spectrometry (ICP-MS), which was developed as a powerful tool for the determination of trace elements, has especially benefited the determination of REEs by providing excellent multi-element detection capability with high sensitivity and wide dynamic range. This has allowed direct determination of trace REEs. Nevertheless, the direct determination of REEs in seawater with ICP-MS is still a challenge owing to the remarkable matrix effect and potential spectral interference from some coexisting elements. In seawater, the concentrations of the matrix ions such as sodium, magnesium, potassium and calcium range from 0.4 to 11 g kg^{-1} [11]. Such a high salt content in seawater causes instrumental drift, signal suppression and clogging of the sample introduction system of the instrument. On the other hand, some coexisting elements in seawater such as barium (Ba), tin (Sn) and antimony (Sb) possibly bring serious spectral interference with the determination of europium (Eu), lanthanum (La) and cerium (Ce) by producing oxide ions and hydroxide ions during ICP ionization [12], for example, ^{134}BaOH/^{136}BaOH and ^{135}BaO/^{137}BaO can interfere with ^{151}Eu/^{153}Eu, ^{137}BaOH/^{138}BaOH and ^{138}BaO with ^{154}Gd/^{155}Gd; ^{123}SbO with ^{139}La, and ^{124}SnO with ^{140}Ce. Besides preconcentration of REEs, rapid separation of the matrix

* Corresponding author at: Department of Chemistry & The MOE Key Laboratory of Modern Analytical Sciences, College of Chemistry and Chemical Engineering, Xiamen University, Xiamen 361005, China. Tel.: +86 592 218 1796; fax: +86 592 218 1796.
E-mail address: qqwang@xmu.edu.cn (Q. Wang).

0039-9140/$ – see front matter © 2007 Elsevier B.V. All rights reserved.
doi:10.1016/j.talanta.2007.01.015

is thus necessary for reducing the matrix effect and spectral interference. Many preconcentration methods have been used such as solvent extraction [13,14], coprecipitation with iron hydroxide [8,15,16], ion exchange with chelating resin [4,17–21], 2-ethylhexylphosphonic acid mono-(2-ethylhexyl) ester levextrel resin [22,23], chelating fiber [24,25] and nanometer-sized titanium dioxide [26]. However, these previously developed systems still have their respective limitations in practice. Coprecipitation and solvent extraction methods involve much manipulation and additional separation steps and are somewhat difficult to be used in a flowing system. Chelation with Chelex-100 resin requires the removal of Ca^{2+} and Mg^{2+} before elution of REEs. The extractant loaded in the levextrel resin may gradually be lost during elution.

On-line preconcentration method coupled with flame atomic absorption spectrometry [27], electrothermal atomic absorption spectrometry [28,29], atomic fluorescence spectrometry [30], inductively coupled plasma atomic emission spectrometry [31,32] and ICP-MS [18–20] have been widely applied for determining trace elements. In this study, a chemical boned alkyl phosphinic acid resin (APAR) was novelly synthesized. It was used to pack a short column for on-line preconcentration of REEs and separation of matrix as well as coexisting metals before ICP-MS determination. The optimum experimental conditions were established based on systematic studies, and the proposed method was successfully applied to the determination of trace REEs in the coastal seawater around Xiamen Island.

2. Experimental

2.1. Apparatus and reagents

A Perkin-Elmer ELAN DRC II ICP-MS (Sciex, Canada) was used throughout for determination of REEs. The operating conditions are summarized in Table 1. The eluant was pumped by a quaternary gradient pump of a Shimadzu LC-2010 system (Kyoto, Japan). The seawater samples were pumped by an YSB-III isocratic pump (Shanghai Institute of Atomic Nucleus of CAS, Shanghai, China). The pH measurements of all solutions were performed using a Mettler Toledo Delta 320 pH meter (Mettler-Toledo instruments Co. Ltd., Shanghai, China).

All solutions used were prepared with ultra pure water (UPW) produced by a high-pressure reverse osmosis water purification system (18 MΩ, Pen-Tung Sah Micro-Electro-Mechanical Systems Research Center of Xiamen University, China). All reagents used in this work were of the highest purity available and at least of analytical grade. The nitric acid solution was obtained by diluting concentrated nitric acid (G. R., Sinopharm Chemical Reagent Co. Ltd., Shanghai, China) with UPW. REE stock solution of 1000 mg L^{-1} was prepared by dissolving the corresponding REE oxide (purity > 99.9999%, Changchun Institute of Applied Chemistry of CAS, Changchun, China) in 1:1 nitric acid by gently heating to near dryness and diluting to the required concentration with UPW. Working solutions of mixed REEs were prepared by mixing and stepwise diluting the stock solutions with UPW. The pH of the solution was adjusted with diluted nitric acid or ammonium acetate buffer.

Table 1
Operation conditions for ICP-MS

RF power	1150 kW
Plasma gas (Ar) flow rate	16 L min^{-1}
Auxiliary gas flow rate	1.2 L min^{-1}
Nebulizer gas flow rate	0.93 L min^{-1}
Sample uptake rate	1 mL min^{-1}
Sampler (nickel) orifice	1.1 mm
Skimmer (nickel) orifice	0.9 mm
Data acquisition mode	Chromera
Selected isotope	^{89}Y, ^{139}La, ^{140}Ce, ^{141}Pr, ^{146}Nd, ^{147}Sm, ^{151}Eu, ^{157}Gd, ^{159}Tb, ^{162}Dy, ^{165}Ho, ^{166}Er, ^{169}Tm, ^{174}Yb, ^{175}Lu

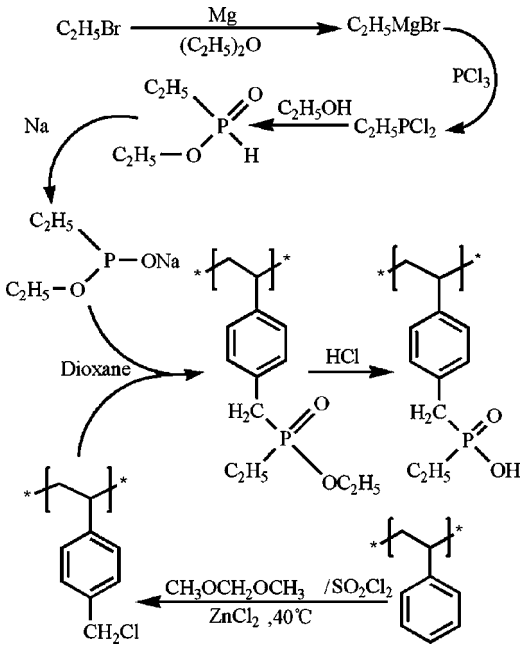

Fig. 1. Synthesis of alkyl phosphinic acid resin.

2.2. Synthesis of the APAR and preparation of the column

The APAR was synthesized by sequential reactions of a chloromethylation, a phosphorylation and an acid catalyzed hydrolytic reaction on styrene-divinylbenzene copolymer beads (diameter: 8 μm, crosslinking degree: 10%, H&E, China). The procedures of the APAR synthesis are presented in Fig. 1. Chloromethylation of the styrene–divinylbenzene copolymer beads was carried out in a three-necked flask with the reactant mixture of methylal, sulfuric chloride and anhydrous zinc chloride as catalyst at 80 °C for 16 h. After chloromethylation the polymer beads were filtered out and were washed with anhydrous aether, and then were sealed in a round flask for next-step use. Grignard reagent was prepared by the Grignard reaction of bromoethane and magnesium chips in aether. The synthesized Grignard reagent was diluted by aether and added dropwise into phosphorus trichloride in aether for alkylation of phosphorus trichloride. After the alkylation of phosphorus trichloride, resulted yellow solid was filtered off, and the liquid

phase was dropped into excessive ethanol at the presence of triethylamine as acid scavenger. After the alcoholysis was completed, the liquid phase was filtered out from the white triethylamine chloride, and was distilled to get the phosphite ester intermediate product. An amount of metallic sodium was dissolved in a mixture of the phosphite ester and dioxane, and then the mixture was poured into a round flask containing the synthesized chloromethyl copolymer beads. After 4 h of refluxing and stirring, the polymer beads were filtered out and followed by refluxing with 1:1 hydrochloric acid for acid catalytic hydrolysis. After 16 h hydrolysis, the resulted APAR was filtered out and sequentially washed with UPW, aether, ethanol and a large volume of UPW. It was characterized by Nicolet FT-IR (Madison, USA) as ν_{max}/cm^{-1} 1162 (P=O) and 937ν_s (P–OH) (KBr) and 400 MHz Varian NMR (Fort Collins, USA) as ^{31}P NMR δP 64.12 ppm ($CDCl_3$; Me_4Si). The column was prepared by packing 0.5 g APAR into a 4.6 mm i.d. × 50 mm in length IT Modular stainless steel column (Isolation Technologies Inc., Hopedail, USA). The adsorption capacity of the column for each REE was measured using the bath method [33].

2.3. Sample preparation

Seawater samples were collected at the south coast of Xiamen Island (24°25″E, 118°08″N). Samples were adjusted to pH 6.0 by adding an appropriate amount of 1% nitric acid, and filtered through a membrane of pore size 0.45 μm to obtain soluble REEs, and then stocked in acid-cleaned polyethylene plastic buckets at 4 °C before analysis.

2.4. On-line preconcentration procedure

The instrumental configuration of on-line preconcentration system is shown schematically in Fig. 2. A six-way valve was used to switch the flow path. Before sample loading, the six-way valve was at position 1. The column was preconditioned with UPW at a flow rate of 1 mL min^{-1} for 1 min. Then, the sample passed through the column for REEs preconcentration and/or matrix and coexisting metals separation. In the elution step, the six-way valve was switched to position 2. After washing with 1 mL of UPW, the REEs retained on the column was eluted with 0.1 mol L^{-1} of nitric acid and directly introduced into the ICP-MS for determination. After the determination, a 0.2 mol L^{-1} nitric acid solution and then a dilute EDTA-Na_2 solution were passed through the column to strip the metal ions that strongly adsorbed on the resin, for example, Sc(III), Hg(II), U(VI) and Th(IV).

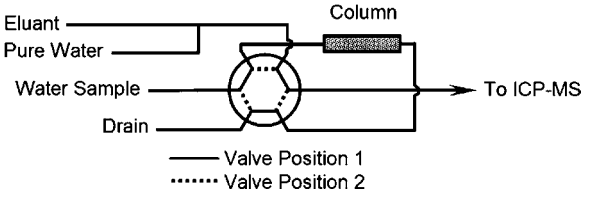

Fig. 2. Schematic diagram of on-line preconcentration and separation system: valve position 1, sample loading; valve position 2, elution and rinse.

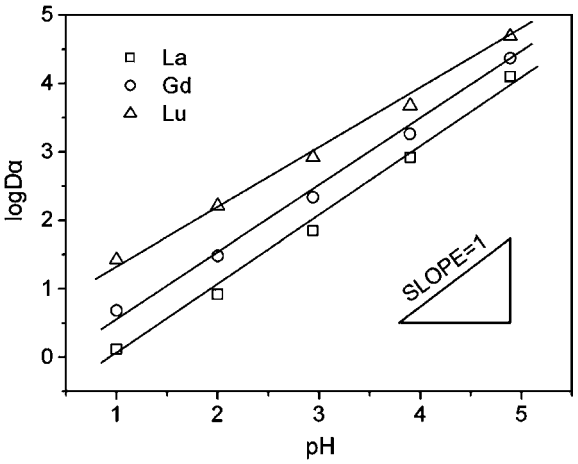

Fig. 3. Log–log plot of pH against $\log D\alpha$: D is the distribution ratio of REE and defined as $D=[(C_0-C)/C][V_{aq}/m_s]$, where C_0 and C are the initial concentration and equilibrium concentration of REE ($\mu g\,mL^{-1}$), respectively; V_{aq} the volume of aqueous phase (mL), and m_s is the mass of the APAR. α is the side reaction coefficient of REE, and can be calculated by $\alpha=1+\beta_1[L]+\beta_2[L]^2+\cdots$,where L indicates $ClCH_2COOH$ or CH_3COOH in buffer solutions, β_1 and β_2 are the successive stability constants of REE–L complexes, respectively. $\log\beta_{1\,La\text{-}HAc}$, 2.02; $\log\beta_{2\,La\text{-}HAc}$, 2.36; $\log\beta_{1\,La\text{-}HAcCl}$, 2.03; $\log\beta_{2\,La\text{-}HAcCl}$, 2.87; $\log\beta_{1\,Gd\text{-}HAc}$, 2.16; $\log\beta_{2\,Gd\text{-}HAc}$, 3.76; $\log\beta_{1\,Gd\text{-}HAcCl}$, 2.06; $\log\beta_{2\,Gd\text{-}HAcCl}$, 3.10; $\log\beta_{1\,Lu\text{-}HAc}$, 2.05; $\log\beta_{2\,Lu\text{-}HAc}$, 3.69; $\log\beta_{1\,Lu\text{-}HAcCl}$, 2.09; $\log\beta_{2\,Lu\text{-}HAcCl}$, 3.37.

3. Results and discussion

3.1. Possible mechanism of the adsorption of REEs on the APAR

Our previous studies showed that alkyl phosphinic acid demonstrated good selectivity in the extraction of REEs and some other metals [33–36]. The adsorption mechanism of REEs on the APAR is supposed to be similar to the extraction mechanism of REEs with bis(1,1,3,3-tetramethylbutyl) phosphinic acid (HMBP). REE can substitute the active hydrogen of the hydroxyl in the phosphinic acid group and follow an ion-exchange mechanism. On the other hand, the oxygen of P=O group in the phosphinic acid is an electron donor which is easy to give its lone paired electron to REE ion through complexation. Nevertheless, there is something different between the adsorption mechanism of the APAR and that of liquid HMBP extractant. In nonpolar solvent, HMBP can form a dimer by hydrogen bond. REE can exchange three H^+ of the three dimers. The molecular ratio of REE to HMBP resulted in 1:6 [33]. However, the alkyl phosphinic acid was chemically bonded on the resin framework in the APAR. It is difficult to form dimer in this case. The result of log–log plot analysis indicated that the interaction between REE and the phosphinic acid on the resin mainly through a cation-exchange mechanism shown in Fig. 3 indicating a slope of 1 when La, Gd and Lu were set as examples of REEs. Moreover, the phosphinic acid functional group was chemically linked to the benzene ring on the resin matrix via a methylene in the APAR. This methylene not only reduced the inductive effect from the aromatic ring resulting in higher electron density on the oxygen atoms of the functional groups,

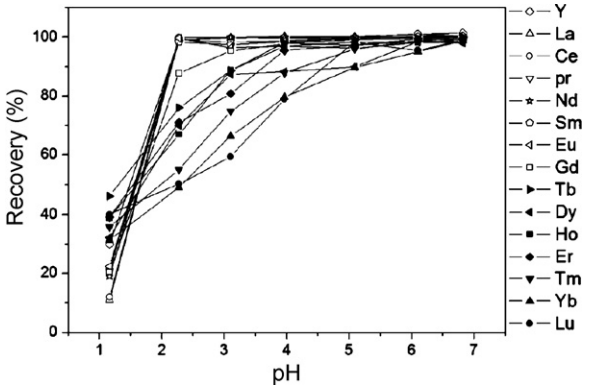

Fig. 4. Effect of pH on the recovery (%) of REEs on the column: concentration of REE each, 1.0 μg L^{-1}; sample volume, 10 mL; sampling flow rate, 2.0 mL min^{-1}; elution time, 0.5 min.

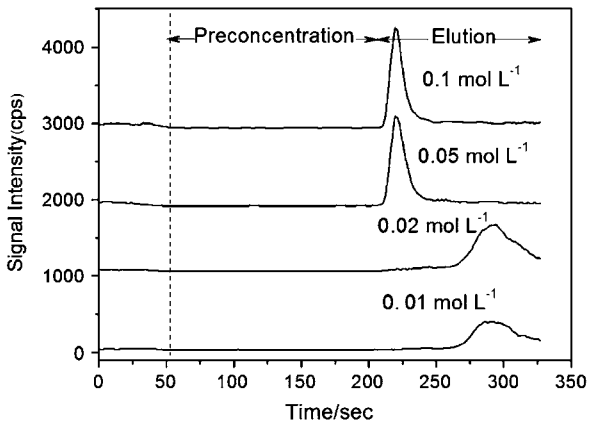

Fig. 5. The elution profile of La by different concentration of HNO_3: La concentration, 1.0 ng L^{-1}; sample flow rate, 2 mL min^{-1}; sample volume, 10 mL; HNO_3 flow rate, 1 mL min^{-1}.

but also acted as "elbow" leading to a more flexible and kinetic ability of the bonded phosphinic acid. Therefore, the adsorption and/or desorption processes are more rapidly. The chemically bonded functional group was very stable, so the column had a long operating life.

3.1.1. Optimization of preconcentration and elution conditions

The effect of the sample acidity on recoveries of REEs by the APAR was studied. The pH values of the sample solutions were adjusted over a range of 1–7 prior to on-line preconcentration and ICP-MS determination. Results are shown in Fig. 4. The retention behaviors of REEs on the APAR were obviously dependent on acidity. It can be seen that all REEs were adsorbed poorly when the pH of the sample was lower than 2. In the range pH 2–5, yttrium and light REEs from La to Gd were quantitatively absorbed on APAR, while heavy REEs from Tb to Lu were still poorly recovered. When the pH value of the sample was higher than 6, the recoveries of all REEs were quantitative. This result implies that seawater samples (normally pH > 7) can be directly passed through the column for REEs concentration just after simply filtration. On the other hand, as can be seen from Fig. 4 that the adsorption of REEs on the APAR column was poorly under high acidity, hence, mineral acids such as nitric acid could be used as an eluant. Various concentrations of nitric acid were tested for eluting REEs from the column. The elution time and peak width of elution profile of REEs increased along with the decrease in the concentration of nitric acid used. The elution profile of La from the column by nitric acid ranging from 0.01 to 0.1 mol L^{-1} is shown in Fig. 5. La as an example can be completely eluted from the column by 0.1 mol L^{-1} nitric acid within 30 s. Increasing the concentration of nitric acid higher than 0.1 mol L^{-1} did not benefit the elution efficiency, but led to the increase of the blank value. The effects of nitric acid concentration upon the elution of yttrium and other lanthanides on the column are similar to La as shown in Fig. 5 and the eluent volume of 0.5 mL was sufficient to quantitatively elute them. Such a small elution volume makes it possible to use relatively smaller sample volume to achieve a high enrichment factor. The effect of eluting flow rate was also studied. But it had no obvious effect on the recoveries of REEs in the range 0.5–2.0 mL min^{-1}; 1.0 mL min^{-1} was thus adopted to suit the sampling rate requirement for ICP-MS.

Besides, the effects of the sample flow rate and volume on the preconcentration efficiencies of REEs were also tested in the range from 0.5 to 3.5 mL min^{-1} and from 10 to 200 mL, respectively. Results obtained indicated that all REEs were recovered quantitatively (>97%) at the flow rate up to 2.0 mL min^{-1} and in the whole range of volume tested. Considering that the concentrations of REEs in seawater are extremely low, a larger sample volume was beneficial to get a bigger enrichment factor. It was desirable to pump the sample as fast as possible to shorten the analysis time. Thus, a flow rate of 2.0 mL min^{-1} was used as the optimum flow rate.

As mentioned above, the REEs adsorbed on column can be quantitatively eluted by 0.5 mL of 0.1 mol L^{-1} nitric acid, and an enrichment factor of nearly 400 was achievable for all REEs when the sample volume was 200 mL. In order to shorten the analysis time, a sample volume of 60 mL was adopted for the preconcentration of REEs in seawater. It should be noted that the sampling is 30 min even a sample volume of 60 mL was adopted at a flow rate of 2.0 mL min^{-1}. Indeed, this problem can be overcome by using an array of columns up to 12 or more with one or two multichannel switches in the on-line preconcentration system. The sampling frequency can also be greatly improved.

3.1.2. Column capacity

The adsorption capacity of the column for each REE was measured using the bath method. 100 mg APAR was equilibrated by shaking for 2 h in the solution containing excess REE (100 mg L^{-1}, 10 mL) at pH 6.0. The APAR was then filtered and the concentration of REE in the aqueous phase was determined using arsenazo III spectrophotometry [33]. The column capacities for Y, La, Ce, Pr, Nd, Sm, Eu, Gd, Tb, Dy, Ho, Er, Tm, Yb, and Lu were found to be 15.7, 14.3, 14.4, 14.3, 14.0, 13.9, 14.1, 13.9, 13.8, 13.7, 13.4, 13.2, 13.4, 13.1 and 13.5 μmol g^{-1}, respectively. These are sufficient for the preconcentration of trace REEs in seawater.

Table 2
Separation of the major matrix and interfering ions[a]

Coexisting element	Concentration in sample ($\mu g\,L^{-1}$)	Concentration in eluent ($\mu g\,L^{-1}$)[b]
Na^+ (NaCl)	1×10^7	350 ± 40
Mg^{2+}($MgCl_2$)	2×10^6	86 ± 10
K^+ (KCl)	5×10^5	120 ± 20
Ca^{2+} ($CaCl_2$)	5×10^5	100 ± 10
Ba^{2+}	10	0.046 ± 0.0001
Sn^{2+}	1	0.015 ± 0.0001
Sb^{3+}	1	0.036 ± 0.0001

[a] Sample volume, 10 mL; sample flow rate, 2.0 mL min^{-1}; eluant, 0.1 mol L^{-1} HNO_3; elution time, 0.5 min.
[b] The concentration of matrix in the eluent was determined by the semi-quantitative mode of ICP-MS; $n = 3$.

3.2. Separation of the matrix and elimination of spectral interference from some coexisting ions

The high salt content and presence of spectral interfering ions in seawater result in an obvious matrix effect and spectral interference during direct determination of trace REEs in seawater by ICP-MS. The separation of the major matrix and the spectrally interfering ions in seawater from REEs in seawater is thus necessary. Therefore, the effects of the major matrix and the spectrally interfering ions on the recovery of REEs were studied. Synthetic seawater [37] containing REEs of totally 1 $\mu g\,L^{-1}$ and Na^+, Mg^{2+}, K^+ and Ca^{2+} respectively of 10,000, 2000, 500 and 500 mg L^{-1} as well as Ba^{2+}, Sn^{2+} and Sb^{2+} respectively of 13.7, 0.15 and 1.48 ng L^{-1} was treated according to the proposed preconcentration procedures. When REEs were retained on the column under the optimum conditions, the matrix and the spectral interfering ions flowed out of the column. The concentrations of REEs, and the matrix ions and the spectrally interfering ions in the eluent were determined by ICP-MS. The results listed in Table 2 indicated that the concentration of the matrix ions and the spectrally interfering ions in the eluent were significantly lower, which is suitable for direct determination of trace REEs by ICP-MS. The recoveries of REEs were acceptable (97–99%), suggesting that the matrix and the spectrally interfering ions can be separated effectively while REEs were concentrated on the column.

The results obtained also suggested that the APAR could adsorb other metals such as Al(III), Ga(III), Pb(II), Bi(III), Fe(III), Co(II), Ni(II), Zn(II), Cd(II), Sc(III), Hg(II), U(VI) and Th(IV), besides REEs. However, these metals can be separated from REEs when using 0.1 mol L^{-1} HNO_3 as an eluant. Although there are some overlap with REEs, they did not interfere the determination of REEs by ICP-MS. It should also be noted that the elements such as Sc(III), Hg(II), U(VI) and Th(IV) in seawater have stronger intensity to adsorb on the column, their adsorption onto the column would occupy some active sites of the resin. However, they could be eluted effectively out of the column by 5 mL of 0.2 mol L^{-1} HNO_3 and dilute EDTA-Na_2, respectively. Furthermore, considering the low concentrations of coexisting absorbable elements in seawater compared with the high column capacity, their adsorption on the column did not influence remarkably on the recovery of REEs. Results obtained indicated that the column could be used for hundreds of replicate preconcentration runs without any decrease in the recovery of REEs.

3.3. Method evaluation

The detection limit (DL) of ICP-MS and method detection limit (MDL) with on-line preconcentration were calculated based on three times of signal to noise ratio of the blank solution. The DLs of ICP-MS for REEs and the MDLs of the APAR on-line preconcentration ICP-MS are shown in Table 3. The MDLs of REEs are much improved and low enough for accurate determination of trace REEs in seawater. The correlation coefficients of the calibration curves (from 0.01 to 100 ng L^{-1}) for all REEs were greater than 0.999. The R.S.D.s ($n = 6$) of REEs were calculated based on the measured values of an artificial

Table 3
Merits of the APAR on-line preconcentration ICP-MS for determination of REEs

Element	DL (ng L^{-1})	MDL (pg L^{-1})	DL/MDL	Enrichment factor	R.S.D. (%) ($n = 6$)	Calibration curve[a]		
						k	b	R^2
Y	0.47	6.49	72.4	398.4	4.3	24.78	21.31	0.9999
La	2.37	12.7	186.6	398.0	5.1	11.90	67.30	0.9997
Ce	1.19	6.93	171.7	396.8	4.8	17.11	120.02	0.9985
Pr	0.44	1.90	231.6	396.4	3.2	28.16	15.95	0.9999
Nd	2.22	10.8	205.5	394.0	3.4	10.58	25.48	0.9996
Sm	2.21	10.4	212.5	393.2	2.6	9.45	2.04	0.9999
Eu	0.69	1.72	401.2	391.3	3.1	18.42	−5.67	0.9999
Gd	1.47	6.08	241.8	388.1	2.0	8.76	6.29	0.9999
Tb	1.10	3.33	330.3	386.6	2.2	32.14	−3.74	0.9999
Dy	1.91	4.04	472.8	385.8	3.1	10.82	−3.54	0.9998
Ho	0.58	1.43	405.6	384.3	1.8	35.51	6.72	0.9999
Er	0.48	2.10	228.6	382.7	1.6	19.19	142.60	0.9999
Tm	0.93	2.96	314.2	381.6	1.2	34.66	−12.19	0.9998
Yb	2.20	4.84	454.5	378.9	2.1	7.59	−3.86	0.9999
Lu	0.08	1.44	55.6	377.8	1.1	33.11	6.33	0.9999

[a] Calibration curve ($y = kx + b$). k: slope (cps/ng L^{-1}); b: intercept (cps).

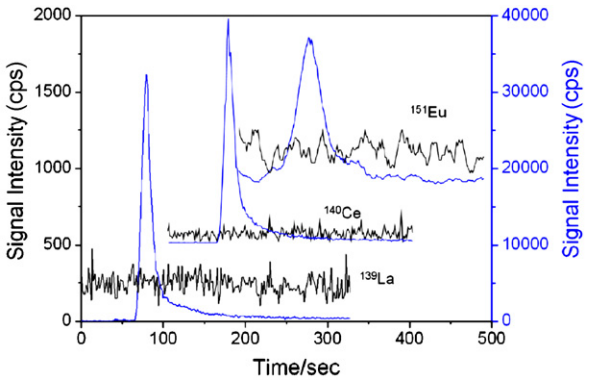

Fig. 6. Signals of ^{139}La, ^{140}Ce and ^{151}Eu before and after on-line preconcentration: direct determined by ICP-MS (—); determined by ICP-MS after the APAR on-line preconcentration (▬); sample volume, 60 mL seawater; sample flow rate, 2 mL min^{-1}; HNO_3 concentration, 0.1 mL min^{-1}; HNO_3 flow rate, 1 mL min^{-1}. (For interpretation of the references to color in this figure legend, the reader is referred to the web version of the article.)

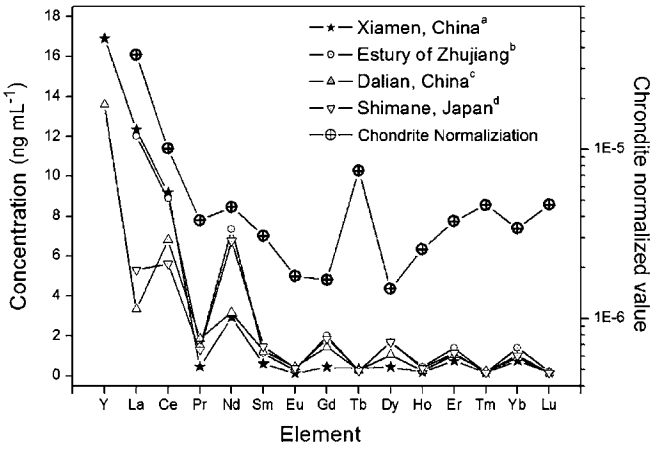

Fig. 7. Comparison of REEs concentration in seawater obtained by the present method with those reported in the literature and the chondrite normalization pattern for REEs in Xiamen seawater: (a) present method; (b) Ref. [22]; (c) Ref. [24]; (d) Ref. [14].

seawater containing 1 μg L^{-1} mixed REEs were smaller than 5%. The comparison of the signals of direct determination and those after on-line preconcentration of real seawater for La, Ce and Eu are also shown in Fig. 6. Obviously, the signals are remarkably enhanced.

3.4. Analytical application

The established integrated method was applied to determine soluble REEs in Xiamen coastal seawater. The sample volume of seawater is 60 mL. Since there was no available certified reference material on hand, trace amount of standard REE ions were spiked into the seawater sample before the preconcentration and determination. The results are given in Table 4. The recoveries of spikes are within 97.9–99.9%. A comparison between the data obtained by this method and those reported in the literature [14,22,24] is presented in Fig. 7, and reasonable agreement was achieved. The chondrite normalized distributions of REEs [38] in seawater shown in Fig. 7 also indicated the obvious positive anomaly of La, Ce and Tb. The positive anomaly of La, Ce and Tb may be caused by human activities in the southern and southeastern parts of China, especially the use of REE fertilizers in the field.

Table 4
Concentrations of REEs in seawater ($n = 6$)[a]

Element	Determined (ng L^{-1})	Added (ng L^{-1})	Totally founded (ng L^{-1})	Recovery (%)
Y	16.90	1.0	17.88	98.0
La	12.35	1.0	13.34	99.2
Ce	9.19	1.0	10.19	99.9
Pr	0.46	1.0	1.46	99.6
Nd	2.92	1.0	3.90	97.9
Sm	0.60	1.0	1.59	99.3
Eu	0.13	1.0	1.11	97.9
Gd	0.44	1.0	1.43	99.8
Tb	0.35	1.0	1.33	97.9
Dy	0.45	1.0	1.44	99.4
Ho	0.20	1.0	1.19	98.9
Er	0.75	1.0	1.74	98.8
Tm	0.15	1.0	1.14	99.3
Yb	0.75	1.0	1.73	98.7
Lu	0.16	1.0	1.16	99.3

[a] Collected at 24°25″E, 118°08″N, the south coast of Xiamen Island.

4. Conclusion

In this work, a novel chemical bonded APAR was synthesized. The APAR packed column was successfully used for on-line preconcentration of trace REEs and separation of the matrix and spectrally interfering metals in seawater prior to accurate ICP-MS determination. Chemically bonded alkyl phosphinic acid on styrene-divinylbenzene copolymer beads is effective and quite stable, and can be used for multiple repetition of preconcentration and elution. The developed method provides an attractive alternative for sensitive and accurate determination of trace REEs in seawater, and is expected to be useful for environment science and marine geochemistry studies in the future.

Acknowledgements

This work is financially supported by the National Natural Science Foundation of China (20535020, 20475046) and the National Basic Research Program of China (2003CD415001, 2003CCA00500). We thank Prof. Benli Huang for valuable discussion and Mr. Dong Yan for assistance with ICPMS determination. The loan of the Shimadzu HPLC 2010 was appreciated very much.

References

[1] G.X. Xu, Rare Earths, 2nd ed., Metallurgical Industry Press of China, Beijing, 1995, pp. 583–590 (in Chinese).
[2] A.V. Gorbunov, M.V. Frontasyeva, S.F. Gundorina, T.L. Onischenko, B.B. Maksjuta, C.S. Pal, Sci. Total Environ. 122 (1992) 337.
[3] E. Diatloff, F.W. Smith, C.J. Asher, J. Plant Nutr. 18 (1995) 1991.
[4] P. Möller, P. Dulski, J. Luck, Spectrochim. Acta 47 (1992) 1379.

[5] E.D. Goldberg, M. Koide, R.A. Schmitt, R.H. Smith, J. Geophys. Res. 68 (1963) 4209.
[6] A. Hirose, K. Kobori, D. Ishii, Anal. Chim. Acta 97 (1978) 303.
[7] H. Elderfield, M.J. Geraves, Nature 126 (1988) 124.
[8] M.J. Geraves, H. Elderfield, G.P. Klinkhammer, Anal. Chim. Acta 218 (1989) 265.
[9] G. Michard, F. Albarede, A. Michard, J.F. Minster, J.L. Carlou, N. Tan, Earth Planet Sci. Lett. 67 (1984) 297.
[10] A. Michard, F. Albarede, Chem. Geol. 55 (1986) 51.
[11] Z.B. Zhang, S.L. Liu, Marine Chemistry, vol. 1, Shandong Education Press, Jinan, 2004, pp. 59–60.
[12] E.H. Evans, J. Giglio, J. Anal. At. Spectrom. 8 (1993) 1.
[13] M.B. Shabani, T. Akagi, H. Shimizu, A. Masuda, Anal. Chem. 62 (1990) 2709.
[14] M.B. Shabani, A. Masuda, Anal. Chem. 63 (1991) 2099.
[15] D.J. Piepgras, S.B. Jacobsen, Geochim. Cosmsochim. Acta 56 (1992) 1851.
[16] T. Yabutani, S. Ji, F. Mouri, A. Itoh, K. Chiba, H. Haraguchi, Bull. Chem. Soc. Jpn. 73 (2000) 895.
[17] H. Haraguchi, A. Itoh, C. Kimata, H. Miwa, Analyst 123 (1998) 773.
[18] O. Vicente, A. Padro, L. Martinez, R. Olsina, E. Marchevsky, Spectrochim. Acta B 53 (1998) 1281.
[19] S.N. Willie, R.E. Sturgeon, Spectrochim. Acta B 56 (2001) 1707.
[20] S. Hirata, T. Kajiya, M. Aihara, K. Honda, O. Shikino, Talanta 58 (2002) 1185.
[21] Y.B. Zhu, A. Itoh, E. Fujimori, T. Umemura, H. Haraguchi, J. Alloys Compd. 408–412 (2006) 985.
[22] H.Z. Zhang, X. Yan, X.L. Wang, Z.T. Chen, L. Xu, Chin. Rock Miner. Anal. 16 (1997) 201 (in Chinese).
[23] J. Ai, S.H. Hu, Q. Shuai, Q.W. Yu, Chin. J. Anal. Chem. 30 (2002) 1226 (in Chinese).
[24] T.H. Zhang, X.Q. Shan, R.X. Liu, H.X. Tang, S.Z. Zhang, Anal. Chem. 70 (1998) 3964.
[25] B. Wen, X.Q. Shan, S.G. Xu, Analyst 124 (1999) 621.
[26] P. Liang, B. Hu, Z.C. Jiang, Y.C. Qin, T.Y. Peng, J. Anal. At. Spectrom. 16 (2001) 863.
[27] R.S. Praveen, S. Daniel, T. Prasada Rao, S. Sampath, K. Sreenivasa Rao, Talanta 70 (2006) 437.
[28] Y. Wang, J.H. Wang, Z.L. Fang, Anal. Chem. 77 (2005) 5396.
[29] F. Sánchez Rojas, C. Bosch Ojeda, J.M. Cano Pavón, Talanta 70 (2006) 979.
[30] Y. Wang, M.L. Chen, J.H. Wang, J. Anal. At. Spectrom. 21 (2006) 535.
[31] T. Sumida, T. Ikenoue, K. Hamada, A. Sabarudin, M. Oshima, S. Motomizu, Talanta 68 (2005) 388.
[32] M. Muzikar, C. Fontàs, M. Hidalgo, J. Havel, V. Salvadó, Talanta 70 (2006) 1081.
[33] Q.Q. Wang, B.L. Huang, K. Tsunoda, H. Akaiwa, Bull. Chem. Soc. Jpn. 72 (1999) 1693.
[34] Q.Q. Wang, K. Tsunoda, H. Akaiwa, Anal. Sci. 13 (Supplement) (1997) 153.
[35] Q.Q. Wang, K. Tsunoda, H. Akaiwa, M. Sugiya, T. Watanabe, Anal. Sci. 12 (1996) 931.
[36] Q.Q. Wang, K. Tsunoda, H. Akaiwa, Anal. Sci. 13 (1997) 27.
[37] K.W. Bruland, Trace elements in seawater, in: J.P. Riley, R. Chester (Eds.), Chemical Oceanography, Vol.8, Academic Press, London, 1983, p. 398.
[38] W.V. Boynton, Cosmochemistry of rare earth elements: meteorite studies, in: P. Henderson (Ed.), Rare Earth Element Geochemistry, Elsevier, Amsterdam, 1984, pp. 63–114.

Available online at www.sciencedirect.com
ScienceDirect
Talanta 72 (2007) 1329–1335
Talanta
www.elsevier.com/locate/talanta

Determination of flunitrazepam and 7-aminoflunitrazepam g in human urine by on-line solid phase extraction liquid chromatography–electrospray-tandem mass spectrometry

Ming-Ren Fuh *, Shi-Wei Lin, Li-Lung Chen, Tzuen-Yeuan Lin

Department of Chemistry, Soochow University, P.O. Box 86-72, Taipei, Taiwan

Received 24 October 2006; received in revised form 16 January 2007; accepted 16 January 2007
Available online 21 January 2007

Abstract

A method using an on-line solid phase extraction (SPE) and liquid chromatography with electrospray-tandem mass spectrometry (LC–ES-MS/MS) for the determination of flunitrazepam (FM2) and 7-aminoflunitrazepam (7-aminoFM2) in urine was developed. A mixed mode Oasis HLB SPE cartridge column was utilized for on-line extraction. A reversed phase C_{18} LC column was employed for LC separation and MS/MS was used for detection. Sample extraction, clean-up and elution were performed automatically and controlled by a six-port valve. Recoveries ranging from 94.8 to 101.3% were measured. For both 7-aminoFM2 and FM2, dual linear ranges were determined from 20 to 200 and 200–2000 ng/ml, respectively. The detection limit for each analyte based on a signal-to-noise ratio of 3 ranged from 1 to 3 ng/ml. The intra-day and inter-day precision showed coefficients of variance (CV) ranging from 4.6 to 8.5 and 2.6–9.2%, respectively. The applicability of this newly developed method was examined by analyzing several urine samples.

Keywords: Flunitrazepam; 7-Aminoflunitrazepam; On-line solid phase extraction; Liquid chromatography–electrospray-tandem mass spectrometry

1. Introduction

Flunitrazepam (FM2) is a fluorinated derivative of 1,4-benzodiazepine and used as a hypnotic and anesthetic induction agent. FM2 is a potent drug with detection difficulty owing to its therapeutically effectiveness at low dose. 7-Aminoflunitrazepam (7-aminoFM2) is the major urinary metabolite of FM2. The structures of 7-aminoFM2 and FM2 are shown in Fig. 1. Due to low dosage and rigorous biotransformation, the concentrations of FM2 and its metabolites found in urine are very low. It has been reported that 7-aminoFM2 concentration reached 50–200 μg/L within 6–24 h after a single 2 mg oral dose [1–3]. In the past few years, the number of illegal user of FM2 has increased dramatically in Taiwan. Urine sample analysis is most commonly applied to drug abused inspection. Therefore, a sensitive and accurate analytical method to measure FM2 and its major metabolite, 7-aminoFM2, in urine is needed.

Various analytical methods for the measurement of FM2 and 7-aminoFM2 have been reported, including immunoassay, gas chromatography-mass spectrometry (GC–MS), high performance liquid chromatography (HPLC) with UV, fluorescence and electrochemical detection [4–10]. The lack of specificity and sensitivity of immunoassay as well as LC-UV methods limit their application. GC–MS is an excellent method that provides unambiguous identification of compounds with good sensitivity; however, time-consuming derivatization prior to analysis is required.

LC–electrospray (ES)-MS has emerged as a sensitive and selective analytical method in drug analysis [11–16]. Tandem-MS further improves the specificity and sensitivity of detection. For the analysis of biological samples by LC–ES-MS, severe matrix effect and ion suppression effect are often observed [17–20]. Thus, an effective sample pre-treatment procedure which removes interfering endogenous components and pre-concentrates the analytical compounds is often needed to improve sensitivity. Some off-line sample preparation procedures, such as, liquid–liquid extraction, solid phase micro extraction, and solid phase extraction (SPE), have been

* Corresponding author. Tel.: +886 2 28819471x6821; fax: +886 2 28812685.
E-mail address: msfuh@mail.scu.edu.tw (M.-R. Fuh).

0039-9140/$ – see front matter © 2007 Elsevier B.V. All rights reserved.
doi:10.1016/j.talanta.2007.01.040

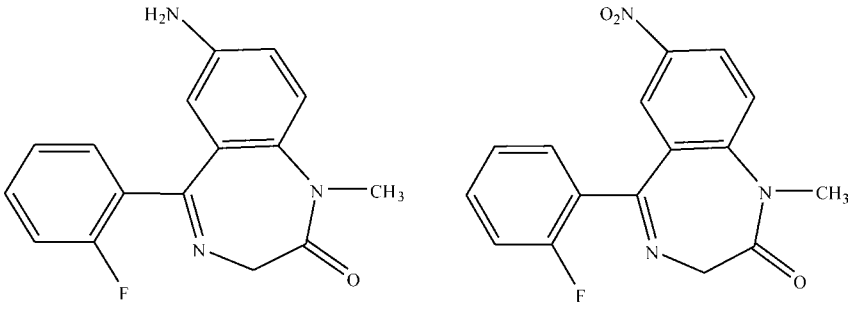

7-aminoFM2 FM2

Fig. 1. Chemical structure of analytical compound.

employed for the measurement of these compounds [21–25]. For the analysis of FM2 and 7-aminoFM2 in biological fluids, liquid–liquid extraction and solid phase extraction are the most commonly used sample pre-treatment methods. They provide excellent sensitivity; however, both techniques require laborious clean-up, evaporation and concentration procedures. Moreover, these methods often require additional instrumentation to be automated.

This paper describes the development and validation of an automated on-line SPE LC–ES-tandem MS method for the analysis of FM2 and 7-aminoFM2 for drug abused urine sample measurement. Diluted urine sample was injected into an on-line SPE column directly for on-line extraction and LC–ES-MS/MS measurement. Sample extraction, clean-up and elution were performed automatically and controlled by a six-port valve. This newly developed method is simple, selective, sensitive and reproducible and is validated for the analysis of urine samples from FM2 drug abused suspects.

2. Experimental

2.1. Chemicals

Purified water was from a Milli-Q system from Millipore Corp. (Bedford, MA, USA). HPLC grade acetonitrile and methanol (Milinckrodt Baker, Paris, KY, USA), were used. Acetic acid was purchased from Riedel-de Haen AG, Germany. Ammonium hydroxide and ethyl acetate were obtained form J.T. Baker (Phillipsburg, NJ, USA). FM2, 7-aminoFM2, and d_4-*N*-desmethylflunitrazepam were from Cerilliant Corp. (Austin, TX, USA).

2.2. Preparation of standard solutions

Stock solutions (100 μg/ml) of FM2, 7-aminoFM2 and internal standard (d_4-*N*-desmethylflunitrazepam) were prepared in methanol. All solutions were kept in a refrigerator (4 °C) when not in use. Spiked urine standard solutions were prepared by spiking appropriate amounts of each analytical component and internal standard (75 ng/ml) into 2 ml of drug-free urine. The standard curve range was 20–2000 ng/ml for both analytes. Drug-free urines collected from five healthy volunteers were used for method development and preparation of calibrators.

2.3. Equipment

An HP1100 LC system (Hewlett-Packard Co., Palo Alto, CA, USA) consisting of a quaternary pump, an on-line degaser, an autosampler, and a six-port autoswitch valve was used. An Oasis HLB extraction column (2.1 mm × 20 mm, 25 μm, Waters Corp., Milford, MA, USA) was utilized for on-line extraction. A symmetry shield RP18 column (2.1 mm × 30 mm, 3.5 μm, Waters Corp.) was used for LC separation.

Mass spectrometric detection was performed using an Agilent series LC/MSD trap SL instrument equipped with an electrospray ionization source that was operated in the positive mode with the spray voltage set at −3.5 kV. The capillary exit voltage was set at 130 V. Agilent 1100 series LC/MSD Trap software (version 4.0) was utilized for system control, data acquisition and data analysis. Heated N_2 gas (350 °C, 10 l/min) was used to evaporate solvent from the electrospray chamber, and compressed N_2 gas (50 psi) was used for nebulization. A second autoswitch valve was utilized to divert eluent from LC column to ES-tandem MS or waste. Multiple reaction monitoring (MRM) was employed for quantitative measurement. The isolation width for precursor ions was 2. The settings for the MRM were: FM2, *m/z* 314 → 300, 286 and 268; 7-aminoFM2, *m/z* 284 → 264, 163 and 135; d_4-*N*-desmethylFM2, *m/z* 304 → 290 and 258. MS/MS data acquisition was performed under the following conditions: normal scan speed, *m/z* range 80–400, ion charge control (ICC) target 30,000 and maximum accumulation time 300 ms.

2.4. On-line sample preparation and LC separation

Each urine sample (2 ml) was diluted with 2 ml of acetonitrile. The mixture was vortexed for 3 min and centrifuged for 5 min at 1500 × *g*. A 10 μl of aliquot of supernatant fluid was used for analysis. Prior to extraction, the HLB extraction column was equilibrated with 1.5% (v/v) of ammonium hydroxide at a flow rate of 1 ml/min for 2 min, with the system in the "extraction" configuration shown in Fig. 2a. Table 1 is the summary of the time program for extraction, washing and elution of the on-line SPE LC system. Urine samples were injected by autosampler, and carried onto the HLB extraction column by 1.5% ammonium hydroxide solution at a flow rate of 1 ml/min. The analytes of interest were retained on the SPE column while the urine

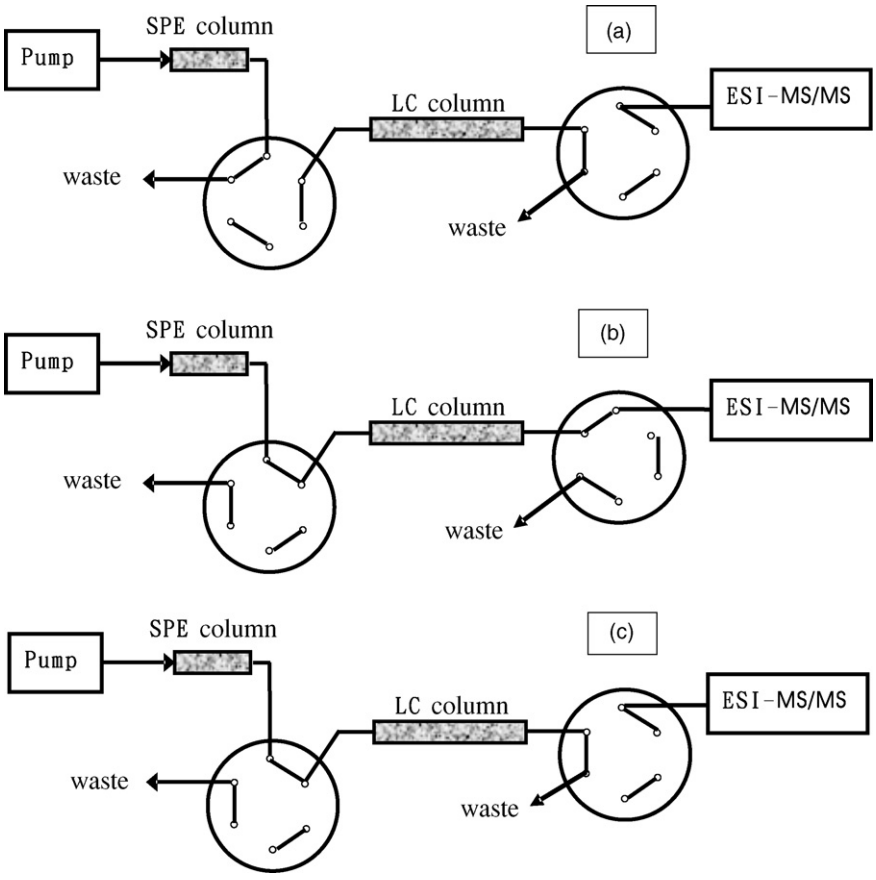

Fig. 2. Configuration of on-line SPE LC–ES-MS/MS: (a) extraction, (b) analysis, and (c) cleaning.

matrix was washed to waste. The extracted components were first washed by a 1.5% ammonium hydroxide/methanol (75/25, v/v) mixture and then by acetonitrile/water (5/95, v/v) mixture. At 6.1 min after sample injection, a gradient elution (at the flow rate of 0.4 ml/min) was employed to separate the analytical compounds. Simultaneously, the system was turned to the "analysis" configuration (shown in Fig. 2b), and the analytical compounds were delivered to the LC/ES/tandem MS instrument for measurement. After the gradient elution (at 13.1 min), both SPE and LC columns were further cleaned with acetonitrile/water (95/5, v/v) mixture while the washing solution was delivered to waste instead of ES-tandem MS (shown in Fig. 2c). After the cleaning procedure, the SPE and LC column was equilibrated with the initial gradient elution solvent for 2 min. At 20.1 min after sample injection, the switch valve was turned back to extraction configuration. The SPE column was re-equilibrated with 1.5% ammonium hydroxide for 2 min and was then ready for next sample injection.

Table 1
Time program of extraction and LC separation (see experimental for detail)

Time (min)	A (%)	B (%)	C (%)	D (%)	Flow rate (ml/min)
0.0	100	0	0	0	1.0
1.0	100	0	0	0	1.0
1.1	0	100	0	0	1.0
4.0	0	100	0	0	1.0
4.1	0	0	100	0	1.0
6.0	0	0	100	0	1.0
6.1	0	0	65	35	0.4
8.5	0	0	65	35	0.4
13.0	0	0	0	100	0.4
13.1	0	0	0	100	0.6
18.0	0	0	0	100	0.6
18.1	0	0	65	35	0.6
20.0	0	0	65	35	0.6
20.1	100	0	0	0	1.0
22.0	100	0	0	0	1.0

A, 1.5% NH_4OH; B, 1.5% NH_4OH/methanol (75/25, v/v); C, acetonitrile/H_2O (5/95, v/v); D, acetonitrile/H_2O (95/5, v/v).

2.5. Investigation of ion suppression effect

A post-column infusion system used in this study is a modification of previously reported configuration [26]. Ion suppression effect of this newly developed method was evaluated by injecting blank human urine samples from five volunteers into the on-line SPE LC–ES-MS/MS while a mixture of FM2 and 7-aminnoFM2 (100 ng/ml each) in acetonitrile/water (50/50, v/v) was continuously infused in parallel at 20 μl/min through a PEEK tee-junction (Upchurch Scientific, Oak Harbor, WA, USA) by a syringe pump (Harvard Apparatus, South Natick, MA, USA).

3. Results and discussion

3.1. ES-MS and ES-MS/MS analysis

The ES with positive mode was used for the detection. The concentration of 100 ng/ml of each analytical compound was used in this study with flow injection. In ES-MS measurement, proton adduct ion $[M+H]^+$ was obtained as base ion for analytes and internal standard. In ES-MS/MS determination, $[M+H]^+$ ion of each component was used as the precursor ion. The tandem MS fragmentations of the analytical compounds were complicated and similar to the results from atmospheric pressure chemical ionization-tandem MS; however, there was no assignment of these ions reported [21]. The tentative assignments of characteristic ESI-MS/MS fragment ions are summarized in Table 2.

3.2. Optimization of on-line SPE LC separation

A mixed mode SPE column packed porous polymer with both hydrophilic and lipophilic functions was utilized as a trapping column. The loading solution, washing solution and elution solution for on-line SPE LC separation were evaluated. For loading solution, an alkaline solution was used to minimize the protonation of amino group in the analytical molecule and maintain the analyte as neutral molecule that was readily retained in the SPE column.

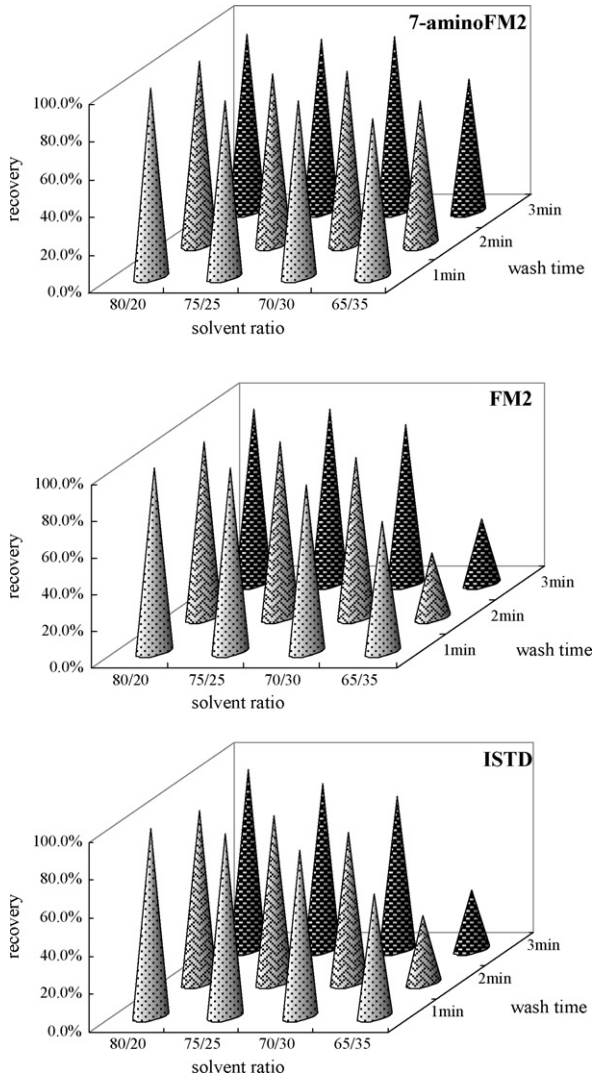

Fig. 3. Effect of solvent composition and washing time on the recoveries of analytical component and internal standard.

Table 2
ES-MS[a] results for analytes and internal standards

Fragmentation energy (V)		MS[a] ion[a,b]
7-AminoFM2	1.30	$[M+H]^+$ (284), **$[M+H–HF]^+$ (264)**, $[M+H–CO]^+$ (256), $[M+H–CO–HF]^+$ (236), $[M+H–CO–NCH_3]^+$ (227), **$[M+H–C_6H_4F–CN]^+$ (163)**, $[M+H–C_6H_4F–CN–CH_3]^+$ (148), **$[H_3NC_6H_4NCO]^+$ (135)**
FM2	1.50	$[M+H]^+$ (314), **$[M+H–CH_2]^+$ (300)**, **$[M+H–CO]^+$ (286)**, **$[M+H–NO_2]^+$ (268)**, $[M+H–NO_2–CO]^+$ (240)
d_4-DesmethylFM2	1.35	$[M+H]^+$ (304), **$[M+H–CH_2]^+$ (290)**, $[M+H–CO]^+$ (276), **$[M+H–NO_2]^+$ (258)**

[a] *m/z* of each ion in parenthesis.
[b] Quantitative ions are in bold.

The purpose of washing solution is to remove endogenous components in urine and minimize the interference of measurement. Strong washing solution can effectively remove interfering components; however, it might also elute the analytical compounds. The effectiveness of various compositions of 1.5% ammonium hydroxide/methanol (80:20, 75:25, 70:30 and 65:35) as washing solution was examined and the recoveries of analytes using different washing solution were evaluated. In this study, the standard solution (100 ng/ml) was injected into SPE column, washed with various washing solution and eluted with acetonitrile/water (40/60, v/v) mixture. The recovery was determined by the ratio of response for standard solution with washing step to that without washing step. The results shown in Fig. 3 indicated that the recovery of each analytical compound decreased as the organic content of washing solvent increased. Moreover, the recovery of each analyte reduced as the washing

time extended. We decided to use 1.5% ammonium hydroxide/methanol (75:25) mixture as the washing solvent since only small amount of each analytical compound (less than 7%) was lost even after 3 min of washing.

Prior to elution, a second washing solution (acetonitrile/water, 5/95) was employed. This step was to remove the residual alkaline washing solvent used in the last step. Without this second washing procedure, the alkaline mixture would enter LC separation column. As a result, the LC resolution lessened and peak broadening was observed.

A gradient elution was developed to effectively elute the analytical components and ISTD. In addition, we also examined the effect of acetic acid (0.01–0.1%) on LC separation and MS detection. Intuitively, the addition of acid in mobile phase will promote the protonation of analytical molecules and enhance the sensitivity. In this study, the addition of acetic acid in mobile phase exhibited little effect on LC separation; however, the addition of acid markedly reduced the sensitivity of ESI-MS/MS detection. This might attribute to the competition of acetic acid molecule for the positive charge on ESI droplet; thus, the reduction of the MS sensitivity was determined. Therefore, no acid was added in LC mobile phase. Fig. 4 shows the typical chromatograms for a spiked urine sample. The retention time of 7-aminoFM2, FM2 and internal standard was 9.9, 11.8 and 10.7 min, respectively. Small amount of endogenous components from urine would remain in the LC column after gradient elution; therefore, additional washing procedure with acetonitrile/water solution (95/5) was employed.

3.3. Evaluation of ion suppression effect

For ion suppression effect evaluation, five volunteer's blank urine samples and acetonitrile/water (50/50, v/v) mixture were injected. Comparing to the responses of analytes in acetonitrile/water, there was less than 6% decreased in either 7-aminoFM2 or FM2 response observed for all five human blank urine samples. The results indicated that the on-line SPE clean-up procedure combined with LC separation effectively remove and separate the potential interfering endogenous components in urine.

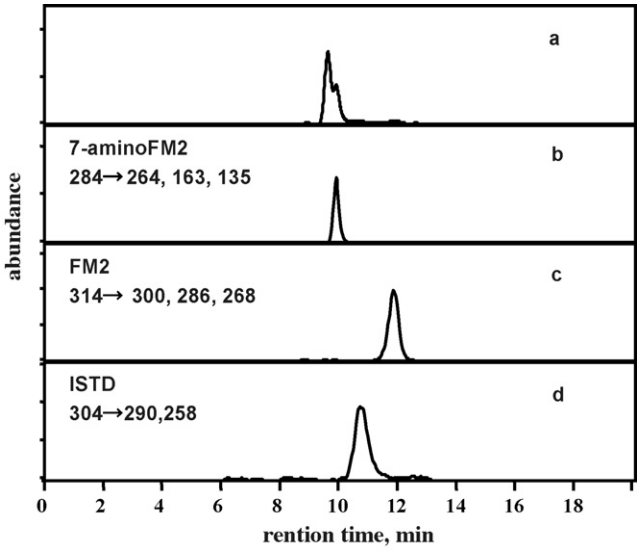

Fig. 4. LC–ES-MS/MS chromatograms of a spiked urine sample (200 ng/ml for each analyte, 75ng/ml for ISTD). (a) Total ion chromatogram; (b–d) extracted ion chromatogram.

Table 3
Recovery[a] of on-line SPE analysis of spiked urine sample

	60 ng/ml	100 ng/ml	400 ng/ml	1000 ng/ml
7-AminoFM2	94.8 ± 5.3	101.1 ± 4.2	99.7 ± 4.4	97.8 ± 3.1
FM2	97.5 ± 4.5	98.1 ± 3.7	98.7 ± 2.8	101.3 ± 3.5

[a] Recovery, %. Average ± standard deviation ($n = 5$).

3.4. Extraction recovery

In order to evaluate the on-line SPE extraction recoveries of this newly developed method, spiked urine samples and standard in acetonitrile/water (50/50, v/v) were analyzed. The recovery was determined by the peak area of a spiked urine sample as a fraction of a corresponding standard in acetonitrile/water solution. The results of this investigation are summarized in Table 3. Good recoveries ranging from 94.8 to 101.3% were obtained. This is another indication that there was no ion suppression effect detected in this newly developed method. In addition, the chromatographic performance and MS/MS spectral quality of urine samples were not less than those of standard in methanol/water. The results indicated that this assay was suitable for the analysis of 7-aminoFM2 and FM2 in urine samples.

3.5. Quantitative analysis and detection limit

A series of spiked urine solutions were utilized to examine the linearity of this newly developed method. The calibration curve for each analyte was constructed using least squares regression of quantities of each analyte versus peak area ratio of analyte peak area to that of its internal standard. The evaluation of linearity is summarized in Table 4. For both 7-aminoFM2 and FM2, dual linear ranges were determined from 20 to 200 and 200–2000 ng/ml, respectively.

The detection limit for each analyte based on a signal-to-noise ratio of 3 was ranged from 1 to 3 ng/ml. Nanogram-per-milliliter detection limits for urinary FM2 and 7-aminoFM2 measurement by GC–MS or LC–MS assays have been reported previously [2,6,21–23]. These methods often required extensive sample preparation procedures and were difficult to automate. The sensitivity of this present method is superior or equal to those previously reported results. Moreover, this newly developed method required minimum sample preparation and was fully automated.

Precision and accuracy were examined by analyzing urine samples with known concentrations of analytes and the results are summarized in Table 5. The intra-day and inter-day precision showed coefficients of variance (CV) ranging from 4.6 to 8.5 and 2.6–9.2%, respectively. The accuracy of the method was expressed by [mean measured concentration/spiked concentration] × 100%; accuracies ranging from 96.0 to 102.8% and 95.8–106.0% was determined for 7-aminoFM2 and FM2, respectively.

Table 4
Retention time, linearity and detection limit

	Calibration curve[a,b]	Range (ng/ml)	r^2	D.L.[c] (ng/ml)
7-AminoFM2	$Y = 0.745X - 2.368$	20–200	0.997	1
	$Y = 0.756X - 2.879$	200–2000	0.996	
FM2	$Y = 0.298X - 2.133$	20–200	0.997	3
	$Y = 0.246X - 5.568$	200–2000	0.998	

[a] Y, peak area ratio of standard and internal standard; X, concentration, ng/ml.
[b] Concentrations of standard: 20–200: 20, 60, 100, 150, 200 ng/ml; 200–2000: 200, 500,1500, 2000 ng/ml.
[c] D.L., detection limit.

Table 5
Precision and accuracy

	Intra-day ($n = 3$)				Inter-day ($n = 3$)			
	20 ng/ml	100 ng/ml	500 ng/ml	1500 ng/ml	20 ng/ml	100 ng/ml	500 ng/ml	1500 ng/ml
7-AminoFM2								
Mean	19.9	101.1	513.0	1466.8	19.2	98.6	514.2	1491.5
Accuracy (%)	99.5	101.1	102.6	97.8	96.0	98.6	102.8	99.4
CV	6.9	6.3	5.7	4.6	9.2	4.4	3.3	2.6
FM2								
Mean	21.2	100.5	478.9	1470.8	21.0	98.1	498.5	1494.5
Accuracy (%)	106.0	100.5	95.8	98.1	105.0	98.1	99.7	99.6
CV	6.4	7.1	8.5	4.8	5.4	5.8	4.3	3.1

Table 6
7-AminoFM2 analysis results of urine analysis

Sample	GC–MS[a] (ng/ml)	On-line SPE LC/MS/MS[a] (ng/ml)	RF[b] (%)
A	1228.2	1115.3	−9.2
B	284.4	277.8	−2.3
C	85.1	82.2	−3.4
D[c]	8642.4	9115.8	13.3
E	645.6	689.3	6.8
F	452.5	422.1	−6.7
G	176.3	181.6	3.0

[a] $n = 3$.
[b] RF, relative difference.
[c] Sample was diluted 10-fold prior to on-line SPE LC/MS/MS analysis.

3.6. Examination of urine samples of illicit drug users

This newly developed analytical assay was applied to urine samples collected from four drug addicts, and the results are summarized in Table 6. These samples were analyzed by a GC–MS method at Taipei Veterans General Hospital. The concentrations of 7-aminoFM2 for these samples measured by this method ranged from 9115.8 to 82.2 ng/ml. Relative differences of the results from GC–MS and on-line SPE LC–tandem MS method ranged from −9.2 to 13.3%. No FM2 was detected in these urine samples. It has been reported that FM2 is seldom found in urine sample [27,28].

4. Summary

A fully automated method was developed for the simultaneous determination of FM2 and 7-aminoFM2 in urine. Minimum sample preparation was needed. This newly developed method consisted of an on-line SPE column for sample extraction and LC–ES-MS/MS for identification and quantization. A switch valve and a time program were utilized to control the extraction, elution and analysis sequences. Each analysis was accomplished in less than 25 min. The detection limit of this assay was comparable with previously reported methods. Good recoveries ranging from 94.8 to 101.3% were determined. This method has been successfully applied to analyze several urine samples. Good agreement between the results from this method and a standard GC–MS method was obtained.

Acknowledgements

This work was financially supported by National Science Council of Taiwan. The authors would like to thank Ms. Wei-Lan Chu of Taipei Veterans General Hospital and Dr. Dong-Liang Lin and Ms Rae-Ming Yin of Institute of Forensic Medicine, Ministry of Justice of Taiwan for providing much assistance in this study.

References

[1] W. Wickstrom, R. Amrein, P. Haefelfinger, D. Hartmann, Eur. J. Clin. Pharm. 17 (1980) 189.
[2] M.A. ElShohy, S. Feng, S.J. Salamone, R. Wu, J. Anal. Toxicol. 21 (1997) 335.
[3] S.J. Salamone, S. Honasoge, J. Anal. Toxicol. 21 (1997) 341.
[4] W. Huang, D.E. Moody, J. Anal. Toxicol. 19 (1995) 333.
[5] K. Walshe, A.M. Barrett, P.V. Kavanagh, S.M. McNamara, C. Moran, A.G. Shattock, J. Anal. Toxicol. 24 (2000) 296.
[6] H. Synder, K.S. Schwenzer, R. Pearlman, A.J. McNally, M. Tsilimidos, S.J. Salamone, R. Brenneisen, M.A. ElSohly, S. Feng, J. Anal. Toxicol. 25 (2001) 699.

[7] F. Berthault, P. KIntz, P. Mangin, J. Chromatogr. B 685 (1996) 383.
[8] W. He, N. Parissis, J. Pharm. Biomed. Anal. 16 (1997) 707.
[9] I. Deinl, G. Mahr, L. Meyer, J. Anal. Toxicol. 22 (1998) 197.
[10] H. Morland, A. Smith-Kielland, Clin. Chem. 43 (1997) 1245.
[11] M.R. Fuh, C.H. Huang, S.L. Ling, W.H.T. Pan, J. Chromatogr. A 1031 (2004) 197.
[12] T.Y. Wu, M.R. Fuh, Rapid. Commun. Mass Spectrom. 19 (2005) 775.
[13] S.A. Chan, S.W. Lin, K.J. Yu, T.Y. Liu, M.R. Fuh, Talanta 69 (2006) 952.
[14] K. Stoob, H.P. Singer, C.W. Goetz, M. Ruff, S.R. Mueller, J. Chromatogr. A 1097 (2005) 138.
[15] A. Gentili, D. Perret, S. Marchese, Trends Anal. Chem. 24 (2005) 704.
[16] C.C. Chou, M.R. Lee, F.C. Cheng, D.Y. Yang, J. Chromatogr. A 1097 (2005) 74.
[17] B.K. Matuszewski, M.L. Constanzer, C.M. Chavez-Eng, Anal. Chem. 75 (2003) 3019.
[18] P.R. Tiller, L.A. Romanyshyn, Rapid. Commun. Mass Spectrom. 16 (2002) 92.
[19] M.J. Avery, Rapid. Commun. Mass Spectrom. 17 (2003) 197.
[20] H. Mei, Y. Hsieh, C. Nardo, X. Xym, S. Wang, K. Ng, W.A. Korfmacher, Rapid. Commun. Mass Spectrom. 17 (2003) 97.
[21] M. Kollroser, C. Schober, J. Pharm. Biomed. Anal. 28 (2002) 1173.
[22] N. Jourdil, J. Bessard, F. Vincent, H. Eysseric, G. Bessard, J. Chromatogr. B 788 (2003) 207.
[23] H. Yuan, Z. Mester, H. Lord, J. Pawliszyn, J. Anal. Toxicol. 24 (2000) 718.
[24] O. Quintela, F.-L. Sauvage, F. Charvier, J.-M. Gaulier, G. Lachatre, P. Marquet, Clin. Chem. 52 (2006) 1346.
[25] B.E. Smink, J.E. Brandsma, A. Dikhuizen, K.J. Lusthof, J.J. de Gier, A.C.G. Egberts, D.R.A. Uges, J. Chromatogr. B 811 (2004) 13.
[26] R. King, R. Bonfiglio, C. Fernandez-Metzler, C. Miller-Stein, T. Olah, J. Am. Soc. Mass Spectrom. 11 (2000) 942.
[27] I.M. McIntyre, M.L. Syrjanen, K. Crump, S. Horomidis, A.W. Peace, O.H. Drummer, J. Anal. Toxicol. 17 (1993) 202.
[28] O.H. Drummer, M.L. Syrjanen, S.M. Cordner, Am. J. For. Med. Pathol. 14 (1993) 238.

Available online at www.sciencedirect.com
ScienceDirect
Talanta 72 (2007) 1453–1457
Talanta
www.elsevier.com/locate/talanta

A selective artemisinin-sensor using metalloporphyrin as a recognition element entrapped in the Au-nanoparticles-chitosan modified electrodes

Fu-Chun Gong *, Zi-Dan Xiao, Zhong Cao, Dao-Xin Wu

College of Chemistry and Environmental Engineering, Changsha University, of Science and Technology, Changsha 410076, PR China

Received 3 December 2006; received in revised form 24 January 2007; accepted 24 January 2007
Available online 6 February 2007

Abstract

An amperometric artemisinin (ARN) sensor based on the supramolecular recognition of glycosylated metalloporphyrin, which is included in the Au-nanoparticles-chitosan film coated on the glass carbon electrodes, was developed. For the improvement of the selectivity of artemisinin detection, 5,10,15,20-tetrakis[2-(2,3,4,6-tetraacetyl-β-D-glucopyranosyl)-1-O-phenyl]porphyrin (T(*o*-glu)PPH) metal complex [FeT(*o*-glu)PPCl] was synthesized and employed as a ARN-sensitive and -selective material in the amperometric sensors. The proposed [FeT(*o*-glu)PPCl]/Au-nanoparticles modified electrodes showed excellent selectivity and sensitivity toward ARN with respect to a number of interferents and exhibited stable current response, which can be attributed to the coordination of ARN with the [FeT(*o*-glu)PPCl] in the electrodes. The calibration graph obtained with the proposed sensor was linear over the range of 1.8×10^{-7}–1.7×10^{-9} mol l^{-1}, with a detection limit of 1.7×10^{-9} mol l^{-1} for ARN. Significant advantages of the proposed procedure over the conventional reductive electrochemical methods are the selective detection and the relatively low applied potential requirement of the ARN-sensor. The prepared sensor is applied for the determination of ARN in plant samples and the results agreed with the values obtained by the pharmacopoeia method.

Keywords: Artemisinin sensor; Supramolecular recognition; Metalloporphyrin; Au-nanoparticles-chitosan

1. Introduction

The incidence of malaria is dramatically increasing since many *Plasmodium falciparum* strains are now resistant to widely used drugs like chloroquine. Artemisinin (qinghaosu, ARN), an unusual sesquiterpene-lactyone endoperoxide from *Artemisia annua* L., is an effective antimalarial drug, particularly against chloroquine-resistant *P. falciparum* infection and cerebral malarial [1,2]. Since artemisinin (Fig. 1) lack a chromophore for direct UV or fluorescence detection, it was not possible to analyze it in biosamples without chemical derivatization. Fortunately, an endoperoxide moiety in ARN and its derivatives allows the electrochemical reduction of the peroxide function. Reductive electrochemical detection is frequently used for ARN and its derivatives detection. In contrast to derivatization-based UV absorbance detection, the use of electrochemical detection allows determinations of ARN and its derivatives without a preceding derivatization. Acton et al. [3] reported a reductive electrochemical HPLC assay with a gold/mercury electrode for ARN detection in *A. annua*. The method was found sensitive, specific and rapid but a gold/mercury electrode requires frequent cleaning, polishing and preparation. An alternative method using a glassy carbon electrode and HPLC with reductive EC detection was developed for the assay of artesunic acid and dihydroartemisinin in blood [4]. The method was validated and applied to pharmacokinetic studies with rabbits after intravenous administration of artesunic acid. However, there are two drawbacks of the insufficient selectivity and the relatively high operating potential requirement in the conventional procedures mentioned for ARN and its derivatives determination.

Recently, synthetic metalloporphyrins have attracted attention in relation to the chemical and biological recognition [5–7]. As far as the application in electrochemical approaches is concerned, porphyrins have been used as the ionophores in potentiometric sensors. Some of them were employed as electroactive components in the membrane of ion-selective electrodes [8]. The methods using [CoT(II)PPCl] and [MnT(III)PPCl] as recognition element for SCN^- and salicy-

* Corresponding author. Fax: +86 731 2618234.
E-mail address: gfc139@yahoo.com.cn (F.-C. Gong).

0039-9140/$ – see front matter © 2007 Elsevier B.V. All rights reserved.
doi:10.1016/j.talanta.2007.01.056

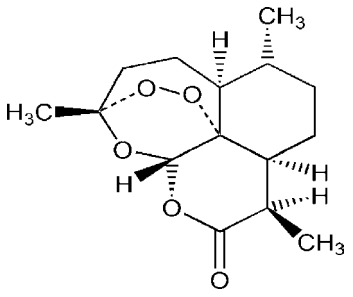

Fig. 1. Structure of artemisinin.

late determination with a potentiometric finish were respectively reported [9,10]. Some efforts have also been focused on the current utility of such compounds as the active material in the development of amperometric electrodes coated with porphyrin. Frey et al. [11] and Duony et al. [12] used TPP-coated glassy carbon electrode for the detection of heavy metal ion (Cu^{2+}) and electropolymerized protoporphyrin based graphite carbon electrode for dopamine determination. To the best of our knowledge, no efforts have been made on the application of the drug electrode incorporated with metalloporphyrin in chitosan modified glass carbon electrode for the detection of endoperoxide bridge analogous species. In a previous report, it was demonstrated that the porphyrin Fe(III) moiety in hemoglobin and synthetic porphyrin Fe(III) display interaction with artemisinin [13–15]. Inspired by the success of the above outlined molecular recognition research, the present authors tried to develop a drug sensor for ARN assay with an amperometric finish. In the present work, we make the first attempt to design and use a Fe(III) coordinating glycosylated porphyrin ([FeT(*o*-glu)PPCl])-based amperometric sensor for selective ARN detection. The ARN sensor has been fabricated by including an active material [FeT(*o*-glu)PPCl] in Au-nanoparticles/chitosan matrices coated on the glass carbon electrodes, which act as working electrodes. The active material [FeT(*o*-glu)PPCl] on electrodes can coordinate with the analyte ARN in samples and the [FeT(*o*-glu)PPCl]/Au-nanoparticles-modified electrodes showed excellent selectivity toward ARN with respect to a number of interferents and exhibited stable response. The proposed amperometric sensor detection for ARN assay offers the advantages derived from the selectivity and sensitivity owing to incorporation of metalloporphyrin and Au-nanoparticles in the chitosan film on the glassy carbon electrodes. A relatively low applied potential for ARN reductive electrochemical detection has also been realized.

2. Experimental

2.1. Materials and reagents

Glycosylated porphyrin (T(*o*-glu)PPH_2, Fig. 2)) and its metal complexes were synthesized by Adler's method [16]. Chitosan and $HAuCl_4$ were purchased from Shanghai Chemicals (Shanghai, China) and used as received from the supplier. Artemisinin and artemisinic acid were provided by Swellxin Science & Technology Lit. Co. (Guangzhou, China). All other reagents were analytical grade and used as received from supplier.

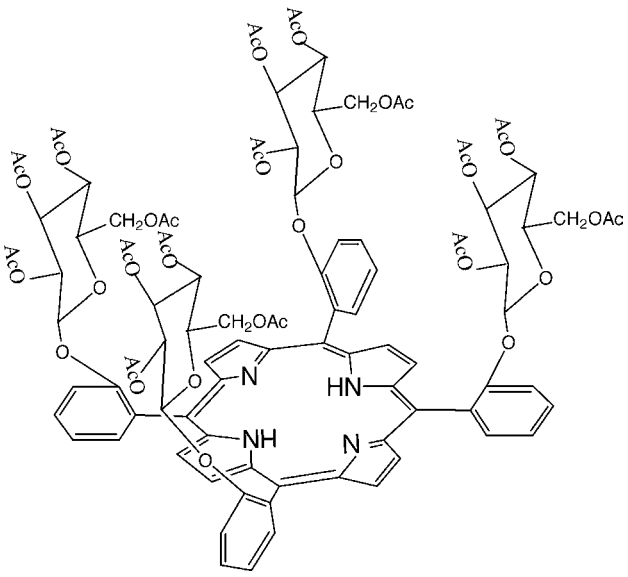

Fig. 2. Structure of glycosylated porphyrin.

2.2. Apparatus

Electrochemical experiments were carried out using a Perkin-Elmer Electrochemical Analyzer System connected with an Echem M 283 data storage system. Cyclic voltammetric (CV) and amperometric measurements were performed with a conventional three-electrode system consisting of SCE as a reference electrode, a Pt counter electrode (2.7 cm^2) and a modified glassy carbon electrode as a working electrode mentioned later. All experimental solutions were thoroughly deoxygenated by bubbling nitrogen through the solution for at least 10 min. Unless otherwise indicated, voltammetry and amperometry were performed at 80 mV/s in Britton-Ribinson (BR) buffer solutions (0.01 mol) containing 20% ethanol, pH 6.8 at 25 °C.

2.3. Preparation of [FeT(o-glu)PPCl]/Au-nanoparticles electrodes

The Au-nanoparticles were prepared according to the method reported elsewhere [17] with slight modifications. All glasswares used in the preparation procedure were thoroughly cleaned in the aqua regia (3 parts of HCl plus 1 part HNO_3) and rinsed with doubly distilled water. One hundred millilitre of 0.01% $HAuCl_4$ solution in a 250 ml beaker was brought to boiling with vigorous stirring, then 2.5 ml of 1% sodium citrate solution was quickly added to give a color change from blue to red-violet. Boiling continued for additional 10 min, the heater was then removed and the resulting mixture was stirred continuously for another 10 min. The cooled Au colloid solution was stored at 4 °C in a dark bottle.

A mixture was prepared by adding a 1 ml of Au colloid solution aforementioned and a 1 ml of [FeT(*o*-glu)PPCl]-containing acetone solution (0.1%, w/v) into a 50 ml of 2% acetic acid solution containing 2% chitosan and mixing them thoroughly. Fifty microlitre of the resulting mixture solution was coated on the cleaned glassy carbon electrodes and left to dry at

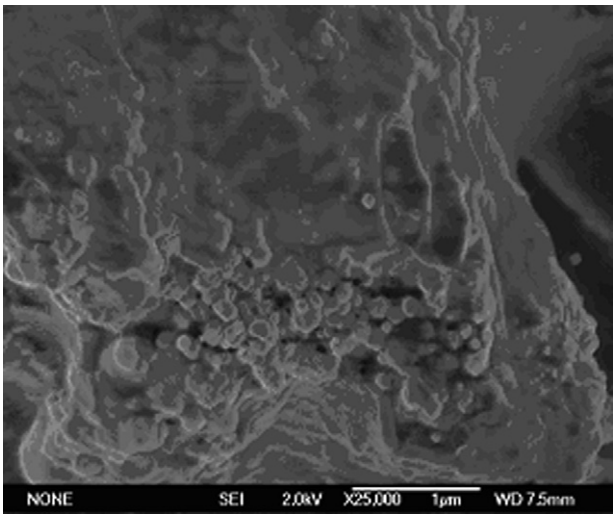

Fig. 3. Scaning electron micrograph of chitosan flim incorporated with nano-Au particles and [FeT(*o*-glu)TTCl].

room temperature for about 1 h. An Au-nanoparticles/[FeT(*o*-glu)PPCl]/chitosan modified electrode was obtained and could be used after washing with distilled water. Fig. 3 shows the scanning electron micrograph of the chitosan film incorporated with nano-Au particles and [FeT(*o*-glu)TTCl].

2.4. Preparation of buffers and solutions

Britton-Ribinson buffer is a 0.01 mol l^{-1} Na_2HPO_4–0.01 mol l^{-1} NaH_2PO_4 solution of pH 6.8. Stock working solution was prepared by dissolving 1.41 g ARN in 500 ml ethanol. The resulting solution (1.0×10^{-2} mol l^{-1}) was stocked in refrigerator at 4 °C. All ARN solutions in this study were prepared by diluting the stock working solution with BR buffer containing 20% ethanol.

2.5. Sample preparation

An amount of 1 g dried leaves of *A. annua* L. was ground into powder. The resulting powder was then extracted with 100 ml of ethanol for three times. After being extracted, the extract was filtered into a calibrated flask and then diluted to 1000 ml for determination.

2.6. Measurement procedure

The determination procedure is as follows. Amperometric measurements were carried out in 10 ml of a BR solution (pH 6.8) containing 20% ethanol using a [FeT(*o*-glu)PPCl]/chitosan modified electrode as a working electrode with an applied potential of −465 mV versus SCE and under magnetic stirrer bar. After the background current was stabilized, the response was subsequently recorded during the addition of 50 μl ARN containing solution. An increase value of current response is calculated and it is taken as the evaluation of the concentration of ARN in samples.

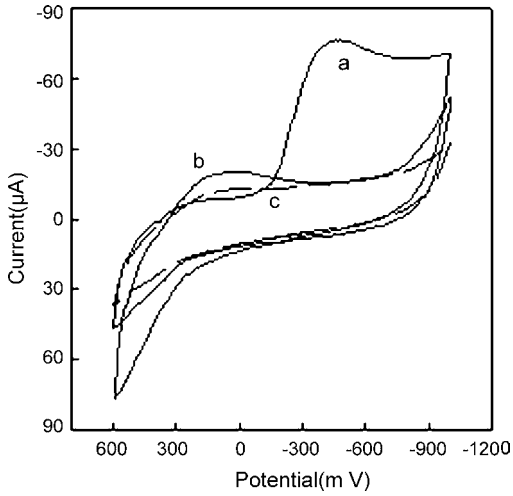

Fig. 4. Cyclic voltammograms obtained with a [FeT(*o*-glu)TTCl]/Au-nanoparticles modified electrode in the presence of 3.5×10^{-8} mol l^{-1} (curve a) and in a blank solution (curve c), and the unmodified electrode in the 3.5×10^{-8} mol l^{-1} ARN solution (curve b).

3. Results and discussion

3.1. Response characteristics of the ARN-sensor

The prepared electrodes were examined with the ARN-containing solution and BR buffer. Fig. 4 shows the cyclic voltammograms obtained with a [FeT(*o*-glu)PPCl]-chitosan modified electrode and a unmodified electrode. One can notice that a significant reduction peak at −465 mV appears when scan with the [FeT(*o*-glu)PPCl]-chitosan modified electrode in the presence of ARN (curve a). The unmodified electrode with the same addition of ARN (curve b) and the [FeT(*o*-glu)PPCl]-chitosan modified electrode in the absence of ARN (curve c) showed sluggish response. It was found that potential of only −465 mV was required for the reduction of ARN with the [FeT(*o*-glu)PPCl]-chitosan modified electrode. This implies that ARN can be reduced at a significantly more positive potential at the metalloporphyrin-modified electrode (−0.465 V) than an unmodified electrode (about −0.950 V). It seems that ARN can react with the [FeT(*o*-glu)PPCl] coated on the electrodes.

3.2. Selection of active materials for recognition element in electrodes

The characteristic performance of the prepared electrodes incorporated with different porphyrins including [MnT(*o*-glu)PPCl], [ZnT(*o*-glu)PPCl], [FeT(*o*-glu)PPCl] and T(*o*-glu)PPH_2 were investigated by amperometry. The results of these electrodes are shown in Table 1. It can be observed that the electrodes based on [MnT(*o*-glu)PPCl], [ZnT(*o*-glu)PPCl] and [FeT(*o*-glu)PPCl] exhibit better response characteristic than that based on T(*o*-glu)PPH_2. It is thought that the interaction of ARN with porphyrin is via the coordination with central metal of metalloporphyrin. T(*o*-glu)PPH_2 does not possess central metal capable of coordinating with ARN. Therefore, the poor amperometric response characteristics of

Table 1
Response characteristics of the modified electrodes incorporated with different active materials

Electrode[a]	Modifier	Working range (mol l^{-1})	Slope (mV/decade)
1	[FeT(*o*-glu)PPCl]	3.4×10^{-9}–1.3×10^{-6}	47.5 ± 1.8
2	[ZnT(*o*-glu)PPCl]	2.8×10^{-9}–6.9×10^{-6}	36.2 ± 1.5
3	[MnT(*o*-glu)PPCl]	5.8×10^{-9}–7.9×10^{-6}	32.2 ± 1.7
4	T(*o*-glu)PPH_2	Sluggish response	–

[a] The concentration of the active materials for electrode modification is 0.1%.

T(*o*-glu)PPH_2 modified electrodes are expected as compared to those of [MnT(*o*-glu)PPCl], [ZnT(*o*-glu)PPCl] and [FeT(*o*-glu)PPCl]. In view of the significant selectivity and sensitivity of the [FeT(*o*-glu)PPCl] modified electrodes compared with [ZnT(*o*-glu)PPCl] and [MnT(*o*-glu)PPCl]-modified electrode as described in the next section, [FeT(*o*-glu)PPCl] was used as the ARN-sensitive material in all further studies.

3.3. Selectivity of ARN-sensor

Five possible interfering substrates were used to evaluate the selectivity of the ARN-sensor. The current recorded for each interfering substrate at a concentration of 5×10^{-8} mol l^{-1} in the presence of 5×10^{-8} mol l^{-1} ARN was used as an indicator for the sensor selectivity in comparison with the ARN readings alone. The results of the interference investigation are listed in Table 2. From the data in Table 2, one can observe that EDTA-Fe^{3+}, Fe^{3+}, H_2O_2 and artemisinic acid do not cause any interference (≤3% change) under the experimental conditions. The most obvious interfering species is CN^-.

The reduction of ARN on the [FeT(*o*-glu)PPCl]-modified electrode takes place in a similar way to that of ARN in the presence of hemin in solution phase. According to the reports [18,19] on reduction mechanism of artemisinin in the presence of hemin, the interaction mode of ARN with [FeT(*o*-glu)PPCl] is thought to follow the reaction scheme:

$$[\text{Fe(II)T}(o\text{-glu})\text{PPCl}] + \text{ARN(ox)}$$
$$\rightarrow [\text{Fe(III)T}(o\text{-glu})\text{PPCl} \cdot \text{ARN}](\text{ox})\,\text{ads}$$
$$\xrightarrow{+e^-} [\text{Fe(II)T}(o\text{-glu})\text{PPCl} \cdot \text{ARN}^*](\text{ox})\,\text{ads}$$
$$\xrightarrow{+e^-} [\text{Fe(III)T}(o\text{-glu})\text{PPCl}] + \text{ARN}\,(\text{red})\,(\text{Product})$$

Table 2
Possible interferences tested with the [FeT(*o*-glu)PPCl]/Au-nanoparticles modified electrodes

Interferents	Current ratio[a]
EDTA-Fe(III)	1.02
Fe^{3+}	1.01
CN^-	0.83
H_2O_2	1.02
Artemisinic acid	1.00

[a] Ratio of currents for mixtures containing 5×10^{-8} mol l^{-1} interfering substrate and 5×10^{-8} mol l^{-1} ARN compared to that for 5×10^{-8} mol l^{-1} ARN.

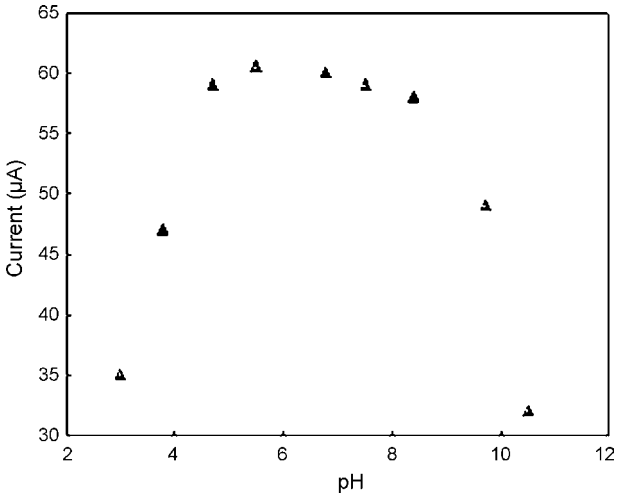

Fig. 5. Effect of pH on the reductive current response of the [FeT(*o*-glu)TTCl]/Au-nanoparticles modified electrode at a concentration of 1×10^{-8} mol l^{-1} of ARN-containing solution. Operating potential: −465 mV vs. SCE.

It seems that CN^- can bind to the central metal Fe(III) of [Fe(III)T(*o*-glu)PPC], and thus, interferes in the determination of ARN.

3.4. Effect of pH

The effect of the electrolyte pH on the response performance of the ARN-sensor was investigated by recording the reduction peak current of ARN at a operating potential of −465 mV (versus SCE) in a concentration of 1×10^{-8} mol l^{-1} over a pH range of 3.0–10.5. Fig. 5 is a plot of I_P versus pH for the reduction of ARN. One can see that the reduction current increases with the increase of pH values up to 6.0, then, tend to stabilize. However, a lower pH less than 3.0 or a higher pH more than 8.5 could cause a decrease of the current response. The lower the pH of the electrolyte, the more favourable for the reduction of the ARN. However, the lower or the higher pH is unfavourable for the stabilization of the metal coordinated with porphyrin and of the chitosan film on electrodes. In the subsequent experiments, a pH 6.8 BR buffer solution was used as an ideal experimental condition.

3.5. Repeatability of ARN-sensor

The repeatability of the prepared ARN sensors was evaluated with 10 amperometric measurements in 5×10^{-8} mol l^{-1} ARN-containing solutions. The sensor exhibited sufficient repeatability with a standard deviation of 3.8%.

3.6. Preliminary analytical application

Fig. 6 shows calibration curve obtained at pH 6.8 with the prepared ARN-sensor. It was linear over the range 1.8×10^{-7}–1.7×10^{-9} mol l^{-1}, with a detection limit of 1.7×10^{-9} mol l^{-1} for ARN. The linear equation was I (μA) = 11.70 + 0.41C ($\times 10^{-9}$ mol l^{-1}), with a correlation coef-

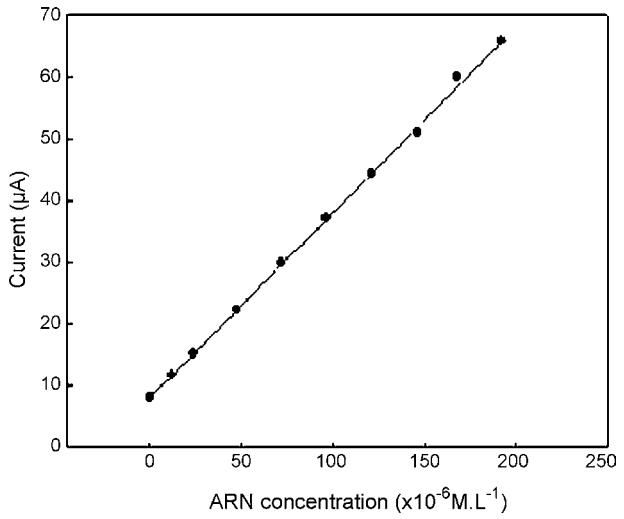

Fig. 6. Calibration curve for the determination of ARN obtained by amperometric measurement. The sample measurements were carried out in a 10 ml BR solution (pH 6.8) containing 20% ethanol using a [FeT(*o*-glu)TTCl] modified electrode as a working electrode with an applied potential of −465 mV vs. SCE and under magnetic stirrer bar.

Table 3
ARN determination with the proposed ARN-sensor in the crude plant extracts

Sample[a]	Proposed method (mg/g dried plant)	UV–visible spectroscopy (at 600 nm)
1	3.72 ± 0.07[b]	3.90
2	4.31 ± 0.05	4.36
3	4.37 ± 0.04	4.25

[a] The sample solutions were obtained by diluting the stock solution prepared as described in Section 2.
[b] Mean ± S.D. of six measurements.

ficient value of 0.996. On this basis, the proposed procedure was applied for the direct determination of ARN in plant extract samples. The sample solutions prepared as described in Section 2 were 10-fold diluted with a BR buffer solution of pH 6.8 followed by amperometric measurements using the prepared ARN sensor. Table 3 shows the results compared with those obtained by the pharmacopoeia method (UV–visible spectroscopy). It indicates that the concentrations of ARN determined by the sensor method are in good agreement with those by the pharmacopoeia method. An another obvious advantage of the proposed procedure is the simple sample preparation with even turbid samples.

4. Conclusions

We have reported here for the first time the application of a new metalloporphyrin-based sensor for ARN assay. The design of the method consists of a glycosylated metalloporphyrin as a supramolecular recognition element and a natural polymer chitosan as an Au-nanoparticles/metalloporphyrin immobilization material. The proposed ARN-sensor detection for ARN offers the advantages derived from the selectivity and the sensitivity owing to incorporation of metalloporphyrin and Au-nanoparticles in the sensitive membrane. The simplicity, sensitivity and selectivity make it capable of replacement of the officially recommended procedure.

Acknowledgments

The authors are grateful for the support of the Foundation for Educational Committee and the Foundation of Science Commission of Hunan Province (Grants No. 05SK3058).

References

[1] World Health Organization, The World Health Report 1996—Fighting Disease, Fostering Development, Geneva, Switzerland, 1996.
[2] WHO, UNDP/World Bank/WHO Special Programme for Research and Training in Tropical Diseases. 1994–1995. The role of artemisinin and derivatives in the current treatment of malaria. Report of an Informal Consultation convened by WHO in Genvea, 1993-09-2729.
[3] N. Acton, D.L. Klayman, I.J. Rollman, Planta Med. 51 (1985) 445.
[4] Z.M. Zhou, J.C. Anders, H. Chung, A.D. Theoharides, J. Chromatogr. 77 (1987) 414.
[5] N.A. Chaniotakis, A.M. Chasser, M.E. Meyerhoff, J.T. Groves, Anal. Chem. 60 (1988) 185.
[6] M.S.M. Quintino, K. Araki, H.E. Toma, L. Angnes, Talanta 68 (2006) 1281.
[7] J. Yoon, J.H. Shin, I.R. Paeng, H. Nam, G.S. Cha, K.J. Paeny, Anal. Chim. Acta 367 (1998) 175.
[8] V.K. Guota, A.K. Jain, L.P. Singh, U. Khurana, Anal. Chim. Acta 355 (1997) 33.
[9] D. Ammann, M. Huser, B. Krautler, P. Schulthess, B. Lindemann, E. Halder, M. Simon, Helv. Chim. Acta 69 (1986) 849.
[10] Q.L. Chang, M.E. Meyerhoff, Anal. Chim. Acta 186 (1986) 81.
[11] H.H. Frey, C.J. McNeil, R.W. Keay, J.V. Bannister, Electroanalysis 10 (1998) 480.
[12] B. Duony, R. Arechabaleta, N.J. Tao, J. Electroanal. Chem. 447 (1998) 63.
[13] A.F.G. Slater, W.J. Swiggard, B.R. Orton, Proc. Natl. Acad. Sci. U.S.A. 88 (1991) 325.
[14] R. Anne, M.J. Bernard, Am. Chem. Soc. 119 (1997) 5968.
[15] L. Messori, F. Piccioli, B. Eitler, M.C. Bergonzi, F.F. Vincieri, Bioorg. Med. Chem. Lett. 13 (2003) 4055.
[16] X.-B. Zhang, C.-C. Guo, J.-B. Xu, J.-B. Yu, J. Mol. Catal. A31 (2000) 153.
[17] K.C. Grabar, R.G. Freeman, M.B. Hommer, M.J. Natan, Anal. Chem. 67 (1995) 735.
[18] Y. Chen, J.-M. Zheng, S.-M. Zhu, H.-Y. Chen, Electrochim. Acta 44 (1999) 2345.
[19] Z.-J. Zhou, P.-H. Yang, D.-X. Feng, Y.-T. Zhu, M.-Y. Zhang, Chin. J. Anal. Labor. 23 (2004) 28.

Available online at www.sciencedirect.com
ScienceDirect
Talanta 72 (2007) 1469–1473
Talanta
www.elsevier.com/locate/talanta

Aluminum(III) selective potentiometric sensor based on morin in poly(vinyl chloride) matrix

Vinod K. Gupta*, Ajay K. Jain, Gaurav Maheshwari

Department of Chemistry, Indian Institute of Technology Roorkee, Roorkee 247667, Uttaranchal, India

Received 22 December 2006; received in revised form 25 January 2007; accepted 25 January 2007
Available online 9 February 2007

Abstract

Al^{3+} selective sensor has been fabricated from poly(vinyl chloride) (PVC) matrix membranes containing neutral carrier morin as ionophore. Best performance was exhibited by the membrane having composition as morin:PVC:sodium tetraphenyl borate:tri-*n*-butylphosphate in the ratio 5:150:5:150 (w/w, mg). This membrane worked well over a wide activity range of 5.0×10^{-7} to 1.0×10^{-1} M of Al^{3+} with a Nernstian slope of 19.7 ± 0.1 mV/decade of Al^{3+} activity and a limit of detection 3.2×10^{-7} M. The response time of the sensor is ~5 s and membrane could be used over a period of 2 months with good reproducibility. The proposed sensor works well over a pH range (3.5–5.0) and demonstrates good discriminating power over a number of mono-, di- and trivalent cations. The sensor can also be used in partially non-aqueous media having up to 20% (v/v) methanol, ethanol or acetone content with no significant change in the value of slope or working activity range. The sensor has also been used in the potentiometric titration of Al^{3+} with EDTA and for its determination in zinc plating mud and red mud.

Keywords: Poly(vinyl chloride) (PVC); Nernstian slope; Aluminum selective sensor; Morin; Ionophore

1. Introduction

Aluminum is third most abundant element and widely used for industrial and domestic purposes. Thus, aluminum is present in environmental samples where its estimation is important in view of its toxicity above certain level. Aluminum is known to cause dementia, anemia, myopathy, bone and joint disease [1–4]. A number of methods such as graphite furnace atomic absorption spectrometry (GF-AAS), inductively coupled plasma-atomic emission spectrometry (ICP-AES) [5–9], liquid chromatography [10], flow-injection [11] and stripping voltammetry [12] have been used to determine aluminum. Though these methods provide accurate results but are not very convenient for the analysis of large number of environmental samples as they require sample pretreatment and sufficient infrastructure back-up. On the other hand, analytical procedures involving ion sensors are most appropriate for such determinations as they require no or minimum sample pretreatment and are fast, convenient and cheap. Of course analysis by ion sensor requires the availability of sensitive and selective aluminum sensor. The literature shows that few aluminum selective sensors have been reported using solid membranes of neutral carriers [13–17]. However, these sensors exhibit some limitations, as they generally show narrow working activity range, some interference to Cu^{2+}, Cd^{2+}, Hg^{2+} and Fe^{3+} and not very low response time. A selective, sensitive and fast responding aluminum sensor with high shelf life time is required. Towards this objective, we have explored morin (**I**) (Fig. 1), known to form strong complex with aluminum, as an aluminum selective ionophore. The present communication reports the results of our investigations on PVC based membranes of (**I**) as Al^{3+} selective sensors.

2. Experimental

2.1. Reagents

Morin (**I**) from SRL (India), dibutyl phthalate (DBP) and dioctyl phthalate (DOP) from Reidal (India), chloronaphthalene (CN) Acros (USA), tri-*n*-butylphosphate (TBP) from Merck (Germany), sodium tetraphenyl borate (NaTBP) from BDH (UK) and high molecular weight poly(vinyl chloride) (PVC) from Aldrich (USA) were obtained and used as such. Other

* Corresponding author. Tel.: +91 1332 285801; fax: +91 1332 273560.
E-mail address: vinodfcy@iitr.ernet.in (V.K. Gupta).

0039-9140/$ – see front matter © 2007 Elsevier B.V. All rights reserved.
doi:10.1016/j.talanta.2007.01.064

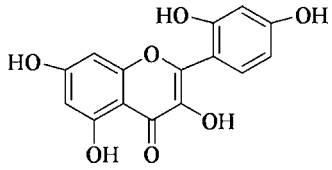

Fig. 1. Structure formula of (**I**).

reagents were of analytical grade. Solutions of metal (nitrates) were prepared in double distilled water and standardized by the reported methods wherever necessary. Working solutions of different activities were prepared by diluting 0.1 M stock solutions.

2.2. Apparatus and potential measurements

The potential measurements were carried out at 25.0 ± 0.1 °C with a digital pH meter (Model 5652 A, ECIL, India) and microvoltmeter, model CVM 301, Century (India). The prepared membranes were equilibrated for 3 days in 0.5 M aluminum nitrate solution. All potential studies were carried out by using the following cell assembly, employing saturated calomel electrodes (SCE) as reference electrodes:

SCE/internal solution (0.1 M Al^{3+})/membrane/

test solutions/SCE

The cell potential was measured by varying the activity of Al^{3+} test solution in the range 1.0×10^{-7} to 1.0×10^{-1} M by serial dilution and after each dilution pH of the solution was checked and maintained between pH 4.0 and 5.0. All pH adjustments were made with dil. HCl or NaOH solution. The response time of membrane sensors, i.e., the time required to reach stable and constant potential was recorded for all membranes. The activity coefficients (γ) of metal ions have been calculated from the modified form of the Debye–Hückel equation [18].

2.3. Preparation of membranes

The PVC based membranes were prepared according to the method proposed by Craggs et al. [19]. Thus, varying amounts of (**I**) and an appropriate amount of PVC were dissolved in minimum amount of THF. The anion excluder; NaTPB and solvent mediators; DBP, DOP, CN and TBP were also added to get membranes of different compositions. After complete dissolution of all the components and thorough mixing, homogeneous mixture was poured into polyacrylates rings placed on a smooth glass plate. THF was allowed to evaporate for about 24 h at room temperature. The transparent membranes of 0.5 mm thickness were removed carefully from the glass plate. A 1.5 cm diameter piece was cut out and glued to one end of a "Pyrex" glass tube with the help of araldite.

2.4. Sample preparation

About 1 g samples of zinc plating mud and red mud (aluminum industries waste) were left overnight in contact with 10 mL of concentrated HCl and mixture of acids (2 mL HCl, 2 mL HNO_3 and 2 mL H_2SO_4), respectively. After filtration both the residues were washed with 10 mL of dilute HCl. The filtrate and washings were combined and finally made up to 100 mL, adjusting the overall pH to ~5 with dilute NH_3. Estimations were done at constant ionic strength of 0.1 M KNO_3.

3. Results and discussion

3.1. Working activity range and slope of Al^{3+} sensor

The potential of the sensors employing different membranes was determined as a function of aluminum activity and the response obtained is depicted in Fig. 2. The working activity range and slope were determined from these plots and compiled in Table 1 along with composition of the membranes and response time. It is worth mentioning that a number of other membranes having different composition were also investigated but the results are given only for those which have performed best in terms of wide working activity range, Nernstian or near-Nernstian slope, low response time and good reproducibility. It is seen from Table 1 that the sensor no. 1 having membrane without plasticizer shows a working activity range of 3.2×10^{-5} to 1.0×10^{-1} M with a slope of 15.5 mV/decade of activity. Thus, slope of this membrane is substantially sub-Nernstian and the working activity range narrow. Therefore, improvement in the performance characteristic of the sensor was attempted by the addition of four plasticizers to the membranes. It is known that the addition of plasticizers generally improves the working activity range, stability and shelf life. However, the selectivity normally remains unaffected because it largely depends on metal–ionophore interaction. The plasticizer to be used in membrane should exhibit high lipophilicity, have high molecular weight, low tendency for exudation from the polymer matrix, low vapor pressure and high capacity to

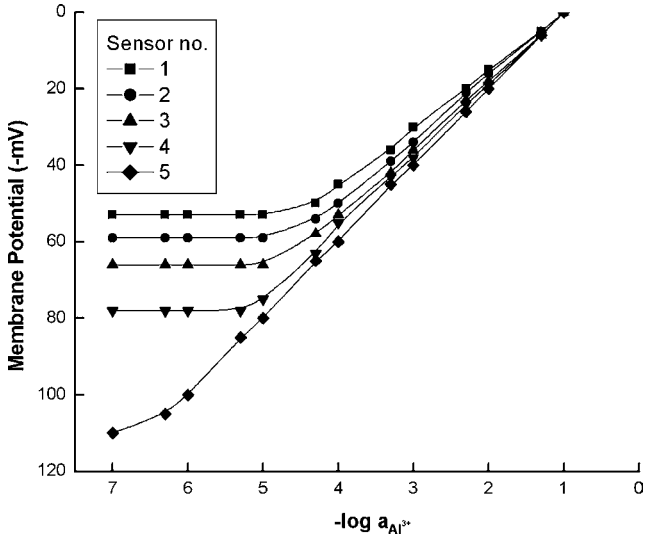

Fig. 2. Variation of membrane potential with molarity of Al^{3+} ions; PVC based membranes of (**I**) without solvent mediator (1), with solvent mediators, DBP (2), DOP (3), CN (4), and TBP (5).

Table 1
Composition of different PVC-membrane sensors based on (**I**) for the determination of Al^{3+} in solution

Sensor no.	Components in membranes (w/w)							Working activity range (M)	Slope (mV/decade of activity)	Response time (s)
	I	PVC	NaTPB	DBP	DOP	CN	TBP			
1	5	150	5	–	–	–	–	3.2×10^{-5} to 1.0×10^{-1}	15.5	28
2	5	150	5	150	–	–	–	2.5×10^{-5} to 1.0×10^{-1}	17.0	23
3	5	150	5	–	150	–	–	1.8×10^{-5} to 1.0×10^{-1}	17.8	18
4	5	150	5	–	–	150	–	8.9×10^{-6} to 1.0×10^{-1}	19.0	12
5	**5**	**150**	**5**	–	–	–	**150**	**5.0×10^{-7} to 1.0×10^{-1}**	**19.7**	5
6	5	125	5	–	–	–	150	7.9×10^{-6} to 1.0×10^{-1}	17.6	16
7	5	175	5	–	–	–	150	5.6×10^{-6} to 1.0×10^{-1}	20.2	14

Bold values indicate to best sensor and its performance characteristics.

dissolve the substrate and other additives present in the membrane. Additionally, its viscosity and dielectric constant should be adequate [20]. Thus, plasticizers namely DBP, DOP, CN and TBP were added to improve the performance of the sensors. It is seen from Table 1 that the addition of plasticizers to the membranes (sensors no. 2–5) has resulted in improvement of the working activity range and the slope of the corresponding calibration curves. Of the four plasticizers used, sensor no. 5 containing TBP plasticizer performs best as it exhibits widest working activity range of 5.0×10^{-7} to 1.0×10^{-1} M with Nernstian slope of 19.7 mV/decade of activity and a limit of detection 3.2×10^{-7} M. The detection limit was taken as the activity corresponding to the point of intersection of the linear portion of the potential response plot at lower activity end. The effect of varying amount of PVC on membrane was also looked into (Table 1) and it is seen that the sensors no. 6 and 7 having lower and higher amount of PVC as compares to sensor no. 5 performs poorly.

3.2. Response and lifetime

The response time of membranes without solvent mediator was found to be ∼28 s. The addition of solvent mediators improved the response time significantly as a sharp reduction in the response time was observed in all the cases, although the effect varied for different solvent mediators. Membranes containing DBP, DOP and CN performed satisfactorily as the response time for these membranes were 23, 18 and 12 s, respectively. The best results were obtained for sensor no. 5 over the entire working activity range (Table 1), as it exhibited lowest (5 s) response time. Potentials remained constant for about 4 min after which a very slow divergence was recorded. The membrane could be used over a period of 2 months without showing any significant variation in the working activity range, slope and response time. The membrane was stored in 0.5 M aluminum(III) solution when not in use. As sensor no. 5 has exhibited widest working activity range, Nernstian slope and lowest response time, all further studies were carried out with this sensor only.

3.3. pH and solvent effect

Hydrogen ions are known to cause interference in the performance of the sensors. Thus, it was necessary to determine useful pH range where the sensor can perform without being affected by H^+ ions. Thus, pH dependence of the membrane sensor no. 5 was investigated at two activities of Al^{3+} 1.0×10^{-3} and 1.0×10^{-4} M and the results obtained are given in Fig. 3. It is seen from the figure that the potential remains constant over a pH range of 3.5–5.0. In view of sharp change in potential below pH 3.5 and above 4.5, it is better to make all measurements at mid point, i.e., 4.5. The change in potential below pH 3.5 is due to interference caused by H^+ while above 5.0 due to hydrolysis of Al^{3+}.

The performance of the sensor was further assessed in partially non-aqueous media, i.e., methanol–water, ethanol–water and acetone–water mixtures. The results obtained are compiled in Table 2. It is seen that with increase in non-aqueous content both the slope and working activity range are reduced. This effect is significantly pronounced above 20% methanol, ethanol and acetone. Thus, the sensor can be used in mixtures containing only up to 20% non-aqueous content.

3.4. Potentiometric selectivity

The selectivity is the most important characteristics as it determines the extent of utility of a sensor in real sample measurement. The selectivity coefficient values were determined by matched potential method (MPM), which was proposed by Gadzekpo and Christian [21] to overcome difficulties in

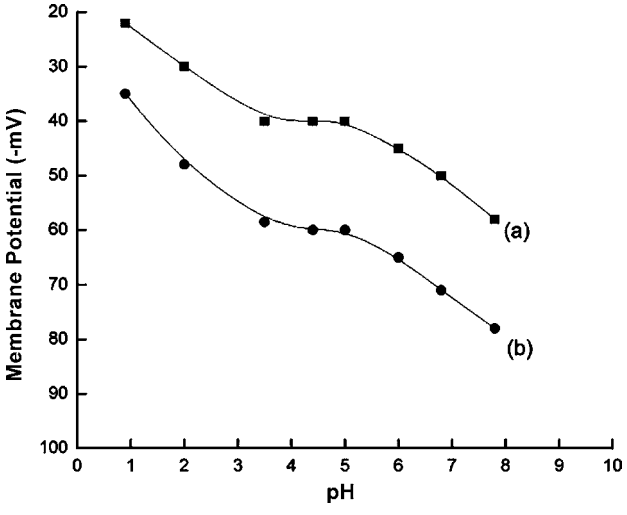

Fig. 3. Effect of pH on cell potential; activity of Al^{3+} (M), 1.0×10^{-3} M (a) and 1.0×10^{-4} M (b).

Table 2
Effect of partially non-aqueous medium on the working activity range of the proposed Al^{3+} selective sensors (no. 5, Table 1)

Non-aqueous content (%, v/v)	Slope (mV/decade of activity)	Working activity range (M)
0	19.7	5.0×10^{-7} to 1.0×10^{-1}
Methanol		
10	19.7	5.0×10^{-7} to 1.0×10^{-1}
20	19.5	2.0×10^{-7} to 1.0×10^{-1}
25	17.5	1.8×10^{-6} to 1.0×10^{-1}
Ethanol		
10	19.7	5.0×10^{-7} to 1.0×10^{-1}
20	19.2	2.0×10^{-7} to 1.0×10^{-1}
25	17.4	1.8×10^{-6} to 1.0×10^{-1}
Acetone		
10	19.7	5.0×10^{-7} to 1.0×10^{-1}
20	19.4	2.5×10^{-7} to 1.0×10^{-1}
25	17.0	5.6×10^{-6} to 1.0×10^{-1}

obtaining selectivity coefficient values when ions of unequal charges are involved. In this procedure, the selectivity coefficient $K^{Pot}_{Al^{3+},B}$ is calculated by the expression:

$$K^{Pot}_{Al^{3+},B} = \frac{a'_{Al^{3+}} - a_{Al^{3+}}}{a_B} = \frac{\Delta a_{Al^{3+}}}{a_B}$$

and is therefore determined by measuring change in potential upon increasing by a definite amount the primary ion activity from an initial values of $a_{Al^{3+}}$ to $a'_{Al^{3+}}$ and a_B represents the activity of interfering ion (B) added to the same reference solution of activity $a_{Al^{3+}}$ which causes the same potential change. The values of $a_{Al^{3+}}$ and $a'_{Al^{3+}}$ were taken to be 1×10^{-3} and 5×10^{-3} M, whereas the values of a_B experimentally determined. The values determined by MPM method are given in Table 3. A value of selectivity coefficient equal to 1.0 indicates that the sensor responds equally to primary as well as interfering ion. However, a value smaller than 1.0 indicates that membrane sensor is responding more to primary ion than interfering ion and in such a case the sensor is said to be selective to primary ion over interfering ion. Further, smaller the selectivity coefficient, higher is the selectivity order. A perusal of Table 3 shows that selectivity coefficient values for present sensor are much smaller than 1.0 over a number of mono-, di- and trivalent cations studied. Hence, the sensor is sufficiently selective over these ions and can therefore be used to estimate aluminum in presence of these interfering ions by direct potentiometry.

Table 3
Selectivity coefficient values ($K^{Pot}_{Al^{3+},B}$) for Al^{3+} selective sensor by matched potential method

Interfering ion (B)	Selectivity coefficients [$K^{Pot}_{Al^{3+},B}$]
K^+	1.0×10^{-3}
Na^+	1.7×10^{-3}
NH_4^+	1.2×10^{-3}
Cd^{2+}	5.0×10^{-4}
Pb^{2+}	8.0×10^{-4}
Cu^{2+}	1.2×10^{-4}
Mn^{2+}	2.5×10^{-4}
Hg^{2+}	1.0×10^{-4}
Ni^{2+}	1.9×10^{-4}
Zn^{2+}	2.8×10^{-4}
Co^{2+}	3.9×10^{-4}
Fe^{3+}	3.9×10^{-3}
Cr^{3+}	2.0×10^{-3}

Table 4
Quantification of aluminum in zinc plating mud and red mud using AAS and Al^{3+} sensor (no. 5, Table 1)

Samples	Aluminum content (mg/g)	
	Sensor no. 5	AAS
Zinc plating mud	0.37 ± 0.02	0.35 ± 0.01
Red mud	9.80 ± 0.70	9.07 ± 0.50

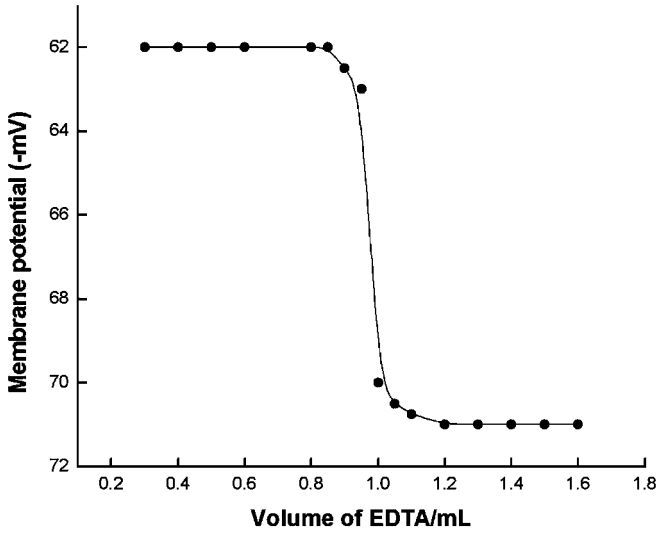

Fig. 4. Potentiometric titration plot of 1×10^{-4} M Al^{3+} solution (10 mL) with EDTA (1.0×10^{-3} M).

4. Analytical application of sensor

The utility of the sensor no. 5 was further investigated to determine aluminum in zinc plating mud and red mud. The results are found to be close agreement with those obtained by AAS (Table 4). Thus, the sensor can be employed for Al^{3+} quantification in real samples. The sensor has also been used as an indicator electrode in the potentiometric titration of Al^{3+} against EDTA. A 10 mL solution of Al^{3+} (1.0×10^{-4} M) was titrated with 1.0×10^{-3} M EDTA solution at pH 5.0. The titration plot obtained (Fig. 4) is of standard sigmoid shape and the end point corresponds to 1:1 stoichiometry of Al-EDTA complex.

5. Conclusion

Of the seven Al^{3+} sensors prepared, the sensor no. 5 having membrane incorporating morin as an ionophore, TBP as a plasticizer and NaTPB as anion excluder in PVC matrix in the ratio 5:150:5:150 was found to give best performance in terms of working activity range, Nernstian slope, pH range and response

Table 5
Comparison of the proposed Al^{3+} ion selective sensor with the existing Al^{3+} selective solid state sensors

Serial no.	Working activity range (M)	Slope (mV/decade of activity)	pH range	Response time (s)	Interference (calculated by MPM)	Life time (days)	Reference no.
1	1.0×10^{-5} to 1.0×10^{-1}	19.5	2.25–3.25	–	NM[a]	30	[13]
2	1.0×10^{-6} to 1.0×10^{-2}	Near-Nernstian	Acidic range	–	Cu^{2+}, Cd^{2+}, Hg^{2+}	60	[14]
3	5.0×10^{-6} to 1.0×10^{-2}	19.3	2.9–5.0	10	NM	70	[15]
4	2.0×10^{-6} to 2.0×10^{-2}	19.6	3.4–5.0	5	Fe^{3+}	90	[16]
5	1.0×10^{-6} to 1.6×10^{-1}	19.6	3.0–8.5	∼5	NM	90	[17]
6	5.0×10^{-7} to 1.0×10^{-1}	19.7	3.5–5.0	∼5	–	60	Proposed sensor

[a] Not mentioned.

time. Its performance has been compared with some important sensors in Table 5. It is seen from the table that this sensor is superior to sensors of ETPTP [13], furil [14], tetradentate Schiff base [15], hydroxy-thio-xanthones [16] and 1-hydroxy-3-methyl-9*H*-xanthen-9-one [17] in terms of wider working activity range and selectivity. Thus, the proposed sensor is an important addition in this field and can be used for the determination of Al^{3+}.

Acknowledgement

The authors are thankful to Ministry of Human Resource and Development (MHRD), New Delhi, India for providing funds to undertake the work.

References

[1] S.W. King, J. Savory, M.R. Willis, Crit. Rev. Clin. Lab. Sci. 13 (1981) 1.
[2] I.S. Parkinson, M.K. Ward, J. Clin. Pathol. 34 (1981) 1285.
[3] A.M. Pierdes, Int. J. Artif. Organs 1 (1978) 206.
[4] M. Sundaram, M.U. Wolverson, A. Heidelberg, R.D. Grider, Am. J. Roentgenol. 13 (1981) 363.
[5] B. Bocca, A. Alimonti, F. Petrucci, N. Violante, G. Sancesario, G. Forte, O. Senofonte, Spectrochim. Acta B 59 (2004) 559.
[6] S. Polizzi, E. Pira, M. Ferrara, M. Bugiani, A. Papaleo, R. Albera, S. Palmi, Neur. Toxicol. 23 (2002) 761.
[7] K. Popińska, J. Kierkuo, M. Lyszkowska, J. Socha, E. Pietraszek, W. Kmiotek, J. Ksiazyk, Nutrition 15 (1999) 683.
[8] N.B. Roberts, A. Clough, J.P. Bellia, J.Y. Kim, J. Inorg. Biochem. 69 (1998) 171.
[9] A. Sanz-Medel, A.B. Soldado-Cabezuelo, R. Milačič, T. Bantan-Polak, Coord. Chem. Rev. 228 (2002) 373.
[10] H. Lian, Y. Kang, S. Bi, Y. Arkin, D. Shao, D. Li, Y. Chen, L. Dai, N. Gan, L. Tian, Talanta 62 (2004) 43.
[11] G. Albendin, M.P. Manuel-vez, C. Moreno, M.R. Garcia-Vargas, Talanta 60 (2003) 425.
[12] A.L. Balbo, V.C.D. Orto, S. Sobral, I. Rezzano, Anal. Lett. 31 (1998) 2717.
[13] M.B. Saleh, S.S.M. Hassan, A.A.A. Gaber, N.A.A. Kream, Anal. Chim. Acta 434 (2001) 247.
[14] M.F. Mousavi, M. Arvand-Barmchi, M.A. Zanjanchi, Electroanalysis 13 (2001) 1125.
[15] A. Abbaspour, A.R. Esmaeilbeig, A.A. Jarrahpour, B. Khajeh, R. Kia, Talanta 58 (2002) 397.
[16] M. Shamsipur, S. Ershad, A. Yari, H. Sharghi, A.R. Salimi, Anal. Sci. 20 (2004) 301.
[17] A. Yari, L. Darvishi, M. Shamsipur, Anal. Chim. Acta 555 (2006) 329.
[18] G.D. Christian, Analytical Chemistry, 6th ed., John Wiley & Sons, Inc., 2003, p. 212 (Chapter 6).
[19] A. Craggs, G.J. Moody, J.D.R.J. Thomas, Chem. Educ. 51 (1974) 541.
[20] M.A. de Los, A. Perez, L.P. Martin, J.C. Quintana, M. Yazdani-Pedram, Sens. Actuators B 89 (2003) 262.
[21] V.P. Gadzekpo, G.D. Christian, Anal. Chim. Acta 164 (1984) 279.

Available online at www.sciencedirect.com
ScienceDirect
Talanta 72 (2007) 1481–1486
Talanta
www.elsevier.com/locate/talanta

On-line sample digestion using an electromagnetic heating column for the determination of zinc and manganese in tea leaf by flame atomic absorption spectrometry

Su-Ping Han, Wu-Er Gan *, Qing-De Su

Department of Chemistry, University of Science and Technology of China, Hefei, Anhui 230026, PR China

Received 12 October 2006; received in revised form 26 January 2007; accepted 26 January 2007
Available online 9 February 2007

Abstract

A new on-line sample digestion system using electromagnetic induction heating technique was developed for the determination of zinc and manganese in tea leaf by flame atomic absorption spectrometry (FAAS). The homemade electromagnetic heating column (EMHC), whose effective diameter was about 1 mm, was composed of a polytetrafluoroethylene (PTFE) outer tube and seven compactly packed PTFE coil-coated iron wires. The pre-digested sample solution was pumped through EMHC and then transferred directly to FAAS for determination. An analytical throughput of 72 samples h^{-1} was obtained in the present system. Under optimal condition, the detection limits (3σ) of zinc and manganese were 4.2 $\mu g\,L^{-1}$ and 3.0 $\mu g\,L^{-1}$, along with relative standard deviations (R.S.D.) of 3.2% and 3.6% respectively for zinc and manganese. Certified reference materials GBW 07602, GBW 07605 and GBW 08505 were analyzed to validate the proposed method, good agreement was achieved between the certified values and the obtained results.

Keywords: Electromagnetic induction heating; On-line digestion; Flow injection; Flame atomic spectrometry; Tea leaf samples

1. Introduction

Flame atomic absorption spectrometry (FAAS) has been shown to be a promising technique for the determination of trace heavy metals in view of its low costs and easy usage [1–4]. Some pretreatment procedures, including sample digestion [5–7,21,22], pre-concentration [8–11], separation [12,13], etc., are necessary for the determination of trace heavy metals in environmental samples. Among them, sample digestion is a critical step.

By using flow injection (FI), it is possible to incorporate on-line sample preparation with detection in an automatic procedure to avoid laborious sample pretreatment [5–7]. Nowadays, focused microwave oven coupled to an on-line flow system is one of the most proposed methods for sample digestion [14–16]. The main characteristic of the focused microwave oven is the possibility to perform reproducible irradiation during a short and controlled reaction time. It has some advantages over classical methods including saving time and reagent consumption. In addition, digesting samples in a closed system can reduce the loss of volatile elements and atmospheric contamination. However, the high cost of instrumental required for safety microwave operations should be mentioned.

Another heating technique, whose virtue can be comparable with focused microwave-assisted heating, is electromagnetic induction heating (EMIH). It has been widely used in many industrial processes such as induction metal melting [17]. There were also reports about EMIH been used in processing silicon wafers [18] and in surface molding [19]. Besides, it is an effective method for the processing of food, drink, wood, etc., to save energy and reduce processing time [20]. Our previous work has successfully applied it to sample preparation for the determination of Hg in fish samples [21] and mainstream cigarette smoke [22].

The main purpose of this study was to develop an on-line sample digestion method of higher heating efficiency and heating rate by employing electromagnetic heating technique. The proposed method was successfully employed for the determination

* Corresponding author. Tel.: +86 5513600021.
E-mail address: wgan@ustc.edu.cn (W.-E. Gan).

0039-9140/$ – see front matter © 2007 Elsevier B.V. All rights reserved.
doi:10.1016/j.talanta.2007.01.061

Table 1
FAAS operational parameters for the determination of Zn and Mn

Parameters	Zn	Mn
Wave length (nm)	213.9	279.5
Lamp current (mA)	1.3	1.5
Band pass (nm)	0.4	0.2
Measuring signal	Peak height absorbance	Peak height absorbance
Flame type	Air acetylene	Air acetylene
Air flow rate (L min^{-1})	5.0	5.0
Acetylene flow rate (L min^{-1})	1.0	1.0

of zinc and manganese in tea leaf samples. Special interests were focused on the study of the parameters influencing the on-line digestion efficiency and FI variables.

2. Experimental

2.1. Apparatus

A Model WFX-120 atomic absorption spectrometer (Ruili Analytical Instruments Factory, Beijing, PR China) was employed throughout. Zinc and manganese hollow cathode lamps (Dianguang Instrument Factory, Shanghai, PR China) were used as radiation source. Air-acetylene flame was adopted for flame atomization. The measurement conditions were optimized on signal-to-background ratio, and the instrumental and operational parameters used in this work are presented in Table 1.

The schematic diagram of the FI-FAAS with on-line digestion manifold is shown in Fig. 1(a). The system consisted of an IFIS-C peristaltic pump (Xi'an Ruimai Electronic Technology Co. Ltd., Xi'an, PR China), an electromagnetic induction oven (EMIO) (Shandong Jiuyang Co. Ltd., Shandong, PR China), and a homemade electromagnetic heating column (EMHC) that was made of a polytetrafluoroethylene (PTFE) outer tube (50 cm length × 4.2 mm i.d.). Seven iron wires (49 cm length × 1.2 mm diameter) sealed in thinner PTFE coil (1.2 mm i.d. × 1.4 mm o.d. × 50 cm length) were filled in the PTFE outer tube compactly and were parallel to the tube. The sectional view was shown in Fig. 1(b). The EMHC was coiled into a loop and placed on the surface of EMIO. The basic working principle of EMIO has been described in our earlier work [22]. One millimeter i.d. PTFE coil was employed as both inlet and outlet tubing of EMHC. This instrument was operated with a personal computer installed with lab-compiled software.

WX-3000 microwave oven (Shanghai EU Chemical Instruments Co. Ltd., PR China) was used for off-line sample digestion as a comparison.

UV-9100 UV/VIS spectrophotometer (Ruili Analytical Instruments Factory, Beijing, PR China) was used to detect the ultraviolet absorption signal of phenol solution.

2.2. Reagents

All solutions were prepared by using high purity de-ionized water (18 M Ω cm^{-1}) obtained from a Milli-Q water purification system (Millipore, Bedford, USA). High purity reagents or analytical reagent-grade were employed for the preparation of all solutions. Stock standard solutions of zinc and manganese (1000 mg L^{-1}) were prepared by dissolving appropriate amount of the solid in 2% HNO_3 (v/v). Working solutions were prepared daily by dilution of stock solutions and adding appropriate amount of nitric acid and perchloric acid. One thousand mg L^{-1} phenol solution was prepared by dissolving appropriate phenol in de-ionized water and then kept at around 0 °C in fridge. When used, the solution was diluted to 25 mg L^{-1}. De-ionized water was used as carrier solution.

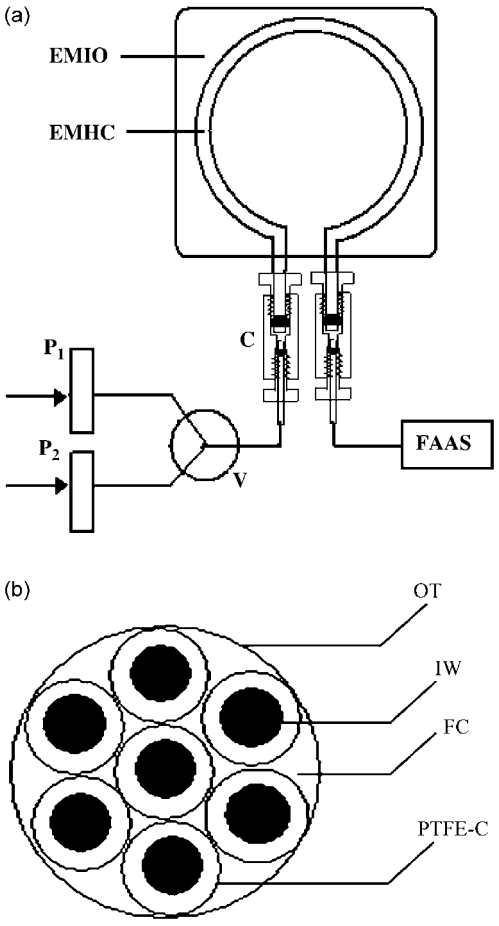

Fig. 1. (a) The schematic diagram of the FI-FAAS with on-line digestion manifold. P_1 and P_2, peristaltic pump; V, three-way valve; C, connector; EMHC, electromagnetic heating column; EMIO, electromagnetic induction oven; FAAS, flame atomic absorption spectrometer. (b) The sectional view of EMHC. OT, outer tube; FC, solution flow channel; PTFE-C, PTFE coil; IW, iron wires.

2.3. Sample preparation

Tea leaf samples were firstly dried at 60 °C to a constant weight. After grinding to pass through a 200-mesh sieve, tea leaf samples were stored in a desiccator. Pre-digested sample solutions were prepared by mixing 0.5000 g and 0.1000 g tea leaf samples with 100 mL acid decomposition solution (3.5 mol L^{-1} HNO_3 + 1.0 mol L^{-1} $HClO_4$) respectively for Zn and Mn determination. GBW 07605 (tea), GBW 08505 (tea) and GBW 07602 (bush branch and leaves) obtained from China National Research Center for Certified Reference Materials were subjected to the same treatment except for grinding.

2.4. General procedure

Before EMIO starting to work, expelled air from digestion coil by pumping de-ionized water and made sure that the digestion coil was full of water, because the high temperature of iron wires would damage the EMHC without water.

The flow system is depicted in Fig. 1(a). Firstly, set the EMIO working power at 150 W and warmed-up for 60 s. The sample solution was drawn by P_1 at a flow rate of 3.6 min L^{-1} for 15 s. Then, P_1 was turned off and the three-way valve was switched over to let water carrier be pumped in by P_2 at the same flow rate for 35 s. After that, another sample solution was drawn from PTFE bottle. Calibration standards were operated in the same way. The main reason for operating in this way was to prevent interaction between two sample zones, which would generate a crossover between two absorption peaks. Besides, samples were transported to the spectrometer by de-ionized water carrier stream can save consumption of samples and acid digestion solution.

Off-line sample digestion was carried out by placing 0.5000 g and 0.1000 g tea leaf samples in PTFE vessels for Zn and Mn determination, respectively. After adding 4 mL conc. HNO_3 and 1 mL 30% H_2O_2, the vessels were placed in the microwave oven for off-line digestion. The digestion program consisted of two stages: stage 1 (120 °C, 0.5 Mpa, 5 min); stage 2 (140 °C, 1.0 Mpa, 10 min). When digestion was complete, the solutions were transferred to 100 mL volumetric flasks and made up to volume by washing the PTFE vessels with de-ionized water.

3. Results and discussion

3.1. Optimization of EMIH parameters

EMIH is a fundamental extension of Maxwell's equations. A magnetic field oscillating transverse to the surface of the heated material and induces eddy currents in a thin-layer region beneath the surface of the heated material, then the material can be directly heated on the basis of Joule's law. The energy required for eddy currents to circulate around the working material within the induction area depends on power absorption p from electric field, which can be written as Eq. (1) [23]:

$$p = 0.5 f\varepsilon_0\varepsilon' E^2 \tan\delta \quad (1)$$

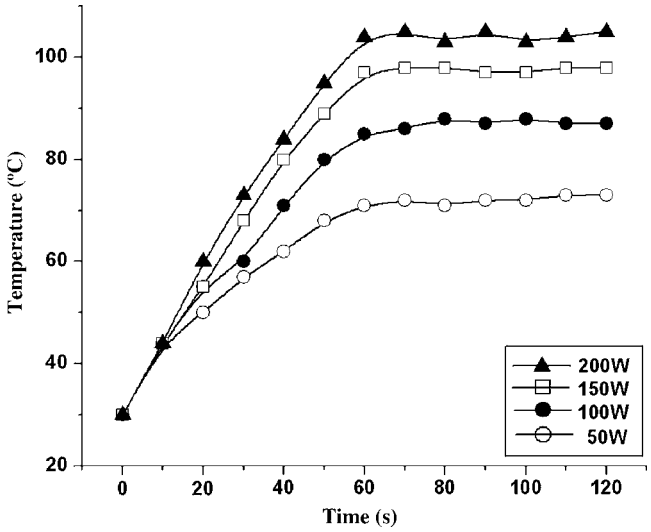

Fig. 2. Relationship between temperature and heating power of EMIO.

where f is the alternating current frequency, ε_0 the permittivity of free space, ε' the real component of the dielectric response, E the electric field intensity, $\tan\delta$ is the loss tangent of the material. The loss tangent can be separated into two parts: dipole relaxation ($\tan\delta_a$) and the conduction current (ohmic) components ($\tan\delta_s$):

$$\tan\delta = \tan\delta_a + \tan\delta_s = \frac{\varepsilon''}{\varepsilon_0\varepsilon'} + \frac{\sigma}{f\varepsilon_0\varepsilon'} \quad (2)$$

where σ represents the material conductivity and ε'' is the imaginary part of the dielectric permittivity associated with polarization relaxation. Eq. (1) in combination with Eq. (2) indicates that power absorption can be increased by increasing f and E, as well as by selecting high conductivity material. Iron and steel are two commonly used ferromagnetic materials. Compared with steel, iron has higher conductivity, so it was selected as the heating material in our work.

The thin-layer region beneath the heated material is defined as the penetration depth, which can be described by:

$$\delta = \frac{1}{\sqrt{\pi\mu\sigma f}} \quad (3)$$

where μ is the magnetic permeability. Calculated by Eq. (3), the penetration depth of iron was about 0.02 mm when the alternating current frequency of EMIO is 20,000 Hz. It indicates that heat energy mainly concentrates on the heated material surface. Therefore, high heating efficiency could be obtained when sample solution flows along the surface of PTFE-coated iron wires in EMHC.

Firstly, we investigated the relationship between temperature and different heating powers (50 W, 100 W, 150 W, 200 W) at a constant flow rate of 3.6 mL min^{-1} (Fig. 2). The results indicated that the required digestion temperatures could be obtained by means of selecting heating powers. The time of reaching equilibrium temperature was about 60 s, so a warm-up period of 60 s was needed before measurement of sample.

Table 2
The appropriate EMHC length for different sample weights

Sample weight (g)	EMHC length (cm)
0.0250	20
0.0500	20
0.1000	25
0.2500	35
0.5000	50
0.8000	90
1.0000[a]	–

[a] Sample caused the clogging of solution flow channel.

The effect of heating temperature on signal intensity was evaluated ranging from room temperature (30 °C) to 105 °C. It was found that the signal intensity increased till the temperature up to 95 °C, then reached a plateau. When the temperature of sample solution was over 100 °C, lots of bubbles would form and affect FAAS determination. Therefore, the heating temperature was set at 98 °C, and the corresponding heating power was 150 W.

The dilution factor and sample zone extension were considered to choose the dimension of EMHC. As for FAAS detection, the appropriate dispersion coefficient of FI system is about 1–2 [24]. Larger EMHC diameter causes obvious expansion of sample zone, which leads to the decrease of absorbance signal. On the other hand, the EMHC should have adequate diameter for sufficient sample digestion time at a certain flow rate. For these reasons, a 4.2 mm i.d. PTFE tube compactly packed with seven 1.4 mm o.d. PTFE-coated iron wires was used as the EMHC. Here, its effective diameter was about 1 mm.

For selecting an appropriate EMHC length, both the stability and the intensity of absorption signal were taken into account in our work. Shorter EMHC length resulted in incomplete digestion and poor absorption intensity stability due to having small particles in solution. Furthermore, the dissolved solids even provoked the problem of burner clogging. The appropriate EMHC length was obtained when the absorption signal reached a plateau and did not increased along with the length of EMHC. The results in Table 2 indicated that the maximum allowance of sample weight was 0.8000 g in present EMHC, and sample weight more than 1.0 g would cause blockage of solution flow channel. Considering the concentrations of Zn and Mn in tea leaf samples, sample weight of 0.5000 g and 0.1000 g were chosen for the determination of Zn and Mn in our experiments. Accordingly, a 50 cm length EMHC was used for further determinations. It should be note that the length of EMHC would need a proper optimization for new applications.

3.2. Optimization of FI parameters

The effect of inner diameters of both inlet and outlet tubing of EMHC on dispersion coefficient was studied by detecting the ultraviolet absorption intensity of 25 mg L^{-1} phenol solution at its absorption peak 270 nm. Inner diameters of 0.5 mm, 0.8 mm, 1.0 mm, 1.2 mm and 1.5 mm tubings were studied. The absorption intensity of phenol solution was shown in Fig. 3. The largest signal intensity could be achieved when the diameters of inlet and outlet tubing were both 1.0 mm, which was in accordance with the effective diameter of EMHC. Thus 1.0 mm i.d. PTFE coil was selected as inlet and outlet tubing.

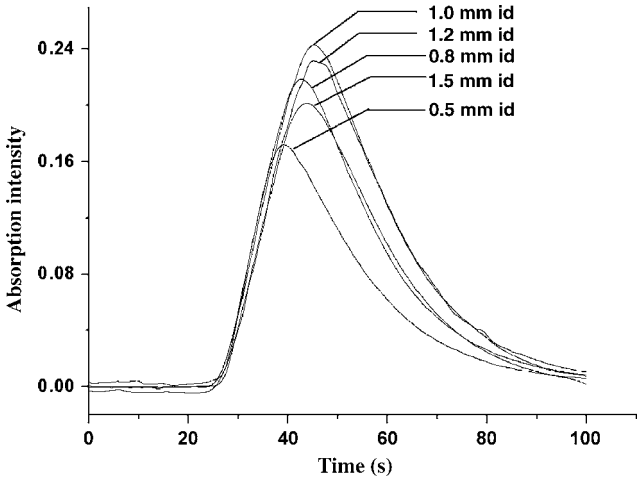

Fig. 3. Effect of different inner diamerers of inlet and outlet tubing of EMHC on dispersion coefficient of FI system by detecting the ultraviolet absorption intensity of 25 mg L^{-1} phenol solution at 270 nm.

Influence of sample volumes on dispersion coefficient was also studied by detecting the ultraviolet absorption intensity of 25 mg L^{-1} phenol solution. It was found that the signal intensity increased as the sample volume increased from 0.3 mL to 1.5 mL (Fig. 4), i.e. increasing sample volume would decrease dispersion coefficient. On the other hand, larger sample volume resulted in a lower analytical throughput. Therefore, 0.9 mL sample volume was chosen in our analytical procedure. Here, the absorption intensity of 25 mg L^{-1} phenol solution was 0.38; the dispersion coefficient of EMHC was 1.80. At the flow rate of 3.6 mL min^{-1}, an integral sample determination needed 50 s, so an analytical throughput of 72 h^{-1} was achieved.

The effect of varying the flow rate on absorption intensity was investigated in the range of 2–6 mL min^{-1}. By increasing flow rate, the absorption intensity could be strengthened. This is

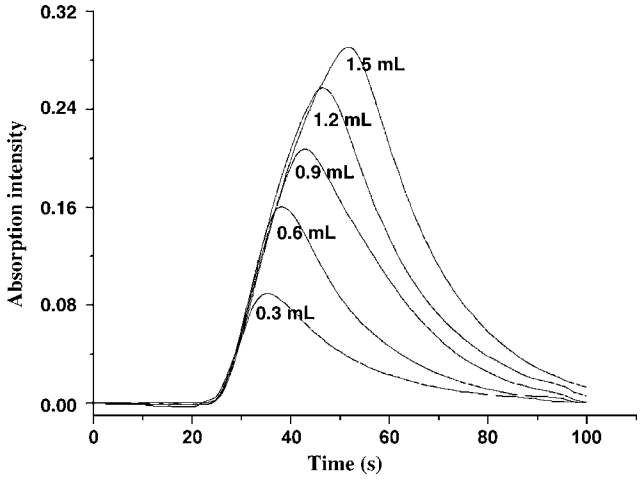

Fig. 4. Effect of different sample volumes on dispersion coefficient of FI system at the flow rate of 3.6 mL min^{-1} by detecting the ultraviolet absorption intensity of 25 mg L^{-1} phenol solution at 270 nm.

Table 3
Recoveries of Zn and Mn from tea certified reference material GBW 07605 by using different digestion media ($n=6$) (%)

Total acid concentration (v/v)	The volume proportion of HNO_3 and $HClO_4$ (HNO_3:$HClO_4$)							
	8:1		4:1		8:3		2:1	
	Zn	Mn	Zn	Mn	Zn	Mn	Zn	Mn
20%	68	53	71	65	80	72	73	68
30%	82	76	86	90	103	98	96	89
40%	88	81	92	89	96	103	94	102
50%	92	101	104	97	102	105	98	101

Table 4
Analytical results of Zn and Mn in tea leaf samples ($n=6$) ($\mu g\,g^{-1}$)

Sample	Found value[a]		Found value[b]		Found value[b,c]		Recovery[c] (%)	
	Zn	Mn	Zn	Mn	Zn	Mn	Zn	Mn
1	46.8 ± 1.5	1075 ± 15	45.0 ± 1.4	1065 ± 22	96.3 ± 1.6	2033 ± 31	103	97
2	50.2 ± 1.9	952 ± 15	48.2 ± 1.2	965 ± 12	98.8 ± 1.5	1922 ± 26	101	96
3	53.1 ± 1.7	757 ± 10	52.5 ± 1.8	740 ± 15	99.7 ± 2.3	1637 ± 19	94	90
4	34.8 ± 0.8	1233 ± 18	35.0 ± 1.1	1225 ± 24	83.5 ± 1.9	2280 ± 27	97	106
5	39.4 ± 1.2	1078 ± 17	38.5 ± 0.8	1090 ± 13	87.3 ± 1.7	2054 ± 25	98	96

[a] Results obtained by using the off-line digestion.
[b] Results obtained by using the proposed method.
[c] Results obtained after adding 50 $\mu g\,g^{-1}$ Zn and 1000 $\mu g\,g^{-1}$ Mn.

similar to the previous report that flow rate higher than the uptake rate of FAAS (3.5 mL min^{-1}) would provide better signals [25]. Higher flow rate was not recommended because the residence time in EMHC was too short for sample to be decomposed well for FAAS detection, whereas lower flow rate would prejudice the analytical throughput. Karlberg and Pacey has pointed out that to a selected FI system, flow rate did not affect dispersion coefficient in the range of 1.6–4 mL min^{-1} [26]. So the flow rate of 3.6 mL min^{-1} was selected in our work.

3.3. Selection of acid decomposition solution

For on-line sample digestion, concentrated nitric acid should be avoided due to fume generation in lab ambient and observed corrosion of equipment. Firstly, three diluted acids (HNO_3, $HNO_3 + HClO_4$, $HNO_3 + HCl$) at a total acid concentration of 50% (v/v) were studied. It was observed that $HNO_3 + HClO_4$ gave better recoveries for tea certified reference material GBW 07605. Then, the concentrations of HNO_3 and $HClO_4$ were selected in a systematic way (as checked the recoveries of Zn and Mn from GBW 07605) (Table 3). The results indicated that HNO_3 and $HClO_4$ at a volume proportion of 8:3 was more efficient, and the total acid concentration of 30% (v/v) was sufficient to allow the interest elements extraction (recoveries of Zn and Mn were 103% and 98%), so it was selected as acid decomposition solution, i.e. the composition of the acid decomposition solution was 3.5 mol L^{-1} HNO_3 + 1.0 mol L^{-1} $HClO_4$.

3.4. Analytical performance and method validation

The calibrations were performed by using standard solutions of Zn and Mn prepared in acid decomposition solution. The regression equations were $A = 0.020 + 0.592C_{Zn}$, $r = 0.997$ and $A = 0.006 + 0.174C_{Mn}$, $r = 0.999$; where C was the concentration expressed in $\mu g\,mL^{-1}$. The calibrations graphs of Zn and Mn were linear up to 0.6 $\mu g\,mL^{-1}$ and 4 $\mu g\,mL^{-1}$. Detection limits (3σ) were 4.2 $\mu g\,L^{-1}$ for Zn and 3.0 $\mu g\,L^{-1}$ for Mn. The repeatabilities, evaluated by the relative standard deviation (R.S.D.) for certified reference material were 3.2% for Zn and 3.6% for Mn ($n=10$).

Table 5
Results of Zn and Mn determination in certified reference material

	Certified value ($\mu g\,g^{-1}$)		Found value ($\mu g\,g^{-1}$)	
	Zn	Mn	Zn	Mn
GBW 07602	20.6 ± 2.2	58 ± 6	19.8 ± 0.5	60 ± 3
GBW 07605	26.3 ± 0.9	1240 ± 40	25.6 ± 0.8	1228 ± 26
GBW 08505	38.7 ± 3.9	766 ± 28	39.2 ± 1.5	745 ± 15

The concentration was defined as mean value ± S.D. ($n=3$).

Analytical results obtained by the proposed method were in good agreement with the results obtained by using off-line digestion (Table 4). The concentrations of Zn and Mn in tea leaf samples were found to range from 33.9 $\mu g\,g^{-1}$ to 54.3 $\mu g\,g^{-1}$ and from 725 $\mu g\,g^{-1}$ to 1249 $\mu g\,g^{-1}$, respectively.

The proposed method was validated by analyzing three certified reference materials: GBW 07605 (tea), GBW 08505 (tea) and GBW 07602 (bush branch and leaves). The results were in good agreement with certified values (Table 5).

4. Conclusion

The present work has demonstrated a new concept for sample digestion based on electromagnetic induction heating technique.

High heating efficiency could be obtained due to heating energy was concentrated just in a thin layer beneath the surface of heated material. The method also exhibited superiority in such characteristics as simple sample preparation, less reagent consumption, high sample throughput as well as lower instrumental and operating costs. It may prove to be a useful new alternative to the conventional used off-line digestion and focused microwave-assisted heating technique.

Acknowledgement

This work is supported by the National Nature Science Foundation of PR China (no. 20675074).

References

[1] Y. Li, Y. Jiang, X.-P. Yan, W.-J. Peng, Y.-Y. Wu, Anal. Chem. 74 (2002) 1075.
[2] I. Karadjova, B. Izgi, S. Gucer, Spectrochim. Acta B 57 (2002) 581.
[3] E. Kenduzler, A.R. Turker, O. Yalcinkaya, Talanta 69 (2006) 835.
[4] V.A. Lemos, E.M. Gama, A.D. Lima, Microchim Acta 153 (2006) 179.
[5] B. Welz, Y.Z. He, M. Sperling, Talanta 40 (1993) 1917.
[6] R.S. Praveen, S. Daniel, T.P. Rao, S. Sampath, K.S. Rao, Talanta 70 (2006) 437.
[7] O. Wurl, O. Elsholz, J. Baasner, Fresenius J. Anal. Chem. 366 (2000) 191.
[8] Y. Wang, J.-H. Wang, Z.-L. Fang, Anal. Chem. 77 (2005) 5396.
[9] K. Prasad, P. Gopikrishna, R. Kala, T.P. Rao, G.R.K. Naidu, Talanta 69 (2006) 938.
[10] Y. Wang, M.-L. Chen, J.-H. Wang, J. Anal. Atom. Spectrom. 21 (2006) 535.
[11] K. Suvardhan, K.S. Kumar, D. Rekha, B. Jayaraj, G.K. Naidu, P. Chiranjeevi, Talanta 68 (2006) 735.
[12] Y.F. Lasheen, A.F. Seliman, A.A. Abdel-Rassoul, J. Chromatogr. A 1136 (2006) 202.
[13] N. Burham, S.M. Abdel-Azeem, M.F. El-Shahat, Anal. Chim. Acta 579 (2006) 193.
[14] S.P. Fill, E. Oliveira, P.V. Oliveira, J. Braz. Chem. Soc. 14 (2003) 435.
[15] J.A. Sweileh, Microchem. J. 65 (2000) 87.
[16] M.D. DeAlmeida, K.C. Leandro, C.V. DaCosta, R.E. Santelli, M. Dela-Guardia, J. Anal. Atom. Spectrom. 12 (1997) 1235.
[17] E.J. Davies, P.G. Simpson, Induction Heating Handbook, Mcgraw-Hill Book, Company Ltd., London, 1995.
[18] K. Thompson, Y.B. Gianchandani, J. Booske, R.F. Cooper, J. Microelectromech. Syst. 11 (2002) 285.
[19] S.-C. Chen, W.-R. Jong, J.-A. Chang, J. Appl. Polym. Sci. 101 (2006) 1174.
[20] R.F. Schiffmann, in: D. Clark, et al. (Eds.), Microwave Theory and Application in Material Processing III (Ceramic Transactions 59), The American Ceramic Society, Westerville, OH, 1995, pp. 7–16.
[21] L.-J. Shao, W.-E. Gan, Q.-D. Su, Anal. Chim. Acta 562 (2006) 128.
[22] L.-J. Shao, W.-E. Gan, W.-B. Zhang, Q.-D. Su, J. Anal. Atom. Spectrom. 20 (2005) 1296.
[23] C.A. Balanis, Advanced Engineering Electromagnetics, Wiley, New York, 1989.
[24] Z.-L. Fang, Flow Injection Analysis Method, Science Press, China, 1999, p. 11.
[25] P. Sooksamiti, H. Geckeis, K. Grudpan, Analyst 121 (1996) 1413.
[26] B. Karlberg, G.E. Pacey, Flow Injection Analysis: A Practical Guide, Elsevier, Amsterdam, New York, 1989.

Available online at www.sciencedirect.com
ScienceDirect
Talanta 72 (2007) 1519–1526
Talanta
www.elsevier.com/locate/talanta

Preparation of luminescent Cy5 doped core-shell SFNPs and its application as a near-infrared fluorescent marker

Xiaoxiao He, Jiyun Chen, Kemin Wang *, Dilan Qin, Weihong Tan

State Key Laboratory of Chemo/Biosensing and Chemometrics, College of Chemistry & Chemical Engineering, Engineering Center for Biomedicine, Institute of Life Science & Biological Technology, Hunan University, Engineering Research Center for Bio-Nanotechnology of Hunan Province, Changsha 410082, PR China

Received 3 December 2006; received in revised form 30 January 2007; accepted 30 January 2007
Available online 13 February 2007

Abstract

Cy5 dye is widely used as a biomarker in the research fields of life science because of its excitation at wavelengths above 600 nm where autofluorescence of bio-matter is much reduced. However, Cy5 dye could not be encapsulate into silica directly to form stable nanoparticles by using of the traditional methods. In this paper, an improved method had been developed to prepare Cy5 dye doped core-shell silica fluorescent nanoparticles (SFNPs), employing biomolecules conjugated Cy5 as the core material and silica coating produced from the hydrolysis TEOS (tetraethyl orthosilicate) in the water-in-oil microemulsion. To obtain stable Cy5 dye doped SFNPs with core-shell structure, five kinds of biomolecules with different iso-electric point (p*I*) have been selected to conjugate Cy5 for preparation of core-shell SFNPs. Results demonstrated that very bright and photostable Cy5 doped core-shell SFNPs could be both prepared by use of positive polysine conjugated Cy5 or IgG conjugated Cy5 as the core material, respectively. IgG conjugated Cy5 doped core-shell SFNPs was selected as a demonstration to be characterized and applied as a near-infrared fluorescent marker in cell recognition. The results showed that Cy5 doped core-shell SFNPs prepared by conjugating with a positive biomolecules IgG as the core material were luminescent and stable. About 110 Cy5 dye molecules could be doped in one nanoparticle with size of 42 ± 5 nm. The breast cancer cells had been selectively recognized by use of the near-infrared fluorescent marker based on the Cy5–IgG doped core-shell SFNPs. And the results demonstrated that this Cy5 doped core-shell SFNPs fluorescence marker was superior to the pure Cy5 dye marker for cell recognition in photostability and detection sensitivity.

Keywords: Cy5 dye; Core-shell SFNPs; Near-infrared fluorescent marker; Cell recognition

1. Introduction

The fluorophore, Cy5 dye, is one of the most important dyes that has been gotten important application in the research fields of life science, such as microarray-based analysis, DNA sequence, fluorescence immunoassay, flow cytometery, clinical diagnose and so on [1–4]. The absorption and the emission wavelengths of Cy5 dye are in the red spectral region, which is sufficiently removed from the intrinsic fluorescence of most biological tissues and the scatter of the glass service or solvent, thereby suppressing the background noise. However, Cy5 dye is also not stable in the ambient environment. Fare et al. reported Cy5 showed significant degradation when it was exposed to ozone levels of 5–10 ppb for periods as short as 10–30 s [5]. This degradation significantly affects the uniformity and reproducibility of fluorescent signals across DNA microarrays. A dye-protecting solution is usually needed to prevent both the Cy5 signal degradation and the associated loss of data quality at elevated ozone concentrations. Cooper and co-workers reported Cy5 was sensitive to proton concentration [6]. So it is important to provide a new technique to enhance the performance of Cy5 dye.

Recently, with development of nanotechnology and nanofabrication techniques, attention has also focused on synthesis of fluorophore-doped core-shell nanoparticles (NPs), which can protect the fluorophore from environmental factors because they are shielded inside a certain shell matrix. The fluorophore doped inside the shell matrix still demonstrated the fluorescence characteristics [7–33]. Among the fluorophore-doped core-shell NPs, fluorophore doped silica fluorescent nanoparticles (SFNPs)

* Corresponding author. Tel.: +86 731 8821566; fax: +86 731 8821566.
E-mail address: kmwang@hnu.cn (K. Wang).

0039-9140/$ – see front matter © 2007 Published by Elsevier B.V.
doi:10.1016/j.talanta.2007.01.069

prepared by nucleation and shell coating through the hydrolysis of silane in water in oil (W/O) microemulsion containing value of facilitating bio-modification, biocompatibility, higher detection sensitivity and photostability has been well applied in cell recognition, bacterial detection, DNA analysis and so on [19–33]. However, the Cy5 dye could not be encapsulate into silica directly to form stable core-shell SFNPs for electrostatic repulsion between the negative Cy5 dye and the negatively charged silica matrix in neutral pH [34]. Zhou [35] had developed a method to prepare cyanine dye-doped silica core-shell NPs by using Au colloid conjugated with dye molecules as the core. The Au colloid core conjugated with dye molecules was first prepared through the thiol functional group of the cyanine dyes labeled oligonucleotide with the surface of the Au colloid, and then embedded in the silica shell produced from the hydrolysis of organosaline. Cy5-doped Au/silica core-shell NPs and Cy3-doped Au/silica core-shell NPs were successfully prepared by this method. While this method suffered from the complicated process and cost of the thiolated oligonucleotide. Herein, there is still considerable incentive to develop simple and economical approaches for preparation of Cy5 dye doped NPs.

In this paper, we demonstrated a method for preparation of an improved class of Cy5 doped core-shell SFNPs and used it as a highly sensitive and photostable label in cells recognition. To successfully entrap Cy5 inside a silica matrix, Cy5 was first conjugated with biomolecules such as protein or peptide. Then the Cy5 doped core-shell SFNPs have been prepared, employing biomolecules conjugated Cy5 as the core and the silica produced from the hydrolysis TEOS (tetraethyl orthosilicate) as the shell by use of the reported water-in-oil microemulsion technique [24]. We have, respectively, investigated five kinds of biomolecules with different p*I* conjugated Cy5 as the core material. The results displayed that very bright and photostable Cy5 doped core-shell SFNPs can be both prepared by use of positive IgG conjugated Cy5 or polysine conjugated Cy5 as the core material. IgG conjugated Cy5 doped core-shell SFNPs was further selected as a demonstration to be characterized and applied as a marker in cell recognition. The results showed that the stable IgG conjugated Cy5 doped core-shell SFNPs were uniform in size and still displayed maximum excitation in the near-infrared spectral region. A novel near-infrared fluorescence marker has been based by use of the Cy5–IgG doped core-shell SFNPs. The breast cancer cells have been selectively recognized by use of this fluorescence marker. And the results demonstrated that this stable Cy5 doped core-shell SFNPs fluorescence marker was superior to the pure Cy5 dye marker in detection sensitivity for its doping about 110 Cy5 dye molecules in one nanoparticle. It would provide a new technology to enhance the application of Cy5 dye in the research of biomedicine.

2. Experimental

2.1. Reagents and materials

Cy5 NHS ester was obtained from Amersham. C-erb-B2 was bought from Beijin Zhongsha Biotechnologies Co. Ltd. All other chemicals were of reagent grade and were used without further purification. Double distilled water was used for all the experiments. Breast cancer cells (MCF-7) were provided by the Cell Center of our lab. Cells were inoculated at a density of 1×10^5 cells/well in six-well plate with a glass slide on the bottom of the plate at 37 °C on the RPMI1640 (GIBCO USA) medium with 10% fetal calf serum in a 5% CO_2.

2.2. Instruments

All fluorescence measurements were performed by Hitachi F-2500 fluorescence spectrophotometer (Kyoto, Japan). The SFNPs were measured with Transmission Electron Microscope (TEM) (JEOL JEM-1230). Cells and SFNPs were visualized by use of FV500-IX70 laser confocal microscopy (Olympus Japan). Cells were cultured by use of CO_2 culture ark (Nu-4750E NUAIR U.S.A.).

2.3. Experimental details

2.3.1. Preparation of Cy5 doped core-shell SFNPs

Cy5 was first conjugated with a kind of biomolecules as the reported methods [36]. In this paper, polylysine (MW 70,000–15,000), IgG (MW 150,000), BSA (MW 68,000), insulin (MW 5,700) and pepsin (MW 42,500) have been used to conjugate Cy5, respectively. Then different NPs was synthesized, respectively, by selecting Cy5–polylysine, Cy5–IgG, Cy5–BSA, Cy5–insulin, Cy5–pepsin and pure Cy5 dye as the core materials, employing water-in-oil microemulsion technique as reported before [21]. Briefly, a solution containing cyclohexane, TritonX-100, *n*-hexanol (with volume ratio 4:1:1) was mixed with adequate water and stirred for 5 min, followed by the addition of aqueous biomolecules conjugated Cy5 dye solutions, respectively, as the core material. In the presence of TEOS, polymerization reaction was initiated by adding concentrated NH_4OH. The reaction was allowed to continue for 24 h to produce silica NPs. Then, the NPs were isolated by acetone and washed with ethanol and water for several times to remove surfactant molecules.

2.3.2. Investigation on formation of stable Cy5 doped core-shell SFNPs

In order to detect whether the stable Cy5 doped core-shell SFNPs can be formed by use of different biomolecule conjugated with Cy5 dye as the core material, the prepared NPs were suspended in water and washed for many times. The relative fluorescence intensity of the water-washed NPs was, respectively, measured. At the same time, the water-washed NPs were all imaged, respectively, with confocal microscopy.

2.3.3. Characterization of the stable Cy5 doped core-shell SFNPs

IgG conjugated Cy5 doped core-shell SFNPs was selected as a demonstration to be characterized. The shape and the size of the Cy5–IgG doped core-shell SFNPs was analyzed with TEM. The leakage of Cy5 from the silica matrix, the photostability and the spectrum characterization of Cy5–IgG doped core-shell SFNPs have also been investigated.

2.3.4. Application of the near-infrared fluorescent marker based on Cy5–IgG doped core-shell SFNPs for cell recognition

2.3.4.1. Biological modification of Cy5–IgG doped core-shell SFNPs. The C-erb-B2 antibody was coupled to the Cy5–IgG doped core-shell SFNPs by using the followed cyanogen bromide (CNBr) method as previous reported [24]. Prepared stable Cy5–IgG doped core-shell SFNPs were suspended in 2 mL 2 mol L^{-1} sodium carbonate solution and ultrasonicated for 10 min. Solution of CNBr in acetonitrile (2 mg mL^{-1}) was then added dropwise to the NPs suspensions under stirring for 10 min at room temperature. The activated particles were washed successively with ice-cold water and PBS buffer (pH 7.6). Then, the activated NPs were re-suspended in the PBS buffer (pH 7.6). 20 μL (1 mg mL^{-1}) C-erb-B2 antibody diluted in PBS buffer was added to these NPs suspension, and the mixture was stirred continuously for 24 h at 4 °C. The final product was washed, re-suspended in PBS buffer and stored at 4 °C for future experiments.

2.3.4.2. Incubation of the C-erb-B2 antibody modified Cy5–IgG doped core-shell SFNPs with breast cancer cells. The cells were cultured until the cover rate on the glass slide reached 70–90%. After the removal of the medium in the six-well plate, the glass slide with cells was washed thrice with PBS buffer, and then fixed with 4% paraformaldehyde solution for 10 min at 4 °C. The cells were first blocked with 500 μL 1% BSA for 1 h at room temperature, and washed with pH 7.4 PBS buffer for three times. Then the cells on the glass slide were incubated with C-erb-B2 antibody modified Cy5–IgG doped core-shell SFNPs suspension for 30 min at 37 °C. After incubation, unbound SFNPs were washed away with PBS buffer. The cells were observed and analyzed with confocal microscopy.

3. Results and discussions

3.1. The effect of different biomolecules conjugated Cy5 dye on formation of stable Cy5 doped core-shell SFNPs

Different NPs was synthesized, respectively, by selecting Cy5–polylysine, Cy5–IgG, Cy5–BSA, Cy5–insulin, Cy5–pepsin and pure Cy5 dye as the core materials. The relative fluorescence intensity of the prepared NPs after washing with water for many times was shown in Fig. 1. The relative fluorescence intensity of the NPs adopted Cy5–polylysine and Cy5–IgG as core material, respectively, still kept over 60% of their initial intensity after washing with water for many times. However, the relative fluorescence intensity of the NPs adopted Cy5–BSA, Cy5–insulin, Cy5–pepsin and pure Cy5 dye as core material, respectively, was all below 20% of its initial intensity. The reason for this is that both of IgG and polylysine demonstrated positive at natural pH because the p*I* of IgG (p*I* = 8.0) and polylysine (p*I* = 9.7) are all over 7. Then the negative core material Cy5 was attached a positive bimolecular, and can be easily doped inside the silica shell to form relatively stable core-shell SFNPs. Especially the p*I* of polylysine is much high, and there is almost no leakage from the shell after it was doped inside to form core-shell SFNPs. While the p*I* of BSA (p*I* = 4.8), insulin (p*I* = 5.3) and pepsin (p*I* = 1.0) is below 7, which caused they are negative at natural pH. Stable core-shell SFNPs all cannot be formed by attaching BSA, insulin or pepsin to Cy5.

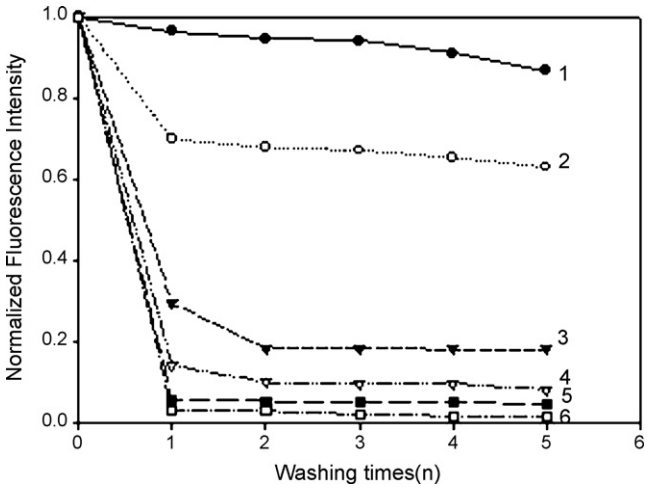

Fig. 1. The relative fluorescence intensity of prepared different Cy5 NPs after washing with water for many times. (Curve 1, 2, 3, 4, 5 and 6 represented the, respectively, prepared Cy5 NPs by using Cy5–PLA, Cy5–IgG, Cy5–BSA, Cy5–pepsin, Cy5–insulin and pure Cy5 dye as the core materials.)

At the same time, the prepared NPs were all imaged with confocal microscopy after washing with water for many times, as shown in Fig. 2. Both sets were collected under the same experimental conditions (PMT 701V, Laser intensity 10.0, gain power 3.5). The fluorescence of the silica NPs adopted Cy5–polylysine and Cy5–IgG as core material, respectively, were both visible after they were washed with water for five times. The NPs prepared adopted Cy5–BSA, Cy5–insulin, Cy5–pepsin as core material, respectively, demonstrated fluorescent when they were not washed with water. However, the fluorescence of the NPs were all invisible after they were washed with water for five times. And no fluorescence can be observed by only use of pure Cy5 dye as the core material for preparation of Cy5 doped core-shell silica NPs. The confocal microscopy imaging of the prepared NPs also demonstrated that very bright and photostable Cy5 doped core-shell SFNPs could be both prepared by use of positive polylysine conjugated Cy5 or IgG conjugated Cy5 as the core material, respectively. In subsequent experiments, IgG conjugated Cy5 doped core-shell SFNPs was selected as a demonstration to be characterized and applied as a near-infrared fluorescent marker in cell recognition.

3.2. The characteristics of stable Cy5–IgG doped core-shell SFNPs

3.2.1. Transmission electron microscope (TEM) images of the Cy5–IgG doped core-shell SFNPs

The Cy5–IgG doped core-shell SFNPs suspension was added dropwise onto the carbon-coated copper membrane, and dried at room temperature. The size was measured by Hitachi-800 transmission electron microscope. The results from TEM

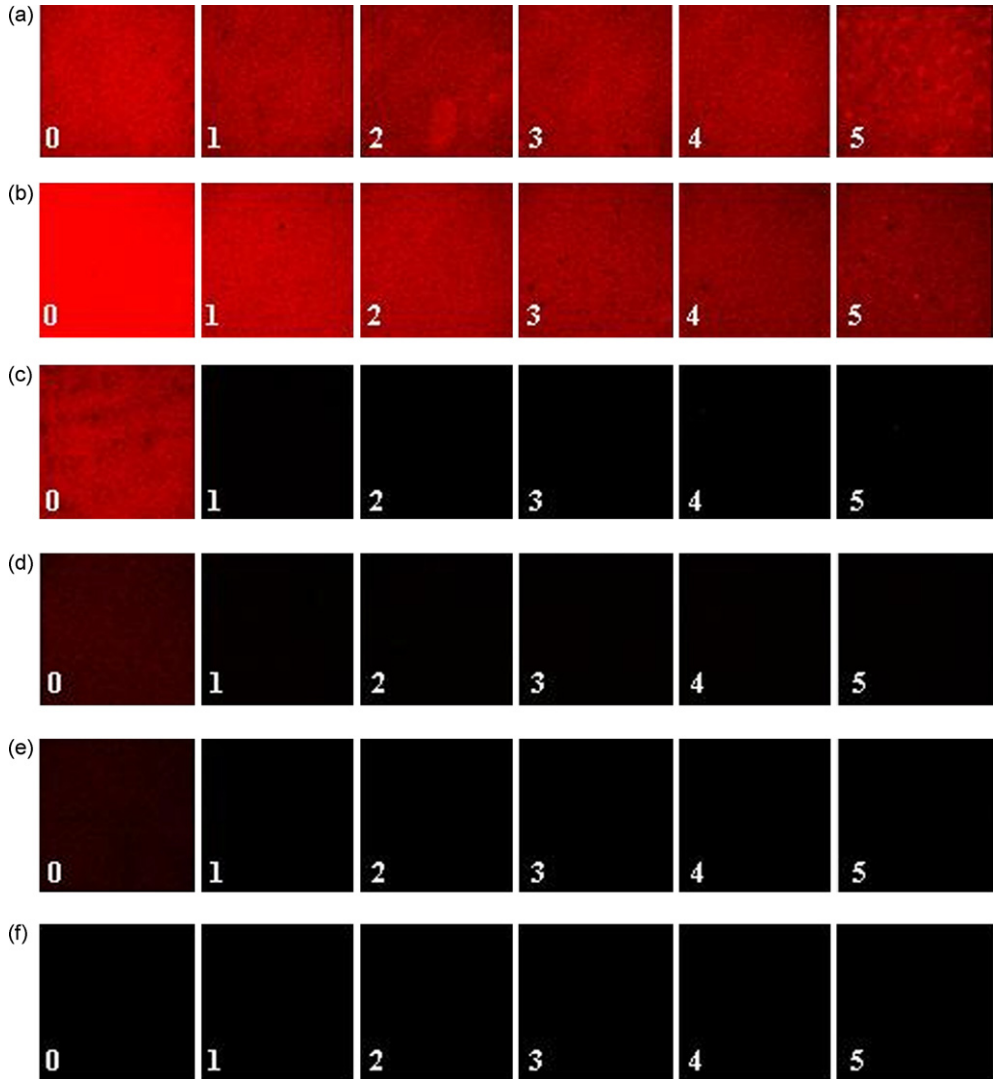

Fig. 2. Fluorescence image of the Cy5 silica NPs washed for five times ((a) Cy5–PLA NPs; (b) Cy5–IgG NPs; (c) Cy5–BSA NPs; (d) Cy5–insulin NPs; (e) Cy5–pepsin NPs; (f) pure Cy5 dye NPs. 0,1,2,3,4,5 were represented, respectively, the prepared NPs after washing with water for different times).

(Fig. 3) showed that the NPs were 42 ± 5 nm in sizes and uniform.

3.2.2. *The amount of the Cy5 dye molecules doped per nanoparticles*

The Cy5 dye molecules per Cy5–IgG doped core-shell SFNPs have been determined by use of viscosity and TEM measurements (viscosity/TEM method) [37]. The viscosity of the NPs suspension was first determined using a cone plate viscometer (LVDV-III+cp) at 25 °C. Then the volume fraction of suspended NPs was derived by Einstein in 1906, see Eq. (1).

$$h/h_0 = 1 + 2.5\,\Phi \tag{1}$$

where h is the viscosity of the NPs suspension, h_0 is the viscosity of the solvent without NPs (so h/h_0 is the relative viscosity), and Φ is the volume fraction of NPs. The viscosity determination showed that viscosity of the Cy5 doped core-shell SFNPs is 1.09, and the solvent is water. So the volume fraction of suspended NPs is 0.036. And the total volume of Cy5 NPs prepared in one time is 0.108 cm^3. As the TEM characterization showed that the Cy5 doped core-shell SFNPs prepared by using Cy5–IgG as core material were uniform in size. To determine the amount of the Cy5 dye molecules per NPs, the number of the Cy5–IgG doped core-shell SFNPs per volume is obtained by dividing the total volume of NPs per volume solution, Φ, by the average volume of a NPs obtained from the TEM, see Eq. (2).

$$N = \Phi/4/3\pi(d/2)^3 \tag{2}$$

where N is the number of NPs/volume, Φ is the volume fraction of particles determined by viscosity, $4/3\pi(d/2)^3$ is the average volume of a Cy5–IgG doped core-shell SFNPs, and d is the volume-weighted diameter determined by TEM. The average size of the Cy5–IgG doped core-shell SFNPs is 42 nm. And then the number of the NPs is 2.79×10^{15}. And the amount of the Cy5 dye molecules per NPs is then equal to the Cy5 dye weight per unit volume, divided by the number of NPs per unit volume. The total amount of the Cy5 dye per unit volume can be derived through the absorption. The result showed that the

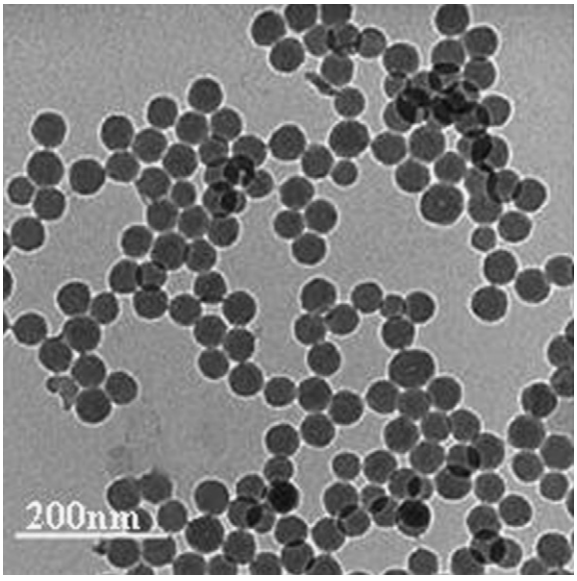

Fig. 3. TEM image of Cy5–IgG doped core-shell SFNPs at 17,5000× magnification.

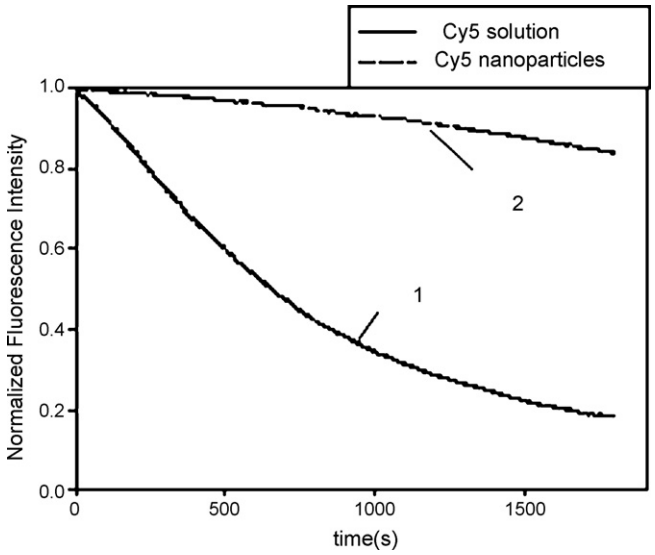

Fig. 4. Photostability experiment of pure Cy5 dye and Cy5–IgG doped core-shell SFNPs. All dispersed in a slide with excitation from a laser confocal microscopy (PMT 701V; Laser intensity 25.0). Curve 1: photostability of Cy5 dye; Curve 2: photostability of Cy5–IgG NPs.

total amount of the Cy5 dye per unit volume is 0.4 mg. So there were about 110 Cy5 dye molecules per SFNPs.

3.2.3. Spectroflurometric measurements of the Cy5–IgG doped core-shell SFNPs suspensions

Spectroflurometric measurements have also been used to characterize Cy5–IgG doped core-shell SFNPs. The maximum excitation and maximum emission of pure Cy5 dye solution were, respectively, at 650 nm and at 664 nm. And the Cy5–IgG doped core-shell SFNPs suspension showed maximum excitation at 653 nm and maximum emission at 667 nm. Compared to the pure Cy5 dye solution, the complete spectrum of the SFNPs suspensions was only red-shifted by 3 nm, indicating that the spectra characterization of the Cy5 dye had not changed greatly when it was conjugated with IgG to be doped inside the silica NPs. Then the Cy5–IgG doped core-shell SFNPs might be used as a near-infrared fluorescent marker in bioanalysis.

3.2.4. Photostability of Cy5 dye in the core-shell SFNPs

We have investigated the photostability of Cy5–IgG doped core-shell SFNPs in aqueous phase. The Cy5–IgG doped core-shell SFNPs was taken for the photobleaching experiment in solution phase with confocal microscopy. Both sets were collected under the same experimental conditions (PMT 701 V, Laser intensity 25.0, gain power 3.5). The samples were excited for 1800 s by successive scans. The average intensity was recorded and normalized to its initial value. With reference to Fig. 4, the Cy5–IgG doped core-shell SFNPs showed a little photobleaching, the emission intensity decreased to 83.9% as that of before excited and the red signal were still clearly distinguished to the eye. However, the intensity of pure Cy5 dye dropped to 18.3% as that of before excited. The results clearly demonstrated that the photostability of Cy5 was gotten increased when it was conjugated to IgG and doped inside the silica matrix. The reason for this may be that the positive Cy5–IgG then can be well doped in the silica network through electrostatic interaction, and then the potential quenching substance was apart from the Cy5 molecules by the silica shell.

3.2.5. Cy5 leakage form the core-shell SFNPs

The leakage of Cy5 from the core-shell SFNPs was determined according to the changing of the fluorescence intensity of the NPs suspension. 0.1 mg prepared Cy5–IgG doped core-shell SFNPs was suspended in 1 mL PBS buffer. At scheduled intervals, SFNPs suspension samples were centrifuged for 15 min at 12,000 rpm and re-suspended in a new 1 mL PBS buffer. The total fluorescence intensity of Cy5 in the NPs suspension was analyzed. The emission intensity of the Cy5–IgG doped core-shell SFNPs suspension still kept 95% as that of initial intensity after incubation for 20 h in PBS buffer and washing six times, suggesting that the Cy5 doped core-shell SFNPs could effectively avoid Cy5 leakage.

3.2.6. Application of Cy5–IgG doped core-shell SFNPs as a near-infrared fluorescent marker for breast cancer cells recognition

3.2.6.1. Recognition of breast cancer cells by use of Cy5 doped core-shell SFNP as a near-infrared fluorescent marker. As shown in Fig. 5A, red aureola around the membrane was obvious in the field of view of the confocal microscopy, due to the binding of the C-erb-B2 labeled Cy5–IgG doped core-shell SFNPs to the membrane. On the contrary, the control experiments with only SFNPs unmodified with C-erb-B2 did not show any labeling signal around the breast cancer cells membrane, as shown in Fig. 5B. The control experiments with C-erb-B2 labeled Cy5 doped core-shell SFNPs did not show any labeling signal around the cos-7 cells membrane either (Fig. 5C). Above results clearly indicated that the Cy5–IgG doped core-shell SFNPs modified with antibody C-erb-B2 was able to perform as a selective

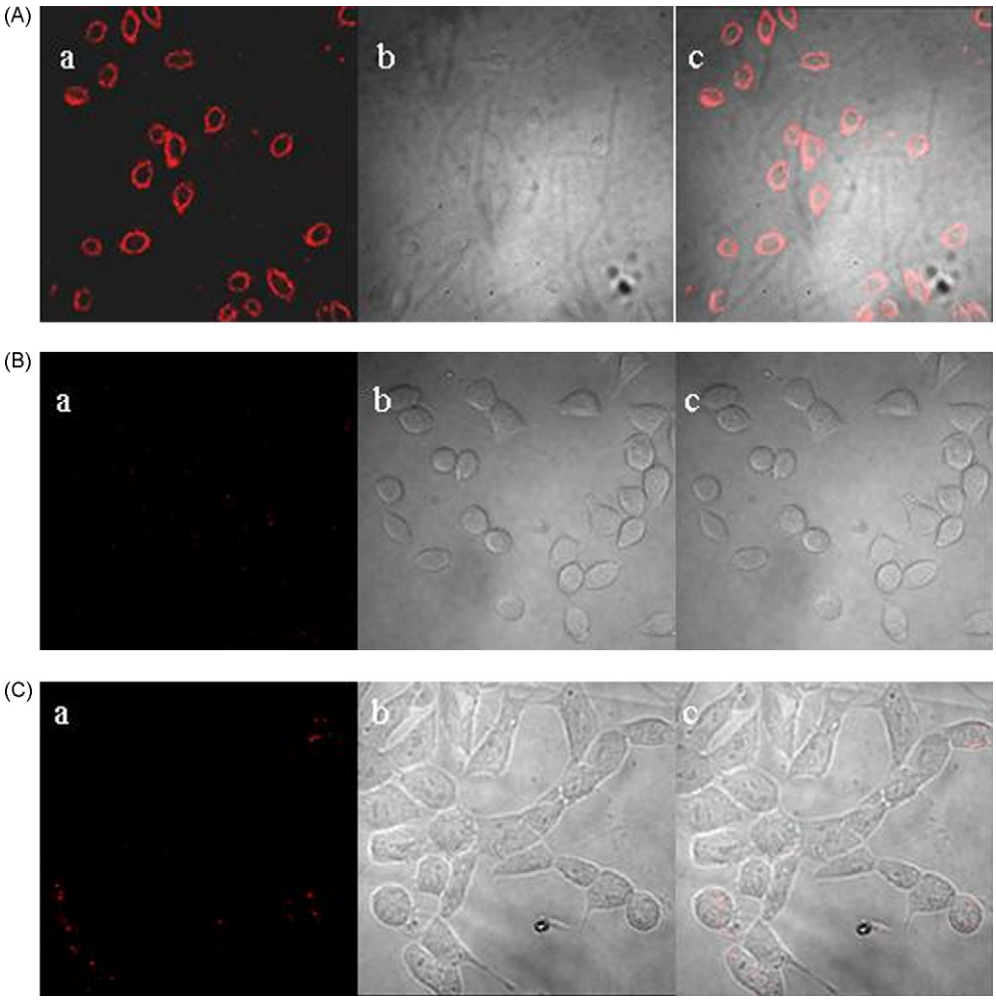

Fig. 5. Confocal microscopy images of recognized breast cancer cell (200×) by use of Cy5–IgG doped core-shell SFNPs as a near-infrared fluorescent marker, (A) breast cancer cell incubated with C-erb-B2 labeled Cy5–IgG doped core-shell SFNPs, (B) breast cancer cell incubated with only Cy5–IgG doped core-shell SFNPs, (C) cos-7 cells incubated with C-erb-B2 labeled Cy5–IgG doped core-shell SFNPs, a, b, and c represented fluorescent image, bright-field image and Merge image, respectively. (PMT 583V; Laser intensity10.0, gain power 1.9).

biomarker for breast cancer cell through receptor–ligand recognition.

At the same time, we have compared the sensitivity of the Cy5–IgG doped core-shell SFNPs conjugated with C-erb-B2 and pure Cy5 dye labeled with C-erb-B2 for recognition of the breast cancer cell. Both sets were collected under the same experimental conditions (PMT583V, Laser intensity 10.0, gain power 1.9). Fig. 6 show the labeled cells images obtained by these two label methods, respectively, strong red fluorescence around the cell membrane in the recognized breast cancer cells demonstrated based on the Cy5–IgG doped core-shell SFNPs label method, and the relative average fluorescence intensity of the label cells is 58.03. While the fluorescence around the cell membrane was a little weaker by use of pure Cy5 dye labeled

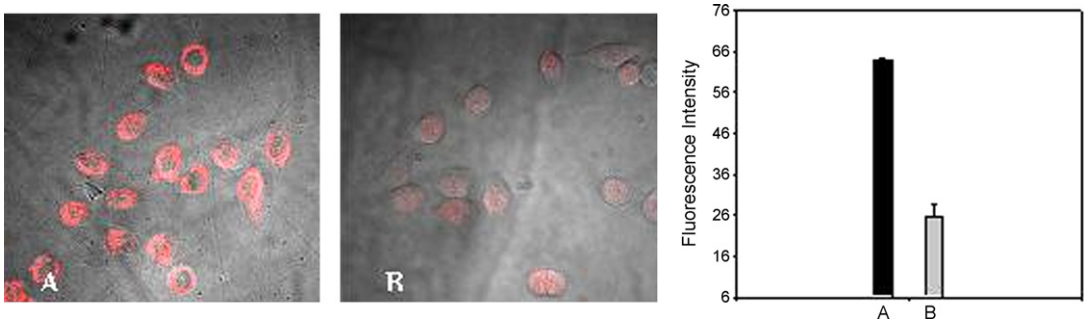

Fig. 6. Detection sensitivity comparison of different label method for recognition of breast cancer cells: (A) recognized cells by use of Cy5–IgG doped core-shell SFNPs label method; (B) recognized cells by use of pure Cy5 dye label method.

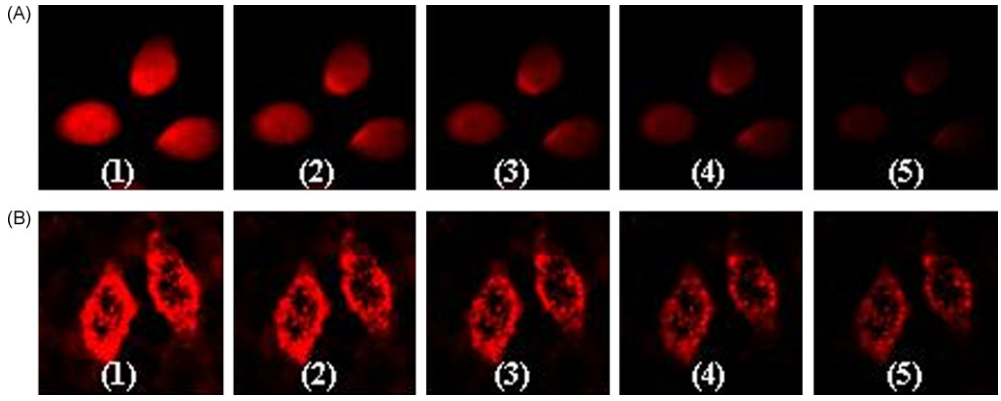

Fig. 7. Photostability comparison of recognized breast cancer cell labeled with pure Cy5 label method and Cy5–IgG doped core-shell SFNPs label method. (A) Photostability of recognized breast cancer cell with pure Cy5 label method. (B) Photostability of breast recognized breast cancer cell with Cy5 doped core-shell SFNP label method ((1) 0 min; (2) 3 min; (3) 5 min; (4) 8 min; (5) 10 min).

C-erb-B2 in the control experiment group, and the relative average fluorescence intensity of the label cells is 19.87. The main reason for higher sensitivity of Cy5–IgG doped core-shell SFNPs labels maybe the number of the dye coupled to the C-erb-B2 antibody. We have just determined there were about 110 Cy5 dye molecules per SFNPs. In this way, one antibody can be coupled to about 110 Cy5 dye molecules indirectly. However, there are only a few dye molecules coupled to one antibody in the pure dye label method.

3.2.6.2. The photostability of the Cy5–IgG doped core-shell SFNPs label method. To test the photostability of the Cy5–IgG doped core-shell SFNPs label method, the breast cancer cell were recognized with Cy5–IgG doped core-shell SFNPs modified C-erb-B2 and pure Cy5 dye labeled C-erb-B2, respectively, and was used for photobleaching experiments with confocal microscopy. Both sets were collected under the same experimental conditions (PMT 643V, Laser intensity 10.0, gain power 1.9). The samples were excited for 10 min by successive intense irradiation. Fluorescent images were acquired every few minutes. As shown in Fig. 7, the fluorescent intensity of breast cancer cell recognized by the pure Cy5 dye label method bleached very quickly after 10 min of continuous illumination, and the red signal of the dye was almost invisible. While cells recognized with Cy5–IgG doped core-shell SFNPs label method had strong fluorescence under the same illumination conditions, the red signal was still clearly distinguished to eyes. The results demonstrated that the Cy5–IgG doped core-shell SFNPs label provided more photostability in comparison with the pure Cy5 label method.

4. Conclusions

In this paper, we have developed a method for preparation of an improved class of Cy5 doped core-shell SFNPs and used it as highly sensitive and photostable label in cells recognition. The stable Cy5 dye doped core-shell silica fluorescent nanoparticles (SFNPs) were be easily prepared, employing positive biomolecules such as IgG or polysine conjugated Cy5 as the core material and silica coating produced from the hydrolysis TEOS (tetraethyl orthosilicate) in the water-in-oil microemulsion. The prepared stable Cy5 doped core-shell SFNPs were luminescent with about 110 Cy5 dye molecules doped in one nanoparticle and still displayed maximum excitation in the near-infrared spectral region, which made it could be used as a near-infrared fluorescent marker in bioanalysis. A fluorescent marker was based using Cy5–IgG doped core-shell SFNPs and has been successfully applied to recognize the breast cancer cells with higher photostability and detection sensitivity. It introduced a new technology to enhance the performance of Cy5 dye, which was very important for the application of Cy5 dye in bioanalysis and biochip.

Acknowledgements

This work was partially supported by the National Key Basic Research Program (2002CB513100-10), Key Project Foundation of China Education Ministry (107084), National Science Foundation of PR China (90606003, 20405005), Major International (Regional) Joint Research Program of Natural Science Foundation of China (20610107) and Outstanding Youth Foundation of Hunan Province (06JJ10004).

References

[1] K. Stadtherr, H. Wolf, P. Lindner, Anal. Chem. 77 (2005) 3437.
[2] P. Angenendt, J.G. kler, Z. Konthur, H. Lehrach, D.J. Cahill, Anal. Chem. 75 (2003) 4368.
[3] B. Ballou, G.W. Fisher, J.S. Deng, T.R. Hakala, M. Srivastava, D.L. Farkas, Cancer Detect. Prev. 22 (1998) 251.
[4] K. Raemdonck, K. Remaut, B. Lucas, N.N. Sanders, J. Demeester,.S.C. De Smedt, Biochemistry 45 (2006) 10614.
[5] T.L. Fare, E.M. Coffey, H.Y. Dai, Y.D.D. He, D.A. Kessler, K.A. Kilian, J.E. Koch, E. LeProust, M.J. Marton, M.R. Meyer, R.B. Stoughton, G.Y. Tokiwa, Y.Q. Wang, Anal. Chem. 75 (2003) 4672.
[6] M.S. Briggs, D.D. Burns, M.E. Cooper, S.J. Gregory, Chem. Commun. (2000) 2323.
[7] X.H. Gao, L. Yang, J.A. Petros, F.F. Marshall, J.W. Simons, S.M. Nie, Curr. Opin. Biotechnol. 16 (2005) 63.
[8] M.Y. Han, X.H. Gao, J.Z. Su, S.M. Nie, Nat. Biotechnol. 19 (2001) 631.
[9] A.P. Alivisatos, Nat. Biotechnol. 22 (2004) 47.
[10] K.P. McNamara, T. Nguyen, G. Dumitrascu, J. Ji, N. Rosenzweig, Z. Rosenzweig, Anal. Chem. 73 (2001) 3240.
[11] M. Nichkova, D. Dosev, S.J. Gee, B.D. Hammock, I.M. Kennedy, Anal. Chem. 77 (2005) 6864.
[12] A.H. Ma, Z. Rosenzweig, Anal. Chem. 76 (2004) 569.

[13] C.D. Jones, J.G. McGrath, L. Andrew Lyon, J. Phys. Chem. B 108 (2004) 12652.
[14] W.C.W. Chan, S.M. Nie, Science 281 (1998) 2016.
[15] J.M. Bruchez, M. Moronne, P. Gin, S. Weiss, A.P. Alivisatos, Science 281 (1998) 2013.
[16] S. Santra, D. Dutta, G.A. Walter, B.M. Moudgil, Technol. Cancer Res. Treat. 4 (2005) 593.
[17] M. Magliulo, E. Michelini, P. Simoni, M. Guardigli, A. Roda, Anal. Bioanal Chem. 384 (2006) 27.
[18] F. Wang, W.B. Tan, Y. Zhang, X.P. Fan, M.Q. Wang, Nanotechnology 17 (2006) R1.
[19] L. Wang, C.Y. Yang, W.H. Tan, Nano Lett. 5 (2005) 37.
[20] X.J. Zhao, D.R. Tapec, W.H. Tan, J. Am. Chem. Soc. 125 (2003) 11474.
[21] X.X. He, K.M. Wang, W.H. Tan, B. Liu, X. Lin, C.M. He, D. Li, S.S. Huang, J. Li, J. Am. Chem. Soc. 125 (2003) 7168.
[22] H. Ow, D.R. Larson, M. Srivastava, Nano Lett. 5 (2005) 113.
[23] S. Santra, P. Zhang, K.M. Wang, R. Tapec, W.H. Tan, Anal. Chem. 73 (2001) 4988.
[24] X.X. He, K.M. Wang, W.H. Tan, J. Li, X.H. Yang, S.S. Huang, D. Li, D. Xiao, J. Nanosci. Nanotechnol. 2 (2002) 317.
[25] Z.Q. Ye, M.Q. Tan, G.L. Wang, J.L. Yuan, Anal. Chem. 76 (2004) 513.
[26] C. Kneuer, M. Sameti, E.G. Haltner, Int. J. Pharm. 196 (2000) 257.
[27] J.K. Herr, J.E. Smith, C.D. Medley, D.H. Shangguan, W.H. Tan, Anal. Chem. 78 (2006) 2918.
[28] R. Bakalova, Z. Zhelev, I. Aoki, H. Ohba, Y. Imai, I. Kanno, Anal. Chem. 78 (2006) 5925.
[29] S. Santra, J.S.X.K.M. Wang, W.H. Tan, J. Nanosci. Nanotechnol. 4 (2004) 590.
[30] J.M. Liu, G.H. Zhu, Z.M. Rao, C.J. Wei, L.D. Li, C.L. Chen, Z.M. Li, Anal. Chim. Acta 528 (2005) 29–35.
[31] M. Qhobosheane, S. Santra, P. Zhang, W.H. Tan, Analyst 126 (2001) 1274.
[32] W.H. Tan, K.M. Wang, X.X. He, X.J. Julia Zhao, T. Drake, L. Wang, R.P. Bagwe, Med. Res. Rev. 24 (2004) 621.
[33] Z.f. Peng, Z.P. Chen, J.H. Jiang, X.B. Zhang, G.L. Shen, R.Q. Yu, Anal. Chim. Acta 583 (2007) 40.
[34] X.X. He, K.M. Wang, W.H. Tan, J.Y. Chen, J.H. Duan, Y. Yuan, X. Lin, China Sci. Bull. 50 (2005) 2185.
[35] X.C. Zhou, J.Z. Zhou, Anal. Chem. 76 (2004) 5302.
[36] R.B. Mujumdar, L.A. Ernst, S.R. Mujumdar, C.J. Lewis, A.S. Waggoner, Bioconj. Chem. 4 (1993) 105.
[37] F. Reynolds, T. O'Loughlin, R. Weissleder, Lee. Josephson Anal. Chem. 77 (2005) 814.

Available online at www.sciencedirect.com
ScienceDirect
Talanta 72 (2007) 1283–1287
Talanta
www.elsevier.com/locate/talanta

A novel fluorescent method for determination of peroxynitrite using folic acid as a probe

Jun-Chao Huang [a], De-Jia Li [b], Jun-Chen Diao [a], Jie Hou [a], Jiang-Lan Yuan [a], Guo-Lin Zou [a,*]

[a] *State Key Laboratory of Virology, College of Life Sciences, Wuhan University, Wuhan, Hubei 430072, China*
[b] *Medical College, Zhengzhou University, Zhengzhou, Henan 450052, China*

Received 10 May 2006; received in revised form 14 January 2007; accepted 14 January 2007
Available online 20 January 2007

Abstract

A novel method for the determination of peroxynitrite using folic acid as a fluorescent probe is described. The method is based on the oxidation of the reduced, low-fluorescent folic acid by peroxynitrite to produce a high-fluorescent emission product. The fluorescence increase is linearly related to the concentration of peroxynitrite in the range of 3×10^{-8} to 5.0×10^{-6} mol L^{-1} with a correlation coefficient of 0.998, and the detection limit is 1×10^{-8} mol L^{-1}. Interferences from some metal ions normally seen in biological samples, and also some anions structurally similar to peroxynitrite were studied. The optimal conditions for the detection of peroxynitrite were evaluated.

Keywords: Peroxynitrite; Folic acid; Fluorimetry; Probe

1. Introduction

Peroxynitrite chemistry is of remarkable interest with increasing evidences showing the importance of peroxynitrite in the development of oxidative damage in various pathologies [1,2]. Peroxynitrite, generated from the diffusion-controlled reaction between the nitrogen monoxide and superoxide radicals [3,4], can cause lipid peroxidation [5], chemical cleavage of DNA [6,7], inactivation of key metabolic enzymes (e.g., aconitase [8,9], succinate dehydrogenase, ribonucleotide reductase, and cytochrome oxidase of the mitochondrial electron transport chain [10,11]), and reduction in cellular antioxidant defenses by oxidation of thiol pools [12]. Peroxynitrite can also nitrate protein tyrosine residues, possibly leading to inactivation of tyrosine kinase [13] or the disruption of key cytoskeletal components that may contribute to the pathogenesis of diseases, including inflammatory processes, ischemia-reperfusion, septic shock, and neurodegenerative disorders [14–16].

Due to the great importance of the research mentioned above, the point of interest was concentrated upon the measurement of peroxynitrite in both pathological and normal conditions in biological systems. However, the peroxynitrite assay is extremely difficult because of the low concentration, high activity, and elusive natures of peroxynitrite. Currently, most of techniques for peroxynitrite measurement are indirectly based on chemical detection of the decomposition products removed from biological systems. Peroxynitrite generation is usually measured by ultraviolet–visible (UV–vis) spectroscopy [17], chemiluminescence [18], immunohistochemistry [19], amperometry [20,21], electron spin resonance (ESR) [22,23], and fluorescence [24–26].

Two fluorogenic probes, dihydrodichlorofluorescein (DCFH) and dihydrorhodamine-123 (DHR-123), which are considered to be ideal, have been widely employed to monitor peroxynitrite in various systems [27,28]. The above methods are based on the oxidation of the reduced, non-fluorescent forms of fluorescent dyes such as fluorescein and rhodamine by peroxynitrite to produce the parent dye molecule, resulting in a dramatic increase in fluorescence response. However, the synthesis of these probe molecules is rather difficult and inconvenient [29]. Additionally, the use of organic dyes is very likely to result in environmental pollution, which should be avoided as possible as we can. Thus, a cheap, fast, and simple method to determine the peroxynitrite is needed.

* Corresponding author. Tel.: +86 27 87645674; fax: +86 27 87669560.
E-mail address: jchuang77@163.com (G.-L. Zou).

0039-9140/$ – see front matter © 2007 Elsevier B.V. All rights reserved.
doi:10.1016/j.talanta.2007.01.033

Folic acid is made up of a pterin moiety (purine and pyrazine fused together) that is linked to the side chain containing *p*-aminobenzoic acid (pteroic acid) and glutamic acid. Folic acid functions as a cofactor in the transfer and utilization of one carbon groups, which plays a key role in the biosynthesis of purines and pyrimidines and regeneration of methionine [30]. Recent studies showed that the pathogenesis of cardiovascular, hematological and neurological diseases and cancer are associated with the antioxidant activity of folic acid. Folic acid can act as a peroxynitrite scanvenger [31,32] due to its high reaction rate with peroxynitrite. Folic acid is a low-fluorescent substance, but the oxidation folic acid by peroxynitrite can give high-fluorescent emission product. Comparing with the above mentioned two dyes, folic acid is relative inexpensive, not toxic to biological system and stable in solution. The present study was designed to build a new fluorometric method for peroxynitrite determination.

2. Experimental

2.1. Chemicals

Folic acid (Shanghai Chem. Agent, Inc., Shanghai, China) was prepared by dissolving appropriate amount of folic acid in 0.001 mol L^{-1} NaOH and kept frozen, and the working barbital buffer solution was prepared by dissolving 4.125 g barbital sodium in 500 mL distilled water and add 0.7 mL 1.0 mol L^{-1} HCl. All the reagents were of analytical reagent grade and were used without further purification, unless stated otherwise. Doubly distilled water was used throughout.

2.2. Synthesis of peroxynitrite

Peroxynitrite was synthesized according to the previous description [33]. An aqueous solution of 0.6 mol L^{-1} sodium nitrite was rapidly mixed with an equal volume of 0.7 mol L^{-1} H_2O_2 containing 0.6 mol L^{-1} HCl and then immediately quenched with the same volume of 1.5 mol L^{-1} NaOH. Then some MnO_2 powder was added to the mixture solution to eliminate the excess H_2O_2, then the mixture was filtered and stored at −18 °C. Peroxynitrite concentration was determined by UV spectrometry at 302 nm ($\varepsilon = 1670$ L mol^{-1} cm^{-1}) [29].

2.3. Apparatus

Absorption spectra were obtained on a cary-100 UV–visible spectrophotometer (Varian, USA). The fluorescence spectra and relative fluorescence intensity were measured with a fluorescence-4500 (Hitachi, Japan) with a 10 mm quartz cuvette, the excitation and the emission wavelength slits were respectively set at 5.0 and 10.0 nm. All pH values were measured with a pH S-301 digital ion meter.

2.4. Procedure

In a set of 10 mL-volumetric tubes containing pH 9.4 barbital buffer solution, 1.0 mL of folic acid (1.0×10^{-4} mol L^{-1}) and different amount of peroxynitrite were added. The tubes were closed and then quickly and carefully shaken. The reaction solution was kept at room temperature for 5 min. The fluorescence intensity of the solution was recorded at 460 nm with the excitation wavelength set at 380 nm.

2.5. Detection of peroxynitrite in biological samples

At first, the Hela cells were maintained in Dulbecco's modified Eagle's medium (Gibco-BRL) which contains 10% heat-inactivated fetal calf serum, penicillin (100 U mL^{-1}) and streptomycin (50 μg mL^{-1}) in a 5% CO_2 environment at 37 °C. Next, these cells were plated on a six-well chamber. When growing up to 80% confluency, they were treated with various concentration of adriamycin for 6 h. Then the adherent cells were detached by trypsin treatment and washed twice with PBS containing 1% BSA. After that, these cells were added to barbital buffer solution containing 1.5×10^{-5} mol L^{-1} folic acid and were broken using an ultrasonic disintegrator. Finally, the suspension was taken for analysis under the optimally experimental conditions.

3. Results and discussion

3.1. Spectra characteristics

Fig. 1 shows the fluorescence excitation and emission spectra of folic acid and the mixture of folic acid with peroxynitrite in barbital buffer solution (pH 9.4). Folic acid has low fluorescence excitation and emission spectra. However, high fluorescence product generated by the introduction of peroxynitrite into the solution of folic acid, resulting in dramatic increase in spectra characteristics with excitation maximum at 380 nm and fluorescence emission maximum at 460 nm.

3.2. Optimization of the general procedure

The effect of pH on the fluorogenic reaction was studied in the range of 7–9.4 in barbital buffer solution, and the results are

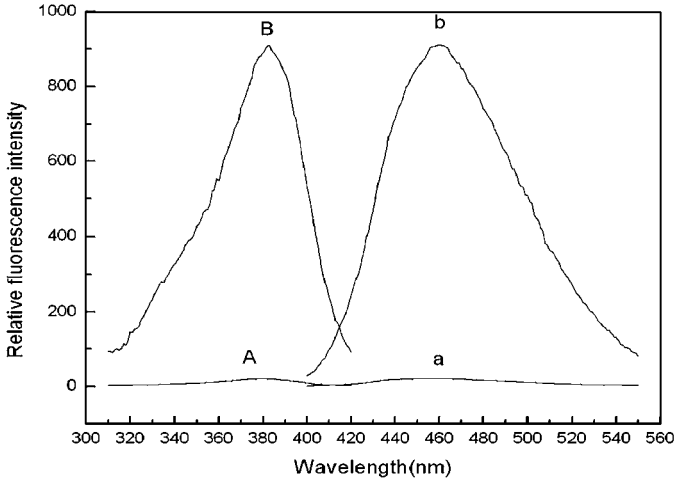

Fig. 1. Fluorescence excitation and emission spectra of the system. (A and a) Folic acid, 1.5×10^{-5} mol L^{-1}; (B and b) folic acid, 1.5×10^{-5} mol L^{-1} + peroxynitrite, 2.0×10^{-6} mol L^{-1}; pH 9.4 barbital buffer solution, 25 °C.

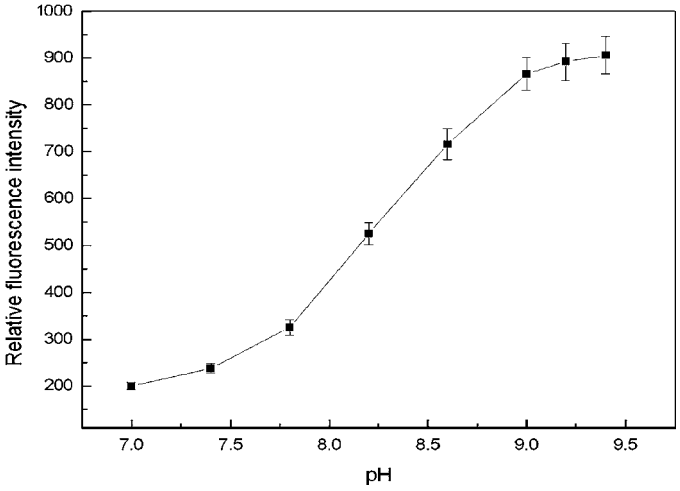

Fig. 2. Effect of pH on the system. Folic acid, 1.5×10^{-5} mol L^{-1} + peroxynitrite, 2.0×10^{-6} mol L^{-1}; barbital buffer solution, 25 °C.

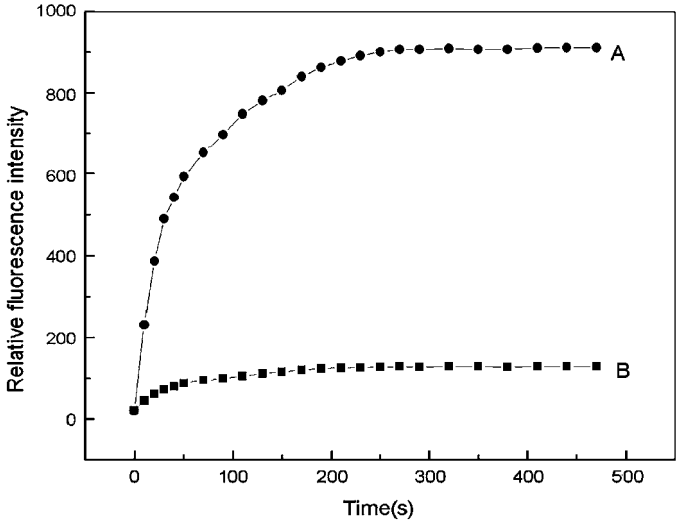

Fig. 3. The kinetic characteristics of the detection system. (A) Folic acid, 1.5×10^{-5} mol L^{-1} + peroxynitrite, 2.0×10^{-6} mol L^{-1}; (B) folic acid, 1.5×10^{-5} mol L^{-1} + peroxynitrite, 2.0×10^{-7} mol L^{-1}; pH 9.4 barbital buffer solution, 25 °C.

shown in Fig. 2. The data shown are average values of three repeated determinations. As can be seen from Fig. 2, fluorescence intensity of the detective system increased greatly with the pH value, and then leveled off as the pH value approached to 9.4, which is near the upper limit pH value of barbital buffer. The fluorescence intensity is pH dependent, because peroxynitrite can only exist for a short moment in neutral environment, but a much longer time in basic environment. For example, the half-life of peroxynitrite is less than 1 s at pH 7.4. Most peroxynitrite decayed before reacting with folic acid in neutral environment, and with pH increased, it can become more stable and react with more folic acid. But when pH was too high, peroxynitrite became too stable to react with folic acid. Hence, pH 9.4 of barbital buffer was chosen for the fluorogenic reaction.

The kinetic characteristics of the proposed detection system were studied. Upon the addition of peroxynitrite to the solution of folic acid in barbital buffer, the fluorescence intensity of the detective system was recorded as a function of reaction time. From Fig. 3, we can see that the fluorescence intensity of the detection system reached its maximum value in about 230 s, then the fluorescence intensity of the detective system almost remained unchanged. Therefore, to obtain a highly sensitive and reproducible results, a 5-min reaction time was selected in the following experiment. Further results showed that the fluorescence intensity of the detective system almost remained unchanged in a few hours.

The effect of the concentration of folic acid on ΔF of the system was studied and the results were shown in Fig. 4. The data shown are average values of three repeated determinations. From Fig. 4, it can be seen that ΔF of the detection system increased when the concentration of folic acid increased from 5.0×10^{-8} to 1.5×10^{-5} mol L^{-1} and the increase slowed down when the concentration of folic acid was up to 1.5×10^{-5} mol L^{-1}, therefore, 1.5×10^{-5} mol L^{-1} of folic acid was recommended for the subsequent experiment.

3.3. Analytical performance

Under the selected conditions given above, the fluorescence increment shows a linear relationship with the concentration of peroxynitrite in the range of 3×10^{-8} to 5.0×10^{-6} mol L^{-1} with a correlation coefficient 0.998, which is shown in Fig. 5. The detection limit, calculated according to the $3S_b/k$ criterion, in which k is the slope of the range of the linearity used and S_b, the standard deviation ($n = 9$) of the blank solution, is found to be 1.0×10^{-8} mol L^{-1}.

In order to demonstrate the accuracy of the new method, a series of peroxynitrite standard solutions are determined by the proposed fluorometric method. The results are shown in Table 1, the detection data reveals a good correlation and no statistical difference compared with the standard data. It can be seen that the new method is comparatively precise.

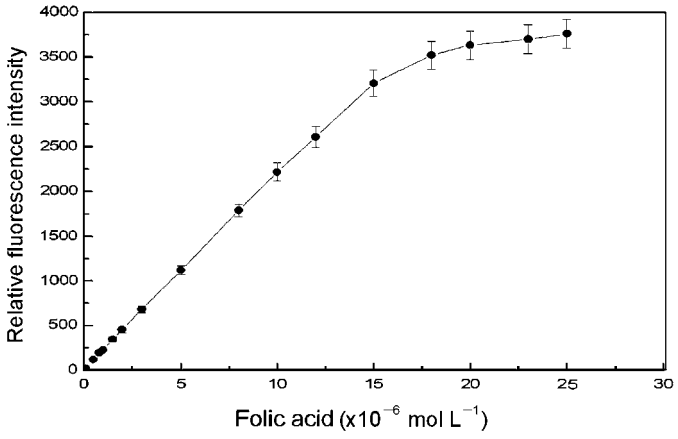

Fig. 4. Effect of the concentration of folic acid on the fluorescence increment of the system. Folic acid (different concentrations) + peroxynitrite (1.0×10^{-5} mol L^{-1}). pH 9.4 barbital buffer solution, 25 °C.

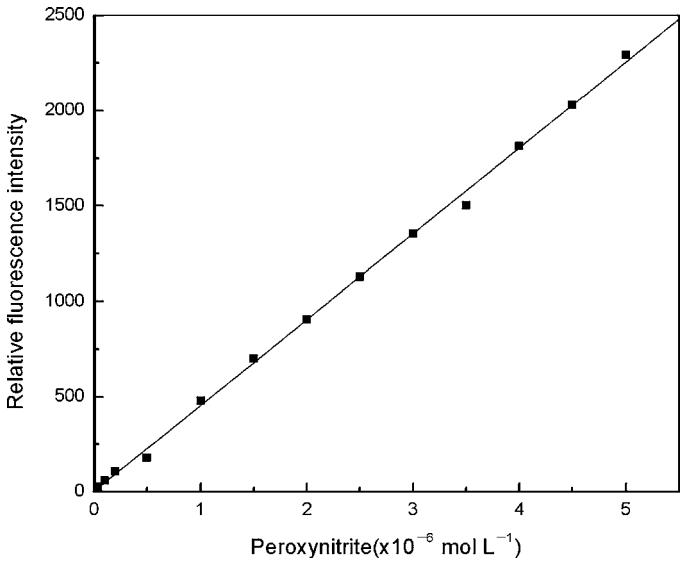

Fig. 5. The calibration curve in the range of 3×10^{-8} to 5.0×10^{-6} mol L^{-1} peroxynitrite. Folic acid, 1.5×10^{-5} mol L^{-1}; pH 9.4 barbital buffer solution, 25 °C.

Table 1
Comparison of determination results (mol L^{-1}) between this method and standard spectrophotometry

Sample no.	Standard method	This method	Relative error (%)
1	5.0×10^{-7}	4.76×10^{-7}	5.0
2	8.0×10^{-7}	7.88×10^{-7}	1.5
3	1.6×10^{-6}	1.61×10^{-6}	−0.6
4	3.6×10^{-6}	3.68×10^{-6}	−2.2
5	4.6×10^{-6}	4.75×10^{-6}	−3

The interferences of the proposed probe for peroxynitrite were studied. A variety of interfering agents from some amino acids, metal ions normally seen in biological samples to anions structurally similar to peroxynitrite were added to the detected system containing 2.0×10^{-6} mol L^{-1} peroxynitrite and 1.5×10^{-5} mol L^{-1} folic acid in pH 9.4 of barbital buffer. Results in Table 2 show a fairly satisfactory selectivity of the method. Especially the interference of H_2O_2 is quite low. Because the reactivity of peroxynitrite is 2000 times greater than H_2O_2 [34]. But the interference of Cu^{2+}, Mn^{2+} and Fe^{3+} is a little high, because these metal ions or their compounds can react with peroxynitrite [35–37]. But these metal ion can be inactivated by the addition of a chelated reagent such as diethylenetriaminepentaacetic acid (DTPA).

Table 2
The response for a variety of potential interferences expressed as a percentage of the ΔF of peroxynitrite in pH 9.4 barbital buffer solution, 25 °C

Interference	Concentration (10^{-6} mol L^{-1})	Peroxynitrite (%)
Peroxynitrite	2	100 (F = 906)
NO_3^-	1000	0.54
NO_2^-	100	−0.29
H_2O_2	100	0.5
NH_2OH	1000	1.1
Glucose	100	−0.2
Methionine	1000	−0.19
Glycine	1000	−4.2
Glutathione	1000	−5.0
Ascorbic acid	1000	−2.2
Uric acid	100	−2.3
Cu^{2+}	20	−3.8
Fe^{3+}	20	−1.9
Mn^{2+}	20	−1.8

Table 3
Standard additions and recovery data of cell samples

Sample no.	Peroxynitrite in samples (10^{-7} mol L^{-1})	Peroxynitrite added (10^{-7} mol L^{-1})	Peroxynitrite found (10^{-7} mol L^{-1})	Recovery (%)
1	3.36	1.0	3 98	91
		10.0	11.15	83
2	2.62	1.0	3 22	88
		10.0	11.33	90
3	1.26	1.0	1.91	85
		10.0	9.68	86

The final adriamycin concentration for samples 1–3 are 50, 30 and 15 μmol L^{-1}, respectively.

3.4. Analysis of biological samples

As is well known that peroxynitrite can be generated from cell injury induced by adriamycin. Results of the fluorescence intensity and the recovery data of addition of external peroxynitrite standard solutions to cells treated with adriamycin, are shown in Table 3, which are average values of three repeated determinations. The recovery data is not good enough, because the substances of broken cells in suspension can react with peroxynitrite, which inhibits the reaction between folic acid and peroxynitrite.

4. Conclusion

In summary, a novel fluorescent probe for the determination of peroxynitrite was proposed in this paper. As an indicator, folic acid is easily available, reasonably inexpensive, and stable in solution. The present method for the determination of peroxynitrite is cheap, simple and sensitive. The response time of the proposed probe for peroxynitrite is less than 5 min. Compared with the commonly used probe DHR-123, the fluorescent probe reported here has some advantages. (I) Higher sensitivity. The oxidation of folic acid by peroxynitrite is linear over the range of 3×10^{-8} to 5.0×10^{-6} mol L^{-1}, while the linear range is within 1.0×10^{-6} mol L^{-1} for DHR-123. In addition, the proposed probe has a detection limit of 1.0×10^{-8} mol L^{-1} whereas DHR-123 has a detection limit of 1.0×10^{-7} mol L^{-1} [38]. This is desirable for probing of peroxynitrite in lower concentrations. These make it ideal for detecting peroxynitrite formation. (II) Higher stability. Folic acid demonstrates greater photostability than those of DCFH and DHR-123, both of which are extremely sensitive to light induced oxidation [39]. (III) The fluorescent probe reported here is commercially available, and less likely to result in environmental pollution. Since folic acid is much likely

to coexist with peroxynitrite within living beings, the oxidation reaction might probably be another pathway of less injury to cells or organisms. Hence, we believe that the proposed probe can be applicable to the study of peroxynitrite in biological systems.

Acknowledgement

The authors gratefully acknowledge the support of this research by a grant (no. 30370366) from the National Natural Science Foundation of China.

References

[1] J.S. Beckman, W.H. Koppenol, Am. J. Physiol. Cell Physiol. 271 (1996) C1424.
[2] C. Ducrocq, B. Blanchard, B. Pignatelli, Cell. Mol. Life Sci. 55 (1999) 1068.
[3] R. Kissner, T. Nauser, P. Bugnon, Chem. Res. Toxicol. 10 (1997) 1285.
[4] T. Nauser, W.H. Koppenol, J. Phys. Chem. A 106 (2002) 4084.
[5] R. Radi, J.S. Beckman, K.M. Bush, Arch. Biochem. Biophys. 288 (1991) 481.
[6] T. Douki, J. Cadet, B.N. Ames, Chem. Res. Toxicol. 9 (1996) 3.
[7] V. Yermiloy, J. Rubio, M. Becchi, Carcinogenesis 16 (1995) 2045.
[8] L. Castro, M. Rodriguez, R. Radi, J. Biol. Chem. 269 (1994) 29409.
[9] A. Hausladen, I. Fridovich, J. Biol. Chem. 269 (1994) 29405.
[10] R. Ridi, M. Rodriguez, L. Castor, Arch. Biochem. Biophys. 308 (1994) 89.
[11] J.P. Bolanos, S.J.R. Heals, J.M. Land, J. Neurochem. 64 (1995) 1965.
[12] M.G. Salgo, E. Bermudez, G.L. Squadrito, Arch. Biochem. Biophys. 322 (1995) 500.
[13] B.L. Martin, D. Wu, S. Jack, J. Biol. Chem. 265 (1990) 7108.
[14] N. Fukuyama, Y. Takebayashi, M. Hida, Free Radic. Biol. Med. 22 (1997) 771.
[15] C. Szado, Shock 6 (1996) 79.
[16] M.A. Packer, J.L. Scarlett, S.W. Martin, Gen. Pharm. 31 (1998) 179.
[17] A. Vandervlite, J.P. Eiserich, C.A. Oneill, Arch. Biochem. Biophys. 319 (1995) 341.
[18] K. Dai, A.G. Vlessidis, N.P. Evmiridis, Talanta 59 (2003) 55.
[19] S.B. Digerness, K.D. Harris, J.W. Kirklin, Free Radic. Biol. Med. 27 (1999) 1386.
[20] J. Xue, X. Ying, J. Chin, Anal. Chem. 72 (2000) 5313.
[21] P. Wang, J.L. Zweier, J. Biol. Chem. 271 (1996) 29223.
[22] S. Dikalov, M. Skatchkov, B. Fink, Nitric Oxide 1 (1997) 423.
[23] S. Dikalov, M. Skatchkov, E. Basseneg, Biochem. Biophys. Res. Commun. 230 (1997) 54.
[24] J. Glebska, W.H. Knoppenol, Free Radic. Biol. Med. 35 (2003) 678.
[25] F.J. Martin-Romero, Y.G. Martin, F. Henao, J. Fluorescence 14 (2004) 17.
[26] S.L. Hempel, G.R. Buettner, D.A. Wessels, Free Radic. Biol. Med. 27 (1999) 146.
[27] N.W. Kooy, J.A. Royall, H. Ischiropoulos, Free Radic. Biol. Med. 16 (1994) 149.
[28] H. Possel, H. Noack, W. Augustin, FEBS Lett. 416 (1997) 175.
[29] X.F. Yang, X.Q. Guo, Y.B. Zhao, Talanta 57 (2002) 883.
[30] O. Stanger, Curr. Drug Metab. 3 (2002) 211.
[31] M. Basshir, FEBS Lett. 555 (2003) 601.
[32] R. Joshi, S. Adhikari, B.S. Patro, Free Radic. Biol. Med. 30 (2001) 1390.
[33] J.S. Beckman, T.W. Beckman, J. Chen, Proc. Natl. Acad. Sci. U.S.A. 87 (1990) 1620.
[34] G.T. Vatassery, Biochem. Pharmacol. 52 (1996) 579.
[35] J.M. Souza, E. Daikhin, M. Yudkoff, Arch. Biochem. Biophys. 371 (1999) 169.
[36] A. Daiber, M. Bachschmid, J.S. Beckman, Biochem. Biophys. Res. Commun. 317 (2004) 873.
[37] P. Salvemini, Z.Q. Wang, M.K. Stern, Proc. Natl. Acad. Sci. U.S.A. 95 (1998) 2659.
[38] H. Ischiropoulos, J.S. Beckman, J.P. Crow, Methods 7 (1995) 109.
[39] J. Liang, Z.H. Liu, R.X. Cai, Anal. Chim. Acta 530 (2005) 317.

Available online at www.sciencedirect.com
ScienceDirect
Talanta 72 (2007) 1298–1301
Talanta
www.elsevier.com/locate/talanta

Simple and rapid determination of sulfonamides in milk using Ether-type column liquid chromatography

Xiaojia Huang [a,*], Dongxing Yuan [a], Benli Huang [b]

[a] State Key Laboratory of Marine Environmental Science, Environmental Science Research Center, Xiamen University, Xiamen, 361005, China
[b] Department of Chemistry & The MOE Key Laboratory of Analytical Sciences, Xiamen University, Xiamen 361005, China

Received 17 October 2006; received in revised form 9 January 2007; accepted 14 January 2007
Available online 20 January 2007

Abstract

A simplified and rapid determining/identifying method for residual sulfonamides (SAs) in milk by using Ether-type stationary phase, which made in our lab, was presented. The target analytes were extracted by mixing with ethanol–acetic acid (97:3, v/v) followed by centrifugation. The procedure used a Ether-type C8 column, isocratic elution with acetonitrile–water (5:95, v/v), and a photo-diode array detector. The linear range of determination was 50–10,000 μg/L for sulfanilamide and 100–10,000 μg/L for sulfadiazine, sulfamerazine, sulfamethazine. Average recoveries of four SAs (spiked 0.5, 1.0 and 1.5 μg/mL) ranged from 80.1% to 87.6%, with relative standard deviations between 3.4% and 5.8%. The total time and solvent required for the analysis of one sample were <15 min and <1.0 mL of ethanol and 0.6 mL of acetonitrile, respectively. The developed procedure was nearly harmless to the human and environment.

Keywords: Sulfonamides; HPLC; Ether-type stationary phase; Milk

1. Introduction

Sulfonamide group of drugs is frequently used for prevention or treatment of diseases to food-producing animals in China and all the countries of the world, respectively [1]. There is a risk of drugs remaining in edible animal products like meat, milk, egg and fish because of illegal use such as an excessive administration and an inappropriate withdrawal period. One of the drugs, sulfamethazine is suspected to be carcinogenic and produce thyroid tumors in rodent [2] and others are known to cause allergic reactions in human. Owing to their potential impact on human health, the European Union has adopted a maximum residue level (MRL) of 100 ng/mL in edible animal tissue [3,4]. Therefore, there is a need for the development of sensitive and selective method for monitoring their residue level in edible animal products.

An acceptable routine method must be simple, reliable, inexpensive, fast, less hazardous to operator and environment and capable of determining residues at concentrations less than the MRL. There are several analytical methods include HPLC [5–9], GC [10,11], CE [12,13] for the determination of sulfonamides. Among them HPLC with ultraviolet detection is the most widely applied [14,15]. Since most sulfonamides (SAs) possess polar group, which can interaction with silanol groups on conventional silica-based stationary phase, and broaden and tailing peaks often appear during separation. Some measures such as increasing the content of organic solvent in mobile phase, using buffer solution and enhance column temperature should be taken to improve separation results. While, using more organic solvent will poison to humans and environment, preparing buffer solution is time consuming, using buffer solution as mobile phase will harm column and instrument and need rinse column after experiment, elevating column will damage column. Furusawa and co-workers [7,16,17] have used ethanol/water as binary mobile phase to separate SAs. Ethanol is less harm to humans and environment than methanol and acetonitrile, but higher column temperature should be used in order to improve separation results and reduce column pressure. They [18] also used PEG (polyethyleneglycol) column to analyse five SAs under 100% water as mobile phase, good separate was obtained but also needed high column temperature.

* Corresponding author at: P.O. Box 1009, Xiamen University, Xiamen 361005, China. Tel.: +86 592 2184860.
E-mail address: hxj@xmu.edu.cn (X. Huang).

0039-9140/$ – see front matter © 2007 Published by Elsevier B.V.
doi:10.1016/j.talanta.2007.01.031

In this study, we use Ether-type C8 column, which made in our lab, to analysis four SAs in milk. Because of the existence of a bulky group in the alkyl ligand of Ether-type C8, the interaction between SAs and residual silanol group on the silica surface was inhibited. The chromatographic conditions are very simple. The mobile phase contains only 5% acetonitrile, which effect on the environment and humans is negligible, not need buffer and high column temperature during separation. The total time and solvent required for the analysis of one sample were <15 min and <1.0 mL of ethanol and 0.6 mL of acetonitrile, respectively, under optimal conditions.

2. Experimental

2.1. Materials and reagents

Paper-packed cow's milk served as a sample, and was stored in a refrigerator until analysis. Sulfanilamide (SAM), sulfadiazine (SDA), sulfamerazine (SMA), and sulfamethazine (SMZ) were supplied by national institute for the control of pharmaceutical and biological products. HPLC-grade acetonitrile was purchased from Tedia Company (Fairfield, USA); Analytical grade ethanol was supplied by Shanghai Chemical Co. Ltd. (Shanghai, China); Water used throughout this study was purified using a Milli-Q water purification system (Millipore, USA).

Ether-type C8 (particle size 5 mm) (150 mm × 4.6 mm i.d.) was prepared in our lab [19]. The structure was showed in Fig. 1.

2.2. Apparatus

HPLC analyses were carried out on a ProStar LC chromatographic system (Varian, USA) equipped with a binary pump (ProStar 218) and a diode array detector (ProStar 335) and Star LC workstation. Sample injection was performed using a RE3725i manual sample injector with a 20 μL loop (Rheodyne, Cotati, CA, USA). All experiments were performed at room temperature.

The following apparatus was used in the sample preparation: a KQ-300B ultrasonic cleaner (Kunshan Instrumental Co. Ltd., Jiangshu, Chian); a microcentrifuge, Biofuge fresco (Kendo Lab. Products, Hanau, Germany).

2.3. Preparation of standard solutions

Stock standard solutions of four SAs were prepared by dissolving each in water to concentration of 100 μg/mL. Mixed standard solutions of these SAs were prepared by diluting the stock solutions with water. The solutions were kept in a refrigerator for up to 1 month.

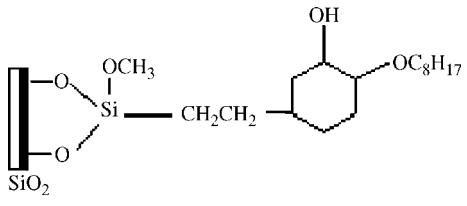

Fig. 1. The structure of Ether-type C8.

2.4. Preparation of sample

The preparation of sample is very simple. A 0.5 mL sample was placed into a microcentrifuge tube together with 0.2 mL of ethanol–acetic acid (97:3, v/v) and homogenized with ultrasonic homogenizer for 30 s. Then the tube was centrifuged at 10,000 × *g* for 5 min at 4 °C with a microcentrifuge. The supernatant was injected directly on the LC column.

2.5. Recovery test

The recoveries of SAM, SDA, SMA and SMZ from blank milk samples spiked at 0.5, 1.0 and 1.5 μg/mL were determined. These fortification concentrations were prepared by adding 20 μL of four mixed standard solutions of SAM, SDA, SMA and SMZ (25, 50 and 75 μg/mL, respectively) to separated 1 mL portions of the sample. Fortified samples were allowed to stand at 4 °C for 1 h after sulphonamide standards addition and then mixed prior to workup.

3. Results and discussion

3.1. Sample preparation

There are two routes to pretreat sample when analysis SAs in milk. One is utilizing acid as precipitator to subside protein in milk [7,20–22]. The other is using Ultrafree–MC membrane to deproteinize the extracted solution [16,17]. Higher recovery can be obtained when use Ultrafree–MC membrane to prepare sample, but the membrane is more expensive than ethanol–acetic acid. After investigation, acceptable recovery (>80%) can be obtained using ethanol–acetic acid as precipitator to deproteinize the milk [7]. Thereafter, using ethanol–acetic acid (97:3, v/v) to pretreat the milk was adopted.

3.2. Optimization of mobile phase

Conventional silica-based stationary phases are the most used columns. A problem that continues to plague those columns is the incomplete reaction of the surface silanols on silica with a silanizing reagent. This may cause severe band tailing, broad bands, low plate numbers and retention that vary from column to column when separating polar samples, especially basic solutes. Most SAs possess polar group, which can interaction with silanol groups. Some boresome measures should be taken in order to improve separation results [7,16–18]. Due to the existence of a bulky group in the alkyl ligand of Ether-type C8, the interaction between polar analytes and residual silanol group on the silica surface was inhibited [23,24]. Thereafter, the Ether-type stationary phase can separate polar analytes under simple mobile phase, such as acetonitrile/water. At the same time, a ether group "embeds" in the alkyl ligand, so the stationary phase of ETBP is more hydrophilic than conventional stationary phase and can be performed under more water as mobile phase while does

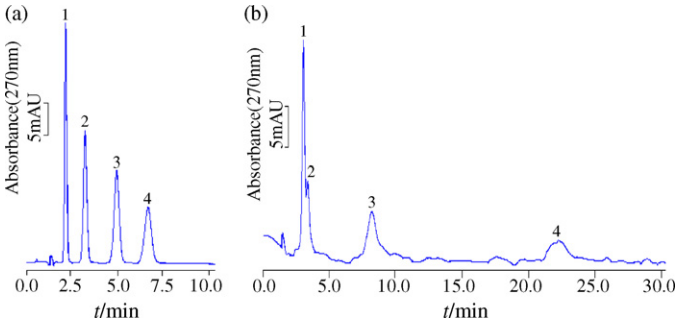

Fig. 2. HPLC chromatograms of four SAs on Ether-type C8 (a) and Agilent-C8 (b). Conditions: mobile phase acetonitrile–water (5:95, v/v); flow rate 1.5 mL/min; injection volume 20 μL; detector number 270 nm. Peaks (1) sulfanilamide; (2) sulfadiazine; (3) sulfamerazine; (4) sulfamethazine.

not damage the column [24]. In this study, acetonitrile/water was used as binary mobile phase to separate four SAs. After regulating the content of acetonitrile, four SAs were separated completely within 8 min when only 5% acetonitrile was used (Fig. 2a). Fig. 2b showed the separated of four SAs on Agilent-C8 under the same chromatographic conditions. It can be seen from Fig. 2b that sulfanilamide and sulfadiazine were eluted almost at the same time, and the peak of sulfamethazine showed as a "bread peak", which indicated that there existed serious interaction between sulfamethazine and silanol groups on the Agilent-C8. Therefore, some measures such as using buffer solution or enhance column temperature should be taken to improve separation results when use above column. While very sharp and symmetrical peaks of the four SAs can be obtained on the Ether-type C8 under simple, low content of organic solvent and need not high column temperature.

Fig. 3 shows the separation result of spiked with four SAs milk under the optimal conditions on Ether-type C8. We can see

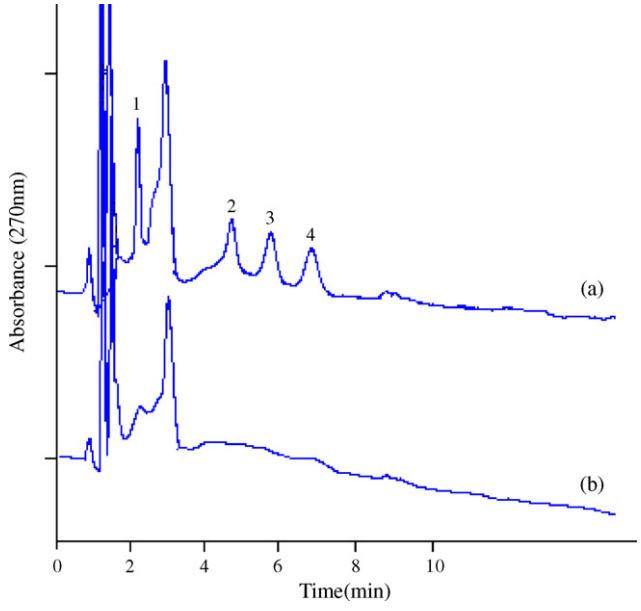

Fig. 3. HPLC chromatograms obtained from milk samples: (a) spiked with four sulfonamides milk sample and (b) blank milk sample. The conditions and peaks the same as Fig. 2.

Table 1
Recoveries and R.S.D. of target compounds from milk

Spiked (μg/mL)	Recovery (%) (mean ± R.S.D., $n = 5$)			
	SAM	SDA	SMA	SMZ
0.5	81.0 (3.5)	85.6 (4.9)	80.8 (5.0)	83.2 (5.8)
1.0	81.2 (4.2)	81.5 (3.8)	84.2 (3.9)	87.6 (4.5)
1.5	86.5 (4.0)	80.1 (3.4)	83.1 (4.6)	81.2 (4.2)

from the figure that the extracts were free from interfering compounds for quantification and identification during separation. The total time required for the analysis of one sample was less than 15 min.

3.3. Calibration

The calibration graphs that generated by plotting peak areas against amount were linear over the range 50–10,000 μg/L for sulfanilamide and 100–10,000 μg/L for sulfadiazine, sulfamerazine, sulfamethazine. The correlation coefficients for each compounds was >0.998. The detected limit for sulfanilamide and sulfadiazine were 30 and 60 ng/mL for sulfamerazine and sulfamethazine. These detected limit were well below the maximum residue limit (MRL) (100 ng/mL) established by European Union [3,4].

3.4. Recoveries

Table 1 summarizes the average recoveries from milk samples at three different spiking levels (0.5, 1.0 and 1.5 μg/mL) and their relative standard deviations (R.S.D.). Average recoveries of four SAs ranged from 80.1% to 87.6%, with relative standard deviations between 3.4% and 5.8%. The recoveries and R.S.D. meet the criteria for residue analysis of the Codex (recovery 70–110% and R.S.D. <20%) [25]. The good results indicate that the proposed procedure is suit to routinely monitor SAs in milk.

4. Conclusions

A simple and rapid method for determining sulfanilamide, sulfadiazine, sulfamerazine and sulfamethazine in milk using Ether-type C8 as separation column was developed. The main characteristics of the proposed procedure are summarized as follows: shorter analysis time (total less 15 min per sample); high precision (R.S.D. <6.0% in the recovery test); nearly harmless to the environment (total solvent consumption <1.0 mL of ethanol and 0.6 mL of acetonitrile, respectively); low cost (low 0.12 US$ per sample). Therefore, this method is useful for practical residue monitoring and studying pharmacokinetics of SAM, SDA, SMA and SMZ in milk.

Acknowledgements

The project was supported by Youth Talent Foundation of Fujian Province (no. 2006F3117), Start-up foundation of Xiamen University and Innovation Foundation of Xiamen University (no. XDKJCX20063007).

References

[1] J.F.M. Nouws, J. Laurensen, Vet. Quart. 12 (1990).
[2] N.A. Littlefield, W.G. Sheldon, R. Allen, D.W. Gaylor, Food Chem.Toxicol. 28 (1990) 157.
[3] Commission of the European Communities, Establishment by the European Community of Maximum Residue Limits (MRLs) for Residues of Veterinary Medical Products in Foodstuffs of Animal Origin, The Rules Governing Medical Products in European Community VI, ECSC-EEC-EAEC, Brussels, Belgium, October 1991.
[4] C. Hartig, T. Storm, M. Jekel, J. Chromatogr. A 854 (1999) 163–173.
[5] S. Babic, D. Asperger, D. Mutavdzic, A.J.M. Horvat, M. Kastelan-Macan, Talanta 70 (2006) 732.
[6] A. Preechaworapun, S. Chuanuwatanakul, Y. Einaga, K. Grudpan, S. Motomizu, O. Chailapakul, Talanta 68 (2006) 1726.
[7] K. Kishida, N. Furusawa, J. Chromatogr. A 1028 (2004) 175.
[8] M.R. Fuh, S.A. Chan, Talanta 55 (2001) 1127.
[9] K. Kishida, N. Furusawa, Talanta 67 (2005) 54.
[10] A. Cannavan, S.A. Hewitt, W.J. Blanchflower, D.G. Kennedy, Analyst 121 (1996) 1457.
[11] V.B. Reevs, J. Chromatogr. B 723 (1999) 127.
[12] M.S. Fuh, S. Chu, Anal. Chim. Acta 499 (2003) 215.
[13] S. Lamba, S.K. Sanghi, A. Asthana, M. Shelke, Anal. Chim. Acta 552 (2005) 110.
[14] V.K. Agarwal, J. Chromatogr. 624 (1992) 411.
[15] A.R. Long, C.R. Short, S.A. Barker, J. Chromatogr. 502 (1990) 87.
[16] N. Furusawa, K. Kishida, Fresen. J. Anal. Chem. 371 (2001) 1031.
[17] N. Furusawa, J. Chromatogr. A 898 (2000) 185.
[18] N. Furusawa, K. Kishida, LC–GC Eur. 18 (2005) 600.
[19] X.J. Huang, J. Wang, X.L. Liu, R. Cong, Anal. Sci. 19 (2003) 1391.
[20] N. Furusawa, Anal. Chim. Acta 481 (2003) 255.
[21] N. Furusawa, LC–GC N. Am. 21 (2003) 362.
[22] N. Furusawa, Chromatographia 57 (2003) 317.
[23] X.J. Huang, J. Wang, X.L. Liu, S.Z. Huang, Chromatographia 54 (2001) 350.
[24] J.J. Kirkland, J.W. Henderson, J.D. Martosella, B.A. Bidlingmeyer, J. Basta-Russell, J.B. Adams Jr., LC–GC 17 (1999) 634.
[25] Codex Alimentarius Commission, Joint FAO/WHO Food Standards Program, Residues of Veterinary Drugs in Food, vol. 3, 2nd ed., Rome, Italy, 1993.

Available online at www.sciencedirect.com
ScienceDirect
Talanta 72 (2007) 1400–1403
Talanta
www.elsevier.com/locate/talanta

Ammonium fluoride as a novel chemical modifier for the elimination of magnesium chloride interference on the determination of lead by graphite furnace atomic absorption spectrometry

Lenka Husáková [a,*], Jitka Šrámková [a], Tomáš Černohorský [b], Martina Bařinová [a]

[a] *Department of Analytical Chemistry, Faculty of Chemical Technology, University of Pardubice, nám. Čs. legií 565, Pardubice CZ-532 10, Czech Republic*
[b] *Department of Environmental Protection, University of Pardubice, nám. Čs. legií 565, Pardubice CZ-532 10, Czech Republic*

Received 9 November 2006; received in revised form 18 January 2007; accepted 19 January 2007
Available online 30 January 2007

Abstract

Ammonium fluoride was found to be very efficient modifier for the elimination of $MgCl_2$ interference on Pb determination. Ammonium fluoride probably converts strongly interfering volatile $MgCl_2$ to less volatile MgF_2 matrix that makes possible the release of Pb analyte at lower temperature, before the matrix starts to vaporize. It was observed likewise that NH_4F removes the interferences mentioned, i.e. caused by $MgCl_2$ presence, much more effectively as compared with some modifiers, before now recommended for this purpose. The application of this modifier to the determination of Pb in 2% (m/v) $MgCl_2$ has ensured the characteristic mass and LOD value in the original sample of 12 pg and 60 ng g^{-1}, respectively (10 μl aliquots of sample). Applying the modifier to standards and samples enables the use of matrix-free standard solutions for attaining accurate analysis as verified by recovery studies.

Keywords: GFAAS; Lead analyte; Magnesium chloride matrix; Ammonium fluoride chemical modifier

1. Introduction

Direct determination of Pb in high salinity matrix by GFAAS is difficult since the matrix components induce both matrix and spectral interferences. Spectral interferences are caused mainly by the molecular absorption of NaCl in the ultraviolet range or by light scattering by sodium chloride particles, while chemical interferences are mainly caused due to the formation of volatile halides or, e.g. by occlusion of the analyte in the chloride matrix [1–5]. The interference effects of $MgCl_2$ matrix have been found more severe than that of NaCl matrix by several authors [2,5,6]. The formation of halides with HCl in the vapor phase has been treated theoretically in ref. [7], and the release of HCl at elevated temperature by the hydrolysis of the hydrated $MgCl_2$ salt was experimentally studied [8]. The release of HCl by the decomposition of MgOHCl was also concluded [9].

To overcome these problems pre-concentration and separation techniques can be used [10]; nevertheless, these procedures are time-consuming. Application of chemical modifiers is frequently used way to overcome these problems [11]. For this purpose, chemical modifiers such as HNO_3 and NH_4NO_3 [12], Pd-nitrate alone or combined with Mg-nitrate or with some other different reagents [13–15] as well as different organic acids, see e.g. ref. [8] have been used. A specific advantage of the oxalic acid modifier is that no carbon residue is left in the graphite tube [8,16].

It is shown in this work that NH_4F is very efficient for the elimination of $MgCl_2$ interference on Pb determination and is superior to some other chemical modifiers previously recommended for this purpose.

2. Experimental

2.1. Reagents

Reagents of analytical grade or higher quality were used. All solutions were prepared using deionized water. Water used in all experiments was purified using the UltraClear (SG, Germany) pure water system to 0.05 μS cm^{-1}.

* Corresponding author. Tel.: +420 466037029; fax: +420 466037068.
E-mail address: Lenka.Husakova@upce.cz (L. Husáková).

0039-9140/$ – see front matter © 2007 Elsevier B.V. All rights reserved.
doi:10.1016/j.talanta.2007.01.048

Lead stock solution (1 g l^{-1}) was obtained from Analytika, Ltd. (Prague, Czech Republic). Nitric acid (65%, m/v) was Selectipur quality (Lach-Ner, Neratovice, Czech Republic). The solution of 1 g l^{-1} of Pd and 2 g l^{-1} of Mg was prepared by dilution of an appropriate amount of a palladium solution of 10 g l^{-1} Pd in 10% (v/v) HNO_3 (CPI International, USA) and 10 g l^{-1} of Mg with water. Magnesium nitrate of 10 g l^{-1} was prepared by dissolving of the appropriate amount of the salt (Lachema, Brno, Czech Republic) in water. Hydrofluoric acid 38–40% (m/v) was pro-analysis grade (p.a.) (Lachema, Brno, Czech Republic). Solutions of 10 and 100 g l^{-1} ammonium fluoride (Sigma-Aldrich Chemie GmbH, Steinheim, Germany) and that of ammonium nitrate (Lachema) were prepared by dissolving of these salts in water. Magnesium chloride (p.a.) was purchased from Fluka (Buchs, Switzerland) and Merck (Darmstadt, Germany) and the working solutions (1, 10 and 50 g l^{-1}) were prepared by dilution of an appropriate amount of the component in water.

2.2. Instrumentation

Avanta P double beam atomic absorption spectrometer (GBC Scientific Equipment Pty. Ltd., Australia) equipped with GF 3000 graphite furnace, autosampler PAL 3000 and deuterium arc background corrector was used. Super lamp (Photron Pty. Ltd., Australia) was the line source (lamp current 8 mA, wavelength 283.3 nm, spectral bandpass 0.5 nm). Peak area absorbance values were measured. Pyrolytically coated graphite tubes (Schunk, Germany, cat. no. 56GB715) with a pre-installed pyrolytic graphite L'vov platform were used. Argon was used as sheating gas; the internal gas flow in the graphite tube was interrupted during the atomization step.

2.3. Procedure

When the interference of $MgCl_2$ matrix on the determination of Pb in the presence of different chemical modifiers was studied, 200 pg of Pb and 10–200 μg of $MgCl_2$ was injected to graphite furnace together with (i) 5 μg Pd + 10 μg $Mg(NO_3)_2$, (ii) 180 μg HNO_3, (iii) 60 μg HF, (iv) 300 μg NH_4NO_3 and (v) 200 μg NH_4F. For this purpose, 10 μl aliquot of the solution of 20 μg l^{-1} of Pb, the appropriate volume of $MgCl_2$ solution and the appropriate volume of individual modifier were injected as a single deposition on the platform by means of autosampler. The same amount of the sample and different volume of modifiers will result in different final volumes injected to the cuvette which would have negative influence on reproducibility. To reach better reproducibility the volume was filled up with water to 20 μl before the injection. Regarding the use of NH_4NO_3, HNO_3, HF and NH_4F, such amounts of modifiers were chosen to ensure the same [F^-/Cl^-] and [NO_3^-/Cl^-] mole concentration ratio. Thus, e.g. for 200 μg of $MgCl_2$ matrix this ratio was 1.8.

In other experiments, e.g. when the analytical recoveries in the presence of $MgCl_2$ matrix were studied, 10 μl of 2% (m/v) $MgCl_2$ alone or spiked with 10 μg l^{-1} of Pb and 2 μl of 100 g l^{-1} of NH_4F were injected on the platform after the volume filling up to 20 μl with water. This procedure ensures that 200 μg of $MgCl_2$ with or without 100 pg of Pb and 200 μg of NH_4F is injected into the cuvette.

Five aqueous standards were used to obtain the calibration curves and two standard additions were also made. The concentrations of solutions used have ranged from 5 to 50 μg l^{-1} of Pb. The calibration curves were linear in the concentration ranges of these standards. The direct calibration and standard addition method were controlled and compared by means of the instrument software. Correlation coefficients found were at least 0.999 for direct calibration and 0.99 for standard additions. The temperature program used throughout this work is presented in Table 1.

Table 1
Optimized electrothermal program with the use of NH_4F modifier

Step	Temperature (°C)	Time (s)		Gas flow (l min^{-1})
		Ramp	Hold	
Injection	20	–	–	–
Drying	95	20	15	3.0
	120	20	15	3.0
Pyrolysis	600[a]	5	10	3.0
	600[a]	0	1	0.0
Atomization	1600[a]	0	2	0.0
Cleaning	2000	1	1	3.0
Cooling down	40	25	5	3.0

[a] The pyrolysis and atomization temperatures were, respectively, 600 and 1500 °C with and without matrix and without chemical modifier, 600 and 1600 °C for NH_4NO_3, 500 and 1700 °C for HF and 1000 and 1900 °C for Pd + $Mg(NO_3)_2$ modifiers.

3. Results and discussion

3.1. Comparison of the selected chemical modifiers

The effect of increasing $MgCl_2$ concentration on the net lead signal in the presence of five different modifiers, Pd (nitrate) + Mg (nitrate), NH_4NO_3, HNO_3, HF and NH_4F was studied. The pyrolysis and atomization temperatures used for measurement in the presence of individual chemical modifiers, based on measurement of pyrolysis and atomization curves, are displayed in Table 1. According to Fig. 1, it is evident that NH_4F is very efficient for the elimination of $MgCl_2$ interference on Pb determination. In the presence of 200 μg of NH_4F the same amount of $MgCl_2$ could be tolerated without changes of sensitivity. Time-scans of net lead and background signals in the presence of matrix (200 pg Pb and 200 μg of $MgCl_2$) without and with applying NH_4F modifier are shown in Fig. 2a and b, respectively. In addition, time-scans of Pb atomic absorption signal with the use of modifier alone (Fig. 2c) and also under matrix-free conditions (Fig. 2d) are shown for comparison.

It can be supposed that NH_4F, similarly to HF [17,18], converts the chloride matrix to fluoride one. Nevertheless, as seen in Fig. 1, NH_4F is much more effective to eliminate $MgCl_2$ interference effect than HF and other previously applied modifiers

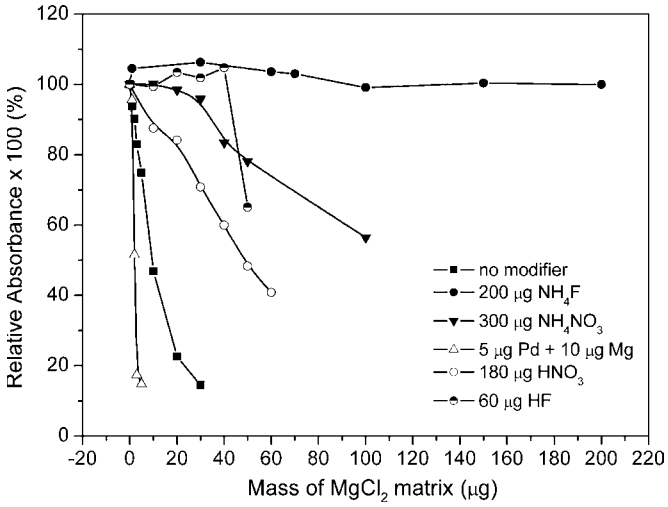

Fig. 1. Influence of $MgCl_2$ amount on the relative absorbance signal of 200 pg of Pb in the absence and in the presence of selected chemical modifiers. Pyrolysis and atomization temperatures in the presence of different modifiers were slightly different, as they appear in Table 1.

in comparison. This high effectiveness must be related to the formation of insoluble and non-interfering MgF_2.

According to Fig. 1, nitric acid is less effective in the elimination of chloride interference effect when compared with NH_4NO_3, in agreement with literature [12]. This lower effectiveness can be attributed to the volatilization loss of nitric acid, which occurs too early during the drying step. On the other hand, NH_4NO_3 added is retained in the drying step and converted to NH_4Cl that is volatilized in the early stage of pyrolysis step. The less effective removal of chloride interference effect with the addition of HNO_3 was also attributed to its volatilization loss by Yin et al. [19] and Daminelli et al. [20]. Similarly, it can be supposed that the higher efficiency of NH_4F in comparison with HF (Fig. 1) is due to the volatilization loss of HF. It is also evident from Fig. 1, in accordance with the literature [14], that interference of $MgCl_2$ could not be removed by the addition of $Pd + Mg(NO_3)_2$ modifier.

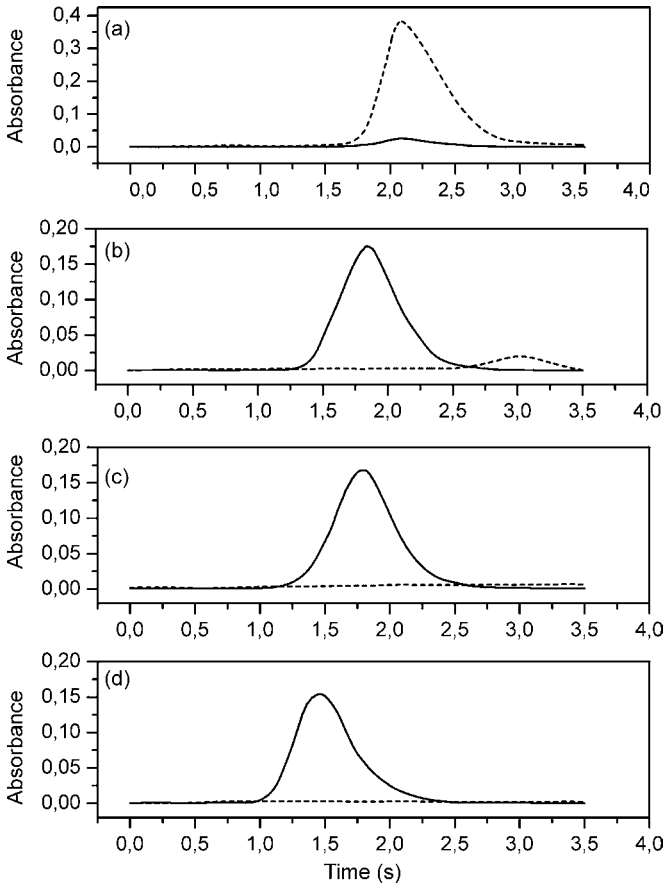

Fig. 2. Atomic (solid lines) and background (dotted lines) absorbance signals for 200 pg of Pb in presence of (a) 200 μg $MgCl_2$, (b) 200 μg $MgCl_2$ + 200 μg NH_4F, (c) 200 μg NH_4F, and under (d) matrix and modifier free conditions.

The elimination of Pb signal depletion by $MgCl_2$ matrix after the addition of NH_4F (Fig. 1) is likely the consequence of formation of non-interfering MgF_2. As it can be seen in Fig. 2, by addition of this modifier the background signal is reduced and also delayed to higher temperatures due to the vaporization of less volatile MgF_2 in comparison with $MgCl_2$ and its hydrolysis products. This can be confirmed based on boiling point data available from literature [21]. In case of NH_4F addition (Fig. 2b), the Pb atomic absorption signal appears earlier (at a lower temperature) than without addition, i.e. when the $MgCl_2$ matrix is present alone. The observation of Pb atomic absorption signal at higher temperatures, when the $MgCl_2$ matrix is present alone, can be explained based on the studies reported in ref. [8]. Accordingly, the hydrated $MgCl_2$ undergoes a partial hydrolysis and the hydrolysis products vaporize as $MgCl_2$ and MgO at elevated temperatures. Under slow heating conditions the vaporization of the chloride and the oxide are well separated, but under fast heating, applied also in this work, they covaporize in a broad temperature range. The background signal (Fig. 2a) corresponds likely to this covaporization and fraction of lead analyte vaporized from MgO residue at higher temperatures might be represented by the small Pb signal in Fig. 2a. On the other hand, this very weak signal can also originate from the imperfection of the applied D_2 lamp background correction, i.e. it is not necessarily Pb AAS signal. As it can be further seen in Figs. 1 and 2, the Pb atomic absorption signal did not decrease by the addition of NH_4F, with or without the presence of $MgCl_2$ although the vaporization of Pb in a fluoride form can result in a limited gas phase atomization as the dissociation energy of the mono-fluoride (PbF) is quite high [21]. The addition of NH_4F to the Pb nitrate solution causes a delay of the Pb atomic absorption signal probably as a consequence of a more refractory Pb species (Fig. 2c versus Fig. 2d).

3.2. Analytical performance

The equation for direct aqueous calibration constructed following the procedure described in Section 2 and applying the temperature program given in Table 1 was as follows: $y = 3.65 \times 10^{-3}$ $(9.73 \times 10^{-5})x$ (where y = integrated absorbance and x concentration of the analyte ($\mu g\,l^{-1}$); standard deviation of the slope is given in parentheses). The slopes of calibration lines of the standard additions method for 2% (m/v) $MgCl_2$ solution in the presence of 200 μg of NH_4F were

very close to that of the aqueous standard. Deviations in slopes for direct aqueous calibration and that of standard addition were found to be within 10%, which means that the effect of matrix was under a good control at conditions described and direct aqueous calibration can be used for quantification.

Limit of detection (LOD) and limit of quantification (LOQ) calculated based on a repeated analysis of 2% (m/v) $MgCl_2$ sample with low Pb concentration as $3S_{blk}/m$ and/or $10S_{blk}/m$, where S_{blk} is the standard deviation of 10 blank measurements and m is the slope of the calibration graph were 1.2 and 4 $\mu g\,l^{-1}$, respectively. The characteristic mass defined as such a mass of analyte which produces an integrated absorbance signal of 0.0044 s was 12 pg. Characteristic mass found in this study is lower than those reported for Pb previously with different modifiers during the analysis of samples containing $MgCl_2$ matrix, e.g. see water samples [13,15].

In order to check the accuracy of the method for the analysis of $MgCl_2$ analytical reagents, we have investigated the recovery of Pb added to a number of such reagents, since no reagents with certified Pb concentrations are available. For this purpose, the solutions of 2% (m/v) $MgCl_2$ spiked with 10 $\mu g\,l^{-1}$ of Pb were used. When solutions with higher concentration of $MgCl_2$ were analyzed, the large amount of a precipitate has created on the platform and problems during the drying and also displacement of the analyte from the cuvette can occur. Recoveries obtained using a direct aqueous calibration method were found in the range of 97–104% indicating that the proposed method permits matrix-free determination of Pb in these analytical reagents. Taking into consideration the LOD and LOQ value corresponding to 60 ng g^{-1}, and/or 200 ng g^{-1} of Pb in original sample, the method can be successfully used for an accurate determination of Pb in $MgCl_2$ analytical reagents with Pb concentration above 200 ng g^{-1}. The precision of the method expressed as the relative standard deviation by five replicate measurements of 10 $\mu g\,l^{-1}$ of Pb in 2% (m/v) $MgCl_2$ was 2%.

4. Conclusions

It is possible to claim from the presented results that NH_4F is very efficient chemical modifier for removing of the interference effect of $MgCl_2.6H_2O$ on the determination of Pb. It can be applied to the direct and accurate determination of Pb in $MgCl_2$ analytical reagents with concentration of Pb above 200 ng g^{-1}. The use of this proposed modifier thus features a quick and elegant solution of problems solved in the time being usually by means of time-consuming separation techniques or by the use of alternative analytical methods. Another advantage of the proposed modifier is that it is available in a high purity and thus no problems with contamination were observed, which impacts positively LOD value. Regarding the mechanism of action of the proposed modifier its successful application can be expected also to the determination of some other elements strongly sensitive on the presence of $MgCl_2$ as well as to sea water analysis.

Acknowledgements

The study was performed thanks to financial support of the Ministry of Education, Youth and Sports of Czech Republic (Project No. 0021627502). The authors would like to thank Prof. Tibor Kántor from the Department of General and Inorganic Chemistry, Eötvös Loránd University, Budapest, Hungary and Associate Prof. Karel Handlíř from the Department of General and Inorganic Chemistry of University of Pardubice, Pardubice, Czech Republic for valuable suggestions and advises during the work.

References

[1] J. Carroll, N.J. Miller-Ihli, J.M. Harnly, T.C. O'Haver, D. Littlejohn, J. Anal. At. Spectrom. 7 (1992) 533.
[2] M.M. Chaudhry, D. Mouillere, B.J. Ottaway, D. Littlejohn, J.E. Whitley, J. Anal. At. Spectrom. 7 (1992) 701.
[3] B.R. Culver, T. Surles, Anal. Chem. 47 (1975) 920.
[4] E.J. Czobik, J.P. Matousek, Anal. Chem. 50 (1978) 2.
[5] J.Y. Cabon, A. Le Bihan, Spectrochim. Acta Part B 51 (1996) 619.
[6] M. Grotti, R. Leardi, R. Frache, Anal. Chim. Acta 376 (1998) 293.
[7] T. Kántor, L. Bezúr, E. Pungor, J.D. Winefordner, Spectrochim. Acta Part B 38 (1983) 581.
[8] T. Kántor, Spectrochim. Acta Part B 50 (1995) 1599.
[9] D.M. Hughes, C.L. Chakrabarti, D.M. Goltz, D.C. Grégoire, R.E. Sturgeon, J.P. Byrne, Spectrochim. Acta Part B 50 (1995) 425.
[10] D. Bohrer, P.C. do Nascimento, M. Guterres, M. Trevisan, E. Seibert, Analyst 124 (1999) 1345.
[11] D.L. Tsalev, V.I. Slaveykova, P.B. Mandjukov, Spectrochim. Acta Rev. 13 (1990) 225.
[12] R.D. Ediger, At. Absorp. Newslett. 14 (1975) 127.
[13] P. Bermejo-Barrera, J. Moreda-Piñeiro, A. Moreda-Piñeiro, A. Bermejo-Barrera, J. Anal. At. Spectrom. 13 (1998) 777.
[14] J.Y. Cabon, A. Le Bihan, Spectrochim. Acta Part B 51 (1996) 1245.
[15] O. Acar, Talanta 65 (2005) 672.
[16] A.B. Volynsky, S.V. Tikhomirov, V.G. Senin, A.N. Kashin, Anal. Chim. Acta 284 (1993) 367.
[17] I. López-García, M. Sánchez-Merlos, M. Hernández-Córdoba, Anal. Chim. Acta 396 (1999) 279.
[18] J.Y. Cabon, Spectrochim. Acta Part B 57 (2002) 513.
[19] X.F. Yin, G. Schlemmer, B. Welz, Anal. Chem. 59 (1987) 1462.
[20] G. Daminelli, D.A. Katskov, P.J.J.G. Marais, P. Tittarelli, Spectrochim. Acta Part B 53 (1998) 945.
[21] D.R. Lide (Ed.), CRC Handbook of Chemistry and Physics, 81st ed., CRC Press, Boca Raton, 2000.

Available online at www.sciencedirect.com
ScienceDirect
Talanta 72 (2007) 1392–1399
Talanta
www.elsevier.com/locate/talanta

A mercury-free electrochemical sensor for the determination of thallium(I) based on the rotating-disc bismuth film electrode

E.O. Jorge [a], M.M.M. Neto [a,b,*], M.M. Rocha [a]

[a] *Departamento de Química e Bioquímica, Centro de Ciências Moleculares e Materiais, Faculdade de Ciências, Universidade de Lisboa, Campo Grande, Ed. C8, 1749-016 Lisboa, Portugal*

[b] *Departamento de Química Agrícola e Ambiental, Instituto Superior de Agronomia, TULisbon, Tapada da Ajuda, 1349-017 Lisboa, Portugal*

Received 25 October 2006; received in revised form 5 January 2007; accepted 19 January 2007
Available online 30 January 2007

Abstract

A bismuth film electrode was tested and proposed as an environmentally friendly sensor for the determination of trace levels of Tl(I) in non-deoxygenated solutions. Determination of thallium was made by anodic stripping voltammetry at a rotating-disc bismuth film electrode plated in situ, using acetate buffer as the supporting electrolyte. The stripping step was carried out by a square wave potential-time excitation signal. A univariate optimisation study was performed with several experimental parameters as variables. Under the selected optimised conditions, a linear calibration plot was obtained in the submicromolar concentration range, allowing the electrochemical determination of thallium in trace amounts; the calculated detection limit was 10.8 nM and the relative standard deviation for 15 measurements of 0.1 μM Tl(I) was ±0.2%, for a 120 s accumulation time. Interference of other metals on the response of Tl(I) was investigated. Application to real environmental samples was tested. The bismuth film electrode appears to be a promising tool for electroanalytical purposes, ensuring the use of clean methodology.

Keywords: Thallium; Bismuth film electrode; Square wave voltammetry; Anodic stripping voltammetry; Mercury-free electrodes

1. Introduction

Thallium is present in the environment in trace amounts. Emissions from cement plants and combustion of fossil-fuel are the main causes of thallium pollution [1]. Thallium is a non-biological element, but it enters cells via K^+ transport systems, since the ionic form of Tl^+ is similar to K^+ due to their resemblance in ionic radii (Tl^+: 164 pm, K^+: 152 pm). Thallium binds more tightly than potassium to N and S ligands [2] and is very harmful for living organisms even at very low concentrations [3]. It is therefore important to develop sensitive and accurate analytical methods to determine trace levels of thallium in environmental and food samples.

Although spectrophotometric techniques have been widely used to determine traces of thallium in different matrices [4–7], electroanalytical methods also appear very suitable [8–13], because they are reliable and sensitive and require less expensive equipment. Anodic stripping voltammetry (ASV) is recognized as a powerful technique for measurement of heavy metals in trace amounts [14]. For this purpose, mercury electrodes, namely the hanging mercury drop and the mercury film electrode (MFE), have been commonly used, due to the high hydrogen overvoltage and the ability to form amalgams. Thallium is very soluble in mercury (43.0 at%) [15] and a good sensitivity is achieved with mercury electrodes because thallium ions are readily reduced and amalgamated during the deposition step of the ASV analytical protocol [16]. However, because of its high toxicity, mercury should be replaced by less toxic or, preferably, non-toxic electrode materials. In several countries, Hg-containing instruments and electrical components have been phased out and the use of mercury compounds has even been banned [17]. A number of alternative and new electrode materials has been investigated, including various forms of carbon, gold, iridium or boron-doped diamond, but none has approached the favourable electrochemical behaviour of mercury [18–22].

* Corresponding author at: Departamento de Química e Bioquímica, Centro de Ciências Moleculares e Materiais, Faculdade de Ciências, Universidade de Lisboa, Campo Grande, Ed. C8, 1749-016 Lisboa, Portugal. Tel.: +351 962763055.
E-mail address: mm.neto@netcabo.pt (M.M.M. Neto).

0039-9140/$ – see front matter © 2007 Elsevier B.V. All rights reserved.
doi:10.1016/j.talanta.2007.01.047

Recently, the bismuth film electrode (BFE) has been developed as a very attractive sensor for ASV of heavy metals to replace mercury electrodes, with an equivalent performance [23,24]. Bismuth can be electroplated onto an inert substrate (e.g. glassy carbon) using the in situ plating procedure introduced by Florence [25] to prepare the MFE. In addition to its low toxicity, the BFE offers other advantages over the MFE. It is less susceptible to oxygen interference, exhibiting lower background currents, not only in square wave stripping voltammetry but also in linear scan voltammetric experiments in non-deaerated media [23]. After measurements, the renewal of the BFE is electrochemically achieved. It must be stressed that the removal of mercury films from glassy carbon is not an easy task [26–28]. Whereas mercury films on glassy carbon consist of finely divided mercury droplets, the bismuth deposits have a completely different morphology [23,29,30]. Using scanning electron microscopy (SEM), Wang et al. observed a highly porous, three-dimensional fibril-like network for a bismuth deposit on glassy carbon, from acetate buffer solutions [23]. Thus, BFE exhibits good mechanical stability, which enhances its potential usefulness to operate under hydrodynamic conditions, e.g. in flow systems. All these attractive features make this sensor a promising replacement for the mercury electrodes in electroanalysis, with additional advantages. A significant number of reports on the analytical utility of the BFE has already been published [31–36]. Glassy carbon [24] and carbon paste [36] have been used as substrates to the development of bismuth-coated electrodes for thallium analysis by ASV. Other mercury-free sensors for the detection of thallium by ASV have also been proposed. Using a chemically modified glassy carbon electrode with Langmuir–Blodget film of *p*-allylcalix [4] arene, Dong et al. determined thallium in environmental water samples [37]. Graphite microelectrodes were applied for the same purpose with low detection and quantification limits, 0.01 and 0.03 $\mu g\,L^{-1}$, respectively [10]. The quantification of thallium in the presence of lead and cadmium was carried out at a silver–gold alloy electrode by subtractive ASV [38].

It is well-known that ASV with hydrodynamic sensors is very advantageous [14,39,40]. The mass transport is controlled by well-defined hydrodynamics, leading to high sensitivity. The rotating-disc electrode is one of the most widely used electrodes of this type. Some electroanalytical studies involving bismuth film electrodes in hydrodynamic configurations have been reported in the literature for analytical purposes [33,34,41]. However, no application of the rotating-disc bismuth film electrode for the quantification of thallium in real samples seems to have been previously published.

In this work, the analytical potentialities of a rotating-disc bismuth film electrode are explored for the determination of Tl(I) in environmental matrices by ASV, using a square wave voltammetric scan in the determination step. Square wave voltammetry enables a fast analysis with high scan rates, and minimises the problems arising from the presence of dissolved oxygen. After the optimisation of the experimental parameters, the sensor was successfully applied to the quantification of thallium in river water and soil samples.

2. Experimental

2.1. Apparatus

Electrochemical experiments were performed using a computer-controlled Autolab Basic PGSTAT 20 potentiostat (Eco Chemie, Utrecht, The Netherlands) driven by GPES software (Version 4.7). A M Series AA atomic absorption spectrophotometer and GF95Z graphite furnace system with sample dispenser (Thermo Electron Corporation, Cambridge; UK) was employed for the photometric determination of thallium.

Electrochemical measurements were made in a glass cell (100 mL) equipped with a platinum wire auxiliary electrode, an Ag|AgCl|3 M KCl reference electrode (Metrohm), and a rotating-disc glassy carbon working electrode (area: 0.385 cm^2) from Oxford Electrodes. Bismuth films were prepared in situ by electrochemical deposition of bismuth onto the surface of the glassy carbon disc. A combined pH electrode pHC 3005-8 with a Radiometer MeterLab PHM201 was used to make pH measurements. All the glassware was carefully cleaned by soaking the pieces, overnight, in a 2% diluted RBS 25 detergent, washed several times with distilled water and finally with Millipore water.

2.2. Reagents and solutions

All solutions were made from analytical grade reagents and Millipore Milli-Q ultrapure water (conductivity <0.1 $\mu S\,cm^{-1}$) and stored in Pyrex glass flasks. The supporting electrolyte was a 0.1 M acetate buffer (pH 4.6) prepared from acetic acid and sodium acetate (Aldrich). The bismuth(III), thallium(I), lead(II) and cadmium(II) stock solutions were prepared from $Bi(NO_3)_3{\cdot}5H_2O$, $TlNO_3$, $Pb(NO_3)_2$ and $Cd(NO_3)_2{\cdot}4H_2O$, respectively, all supplied by Merck. The working solutions were obtained by adding the appropriate amount of stock solution to the supporting electrolyte.

2.3. Procedure

Prior to each experiment, the glassy carbon electrode was polished on a polishing pad with Alpha Micropolish alumina 0.3 μm particle size (Büehler), rinsed with Milli-Q water and dried. The electrode surface was then activated by continuous potentiodynamic cycling ($n = 10$), at 50 $mV\,s^{-1}$, between −1.0 V and +0.8 V, in supporting electrolyte without the removal of oxygen. The bismuth film was prepared in situ, by co-deposition of bismuth and the target species at −1.4 V for 120 s, from 1.9 μM bismuth(III) nitrate in acetate buffer (pH 4.6). After an equilibration period of 5 s, a positive going square wave scan to a final potential of −0.5 V was applied on the BFE while the anodic stripping voltammogram was being recorded. The electrode was continuously rotating at a rotation speed of 240 rpm. The selected square wave parameters were: frequency 40 Hz, amplitude 80 mV and scan increment 5 mV. After measurements, the electrode potential was held at +0.3 V for 30 s to clean its surface electrochemically. All potentials are referred to Ag|AgCl reference electrode.

In cyclic voltammetry tests, solutions were previously deaerated with oxygen-free nitrogen for 15 min.

The standard addition method was used to evaluate the content of Tl(I) in real samples. All experiments were carried out at temperatures of 25 ± 1 °C.

2.4. Real samples pre-treatment

Water samples were analysed after a minor pre-treatment, consisting of filtration through Whatman filter no. 1, followed by pH adjustment to 4.6 with acetate buffer.

The soil samples were simply washed, since thallium compounds are very soluble in water. Owing to their high volatility [42], it was decided to avoid digestion procedures. Air-dried soil (50 g) was thus shaken for 1 h at room temperature with 150 mL of Milli-Q ultrapure water, using magnetic stirring. The liquid phase was then decanted and successive filtrations under vacuum with numbers 1, 41 and 42 Whatman filters were carried out and followed by a final filtration with a Minisart 0.20 μm filter. The pH of the collected colourless filtrate was then adjusted to 4.6 with acetate buffer solution. Prior to voltammetric determinations, test solutions were transferred to the cell and an aliquot of bismuth(III) salt solution was added to obtain a Bi(III) concentration of 1.9 μM.

3. Results and discussion

3.1. Electrochemical behaviour of Tl(0)/Tl(I) at the BFE

The accessible potential window of the bismuth-coated electrode in acetate buffer was firstly investigated. The current response of a rotating-disc glassy carbon electrode, immersed in a solution containing 1.9 μM bismuth(III) nitrate, was analysed after holding the potential at four different values (−0.8, −1.0, −1.2 and −1.4 V) for 120 s deposition time (t_{dep}). The recorded anodic stripping voltammograms indicate that the stripping potential of bismuth ($E_p = -0.23$ V) was not affected, but the peak current increased as the deposition potential became more negative, denoting that a better coverage of the electrode surface was attained at −1.4 V. The potential window of the bismuth-coated glassy carbon electrode is limited in the anodic region by the oxidation of bismuth, starting around −0.4 V; the hydrogen overvoltage, which limits the cathodic range, is quite high (starting around −1.2 V).

Cyclic voltammetry of thallium in the presence of 1.9 μM Bi(III) was performed in 0.1 M acetate buffer solutions (pH 4.6), to characterize the voltammetric signal of thallium at an in situ plated bismuth film electrode. A well-defined stripping peak ($E_p = -0.78$ V) due to the oxidation of thallium at the BFE was obtained. The shape of a typical voltammogram, which is illustrated in Fig. 1, reflects the irreversibility of the electrode process. The effect of potential scan rate (ranging between 10 and 150 mV s^{-1}) on the peak potential and the peak current of thallium was studied. A slightly positive shift in the peak potential was observed, which confirms the irreversibility of the redox process. The anodic peak heights markedly increased with increasing scan rate, yielding a linear relationship between peak current and the scan rate up to 100 mV s^{-1}, with a correlation coefficient of 0.998.

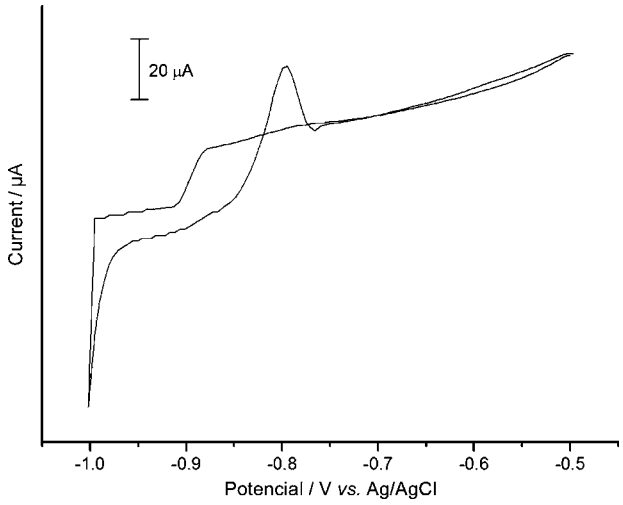

Fig. 1. Typical cyclic voltammogram of 100 μM Tl(I) + 1.9 μM Bi(III) in 0.1 M acetate buffer (pH 4.6) at a glassy carbon rotating-disc electrode. $E_i = -0.5$ V (vs. Ag|AgCl), sweep rate: 100 mV s^{-1}, rotation speed: 240 rpm.

As expected for film electrodes, the signal of the target species is supposed to be affected by the film thickness. This can be controlled by varying the Bi(III) concentration in the test solution, at a fixed deposition time. Bismuth was co-deposited with thallium on the rotating-disc glassy carbon electrode at −1.4 V, for 120 s, after adding different bismuth(III) concentrations at the micromolar level to an acetate solution containing 0.1 μM Tl(I). As shown by the obtained square wave stripping voltammograms exhibited in Fig. 2a, the thallium peak potential remained constant (at −0.76 V) up to 1.9 μM Bi(III), and deviates to more negative values for higher Bi(III) concentrations. In which concerns peak current, I_p, it increased with increasing bismuth concentration between 0.6 and 1.9 μM, and then decreased at higher concentrations (Fig. 2b). This behaviour, and also the peak shape observed for the higher bismuth concentrations, strongly suggest the occurrence of multilayer deposition, that may cause a weak adhesion of bismuth to the glassy carbon surface. A fixed Bi(III) concentration of 1.9 μM, capable of generating reproducible bismuth film electrodes, which enable good sensitivity, was used in the analytical experiments.

3.2. Optimization of experimental conditions for anodic stripping voltammetric determination of thallium(I) at a BFE

Aiming to establish the most suitable experimental conditions for the square wave anodic stripping voltammetric measurements of thallium(I) at the rotating-disc bismuth film electrode in acetate buffer, a univariate optimization study was performed with the deposition time, the deposition potential, the electrode rotation speed and the square wave parameters as variables.

Square wave anodic stripping voltammograms of 0.1 μM Tl(I) at the BFE were recorded, after holding the electrode at 6 different deposition times, starting from 60 s. Peak current increased rapidly with deposition time up to 120 s, and increased

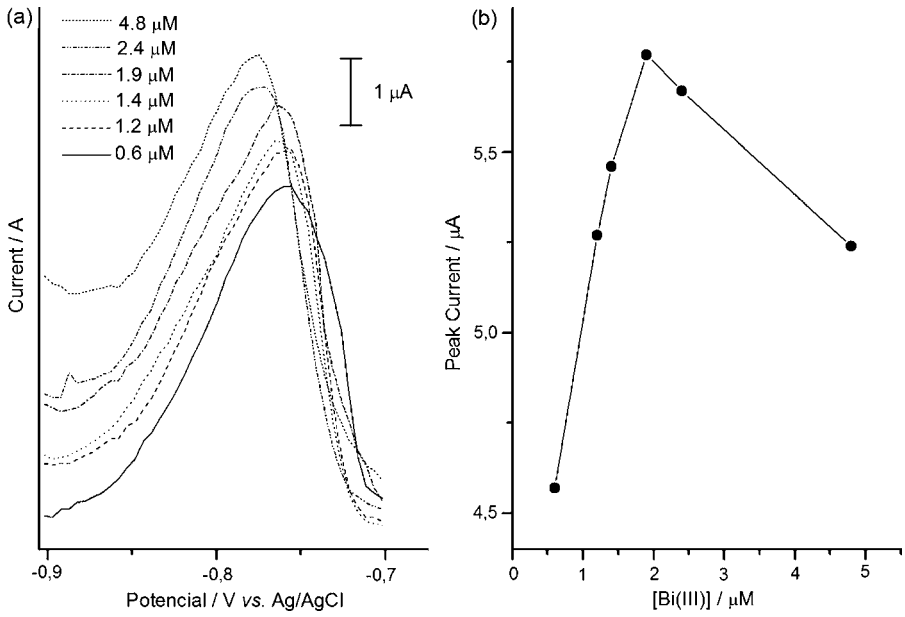

Fig. 2. (a) Square wave stripping voltammograms of 0.1 μM Tl(I) at a glassy carbon rotating-disc electrode, in the presence of increasing levels of Bi(III). Supporting electrolyte: 0.1 M acetate buffer (pH 4.6). E_{dep}: −1.4 V; t_{dep}: 120 s; t_{eq}: 5 s; rotation speed: 240 rpm, square wave amplitude: 25 mV, ΔE_s: 5 mV, square wave frequency: 20 Hz. (b) The influence of Bi(III) concentration on thallium peak current.

more slightly for longer accumulation periods, reflecting the gradual saturation of the electrode surface. Hence, a deposition time of 120 s was adopted. The influence of the deposition potential was also analysed. A remarkable enhancement in sensitivity was observed upon changing the deposition potential from −0.9 to −1.5 V. At more negative potentials, the reduction of the positively charged thallium(I) ions is more effectively accomplished. A deposition potential of −1.4 V was chosen in all subsequent work. This value is in agreement with the suitable potential for co-deposition of bismuth films.

The effect of increasing mass transport to the in situ plated BFE was examined. The flux of solution to the electrode surface, generated by forced convection, causes a significant improvement in sensitivity. For example, an 8-fold enhancement of the thallium peak is observed at an electrode rotation speed of 480 rpm, when compared with the one obtained at static conditions. According to Levich equation [43], which predicts that the thickness of the diffusion layer decreases linearly with the increment of the square root of the electrode rotation speed, ω, a linear plot of thallium stripping peak current versus $\omega^{1/2}$ was obtained from 60 to 1600 rpm, with a correlation coefficient of 0.998, confirming that the overall diffusion rate of the target species to the electrode surface is controlled by convective mass transfer. However, at high rates of convective mass transport ($\omega > 1800$ rpm), the electrode response became poorly reproducible, exhibiting oscillations in current. Despite the enhanced sensitivity achieved using a hydrodynamic electrode, these results indicate that, at high rotation speeds, the BFE is more susceptible to mechanical disruption during convective accumulation with obvious implications on its analytical performance. The speed of 240 rpm was selected as giving the best compromise between sensitivity, mechanical stability and reproducibility of the bismuth film.

The normal square wave parameters frequency, scan increment and amplitude were also optimised in order to perform fast analysis with high sensitivity. The variation of peak current with square wave frequency is illustrated in Fig. 3. There is a considerable increase up to 40 Hz, but at higher frequencies the current starts to increase slowly, tending to level off, owing to the influence of the capacitive background current on the total measured current. As a result of this hindering capacitive contribution, sensitivity decreases. A square wave frequency of 40 Hz was chosen so as to provide large peaks with a good definition and fast scan rates. Scan increment, ΔE_s, was varied from 1 to 10 mV. No significant improvement was achieved above 5 mV; although peak currents were slightly increased, peak broadening occurred.

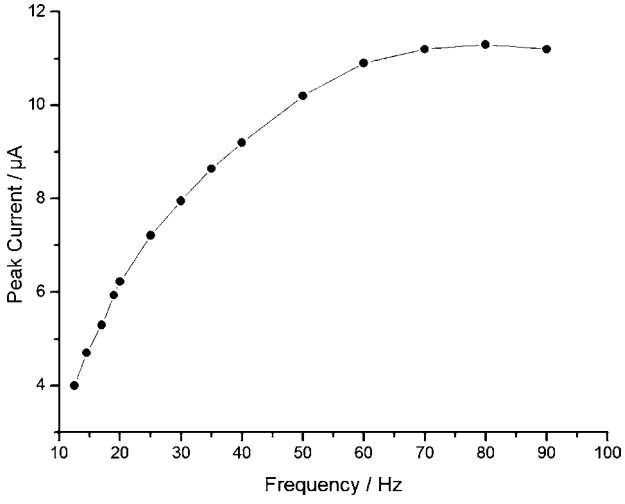

Fig. 3. The dependence of the stripping response of Tl(I) at a BFE on the square wave frequency. [Bi(III)] = 1.9 μM. Other conditions as in Fig. 2.

The best value of scan increment consistent with both adequate peak definition and evaluation was therefore 5 mV. In combination with the selected frequency, a scan rate of 200 mV s^{-1} was produced. The effect of square wave amplitude was studied in the range 10–140 mV. Greater peak currents were recorded for higher square wave amplitudes. Although a linear plot was obtained, deviation from linearity was observed at amplitudes above 90 mV.

The selected square wave parameters for quantitative measurements of traces of thallium(I), in 0.1 M acetate buffer, by square wave ASV at an in situ plated rotating-disc bismuth film electrode were: square wave frequency, 40 Hz; scan increment, 5 mV; square wave amplitude, 80 mV.

Equilibration time (t_{eq}) values up to 5 s proved to have a very slightly positive effect on the electrode signal (about 4%); higher t_{eq} gave rise to lower peak heights. An equilibration time of 5 s was chosen.

3.3. Calibration curve and precision

Under the experimental conditions selected on the optimisation studies, a calibration plot of thallium stripping peak current, measured at −0.8 V, against concentration was constructed using standard additions (Fig. 4). There is a close fit to linearity from 12 to 150 nM. Least-squares treatment yielded a slope of 188 ± 4.01 A/M, an intercept of 0.855 ± 0.337 μA and a correlation coefficient of 0.998 ($N = 12$). For more diluted solutions, the plotted values do not fit the straight line. For concentrations under 1.2 nM the results are poorly reproducible. The calculated limits of detection (LOD) and quantification (LOQ) [44] were 10.8 and 36.1 nM, respectively.

The assessments of the reproducibility of the generated bismuth film electrode itself as well as its response are very important for the reliability of data in future analytical applications. For this purpose, a test solution containing 0.1 μM Tl(I) in 1.9 μM Bi(III)/0.1 M acetate buffer was employed. The electrode was continuously rotating at 240 rpm. A series of 15 consecutive measurements performed every 30 min, after 120 s co-deposition of thallium and bismuth at −1.4 V, yielded a very stable response for thallium with a relative standard deviation of 0.2%, with a mean peak current of 29.5 μA. Between runs, the electrode was potentiostatically conditioned at +0.3 V for 30 s, to remove the metallic film, before renewing it. Well-shaped and reproducible peaks have been obtained with no apparent deterioration of the signal quality for at least 7 h. We can conclude that the rotating-disc bismuth film electrode plated in situ has very good reproducibility and allows a satisfactory repeatability of the results.

3.4. Interferences of Pb(II) and Cd(II)

Possible interferents include electroactive trace metals. Lead(II) and cadmium(II) are generally considered as the major interferences in the determination of thallium on mercury [9,45] and carbon electrodes [10] by ASV. The use of the BFE significantly contributes to overcome this problem.

Successive additions of lead acetate were performed in a background electrolyte solution containing 0.1 μM Tl(I) and 1.9 μM Bi(III). The stripping voltammograms have exhibited excellent peak resolution, with stripping potentials occurring at −0.79 and −0.62 V, for Tl(I) and Pb(II), respectively. No interference has been found in ASV of thallium up to 200 μM Pb(II). The interference of cadmium was found to be more problematic. Cadmium and thallium peaks partially overlap, since the corresponding oxidation potentials are in close proximity to one another. However, the oxidation processes of Cd and

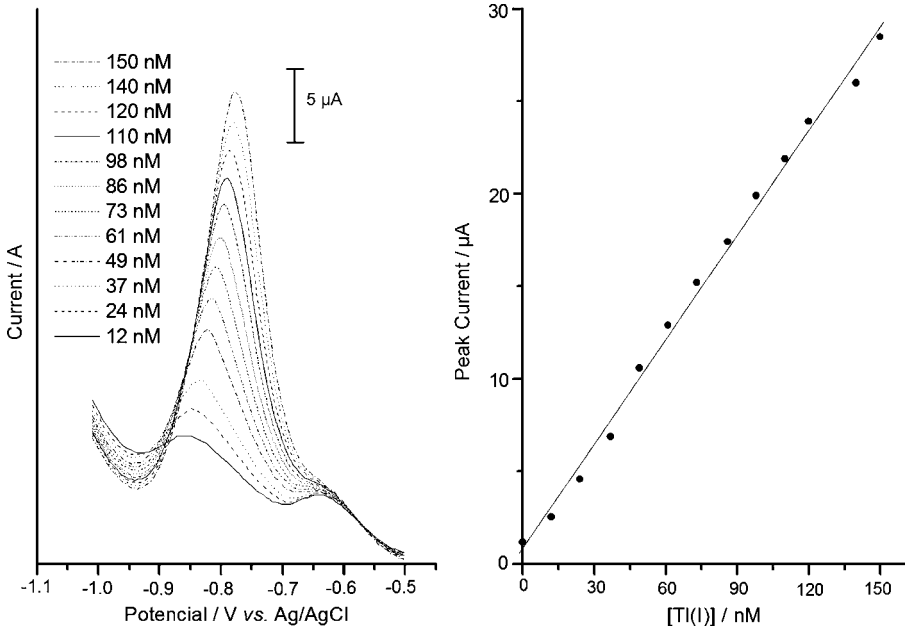

Fig. 4. Square wave voltammetry at a BFE for increasing concentrations of Tl(I). $E_i = -1.0$ V to $E_f = -0.5$ V (vs. Ag|AgCl), square wave frequency = 40 Hz, square wave amplitude = 80 mV. Other conditions as in Fig. 2. Also shown on the right is the resulting calibration plot.

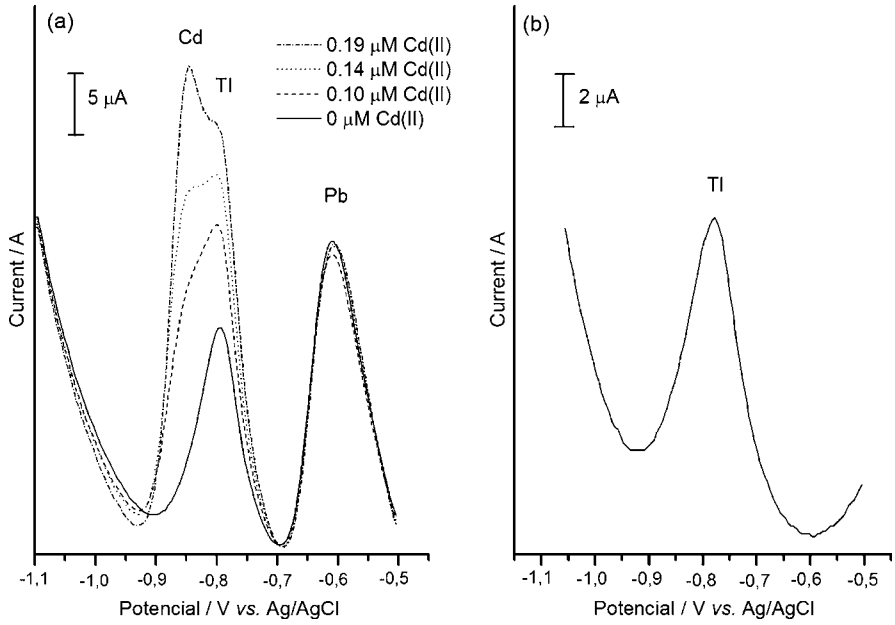

Fig. 5. Square wave ASV of 0.1 μM Tl(I) + 0.1 μM Pb(II) at a BFE (a) in the absence (solid line) and presence (broken lines) of Cd(II) (b) in the presence of 0.19 μM Cd(II) + 1.0 mM EDTA. Other conditions as in Fig. 4.

Tl at the BFE, in acetate buffer, lead to a slight improvement in peak resolution when compared with that obtained at bare carbon electrodes [10]. As seen in Fig. 5a, stripping voltammograms registered after making successive additions of Cd(II) in a solution containing fixed concentrations of Tl(I) and Pb(II) show that Pb(II) peak remains practically inalterable, while Tl(I) peak raises with increasing cadmium concentration. Although exhibiting poor resolution, it should be pointed out that no shift of peak potentials occurred for thallium and cadmium.

The interference of Pb(II) in the ASV of Tl(I) is actually largely overcome with the use of the proposed BFE. However, when cadmium is present in the solutions under analysis, the addition of complexing agents is recommended [10,14,45] to minimize the interference of cadmium in ASV measurements of thallium. As shown in Fig. 5b, the addition of 1.0 mM EDTA in acetate buffer enabled the detection of 0.1 μM Tl(I), with no cadmium and lead interferences. The presence of excess of Cd(II) and Pb(II) in the quantification of 98 nM Tl(I) at the BFE was allowed for ratios of Cd:Tl and Pb:Tl of 2500:1 and 10,000:1, respectively, which mean an important improvement in comparison with the data obtained using different electrode materials [9,10,45]. The interfering effects of Cu(II) and Zn(II) were also examined. In the presence of 1.0 mM EDTA, for 98 nM Tl(I), zinc is tolerated when present at 1000-fold

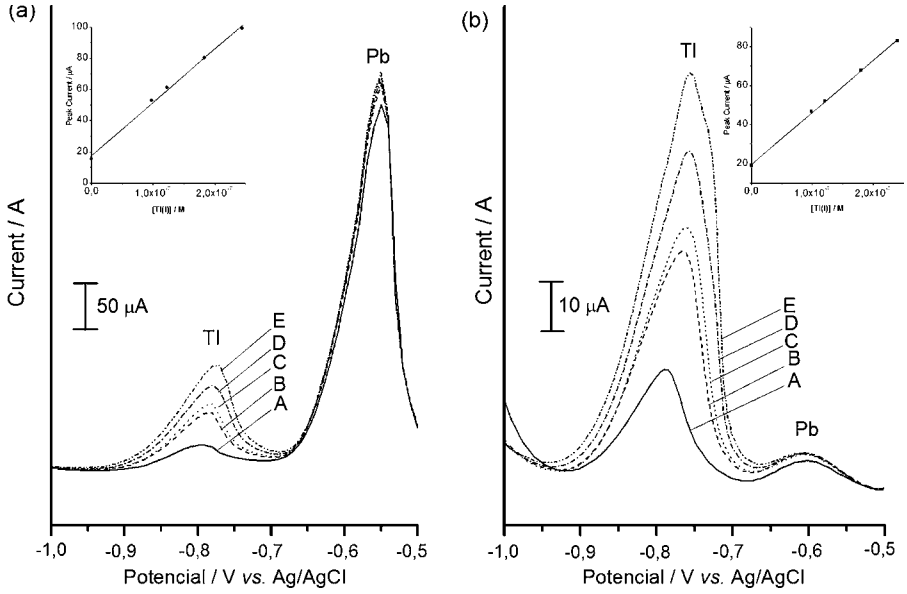

Fig. 6. Standard additions for (a) river water and (b) soil extract samples in acetate buffer. Curves: A, sample; B, C, D and E, sample +98, 120, 180 and 240 nM, respectively, of Tl(I). Other conditions as in Fig. 4.

more than the Tl(I) concentration, and copper over 100-fold more.

3.5. Application to real samples

The analytical utility of the rotating-disc BFE for the determination of Tl(I) in environmental samples was tested with river Tagus water and soil samples collected from polluted sites of the river bank on the outskirts of Lisbon, where a cement plant is in operation nearby. It is interesting to check the thallium levels at this place, since there is some population density together with some agricultural and fishing activities. The anthropogenic activities may cause enrichment of Tl in the environment, leading to abnormally high levels in natural matrices, as reported elsewhere [46].

The suitability of the BFE for the determination of thallium in the samples is illustrated in Fig. 6. The thallium peak in river water and soil extract samples can thus be easily quantified following four standard additions of thallium nitrate solution. The considerably high thallium concentration found in the river water and soil samples, $2.2 \pm 0.1\ \mu g\ L^{-1}$ and $15.0 \pm 0.6\ ng\ g^{-1}$, respectively, has confirmed the suspicion of heavy pollution in this case study. These results demonstrated good agreement compared with independent analysis by graphite furnace atomic absorption spectroscopy (AAS): $2.5 \pm 0.64\ \mu g\ L^{-1}$ and less than $30\ ng\ g^{-1}$, for the water and soil samples, respectively. No appreciable cadmium content was found using the reference method (LOQ for the AAS method: $0.5\ \mu g\ L^{-1}$ Cd). Each analytical measurement was replicated five times using both the ASV and AAS methods.

The high lead content found in the river water (not calculated) is clearly shown by the presence of a sharp stripping peak at ~ -0.6 V in the recorded voltammograms (see Fig. 6a). It is well-known that lead is a contaminant usually present in environmental matrices. The significantly smaller amount of lead shown by the voltammogram obtained for the soil extract was attributed to the very low solubility of lead compounds in water. Thus, lead was not easily transferred to the aqueous phase during the soil treatment procedure employed in the present work.

4. Conclusions

We have demonstrated that BFE's are very suitable to determine trace amounts of thallium in environmental samples by square wave ASV, avoiding the use of mercury. The presented data strongly suggest that BFE will play an important role in electroanalysis in the near future, allowing direct measurements in non-deaerated solutions. The potentialities to operate in flow systems are reinforced by the success of its performance under hydrodynamic conditions, based on the use of the rotating-disc electrode. Ion-exchanger polymeric coatings on the bismuth films [9] should be considered in order to improve the voltammetric signal, lowering detection limits.

The combination of low toxicity of bismuth with good performance of the rotating-disc BFE in voltammetric measurements makes it an attractive and promising sensor to monitor toxic chemical species in environmental matrices using a clean methodology.

Acknowledgements

The authors acknowledge FCT (Fundação para a Ciência e a Tecnologia) for support. We thank Dr. M.A. Trancoso from INETI for the AAS measurements.

References

[1] I. Liem, G. Kaiser, M. Sager, G. Tölg, Anal. Chim. Acta 158 (1984) 179.
[2] R.J.P. Williams, J.J.R. Fraústo da Silva, The Natural Selection of the Chemical Elements, Clarendon Press, Oxford, 1996, p. 626.
[3] A. Leonard, G.B. Gerner, Mutat. Res. 387 (1997) 47.
[4] R.C. Carpenter, Anal. Chim. Acta 125 (1981) 209.
[5] M.A. Floyd, V.A. Fassel, R.K. Winge, J.M. Katzenberger, A.P.D. Silva, Anal. Chem. 52 (1980) 431.
[6] W. Schmidt, V. Dietl, Fresenius Z. Anal. Chem. 315 (1983) 690.
[7] P. Schramel, I. Wendler, J. Angerer, Int. Arch. Occup. Environ. Health 69 (1997) 219.
[8] A. Ciszewski, Z. Lukaszewski, Anal. Chim. Acta 146 (1983) 51.
[9] T.-H. Lu, H.-Y. Yang, I. Wen Sun, Talanta 49 (1999) 59.
[10] N. Spano, A. Panzanelli, P.C. Piu, M.I. Pilo, G. Sanna, R. Seeber, A. Tapparo, Anal. Chim. Acta 553 (2005) 201.
[11] A.K. Das, M. Dutta, M.L. Cervera, M. de la Guardia, Microchem. J. 86 (2007) 2.
[12] R. Cleven, L. Fokkert, Anal. Chim. Acta 289 (1994) 215.
[13] I. Svancara, P. Ostapczuk, J. Arunachalam, H. Emons, K. Vytras, Electroanalysis 9 (1997) 26.
[14] J. Wang, Stripping Analysis, VCH, New York, 1995.
[15] T.R. Copeland, R.K. Skogerboe, Anal. Chem. 46 (1974) 1257A.
[16] B. Krasnodebska-Ostrega, E. Stryjewska, Chem. Anal. (Warsaw) 49 (2004) 519.
[17] E. Gustafsson, Water Air Soil Pollut. 80 (1995) 99.
[18] E.P. Achterberg, C. Braungardt, Anal. Chim. Acta 400 (1999) 381.
[19] O.M.S. Filipe, C.M.A. Brett, Talanta 61 (2003) 643.
[20] J. Wang, B. Tian, Anal. Chem. 65 (1993) 1529.
[21] M.A. Nolan, S.P. Kounaves, Anal. Chem. 71 (1999) 3567.
[22] Y.-C. Tsai, B.A. Coles, K. Holt, J.S. Foord, F. Marken, R.G. Compton, Electroanalysis 13 (2001) 831.
[23] J. Wang, J. Lu, S.B. Hocevar, P.A.M. Farias, Anal. Chem. 72 (2000) 3218.
[24] J. Wang, J. Lu, U.A. Kirgoz, S.B. Hocevar, B. Ogorevc, Anal. Chim. Acta 434 (2001) 29.
[25] T.M. Florence, J. Electroanal. Chem. 27 (1970) 273.
[26] W. Frenzel, Anal. Chim. Acta 273 (1993) 123.
[27] N.F. Zakharchuk, Kh.Z. Brainina, Electroanalysis 10 (1998) 379.
[28] F. Ribeiro, M.M.M. Neto, M.M. Rocha, I.T.E. Fonseca, Anal. Chim. Acta 579 (2006) 227.
[29] A. Królicka, A. Bobrowski, Electrochem. Commun. 6 (2004) 99.
[30] M. Yang, Z. Hu, J. Electroanal. Chem. 583 (2005) 46.
[31] J. Wang, J. Lu, S.B. Hocevar, B. Ogorevc, Electroanalysis 13 (2001) 13.
[32] Z. Guo, F. Feng, Y. Hou, N. Jaffrezic-Renault, Talanta 4 (2005) 1052.
[33] G. Kefala, A. Economou, A. Voulgaropoulos, M. Sofoniou, Talanta 61 (2003) 603.
[34] M. Morfobos, A. Economou, A. Voulgaropoulos, Anal. Chim. Acta 519 (2004) 57.
[35] G. Kefala, A. Economou, A. Voulgaropoulos, Analyst 129 (2004) 1082.
[36] I. Svancara, L. Baldrianova, E. Tesarova, S.B. Hocevar, S.A.A. Elsuccary, A. Economou, S. Sotiropoulos, B. Ogorevc, K. Vytras, Electroanalysis 18 (2005) 177.
[37] H. Dong, H. Zheng, L. Lin, B. Ye, Sens. Actuators B 115 (2006) 303.
[38] Y. Bonfil, M. Brand, E. Kirowa-Eisner, Electroanalysis 15 (2003) 1369.
[39] M.M.G.S. Rocha, M.M.P.M. Neto, M.O. Torres, A. de Varennes, Electroanalysis 9 (1997) 145.
[40] M.M.P.M. Neto, M.M.G.S. Rocha, C.M.A. Brett, Talanta 41 (1994) 1597.

[41] E. Chatzitheodorou, A. Economou, A. Voulgaropoulos, Electroanalysis 16 (2004) 1745.
[42] B. Griepink, M. Sager, G. Tölg, Pure Appl. Chem. 60 (1988) 9.
[43] V.G. Levich, Physicochemical Hydrodynamics, Prentice-Hall, Englewood Cliffs, NJ, 1962.
[44] J.N. Miller, J.C. Miller (Eds.), Statistics and Chemometrics for Analytical Chemistry, fourth ed., Prentice-Hall, Upper Saddle River, NJ, 2000 (Chapter 5).
[45] J.-M. Zen, J.-W. Wu, Electroanalysis 9 (1997) 302.
[46] A.L. John Peter, T. Viraraghavan, Environ. Int. 31 (2005) 493.

Available online at www.sciencedirect.com
ScienceDirect
Talanta 72 (2007) 1474–1480
Talanta
www.elsevier.com/locate/talanta

Improve the signal-to-noise ratio of a quartz crystal microbalance in an impedance analysis method

Qi Kang, Yong Qi, Ping Zhang, Dazhong Shen *

School of Chemistry, Chemical Engineering and Material Science, Shandong Normal University, Jinan 250014, People's Republic of China

Received 12 September 2006; received in revised form 26 January 2007; accepted 26 January 2007
Available online 9 February 2007

Abstract

A new data treatment method for the improvement of the signal-to-noise ratio of a quartz crystal microbalance (QCM) was proposed, where an averaged resonant frequency was calculated according to its conductance peak in an impedance analysis method. The relationship between the averaged resonant frequency and the medians of the conductance peak at different sampling heights was derived. It was shown that the signal-to-noise ratio of the averaged resonant frequency was about eight times of that of the resonant frequency calculated directly from its equivalent circuit parameters. The averaged resonant frequency of the QCM was applied to monitor the self-assembled process of a 6-*O*-(2′-(α-thiohydroxyacetamide)-ethyl)-diethoxylsilyl-β-cyclodextrin (OTED-β-CD), on gold surface as well as the adsorption of nitrophenol isomers onto the OTED-β-CD self-assembled monolayer film.

Keywords: Quartz crystal microbalance; Impedance analysis; Signal-to-noise ratio; Cyclodextrin

1. Introduction

A quartz crystal microbalance (QCM) is a mass sensitive device being widely used for monitoring the solid/liquid interface processes in the past two decades [1–5]. It has been successfully demonstrated that the QCM can be applied in electrochemistry [6], DNA biosensors [7,8], immunosensor [9,10], biomimetic sensor [11,12], organic vapor sensing [13], humidity sensor [14], etc. In the signal measurements of the QCM, an active or a passive methods were employed. In the active method, the oscillating frequency of the oscillating circuit with the QCM as the frequency control element is measured. The active method has the advantage of simplification in apparatus [15]. But the oscillating frequency was related to the oscillating circuit employed and could be not measured in certain situation such as heavy mass loading or highly viscous damping [16]. In the passive method, the values of magnitude and phase of the impedance of the QCM were measured at a group of given frequencies from the externally applied voltages. The electrical properties of the QCM can be found from the impedance–frequency curves [17,18]. Hence, the impedance analysis method can provide more information for the QCM in a liquid phase. Under highly damping conditions, an active oscillation of the QCM is broken down but the forced oscillation from the impedance analyzer still provides valuable information about the coating onto the QCM.

Usually, the motional resistance (R_m), motional inductance (L_m), motional capacitance (C_m) and static capacitance (C_0) of the QCM are measured in the impedance analysis method according to the Butterworth–van Dyke equivalent circuit model [19]. Accordingly, the resonant frequency of the QCM (f_0) is calculated by [1]:

$$f_0 = \frac{1}{2\pi\sqrt{L_m C_m}} \quad (1)$$

It should be noted that a time of about 2–3 s is needed in the calculation of the four equivalent circuit parameters by the single chip micyoco in an impedance analyzer. On the other hand, the noise level of the resonant frequency obtained from Eq. (1) is about ±1 Hz for the QCM with one side facing an aqueous solution. In this work, the signal-to-noise ratio of the resonant frequency of the QCM was improved by using an averaged technique in a user program. The averaged resonant frequency was calculated according to the medians and spans of the conductance peak at different sampling heights, which had a

* Corresponding author. Fax: +86 531 82615258.
E-mail address: dzshen@sdnu.edu.cn (D. Shen).

0039-9140/$ – see front matter © 2007 Elsevier B.V. All rights reserved.
doi:10.1016/j.talanta.2007.01.060

much lower noise level than the commonly used f_0 in Eq. (1) by using the L_m and C_m values provided directly by an impedance analyzer. The calculation time is less than 0.1 s in a personal computer for the averaged resonant frequency and the equivalent circuit parameters of the QCM in the user program. The correlation between the averaged frequency and the medians and spans of the conductance peak at different sampling heights was analyzed.

As a model example of the applicability of the averaged frequency, the self-assembled process of a thiol-terminated β-cyclodextrin derivative, 6-*O*-(2′-(α-thiohydroxyacetamide)-ethyl)-diethoxylsilyl-β-cyclodextrin (OTED-β-CD) on gold surface, as well as the adsorption of nitrophenol isomers onto the OTED-β-CD self-assembled monolayer (SAM) film, were investigated by the QCM. The OTED-β-CD was chosen as the model system because cyclodextrin derivatives were attractive for the constructions of supramolecular recognition systems, thanks to their structural characteristics and special functions [20,21]. The cyclodextrin derivatives had been found applications in fluorometry [22–24], spectrophotometry [25], sensors [26–28], enantioseparation [29,30], etc. The mass changes during the processes of the OTED-β-CD self-assembled onto gold surface and nitrophenol isomers adsorbed onto the OTED-β-CD SAM films were monitored in situ by the averaged frequency shifts of the QCM. The adsorption equilibrium constants of nitrophenol isomers onto the OTED-β-CD SAM film were estimated. The new data treatment method shows a good applicability for QCM in liquid phases.

2. Experiment

2.1. Apparatus and reagents

The experimental set-up was similar to that described in a previous work [31]. AT-cut 10 MHz QCM crystals with polished gold electrodes (diameter 5.1 mm) were purchased from International Crystal Manufacturer (OK, USA). The QCM was attached to the detection cell with one side exposed to the liquid phase by two O rings. The quartz wafer was in an angle of ca. 60° to the horizontal surface to eliminate the possible longitudinal wave effect of the QCM [32]. The temperature of the detection cell was controlled at 25 ± 0.1 °C by a thermostatic water bath. The leading wires from the two gold electrodes were connected to a precision impedance analyzer (Agilent 4294A) through 16047E test fixture for axial lead components. The parasitic capacitance and inductance of the test fixture and leading wires were corrected in the calibration step prior to measurements. A user program written in Visual Basic 6.0 was used to control the impedance analyzer and to acquire and process the impedance data. The conductance (G) of the QCM was scanned at 801 measuring frequencies in its resonance region. The resonant frequencies of the QCM were estimated from the medians and spans of the conductance peak at different sampling heights (see Fig. 1). A weighting averaged resonant frequency was obtained according to the proposed method.

Analytical-reagent grade chemicals and double-distilled water were used. Nitrophenol isomers (*o*-, *m*- and *p*-) were purchased from Shanghai Chemicals. β-Cyclodextrin was purchased from Jinan Chemicals and was re-crystallized from water for three times. OTED-β-CD was synthesized in this lab according to Refs. [33,34].

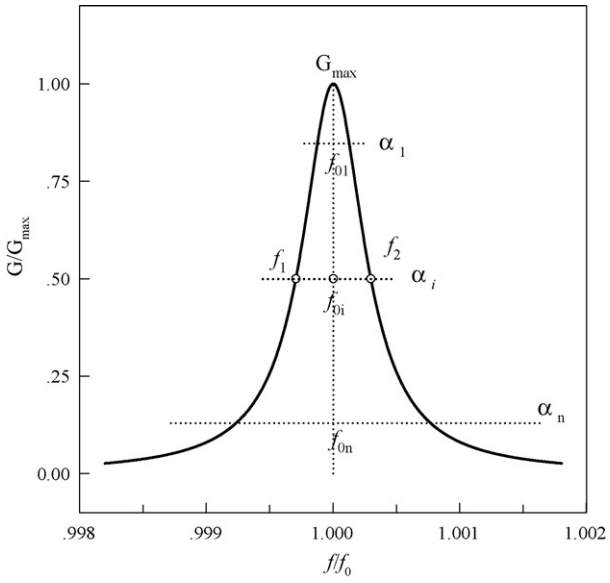

Fig. 1. Relationship between the resonant frequency (f_0) and measuring frequencies (f_1 and f_2) at different sampling heights (α_i) in the conductance peak of the QCM.

2.2. Monitoring the adsorption processes of nitrophenol onto OTED-β-CD film by QCM

Before the self-assembled experiment, the detection cell was cleaned by acetone and water, respectively. The cell was dried by N_2 stream and rotated to keep the QCM in horizontal. Ten microlitres of Piranha solution (75% H_2SO_4, 25% H_2O_2) was spread on the gold electrode inside the cell for 5 min. The detection cell was cleaned by water and ethanol then rotated back to normal position with the quartz wafer was in an angle of ca. 60° to the horizontal surface. Twenty-five millilitres of ethanol was added into the sealed detection cell. After the stability of the baseline of the QCM, an OTED-β-CD stock solution in ethanol was added in the closed detection cell by a microsyringe. The initial concentration of OTED-β-CD in the cell was 2.5×10^{-5} mol/L. The frequency shifts (Δf) during the early self-assembled processes of OTED-β-CD on gold electrode surface was monitored with a time interval of 7.8 s. The observed adsorption mass (Γ) was calculated according to the Sauerbrey equation as follows:

$$\Gamma = \frac{-\Delta f}{2.26 \times 10^{-6} F_0^2} \quad (2)$$

where F_0 is the fundamental frequency of the QCM.

After a self-assembled time of overnight, the gold electrode surface and detection cell were cleaned by ethanol and water, respectively. Then 25 mL phosphate buffer (8.8 mmol/L KH_2PO_4 + 1.2 mmol/L Na_2HPO_4, pH 6) was added in the detection cell. The stable frequency was recorded as the reference. A

desired amount of nitrophenol stock solution was added into the detection cell. In the kinetics experiments, the frequency shifts in solutions of given concentration of nitrophenol were followed. In the adsorption isotherm experiments, nitrophenol was sequentially added and the stable frequency shifts were record to estimate the adsorbed mass. After the adsorption of nitrophenol, the OTED-β-CD SAM film was regenerated by thoroughly rinsing with the phosphate buffer.

3. Results and discussion

3.1. Evaluating the resonant frequency of QCM in impedance analysis method

In an impedance analysis method, the magnitude and phase of the impedance of the QCM were scanned at a series of measuring frequencies in its resonance region. And four equivalent circuit parameters of a QCM were provided by the impedance analyzer itself in 2–3 s. According to Eq. (1), the resonant frequency of the QCM was obtained. As shown in Fig. 2, the noise level of this resonant frequency is about ±1 Hz for the QCM with one side facing an aqueous solution. To improve the signal-to-noise ratio of resonant frequency of the QCM and to speed up the calculation, a user program was written to analyze the impedance data in a personal computer. The method to estimate the resonant frequency of the QCM was discussed below.

In the frequency region near the resonance of the QCM, the conductance of the QCM was given by [1]:

$$G = \frac{R_m}{R_m^2 + (\omega L_m - \omega^{-1} C_m^{-1})^2} \tag{3}$$

where $\omega = 2\pi f$, f is the measuring frequency.

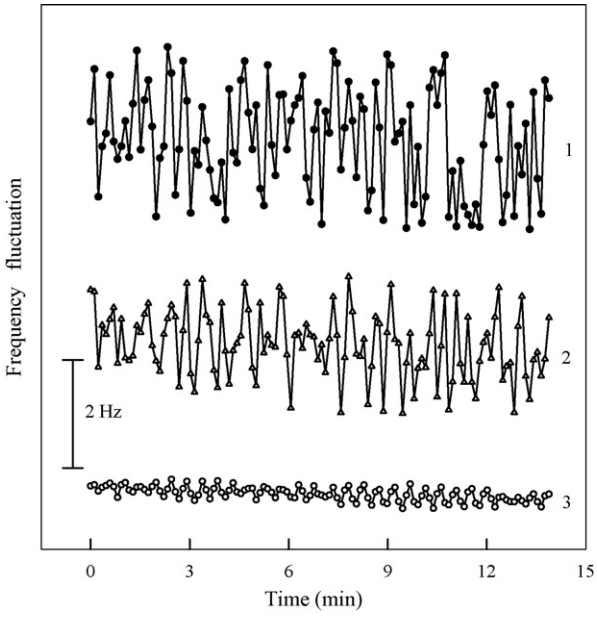

Fig. 2. Comparison of the noise level of the stable baseline of QCM in water. (1) Frequency calculated by $f_0 = 1/(2\pi\sqrt{L_m C_m})$; (2) frequency estimated from Eq. (9) at $\alpha_i = 0.5$; (3) averaged frequency from 200 sampling heights estimated from Eq. (10) with $\alpha_i = 0.15$–0.95.

According to Eq. (3), the resonant frequency is corresponded to the measuring frequency at the point of $(\omega L_m - \omega^{-1} C_m^{-1}) = 0$, where the maximum conductance, $G_{max} = R_m^{-1}$, is obtained. Fig. 1 depicts a typical conductance–frequency spectrum of a QCM in water. Theoretically, an f_0 was obtained by searching the measuring position of G_{max} in the conductance peak. But the precision of f_0 was rather poor as the frequency resolution was limited by the scanning interval used. Hence, a time-consuming stepwise scanning method was needed, where the frequency span was reduced step-by-step, and the center frequency was changed to find more accurate corresponding frequency [35].

As shown in Fig. 1, the conductance peak is in a good symmetry. The f_0 value should be very close to the middle line of the conductance peak. At a given sampling height of $\alpha_i = G_i/G_{max}$, the frequencies at the two intersections, f_1 and f_2, can be calculated with high precision by an interpolation arithmetic. Hence, the median, $f_{12} = (f_1 + f_2)/2$, has a much better precision than that of f_0 at the point of G_{max} in the experimental curve. According to Eq. (3), the following equation was given at the given height:

$$(\omega L_m - \omega^{-1} C_m^{-1})^2 = (\alpha_i^{-1} - 1) R_m^2 \tag{4}$$

From the two roots for ω in Eq. (4), the expressions of the two intersections were given by:

$$f_1 = f_0[1 - \pi f_0 C_m R_m (\alpha_i^{-1} - 1)^{0.5} + 0.5\pi^2 f_0^2 R_m^2 C_m^2 (\alpha_i^{-1} - 1)] \tag{5}$$

$$f_2 = f_0[1 + \pi f_0 C_m R_m (\alpha_i^{-1} - 1)^{0.5} + 0.5\pi^2 f_0^2 R_m^2 C_m^2 (\alpha_i^{-1} - 1)] \tag{6}$$

Accordingly, median and the span $(f_2 - f_1)$ were expressed as:

$$f_{12} = f_0[1 + 0.5\pi^2 f_0^2 R_m^2 C_m^2 (\alpha_i^{-1} - 1)] \tag{7}$$

$$f_2 - f_1 = 2\pi f_0^2 C_m R_m (\alpha_i^{-1} - 1)^{0.5} \tag{8}$$

From Eqs. (7) and (8), the resonant frequency was obtained from the combination of the median and span of the conductance peak at a given sampling height:

$$f_0 = f_{12} - \frac{(f_2 - f_1)^2}{8 f_{12}} \tag{9}$$

It can be seen that there is a slight difference between the values of f_0 and f_{12}. As the span increases, this difference becomes larger. According to Eq. (8), the span increases with increasing R_m or reducing α_i. Hence, the difference between f_0 and f_{12} was related to the sampling height and the viscodensity of the liquid phase, which is supported by the experimental results in Fig. 3. For example, the difference between Δf_0 and Δf_{12} can be neglected for a QCM in air because the R_m is small (ca. 5 Ω). When the QCM was in contact with a viscous liquid (56% glycerin, $R_m = 950$ Ω), the difference between Δf_0 and Δf_{12} was not negligible, especially in the bottom of the conductance peak with a small α_i used.

It should be noted that the difference between f_0 and f_{12} was quite small for a QCM with one side in contact with water

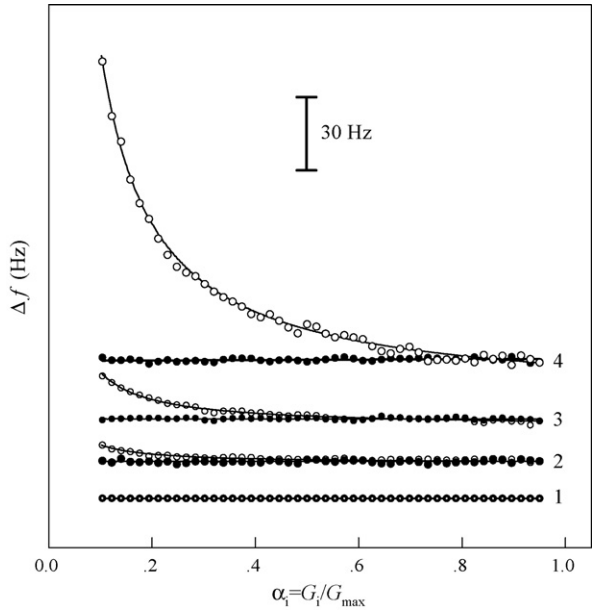

Fig. 3. Dependence of the shifts between the resonant frequency (●) and middle frequency (◯) of the QCM in the impedance analysis method. (1) In air; (2) in water; (3) in 30% glycerin; (4) in 56% glycerin.

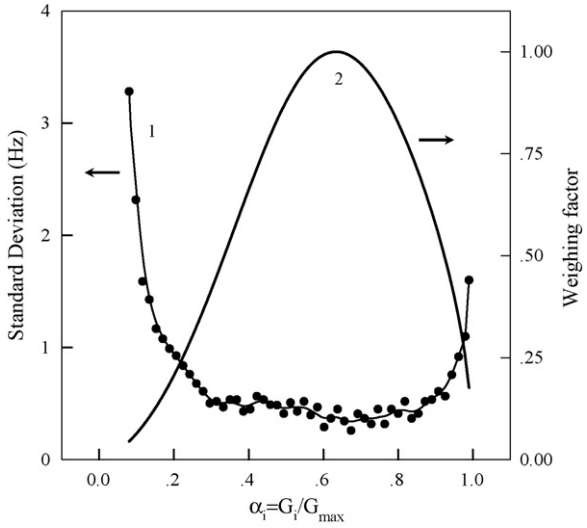

Fig. 4. (1) Dependence of the standard deviation of the baseline of QCM in water on the sampling heights. (2) Weighing factors used in averaged resonant frequency at different sampling heights.

($R_m = 330\,\Omega$). The value of f_{12} can be used as f_0 in most of cases except in the theoretical simulation of the impedance of the QCM. On the other hand, the motional parameters of the QCM can be calculated by: $R_m = 1/G_{max}$, $L_m = (\alpha_i^{-1} - 1)R_m/2\pi(f_2 - f_1)$, $C_m = (4\pi^2 f_0^2 L_m)^{-1}$. At the half height of the conductance peak, $\alpha_i = 0.5$, the calculation for L_m was simplified as $L_m = R_m/2\pi(f_2 - f_1)$.

3.2. Improving the signal-to-noise ratio of QCM by a mean technique

As shown in Fig. 2, the noise level of f_0 at one sampling height ($\alpha_i = 0.5$) was about ±0.7 Hz in the measurement of the baseline of QCM in water, which is a little less than that of f_0 calculated by Eq. (1) in the classical method. It should be noted that only the data at four measuring points were used to estimate the f_0 by Eq. (9) at a given sampling height on the conductance peak. In fact, much more points were measured to complete a conductance spectrum. In this work, the conductance of the QCM was scanned at 801 measuring frequencies. Thus, many sampling heights can be used to calculate f_0, which is equivalent to the reduplicative measurements of f_0 in a scan. Hence, an averaged resonant frequency was proposed as a new measuring parameter in the impedance analysis method. As shown in Fig. 2, the noise level of an averaged resonant frequency is much reduced. In this figure, the standard deviation (S.D.) of the averaged resonant frequency was 0.12 Hz, which was about 1/6 and 1/8 of that of f_0 at $\alpha_i = 0.5$ and f_0 from Eq. (1), respectively. Therefore, the signal-to-noise ratio of QCM was expected to improve by using the averaged resonant frequency method.

Fig. 1 illustrates the principle of the averaged resonant frequency method. In short, the resonant frequencies from different sampling heights in the conductance peak were averaged according to the following equation in order to decrease the random noise:

$$f_0 = \frac{\sum_{i=1}^{n} w_i f_{0i}}{\sum_{i=1}^{n} w_i} \tag{10}$$

where n is the number of sampling heights, w_i the weighing factor, and f_{0i} the resonant frequency at given sampling height of α_i, respectively. The value of w_i was related to the sampling height.

Fig. 4 shows the S.D. values of the baseline presented by f_0 in Eq. (9) at different sampling heights. It can be seen that the S.D. values were similar in the range of $\alpha_i = 0.25$–0.9. In the bottom of the conductance peak ($\alpha_i < 0.25$), the S.D. values increase as α_i decreases. But in the top of the conductance peak ($\alpha_i > 0.9$), the S.D. values increase slightly as α_i increases. The dependence of S.D. on the sampling height can be interpreted from the first derivative of conductance with respect to frequency ($\partial G/\partial f$):

$$\frac{\partial G}{\partial f} = -\frac{8\pi R_m L_m(\omega L_m - \omega^{-1}C_m^{-1})}{[R_m^2 + (\omega L_m - \omega^{-1}C_m^{-1})^2]^2} = \pm\frac{8\pi L_m(\alpha_i^{-1} - 1)}{[1 + (\alpha_i^{-1} - 1)^2]^2 R_m^2} \tag{11}$$

As shown in Eq. (11), the value of $\partial G/\partial f$ is sensitive to the sampling height. At the top of the conductance peak ($\alpha_i = 1$), we have $\partial G/\partial f = 0$ because of $(\alpha_i^{-1} - 1) = 0$. As the sampling height decreases, the value of $|\partial G/\partial f|$ increases until reaches its maximum of $8.16L_m/R_m^2$ at $\alpha_i = 0.634$ then decreases. In the bottom of the conductance peak, the value of $|\partial G/\partial f|$ is much reduced. For example, we have $|\partial G/\partial f| = 0.03L_m/R_m^2$ at $\alpha_i = 0.1$. The larger the value of $|\partial G/\partial f|$, the less the influence of a random error in G on the estimation of f_0 from Eq. (9). Hence, the S.D. values of f_0 estimated from the bottom and top parts of the conductance peak were larger than those from the middle of the conductance peak.

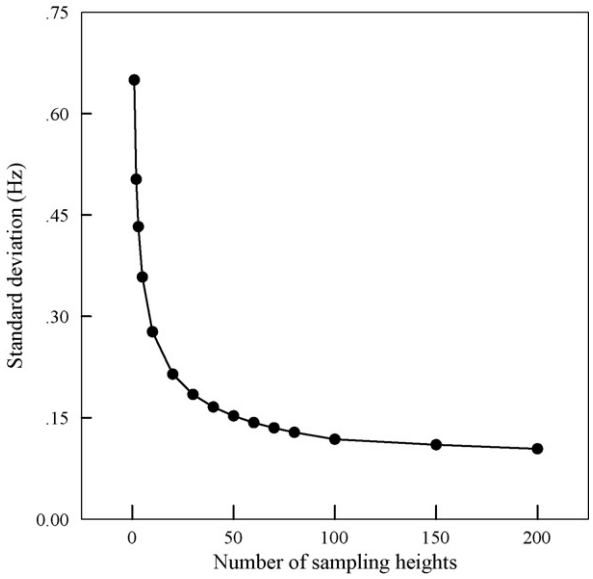

Fig. 5. Dependence of the standard deviation of the baseline of QCM in water on the number of sampling heights.

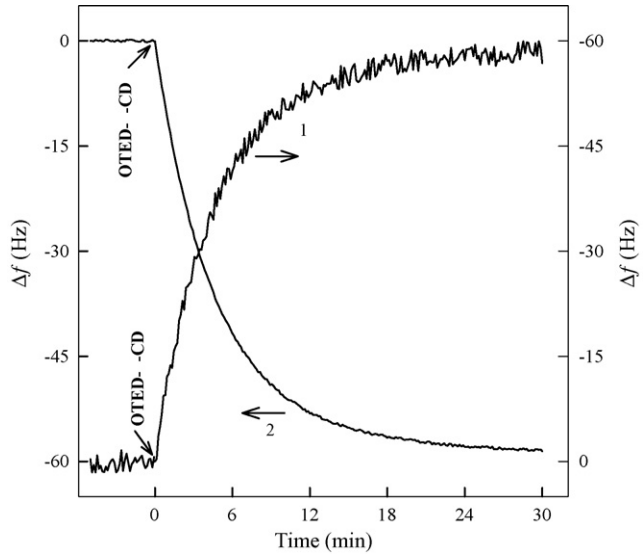

Fig. 6. Frequency shifts of QCM during the self-assembled process of OTED-β-CD (2.5×10^{-5} mol/L in ethanol) on the surface of gold electrode. (1) Frequency shifts calculated by $f_0 = 1/(2\pi\sqrt{L_m C_m})$; (2) averaged frequency shifts estimated by Eq. (10) from 200 sampling heights with α_i in the range of 0.15–0.95. The two curves were measured at the same experiment and shown in contrary directions for drawing clarity.

Based on the values of $|\partial G/\partial f|$ and the S.D. in Fig. 4, the weighing factors, which were proportional to $|\partial G/\partial f|^{1/2}$ and shown in Fig. 4, were used in this work. By using the weighing factors, the S.D. of the averaged resonant frequency was a little lower than the classical mean method with $w_i = 1$ at all sampling heights.

Fig. 5 illustrates the dependence of the S.D. of the baseline of the QCM in water on the number of sampling heights. In the choice of the sampling height, the co-linearity among the measuring points was avoided by using suitable α_i interval between two adjacent sampling heights. It can be seen that the S.D. values decrease as the number of sampling height increases, especially in the region of low sampling number. When the number of sampling heights was reached to 100, the S.D. value approached to a stable level. In this work, the averaged resonant frequency from 200 sampling heights with α_i in the range of 0.15–0.95 was used. The averaged frequency with lower noise level was expected to increases the signal-to-noise ratio of the QCM, which, in turn, yields a lower detection limit. To demonstrate the applicability of the averaged resonant frequency, the interaction between β-cyclodextrin and nitrophenol was investigated by the QCM technique.

3.3. Monitoring the formation of OTED-β-CD SAM on gold

A β-cyclodextrin (β-CD) is a cyclic oligosaccharide consisting of seven glucose units. This cone shaped molecule is known to form inclusion complexes with a variety of guest compounds containing hydrophobic groups. To study the inclusion interaction by the QCM technique, it is needed to immobilize the β-CD onto the electrode surface of the QCM. In this work, a thiol-terminated β-cyclodextrin derivative, OTED-β-CD, was chosen since it was adsorbed onto the Au surface as a result of the chemical bonding between S atoms in the molecules and the Au surface. The OTED-β-CD SAM is considered to be located on the Au surface with their cavity axis aligned perpendicular to the surface. The mass changes in the self-assembled processes of the OTED-β-CD on gold surface were monitored in real time from the frequency shifts of the QCM.

As can be seen in Fig. 6, the self-assembled process is quite rapid. The frequency shifts were approached to stable value within 30 min. Again, the averaged resonant frequency shifts have a much less noise level than the resonant frequency shifts calculated according to Eq. (1). The stable averaged frequency shift for the self-assembled process was 58.4 ± 4.7 Hz, which corresponds to an observed binding mass of 0.258 μg/cm^2.

3.4. Monitoring the adsorption of nitrophenol onto OTED-β-CD SAM film

Molecular recognition phenomena have been extensively studied for various applications ranging from sensing to separations. Chemical sensors based on host–guest interactions have attracted increasing attentions [21]. Cyclodextrins have drawn much attention due to their capability of molecular recognition, owing to their well-defined cavities, whose sizes are different depending on the number of amylose units in cyclic oligomers.

With OTED-β-CD self-assembled on the electrode surface of the QCM, the mass changes during the adsorption processes of nitrophenol isomers onto the OTED-β-CD SAM film were followed according the resonant frequency shifts. The main forces for the adsorption include the penetration of the hydrophobic part of the nitrophenol into the cyclodextrin cavity and the intermolecular hydrogen bind between OTED-β-CD SAM film and nitrophenol. The inclusion complex was expected to form

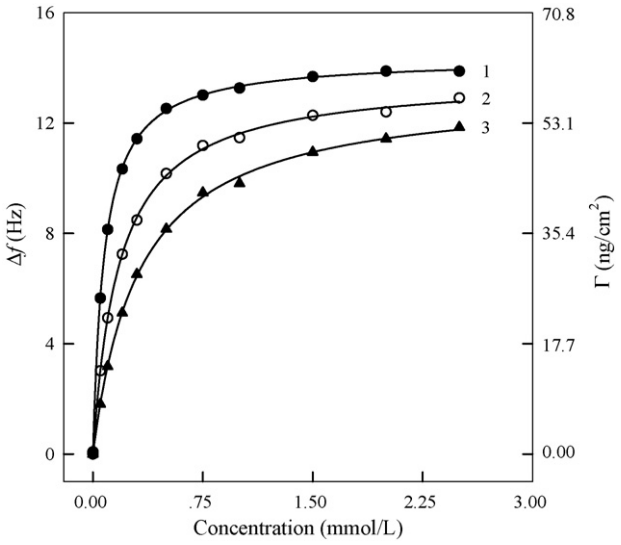

Fig. 7. Observed adsorption isotherms of nitrophenol isomers on OTED-β-CD SAM film. (1) *p*-Nitrophenol; (2) *m*-nitrophenol; (3) *o*-nitrophenol.

on the OTED-β-CD SAM film. It was shown that the adsorption process of 1 mmol/L nitrophenol onto OTED-β-CD film was finished within 4 min. As the concentration of nitrophenol increases, adsorption equilibrium is reached in a shorter time. After the adsorption, the detection cell was rinsed with nitrophenol-free buffer, the resonant frequency of the QCM increased and approached to the previous baseline. This result indicated that the adsorption of nitrophenol onto the OTED-β-CD film was reversible with respect the dilution of the bulk phase.

According to the frequency decreases of the QCM, the adsorbed masses were calculated from Eq. (2). Fig. 7 illustrates the observed adsorption isotherms of three nitrophenol isomers onto the OTED-β-CD SAM film. The adsorption isotherms can be fitted well with the Langmuir isotherm in the following equation:

$$\Gamma = \frac{\Gamma_\infty KC}{1 + KC} \tag{12}$$

where Γ_∞ was the saturated adsorption mass, K the adsorption equilibrium constant. Fitting Langmuir isotherms to the plots in Fig. 7 yielded the adsorption equilibrium constants were regressed to be 1.37×10^3, 5.62×10^3, 1.31×10^4 L mol^{-1} for *o*-, *m*- and *p*-nitrophenol, respectively.

The difference in adsorption equilibrium constants may be due to the molecular structure of the nitrophenol isomers. The top and bottom diameters of the cavity of β-CD are 6.0 and 6.5 Å, respectively [36]. A *p*-nitrophenol molecular has the minimum structure resistance for entrancement the CD cavity. Hence, the adsorption equilibrium constant is the biggest among the three isomers. An *o*-nitrophenol molecular has the maximum structure resistance for entrancement the CD cavity. The hydrogen bind in the *o*-nitrophenol molecular weakens its interaction with the CD film. Thus, the adsorption equilibrium constant for *o*-nitrophenol was less than that for *p*- and *m*-nitrophenols.

3.5. Estimating the absorption kinetic parameters for nitrophenols onto OTED-β-CD film

As discussed above, the adsorption processes of nitrophenols onto the OTED-β-CD film were reversible and the adsorption isotherms were in Langmuir type. Hence, the adsorption processes were analyzed by the Langmuir adsorption model. The adsorption rate is assumed to be proportional to the concentration of nitrophenol in solution and to the free surface area. The desorption rate is proportional to the number of adsorbed nitrophenol. In the adsorption process, we have:

$$\frac{\mathrm{d}\theta}{\mathrm{d}t} = k_\mathrm{a}C(1-\theta) - k_\mathrm{d}\theta \tag{13}$$

where θ denotes the fraction of surface area covered by nitrophenol, k_a and k_d the rate constants for adsorption and desorption, respectively, t is the adsorption time. For all experiments carried out here, the amount of nitrophenol in solution is much large compared to the amount on the surface. Hence, C is constant and $k_\mathrm{a}C$ is a pseudo-first-order rate constant with units of reciprocal seconds.

According to Eq. (13), the expression of θ was obtained. Under certain conditions, the frequency shifts of a QCM are in a linear correlation with the adsorption amounts. If the adsorption layer is homogenous, the frequency shift of the sensor is in a linear relationship with θ, i.e., $\Delta f = \theta\,\Delta f_\mathrm{sat}$. Here Δf_sat was the frequency shift corresponding to the adsorption mass of a saturation adsorption layer of nitrophenol. Accordingly, the frequency shift of the QCM in the adsorption processes is expressed as:

$$\Delta f = \frac{\Delta f_\mathrm{sat} KC}{1 + KC}[1 - \exp(-(k_\mathrm{a}C + k_\mathrm{d})t)] \tag{14}$$

By using Eq. (14) as the fitting model, an observed rate constant, $k_1 = k_\mathrm{a}C + k_\mathrm{d}$, was obtained from the frequency shifts of the QCM in a given concentration of nitrophenol. It was revealed that the k_1 values were in good linearity with the concentration of nitrophenol in solution. According to the slopes of the plottings of k_1 versus C, the adsorption rate constants were estimated. Under our experimental conditions, the adsorption rate constants were 11.6, 17.4 and 21.9 L mol^{-1} s^{-1} for *o*-, *m*- and *p*-nitrophenol, respectively. The desorption rate constants were estimated by $k_\mathrm{d} = k_\mathrm{a}/K$, to be 8.47×10^{-3}, 3.10×10^{-3} and 1.67×10^{-3} s^{-1} for *o*-, *m*- and *p*-nitrophenol, respectively.

4. Conclusions

The results described above indicated that the proposed data treatment method is a simple and efficient way to improve the signal-to-noise ratio of a QCM in an impedance analysis method. The signal-to-noise ratio of the averaged resonant frequency was about eight times of classical resonant frequency from equivalent circuit parameters. The difference between the resonant frequency and the center frequency of the conductance peak was discussed. In contact with low viscous liquid phase, the two frequencies were very close. As the viscosity of the liquid phase increases, the difference becomes larger, especially in the bottom part of the conductance peak. The averaged resonant fre-

quency is a useful parameter for the application of the QCM to monitor the interface process with a relatively small frequency shift, such as the adsorption of nitrophenol isomers onto the OTED-β-CD SAM film. It was shown that adsorption processes of nitrophenols onto the OTED-β-CD film were reversible and the adsorption isotherms were in Langmuir type. The adsorption equilibrium constants were estimated to be 1.37×10^3, 5.62×10^3, 1.31×10^4 L mol^{-1} for *o*-, *m*- and *p*-nitrophenol, respectively. And the adsorption rate constants were evaluated to be 11.6, 17.4 and 21.9 L mol^{-1} s^{-1} for *o*-, *m*- and *p*-nitrophenol, respectively.

Acknowledgements

The authors gratefully acknowledge financial support of the National Natural Science Foundation of China (no. 20275021, no. 20527005) and the Natural Science Foundation of Shandong Province (no. 2004B01).

References

[1] D.A. Buttry, M.D. Word, Chem. Rev. 92 (1992) 1355.
[2] A. Janshoff, H.J. Galla, Angew Chem. Int. Ed. 39 (2000) 4004.
[3] K.A. Marx, Biomacromolecules 4 (2003) 1099.
[4] V.M. Mecea, Sens. Actuators A 128 (2006) 270.
[5] E.A. Mothershed, A.M. Whitney, Clin. Chim. Acta 363 (2006) 206.
[6] A.R. Hillman, in: A.J. Bard, M. Stratmann (Eds.), Encyclopaedia of Electrochemistry, vol. 3, Wiley, New York, 2003, pp. 230–289.
[7] S. Tombelli, M. Minunni, A. Santucci, M.M. Spiriti, M. Mascini, Talanta 68 (2006) 806.
[8] X.L. Su, R. Robelek, Y. Wu, G.Y. Wang, W. Knoll, Anal. Chem. 76 (2004) 489.
[9] Y.G. Lee, K.S. Chang, Talanta 65 (2005) 1335.
[10] Y. Zhang, V. Telyatnikov, M. Sathe, X. Zeng, P.G. Wang, J. Am. Chem. Soc. 125 (2003) 9292.
[11] B.S. Ebarvia, S. Cabanilla, F. Sevilla III, Talanta 66 (2005) 145.
[12] Z.H. Zhang, H. Li, H.P. Liao, L.H. Nie, S.Z. Yao, Sens. Actuators B 105 (2005) 176.
[13] I. Goubaidoulline, G. Vidrich, D. Johannsmann, Anal. Chem. 77 (2005) 615.
[14] P.G. Su, Y.L. Sun, C.C. Lin, Talanta 69 (2006) 946.
[15] S. Bruckenstein, M. Shay, Electrochim. Acta 30 (1985) 1295.
[16] D.Z. Shen, Q. Kang, Y.H. Xue, L.Z. Wang, Sens. Actuators B 50 (1998) 253.
[17] D.S. Ballantine, R.M. White, S.J. Martin, Acoustic Wave Sensors, Theory, Design and Physico-chemical Applications, Academic Press, San Diego, 1997.
[18] S.Z. Yao, Piezoelectric Chemistry and Biosensors, Hunan Normal University Press, Changsha, 1997.
[19] M.A.M. Noel, P.A. Topart, Anal. Chem. 66 (1994) 484.
[20] A. Douhal, Chem. Rev. 104 (2004) 1955.
[21] J. Szejtli, T. Osa, Comprehensive Supramolecular Chemistry, vol. 3, Pergamon/Elsevier, Oxford, 1996.
[22] Y. Yang, X. Yang, C.X. Jiao, H.F. Yang, Z.M. Liu, G.L. Shen, R.Q. Yu, Anal. Chim. Acta 513 (2004) 385.
[23] B. Tang, Z.Z. Chen, N. Zhang, J. Zhang, Y. Wang, Talanta 68 (2006) 575.
[24] X. Wang, H.L. Zeng, L.X. Zhao, J.M. Lin, Anal. Chim. Acta 556 (2006) 313.
[25] S.O. Fakayode, M.A. Busch, K.W. Busch, Talanta 68 (2006) 1574.
[26] R.I.S. Staden, A.A. Ratko, Talanta 69 (2006) 1049.
[27] B. Kieser, C. Fietzek, R. Schmidt, G. Belge, U. Weimar, V. Schurig, G. Gauglitz, Anal. Chem. 74 (2002) 3005.
[28] M.A.A. Lomillo, O.D. Renedo, M.J.A. Martinez, Electrochim. Acta 50 (2005) 1807.
[29] N. Na, Y. Hu, J. Ouyang, W.R.G. Baeyens, J.R. Delanghe, Y.E.C. Taes, M. Xie, H. Chen, Y. Yang, Talanta 69 (2006) 866.
[30] V. Schurig, S. Mayer, J. Biochem. Biophys. Methods 48 (2001) 117.
[31] D.Z. Shen, Q. Kang, M.H. Huang, H.T. Zhang, M.S. Yang, Anal. Chim. Acta 551 (2005) 15.
[32] D.Z. Shen, Q. Kang, P. Zhang, C.Y. Guo, Anal. Chim. Acta 525 (2004) 205.
[33] Y. Inoue, T. Hakushi, L. Yu, J. Am. Chem. Soc. 115 (1993) 475.
[34] P. Fugedi, P. Nanasi, J. Szejtli, Carbohydr. Res. 175 (1988) 173.
[35] A.L. Kipling, M. Thompson, Anal. Chem. 62 (1990) 1514.
[36] M.V. Rekharsky, Y. Inoue, Chem. Rev. 98 (1998) 1875.

Available online at www.sciencedirect.com
ScienceDirect
Talanta 72 (2007) 1348–1356
Talanta
www.elsevier.com/locate/talanta

Liquid chromatographic/electrospray mass spectrometric determination (LC/ESI-MS) of chelerythrine and dihydrochelerythrine in near-critical CO_2 extracts from real and spiked plasma samples

Bořivoj Klejdus [a], Lea Lojková [a], Pavel Kosina [b], Jitka Ulrichová [b], Vilím Šimánek [a], Vlastimil Kubáň [a,*]

[a] *Department of Chemistry and Biochemistry, Mendel University of Agriculture and Forestry Brno, Zemědělská 1, CZ-613 00 Brno, Czech Republic*
[b] *Institute of Medical Chemistry and Biochemistry, Faculty of Medicine, Palacký University, Hněvotínská 3, 775 15 Olomouc, Czech Republic*

Received 11 August 2006; received in revised form 11 January 2007; accepted 19 January 2007
Available online 2 February 2007

Abstract

Two polar benzo[*c*]phenanthridine alkaloids, chelerythrine (CHE) and dihydrochelerythrine (DHCHE), were extracted at 35 °C and 10 MPa (15 MPa for real samples) from real and spiked plasma samples with acceptable recoveries (95.1% and 81.0%, respectively) using near-critical CO_2 modified with aqueous (1:1, v/v) methanol. The alkaloids were quantified by a liquid chromatographic/electrospray mass spectrometric (LC/ESI-MS) method on a Zorbax SB-CN column (75 mm × 4.6 mm, 3.5 μm particle size) using methanol (organic phase) and 50 mM ammonium formiate (aqueous phase) as a mobile phase. A linear gradient 0–1 min, isocratic at 60% organic phase (v/v); from 1.0 to 7.0 min, 60–71% organic phase (v/v); from 7.0 to 18.0 min, 71–60% organic phase (v/v) was applied. The limit of detection was 1.22 ng (3.50 pmol) for CHE and 0.95 ng (2.72 pmol) for DHCHE per 1 ml of the sample. The linearity of the calibration curves was satisfactory as indicated by coefficients of determination 0.9979 and 0.9995 for CHE and DHCHE, respectively. Repeatability and intermediate precision (average R.S.D.s) were 1.0–1.5%, accuracy was in the range 99.7–100.3%. Average recovery was 100.1% for both, standard solutions and spiked plasma extracts. Three samples of real rat plasma were extracted and analysed to test the method.

Keywords: Liquid chromatography/electrospray mass spectrometry; Benzo[*c*]phenanthridine alkaloids; Chelerythrine; Dihydrochelerythrine; Near-critical CO_2 extraction; Spiked and real samples; Plasma matrix

1. Introduction

Quaternary benzo[*c*]phenanthridine alkaloids (QBA), originating from aromatic amino acid tyrosine, are found within the families Fumariaceae, Papaveraceae, Ranunculaceae and Rutaceae, where they act as phytochemicals with a broad spectrum of biological activity [1,2]. Plants containing QBA are used in traditional medicine and homeopathy. Standardized extracts from *Sanguinaria canadensis* and *Macleaya cordata* are used in oral hygiene products and for treatment of periodontal disease for their supposed antimicrobial and anti-inflammatory effects [3]. Aqueous extract of the bark of *Bocconia arborea*, common Mexican tree, has been used in traditional medicine to cure diabetes, cancer, inflammatory affections and bacterial infections. It is generally believed to produce beneficial effects [4].

The QBA were found also in the oil extracted from *Argemone mexicana* [5]. Several cases of intoxication by argemone-containing edible oil [6], referred to as epidemic dropsy, were registered in India (2900 hospitalized people and more than 67 deaths in August 1998). In China, sanguarine and chelerythrine contamination was found in honey due to bees gathering nectar and pollen from *M. cordata* [7]. Alkaloids were proclaimed to change the product taste, reduce its quality and posses a health risk to consumers.

There are a lot of analytical procedures for determination of QBA in biological materials (plant extracts, animal tissues, etc.), pharmacological and veterinary preparations and for studies of their biotransformations. Gas chromatography with mass spectrometric detection [8], high-performance liquid chromatography utilizing UV–vis spectrophotometric and

* Corresponding author. Tel.: +420 545133285; fax: +420 545212044.
E-mail address: kuban@mendelu.cz (V. Kubáň).

0039-9140/$ – see front matter © 2007 Elsevier B.V. All rights reserved.
doi:10.1016/j.talanta.2007.01.055

fluorimetric [9–11], mass spectrometric [7,12,13] and other detection systems and even electromigration methods, including isotachophoresis [14] and capillary zone electrophoresis [5,9,11] are the most widely used.

Methods for QBA isolation from biological materials rich in these substance(s) are well known. Rapid and reliable solid-phase extractions (SPE) for isolation of QBA from plants were established. Usually methanol, ethanol or acetonitrile acidified with HCl, acetic or formic acids are successfully employed with recoveries 80–95%, except of 65% recoveries for sanguarine (SA) in in vitro cells. Quantitative (nearly 100%) recovery was reached via sonication of dried and powdered plant samples [15]. A microwave-assisted extraction (MAE) was found to be the most effective method capable of yielding sanguinarine and chelerythrine from fruits of *M. cordata* with a short extraction time [16]. Supercritical fluid extraction (SFE) was successfully used to extract biologically active compounds of lower polarity from plant materials. A high flow-rate modification of the method is good even for the extraction of polar compounds [17,18] from complex matrices. In addition to that, complex matrices like soils contain molecules able to act as entrainers that further enhance the method recovery.

Isolation of alkaloids from animal tissues is much more complicated, especially when intact tissues with multiple cell types are present. Recoveries close to 20% are typically obtained. One of our goals was to find out appropriate conditions for quantitative and reproducible recovery and highest possible selectivity of chelerythrine, sanguinarine and their dihydroderivatives (see Fig. 1 for the chemical formulas) from spiked and real plasma matrices. The second aim of this work was to use a rapid and sensitive LC/ESI-MS for the determination of chelerythrine (CHE) and dihydrochelerythrine (DHCHE), to develop a robust and sensitive analytical procedure combining efficient extraction and quantification, to validate it properly and to apply it for precise and sensitive determination of both analytes in real and spiked animal plasma samples.

2. Experimental

2.1. Chemicals

Chelerythrine was supplied by Fluka (Buchs, Switzerland), dihydrochelerythrine was prepared from CHE by reaction with $NaBH_4$ in methanol [12]. The stock standard solutions of CHE and DHCHE at 10 μg ml^{-1} were prepared in methanol and stored at 4 °C in dark. The working standard solutions were prepared daily by dilution of the stock solutions with methanol (1:10, v/v). All solutions were filtered through a 0.45 μm Teflon membrane filter (MetaChem, Torrance, CA, USA) prior to LC/ESI-MS separations. All other chemicals were of analytical grade.

2.2. Samples and sample preparation

A standard solution of a given concentration (10, 20 or 50 μl of the stock solution containing 8.82 mg l^{-1} of CHE and 11.15 mg l^{-1} of DHCHE diluted 1:10) was spiked to a dry glass wool in an empty extraction cartridge prior to addition of an in situ modifier to perform "model" extractions. Spiked and naturally contaminated plasma samples (200, 150 and 100 μl) were added directly on nylon membrane filter (0.45 μm, MetaChem, Torrance, CA, USA) in the extraction cartridge together with or after the in situ modifier addition.

Experimental animals handling and rat plasma samples preparation is described in our previous study [12]. The samples of human plasma were obtained from the Faculty Hospital Bohunice (Brno, Czech Republic). De-frozen rat and human plasma samples were spiked at laboratory temperature with 10–50 μl of standard solution, equilibrated for 30 or 60 min in Eppendorf vials and dosed to extraction cells.

2.3. Near-critical CO_2 extraction

Model experiments and spiked plasma samples were prepared as described above. Content of Eppendorf vial was

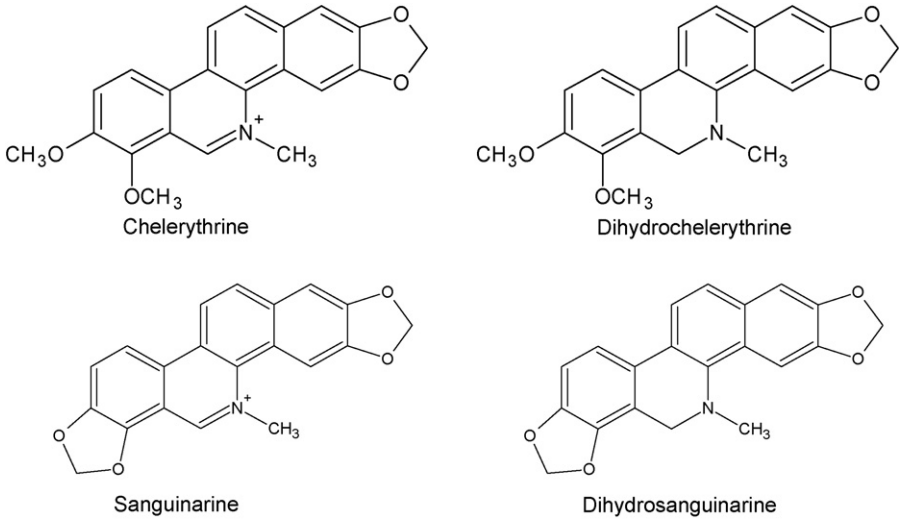

Fig. 1. Chelerythrine, sanguinarine and their dihydroderivatives formulas. Although chelerythrine and dihydrochelerythrine are considered polar analytes for SFE, recoveries 95.1 and 81.0%, resp., were achieved from plasma sample.

quantitatively transferred to the extraction cartridge using 0.5 ml of an in situ modifier. As for real plasma samples (rats fed with the analytes), 100 or 150 μl of the plasma was dosed to the extraction cartridge. The cartridge contained modifier to avoid the plasma sticking on the extraction cell walls. The cartridge was immediately sealed after the sample addition and fastened in the extraction cell-heating block.

All extractions were carried out using an SE-1 instrument (SEKO-K, Brno, Czech Republic) equipped with a Valco valve (VICI, Schenkon, Switzerland, loop 1 ml) for continuous modifier addition [19]. The extraction cell was pressurized at 35–50 °C up to 7–38 MPa using SFC/SFE grade CO_2 (Siad, Brno, Czech Republic) with 5% (v/v) of a modifier added via the Valco valve to the instrument piston pump.

The modified supercritical fluid went through the extraction cartridge filled with the sample for 15 min (dynamic extraction). Additional period (15 min) without modifier addition followed after each extraction to get water out of the piston micropump. Real sample extractions were carried out for total time 45 min (trapping) with 30 min modifier addition. Extraction time for kinetic studies was prolonged to 75 min. The extraction medium containing analytes was led through a fused silica restrictor (12 cm, 50 μm i.d., gas flow-rate of 650–750 ml/min). Analytes were quantitatively trapped in 20 ml of a trapping solvent (methanol) at the laboratory temperature. Smaller amount of the trapping solvent would be sufficient, but due to the high gas flow-rate a 50 ml glass vial with a flexible foil seal was used to prevent splashing the solvent out of the trapping vial and so much solvent was needed to achieve sufficient solvent column height.

Prior to the analyses, the extracts were pre-concentrated in a rotary vacuum evaporator IKA RV 05-ST with a HB 4 water bath (all from IKA-Werke, Staufen, Germany) to dryness, dissolved in 500 μl of 0.1 M HCl and injected directly into the LC system (model solution samples, some real samples) or filtered through the 0.45 μm filter (MetaChem, Torance, CA, USA) before the injection (most of real plasma samples) to protect a LC column.

2.4. High-performance liquid chromatography/electrospray mass spectrometry

An HP 1100 chromatographic system [16] was controlled with the ChemStation software (Rev. A 07.01). The Zorbax SB-CN chromatographic column (75 mm × 4.6 mm, 3.5 μm, Agilent Technologies, Palo Alto, CA, USA) was used. Injection volume was 5 μl. A mobile phase consisted of 50 mM ammonium formiate (aqueous phase) and methanol (organic phase). A linear gradient was applied as follows: from start to 1 min, 60% organic phase (v/v); from 1.0 to 7.0 min, 60–71% organic phase (v/v); from 7.0 to 18.0 min, 71–60% organic phase (v/v). Flow-rate was 0.7 ml min^{-1} and the temperature of the column oven was set at 15 °C. The signal was monitored with the diode array detector at 285 nm. Spectra were registered in the range of 190–400 nm (SBW 100 nm).

The column effluent was directly introduced into a single quadruple mass-selective HP MSD detector (G1946A, Hewlett-Packard, Palo Alto, CA, USA) operated in a positive ESI mode. The mass spectrometer was calibrated with an ESI tuning solution obtained from the same manufacturer. The nebulizer gas pressure was 50 psi, the drying gas was nitrogen at 12 l min^{-1}, the temperature was 350 °C and the capillary voltage was 1500 V. The fragmentor voltage was set to 100 eV (CID 200 V) and the gain was 1. Additional structural information, gained at 200 V fragmentor voltage, were obtained by detecting diagnostic product-ions obtained by in-source CID of the precursor ion. The *m/z* spectra were acquired at *m/z* 100–400 for both analytes in full scan mode and the data for selected ion monitoring (SIM) mode were acquired at *m/z* 348 → 332 for CHE and at *m/z* 350 → 335 for DHCHE. The dwell time for each analyte was 199 ms.

2.5. Accuracy, precision and recovery

Accuracy, precision and recovery of the determination of QBA analytes were evaluated with the plasma extracts spiked with CHE and DHCHE standards (seven concentrations varying from 20 to 200 ng ml^{-1}, five replicates each). Regression parameters of a calibration curve were calculated automatically in the programme ChemStation Version 08. Coefficients of variations (% C.V.) of intra-day assay were determined in six spiked extracts. Intermediate precision was determined by analysing six spiked extracts during a 5-day period (three replicates). Ana-

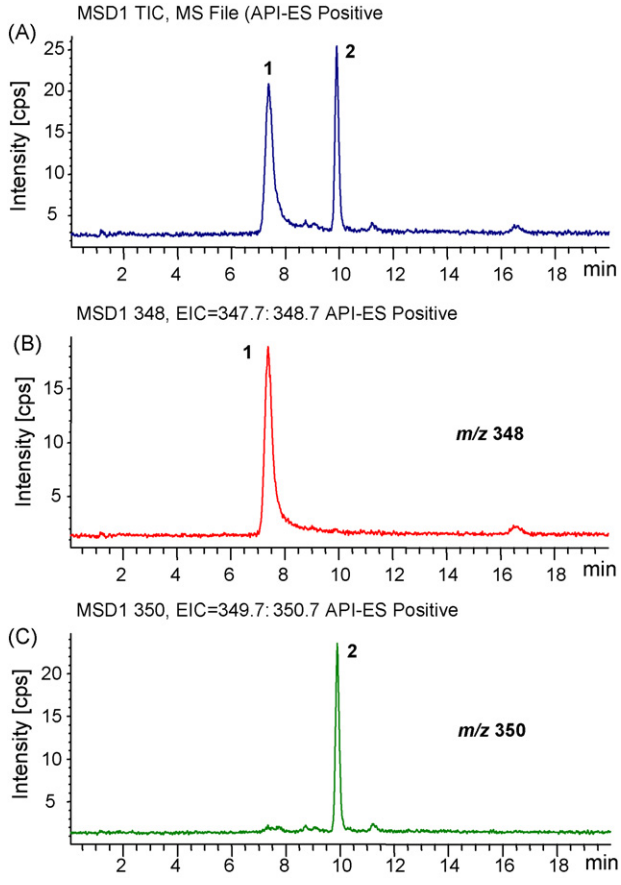

Fig. 2. LC/ESI-MS chromatograms of the standard solution with chelerythrine (peak 1) and dihydrochelerythrine (peak 1). (A) Total ion monitoring, (B) SIM mode for CHE (*m/z* 348), (C) SIM mode for DHCHE (*m/z* 350).

lyte concentrations were calculated from the calibration curves. The standard addition method was used also in real samples. Accuracy (in %) was evaluated by comparing calculated concentrations of the individual analytes with measured ones.

3. Results and discussion

3.1. Liquid chromatography/mass spectrometry optimization

The Zorbax SB-CN chromatographic column was found very suitable for CHE and DHCHE separation, as well as mobile phase containing 50 mM ammonium formiate and methanol. Previously described method [8] used mobile phase containing 10 mM ammonium formiate. However, for the chromatographic determination of CHE, given mobile phase composition was not quite proper due to a high tailing factor of CHE (at retention time 8.19 min, the end of the peak nearly touches next analyte peak of DHCHE with retention time 10.02 min, so the CHE peak symmetry is unsatisfactory). The mobile phase containing 50 mM of ammonium formiate suppressed the tailing and thus dramatically increased the peak symmetry. Proper gradient was found to achieve short time of analysis and best peak resolution (see Section 2.4) with retention times 7.37 and 10.08 min for CHE and DHCHE, respectively. Resolution 0.71 between CHE (1) and SA (2) peaks and resolution 0.93 between DHCHE (3) and dihydrosanguarine (4) peaks (see Fig. 2.) were obtained. With the new mobile phase composition, the method can be used for the simultaneous determination of both, CHE and DHCHE, and sanguarine plus its dihydrosanguarine derivative. Fig. 2 shows the chromatogram of standard solution, Fig. 3 represents the influence of the mobile phase composition, and simultaneous determination of four analytes.

Quadruple mass spectrometric detector with electrospray ionization (ESI-MS) in the positive ion selective mode (SIM: selected ion monitoring) was used in the commonly optimised range of parameters: drying gas temperature (100–350 °C with 50 °C steps) and nitrogen flow (3–13 l min^{-1} in 1 l min^{-1} steps), nebulizer pressure (20–60 psi in 5 psi steps), capillary voltage (1000–6000 V in 500 V steps) and fragmentor voltage (20–200 eV in 20 eV steps). To minimize fragmentation of analytes, gain 1 was kept constant for all experiments. At fragmentor voltage 200 V, diagnostic product-ions obtained by in-source CID of the precursor ion were detected at m/z 348 → 332 for CHE and at m/z 350 → 335 for DHCHE. The optimisation was carried out by flow injection analysis (FIA) of several solutions containing the 1 ng μl^{-1} of a single analyte. Optimum values of detector parameters are given in Section 2.4.

Most of the parameter optimisations were in good agreement with the data obtained for sanguarine, dihydrosanguarine or benz(*c*)acridine [8]. However, in contrast to the other QBA, CHE and DHCHE required mobile phase containing 50 mM of ammonium formiate to achieve higher ionisation sensitivity (See Fig. 4.) The efficiency of ionization processes in LC/ESI-MS

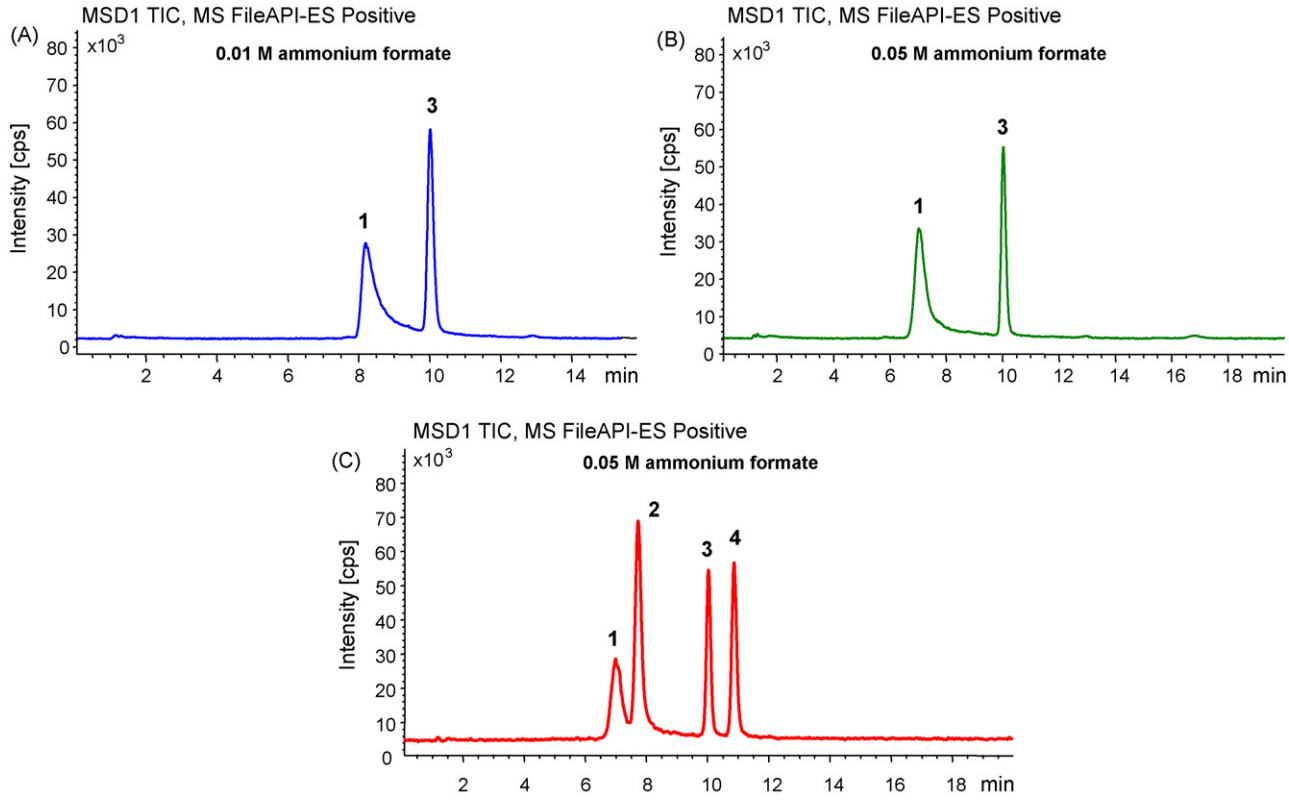

Fig. 3. The influence of a mobile phase composition to the efficiency of chromatographic separation: (A) 10 mM ammonium formiate, (B) 50 mM of ammonium formiate, (C) chromatogram of standards solution of CHE (1), sanguarine (2), DHCHE (3) and dihydrosanguarine (4).

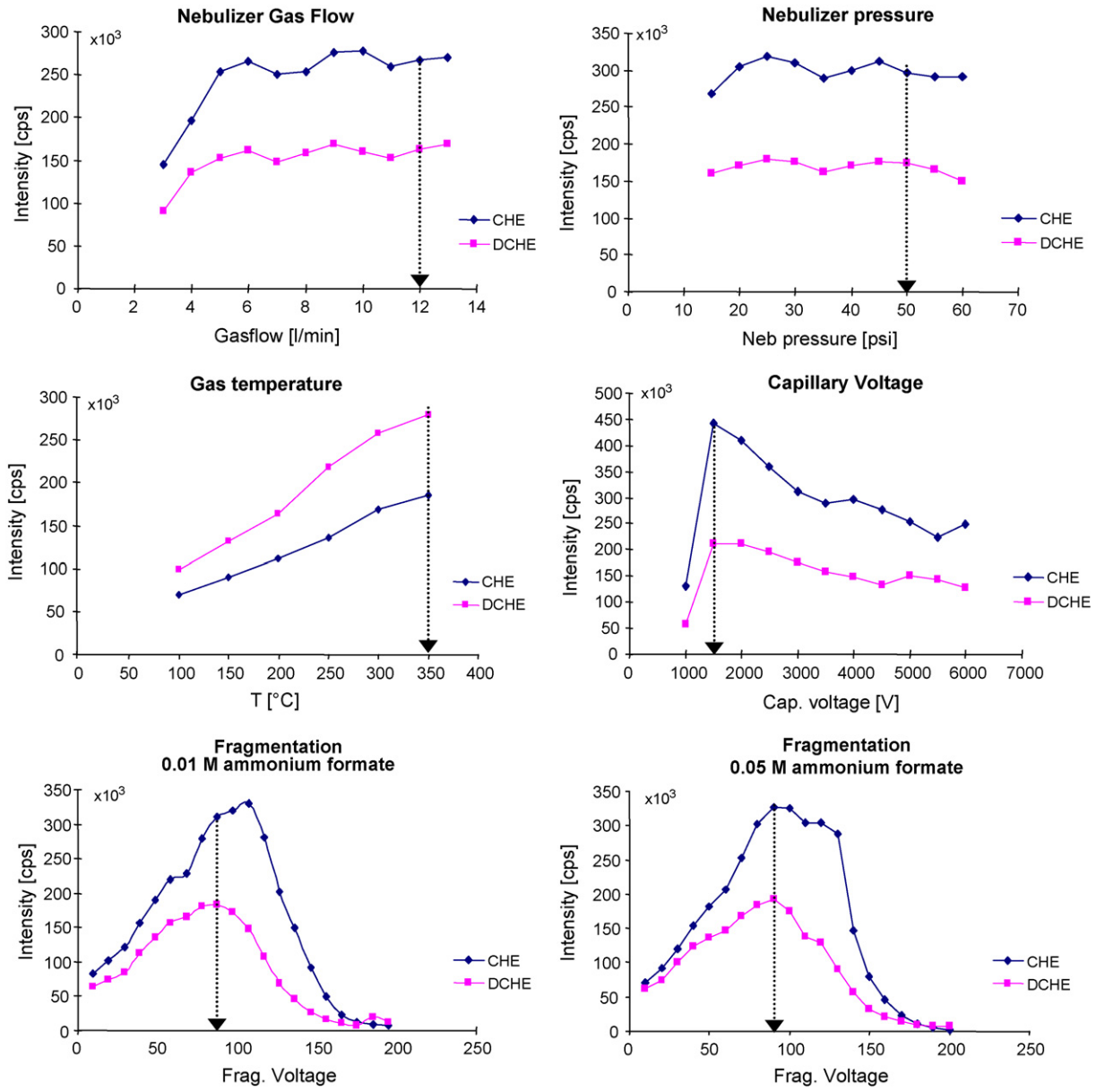

Fig. 4. FIA studies for optimisation of the ESI-MS positive mode signal. Influence of nebulizer gas flow, nebulizer pressure, gas temperature, capillary voltage and fragmentation were examined. Influence of both fragmentor voltage and ammonium formiate concentration on the intensity of analytical ion current was also examined.

is seriously influenced by electrolyte composition and by fragmentor voltage. The effect of ammonium formiate concentration on the ionization efficiency was tested. The highest intensity for CHE and DHCHE were achieved in 50 mM of ammonium formiate.

The mass spectra of CHE and DHCHE (Fig. 5) were scanned in the range 100–400 *m/z* at 1500 V capillary voltage and collision energy set at 100 and 200 eV, respectively. The molecular ion CHE $[M+H]^+$ was measured at *m/z* 348 and specific products of fragmentation at *m/z* 332 $[M–CH_3]^+$, the molecular ion DHCHE $[M+H]^+$ was measured at *m/z* 350 and specific products of fragmentation at *m/z* 335 $[M+H–CH_3]^+$. The fragments were in good coincidence with so far published data [4,20] (Fig. 6).

3.2. *Near-critical CO_2 extraction*

3.2.1. *Optimisation of extraction conditions*

During the optimisation of extraction conditions, selectivity was in the spotlight, because of the plasma is very complex matrix. Our aim was to separate CHE and DHCHE from endogenous components present in plasma and enable direct LC/ESI-MS analysis without the need of cleanup. Thus, the experiments started at the mildest extraction conditions (35 °C, 7 MPa—lowest working conditions of the instrument) and were enhanced consecutively to see prospective increase of recovery.

All extractions from spiked plasma samples were carried out for 15 min. Study of extraction kinetics was prolonged to 75 min.

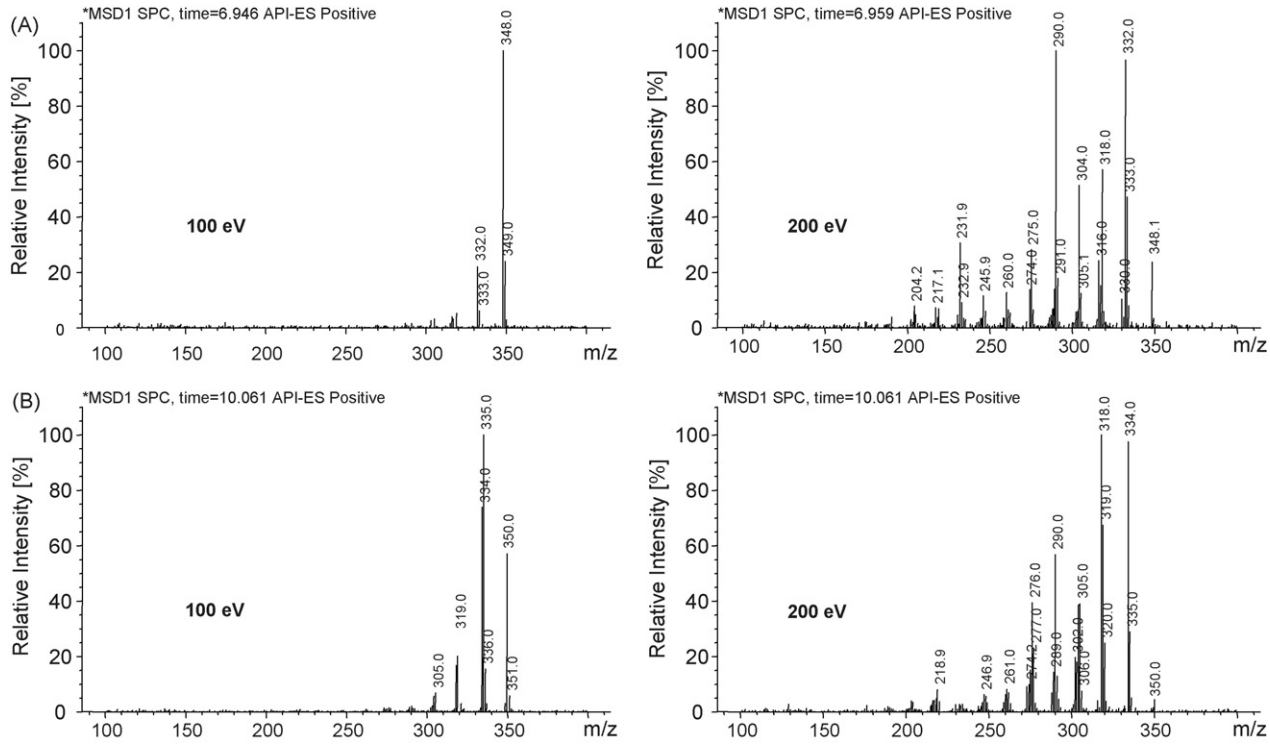

Fig. 5. ESI-MS spectral characteristics of (A) chelerythrine and (B) dihydrochelerythrine for the fragmentor voltage 100 and 200 eV. For chromatographic conditions see Sections 2.4 and 3.1.

Approximately, 90% of CHE and 63% of DHCHE was extracted during the first 10 min and the concentration of both analytes was at the LOQ level in the fraction from 15–20 min. Also the trapping efficiency and stripping effect were tested, as the gas flow-rate was relatively high. Most of non-volatile QBA analytes were trapped quantitatively into foil-sealed 50 ml vial with 20 ml of MeOH. Stripping effect was insignificant during the extraction time.

Table 1
Near-critical CO_2 extraction parameters optimisation (spiked plasma samples). All extractions were carried out under following conditions: 10 MPa, 35 °C, 15 min, 0.5 ml of in situ MeOH/H_2O mixture 1:1 (v/v) plus 0.5 ml of MeOH/H_2O mixture 1:1 (v/v) per one pump filling, 12 cm restrictor 50 μm i.d., analytes trapped to 20 ml of MeOH (50 ml flask, foil seal); unless other parameters are given in the table

Temperature [°C] optimization	Recovery [%]		Pressure optimisation [MPa]	Recovery [%]	
	CHE	DHCHE		CHE	DHCHE
35	**94.9**	**79.6**	7.5	86.1	77.8
37.5	92.3	81.4	10	**96.6**	**80.5**
40	94.1	80.9	12.5	93.0	81.2
45	94.4	78.5	15	95.1	78.8
50	90.0	82.8	17.5	92.7	80.3
55	93.4	80.3	20	94.4	80.2
60	96.2	79.5	25	93.5	79.9
75	93.8	81.0	30	95.6	78.3
100	91.6	80.4	38	94.8	81.4

Modifier composition	Recovery [%]		In situ modifier [μl]	Recovery [%]		On-line modifier [μl]	Recovery [%]	
	CHE	DHCHE		CHE	DHCHE		CHE	DHCHE
100% MeOH	62.2	76.4	100	62.9	75.5	100	79.9	76.2
10% H_2O	86.4	83.5	250	75.2	83.6	250	86.3	80.4
25% H_2O	88.5	85.6	400	91.4	83.0	400	93.5	82.1
40% H_2O	91.6	82.5	500	**93.7**	**82.2**	500	**95.0**	**81.4**
50% H_2O	**95.2**	**81.0**	600	94.0	81.3	600	96.3	80.0
60% H_2O	94.3	80.7	750	94.6	80.7	750	94.1	82.3
75% H_2O	91.0	76.1	1000	93.7	83.8	1000	96.5	81.5

Optimum values are given in bold. All R.S.D.s are in the range 1.4–3.9%, except the 600, 750 μl and 1 ml of on-line modifier, where R.S.D.s are in the range 2.7–7.5%.

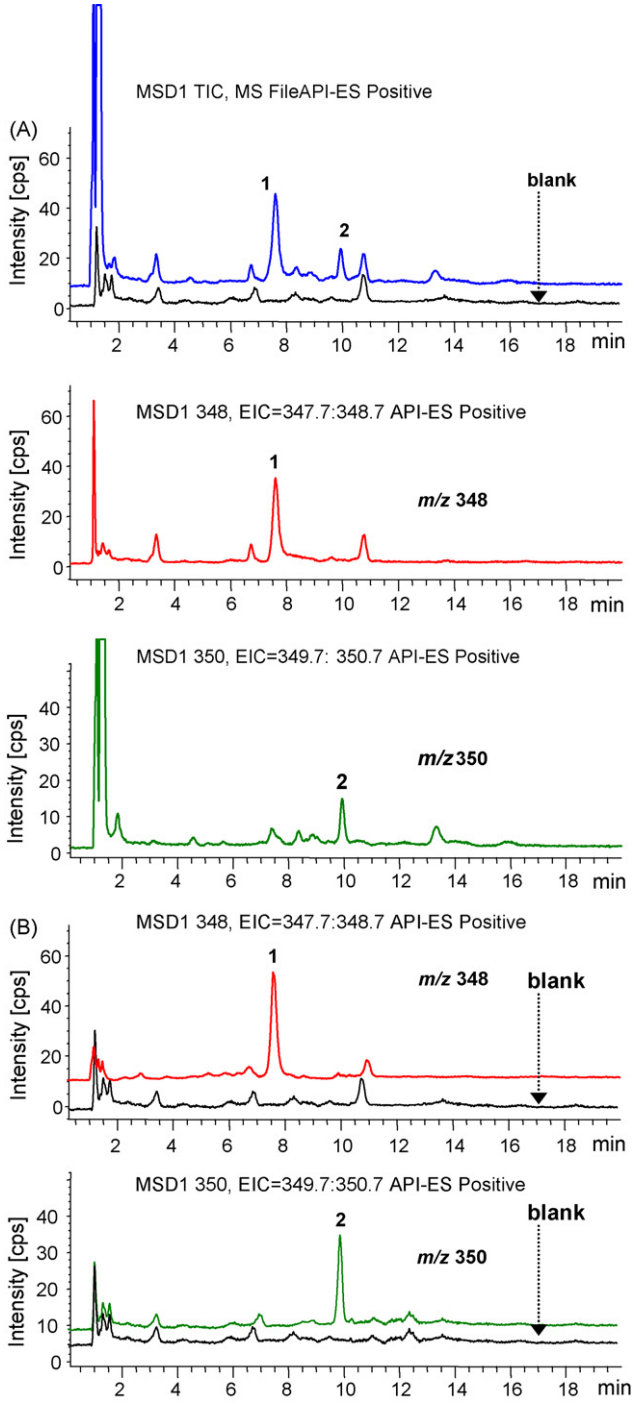

Fig. 6. LC/ESI-MS chromatograms of real samples (rat plasma naturally containing analytes, (A) and spiked samples (human plasma, (B): SIM mode for CHE (peak 1) at *m/z* 348 and for DHCHE (peak 2) at *m/z* 350.

Starting extraction temperature, 35 °C, was found sufficient. Temperature enhancement above the critical point did not improve recovery; it only led to lower selectivity. On the other hand, mild pressure increase – to 10 MPa – proved to be helpful to the recovery. Further pressure increase (12.5, 15, 20, etc. up to 40 MPa) did not improve much the recovery and also lowered the selectivity. Then, temperature optimisation was verified again at the 10 MPa pressure. In fact, both analytes were extractable well in a wide range of temperatures and pressures, and optimal conditions were chosen on the base of selectivity. Selectivity tests for model samples were performed with 150 μl of blank human plasma in the extraction cell and analytes spiked freshly to glass wool placed in upper part of extraction cartridge to avoid analyte-matrix interaction.

As a next step, modifier composition was optimised. Pure MeOH, known to be good for lignans, gave non-quantitative results. Small percentage of water (10%, v/v) led to recoveries 86 and 83% for CHE and DHCHE, respectively. In the end, MeOH/H_2O mixture 1:1 (v/v) was selected as a good modifier. Both in situ and on-line modifier volume was optimised in cross-linked study. A 0.5 ml of in situ MeOH/H_2O mixture 1:1 (v/v) and 0.5 ml of the same on-line modifier was selected as the best choice. Under these conditions, average recoveries 94.9 and 79.6% for CHE and DHCHE, respectively, were achieved. Smaller percentage of water is slightly more favourable for DHCHE, but not so good for CHE. Higher amount of modifier can be used too with similar recoveries. But surprisingly it caused increase of R.S.D.s, probably due to the fluctuation of restrictor flow-rate. For more optimisation details, see Table 1.

3.2.2. Application to real samples

Some optimisations were verified for real plasma samples to exclude prospective matrix effect, but the results were in good agreement with the model extractions data. Pressure enhancement to 15 MPa did not decrease selectivity, and thus the value

Table 2
Retention factors, calibration data, LODs and LOQs for CHE and DHCHE obtained under optimised separation conditions of ESI-MS detection (injection volume 5 μl) and near-critical CO_2 extraction and LC/ESI-MS determination of CHE and DHCHE in real rat plasma samples. R.S.D.s are quite high, as the total amount of sample allowed only three repetitions at 100 μl injections

	CHE	DHCHE
Retention factor	4.42	6.75
Coefficient of determination R^2 ($n=6$)	0.9979	0.9995
LOD	1.22 ng/ml 3.50 pmol/ml	0.95 ng/ml 2.72 pmol/ml
LOQ	4.06 ng/ml 11.7 pmol/ml	3.20 ng/ml 9.06 pmol/ml
Calibration equation	$y = 1606716.59\,x$	$y = 964552.67\,x$
Sample 1 ($n=3$)		
Concentration ± S.D. [ng/ml][a]	0.22 ± 0.01	2.28 ± 0.07
R.S.D. [%]	4.28	3.19
Sample 2 ($n=3$)		
Concentration ± S.D. [ng/ml]	0.51 ± 0.02	3.51 ± 0.15
R.S.D. [%]	3.63	4.40
Sample 3 ($n=3$)		
Concentration ± S.D. [ng/ml]	0.47 ± 0.03	2.52 ± 0.15
R.S.D. [%]	5.79	5.91

Spiked samples with 200 μl injections and $n=6$ brought better R.S.D. results.
[a] Low concentration of analytes was expected to be another reason, why the R.S.D.s are quite high. Although real measured concentrations were 10-times higher (lower amount of mobile phase was used as a solvent and values were re-calculated to be comparable), the concentration of CHE in sample 1 was under the LOQ. However, R.S.D.s found for CHE were on the same level as those of DCHE, which were safely over the quantification limit.

was applied. Extraction time was prolonged to 45 min, because of the strong bonds with the matrix were expected. However, neither of analytes was found in concentration higher than LOQ (but traces were detected indicatively) in the fraction 30–45 min.

Samples were taken out of the freezer to laboratory temperature and immediately after plasma became liquid 100 μl aliquots were injected to the extraction cell. Rest of the sample was immediately frozen. All samples were analysed in triplicate, as there was not enough plasma in Eppendorf vials for more experiments. Measured concentrations are given in Table 2. Calibration curves and standard addition method were used for the quantification. Due to unknown concentrations of CHE and DHCHE in the samples and lack of certified reference materials no comparison with other methods is offered.

3.3. Validation of the LC/ESI-MS method

Validation of chromatographic method was performed according to common principles of good laboratory practice. The limits of detection (LOD for S/N = 3) were estimated at 1.22 ng/ml (3.50 pmol/ml) and 0.95 ng/ml (2.72 pmol/ml) and limit of quantification (LOQ for S/N = 10) at 4.06 ng (11.7 pmol/ml) and 3.20 ng/ml (9.06 pmol/ml) for CHE and DHCHE, respectively. The calibration curves constructed from 5 points ($n = 12$) were linear in required concentration ranges (4–400 ng/ml) with coefficients of determination $r^2 = 0.9979$ and $r = 0.9995$ for CHE and DHCHE, respectively. Most important parameters, like retention factors, limits of detection (LOD), limits of quantification (LOQ), equations of calibration curves and their correlation coefficients for both analytes are given in Table 2.

Accuracy was determined for standard solutions with concentrations 20, 40, 100 and 200 ng ml^{-1} and for plasma extract spiked with the same concentrations of analytes ($n = 6$). For standard solutions, R.S.D.s varied in the range 0.66–1.15% for lower concentrations and 0.55–0.87% for higher concentrations (avg. 0.84%), with recoveries 98.5–101.8% (avg. 100.1%). For spiked plasma extracts, R.S.D.s varied in the range 0.81–1.71% for lower concentrations and 0.60–1.66% for higher concentrations (avg. 1.14%), with recoveries 99.1–101.8% (avg. 100.1%).

As for repeatability, R.S.D.s were in the range 0.73–1.90% (avg. 1.51%) and recovery was 98.5–101.0% (avg. 99.8%) for standard solutions. For spiked plasma extracts, R.S.D.s were in the range 0.73–1.98% (avg. 1.04%) and recovery was 98.8–100.9% (avg. 99.8%). Intermediate precision R.S.D.s were in the range 1.10–1.79% (avg. 1.33%) and recovery was 99.2–101.7% (avg. 100.3%) for standard solution, for spiked plasma extracts R.S.D.s were in the range 0.89–1.74% (avg. 1.34%) and recovery was 98.2–101.0% (avg. 100.3%). All validation data are given in Table 3.

Table 3
LC/ESI-MS accuracy: determination of CHE and DHCHE in plasma extracts, standard solutions and plasma extracts spiked with known concentrations of analytes ($n = 6$) and repeatability and intermediate precision of CHE and DHCHE determination for the plasma extract spiked with the standard solution ($n = 6$, $n = 30$)

STD volume (μl)	10		20		50		100	
	CHE	DHCHE	CHE	DHCHE	CHE	DHCHE	CHE	DHCHE
Standard solutions in ultra-pure water (accuracy, $n = 6$)								
Calc. content [ng/ml]	17.6	23.1	35.3	46.2	88.2	115.5	176.4	231.0
Conc. [ng/ml]	17.4	23.5	35.4	45.5	88.4	116.3	175.9	233.0
S.D. [ng/ml]	0.20	0.26	0.24	0.49	0.77	0.68	0.97	1.66
R.S.D. [%]	1.15	1.12	0.66	1.08	0.87	0.58	0.55	0.71
Recovery [%]	98.6	101.8	100.4	98.6	100.3	100.7	99.7	100.9
Plasma extract spiked with standard solution (accuracy, $n = 6$)								
Calc. content [ng/ml]	51.1	59.9	68.8	82.98	121.7	152.3	209.9	267.8
Conc. [ng/ml]	52.1	60.1	68.1	82.5	121.3	153.1	210.5	265.9
S.D. [ng/ml]	0.89	0.80	0.55	1.22	2.02	1.34	1.42	1.59
R.S.D. [%]	1.71	1.33	0.81	1.48	1.66	0.88	0.68	0.60
Recovery [%]	101.8	100.3	99.1	99.4	99.7	100.5	100.3	99.3
Plasma extract spiked with the standard solution (repeatability, $n = 6$)								
Calc. content [ng/ml]	51.1	59.9	68.8	83.0	121.7	152.3	209.9	267.8
Conc. [ng/ml]	50.8	59.2	69.2	82.1	122.0	153.6	209.1	268.3
S.D. [ng/ml]	1.00	0.52	0.54	0.92	0.98	1.60	1.54	2.63
R.S.D. [%]	1.98	0.89	0.79	1.12	0.81	1.04	0.73	0.98
Recovery [%]	99.3	98.8	100.6	98.9	100.2	100.9	99.7	100.2
Plasma extract spiked with the standard solution (intermediate precision, $n = 30$)								
Calc. content [ng/ml]	51.1	59.9	68.8	83.0	121.7	152.3	209.9	267.8
Conc. [ng/ml]	50.9	60.5	67.5	82.3	120.8	153.4	209.4	268.0
S.D. [ng/ml]	0.54	0.73	0.96	1.43	1.07	1.99	3.17	4.35
R.S.D. [%]	1.05	1.20	1.43	1.74	0.89	1.30	1.51	1.62
Recovery [%]	99.6	101.0	98.2	99.2	99.2	100.8	99.8	100.1

Spiked plasma extract from temperature optimisation study (200 μl of plasma spiked with 20 μl of standard solution, concentrations 33.5 ± 0.42 and 36.8 ± 0.28 ng/ml, R.S.D.s 1.25 and 0.76%, recoveries 94.9 and 79.6% for CHE and DHCHE, respectively) was used for validation purposes. Long-time contaminated plasma was not available at the time of method optimisation.

4. Conclusions

Chelerythrine and dihydrochelerythrine were successfully extracted from plasma and determined by means of LC/ESI-MS within 15 min with the very good accuracy, repeatability and intermediate precision. Recovery achieved in optimisation studies was 95 and 81%, resp., extraction time was 15 min for spiked samples and 30 min for real plasma samples.

Although the aim (a quantitative extraction of both analytes) was not achieved (95% of CHE seems good, but 81% of DHCHE cannot be called quantitative recovery), still the method offers serious enhancement in comparison to QBA recoveries from plasma reported in literature. Usually, recovery of QBA from plant material is quantitative, but extractions from plasma and animal tissues reported in papers did not reach 50% (20% typically).

As for the extraction selectivity, thanks to the nylon filter in the extraction cell, most of the extracts were clean enough to be analysed directly, without the cleanup. Most of the ballast compounds were separated from the analytes. To tell the truth, most of the samples went through the cleanup step anyway, as it did not cause much trouble in comparison with the risk of chromatographic column damage. But it was proved that the risk of filter rupture is completely avoided with the use of brand new disposable filters for each extraction.

At the same time, the portfolio of chromatographic methods for QBA analysis was enhanced for two more analytes. Newly developed method, optimised for CHE and DHCHE, is highly sensitive tool for the determination of both analytes in plasma extracts. It is robust, with very good accuracy and precision, and allows also simultaneous determination of sanguinarine and dihydrosanguinarine.

Nowadays, CHE and DHCHE are analytes of much interest. There are over 1440 papers on CHE listed on ISI Web of knowledge, but only 13 of them has something to do with LC. Let the quick and reliable method for extraction and analysis of CHE and DHCHE from plasma samples is a useful contribution for all further investigation of QBA analytes.

Acknowledgements

This work was supported by the Grant Agency of the Czech Republic (GA ČR 525/07/0871) and the Grant Agency of the MŠMT (Grant No. MSM 6198959216).

References

[1] V. Šimánek, in: A. Brossi (Ed.), The Alcaloids, vol. 26, Academic Press, New York, 1985, pp. 185–234.
[2] R. Verpoorte, in: M.F. Roberts, M. Wink (Eds.), Alkaloids. Biochemistry, Ecology and Medicinal Applications, Plenum Press, New York, 1998, pp. 397–426.
[3] B.D. Krane, M.O. Fagbule, M. Shamma, B. Gozler, J. Nat. Prod. 47 (1984) 1.
[4] R.M. Perez Gutierrez, R. Vargas Solis, G. Diaz Gutierrez, F.J. Martinez-Martinez, Phytochem. Anal. 13 (2002) 177.
[5] S. Husain, R. Narsimba, R. Nageswara, J. Chromatogr. A 863 (1999) 123.
[6] H. Holeeinger, R. Micheline, A. Deroussent, R.P. Singh, T. Cresteil, J. Chromatogr. B 799 (2004) 195.
[7] X. Luo, B. Chen, S. Yao, Chromatografia 60 (2004) 347.
[8] R.M.P. Gutierrez, R.V. Solis, G.D. Gutierez, F.J. Martinez-Martinez, Phytochem. Anal. 13 (2002) 177.
[9] P. Kosina, J. Ševčík, M. Modriansky, A. Gavenda, P. Bednář, P. Barták, D. Walterová, J. Ulrichová, J. Sep. Sci. 26 (2003) 679.
[10] N. Chauret, J. Archambault, Anal. Chim. Acta 249 (1991) 231.
[11] J. Ševčík, J. Vičar, J. Ulrichová, I. Válka, K. Lemr, V. Šimánek, J. Chromatogr. A 866 (2000) 293.
[12] J. Psotová, B. Klejdus, R. Večeřa, J. Kosina, V. Kubáň, J. Vičar, V. Šimánek, J. Ulrichová, J. Chromatogr. B 830 (2006) 165.
[13] S. Frick, R. Krammel, K. Schmidt, A.J. Fist, T.M. Kutchan, J. Nat. Prod. 68 (2005) 666.
[14] D. Walterová, Z. Stránský, V. Preininger, V. Šimánek, Electrophoresis 6 (1985) 128.
[15] K. Yoshimatsu, F. Kiuchi, K. Shimomura, Y. Makino, Chem. Pharmacol. Bull. 53 (2005) 1446.
[16] F. Zhang, B. Chen, S. Xiao, S.Z. Yao, Sep. Purif. Technol. 42 (2005) 283.
[17] B. Klejdus, L. Lojková, O. Lapčík, R. Koblovská, J. Moravcová, V. Kubáň, J. Sep. Sci. 28 (2005) 1334.
[18] L. Lojková, B. Klejdus, P. Formánek, V. Kubáň, J. Agric. Food Chem. 54 (2006) 000.
[19] M. Adam, K. Ventura, P. Jandera, J. Churáček, J. Liq. Chromatogr. Rel. Technol. 23 (2000) 1511.
[20] L. Mingjin, Z. Weidong, H. Jiang, L. Runhui, Z. Chuan, J. Pharm. Biomed. Anal. 42 (2006) 178.

Available online at www.sciencedirect.com
ScienceDirect
Talanta 72 (2007) 1581–1585
Talanta
www.elsevier.com/locate/talanta

Solid-phase microextraction coupled to gas chromatography for the determination of 2,3-dimethyl-2,3-dinitrobutane as a marking agent for explosives

Xiujuan Li [a], Zhaorui Zeng [b,*], Yi Zeng [c]

[a] *College of Food Science & Technology, Huazhong Agricultural University, Wuhan 430070, China*
[b] *Department of Chemistry, Wuhan University, Wuhan 430072, China*
[c] *Beijing Public Security Bureau, Beijing 100007, China*

Received 29 September 2006; received in revised form 5 February 2007; accepted 6 February 2007
Available online 20 February 2007

Abstract

This paper investigates the detection of 2,3-dimethyl-2,3-dinitrobutane (DMNB), a marking agent in explosives, by gas chromatography (GC) with electron capture detection using solid-phase microextraction (SPME) as a sample preparation technique. The 25,27-dihydroxy-26,28-oxy (2′,7′-dioxo-3′,6′-diazaoctyl) oxy-*p-tert*-butylcalix[4]arene/hydroxy-terminated silicone oil coated fiber was highly sensitive to trap DMNB from ammonium nitrate matrix. The analysis was performed by extracting 2 g of explosives for 30 s at room temperature and then immediately introducing into the heated GC injector for 1 min of thermal desorption. The method showed good linearity in the range from 0.01 to 1.0 μg/g. The relative standard deviations for these extractions were <8%. The calculated limit of detection for DMNB (S/N = 3) was 4.43×10^{-4} μg/g, which illustrates that the proposed systems are suitable for explosive detection at trace level. This is the first report of an SPME–GC system shown to extract marking agent in explosives for subsequent detection in a simple, rapid, sensitive, and inexpensive manner.

Keywords: Gas chromatography; Solid-phase microextraction; Calixarene; 2,3-Dimethyl-2,3-dinitrobutane (DMNB); Explosives

1. Introduction

In recent years identification and quantification of traces of explosives has constituted an emerging and important topic of interest due to their relevant role in many areas concerning the security and health of the population, including environmental and toxicological effects, land mine detection, aviation security or the prevention of terrorist attacks [1,2]. Different kinds of methods including gas chromatography-electron capture detection (GC–ECD) [3], GC–tandem mass spectrometry (GC/MS/MS) [4], ion mobility spectrometry (IMS) [5], capillary electrophoresis [6], high performance liquid chromatography [7], liquid chromatography–MS [8], voltammetry [9], flow-injection/electrochemistry analysis [10], X-ray systems and a number of chemical sensors [11,12] are involved for explosive analysis.

Some explosives, such as dynamite, can be detected directly by vapor-phase detectors, but plastic explosives (defined as malleable at room temperature with explosive component vapor pressures $<10^{-4}$ Pa at 25 °C), which have been used extensively by terrorists, contain only explosive ingredients of very low vapor pressure. Therefore, the International Civil Aviation Organization (ICAO) adopted the "Convention on the Marking of Plastic Explosives for the Purpose of Detection" in 1991 (ratified in 1998) that requires the addition of certain marking agents, which have a sufficient vapor pressure that, when mixed into the explosives, allows their detection [13]. 2,3-Dimethyl-2,3-dinitrobutane (DMNB) has been identified as the most suitable marking agent, as it does not affect explosive characteristics, such as shelf life and stability.

A few analytical methods have been developed for detecting DMNB. The detection has been previously demonstrated using IMS [14]. It is effective but often requires the manual transfer of samples from a suspect area and thermal desorption into the spectrometer. A sensitive voltammetric detection is newly described [15]. Under the optimal conditions, a linear

* Corresponding author. Fax: +86 27 8764 7617.
E-mail address: zrzeng@whu.edu.cn (Z. Zeng).

0039-9140/$ – see front matter © 2007 Elsevier B.V. All rights reserved.
doi:10.1016/j.talanta.2007.02.018

response is observed over the 300–3000 mg/l DMNB concentration range, with a detection limit of 60 mg/l. MS [16] and fluorescent quenching detection in connection to the polyphenylene conjugated polymer [17] have also been developed, aiming to improve the sensitivity, selectivity and reliability. Nevertheless, the demand for rapid, sensitive, selective, inexpensive and field portable device is high.

According to ICAO, the content of DMNB incorporated in explosives is very low (1:1000, w/w), and there is generally no time for using many traditional sample pre-concentration techniques, which are unfortunately often an important operation of ultra-high-sensitivity detection. Since DMNB continues to release its vapor at a steady rate for several years, and it does not readily adhere to common substances the taggant may come in contact with [18], solid-phase microextraction (SPME) [19] will be a very effective tool for the detection of explosives in the future. This technique was developed to address the need to facilitate rapid sample preparation both in the laboratory and on-site where the investigated system is located. It successfully overcomes the inherent shortcomings of traditional sample preparation methods by integrating sample extraction, concentration, and introduction for instrumental analysis into a single step. SPME eliminates use of organic solvents, and substantially shortens the time of analysis and allows convenient automation of the sample preparation step. Additionally, the often-lower detection limits possible using SPME allow for confirmation of positive samples that previously went undetected. Perr et al. [20] used SPME to extract explosive and taggant for IMS vapor detection. The utility of IMS was greatly enhanced by using SPME vapor sampling because of the increase in sampling efficiency and improved sensitivity. However, a SPME-IMS interface was necessary to couple the extraction efficiency of SPME to the detection capability of IMS. In this sense, GC will be a good choice as the fiber of SPME can be inserted directly into the injector of a gas chromatograph without any interface.

SPME fiber coating plays the most important role in the extraction and the coating based on host–guest interactions have attracted increasing attention [21,22]. Calixarenes are best known to form host–guest complexes with organic species [23]. By changing the functionality and the cavity sizes of calixarenes, chemical specificity of host–guest interaction can therefore be achieved. 25,27-Dihydroxy-26,28-oxy (2′,7′-dioxo-3′,6′-diazaoctyl) oxy-*p-tert*-butylcalix[4]arene (amide bridged-C[4]) [24] offers simultaneous polar (lower-rim) and nonpolar (upper-rim) features, which should represent enhanced binding toward DMNB owing to its polar nitro substituents and nonpolar alkyl chain.

The purpose of our work is to assess the feasibility of the headspace-SPME technique combined with GC with electron capture detection (ECD) for effective determination of DMNB in explosives using laboratory-made amide bridged-C[4]/hydroxy-terminated silicone oil coated fiber (amide bridged-C[4]/OH-TSO) [24]. Ammonium nitrate is used as sample matrix as it is an explosive in its purest form and is often used by terrorists in China. Parameters affecting the sorption of DMNB to the fiber, including extraction time, extraction temperature and desorption time were optimized. Interferences from other compounds and different solvents were discussed. The extraction ability of this new fiber to DMNB was compared with those of commercial polyacrylate (PA), poly(dimethylsiloxane) (PDMS) and PDMS/divinylbenzene (PDMS/DVB) fibers. At last, linearity, detection limit, and precision of the whole procedure were validated.

2. Experimental

2.1. Instrumentation

The experiments were performed using a SP-6800A capillary GC system (Shangdong Lunan Ruihong Chemical Instrument Corporation, Tengzhou, China) equipped with a capillary split injector system and an electron capture detector (ECD, ^{63}Ni), on an SE-54 capillary column (30 m × 0.25 mm i.d., 0.33 μm film thickness). Online data collection and processing was done on Chromatopac model SISC-SPS (Beijing, China). The oven temperature was programmed from 190 °C, and then increased to 230 °C at 15 °C/min (held 6 min). The temperatures were 320 °C for the injector and 300 °C for the ECD detector. Ultrapure nitrogen (>99.999%) was used as the carrier gas and make-up gas. The flow-rate of make-up gas was 20 ml/min and the column flow-rate was 1 ml/min in the 1:20 split mode for all the analyses except the experiments in Section 3.6, which were splitless.

A laboratory-made SPME with amide bridged-C[4]/OH-TSO fiber (30 mg, 85 μm) syringe was used to transfer the extracted sample to the GC injector for analysis. The commercially available PA (85 μm), PDMS (100 μm) and PDMS/DVB (65 μm) coated fibers were obtained from Supelco (Bellefonte, PA, USA).

2.2. Preparation of amide bridged-C[4]/OH-TSO fiber

The fiber was prepared according to Ref. [24]. In brief, 30 mg of amide bridged-C[4] was dissolved in 200 μl of methylene chloride, and then 90 mg of OH-TSO, 100 μl of tetraethoxysilane (TEOS), 50 μl of 3-(2-cyclooxypropoxyl)-propyltrimethoxysilane (KH-560) and 10 mg of poly(methylhydrosiloxane) (PMHS) were added and mixed thoroughly by ultrasonic agitation in a plastic tube. A 38 μl volume of trifluoroacetic acid containing 5% water was sequentially added to the resulting solution with ultrasonic agitation for another 3 min. The mixture was centrifuged at 12,000 rpm for 8 min. The top clear sol solution was used for fiber coating. After the treated fiber was dipped vertically into the sol–gel solution for 30 min, a sol–gel coating was formed on the bare outer surface of the fiber end (about 1 cm). For each fiber, this coating process was repeated several times until the desired thickness of the coating was obtained. The fiber was then placed in a desiccator at room temperature for 12 h and then conditioned at 280 °C under nitrogen for 2.5 h in the GC injection port.

2.3. Reagents and standards

2,3-Dimethyl-2,3-dinitrobutane (DMNB) was synthesized by Beijing General Research Institute of Mining and Metallurgy,

Beijing, China. Ammonium nitrate (AR) was purchased from Shanghai Chemical Factory, China. Certain amounts of DMNB and dried ammonium nitrate were mixed and mortared to get standard sample with a concentration of 0.01–1.0 μg/g, respectively. The optimization of SPME conditions was performed in the mixture with a concentration of 1.0 μg/g. All solvents used in this study were analytical-reagent grade.

2.4. Headspace-SPME procedure

Before the initial application, the fibers were conditioned according to the recommendations of the producer. Each day, before analysis, the amide bridged-C[4]/OH-TSO fiber was conditioned for 20 min in the GC injector to verify that no extraneous compounds were desorbed from the fiber. To prevent the analytes from being adsorbed on the glass wall, the amber vials were acid washed and silanized with trimethylchlorosilane prior to the experiments.

For the analysis of DMNB, a 2 g of mixture was added in a 10-ml amber vial. The vial was closed with butyl rubber stoppers wrapped with PTFE sealing tape, and then sealed with aluminum caps. The extraction was performed by exposing the coated fiber end to the headspace of the vial for 30 s at room temperature (23–27 °C). The fiber was then immediately inserted into the heated GC injector for 1 min of thermal desorption. All the determinations were performed in duplicate except extra explanations and the average values were reported.

3. Results and discussion

3.1. Investigation of the vapor pressure of DMNB in ammonium nitrate

In order to investigate the vapor pressure of DMNB in ammonium nitrate, the experiments were divided into two groups: in one group, five extractions were performed from five separate vials (freshly prepared samples); in the other group, five extractions were performed from the same vial. And then, the relative standard deviations of peak areas were obtained for each group. As shown in Table 1, the result that there were no obvious differences between the two groups shows the vapor pressure of DMNB in ammonium nitrate can be considered invariable during that period, which is consistent with the known facts that DMNB continues to release its vapor at a steady rate for 5–10 years [18]. Consequently, some of experiments could be performed using one sample vial, such as the investigation of extraction time, desorption time and the precision of the method. These results also illustrate that SPME is very suitable for analysis of DMNB.

Table 1
Peak areas of extracting from the same vial vs. extracting from different vials

Peak areas from different vials (μv s)	Peak areas from the same vial (μv s)
6.97×10^7	7.07×10^7
7.25×10^7	7.51×10^7
7.34×10^7	6.82×10^7
7.11×10^7	7.10×10^7
6.59×10^7	6.86×10^7
Average value = 7.06×10^7, R.S.D.[a] = 4.17%	Average value = 7.07×10^7, R.S.D. = 3.89%

[a] R.S.D. (%) = relative standard deviations.

3.2. Optimization of SPME operating conditions

3.2.1. Extraction temperature

The extraction temperature profile of DMNB in ammonium nitrate was investigated. By increasing the temperature of the sample, the vapor pressure of the analyte is increased, allowing the partitioning of the analyte between the sample and the headspace to reach equilibrium more quickly. However, at the excessively high temperatures, the affinity of the analyte for the fiber coating diminishes. An optimum temperature exists for the partitioning of the analyte among the sample matrix, headspace and fiber coating, with the maximum loading onto the fiber. The results showed that the highest yield was obtained at 70 °C, which is 1.7 times more than that at 27 °C (room temperature). But in this paper, all experiments were carried out at room temperature (23–27 °C) for the convenience of the real sample analysis.

3.2.2. Extraction time

Fig. 1 shows the adsorption time profile of DMNB in ammonium nitrate. From this figure, it can be seen that the extraction yield increased significantly with the increase of extraction time. The extraction amount at 180 s was 6.14 times more than that at 5 s, and was 1.93 times more than that at 30 s. Since the response was acceptable, an extraction time of 30 s was set to meet the demand for fast determination of explosives.

3.2.3. Desorption time

The influence of desorption time on the extraction efficiency was studied by placing the fiber with the adsorbed analyte in the injector for progressively longer periods of time. Thanks to

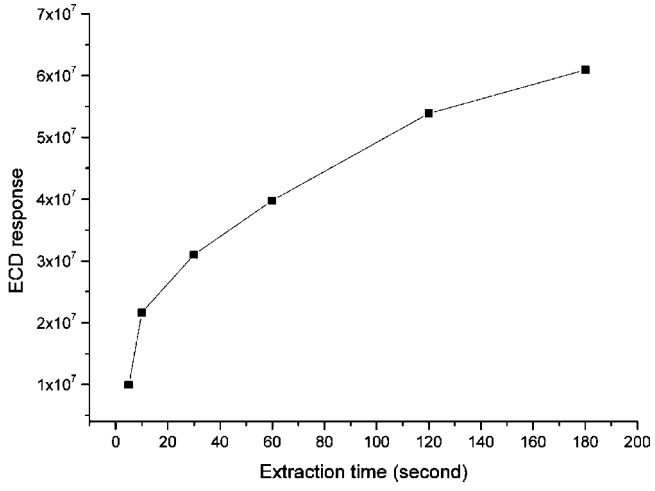

Fig. 1. The extraction time profile of DMNB in ammonium nitrate.

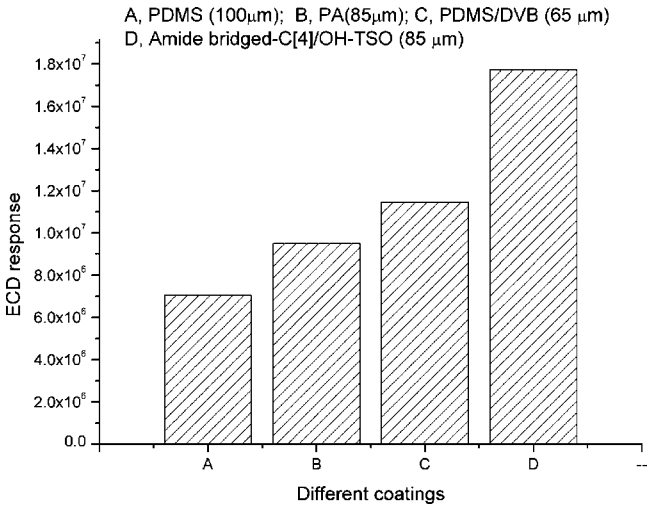

Fig. 2. Comparison of the extraction ability to DMNB by use of amide bridged-C[4]/OH-TSO fiber and commercial PDMS, PA and PDMS/DVB fibers.

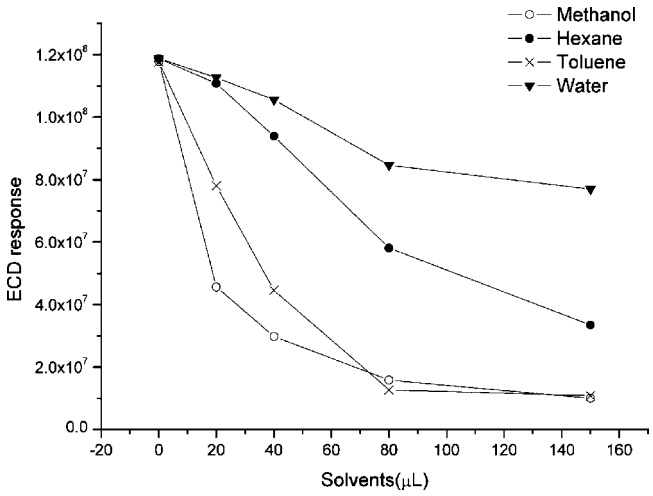

Fig. 3. The effect of solvents on the extraction amounts of DMNB.

the high thermal stability of amide bridged-C[4]/OH-TSO fiber (up to 380 °C), the experiments were performed by setting the injector temperature to 320 °C. It was observed that DMNB was fully desorbed into the injector after 1 min. And then a desorption time of 1 min was selected in this study.

3.3. Extraction efficiency of Diglycidyloxy-C[4]/OH-TSO fiber

Fig. 2 compared the extraction capability of DMNB by use of our laboratory-made sol–gel amide bridged-C[4]/OH-TSO fiber and commercial PDMS, PA and PDMS/DVB fibers. The result revealed that amide bridged-C[4]/OH-TSO fiber represented the highest efficiency for DMNB among these fibers. Firstly, the introduction of the polar amide bridge in calixarene molecules enhances the polarity of the sol–gel coating and increases the hydrogen bonding and dipole–dipole interactions with DMNB. Secondly, it is due to the cavity-shaped cyclic molecular structure and hydrophobic interactions between DMNB and calixarene resulting from the cavity and the hydrophobic *tert*-butyl groups. Thirdly, this becomes possible also thanks to the outstanding material properties of sol–gel coating, which provides sorption sites for both the polar and nonpolar analytes.

3.4. Effect of solvents

The effect originated from different volumes of solvents (methanol, hexane, toluene and water) added to the sample was studied. The experiment was done by injecting each solvent to a closed sample vial. As shown in Fig. 3, the addition of small amounts of solvents greatly decreased the extraction amounts of DMNB. When the volume of water exceeded 2 ml in 2 g of mixtures, the extraction amount of DMNB was less than 7.13% of that with no water added. That is to say, the determination of DMNB with SPME technique should avoid any addition of solvents; otherwise, positive samples may go undetected.

3.5. Interference from other compounds

Interference from organics such as nitrobenzenes explosives (nitrobenzene, *p*-nitrotoluene, *p*-nitroethylbenzene, *m*-dinitrobenzene and *o*-dinitrobenzene), aroma substances in drinks (*n*-propanol, isobutanol, isoamyl alcohol, *n*-hexanol, linalool, β-phenylethanol, ethyl acetate, isobutyl acetate, ethyl butyrate, isoamyl acetate, ethyl hexanoate, ethyl lactate, ethyl octanoate, ethyl decanoate, diethyl succinate, acetic acid, hexanoic acid, octanoic acid and decanoic acid) and nitroglycerin tablets (a kind of medicine often used by air) were studied. Apart from nitrobenzenes, all these compounds showed no peaks in the chromatograms under that condition. Although some of these nitrobenzenes could be determined, and the response of DMNB was suppressed by adding the organics, they showed no interference in the identification of DMNB with a concentration of 1.0 μg/g (as shown in Fig. 4).

3.6. Limit of detection, linearity, correlation coefficient and the relative standard deviations (R.S.D., %)

The linearity of the method was tested by extracting 2 g of DMNB samples with increasing concentrations (from 0.01 to

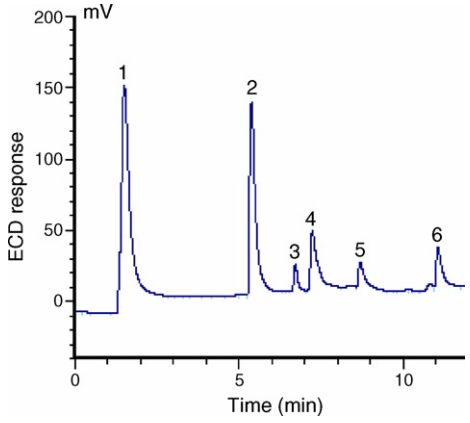

Fig. 4. Chromatogram of extraction of DMNB in ammonium nitrate spiked with 0.05 mg/g of nitrobenzenes compounds. Peaks: 1, methanol; 2, nitrobenzene; 3, DMNB; 4, *p*-nitrotoluene; 5, *p*-nitroethylbenzene; 6, *m*-dinitrobenzene.

1.0 μg/g). The headspace-SPME procedure with sol–gel-coated amide bridged-C[4]/OH-TSO fiber showed extraordinarily wide linear ranges with a correlation coefficient of 0.999. The calculated limit of detection (LOD) was 4.43×10^{-4} μg/g, estimated on the basis of 3:1 signal to noise ratios. The linearity was broader and the LOD was much lower than those described in Ref. [15]. In contrast to SPME-GC, no DMNB in the chromatogram was obtained by direct injection of 60 μl of gas in the headspace of the vial containing DMNB sample with a concentration of 1.0 μg/g.

The precision of the method was determined by performing five consecutive fiber extractions from DMNB samples with each concentration. The corresponding standard deviation, calculated for these extractions and expressed as a percentage, was below 8%.

In order to demonstrate the practical suitability of the procedure, DMNB mixture with a concentration of 0.1 μg/g was packaged in two plastic bags. One bag was tied securely and the other was unsealed and both of these samples were placed in a desiccator at room temperature. The samples were analyzed at intervals of 15 days. Results showed DMNB in the tied bag was detectable by SPME-GC system even after 6 months, but it was undetectable in the unsealed one only after 3 months because of the moisture absorption of ammonium nitrate.

4. Conclusions

A sensitive and effective method to identify and detect marking agent in explosives is proposed by combination GC with ECD using SPME as a sample preparation technique. Using SPME technique simplifies the detection process, and allows for rapid field sampling. The laboratory-made sol–gel amide bridged-C[4]/OH-TSO fiber was very sensitive to trap DMNB from ammonium nitrate and LOD of 4.43×10^{-4} μg/g was achieved. The explosive or non-explosive compounds do not interfere with detection and identification. Considering the good characteristics owned by calixarene-based sol–gel coatings such as stability, uniform, high sensitivity and long lifetime, a chemical sensor based on calixarenes-containing polymer film proceeded with optical instruments will be introduced for improved selectivity, sensitivity and availability.

Acknowledgements

This work was kindly supported by the National Natural Science Foundation of China (Grant No. 20375028). The authors would also like to acknowledge Prof. Helin Luan (Beijing General Research Institute of Mining and Metallurgy, Beijing, China) for donation of DMNB used in this research.

References

[1] J. Yinon, Trends Anal. Chem. 21 (2002) 292.
[2] G. Reid Asbury, J. Klasmeier, H.H. Hill Jr., Talanta 50 (2000) 1291.
[3] B. Zhang, et al., Talanta 72 (2007) 612.
[4] J.M. Perr, K.G. Furton, J.R. Almirall, Talanta 67 (2005) 430.
[5] R.G. Ewing, D.A. Atkinson, G.A. Eiceman, G.J. Ewing, Talanta 54 (2001) 515.
[6] K.G. Hopper, H. LeClair, B.R. McCord, Talanta 67 (2005) 304.
[7] R.L. Marple, W.R. LaCourse, Talanta 66 (2005) 581.
[8] X. Pan, K. Tian, L.E. Jones, G.P. Cobb, Talanta 70 (2006) 455.
[9] N. Pon Saravanan, S. Venugopalan, N. Senthilkumar, P. Santhosh, B. Kavita, H. Gurumallesh Prabu, Talanta 69 (2006) 656.
[10] J. Wang, M. Pumera, Talanta 69 (2006) 984.
[11] M. Nambayah, T.I. Quickenden, Talanta 63 (2004) 461.
[12] D.R. Shankaran, K.V. Gobi, K. Matsumoto, T. Imato, K. Toko, N. Miura, Sens. Actuators B 100 (2004) 450.
[13] Doc. 9571 ICAO Convention, International Civil Aviation Organization, Montreal, Canada, March 1, 1991.
[14] R.G. Ewing, C.J. Miller, Field Anal. Chem. Technol. 5 (5) (2001) 215.
[15] J. Wang, S. Thongngamdee, D. Lu, Electroanalysis 18 (10) (2006) 971.
[16] L.G. Cabrini, R. Sparrapan, M.A. Mendes, L.A.B. Moraes, M.N. Eberlin, J. Mass Spectrom. 40 (2005) 1506.
[17] S.W. Thomas III, J.P. Amara, R.E. Bjork, T.M. Swager, Chem. Commun. (2005) 4572.
[18] J. Yinon, Forensic Applications of Mass Spectrometry, CRC Press, Boca Raton, FL, 1995.
[19] R.P. Belardi, J. Pawliszyn, J. Water Pollut. Res. J. Can. 24 (1989) 179.
[20] J.M. Perr, K.G. Furton, J.R. Almirall, J. Sep. Sci. 28 (2005) 177.
[21] Z.R. Zeng, W.L. Qiu, Z.F. Huang, Anal. Chem. 73 (2001) 2429.
[22] Z.R. Zeng, W.L. Qiu, M. Yang, X. Wei, Z.F. Huang, F. Li, J. Chromatogr. A 934 (2001) 51.
[23] M. Vincenti, A. Irico, Int. J. Mass Spectrom. 214 (2002) 23.
[24] W. Wang, S.L. Gong, Q.H. Cao, Y.Y. Chen, X.J. Li, Z.R. Zeng, Chromatographia 61 (2005) 78.

Available online at www.sciencedirect.com
ScienceDirect
Talanta 72 (2007) 1404–1409
Talanta
www.elsevier.com/locate/talanta

Optimization of phenolic compounds analysis by capillary electrophoresis

Diana L.D. Lima, Armando C. Duarte, Valdemar I. Esteves *

CESAM—Department of Chemistry, University of Aveiro, Campus de Santiago, 3810-193 Aveiro, Portugal

Received 10 November 2006; received in revised form 17 January 2007; accepted 19 January 2007
Available online 30 January 2007

Abstract

Operational parameters like migration time, temperature, voltage, composition of background electrolyte and content of organic modifier were optimized in CZE for the determination of lignin-like phenolic compounds.

The applied background electrolyte buffer consisted of a $Na_2B_4O_7$, KH_2PO_4 aqueous solution, pH 9.15 using acetonitrile as organic modifier with UV-detection. Compounds, such as acetosyringone, acetovanillone, syringealdehyde, *p*-hydroxyacetophenone, vanillin, syringic acid, ferulic acid, *p*-hydroxybenzaldehyde, *p*-coumaric acid, vanillic acid and *p*-hydroxybenzoic acid were applied as reference compounds.

The quality and quantity of different phenolic compounds obtained upon alkaline CuO oxidation of a commercial humic acid were determined with CZE using ethylvanillin as internal standard.

The optimized CZE revealed has being an appropriate method since it is quick, sensitive and quantitative and does not require a time-consuming sample preparation.

Keywords: Capillary zone electrophoresis; Humic acids; Phenols; CuO oxidation

1. Introduction

Humic substances (HS) are the most important natural sunlight-absorbing components in aquatic environments. The major proportion of carbon on earth's surface is present as humic substances, resulting of the decomposition of organic materials which can be found as colloidal or dissolved matter as well as soils constituents.

According to general adopted procedure, HS can be divided into three fractions based on water solubility: (a) humin, the fraction that is not water soluble at any pH; (b) humic acids (HA), the fraction that is not soluble under acidic conditions (pH bellow 2) but becomes soluble at higher pH; finally, fulvic acid (FA), the fraction that is soluble under all pH conditions.

Analytical methods have been used in order to develop structural models that allow a better understanding of the environmental role and basic functions of HS. The structural models suggest a relative biologically resistant and highly substituted core of aromatic nature with the presence of heterocyclic structures. The units are linked to each other by alkyl chains of different lengths that are highly substituted with functional groups, such as carboxylic, aliphatic, aromatic, hydroxyl and amino groups [6,12–15].

Lignin is an abundant and stable phenolic macromolecule, hardly accessible to most organisms, found in vascular plants, with an important role on plants structure and essentially absent in all other living organisms. A large number of phenolic compounds presents in lignin are also present in humic substances.

Lignin has been used as a fingerprint of terrestrial input for marine organic matter, namely humic substances.

Analyses of phenolic compounds derived from humic substances or lignin gives evidence of the presence of terrigenous vascular plant material in marine samples and provides information on the taxonomic source and diagenetic state of humic substances, making a unique tracer for vascular plant matter, suitable even for the chemotaxonomic distinction between angiosperms, gymnosperms and non-woody vascular plants. Phenols in these substances are considered fingerprints of the organic matter of terrestrial samples [1,2,10,11].

Due to the complexity of the sample, identification and quantification of phenols lignin-derived from humic substances require a previous oxidative hydrolysis with CuO, followed by extraction with an organic solvent—ethyl ether [1,2].

* Corresponding author. Tel.: +351 234401408.
E-mail address: Valdemar@dq.ua.pt (V.I. Esteves).

0039-9140/$ – see front matter © 2007 Elsevier B.V. All rights reserved.
doi:10.1016/j.talanta.2007.01.049

The compounds obtained by CuO-oxidation procedure can be analysed and identified using different techniques that usually have a complex sample preparation protocol [7]. Usually, derived lignin-phenols obtained from CuO oxidation are analysed by gas chromatography after derivatization, resulting in a long analysis time [8].

Commonly used techniques for the characterization of lignin-derived phenols are either gas capillary chromatography with fused-silica columns as used by Hedges and Ertel [3], Tareq et al. [10], Hautala et al. [16], or high-performance liquid chromatography as used by Štěrbová et al. [17], Sjöberg et al. [18], Lobbes et al. [19]. These methods either suffer from low sensitivity, time-consuming procedures or chemical modification procedures. Thus, there is a need for the development of highly specific, quantitative methods, but without any derivatization process, like the one used in gas chromatography. Capillary zone electrophoresis is becoming a commonly applied analytical method for the analysis of various lignin degradation products [1,8]. The main advantage of capillary electrophoresis in phenols analysis is the high separation power, leading to fast and well resolved separation of similar compounds by adjusting the main parameters that affect electrophoretic behaviour, including buffer concentration, pH, applied potential and cartridge temperature [7–9]. CZE also allows the use of small amounts of sample, which sometimes can be a very important issue. [6] This technique avoids the derivatization procedure and allows the accomplishment of well-resolved separations in less time than the usually taken by chromatographic methods.

This work reports the separation, identification and quantification of phenolic compounds obtained by CuO oxidation of humic substances, using ethylvanillin as an internal standard, by capillary zone electrophoresis coupled to a diode array detector.

2. Materials and methods

2.1. Instrumentation

All experiments were performed using a Beckman P/ACE MDQ capillary electrophoresis system equipped with a diode array detector. Separation was carried out on an 42.8 cm long fused-silica capillary (36 cm effective length to the detector), 75 μm internal diameter and 375 μm of external diameter. To optimize the separation and to obtain a more stable baseline, ca. 1 mm of the polyimide coating was removed by burning both ends of the capillary and then polishing them.

2.2. Buffer and standards

The run buffer consisted of a daily prepared 4.3×10^{-2} M $Na_2B_4O_7 + 2.7 \times 10^{-2}$ M $KH_2PO_4 + 8.5\%$ CH_3CN solution with a final pH of 9.15. The buffer was prepared with ultra-pure water and using acetonitrile as an organic modifier.

An internal standard stock solution of ethylvanillin (99%, Aldrich) was prepared at a concentration of 0.01 M. A stock standard solution was also prepared containing all of the following reagents at a 0.01 M concentration: acetosyringone (97%, Aldrich), acetovanillone (98%, Aldrich), syringealdehyde (99%, Aldrich), *p*-hydroxyacetophenone (99%, Aldrich), vanillin (99%, Merck), syringic acid (98%, Sigma), ferulic acid (99%, Aldrich), *p*-hydroxybenzaldehyde (99%, BHD), *p*-coumaric acid (98%, Sigma), vanillic acid (97%, Aldrich), *p*-hydroxybenzoic acid (99%, Aldrich). Standards calibration solutions, with concentrations ranging 1.25×10^{-5} to 2.5×10^{-3} M, were prepared upon dilution of the stock solution. Internal standard was added to these standards in order to obtain a final concentration of 2.5×10^{-5} M.

Stock solutions were prepared by dissolving the reagents in a small quantity of acetonitrile and then by completing the volume with ultra-pure water. Calibration solutions were then prepared by dilution of the previous stock solution. The dissolution of the reagents was not made in methanol in order to avoid the oxidation of aldehydes and the isomerization of ferulic and *p*-coumaric acids. All the solutions were kept on closed vials, under N_2 atmosphere, at 4 °C.

Buffer, standards and samples were filtered through a 0.22 μm membrane filter.

2.3. Sample preparation

The humic acids derived phenols were obtained according to the method described by Hedges and Ertel [3], which involves CuO oxidation of 100 mg of Fluka humic acids. Humic acids were placed in an air tight Teflon vial protected by a steel bomb fitted with a screw cap with 100 mg of ammonium iron(II) sulphate hexahydrate $[Fe(NH_4)_2(SO_4)_2{\cdot}6H_2O]$, 250 mg of CuO and 6 mL NaOH 2 M (purged with N_2). The Teflon vial and the bomb were sealed under nitrogen atmosphere in a glove box, after being one night in this atmosphere.

The oxidation was carried out by heating the bombs at 155 °C for 3 h in an oven. After cooling the bomb under running tap water and adding 10 μL of internal standard 0.01 M, the supernatant of the Teflon vial was saved and the sediment washed with four portions of 5 mL NaOH 1M (purged with N_2). The supernatants and washings were acidified with HCl 6 M to pH 1, transferred to a 50 mL centrifuge tube and centrifuged at 4000 rpm for 10 min. The precipitate was washed with acidified water (pH 1) and the centrifugation repeated.

The combined supernatants were extracted for three successive times with 20 mL of ethyl ether and then these ether extracts were passed through an anhydrous Na_2SO_4 column. Finally, the ethyl ether was evaporated under a N_2 stream and the obtained solid residue dissolved in 2 mL of acetonitrile plus 2 mL of buffer.

2.4. Capillary column conditioning

New capillaries were conditioned with NaOH 1 M for 10 min, followed by 30 min, with NaOH 0.1 M, 5 min with ultra-pure water and finally 10 min with electrolyte.

The capillary was conditioned every day with NaOH 1 M, NaOH 0.1 M, ultra-pure water and electrolyte for 5 min each, in order to obtain a stable baseline and to improve the reproducibility of the migration time. Before each injection, the capillary was flushed with NaOH 0.1 M for 5 min, ultra-pure water for

2 min and electrolyte for 3 min. All flushing was performed using 20.0 psi pressure.

2.5. Separation conditions

Injection times varied from 4 s for the less concentrated standards to 2 s for the most concentrated; samples were injected for 5 s.

Electrophoretic separations were carried out at positive power supply of 25 kV for 15 min, maintaining the capillary temperature at 25 °C, resulting in a current of ~250 μA.

Solutes were monitored by detection at 214 nm or in the range 190–300 nm for multi-wavelength detecting.The run buffer vials were used for four consecutive injections before replacement with new vials.

3. Results and discussion

3.1. Optimization of capillary zone electrophoresis

Factors, such as electrolyte composition, applied voltage, injection time, temperature and stability of the hydrodynamic injection have a great influence on the migration behaviour of phenolic compounds. Therefore, it is important to study these factors deeply. Using optimum separation conditions, it is possible to control the electrophoretic mobilities of the solutes or the electrophoretic flow (EOF) in order to obtain higher resolutions.

3.1.1. Effect of organic modifiers

The effect of organic solvents within the buffers, on the resolution, was evaluated using a buffer with 4.3×10^{-2} M $Na_2B_4O_7$ and 2.7×10^{-2} M KH_2PO_4, a temperature of 25 °C and a voltage of 30 kV. As organic modifier, 8.5, 12 and 15% of acetonitrile were used in our study.

Electrophoretic mobility, as a normalized parameter it permits, in principle, the comparisons with similar literature samples, was calculated using the following expression:

$$\mu_{i(\text{net})} = \frac{V_{i(\text{net})}}{E} = \frac{L_D \times L_T}{M_t \times V} \ (\text{cm}^2\ \text{s}^{-1}\ \text{V}^{-1})$$

where L_D is the length to the detector, L_T the total length, M_t the migration time and V is the voltage applied.

The electrophoretic mobility of phenolic acids decreases with the increasing of the organic modifier content, resulting in an increase on the migration time and analyses time (Fig. 1).

Using 8.5% of acetonitrile in buffer composition we can achieve a good separation in less than 15 min. On the other hand, if we use 15%, the time of analyses is greater than 20 min.

Generally, the resolution is higher when is used a electrolyte with higher percentage of acetonitrile, but due to the broadening of the last peaks, the resolution between two consecutives peaks that have similar migration times, like *p*-coumaric acid and vanillic acid, decreases to values lower than 2.5.

In order to obtain values of resolution higher than 2.5 for all the compounds, and to obtain the highest values of efficiency, it was decided to use an electrolyte with 8.5% of acetonitrile. The values of efficiency obtained with this electrolyte composition were found to be between 130,000 and 25,000 theoretical plates.

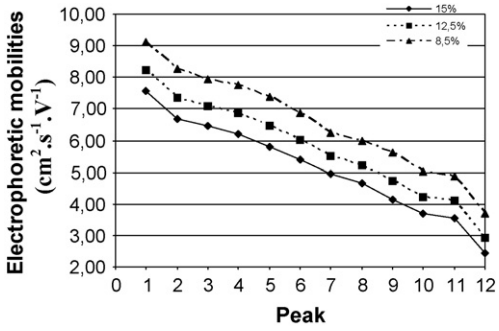

Fig. 1. Influence of the percentage of organic modifier in buffer composition on the migration time. Peak identification: (1) acetosyringone, (2) acetovanillone, (3) syringealdehyde, (4) ethylvanillin, (5) *p*-hydroxyacetophenone, (6) vanillin, (7) syringic acid, (8) ferulic acid, (9) *p*-hydroxybenzaldehyde, (10) *p*-coumaric acid, (11) vanillic acid and (12) *p*-hydroxybenzoic acid.

3.1.2. Effect of applied temperature

Temperature is an important factor in the evaluation of the stability of the migration times. We studied the use of two different temperatures, 20 and 25 °C maintaining a constant voltage of 20 kV. From Fig. 2, we can observe that increasing the temperature, the mobility of the compounds also increases. For this reason, it would be better to choose 25 °C in order to have a less time-consuming analysis. But there are others parameters to have in consideration, such as the reproducibility of the migration times, resolution between peaks and efficiency.

The reproducibility of migration time and related areas were tested through the coefficient of variation (CV):

$$\text{CV} = \frac{S}{x_{\text{med}}} \times 100\ \%,$$

where S is the standard deviation and x_{med} the mean value.

Comparing the values of the CV (Table 1) is possible to observe that the reproducibility of the migration time is higher at 25 °C for the shorter migration time, since most of the values of CV are smaller, decreasing for the higher migration times.

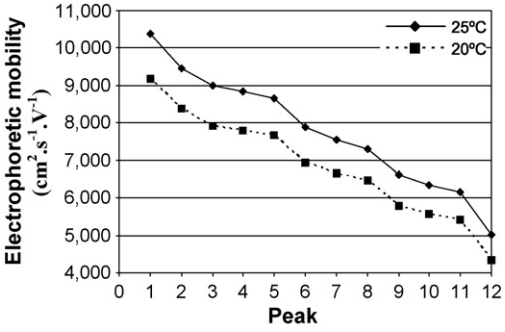

Fig. 2. Influence of the temperature on the migration time of the analytes ($n = 6$). Peak identification: (1) acetosyringone, (2) acetovanillone, (3) syringealdehyde, (4) ethylvanillin, (5) *p*-hydroxyacetophenone, (6) vanillin, (7) syringic acid, (8) ferulic acid, (9) *p*-hydroxybenzaldehyde, (10) *p*-coumaric acid, (11) vanillic acid and (12) *p*-hydroxybenzoic acid.

Table 1
Coefficient of variation of the migration times and of the ratio areas of analyte and of IS for each compound at 20 and 25 °C ($n = 6$)

Analyte	CV (%)			
	Migration time		Ratio areas	
	25 °C	20 °C	25 °C	20 °C
Acetosyringone	0.39	0.71	1.68	2.30
Acetovanillone	0.49	0.73	1.63	3.66
Syringealdehyde	0.09	1.02	1.61	1.42
Ethylvanillin (IS)	0.19	0.95	–	–
p-Hydroxyacetophenone	0.84	0.73	1.01	1.58
Vanillin	0.13	1.10	3.83	1.20
Syringic acid	1.02	0.84	1.71	2.38
Ferulic acid	1.26	0.89	2.15	1.34
p-Hydroxybenzaldehyde	0.41	1.12	2.36	12.90
p-Coumaric acid	1.46	1.06	3.04	3.81
Vanillic acid	1.47	1.09	1.42	2.29
p-Hydroxybenzoic acid	1.90	1.38	1.98	11.75

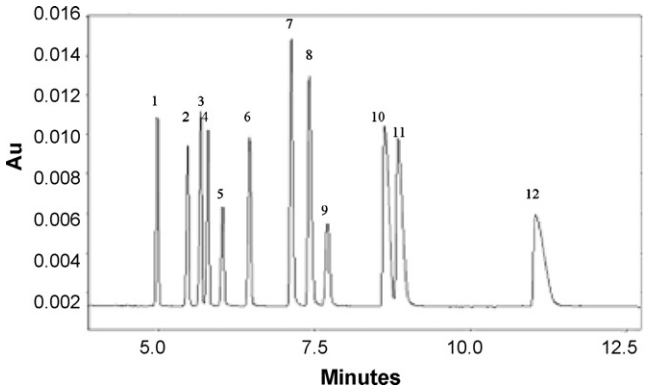

Fig. 3. Electropherogram of a standard solution with a concentration of 0.001 M for each compound. Peak identification: (1) acetosyringone, (2) acetovanillone, (3) syringealdehyde, (4) ethylvanillin, (5) *p*-hydroxyacetophenone, (6) vanillin, (7) syringic acid, (8) ferulic acid, (9) *p*-hydroxybenzaldehyde, (10) *p*-coumaric acid, (11) vanillic acid and (12) *p*-hydroxybenzoic acid. Injection time: 2 s; injection pressure: 0.3 psi; voltage: 25 kV; temperature: 25 °C; detection: 214 nm.

In what concerns area ratios, the reproducibility is, for most analytes, higher at 25 °C.

The resolution between two consecutive points is also important, and it should be greater than 2.0. The smallest values obtained for the resolution were between the following pairs of compounds: syringealdehyde/ethylvanillin, ethylvanillin/*p*-hydroxyacetophenone and *p*-coumaric acid/vanillic acid. For the first two pairs, the resolution was higher at 25 °C, while for the last considered pair, the value was smaller, yet higher then 2.0. In order to obtain resolution values higher than 2.0 for all compounds, better reproducibility of area ratios and shorter analysis time the experimental temperature was set at 25 °C.

3.1.3. Effect of applied voltage

The ideal separation in CZE is usually obtained by using a voltage as high as possible, in order to obtain the best separation, in the shortest time, with the best efficiency. High voltages lead to difficult heat dissipation during the electrophoretic separation due to the Joule effect. Joule heating is known to affect the electroosmotic flow (EOF), diffusion of analytes and therefore the efficiency and reproducibility of the separation. For this last reason, is then important to control this phenomenon.

To choose the most appropriate voltage in the electrophoretic separation, a study was made using different values of voltage: 20, 25 and 30 kV at a temperature of 25 °C, using an electrolyte composed by 4.3×10^{-2} M $Na_2B_4O_7$, 2.7×10^{-2} M KH_2PO_4 and 8.5% of acetonitrile and an injection of 0.3 psi 3 s.

Comparing the results obtained at different values of voltage, it is possible to conclude that increasing the voltage we decreased the migration time, leading to a faster analysis. For this reason, we could choose a voltage of 30 kV. However, this high voltage leads to an intense Joule effect and thus efficiency lost.

Choosing 30 kV as the separation voltage, the resolution between *p*-coumaric acid and vanillic acid (most critical pair of compounds) is smaller than 2. However, for a voltage of 25 kV, the resolution between the two peaks mentioned is higher than 2, which is an acceptable value. The resolution obtained performing the separation at 20 kV is higher, but in some cases the efficiency decreases due to the broadening of the peaks.

A compromise was made between a poorer separation at a high voltage and a longer time analyses at too low voltage, by adopting 25 kV for the separation of the phenolic compounds.

3.2. Electrophoretic separation of phenolics

Under optimized conditions, it was possible to separate and determine all compounds present in the standard solutions (Fig. 3). These compounds can be obtained after alkaline CuO oxidation of humic substances, for which lignin can be an important source.

Under the optimized conditions of CZE described, the migration times of the compounds in study are the ones indicated in Table 2.

3.3. Performance of the method

Regression analysis for each compound was performed with seven standards, with the concentrations ranging between

Table 2
Summary of the migration times and 95% confidence interval of the compounds under optimized conditions (each migration time was obtain by the mean of eleven values)

Compound	Migration time (min)
Acetosyringone	5.34 ± 0.02
Acetovanillone	5.89 ± 0.02
Syringealdehyde	6.13 ± 0.02
Ethylvanillin	6.29 ± 0.03
p-Hydroxyacetophenone	6.53 ± 0.03
Vanillin	7.04 ± 0.03
Syringic acid	7.73 ± 0.05
Ferulic acid	8.07 ± 0.06
p-Hydroxybenzeldehyde	8.50 ± 0.04
p-Coumaric acid	9.49 ± 0.09
Vanillic acid	9.73 ± 0.09
p-Hydroxybenzoic acid	12.4 ± 0.2

Table 3
Summary of calibration and precision data for the method

Compound	Equation of regression line	r	LOD (mol/dm^3)	Lin (%)	AS
Acetosyringone	$y = (0.96 \pm 0.02) \times -0.01 \pm 0.02$	0.999	1.12×10^{-4}	99.985	0.037
Acetovanillone	$y = (0.91 \pm 0.01) \times -0.00 \pm 0.01$	0.999	9.11×10^{-5}	99.989	0.030
Syringealdehyde	$y = (1.16 \pm 0.01) \times -0.02 \pm 0.02$	0.999	8.16×10^{-5}	99.987	0.027
p-Hydroxyacetophenone	$y = (0.584 \pm 0.006) \times +0.019 \pm 0.008$	1.000	7.62×10^{-5}	99.994	0.025
Vanillin	$y = (1.12 \pm 0.01) \times -0.00 \pm 0.01$	1.000	6.95×10^{-5}	99.989	0.023
Syringic acid	$y = (2.03 \pm 0.03) \times -0.07 \pm 0.04$	0.999	1.15×10^{-4}	99.968	0.038
Ferulic acid	$y = (1.87 \pm 0.02) \times +0.01 \pm 0.02$	1.000	7.41×10^{-5}	99.981	0.025
p-Hydroxybenzeldehyde	$y = (0.70 \pm 0.01) \times +0.03 \pm 0.01$	0.999	1.12×10^{-4}	99.989	0.037
p-Coumaric acid	$y = (2.20 \pm 0.03) \times +0.05 \pm 0.04$	0.999	1.08×10^{-4}	99.968	0.036
Vanillic acid	$y = (2.34 \pm 0.02) \times -0.01 \pm 0.03$	1.000	$6{,}17 \times 10^{-5}$	99.980	0.020
p-Hydroxybenzoic acid	$y = (2.23 \pm 0.04) \times -0.03 \pm 0.05$	0.999	1.18×10^{-4}	99.961	0.039

1.25×10^{-5} and 2.5×10^{-3} M, and four replicates each. The linearity of response of the method was confirmed making analysis of standard solutions containing a mixture of the phenols that are expected to be found in humic acids samples (Table 3). Correlation coefficients ranging between 0.999 and 1.000 (Table 3) suggest that the method used is linear for the range of concentration used in this study.

The linearity (Lin) was calculated by the equation:

$$\text{Lin}\,(\%) = 100 - \text{R.S.D.}_\text{b}$$

where R.S.D._b is the relative standard deviation of the slope. Linearity ranged between 99.961 and 99.994. Another analytical parameter was calculated, the analytical sensitivity (AS), calculated as the standard deviation of the residual divided by the slope.

3.4. Determination of phenolic compounds in humic acids

An electropherogram of a humic acid sample is shown in Fig. 4. Peaks were assigned not only by comparing the migration times with those of standards, but also by multi-wavelength scanning of the peaks between 190 and 300 nm with a UV-photodiode array detector and by spiking the sample with standard compounds.

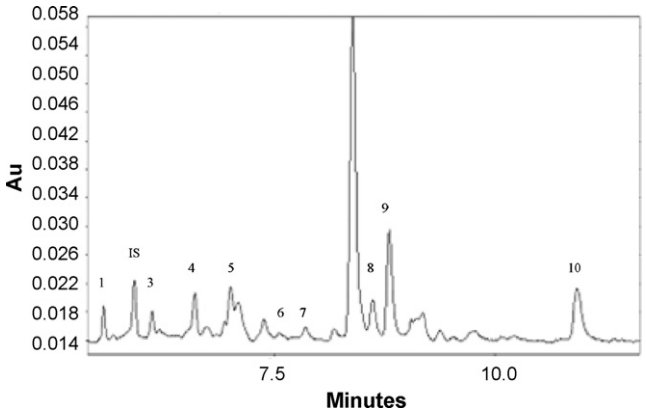

Fig. 4. Electropherogram of a Fluka humic acid sample. Peak identification: (1) acetovanillone, (IS) ethylvanillin, (3) *p*-hydroxyacetophenone, (4) vanillin, (5) syringic acid, (6) ferulic acid, (7) *p*-hydroxybenzaldehyde, (8) *p*-coumaric acid, (9) vanillic acid and (10) *p*-hydroxybenzoic acid. Injection time: 5 s; injection pressure: 0.3 psi; voltage: 25 kV; temperature: 25 °C; detection: 214 nm.

Table 4
Summary of the concentrations of phenols in Fluka humic acids with 95% confidence limits

Compound	[Humic acids] (μg/gsample)	Number of replicates
Acetosyringone	n.d.	–
Acetovanillone	83 ± 5	15
Syringealdehyde	n.d.	–
p-Hydroxyacetophenone	104 ± 3	15
Vanillin	121 ± 4	15
Syringic acid	123 ± 9	10
Ferulic acid	14 ± 6	14
p-Hydroxybenzeldehyde	49 ± 7	15
p-Coumaric acid	49 ± 6	7
Vanillic acid	189 ± 4	15
p-Hydroxybenzoic acid	104 ± 5	15

n.d.: Not determined.

The results obtained for the sample of Fluka humic acids are shown in Table 4 and show a large predominance of vanillyl phenols, indicating an unambiguous general tracer of terrestrially derived material.

Compounds, such as *p*-hydroxybenzoic acid, *p*-hydroxyacetophenone and syringic acid are also present in large quantities. The low concentration of ferulic acid makes the analysis difficult due to the high value of its confidence limit. Acetosyringone and syringealdehyde were not determined.

The presence of cinnamyl phenols denotes the presence of non-woody tissues, while the presence of vanillyl, syringyl and sometimes *p*-hydroxyl-phenols indicates that this sample comes from tissues of angiosperms plants [5]. Vanillic acid dominates over vanillin indicating extensive oxidative biodegradation of the lignin structural units [4].

4. Conclusion

A simple and rapid (less than 15 min) CE method with UV detection can be used for the analyses of phenolic compounds from humic acids, being an alternative to methods, such as gas capillary chromatography on fused-silica columns or

high-performance liquid chromatography, avoiding the step of derivatization. The compound identification problems, due to poor accuracy of migration time, were overcame by spiking 2 mL of sample with 25 μL of 0.01 M solutions of each compound and by comparing the UV–vis spectra from standards and sample compounds.

References

[1] O. Maman, F. Marseille, B. Guillet, J.R. Disnar, P. Morin, J. Chromatogr. A 755 (1996) 89.
[2] T. Javor, W. Buchberger, I. Tanzcos, Mikrochim. Acta 135 (2000) 45.
[3] J.I. Hedges, J.R. Ertel, Anal. Chem. 54 (1982) 174.
[4] K.J.M. Schulte, J.I. Hedges, Nature 321 (1986) 61.
[5] J.I. Hedges, P.L. Parker, Geochim. Cosmochim. Acta 43 (1979) 1803.
[6] P.S. Kopplin, A.W. Garrison, E.M. Perdue, D. Freitag, A. Kettrup, J. Chromatogr. A 807 (1998) 101.
[7] M. Bonoli, M. Montanucci, T.G. Toschi, G. Lercker, J. Chromatogr. A 1011 (2003) 163.
[8] T. Javor, W. Buchberger, O. Faix, Anal. Chim. Acta 484 (2003) 181.
[9] J. Kronholm, P.R. Ruiz, S.P. Porras, K. Hartonen, R.C. Martínez, M.-L. Riekkola, J. Chromatogr. A 1022 (2004) 9.
[10] S.M. Tareq, N. Tanaka, O. Keiichi, Sci. Total Environ. 324 (2004) 91.
[11] T. Dittmar, J.R. Lara, Geochim. Cosmochim. Acta 65 (2001) 1417.
[12] M.N. Jones, J.W. Birkett, A.E. Wilkinson, Anal. Chim. Acta 314 (1995) 149.
[13] I. Rozenbaha, G. Odham, U. Jarnberg, T. Alsberg, M. Klavins, Anal. Chim. Acta 452 (2002) 105.
[14] J. Peuravuori, N. Paaso, K. Pihlaja, Anal. Chim. Acta 391 (1995) 331.
[15] K.D. Jones, W.-H. Huang, J. Hazard. Mater. 103 (2003) 93.
[16] K. Hautala, J. Peuravuori, K. Pihlaja, Environ. Int. 24 (1998) 527.
[17] D. Štěrbová, D. Matějíček, J. Vlček, V. Kubáň, Anal. Chim. Acta 513 (2004) 435.
[18] G. Sjöberg, H. Knicker, S.I. Nilsson, D. Berggren, Soil Biol. Biochem. 36 (2004) 609.
[19] J. Lobbes, H.C. Fitznar, G. Kattner, Anal. Chem. 71 (1999) 3008.

Available online at www.sciencedirect.com
ScienceDirect
Talanta 72 (2007) 1307–1315
Talanta
www.elsevier.com/locate/talanta

QSPR study of GC retention indices for saturated esters on seven stationary phases based on novel topological indices

Fengping Liu [a,b], Yizeng Liang [a], Chenzhong Cao [b,*], Neng Zhou [a]

[a] School of Chemistry and Chemical Engineering, Central South University, Changsha 410083, China
[b] School of Chemistry and Chemical Engineering, Hunan University of Science and Technology, Xiangtan 411201, China

Received 27 October 2006; received in revised form 12 January 2007; accepted 14 January 2007
Available online 20 January 2007

Abstract

The novel topological indices, polarizability effect index (PEI), odd–even index (OEI) and steric effect index (SV_{ij}), previously developed in our team, were extended to predict the gas chromatographic retention indices (RI) of saturated esters on seven stationary phases (SE-30, OV-7, DC-710, OV-25, XE-60, OV-225 and Silar-5CP). The sets of molecular descriptors were derived directly from the structure of the compounds based on graph theory. Multiple linear regression (MLR) models between the RI and the topological indices were established for each stationary phase with a correlation coefficient between 0.9989 and 0.9977 and a leave-one-out cross-validation correlation coefficient between 0.9988 and 0.9975. The average prediction errors over seven phases are within the range of 0.5–0.7%. Statistical analysis showed that the polarizability effect, the molecular size and the branching make dominant contributions to RI of ester compounds, but steric effect also provides separate contribution. The models with topological indices were compared with recently proposed QSRR models of the similar data. It is found that the present indices produce better correlations with Kováts retention indices than the previous topological indices. The significant improvement demonstrates the efficiency of the current study in the quantitative structure retention indices correlations of complex compounds with polar functional group.

Keywords: Gas chromatographic retention indices; Topological indices; Saturated esters; Quantitative structure retention relationships

1. Introduction

The ester compound is a sort of important medical material. An effective method for determination of the esters is gas chromatography. If the retentions of these substances on chromatographic systems can be theoretically predicted relatively well, a fast theoretical approach could (partly) replace the time-consuming experimental one. Therefore, it is necessary to study the retention mechanism of esters on different stationary phases in order to predict the retention property of these compounds. Among all methods, quantitative structure-retention relationships (QSRR) are the most popular.

In QSRR research, chemical compounds must be presented in computer readable form, and afterward the quantitative correlation between a chemical structure and its retention can be obtained using different statistical and learning procedures. The QSRR models described in the literature usually apply multiple linear regression (MLR) methods, often combined with genetic algorithms (GA) for feature selection [1–3]. Other frequently used approaches include artificial neural networks, partial least squares (PLS) and principal component regression (PCR) [4–6]. But the major problem in QSRR studies still remains a mathematical representation of molecular structure, that is, translation of the molecular structure into the computer readable form retaining as much structural information as possible.

In QSRR studies, the chemical compounds can be presented by empirical physicochemical parameters or non-empirical structural descriptors [7,8]. Because it is not always possible to obtain physicochemical parameters for each compound of interest, the development of non-empirical structural representation that is able to give a satisfactory correlation with the retention properties would be beneficial. Several topological, geometric, electronic and quantum chemical indices have been already used in QSRR research. Song et al. studied the chromatographic behavior of alcohols employing semi-empirical quantum chemical method (AM1) in MOPAC and Hartree–Fock (HF) method

* Corresponding author. Tel.: +86 7328291336; fax: +86 7328291001.
E-mail address: czcao@hnust.edu.cn (C. Cao).

0039-9140/$ – see front matter © 2007 Elsevier B.V. All rights reserved.
doi:10.1016/j.talanta.2007.01.038

in Gaussian 98 implemented [9]. Zhai et al. derived QSRR model to correlate the GC retention indices for PCDFs using specific structural and thermodynamic parameters [10]. Based on the topologic, topographic and quantum-chemical descriptors, Martínez et al. predicted the Kováts retention indices of the imine family [11]. QSPR equations have been established to model gas chromatographic retention data of alkyl pyridines on apolar and polar stationary phases by Tulasamma and Reddy [12]. Wang et al. proposed quantitative structure-gas chromatographic relative retention time models on seven stationary phases for 209 polybrominated diphenyl ether congeners [13].

Topological indices are numerical representations of the chemical structure computed on the basis of molecular graph [14]. Many topological indices have been proposed since the pioneering work of Wiener [15]. Because topological indices can be easily calculated and they still give good correlation with retention properties, their use in QSRR studies instead of more complicated geometric, electronic and quantum chemical descriptors is promising. Many investigators have obtained good correlations between the experimental gas chromatographic RI and structural characteristics of molecules by using different topological indices as structural descriptors [16–18]. However, previous QSRR studies targeted mainly for modeling the retention correlation with separate equations for each different columns.

Due to the simplicity and efficiency of graph-theoretical approaches, our group recently introduced a set of novel topological indices (PEI, OEI, SV_{ij} and χ_{eq}) to establish the quantitative relationships between the physicochemical properties and molecular structure (QSPR) for alkane compounds [19–21]. It is therefore expected that these indices would make a breakthrough in structure-gas chromatographic RI correlations of complex compounds.

The main aim of this study is to further explore the potential of these topological indices in structure-retention indices correlations. The other goal of this study is to use these indices as an aid in interpreting molecular mechanism of interactions between eluents and stationary phases with different polarities. First, the range of these indices are further extended into other groups containing more than carbon and hydrogen atom in a molecule; second, the multiple linear regression models including the extended indices are developed to correlate Kováts retention indices of saturated esters on seven different stationary phases; third, the models are compared with a recent work to show the efficiency of the present indices in QSRR modeling of the saturated ester molecules. Finally, the leave-one-out cross-validation method is used to test the validity of the final models.

2. Methodology

2.1. Data and software

2.1.1. Database

The Kováts retention indices of ester compounds on seven stationary phases for this investigation were extracted from the report of Ashes and Haken [22]. The database contains RI for 90 saturated acids esters on seven GC columns of different stationary phases including SE-30, OV-7, DC-710, OV-25, XE-60, OV-225 and Silar-5CP. The esters and their retention indices are shown in Table 1. The retention data were obtained isothermally at 150 °C using 12 ft × 1/4 in O.D. aluminum columns packed with 10% stationary phase on 62–72 mesh acid-washed and silanized celatom.

2.1.2. Software

Statistical evaluation of the data and multivariate data analysis has been performed mainly by the software products Origin program packages [23]. Additional calculation programs have been developed in Matlab 6.0. All work has been performed on personal computers running under operating system Microsoft Windows.

2.2. Molecular descriptors generation and calculation

As is well known, the chromatographic retention is based on the interaction between the solute and the stationary phase. The difference of the retention is the macrocosmic reflection of the molecular structure of the solute and the property of the stationary phase. Thus, descriptors encoding significant structural information are used to present the unique retention characteristics of compounds and to build the relationship between structure and retention in this study. Here, the novel topological indices, PEI, OEI, SV_{ij}, and χ_{eq}, introduced recently by our group, are extended and employed to establish the QSRR models. The descriptors that appear in the best MLR equations for the seven different stationary phases are identical. A complete list of the esters and the calculated values of the molecular descriptors appearing in the QSRR models are summarized in Table 2.

2.2.1. The polarizability effect index PEI of alkyl groups

In the preceding paper [19], the polarizability effect index (PEI) for alkyl groups of alkane molecules has been developed and calculated. It quantitatively indicates the relative proportion polarizability effect of the alkyl groups. The PEI values of some normal alkyls and the increments ΔPEI are listed in Table 3. As with saturated esters, the contribution of the chromatographic retention arising from relative proportion polarizability effect of alkyl groups is expressed as:

$$\mathrm{PEI} = \sum \left[\sum \Delta\mathrm{PEI} \right] \tag{1}$$

where ΔPEI is the polarizability effect index increment of *i*th essential unit and can be directly taken from Table 3. The molecule of propyl propionate ($C_6H_{12}O_2$) is taken as an example to illustrate the calculation of the polarizability effect index of alkyl groups. Fig. 1 shows its hydrogen-suppressed molecular graph, where the numbers are the numberings of each carbon atom according its distance to the carbon atom of ester bond. Take the carbon atom of ester bond as the beginning to calculate the PEI index as below:

$$\mathrm{PEI} = \sum \left[\sum \Delta\mathrm{PEI} \right] = 1.0000 + 0.1405 \times 2 + 0.04813 \times 2 + 0.02350 = 1.4008 \tag{2}$$

Table 1
Data set and the corresponding experimental and calculated retention indices on seven stationary phases of 90 saturated esters

No.	SE-30		OV-7		DC-710		OV-25		XE-60		OV-225		Silar-5CP	
	Experimental	Calculated	Experimental	Calculated	Experimental	Calculated	Experimental	Calculated	Experimental	Calculated	Experimental	Calculated	Experimental	Calculated
1	509	527	559	583	609	624	693	691	737	749	759	762	850	861
2	592	615	648	673	690	712	760	774	815	833	835	845	923	938
3	695	704	755	764	796	802	853	860	920	923	932	935	1013	1023
4	794	807	855	870	895	908	946	962	1022	1034	1030	1046	1116	1131
5	891	895	958	961	996	997	1044	1046	1122	1122	1132	1134	1212	1214
6	988	992	1056	1061	1092	1096	1133	1142	1221	1225	1229	1237	1301	1312
7	643	663	686	716	722	753	782	809	842	869	840	876	914	959
8	750	754	810	810	846	846	898	898	976	967	977	974	1063	1054
9	859	859	922	918	955	954	1001	1002	1086	1078	1087	1086	1172	1162
10	617	615	667	673	710	712	775	774	837	833	851	845	947	938
11	692	693	743	752	783	789	845	846	897	905	905	915	998	1001
12	789	786	851	847	884	882	934	935	1003	998	1013	1008	1098	1089
13	886	878	949	942	984	976	1032	1025	1104	1093	1113	1103	1195	1180
14	980	974	1047	1041	1082	1074	1125	1119	1202	1194	1211	1204	1289	1276
15	1074	1069	1142	1139	1176	1171	1215	1212	1300	1293	1307	1303	1378	1372
16	733	732	785	785	817	819	871	871	920	930	928	935	1001	1011
17	848	840	906	896	938	930	985	977	1057	1045	1062	1052	1141	1124
18	948	932	1014	992	1042	1025	1086	1068	1156	1143	1169	1149	1243	1218
19	702	704	767	764	803	802	868	860	923	923	938	935	1032	1023
20	778	786	840	847	876	882	931	935	986	998	999	1008	1085	1089
21	875	874	938	937	973	971	1022	1019	1089	1086	1098	1096	1179	1171
22	969	968	1036	1034	1069	1066	1114	1111	1187	1183	1193	1192	1272	1264
23	1062	1062	1131	1130	1164	1162	1208	1203	1284	1281	1288	1290	1362	1357
24	1156	1158	1225	1229	1258	1261	1292	1297	1380	1381	1388	1391	1451	1454
25	820	829	878	884	905	917	955	964	1010	1027	1019	1032	1091	1103
26	933	924	993	982	1023	1014	1065	1057	1143	1128	1146	1134	1217	1201
27	1029	1024	1093	1086	1124	1117	1163	1156	1243	1235	1247	1241	1316	1304
28	807	801	871	864	907	901	961	954	1027	1024	1042	1035	1131	1119
29	876	878	941	942	975	976	1014	1025	1085	1093	1105	1103	1180	1180
30	971	968	1036	1034	1069	1066	1111	1111	1179	1183	1196	1192	1221	1264
31	1063	1060	1130	1128	1163	1160	1205	1200	1279	1277	1289	1286	1361	1353
32	1155	1155	1222	1226	1257	1257	1304	1293	1375	1376	1382	1385	1451	1447
33	1247	1250	1316	1324	1349	1353	1382	1385	1470	1475	1476	1484	1539	1542
34	915	917	971	975	1000	1006	1046	1049	1105	1117	1116	1122	1180	1188
35	1027	1020	1087	1081	1117	1112	1156	1151	1235	1227	1240	1233	1307	1295
36	1132	1114	1185	1178	1217	1208	1253	1243	1333	1326	1340	1332	1405	1390
37	902	895	974	961	1006	997	1056	1046	1133	1122	1140	1134	1225	1214
38	976	974	1045	1041	1073	1074	1118	1119	1196	1194	1203	1204	1275	1276
39	1064	1062	1138	1130	1164	1162	1207	1203	1283	1281	1295	1290	1363	1357
40	1156	1155	1231	1226	1256	1257	1295	1293	1377	1376	1383	1385	1451	1447
41	1246	1249	1325	1322	1349	1352	1384	1384	1471	1473	1508	1482	1539	1540
42	1337	1345	1417	1421	1440	1450	1470	1477	1565	1573	1575	1582	1626	1636
43	1008	1016	1074	1076	1115	1107	1131	1145	1207	1220	1206	1225	1275	1287
44	1119	1112	1189	1175	1211	1206	1246	1240	1332	1323	1333	1328	1397	1386

Table 1 (*Continued*)

No.	SE-30		OV-7		DC-710		OV-25		XE-60		OV-225		Silar-5CP	
	Experimental	Calculated	Experimental	Calculated	Experimental	Calculated	Experimental	Calculated	Experimental	Calculated	Experimental	Calculated	Experimental	Calculated
45	1212	1215	1287	1284	1308	1314	1342	1346	1430	1433	1432	1441	1494	1497
46	665	663	723	716	764	753	812	809	870	869	885	876	957	959
47	732	732	793	785	831	819	875	871	968	930	935	935	1016	1011
48	836	829	891	884	925	917	968	964	1035	1027	1041	1032	1107	1103
49	931	917	987	975	1019	1006	1059	1049	1130	1117	1136	1122	1201	1188
50	1024	1016	1082	1076	1115	1107	1155	1145	1225	1220	1230	1225	1294	1287
51	1117	1109	1177	1172	1208	1202	1238	1236	1323	1317	1323	1322	1383	1380
52	780	763	829	809	849	841	889	886	953	945	947	945	1014	1010
53	899	887	946	939	975	970	1008	1011	1096	1079	1086	1080	1149	1142
54	994	983	1045	1036	1075	1068	1109	1104	1196	1190	1188	1192	1249	1250
55	763	753	823	809	854	845	902	897	969	966	982	973	1063	1053
56	839	840	893	896	925	930	967	977	1033	1045	1042	1052	1114	1124
57	929	924	987	982	1018	1014	1059	1057	1129	1128	1137	1134	1206	1201
58	1021	1020	1081	1081	1111	1112	1149	1151	1224	1227	1231	1233	1296	1295
59	1112	1112	1174	1175	1204	1206	1238	1240	1318	1323	1325	1328	1386	1386
60	1204	1214	1267	1283	1296	1313	1326	1345	1414	1432	1417	1439	1474	1495
61	874	887	923	939	950	970	989	1011	1049	1079	1064	1080	1127	1142
62	985	985	1039	1038	1066	1071	1096	1107	1177	1194	1184	1196	1246	1254
63	1081	1078	1136	1136	1164	1166	1196	1199	1278	1282	1281	1284	1343	1338
64	875	864	936	925	970	961	1019	1009	1094	1089	1104	1097	1177	1174
65	943	938	1004	998	1036	1032	1078	1076	1158	1153	1163	1160	1219	1230
66	1035	1030	1094	1093	1128	1125	1165	1164	1249	1245	1253	1252	1313	1316
67	1125	1114	1189	1178	1220	1208	1252	1243	1340	1326	1345	1332	1402	1390
68	1215	1215	1281	1284	1313	1314	1340	1346	1433	1433	1438	1441	1490	1497
69	1306	1304	1374	1373	1404	1402	1427	1428	1527	1524	1529	1529	1578	1579
70	979	968	1028	1019	1059	1050	1095	1086	1169	1165	1172	1165	1229	1221
71	1089	1078	1147	1136	1175	1166	1200	1199	1296	1282	1309	1284	1340	1338
72	1181	1197	1244	1259	1272	1288	1298	1316	1393	1407	1394	1410	1442	1460
73	853	847	908	902	945	936	989	981	1054	1053	1065	1058	1131	1128
74	917	916	973	971	1006	1002	1053	1043	1118	1113	1121	1117	1173	1179
75	1009	1011	1064	1068	1096	1097	1136	1134	1204	1208	1213	1211	1266	1268
76	1097	1096	1157	1152	1189	1180	1222	1212	1296	1292	1303	1293	1352	1344
77	1187	1197	1246	1259	1279	1286	1310	1314	1389	1399	1394	1402	1440	1450
78	1277	1288	1337	1352	1370	1379	1398	1403	1483	1494	1486	1497	1527	1541
79	952	947	999	995	1021	1024	1060	1059	1121	1128	1128	1127	1176	1179
80	1064	1064	1116	1114	1144	1142	1179	1172	1254	1252	1257	1249	1306	1296
81	1153	1149	1208	1204	1238	1231	1267	1258	1352	1343	1350	1342	1394	1386
82	845	846	899	897	934	931	979	974	1049	1047	1053	1050	1116	1116
83	914	924	969	976	1000	1006	1037	1045	1122	1116	1113	1117	1171	1176
84	1005	1013	1060	1066	1092	1095	1130	1129	1204	1204	1206	1205	1260	1258
85	1093	1105	1150	1161	1182	1189	1217	1219	1295	1299	1296	1299	1343	1348
86	1183	1194	1241	1253	1273	1280	1303	1306	1390	1391	1387	1391	1434	1436
87	1273	1287	1332	1348	1364	1374	1393	1396	1482	1488	1478	1488	1520	1528
88	954	964	996	1009	1022	1037	1058	1069	1120	1141	1125	1137	1174	1185
89	1060	1063	1112	1112	1139	1140	1167	1168	1253	1247	1249	1244	1294	1288
90	1149	1160	1202	1212	1232	1239	1263	1263	1352	1349	1343	1346	1387	1386

Table 2
The values of the topological indices of the 90 saturated ester molecules that were used in this work

No.	Compounds	OEI	SV*ij*	PEI × χ_{eq}
1	Methyl acetate	3.5000	8	3.1418
2	Ethyl acetate	5.2222	24	3.2159
3	Propyl acetate	6.8194	40	3.2445
4	Butyl acetate	8.4967	56	3.2250
5	Pentyl acetate	10.1183	72	3.2649
6	Hexyl acetate	11.7808	88	3.2689
7	Isopropyl acetate	6.4444	58	3.3036
8	Isobutyl acetate	7.9167	74	3.2810
9	Isopentyl acetate	9.6739	90	3.2762
10	Methyl propionate	5.2222	24	3.2159
11	Ethyl propionate	6.8194	40	3.3036
12	Propyl propionate	8.4967	56	3.3397
13	Butyl propionate	10.1183	72	3.3577
14	Pentyl propionate	11.7808	88	3.3677
15	Hexyl propionate	13.4120	104	3.3737
16	Isopropyl propionate	7.9167	74	3.3984
17	Isobutyl propionate	9.6739	90	3.3807
18	Isopentyl propionate	11.2400	106	3.3789
19	Methyl butyrate	6.8194	40	3.2445
20	Ethyl butyrate	8.4967	56	3.3397
21	Propyl butyrate	10.1183	72	3.3807
22	Butyl butyrate	11.7808	88	3.4019
23	Pentyl butyrate	13.4120	104	3.4141
24	Hexyl butyrate	15.0680	120	3.4217
25	Isopropyl butyrate	9.6739	90	3.4392
26	Isobutyl butyrate	11.2400	106	3.4248
27	Isopentyl butyrate	12.9433	122	3.4253
28	Methyl pentanoate	8.4967	56	3.2579
29	Ethyl pentanoate	10.1183	72	3.3577
30	Propyl pentanoate	11.7808	88	3.4019
31	Butyl pentanoate	13.4120	104	3.4253
32	Pentyl pentanoate	15.0680	120	3.4391
33	Hexyl pentanoate	16.7039	136	3.4480
34	Isopropyl pentanoate	11.2400	106	3.4601
35	Isobutyl pentanoate	12.9433	122	3.4482
36	Isopentyl pentanoate	14.5433	138	3.4503
37	Methyl hexanoate	10.1183	72	3.2649
38	Ethyl hexanoate	11.7808	88	3.3677
39	Propyl hexanoate	13.4120	104	3.4141
40	Butyl hexanoate	15.0680	120	3.4391
41	Pentyl hexanoate	16.7039	136	3.4542
42	Hexyl hexanoate	18.3563	152	3.4640
43	Isopropyl hexanoate	12.9433	122	3.4722
44	Isobutyl hexanoate	14.5433	138	3.4620
45	Isopentyl hexanoate	16.2239	142	3.4654
46	Methyl isobutyrate	6.4444	58	3.3036
47	Ethyl isobutyrate	7.9167	74	3.3984
48	Propyl isobutyrate	9.6739	90	3.4392
49	Butyl isobutyrate	11.2400	106	3.4601
50	Pentyl isobutyrate	12.9433	122	3.4722
51	Hexyl isobutyrate	14.5433	138	3.4797
52	Isopropyl isobutyrate	8.8889	108	3.4976
53	Isobutyl isobutyrate	10.9311	124	3.4831
54	Isopentyl isobutyrate	12.3061	154	3.3698
55	Methyl isopentanoate	7.9167	74	3.2837
56	Ethyl isopentanoate	9.6739	90	3.3807
57	Propyl isopentanoate	11.2400	106	3.4248
58	Butyl isopentanoate	12.9433	122	3.4482
59	Pentyl isopentanoate	14.5433	138	3.4620
60	Hexyl isopentanoate	16.2239	142	3.4708
61	Isopropyl isopentanoate	10.9311	124	3.4831
62	Isobutyl isopentanoate	12.3061	154	3.3575
63	Isopentyl isopentanoate	14.1466	156	3.4732
64	Methyl isohexanoate	9.6739	90	3.2434

Table 2 (*Continued*)

No.	Compounds	OEI	SV*ij*	PEI × χ_{eq}
65	Ethyl isohexanoate	11.2400	106	3.3463
66	Propyl isohexanoate	12.9433	122	3.3927
67	Butyl isohexanoate	14.5433	138	3.4503
68	Pentyl isohexanoate	16.2239	142	3.4654
69	Hexyl isohexanoate	17.8398	170	3.4751
70	Isopropyl isohexanoate	12.3061	154	3.4508
71	Isobutyl isohexanoate	14.1466	156	3.4732
72	Isopentyl isohexanoate	16.1433	172	3.4765
73	Methyl 2-methylpentanoate	9.8161	105	3.3577
74	Ethyl 2-methylpentanoate	11.3128	121	3.4601
75	Propyl 2-methylpentanoate	13.0553	137	3.5063
76	Butyl 2-methylpentanoate	14.6309	163	3.5311
77	Pentyl 2-methylpentanoate	16.3277	169	3.5460
78	Hexyl 2-methylpentanoate	17.9115	185	3.5557
79	Isopropyl 2-methylpentanoate	12.3094	155	3.5644
80	Isobutyl 2-methylpentanoate	14.2977	181	3.5540
81	Isopentyl 2-methylpentanoate	15.7066	187	3.5572
82	Methyl 2-ethylbutyrate	9.9583	120	3.3807
83	Ethyl 2-ethylbutyrate	11.5906	136	3.4831
84	Propyl 2-ethylbutyrate	13.2367	152	3.5292
85	Butyl 2-ethylbutyrate	14.8844	168	3.5540
86	Pentyl 2-ethylbutyrate	16.4452	184	3.5688
87	Hexyl 2-ethylbutyrate	18.0452	200	3.5784
88	Isopropyl 2-ethylbutyrate	12.7228	170	3.5873
89	Isobutyl 2-ethylbutyrate	14.3828	186	3.5768
90	Isopentyl 2-ethylbutyrate	16.0322	202	3.5800

2.2.2. The odd–even index OEI

Odd–even index has been defined for the alkane molecule in our previous paper [20], which reflects the size of the molecule and the connection of each atom. The index is restated briefly as follows:

$$\mathrm{OEI} = \sum_{i=1}^{N}\sum_{j\neq i}^{N}[(-1)^{D_{ij}-1}S] \tag{3}$$

where N is the number of vertices in molecular graph and S is the derivative matrix from distance matrix D. The elements of S are the squares of the reciprocal distances $(D_{ij})^{-2}$, i.e., $S = [1/D_{ij}^2]$ (when $i=j$, let $1/D_{ij}^2 = 0$). Take propyl propionate (Fig. 1) as an example to illustrate the calculation of OEI. Because the ester bonds are common to all molecules studied in this work, it is excluded from the calculation of OEI. We use matrices D to represent D_{ij} of the molecule.

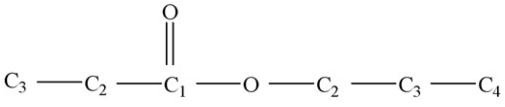

Fig. 1. The hydrogen-suppressed molecular graph of propyl propionate.

$$D = \begin{bmatrix} 0 & 1 & 2 & 3 & 4 & 5 \\ 1 & 0 & 1 & 2 & 3 & 4 \\ 2 & 1 & 0 & 1 & 2 & 3 \\ 3 & 2 & 1 & 0 & 1 & 2 \\ 4 & 3 & 2 & 1 & 0 & 1 \\ 5 & 4 & 3 & 2 & 1 & 0 \end{bmatrix}$$

$$S = \begin{bmatrix} 0 & 1 & 1/4 & 1/9 & 1/16 & 1/25 \\ 1 & 0 & 1 & 1/4 & 1/9 & 1/16 \\ 1/4 & 1 & 0 & 1 & 1/4 & 1/9 \\ 1/9 & 1/4 & 1 & 0 & 1 & 1/4 \\ 1/16 & 1/9 & 1/4 & 1 & 0 & 1 \\ 1/25 & 1/16 & 1/9 & 1/4 & 1 & 0 \end{bmatrix}$$

According to Eq. (3), OEI is computed as follows:

$$\mathrm{OEI} = 1 \times 10 + \left[-\tfrac{1}{4}\right] \times 8 + \left[\tfrac{1}{9}\right] \times 6 + \left[-\tfrac{1}{16}\right] \times 4 + \left[\tfrac{1}{25}\right] \times 2 = 8.4967 \tag{4}$$

Table 3
PEI and ΔPEI values of normal alkyl $H(CH_2)_N$

N_i	PEI	ΔPEI
1	1.0000	1.0000
2	1.1405	0.1405
3	1.1887	0.04813
4	1.2122	0.02350
5	1.2260	0.01380
6	1.2350	0.009052
7	1.2414	0.006388
8	1.2461	0.004748
9	1.2498	0.003666
10	1.2527	0.002916

Table 4
Regression coefficients of the final models for RI based on seven stationary phases

Stationary phase	Constant	OEI	SV_{ij}	PEI × χ_{eq}
SE-30	879.1623 ± 62.9095	62.4952 ± 0.5784	−0.3654 ± 0.0597	−180.7950 ± 19.7132
OV-7	1003.1880 ± 71.5521	66.6275 ± 0.6579	−0.5971 ± 0.0679	−206.3300 ± 22.4214
DC-710	1106.2880 ± 63.7493	66.3712 ± 0.5861	−0.6123 ± 0.0605	−225.7310 ± 19.9764
OV-25	1196.3860 ± 60.0167	65.0259 ± 0.5518	−0.7301 ± 0.0569	−231.4060 ± 18.8067
XE-60	1506.3940 ± 76.8809	67.9642 ± 0.7069	−0.5839 ± 0.0729	−315.3410 ± 24.0913
OV-225	1568.0250 ± 71.5898	69.4442 ± 0.6582	−0.7237 ± 0.0679	−332.1940 ± 22.4333
Silar-5CP	1768.3200 ± 84.5626	69.0985 ± 0.7775	−0.9332 ± 0.0803	−363.4950 ± 26.4984

2.2.3. The steric effect index SV_{ij}

The chromatographic property of esters is influenced by the steric effect, which reflects the bulkiness of the molecule. Here, as our preceding study did [21], a steric effect index SV_{ij} is developed to scale steric effect of ester molecules. We define $SV_{ij} = \sum V_{ij}$ and $V_{ij} = (V_i \times V_j)^2$, V_i and V_j are the vertex degree of vertex i and vertex j in a C_i–C_j bond, respectively. The ester bonds are common to all molecules studied here, so the calculation of SV_{ij} only includes C–C bonds. As for propyl propionate molecule (Fig. 1), there are five carbon–carbon bonds: C_3–C_2, C_2–C_1, C_1–C_2, C_2–C_3 and C_3–C_4. Their V_{ij} are $V_{32} = (1 \times 2)^2 = 4$, $V_{21} = (2 \times 2)^2 = 16$, $V_{12} = (2 \times 2)^2 = 16$, $V_{23} = (2 \times 2)^2 = 16$ and $V_{34} = (2 \times 1)^2 = 4$, respectively. Thus, the $SV_{ij} = \sum V_{ij} = 4 + 16 + 16 + 16 + 4 = 56$.

2.2.4. Molecular electronegativity χ_{eq}

The molecular electronegativity χ_{eq} corresponding to equalization of chemical potentials in a compound is calculated by Bratsch's electronegativity equalization method [24] (harmonic mean, with Pauling electronegativity scale), which characterizes the property of the bond. It is known that the Pauling electronegativities χ_p for H, C and O elements are 2.20, 2.55, 3.44, respectively, thus the molecular electronegativity of the molecule $C_6H_{12}O_2$ (propyl propionate) is

$$\chi_{eq} = \frac{N}{\sum n_i/\chi_P} = \frac{20}{[(6/2.55) + (12/2.20) + (2/3.44)]} = 2.3841 \quad (5)$$

where N is the total atom number of the molecule, and n_i is the number of the ith atom.

2.3. Statistical analysis method

Multiple linear regression is used through the paper to build QSRR models, the intercepts and coefficients of which are reported with their 95% confidence intervals. The goodness of the correlation is examined by the correlation coefficient (R), the F-test (F) and the standard error (s). To verify the validity and stability of the models obtained, the cross-validation test using the "leave-one-out" method is performed. The predictive ability of the model is quantified in terms of the corresponding leave-one-out cross-validated parameters, R_{cv} and s_{cv} values.

3. Results and discussion

3.1. Linear regression models with the topological indices

Multiple linear regression analysis using the novel PEI, OEI, SV_{ij} and χ_{eq} topological indices is performed for the

Table 5
Statistical results of MLR models for RI based on seven stationary phases with topological indices

Stationary phase	Descriptors	R	s	F	R_{cv}	s_{cv}
SE-30	OEI, SV_{ij}, PEI × χ_{eq}	0.9989	8.53	12666	0.9988	8.79
	Lu, DAI(–CH_3), DAI(–O–) [18]	0.9983	10.25	8533	0.9981	10.00
OV-7	OEI, SV_{ij}, PEI × χ_{eq}	0.9986	9.71	10169	0.9984	10.02
	Lu, DAI(–CH_3), DAI(–O–) [18]	0.9982	10.86	7895	0.9980	11.30
DC-710	OEI, SV_{ij}, PEI × χ_{eq}	0.9988	8.65	12433	0.9988	8.89
	Lu, DAI(–CH_3), DAI(–O–) [18]	0.9979	11.56	6795	0.9977	12.10
OV-25	OEI, SV_{ij}, PEI × χ_{eq}	0.9989	8.14	12673	0.9988	8.33
	Lu, DAI(–CH_3), DAI(–O–) [18]	0.9972	12.66	5111	0.9970	12.80
XE-60	OEI, SV_{ij}, PEI × χ_{eq}	0.9983	10.43	8564	0.9981	10.73
	Lu, DAI(–CH_3), DAI(O), DAI(–O–) [18]	0.9962	15.65	2717	0.9957	16.10
OV-225	OEI, SV_{ij}, PEI × χ_{eq}	0.9985	9.71	9754	0.9984	9.93
	Lu, DAI(–CH_3), DAI(O), DAI(–O–) [18]	0.9951	17.25	2191	0.9945	18.30
Silar-5CP	OEI, SV_{ij}, PEI × χ_{eq}	0.9977	11.47	6222	0.9975	11.68
	Lu, DAI(–CH_3), DAI(O), DAI(–O–) [18]	0.9940	18.26	1784	0.9932	19.30

Table 6
The relative and fraction contribution (Ψ_r and Ψ_f)of individual topological index to RI based on seven stationary phases

Stationary phase	OEI (Ψ_r and Ψ_f)	SV_{ij} (Ψ_r and Ψ_f)	PEI × χ_{eq} (Ψ_r and Ψ_f)
SE-30	750.08 (53.1)	−41.54 (2.9)	−617.22 (43.7)
OV-7	799.68 (50.7)	−67.86 (4.3)	−704.39 (44.7)
DC-710	796.60 (48.6)	−69.59 (4.2)	−770.63 (46.9)
OV-25	780.46 (47.1)	−82.98 (5.0)	−790.00 (47.7)
XE-60	815.72 (41.5)	−66.36 (3.4)	−1076.55 (54.8)
OV-225	833.48 (40.5)	−82.26 (4.0)	−1134.09 (55.2)
Silar-5CP	829.34 (37.9)	−106.07 (4.8)	−1240.95 (56.8)

Values in parentheses are in percent.

development of the final three-parameters QSRR models. The descriptors that appear in the best MLR equations for all stationary phases are identical. The final model is obtained in the form of Eq. (6).

$$RI = a_0 + a_1 OEI + a_2 SV_{ij} + a_3 PEI \times \chi_{eq} \quad (6)$$

where a_0 is a constant, a_1, a_2, a_3 is the contribution coefficient of the OEI, SV_{ij} and PEI × χ_{eq} index, respectively. Each coefficient describes the sensitivity of a stationary phase to each of the individual index, so the coefficient of these parameters would reflect the relative importance of each index. The regression coefficients of the final models are shown in Table 4, and the statistical results for the final models are listed in Table 5.

In all cases, the correlation coefficient R is larger than 0.9977, especially for stationary phases SE-30, DC-710 and OV-25, excellent correlations are obtained ($R \geq 0.9988$). According to the statement of Mihalic and Trinajstic [25], the models we have constructed represent excellent QSRR models judging from the statistics.

Cross-correlation analysis shows that the indices in the model are not highly correlated with each other (the pair-wise correlation coefficients $R \leq 0.88$). Furthermore, in all cases, the cross-validated R_{cv} values ($R_{cv} \geq 0.9975$) are very close to the corresponding R values and the cross-validated s_{cv} values ($s_{cv} \leq 11.7$) are only slightly larger than the corresponding s values. Clearly, the cross-validation demonstrates the final models to be statistically significant. The MLR models are also compared with a recent work obtained in terms of the topological descriptors for the same compounds [18]. The results are summarized in Table 5. It can be seen in Table 5 that the combination of the present indices produces better correlations than the Lu index for all the columns, especially for the medium–high polar stationary phases. The significant improvement of 10.1–43.7% in average error relative to the linear models with the Lu index over seven phases evidently demonstrates the efficiency of the present novel indices in structure-retention correlations.

3.2. Structural interpretation of retention indices

By the interpreting of the descriptors in the linear model, it is possible to gain some insight into factors that are likely to govern the chromatographic retention of saturated ester compounds on different stationary phases. As is well known, the chromatographic retention is based on the interaction between the solute and the stationary phase, which include directional force, induction force, dispersion force, hydrogen bond and so on.

In order to obtain insights into the molecular mechanism of interactions between eluents and stationary phases, the relative importance of structural features in molecules is analyzed from the relative contributions (Ψ_r) or fraction contributions (Ψ_f) of the corresponding topological indices to RI [26]:

$$\Psi_r(i) = \alpha_i \bar{T} I_i \quad (7)$$

$$\psi_f(i) = \frac{R^2 |\psi_r(i)|}{\sum_i |\psi_r(i)|} \times 100\% \quad (8)$$

where α_i and $\bar{T} I_i$ are the coefficient and the average value of the ith topological index in the model and R is the coefficient of determination of the model. The sum is over all indices in the model. The results for above seven models are shown in Table 6.

It can be observed in Table 6 that the retention of saturated ester is primarily influenced by size, steric factors and polar effects of the molecule. Contributions of individual index to the seven stationary phases cover a wide range of values dependent on the polarity of the columns.

In general, the OEI index makes a major contribution to RI, and the range of Ψ_f values is within 37.9–53.1%. Because the OEI index characterizes the information of molecular branching and size, the results indicate that the position of the substituent and size of a probe molecule play a leading role in determining Kováts retention indices of saturated esters on all columns with different polarities. That is, the larger the size of a molecule is, the greater the RI value is. It should be noted that the relative importance of the molecular property coded by the OEI index to retention become more and more weak with the increasing polarity of the stationary phase molecules.

The other significant factor for the retention of the saturated ester is the PEI × χ_{eq} index, and the range of Ψ_f values is within 43.7–56.8%. According to the electronegativity equalization method [24], the charge q_e on the ester bond is proprtional to the molecular electronegativity χ_{eq}. In fact, the item PEI × χ_{eq} scales the inductive dipole between the charge q_e on the ester bond and the polarizability effect PEI of alkyl groups. The larger the PEI × χ_{eq} is, the lager the intramolecular inductive dipole is, and the less the molecular polar is. Thus, for the same stationary phase, the increase of PEI × χ_{eq} will decrease the RI value of saturated esters. On the contrary, theΨ_f values for this index steadily increase, with the increasing polarity of the columns.

On the other hand, the SV_{ij} index characterizing the bulkiness of the molecule has smaller contribution to RI on different polar columns. The Ψ_f values for individual SV_{ij} index are 2.9–5.0%. Obviously, branching prevents eluents from close contact with stationary phases in space and reduces the interactions between eluents and columns. The descriptor shows the negative effect on the retention indices, consequently, RI of eluents decrease. For example, the RI on the OV-7 column decreases in the order: pentyl pentanoate (1222) > isopentyl pentanoate (1185) > isopentyl isopentanoate (1136).

From the above discussion, it can be seen that the intramolecular inductive dipole and the molecular size are likely two major factors controlling the retention behavior of saturated ester compounds on different stationary phase. All the descriptors involved in the model, which have explicit physical meaning, may account for the structural features responsible for the retention behaviors of these compounds.

4. Conclusion

Based on novel topological indices, quantitative structural-retention relationship models were built to study the retention behaviors of 90 saturated esters for seven GC columns by the MLR method. The cross-validation using the general leave-one-out method demonstrated the final models to be statistically significant and reliable.

This paper provided a simple and straightforward way to predict the retention indices of saturated esters from their structures and gave some insight into structural features related to the retention of the compounds. This study also showed that the utility of the QSPR treatment involving descriptors derived solely from chemical structure and the correlation equation can be used for the prediction of the retention indices for similar compounds in cases where retention values were not readily available. Furthermore, the proposed approach can also be expected to extend in other QSRR/QSAR investigation in the future.

Acknowledgements

The project is supported by the Natural Science Foundation of Hunan Province No. 06JJ2002 (NSFH) and the Scientific Research Fund Provincial Education Department No. 04A015 (HPED).

References

[1] R. Kaliszan, J. Chromatogr. A 656 (1993) 417.
[2] R. Kaliszan, Quantitative Structure-Chromatographic Retention Relationships, Wiley-Interscience, New York, 1987.
[3] Y. Wang, X. Zhang, X. Yao, Y. Gao, M. Liu, Z. Hu, B. Fan, Anal. Chim. Acta 463 (2002) 89.
[4] B.G.M. Vandeginste, D.L. Massart, L.C.M. Buydens, S. De Jong, J. Smeyers-Verbeke, Handbook of Chemometrics and Qualimetrics: Part B, Elsevier, Amsterdam, 1998.
[5] R. Kramer, Chemometric Techniques for Quantitative Analysis, Marcel Dekker, New York, 1998.
[6] S. Wold, M. Sjöström, L. Eriksson, P. Schleyer, N.L. Allinger, T. Clark, J. Gasteiger, P.A. Kollman, H.F. Schaefer III, P.R. Schreiner (Eds.), The Encyclopedia of Computational Chemistry, Wiley, Chichester, 1998.
[7] R. Kaliszan, CRC Crit. Rev., Anal. Chem. 16 (1986) 323.
[8] R. Hu, H. Liu, R. Zhang, C. Xue, X. Yao, M. Liu, Z. Hu, B. Fan, Talanta 68 (2005) 31.
[9] Y. Song, J. Zhou, S. Zi, J. Xie, Y. Ye, Bioorg. Med. Chem. 13 (2005) 3169.
[10] Z. Zhai, Z. Wang, L. Wang, J. Mol. Struct. (Theochem.) 724 (2005) 115.
[11] J.A. Martínez, J.C. Escalona-Arranz, A. Villar-Rojas, F. Téllez-Palmero, R. Pérez-Rosés, L. González, R. Carrasco-Velar, J. Chromatogr. A 1102 (2006) 238.
[12] P. Tulasamma, K.S. Reddy, J. Mol. Graphics Modell. 25 (2006) 507.
[13] Ya. Wang, A. Li, H. Liu, Q. Zhang, W. Ma, W. Song, G. Jiang, J. Chromatogr. A 1103 (2006) 314.
[14] O. Ivanciuc, T. Ivanciuc, A.T. Balaban, Tetrahedron 54 (1998) 9129.
[15] N. Guevara, F. Graph, J. Mol. Struct. (Theochem.) 493 (1999) 29.
[16] M. Pompe, M. Novic, J. Chem. Inf. Comput. Sci. 39 (1999) 59.
[17] B.S. Junkes, R.D.M.C. Amboni, R.A. Yunes, V.E.F. Heinzen, Anal. Chim. Acta 477 (2003) 29.
[18] C. Lu, W. Guo, C. Yin, Anal. Chim. Acta 561 (2006) 96.
[19] C. Cao, Z. Li, J. Chem. Inf. Comput. Sci. 38 (1998) 1.
[20] C. Cao, H. Yuan, J. Chem. Inf. Comput. Sci. 41 (2001) 867.
[21] C. Cao, L. Jiang, H. Yuan, Internet Electron. J. Mol. Des. 3 (2004) 150, http://www.biochempress.com/.
[22] J.R. Ashes, J.K. Haken, J. Chromatogr. 101 (1974) 103.
[23] H. Kabinyi, in: R. Mannhold, P. Krogs Gaad-Larsen, H. Timmerman (Eds.), QSAR: Hansch Analysis and Related Approaches, VCH, Weinheim, 1993.
[24] S.G. Bratsch, J. Chem. Educ. 61 (1984) 588.
[25] M. Mihalic, N. Trinajstic, J. Chem. Educ. 69 (1992) 701.
[26] D.E. Needham, I.C. Wei, P.G. Seybold, J. Am. Chem. Soc. 110 (1988) 4186.

Available online at www.sciencedirect.com
ScienceDirect
Talanta 72 (2007) 1458–1468
Talanta
www.elsevier.com/locate/talanta

UV–visible spectroscopic and electrochemical study of the complex formation between Fe(II) and 5-amino-1,10-phenantroline (5-Aphen) in aqueous solution

María Luisa Lozano-Camargo [a], Alberto Rojas-Hernández [a,*], Martín Gómez-Hernández [b], Ma de Lourdes Pacheco-Hernández [a], Laura Galicia [a], María Teresa Ramírez-Silva [a]

[a] *Universidad Autónoma Metropolitana-Iztapalapa, Departamento de Química, Apartado Postal 55-534, 09340 México, D.F., México*
[b] *Universidad Autónoma Metropolitana-Xochimilco, Departamento de Sistemas Biológicos, Calzada del Hueso 1100, Col. Villa Quietud, Coyoacán, 04960 México, D.F., México*

Received 5 January 2007; accepted 24 January 2007
Available online 12 February 2007

Abstract

The system Fe(II)–5-Aphen–H_2O was studied. The spectroscopic and electrochemical results show that only one stable complex between Fe(II) and 5-Aphen forms, having a 1:3 stoichiometric ratio. The spectrophotometry study allowed determination of the formation constant of the complex ($\log \beta_3 = 23.42 \pm 0.06$). Also, the stability of the complex was evaluated as a function of pH; it was found that it decomposed at low pH values depending on the concentration and a pseudo-first order kinetics constant associated with $k' = 0.011\ \text{min}^{-1}$. The results are in agreement with the electrochemical behaviour observed in the system, which indicated that at pH 1.33 the destruction of the complex $[Fe(5\text{-Aphen})3]^{2+}$ took place as a function of time; however, when the experiments were carried out at pH 6.19 the complex was stable. The thermodynamic data obtained through the use of MEDUSA allowed construction of predominance zone diagrams of the system Fe(II)–5-Aphen–H_2O under the experimental conditions used. The thermodynamic results represented in the PZD describe the experimental behaviour reported in this work.

Keywords: Equilibrium constant; SQUAD; 5-Amino-1,10-phenantroline; Fe(II)

1. Introduction

Nowadays, the field of research of potentiometric and amperometric sensors is growing. The need to monitor substances in order to establish reliable pollution control processes, has oriented research to develop new materials. This is the case of detection and destruction, by means of some metal complexes, of toxic gases like nitrogen, sulphur and carbon oxides (NO_x, SO_x, CO and CO_2) [1–6]. Some of these complexes have 5-amino-1,10-phenantroline (5-Aphen) as ligand, because it may act a bidentade ligand with metal ions like Mn(II), Fe(II), Co(II), Ni(II), Cu(II), Zn(II), Ru(II) and Os(II) [1,2,7].

The system Fe(II)/5-Aphen has been studied also as electrocatalyst and as sensor, the latter because it is capable of electropolimerizing [8,9], and because of the possibility to build in metal complexes in the electrode sensor for monitoring species on a continuous flow.

In future, we want to synthesize and electropolimerize the possible Fe(II)/5-Aphen complexes in aqueous media, where pH control is likely to be crucial. To the best of our knowledge there is no precise information on the formation constants of these species [10]. Then, the goal of the present work is to characterize the kinetic and thermodynamic behaviour of these complexes in solution, by spectrophotometric and electrochemical methods.

2. Materials and methods

2.1. Reagents and aqueous solutions

The 5-Aphen and Fe(II) aqueous solutions were prepared from 5-Aphen (Polysciences Inc.) and from $FeSO_4 \cdot 7H_2O$ (100%, J.T. Baker), with deionized water Type I (18 MΩ), CO_2-

* Corresponding author. Tel.: +52 55 58044670; fax: +52 55 58044666.
E-mail address: suemi918@xanum.uam.mx (A. Rojas-Hernández).

0039-9140/$ – see front matter © 2007 Elsevier B.V. All rights reserved.
doi:10.1016/j.talanta.2007.01.065

free and saturated with nitrogen at a pH near 6.0. pH changes were made with HCl (37%, Merck) or NaOH (99%, Merck) aqueous solutions.

2.2. pH measurements

pH measurements were obtained with a Tacussel potentiometer LPH430T, ΔpH 0.001, equipped with a combined pH electrode. The temperature was controlled with a Cole Parmer bath at $(25.0 \pm 0.1)\,^{\circ}C$. An inert atmosphere (nitrogen) was maintained during the experiments in order to avoid the possibility of Fe(II) oxidation.

2.3. Spectrophotometric measurements

The spectra for all solutions were obtained with a Lambda 20 Perkin Elmer spectrophotometer with quartz cells of pathlength of 1.0 cm in the 200–600 nm wavelength range at a 240 nm/min sweep rate.

2.4. Electrochemistry measurements

The electrochemical studies were carried out using a BAS-100 W potentiostat, coupled to the typical three-electrode cell, with the carbon paste electrode, CPE, as working electrode, a graphite rod as counter electrode and a Radiometer saturated mercury sulphate as reference, SSE. The CPE was prepared mixing 99.99% single crystal graphite powder from Alfa Aesar and nujol Fluka in 1:1 proportion to ensure easy manipulation. All potentials herein reported are referred to the SSE. The voltammogram studies were conducted using 7.5×10^{-4} M 5-Aphen and 2.5×10^{-4} M for Fe(II) in 0.5 M of H_2SO_4.

2.5. Kinetic studies

An aqueous solution of final concentrations of 7.5×10^{-5} M for 5-Aphen and 2.5×10^{-5} M for Fe(II). Absorption spectra of the red solution acidified to pH 0.291 with HCl were obtained with the spectrophotometer as a function of time during 7 h.

2.6. Stoichiometry of the Fe(II)/5-Aphen′ complex

Several solutions were obtained by mixing the former systems in such a way that final concentration of Fe(II) were 2.5×10^{-5} and 2.5×10^{-4} M, both for variable final concentrations of 5-Aphen covering the 0–5 [5-Aphen]/[Fe(II)] ratio range, and acidulating the system to pH 1.1 with HCl. One absorption spectrum was obtained with a spectrophotometer for each final system 5 min after its preparation.

2.7. Formation constant of the Fe(II)/5-Aphen complex

An aqueous solution was prepared having 5-Aphen 7.5×10^{-5} M and Fe(II) 2.5×10^{-5} M final concentrations. The pH of several portions of this solution was changed in the $0.2 < pH < 8.4$ range, either with HCl or NaOH as suitable. The solutions thus prepared were left to rest at least for 24 h in plastic beakers hermetically closed; after this, the final pH of each solution was measured. Absorption spectra were acquired at 24 and 240 h for each solution. The experimental data were analyzed with the aid of TRIANG [11] and SQUAD [12,13] data processing software.

3. Dissociation kinetics of the Fe(II)/5-Aphen complex

3.1. Spectrophotometric study

It was observed that the Fe(II) and 5-Aphen mixture in a very acid medium at pH 0.291 does not give the formation of Fe(II)/5-Aphen complexes, because the solution shows the same aspect than the aqueous solutions with 5-Aphen alone. Nevertheless, a NaOH basification of the solution to pH values greater than 2.0, produces a red color.

On the other hand, if Fe(II) and 5-Aphen are mixed in water at $pH \approx 6.0$, suddenly an intense red color appears. Then if HCl is added the red color remains for some time, even at pH values near 0.1. Presently, these experiments revealed a difference indicating that the species formed at neutral pH decompose slowly at acid pH values, due to competition of Fe^{2+} and H^+ to react with the 5-Aphen's nitrogen atoms. Fig. 1a shows the initial absorption spectrum of the Fe(II)/5-Aphen′ aqueous system

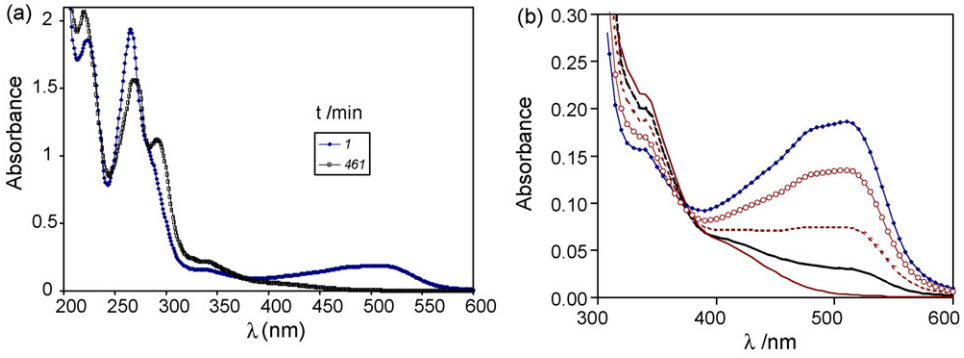

Fig. 1. Absorption spectra as a function of time for the Fe(II)/5-Aphen system, formed at $pH \approx 6.0$ and acidulated at pH 0.291. (a) Initial and final absorption spectra in the 200–600 nm wavelength range. (b) Disappearance of the absorption band of the complex in the 380–600 nm wavelength range during 461 min.

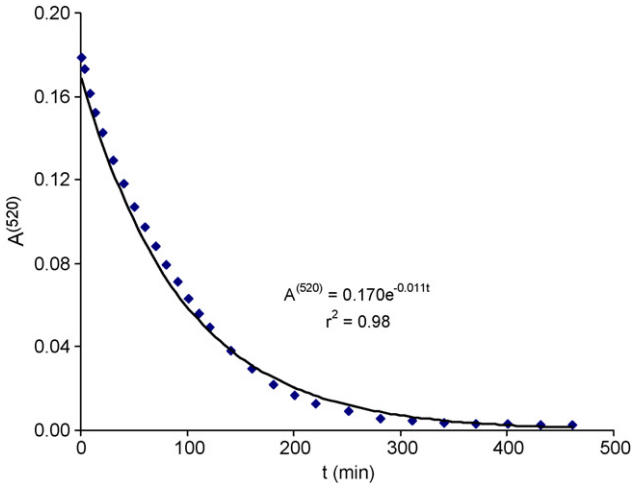

Fig. 2. Absorbance measured at a wavelength of 520 nm as a function of time for the Fe(II)/5-Aphen system, formed at pH ≈ 6.0 and acidulated at pH 0.291. The chemical kinetics of the system may be fitted to a pseudo-first order model for the irreversible dissociation of only one complex.

at pH 0.291 acquired after 461 min from the beginning of the experiment, and Fig. 1b presents the evolution of the absorption spectrum of the same system with time. As can be seen in the former figure, the shape of the absorption spectrum at 461 min is very similar to that of (5-Aphen)H_2^{2+} species [14]. On the other hand, Fig. 1b indicates that the absorbance at 520 nm diminishes with time but it increases at 340 nm, forming a time-independent isosbestic point at 375 nm. This behaviour may be due to an overall dissociation of a single complex at this pH value.

Fig. 2 shows the absorbance behaviour of the system at 520 nm as a function of time, where the absorbance decays exponentially with time. This is consistent with the hypothesis that there is only one complex that dissociates to Fe′(II) and (5-Aphen)H_2^{2+} species.

Then, if an irreversible dissociation of pseudo-first order [15] is considered for a Fe(5-Aphen)$_n$ complex, in agreement with Eq. (1):

$$\text{Fe(5-Aphen)}'_n \rightarrow \text{Fe}'(\text{II}) + n(\text{5-Aphen}') \quad (1)$$

it can be shown that the concentration of the complex will decay as predicted by Eq. (2):

$$[\text{Fe(5-Aphen)}'_n] = [\text{Fe(5-Aphen)}'_n]_o \, e^{-k't} \quad (2)$$

where k' is the apparent rate constant at pH 0.291 and t the elapsed time in minutes.

For a 520 nm wavelength, where only the complex can absorb electromagnetic radiation, an equation similar to Eq. (2) may be deduced, but with absorbance values at this wavelength ($A^{(520)}$) instead of [Fe(5-Aphen)′$_n$].

The regression analysis gave $k' = 0.011\ \text{min}^{-1}$ at pH 0.291, with an acceptable correlation coefficient of 0.98. If it is considered a kinetic model with a pseudo-second order model the fit is not as good.

3.2. Electrochemical study

3.2.1. Stability study of the complex at pH 1.33

In order to corroborate the pH effect on the stability of the Fe(II)/5-Aphen and because only one species exists associated to the red color, as observed in the spectrophotometry study, it seemed adequate to perform an electrochemical study. Therefore, a triangular sweeping voltammetry study was carried out at pH 1.33 at a 0.1 V s^{-1} potential scan rate to assess the stability of the Fe(II)–5-Aphen as a function of time. The potential program applied was initiated at the null current potential sweeping in the anodic sense within the 0.1–0.8 V/SSE potential range.

Fig. 3a shows the voltammograms obtained on a carbon paste electrode in H_2SO_4 0.5 M at pH 1.33 for the Fe(II) 2.5×10^{-4} M and 5-Aphen 7.5×10^{-4} M. The Fe(II) system corresponding to the continuous thick line exhibits an oxidation process at 515 mV, associated to the Fe(II) to Fe(III) step: in this system the solution was colorless. Also in Fig. 3a, the continuous thin line represents the electrochemical behaviour of the ligand 5-Aphen that displayed two clearly defined oxidation peaks at 481 and 650 mV, and a colorless solution as well.

When the Fe(II) was mixed with the 5-Aphen, the resulting voltammogram is shown in Fig. 3b where at $t = 0$, depicted by the broken line, there appeared three oxidation processes and the solution became reddish. However, with elapsing time the overall shape was lost and after 72 h, the resulting voltammogram is shown in Fig. 3b depicted by the dot-line trace, also with a colorless solution. Fig. 3c compares the mix Fe/5-Aphen at 72 h and the 5-Aphen alone, which gives evidence that the complex has dissociated thus returning to the unmixed 5-Aphen profile. The current increase observed in the voltammogram of the complex at 72 h is due to the free Fe(II) contribution in solution which oxidizes in the same potential range. When the dissociation of the complex is followed as a function of time, as shown in Fig. 3d, a significant current decrease is noted during the first few minutes and as time elapses further, changes set in due to contribution from processes of the Fe(II) and 5-Aphen that are left free. Therefore, with these data, it is not possible to obtain the dissociation kinetics of the complex at pH 1.33 because several processes exist associated within the electrochemical response obtained, however, the complex's signal can be clearly seen to disappear. This study provided experimental that evidence the Fe(II)–5-Aphen complex is not stable under the pH conditions chosen, and that only one species is formed upon mixing the solutions.

3.2.2. Stability study of the complex at pH 6.19

Fig. 4a shows the voltammograms corresponding (*) to the Fe(II) in solution at pH 6.19. In this case, the oxidation peak appeared at 515 mV. The voltammogram (Δ) shows the 5-Aphen pH 6.19 aqueous solution. Two oxidation peaks were observed at 338 and 538 mV.

The (♦) plot in Fig. 4b depicts the electrochemical response behaviour of the Fe(II)–5-Aphen fresh mix solution at time 0 h, showing also an irreversible oxidation peak at 455 mV. The same voltammetric response is observed for the 72 h stabilized solution (◯), the oxidation peak was shifted 14 mV in the cathodic

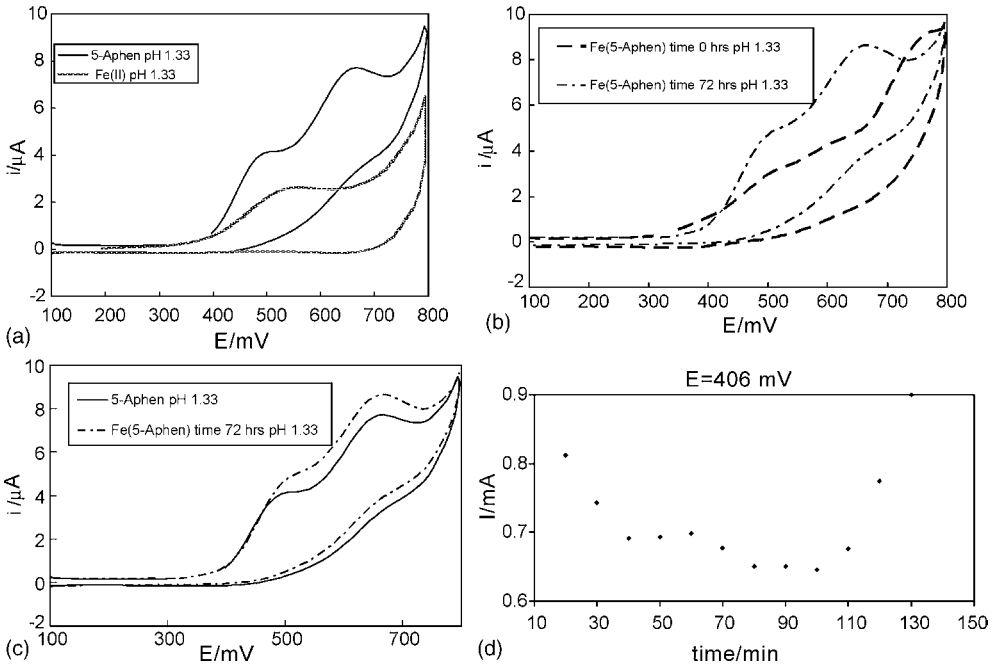

Fig. 3. Typical cyclic voltammograms obtained in 0.5 M H_2SO_4 at pH 1.33. (a) 2.5×10^{-4} Fe(II) M and 7.5×10^{-4} M 5-Aphen separate solution. (b) 2.5×10^{-4} M Fe(II) and 7.5×10^{-4} M 5-Aphen mix; solution time 0 and 72 h. (c) 7.5×10^{-4} M 5-Aphen and complex Fe(5-Aphen), time 72 h. (d) Behaviour of $I = f(t)$ for complex at $E = 406$ mV.

sense with respect to the fresh solution. The results show that the Fe(II)–5-Aphen complex formation is stable in the experimental conditions used for the study, pH 6.19, because the oxidation peaks obtained for the fresh solution after 72 h stabilization were not modified with time.

When comparing the electrochemical response of the Fe(II) and the Fe(II)–5-Aphen complex, as shown in Fig. 4c, a 60 mV shift toward cathodic potentials can be noted of the complex's oxidation peak, which confirms its presence in the solution. Further, the comparison of the Fe(II)–5-Aphen response with that of the 5-Aphen alone, shown in Fig. 4d, shows that a 119 mV potential difference can be noted between the complex oxidation peak and the 5-Aphen's peak at 338 mV at pH 6.19. The results obtained at this pH confirm the formation of the Fe(II)–5-Aphen complex and that it was stable.

3.2.3. Comparison of the electrochemical behaviour at pH 1.33 and 6.19

In order to analyze the changes exhibited during the electrochemical studies of the Fe^{2+} and 5-Aphen species at the different

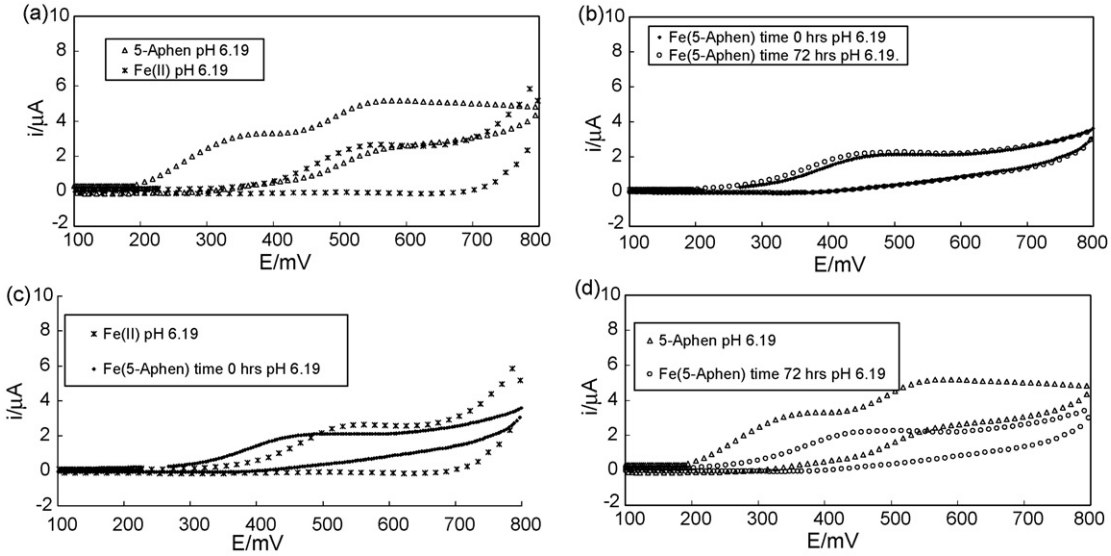

Fig. 4. Typical cyclic voltammograms obtained at pH 6.19. (a) 2.5×10^{-4} M Fe(II) and 7.5×10^{-4} M 5-Aphen separate solution. (b) 2.5×10^{-4} M Fe(II) and 7.5×10^{-4} M 5-Aphen mix solution; time 0 and 72 h. (c) 2.5×10^{-4} M Fe(II) and 2.5×10^{-4} M Fe(II) and 7.5×10^{-4} M 5-Aphen mix solution; time 0. (d) 7.5×10^{-4} M 5-Aphen and complex Fe(5-Aphen); time 72 h.

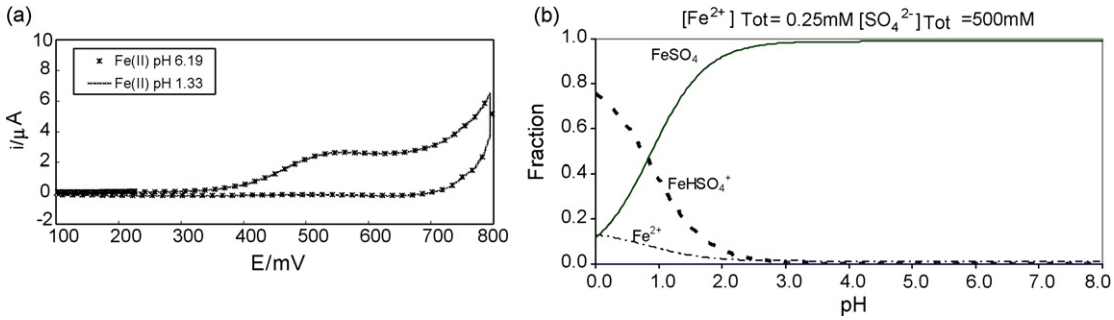

Fig. 5. (a) Typical cyclic voltammograms obtained at pH 1.33, 6.19 and [Fe(II)] = 2.5×10^{-4} M. (b) Molar fractions diagram for the Fe(II) species.

pH values used, a chemical speciation analysis was performed under the different conditions employed.

The Fe(II) oxidation behaviour at pH 1.33 and 6.19 was the same, as shown in Fig. 5a, which is because at both conditions the Fe(II) predominant chemical species is the same as that indicated by the distribution diagram shown in Fig. 5b, where the species at both pH values was Fe(SO_4) at [SO_4] 500 mM.

Fig. 6a shows the results concerning the 5-Aphen's behaviour, which shows that the change in the electrochemical response is due to the pH value, because the molar fractions of the species present at pH 1.33 was 0.68 for 5-Aphen H^+ and 0.32 for 5-Aphen H_2^{2+}, and at pH 6.19 it was 0.725 for 5-Aphen and 0.225 for 5-Aphen H^+, which is clearly appreciable in the molar fractions diagram for the 5-Aphen in Fig. 6b. Fig. 6c shows that the pH effect on the 5-Aphen makes the difference in the electrochemical response of the complex formed at the different pH values studied.

Voltammetric studies confirm that the Fe(II)–5-Aphen complex is the same one in both values of pH studied.

4. Thermodynamics of the formation of the complex between Fe(II) and (5-Aphen)

4.1. Molar ratio method and stoichiometry of the complex [16,17]

The knowledge of the kinetic behaviour of the system permitted to design suitable experiments to undertake the thermodynamic studies, because it was possible to obtain systems in thermodynamic equilibrium. Nevertheless, the stoichiometric ratio of the complex was investigated first by means of the molar ratio method [16,17].

Fig. 7 shows the evolution of absorption spectra with the molar ratio of 5-Aphen to Fe(II) at pH 1.1 5 min after preparation of each system. It is remarkable that the shape of these spectra is very similar to the initial absorption spectrum shown in Fig. 1a. This fact indicates that the same complex is forming at all the pH values studied. The latter is corroborated through the electrochemical studies.

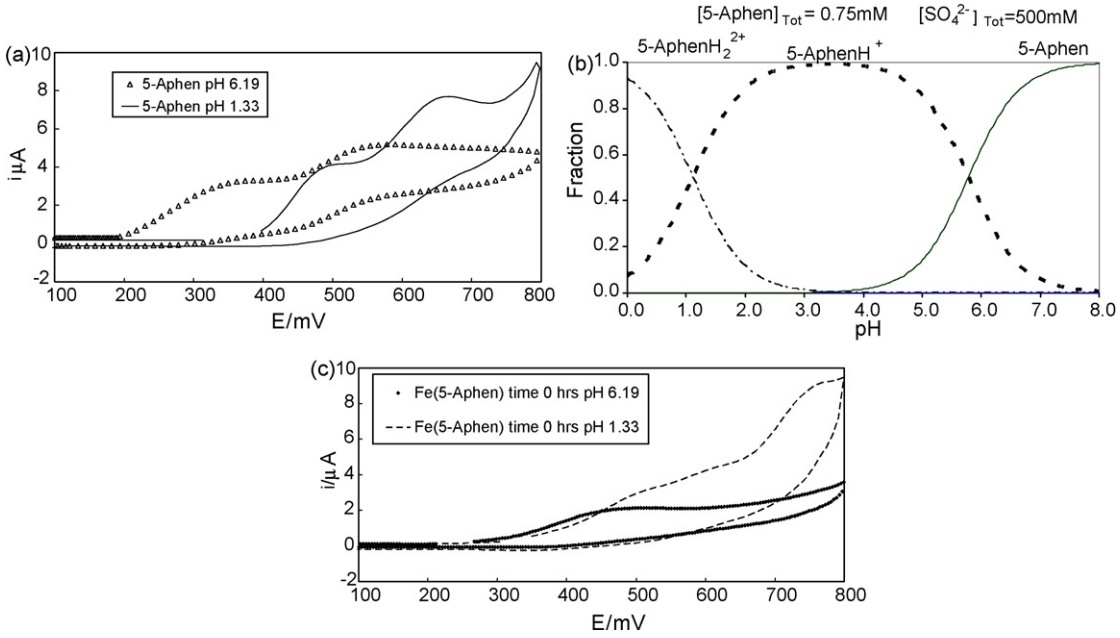

Fig. 6. (a) Typical cyclic voltammograms obtained at pH 1.33 and 6.19 for 7.5×10^{-4} M 5-Aphen. (b) Molar fraction diagram for 5-Aphen′ species. (c) Typical cyclic voltammograms obtained at pH 1.33 and 6.19 for 2.5×10^{-4} M Fe(II) and 7.5×10^{-4} M 5-Aphen mix solution at time 0.

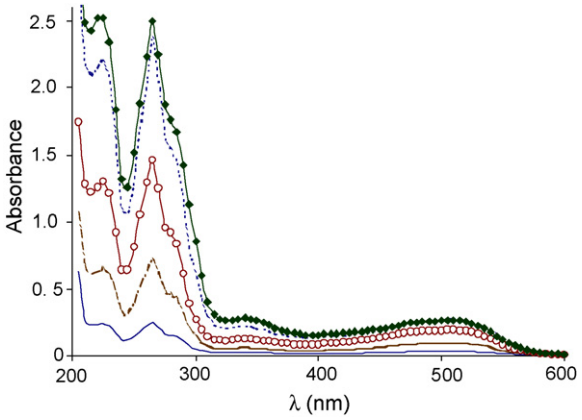

Fig. 7. Evolution of absorption spectra of different systems with [5-Aphen′]/[Fe(II)] molar ratio at pH 1.1 [is this value correct, because 1.33 has been mostly cited] and 5 min after preparation of each system. For all systems, the molar concentration of Fe(II) was equal to 2.5×10^{-5} M and the [5-Aphen′]/[Fe(II)] molar ratios shown are: (—) 0.25, (–·–·–) 0.75, (—o—) 1.50, (– – – –) 2.5, (—◆—) 3.0.

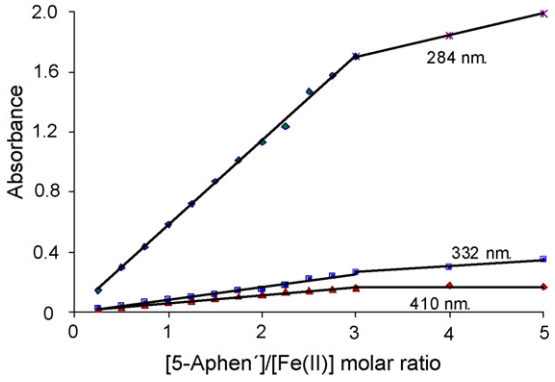

Fig. 8. Plot of the absorbance as a function of [5-Aphen′]/[Fe(II)] molar ratio for several wavelength values. The Fe(II) molar concentration was equal to 2.5×10^{-5} M, the pH 1.1. The data were recorded 5 min after preparation of each system.

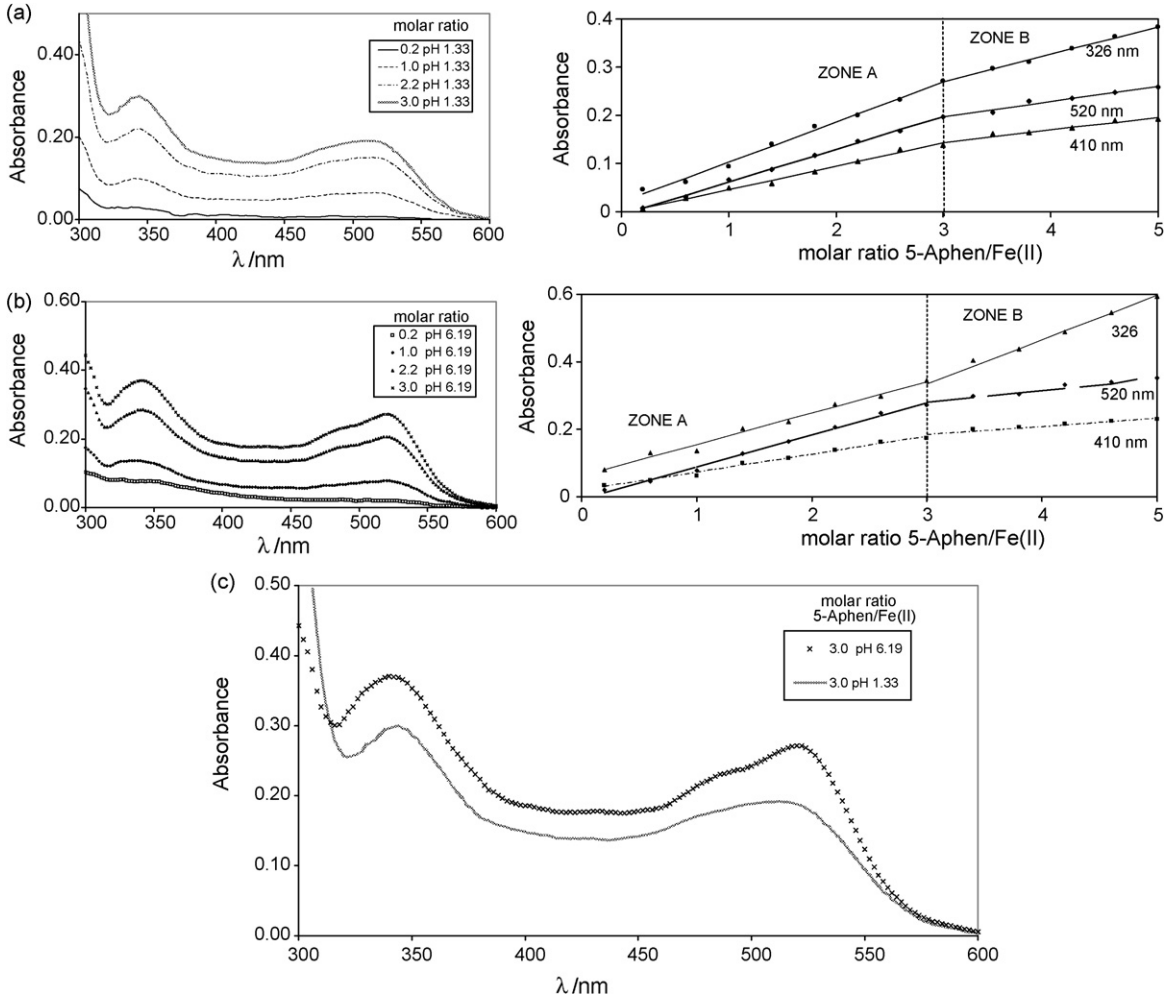

Fig. 9. Absorbance spectra and molar relations plot for 5-Aphen/Fe(II). (a) pH 1.33, (b) 6.19, and (c) comparison of the absorbance spectra at a molar relation of 3 at pH 1.33 and 6.19.

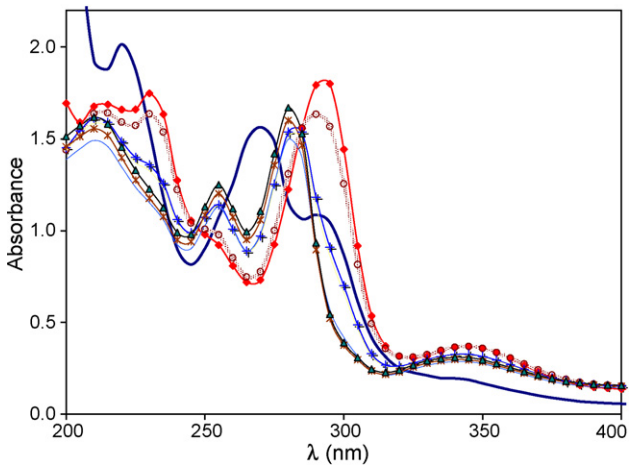

Fig. 10. Absorption spectra for the Fe(II)/5-Aphen systems (UV region), at different pH values: (▬) 0.29, (◆) 1.64, (▬▪▬▪▬) 2.20, (●) 2.89, (▬) 3.93, (✳) 5.39, and (▲) 6.31. The Fe(II) concentration was 2.5×10^{-5} M and the 5-Aphen concentration was 7.5×10^{-5} M in all the systems.

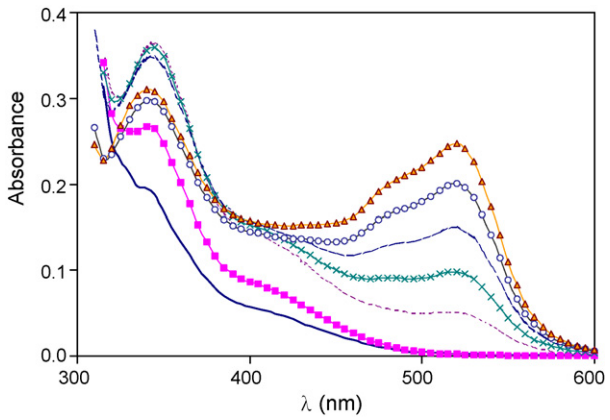

Fig. 11. Absorption spectra for the Fe(II)/5-Aphen systems (near UV and visible regions), at different pH values: (▬) 0.29, (■) 0.61, (▬ ▬ ▬) 2.06, (✕) 2.38, (▬ ▬ ▬) 2.72, (○) 3.41 and (△) 6.31. The Fe(II) concentration was 2.5×10^{-5} M and the 5-Aphen′ concentration was 7.5×10^{-5} M in all the systems.

Fig. 8 shows the functional relationship between absorbance and the [5-Aphen′]/[Fe(II)] molar ratio. For all the wavelengths studied, the curves obtained are practically formed by two straight lines with an intersection point at a [5-Aphen′]/[Fe(II)] molar ratio of 3. This fact indicates that the formulae of the only complex formed is Fe(5-Aphen)$_3$′. Although the degree of protonation is yet unknown, it is very probable that the complex is not protonated nor hydroxilated, like is the case of a similar complex formed between Fe(II) and 1,10-phenantroline (*o*-phen) [10].

Given the low absorbance values at 520 nm wavelength where the complex absorbs, it became necessary to prepare more concentrated solutions, namely 10 times, as compared to the previous experiments with Fe(II) 2.5×10^{-4} M and 5-Aphen 7.5×10^{-4} M; under these conditions the absorption spectra were obtained for different molar ratios, considering only the 300–600 nm range to focus on the complex's behaviour. The inset in Fig. 9a shows the absorption spectra obtained for the mix at pH 1.33 at different 5-Aphen/Fe(II) molar ratios. An increment is noted in the absorbance band at 520 nm that is associated to complex formation, while in Fig. 9a the slope changes for a relation of 1:3 of the complex. A slight increment was also observed at ratios greater than 3 that may be due to the complex's dissociation effect at this pH value or to a small contribution of 5-Aphen species to the absorbance. The inset in Fig. 9b shows the absorption spectra obtained at pH 6.19, where the absorbance values shown for the complex were greater for the different molar ratios. Nevertheless, Fig. 9b confirms the ratio 1:3 for the different wavelengths plotted. Fig. 9c indicates that at pH 1.33 the same spectroscopic behaviour was obtained as at pH 6.19, except that the absorbance values for the whole of the spectrum were greater at pH 6.19, which confirms that the complex formed was more stable at this pH value.

4.2. Determination of the formation constant of the complex with the aid of the data processing software SQUAD [12,13]

Figs. 10 and 11 show the evolution of absorption spectra at different pH values 24 h after the preparation of each system. The scale used in each figure is different in order to realize better the details of the shape of the set of spectra.

The set of spectra obtained 240 h after preparation of each system is very similar to that shown in Figs. 10 and 11.

In order to appreciate the validity of this statement, Fig. 12 shows a comparison of the relationship of absorbance as a function of pH at 520 nm wavelength for the systems 1 and 10 days after preparation. It can be observed that for pH values lesser than 6.5, the absorbance is practically the same at each pH value, which it was taken as an indication that these systems are in thermodynamic equilibrium.

Absorbance data, between 200 and 600 nm, of several systems in thermodynamic equilibrium for pH < 6.5 were fed into the software TRIANG [11]. The results obtained with this study permit to conclude that the observed behaviour is due to three

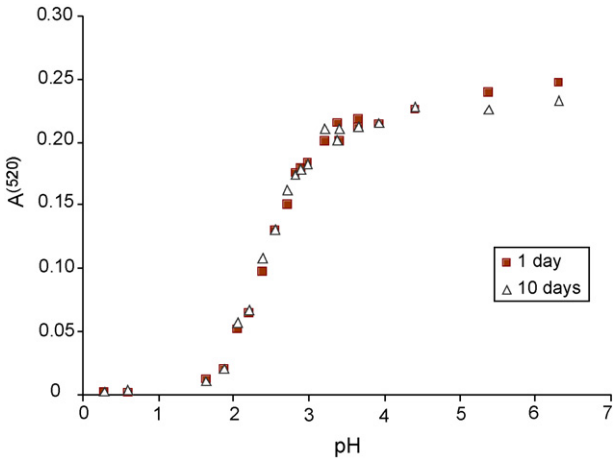

Fig. 12. Plot of the absorbance at 520 nm wavelength as a function of pH for Fe(II)/5-Aphen systems (■) 24 h and (△) 240 h after their preparation.

Table 1
Best refined models by SQUAD for the Fe(II)/5-Aphen′ sytems with absorption spectra obtained 24 h after their preparation, as explained in the text

Wavelength range (nm)	Chemical model	$\log \beta \pm \sigma$	σ[a]	U[b]
208–584	$H^+ + (5\text{-Aphen}) = (5\text{-Aphen})H^+$	5.78[c]	0.022	0.375
	$2H^+ + (5\text{-Aphen}) = (5\text{-Aphen})H_2^{2+}$	6.89[c]		
	$Fe^{2+} + 3(5\text{-Aphen}) = Fe(5\text{-Aphen})_3^{2+}$	23.155 ± 0.036		
464–584	$H^+ + (5\text{-Aphen}) = (5\text{-Aphen})H^+$	5.78[d]	0.008	0.016
	$2H^+ + (5\text{-Aphen}) = (5\text{-Aphen})H_2^{2+}$	6.89[d]		
	$Fe^{2+} + 3(5\text{-Aphen}) = Fe(5\text{-Aphen})_3^{2+}$	23.447 ± 0.024		

Nineteen absorption spectra with pH values ranging from 0.2 to 6.4 with wavelength increments of 8 nm for each spectrum.
[a] Total standard deviation for absorbance data.
[b] Sum of squares of absorbance residuals.
[c] These equilibrium constants were fixed during refining at the values previously obtained [14] and the molar absorptivity coefficients for $(5\text{-Aphen})H^+$ and $(5\text{-Aphen})H_2^{2+}$ were varied, but those of (5-Aphen) were fixed to zero due to its low concentration in the studied systems.
[d] These equilibrium constants were fixed during refining at the values previously obtained [14] and the molar absorptivity coefficients for (5-Aphen), $(5\text{-Aphen})H^+$ and $(5\text{-Aphen})H_2^{2+}$ were fixed to zero due to the very low absorption in the visible region.

absorbing species in the system. Taking into consideration all the information described before, these species could be $(5\text{-Aphen})H_2^{2+}$, $(5\text{-Aphen})H^+$ and $Fe(5\text{-Aphen})_3^{2+}$.

Then, both sets of absorption spectra (those for 24 and 240 h) were introduced into the software SQUAD [12,13], in order to refine the equilibrium constant of the complex and to obtain the molar absorptivity coefficients of the species.

The following chemical model was also introduced into SQUAD:

$$H^+ + 5\text{-Aphen} = (5\text{-Aphen})H^+ \ldots \beta_1$$
$$2H^+ + 5\text{-Aphen} = (5\text{-Aphen})H_2^{2+} \ldots \beta_2$$
$$Fe^{2+} + 3(5\text{-Aphen}) = Fe(5\text{-Aphen})_3^{2+} \ldots \beta_3$$

Table 1 presents the results obtained by processing absorbance data after 24 h after preparation of the systems and Table 2 presents the results obtained with data 240 h after preparation.

Fig. 13 shows the plots of the molar absorptivity coefficients obtained through the use of SQUAD for the refinement described and shown in the first row of Table 1.

It is important to underline than the coefficients obtained for $(5\text{-Aphen})H^+$ and $(5\text{-Aphen})H_2^{2+}$ with this data refinement have the same shape previously obtained [14]; the deviation in this calculation was less than 26% at the coefficients main maxima.

The great similitude of the values obtained through different refinements of the formation constant of the complex (Tables 1 and 2) and the goodness of the fit of the experimental absorption spectra in thermodynamic equilibrium, considering only the formation of $(5\text{-Aphen})H^+$, $(5\text{-Aphen})H_2^{2+}$ and $Fe(5\text{-Aphen})_3^{2+}$, permit to establish that the value of the formation constant of the $Fe(5\text{-Aphen})_3^{2+}$ complex was $\log \beta \approx 23.4 \pm 0.1$. Furthermore, the value of this formation constant is very similar to that reported for de complex of Fe(II) with *o*-phen (21.3 [10]).

5. Spectroscopic features of the $Fe(5\text{-Aphen})_3^{2+}$ complex

The $Fe(5\text{-Aphen})_3^{2+}$ complex presents characteristic absorption bands related with electronic transitions of the 5-Aphen species and the charge-transfer from metal to ligand in the visible region of electromagnetic spectrum.

Table 3 resumes the wavelength values of the absorption bands and the values of the molar absorptivity coefficients for these wavelengths, for some of the absorbing species in the system. For the complex, the refining values obtained in the present work were used except that for the 5-Aphen species the results previously obtained [14] were employed. In general, it can be observed that the location of the maximum absorp-

Table 2
Best refined models by SQUAD for the Fe(II)/5-Aphen′ sytems with absorption spectra obtained 240 h after their preparation, as explained in the text

Wavelength range (nm)	Chemical model	$\log \beta \pm \sigma$	σ[a]	U[b]
365–600	$H^+ + (5\text{-Aphen}) = (5\text{-Aphen})H^+$	5.78[c]	0.009	0.078
	$2H^+ + (5\text{-Aphen}) = (5\text{-Aphen})H_2^{2+}$	6.89[c]		
	$Fe^{2+} + 3(5\text{-Aphen}) = Fe(5\text{-Aphen})_3^{2+}$	23.513 ± 0.040		
485–600	$H^+ + (5\text{-Aphen}) = (5\text{-Aphen})H^+$	5.78[d]	0.008	0.038
	$2H^+ + (5\text{-Aphen}) = (5\text{-Aphen})H_2^{2+}$	6.89[d]		
	$Fe^{2+} + 3(5\text{-Aphen}) = Fe(5\text{-Aphen})_3^{2+}$	23.563 ± 0.024		

Twenty-three absorption spectra with pH values ranging from 0.2 to 6.4 with wavelength increments of 5 nm for each spectrum.
[a] Total standard deviation for absorbance data.
[b] Sum of squares of absorbance residuals.
[c] These equilibrium constants were fixed during refining at the values previously obtained [14] and the molar absorptivity coefficients for $(5\text{-Aphen})H^+$ and $(5\text{-Aphen})H_2^{2+}$ were varied, but those of (5-Aphen) were fixed to zero due to its low concentration in the studied systems.
[d] These equilibrium constants were fixed during refining at the values previously obtained [14] and the molar absorptivity coefficients for (5-Aphen), $(5\text{-Aphen})H^+$ and $(5\text{-Aphen})H_2^{2+}$ were fixed to zero due to the very low absorption in the visible region.

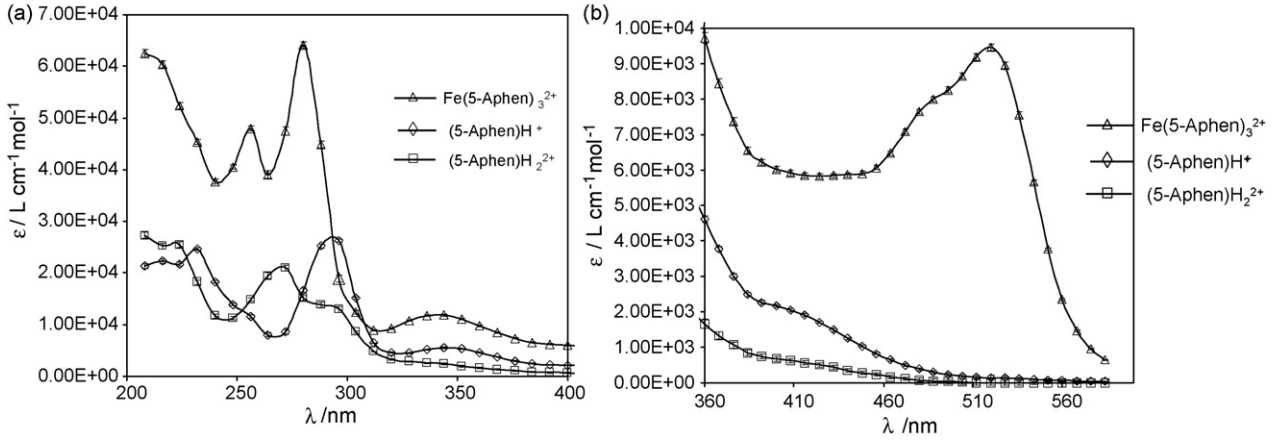

Fig. 13. Plots of the molar absorptivity coefficients (ε) calculated with the aid of SQUAD for the refinement shown in the first row of Table 1. (a) 208–400 nm wavelength range. (b) 360–584 nm wavelength range.

tion wavelengths is almost the same as for (5-Aphen)H^+ or (5-Aphen)$H_2{}^{2+}$ and Fe(5-Aphen)$_3{}^{2+}$. This fact suggests that the spectroscopic effect is practically the same for the H^+ substitution with Fe^{2+}. Also it can be seen that the maxima of the molar absorptivity coefficients on the UV region of the complex are approximately three times those of (5-Aphen) or (5-Aphen)H^+ species, as expected by the three ligands in the formulae of the complex.

The absorption bands located at 480 and 520 nm may be associated to the charge-transfer of the d orbitals of the metal ion to the unoccupied orbitals of the ligand. This absorption bands are similar to those observed in the case of the Fe(*o*-phen)$_3{}^{2+}$ complex (e.g. 9.3×10^3 L cm^{-1} mol^{-1} at 520 nm for Fe(5-Aphen)$_3{}^{2+}$ and 11.0×10^3 L cm^{-1} mol^{-1} at 510 nm for Fe(*o*-phen)$_3{}^{2+}$) [18].

In order to analyze the behaviour of the Fe/5-Aphen complex, the predominance zone diagrams were constructed from thermodynamic data estimated for the 5-Aphen′ [19] and the complex (see Table 1); whereas for the Fe-SO_4–H_2O complexes the data were taken from the HYDRA data base included in MEDUSA (19). Fig. 14 shows the diagrams log [5-Aphen′]$_{TOT}$ as a function of pH for the [Fe(II)]$_{TOT}$ = 25.0 μM y [$SO_4{}^{2-}$]$_{TOT}$ = 500mM concentrations obtained by means of MEDUSA. The PZD for the iron species are presented in Fig. 14a and c, whereas the diagrams corresponding to the 5-Aphen′ species are shown in Fig. 14b and d under the experimental conditions used.

In the case of the spectrophotometry studies a [5-Aphen′]$_{TOT} = 7.5 \times 10^{-5}$ M solution was used as indicated in Fig. 14a and b by means of a broken line. Fig. 14a shows that at pH values smaller than 3 the complex Fe(5-Aphen)$_3{}^{2+}$ does not predominate, however, at greater pH values the reverse is true. Further analysis corroborated that the predominating species at acid pH in the 5-Aphen PZD (see Fig. 14b) are those without Fe(II); when the pH reached 6 the 5-Aphen associated to Fe

Table 3
Comparison of the wavelengths of maximium absorption and the molar abosptivity coefficient values for Fe(5-Aphen)$_3{}^{2+}$, (5-Aphen) and (5-Aphen)H^+ species

Spectroscopic features	Species		
	Fe(5-Aphen)$_3{}^{2+}$	(5-Aphen)	(5-Aphen)H^+
λ_{max1} (nm)	208, 232^{sh}	232	215
$\epsilon_{\lambda_{max\,1}} \times 10^4$ (L mol^{-1} cm^{-1})	6.39 ± 0.11, 4.73 ± 0.16	2.07 ± 0.04	1.99 ± 0.03
λ_{max2} (nm)	256	256^{sh}	256^{sh}
$\epsilon_{\lambda_{max\,2}} \times 10^4$ (L mol^{-1} cm^{-1})	4.93 ± 0.10	1.00 ± 0.02^{sh}	1.09 ± 0.03^{sh}
λ_{max3} (nm)	280	280	295
$\epsilon_{\lambda_{max\,3}} \times 10^4$ (L mol^{-1} cm^{-1})	6.70 ± 0.19	1.95 ± 0.03	2.13 ± 0.11
λ_{max4} (nm)	344	328	344
$\epsilon_{\lambda_{max\,4}} \times 10^4$ (L mol^{-1} cm^{-1})	1.27 ± 0.06	0.40 ± 0.04	0.43 ± 0.02
λ_{max5} (nm)	416^{pl}		416^{sh}
$\epsilon_{\lambda_{max\,5}} \times 10^4$ (L mol^{-1} cm^{-1})	0.62 ± 0.02		0.15 ± 0.01
λ_{max6} (nm)	480^{sh}		
$\epsilon_{\lambda_{max\,6}} \times 10^4$ (L mol^{-1} cm^{-1})	0.77 ± 0.01		
λ_{max7} (nm)	520		
$\epsilon_{\lambda_{max\,7}} \times 10^4$ (L mol^{-1} cm^{-1})	0.93 ± 0.01		

sh = Shoulder; pl = Plateau.

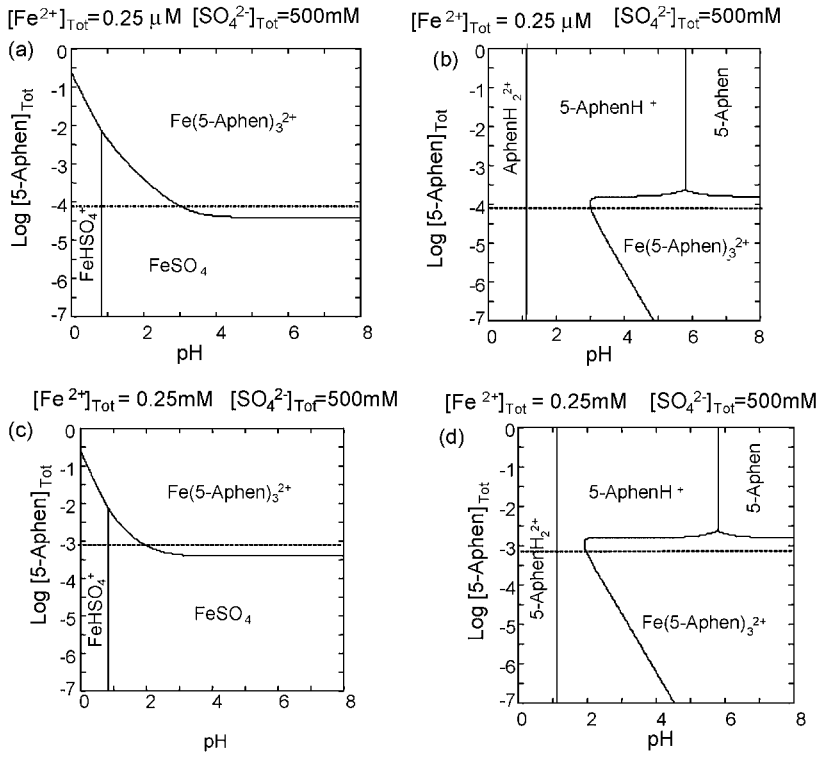

Fig. 14. Predominance zone diagram for (a) Fe(II) and [5-Aphen′]$_{TOT}$ = 7.5 × 10^{-5} M, (b) 5-Aphen′ and [5-Aphen′]$_{TOT}$ = 7.5 × 10^{-5} M, (c) Fe(II) and [5-Aphen′]$_{TOT}$ = 7.5 × 10^{-4} M, (d) 5-Aphen′ [5-Aphen′]$_{TOT}$ = 7.5 × 10^{-4} M.

predominated. The results predict the experimental behaviour, where at basic pH the absorption band associated to the Fe(5-Aphen)$_3^{2+}$ complex predominated, while upon decreasing the pH to 0.29, the band disappears as a function of time till equilibrium is reached, whereby the spectrum only shows the absorption bands associated to the 5- Aphen′ species.

The working conditions to be used for the voltammetry studies were obtained likewise, with a [5-Aphen′]$_{TOT}$ = 7.5 × 10^{-4} M concentration, as is indicated in Fig. 14c and d by the broken line. Thus, Fig. 14c shows that under these ligand and acid pH conditions there is no complex. This explains why the voltammograms obtained at acid pH show the 5-Aphen′ oxidation profile, which was also corroborated in Fig. 14d where the complex only predominates at pH greater than 2. A comparison between both diagrams reveals that the complex predominance zone is greater at higher Fe(II) and 5-Aphen′ concentrations.

6. Conclusions

The kinetic and thermodynamic studies obtained through application of spectrophotometry and electrochemistry methods allowed analysis of the behaviour of the Fe(II)–5-Aphen system in aqueous solution. The influence of the pH was studied, giving an adequate insight on the time-stability of the species in the system. The experimental conditions were determined for values near neutrality, where the complex with a stoichiometry [Fe(5-Aphen)$_3$]$^{2+}$ is stable as a function of pH. Also, it was found that for acid pH values there was a coupled reaction associated to competence of the H$^+$ for the coordination sites of the 5-Aphen, thus proving dissociation of the complex, as shown by the spectrophotometry and electrochemical results. The formation of the Fe(5-Aphen)$_3^{2+}$ complex alone has been studied; namely, it was slowly destroyed in very acidic milieu, in such a way that a red color may be observed during 7 h. The apparent rate constant, global formation constant and spectroscopic features have been characterized.

The PZD presented with the thermodynamic constant obtained in this work describe perfectly the chemical and electrochemical behaviour of the [Fe(5-Aphen)$_3$]$^{2+}$ as a function of pH.

Acknowledgements

We want to acknowledge CONACyT for partial financial support through the postgraduate fellowships of MLLC and through project 46124. We also acknowledge PROMEP (SEP) for partial financial support to the Analytical Chemistry and Electrochemistry Academic Groups of UAM-I (Cuerpos Académicos de Química Analítica y Electroquímica de la UAM-I). We are in debt with Mario Romero for English translation.

References

[1] P.G. Pickup, R.A. Osteryoung, Inorg. Chem. 24 (1985) 2707–2712.
[2] I. De Gregori, F. Bedioui, J. Devinck, J. Electroanal. Chem. 238 (1987) 197–214.
[3] V. Rivera, A.R. Guadalupe, J.L. Colón, Memorias del Congreso Iberoamericano de Electroquímica (1996) 235–236.
[4] W. Frazier, M. Nyasulu, H. Motola, J. Electroanal. Chem. 239 (1988) 175–186.

[5] Ch.D. Ellis, D.L. Margerum, R.W. Murray, T.J. Meyer, Inorg. Chem. 22 (1983) 1283–1291.
[6] P. Nunciante, G. Pistola, Electrochim. Acta 34 (1989) 223–228.
[7] L.G. Bachas, L. Cullen, R.S. Hutchins, D.L. Scott, J. Chem. Soc. Dalton Trans. (1997) 1571–1577.
[8] Y.-W. Liou, Ch.M. Wang, J. Electroanal. Chem. 495 (2001) 126–133.
[9] W.T. Chuang, C.H. Wang, Ch.M. Wang, J. Electroanal. Chem. 521 (2002) 175–182.
[10] W.A.E. Mc. Bride, Critical Review of Equilibrium Data for Proton and Metal Complexes of 1,10-phenantroline, 2,2′-bipyridil and Related Compounds, IUPAC, Chemical Series No. 17, Pergamon, UK, 1978.
[11] F.R. Hartley, C. Burgess, R.M. Alcock, Solution Equilibria, Wiley, New York, 1980.
[12] D.J. Legget, in: D.J. Legget (Ed.), Computational Methods for the Determination of Formation Constants, Plenum Press, New York, 1985, p. 159.
[13] A. Morales, M.Sc. Thesis, FES-Cuautitlán, UNAM, Mexico, 1993.
[14] M.T. Ramírez-Silva, M. Gómez-Hernández, M.L. Pacheco-Hernández, A. Rojas-Hernández, L. Galicia, Spectrochim. Acta Part A 60 (2004) 781–789.
[15] G.W. Castellan, Fisicoquímica, Addison, New York, 1987.
[16] D.C. Harris, Quantitative Chemical Analysis, Freeman, New York, 2002.
[17] D.A. Skoog, D.M. West, F.J. Holler, S.R. Crouch, Fundamentals of Analytical Chemistry, Thomson, Belmont, 2004.
[18] C.J. Ballhausen, Ligand Field Theory, MacGraw-Hill, New York, 1962.
[19] I. Puigdomenech, MEDUSA (Making equilibrium diagrams/using sophisticated algorithms), Royal Institute of Technology, Stockholm, Sweden, 2004.

Available online at www.sciencedirect.com
ScienceDirect
Talanta 72 (2007) 1293–1297
Talanta
www.elsevier.com/locate/talanta

The study of a chemiluminescence immunoassay using the peroxyoxalate chemiluminescent reaction and its application

Lirong Luo, Zhujun Zhang *, Lingyan Hou, Jinli Wang, Wei Tian

School of Chemistry and Materials Science, Shaanxi Normal University, Xi'an 710062, PR China

Received 13 October 2006; received in revised form 12 January 2007; accepted 14 January 2007
Available online 20 January 2007

Abstract

The paper presented a novel chemiluminescence (CL) immunoassay method, which combines the advantages of traditional enzyme-linked immunosorbent assays (ELISA) and bis (2,4,6-trichlorophenyl) oxalate (TCPO)–hydrogen peroxide CL detection system. A fluorescent product 2,3-diaminophenazine (DAPN) was produced by reaction between *o*-phenylenediamine (OPDA, 1,2-diaminobenzene) and H_2O_2 catalyzed by horseradish peroxidase (HRP). DAPN was excited by the reactive intermediate of TCPO–H_2O_2 chemiluminescent reaction, and led to CL. The dependence of the CL intensity on the concentrations of antigen was studied. As analytical application, the proposed method was used for determination of recombinant human interleukin 6 (rHu IL-6) and β-human chorionic gonadotropin (β-HCG). Under the selected experimental conditions, a linear relationship was obtained between the CL intensity and the concentration of rHu IL-6 in the range of 4.0–625.0 pg/ml, and β-HCG in the range of 12.5–400.0 mIU/ml. The detection limits were 0.5 pg/ml for rHu IL-6 and 3 mIU/ml for β-HCG with relative standard deviation of 2.3 for 78.0 pg/ml rHu IL-6, and 3.9 for 50.0 mIU/ml β-HCG. This method has been applied to the determination of rHu IL-6 in human serum and β-HCG in urine with satisfactory results.

Keywords: Chemiluminescence; Immunoassay; ELISA; TCPO

1. Introduction

An immunoassay is an analytical technique, which is capable of specifically detecting very small quantifies of a particular compound. Today, immunoassays play a prominent role in the analysis of many clinical laboratory analytes such as proteins, hormones, drugs, and nucleic acids because of its high specificity, versatility and sensitivity. The future involves development of assays with higher sensitivities [1–5]. Radio immunoassay (RIA) had been the most widely used immunoassay since it was first introduced in 1959. However, the known drawbacks of radioisotopes, health hazard, waste disposal problems and short half-life have induced intensive search for alternative methods [6,7]. Enzyme-linked immunosorbent assays (ELISAs) are among the most extensively used types of immunoassays, and their application in environmental, food, and medical analysis is an area with an enormous potential for growth [4,8]. ELISA assays were found to be safer and easier than the early RIA, and could be based either on colorimetric, fluorescent or chemiluminescent detection. Moreover, the sensitivity of an ELISA assay strongly depends on the affinity of specific antibodies and on the sensitivity of the detection method. However, the sensitivity of conventional colorimetric detection is relatively low [9,10].

Chemiluminescence (CL) is now commonly used for immunoassay in the form of a chemiluminescent label or as a chemiluminescent detection reaction for an enzyme label. CL immunoassays have become very popular in recent years, as they offer significant gains in sensitivity over most other methods at a low cost [11–13]. Advances in sensitivity have been achieved by using chemiluminescent detection of enzyme labels. HRP was employed as label frequently in immunoassay, and it was detected with the luminol-based enhanced chemiluminescence (ECL) system, the ECL reaction offers the possibility of improving the sensitivity of immunoassays to at least 2–3 orders of magnitude compared to conventional colorimetric detection [10,14]. However, the quantum yield of luminol does not exceed 5% in dimethyl-sulphoxide and 1–1.5% in aqueous systems [3].

* Corresponding author. Tel.: +86 29 85308748; fax: +86 29 85307774.
E-mail address: zzjl8@hotmail.com (Z. Zhang).

0039-9140/$ – see front matter © 2007 Elsevier B.V. All rights reserved.
doi:10.1016/j.talanta.2007.01.030

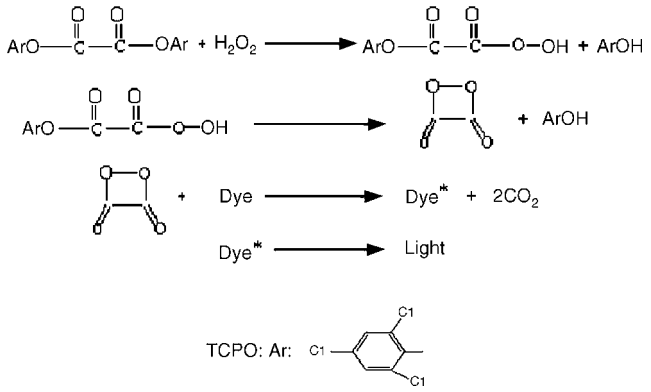

Fig. 1. Possible reaction pathway for the PO–CL system—dye: fluorophore; TCPO: bis-(2,4,6,-trichlorophenyl) oxalate.

The simplest way to increase the sensitivity is to use a system with high emission quantum yield. The TCPO–H_2O_2 chemiluminescent reaction is very efficient, having a quantum yield higher than that observed for most of the chemiluminescent reaction discovered to date. This reaction requires the presence of a suitable fluorophore and has a quantum yield of 5–50% [15,16]. Like many CL reactions, the PO–CL reaction can be schematized in three basic steps (Fig. 1). In the first step, an aryl oxalate ester like TCPO reacts with H_2O_2 to produce a key chemical intermediate, 1,2-dioxetanedione (C_2O_4), containing the necessary excitation energy. The second step involves the chemiexcitation of a fluorophore to electronically excited states by the reactive intermediate via conversion of the chemical energy into electronic excitation energy. The final step is the emission of light energy by returning the excited fluorophore molecule to the ground state [17,18].

In this paper, the traditional ELISA assay by using HRP as the enzyme label was coupled with TCPO–H_2O_2 chemiluminescent reaction. HRP be an excellent enzyme for catalyzing the reaction between OPDA and H_2O_2 to form DAPN [19,20]. The fluorescent product DAPN could be excited by the reactive intermediate of TCPO–H_2O_2 chemiluminescent reaction, and the emission of light could be detected by a high sensitive cooled CCD. Therefore, the amount of an enzyme-labeled analyte or labeled specific binding partner for an analyte could be detected.

As analytical application, the proposed method was used for determination of rHu IL-6 and β-HCG. The proposed method has the advantage of showing the specificity of ELISA (non-chemiluminescent assays), sensitivity of TCPO–H_2O_2 system and high throughput of CL imaging assay. In addition, fluorescent peroxidase substrates and oxalates could be chosen independently, efficiency and flexibility are therefore the main advantages of this system.

2. Experimental

2.1. Reagents and solutions

Recombinant human interleukin 6 (rHu IL-6), two monoclonal antibodies against rHu IL-6 were kindly donated by Prof. B.Q. Jin (Department of Immuno, The Fourth Military Medical University, Xi'an, China). β-Human chorionic gonadotropin (β-HCG) ELISA kits were purchased from Biocell Laboratory Ltd. (Zhengzhou, China). All chemicals and reagents used in this study were of analytical grade quality. Solutions were prepared in deionized, distilled water. Citric acid ($C_6H_8O_7{\cdot}H_2O$), H_2O_2, Na_2CO_3, $NaHCO_3$, KH_2PO_4, $Na_2HPO_4{\cdot}12H_2O$, NaCl, KCl, Tween 20, and NaH_2PO_4 were obtained from Shanghai Chemical Plant (Shanghai, China). *o*-Phenylenediamine (OPDA), HRP (250 IU/mg) were obtained from LaiBo Technology Development Company (Xi'an, China). Bis (2,4,6-trichlorophenyl) oxalate (TCPO) was synthesized as described by Mohan [21]. The coating solution was 0.05 mol/l Na_2CO_3–$NaHCO_3$ buffer, pH 9.6. 0.15 mol/l PBS buffer, pH 7.4 was prepared by dissolving 0.2 g KH_2PO_4, 2.9 g $Na_2HPO_4{\cdot}12H_2O$, 8.0 g NaCl, 0.2 g KCl in 1 l water. 96-well plates were rinsed with PBST solution (PBST: PBS solution containing 0.05% (v/v) Tween-20). Antigen and antibody were diluted with PBSTB solution (PBSTB: PBST containing 0.1% (w/v) BSA). A 1 mg/ml OPDA stock solution was prepared by dissolving 10 mg OPDA in 10 ml distilled water. The reagents for conventional ELISA colorimetric reaction were prepared by appropriate dilution of the stock solution of OPDA, H_2O_2 (30%) with Na_2HPO_4–citric acid (pH 5.0) buffer solution. HRP solutions were prepared by dissolving a certain amount of HRP in deionized water and stored below 4 °C.

The PO–CL reagents were prepared in volumetric glass flasks by dissolving H_2O_2 (30%), TCPO in dried acetonitrile before use. Imidazole stock solution was prepared by dissolving a certain amount of imidazole in ethanol.

2.2. Instrumentation

The 96 well transparent microtiter plates were imaged using a FluorchemTM IS-8800 system (Alpha Innotech, CA). The Fluochem imaging system is a powerful digital system ideal for instant photography of a wide variety of samples. Thermoelectric cooling of the CCD camera allows imaging of low light samples in UV-illuminated, chemiluminescent and fluorescent applications. The instrument is controlled by Alpha Ease FC software. Imaging analysis and archiving treatment were performed with Alpha Ease FC software running under Windows 2000.

2.3. Procedures

2.3.1. Procedures for oxidation reaction based on HRP

In this paper, HRP was used as model analytes to optimize the reaction conditions. Fifty microlitres of 3.0×10^{-2} mol/l H_2O_2, 50 μl of a certain concentration of HRP, and 50 μl of 0.5 mg/ml OPDA were added to the wells of 96 well transparent microtiter plates. The oxidation reaction was performed at 37 °C, and the time for oxidation reaction was 10 min. A yellow fluorescent product (DAPN) could be obtained.

2.3.2. Procedures for CL immunoassay of rHu IL-6

A typical "sandwich" type immunoassay was used. A pair of antibodies that recognize different epitopes of same antigen

was used to capture and detect a certain antigen. The assay protocols were as follows: (a) the 96 well plates were coated with anti-rHu IL-6 monoclonal antibody (100 μl/well) diluted 100-fold in 0.05 mol/l carbonate buffer pH 9.6 overnight at 4 °C. All further steps were performed at 37 °C. These wells were washed three times with PBST solution; (b) addition of the rHu IL-6 standard or sample (100 μl/well), incubation for 30 min, wash four times; (c) addition of HRP-conjugated anti-rHu IL-6 monoclonal antibody (100 μl/well). After a final washing step, 50 μl of 3.0×10^{-2} mol/l H_2O_2 and 50 μl of 0.5 mg/ml OPDA were added, and the reaction solution was incubated at 37 °C for 15 min. Then 5 μl of fluorescent product (DAPN) was added to the wells of another microtiter plate, and TCPO CL reagents were added.

2.3.3. Procedures for CL immunoassay of β-HCG

The wells of microtiter plate have been coated by anti-β-HCG monoclonal antibody. All further steps were performed at 37 °C. PBST solution was used as washing solution. The assay protocols were the following: (a) additions of the β-HCG standard or sample (100 μl/well), incubation for 10 min, wash four times; (b) addition of HRP-conjugated anti-β-HCG monoclonal antibody, incubation for 10 min (100 μl/well), wash four times. The following steps were same as 2.3.2.

2.3.4. Procedure for CL imaging assay

CL imaging measurements were performed in Fluorchem TM IS-8800 system. This system was connected to a PC for quantitative imaging and a sample dark box was provided to prevent contact with external light. The system operates in the following steps: (a) samples in transparent microtiter plates were recorded as transmitted light; (b) the luminescent signal was measured with an optimized photon accumulation lasting 8 min; (c) the light emission from each well was quantified by defining a fixed area and counting the number of photon fluxes within this area, the user can manually draw an area of interest through the three OBJECT buttons of software. In this work the area of each well was enclosed with a box (rectangle). The background value was obtained by imaging an equally sized region outside the region of interest and was subtracted from each measurement. Finally, the intensity of the spots was determined using the Spot Denso function of the software, which combines the pixel intensities. The wells were individually analyzed and the intensities (AVG) were plotted as a function of analytes concentration to yield the calibration curve. IDV is the sum of all the pixel values after background correction: IDV = ∑(each pixel value-BACK), AREA is the size (in pixels) of the region enclosed by the box, AVG is the average value after background correction of the pixels enclosed, AVG = IDV/AREA, BACK is the background value that will be subtracted from all the pixels in the object.

2.4. Sample preparation

Fresh blood was collected in clean plastic tubes; no anticoagulant was added to the blood samples allowing the blood coagulation naturally and then centrifuged at 3000 rpm for 5 min. The supernatant part was extracted as serum with a mini sample collector. Serums were stored at −20 °C until assayed. The urine of women could be used directly.

3. Results and discussion

3.1. Optimization of experimental variables of enzyme catalyzed reaction

CL immunoassay depends on both oxidation reaction catalyzed by HRP and the TCPO detection system. CL emission intensity is sensitive to a variety of environmental factors such as solvent, temperature, solution pH and other species present in the system. Different kinds of buffer solutions with varying pH values were tested for the reaction. The maximum CL intensity could be obtained in Na_2HPO_4–citric acid buffer with pH 5.0. Therefore, Na_2HPO_4–citric acid buffer (pH 5.0) was chosen for subsequent experiments (Fig. 2)

Temperature is a very important factor that cannot be neglected in reaction catalyzed by HRP. The optimum temperature for HRP is 37 °C, and the incubation time of HRP and fluorescent substrates was 10 min, increasing of the incubation time led to an increasing background, the relative CL intensity decreased when incubation time was longer than 10 min.

As fluorescent peroxidase substrates, OPDA concentration affected the CL intensity. The effect of the concentration of OPDA on the CL intensity was investigated over the range of 0.06–1 mg/ml. It was found (Fig. 3) that CL intensity reached a maximum value when OPDA concentration was 0.5 mg/ml. Therefore, the OPDA concentration of 0.5 mg/ml was chosen for consequent research work.

In this HRP-catalyzed fluorogenic reaction between H_2O_2 and OPDA, the concentration of H_2O_2 affect the oxidation reaction, and the effect of the concentration of H_2O_2 on the detected CL signal was studied over the range of 5.0×10^{-3} to 5.0×10^{-2} mol/l. Experimental results showed that CL intensity reached a maximum value when H_2O_2 concentration was 3.0×10^{-2} mol/l.

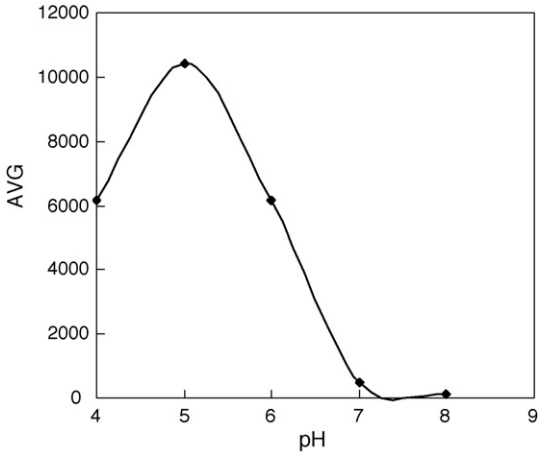

Fig. 2. Effect of pH on the CL intensity—OPDA: 0.5 mg/ml; H_2O_2: 3.0×10^{-2} mol/l; HRP: 1.0×10^{-8} g/ml; TCPO: 7.0×10^{-3} mol/l; H_2O_2: 0.5 mol/l; imidazole: 3.0×10^{-3} mol/1.

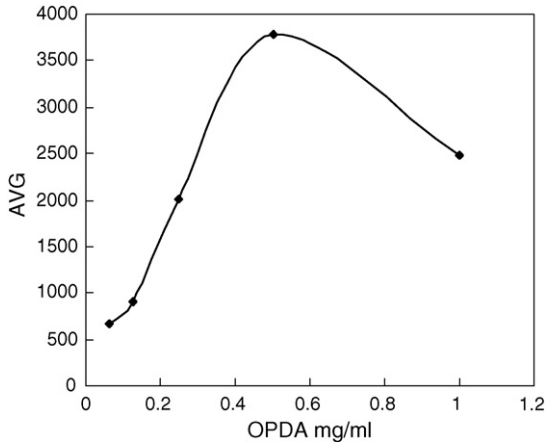

Fig. 3. Effect of concentration of OPDA on the CL intensity—H_2O_2: 3.0×10^{-2} mol/l; HRP: 1.0×10^{-8} g/ml; TCPO: 7.0×10^{-3} mol/l; H_2O_2: 0.5 mol/l; imidazole: 3.0×10^{-3} mol/l.

3.2. Optimization of the CL reaction conditions

As expected, the intensity of the PO–CL emission peak was found to be proportional to the initial concentration of the reactants. It is known that CL intensity increases with the increase in TCPO and H_2O_2 concentration. However, increasing of the concentration led to an increasing background, the relative CL intensity decreased. In this paper, the effect of the concentration of TCPO on the CL intensity was investigated over the range of 1.5×10^{-4} to 8.0×10^{-3} mol/l. Experimental results showed that when TCPO concentration was 7.0×10^{-3} mol/l, a maximum CL signal could be obtained. The effect of H_2O_2 concentration on the CL intensity was also investigated. It was found (Fig. 4) that CL intensity reached a maximum value when H_2O_2 concentration was 0.5 mol l^{-1} In the presence of imidazole (5.0×10^{-3} mol/l), the light intensity is much higher than that in the absence of the base. The observed behavior is clearly indicative of the catalytic effect of imidazole on the PO–CL system studied [22]. However, further addition of imidazole revealed a gradual decrease of the CL intensity. This is most probably due to the quenching effect of the base at higher concentrations, which begins to decompose the reactive intermediate, dioxetanedione, and hence reduces the CL light.

The TCPO–H_2O_2 chemiluminescent reaction in organic solvents has a very high quantum yield; the aqueous solutions currently used in oxidation reaction catalyzed by HRP reduce dramatically the efficiency of this reaction. The volume of fluorescent product (DAPN) used in TCPO–H_2O_2 chemiluminescent reaction was studied. Finally, 5 μl fluorescent products were chosen for consequent CL detection. In addition, different organic media such as acetone, ethyl acetate, dimethyl phthalate, *tert*-butyl alcohol, ethanol and acetonitrile were chosen as solvent of TCPO and H_2O_2. Experimental results showed that when dimethyl phthalate was chosen as solvent, the strongest CL signal could be obtained, however, the CL signal of reagent blank was high. When acetonitrile was chosen as solvent of TCPO and H_2O_2, CL signal with biggest S/N (signal to noise ratio) could be obtained, and CL signal could be enhanced by imidazole (5.0×10^{-3} mol/1 in ethanol).

3.3. Performance of CL imaging assay for rHu IL-6 measurements

Under the selected conditions, CL response to rHu IL-6 solution was linear in the concentration range of 4.0–625.0 pg/ml, and the detection limit was 0.5 pg/ml, (3σ). The image of different concentration of rHu IL-6 was shown in Fig. 5. The regression equation of calibration curve for rHu IL-6 was $\Delta I_{Cl} = 14.534$ [rHu IL-6] + 3518, with a correlation coefficient of $R^2 = 0.9945$ ($n = 5$). The relative standard deviation (R.S.D.) for nine parallel measurements of 78.0 pg/ml was 2.3%.

3.4. Performance of CL imaging assay for β-HCG measurements

Under the selected conditions, CL response to β-HCG solution was linear in the concentration range of 12.5–400.0 mIU/ml, and the detection limit was 3 mIU/ml, (3σ). The regression equation of calibration curve for β-HCG was $\Delta I_{Cl} = 1.7196$[β-HCG] + 78.299, with a correlation coefficient of $R^2 = 0.9928$

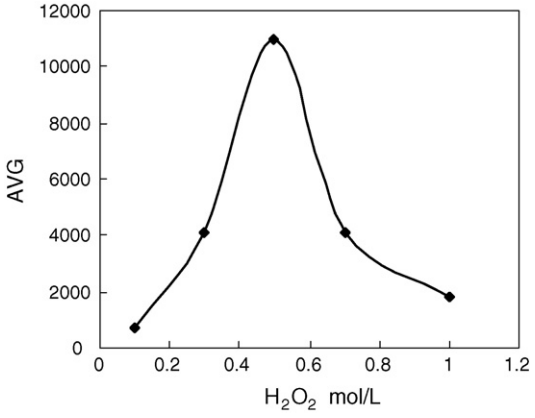

Fig. 4. Effect of concentration of H_2O_2 on the CL intensity—OPDA: 0.5 mg/ml; HRP: 1.0×10^{-8} g/ml; TCPO: 7.0×10^{-3} mol/l; imidazole: 3.0×10^{-3} mol/l.

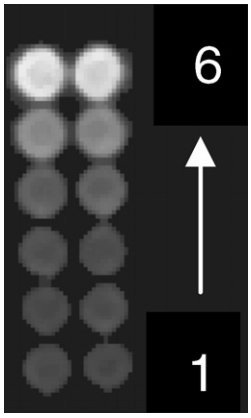

Fig. 5. RHu IL-6 imaging assay using a 96-well transparent microtiter plate: 1–6 represent reagent blank and 4.0–625.0 pg/ml rHu IL-6.

Table 1
Results of recovery test of rHu IL-6

Sample no.	Original (pg/ml)	Added (pg/ml)	Total (pg/ml)	Found (pg/ml)	R.S.D. (%)[a]	Recoveries
1	240.0	312.0	552.0	341.2	4.9	109.4
2	0	312.0	312.0	296.5	3.8	95.0
3	69.1	156.0	225.1	142.7	2.7	91.5
4	131.6	78.0	209.6	72.4	3.5	92.8
5	0	78.0	78.0	84.3	4.7	108.1

[a] R.S.D. represents relative standard deviation (average of three determinations).

Table 2
Results of analysis of β-HCG in urine

Sample no.	1	2	3	4	5
Result of proposed method (mIU/ml)[a]	6080	7380	8926	7589	0
R.S.D (%)	4.3	3.9	3.5	4.7	
Result of hospital	Pregnant	Pregnant	Pregnant	Pregnant	Normal

[a] Concentration (mIU/ml): average of three determinations.

Table 3
Results of recovery test of β-HCG

Sample no.	Original (mIU/ml)	Added (mIU/ml)	Total (mIU/ml)	Found (mIU/ml)	R.S.D. (%)[a]	Recoveries (%)
1	0	25.0	25.0	27.2	3.9	108.8
2	0	50.0	50.0	55.0	4.8	110.0
3	0	100.0	100.0	102.3	3.5	102.3
4	0	100.0	100.0	98.7	4.9	98.7
5	0	200.0	200.0	180.3	3.7	90.2

[a] R.S.D. represents relative standard deviation (average of three determinations).

($n = 6$). The relative standard deviation (R.S.D.) for nine parallel measurements of 50.0 mIU/ml was 3.9%.

3.5. Sample analysis

3.5.1. Sample analysis of rHu IL-6

According to the procedure detailed in Section 2.3.2, the proposed method was applied to the determination of rHu IL-6 in human serum and the accuracy of the rHu IL-6 was evaluated by determining the recoveries of rHu IL-6 after adding to fresh human serum. The results were shown in Table 1.

3.5.2. Sample analysis of β-HCG

According to the procedure detailed in Section 2.3.3, the proposed method was applied to the determination of β-HCG in women urine and the experiments results agreed well with those obtained from hospital (Table 2). The concentration of β-HCG of pregnant women was obvious higher than reference value of normal women (0–5 mIU/mL), and the accuracy of the β-HCG was further evaluated by determining the recoveries of β-HCG after adding to fresh human serum. The results were shown in Table 3.

4. Conclusions

A novel CL immunoassay was presented in this paper, which was based on the principle of HRP catalyzed oxidation reaction and TCPO CL detection system. High emission intensity and better specificity were obtained based on this model. It provides a TCPO–H_2O_2 model for CL imaging assay and implies the preferable use for immunoassay.

Acknowledgement

This study was supported by the National Natural Science Foundation of China (No. 30470886).

References

[1] M.Z. Zheng, J.L. Richard, J. Binder, Mycopathologia 161 (2006) 261.
[2] C. Dodeigne, L. Thunus, R. Lejeune, Talanta 51 (2000) 415.
[3] W.R.G. Baeyens, S.G. Schulman, A.C. Calokerinos, Y. Zhao, A.M. García Campaña, K. Nakashima, D. De Keukeleire, J. Pharmaceut. Biomed. 17 (1998) 941.
[4] V.S. Morozova, A.I. Levashova, S.A. Eremin, J. Anal. Chem. 60 (2005) 202.
[5] Y. Fintschenko, G.S. Wilson, Microchim. Acta 129 (1998) 7.
[6] Z.P. Li, Y.C. Wang, C.H. Liu, Y.K. Li, Anal. Chim. Acta 551 (2005) 85.
[7] I. Surugiu, J. Svitel, L. Ye, K. Haupt, B. Danielsson, Anal. Chem. 73 (2001) 4388.
[8] P.F. Bolado, M. Begoña, G. García, A.C. García, Anal. Chim. Acta 534 (2005) 231.
[9] A.E. Botchkareva, S.A. Eremin, A. Montoya, J.J. Manclus, B. Mickova, P. Rauch, F. Fini, S. Girotti, J. Immunol. Meth. 283 (2003) 45.
[10] C.A. Marquette, P. Hezard, A. Degiuli, L.J. Blum, Sens. Actuators B: Chem. 113 (2006) 664.
[11] L.J. Kricka, Anal. Chim. Acta 500 (2003) 279.
[12] A. Pasha, N.G.K. Karanth, N.G. Karanth, Biosens. Bioelectron. 21 (2006) 1264.
[13] L. Gámiz-Gracia, A.M. García-Campaña, J.J. Soto-Chinchilla, J.F. Huertas-Pérez, A. González-Casado, TRAC-Trend Anal. Chem. 24 (2005) 927.
[14] N. Díaz, K.G. Sánchez, J. Lovillo, J.A. González García, Anal. Chim. Acta 321 (1996) 219.
[15] A. Kamyshny, S. Magdassi, Colloid Surf. B 11 (1998) 249.
[16] D. Salerno, J.R. Daban, J. Chromatogr. B 793 (2003) 75.
[17] M. Shamsipur, M.J. Chaichi, A.R. Karami, H. Sharghi, J. Photochem. Photobiol. A 174 (2005) 23.
[18] A.G. Mohan, N.J. Turro, J. Chem. Educ. 51 (1974) 528.
[19] K. Zhang, L.Y. Mao, R.X. Cai, Talanta 51 (2000) 179.
[20] H. Akhavan-Tafti, R. deSilva, R. Eickholt, R. Handley, M. Mazelis, M. Sandison, Talanta 60 (2003) 345.
[21] M. Shamsipur, A. Yeganeh-Faal, M.J. Chaichi, M. Tajbakhsh, A. Parach, Dyes Pigments 72 (2007) 113.
[22] M. Emteborg, E. Pontén, K. Irgum, Anal. Chem. 69 (1997) 2109.

Available online at www.sciencedirect.com
ScienceDirect
Talanta 72 (2007) 1446–1452
Talanta
www.elsevier.com/locate/talanta

Multicolor quantum dot-encoded microspheres for the detection of biomolecules

Qiang Ma, Xinyan Wang, Yabing Li, Yuhua Shi, Xingguang Su *

Department of Analytical Chemistry, College of Chemistry, Jilin University, Changchun 130012, China

Received 3 November 2006; received in revised form 24 January 2007; accepted 24 January 2007
Available online 6 February 2007

Abstract

The biocompatible semiconductor quantum dots (QDs) have unique photophysical properties, which provide important advantages over organic dyes and lanthanide probes in fluorescence labeling applications. In this work, multicolor quantum QD-encoded microspheres have been prepared via the layer-by-layer (LbL) assembly approach. Polystyrene microspheres of 3 μm diameter were used as templates for the deposition of different sized CdTe QDs/polyelectrolyte multilayers via electrostatic interactions. Two kinds of biofuntional multicolor microspheres with two different antibodies, anti-human IgG and anti-rabbit IgG were prepared. Human IgG and rabbit IgG can be detected as target antigens in the multiplexed fluoroimmunoassays. Furthermore, a novel microfluidic on-chip device was developed to detect two kinds of antigen-conjugated multicolor QD-encoded microspheres; the microspheres can be distinguished from each other based on their fluorescence signals.

Keywords: Quantum dots; Fluorescent polystyrene microspheres; Fluoroimmunoassay

1. Introduction

An array of detection probes, which employed for detection of a large number of analytes simultaneously is needed for both public health improvement and biothreat reduction purpose. Although fluoroimmunoassays using conventional fluorophores can be multiplexed to screen for multiple analytes simultaneously, multicolor analysis of more than one or two color is often complicated by the requirement of an elaborate excitation and detection scheme and challenging data collection and analysis [1,2]. Problems with organic fluorophores include narrow excitation bands and broad emission spectra, which can make detection of multiple light emitting probes difficult due to spectral overlap and photodegradation [3].

Colloidal semiconductor CdTe quantum dots (QDs) are nanoscale spherical particles that have the potential to overcome some of the functional limitations encountered by organic dyes in fluorescence labeling applications [4]. The luminescent QDs fluorescence emission wavelength can be continuously tuned by changing the particle size [5]. With narrow emission spectra, broad excitation bandwidth, different-sized QDs can be excited simultaneously by a single wavelength. In addition, QDs have a good quantum yield and high photochemical stability against photobleaching. Although QDs have wider emission spectra compared with lanthanides, they are most attractive luminescent materials based on their high absorptivities. These features make QDs have been shown to be ideal for use as spectral labels in multiplexed bioanalysis. Multicolor optical "bar codes" have been generated by embedding different sized QDs into microspheres at precisely controlled ratios [5,6].

On the surfaces of encoded microspheres, capture regents have been immobilized in the suspension array [7,8]. Compare to planar array which spot antibodies onto a slide, membrane, well or other planar surface at different location, suspension array offers greater flexibility, reduced antibody denaturation occurrence and faster reaction kinetics [9]. The high binding capacity of three-dimensional microspheres makes the suspension array a very sensitive platform for immunoassays [10]. Each 5.5 μm sphere could provide a large surface area that can accommodate up to 100,000 capture antibodies, the high density of capture antibodies ensures maximum antigen binding, and also to avoid such problems as target object aggregation or inactivation due

* Corresponding author. Tel.: +86 431 5168352; fax: +86 431 8499805.
E-mail address: suxg@mail.jlu.edu.cn (X. Su).

0039-9140/$ – see front matter © 2007 Elsevier B.V. All rights reserved.
doi:10.1016/j.talanta.2007.01.058

to the overloading with fluorescent labels [11]. By integrating molecular recognition with optical coding, each microsphere could be considered as "chemical lab" that detects and analyzes a unique sequence or compound in a complex mixture. Multiple QD-encoded microspheres can be potential fluorescent probes to encode even thousands of genes, proteins, and small-molecule compounds. Recently, mesoporous sllica beads or polystyrene beads doped with multicolor QDs have been used for biological applications, including DNA detection [5,12], multiplexed bioassays, [13] and immunoassays of immunoglobulin G (IgG) [14].

Fluorescent microspheres are usually prepared through hydrophobic mescoporous (silica or polystyrene) microspheres embedded with hydrophobic QDs via porosity partitioning and entrapment or swelling [5,6], phase transfer or coating with an amphiphilic polymer are essential and nontrivial step for this kind of microspheres to be used as biological reporters. Although the fluorescent efficiency of the QDs produced in high-temperature coordinating solvents (organic solvents) is usually high, current phase transfer schemes still require many experimental steps, and ligand exchange is commonly associated with decreased fluorescent efficiency and a propensity to aggregate and precipitate in biological buffer.

In the current work, we employ the layer-by-layer (LbL) method for the construction of biofunctional QD-encoded microspheres. The negatively charged CdTe QDs were deposited in alternation with poly (allylamine hydrochloride) (PAH)/poly (sodium 4-styrensulfonate) (PSS)/PAH polyelectrolyte (PE) multilayers on the surface of polystyrene (PS) microspheres, followed by an outermost layer of antibodies to render the particles biospecific [14,15]. The number of different-colored QDs layers was adjusted experimentally to achieve the different multicolor codes. The bioactivity of QD-encoded microspheres/antibodies was proved by antigen–antibody immunoreaction. The immunoassays adopted a sandwich immunoassay format where antigens were captured by QD-encoded microspheres/antibodies, and recognized subsequently by corresponding antibodies. Moreover, a novel microfluidic chip system was established to confirm and identify the encoded microsohere-based immunoassays in this study. With the excitation of 488 nm laser, the fluorescent emission of the immunocomplexes at 520 nm (FITC), 600 nm (QDs_{orange}) and 650 nm (QDs_{red}) can be detected synchronously.

2. Experimental

2.1. Instrumentation

Fluorescence experiments were performed on a RF-5301 PC spectrofluorophotometer (Shimadzu Co., Japan). A 1 cm path length quartz cuvette was used to measure the fluorescence spectrum. A bath ultrasonic cleaner (Autoscience AS 3120, Tianjin, China) was used to disperse the spheres. All optical measurements were carried out at room temperature under ambient conditions.

In this experiment, mean fluorescence values are reported in arbitrary units that are internally consistent within a given experiment; however, these units are not absolutely comparable between experiments. All samples were prepared in triplicate and average values at each concentration were calculated.

2.2. Reagents and chemicals

All chemicals used were of analytical reagent grade without further purification. The negatively charged sulfate-stabilized polystyrene (PS) particles (wt 10%, average diameter 3 μm), Poly (allylamine hydrochloride) (PAH, $M_w = 70{,}000\ g\ mol^{-1}$), and poly (sodium 4-styrenesulfonate) (PSS, $M_w = 70{,}000\ g\ mol^{-1}$) were also obtained from Sigma–Aldrich and used as received. The PAH and PSS deposition solution was prepared to a polymer concentration of 2 mg/mL in 0.2 M sodium chloride. Rabbit IgG (10 mg), goat-anti-rabbit IgG (1.5 mg/mL), and goat-anti-rabbit IgG/FITC conjugate (1.5 mg/mL), human IgG (10 mg), goat-anti-human IgG (1.5 mg/mL) and goat-anti-human IgG/FITC conjugate (1.5 mg/mL) were obtained from Beijing Dingguo Biotechnology Ltd., China. Bovine serum albumin (BSA, 5 g) was obtained from Genview. Bovine viral diarrhea virus (BVDV, 2 mg/mL) stocks and FITC labeled pig anti-BVDV (1.5 mg/mL) were obtained from Changchun Commodity Inspection Bureau. Hydroxypropyl methyl cellulose (HPMC) was obtained from Shandong Tairui Chemical Co. China. All antigen powders were diluted by 2 mmol/L phosphate buffered saline solution (PBS, pH 7.4) to obtain 1 mg/mL solution and all the solutions were stored at 0–4 °C, diluted only prior to immediate use. The water used in all experiments had a resistivity higher than 18 MΩ cm.

2.3. Microchip device and detection

The integrated microfluidic chip laser-induced fluorescence (LIF) system contains a laser excitation source (488 nm, 20 mW) and four photo-multiplier tubes. For coincidence measurements, light-scattering and LIF signals were obtained simultaneously from the chip using optical fiber, filtered by 520, 600 and 650 nm filters to receive corresponding single fluorescent signals. The signals were amplified and digitized with the multifunction I/O cards.

The polydimethyl siloxane (PDMS) chips were obtained from Dalian Institute of Chemical Physics, Chinese Academy of Sciences. The channels on the microchip were 100 μm wide and 30 μm deep. Probe region was design at 50 μm down stream of the focusing chamber. The waste reservoir was grounded. HPMC (1%, v/v) solution was added from the focus reservoirs for reducing the microspheres adhesion, when sample was continuously infused into the focusing chamber.

2.4. Preparation of biofunctional fluorescent microspheres

Water-compatible CdTe quantum dots used in our studies were synthesized as described in previous papers [16]. The final nanocrystal dispersions are stable in basic aqueous solutions (pH

>6). A luminescence quantum yield of ~25% was measured for the CdTe nanoparticles at room temperature by comparing with the fluorescence emission of Rhodamine 6G [17]. Stable water-compatible 3-mercaptopropyl-capped CdTe QDs (0.3 mmol/L) with emission maximum at about 590 and 650 nm were used in the present experiments.

Fabrication of the biofunctional QD-encoded microspheres used the layer-by-layer method. The first step is the deposition of 200 μL 2 mg/mL PAH and PSS onto the PS spheres alternately [18]. Then three-layer (PAH/PSS/PAH) polyelectrolyte film provides both a smooth and uniform, positively charged outer surface to facilitate the adsorption of the negatively charged CdTe nanocrystals capped with mercaptopropyl acid utilizing the electrostatic interaction [19–23]. After each deposition, the microspheres were washed three times with 500 μL PBS by centrifugation (3000 rpm, 10 min), with sonication (1 min) between each wash step. PE_3/different color QDs layers were deposited repeatedly by using the above-mentioned procedures, thus yielding two kinds of QD-encoded fluorescent microspheres.

Then 1 mg/mL goat-anti-rabbit IgG and 1 mg/mL goat-anti-human IgG were deposited, respectively, to form the biofunctional multicolor QD-encoded fluorescent microspheres by electrostatic deposition, and the antibody layer was separated from the outermost QDs layer by $(PAH/PSS)_2$. After washed three times with 500 μL PBS and blocked by BSA solution, the two types of biofunctional QD-encoded fluorescent microspheres were stored at 4 °C before use.

2.5. Sandwich immunoassay on the QD-encoded microspheres

The sandwich immunoassay was adopted to test the bioactivity of biofunctional QD-encoded fluorescent microspheres. The biofunctional multicolor microspheres and different concentration antigen solutions were mixed and incubated on a shaker for 3 h, and then wash steps were carried out twice to remove the unbound antigens. The QD-encoded $microspheres_1$/goat anti-rabbit IgG/rabbit IgG and QD-encoded $microspheres_2$/goat anti-human IgG/human IgG immunocomplexes can be obtained. Then corresponding FITC-labeled antibodies (goat-anti-rabbit IgG/FITC and goat-anti-human IgG/FITC) with the concentration of 1 mg/mL were added to the microspheres immunoassay system, respectively. The reaction mixture was incubated with gentle vortex for 3 h and followed by centrifugation (3000 rpm, 10 min). After centrifugation, the microspheres were resuspended in PBS buffer for further studies.

To avoid the influence of free IgG (goat-anti-rabbit IgG or goat-anti-human IgG) in the solution of QDs labeled IgG on the immunoreaction of rabbit IgG (or human IgG)/goat-anti-rabbit IgG (or goat-anti-human IgG)/fluorescent microspheres with QDs labeled IgG, we employed FITC labeled IgG in the sandwich structure to identify a hit for the IgG. Furthermore, two QDs and one organic dye in this sandwich structure can also be excited simultaneously by a single wavelength, and the use of organic dye does not affect the multiplexed bioanalysis.

3. Results and discussion

3.1. The fluorescence spectra of multicolor QD-encoded microspheres

Evidence for the formation of PE/CdTe QDs multilayer films on microspheres was provided by fluorescence spectroscopy. Fig. 1 shows the fluorescence emission spectra of the QDs-encoded microspheres. It can be seen that the first deposited QDs layer (590 nm emission) on the microspheres generated a luminescence peak. Then PAH/PSS/PAH/QDs (650 nm emission) layers were assembled for the followed deposition cycle. With the number of QDs (650 nm emission) adsorbed layers increasing, the luminescence peak at 650 nm emerged and grew obviously. The luminescence peak at 590 nm decreased slowly due to the deposited PE layers, which weakened the inner QDs (590 nm emission) fluorescence. The red shift in the peak emission of the CdTe QDs in the multilayer shell was also observed in Fig. 1. This is due to enhancement of directional polarizability of molecules around, when the carboxyl on the water-compatible CdTe QDs bound with PAH layer. As shown in Fig. 1, PS microspheres can be coated with the nearly code 10:0, 8:3, 6:6, 4:8 as well as 12:3 (the relative intensities ratio of fluorescence peaks). We chose fluorescent PS microspheres with the code 6:6, 4:8 and 12:3 for the further use.

3.2. Immunoreaction on the surface of biofunctional QD-encoded microspheres

The immunoreactions between antibodies immobilized on the functional microspheres and antigens can be confirmed

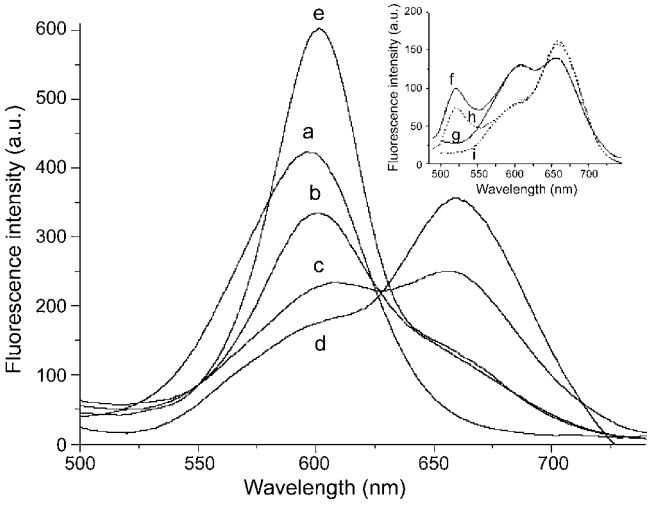

Fig. 1. Fluorescence emission spectra of QD-encoded PS microspheres: $PE_3/QDs_{590\ nm}$ multilayer films with the code 10:0 (a); $PE_3/QDs_{590\ nm}/PE_3/QDs_{650\ nm}$ multilayer films with the code 8:3 (b); $PE_3/QDs_{590\ nm}/(PE_3/QDs_{650\ nm})_2$ multilayer films with the code 6:6 (c); $PE_3/QDs_{590\ nm}/(PE_3/QDs_{650\ nm})_3$ multilayer films with the code 4:8 (d) and $(PE_3/QDs_{590\ nm})_2/PE_3/QDs_{650\ nm}$ multilayer films with the code 12:3 (e). The inset shows the fluorescence spectra of fluorescent microspheres (code 6:6) after immunoreaction (f); no rabbit IgG added (g); the fluorescent microspheres (code 4:8) after immunoreaction (h) and no human IgG added (i). Excitation wavelength is 465 nm. The concentrations of microspheres are 1 μg/mL. The concentrations of FITC labeled antibody are 1 mg/mL.

in this study. For this purpose, antigens of rabbit IgG and human IgG were added to the systems of functional fluorescent miscrospheres with goat-anti-rabbit IgG and goat-anti-human IgG, respectively. Then, FITC-labeled goat-anti-rabbit IgG and FITC-labeled goat-anti-human IgG antibodies were added, respectively. If the immunoreactions between antibodies immobilized on the functional fluorescent microspheres and antigens occurred, the FITC-labeled antibodies can be captured by antigen which was on the surface of biofunctional QD-encoded fluorescent microspheres. From the inset of Fig. 1, it can be seen that the green emitting FITC peak (520 nm) of FITC labeled goat-anti-rabbit IgG appeared in the fluorescence spectra of rabbit IgG/goat-anti-rabbit IgG/fluorescent microspheres with the code 6:6 system obviously, and the green emitting FITC peak of FITC labeled goat-anti-human IgG also appeared in the fluorescence spectra of human IgG/anti-human IgG/fluorescent microspheres with the code 4:8 system.

PBS with no antigen was added to the biofunctional QD-encoded microspheres as non-specific binding control. After incubated with corresponding FITC-labeled antibodies and washed, no FITC signal was found in the fluorescence emission spectra of the biofunctional microspheres with the code 6:6 and 4:8 (see Fig. 1). It indicates that the immunoreaction between QD-encoded fluorescent microspheres/antibodies and antigens really occurred on the surface of fluorescent microspheres in this study.

3.3. Detection with the microfluidic on-chip device

Figs. 2 and 3 show typical scatter/fluorescence coincidence data when the QD-encoded fluorescent microspheres flowed through the channel of microchip. Each peak in the scatter channel represents a microphere passing through the interrogation region. The fluorescent signals can be detected by 520, 600 and 650 nm channels synchronously. From Fig. 2a, it can be seen that the fluorescent signals of functional fluorescent microspheres (code 6:6) with goat-anti-rabbit IgG can be observed at 600 and 650 nm channel, respectively. But no fluorescent signal was detected at 520 nm channel. When the system of fluorescent microspheres (code 6:6)/goat-anti-rabbit IgG/rabbit IgG/FITC labeled goat-anti-rabbit IgG flowed on the microchip, the fluorescent signal of FITC labeled goat-anti-rabbit IgG at 520 nm can be detected (see Fig. 2b). It indicates that the FITC labeled goat-anti-rabbit IgG was captured by the rabbit IgG on the surface of functional fluorescent microspheres. It also demonstrates that the immunoreactions between goat-anti-rabbit IgG and rabbit IgG, rabbit IgG and FITC labeled goat-anti-rabbit IgG occurred on the surface of the functional fluorescent microspheres.

The same phenomenon can be observed for the functional microspheres (code 4:8) with goat-anti-human IgG. When fluorescent microspheres (code 4:8) with goat-anti-human IgG flowed on the microchip, the fluorescent signals can be observed at 600 and 650 nm channel, respectively. But no fluorescent

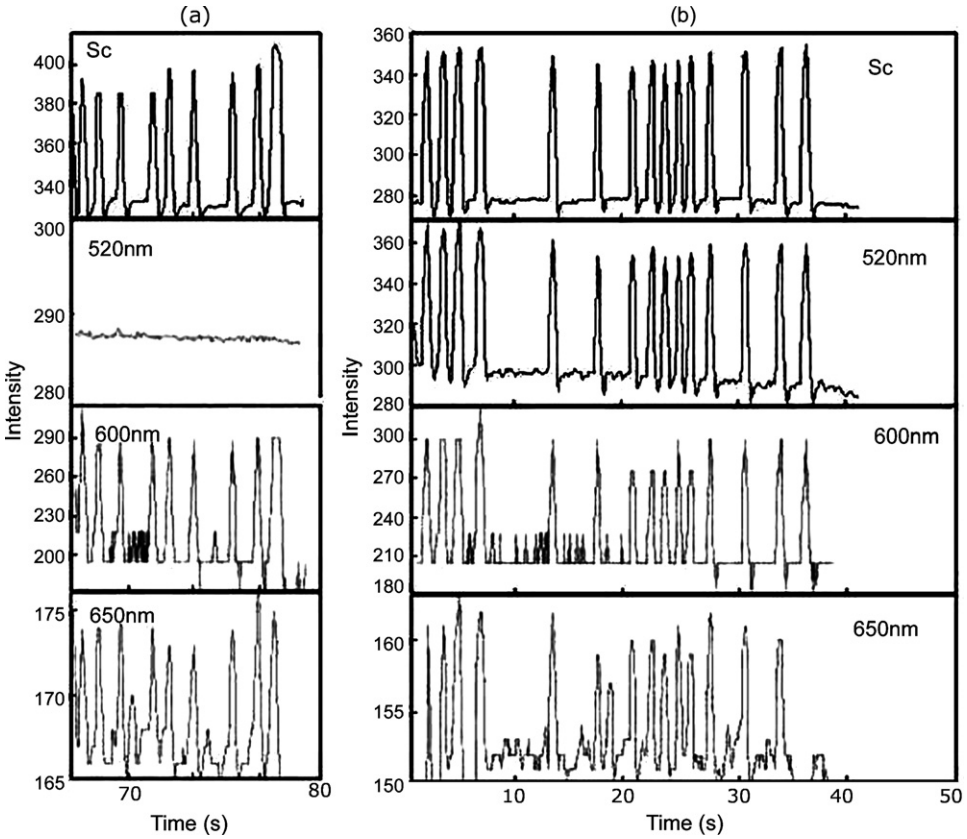

Fig. 2. (a) Light scattering (Sc) and fluorescence signals of 1 μg/mL fluorescent microspheres (code 6:6) with goat-anti-rabbit IgG system flowed on the microchip. (b) Light scattering (Sc) and fluorescence signals of 1 μg/mL fluorescent microspheres (code 6:6)/goat-anti-rabbit IgG/rabbit IgG/FITC labeled goat-anti-rabbit IgG system flowed on the microchip.

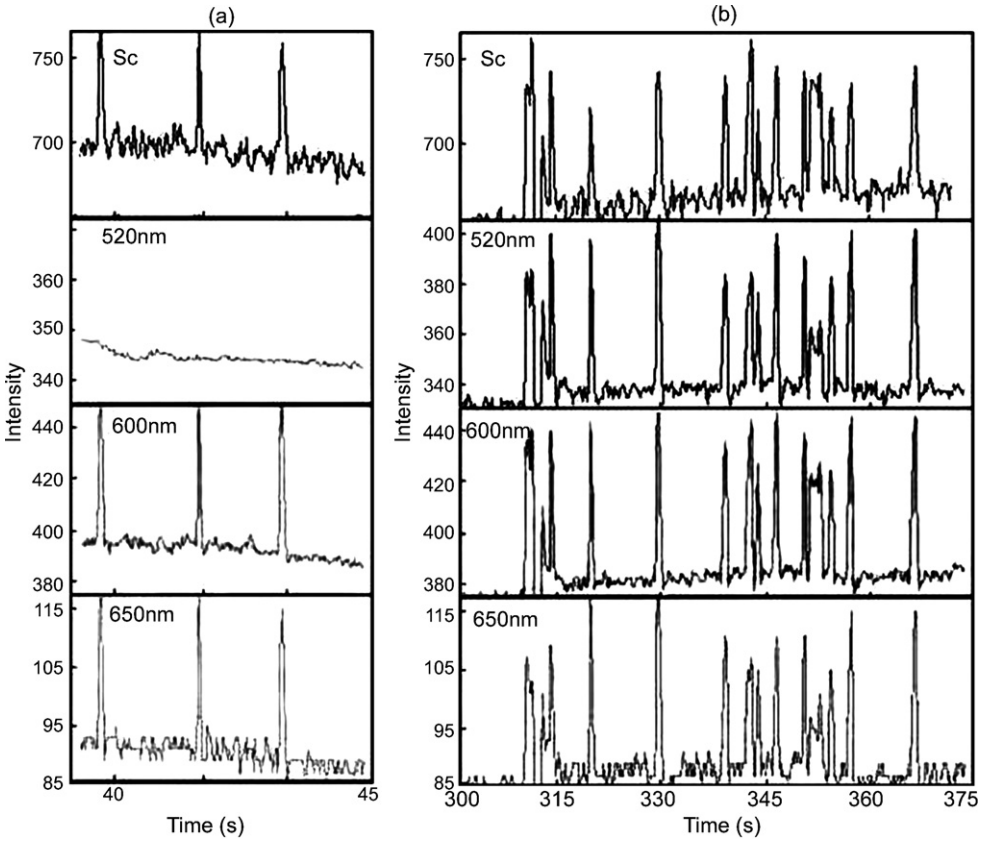

Fig. 3. (a) Light scattering (Sc) and fluorescence signals of 1 μg/mL fluorescent microspheres (code 4:8) with goat-anti-human IgG system flowed on the microchip. (b) Light scattering (Sc) and fluorescence signals of 1 μg/mL fluorescent microspheres (code 4:8)/goat-anti-human IgG/human IgG/FITC labeled goat-anti-human IgG system flowed on the microchip.

signal was detected at 520 nm channel. When the system of fluorescent microspheres (code 4:8)/goat-anti-human IgG/human IgG/FITC labeled goat-anti-human IgG flowed, the fluorescent signal of FITC labeled goat anti-human IgG at 520 nm can be detected (see Fig. 3b). This also confirms the immunoreaction on the surface of the functional fluorescent microspheres.

3.4. Sandwich immunoassay for the detection of rabbit IgG and human IgG

In order to detect rabbit IgG and human IgG, different concentrations of free rabbit IgG and human IgG were added to the biofunctional fluorescent microspheres (code 6:6 and 4:8) with goat-anti-rabbit IgG and goat-anti-human IgG, respectively. Fluorescent intensities were measured after the corresponding FITC-labeled goat-anti-rabbit IgG or FITC-labeled goat-anti-human IgG antibodies were added. Figs. 4 and 5 show the fluorescence emission spectra of the sandwich immunoassay. For the system of fluorescent microspheres (code 6:6)/goat-anti-rabbit IgG/rabbit IgG/FITC labeled goat-anti-rabbit IgG, it can be seen that the fluorescent intensity of FITC labeled goat-anti-rabbit IgG at 520 nm increased gradually with the increasing concentration of rabbit IgG added (see Fig. 4), the ratio of the fluorescent intensity at 520 nm and encoded microspheres ($I_{520\,nm}/I_{609\,nm}$) increases linearly with the increasing concentration of rabbit IgG in the range

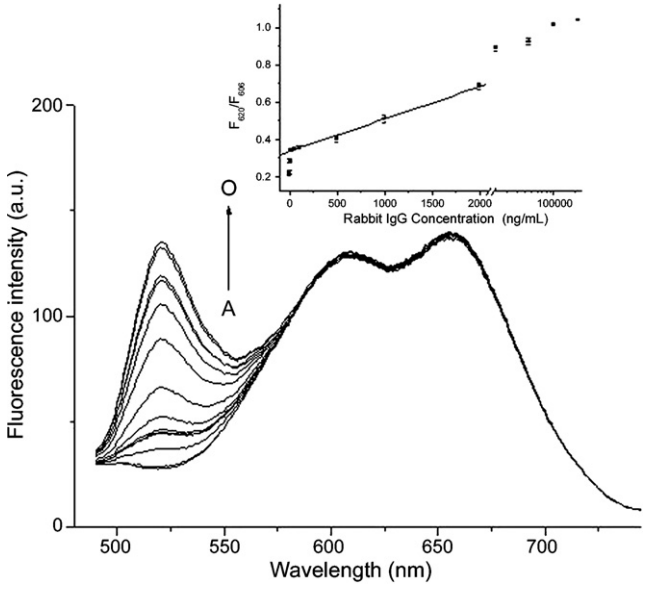

Fig. 4. The fluorescence emission spectra of 1 μg/mL fluorescent microsphere (code 6:6) in the sandwich assay with a series of different concentration of rabbit IgG added: (A) 0 ng/mL; (B) 1 ng/mL; (C) 5 ng/mL; (D) 10 ng/mL; (E) 20 ng/mL; (F) 50 ng/mL; (G) 100 ng/mL; (H) 500 ng/mL; (I) 1 μg/mL; (J) 2 μg/mL; (K) 10 μg/mL; (L) 20 μg/mL; (M) 50 μg/mL; (N) 100 μg/mL and (O) 200 μg/mL rabbit IgG. The inset shows the linearly relation between concentration of rabbit IgG and fluorescent intensity. The error bars show the standard deviations obtained from multiple experimental repeats ($n = 3$).

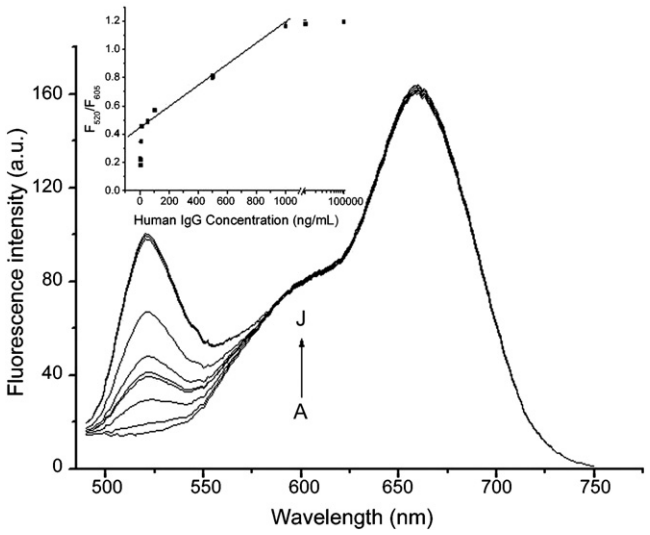

Fig. 5. The fluorescence emission spectra of 1 μg/mL fluorescent microsphere (code 4:8) in the sandwich assay with a series of different concentration of human IgG added: (A) 0 ng/mL; (B) 1 ng/mL; (C) 5 ng/mL; (D) 10 ng/mL; (E) 50 ng/mL; (F) 100 ng/mL; (G) 500 ng/mL; (H) 1 μg/mL; (I) 10 μg/mL and (J) 100 μg/mL human IgG. The inset shows the linearly relation between concentration of human IgG and fluorescent intensity. The error bars show the standard deviations obtained from multiple experimental repeats ($n = 3$).

of 10–2000 ng/mL. The linear regression equation is as follows: $I_{520\,nm}/I_{609\,nm} = 0.338 + 1.71 \times 10^{-4}\, C_{R\text{-}IgG}$ (ng/mL), and the coefficient of correlation is 0.999, the detection limits of this assay is 5.8 ng/mL rabbit IgG.

As for the system of fluorescent microspheres (code 4:8)/goat-anti-human IgG/human IgG/FITC labeled goat-anti-human IgG, the fluorescent intensity of FITC labeled goat-anti-rabbit IgG at 520 nm also increased linearly with the increasing concentration of human IgG in the range of 5–1000 ng/mL (see Fig. 5). The linear regression equation is as follows: $I_{520\,nm}/I_{609\,nm} = 0.476 + 6.88 \times 10^{-4}\, C_{H\text{-}IgG}$ (ng/mL) and the coefficient of correlation is 0.997, the detection limits of this assay is 1.5 ng/mL human IgG.

3.5. The detection of bovine viral diarrhea virus

Biofunctional QD-encoded fluorescent microspheres (code 12:3) were prepared as described above, with different amounts of bovine viral diarrhea virus coupled to the microspheres. BVDV-modified microspheres were blocked by BSA and washed before detection. Fluorescent intensities were measured after the FITC-labeled pig-anti-BVDV was added to the QD-encoded fluorescent microspheres solution. Fig. 6 shows the fluorescence emission spectra of the immunoreaction system. It can be seen that the fluorescent peaks of FITC-labeled pig-anti-BVDV at 520 nm can be observed over a concentration range of BVDV from 20 to 1000 ng/mL. The fluorescent intensity at 520 nm increases with the increasing concentration of BVDV. It indicates that the FITC-labeled pig-anti-BVDV was captured on the surface of the functional fluorescent microspheres. This result also suggests that the QD-encoded fluorescent microspheres could be used in fluoroimmunoassays for real sample.

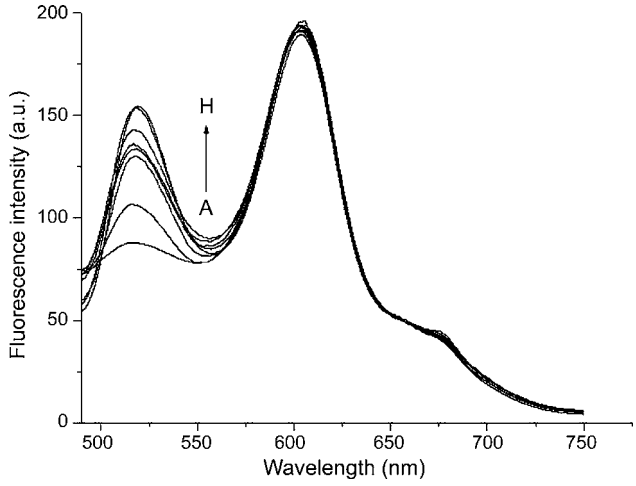

Fig. 6. The fluorescence emission spectra of 1 μg/mL fluorescent microsphere (code 12:3) in the fluoroimmunoassay with a series of different concentration of BVDV added: (A) 20 ng/mL; (B) 40 ng/mL; (C) 60 ng/mL; (D) 100 ng/mL; (E) 200 ng/mL; (F) 400 ng/mL; (G) 600 ng/mL and (H) 1000 ng/mL.

4. Conclusions

In the present study, multicolor QD-encoded fluorescent microspheres were prepared by deposition of different colors water soluble CdTe QDs through layer-by-layer self-assembly. This method avoids elaborate chemical reactions, and it is easy to control the QD-loading and microspheres composition. The CdTe QDs used here were prepared in aqueous solution. It can labels biomolecules such as protein without any post-preparative treatment. The biofunctional QD-encoded fluorescent microspheres were used to detect different antigens effectively in fluro-immunoassays in this study. In comparison with other fluorescent microsphere-based immunoassays, the use of QDs provides a new approach to make probes that fluoresce at different wavelengths with a single excitation wavelength. It will be particularly useful in the development of fluoroimmunoassays and immunosensor devices. Thus, the multicolor QD-coded fluorescent microspheres can be visualized as a fluorescent label for sensitive detections using suspension arrays or microinfludic devices.

Acknowledgements

This work was financially supported by the National Natural Science Foundation of China (No. 20075009, No. 20475020). The authors thank Prof. Shuming Nie (Wallace H. Coulter Department of Biomedical Engineering, Emory University and Georgia Institute of Technology) for the helpful suggestions.

References

[1] E.E. Swartzman, S.J. Miraglia, J. Mellentin-Michelotti, L. Evangelista, P.M. Yuan, Anal. Biochem. 271 (1999) 143.
[2] D.J. Graves, H.J. Sue, S. Addya, S. Surrey, P. Fortina, Biotechniques 32 (2002) 346.
[3] G.T. Hermanson, Bioconjugate Techniques, Academic Press, London, UK, 1996 (Chapter 8).

[4] E.R. Goldman, E.D. Balighian, H. Mattoussi, M.K. Kuno, J.M. Mauro, P.T. Tran, G.P. Anderson, J. Am. Chem. Soc. 124 (2002) 6378.
[5] M.Y. Han, X.H. Gao, J.Z. Su, S.M. Nie, Nat. Biotechnol. 19 (2001) 631.
[6] Y.P. Ho, M.C. Kung, S. Yang, T. Wang, Nano Lett. 5 (2005) 1693.
[7] K.L. Kellar, J. Clin. Ligand. Assay 26 (2003) 76.
[8] D.A. Vignali, J. Immunol. Methods 243 (2000) 243.
[9] J.P. Nolan, I.A. Sjlar, Trends Biotechnol. 20 (2002) 9.
[10] K.L. Kellar, M.A. Iannone, Exp. Hematol. 30 (2002) 1227.
[11] V. Stsiapura, A. Sukhanova, M. Artemyev, M. Pluot, J.H.M. Cohen, A.V. Baranov, V. Oleinikov, I. Nabiev, Anal. Biochem. 334 (2004) 257.
[12] W.J. Parak, D. Gerion, D. Zanchet, A.S. Woerz, T. Pellegrino, C. Micheel, S.C. Williams, M. Seitz, R.E. Bruehl, Z. Bryant, C. Bustamante, C.R. Bertozzi, A.P. Alivisatos, Chem. Mater. 14 (2002) 2113.
[13] Y.C. Cao, Z.L. Huang, T.C. Liu, H.Q. Wang, X.X. Zhu, Z. Wang, Y.D. Zhao, M.X. Liu, Q.M. Lu, Anal. Biochem. 35 (2006) 193.
[14] D.Y. Wang, A.L. Rogach, F. Caruso, Nano Lett. 2 (2002) 857.
[15] F. Caruso, K. Niikura, D.N. Furlong, Y. Okahata, Langmuir 13 (1997) 3427.
[16] Q. Ma, X.G. Su, X.Y. Wang, Y. Wan, C.L. Wang, B. Yang, Q.H. Jin, Talanta 67 (2005) 1029.
[17] J. Georges, N. Arnaud, L. Parise, Appl. Spectrosc. 50 (1996) 1505.
[18] A. Bange, H.B. Halsall, W.R. Heineman, Biosens. Bioelectron. 20 (2005) 2488.
[19] G. Decher, Science 277 (1997) 1232.
[20] F. Caruso, R.A. Caruso, H. Mo¨hwald, Science 282 (1998) 1111.
[21] E. Donath, G.B. Sukhorukov, F. Caruso, S.A. Davis, H. Mo¨hwald, Angew. Chem. 37 (1998) 2201.
[22] F. Caruso, Adv. Mater. 13 (2001) 11.
[23] F. Caruso, M. Spasova, A. Susha, M. Giersig, R.A. Caruso, Chem. Mater. 13 (2001) 109.

Available online at www.sciencedirect.com
ScienceDirect
Talanta 72 (2007) 1507–1518
Talanta
www.elsevier.com/locate/talanta

Extraction and speciation of arsenic in plants grown on arsenic contaminated soils

Kalam A. Mir [a], Allison Rutter [b,*], Iris Koch [c], Paula Smith [c], Ken J. Reimer [c], John S. Poland [b]

[a] *Department of Chemistry, Queen's University, Kingston, ON, Canada*
[b] *School of Environmental Studies, Queen's University, Kingston, ON K7L 3N6, Canada*
[c] *Environmental Sciences Group (ESG), Royal Military College, Kingston, ON, Canada*

Received 18 October 2006; received in revised form 26 January 2007; accepted 28 January 2007
Available online 13 February 2007

Abstract

A sequential arsenic extraction method was developed that yielded extraction efficiencies (EE) that were approximately double those using current methods for terrestrial plants. The method was applied to plants from two arsenic contaminated sites and showed potential for risk assessment studies. In the method, plants were extracted first by 1:1 water–methanol followed by 0.1 M hydrochloric (HCl) acid. Total arsenic in plant and soil samples collected from contaminated sites was mineralized by acid digestion and detected by inductively coupled plasma-atomic emission spectrometry (ICP-AES) and hydride generation-atomic absorption spectrometry (HG-AAS). Arsenic speciation was done by high performance liquid chromatography coupled with HG-AAS (HPLC–HGAAS) and by HPLC coupled with ICP-mass spectrometry (HPLC–ICP-MS). Spike recovery experiments with arsenite (As(III)), arsenate (As(V)), methylarsonic acid (MA) and dimethylarsinic acid (DMA) showed stability of the species in the extraction processes. Speciation analysis by X-ray absorption near edge spectroscopy (XANES) demonstrated that no transformation of As(III) and As(V) occurred due to sample handling. Dilute HCl was efficient in extracting arsenic from plants; however, extraction and determination of organic species were difficult in this medium. Sequential extraction with 1:1 water–methanol followed by 0.1 M-HCl was most useful in extracting and speciating both organic and inorganic arsenic from plants. Trace amounts of MA and DMA in plants could be detected by HPLC–HGAAS aided by the process of separation and preconcentration of the sequential extraction method. Both organic and inorganic arsenic compounds could be detected simultaneously in synthetic gastric fluid extracts (GFE) but EEs by this method were lower than those of the sequential method. The developed sequential method was shown to be reliable and applicable to various terrestrial plants for arsenic extraction and speciation.

Keywords: Arsenic; Plants; Extraction; Speciation; Sequential extraction

1. Introduction

Arsenic has been known to be toxic since ancient times. This toxicity can make the high levels of arsenic found in plants growing on many contaminated sites [1,2] problematic for plant consumers. Many arsenic compounds present in the terrestrial and marine environments have been detected [3,4]. As(III), As(V), methylarsonic acid (MA) and dimethylarsinic acid (DMA) are the predominant arsenic species found in terrestrial biota, including plants [2,3]. Chronic exposure to arsenic, particularly inorganic arsenite (As(III)) and arsenate (As(V)), has been implicated in many physiological disorders and various types of cancers [5–7]. Since the toxicity of arsenic is dependent on its chemical form, both speciation and quantitative determination of arsenic are essential [8–10]. Furthermore, arsenic must be extracted from solid samples and presented in an aqueous form for speciation analysis by the more common methods such as high performance liquid chromatography (HPLC) with element specific detection [3,11]. The extraction of arsenic from solid matrices is a critical step since high recoveries as well as species preservation are required [3,11–14]. The diversity of arsenic and plant species in the environment as well as locations of sampling only further complicate the situation [15–18].

Solvent extractions aided by physical shaking or sonication have been the traditional methods for extracting arsenic from the solid matrices. A number of extraction methods are based

* Corresponding author. Tel.: +1 613 533 2642; fax: +1 613 533 2897.
E-mail address: ruttera@biology.queensu.ca (A. Rutter).

0039-9140/$ – see front matter © 2007 Elsevier B.V. All rights reserved.
doi:10.1016/j.talanta.2007.01.068

on mixtures of methanol and water, a relatively mild extractant, aimed at maintaining the integrity of arsenic species in the samples [3]. Despite the popularity of methanol–water as an extractant for most terrestrial plants, it has a poor extraction efficiency [12,16–18]. Dilute (0.3 M) phosphoric acid was found to be a convenient extractant of arsenic species from terrestrial plants [15]. Combinations of acetonitrile–water [13,14] and methanol–water–chloroform [10] have been used as well. Extraction efficiency varies widely depending on matrix and extractant.

Pressurized liquid extraction (PLE), also known as accelerated solvent extraction (ASE), is a rapid technique of solvent extraction at elevated pressure and temperature. The extraction efficiencies of PLE varied widely depending on sample matrix; extraction efficiencies of 80–102% for freeze-dried carrots [13], 33% for rice [19] and 30% for fresh plant materials [20] were obtained. Modification of sample matrix with chemical reagents such as acid [14,19] and base [14] for the improvement of extraction efficiency is another approach that may, however, compromise species integrity.

Enzymes such as alpha-amylase for cellulose have also been used for the modification of the plant matrices [13,19,21]. Treatment by the cellulase yielded an extraction efficiency of 104% for freeze-dried apples [13] and 59% for rice samples [19]. The enzymatic treatment did not improve the extraction efficiency in seaweed (kelp) [21] and enzymes are generally expensive.

Even if all the arsenic in a sample can be extracted and characterized, the toxicological risk of arsenic to either humans or ecological receptors is dependent on its bioavailability. Bioaccessibility, the fraction of a dose that is soluble in the gastrointestinal environment [22] is considered to be a good estimate of arsenic bioavailability, since dissolved arsenic is almost completely absorbed into the bloodstream from the gastrointestinal tract [23]. Most bioaccessibility methods involve the extraction of a matrix (predominantly soils) with synthetic gastric fluid (e.g., diluted HCl at pH 1.5–4.0) at typical solid/liquid mixtures (e.g., 1:100) and at body temperature (37 °C for humans) for appropriate lengths of time (1 h for gastric phase, 4 h for small intestinal phase) [24–27]. Bioaccessibility ranges widely for soils (<1–100%) and may be linked to pH and iron oxide content; ranges are smaller for algae (30–80%) and are dependent on algal species [27].

Although many individual plant species and foods have been extracted using the various methods, there remains a need for more effective extraction methods that can be applied to terrestrial plants [3,28]. The goal of the present work was to develop more effective but simple methods for arsenic extraction from terrestrial plants, particularly for plants from sites with high levels of arsenic contamination. In order to be applicable to risk assessment approaches to arsenic impacted sites, these methods need to be highly reproducible, rugged, and use instrumentation that is readily available, and cost effective, in commercial laboratories. In the present study, various extractants were tested for arsenic extraction, and a sequential extraction method with 1:1 water–methanol and dilute HCl was developed and applied to extract and speciate arsenic from terrestrial plant samples.

2. Experimental section

2.1. Reagents and apparatus

All solutions were prepared with distilled deionized water (DDW) (Barnstead, E-pure, 18 MΩ or Millipore 18 MΩ). Methanol was Fisher Scientific pesticide or HPLC grade. ICP-AES standards were procured from commercial sources. HNO_3 and HCl were ACS reagents from Fisher Scientific. H_3PO_4, NH_3 and HCl used for HPLC–HGAAS experiments were Fluka analytical reagents. $NaBH_4$ (BDH analytical reagent) solutions were prepared fresh before each analysis. Arsenic standards were procured from commercial vendors. Arsenic species standards were from different sources; As(III) was from arsenic oxide AAS standard (SCP Science and Fluka Chemica), As(V) was from sodium arsenate ($Na_2HAsO_4{\cdot}7H_2O$, Sigma–Aldrich), MMA was monomethylarsonic acid (CH_5AsO_3, Pfaltz and Bauer), DMA was dimethylarsinic acid (cacodylic acid, $C_2H_7AsO_2$, Fluka Chemica).

The plant samples were weighed in 15 mL extraction tubes (Corning plastic), mixed with solvent by vortexing (Thermolyne Maxi Mix II) and sonicated in a Fisher Scientific FS 28 (50/60 Hz) sonicator. Solid and liquid phases were separated by centrifuging at 3000 rpm (IEC/Centra®/MP4 International Equipment Company, USA). The HG-AAS analysis for total arsenic was carried out with an AA/AE spectrophotometer (Instrumentation Laboratory, Allied Analytical Systems, USA) equipped with a vapor generation accessory (VGA-76, Varian) for hydride generation and separation; atomization was performed in an air–acetylene flame. The ICP analyses were conducted by a simultaneous ICP-AES instrument (VISTA AX CCD, Varian). HPLC–HGAAS experiments were performed using an anion exchange column (Hamilton PRP-x100 250 mm × 4.6 mm). Mobile phase was 20 mM ammonium phosphate buffer at pH 6.0 and flow rate 1.5 mL min^{-1}. Arsines were detected by a SOLAAR 969 AAS instrument equipped with VP90 vapor generator accessory, an EC90 furnace and quartz T-tube and run using SOLAAR software (Thermo Instruments, Canada). HPLC–ICPMS analyses were performed by connecting the HPLC to a PQ Excell ICPMS. All instrument operating conditions were given elsewhere [29].

2.2. Samples

Plant samples used for the method development were collected from an abandoned gold mining area at Deloro, ON, Canada. The plant samples used to test the developed sequential extraction method were from Deloro and from gold mining areas in Yellowknife, NWT, Canada. Plant samples were hand picked and stored for 1–3 days in plastic bags at 4 °C until processing. Surface (0–10 cm) soil samples from Deloro were collected in Whirlpaks® and stored at 4 °C. Plants were cut to remove roots from stems and washed with copious amounts of distilled water to remove the adhered soil and dust particles. Washed plant and soil samples were air dried in the laboratory. Dried plants were ground with a laboratory grinder and were stored in plastic bags in the freezer for up to one year at −20 °C to ensure stability

of the arsenic species. Dried soil samples were homogenized by mortar and pestle before sampling for analysis.

3. Determination of total arsenic

Total arsenic in all plant and soil samples was determined by acid digestion. Portions of ground plant samples were weighed accurately (0.5 ± 0.0001 g) in 30 mL Vycor® glass crucibles and ashed in the muffle furnace (Isotemp® Programmable Muffle Furnace, Fisher Scientific) using a temperature ramp to 500 °C. The ashed plant samples were digested with 4 mL 1:3 HNO_3/HCl (aqua regia) solution for 4 h on a hot plate under watch glass covers. After removing the watch glass covers, 2–3 drops of 50% H_2O_2 were added and the volumes reduced to approximately 2 mL. All samples were then quantitatively transferred to graduated glass tubes and volumes were made up to 12.5 mL with DDW, filtered (Fisherbrand® Quantitative, medium porosity) and analyzed by ICP-AES or HG-AAS depending on arsenic concentration. All dissolved arsenic in the calibration standards and sample solutions were reduced to As (III) in the prereduction step using hydroxylamine hydrochloride (masking agent), potassium iodide and concentrated HCl to ensure maximum HG-AAS sensitivity. HG-AAS was used for the low arsenic samples because of its higher sensitivity. Certified reference plant materials (CRM GBW 07603: Bush Branches and Leaves and SRM NIST 1575: Pine Needles) were analyzed following the above procedure. Dried soil samples (0.5 ± 0.0001 g) were digested with 8 mL aqua regia solution overnight in graduated digestion tubes heated on an aluminum block. Digested residues were made up to 25 mL with DDW and after filtration analyzed by ICPAES. The 1:1 water–methanol extracts in batches were completely dried at ∼60 °C in an oven to remove solvent and regenerated in distilled-deionized water (DDW) in preparation for total arsenic analysis and speciation. All other extracts were analyzed directly by HGAAS, ICPAES or HPLC–HGAAS.

4. Extraction of arsenic from plants

4.1. Solvent-sonication extraction

The solvents used to extract arsenic from plant matrices were water (DDW), methanol, 1:1 water/methanol, 0.1 M-, 0.05 M-, 0.02 M- and 0.01 M-HCl solutions, and 0.1 molar sodium hydroxide (M-NaOH). Initially, 0.5 g, and after method optimization 0.25 g, of powdered samples were accurately weighed into 15 mL extraction tubes and 10 mL of extractant was introduced to the samples. After closing the lids securely, samples and extractants were mixed thoroughly by a vortex apparatus for a minute. The samples were then sonicated for 20 min in the first step of extraction. The resulting mixtures were centrifuged at 3000 rpm for 10 min for all extraction steps. In the subsequent steps of extraction, undissolved sample matrices that settled at the bottom of the tube due to centrifugation were redispersed into the extractant solvent by vortexing and tapping/shaking if necessary, and were sonicated for 10 min. The supernatant solutions from centrifugation from each step were collected in respective sample vials. Extraction of samples was carried out five times (5 steps) initially, and then three times (3 steps) after method optimization. The extraction solutions were filtered before analysis. After the initial trial of the time-consuming roto-evaporation technique, the 1:1 water–methanol extracts were dried in batches in the oven (∼65 °C) to remove methanol and regenerated in smaller volume (3–5 mL) of DDW than the extractant volume (30 mL). Spike recoveries were not affected by this process; the individual standard spike results were within ±10% of the introduced concentrations. The drying and regeneration processes improved the detection limits of the trace organic species by a factor of ten.

4.2. Solvent-Soxhlet extraction

The powdered samples, 0.5 or 0.25 g portions, were accurately weighed into cellulose thimbles (Fisherbrand® 25 mL) for Soxhlet extraction. About 70 mL solvent was employed in 125 mL distillation flasks and heated on electric coils to achieve four cycles per hour. Water (DDW), methanol and 1:1 water–methanol were used as solvents for Soxhlet extractions that lasted for 6 h for each batch. Exhaustive Soxhlet extraction was demonstrated by extracting for 2, 4, 6 and 12 h with water as solvent.

4.3. Gastric fluid extraction (GFE)

GFE was carried out using synthetic gastric fluid solution consisting 1.25 g L^{-1} pepsin (Sigma P7000: activity 1:10000) and 8.77 g L^{-1} NaCl. The pH of solution was adjusted to 1.8 with concentrated HCl [30]. Powdered plant samples were weighed (0.5 ± 0.0001 g) into 50 mL centrifuge tubes and 20 mL portions of gastric fluid were added. The samples were vortexed for one minute and then shaken at 250 rpm for 60 min at 37 °C in an incubator shaker (Innova Refrigerated Incubator Shaker, Brunswick). The resulting solutions were centrifuged at 3000 rpm for 10 min and the supernatants were decanted in 100 mL plastic bottles. The extracts were filtered and analyzed for total arsenic and arsenic species.

5. Arsenic speciation analysis (HPLC–HGAAS)

Standards and plant extracts were introduced in a 100 μL sample loop using 1 mL syringes fitted with the syringe filters (Millipore Milex-HV Hydrophilic PVDF 0.45 μm) and injected into the HPLC column. The elution order in retention time was As(III) < DMA < MA < As(V), as reported in Fig. 3(A). Hydride generation was achieved by mixing the eluent from HPLC column with 1 M-HCl and 1% $NaBH_4$ stabilized in 0.1% NaOH. HPLC chromatograms were generated from AAS data by using a macro in MS Excel. Mixed standards of As(III), As(V), MA and DMA were prepared from concentrated stocks in 50, 100, 200 and 500 μg L^{-1} concentrations by mixing appropriate volumes in DDW. Identification of arsenic species in extracts was accomplished by matching the peak retention times of standards with those in the sample extracts. The reliable detection limits (RDL = 2(t-stat)(S.D.)) were determined to be 7, 31, 15 and

14 μg L^{-1} for As(III), As(V), MA and DMA, respectively. The *t*-stat is the value (at $n-1$ degree of freedom and single-sided 95% confidence limit) taken from Student's *t*-table and S.D. is standard deviation of *n* (8) replicate runs of the lowest concentration (50 μg L^{-1}) of calibration standards.

6. Quality assurance and quality control (QA/QC)

The sample preparations and analytical procedures were accompanied by blanks and spiked standards. Samples were analyzed in two or three independent replicates to ascertain reproducibility of the analytical results. The number of duplicates and blanks in each analysis ranged from 15% to 25% of the samples analyzed. Sample and spike concentrations were calculated using linear equations ($r^2 \geq 0.999$) obtained from the external calibration curves. The total amounts of arsenic in a number of reference materials [CRM GBW 07603 Bush Branches and Leaves, 1.25 μg g^{-1} total As; SRM NIST 1575 Pine Needles, 0.21 μg g^{-1} total As; and IAEA-140/TM Seaweed (*Fucus* sp.), 42.2–46.4 μg g^{-1} total As] were determined. The four-point linear calibration range of ICP-AES was 0.10–5.0 μg g^{-1}. Except for the concentrations close to the detection limits, results were within 10% of the certified values.

The results of total arsenic in a number of plants determined by the ashing and aqua regia digestion method and a concentrated HNO_3 acid digestion method [31] were compared. The concentrations of arsenic of the CRM by the wet method ranged from 90% to 100% of the certified results and no significant difference was found between the results from the two methods; and therefore the ashing method that removed plant organic materials by dry ashing was used as it was more convenient to follow in this lab than the wet HNO_3 method.

Mass balance experiments comprising determinations of arsenic in the extracts and plant residues accounted for the total arsenic (99–111% recovery) and showed insignificant loss or gain of arsenic during analyses involving several steps.

7. X-Ray absorption near-edge spectroscopy (XANES)

XANES spectra of plant samples containing arsenic levels above the XANES detection limit of approximately 10 μg g^{-1} were collected at the bending magnet beamline of Pacific Northwest Consortium Collaborative Access Team (PNC-CAT), Sector 20, at the Advanced Photon Source, Argonne National Laboratory in Illinois [32].

Subsamples were loaded into wells of an aluminum sample holder, and sealed in place using Kapton^{TM} tape. The plate containing the samples was positioned in the path of the X-ray beam, at a 45° angle to both the beam and the detector (the latter was positioned 90° to the beam). A silicon (1 1 1) double-crystal monochromator (resolution ~5000 E/dE at 12 keV, detuned to 85% of maximum at 12,100 eV) and a rhodium-coated harmonic rejection mirror provided X-rays for measurement. The monochromator was calibrated using the gold L3 absorption edge (11919.7 eV)) [33] for measurements at the arsenic K-edge (11,868 eV). Incident X-ray beam size was defined by a 1 mm vertical and 4 mm horizontal slit after the mirror. Nitrogen-filled transmission ionization chambers were present before and after the samples for normalization to the incident intensity and transmission measurements, respectively. Fluorescence data were collected using a solid-state Ge(Li) detector (Canberra model GL0055PS) or an argon-filled fluorescence ionization chamber. Typically, five scans were collected and averaged before background-removal and normalization-to-edge-jump. The WinXAS program [34] was used for processing the spectra.

8. Results and discussion

8.1. Extraction efficiencies of solvents by Soxhlet and sonication processes

Arsenic concentrations in soil samples collected from the Deloro site ranged from 335 to 100,000 μg g^{-1}. The very high As concentration was found in the soil of an arsenic tailing pond near the gold mining and processing area. Plant samples had concentrations ranging from 2.3 to 241 μg g^{-1} (dry weight) arsenic. Three plants were selected for further extraction experiments because the species were representative of plants grown on the arsenic contaminated soils at this site and because their high concentration would simplify the analysis of arsenic species within the plant. The three Deloro plants were P-1, field horsetail (*Equisetum arvense*, 241 μg g^{-1} total As), P-3, an alkali grass (*Puccinellia* sp., 146 μg g^{-1} total As) and P-6, variegated horsetail (*Equisetum variegatum*, 24.4 μg g^{-1} total As).

Soxhlet and sonication methods are used in the extraction of metals from plant matrices [35,36]. Of the two, currently the sonication technique has been more commonly employed in toxic metal extractions [3]. The extraction efficiency (EE) of a particular solvent is defined as the percentage of total arsenic extracted by the solvent from a plant sample. Results of extraction experiments for a number of solvents are shown in Figs. 1 and 2 for the Soxhlet and sonication experiments, respectively. Of the three solvents tested in the 6-h Soxhlet extractions, water extracted the most arsenic from the plant samples. In contrast, methanol showed considerably lower extraction efficiencies (Fig. 1).

Fig. 2 illustrates extraction efficiencies for solvent–sonication extractions using methanol, 1:1 water/methanol, water (DDW), GFE extractant, and 0.1 M-NaOH and HCl solutions of 0.1 M-, 0.05 M-, 0.02 M- and 0.01 M concentrations. The extraction

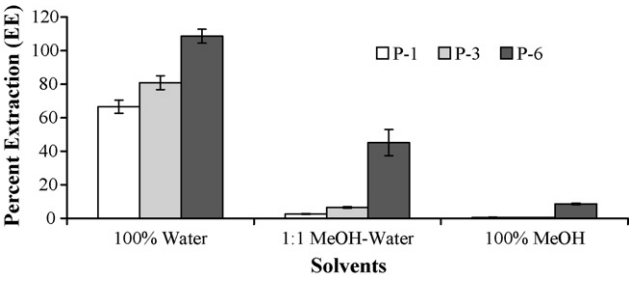

Fig. 1. Extraction efficiencies (EE) of different solvents in solvent-Soxhlet method for three plants are presented. Error bars are ±1 S.D. from three independent determinations.

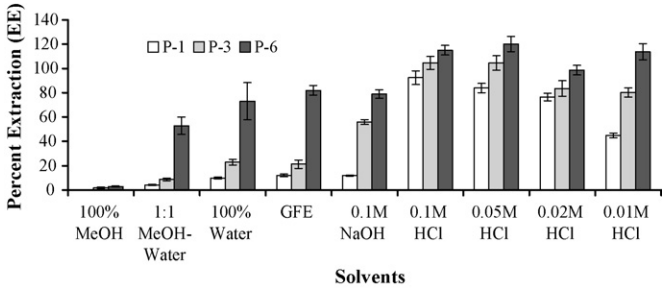

Fig. 2. Extraction efficiencies (EE) of different solvents in solvent-sonication method for three plants are shown. Error bars represent ±1 S.D. from three independent determinations.

results showed that the water-Soxhlet method was more effective than water-sonication method. The higher efficiency of the water-Soxhlet method was likely because the former was an exhaustive extraction technique carried out at a higher temperature. The water–methanol solvent has been traditionally used as an extractant in terrestrial plant studies, particularly for the environmentally focused studies [20,37]. While water–methanol has been shown to be effective for biological samples such as lobster tissues [36], the data presented here indicated that other solvents were more effective for terrestrial plants.

In another study [14] NaOH solution has been shown to provide higher EE compared to the other extractants (e.g., acetic acid, EDTA, tetrabutylammonium hydroxide, acetonitrile/H_2O, and MeOH/H_2O) in the extraction of arsenic from plant materials. EE's of 22%, 32% and 36% were obtained from freeze-dried poplar leaves, pine shoots, and spruce shoots, respectively. In the present study, 0.1 M-NaOH performed similarly to water with EE's 12%, 56% and 79% for plants P-1, P-3 and P-6, respectively. In contrast, introduction of 0.1 M-HCl induced a marked improvement (92%, 104% and 115%) in the EE's for the plants (Fig. 2). Concentrated HCl has been used to extract inorganic arsenic from biological samples [38,39] where HCl helped to solubilize the sample and aided in breaking up the bonds between As(III) and the thiol groups of proteins [13]. Dilute HCl solutions have not been used as an extractant for arsenic from terrestrial plants. However, our data indicated that it was an effective extractant for arsenic in terrestrial plants.

In a previous study [11], it was observed that the percent of arsenic extracted was inversely related to the total arsenic content of the plant. A reason for this trend was thought to be due to the induced chemical and/or physical bonding of arsenic to the plant matrix and/or sequestration in vascular plant tissues due to the increased exposure of the plant to arsenic. In other studies, it has been demonstrated that both As(III) and As(V) efficiently induced the biosynthesis of phytochelatins ([γ-glutamate-cysteine]$_n$-glycine) synthesized from reduced glutathione (GSH) in plants and that arsenic–phytochelatin (As–PC) were present in weak acid extracts [40,27,41]. As(III) is found to coordinate with the sulphur (S) of thiol groups (SH) of the PC in various proportions. The cause of higher arsenic extraction efficiency of dilute HCl may be due to its ability to break up the As–S bond of the various As–S bond-containing complexes in plant tissues. Interestingly, much less arsenic was complexed to phytochelatins in an arsenic hyperaccumulator plant, which is presumably more tolerant to arsenic [41].

8.2. Study of arsenic species spiked on a plant matrix

Given the relationship between arsenic species and toxicity, it is critical to assess the effect any extraction method has on the individual arsenic species. The arsenic concentrations in these plants are high and there are no similar terrestrial plant reference materials with comparable arsenic values. Because there is no agreement on extraction methods, there are no reference values for individual species in any of the available terrestrial plant reference materials. Marine algae, which have proportions of carbohydrates, lipids and proteins similar to terrestrial plants, are available but their speciation is vastly different. The predominant arsenic species found in terrestrial plants are As(III), As(V), MA and DMA; therefore, these four compounds were spiked onto a plant matrix in a series of experiments designed to assess the effect of the solvents and extraction processes on speciation. Spiking was done with prepared solutions of these four individual arsenic species and results are shown in Table 1.

Recovery experiments were conducted using a plant matrix having comparatively low arsenic concentration (1.8 μg g^{-1}) and spiking with the standard arsenic species. The spiked concentrations, which ranged from 6.0 to 120 μg g^{-1}, were determined on the basis of 0.5 g dry plant sample. Spikes were extracted following the same procedures that were used for the extraction of plant matrices. Soxhlet extractions with water and sonication extractions with water, 1:1 water–methanol and 0.05 M-HCl as extractants were carried out.

Total concentrations of the inorganic arsenic species, As(III) and As(V), were determined by HG-AAS and those of the organoarsenic species, DMA and MA, were done by ICP-AES for the spike-experiments. The spike-speciation experiments were performed by HPLC–HGAAS. Results of spike recovery (total arsenic), reported in Table 1, show quantitative recovery of arsenic species ranging from 90 to 110% for the extraction media and methods employed. Overall, the HPLC–HGAAS speciation data also showed good total arsenic recovery (sum of species concentrations), suggesting that the extraction procedures used were mild and did not significantly alter the arsenic speciation. Oxidized or reduced forms of the introduced inorganic species were not detected in the 1:1 water–methanol sonication and 100% water-sonication extracts.

However, in the 0.05 M-HCl sonication and 100% water-Soxhlet extracts a small amount of interconversion (2.5–5%) of the inorganic arsenic species was observed. The reduced form of As(V), that is As(III), was detected in the extracts of 0.05 M HCl-sonication (Table 1). The source of the arsenite could be the plant matrix spiked, but since As(III) was not observed in the other extracts analyzed, it is likely that in this case the extraction process caused the reduction of arsenate to arsenite. It has been shown that under slightly reducing conditions and/or lower pH, As(III) can become more stable mainly as neutral H_3AsO_3 [42]. It appeared that species interconversion occurred also in the 100% water-Soxhlet extraction where As(V) was detected in the As(III) spike. Interconversion between As(III) and As(V)

Table 1
Results of spike recovery experiments

Extraction medium-method	Spikes	Spiked conc.	Recovered spike conc. (HG-AAS/ICP-AES)	Recovered spike conc. (HPLC–HGAAS)			
				As(III)	As(V)	DMA	MA
1:1 Water–methanol-sonication	As(III)	120	132 ± 6	144 ± 6	nd	nd	nd
	As(V)	120	120 ± 12	nd	132 ± 6	nd	nd
	DMA	60.0	58.8 ± 3.6	nd	nd	56.4 ± 6.6	nd
	MA	12.0	11.4 ± 1.2	nd	nd	nd	14.4 ± 0.6
0.05 M-HCl-sonication	As(III)	120	132 ± 6	144 ± 6	nd	nd	nd
	As(V)	120	126 ± 6	7.8 ± 1.8	144 ± 6	nd	nd
	DMA	12.0	11.7 ± 0.2	nd	nd	13.2 ± 0.6	nd
	MA	12.0	11.9 ± 0.1	nd	nd	nd	16.2 ± 0.6
100% Water-sonication	As(III)	120	126 ± 6	144 ± 6	nd	nd	nd
	As(V)	120	129 ± 2	nd	132 ± 6	nd	nd
	DMA	12.0	12.0 ± 0.6	nd	nd	12.6 ± 0.6	nd
	MA	12.0	12.2 ± 0.2	nd	nd	nd	16.3 ± 0.2
100% Water-Soxhlet	As(III)	120	120 ± 1	137 ± 1	3.6 ± 1.8	nd	nd
	As(V)	120	120 ± 6	nd	108 ± 6	nd	nd
	DMA	60.0	52.8 ± 2.4	nd	nd	60.0 ± 6.0	nd
	MA	6.0	6.5 ± 0.1	nd	nd	nd	7.8 ± 0.6

Spiked and recovered spike concentrations (average ± 1 S.D. from three independent determinations) are reported in $\mu g\,g^{-1}$ dry sample. nd indicates species not detected.

in water [43] and the influence of pH and matrix on the stability of inorganic arsenic species has been demonstrated by spiking the species in wastewater samples [44].The transformation and underlying uncertainties in predicting such transformations of the inorganic arsenic species in aqueous samples have been discussed [3].

8.3. Speciation of arsenic species in plant extracts

The results of arsenic in the extracts of P-1, P-3 and P-6 by the various extraction methods have already been discussed (see Figs. 1 and 2). The extracts were analyzed for arsenic species by HPLC–HGAAS, and the concentrations of individual species as well as total arsenic concentrations in the extracts are reported in Table 2. The sums of arsenic concentrations of the species agree well with the totals determined by ICP-AES. The majority of arsenic extracted was inorganic arsenite and arsenate. The organoarsenic species, MA, was detected in 1:1 water–methanol extracts of P-1 (Table 2).

Although the EE of 1:1 water–methanol was low, only the organoarsenic species (MA) that was detected in the target plant P-1 was extracted in this medium. This observation was important since it indicated that small concentrations or trace organoarsenic species could be detected in the water–alcohol medium which suppressed the extraction of inorganic species. Representative chromatograms of standard arsenic species along with the chromatogram of arsenic in two plant extracts of 1:1 water–methanol are presented in Fig. 3. In terrestrial plants, the organoarsenic species that are usually encountered are MA and DMA [45]. For example, up to 2% MA and DMA were measured in shoots and roots of *Holcus lanatus* and *Arabidopsis thaliana* [46].

In the acid media, concentrations of As(V) predominated over those of As(III) in all cases except for plant P-6. For P-6, As(III) predominated over As(V) in all but the 0.1 M-HCl medium. No As(III) was detected in water-Soxhlet extracts. This may be due to the oxidizing capability of Soxhlet extraction and is consistent with the As(III) spike data for water-Soxhlet where some conversion of As(III) to As(V) was observed. The reducing and/or stabilizing nature of chloride ion for As(III) was shown by the presence of As(III) in all HCl media. Both As(III) and As(V)

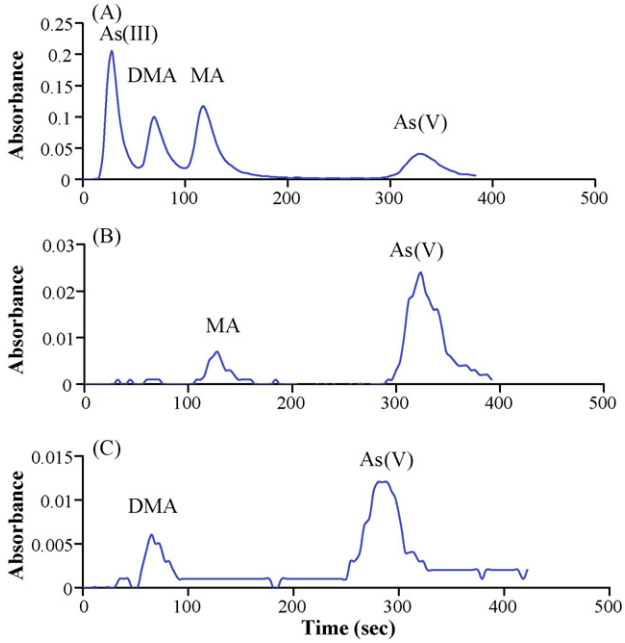

Fig. 3. Representative HPLC–HGAAS chromatograms. (A) Standard arsenic species, (B) 1:1 water–methanol extract of plant YK-11, and (C) DL-129 (see Tables 4 and 5 for plant information). HPLC was performed with anion exchange column (Hamilton PRP-X100 250 mm × 4.6 mm column), 20 mM ammonium phosphate, pH 6.0 at 1.5 mL min^{-1}.

Table 2
Speciation of arsenic extracted from plant samples

Extraction method	Plant ID	Amount of As extracted	As by HPLC–HGAAS[a]		Sum of species
			As(III)	As(V)	
100% water-sonication	P-1	24 ± 2	nd	21 ± 1	21 ± 1
	P-3	34 ± 3	nd	29 ± 3	29 ± 3
	P-6	18 ± 4	13 ± 1	6.3 ± 0.2	19 ± 1
0.01 M-HCl-sonication	P-1	108 ± 2	5.9 ± 1.1	96.1 ± 0.2	102 ± 1
	P-3	117 ± 4	11.9 ± 0.9	97 ± 5	109 ± 9
	P-6	28 ± 2	16.7 ± 0.1	10 ± 1	27 ± 1
0.02 M-HCl-sonication	P-1	184 ± 3	24 ± 14	169 ± 24	193 ± 38
	P-3	122 ± 8	36 ± 3	100 ± 21	136 ± 24
	P-6	24 ± 1	15 ± 1	12.3 ± 0.2	27 ± 1
0.05 M-HCl-sonication	P-1	202 ± 6	15 ± 1	184 ± 6	199 ± 7
	P-3	153 ± 6	29 ± 1	114 ± 6	143 ± 7
	P-6	29.3 ± 1.3	21.6 ± 0.3	12.5 ± 1.4	34 ± 2
0.1 M-HCl-sonication	P-1	223 ± 11	12 ± 1	208 ± 8	220 ± 9
	P-3	153 ± 7	31 ± 8	143 ± 8	174 ± 16
	P-6	28 ± 1	8 ± 2	27 ± 1	35 ± 3
100% water-Soxhlet	P-1	160 ± 7	nd	150 ± 16	150 ± 16
	P-3	118 ± 4	nd	100 ± 14	100 ± 14
	P-6	26 ± 1	nd	22 ± 4	22 ± 4
1:1 water–methanol-sonication	P-1	7.7 ± 1.0	1.7 ± 0.8	5.6 ± 0.4	8.8 ± 1.2[b]
	P-3	10.0 ± 0.5	5.6 ± 1.5	6.5 ± 0.8	12 ± 2
	P-6	9.7 ± 0.5	10.8 ± 0.6	2.1 ± 0.3	13 ± 1

Results are average ±1 S.D. from three independent determinations. Concentrations are in $\mu g\,g^{-1}$. nd = not detected.
[a] MA was detected only in the water–methanol extracts of P-1 ($1.51 \pm 0.04\ \mu g\,g^{-1}$).
[b] Sum includes MA concentration. DMA was not detected in any extract.

were present in 1:1 water–methanol extracts of all plants indicating the milder nature of the solvent. HPLC–ICPMS speciation of arsenic in Deloro plants was performed to look for additional arsenic species, however, only As(III), As(V), MA and DMA were detected, confirming the HPLC–HGAAS results. In Fig. 4, HPLC–ICPMS chromatograms of two plants DL-119 (Canada goldenrod, *Solidago Canadensis*) and DL-207 (field horsetail, *Equisetum arvense*) are shown.

8.4. Gastric fluid extraction

Extraction efficiencies of synthetic gastric fluid are used to estimate the bioavailability of arsenic in the human stomach and intestines [47,48]. Gastric fluid extractions, modeling human gastrointestinal conditions, have been carried out to extract arsenic from plant matrices [11]. GFE extractions are currently being used in risk assessments of arsenic contaminated sites [49]; therefore, it is important to compare the extraction efficiency of the various extracts used in this study to GFE. The speciation results of the GFE experiments are presented in Table 3. The EE of GFE was comparable to that of 100% water as was shown earlier in Fig. 2.

The average ($n = 3$) amount of MA extracted from P-1 was $1.4 \pm 0.1\ \mu g\,g^{-1}$ and compared favourably with the amount extracted by the 1:1 water–methanol sonication method of $1.51 \pm 0.04\ \mu g\,g^{-1}$. Thus, the synthetic gastric fluid showed potential for simultaneous analysis of the organic and inorganic arsenic in plant samples. Although GFE extracted significantly less arsenic from the terrestrial plants than 0.05 M-HCl did, it had the advantage of extracting both organic and inorganic arsenic in one extraction. Unlike water–methanol extracts where methanol was removed prior to analysis, GFE extracts were introduced directly to the ICP and HPLC column for analysis. Further experiments with GFE, however, showed generally low extraction efficiencies from the various terrestrial plants, suggesting it could not be used to characterize the speciation of all the arsenic in a plant sample.

8.5. Sequential extraction of arsenic from plants

Although As(III) and As(V) are known to be the predominant species in terrestrial plants [3,10,20], MA and DMA are also detected in lower concentrations [3,13,45], and other organoarsenic compounds such as arsenobetaine (AB), arsenocholine (AC), and different arsenosugars have been detected in plant tissues [3,50]. Therefore, it is important to extract both inorganic and organic arsenicals to obtain a broader picture of the species in plants.

The present study has revealed that while the water–methanol mixture can extract organoarsenic species that dilute HCl apparently cannot, HCl is more efficient in extracting inorganic arsenic, and therefore, an extraction that includes both is desirable. In addition, the organoarsenic species in general exist in much smaller amounts than the inorganic species in the ter-

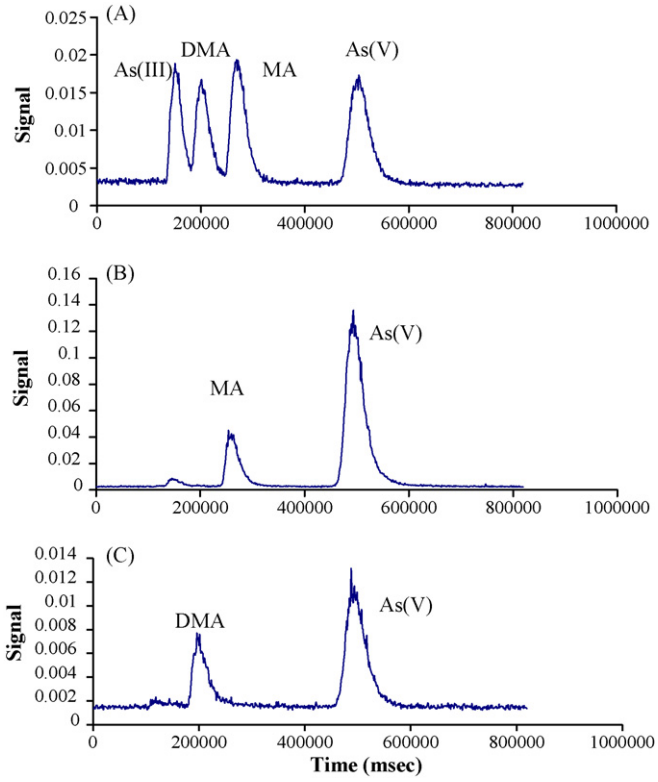

Fig. 4. HPLC–ICPMS anion exchange chromatograms of: (A) standard solution (20 μg L^{-1}), (B) Deloro plant DL-207 (field horsetail, *Equisetum arvense*) and (C) DL-119 (Canada goldenrod, *Solidago Canadensis*). HPLC–ICPMS confirmed MA in DL-207 and DMA in DL-119 previously determined by HPLC–HGAAS.

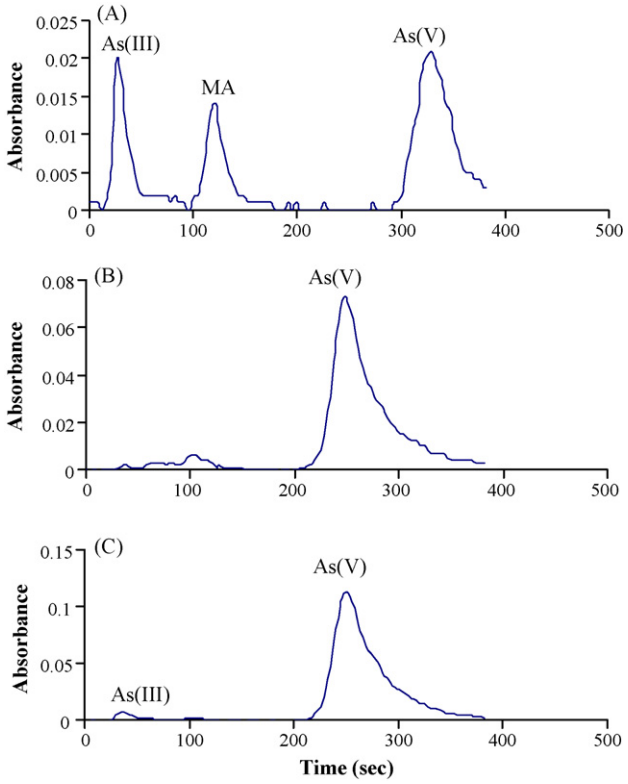

Fig. 5. HPLC–HGAAS chromatograms of field horsetail (P-1): 1:1 water–methanol extract (A), water extract (B), and 0.1 M-HCl extract (C). Analyses of water extract (B) and acid extract (C) were performed in June (same day); analysis of 1:1 water–methanol extract (A) was performed in August of the same year. Difference in the retention time of As(V) in the chromatograms was due to difference in the HPLC conditions (given in Fig. 3).

restrial plants which makes their determination difficult in the presence of concentrated inorganic species. This was evident in the case of organoarsenic species MA in field horsetail as was demonstrated in the chromatograms in Fig. 5. The chromatogram of the field horsetail 1:1 water–methanol extract (Fig. 5A) has a prominent peak of organic MA as compared to the water and 0.1 M-HCl extracts in Fig. 5B and C, respectively.

In the procedures for optimization of the sequential method, experiments were conducted to find out if a 1:1 v/v combination of 0.1 M-HCl and methanol could be used as a potential extractant of both inorganic and organic arsenicals. The results showed that the total arsenic extracted by the experimental solvent was less than 50% of the amount extracted by 0.05 M-HCl. Arsenic speciation by HPLC–HGAAS revealed no MA in the HCl–methanol extracts of P-1 indicating a suppressing effect of HCl on the extraction of the organoarsenic compound. Interestingly, HCl was a component of GFE solvent, which released MA; this contradictory behaviour is unexplained at present.

Consequently, a sequential method in which extraction with 1:1 water–methanol followed by 0.1 M-HCl was developed to extract both organic and inorganic arsenic from plant matrices. The extraction by acid prior to water–alcohol was found to be unfavourable to the extraction or determination of organoarsenic species; therefore, the extraction sequence of water–methanol followed by acid was adopted.

8.6. Application of the sequential method to terrestrial plants

The sequential extraction results of fifteen plant samples from arsenic contaminated areas in Yellowknife, NWT and nine plant

Table 3
Arsenic extracted by GFE

Sample ID	Total As	As extracted by GFE	Species in GFE extracts				Sum of species in GFE
			As(III)	As(V)	MA	DMA	
P-1	241 ± 9	29.4 ± 2.4	nd	28.4 ± 0.1	1.4 ± 0.1	nd	29.8 ± 0.2
P-3	146 ± 5	31.3 ± 5.1	4.8 ± 0.1	26.8 ± 0.2	nd	nd	31.6 ± 0.3
P-6	24 ± 1	20.0 ± 0.8	16.5 ± 0.4	6.1 ± 1.3	nd	nd	22.6 ± 1.7

Arsenic speciation in GFE extracts was done by HPLC–HGAAS. Results are mean ± 1 S.D. (μg g^{-1}) from three independent determinations and nd = not detected.

Table 4
Extraction of arsenic from the Yellowknife (YK) and Deloro (DL) plants by sequential extraction method

Plant ID	Latin name	Common name	Total As in plant ($\mu g\,g^{-1}$)	As in 1:1 water–MeOH, ($\mu g\,g^{-1}$)	As in 0.1 M-HCl, ($\mu g\,g^{-1}$)	EE of 1:1 water–MeOH	EE of sequential method
YK-1	*Agropyron trachycaulum*	Slender wheat grass	95.2	8.2	20.2	9	30
YK-2	*Epilobium angustifolium*	Fireweed	4.6	1.5	nd	33	33
YK-3	*Archtostaphytos uva-ursi*	Common bearberry	18.5	1.8	4.8	10	36
YK-4	*Agropyron trachycaulum*	Slender wheat grass	8.0	1.5	1.5	19	38
YK-5	*Senecio vulgaris*	Common groundsel shoots	38.5	5.8	20.6	15	69
YK-6	*Agrostis scabra*	Rough hair grass shoots	47.5	24.9 ± 0.8	25.0 ± 0.8	52 ± 2	105 ± 3
YK-7	*Picea mariana*	Black spruce bough/cones	12.6	0.78 ± 0.20	2.8 ± 0.1	6.2 ± 1.5	29 ± 2
YK-8	*Hordeum jubatum*	Foxtail barley	4.4	1.2	nd	27	27
YK-9	*Calamagrostis canadensis*	Blue joint-1	4.0	2.5	nd	63	63
YK-10	*Calamagrostis canadensis*	Bluejoint-2	8.1	3.7 ± 0.2	nd	46 ± 2	46 ± 2
YK-11	*Calamagrostis canadensis*	Bluejoint-3	77.7	3.4 ± 0.4	20.2 ± 1.1	4.4 ± 0.5	30 ± 2
YK-12	*Calamagrostis canadensis*	Bluejoint-4	3.8	1.1	1.3	29	64
YK-13	*Calamagrostis canadensis*	Bluejoint-5	3.0	1.4	1.7	48	105
YK-14	*Hordeum jubatum*	Foxtail barley	0.90	0.80	nd	89	89
YK-15	*Epilobium angustifolium*	Fireweed	2.1	1.1	1.5	52	128
DL-60	*Equisetum arvense*	Field horsetail	24.9	18.5	3.3	74	88
DL-101	*Equisetum arvense*	Field horsetail	410	126 ± 12	222 ± 6	30	85
DL-105	*Verbena hastata*	Blue vervain	8.4	2.5	0.82	30	40
DL-129	*Solidago canadensis*	Canada goldenrod	8.2	1.6	nd	19	19
DL-201	*Onoclea sensibilis*	Sensitive fern	48.4	7.8	11.6	16	40
DL-204	*Equisetum arvense*	Field horsetail	19.4	6.4	13.4	33	102
DL-205	*Aster lanceolatus*	Panicle aster	2.9	0.37	13	nd	13
DL-220	*Lythrum salicaria*	Purple loosestrife	18.7	0.67	3.6	2.9	19
Dl-221	*Equisetum arvense*	Field horsetail	26.3	9.7	10.8	37	78

Results of mean ± average deviation from two independent analyses for a number of plants show reproducibility of analyses and nd = not detected.

samples from abandoned gold mining areas at Deloro, ON, Canada are reported in Table 4. The total arsenic concentrations determined by ICP-AES ranged from 1 to 95 $\mu g\,g^{-1}$ and from 1 to 530 $\mu g\,g^{-1}$ in the Yellowknife and Deloro plants, respectively. Most of the Yellowknife plants were grass species; the grasses usually consist of silica-rich hard-tissues and are difficult to process [51]. The 1:1 water–methanol extraction of the Yellowknife plants yielded EEs ranging from 4 to 89% with a median at 29%. The sequential extraction followed by 0.1 M-HCl extracted more arsenic from the plants. Had the extractions been carried out only with 1:1 water–methanol, the traditional solvent used for plant arsenic extractions, low extraction efficiency would have been achieved. From these plants which were mostly grasses, the overall EE from sequential extractions ranged from 27 to 128% with a median at 46% that was almost double of the median EE of 1:1 water–methanol extractions. The arsenic extraction efficiencies of Deloro plants obtained using the sequential method ranged from 13 to 106% with a median at 70%.

Arsenic in selected plant extracts was speciated by HPLC–HGAAS and the results are reported in Table 5. The results showed that most of the arsenic in plants was inorganic. The overall predominance of As(V) was observed in the extracts of the plants from both locations. The organoarsenic species were detected in the 1:1 water–methanol extracts of the plants; MA in YK-1, YK-4, YK-11, DL-204 and DL-221 and DMA in DL-105, DL-129, DL-205 and DL-220.

The knowledge of chemical and physical states of the unextracted arsenic in these plants may provide insight into understanding the factors that influence extraction of arsenic from the plant matrix. It is generally believed that the low EE is due to a number of factors such as the insoluble forms of arsenic, the chemical and/or physical bonding of As to the plant matrix, and the trapping of arsenic compounds inside the plant vascular tissues [20,28]. A number of plant samples were examined by XANES to better understand the arsenic speciation in the plant samples.

8.7. XANES experiments

The XANES method has been described in Section 7. XANES spectra were collected for a variety of plant samples at different stages of preparation including: frozen fresh plants (plants frozen after sampling without drying), dry-ground samples, and dried residues from the sequential extraction of plants. XANES spectra of three plants are compared to standard arsenic species in Fig. 6. The arsenic species in XANES spectra are generally identified using the position of the main peak feature in the spectra (Fig. 6).

A comparison of the X-ray absorption peaks of arsenic species in the arsenic standards and the fresh frozen and dry ground samples of three plants in Fig. 6 revealed no significant transformation in the oxidation states of arsenic species from the fresh frozen to the dry ground plant samples. This demonstrated, within the sensitivity of the XANES method, the stability of As(III)/As(V) species in plant samples during handling and sample preparations. However, within the As(III) oxidation state ($As(Glu)_3$ and As_2O_3) some shifts, indicative of transformation,

Table 5
Speciation of arsenic in Yellowknife and Deloro plants (see Table 4 for plant details) by HPLC–HGAAS

Plant ID	As(III)		DMA		MA		As(V)		Sum of species	Total As in plant
	1:1 water-MeOH	0.1 M-HCl	1:1 water–MeOH	0.1 M-HCl	1:1 water–MeOH	0.1 M-HCl	1:1 water–MeOH	0.1 M-HCl		
YK-1	3.1	nd	nd	nd	0.36	nd	4.3	19.5	27.3	95.2
YK-3	nd	nd	nd	nd	nd	nd	1.0	5.6	6.6	18.5
YK-4	0.53	nd	nd	nd	0.23	nd	0.83	2.1	3.6	8.0
YK-5	1.5	7.6	nd	nd	nd	nd	3.4	20.9	33.4	38.5
YK-6	9.4 ± 1.4	0.49 ± 0.13	nd	nd	nd	nd	11 ± 1	29 ± 2	50 ± 5	47.5
YK-11	0.50 ± 0.11	0.49 ± 0.08	nd	nd	0.25 ± 0.02	nd	2.1 ± 0.2	24 ± 1	27 ± 1	77.7
DL-60	10.7	0.46	nd	nd	nd	nd	7.7	2.9	21.8	24.9
DL-101	15.8 ± 0.2	150 ± 6	nd	nd	nd	nd	110 ± 12	71.60 ± 0.04	347 ± 18	410
DL-105	nd	0.82	0.40	nd	nd	nd	2.1	nd	3.3	8.4
DL-129	nd	nd	0.23	nd	nd	nd	1.3	nd	1.5	8.2
DL-201	0.18	9.5	nd	nd	nd	nd	7.6	2.1	19.4	48.4
DL-204	0.96	1.7	nd	nd	0.13	nd	5.3	11.7	19.8	19.4
DL-205	0.27	nd	0.11	nd	nd	nd	nd	nd	0.38	2.9
DL-220	nd	2.9	0.21	nd	nd	nd	0.46	nd	4.0	18.7
DI-221	3.8	1.9	nd	nd	2.2	nd	3.8	9.0	20.7	26.3

Mean ± average deviation from two independent determinations shows reproducibility of analyses. Concentrations are in $\mu g\,g^{-1}$ and nd = not detected.

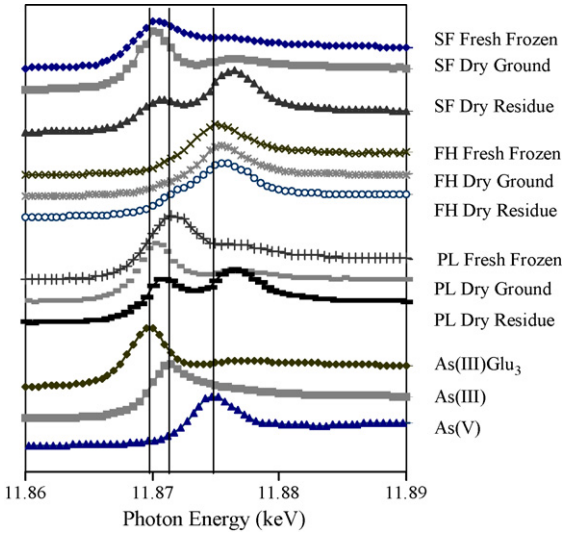

Fig. 6. XANES spectra of fresh frozen, dry ground and dry residue of sequential extraction of sensitive fern (SF), field horsetail (FH) and purple loosestrife (PL). Aqueous standards of arsenic(III)-gluatathione ($As(Glu)_3$ synthesized, see acknowledgement), arsenite (As_2O_3–Fluka reagent grade) and arsenate (KH_2AsO_4–Fluka reagent grade) are shown for reference. Extraction details in Tables 4 and 5.

were evident particularly in purple loosestrife (PL). A comparison of the XANES spectra of dry ground and dry residues of extraction of the same plants showed significant shifts in the peak intensities as well as absorption positions between the corresponding spectra of PL and sensitive fern (SF). It is clear that the profile of the arsenic species remaining in the PL and SF residues of extract are not consistent with that of the original plants. Further study will be required to come to any conclusions regarding the transformation of arsenic species in plant matrices due to extraction.

9. Conclusions

The traditional method of arsenic extraction by water–methanol mixtures from terrestrial plants was augmented by the sequential extraction with dilute hydrochloric acid. Almost double the amount of arsenic was extracted by the sequential method compared to the traditional method. Arsenic spike recovery experiments demonstrated stability of the species during the extraction processes and XANES results showed that no species (As(III)/As(V)) transformation occurred due to sample preparations (prior to extraction). Trace amounts of organoarsenic species could be detected by HPLC–HGAAS aided by the process of separation and preconcentration: the organoarsenic species were separated from the large inorganic fractions by extracting them first in the water–methanol mixture, which was concentrated. We demonstrated the applicability of the developed sequential method to various terrestrial plants for arsenic speciation.

Acknowledgements

We would like to thank the Ministry of Environment, Ontario and in particular Robert A. Helliar, Project Engineer, Regional Program Unit, for allowing access to the Deloro site and Dr. W. Cullen and Dr. H. Sun of the University of British Columbia for providing the $As(Glu)_3$ standard. PNC-CAT facilities at the Advanced Photon Source, and research at these facilities, are supported by the US DOE Office of Science Grant No. DEFG03-97ER45628, the University of Washington, a major facilities access grant from NSERC, Simon Fraser University and the Advanced Photon Source. Use of the Advanced Photon Source is also supported by the U. S. Department of Energy, Office of Science, Office of Basic Energy Sciences, under Contract No. W-31-109-Eng-38. We thank Dr. Robert Gordon for his assistance with XANES analyses.

References

[1] R. Eisler, Rev. Environ. Contamin. Toxicol. 180 (2004) 133–165.
[2] I. Koch, C.A. Ollson, J. Potten, K.J. Reimer, in: V.R. Preedy, R.R. Watson (Eds.), Rev. Food Nutrition Toxicity, vol. 1, Taylor & Francis, London, 2003, pp. 16–40.
[3] K.A. Francesconi, D. Kuehnelt, Analyst 129 (2004) 373–395.
[4] Z. Gong, X. Lu, M. Ma, M.C. Watt, X.C. Le, Talanta 58 (2002) 77–96.
[5] Y. Jin, G. Sun, X. Li, G. Li, C. Lu, L. Qu, Toxicol. Appl. Pharmacol. 196 (3) (2004) 396–403.
[6] J.S. Petrick, F. Ayala-Fierro, W.R. Cullen, D.E. Carter, A.H. Vasken, Toxicol. Appl. Pharmacol. 163 (2) (2000) 203–207.
[7] J.C. Ng, J. Wang, A. Shraim, Chemosphere 52 (9) (2003) 1353–1359.
[8] C. B'Hymer, J.A. Caruso, J. Chromatogr. A 1045 (1–2) (2004) 1–13.
[9] S.B. Rasul, Z. Hossain, A.K.M. Munir, M. Alauddin, A.H. Khan, A. Hussam, Talanta 58 (1) (2002) 33–43.
[10] R.A. Pyles, E.A. Woolson, J. Agric. Food Chem. 30 (1982) 866.
[11] I. Koch, C. Hough, S. Mousseau, K. Mir, A. Rutter, C. Olson, E. Lee, P. Andrewes, S. Granhchino, B. Cullen, K. Reimer, Can. J. Anal. Sci. Spectrosc. 47 (4) (2002) 109.
[12] B. He, Y. Fang, G. Jiang, Z. Ni, Spectrochim. Acta Part B: Atom. Spectrosc. 57B (11) (2002) 1705–1711.
[13] J.A. Caruso, D.T. Heitkemper, C. B'Hymer, Analyst 126 (2) (2001) 136.
[14] M. Krachler, H. Emons, Fresenius J. Anal. Chem. 368 (2000) 702.
[15] Y. Bohari, G. Lobos, H. Pinochet, F. Pannier, A. Astruc, M. Potin-Gautier, J. Environ. Monit. 4 (2002) 596.
[16] A. Geiszinger, W. Goessler, W. Kosmus, Appl. Organometal. Chem. 16 (2002) 245–249.
[17] I. Koch, J. Feldmann, L. Wang, P. Andrewes, K.J. Reimer, W.R. Cullen, Sci. Tot. Environ. 236 (1–3) (1999) 101–117.
[18] I. Koch, L. Wang, C.A. Ollson, W.R. Cullen, K.J. Reimer, Environ. Sci. Technol. 34 (1) (2000) 22–26.
[19] D.T. Heitkemper, N.P. Vela, K.R. Stewart, C.S. Westphal, J. Anal. Atom. Spectrom. 16 (2001) 299.
[20] I. Koch, L. Wang, K.J. Reimer, W.R. Cullen, Appl. Organomet. Chem. 14 (5) (2000) 245–252.
[21] A. Montilla, Sample Treatment for Arsenic Speciation. Master's Thesis, 2000, Univ. Alberta, Canada.
[22] M.V. Ruby, R. Schoof, W. Brattin, M. Goldade, G. Post, M. Harnois, D.E. Mosby, S.W. Casteel, W. Berti, M. Carpenter, D. Edwards, D. Cragin, W. Chappell, Environ. Sci. Technol. 33 (21) (1999) 3697–3705.
[23] G.B. Freeman, R.A. Schoof, M.V. Ruby, A.O. Davis, J.A. Dill, S.C. Liao, C.A. Lapin, P.D. Begstrom, Fundam. Appl. Toxicol. 28 (1995) 215–222.
[24] J.M. Laparra, D. Velez, R. Montoro, R. Barbera, R.J. Farre, Agric. Food Chem. 51 (2003) 6080–6085.
[25] J.-K. Yang, M.O. Barnett, P.M. Jardine, N.T. Basta, S.W. Casteel, Environ. Sci. Technol. 36 (2002) 4562–4569.
[26] J.M. Laparra, D. Velez, R. Montoro, R. Barbera, R. Farre, Chemistry 18 (2004) 662–669.
[27] M. Montes-Bayon, J. Jeija, D.L. LeDuc, N. Terry, J.A. Caruso, A. Sanz-Medel, J. Anal. At. Spectrom. 19 (2004) 153–158.

[28] J. Zheng, H. Hintelmann, B. Dimock, M.S. Dzurko, Anal. Bioanal. Chem. 377 (1) (2003) 14–24.
[29] I. Koch, J.V. Mace, K.J. Reimer, Environ. Toxicol. Chem. 24 (2005) 1468–1474.
[30] R.R. Rodriguez, N.T. Basta, S.W. Casteel, L.W. Pace, Environ. Sci. Technol. 33 (1999) 642–649.
[31] I. Rodushkin, T. Ruth, A. Huhtasaari, Anal. Chim. Acta 378 (1–3) (1999) 191–200.
[32] S.M. Heald, D.L. Brewe, E.A. Stern, K.H. Kim, F.T. Brown, D.T. Jiang, E.D. Crozier, R.A. Gordon, J. Synchrotr. Radiat. 6 (1999) 347.
[33] S. Kraft, J. Stumpel, P. Becker, U. Kuetgens, Rev. Sci. Instrum. 67 (1996) 681.
[34] T. Ressler, J. Phys. IV 7 (1997) C2–C269.
[35] J.L. Gomez-Ariza, D. Sanchez-Rodes, I. Giraldez, E. Morales, Analyst 125 (2000) 401.
[36] J.A. Brisbin, J.A. Caruso, Analyst 127 (7) (2002) 921.
[37] H. Helgensen, E.H. Larsen, Analyst 123 (1998) 791.
[38] O. Munoz, V. Devesa, M.A. Suner, D. Velez, R. Montoro, I. Urieta, M.L. Macho, M. Jalon, J. Agric. Food Chem. 48 (2000) 4369–4376.
[39] J.L. Capelo, I. Lavilla, C. Bendicho, Anal. Chem. 73 (2001) 3732.
[40] M.E.V. Schmoger, M. Oven, E. Grill, Plant Physiol. 122 (2000) 793.
[41] A. Raab, J. Feldmann, A.A. Meharg, Plant Physiol. 134 (2004) 1113–1122.
[42] W.R. Cullen, K.J. Reimer, Chem. Rev. 89 (1989) 713.
[43] X.C. Le, S. Yalcin, M.S. Ma, Environ. Sci. Technol. 34 (2000) 2342–2347.
[44] M. Segura, J. Munoz, Y. Madrid, Anal. Biol. Chem. 374 (2002) 513.
[45] R.A. Schoof, L.J. Yost, J. Eickhoff, E.A. Crecelius, D.W. Cragin, D.M. Meacher, D.B. Menzel, Food Chem. Toxicol. 37 (1999) 839.
[46] M. Quaghebeur, Z. Rengel, M. Smirk, J. Anal. Atom. Spectrom. 18 (2) (2003) 128–134.
[47] R.R. Rodriguez, N.T. Basta, S.W. Castel, L.W. Pace, Environ. Sci. Technol. 33 (1999) 642–649.
[48] M.V. Ruby, A. Davis, R.D. Schoof, S. Eberle, C.M. Sellstone, Environ. Sci. Technol. 30 (1996) 422–430.
[49] I. Koch, A Duso, C Haug, C Miskelly, M Sommerville, P Smith, K.J. Reimer, Environ. Forensics 6 (4) (2005) 335–344.
[50] P.A. Gallagher, X. Wei, J.A. Shoemker, C.A. Brockhoff, J.T. Creed, J. Anal. At. Spectrom. 14 (1999) 1829.
[51] J. Williamsonia, H. Eklundia, Paperi ja Puu 78 (10) (1996) 597–604.

Available online at www.sciencedirect.com
ScienceDirect
Talanta 72 (2007) 1261–1268
Talanta
www.elsevier.com/locate/talanta

Evaluation of unfolded-partial least-squares coupled to residual trilinearization for four-way calibration of folic acid and methotrexate in human serum samples

A. Muñoz de la Peña [a,*], I. Durán Merás [a], A. Jiménez Girón [a], H.C. Goicoechea [b]

[a] *Department of Analytical Chemistry, University of Extremadura, 06071 Badajoz, Spain*
[b] *Laboratorio de Desarrollo Analítico y Quimiometría (LADAQ), Cátedra Quimica Analítica I, Facultad de Bioquímica y Ciencias Biológicas, Universidad Nacional del Litoral, S3000ZAA Santa Fe, Argentina*

Received 28 September 2006; received in revised form 21 December 2006; accepted 9 January 2007
Available online 16 January 2007

Abstract

The combination of unfolded-partial least-squares (U-PLS) with a recently proposed separate procedure, known as residual trilinearization (RTL), has been successfully employed for four-way data calibration. The chemometric method employs the evolution of excitation–emission matrices (EEMs) with time, for the resolution of folic acid–methotrexate mixtures, in human serum samples. The fluorogenic products monitored correspond to the oxidation of the studied analytes with potassium permanganate, in slightly acidic medium. The reaction is developed in 7 min and followed using a fast-scanning spectrofluorimeter, capable of recording each complete EEM in 12 s. This allows the acquisition of 10 successive EEMs, at different reaction times, during the development of the oxidation reaction, given rise to the four-way data set employed. The procedure, which had been previously reported for urine determination, is extended to serum analysis in this work. The combination of U-PLS/RTL is providing enhanced predictive results in comparison with standard methods as PARAFAC and N-PLS, in the presence of human serum, where significant unexpected components and or inner filter effects may occur.

Keywords: Four-way data; Unfolded-partial least-squares; Residual trilinearization; Folic acid; Methotrexate; Human serum

1. Introduction

Methotrexate (MTX, 2,4-diamine-*N*,10-methylpteroyl glutamic acid) is a drug included into the antineoplastic and antirheumatic therapeutic categories. It belongs to the antifolates family which produced the first striking, although temporary remission in leukemia and the first cure of a solid tumor, choriocarcinoma [1–5]. At low doses, it is also used in the treatment of psoriatic arthritis and rheumatoid arthritis. Although very effective, its use potentially may produce serious side effects including nausea, mouth ulcers, blood problems, liver cirrhosis, and hair loss. Prolonged treatment with MTX may also lead to folic acid deficiency. To reduce the risk of these side effects, without fear of interfering with its efficacy, a daily dose of folic acid is recommended for those patients taking MTX on a regular weekly basis.

On the other hand, low levels of folic acid (FA, 4-(2-amino-4-hydroxypteridin-6-yl)methylamino-benzoyl-L-glutamic acid), may play a role in cancer development, particularly cancers of cervix, lung and colon [2]. It was found that patients who took folic acid supplements, along with the arthritis drug methotrexate, were less likely to have a malfunctioning liver and less side effects, than those taking just methotrexate [3–5].

In this context, Baker et al. have designed a nanoparticle drug that contains folic acid, methotrexate and fluorescein, with the object of increasing methotrexate antitumor activity and decreasing its toxicity, in the first in vivo study of the therapeutic effect of targeted drug–dendrimer conjugates [6].

The first studies about spectrofluorimetric methods based on oxidation of MTX to pteridine carboxylic, using permanganate, date from 1969 [7]. This reaction was applied to study plasma levels in cancer patients [8] and a kinetic method was

* Corresponding author.
E-mail address: arsenio@unex.es (A. Muñoz de la Peña).

0039-9140/$ – see front matter © 2007 Elsevier B.V. All rights reserved.
doi:10.1016/j.talanta.2007.01.018

developed in our laboratory for its determination in human serum [9].

Its determination by HPLC with fluorimetric detection, also involves derivatization reactions, such as photo-oxidative irradiation at 254 nm in presence of hydrogen peroxide [10–13], oxidation with permanganate in slightly acid medium [14,15], and oxidative cleavage using hydrogen peroxide in presence of phosphate buffer [16–18] or cerium (IV) trihydroxyhydroperoxide [19,20]. Another possibility is the degradation reaction of MTX in acidic solution and the conversion in its degradation product 4-amino-4-deoxy-10-methylpteroic acid [21].

Folic acid itself has little native fluorescence but, by oxidation, it can be turned into a strongly fluorescent compound. Manual fluorimetric methods based on oxidation with permanganate [22] and hydrogen peroxide [23] have been reported. Flow-injection was also used for the oxidation of folic acid using a lead dioxide solid-phase reactor for on-line oxidation [24], or by photochemical reaction [25].

There are no reported methods for the simultaneous determination of both compounds in serum and the analytical methods proposed are mainly applied to urine samples. A simple procedure using capillary zone electrophoresis to determine methotrexate, folinic acid and folic acid in human urine has been developed [26]. In addition, a chromatographic and densitometric method for the determination of folic acid as impurity in methotrexate has been also proposed [27].

The availability of high-order instrumental data coupled to newly chemometric algorithms for data processing, is increasing the regular use of multi-way analysis for solving complex analytical problems. Multi-way data posses an interesting property: the second-order advantage [28]. This property describes the analysis in the presence of unexpected components. Second-order, i.e., matrix data for a given sample, can be produced in a variety of ways, among which one of the simpler is an excitation–emission fluorescence matrix (EEM). When a sample produces a data matrix (a second-order tensor), such as an EEM, the corresponding set obtained by 'stacking' the training matrices is a three-way array.

On the other hand, four-way arrays can be obtained by stacking three-way data obtained when the evolution of a kinetic reaction is followed recording EMMs. The latter data have scarcely been employed to date for developing analytical methodologies. The only reported applications are related to chlorophylls *a* and *b* [29], adrenaline and noradrenaline [30], benzo[*a*]anthracene, benzo[*k*]fluoranthene and dibenzo[*a*,*h*]anthracene [31], 2,3,7,8-tetrachloro-dibenzo-*para*-dioxin [32], methotrexate and leucovorin [33,34], folic acid and methotrexate [35] and femvalerate [36].

This kind of data has been usually processed by resorting to the well-known parallel factor analysis (PARAFAC) method [37]. Very recently, the combination of trilinear least-squares with residual trilinearization (TLLS/RTL) has also been proposed as a new algorithm for four-way data treatment, and shown to be useful for the analysis of complex samples [33,34]. Alternative methodologies based on the use of latent variables do also exist for processing four-way data, such as multi-way partial least-squares (N-PLS), and the unfolded variant of PLS (U-PLS), both of them lacking the second-order advantage [38]. On the other hand, a lately variant, U-PLS coupled to RTL [34], appears to be more suitable than PARAFAC when analytes present strong overlapping with the serum signal or inner filter effects occur. This fact has been already demonstrated for second order data with the counterpart U-PLS residual bilinearization (RBL) approach [39,40].

The aim of the present report was to exploit the potentiality of U-PLS/RTL, as a multi-way modelling approach, for the simultaneous quantitation of MTX and FA in a complex biological sample (human serum), when no satisfactory results are obtained by application of PARAFAC or N-PLS modelling. It is interesting to note that this is the first time where U-PLS/RTL is demonstrated to perform better than PARAFAC or N-PLS in a real biological problem. To perform the determination, both analytes were converted into highly fluorescent compounds, by oxidation with potassium permanganate, and the time evolution of excitation–emission matrices (EEMs) was recorded in order to apply the third-order calibration method.

2. Experimental

2.1. Apparatus and software

Fluorescence spectral measurements were performed on a Varian Cary Eclipse fluorescence spectrophotometer, equipped with two Czerny–Turner monochromators and a xenon flash lamp, and connected to a PC microcomputer via an IEEE 488 (GPIB) serial interface. The Cary Eclipse software was used for data acquisition. Fluorescence measurements were recorded in a 10 mm quartz cell at 20 °C, by use of a thermostatic cell holder and a Selecta thermostatic bath.

All calculations were done using MatLab 5.3, using different routines and graphical interfaces: MVC3, an integrated MatLab toolbox for third-order calibration, developed by Olivieri [33], which allow to perform third-order calibration, with different methods, including PARAFAC [37], unfolded-PLS coupled to residual trilinearization (RTL) [34], N-PLS [38] and TLLS coupled to RTL [34].

2.2. Reagents

All experiments were performed with analytical reagent grade chemicals. Folic acid and methotrexate were obtained from Sigma. Ultra pure water was obtained from a Milli-Q system (Waters Millipore). Stock standard solutions of FA and MTX were prepared by dissolving 0.010 g of these compounds in 100 mL of alkalinized ultra pure grade water. Exposure to direct sunlight was avoided. Working FA and MTX solutions of different concentrations were prepared by dilution of stock solutions with ultra pure water. Buffer solution (pH 3.4, $C_t = 0.5$ M) was prepared from chloroacetic acid and sodium chloroacetate (Panreac). A 4.2×10^{-4} M $KMnO_4$ (Panreac) stock solution was also prepared with ultra pure water.

2.3. Calibration and test sets

In this work, the method of external calibration was employed. For this purpose, a calibration set of 13 samples was constructed, using a central composite design combined with a three level full factorial design. The levels correspond to values in the range 0–1 mg L^{-1} for FA and MTX. Reagents were mixed in the measuring cell, by pipetting an appropriate volume of FA and MTX solution, add deionised water, if necessary, to complete1 mL, 1 mL of 0.12 M chloroacetic/chloroacetate buffer solution and 1 mL of 1.4×10^{-4} M $KMnO_4$ solution. The instrument was set up as follows: monochromators band pass ex/em (nm/nm) = 5/10, detector voltage 550 V and 20 °C of temperature.

The time evolution of EEMs of these solutions was then recorded, and the obtained data were subjected to four-way analysis, as described later. EEMs were recorded at 6 nm intervals for excitation, and at 5 nm intervals for emission. The rapid-scanning instrument allows the acquisition of a complete EEM in 0.2 min at a wavelength scanning speed of 24,000 nm/min. Ten EEMs were obtained at intervals of 0.7 min. It should be noticed that, if reaction significantly evolves during spectral acquisition, the data sample would not be strictly trilinear. In our case, we did not find this problem to be important.

First, the EEMs were recorded in wide spectral excitation, from 200 to 400 nm, and emission ranges, from 350 to 600 nm, respectively, and show Rayleigh scattering and second harmonics from the diffraction grating. These wide ranges were optimized to avoid the Rayleigh scattering and diffraction grating harmonics. These latter signals are undesirable because they are not correlated with the target concentrations of the analytes studied. Therefore, for calibration and prediction purposes, the EEMs were subsequently recorded, as a function of time, in sensible restricted excitation, from 260 to 380 nm, and emission, from 400 to 510 nm, respectively.

2.3.1. Serum samples

Volumes of 100 μL of serum samples (a pool of serum taken from healthy individuals, obtained from the Hospital Infanta Cristina, Badajoz, Spain) were centrifuged for 5 min. Then, 10 μL of the supernatant were placed in the quartz cell and spiked with concentrations of both analytes, selected a random from their corresponding calibration ranges and treated as described for the calibration set. The level of serum dilution implies that the present calibration scheme covers concentration ranges up to 300 mg L^{-1} for FA and MTX, which are within the serum levels for MTX and FA treatment [41,42].

2.4. Theory

2.4.1. U-PLS/RTL

The theory corresponding to the U-PLS algorithm, in combination with residual bilinearization (RBL) was recently published [43]. The U-PLS/RBL model constitutes a second-order multivariate calibration method capable of achieving the second-order advantage [43–45]. For four-way calibration, U-PLS, combined with residual trilinearization (RTL) constitutes an extension of U-PLS/RBL one further dimension [34] and will be briefly described in this section. When using four-way data, in the U-PLS method, the original matrix data is transformed into uni-dimensional arrays (vectors) by concatenating (unfolding) the original three-dimensional information, and concentration information is first employed into the calibration step (without including data for the unknown sample) [46]. The I calibration third order array $\underline{\mathbf{X}}_{c,i}$ (size $J \times K \times L$, where J, K and L are the number of channels in each dimension) are vectorized (unfolded) and a usual U-PLS model is calibrated with these data and the vector of calibration concentrations $\mathbf{y}$ ($I \times 1$, where I is the number of calibration samples). This provides a set of loadings $\mathbf{P}$ and weight loadings $\mathbf{W}$ (both of size $JKL \times A$, where A is the number of latent factors), as well as regression coefficients $\mathbf{v}$ (size $A \times 1$). The parameter A can be selected by techniques such as leave-one-out cross-validation [47]. If no unsuspected interferences occur in the test sample, $\mathbf{v}$ can be employed to estimate the analyte concentration:

$$y_u = \mathbf{t}_u^T \mathbf{v} \tag{1}$$

where $\mathbf{t}_u$ (size $A \times 1$) is the test sample score, obtained by projection of the (unfolded) data for the test sample $\underline{\mathbf{X}}_u$ [vec($\underline{\mathbf{X}}_u$), size ($JKL \times 1$)] onto the space of the A latent factors:

$$\mathbf{t}_u = (\mathbf{W}^T\mathbf{P})^{-1}\,\mathbf{W}^T\,\mathrm{vec}(\underline{\mathbf{X}}_u) \tag{2}$$

When uncalibrated constituents occur in $\underline{\mathbf{X}}_u$, then the sample scores given by Eq. (1) are not suitable for analyte prediction using Eq. (2). In this case, the residuals of the U-PLS prediction step will be abnormally large in comparison with the typical instrumental noise assessed by replicate measurements:

$$S_p = \frac{\|\mathrm{vec}(\underline{\mathbf{E}}_p)\|}{(JKL-A)^{1/2}} = \frac{\left\|\mathrm{vec}(\underline{\mathbf{X}}_u) - P(\mathbf{W}^T\mathbf{P})^{-1}\mathbf{W}^T\,\mathrm{vec}(\underline{\mathbf{X}}_u)\right\|}{(JKL-A)^{1/2}} = \frac{\|\mathrm{vec}(\underline{\mathbf{X}}_u - \mathbf{P}\mathbf{t}_u)\|}{(JKL-A)^{1/2}} \tag{3}$$

where $\|\cdot\|$ indicates the Euclidean norm, and $JKL-A$ corresponds to the degree of freedom (number of variables minus number of adjustable parameters).

If interferent components occur in the test sample, the situation can be handled by a separate procedure called residual trilinearization, based on a Tucker3 decomposition, that models the interferent effects, as already described [34]. RTL aims at minimizing the norm of the residual vector $\mathbf{e}_u$, computed while fitting the sample data to the sum of the relevant contributions to the sample signal. For a single interferent the relevant expression is:

$$\mathrm{vec}(\underline{\mathbf{X}}_u) = \mathbf{P}\mathbf{t}_u + g_{int}(\mathbf{d}_{int} \otimes \mathbf{c}_{int} \otimes \mathbf{b}_{int}) + \mathbf{e}_u \tag{4}$$

where $\mathbf{b}_{int}$, $\mathbf{c}_{int}$ and $\mathbf{d}_{int}$ are normalized profiles in the three modes for the interference and g_{int} is the first core element obtained for Tucker3 analysis of $\underline{\mathbf{E}}_p$ in the following way:

$$(g_{int}, \mathbf{b}_{int}, \mathbf{c}_{int}, \mathbf{d}_{int}) = \mathrm{Tucker3}(\underline{\mathbf{E}}_p) \tag{5}$$

During this RTL procedure, $\mathbf{P}$ is kept constant at the calibration values and $\mathbf{t}_u$ is varied until $\|\mathbf{e}_u\|$ is minimized. The

minimization can been carried out using either a Gauss–Newton (GN) procedure or an alternating least squares algorithm, in both cases starting with $\mathbf{t}_u$ from Eq. (2). Once $\|\mathbf{e}_u\|$ is minimized in Eq. (4), the analyte concentrations are provided by Eq. (1), by introducing the final $\mathbf{t}_u$ vector found by the RTL procedure.

The number of interferents N_i can be assessed by comparing the final residuals s_u with the instrumental noise level:

$$s_u = \frac{\|\mathbf{e}_u\|}{[JKL - (N_c + N_i)]^{1/2}} \quad (6)$$

where $\mathbf{e}_u$ is from Eq. (4) and N_c is the number of calibrated analytes. Typically, a plot of s_u computed for trial number of components will show decreasing values, starting at s_p when the number of components is equal to A (the number of latent variables used to described the calibration data), until it stabilizes at a value compatible with the experimental noise, allowing to locate the correct number of components.

2.4.2. PARAFAC

The I calibration third order array $\underline{\mathbf{X}}_{c,i}$ (size $J \times K \times L$) can be joined with the unknown sample array $\underline{\mathbf{X}}_u$ into a four-way data array $\boldsymbol{X}$, whose dimensions are $[(I_{cal} + 1) \times J \times K \times L]$. In the PARAFAC model, a generic element X_{ijk} of the four-dimensional array $\boldsymbol{X}$ can be written as follows [37]:

$$X_{ijk} = \sum_{n=1}^{N} a_{in} b_{nj} c_{nk} d_{nl} + E_{ijkl} \quad (7)$$

where N is the total number of responsive components, $\underline{E}_{ijkl}$ an element of a residual error array $\boldsymbol{E}$ of the same dimensions as $\boldsymbol{X}$, a_{ni}, b_{nj}, c_{nk} and d_{nl} are the elements of the column vectors $\mathbf{a}_n$, $\mathbf{b}_n$, $\mathbf{c}_n$ and $\mathbf{d}_n$, which are the relative concentration $[(I+1) \times 1]$, emission $(J \times 1)$, excitation $(K \times 1)$ and time channel $(L \times 1)$ profiles for component n, respectively. The column vectors $\mathbf{a}_n$, $\mathbf{b}_n$, $\mathbf{c}_n$ and $\mathbf{d}_n$ are collected into the four loading matrices **A**–**D** ($\mathbf{b}_n$, $\mathbf{c}_n$ and $\mathbf{d}_n$ are usually normalized to unit length). Decomposition of the four-way array provides the profiles **B**–**D**, corresponding to the emission and excitation wavelengths, the time channel, and the relative concentrations (**A**) of individual components in the $(I+1)$ mixtures, whether they are chemically known or not, comprising the basis of the so-called second-order advantage.

To estimate the number of responsive components (N), the consideration of the PARAFAC internal parameter known as core consistency [48] is a useful technique. The parameter known as Concordia (%) is obtained through the following equation:

$$C(\%) = 100\% \times \left(1 - \frac{\sum_{d=1}^{N}\sum_{e=1}^{N}\sum_{f=1}^{N}(g_{def} - t_{def})^2}{\sum_{d=1}^{N}\sum_{e=1}^{N}\sum_{f=1}^{N} t_{def}^2}\right) \quad (8)$$

where g_{def} and t_{def} are the elements of the calculated core and of the intrinsic super-diagonal core, respectively, and N is the number of components of the model, defined by dimensions $(d \times e \times f)$. If they are equal, the core consistency is perfect and has a value of unity (100%). The appropriate number of components is accessed by the model with the highest number of components and a valid value of core consistency diagnostic test.

In the present case, the number of components is equal to the number of different species in the sample. For binary mixture standards, this number is 2, while for serum samples spiked with the analytes this number reaches 3 or 4 on account of the presence of the two analytes plus the background signal originated by serum components (presence of unexpected components).

Identification of the chemical constituent under investigation is done with the aid of the profiles **B**–**D**, as extracted by PARAFAC, and comparing them with those for a standard solution of the analyte of interest. On the other hand, absolute analyte concentrations are obtained after proper calibration, since only relative values (**A**) are provided by decomposing the three-way data array. Experimentally, this is done by using the information for the set of standards of known composition. The calibration procedure involves decomposing an array formed by joining the matrices for the I training samples with that for the unknown. Resorting to Eq. (7), once the component profiles have been obtained, the scores for the standard samples associated with a particular component are linearly related to the nominal concentrations of the analyte:

$$[a_{n1}|a_{n2}|\cdots|a_{n1}] = k_{PARAFAC}\mathbf{y} \quad (9)$$

where n identifies a PARAFAC component, and $\mathbf{y}$ is an $I \times 1$ vector holding the nominal analyte concentrations in the I calibration standards. It should be noticed that employment of this joined calibration mode implies that the array decomposition should be repeated for each newly analyzed sample.

2.4.3. N-PLS

Multiway regression methods such as N-PLS extend the traditional PLS algorithm to higher orders, using the multidimensional structure of the data for model building and prediction [38]. In the case of four-way data, the model is given by the following equation:

$$x_{ijkl} = \sum_{f=1}^{F} t_{if} w_{jf}^{J} w_{kf}^{K} w_{lf}^{L} + e_{ijkl} \quad (10)$$

where x_{ijkl} is the fluorescence intensity measured for sample i at emission wavelength j and excitation wavelength k and time l. The scalar F is the number of components, t_{tf} is an element of the score matrix $\mathbf{T}$, w_{jf}^{J}, w_{kf}^{K} and w_{lf}^{K} are elements of three $\mathbf{W}$ loading matrices, and e_{ijkl} is a residue not fitted by the model. The model finds the scores yielding maximum covariance with analyte concentrations as the dependent variable, in a four-dimensional sense. The advantage of using N-PLS is a stabilization of the decomposition involved in Eq. (10), which potentially gives increased interpretability and better predictions. However, this methodology does not exploit the second-order advantage, and in principle, it should lead to results of a lower quality as compared to PARAFAC or U-PLS/RTL in samples of complex composition like the analyzed in the present work.

2.4.4. Figures of merit

Figures of merit are analytical parameters used for the comparison of methods. In order to calculate the sensitivity, Eq. (11) was applied to a similar case than the one studied herein [33]:

$$\mathrm{SEN} = k\{[[(\mathbf{B}^{\mathrm{T}}\mathbf{B}) * (\mathbf{C}^{\mathrm{T}}\mathbf{C}) * (\mathbf{D}^{\mathrm{T}}\mathbf{D})]^{-1}]_{nn}\}^{-1/2} \quad (11)$$

where "∗" is the element-wise product operator and k is an appropriate scaling actor. In PARAFAC, k is identified with the proportionality constant between scores and concentrations (Eq. (9)), while in U-PLS/RBL it can be obtained by regressing the g_{int} values (Eq. (4)) against **y**. Note that when serum is included in the samples, **B**–**D** include interference profiles and hence a decrease in sensitivity is expected. When the second-order advantage is achieved, Eq. (11) implies a SEN value that is sample-specific and that cannot be defined for the multivariate method as a whole. We thus report average values for a set of representative samples.

On the other hand, the LOD can be estimated using the expression [33]:

$$\mathrm{LOD} = \frac{3.3 s_{\mathrm{r}}}{\mathrm{SEN}} \quad (12)$$

where s_{r} is the instrumental noise level and the appropriate SEN value is employed. Eq. (12) does not account for calibration uncertainties, and hence, it generally provides overoptimistic values. In the case of serum samples, because the value of SEN is given as an average value over a test sample set, LOD is also reported as an average figure.

3. Results and discussion

3.1. Fluorimetric kinetics study of the analytes

FA and MTX are weakly fluorescent compounds but their oxidation, in presence of potassium permanganate, generated two products which are strongly fluorescent. The instrumental and experimental parameters of the corresponding oxidation reactions were already studied and optimized, in order to obtain the appropriate kinetics and fluorescence properties of the products originated. Wittle et al. [49] described how permanganate oxidation of folic acid gives rise to two main fragments, a strongly fluorescent substance identified as 2-amino-4-hydroxy-pteridine-6-carboxylic acid and a second, non-pteridine component. The excitation and emission spectra of the oxidation products, in presence of potassium permanganate, obtained at 7 min of reaction time, show maxima at 350 and 336 nm, for excitation and at 446 and 469 nm, for emission, for FA and MTX, respectively [35]. A strong overlap between their fluorescence spectra can be noted.

As already stated, the determination of mixtures of FA and MTX in urine samples has been previously proposed [35]. First-, second- and third-order methods were investigated and, owing to the complexity of the problem to be solved, third-order calibration was necessary to resolve the mixture. The four-way data used were obtained by recording the evolution with the time of EEM fluorescence measurements, and four-way parallel factor analysis (PARAFAC) or multi-way partial least squares (N-PLS) chemometric calibration.

The proposed method of determination, of mixtures of FA and MTX, was performed at pH 3.4, using a 0.04 mol L^{-1} chloroacetic/sodium chloroacetate buffer solution, and $KMnO_4$ 1.4×10^{-4} mol L^{-1}, at 20 °C [35].

The four-way data used were obtained by recording the evolution with the time of EEM fluorescence measurements, and four-way parallel factor analysis (PARAFAC) and multi-way partial least squares (N-PLS) chemometric calibration were applied satisfactorily, in urine samples. No significant differences were found using the two approaches in this particular case.

It is necessary to remark that, in Ref. [35], the proposed method was applied to urine samples and, in this manuscript, the method was applied to serum samples. As serum background is more complex than urine background and significant unexpected components and or inner filter effects may occur, PARAFAC and N-PLS fail in given adequate prediction results. This is different to the case of urine samples, where the above mentioned methods work properly. This was the reason of investigating in this work a new approach, U-PLS in combination with RTL that has demonstrated its utility in similar situations [39,40].

3.2. Third-order calibration methods

Fig. 1 shows the four-way data array structure used in this work, following the time evolution of the EEM of one of the calibration mixtures, in the presence of potassium permanganate. It can be appreciated that the fluorescence intensity of the analytes increases considerably as a function of reaction time. This provided sensitivity for the determination which is significantly larger than that achieved in the absence of oxidant.

Taking into account the results previously found, we should use the four-way data, following the evolution with time of the EEM of binary mixtures of MTX and FA, for the determination of the analytes in serum samples. The ranges selected were 420–505 nm for emission, 266–374 nm for excitation and 0–5 min for time, for FA and, 455–510 nm for emission, 302–362 nm for excitation and 0–5 min for time, for MTX. The investigated calibration methods were N-PLS, PARAFAC and U-PLS/RTL, a new methodology, recently proposed [34], which applications are practically unexplored.

Fig. 2 shows the experimental design composed of 13 calibration samples, using a central composite design combined with a three level full factorial design, used to generate the data array. The serum samples test set was generated using a random design, i.e., selecting the target concentrations of both analytes at random from the calibration range of each analyte (see Table 1 for details on the composition of these samples).

The number of latent variables was established in N-PLS by resorting to the well-known cross-validation leave-one-sample-out procedure, according to the criterion of Haaland and Thomas [47]. The optimum number of factors was estimated by calculating the ratios $F(A) = \mathrm{PRESS}\ (A < A^*)/\mathrm{PRESS}\ (A)$ (where $\mathrm{PRESS} = \sum(C_{i,\mathrm{act}} - C_{i,\mathrm{pred}})^2$, A is a trial number of factors and A^* corresponds to the minimum PRESS) and selecting the num-

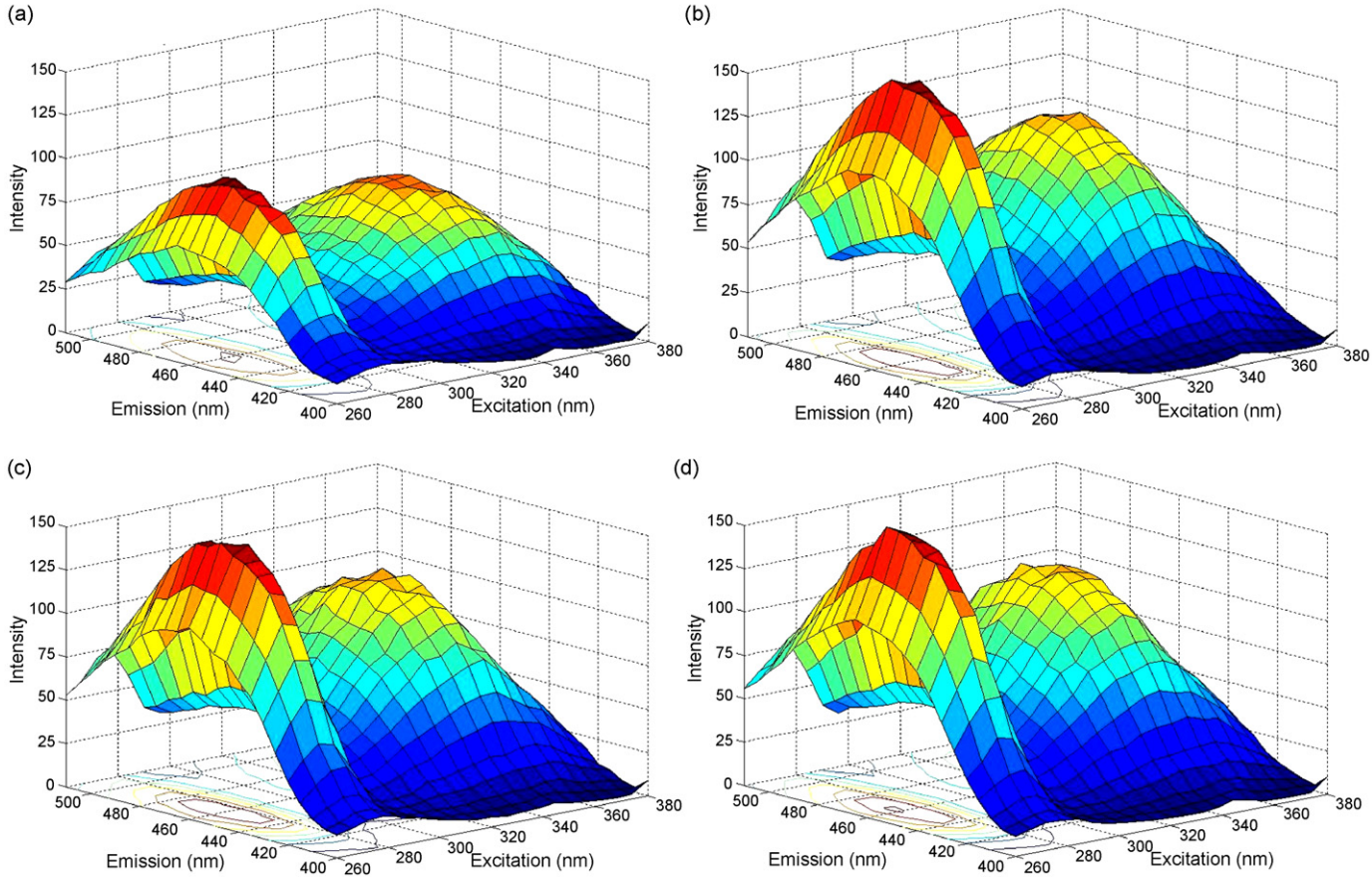

Fig. 1. Excitation–emission matrices (EEMs) for an aqueous solution (pH 3.4) containing 0.5 mg L^{-1} FA and 0.5 mg L^{-1} MTX, as a function of the time of permanganate oxidation. Time selected for illustrating the kinetic evolution of the EEMs (in min): (a) 0, (b) 2.1, (c) 4.2 and (d) 6.3.

ber of factors leading to a probability of less than 75% that $F > 1$. This analysis led to the conclusion that the later number was 2 for both calibration models corresponding to each analyte. On the other hand, the core consistency analysis (see above) was applied for selecting the number of spectral components in PARAFAC

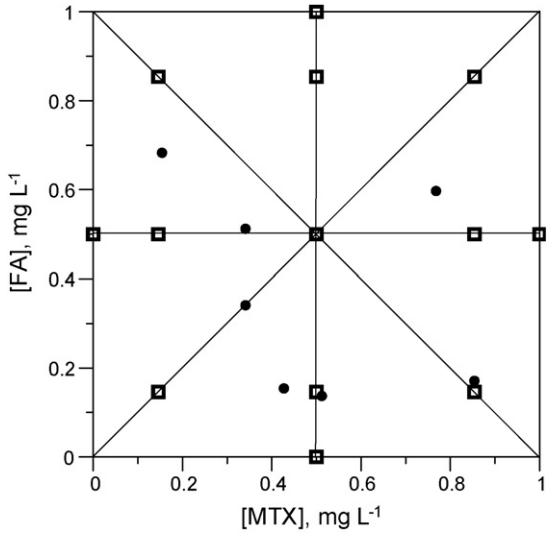

Fig. 2. Experimental design used in the studies of MTX and FA mixtures. (■) Calibration set and (●) serum test set.

[49]. This latter test allowed us to find the optimum number of factors to be used when predicting the analytes concentration in both validation and test samples. Interestingly, for the calibration set, which was prepared with pure standard mixtures, the number of factors was 2, while this number reached 3 or 4 for those samples prepared by spiking real serum. This explains that unexpected components are present in the latter samples. However, unsatisfactory results were obtained from this complicated mixture by PARAFAC or N-PLS (relative error of prediction values higher than 30%). These results are quite different to those obtained when analysing this mixture in synthetic samples (REP = 4–8%), although REP values among 9–23% were found in urine samples [35].

Afterwards, U-PLS/RTL was applied in order to evaluate if an improvement of the results can be obtained respect to PARAFAC and N-PLS. When U-PLS was applied, two latent variables were estimated by means of cross validation [47], fact that agrees well with the number of factors for N-PLS analysis. Subsequently, two additional components were necessary to consider in the RTL procedure when the test set was analysed, suggesting two unexpected components in the serum samples. Fig. 3 shows the variation of prediction residuals (s_u) as a function of trial values of the number of interferents (N_i). The plot shows that when the analysed sample is one corresponding to the test set (sample #2), the necessary number of

Table 1
Results obtained when applying U-PLS/RTL in the analysis of serum samples

FA			MTX		
Actual (mg L^{-1})	Predicted (mg L^{-1})	Rec. (%)	Actual (mg L^{-1})	Predicted (mg L^{-1})	Rec. (%)
0.51	0.56	110	0.34	0.30	88
0.34	0.33	97	0.34	0.36	106
0.68	0.52	76	0.15	0.18	120
0.00	–	–	0.96	1.10	115
0.99	0.86	87	0.00	–	–
0.43	0.45	81	0.84	0.88	105
0.68	0.71	104	0.71	0.67	94
Av. Rec.[a] (%)		93 (13)	Av. Rec.[a] (%)		105 (12)
REP[b] (%)		12	REP[b] (%)		11

[a] Average recovery. Values between parentheses correspond to the standard deviations computed for the recoveries of the seven serum samples.
[b] REP (%): relative error of prediction.

factors for interferences (N_i) reaches 2. As can be seen, this model shows a prediction residual comparable to the instrumental noise level (ca. 1.5 fluorescence units). Predictions using the U-PLS/RTL model are collected in Table 1. As regard the figures of merit for the proposed methodology, LODs were calculated as average values (see above) for a set of representative samples. The obtained values are the following: FA, 0.014 mg L^{-1} and MTX, 0.085 mg L^{-1}. Also, the lineal range was studied and it was found from 0 to 10 mg L^{-1} for FA and to 4 mg L^{-1} for MTX.

In order to get further insight into the accuracy and precision of the algorithm analysed, nominal versus found concentration values were compared by application of the EJCR test. This approach based on the bivariate least squares (BLS) calibration method, computes the joint confidence interval for the intercept and the slope [50,51]. The estimated intercept and slope ($\hat{a}$ and $\hat{b}$, respectively) were compared with their ideal values of 0 and 1 using the elliptical joint confidence region test [52]. Fig. 4 shows the EJCR plots for FA and MTX analysis. As can be seen, the ellipses contain the theoretical ($a = 0$ and $b = 1$) point, what means that no significant differences were found for the confidence level proposed (95%). When U-PLS/RTL was applied, all predictions are seen to be reasonable for samples of the complexity of human serum.

The improved analytical results of U-PLS/RTL over the classical PARAFAC and N-PLS models could probably be understood considering that U-PLS takes better account of the analyte-background interactions due to its latent variable properties. On the other hand, N-PLS does not resort to the second order advantage, as was previously mentioned. Similar results have been already reported in the analysis of complex biological samples, for second order data, in the cases where matrix interferents and/or inner filter effects occur [39,40,53].

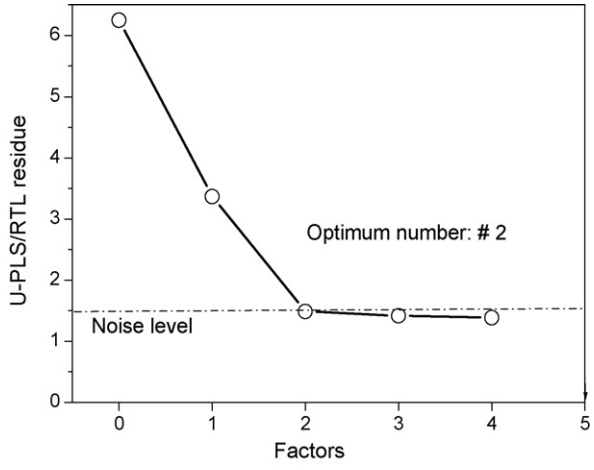

Fig. 3. Plot of the prediction residuals (s_u) a function of a trial number of interferent components (N_i) for serum sample 2, containing 0.34 mg L^{-1} FA and 0.34 mg L^{-1} MTX concentrations. The noise level in this system is ca. 1.5 fluorescence intensity units (–·–·–).

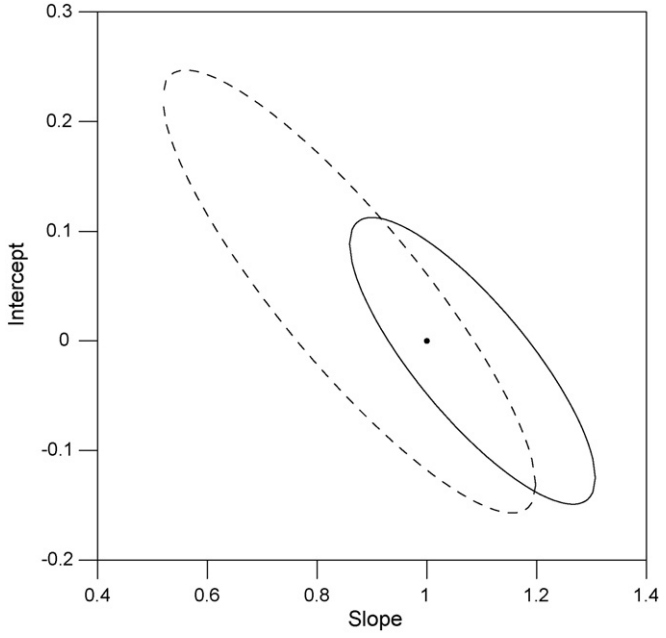

Fig. 4. Plots of the elliptical joint regions (at 95% confidence level), for the slope and intercept, of the least squares regression of the FA (—) and MTX (– – –) plots, of concentrations predicted by the U-PLS/RBL model, in the serum sample set, as a function of the corresponding nominal values. The black point marks the theoretical (1, 0) point.

4. Conclusions

Different multi-way calibration methods have been employed in order to solve methotrexate and folic acid mixtures in a complex biological sample, in which the fluorescence spectra of the mixture components are highly overlapped. Third-order calibration methods were necessary for the determination of these analytes in serum samples and, due to the complexity of the matrix background, only the U-PLS/RTL method was capable to resolve the problem, obtaining satisfactory results. The use of four-way arrays of data exploiting the information contained in a full fluorescence EEM spectrum, in combination with kinetic methods, is a promising tool for complex multicomponent analysis. The time-dependent formation of fluorescent products, by permanganate oxidation, provides and additional order of selectivity with which to determine the analytes of interest. The calibration by U-PLS, including additional latent variables in the model, in combination with RTL, achieving the second-order advantage, considerably improved the analytical results, allowing the folic acid and methotrexate calibration in serum samples.

Acknowledgements

Financial support from the Ministerio de Educación y Ciencia of Spain (Project CTQ 2005-02389) is acknowledged. HCG thanks Universidad Nacional del Litoral (Project CAI + D No. 4-30) and CONICET (Consejo Nacional de Investigaciones Científicas y Técnicas) for financial support.

References

[1] J.R. Bertino, J. Clin. Oncol. 11 (1993) 5–14.
[2] Cancers, Nutrition, Food, World Cancer Research Fund/American Institute for Cancer Research, Washington, DC, 1997.
[3] G.K. Endresen, G. Husby, Tidsskr Nor Laegeforen 119 (1999) 534–537.
[4] Z. Ortiz, B. Shea, M.E. Suarez-Almazor, D. Moher, G.A. Wells, P. Tugwell, J. Rheumatol. 25 (1998) 36–43.
[5] O.K. Jensen, C. Rasmussen, F. Mollerup, P.B. Christensen, H. Hansen, S. Ekelund, A.M. Thulstrup, J. Rheumatol. 29 (2002) 1615–1618.
[6] J.F. Kukowska-Latallo, K.A. Candido, Z. Cao, S.S. Nigavekar, I.J. Majoros, T.P. Thomas, L.P. Balogh, M.K. Khan, J.R. Baker Jr., Cancer Res. 65 (2005) 5317–5324.
[7] S.G. Chakrabarti, I.A. Bernstein, Clin. Chem. 15 (1969) 1157–1161.
[8] J.M.J. Kinkade, W.R. Vogler, P.G. Dayton, Biochem. Med. 10 (1974) 337–350.
[9] A. Espinosa-Mansilla, I. Durán Merás, A. Zamoro, L. Pedano, C. Ferreyra, J. Pharm. Biomed. Anal. 29 (2002) 851–858.
[10] Z. Yu, D. Westerlund, K.S. Boos, J. Chromatogr.: Biomed. Appl. 689 (1997) 379–386.
[11] O. Beck, P. Seideman, M. Wennberg, C. Peterson, Ther. Drug Monit. 13 (1991) 528–532.
[12] J. Salamoun, M. Smrz, F. Kiss, A. Salamounova, J. Chromatogr.: Biomed. Appl. 419 (1987) 213–223.
[13] J. Salamoun, J. Frantisek, J. Chromatogr.: Biomed. Appl. 378 (1986) 173–181.
[14] T. Suzuki, H. Hashimoto, N. Ichinose, Fresen. J. Anal. Chem. 351 (1995) 806–807.
[15] I. Durán Merás, A. Espinosa Mansilla, M.J. Rodríguez Gómez, Anal. Biochem. 346 (2005) 201–209.
[16] E.A. McCrudden, S.E. Tett, J. Chromatogr.: Biomed. Appl. 721 (1999) 87–92.
[17] F. Albertioni, C. Rask, S. Eksborg, J.H. Poulsen, B. Pettersson, O. Beck, H. Schroeder, C. Peterson, Clin. Chem. 42 (1996) 39–44.
[18] F. Albertioni, B. Pettersson, O. Beck, C. Rask, P. Seideman, C. Peterson, J. Chromatogr.: Biomed. Appl. 665 (1995) 163–170.
[19] S. Emara, S. Razee, A. Khedr, T. Masujima, Biomed. Chromatogr. 11 (1997) 42–46.
[20] S. Emara, H. Askal, T. Masujima, Biomed. Chromatogr. 12 (1998) 338–342.
[21] S.M. Sabry, M. Abdel-Hady, M. Elsayed, O.T. Fahmy, H.M. Maher, J. Pharm. Biomed. Anal. 32 (2003) 409–423.
[22] N. Ichinose, T. Tsuneyoshi, M. Kato, T. Sukuzi, S. Ikeda, Fresen. J. Anal. Chem. 346 (1993) 841–846.
[23] X. Liu, H.G. Huang, Fenxi-Huaxue, Chin. J. Anal. Chem. 30 (2002) 1018.
[24] Z.Q. Zhang, Y. Tang, Anal. Bioanal. Chem. 381 (2005) 932–936.
[25] R.A.S. Lapa, J.L.F.C. Lima, B.F. Reis, J.L.M. Santos, E.A.G. Zagatto, Anal. Chim. Acta 351 (1997) 223–228.
[26] J. Rodríguez Flores, G. Castañeda Peñalvo, A. Espinosa Mansilla, M.J. Rodríguez Gómez, J. Chromatogr. B 819 (2005) 141–147.
[27] J. Krzek, A. Kwiecien, Chem. Anal. 45 (2000) 551–559.
[28] K.S. Booksh, B.R. Kowalski, Anal. Chem. 66 (1994) 782A.
[29] Y. Tan, J.H. Jiang, H.L. Wu, H. Cui, R.Q. Yu, Anal. Chim. Acta 412 (2000) 2798–2806.
[30] R.P.H. Nikolajsen, K.S. Booksh, A.M. Hansen, R. Bro, Anal. Chim. Acta 475 (2003) 137–150.
[31] Y.C. Kim, J.A. Jordan, M.L. Nahorniak, K.S. Booksh, Anal. Chem. 77 (2005) 7679–7686.
[32] H.C. Goicoechea, S. Yu, A.C. Olivieri, A.C. Campiglia, Anal. Chem. 77 (2005) 2608–2616.
[33] A.C. Olivieri, J.A. Arancibia, A. Muñoz de la Peña, I. Durán Merás, A. Espinosa Mansilla, Anal. Chem. 76 (2004) 5657–5666.
[34] J.A. Arancibia, A.C. Olivieri, D. Bohoyo Gil, A. Espinosa Mansilla, I. Durán-Merás, A. Muñoz de la Peña, Chemom. Intell. Laborat. Syst. 80 (2006) 77–86.
[35] A. Muñoz de la Peña, I. Durán Merás, A. Jiménez Girón, Anal. Bioanal. Chem. 385 (2006) 1289–1297.
[36] M.L. Nahorniak, G.A. Cooper, Y.-C. Kim, K.S. Booksh, Analyst 130 (2005) 85–93.
[37] C.M. Andersen, R. Bro, J. Chemom. 17 (2003) 200–215.
[38] R. Bro, J. Chemom. 10 (1996) 47–61.
[39] M.J. Culzoni, H.C. Goicoechea, A.P. Pagani, M.A. Cabezon, A.C. Olivieri, Analyst 131 (2006) 718–723.
[40] G.N. Piccirilli, G.M. Escandar, Analyst 131 (2006) 1012–1020.
[41] A. Espinosa Mansilla, I. Durán Merás, M.J. Rodríguez Gómez, A. Muñoz de la Peña, F. Salinas, Talanta 58 (2002) 255–263.
[42] S.L. Morgan, J.Y. Lee, G.S. Alarcon, Ann. Int. Med. 124 (1996) 74.
[43] A.C. Olivieri, J. Chemom. 19 (2005) 253–265.
[44] J. Øhman, P. Geladi, S. Wold, J. Chemom. 4 (1990) 79–90.
[45] J. Øhman, P. Geladi, S. Wold, J. Chemom. 4 (1990) 135–146.
[46] S. Wold, P. Geladi, K. Esbensen, J. Øhman, J. Chemom. 1 (1987) 41–56.
[47] D.M. Haaland, E.V. Thomas, Anal. Chem. 60 (1988) 1193–1202.
[48] R. Bro, H.A.L. Kiers, J. Chemom. 17 (2003) 274–286.
[49] E.L. Wittle, B.L. O'Dell, J.M. Vandenbelt, J.J. Pfiffner, J. Am. Chem. Soc. 69 (1947) 1786–1792.
[50] J. Riu, F.X. Rius, Trends Anal. Chem. 16 (1997) 211–216.
[51] F.J. del Río, J. Riu, F.X. Rius, Anal. Chim. Acta 446 (2001) 49–58.
[52] A.V. González, M.A. Herrador, A.G. Asuero, Talanta 48 (1999) 729–736.
[53] D. Bohoyo Gil, A. Muñoz de la Peña, J.A. Arancibia, G.M. Escandar, A.C. Olivieri, Anal. Chem. 78 (2006) 8051–8058.

Available online at www.sciencedirect.com
ScienceDirect
Talanta 72 (2007) 1533–1539
Talanta
www.elsevier.com/locate/talanta

Application of high performance liquid chromatography for the profiling of complex chemical mixtures with the aid of chemometrics

Yongnian Ni [a,b,*], Liangsheng Zhang [a], Jane Churchill [c], Serge Kokot [c]

[a] *Department of Chemistry, Nanchang University, Nanchang 330047, China*
[b] *The Key Laboratory of Food Sciences of MOE of Nanchang University, Nanchang 330047, China*
[c] *Inorganic Materials Research Program, School of Physical and Chemical Sciences, Queensland University of Technology, Brisbane, Queensland 4001, Australia*

Received 1 October 2006; received in revised form 2 February 2007; accepted 3 February 2007
Available online 11 February 2007

Abstract

In this paper, chemometrics methods were applied to resolve the high performance liquid chromatography (HPLC) fingerprints of complex, many-component substances to compare samples from a batch from a given manufacturer, or from those of different producers. As an example of such complex substances, we used a common Chinese traditional medicine, Huoxiang Zhengqi Tincture (HZT) for this research. Twenty-one samples, each representing a separate HZT production batch from one of three manufacturers were analyzed by HPLC with the aid of a diode array detector (DAD). An Agilent Zorbax Eclipse XDB-C18 column with an Agilent Zorbax high pressure reliance cartridge guard-column were used. The mobile phase consisted of water (A) and methanol (B) with a gradient program of 25–65% (v/v, B) during 0–30 min, 65–55% (v/v, B) during 30–35 min and 55–100% (v/v, B) during 35–60 min (flow rate, 1.0 ml min^{-1}; injection volume, 20 μl; and column temperature-ambient). The detection wavelength was adjusted for maximum sensitivity at different time periods. A peak area matrix with 21 objects × 14 HPLC variables was obtained by sampling each chromatogram at 14 common retention times. Similarities were then calculated to discriminate the batch-to-batch samples and also, a more informative multi-criteria decision making methodology (MCDM), PROMETHEE and GAIA, was applied to obtain more information from the chromatograms in order to rank and compare the complex HZT profiles. The results showed that with the MCDM analysis, it was possible to match and discriminate correctly the batch samples from the three different manufacturers. Fourier transform infrared (FT-IR) spectra taken from samples from several batches were compared by the common similarity method with the HPLC results. It was found that the FT-IR spectra did not discriminate the samples from the different batches.

Keywords: Multi-criteria decision making methods; High performance liquid chromatography; FT-IR; Fingerprinting; Profiling; Complex; Many-component substances; PROMETHEE and GAIA

1. Introduction

Quality assurance (QA) is an integral part of many chemical industries including that of the pharmaceuticals. In general, many products have a complex composition consisting of several active components carefully formulated to specific dosages, and delivered in a controlled, benign matrix. However, in many cases, the composition may be less well defined, and the product is prepared to a general or traditional recipe. A good example of such substances is the alternative or traditional medicines, the application of which is on the increase worldwide [3]. In cases of such preparations, often the composition of the product is so complex that the usual practice of using certified or accepted marker compounds, e.g. [1,2], is no longer feasible. Herbal mixtures (HM) form the basis of many traditional medicines, and the common claim with such medicines is that part of their therapeutic effect arises from a synergistic interaction of the many constituents [4,5]. Apart from the complex composition of their ingredients [6], the contents of an HM may vary with climate and soil of the area of cultivation as well as the age of the plants [7]. In addition, this complexity in composition may be compounded by differences in the exact nature of raw ingredients and the final processing strategy [8].

* Corresponding author.
E-mail address: ynni@ncu.edu.cn (Y. Ni).

0039-9140/$ – see front matter © 2007 Published by Elsevier B.V.
doi:10.1016/j.talanta.2007.02.003

The World Health Organization (WHO) has now accepted the profiling or fingerprinting method as a possible alternative for quality assurance purposes for many complex mixtures including HMs [9], and this approach is recommended in the Chinese Pharmacopoeia [10] for quality control of raw materials for such preparations.

In this paper, we explore some profiling approaches with the use of a well known traditional Chinese medicine (TCM), which is widely produced, and is subject to a lack of control of the many variables referred to above. It is commonly known as the Huoxiang Zhengqi Tincture (HZT) [10], and is a complex mixture of more than ten crude drugs or their extracts.

Central to the fingerprint approach is the collection of information from the complex sample such as an HM mixture as a whole. This typically utilizes results from chromatographic or spectral responses, which represent such a mixture [11], thereby offering an integral characterization of a complex system on a quantitatively and qualitatively comparative basis [12]. Many different techniques have been applied for the fingerprinting of complex preparations, plant extracts and TCMs. They include thin-layer chromatography (TLC) [6], high performance liquid chromatography (HPLC) [11,13], gas chromatography (GC) [14], high-speed counter-current chromatography (HSCCC) [15], capillary electrophoresis (CE) [16] and nuclear magnetic resonance (NMR) [17]. Fourier transform infrared (FT-IR) spectroscopy has become an important tool for rapid analysis of complex samples. The infrared absorbance spectrum can be regarded as a "fingerprint", which is characteristic of a complex substance being analyzed [18]. TLC, HPLC, GC and FT-IR are commonly used instrumental techniques either singly or collectively, for obtaining characteristic profiles of complex substances, and have been recommended for fingerprinting in the literature, e.g. [10,19].

Given the complexity and the multivariate nature of the fingerprinting responses, chemometrics has been utilized for matching and discrimination of the profiles, e.g. similarity calculations [20], fingerprint peak identification [21], chromatographic signal processing [22], multiple chromatographic fingerprint generation [23], chromatographic method optimization [24] and chemical pattern recognition [19,25].

There is no particular clustering method that is entirely satisfactory by itself for fingerprinting analysis, and the suggestion has been made to use such methods in combination, especially when large data sets are involved. For example a, two-stage clustering method was proposed by Punj and Steward [26], which combined Ward's minimum variance method and the *K*-means method. The main reason for such method combination was that the Ward's procedure establishes the number of clusters in the data set, and this cluster number can be used for the *K*-means method calculations as required. It has also been suggested that integration of the hierarchical method with non-hierarchical ones can provide better solutions [27]. This would involve methods such as principal component analysis (PCA), *K*-means cluster and hierarchical cluster analysis (HCA).

Other available methods obviate the need to combine simpler methods as above. Such methods focus on the decision making approaches ordering or ranking objects according to a set of multivariate criteria. These procedures are known as the multi-criteria decision making methods (MCDM) and include, for example, SMART, ELECTRE II and PROMETHEE. Their comparative performance has been studied by Salminen et al. [28], and a broader summary of such methods was made by Kokot and Ayoko [29] who pointed out that the object ranking method, PROMETHEE, coupled with a visual display biplot from the GAIA procedure, have performed consistently well in the MCDM comparative studies. In general, the combination of the two methods has been used sparingly for data analysis. However, more recently, their potential power has been successfully demonstrated across many fields of scientific and technological applications. Thus, after the initial work of Keller et al. [30], Kokot and Phuong [31] compared the performance of Vietnamese and Australian brown rice samples on the basis of their elemental concentrations and physico-chemical properties with the use of these methods, and Khalil et al. [32] applied them for the selection of sites for sustainable on-site sewage effluent disposal as well as for selection of hydrothermal pretreatment methods for the destruction of waste sludge [33]; Purcell et al. [34,35] showed that these MCDM methods were particularly effective for investigating the performance of sugar cane varieties on the basis of the composition of the epicuticular wax on the basis GC–MS, and NIR data profiles, respectively. Zhang et al. [36] have recently demonstrated how PROMETHEE and GAIA methods can be used to compare the quality of pure, adulterated and rancid vegetable oils. These were rank-ordered and directly related to selected marker standards of the oils, the criteria values of which were included in the data matrix. In principle, other international, national or local reference criteria values may be added to this data matrix as required, and the oil samples could be compared against these additional standards as well. Thus, this latter paper opens the possibility to explore the utilization of the PROMETHEE and GAIA methods for the development of reference profiles for HM and TCM materials.

In this work, we researched how HPLC profiling or fingerprinting of complex, many-component substances may be applied to compare samples from a batch from a given manufacturer, or from samples from different producers. We used a Chinese traditional medicine, HZT, as an example of such a substance, which has been applied over many, many years. We particularly investigated how the PROMETHEE II HPLC response modeling could be used for the development of profiling of complex substances and mixtures where the composition is often too complex and costly to resolve by the well known methods of analysis.

2. Experimental

2.1. Materials and reagents

Twenty-one HZT samples were obtained from three different manufacturers: (A) samples A1–7, (B) samples B8–15, and (C) samples C16–21, respectively. Each number identified a single grab sample from a different batch.

Table 1
Original data matrix of the HPLC fingerprints of the HZT samples (peak area × 10^3)

HZT	HPLC peaks at consecutive retention time points													
	1	2	3	4	5	6	7	8	9	10	11	12	13	14
A1	0.878	8.774	8.486	2.587	2.331	3.044	2.845	2.098	1.069	0.717	2.537	1.065	3.713	3.998
A2	0.654	6.972	8.644	3.195	1.997	2.511	2.456	1.972	1.151	1.145	5.907	1.168	3.954	4.507
A3	0.798	8.794	9.872	3.214	2.350	3.166	3.078	2.576	1.996	0.997	4.922	1.251	3.600	1.747
A4	0.503	5.098	7.650	2.680	1.797	2.540	2.606	2.648	1.574	0.725	5.411	1.454	3.355	1.568
A5	0.671	5.262	7.837	2.685	1.845	2.471	2.543	2.216	1.485	0.667	5.561	1.542	3.332	1.550
A6	0.581	6.758	7.337	2.106	2.181	2.491	2.498	1.886	1.370	0.745	6.318	1.295	3.845	4.014
A7	0.504	7.063	6.335	2.250	2.254	2.130	2.056	1.818	0.905	0.520	2.828	1.365	4.297	3.359
B8	0.705	1.866	1.255	1.311	4.187	0.648	0.762	0.790	0.911	0.757	0.194	3.198	1.378	1.063
B9	0.400	0.558	0.804	1.180	1.362	0.090	0.068	0.302	0.578	0.416	0.104	2.900	1.352	1.283
B10	0.331	0.592	0.908	0.682	3.389	0.115	0.105	0.230	0.660	0.358	0.188	2.615	0.881	0.872
B11	0.250	0.211	0.434	0.722	1.977	0.096	0.034	0.229	0.930	0.232	0.064	2.405	0.702	0.921
B12	0.308	0.345	0.540	0.718	3.819	0.078	0.080	0.172	0.549	0.192	0.089	2.176	0.696	1.059
B13	0.235	0.308	0.552	0.757	3.554	0.036	0.097	0.154	0.577	0.090	0.088	2.811	0.981	1.325
B14	0.337	0.863	1.358	0.932	3.126	0.306	0.636	0.581	0.906	0.435	0.167	3.221	0.960	1.031
B15	0.416	0.558	1.047	0.890	4.539	0.215	0.153	0.228	0.717	0.346	0.196	3.200	0.965	1.047
C16	0.488	2.348	7.203	1.193	1.400	3.011	1.474	0.712	0.453	0.675	0.596	0.294	0.091	0.110
C17	1.004	3.132	6.285	0.991	1.482	3.064	2.158	0.885	0.424	0.649	0.623	0.261	0.071	0.238
C18	0.566	1.203	7.274	0.971	1.740	2.762	1.469	0.571	0.426	0.710	0.888	0.341	0.076	1.149
C19	0.652	2.927	6.486	0.468	1.328	2.680	1.456	0.406	0.434	0.698	0.590	0.293	0.087	0.778
C20	0.589	1.794	5.243	2.574	2.146	3.059	2.537	0.681	0.203	0.357	0.526	0.216	0.064	0.193
C21	1.236	2.407	7.166	3.712	1.087	2.956	2.535	0.788	0.640	0.396	0.496	0.231	0.067	0.088

HPLC grade methanol (Fuchen Chemical Reagent Factory, Tianjin, China) was the mobile phase, and freshly double distilled water was used throughout the experiments.

2.2. Instrumentation and chromatographic procedures

HPLC chromatograph (Agilent 1100 Series HPLC-DAD system) was equipped with a vacuum degasser, quaternary pump, autosampler, injector with a 100 μl loop and a DAD detector. An Agilent Zorbax Eclipse XDB-C18 column (4.6 mm × 250 mm, 5 μm) with an Agilent Zorbax high pressure reliance cartridge guard-column (C18, 12.5 mm × 4.6 mm, 5 μm) were used. Chromatographic procedures: the mobile phase consisted of water (A) and methanol (B) with a gradient program of 25–65% (v/v, B) during 0–30 min, 65–55% (v/v, B) during 30–35 min and 55–100% (v/v, B) during 35–60 min. The flow rate was 1.0 ml min^{-1}, the injection volume was 20 μl and the column was maintained at ambient temperature. The detection wavelength for the different retention time periods was adjusted so as to obtain maximum sensitivity for all components detected in a given time period, and the Agilent Chemstation was programmed to control the DAD detector accordingly: 320 nm, 0–5 min; 280 nm, 5–30 min; 320 nm, 30–60 min.

2.3. FT-IR spectroscopy

Approximately 2 ml of each liquid HZT sample was placed on a 10 cm watch glass, and evaporated to dryness under an infrared lamp (ca. 2 h). This powder (1–2 mg) was mixed with KBr crystals (IR grade), finely ground, and pressed into a pellet from which a spectrum was collected.

FT-IR measurements were carried out at room temperature on a Nicolet 5700 FT-IR spectrometer (Thermo Electron Cooperation, USA), a deuterated triglycine sulfate (DTGS) KBr detector and a KBr beam splitter. The IR spectra were recorded in the range of 400–4000 cm^{-1} with a resolution of 4 cm^{-1} and 32 scans.

2.4. Samples and data analysis

For HPLC analysis, each HZT sample-solution was filtered through a 0.45 μm membrane filter, and its chromatogram was obtained according to the experimental conditions (Section 2.2.) Every HPLC run was sampled at 14 common retention times based on the presence of clearly discernible peaks and peak areas were computed accordingly. The corresponding 21 objects (HPLC fingerprints) × 14 variables (HPLC peaks) of the HZT matrix (Table 1) were submitted for data processing with the use of: (i) the similarity evaluation system software for chromatographic fingerprinting of TCM (Chinese Pharmacopoeia Committee, 2004A) [37], and (ii) PROMETHEE and GAIA procedures (Decision Lab 2000 (Visual Decision 2000)) [38].

3. Results and discussion

The HPLC chromatographic fingerprints of the 21 HZT samples (Fig. 1) showed significant differences between the three manufacturers, but the samples from different batches of a given manufacturer were qualitatively similar. It is apparent that sample origin is an important variable for the HZT product.

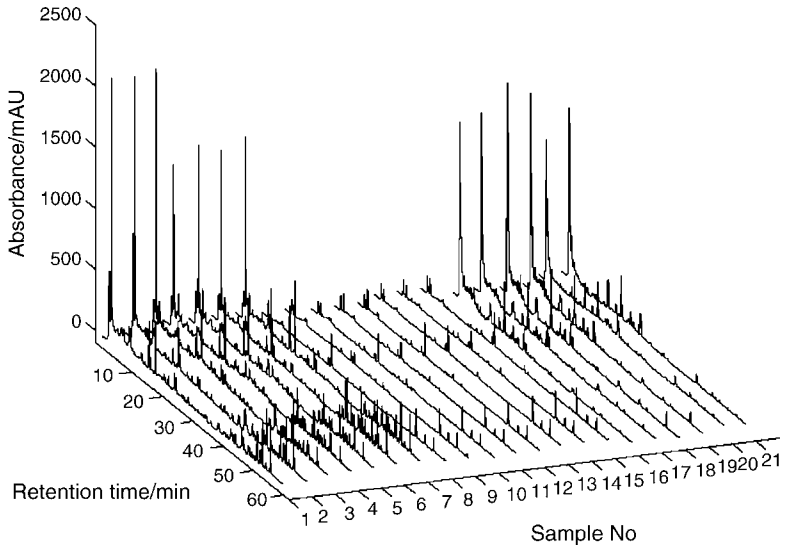

Fig. 1. Chromatographic fingerprints of HZT samples from manufacturers A (1–7), B (8–15) and C (16–21).

3.1. Similarity calculations

A simple similarity calculation [37] may be performed with the use of the Euclidean distance and correlation coefficient (or the cosine value of original data) [24]. In this work, the cosine value method was applied:

$$\cos\ \alpha_{ij} = \frac{\sum_{k=1}^{p} x_{ik}x_{jk}}{\sqrt{\left(\sum_{k=1}^{p} x_{ik}^2\right)\left(\sum_{k=1}^{p} x_{jk}^2\right)}} \quad (1)$$

where x_{ik} and x_{jk} represent the area of the kth peak of the two chromatographic fingerprints, i and j, and p is the number of peaks. The cosine value lies in the range of $0 < \cos\alpha_{ij} \leq 1$. The larger its value, the higher is the similarity between the two fingerprints. When $\cos\alpha_{ij}$ equals 1, they are identical.

The mean of all the available peaks for the seven HZT samples (manufacturer A) was defined as the data vector of the standard chromatographic fingerprint, and the other HZT samples compared against it. The standard chromatographic fingerprints for the products from manufacturers B and C were established in the same way, and comparisons made. In addition, similarities for all of the 21 HZT samples were calculated (Table 2). An example of a histogram, which indicates the similarities and differences between samples, is shown with reference to manufacturer A (Fig. 2). In general, the samples from manufacturer A had high similarity values (>0.94), while those from manufacturers B and C (<0.9) were somewhat lower. Similar conclusions were reached for histograms based on the HPLC fingerprints of samples from manufacturers B and C.

3.2. MCDM: PROMETHEE and GAIA analysis

PROMETHEE, is a non-parametric object-ranking method, and is normally complemented by a PCA biplot method, GAIA. The PROMETHEE procedure requires each matrix variable or criterion, to be modeled independently: (i) select the preferred order of ranking of objects on each variable—either top-down or bottom-up (referred to as maximize or minimize, respectively); (ii) define a preference function, $P(a, b)$ for each variable, which then allows the order of each object on a given variable to be defined by a computed preference index; (iii) set a weighting for the variable (default set to 1).

A summary of the main steps in the PROMETHEE algorithm for the calculation of the ranking indices of objects in a matrix are set out below. Detailed discussion and applications may be found elsewhere [29,30].

Table 2
Results of similarity method calculations

Sample no. (origin)	Comparison of chromatographic fingerprints			
	Manufacturer A	Manufacturer B	Manufacturer C	Common pattern
A1	0.9781	0.5199	0.8527	0.9559
A2	0.9927	0.5103	0.8205	0.9525
A3	0.9907	0.4917	0.8754	0.9634
A4	0.9851	0.5096	0.8489	0.9564
A5	0.9863	0.5115	0.8514	0.9583
A6	0.9889	0.5183	0.7858	0.9417
A7	0.9824	0.5676	0.7972	0.9529
B8	0.6340	0.9754	0.5270	0.7623
B9	0.5600	0.9167	0.3979	0.6659
B10	0.5037	0.9958	0.4191	0.6578
B11	0.4480	0.9766	0.3350	0.5951
B12	0.4204	0.9743	0.3482	0.5823
B13	0.4271	0.9879	0.3254	0.5826
B14	0.5914	0.9886	0.5105	0.7353
B15	0.4681	0.9900	0.4031	0.6306
C16	0.8285	0.3937	0.9938	0.8804
C17	0.8604	0.4119	0.9895	0.9022
C18	0.8094	0.4338	0.9784	0.8740
C19	0.8583	0.4087	0.9828	0.8982
C20	0.8110	0.4788	0.9719	0.8836
C21	0.8158	0.3909	0.9741	0.8664

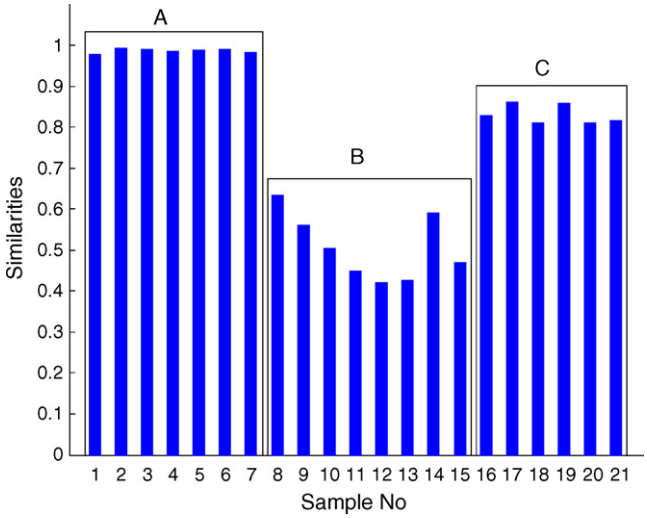

Fig. 2. Similarity histogram using the reference generated by chromatograms of samples (A1–A7) from manufacturer A.

- Step 1: The raw data matrix is converted into a difference, d, matrix by subtracting the entries in each column from one another in all possible combinations.
- Step 2: The selected preference function, $P(a, b)$, for each variable is applied to determine how much each object is preferred to another. In the Decision Lab 2000 (Visual Decision 2000) [38] software, there are six different preference functions available, and on the basis of the selected preference function a preference index, $\pi(a, b)$, is calculated for each object Eq. (2):

$$\pi(a,b) = \sum_{j=1}^{k} w_j P_j(a,b) \tag{2}$$

where w_j is the weight for each criterion.
- Step 3: An overall index, Π, is calculated for each object in order to compare them.
- Step 4: Positive and negative outranking flows, $\varphi^+$and φ^-, are then calculated Eqs. (3) and (4). The former reflects how an object outranks all others, while the latter indicates how other objects outrank a particular one:

$$\varphi^+(a) = \frac{1}{n-1}\sum_{b\varepsilon A}\pi(a,b) \tag{3}$$

$$\varphi^-(a) = \frac{1}{n-1}\sum_{b\varepsilon A}\pi(b,a) \tag{4}$$

- Step 5: A partial preorder can be computed to demonstrate alternative objects, on the basis of the $\varphi^+$and φ^- ranking values, i.e. the PROMETHEE I ranking. This involves the application of comparative rules [29,30].
  (1) a outranks b if: $\varphi^+(a) > \varphi^+(b)$ and $\varphi^-(a) < \varphi^-$ or $\varphi^+(a) > \varphi^+(b)$ and $\varphi^-(a) = \varphi^-(b)$ or $\varphi^+(a) = \varphi^+(b)$ and $\varphi^-(a) < \varphi^-(b)$;
  (2) a is indifferent to b if: $\varphi^+(a) = \varphi^+(b)$ and $\varphi^-(a) = \varphi^-(b)$;
  (3) a cannot be compared to b: in all cases where b does not outrank a (using rules similar to those in 1).
- Step 6: From the partial net flow of each alternative, net outranking flow (φ), values (PROMETHEE II) can be calculated Eq. (5) to give a complete order, i.e. the partial preorder option is omitted:

$$\varphi(a) = \varphi^+(a) - \varphi^-(a) \tag{5}$$

The complementary GAIA method consists of a PCA biplot, which is generated from a matrix formed by the decomposition of the PROMETHEE II rankings [30]. The biplot is interpreted as a normal PCA display, and it can provide guidance for the relative importance of the criteria for the ranking of the objects.

The HPLC fingerprints of the HZT batches from manufacturers A and B (samples A1–A7, and B8–B15, respectively) appear to be strickingly different (Fig. 1). However, they are traditionally well recognised as typical HZT products. We designated these two sets as nominal profile markers for the HZT product, and submitted them for ranking by the PROMETHEE method.

Thus, every criterion in the 15 object × 14 criteria data matrix was set to maximize because for each variable, a higher peak intensity indicated a higher presence of the constituent. Since the samples from the different batches of each manufacturer were intended by the manufacturer to be similar, the Gaussian preference function, $P(a, b)$, was utilized for each peak criterion and the computed standard deviation was set as the required 'threshold' value. The weighting for each criterion was set to 1. PROMETHEE II net outranking flows (φ) were used for the comparison of objects and decision making.

The A and B sets of batches were clearly distinguished from each other with all fingerprints from set A (A1–A7) having negative net outranking flows, φ, and those from the B set (B8–B15) positive ones (Fig. 3, Model a). The standard deviation thresholds, $\pm 2s$ and $\pm 3s$ bars, for each set indicated that the two data sub-sets did not overlap on this basis of comparison. If set C fingerprints were now to be introduced as a test case of HZT samples, then if they were to fall inside the two profile markers, A and B, this set could be classed as exhibiting acceptable HZT properties. If the C set or some of its batch samples were to fall outside the two profile markers then, it could be established with the use of the standard deviation estimates (or further statistical processing, as required) whether these apparently different HPLC fingerprints were significantly different or otherwise. The user is then able to decide if the fingerprints of the test batch conformed to the broad profile of the HZT mixtures as defined by the sets A and B.

When the set C (samples C16–C21) of the HPLC fingerprints of HZT was similarly processed, PROMETHEE II net outranking flows (φ) (Fig. 3, Model b), showed that it overlapped with set B batch of samples with positive (φ) values. Set A batch of fingerprints (A1–A7) had negative φ values, and on the basis of the $\pm 3s$ criterion, was separated from the other two sets of HZT batches. Consequently, in this case the set C HPLC fingerprints may be regarded as similar to the two profile markers.

In principle, the two profile markers, sets A and B of HPLC fingerprints for HZT can now be used as the first notional profile markers for assessing the quality of other HZT mixtures from the same or different manufacturers. Provided the sam-

Model(a)	φNet	2s	3s
B11	0.33	0.38(B)	0.44(B)
B9	0.31		
B12	0.29		
B10	0.28		
B13	0.27		
Bavg	***0.26***		
B14	0.23		
B15	0.22		
B8	0.13	0.14(B)	0.08(B)
A7	-0.21	-0.18(A)	-0.12(A)
A5	-0.23		
A4	-0.23		
Aavg	***-0.30***		
A6	-0.30		
A1	-0.32		
A2	-0.35		
A3	-0.38	-0.42(A)	-0.48(A)

Model(b)	φNet	2s	3s
B11	0.30	0.34(B)	0.40(B)
B9	0.26		
B12	0.25		
B10	0.23		0.24(C)
B13	0.23		
Bavg	***0.22***		
B14	0.19	0.19(C)	
B15	0.18		
C19	0.16		
C16	0.14		
C18	0.14		
Cavg	***0.11***		
C17	0.11		
C20	0.10	0.10(B)	
B8	0.09		0.04(B)
C21	0.03	0.03(C)	-0.02(C)
A7	-0.26	-0.24(A)	-0.18(A)
A5	-0.29		
A4	-0.30		
A6	-0.34		
Aavg	***-0.35***		
A1	-0.37		
A2	-0.39		
A3	-0.43	-0.46(A)	-0.52(A)

Fig. 3. Demonstration of PROMETHEE II overall ranking for the comparison of HZT samples from manufacturers A–C against the respective average quality criteria, Aavg–Cavg. (a) Sets A and B (the nominal extreme threshold profile sets), and (b) comparison of set C against the nominal threshold sets A and B. 2*s* and 3*s* are standard deviations with respect to the various mean values.

pling and the analytical methodologies are the same, then the resulting HPLC fingerprints sampled at the same points may be added to the data matrix of set A and B HPLC batches and a PROMETHE II net outranking flow order obtained. Decision regarding to similarity or otherwise of the new samples with respect to these notional profile markers can then be made with the aid of statistical information discussed previously.

The complementary GAIA PC1 *versus* PC2 biplot (91% data variance described, Fig. 4) showed that the data could be quite crisply segregated into three groupings commensurate with the spectral batches from manufacturers A–C. Thus, the plot provides support for the PROMETHEE II results, but as the molecular origins of the HPLC peaks in the fingerprints are unknown, the criteria vectors cannot be defined and utilized.

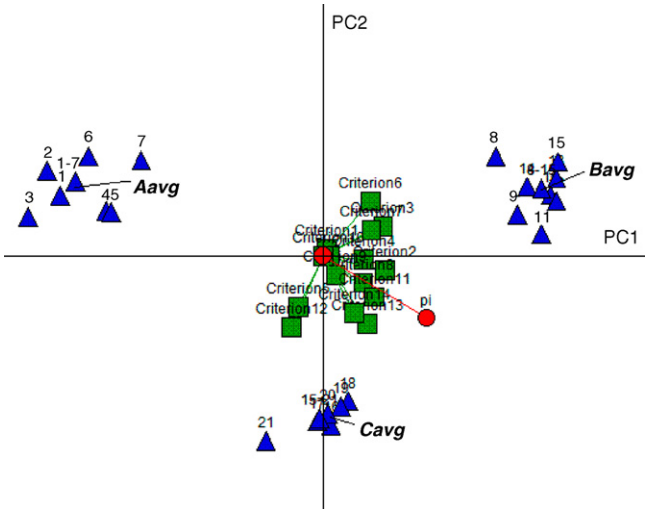

Fig. 4. GAIA biplot including the average samples, Aavg–Cavg, from manufactures A–C (91% of data variance accounted).

3.3. FT-IR analysis

Three representative samples, A1, B8, and C16, were randomly selected from the 21 tested samples corresponding to the three different manufacturers (A–C) and their FT-IR spectra were measured (Fig. 5). It can be seen that the three IR spectra of HZT from different manufactures are almost the same and the similarities calculated between each sample (Table 3) are larger than 0.98. This contrasts clearly with the similarity analysis results based on the HPLC responses. Thus, it appears to be difficult to distinguish the samples from different manufacturers from their FT-IR fingerprints, and a simple FT-IR approach to discriminate between the different HZT samples is inappropriate.

Table 3
Similarities of the selected samples obtained by HPLC and FT-IR

Sample pair	Similarity	
	HPLC method	FT-IR method
A1, B8	0.6414	0.9889
A1, C16	0.8337	0.9903
B8, C16	0.4907	0.9835

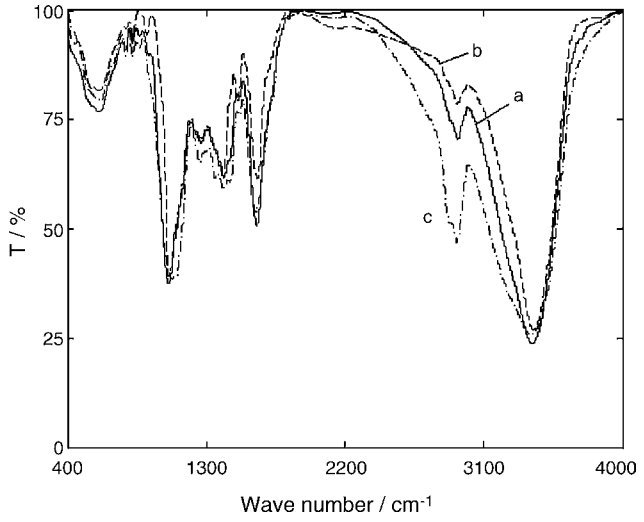

Fig. 5. FT-IR spectra of selected samples from different manufactures: (a) A1, (b) B8, and (c) C16.

4. Conclusion

This study focused on the characterization of complex, many-component substances by means HPLC profiling interpreted by chemometrics. As an example of this approach, a well known, many-component Chinese traditional medicine, HZT, was chosen to demonstrate how HPLC fingerprinting may be interpreted with the aid of chemometrics to compare samples from a batch from a given manufacturer, or samples from different producers.

Simple similarity models provided some uncomplicated information for such comparisons, but the application of the more sophisticated MCDM methods such as PROMETHEE and GAIA, allowed for the inclusion of notional thresholds of HZT profiles on the basis of HPLC measurements. This enabled relative numerical comparisons of each batch, and each manufacturer's profile, with the aid of the net outranking flow, φ, values. In addition, some statistical analysis with the use of the φ values can enhance the quality assurance information on the products. Thus, in principle, the MCDM methods may be applied for QA comparisons of similar complex product profiles.

Acknowledgements

The authors gratefully acknowledge the financial support of this study by the Natural Science Foundation of China (NSFC20365002 and NSFC20562009), the State Key Laboratories of the Electroanalytical Chemistry of Changchun Applied Chemical Institute (SKLEAC2004-3) and the Chemo/Biosensing and Chemometrics of Hunan University (SKLCBC2005-22), the Jiangxi Province Natural Science Foundation (JXNSF0620041), the program for Changjiang Scholars and Innovative Research Team in Universities (IRT0540).

References

[1] X. Zhou, J.Y. Peng, G.R. Fan, Y.T. Wu, J. Chromatogr. A 1092 (2005) 216–221.
[2] V. Schulz, R. Hansel, V.E. Tyler, Rational Phytotheraphy: A Physician's Guide to Herbal Medicine, 3rd ed., Springer Verlag, Berlin, 1998.
[3] D. Normile, Science 299 (2003) 188–190.
[4] S. Wang, H.Q. Ma, Y.J. Sun, C.D. Qiao, S.J. Shao, S.X. Jiang, Talanta 72 (2007) 434.
[5] Note for Guidance on Quality of Herbal Medicinal Products, European Medicines Agency, London, 2001, p. 6.
[6] Y. Dai, K. Miki, T. Fukuoka, A. Tokunaga, T. Tachibana, E. Kondo, K. Noguchi, Life Sci. 66 (2000) 19–29.
[7] Y.X. Zhou, H.M. Lei, Y.H. Xu, L.X. Wei, X.F. Xu, Research Technology of Fingerprint of Chinese Traditional Medicine, Chinese Chemical Engineering Press, Beijing, 2002.
[8] M.M.W.B. Hendriks, L. Cruz-Juarez, D. De Bont, R.D. Hall, Anal. Chim. Acta 545 (2005) 53–64.
[9] World Health Organization, Guidelines for the Assessment of Herbal Medicines, Munich, June 28, 1991, WHO, Geneva, 1991.
[10] Committee of National Pharmacopoeia, Pharmacopoeia of PR China, Chinese Chemical Engineering Press, Beijing, 2005, pp. 661–662.
[11] M. Gu, F. Ouyang, Z.G. Su, J. Chromatogr. A 1022 (2004) 139–144.
[12] P. Drasar, J. Moravcova, J. Chromatogr. B 812 (2004) 3–21.
[13] H.Z. Lian, Y.N. Wei, Talanta 71 (2007) 264–269.
[14] M. Hajimahmoodi, Y.V. Heyden, N. Sadeghi, B. Jannat, M.R. Oveisi, S. Shahbazian, Talanta 66 (2005) 1108–1116.
[15] M. Gu, G.F. Zhang, Z.G. Su, F. Ouyang, J. Chromatogr. A 1041 (2004) 239–243.
[16] S.K. Yan, W.F. Xin, G.A. Luo, Y.M. Wang, Y.Y. Cheng, J. Chromatogr. A 1090 (2005) 90–97.
[17] S. Rezzi, D.E. Axelson, K. Heberger, F. Reniero, C. Mariani, C. Guillou, Anal. Chim. Acta 552 (2005) 13–24.
[18] W.E. Huang, D. Hopper, R. Goodacre, M. Beckmann, A. Singer, J. Draper, J. Microbiol. Method 67 (2006) 273–280.
[19] Y.Q. Xu, S.Q. Sun, Z.M. Yuan, Y. Bai, Chin. J. Anal. Chem. 30 (2002) 1231–1233.
[20] L.X. Wang, H.B. Xiao, X.M. Liang, K.S. Bi, Acta Pharm. Sin. 37 (2002) 713–717.
[21] M.J. Chen, Y.Y. Cheng, Chin. J. Anal. Chem. 31 (2003) 513–517.
[22] F. Gong, Y.Z. Liang, Y.S. Fung, F.T. Chau, J. Chromatogr. A 1029 (2004) 173–183.
[23] M. Gu, S.F. Zhang, Z.G. Su, Y. Chen, F. Ouyang, J. Chromatogr. A 1057 (2004) 133–140.
[24] F. Gong, Y.Z. Liang, P.S. Xie, F.T. Chau, J. Chromatogr. A 1002 (2003) 25–40.
[25] G.H. Lu, K. Chan, Y.Z. Liang, K. Leung, C.L. Chan, Z.H. Jiang, Z.Z. Zhao, J. Chromatogr. A 1073 (2005) 383–392.
[26] G. Punj, D.W. Steward, J. Market. Res. 20 (1983) 134–148.
[27] R.J. Kuo, L.M. Ho, C.M. Hu, Comput. Ind. Eng. 42 (2002) 391–399.
[28] P. Salminen, J. Hokkanen, R. Lahdelma, Eur. J. Oper. Res. 104 (1998) 485–496.
[29] S. Kokot, G. Ayoko, in: P.J. Worsfold, A. Townshend, C.E. Poole (Eds.), Chemometrics-(I) Multi-criteria Decision Marking, Encyclopaedia of Analytical Sciences, vol. 2, 2nd ed., Elsevier, Oxford, 2005, pp. 40–45.
[30] H.R. Keller, D.L. Massart, J.P. Brans, Chemom. Intell. Lab. Syst. 11 (1991) 175–189.
[31] S. Kokot, T.D. Phuong, Analyst 124 (1999) 561–569.
[32] W.A.S. Khalil, A. Goonetilleke, S. Kokot, S. Carroll, Anal. Chim. Acta 506 (2004) 41–56.
[33] W.A.S. Khalil, A. Shanableh, P. Rigby, S. Kokot, J. Environ. Manage. 75 (2005) 53–64.
[34] D.E. Purcell, G.J. Leonard, M.G. O'Shea, S. Kokot, Chemom. Intell. Lab. Syst. 76 (2005) 135–147.
[35] D. Purcell, M. O'Oshea, S. Kokot, Chemom. Intell. Lab. Syst., in press.
[36] G.W. Zhang, Y.N. Ni, J. Churchill, S. Kokot, Talanta 70 (2006) 293–300.
[37] China Pharmacopoeia Committee, http://www.chp.org.cn/.
[38] Decision Lab 2000. Executive edition, Visual Decision Inc., Montreal, Canada.

Available online at www.sciencedirect.com
ScienceDirect
Talanta 72 (2007) 1386–1391
Talanta
www.elsevier.com/locate/talanta

On-line solid-phase extraction and high performance liquid chromatography determination of polycyclic aromatic hydrocarbons in water using polytetrafluoroethylene capillary

Lubov Oliferova, Mikhail Statkus, Grigoriy Tsysin *, Yury Zolotov

Analytical Chemistry Division, Chemistry Department, Lomonosov Moscow State University, Vorob'evy Gory, 119992 Moscow, Russia

Received 20 October 2006; received in revised form 15 January 2007; accepted 19 January 2007
Available online 30 January 2007

Abstract

Naphthalene, biphenyl, acenaphtene, anthracene and pyrene were extracted from water samples using inner walls of polytetrafluoroethylene capillary. Optimum conditions for sorption, desorption and heart-cutting of the analyte zone were found. Combined on-line solid-phase extraction and HPLC method for determination of these compounds was proposed. Limits of detection were: ($\mu g\,L^{-1}$): 0.4 (naphthalene), 0.3 (biphenyl), 0.6 (acenaphtene), 0.2 (anthracene) and 0.1 (pyrene).

Keywords: On-line solid-phase extraction; High performance liquid chromatography; Polycyclic aromatic hydrocarbons; Polytetrafluoroethylene capillary

1. Introduction

The determination of small amounts of organic substances in natural and waste waters still remains one of the important problems of analytical chemistry. Sometimes it could not be solved even with modern instruments, such as HPLC or GC. These difficulties could be overcome by the development of combined methods of analysis including preconcentration step. Preconcentration by means of on-line solid-phase extraction (SPE) enhances selectivity and sensitivity of the instrument thus extending the range of analytical problems that could be solved with the combined method. Alkyl-bound silica gels, synthetic polymers and carbon sorbents are widely used for on-line SPE of organic substances. A number of examples of application of fluoropolymers (FPs) for SPE of hydrophobic compounds were published recently [1–3].

FPs are usually considered as one of the most chemically inert polymer materials; various analytical equipment parts (vessels, tubing, membranes, etc.) are made of FPs. However, FPs are inert only towards hydrophilic components of water solutions; while hydrophobic ones are readily adsorbed on FP surface. This phenomenon could be used for SPE in various analytical methods, including on-line ones.

A common approach for preconcentration of non-charged complexes of metals with organic reagents is application of polytetrafluoroethylene (PTFE) "knotted reactor" (KR) that is a long tied capillary. Analytes are adsorbed by KR inner walls [4–6], then desorbed by polar organic solvent and analyzed by atomic spectrometry. The used chelating reagents were various dithiocarbamates, dithiophosphates, 8-hydroxyquinoline, nitroso-R-salt, etc.

In our opinion, the main advantages of PTFE capillary over similar PTFE powder sorbents [3] are better material properties (rigidity), lower back-pressure and long-term stability (absence of sorbent compression). Moreover, capillary are cheaper and more readily available than powder PTFE sorbents.

Two common approaches to SPE are known: first one (and the most popular one) supposes that experimental conditions are chosen in such a way that analyte recovery is 95–100%. Both static (batch) and dynamic (on-line) variants of this approach require application of high capacity sorbents and strict control of sample volume. The second approach (it is known as "solid phase microextraction", SPME [7]) is performed in static conditions: a small amount of sorbent (usually fibrous, fixed at the syringe needle tip) is introduced to the sample solution. After the establishment of the equilibrium the sorbent is removed

* Corresponding author. Tel.: +7 495 939 5518; fax: +7 495 939 4675.
E-mail address: tsisin@analyt.chem.msu.ru (G. Tsysin).

0039-9140/$ – see front matter © 2007 Elsevier B.V. All rights reserved.
doi:10.1016/j.talanta.2007.01.046

and analyzed. Analyte recovery is usually very low, not more than 1–2% of the initial analyte content, thus recovery is rarely used for evaluation of SPME method performance. The amount of extracted analyte is independent from sample volume and proportional to the concentration of the analyte in the sample [7,8]. This approach allows to use sorbents with moderate and low capacity, and it is commonly used in conjunction with GC for determination of trace organic compounds [7,8]. There are several examples of on-line SPME methods [7,9].

Polycyclic aromatic hydrocarbons (PAHs) are toxic water pollutants and for 16 of them maximum admissible concentrations for tap and natural waters are established by various regulation organizations [10]. HPLC combined with preconcentration is often used for determination of PAHs in waters. These compounds are hydrophobic, their $\log P$ is varied from 3.4 for naphthalene up to 7.7 for indeno[1,2,3-cd]pyrene [10]. Certainly, such a wide range of $\log P$ makes group preconcentration of PAHs quite a complicated task. In the current research we have chosen several PAHs with their $\log P$ varying from 3.4 (naphthalene) to 5.3 (pyrene) for demonstrating that PTFE capillary could be used for extraction of hydrophobic organic compounds from waters.

The aim of the current paper is to present a new on-line hybrid SPME-HPLC method for determination of hydrophobic organic compounds with the use of PTFE capillary as a SPME device.

2. Experimental

2.1. Reagents and materials

All substances and reagents were of analytical grade quality. Distilled and deionized (18.2 MΩ) water was used for preparation of solutions. Stock solutions of PAHs (naphthalene, acenaphtene, anthracene and pyrene) and biphenyl (0.1 g L^{-1}) and solution of $K_4Fe(CN)_6$ (also 0.1 g L^{-1}) were prepared by dissolution of weighted amounts of these substances. Standard solutions were prepared from stock ones by dilution with water and acetonitrile directly prior the experiment. Sorption of biphenyl and PAHs on vessels and tubing was suppressed by introduction of 5% (v/v) acetonitrile to the samples.

2.2. Equipment

On-line SPE-HPLC equipment was based on commercially available HPLC system (Aquilon, Moscow, Russia). It included two chromatographic solvent delivery units; custom-made automatic preconcentration system based on two actuated Rheodyne 9900-500 injection valves, spectrophotometric detector UVV-104. All units were controlled automatically by "Multichrom 2.4" Software (Ampersand Ltd., Moscow, Russia) run on a PC. Analytes were preconcentrated on PTFE capillary (i.d. 0.5 mm, o.d. 1.6 mm, length 5 m). Directly prior to the analysis capillary was conditioned with 5% (v/v) acetonitrile. HPLC runs were performed on Synergi Hydro RP-18 250 mm × 4.6 mm steel column (Phenomenex, Torrance, CA, USA) packed with 4 μm octadecyl silica gel particles. Conditions of HPLC runs were chosen according to [11,12]: isocratic elution with 75% (v/v) acetonitrile–water mixture. Detection was carried out at 254 nm (PAHs, biphenyl) or 420 nm ($K_4Fe(CN)_6$).

Solvents were degassed using ultrasonic bath UZV (Saphire, Moscow, Russia). The same procedure was used for dissolution of the compounds.

Off-line optical absorption measurements were carried out using SF-103 spectrophotometer (Aquilon, Moscow, Russia), 10 mm thick quartz cells were used.

3. Results and discussion

3.1. Dead volume evaluation

Dead volume (DV) should be taken into account for correct evaluation of sorption experiments. For example, the initial part of dynamic breakthrough curve (DBC) recorded by optical HPLC detector is caused by conditioning solvent remaining in the SPE column and tubing after conditioning step. To evaluate the DV of our SPE system we used a solution of $K_4Fe(CN)_6$, that is not adsorbed on PTFE and has an intensive color, thus increasing the sensitivity of detection. Solution of $K_4Fe(CN)_6$ (0.1 g L^{-1}) was injected into PTFE capillary by means of 20 μL chromatographic loop. Retention volume of $K_4Fe(CN)_6$ was equal to 1.0 mL and was considered as a DV of the SPE system. This value was used further for correction of experimental data: the initial part of DBC (equivalent to 1.0 mL) was cropped.

3.2. Investigation of sorption

Sorption isotherms were obtained for investigation of thermodynamic aspects of SPE (i.e. distribution coefficients). Distribution coefficients for plotting the isotherm were evaluated by method of DBC [13]. A series of naphthalene solutions in 5% acetonitrile was prepared, with analyte concentration ranging from 0.1 to 1.0 mg L^{-1}. Then each solution was pumped through PTFE capillary at a flow rate of 1 mL min^{-1} and a DBC was recorded. PTFE capillary was connected directly to the HPLC detector for these experiments. The area above DBC corresponds to the amount of analyte (mg) adsorbed on the inner surface (m^2) of the capillary. Isotherm was linear in the whole studied concentration range (from 0.1 to 1.0 mg L^{-1}), distribution coefficient was 191 L m^{-2}.

Kinetics of PAH sorption on PTFE capillary was also studied; for this purpose a series of DBCs of naphthalene solution with a constant concentration (1.0 mg L^{-1} in 5% acetonitrile) was recorded at a range of flow rates (1.0, 1.5, 2.0, 2.5, 3.0 mL min^{-1}). Some of the obtained DBCs are presented on Fig. 1. The time required for establishment of dynamic equilibrium (i.e. inlet and outlet analyte concentrations are equal) was approximately 6 min for the whole flow rate range. The flow rate of 1 mL min^{-1} was chosen for the subsequent experiments.

DBCs of biphenyl, acenaphtene, anthracene and pyrene were also recorded and evaluated to prove that chosen optimum conditions are also suitable for preconcentration of more hydrophobic compounds. Concentration of analytes was 1.0 mg L^{-1} in 5% acetonitrile. We have found that the sample volume required for establishment of dynamic equilibrium of these compounds

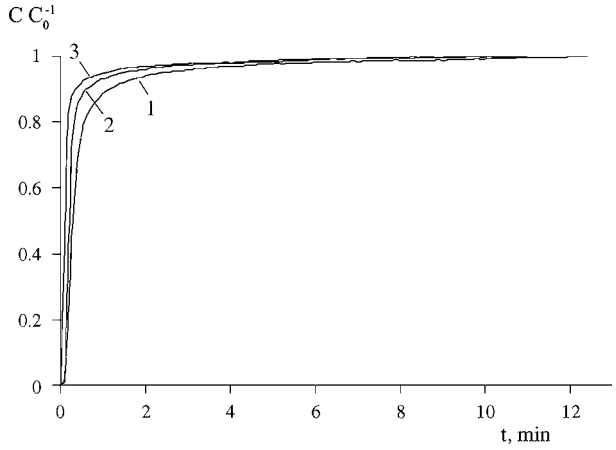

Fig. 1. Sorption of naphthalene on PTFE capillary. Dynamic breakthrough curves, flow rates were: (1) 1.0, (2) 2.0 and (3) 3.0 mL min^{-1}.

with PTFE capillary was not more than for naphthalene (Fig. 2). The time required for establishment of dynamic equilibrium was approximately 8 min.

3.3. Investigation of desorption

The development of an on-line SPE-HPLC method with good analytical performance requires knowledge about the size and shape of analyte peak after desorption. Desorption curves were recorded to evaluate these parameters. Naphthalene and pyrene were adsorbed from 1.0 mg L^{-1} solutions in 5% acetonitrile; afterwards the capillary was washed with 1.0 mL of 5% acetonitrile for 1 min. Subsequently, the analytes were desorbed with 75% acetonitrile at a flow rate of 1.0 mL min^{-1}. The chart of the equipment used for these experiments is presented on Fig. 3. Desorption curve contained two nearly positioned peaks (Fig. 4). To investigate the nature of these two peaks, effluent fractions were collected and then analyzed off-line with the aid of spectrophotometer at 254 nm wavelength. It was found that the first peak was related to so-called shlieren effect (an optical artifact [14]), and the second one—to the analyte itself. From Fig. 4 it may be seen that quantitative desorption of naphthalene as well

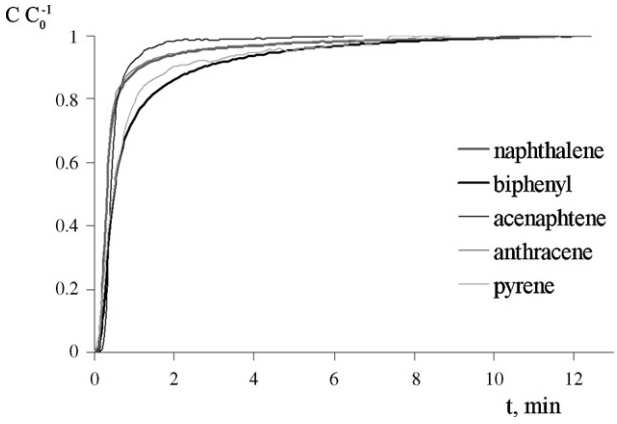

Fig. 2. Dynamic breakthrough curves for sorption of naphthalene, biphenyl, acenaphtene, anthracene and pyrene on PTFE capillary; concentration of PAHs and biphenyl 1 mg L^{-1}, all flow rates were 1 mL min^{-1}.

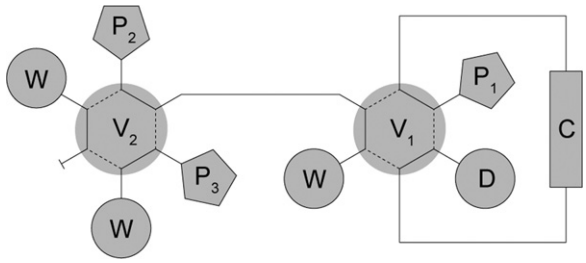

Fig. 3. The experimental set-up used for recording desorption curves. D, HPLC spectrophotometric detector, C, PTFE capillary, P_1, P_2 and P_3, HPLC pumps, V_1 and V_2, injection valves, W, waste.

as pyrene could be achieved with a volume of 75% acetonitrile not exceeding 1.0 mL (that is one dead volume of the capillary).

3.4. Heart-cutting of the analyte after desorption

On-line combination of SPE and HPLC could be performed in various ways. The most common one is desorption of analytes by chromatographic eluent and direct transfer to the chromatographic column. A significant drawback of this approach is related to introduction of sample remaining after preconcentration in the SPE device into the chromatographic column, thus disturbing the equilibrium between column and eluent. This results in large injection peaks, possible shifts in retention volumes and baseline disturbances. Heart-cutting of the analytes after desorption with the aid of HPLC injection loop is one of the ways to overcome these difficulties.

During preliminary experiments, we have found out that maximum loop volume for separation of PAHs on Synergi Hydro RP-18 column was 300 μL; application of larger loops resulted in poorly separated peaks and disturbances of baseline. We have

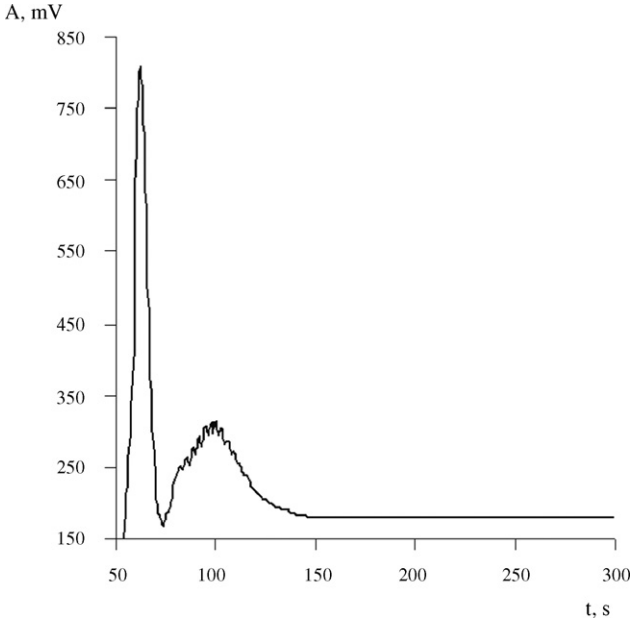

Fig. 4. Desorption curve: naphthalene desorbed with acetonitrile from PTFE capillary. Sample volume was 20 mL, naphthalene concentration 1 mg L^{-1}, all flow rates were 1 mL min^{-1}. Desorption was carried out with 75% acetonitrile.

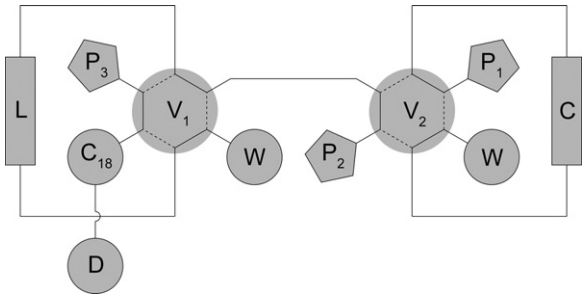

Fig. 5. The experimental set-up used for on-line SPE-HPLC determination of PAHs. D, HPLC spectrophotometric detector, C, PTFE capillary, P_1, P_2 and P_3, HPLC pumps, V_1 and V_2, injection valves, L, injection loop (300 μL volume), C_{18}, HPLC column, W, waste. V_1 is in B position, V_2 is in A position.

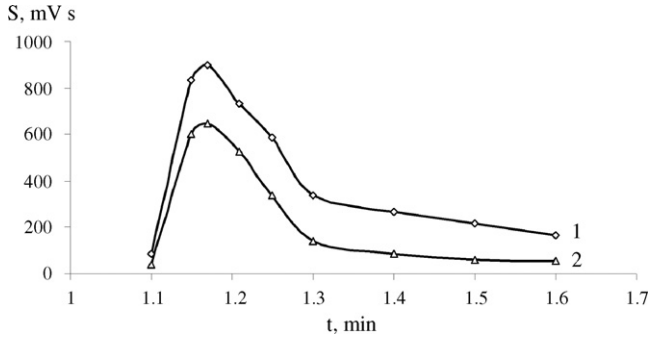

Fig. 6. The dependence of chromatographic peaks area on the delay between start of desorption and injection of the analytes into HPLC column. Naphthalene (1) and pyrene (2) were desorbed with 75% acetonitrile. Sample volume was 20 mL, PAH concentration 0.1 mg L^{-1}. Sample flow rate was 1 mL min^{-1}. Analytes were heart-cut with 300 μL injection loop.

optimized heart-cut conditions to capture analytes in 300 μL injection loop. The chart of the equipment used for these experiments is presented on Fig. 5. A mixture of PAHs (naphthalene and pyrene, 0.1 mg L^{-1} each, in 5% acetonitrile) was pumped (flow rate 1 mL min^{-1}) through capillary for 20 min, then 1 mL of washing solution (5% acetonitrile) was introduced into the capillary at the same flow rate. Desorption was carried out with 75% acetonitrile. Analytes were heart-cut by means of loop installed on an automated injection valve and then introduced into HPLC column. The delay between start of desorption and switching of the valve was varied from 1.1 to 1.6 min. The dependence of chromatographic peaks area on the delay is presented on Fig. 6. Maximum peak area was obtained when delay was 1.17 min.

3.5. On-line SPE-HPLC determination of PAHs

The total duration of the single SPE-HPLC run was 47 min (Table 1). However, the chosen experimental set-up (Fig. 5) allows simultaneous HPLC (for the previous sample) and SPE runs (for the next one), thus reducing overall time required for several analyses.

Calibration plots were constructed: 20 ml of distilled water containing various concentrations of analytes (0.5–2.0 μg L^{-1} for naphthalene and pyrene and 0.5–10.0 μg L^{-1} for others) was analyzed according to the scheme presented in Table 1. Each concentration point was repeated three times for evaluation of precision (Table 2). Calibration graphs were linear in the chosen concentration ranges. Detection limits were evaluated according to the 3s-criterion after several SPE-HPLC runs with blank sample (distilled water).

The long-term reproducibility of technique was not studied specially, but analysis of standard samples after 4 months of the experimental work (around 200 analyses performed) gave no significant deviations (not more than 3–7%) from initial calibration runs.

The results of direct HPLC analysis and the developed on-line SPE-HPLC techniques (preconcentration on PTFE capillary and FP sorbents [3]) were compared, Table 2. It was found out that the application of PTFE capillary for SPE results in detection limits comparable with that for powder FP sorbents [3]; and one order of magnitude lower than for direct HPLC runs.

The results of determination of analytes in spiked and non-spiked water samples are presented in Table 3. Water samples from Black sea and Moskva river, as well as tap water, were spiked with mixture of PAHs and biphenyl. A typical chromatogram for river water sample is presented on Fig. 7. Peaks were identified according to their retention volumes established on model deionized water samples. Recovery of spikes varies from 53 to 120% (naphthalene was recovered poorly from nat-

Table 1
Time schedule of the on-line SPE-HPLC determination of PAHs and biphenyl

Time interval (min)	Step description	Injection valves position		Flow rates (mL min^{-1}) and composition of pumped solutions		
		Valve 1	Valve 2	Pump 1 (sample)	Pump 2	Pump 3 (75% AN[a])
0–5	Flushing of all equipment tubing with 100% AN	B	A	1	1 (100% AN)	0
5–6	Conditioning of capillary with 5% AN	B	A	1	1 (5% AN)	0
6–18	Preconcentration	A	A	1	0	0
18–26	Conditioning of HPLC column 75% AN	A	A	1	0	1
26–27	Flushing of capillary with 5% AN	B	A	0	1 (5% AN)	1
27–28	Filling of tubing with 75% AN	A	B	0	1 (75% AN)	1
28–29.17	Desorption of analytes with 75% AN and heart-cutting	B	B	0	1 (75% AN)	1
29.17–47	Introduction of analytes to HPLC column; HPLC run	B	A	0	0	1

[a] AN, acetonitrile.

Table 2
Performance of the on-line SPE-HPLC determination of PAHs and biphenyl (sample volume 20 mL)

Analyte	Direct HPLC determination		On-line SPE with fluoropolymer F2-M and HPLC determination [3]		On-line SPE with PTFE capillary and HPLC determination	
	R.S.D.[a]	DL[b] ($\mu g\,L^{-1}$)	R.S.D.[c]	DL ($\mu g\,L^{-1}$)	R.S.D.[c]	DL ($\mu g\,L^{-1}$)
Naphthalene	0.02	3	0.01	0.2	0.01	0.4
Biphenyl	0.03	5	0.04	0.4	0.06	0.3
Acenaphtene	0.1	5	0.06	0.3	0.06	0.6
Anthracene	0.03	1	0.09	0.2	0.06	0.2
Pyrene	0.05	2	0.05	0.2	0.03	0.1

[a] $100\,\mu g\,L^{-1}$, $n=3$.
[b] DL, detection limit.
[c] $1\,\mu g\,L^{-1}$, $n=3$.

Table 3
Analysis of spiked samples (sample volume 20 ml)

Sample	Spike ($\mu g\,L^{-1}$)	Found ($\mu g\,L^{-1}$)			
		Biphenyl	Acenaphtene	Anthracene	Pyrene
River water	0	0.0 ± 0.1	–[a]	0.0 ± 0.1	1.3 ± 0.4
(Moskva river)	3	3.0 ± 0.4	–[a]	2.8 ± 0.9	5.0 ± 0.6
Tap water	0	0.2 ± 0.2	0.0 ± 0.3	0.0 ± 0.1	1.8 ± 0.6
	3	2.8 ± 0.3	2.9 ± 0.4	2.7 ± 0.3	4.2 ± 0.4
Seawater	0	0.1 ± 0.2	1.0 ± 0.8	0.2 ± 0.7	1.5 ± 0.9
(Black sea)	3	3.0 ± 0.5	2.6 ± 0.9	3.3 ± 0.7	4.8 ± 0.5

[a] No data available.

ural waters, $R<50\%$, and these results are not presented in the table). We suppose that recovery being not 100% is related in general to the interfering matrix components of waters: for example, sorption of humic and fulvic acids (contained in river water) on inner walls of capillary competes with PAHs sorption and thus decreases recovery. Sea water, on the other hand, contains inorganic ions that could result in so-called "salting out" of hydrophobic compounds thus increasing recovery and affecting the accuracy of results. Such negative effects could be taken into account and minimized by either introduction of internal standard or making calibration runs not with distilled water but with the real sample. The first approach is preferable, being less time and labor-consuming, but requires careful choice of internal standard itself. In our case, the application of internal standard is complicated because it should be used to correct variations in recovery of analytes significantly varying in terms of log *P*.

Increased concentration (as compared to other PAHs) of pyrene in blank water samples might be an indicator of so-called memory effect—incomplete desorption of this analyte during the course of previous experiments. However, it is worthy to note that accurate determination of spike is still possible.

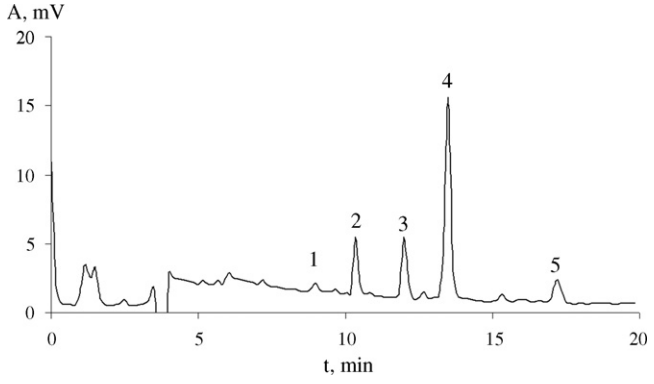

Fig. 7. A typical chromatogram for on-line SPE-HPLC analysis of river water sample; PAHs were preconcentrated on PTFE capillary. Peaks correspond to naphthalene (1), biphenyl (2), acenaphtene (3), anthracene (4) and pyrene (5). Sample volume was 20 mL, analyte concentrations were $10\,\mu g\,L^{-1}$ each. Desorption and HPLC separation was carried out with 75% acetonitrile. Analytes were heart-cut with 300 μL injection loop after 1.17 min delay.

4. Conclusions

To sum up, we developed on-line SPE-HPLC technique for determination of PAHs and biphenyl in waters that includes preconcentration on inner walls of PTFE capillary.

Acknowledgements

Authors are grateful for Russian Foundation of Basic Research for financial support (grants RFBR 06-03-32178 and 04-03-39002).

References

[1] M.J. Clarence, B.J. James, T. Richard, Anal. Chem. 56 (1984) 764.
[2] E. Ivanova, K. Benkhedda, F. Adams, J. Anal. At. Spectrom. 13 (1998) 527.
[3] L. Oliferova, M. Statkus, G. Tsysin, O. Shpigun, Yu. Zolotov, Anal. Chim. Acta 538 (2005) 35.
[4] Zh. Fang, L. Dong, J. Anal. At. Spectrom. 7 (1992) 439.

[5] X.-P. Yan, R. Kerrish, M.J. Hendry, Geochim. Cosmochim. Acta 64 (2000) 2637.
[6] E. Ivanova, X.-P. Yan, F. Adams, Anal. Chim. Acta 354 (1997) 7.
[7] J. Pawliszyn, Solid-Phase Microextraction—Theory and Practice, Wiley-Interscience Publ, New York, 1997, 264 pp.
[8] E.M. Thurman, M.S. Mills, Solid-Phase Extraction, J.Wiley & Sons, New York, 1998, 344 pp.
[9] Y. Saito, M. Nojiri, M. Imaizumi, Y. Nakao, Y. Morishima, H. Kanehara, H. Matsuura, K. Kotera, H. Wada, K. Jinno, J. Chromatogr. A 975 (2002) 105.
[10] E. Manoli, C. Samara, Trends Anal. Chem. 18 (1999) 417.
[11] E. Marengo, M.C. Gennaro, C. Baiocchi, P.L. Bertolo, Anal. Chim. Acta 258 (1992) 93.
[12] S.J. Hart, G.J. Hall, J.E. Kenny, Anal. Bioanal. Chem. 372 (2002) 205.
[13] G. Guiochon, S.G. Shirazi, A.M. Katti, Fundamentals of Preparative and Nonlinear Chromatography, Academic Press, Boston, 1994, 701 pp.
[14] Z. Fang, Flow Injection Separation and Preconcentration, VCH Verlagsgesellschaft mbH, Weinheim, 1993, 259 pp.

Available online at www.sciencedirect.com
ScienceDirect
Talanta 72 (2007) 1370–1377
Talanta
www.elsevier.com/locate/talanta

Speciation of chromium in natural waters by micropumping multicommutated light emitting diode photometry

Cherrine K. Pires [a], Boaventura F. Reis [b], Angel Morales-Rubio [a,*], Miguel de la Guardia [a]

[a] *Department of Analytical Chemistry, University of Valencia, 50 Dr. Moliner Street, 46100 Burjassot Valencia, Spain*
[b] *Centre for Nuclear Energy in Agriculture, University of Sao Paulo, P.O. Box 96, Piracicaba SP 13400-970, Brazil*

Received 10 October 2006; received in revised form 15 January 2007; accepted 19 January 2007
Available online 30 January 2007

Abstract

A simple and sensitive multicommutated flow procedure, implemented by employing a homemade light emitting diode (LED) based photometer, has been developed for the determination of chromium (VI) and total chromium in water. The flow system comprised a set of four solenoid micropumps, which were assembled to work as fluid propelling and as commutating devices. The core of the detection unit comprised a green LED source, a photodiode and a homemade flow cell of 100 mm length and 2 mm inner diameter. The photometric procedure for the speciation of chromium in natural waters was based on the reaction of Cr (VI) with 1,5-diphenylcarbazide. Cr (III) was previously oxidized to Cr (VI) and determined as the difference between total Cr and Cr (VI). After carrying out the assays to select the best operational conditions the features of the method included: a linear response ranging from 10 to 200 $\mu g\,l^{-1}$ Cr (III) and Cr (VI) ($r = 0.999$, $n = 7$); limits of detection of 2.05 and 1.0 $\mu g\,l^{-1}$ for Cr (III) and Cr (VI), respectively; a relative standard deviation lower than 2.0% ($n = 20$) for a typical solution containing 50 $\mu g\,l^{-1}$ Cr; a sampling throughput of 67 and 105 determinations per hour for total Cr and Cr (VI), respectively, and recovery values within the range of 93–108% for spiked concentrations of the order of 50 $\mu g\,l^{-1}$.

Keywords: Flow analysis; Multi-pumping; Chromium speciation; Natural waters; LED-spectrophotometry

1. Introduction

Chromium is an element naturally found in rocks, animals, plants, soil, in volcanic dust and gases. Cr (III) occurs naturally in the environment and it is considered an essential nutrient for plants and animals, while Cr (VI) is generally produced by industrial processes and presents potential risks for living organisms like stomach upsets and ulcers, convulsions, kidney and liver damage, and even death. Skin contact with Cr (VI) compounds can cause skin damages [1,2].

So, in spite of the fact that Cr is considered an essential element for human life, the official agencies devoted to water quality control had been established the highest concentration level of Cr that can be acceptable in water for human consumption. However, since the risk for health caused by Cr is dependent of its chemical species, it is desirable that procedures for Cr determination present high sensitivity and ability to differentiate between Cr (III) and Cr (VI).

The most frequent sample pre-treatments used for Cr speciation are complex formation and pre-concentration by column/ionic exchange. In some cases, Cr speciation is based on oxidation–reduction processes [3].

Analytical procedures proposed for the determination of Cr involve chromatography [4], spectrophotometry [5,6] and chemiluminescence [7] and procedures based on flow injection analysis (FIA) [8,9] have been also proposed.

Generally, analytical procedures based on FIA present high throughput as an inherent advantage; nevertheless the continuous pumping pattern causes a high consumption of the reagent solutions, and a great volume of generated wastes. These disadvantages have been surpassed developing analytical procedure based on multicommutation [10]. In this case, the core of the flow system manifold is constituted by a set of solenoid valves assembled to work as independent commutation units. Exploiting these features, analytical procedures requiring two or more reagent solutions were accomplished using a single pumping

* Corresponding author. Tel.: +34 96 3543997; fax: +34 96 3544838.
E-mail address: angel.morales@uv.es (A. Morales-Rubio).

0039-9140/$ – see front matter © 2007 Elsevier B.V. All rights reserved.
doi:10.1016/j.talanta.2007.01.044

channel [11,12], while in the classical FIA system each reagent required one pumping channel. Furthermore, the intermittent pattern due to the multicommutation process to insert reagent solutions into the reaction coil caused a high decrease of reagent consumption and waste generation [13,14].

Albeit reagent solutions could be handled using a single pumping channel in multicommutated flow systems it does not avoids the use of a peristaltic pump, which is commonly the device used to perform this task. Peristaltic pumps are the most expensive equipment required to implement a flow system, and because of that, an interesting alternative to propel reagent solutions was introduced by Lapa et al. [15] using solenoid micro-pumps. In this study, the flow system manifold was designed nesting a set of micro-pumps to work as solutions propelling and commutating device, thus avoiding the use of a peristaltic pump [16,17], and allowing a reduction of the manifold cost and dimensions and energy requirements.

1,5-Diphenylcarbazide has been employed in more than 70 works appeared in the bibliography for chromium determination [1], but for Cr (III) determination by using this reagent it is necessary a previous oxidative step. The oxidation could be made using FIA [8,18] or SIA [19,20], being the oxidant reagent employed Ce (VI) [19,20] or H_2O_2 in basic medium [8], and sometimes the reaction has been made in a heating water bath at 45 °C [19,20] or in a heating oil bath at 80 °C [18]. From all of these previous procedures it surprises the differences of the LOD values reported, from 0.009 [18] to 5900 $\mu g\,l^{-1}$ [8]. This great variability of the LOD values could be explained by the volume of the sampling loop and it could suppose that sample zone underwent high dispersion, thus affecting the magnitude of the generated signal.

The cheap availability of high luminous light emitting diodes (LED), presenting emission at the required wavelength, and high sensitivity photodiodes, allows us the possibility to develop a homemade photometer with high performance and little dimensions [21,22].

In this work, we have developed a compact equipment set up employing solenoid micro-pumps to handle reagent solutions and a LED base photometer. The solutions handling unit and the photometer detector are assembled together in order to obtain a downsized analytical instrument dedicated for the determination of total Cr and Cr (VI) in water using 1,5-diphenylcarbazide as chromogenic reagent. To attain the concentration level established by the governmental agencies, that is at $\mu g l^{-1}$, it was used a home-made flow cell with an optical path-length of 100 mm and the radiation source (LED) and the photodiode, were attached at the observation windows of the flow cell in order to improve the analytical sensitivity.

2. Experimental

2.1. Standards, reagents and samples

All solutions were prepared with analytical-grade chemicals and with deionized water (resistivity > 18.2 MΩ cm) obtained in a Milli-Q system from Millipore.

A 100 $mg\,l^{-1}$ stock standard solution of Cr (VI) was prepared by dissolving 0.3753 g of potassium dichromate from Scharlau Chemie S.A. (Barcelona, Spain) in 1000 ml of water. Working standard solutions (10–200 $\mu g\,l^{-1}$ Cr (VI)) were prepared weekly in 0.5 $mol\,l^{-1}$ hydrochloric acid from Merck (Darmstadt, Germany) by appropriate dilution.

The 0.012% (w/v) 1,5-diphenylcarbazide from UCB (Brussels, Belgium) solution was prepared by dissolving 0.012 g in 2 ml of 99.5% (v/v) ethanol from Scharlau Chemie S.A. and making the volume up to 100 ml with 0.5 $mol\,l^{-1}$ sulphuric acid from Merck. This solution was stored in the refrigerator and could be used for at least 1 week.

A 100 $mg\,l^{-1}$ stock standard solution of Cr (III) was prepared by dissolving 0.7696 g of chromium nitrate from Panreac (Barcelona, Spain) in 1000 ml of water. Working standard solutions (10–200 $\mu g\,l^{-1}$ Cr (III)) were prepared in 0.5 $mol\,l^{-1}$ hydrochloric acid from Merck.

A 0.15% hydrogen peroxide solution in alkaline medium was daily prepared by dilution from a 30% (v/v) H_2O_2 from Scharlau Chemie S.A. using a 0.2 $mol\,l^{-1}$ NaOH solution freshly prepared.

The potential interferents, such as Al^{3+}, Mn^{2+}, Cd^{2+}, Ba^{2+}, Pb^{2+}, Ca^{2+}, Ni^{2+}, Fe^{2+}, Fe^{3+}, Cu^{2+}, V(V), Co^{2+}, Mo(VI), Na^{+},

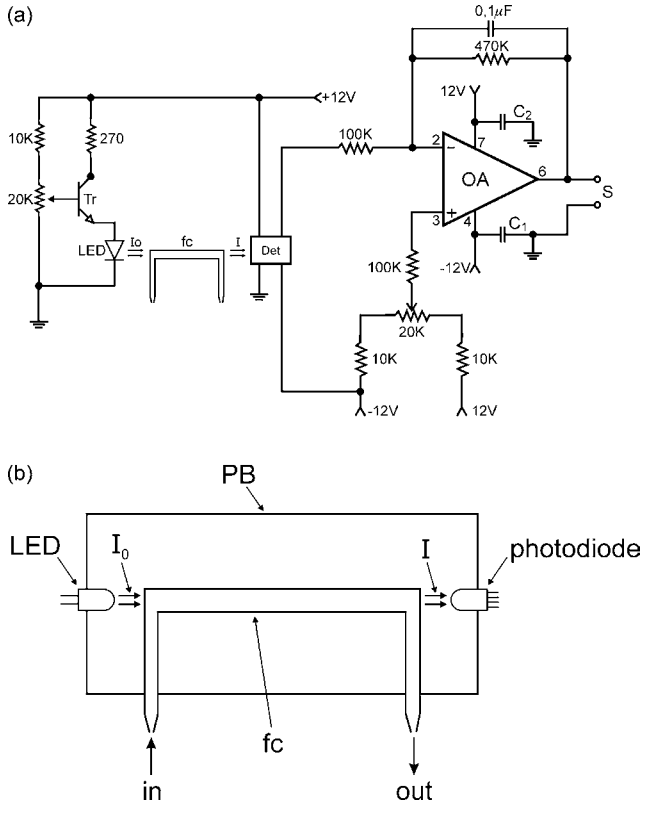

Fig. 1. Structure of the LED photometer. (a) Electronic diagram of the homemade photometer. Tr, transistor BC547; LED, λ = 548 nm; I_0 and I, radiation beam coming and leaving the flow cell, respectively; fc, flow cell; Det, photodiode (IPL 10530 DAL); OA, OP07 operational amplifier; C_1 and C_2 = 2 μF Tantalum capacitor; S, output signal. (b) Long section view of the flow cell, LED and photodiode arrangement. PB, PVC block; I_0 and I, radiation beam coming and leaving the flow cell, respectively; fc, flow cell; glass tube 100 mm long and 2.0 mm inner diameter.

F^-, PO_4^{3-}, CO_3^{2-}, SO_4^{2-}, NO_3^-, Cl^-, citrate, EDTA and acetate were evaluated preparing a 50 μg l^{-1} Cr (III) and Cr (VI) standard solutions plus the investigated substance. It was assured that the interferent concentration was at least 20-times higher than Cr concentration.

Natural water samples were filtered through 0.45 μm cellulose membrane filters and stored into polyethylene bottles before their analysis [23].

2.2. Apparatus

The flow system comprised four solenoid micro-pumps from Bio-Chem Valve Inc. (Boonton, NJ, USA) with nominal volume of 8-μl per pulse; a microcomputer equipped with an electronic interface card Advantech, PCL-711S (San Jose CA, USA); an homemade electronic interface to drive the micro-pumps similar to that described elsewhere [24]; one 3-channels joint device and another 2-channels joint device both machined in acrylic and flow lines of 0.8 mm i.d. PTFE tubing. The flow system control and data acquisition were performed by the microcomputer running software written in Quick BASIC 4.5.

A Hewlett-Packard (Waldbronn, Germany) model 8452A diode-array spectrophotometer equipped with a 50-μl inner volume and 10-mm optical pathway flow cell, and the homemade LED-based photometer, designed to work employing a flow cell with a long optical path-length presented below, were used to carry out spectrometric measurements, using in this case a green LED with an emission wavelength of 540 ± 10 nm.

The electronic diagram of the photometer is shown in Fig. 1 and also this figure indicates the structure of the LED-photometer. The flow cell was made from a boron-silicate glass tube with an inner diameter of 2.0 mm and was machined to

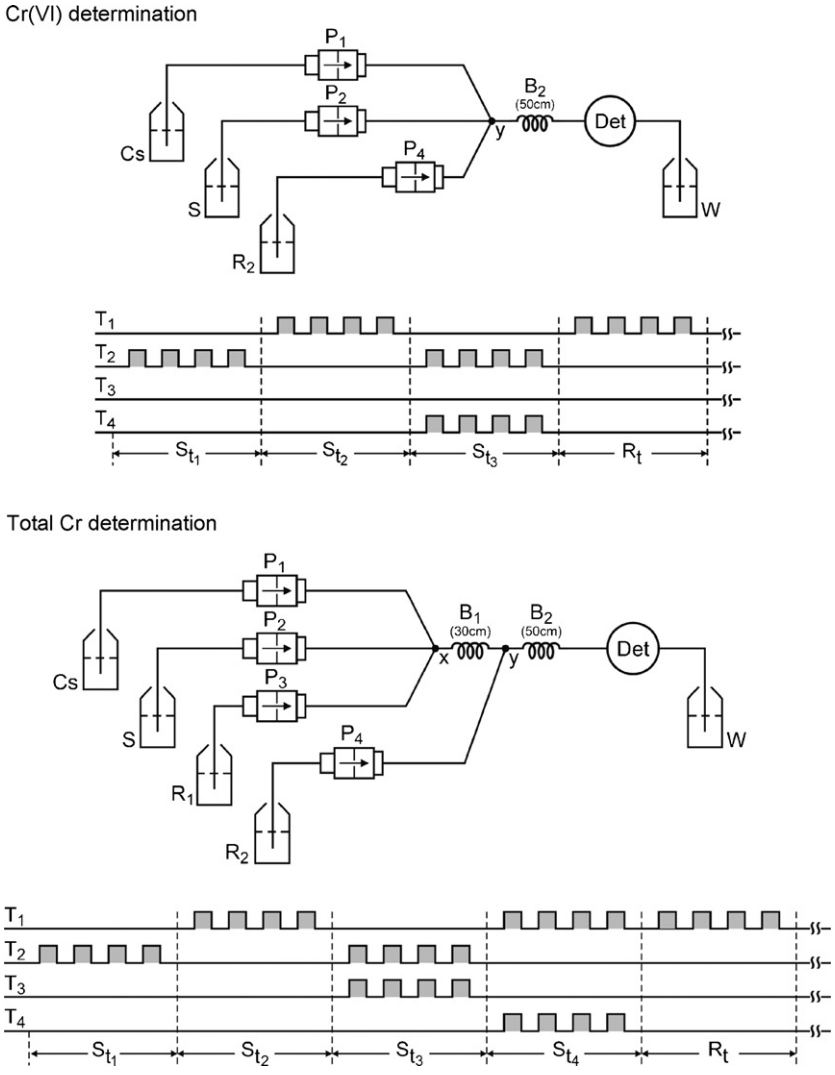

Fig. 2. Diagram of the flow system. Cs, carrier solution, flow rate at 40 μl s^{-1}; S, sample or standard solution; R_1 = 0.15% (w/v) peroxide solution; R_2 = 0.012% (v/v) 1,5-diphenylcarbazide solution; P_1, P_2, P_3 and P_4, solenoid micro-pump; *x* and *y*, flow lines joint devices; B_1 and B_2, reaction coils; Det, homemade photometer; W, waste. The *a* and *b* diagrams show the micro-pumps switching sequence and manifolds for the determination of Cr (VI) and total Cr, respectively. T_1, T_2, T_3, and T_4, timing course for switching micro-pumps P_1, P_2, P_3 and P_4, respectively; St_i, sampling steps (*i* = 1–5); Rt, signal reading step. Shadow surfaces indicate that the corresponding micro-pump is switched ON.

Table 1
Operational conditions of the multicommutation flow system for speciation of chromium in waters

Determination	Step	Event	P_1	P_2	P_3	P_4	Pulses
Cr (VI)	1	Sample/standard replacing	0	1	–	0	40
	2	Analytical path washing	1	0	–	0	90
	3	Introduction of S and R_2	0	1	–	1	12
	4	Transport to the cell	1	0	–	0	30
Total Cr	1	Sample/standard replacing	0	1	0	0	40
	2	Analytical path washing	1	0	0	0	160
	3	Introduction of S and R_1	0	1	1	0	12
	4	Introduction of R_2	1	0	0	1	30
	5	Transport to the cell	1	0	0	0	30

S: Sample or standard solution. R_1: Oxidant reagent (H_2O_2 + NaOH). R_2: 1,5-Diphenylcarbazide (DPC). P_i: Solenoid micro-pumps. 0: Switch OFF. 1: Switch ON. (–): Not employed.

provide two plane windows of approximately 0.15 cm^2 surface close to which both, the LED source and the detector, were mounted.

The flow cell was installed in a PVC block that was machined to allow that both, LED and photodiode, were attached in front of flow cell observation windows. When the photometer was switched ON the base line can be adjusted as follow. Maintaining the dark condition (LED disable for radiation emission) and flow cell filled with carrier solution, the output signal (S) was adjusted to 0.0 mV by means of the variable resistor wired to the no inverting input of the operational amplifier. Afterwards, the LED was enabled to emit radiation turning the variable resistor wired to the base of the transistor (BC547). The radiation emission intensity was increased up till the output signal (S) attained a potential difference of 2000 mV.

The flow system was designed considering that the main focus was the development of the automatic procedure for Cr speciation in natural water. The flow diagrams of the manifolds employed are shown in Fig. 2. As can be see, it comprises four solenoid pumps, each one dedicated to handle the indicated solution. The P_1, P_2, P_3 and P_4 pumps were used for inserting the carrier stream (Cs), the sample or standard (S), the oxidant (diluted H_2O_2 and NaOH) reagent (R_1), and the 1.5-diphenylcarbazide reagent (R_2), respectively.

The violet colour of the reaction product is highly specific for Cr (VI) determination at 548 nm. The micro-pumps switching frequency was 5 Hz defining equal time interval (0.1 s) to switch ON and OFF the system as it was settled in the earlier work [16].

2.3. Recommended procedure

For the spectrophotometric determination of total Cr and Cr (VI) the flows set up shown in Fig. 2 were designed, being the logical operation indicated in the time switching micro-pumps diagrams.

As indicated in Table 1 for the direct determination of Cr (VI), the analytical cycle starts by filling the sample coil with the corresponding sample/standard solution by switching P_2 and further, the carrier solution was employed to wash the analytical path by switching P_1, thus establishing the baseline. For the analytical run, P_2 and P_4 were switched ON simultaneously to insert 96 μl of sample/standard and 96 μl of reagent R_2 (4.8×10^{-6} mol l^{-1} DPC), into the B_2 coil to allow the development of the reaction. Finally, after the established time interval, the pumps P_2 and P_4 were switched OFF, and only P_1 was activated for insertion of the carrier stream (0.5 mol l^{-1} hydrochloric acid solution) for push-

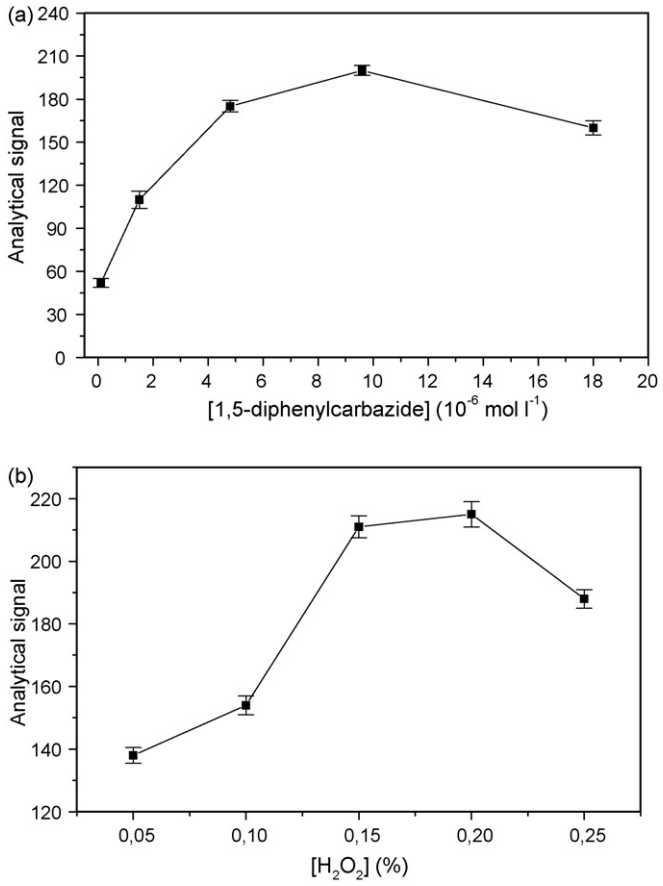

Fig. 3. Effect of the reagent concentration on the analytical signal. (a) Effect of the 1,5-diphenylcarbazide concentration. *Experimental conditions*: sample slug volume = 96 μl, reagent R_2 slug volume = 96 μl, standard solution concentration = 50 μg l^{-1} Cr (VI). (b) Effect of the hydrogen peroxide concentration. *Experimental conditions*: Sample slug volume = 96 μl, reagent R_1 slug volume = 96 μl, reagent R_2 slug volume = 240 μl, standard solution concentration = 50 μg l^{-1} Cr (III). Results are the average of five consecutive measurements and brackets indicate the ± standard deviation of values obtained.

ing the coloured product zone towards the detector, and to wash the system. For different replicates of the same sample/standard solution only steps 3 and 4 should be repeated.

The length of B_2 reactor was set as only 50 cm (250 μl), yet enough for attaining good mixing conditions under all the investigated situations.

Total Cr was determined after treatment of the sample by mixing it with the oxidant reagent R_1 (H_2O_2 and NaOH). Like Cr (VI) determination, the analytical cycle starts by filling the coil sample with the corresponding sample/standard solution by switching P_2 and further, the carrier solution was employed to wash the analytical path by switching P_1, thus establishing the baseline. For the analytical run, P_2 and P_3 were switched ON simultaneously to insert sample and oxidizing reagent R_1 (0.15% H_2O_2 in 0.2 mol l^{-1} NaOH) into the B_1 coil to allow the oxidation of Cr (III) to Cr (VI). Afterwards, P_1 and P_4 were activated simultaneously to transport oxidized sample and to insert R_2 reagent, respectively to the "*y*" joint point and to allow the development of the reaction into the coil B_2. After the established time interval, the pumps P_2 and P_4 were switched OFF, and only P_1 was maintained for pushing the coloured product zone towards the detector.

The length of B_1 reactor was set as 30 cm (150 μl), yet enough to complete Cr (III) oxidation.

Absorbance data obtained for samples were interpolated in a calibration line, prepared in the range between 10 and 200 μg l^{-1} Cr (VI) and Cr (VI) and total Cr determined before and after sample oxidation. The Cr (III) concentration was established from the difference between total Cr and Cr (VI).

3. Results and discussion

3.1. Effect of reagents concentration

For a sample volume of 96 μl and a Cr (VI) concentration of 50 μg l^{-1} it was evaluated the effect of reagents concentration.

Influence of 1,5-diphenylcarbazide concentration was investigated within the 0.1×10^{-6} to 18×10^{-6} mol l^{-1} range, and as can be seen in Fig. 3a the highest signal was achieved for 9.6×10^{-6} mol l^{-1} 1,5-diphenylcarbazide. However, in these conditions double peaks were obtained, which could be caused by variations during the solutions mixing time. This effect could be minimized by increasing the length of reaction coil B_2. Under these conditions, a sample zone broadening caused by dispersion

Table 2
Effect of interfering ions on the determinations of 50 μg l^{-1} Cr (VI)

Added species	Tolerance limit (μg ml^{-1})[a]	Mass ratio	Molar ratio	Recovery (%)
Na^+	1,000	20,000	45,200	96
Ba^{2+}			7,600	95
F^-			54,700	99
PO_4^{3-}			10,900	98
CO_3^{2-}			17,300	99
SO_4^{2-}			10,800	97
Cl^-			29,300	96
NO_3^-			16,800	96
Citrate			5,500	97
EDTA			570	95
Acetate			2,900	97
Al^{3+}	500	10,000	19,300	96
Mn^{2+}			106,000	98
Cd^{2+}			4,600	97
Pb^{2+}			2,500	98
Ca^{2+}	100	2,000	2,600	95
Ni^{2+}			1,800	99
Co^{2+}			1,800	97
Mo(VI)			1,100	95
Fe^{2+}	10	200	200	96
Fe^{3+}			200	98
Cu^{2+}			160	96
V(V)			30	95

[a] No interference was considered for signal variation lower than 5% in the presence of the interfering species.

Table 3
Comparison between analytical figures of merit of the proposed procedure and those achieved using conventional diode array instrumentation

Parameters	Procedure proposed (10 cm optical path cell) (total Cr/Cr (VI))	Diode (1 cm, flow cell) (total Cr/Cr (VI))	Diode (10 cm optical path cell) (total Cr/Cr (VI))
Range (μg l^{-1})	10–200	50–150	10–150
LOD (μg l^{-1})	2.0/1.4	6.7/5.5	4.7/3.5
R.S.D. (%)	<2	2.8/2.3	1.9/2.4

was inevitable, thus a decrease in signal could occur. Furthermore, the number of pumping pulses to displace the sample zone to waste must be increased, thus affecting also the throughput. In this sense, the 4.8×10^{-6} mol l^{-1} 1,5-diphenylcarbazide solution was selected as the R_2 reagent concentration.

Effects of hydrogen peroxide and sodium hydroxide concentrations were investigated within the range of 0.05–0.25% and 0.1–0.5 mol l^{-1}, respectively. As can be seen in Fig. 3b, the highest analytical signals were attained with 0.15% H_2O_2. On the other hand, no significant signal variation was found as a function of NaOH concentration, being considered 0.2 mol l^{-1} NaOH the most appropriate concentration. So, the aforementioned conditions were selected for the preparation of R_1.

3.2. Multicommutation system parameters

Inserted volumes of sample and reagent solutions proved to be relevant parameters in the system design. Influence of the sample and reagent volume was defined by pump stroke volume (8 μl) and number of pulses [16]. The sample and reagent R_2 volumes for Cr (VI) determination were investigated by varying the number of pulses between 2 and 15. Increasing the number of pulses up to 15 led to an increase in analytical signal, but no further increase was found for higher inserted volumes. As a compromise between sensitivity and sampling rate, 12 pulses were selected.

For total Cr determination, sample and reagent R_1 volumes were maintained to 12 pulses, respectively, and reagent R_2 was varied by changing the number of pulses from 4 to 40. Nevertheless, when the number of sampling pulses was higher than 30, no significant signal increase was observed. In this case, 30 pulses for introduction of sample/oxidant mixed solution and 1,5-diphenylcarbazide were selected for further experiments. Considering these results, the operational conditions selected are shown in Table 1. The sequence of events was controlled according to the micro-pumps switching pattern depicted in Fig. 2.

The length of the reaction coils B_1 and B_2 was varied from 10 to 50 cm and from 10 to 100 cm, respectively, thus the inner volume of these of coils varied from 50 to 500 μl.

Results found as a function of the length of the reaction coil B_1 indicate that analytical signals increased up to a 30 cm coils, and decrease for longer coils. The use of such a short reactor was possible in view of the improved mixing conditions guaranteed by the multicommutated sample and reagent introduction.

Absorbance signals increase on increasing the B_2 reactor length from 10 till 50 cm therefore indicating that mixing between oxidized solutions and 1,5-diphenylcarbazide was efficient.

Considering the aforementioned results and aiming to save time of analysis the lengths of coils B_1 and B_2 were fixed at 30 and 50 cm, respectively.

3.3. Potential interfering ions

Natural water is a complex matrix presenting several chemical species, which could cause interferences in the photometric determination of chromium. In this sense, a set of assays was performed in order to establish the tolerance limit of the proposed method. It was considered as a tolerable limit the interferent concentration of foreign ions that produced an error up to a 5% deviation in the determination of Cr (VI) on comparing with measurements obtained in the absence of the assayed substance.

It was selected twenty-three common species usually found in water and results obtained are summarized in Table 2. As can be see, the multicommutation photometric procedure has a wide tolerance for the assayed chemical species and severe interferent effects do not take place. The worst results were obtained for Fe^{2+}, Fe^{3+}, V(V) and Cu^{2+}, but taking into account that the tolerance limit found for these species are higher than those established as the maximum concentration acceptable for the considered compounds in surface waters, the procedure could be useful for chromium determination in waters.

As compared with others studies found in the literature the mass ratio tolerance level of interferent ions found in the present study were of the same order than those obtained by Luo et al. [19] and Noroozifar and Khorasani [25], and better than those found by Themelis et al. [26] and Watanabe et al. [27].

3.4. Figures of merit of the procedure

Determination of both Cr (VI) and total Cr was based on the complexation with 1,5-diphenylcarbazide directly or after oxidation of the sample with H_2O_2 in NaOH. So, the figures of merit correspond to those of the analytical curve established for Cr (VI). Calibration lines were linear within 10 and 200 μg l^{-1}, and a typical equation was $y = (3.348 \pm 0.009)\,x + (20.80 \pm 0.03)$ $r = 0.995$, $n = 7$ in the presence of H_2O_2 and NaOH and; $y = (2.724 \pm 0.004)\,x + (11.15 \pm 0.01)$ $r = 0.999$, $n = 7$ in the absence of H_2O_2, being x the Cr (VI) concentration in μg l^{-1}.

The colorimetric reaction between Cr (VI) and 1,5-diphenylcarbazide (H_4L) is a redox reaction in which Cr (VI) oxidizes it to 1,5-diphenylcarbazone (H_2L). The high slope in the presence of H_2O_2 could be explained by the oxidant action of H_2O_2 over the H_4L. This additional oxidant will increases the concentration of 1,5-diphenylcarbazone (H_2L) and consequently the concentration of the coloured complex $[Cr(HL)_2]^+$.

The relative standard deviation of results was estimated as 1.0 and 1.8% for Cr (VI) and total Cr, respectively, for 20 measurements of a 50 μg l^{-1} Cr concentration, emphasizing the good analytical repeatability of photometric signals. Other favourable characteristics; such as consumption of 0.006 μg 1,5-diphenylcarbazide and 0.240 ml of oxidizing reagent per determination were achieved. The sampling throughput was 67 and 105 determinations per hour, for total Cr and Cr (VI) determination, respectively. Detection limits of 2.0 and 0.97 μg l^{-1} for Cr (III) and Cr (VI), respectively, were found; taking into account that Cr (III) was determined by the difference between total Cr and Cr (VI).

On comparing the aforementioned procedure, based on the use of a home-made LED-photometry, with a spectrophotometric method using a diode array commercial instrument, the analytical features summarized in Table 3 were found. As can be seen the dynamic range depends basically on the length of the flow cell and the R.S.D. and LOD are better for the multicommutation approach than for the measurements based on the use of a diode array instrument.

Table 4 shows the comparison of the analytical characteristics of the method developed for Cr speciation with those of flow photometric procedures previously published based on the use of DPC and also chromotropic acid.

The limit of detection achieved for total chromium and chromium (VI), respectively, by the developed procedure are higher than those obtained by FIA using diphenylcarbazide after 20 min oil bath heating [18], but of the same order than those obtained by FIA using KIO_4/NaOH [26] and SIA using Ce (IV) and 5 min heating [19] and 20 and 500–4000 times lower than those obtained by SIA measurements with Ce (IV) [20] and FIA measurements with H_2O_2/NaOH [8]. It must be noticed that the method that provides the lowest limit of detection involves a heating step for Cr (III) oxidation and 15 times higher sample consumption [18].

The repeatability obtained by using the developed micropumping multicommutation procedure is comparable to those found for the rest of methods. Besides, the Cr (VI) sampling frequency was 105 h^{-1}, it can be seen that it is higher than that found by SIA procedures [19,20] and of the same order than that obtained by FIA procedures [26].

As compared with atomic spectrometric procedures also proposed in the literature for Cr determination in water [1–3] the developed procedure provides a LOD and repeatability features of the same order than atomic ones and a sampling throughput better than that obtained by atomic spectroscopy.

As can be seen in Table 4 the micro-pumping multicommutation procedure generates a reagent waste of 96 to 336 μl per determination and provides 2 to 15 times reduction of wastes as compared to the SIA procedures [19,20], and 5 times reduction as compared with the FIA method [26].

In short, taken in consideration the parameters shown in Table 4, the developed procedure is a suitable and environmentally friendly mechanized alternative to SIA and FIA methods available in the literature and it has improved the previous data obtained [15] about the use of multi-pumping in flow analysis for the determination of Cr in waters.

3.5. Applications

In order to evaluate the applicability of the proposed system, nine natural waters samples, from different origin, were analyzed and results are shown in Table 5. In order to get an additional accuracy assessment, the natural samples were spiked with 50 μg l^{-1} of Cr (III) and 50 μg l^{-1} Cr (VI) and recovery data found are also reported.

As can be seen, recovery data varied from 93 to 107% without any systematic bias for the two species of Cr determined.

Table 4
Analytical performance of flow photometric procedures proposed in the literature for determination of total Cr and Cr (VI)

Parameter	Proposed procedure multicommutation total Cr/Cr (VI)	Reference [19] SIA total Cr/Cr (VI)	Reference [20] SIA total Cr/Cr (VI)	Reference [8] FIA total Cr/Cr (VI)	Reference [18] FIA total Cr/Cr (VI)	Reference [26] FIA total Cr/Cr (VI)	Reference [15] FIA only Cr (VI)
Dynamic range (μg l^{-1})	10–200/10–200	NA/25–100	850–25,000/160–20,000	1000–20,000/1000–20,000	0.1–2.0/0.0125–1.25	30–1200/3–4000	NA
R.S.D. (%)	1.8/1.0	NA/2.0	0.7	<5	<5	4/3	<0.5
LOD (μg l^{-1})	2.0/1.4	NA/2.0	42/23	1100/5900	0.02/0.009	10/1	NA
Throughput (h^{-1})	67/105	NA/17	30	NA	NA	90	80
Sample consumption (μl)[a]	96/96	NA/6000	240	50/50	7900	100	120
Reagents consumption (μl)[a]	336/96	NA/1500	160	NA	NA	536	NA
Reagent used	1,5-Diphenylcarbazide	1,5-Diphenylcarbazide	1,5-Diphenylcarbazide	1,5-Diphenylcarbazide	1,5-Diphenylcarbazide	Chromotropic acid	1,5-Diphenylcarbazide
Cr (III) → Cr (VI) treatment	Oxidant (H_2O_2 + NaOH)	Oxidant Ce (IV) heating water bath at 45 °C for 5 min	Oxidant Ce (IV) heating water bath at 45 °C	Oxidant (H_2O_2 + NaOH)	Heated in an oil bath at 80 °C for 20 min	Oxidant KIO_4/NaOH	–

NA: Not available.
[a] Sample and reagents consumption corresponding to each analysis.

Table 5
The analytical results of Cr (VI) and total Cr concentrations in natural water samples

Sample	Total Cr	Cr (VI)	Cr (III)	Cr (III)/Cr (VI)	Recovery (%)[a] Cr (III)/Cr (VI)
River 1	62 ± 3	18 ± 1	44 ± 1	2.4	106/103
River 1	40 ± 1	14.2 ± 0.1	26 ± 1	1.8	105/105
River 2	55 ± 2	16.1 ± 0.5	39 ± 1	2.4	95/96
River 2	28.6 ± 0.6	13.3 ± 0.6	15.3 ± 0.4	1.2	107/98
River 3	32.6 ± 0.2	14.5 ± 0.6	18.1 ± 0.5	1.2	103/94
River 4	28.3 ± 0.3	12.1 ± 0.2	16.2 ± 0.1	1.3	96/103
River 4	27 ± 2	16.6 ± 0.5	10 ± 1	1.5	105/98
Spring water	26.7 ± 0.2	11.5 ± 0.4	15.2 ± 0.3	1.3	94/95
Tank water	28.2 ± 0.4	13.1 ± 0.2	15.1 ± 0.2	1.1	93/94

Note: Concentration data, expressed in $\mu g\,l^{-1}$, are based on three replicate analysis ± the corresponding standard deviation.
[a] Recovery percentage obtained after spiking the samples with 50 $\mu g\,l^{-1}$ Cr (III) and 50 $\mu g\,l^{-1}$ Cr (VI).

4. Conclusions

In spite of the large numbers of papers dealt with the determination of Cr (VI) by using DPC, the present study offer an interesting alternative to downsized the equipment for Cr speciation in waters.

The use of micro-pumping multicommutation together with a low cost homemade LED-photometric detector with a long path length cell improves the miniaturization of the system and its automatization also enhancing the sensitivity of measurements as compared with previous studies (see Table 4).

The proposed procedure is simple, low-cost and rapid, 54 s per sample for total chromium and 34 s for chromium (VI) determination. The low reagent consumption, and low waste generation are additional advantages, as compared with other flow alternatives. The low weight and reduced power requirements also provide a way to do in situ measurements and additional work is in due course in this sense.

Considering that the permissible maximum limit of total chromium established by the European Community is of 50 $\mu g\,l^{-1}$ in natural waters, the proposed flow system could be employed for Cr screening purpose in station for water purification, without using neither expensive nor sophisticated instrumentation.

Acknowledgements

The authors thank the financial support of the CAPES/MECD (Brazil) n. process 042/03, Ministerio de Educacion, Cultura y Deporte (Spain) ref. PHB 2002-0054-PC and CNPq (Brazil).

References

[1] M. de la Guardia, A. Morales-Rubio, Sample Preparation of Trace Element Analysis, Elsevier, 2003 (Chapter 35, p. 1115).
[2] M.J. Marqués, A. Salvador, A. Morales-Rubio, M. de la Guardia, Fresenius J. Anal. Chem. 362 (1998) 239.
[3] M.J. Marqués, A. Salvador, A. Morales-Rubio, M. de la Guardia, Fresenius J. Anal. Chem. 367 (2000) 601.
[4] J.M. Carey, N.P. Vela, J.A. Caruso, J. Chromatogr. A 662 (1994) 329.
[5] P.K. Tarafder, S.B. Singh, D.P. Rathore, Fresenius J. Anal. Chem. 354 (1996) 124.
[6] T. Cherian, B. Narayana, Ind. J. Chem. Technol. 12 (2005) 596.
[7] L.A. Tortajada-Genaro, P. Campins-Falco, F. Bosch-Reig, Anal. Chim. Acta 446 (2001) 385.
[8] J.E.T. Andersen, Anal. Chim. Acta 361 (1998) 125.
[9] I. Lopez-Garcia, B. Merino-Meroño, N. Campillo, M. Hernandez-Cordoba, Anal. Bioanal. Chem. 373 (2002) 98.
[10] B.F. Reis, A. Morales-Rubio, M. de la Guardia, Anal. Chim. Acta 392 (1999) 265.
[11] F.R.P. Rocha, P.B. Martelli, B.F. Reis, Anal. Chim. Acta 438 (2001) 11.
[12] F.R.P. Rocha, O. Fatibello, B.F. Reis, Talanta 59 (2003) 191.
[13] B.F. Reis, M.F. Gine, E.A.G. Zagatto, J.L.F.C. Lima, R.A. Lapa, Anal. Chim. Acta 293 (1994) 129.
[14] F.R.P. Rocha, B.F. Reis, E.A.G. Zagatto, J.L.F.C. Lima, R.A.S. Lapa, J.L.M. Santos, Anal. Chim. Acta 468 (2002) 119.
[15] R.A.S. Lapa, J.L.F.C. Lima, B.F. Reis, J.L.M. Santos, E.A.G. Zagatto, Anal. Chim. Acta 466 (2002) 125.
[16] A.F. Lavorante, A. Morales-Rubio, M. de la Guardia, B.F. Reis, Anal. Bioanal. Chem. 381 (2005) 1305.
[17] E. Rodenas-Torralba, A. Morales-Rubio, M. de La Guardia, Anal. Bioanal. Chem. 383 (2005) 138.
[18] S. Matsuoka, Y. Tennichi, K. Takehara, K. Yoshimura, Analyst 124 (1999) 787.
[19] Y. Luo, S. Nakano, D.A. Holman, J. Ruzicka, G.D. Christian, Talanta 44 (1997) 1563.
[20] L.V. Mulaudzi, J.F. van Staden, R.I. Stefan, Anal. Chim. Acta 467 (2002) 51.
[21] F.R.P. Rocha, E. Rodenas-Torralba, B.F. Reis, A. Morales-Rubio, M. de La Guardia, Talanta 67 (2005) 673.
[22] M.A. Feres, B.F. Reis, Talanta 68 (2005) 422.
[23] L.S. Clesceri, A.E. Greenberg, A.D. Eaton, Standard Methods for the Examination of Water and Wastewater, 20th ed., American Public Health Association, Washington DC, 1998, p. 108.
[24] E. Rodenas-Torralba, F.R.P. Rocha, B.F. Reis, A. Morales-Rubio, M. de la Guardia, J. Autom. Meth. Mgmt. Chem. 2006 (2006) 1.
[25] N. Noroozifar, M. Khorasani-Motlagh, Anal. Sci. 19 (2003) 705.
[26] D.G. Themelis, F.S. Kika, A. Economou, Talanta 69 (2006) 615.
[27] K. Watanabe, M. Tojo, M. Itagaki, Bunseki Kagaku 55 (2006) 781.

Available online at www.sciencedirect.com
ScienceDirect
Talanta 72 (2007) 1564–1572
Talanta
www.elsevier.com/locate/talanta

Investigation of Cd(II), Pb(II) and Cu(I) complexation by glutathione and its component amino acids by ESI-MS and size exclusion chromatography coupled to ICP-MS and ESI-MS

Kasia Połeć-Pawlak *, Rafał Ruzik, Elżbieta Lipiec

Warsaw University of Technology, Faculty of Chemistry, Department of Analytical Chemistry, ul. Noakowskiego 3, 00-664 Warszawa, Poland

Received 27 September 2006; received in revised form 30 January 2007; accepted 5 February 2007
Available online 16 February 2007

Abstract

The elucidation of structures of glutathione (GSH) complexes play an important role in the fundamental understanding of biochemical pathways of metal ion deactivation in plants. This article attempts to feature key studies for stoichiometry of metal complexes with glutathione and its constituent amino acids to obtain a better understanding of the different metal affinities of the complexation sites of glutathione. The SEC–ICP-MS experiments have indicated that oxidation process of glutathione was accelerated by metal ion presence in following order Cu^{+}, Pb^{2+} and Cd^{2+}. The redox activity of metal ions was confirmed by ESI-MS experiments, which allowed to observe formation of glutathione disulphide (GSSG) in time. The stoichiometry of Cd^{2+}, Cu^{+} and Pb^{2+} complexes with GSH was defined by observing the isotope pattern of investigated metals and hydrogen loss or transfer during binding. The complexes with metal bound to sulphur of 1:1 and 1:2 stoichiometry were found in case of cadmium and lead. The number of hydrogen atoms lost during metal binding and the SEC–ESI-MS results allowed to elucidate that copper is bound by GSSG in ratio 1:1 and 1:2. Additionally, size exclusion chromatography coupled to electrospray MS allowed to differentiate more stable complexes from weak ones that could be created in the gas phase.

Keywords: Glutathione; Oxidative stress; Toxic metal deactivation; Size exclusion chromatography; Electrospray mass spectrometry

1. Introduction

Glutathione (γ-Glu-Cys-Gly, GSH) is one of the major cellular safeguards, which plays a triple protective role as a key antioxidant, antitoxin and enzyme cofactor. It is also known as a chelating bioligand responsible for detoxification of heavy metals, similarly to phytochelatins in plants (polymers of γ-Glu-Cys, PCs) [1] and metallothioneins in animals. Glutathione as a chelating agent contains one thiol group creating mercaptide bond with heavy metal ions like Zn, Cu, Cd, Pb and Ag [2]. In many cases, those metals were reported to be responsible for induction of oxidative stress in plants observed by higher production of reactive oxygen species (ROS) [3]. The literature survey allows to distinguish two different mechanisms, based on heavy metals chemical properties: (1) production of ROS by auto-oxidation and Fenton reaction induced by transition metals such as iron or copper and (2) blocking of essential thiol groups by non-redox-reactive heavy metals [3]. In both cases the glutathione is involved as a: (1) antioxidant responsible for reduction of dehydroascorbate to ascorbate or disulphide bonds of proteins by creation of oxidised GSH dimer (GSSG) [4] and (2) precursor for synthesis of phytochelatins responsible for binding of heavy metals. Additionally, it was proved that induction of PCs synthesis was achieved in presence of metal complex with glutathione, not metal ion itself [5]. The structures of $Cd(GSH)_2$ and $Zn(GSH)_2$, based on mercaptide bond were postulated as a most probable. There are three factors representing efficiency of plant in metal deactivation of heavy metals: (1) the ratio of reduced glutathione against its oxidised counterpart (GSH/GSSG), (2) the affinity of heavy metal to thiol group and (3) the level of amino acids composing GSH such as glutamic acid and cysteine and their affinity to those metals [6]. Thereby, it is not surprising that coordination and stability of glutathione complexes with heavy metals

* Corresponding author. Tel.: +48 22 660 71 09; fax: +48 22 660 74 08.
E-mail address: kasiap@rpi.pl (K. Połeć-Pawlak).

0039-9140/$ – see front matter © 2007 Elsevier B.V. All rights reserved.
doi:10.1016/j.talanta.2007.02.008

are ambiguous and their characterisation is very difficult to be performed. Despite these problems some experiments were carried out by differential pulse polarography trying to clarify some aspects of cadmium complexation by glutathione and its amino acids [7]. The authors suggested the occurrence of two types of coordination modes attributed to cadmium bond to one or two sulphur atoms. The proposed stoichiometry of the complex of tetrahedral cadmium with glutathione (1:1 or 1:2) was explained by involving two deprotonated carboxylic groups in pH 7.5 and proton transfer to amine group. Electrospray ionisation mass spectrometry (ESI-MS), widely used for the analysis of polar and ionic compounds like metal complexes with proteins [8], peptides [9] and even non-covalent complexes [10], in the field of interest was applied to confirm the complexation of arsenic by glutathione in ratio 1:3 [11]. The cadmium and lead complexes with Me/GSH molar ratios $Cd_1(GSH)_1$ and $Pb_1(GSH)_{1/2}$ were also proposed in the comprehensive study of ESI-MS application for identification of GSH complexes with different metal ions [12]. Non-stoichiometric complex of glutathione with cadmium (Cd:S = 1:1) was observed also by ion pairing liquid chromatography coupled to high resolution mass spectrometer with ionisation in inductively coupled plasma (ICP-MS) [13]. Copper, most problematic transition metal, was investigated only during binding to aromatic and α-amino acids and was found to create complexes with molar ratio 1:1. Additionally, in the presence of copper and alkali metal ion intramolecular redox processes or reduction of Cu(I) to Cu(0), noted by the loss of neutral CO_2, were observed in the gas phase [14]. Previously reported results still needed to be confirmed, because interactions of the complex with reversed phase silica based stationary phase and ion pairing agent present in the mobile phase could change its stoichiometry. Moreover, the influence of pH on the complexation equilibria was completely neglected in the case of ESI-MS studies. For this reason the size exclusion chromatography (SEC), widely used for separation of metal–protein/peptide complexes extracted from animal or plant tissue, was chosen as a favourable experimental approach with ICP-MS and ESI-MS detection [15–17]. However, less stable complexes can dissociate during chromatographic separation causing shifts of the retention times or loss of the resolution and sensitivity due to metal sorbing [18]. Still, the purification and fast screening of low stability metal complexes with glutathione and phytochelatins extracted from plant tissue are usually carried out by this method [19–22].

In this work, the SEC–ICP-MS was used to examine the oxidation process of glutathione in presence of selected metals with different chemical properties (Cd(II), Cu(I) and Pb(II)). The electrospray ionisation mass spectrometry was used (1) to perform comparative study of interactions between selected metals, glutathione and its component amino acids (glutamic acid, cysteine and glycine), (2) to demonstrate the influence of oxidation process on the complexation equilibria. Size exclusion chromatography with on-line ESI-MS detection was also used to individuate and characterise reduced and oxidised glutathione complexes with metal ions and to distinguish most stable forms from labile ones.

2. Experimental

2.1. Instrumentation and chemicals

Metal complexes were characterized by ESI-MS and SEC–ESI-MS with the use of a LC–MSD 1100 mass spectrometry detector system (Agilent Technologies, Wilmington, NC, USA). Optimisation of ESI source parameters was carried out using standard solutions of bioligands and their mixtures with metal ions admitted to the detector by light aspiration (10 μL min^{-1}) achieved by the nebulizing gas flow (6 L min^{-1}) transported under pressure of 30 psi. Only orifice voltage was found to influence stability of ions of metallocomplexes. The lowest voltage (60 V) was applied to prevent complex decomposition and to ensure efficient transport of the generated ions to the analysing module. Calculation of isotope patterns was carried out by IsoPro 3.0 MS/MS Software.

Separation of the bioligands and their complexes with metal ions was performed with size exclusion Superdex Peptide HR 10/30 column containing dextran covalently bond to highly cross-linked porous agarose beads (Amersham Pharmacia Biotech, Uppsala, Sweden). Injections were carried out using a model 7725 injection valve with 100 μL injection loop. The eluent was supplemented with methanol stream supplied by Perkin-Elmer HPLC pump (model LC-95, Perkin-Elmer, Norwalk, CT, USA) by T-connector placed between chromatographic column and capillary of ESI source; it was found to be necessary for ensuring efficient ionisation. The Agilent ChemStation for LC/MS System 2000 was used for MS data acquisition and processing. The results obtained by SEC–ESI-MS were verified by the SEC–ICP-MS ones, which were achieved by connection of column outlet to commercial ICP-MS sample introduction system (HP 7500a, Agilent Technologies, Tokio, Japan). A Branson Model 1210 ultrasonic bath (Danbury, CT, USA) was used for degassing buffer and HPLC eluents used for sample preparation and separation.

All reagents used were of analytical grade purchased from Sigma–Aldrich (Sigma–Aldrich, Buchs, Switzerland). The methanol (MeOH) of HPLC gradient grade purchased from Lab-Scan (Lab-Scan Analytical Science, Dublin, Ireland) was used as makeup liquid for SEC–ESI-MS method. Water (18 mΩ) prepared with Mili-Q system (Milipore Elix 3; Milipore, Saint-Quentin, France) was used throughout.

2.2. Sample preparation and analytical procedures

Stock solutions of glutathione, cysteine, glutamic acid, glycine, cadmium(II) and lead(II) (as nitrates) were prepared daily by dissolving of standard materials in degassed solution of 5 mM ammonium acetate buffer (pH 8.0). The obtained stock solutions (0.01 M) were purged with argon stream and sealed for storage in order to avoid oxidation of glutathione and cysteine. A copper(I) solution was prepared from the $[Cu(CH_3CN)_4]ClO_4$ complex synthesized according to the procedure of Hemmerich and Signart [23]. The stock solution (0.01 M) was prepared in the water–acetonitrile mixture (70:30, v/v) with addition of perchloric acid to obtain pH 3, purged with argon and sealed.

Appropriate molar equivalents (1.0, 0.75, 0.5, 0.25) of metals to bioligands, present in concentration of 1 mM, were mixed and incubated in 37 °C. Samples were stabilized with 10 mM ammonium acetate buffer, pH 8.0, for 10 min to reach the equilibrium of the complexation reaction. The ammonium acetate buffer was used, in spite of its different pH range for the best buffering capacity, due to its volatility and good protonation capacity. Cadmium(II) ions introduced in higher concentrations to the solutions, which were directly admitted to the ESI source have been registered also as background ions making difficulties in recognizing signals with isotopic patterns related to their complexes. For this reason glutathione and amino acid complexes with Cd(II) and other metal ions were investigated for the highest excess of the bioligand (Cd/Cu/Pb:ligand = 0.25:1) and under such conditions S/N ratio was 6–57 for signals with cadmium isotope pattern. In samples for SEC–ICP/ESI-MS molar ratio:bioligand was kept as 1:1. Mixture of the reagents was purged with argon and left for 10 min to reach equilibrium of the complexation reaction.

Intensity of negative ions related to metal complexes were 10 times higher than positive ones due to favoured deprotonation of molecule assisted by pH > 7 of the incubation solution. Although, the whole study was carried out in negative ion mode considering the specific isotope patterns of investigated metals, mass spectra obtained for positively charged ions were also investigated. The optimised detection and separation conditions are summarized in Table 1.

Table 1
Optimum ESI-MS, ICP-MS and SEC conditions

ESI-MS detection conditions	
Ionspray voltage	−4000 V
Orifice voltage	60 V
m/z range scanned	100–1500 u
Dwell time	50 ms
Step size	0.1 u
Nebulizing gas temperature	300 °C
Nebulizing gas flow	6.0 L min^{-1} (13.0 L min^{-1} for SEC)
Nebulizing gas pressure	30 psi (60 psi for SEC)
ICP-MS detection conditions	
RF Power	1220 kW
Plasma gas flow rate	15 L min^{-1}
Auxiliary gas flow rate	1 L min^{-1}
Nebulizer gas flow rate	1.13 L min^{-1}
Isotopes monitored	^{63}Cu, ^{114}Cd, ^{207}Pb
Dwell time	100 ms
SEC separation conditions	
Column	Superdex Peptide HR 10/30
Column dimensions	300 × 10 mm, 13 μm
Exclusion limit	20 kDa
Mobile phase composition	5 mM ammonium acetate, pH 7.6
Mobile phase flow	0.7 mL min^{-1}
Post column makeup flow for ESI-MS	0.2 mL min^{-1} of MeOH
Sample volume	100 μL

3. Results and discussion

3.1. Metal binding by selected amino acids and glutathione by SEC–ICP-MS; oxidation of glutathione in presence of Cd(II), Cu(I) and Pb(II)

Due to the possibility of interactions of metal with bioligand in the gas phase during electrospray ionisation, the presence of metal complexes with investigated amino acids and glutathione was checked by injection of appropriate mixtures of GSH with metal ions on SEC column. The column was carefully washed with 0.1% solution of acetic acid to remove sodium and other metal ions sorbed on the stationary phase, which could interact with ligands and compete with studied metals. The incubation buffer with addition of cadmium(II) and lead(II) nitrates or copper(I) complex was used as a blank sample. In the case of each metal ion only baseline was observed without any chromatographic peak, probably due to the sorption of metal on the stationary phase (not shown).

The chromatogram obtained for injected cadmium(II) mixture with glutathione just after its preparation consisted of two peaks. The first peak (t_R 16.0 min), corresponding to complex with higher molecular mass, was significantly increasing in time contrary to the second one (t_R 21.5 min), which completely vanished after 10 h of incubation (Fig. 1a and b). The presence of 5 mM of beta-mercaptoethanol (BMSH) in the starting sample of glutathione with cadmium(II) augmented the second peak twice and restrained investigated complex transformation into the higher molecular mass compound. This could indicate that first peak corresponds to oxidised form of glutathione with created disulphide bridge. Although, two chromatographic peaks were observed also for mixture of glutathione with lead(II) the first peak was dominating already after 15 min of incubation. Only one signal (t_R 15.3 min) was observed in case of mixture of glutathione with copper(I) and was corresponding only to oxidised GSH (Fig. 1a). Similar effect of oxidation was observed for cysteine after addition of metal ions. In case of glutamic acid and glycine for Cd(II) and Pb(II) only one peak was observed at 16.7 min, and two for Cu(I) at 16.6 min and 18.4 min (Fig. 1c). Surprisingly, the peak area of the second one was stable in time while the first peak corresponding to bigger compound containing copper disappeared after 4 h of incubation. The precision for retention times was established for five injections of glutathione mixture with Cd(II) and Cu(I) after 4 h of incubation and was 3.7% and 4.2%, respectively. Although peak areas are somewhat variable (almost 20% for three fresh prepared samples), due to the sorption of metal ions on the stationary phase, registered peaks confirm the presence of metal complexes in the solution. Still, the effect of oxidation process of glutathione and cysteine need to be verified and the polymorphism of Cu–Gly/Glu complexes manifested by two chromatographic peaks should be elucidated.

3.2. ESI-MS investigation of cadmium binding to GSH, Cys, Glu and Gly

The discussion on stoichiometry of the metal complexes with bioligands is based on the accurate calculation of their molecular masses including isotope pattern. The comparison of registered signals on the mass spectrum with theoretical isotope pattern made possible to specify charge of the complex and the number

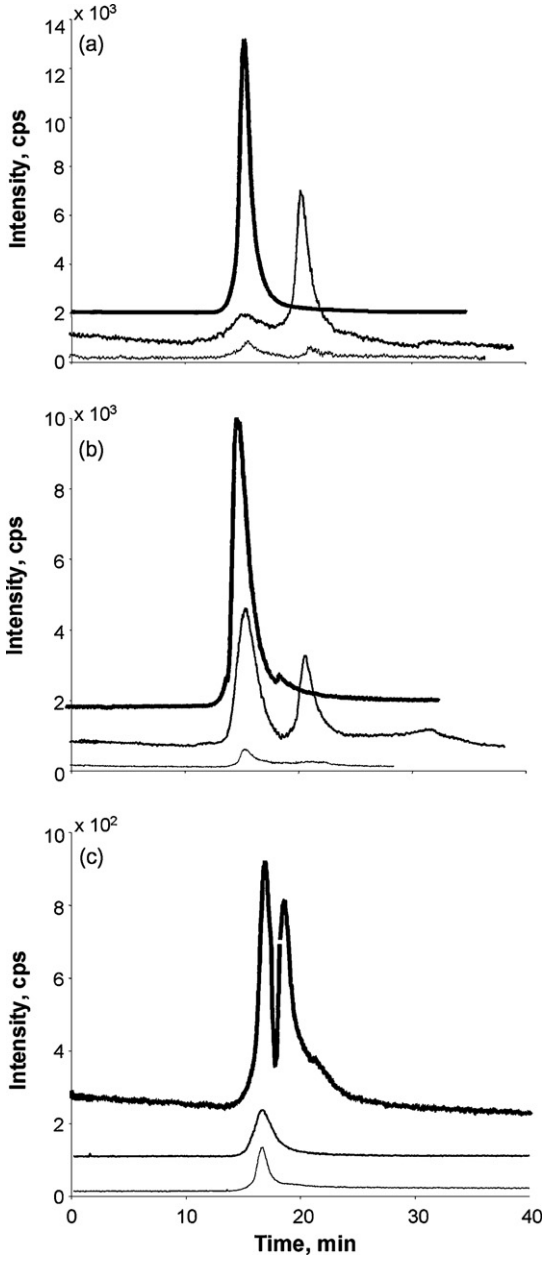

Fig. 1. Chromatograms (SEC–ICP-MS) obtained for mixtures of copper(I) (top, bold lines), cadmium(II) (medium, regular lines) and lead(II) (bottom, dashed lines) with glutathione (a), cysteine (b), and glutamic acid (c) 15 min after preparation. Chromatograms obtained for mixture of cadmium with glutathione after 4 h (bottom line) and 17 h of incubation (top line).

of hydrogen atoms that must be removed to give the observed *m/z* values. In the mass spectrum obtained for glutathione mixture with Cd(II) three signals at *m/z* 306 (not shown), 613 and 611 were found (Fig. 2a), which correspond to conjugate base of glutathione $[GSH\text{-}H]^-$, proton bound cluster $[(GSH)_2\text{-}H]^-$ and its oxidised form with disulphide bridge $[GSSG\text{-}H]^-$, respectively. In spite of degassing of solvents and addition of metal ion in inert gas atmosphere, the oxidation of glutathione is difficult to avoid. In this case the addition of BMSH is unwanted because it is expected to interrupt the equilibrium of the complexation reaction. Oxidation of glutathione in presence of Cd(II) is relatively slow. After 10 min of incubation at 37 °C intensity of the signal at *m/z* 611 achieved only 57000 cps, which was 5% of the intensity of deprotonated quasi-molecular ion of glutathione $[GSH\text{-}H]^-$ and increased linearly during 8 h of incubation to reach plateau for next 17 h, when intensity of $[GSH\text{-}H]^-$ constantly decreased. Signal of theoretically most probable cadmium complex of tetrahedral geometry with four glutathione molecules was registered as a weak signal at *m/z* 1339. The comparison of the registered signal to the theoretical isotope pattern indicated loss of only three protons instead of expected five. This phenomena could be explained by deprotonation of carboxylate groups accompanied by hydrogen transfer to amine group which can be expected at pH 7.4 and were suggested already by other researchers [7]. The same mechanism with hydrogen transfer could be proposed for the formation of ion $[Cd(GSH)_3\text{-}3H]^-$ at *m/z* 1032, which can also be a product of partial fragmentation in the gas phase of ion at *m/z* 1339. To verify the role of reactions in the gas phase, the influence of orifice (nozzle-skimmer) voltage in the range 40–120 V and incubation time in 37 °C on signal stability were checked. The intensity of signals at *m/z* 1032, 1339 and 1450 was decreasing for higher energies and was not registered at all after 24 h of incubation. The intensity of signal at *m/z* 725 corresponding to $[Cd(GSH)_2\text{-}3H]^-$ was found to rise with orifice voltage until maximum reached for 80 V and to decrease slightly (30% loss of intensity after 10 h). After 24 h the signal at *m/z* 723 instead of 725 was found which could correspond to the loss of two hydrogen atoms during creation of glutathione disulphide (GSSG). Acidification of the solution with acetic acid (to pH 5.0) resulted in only slight loss in intensity (20%) of the signal at *m/z* 725 when other ions containing three or four glutathione molecules were completely decomposed. This could indicate, that cadmium complex in which metal ion is bound by two thiolate groups is dominant and most stable form among discussed above. The smallest, singly charged ion $[Cd(GSH)\text{-}3H]^-$ at *m/z* 418 exhibited similar stability in time as well as other observed clusters $[Cd_2(GSH)_2\text{-}5H]^-$ registered at *m/z* 835 and $[Cd_2(GSH)_3\text{-}5H]^-$ at *m/z* 1142, but their intensity was constantly increasing with nozzle-skimmer voltage. Such ions can be suspected to be a product of gas phase reactions in the ions source. The influence of time and pH on the identified cadmium complexes indicates, that only stable signals observed in the mass spectrum correspond to the equilibrium reached in the solution. The changes of the orifice voltage allowed to distinguish most stable forms of the complexes with Cd/GSH molar ratio 1:S, where $S \leq 2$.

Similar characteristic of Cd(II) binding, accompanied by loss of two hydrogen atoms per one coordination centre, can also be observed for its simple complexes with amino acids like cysteine (ion registered at *m/z* 353) and glutamic acid (*m/z* 405) (Fig. 2b and c). Despite the fact that glutamic acid does not contain thiol group, both amino acids form clusters containing two Cd atoms $[Cd_2L_3\text{-}5H]^-$ at *m/z* 584 for cysteine and 662 for glutamic acid. This indicates that complexes with examined bioligands can be formed without participation of thiol group as it was observed by SEC–ICP-MS. Cadmium also creates unstable clusters with glutamic acid and glycine observed as an ion $[CdL_3\text{-}3H]^-$ (registered at *m/z* 552 for Glu and 336 for

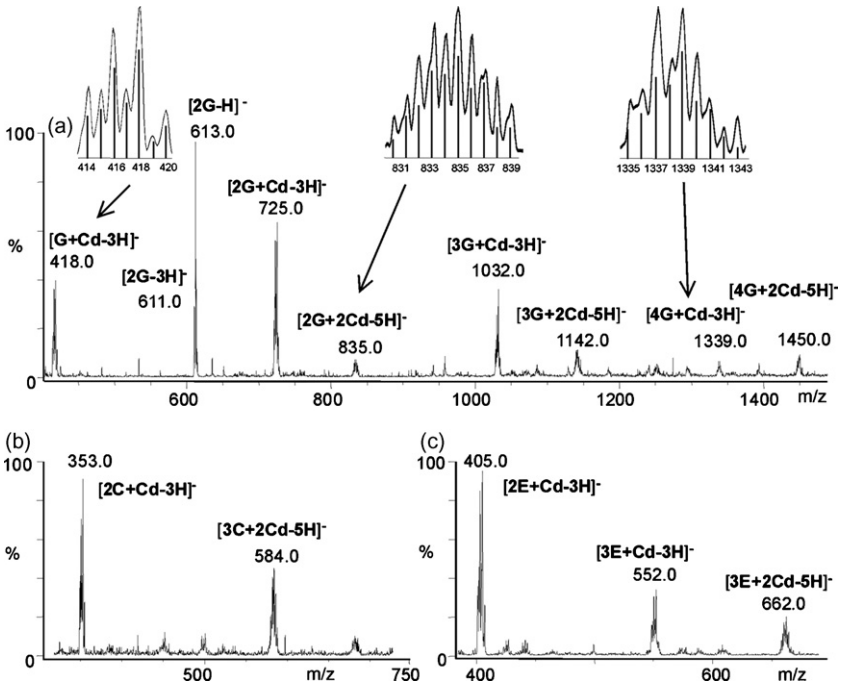

Fig. 2. Mass spectra of cadmium complexes in solutions containing 2.5 mM of Cd(II) and 10 mM of ligands: (a) glutathione-G, (b) cysteine-C and (c) glutamic acid-E. In the inset of mass spectrum of glutathione (a) the comparison of enlarged experimental isotopic pattern (solid line) and theoretical one (histogram) for selected cadmium complexes is presented.

Gly – the last is not shown). The intensity of ions at *m/z* 405, 552 and 662 was slightly decreasing in time simultaneously to strong rise of signal at *m/z* 146 corresponding to quasi-molecular ion $[Glu\text{-}H]^-$. Similar behaviour was observed for glycine. The alteration of the orifice voltage helped to distinguish most stable forms with Cd/Glu molar ratios Cd_1/Glu_2 and Cd_2/Glu_3. Although, signal corresponding to ion $[Cys\text{-}H]^-$ was stable in time, signal at *m/z* 239 for ion $[(Cys)_2\text{-}H]^-$ was increasing significantly, which could be due to releasing cystine instead of cysteine from complexes. An ion at *m/z* 584 corresponding to cluster $[Cd_2Cys_3\text{-}5H]^-$ was found to be more resistant to voltage applied at the orifice than ion $[Cd_1Cys_2\text{-}3H]^-$ registered at *m/z* 353. Both of them were found to be equally stable during 10 h of incubation.

The obtained results have allowed to classify the complexes according to the decreasing stability in the following order: $(GSH)_{1/2}Cd_1 \geq Cys_{1/2}Cd_1 \gg Glu_2Cd_1/Gly_2Cd_1$. Complexes suspected to be created through the proton transfer from carboxylic group to amine one exhibited lower stability than complexes created through the loss of hydrogen atom. The proposed order of stability clearly indicates that thiol group reveals the highest affinity to cadmium.

3.3. ESI-MS investigation of copper binding to GSH, Cys, Glu and Gly

In order to avoid oxidation of cysteine residue in glutathione, copper ions were used as Cu(I). The 0.25 molar equivalent of copper(I) to glutathione guaranteed optimal signal intensity against the noise (S/N = 17–400, for signals of copper isotope pattern). In spite of preparation of the reaction mixture in atmosphere of argon, the oxidation of glutathione was significantly fast. Two minutes after mixing of the reagents, quasi-molecular ion at *m/z* 611 of $[GSSG\text{-}H]^-$ reached intensity of 450 000 cps, after 1 h – 500 000 cps while signal at *m/z* 306 reached only 6% of that intensity. The oxidation process of glutathione after addition of copper(I) ($E_{Cu(II)/Cu(I)} = 0.15$ V [23]) takes place immediately and is difficult to prevent, especially during admission of the sample into the ion source. Due to that fact two molecules of oxidised glutathione with disulphide bridge (GSSG) can be expected to create cluster with copper instead of GSH. In the mass spectra obtained for the mixture of glutathione with copper(I), two main singly charged ions were observed at *m/z* 672 and 1284 (Fig. 3a). In both cases the isotopic pattern corresponding to only one copper atom was observed. For the first ion the molar ratio Cu:GSH = 1:2 was proposed with loss of five hydrogen atoms and for the second Cu:GSH = 1:4 with the loss of six hydrogen atoms, which could suggest the presence of Cu(II) in the solution. The observed complexes were stable during 24 h of incubation and were found to be resistant to higher energies applied in the interface zone and to lower pH (4.2) of the solution for which signals corresponding to cadmium complexes could not be found.

In the case of cysteine, oxidation of its molecule in the system with copper(I) is also observed. Cystine $(Cys)_2$, dimer of cysteine with disulphide bridge was found as a dominant form in solution. This may suggest, that most of the signals corresponding to complexes containing more than one cysteine molecule should be rather attributed to compounds with cystine. This can be confirmed by the fact, that formation of the smallest registered ion at *m/z* 540 is accompanied by the loss of six hydrogen atoms. Of course, electrospray experiments cannot define exact coordi-

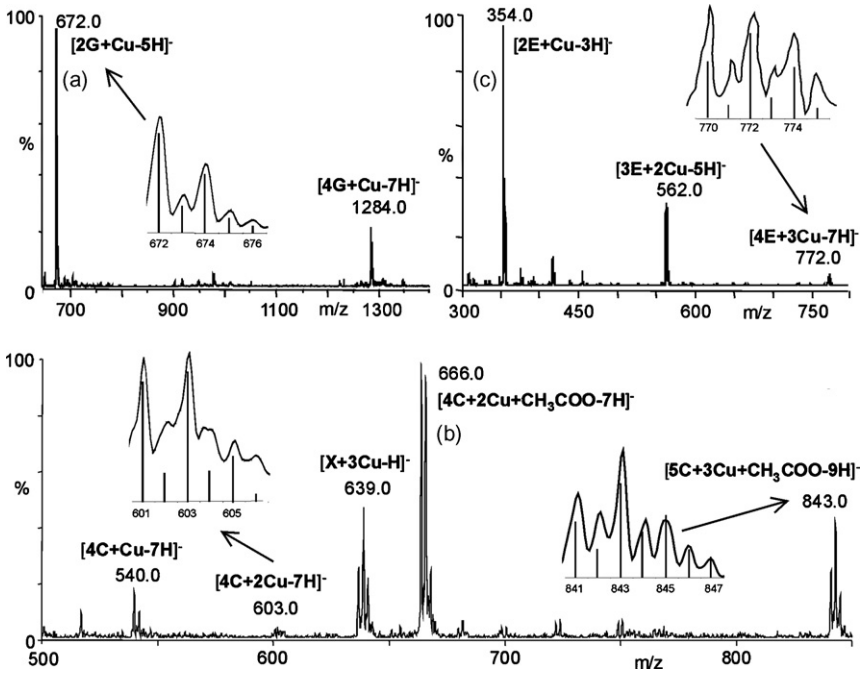

Fig. 3. Mass spectra obtained for solutions containing Cu(I) and R in molar ratio Cu: R = 1:4 of (a) R = glutathione-G, (b) R = cysteine-C and (c) R = glutamic acid-E. The comparison of theoretical isotopic pattern (histogram) obtained for complex with one, two and three atoms of copper and experimental one (solid line) is presented in inset of mass spectra.

nation of metal ion, because proposed structure is limited to exact molecular mass balance. Very weak but stable signal at *m/z* 603 (registered also in positive ion mode at *m/z* 605) corresponds to the ion consisting of two copper atoms and four cysteine residues (or two cystine residues) obtained by loss of six hydrogen atoms (Fig. 3b). According to isotope patterns, signals registered at *m/z* 639, 666 and 843 correspond to three, two and three copper atoms, respectively. The most abundant and unstable ion, at *m/z* 666 can be attributed to the adduct with acetate. The ion registered at *m/z* 843 can be formed from the latter by incorporation of Cu–Cys unit (Fig. 3b). The presence of acetate (main ingredient of incubation buffer) in copper clusters can be explained by higher affinity of copper ions to carboxylic group than to thiol one. Copper creates clusters with glutamic acid and glycine (not shown) similarly to cadmium (Fig. 3c), but in this case longer incubation time enhances their intensity. Smaller ions, formed both for glutamic acid and glycine $[CuL_2\text{-}3H]^-$ registered at *m/z* 354 for Glu and 210 for Gly and $[Cu_2L_3\text{-}5H]^-$ registered at *m/z* 562 for Glu and 346 for Gly (glycine not shown) could not be classified as fragment ions because of their smaller resistance to fragmentation voltage than ion $[Cu_3L_4\text{-}7H]^-$ – *m/z* 772 for Glu and 482 for Gly, whose intensity was linearly increasing. Moreover, signal at *m/z* 208 was found to correspond to ion $[CuGlu\text{-}H]^-$ but its intensity was very low (S/N = 3) and its susceptibility to different ionisation conditions and incubation time could not be discussed. Stability of copper complexes changes in time as follows: Glu–Cu/Gly–Cu > GSSG–Cu > Cys_2–Cu or Cys–Cu and proves more hard character of copper ion in comparison to soft Cd^{2+}. Although, the experiments carried by ESI-MS do not allow to state the charge of copper ion, the involvement of Cu(II) in formation of clusters cannot be excluded. The loss of neutral molecule CO_2 typical of gas phase reduction of copper was observed neither for positive nor negative ion mode [14]. Although the high ability of copper to oxidise GSH is certain, the creation of Cu–GSSG clusters should be confirmed.

3.4. ESI-MS investigation of lead binding to GSH and Cys

The influence of lead(II) addition on glutathione oxidation was found to be intermediate in comparison to metal ions studied above (Fig. 4). The signal at *m/z* 611 measured for the initial mixture of Pb(II) and GSH achieved 15% of the signal at *m/z* 306 and was increasing in time obtaining 30%, 60% and finally 80% after 2, 6 and 24 h, respectively. The simplest cluster with

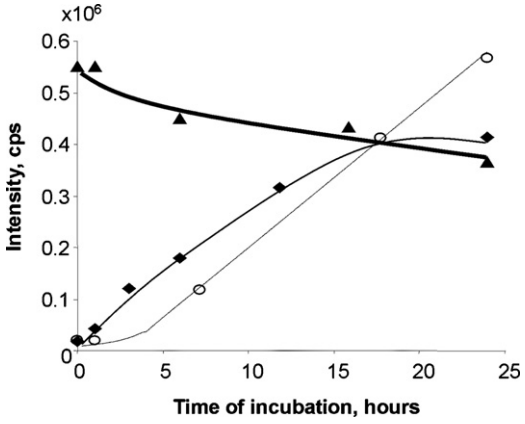

Fig. 4. The influence of incubation time on intensity of $[GSSG\text{-}H]^-$ ion registered at *m/z* 611 after addition of cadmium(II) (regular line with rhombus), copper(I) (bold line with triangles) and lead(II) (thin line with circles).

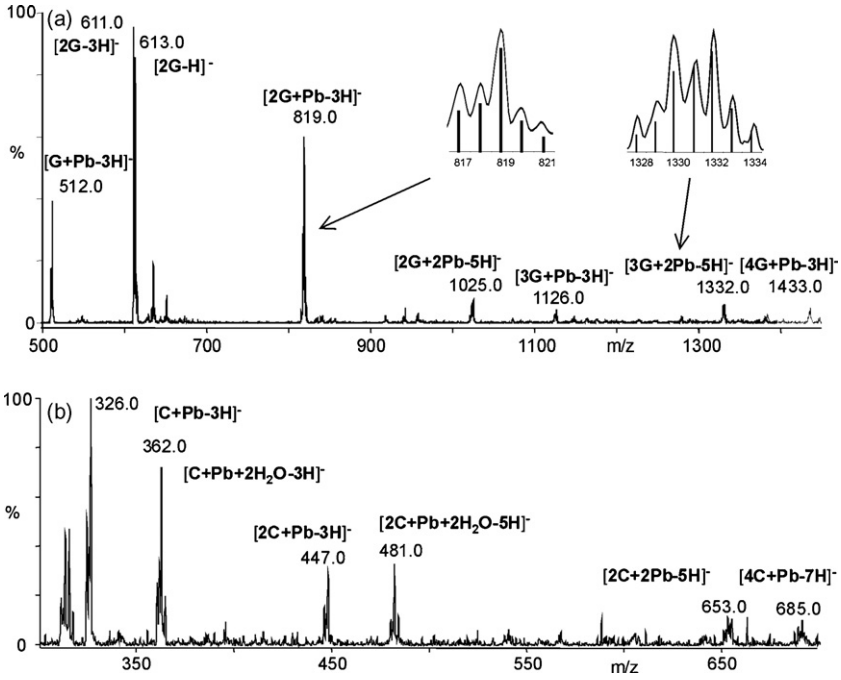

Fig. 5. Mass spectra of lead complexes solutions containing Pb(II) and R in molar ratio Pb:R (10 mM) = 1:4 of (a) R = glutathione–G and (b) R = cysteine-C. The influence of number of lead atoms on isotopic pattern for complexes $[2G + Pb - 3H]^-$ and $[3G + 2Pb - 5H]^-$ (solid line) in comparison to theoretical one (histogram) is presented in inset of mass spectrum obtained for glutathione complex.

molar ratio 1:1 with maximum intensity for 100 V was registered at *m/z* 512 (Fig. 5a). The loss of three hydrogen atoms and good stability of this complex indicate that not only thiol group takes part in binding of metal. Another, less stable cluster $[Pb(GSH)_2\text{-}3H]^-$ (at *m/z* 819 with maximum intensity for 60 V) was decomposing during incubation and transferring into ion observed as a signal at *m/z* 817, probably due to the loss of two hydrogen atoms during creation of sulphur bridge. Hence, the activity of GSSG in lead binding cannot be omitted for ions registered at *m/z* 1025 and *m/z* 817. Additionally, the intensity of both signals was increasing in time as well as signal corresponding to dimer of the glutathione, providing confirmation for proposed structures (Fig. 5a). Signals at *m/z* 1126, 1433 correspond to complexes with Pb/GSH molar ratios 1:3 and 1:4 created with the loss of only two hydrogen atoms, which indicates the necessity of proton transfer. Discussed ions are stable in contrast to equivalent ones with cadmium, which could indicate bigger influence of reactions in the gas phase of ion source.

The importance of thiol group in complexation of lead(II) was investigated in the system Pb(II)–cysteine. After addition of metal ion signal corresponding to quasi-molecular ion of cystine at *m/z* 239 achieved 40% of intensity of cysteine's one at *m/z* 120. After 24 h of incubation signal at *m/z* 239 became dominant and the signal at *m/z* 120 dropped to 10% of cystine peak intensity. Signals related to complexes with one atom of lead registered at *m/z* 326, 362, 447 and 481 with maximum intensity for 80 V were found to be unstable in time (Fig. 5b). For signals at *m/z* 362 and 481 the presence of two neutral molecules of water in the complex was suggested but their stability in spite of variation of fragmentation energy is rather surprising. Signals at *m/z* 653 and 685 with Pb/Cys molar ratio Pb_2Cys_2 and Pb_1Cys_4 became dominant after 24 h of incubation. The loss of four and six hydrogen atoms, respectively, suggests the participation of cystine in the second complex. The complexes of Pb(II) with glutamic acid and glycine were not discussed because signals with isotope pattern of lead were impossible to distinguish from noise.

3.5. Size exclusion chromatography coupled to ESI-MS as an approach for verification of proposed glutathione disulphide structures

With the aim to confirm the structures proposed for the examined metal complexes, size exclusion chromatography was coupled to ESI mass spectrometer. SEC column was prepared in the same way as for SEC–ICP-MS experiments. In spite of dilution of eluate with methanol (0.3 mL min^{-1}), the intensity for observed ions increased 10 times due to better efficiency of ionisation process. Mixtures of cadmium(II), copper(I) or lead(II) ions in molar equivalent to glutamic acid were injected on the column. Only signals corresponding to small metal complexes $[MeGlu_2\text{-}3H]^-$ (at *m/z* 354, 405 and 819 for Cu, Cd and Pb, respectively) were found to coelute with free ligand. Although column was devoted to compounds with molecular mass between 3–10 kDa, glutathione (M_w 307 Da) and cysteine (M_w 120 Da) were efficiently separated from their dimeric species with disulphide bridges (Fig. 6a). Mixture of glutathione with molar equivalent of cadmium was separated and selected signals were observed in negative ion mode. Only peaks corresponding to low molecular complexes were found, at *m/z* 418, 725 and 835. Reconstructed chromatograms for these free signals (*m/z* 835 not shown) indicated that they coeluted with GSH,

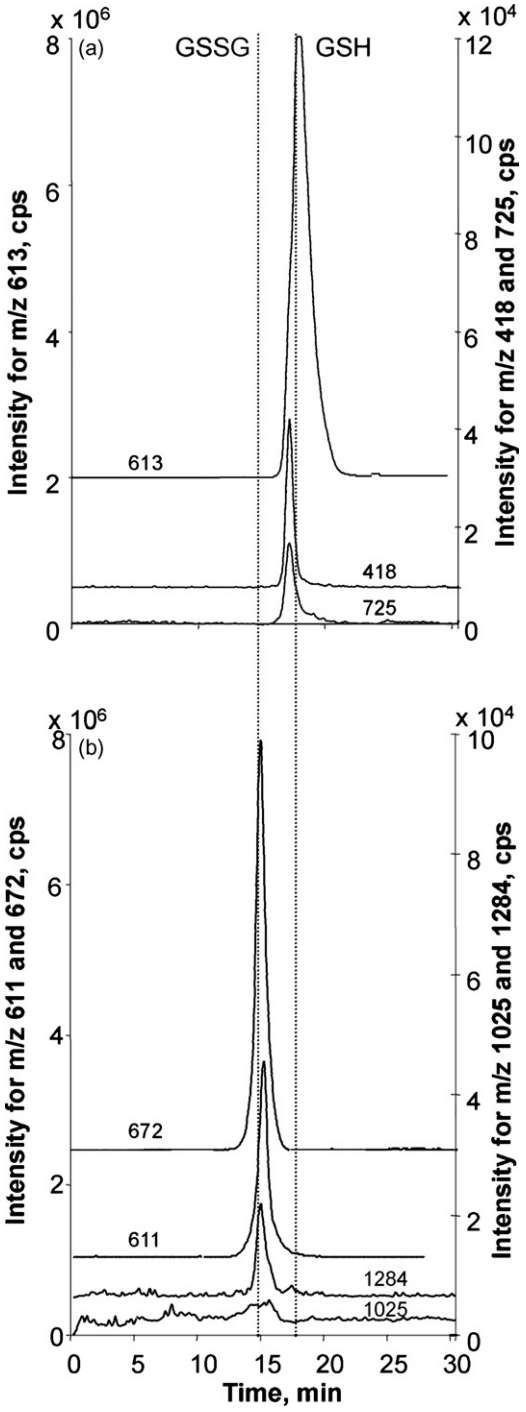

Fig. 6. Chromatograms reconstructed for the ions of cadmium complexes Cd = SG (*m*/*z* 418) and GS–Cd–SG (*m*/*z* 725) complexes in comparison to glutathione (*m*/*z* 613) peak (a). Chromatograms reconstructed for the ions of copper complexes Cu = GSSG (*m*/*z* 672) and GSGS–Cd–GSSG (*m*/*z* 1284) and for lead complex Pb–GSSG–Pb (*m*/*z* 1025) complexes in comparison to glutathione dimer with disulphide bridge (*m*/*z* 611) peak (b).

while copper complexes registered at *m*/*z* 672 and 1284 coeluted with glutathione dimer GSSG (Fig. 6b). Similar phenomenon was observed for signal at *m*/*z* 1025, when lead complexes were investigated.

The results obtained for cysteine mixture with cadmium, copper or lead followed the same pattern and indicated the role of non-oxidised ligand as a complexing agent in the case of cadmium and lead and its dimer with disulphide bridge in the case of copper. Reducing agent (BMSH) responsible for breaking sulphur bridge introduced to the system increased peak areas for Cd–GSH complexes and forced the decomposition of Cu–GSSG ones. It is known that these agents commonly used for the reduction of free phytochelatins and glutathione, were usually avoided in case of investigation of metal complexes due to their competitive character [19–22]. The obtained results proved that in the case of cadmium binding to thiol groups, the addition of reducing agent should be recommended to prevent the creation of disulphide bridges during isolation of cadmium complexes with glutathione and phytochelatins from biological tissue.

4. Conclusions

Both, the SEC–ICP-MS and ESI-MS experiments have indicated copper(I) as a strongest redox agent which leads to fast and complete oxidation of glutathione. The ESI-MS experiments supported by size exclusion chromatography have indicated that instead of Cu–GSH complex stabilised with mercaptide bond the Cu–GSSG complex is created due to high affinity of the metal to amine and carboxylic group. It can be proposed due to presence of clusters with acetate. The lack of $Cu(GSH)_n$ complex and reported low activity of phytochelatin synthetase in literature survey could confirm the theory that presence of mercaptide bond is necessary to induce synthesis of PCs.

SEC–ICP-MS experiments have proved that cadmium(II) can be responsible for oxidative stress. However, the presence of stable $Cd(GSH)_2$ complex showed by ESI-MS and confirmed by SEC–ESI-MS suggests that Cd(II) is rather responsible for depletion of GSH by induction of PCs synthesis.

Lead has been found as an intermediate metal which has been responsible for slow oxidation of GSH illustrated by SEC–ICP-MS and electrospray experiments. Low stability of $Pb(GSH)_2$ complex with mercaptide bond, in contrast to cadmium, and low speed of oxidation process, in contrast to copper, do not allow to postulate which toxic effect is more probable. However, it can be proposed that lead has much lower capacity for induction of both stress effects than cadmium and copper.

Electrospray MS has been found to be prospective tool for the investigation of both weak and stable complexes of metal ions with bioligands. The evaluated molecular masses of the complexes with confirmed lack or presence of disulphide by SEC–ESI-MS allow to determine their stoichiometry. The role of amine or deprotonated carboxylic group presented in the molecule of bioligand in the case of each investigated metal ion cannot be neglected especially in the case of glycine, glutamic acid, cystine and oxidised glutathione. The affinity of metal ions to thiol group can be put in the order: $Cd^{2+} > Pb^{2+} > Cu^{+}/Cu^{2+}$. Such a behavior can be confirmed using HSAB concept [24]. Size exclusion chromatography has led to the elution of only most stable forms and has allowed to distinguish cadmium and lead complexes with GSH and cysteine from copper complexes with GSSG and cystine. Although, it has not been proved that each ion analyzed by ESI-MS was not the gas phase product, at least the signals found by SEC–ESI-MS and confirmed by

SEC–ICP-MS can be proposed as to be related to the specific nature of the interaction in the solution.

Acknowledgments

Kasia Połeć-Pawlak and Rafał Ruzik are grateful to the Polish State Committee for Scientific Research, for financial support within the grant no. 4 T09A01425.

References

[1] Ch.H. Foyer, F.L. Theodoulou, S. Delrot, Trends Plant Sci. 10 (2001) 486.
[2] Ch. Cobbett, P. Goldsbrough, Annu. Rev. Plant Biol. 53 (2002) 159.
[3] A. Schützendübel, A. Polle, J. Exp. Bot. 372 (2002) 1351.
[4] J.L.E. Reubsaet, J.H. Beijnen, A. Bult, R.J. Van Maanen, J.A.D. Marchal, W.J.M. Underberg, J. Pharm. Biomed. Anal. 17 (1998) 955.
[5] O.K. Vatamaniuk, S. Mari, Y.-P. Lu, Ph.A. Rea, J. Biol. Chem. 275 (2000) 31451.
[6] D.G. Mendoza-Cózatl, R. Moreno-Sánchez, J. Theor. Biol. 238 (2006) 919.
[7] B.H. Cruz-Vásquez, J.M. Díaz-Cruz, C. Ariño, M. Esteban, R. Tauler, Analyst 127 (2002) 401.
[8] J.L. Gómez-Ariza, T. García-Barrera, F. Lorenzo, V. Bernal, M.J. Villegas, V. Oliveira, Anal. Chim. Acta 524 (2004) 15.
[9] S. McSheehy, Z. Mester, Trends Anal. Chem. 22 (2003) 311.
[10] J.A. Loo, Int. J. Mass Spectrom. 200 (2000) 175.
[11] M. Montes-Bayón, J. Meija, D.L. LeDuc, N. Terry, J.A. Caruso, A. Sanz-Medel, J. Anal. At. Spectrom. 19 (2004) 153.
[12] N. Burford, M.D. Eelman, K. Groom, J. Inorg. Biochem. 99 (2005) 1992.
[13] V. Loreti, D. Toncelli, E. Morelli, G. Scarano, J. Bettmer, Anal. Bioanal. Chem. 383 (2005) 398.
[14] H. Lavanant, Y. Hoppilliard, J. Mass Spectrom. 32 (1997) 1037.
[15] R.E. Shepherd, Coord. Chem. Rev. 247 (2003) 147.
[16] E. Rosenberg, J. Chromatogr. A 1000 (2003) 841.
[17] S. Hann, G. Koellensperger, C. Binger, P.G. Furtmuller, G. Stingeder, J. Anal. At. Spectrom. 19 (2004) 74.
[18] A. Sanz-Medel, Spectrochim. Acta Part B 53 (1998) 197.
[19] I. Leopold, D. Günther, J. Schmidt, D. Neumann, Phytochemistry 50 (1999) 1323.
[20] V. Vacchina, K. Połeć, J. Szpunar, J. Anal. At. Spectrom. 14 (1999) 1557.
[21] E. Moreli, B.H. Gruz, S. Somovigo, G. Scarano, Plant Sci. 163 (2002) 807.
[22] K. Połeć-Pawlak, R. Ruzik, K. Abramski, M. Ciurzyńska, H. Gawrońska, Anal. Chim. Acta 540 (2005) 61.
[23] P. Hemmerich, C. Signart, Experientia 19 (1963) 488.
[24] R.G. Pearson, J. Am. Chem. Soc. 85 (1963) 3533.

Available online at www.sciencedirect.com
ScienceDirect
Talanta 72 (2007) 1432–1437
Talanta
www.elsevier.com/locate/talanta

Localized surface plasmon resonance sensing detection of glucose in the serum samples of diabetes sufferers based on the redox reaction of chlorauric acid

Xiao Wei Shen, Cheng Zhi Huang, Yuan Fang Li *

College of Chemistry and Chemical Engineering, Southwest University, Chongqing 400715, People's Republic of China

Received 22 October 2006; received in revised form 20 January 2007; accepted 23 January 2007
Available online 12 February 2007

Abstract

In this paper, the formation of gold nanoparticles (Au NPs) as a result of the thermo-active redox reaction of chlorauric acid ($HAuCl_4$) and glucose in alkaline medium was identified by measuring the plasmon resonance absorption, localized surface plasmon resonance (LSPR), and transmission electron microscopy (TEM) images, for the formation of Au NPs displays characteristic plasmon resonance absorption bands and corresponding LSPR signals. It was found that the resulted LSPR signals could be easily detected with a common spectrofluorometer. With increasing glucose concentration, the LSPR intensity displays linear response with the glucose content over the range from 2.0 to 250.0 $\mu mol\,l^{-1}$. Thus, a novel assay of glucose was established with the limits of determination (3σ) being 0.21 $\mu mol\,l^{-1}$, and the detection of glucose could be made easily in the serum samples of diabetes sufferers. Mechanism investigations showed that the activation energy and molar ratio of the reaction were 34.8 $kJ\,mol^{-1}$ and 3:2, respectively.

Keywords: Glucose; Chlorauric acid ($HAuCl_4$); Gold nanoparticles (Au NPs); Localized surface plasmon resonance (LSPR); Activation energy

1. Introduction

Diabetes has historically been, and remains a persistent disease associated with the serum glucose content. So, it is very important to develop a simple and convenient assay for glucose. To date, a number of different glucose sensors using glucose oxidase have been reported [1–4]. These sensors, however, lack stability due to the intrinsic nature of enzyme, and the activity of modified electrode decreases quickly owing to the accumulation of chemisorbed intermediates that block the catalystic surface [5]. There are also methods for glucose assay based on the competition between glucose and a sugar-containing macromolecule, such as dextran for binding to concanavalin A (Con A) [6–8]. The limitation of these methods, however, is that Con A is not specific to glucose, and may tend to agglutinate and precipitate in a few hours. In addition, the agglutinating property of Con A greatly reduces its specificity and applicability [9]. At the same time, several advanced nanomaterial, such as C/Fe nanocomposite (CFN) [10], boron-doped diamond (BDD) electrodes [11], Pt nanoparticles modified carbon nanotubes [12], the flow-injection analysis of glucose without enzyme based on electrocatalytic oxidation of glucose at a nickel electrode [13], all of them are nonenzymatic glucose sensor, and can reduce the affect of oxygen, ascorbic acid and uric.

Gold nanoparticles (Au NPs) have been studied greatly for centuries due to their interesting optical properties [14,15] and promising applications [16–20]. One important aspect of the studies involves the attachment of biomolecules or ligands to the nanoparticles' surface through thio-groups or amino-groups, which lead to absorption changes of gold colloids, and could be applied for the investigations of DNA hybridization [21], immunoassay [22], protein [23], and preparation of multifunctional NPs [24]. Nowadays, there is also proposed some simple and fast methods for the detection of glucose based on SERS (surface-enhanced Raman spectroscopy) signals of the enzyme reaction product [25].

Pasternack et al. have first reported that resonance light scattering (RLS) technique could be used to investigate the

* Corresponding author. Tel.: +86 23 68254659; fax: +86 23 68866796.
E-mail address: liyf@swu.edu.cn (Y.F. Li).

0039-9140/$ – see front matter © 2007 Elsevier B.V. All rights reserved.
doi:10.1016/j.talanta.2007.01.066

formation of aggregated choromophores with a common spectrofluorimeter [26,27], and it has been proved that the technique could be applied to the characterizations of aggregations or self-assemblies of porphyrin–porphyrin [28] and nucleic acids [29], and to the interactions of small organic molecules (OSMs) with biological molecules such as protein [30–32]. In these investigations, RLS technique not only shows high sensitivity but also offers additional benefits of simplicity and versatility [33]. In principle, the spherical gold nanoparticles characteristically exhibit a single strong absorption band that is not present in the spectrum of the bulk gold, and this absorption band occurs when the incident photon frequency is resonant with the collective oscillation of the free electron cloud of the particle and is known as localized surface plasmon resonance (LSPR) [34]. We expect that the light scattering signals resulted from the LSPR could be detected using a common spectrofluorometer, and we herein propose a visual light scattering detection method of glucose in the serum samples of diabetes based on the measured LSPR signals. With the Au NPs resulted from the reaction of glucose and $HAuCl_4$ in this contribution, we detect the glucose without any modification based on the strong LSPR signals of the Au NPs.

2. Experimental

2.1. Apparatus

The LSPR measurements were made with a Hitachi F-4500 spectrofluorometer (Tokyo, Japan), the absorption ones with Hitachi 3010 spectrophotometer (Tokyo, Japan). The galvanothermy constant temperature bath was used to control the temperature (Shanghai Apparatus Company, China). A Tecnai 10 electron microscope (FEA, America) was used to detect the TEM images. The Hitachi 7060 automatic analyzer (Tokyo, Japan) was used to detect the glucose in blood serum with enzyme linked immunosorbant assay (ELISA).

2.2. Reagent

$HAuCl_4{\cdot}3H_2O$ (99.9%) was commercially purchased from Beijing Hengye Zhongyuan Co. (Beijing, China), glucose from Beibei Chemical Reagent Co. (Chongqing, China), and 10.0 nm Au NPs (1/10,000) from Sino-American Biotechnology Co. (Luoyang, China).

Stock solutions of 1.0×10^{-3} mol l^{-1} glucose and 1.0×10^{-2} mol l^{-1} $HAuCl_4$ were prepared by directly dissolving their solid into doubly distilled water. The working solution was obtained by directly diluting the stock solutions with doubly distilled water. Britton–Robinson (BR) buffer solution was used to control the pH values of the interacting system. All the other reagents were of analytical grade. Doubly distilled water was used to prepare all the solutions.

2.3. Procedures

Into a 10.0-ml flask, 1.0 ml BR buffer (pH 11.20), 1.0 ml 2.0 mmol l^{-1} $HAuCl_4$, an appropriate volume of the glucose solution and 10.0 μl commercial standard 10-nm Au NPs (1/10,000) were added, the solution was mixed thoroughly in each of these steps. After diluted to the scale and mixed thoroughly again, the mixture was incubated for 5 min at 373 K, and cool to room temperature.

The LSPR spectra were obtained by scanning simultaneously the excitation and emission monochromators of the F-4500 spectrofluorometer from 220 to 700 nm (namely, $\Delta\lambda$=0 nm). All measurements were made with 5.0 nm slit-width of the excitation and the emission of the spectrofluorometer. Herein, in order to observe the red shift of the resulted spectra more clearly, we chose 420 nm as the beginning of both their absorption and scattering spectra.

3. Results and discussion

3.1. Spectra characteristics and color changes

Fig. 1 shows the absorption of Au NPs resulting from the reaction between $HAuCl_4$ and glucose. It could be found that the absorption of $HAuCl_4$ is very low over the range of 420–700 nm. By the addition of glucose, an absorption peak appearing nearby 522 nm can be found, indicating the formation of Au NPs, which could be identified with the TEM images showing in Fig. 2. Au NPs are well known to display strong plasmon absorption bands due to electron oscillations induced by the incident light [35]. We can educe that the resulted Au NPs should be spherical as they has only one strong plasmon absorption band [36]. In addition, it was found that plasmon absorption bands get red-shifted from 528 to 546 nm with the increasing glucose concentration, and accompany with color changes from orange red to wine red, then to red purple (the inset picture in Fig. 1), indicating that the size of Au NPs gets larger and larger [35]. TEM images (Fig. 2) showed the spherical Au NPs in the presence of 4.0 μmol l^{-1} glucose is about 17.6 nm (left), while that in the presence of 40.0 μmol l^{-1} glucose is 59.3 nm (right).

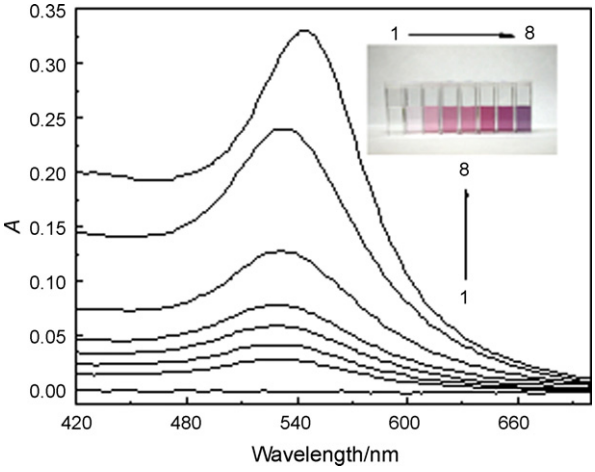

Fig. 1. The absorption of Au NPs resulting from the reaction of $HAuCl_4$ and glucose (the inset picture shows the color change of the solution). Concentrations: glucose (1–8, μmol l^{-1}), 0.0, 2.0, 4.0, 6.0, 8.0, 10.0, 20.0, 40.0; BR (pH 11.20), 1.0 ml; $HAuCl_4$, 0.20 mmol l^{-1}; Au seeds (10 nm, 1/1000), 10.0 μl.

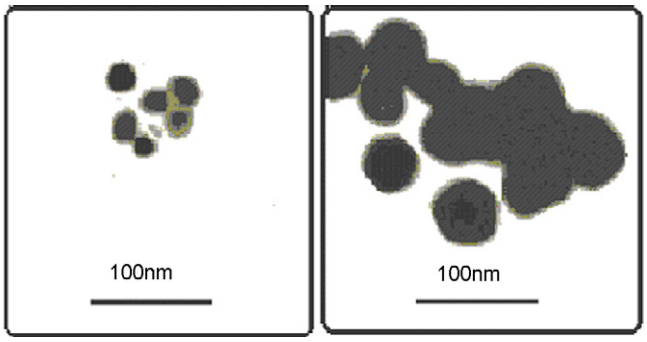

Fig. 2. TEM images of Au NPs produced in the reaction. Concentrations: $HAuCl_4$, 0.20 mmol l^{-1}; glucose, 4.0 μmol l^{-1} (left), 40.0 μmol l^{-1} (right); BR buffer (pH 11.20), 1.0 ml; Au seeds (10 nm, 1/1000), 10.0 μl.

Fig. 3 shows the light scattering signals before and after the reaction. The light scattering signals of glucose or $HAuCl_4$ alone detected with a common spectrofluorometer are very weak, but that after the reaction are very strong. Also, we could find that the LSPR signals of Au NPs in Fig. 3 got red-shifted from 553 to 563 nm with the increasing concentration of glucose from 8.0 to 40.0 μmol l^{-1}. Therefore, the LSPR signals could identify the size-increasing tendency of the formed Au NPs with increasing glucose concentration, identical with the results measured by the absorption and TEM.

3.2. Optimal conditions of the assay

It was observed that Au NPs could not be formed under neutral or acidic pH conditions. LSPR signals of Au NPs indicating the formation of Au NPs from the reaction of glucose and $HAuCl_4$ began to increase only in the medium of pH higher than 10.38, and the maximal of LSPR signals could be available in the medium of pH 11.20, then, began to decrease. Under such conditions, the LSPR intensity of $HAuCl_4$ or glucose alone was very low over the all pH range (Fig. 4). Without any addition of surfactant in the room temperature, we traced the absorption

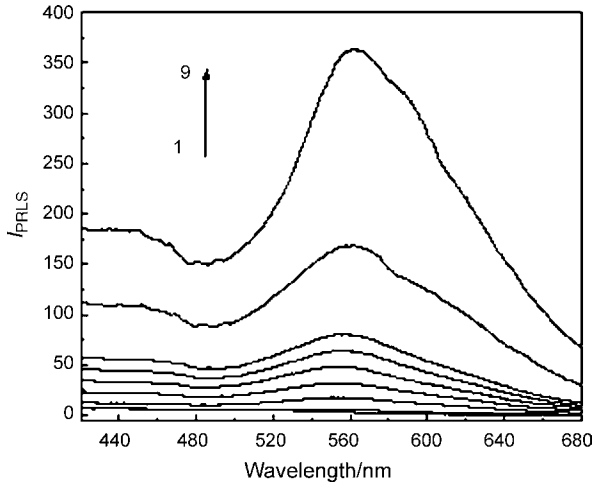

Fig. 3. LSPR spectra of Au NPs resulting from the reaction of glucose and $HAuCl_4$. Concentrations: $HAuCl_4$, 0.2 mmol l^{-1}; BR buffer (pH 11.20) 1.0 ml; glucose (from 1 to 9, μmol l^{-1}), 0.0, 0.0 (without $HAuCl_4$), 2.0, 4.0, 6.0, 8.0, 10.0, 20.0, 40.0; Au seeds (10 nm, 1/1000), 10.0 μl.

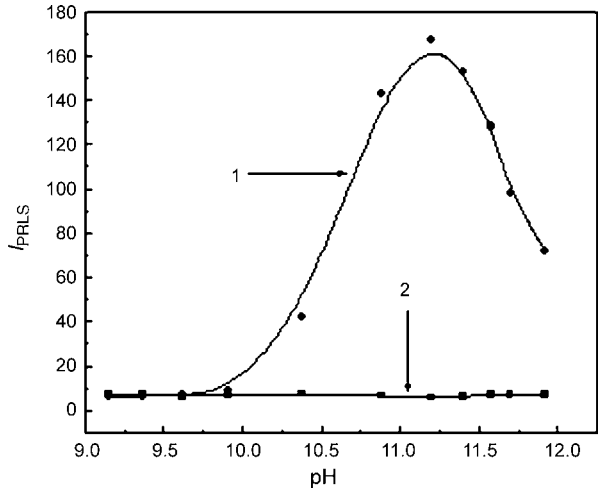

Fig. 4. Effect of pH on the LSPR intensity. Concentrations: $HAuCl_4$, 0.20 mmol l^{-1}; glucose, 20.0 μmol l^{-1}; Au seeds (10 nm, 1/1000), 10.0 μl.

spectra of the Au NPs, and found that the resulted absorption spectra almost have no change at least in 1 month.

It was found that the initial concentration of glucose has strong effect on the reaction velocity. The reaction proceeded very slowly even if the glucose concentration reaches 10.0 μmol l^{-1} at room temperature. Although increasing temperature could prompt the reaction, more than 20 min in boiling water bath was needed if the concentration of glucose is lower than 4.0 μmol l^{-1}. Inspired by the catalytic effect of metallic seeds on the synthesis of gold and silver NPs [37], we added 10.0 μl Au NPs (10.0 nm, 1/10,000) to catalyze this reaction. Fig. 5 shows the time course of this reaction, indicating that the reaction can be finished in 5 min with the catalysis of Au seeds.

3.3. Activation energy of this reaction

As the temperature could prompt this reaction, we measured its activation energy. According to Arrhenius experiential formula, the activation energy is a constant when the temperature is

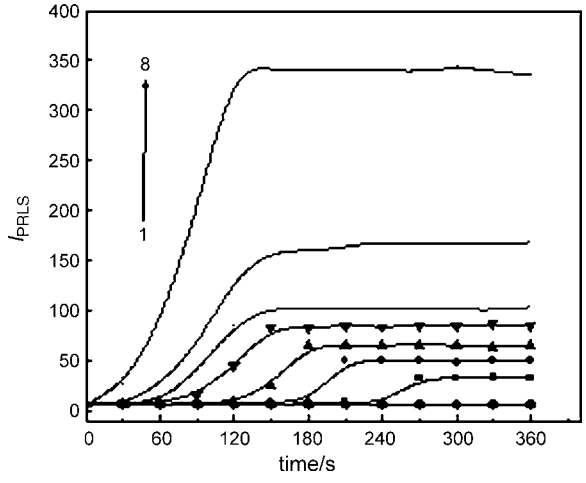

Fig. 5. Effect of time on the LSPR intensity. Concentrations: glucose (1–8, μmol l^{-1}) 0.0, 2.0, 4.0, 6.0, 8.0, 10.0, 20.0, 40.0; $HAuCl_4$, 0.20 mmol l^{-1}; BR buffer (pH 11.20), 1.0 ml; Au seeds (10 nm, 1/1000), 10.0 μl.

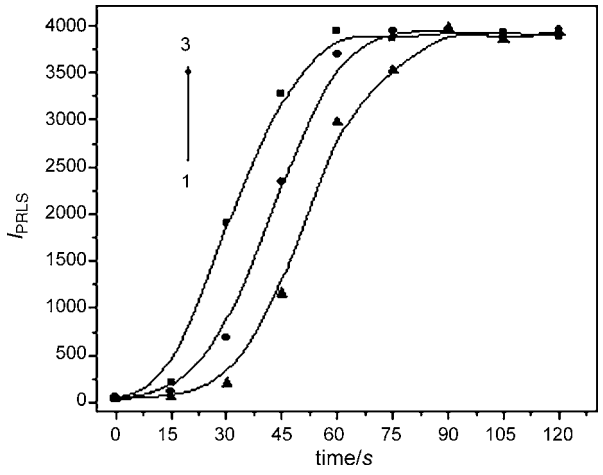

Fig. 6. Effect of temperature on the LSPR intensity. Concentrations: glucose, 0.30 mmol l^{-1}; $HAuCl_4$, 0.20 mmol l^{-1}; BR buffer (pH 11.20), 1.0 ml; Au seeds (10 nm, 1/1000), 10.0 μl. Temperature (1–3): 360 K, 366 K, and 373 K.

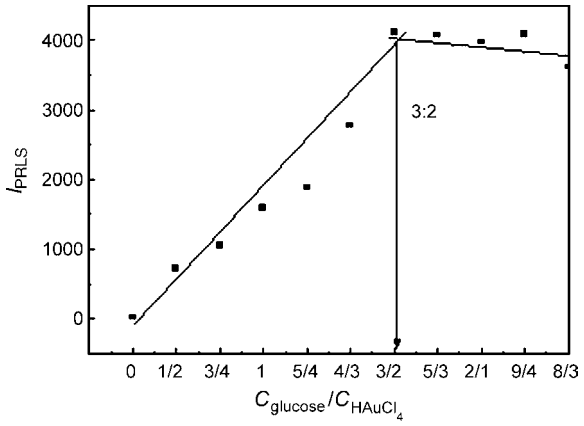

Fig. 7. Effect of the ratio between glucose and $HAuCl_4$ on the LSPR intensity. Concentrations: $HAuCl_4$, 0.20 mmol l^{-1}; BR buffer (pH 11.20) 1.0 ml; Au seeds (10 nm, 1/1000), 10.0 μl.

within a given range. To obtain the activation energy, we chose three temperatures of 373, 366 and 360 K.

According to the former referrence [38], if the initial concentrations of the reactants are uniform, we can obtain the E_a value of an equation as following:

$$\ln\left(\frac{t_1}{t_2}\right) = \frac{E_a}{R}\left(\frac{1}{T_1} - \frac{1}{T_2}\right)$$

It means that we can work out the E_a value by the time needed to finish the reaction in two or more given temperature. Wherein E_a is activation energy. Here, T_1 and T_2 are the reaction temperatures, k_1 and k_2 are the reaction rate, t_1 and t_2 are the reaction time, and n is the reaction order.

As the experimental conditions are unchanged, it is reasonable to suppose that stable LRLS signals can indicate the end of the reaction. As Fig. 6 shows, the ultimate intensity of LRLS signals were the same at these different temperatures, and the reaction could be finished within 60, 75 and 90 s for 0.30 mmol l^{-1} glucose. Thus, we can calculate out that the activation energy are 36.2, 33.3 and 34.8 kJ mol^{-1}, respectively, with the average value is 34.8 kJ mol^{-1}, indicating that the reaction needs a high temperature to prompt this reaction.

3.4. The reaction ratio between glucose and $HAuCl_4$

We can educe that different pH values could affect the LSPR intensity of the solution according to Fig. 4, at the same time, as one mole of $HAuCl_4$ contains one mole of HCl, it means that the concentration of $HAuCl_4$ can strongly affect LSPR intensity of the solution. Thus, in order to obtain steady experimental results, we chose to keep the concentration of $HAuCl_4$ constant and added a series of glucose for the determination of reaction ratio between glucose and $HAuCl_4$. Finally, it was found that maximal LSPR signals could be available when glucose and $HAuCl_4$ were close to proportion of 3:2 (Fig. 7), which was probable the the reaction ratio between glucose and $HAuCl_4$, and indicates the glucose changes to glucose acid in this reaction, this result is consistent with reference [39]. In addition, the repulsion of carboxyl group of the glucose acid absorbed around the Au

Table 1
Tolerance of foreign substances

Substance	Concentration (10^{-5} mol l^{-1})	Change in I_{RLS} (%)	Substance	Concentration (10^{-5} mol l^{-1})	Change in I_{RLS} (%)
Al^{3+}, Cl^-	0.6	6.72	L-Arginine	100.0	−2.95
Pb^{2+}, NO_3^-	0.6	8.93	L-Glycin	100.0	−3.72
Ca^{2+}, Cl^-	5.0	5.71	L-phenylalanine	100.0	−4.32
Cu^{2+}, SO_4^{2-}	0.6	7.26	L-serine	100.0	−3.85
Fe^{3+}, Cl^-	0.8	4.52	L-Cystine	100.0	−2.45
Ba^{2+}, Cl^-	5.0	7.56	L-Lysine	100.0	−3.88
Mg^{2+}, Cl^-	1.0	1.32	Creatine	100.0	1.50
EDTA	5.0	3.45	HSA[a]	2.0×10^{-4}	4.65
K^+, Cl^-	10.0	5.61	BSA[a]	2.0×10^{-4}	5.02
NH_4^+	10.0	−3.25	TritonX-100[b]	0. 08	−5.1
L-Tyrosine	100.0	−0.38	Tween-80[b]	0. 08	−7.61
L-Tryptophan	100.0	−3.14	SDBS[c]	2.0	−4.51
Sucrose	0.1	7.68	Fructose	0.1	3.23

[a] Values in mg ml^{-1}.
[b] Values in percent. Concentrations: $HAuCl_4$, 0.20 mmol l^{-1}; BR (pH 11.20); glucose, 5.0 μmol l^{-1}; EDTA, 50.0 μmol l^{-1}; Au seeds (10 nm, 1/1000), 10.0 μl.
[c] SDBS represents sodium dodecyl benzene sulfonate.

Table 2
The content of glucose in real samples ($n = 5$)

Sample	Found (μmol l^{-1})	R.S.D. (%)	Reference method (μmol l^{-1})	Error (%)
1	5.83	4.63	6.30	7.46
2	6.52	2.85	7.10	8.17
3	9.73	3.15	10.80	9.84

Concentrations: $HAuCl_4$, 0.20 mmol l^{-1}; EDTA, 50.0 μmol l^{-1}; BR buffer (pH 11.20), 1.0 ml; Au seeds (10 nm, 1/1000), 10.0 μl. The serum of diabetes suffer was brought from the Ninth People Hospital of Chongqing (Chongqing, China).

NPs makes them very stable. On the other hand, the alkaline condition for the reaction could also make the formed Au NPs much stable [40], that is the reason the experiment need not surfactant.

3.5. Effect of foreign substance on the reaction

The influences of foreign coexisting substances such as proteins, amino acids, surfactants and metal ions were tested. The results are showed in Table 1. Of all the tested substances, NH_4^+, Ca^{2+}, K^+, amino acids, EDTA, SDBS and Tween-80 can be allowed at higher concentration level; while Mg^{2+}, Pb^{2+}, Fe^{3+}, Cu^{2+}, Al^{3+}, Ba^{2+}, BSA and HSA can be allowed at lower concentration level, which are possibly due to the hydrolyzation of metal ions and the denaturalization of protein in the this alkaline medium. Sucrose and fructose cannot be allowed at high concentration because they are homologs to glucose. However, it is known that glucose is the only free sugar in blood found at high concentration [3], so only a small quantity of free sucrose and fructose exists in the human blood serum. If adding EDTA to reduce the hydroxylation of metal ions, and trichloroacetic acid to exclude the proteins, the affect of metal ions and proteins can be reduced. So, we chose adding an appropriate concentration of EDTA and trichloroacetic acid into the work solution, then, a method for the detection of glucose in serum sample was constructed.

3.6. Calibration curves and sample determinations

According to the above standard procedures, series concentrations of glucose were used to construct the calibration curves. As the red shift only have trivial affect on the LSPR intensity near 550 nm, in order to work out linearity between glucose and the LSPR intensity expediently, we chose 550 nm as the final intensity values. There were linear relationships between the LSPR intensities and the glucose concentrations over the range from 2.0 to 250.0 μ mol l^{-1}(Fig. 8), and the linear regression equation is $\Delta I = 2.58 + 7.53c$ (c, μmol l^{-1}) with the correlation coefficient of 0.9984 and the limit of determination (LOD, 3σ) of 0.21 μmol l^{-1}, showing our present method is very sensitive for the detection of glucose.

To test the method, we detected three serum samples (collected from the Ninth People Hospital of Chongqing, Chongqing, China) of the diabetes suffers. These samples only experienced easy pretreatments by using 2.0 mol l^{-1} trichloroacetic acid to precipitate and remove the proteins in fresh human serum samples [41] with centrifugation, and by diluting the supernatant solution 1000-fold. Considering that metal ions in the samples might exist, an appropriate of EDTA was added into both of the real samples. The subsequent detection showed that the results with standard addition method are identical to those of the enzyme linked immunity technique used by the hospital, indicating our method is reproducible and reliable (Table 2).

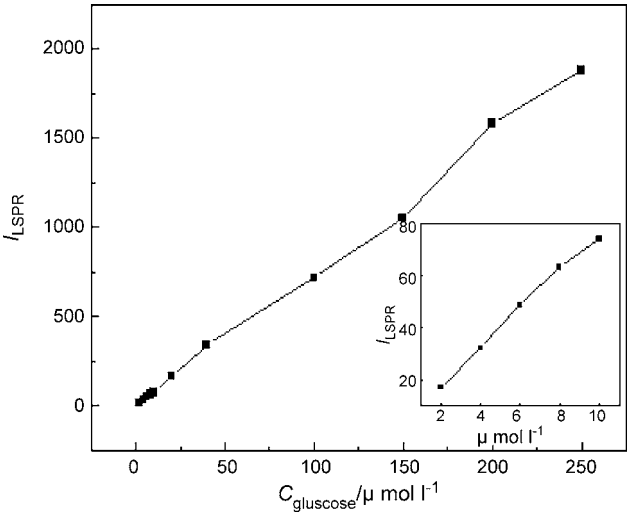

Fig. 8. calibration curve of the relationship between the LSPR intensities and the glucose concentration. Concentrations: $HAuCl_4$, 0.20 mmol l^{-1}; BR buffer (pH 11.20) 1.0 ml; Au seeds (10 nm, 1/1000), 10.0 μl.

4. Conclusion

In this contribution, a glucose method was proposed based on the fomration of gold nanoparticles with a common spectrofluorometer. The detection of real samples in diabetic serum shows our method is sensitive, effective, reliable, simple, and convenient. This reaction makes it easy to presumably judge without any help of apparatus whether there is glucose in our serum by observing the color change of the reaction solution. Furthermore, the formation of Au NPs was very stable by this method, so it may aslo be a valuable approach for the developments of Au NPs preparation for the demands of other researches.

Acknowledgements

All authors herein are grateful to the supports from the National Natural Science Foundation of China (NSFC, No: 20425517; 30570465).

References

[1] K. Wang, J.J. Xu, D.C. Sun, H. Wei, X.H. Xia, Biosens. Bioelectron. 20 (2005) 1366.
[2] J.W. Liu, C. Bian, J.H. Han, S.F. Chen, S.H. Xia, Sens. Actuators B Chem. 106 (2005) 591.
[3] S. Kabilan, A.J. Marshall, F.K. Sartain, M.C. Lee, A. Hussain, X.P. Yang, J. Blyth, N. Karangu, K. James, J. Zeng, D. Smith, A. Domschke, C.R. Lowe, Biosens. Bioelectron. 20 (2005) 1602.
[4] G.A.M. Mersal, M. Khodari, U. Bilitewski, Biosens. Bioelectron. 20 (2004) 305.
[5] Y.X. Huang, W.J. Zhang, H. Xiao, G.X. Li, Biosens. Bioelectron. 21 (2005) 817.
[6] L.J. McCartney, J.C. Pickup, O.J. Rolinski, D.J.S. Birch, Anal. Biochem. 292 (2001) 216.
[7] O.J. Rolinski, D.J.S. Birch, L.J. McCartney, J.C. Pickup, Spectrochim. Acta 57 (2001) 2245.
[8] L. Tolosa, H. Szmacinski, G. Rao, J. Lakowicz, Anal. Biochem. 250 (1997) 102.
[9] X.D. Ge, L. Tolosa, G. Rao, Anal. Chem. 76 (2004) 1403.
[10] J. Wu, Y.H. Zou, N. Gao, J.H. Jiang, G.L.S.R.Q. Yu, Talanta 68 (2005) 12.
[11] J. Lee, S.M. Park, Anal. Chim. Acta 545 (2005) 27.
[12] L.Q. Rong, C. Yang, Q.Y. Qian, X.H. Xia, Talanta, in press.
[13] P.A. Fiorito, C.M.A. Brett, S.I.C. de Torresi, Talanta 69 (2006) 403.
[14] G. Schmid, Chem. Rev. 92 (1992) 1709.
[15] P. Mulvaney, Langmuir 12 (1996) 788.
[16] B. Kim, S.L. Tripp, A. Wei, J. Am. Chem. Soc. 123 (2001) 7955.
[17] L. He, M.D. Musick, S.R. Nicewarner, F.G. Salinas, S.J. Benkovic, M.J. Natan, C.D. Keating, J. Am. Chem. Soc. 122 (2000) 907.
[18] M. Lahav, V. Heleg-Shabtai, J. Wasserman, E. Katz, I. Willner, H. Dürr, Y.Z. Hu, S.H. Bossmann, J. Am. Chem. Soc. 122 (2000) 11480.
[19] X.M. Lin, H.M. Jaeger, C.M. Sorensen, K.J. Klabunde, J. Phys. Chem. B 105 (2001) 3353.
[20] B.M.I. van der Zande, L. Pages, R.A.M. Hikmet, A. Van Blaaderen, J. Phys. Chem. B 103 (1999) 5761.
[21] J.J. Storhoff, C.A. Mirkin, Chem. Rev. 99 (1999) 1849.
[22] L.A. Lion, M.D. Musick, M.J. Natan, Anal. Chem. 70 (1998) 5177.
[23] H. Matsui, P. Porrata, G.E. Douberly, Nano Lett. 9 (2001) 461.
[24] J. Zhu, Y.C. Wang, Y. Lu, Surface A 232 (2004) 155.
[25] Z.S. Wu, G.Z. Zhou, J.H. Jiang, G.L. Shen, R.Q. Yu, Talanta 70 (2006) 533.
[26] R.F. Pasternack, C. Bustamante, P.J. Collings, A. Giannetto, E.J. Gibbs, J. Am. Chem. Soc. 115 (1993) 5393.
[27] R.F. Pasternack, K.F. Schaefer, P. Hambright, Inorg. Chem. 33 (1994) 2062.
[28] R.F. Pasternack, P.J. Collings, Science 269 (1995) 935.
[29] P.J. Collings, E.J. Gibbs, T.E. Starr, O. Vafek, C. Yee, L.A. Pomerance, R.F. Pasternack, J. Phys. Chem. B 103 (1999) 8474.
[30] C.Z. Huang, K.A. Li, S.Y. Tong, Anal. Chem. 69 (1997) 514.
[31] X.Z. Cong, X. Guo, X.X. Wang, H.X. Shen, Anal. Chim. Acta 444 (2001) 205.
[32] Z.X. Guo, H.X. Shen, Anal. Chim. Acta 408 (2000) 177.
[33] X.L. Liu, H. Yuan, D.W. Pang, R.X. Cai, Spectrochim. Acta A 60 (2004) 385.
[34] C.D. Chen, S.F. Cheng, L.K. Chau, C.R.C. Wang, Biosens. Bioelectron. 22 (2007) 926.
[35] Y.Q. He, S.P. Liu, L. Kong, Z.F. Liu, Spectrochim. Acta A 61 (2005) 2861.
[36] K. Aslan, P. Holley, L. Davies, J.R. Lakowicz, C.D. Geddes, J. Am. Chem. Soc. 127 (2005) 12115.
[37] N.R. Jana, L. Gearheart, C.J. Murphy, J. Phys. Chem. B 105 (2001) 4065.
[38] X.C. Fu, W.X. Shen, T.Y. Yao, Physical Chemistry, fourth ed., Higher Education Press, 1990, p. 755.
[39] Z.M. Qi, H.S. Zhou, M. Naoki, H. Itaru, S. Kayori, T. Akiko, K. Kenji, J. Phys. Chem. B 108 (2004) 7006.
[40] X.P. Sun, M.H. Huang, Z.J. Dong, E.K. Wang, J. Fudan Univ. 43 (2004) 477.
[41] X.L. Hu, S.P. Liu, H.Q. Luo, Acta Chin. Sci. 61 (2003) 1287.

Available online at www.sciencedirect.com
ScienceDirect
Talanta 72 (2007) 1378–1385
Talanta
www.elsevier.com/locate/talanta

A chemiluminescence sensor for the determination of hydrogen peroxide

Azra Tahirović [a,b,*], Amira Čopra [a,c], Enisa Omanović-Mikličanin [a,d], Kurt Kalcher [a]

[a] *Institute for Chemistry, Karl-Franzens University, Universitaetsplatz 1, Graz, Austria*
[b] *Faculty of Forestry, University of Sarajevo, Zagrebacka 20, Sarajevo, Bosnia and Herzegovina*
[c] *Faculty of Natural Science, University of Sarajevo, Zmaja od Bosne 33, Sarajevo, Bosnia and Herzegovina*
[d] *Faculty of Agriculture, University of Sarajevo, Zmaja od Bosne 8, Sarajevo, Bosnia and Herzegovina*

Received 16 October 2006; received in revised form 12 January 2007; accepted 19 January 2007
Available online 20 February 2007

Abstract

A chemiluminescence one-shot sensor for hydrogen peroxide is described. It is prepared by immobilization of cobalt chloride and sodium lauryl sulphate in hydroxyethyl cellulose matrix cast on a microscope cover glass. Luminol, sodium phosphate and the sample are mixed before use and applied on the membrane by a micropipette. The calibration graph is linear in the range 20–1600 μg/L, and the detection limit of the method (3σ) is 9 μg/L. A relative standard deviation of 4.5% was obtained for 100 μg/L H_2O_2 ($n = 11$). The sensor has been applied successfully to the determination of hydrogen peroxide in rainwater.

Keywords: Chemiluminescence; Sensors; Hydrogen peroxide; Rainwater

1. Introduction

Hydrogen peroxide, H_2O_2, plays an important role in atmospheric and biochemical processes. It is formed in the reaction of hydroperoxyl radicals ($HO_2^{\bullet}$) and their hydrated form, produced by the photochemical reactions of atmospheric trace gases, such as ozone and volatile organic compounds [1]. Hydrogen peroxide is considered as the most efficient oxidant for the conversion of dissolved sulphur dioxide (SO_2) to sulphuric acid (H_2SO_4) as the main contributor to the acidification of rainwater [2–6]. H_2O_2 can be decomposed by various aqueous chemical processes such as reaction with dissolved SO_2, catalyzed destruction by transition metals such as Fe, Cu, Mn, oxidation by OH radicals, and photolysis [3,7–9]. Concentrations of H_2O_2 within a range 0.01–199 μM for continental rainwater were reported in studies [2]. Generally, the levels of hydrogen peroxide are higher in the summer and lower in the winter [10–12]. It was found that levels of H_2O_2 were higher in the afternoon and low at night [10,12,13].

Different researches have studied the effects of meteorological and chemical factors that can effect the concentration of hydrogen peroxide in clouds and rainwater [2,8,10,13,14].

A number of methods have been used for the determination of hydrogen peroxide, spectrophotometry [15–17], fluorimetry [18,19], amperometry [20,21], and chemiluminescence (CL) [10,22–24]. Chemiluminescence has many advantages in comparison to other methods due to its high sensitivity, low cost, and simple instrumentation.

Chemical sensors with immobilized or solid-state reagents have been used for the determination of hydrogen peroxide; most of them are based on chemiluminescence with luminol or oxalic esters as reagents [25–27]. The Co(II) catalyzed CL reaction of luminol with hydrogen peroxide in alkaline solution has been used quite widespread for the determination of hydrogen peroxide. This reaction has been applied to the determination of gaseous hydrogen peroxide [28], hydrogen peroxide in seawater [29] and rainwater [30] with detection limits in the nanomolar and sub-nanomolar range in seawater [24].

Chemiluminescence flow sensors with immobilized luminol and Co(II) ions onto ion-exchange columns using hydrolysis technique have been applied to the determination of hydrogen peroxide in rainwater [31]. The reported detection limit was 1.2×10^{-8} mol/L.

* Corresponding author at: Faculty of Forestry, University of Sarajevo, Zagrebacka 20, Sarajevo, Bosnia and Herzegovina. Tel.: +387 33 614 003; fax: +387 33 611 349.
E-mail address: atahirovic2001@yahoo.com (A. Tahirović).

0039-9140/$ – see front matter © 2007 Elsevier B.V. All rights reserved.
doi:10.1016/j.talanta.2007.01.072

An approach with immobilization of the Co(II)–ethanolamine complex on a resin, Dowex-50W, lead to the construction of sensitive flow sensors for the determination of hydrogen peroxide in rainwater allowing the use of luminol in neutral or weakly alkaline solutions with a detection limit of 1×10^{-7} mol/L [32].

The use of periodate in designing sensitive and interferences free flow-through sensors for the determination of hydrogen peroxide in rainwater by immobilization of the reagents on an ion-exchange resin have been also reported by the same author [33]. The detection limit of the method was 1×10^{-7} mol/L.

Although some disadvantages of the CL method have been reported due to the interfering effect of transition metal ions [10], this reaction offers some advantages in comparison to enzyme based sensors. Enzymes are usually expensive, pH sensitive, and enzyme based biosensors are often difficult to store over a longer period.

The aim of this work was to develop low cost disposable sensors for the determination of hydrogen peroxide in rainwater based on the reaction of luminol in the presence of Co(II) ions as a catalyst. The sensors are simple and sensitive with a rapid response.

2. Experimental

2.1. Apparatus

A portable laboratory-built luminometer was employed in this work [34]. It consists of a measurement cell and the main electronic board, placed in a separate box. The body of the measurement cell was made from aluminium in two parts, a cylindric containment for the photodiode (light-sensitive detector) and another cylindric support for a micropipette. The latter can be mounted on the former, where light tightness and mechanical stability was achieved by using rubber sealings. The amplifiers were designed in a way that four circuits with different gains amplified simultaneously the signal obtained from the detector, thus allowing the monitoring of the signal without changing the sensitivity range of the instrument. The printed circuit boards were assembled in surface mounted technology and directly incorporated in the measurement cell in order to avoid electrical disturbances.

The photodiode was a type (OSD35 mm, Centronics) offering enhanced sensitivity in the near ultraviolet to blue range of the electromagnetic spectrum making it suitable for measurements with luminol (emission maximum at around 425 nm). The photocurrent of the photodiode was converted into four differently amplified voltages (channels) by four operational amplifiers (LTC 1050CS8, Linear Technology). The amplification ratio between ensuing channels was around 10. The main electronic board with four microprocessors (PIC 16F874, Microchip) provided digitalization (10 bits A/D converter on chip) and storage of the signals, as well as data transfer to a personal computer via a serial interface (RS 232). The tasks were performed with four microprocessors allowing the measurements of all channels simultaneously. Data were evaluated on a personal computer with a laboratory-made software written in Visual Basic. The maximum height of the peak and the integration area were calculated by the software. Usually the two channels with highest sensitivity were used for the data evaluation.

Spectrophotometric determinations were carried out by a UV–VIS spectrophotometer (Hitachi, model V-1500, $\lambda = 200$–1100 nm).

2.2. Reagents

A stock solution of H_2O_2 (10,000 mg/L) was prepared by diluting a standardized 30% solution of hydrogen peroxide. The solution was standardized by titration with $KMnO_4$. Standard solutions of lower concentrations were prepared daily by appropriate dilution of the stock. A 56.4 mmol/L luminol solution was prepared by dissolving appropriate amount of luminol and 0.250 g of $Na_3PO_4{\cdot}12H_2O$ in water to 10 mL volume. The solution was allowed to stand for 48 h before use at 4 °C in the refrigerator.

An aqueous solution of cobalt chloride (0.1 mol/L) was prepared by dissolving $CoCl_2{\cdot}6H_2O$ (1.1896 g) in water up to 50 mL.

Aqueous solutions of EDTA (0.1 mol/L) were prepared by dissolving proper amounts of $Na_2H_2Y{\cdot}2H_2O$ in water. Hydroxyethyl cellulose (HEC) was purchased from Fluka. A stock solution of potassium titanium oxalate (25.0 g) was dissolved in 400 mL of warm water. After cooling, the solution was diluted to 500 mL. The surfactant, sodium lauryl sulphate (SLS, 100 mg), was dissolved in water and made up to 10 mL.

All other chemicals were of analytical grade. Highly purified water prepared with a Milli-Q system (Brenstend, USA) was used for the preparation of solutions.

Trisodium phosphate dodecahydrate was purchased from Fluka.

2.3. Preparation of the sensor

Hydroxyethyl cellulose (150 mg) was weighed into a centrifuge tube, and then cobalt chloride solution (100 μL, 0.1 M) was added, and filled up to 8 mL with water. The solution was placed on a vertical shaker for 48 h. Afterwards 400 μL of the solution of sodium lauryl sulphate was added and the volume was adjusted to 10 mL; the final solution was shaken for additional 30 min.

Ten microlitres of polymer solution was dispensed onto a microscope cover glass (18 mm × 18 mm, Menzel-Gläser, Germany) which was previously rinsed thoroughly with ethanol (96%). The glass was equipped with a self-adhesive reinforcement ring (polypropylene, inner diameter 5.2 mm; Avery Zweckform 5308) in order to get a defined area for the membrane formation. The membranes were dried in the drying oven at 70 °C for 4 h. They were stored in a desiccator over sodium hydroxide at room temperature protected from ambient light. Sodium hydroxide was used as a drying agent in order to prevent possible influence of gasses present in the atmosphere such as CO_2.

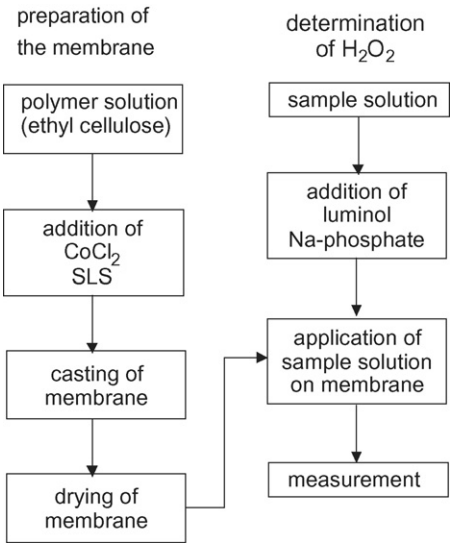

Fig. 1. Determination of hydrogen peroxide with chemiluminescence sensors.

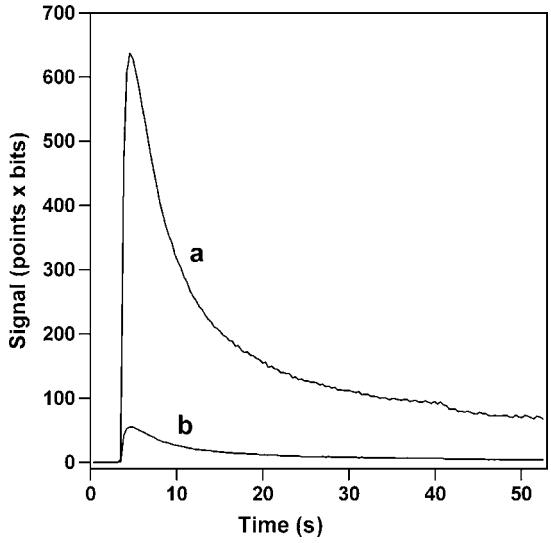

Fig. 2. Response curve of CL reaction for 100 μg/L H_2O_2. (a) Highest amplification (channel 4) and (b) second highest amplification (channel 3).

2.4. Procedure

A sensor (glass support with membrane) was fixed directly on the photodiode, and then the pipette holder was mounted over it. Luminol and sodium phosphate were added to a concentration of 1.4 mmol/L and 53 mmol/L, respectively, to the sample solution immediately before measurements. Recording of the signal was started immediately before 10 μL of the sample solution were dispensed onto the membrane by a 10 μL micropipette. For each measurement one new sensor was used (one-shot sensors). Data were evaluated by summing 100 data points starting with the data when the chemiluminescence reaction started. A schematic sketch of the whole procedure is given in Fig. 1.

Spectrophotometric determination of hydrogen peroxide with potassium titanium oxalate was done after adding 100 μL of H_2SO_4 and 200 μL of potassium titanium oxalate solution to a defined volume of sample solution and diluting up to 10 mL with water. Absorbance was measured at 400 nm in a 1 cm quartz cell.

2.5. Sample collection

Samples of rainwater were collected at the roof-top level of the Institute for Analytical Chemistry, located in the urban area in Graz during June 2005. The samples were collected in polyethylene containers and transported to the laboratory immediately after the rain. They were filtered through 0.45 μm filter membranes to remove insoluble particles. A defined amount of EDTA (1×10^{-5} mol/L) was added to each sample. The samples were stored in the freezer at −20 °C until analysis.

3. Results and discussion

3.1. Instrumental parameters

For registering the response curve the instrumental parameters were optimized. They comprise the number of repetitions of A/D conversions per data point and the time increment between two data.

For the first it was found that 150 conversions yielded responses which were very low in noise; thus the recording of one data lasted a few milliseconds only. The second parameter, the waiting period between two subsequent data, was chosen in order to keep the transfer time of the intermediately stored data to the PC reasonably short. It was found that with a period of 350 ms the whole response curve could be represented with around 150 points of which 100 from the start of the signal were used for integration because the actual signal lasted around 35 s or even less. Fig. 2 shows a typical response as registered after the injection of a test solution.

3.2. Composition of the membrane and polymer solution

In order to prepare chemical sensors useful for the determination of hydrogen peroxide in rainwater, the signal of the sensors should be high enough to detect low concentrations of the analyte. Preliminary investigations carried out on membranes with different combination of constituents in the membrane and in the analyte solution showed that the highest signals were obtained with membranes containing the polymer, cobalt chloride and the surfactant, whereas lower signals were observed with membranes containing all components incorporated in the matrix [35]. The transparency of the membrane is also a very important factor which can influence the signal. Membranes with Co(II) are highly transparent in the absence of sodium phosphate but get very opaque in its presence. Therefore, membranes containing the catalyst and the surfactant in the polymer matrix were chosen, because they are sensitive enough for measurements in the μg/L concentration range of hydrogen peroxide; on the other hand sodium phosphate to achieve alkalinity and luminol were added to the sample solution. A microscopic picture of a typical membrane is shown in Fig. 3.

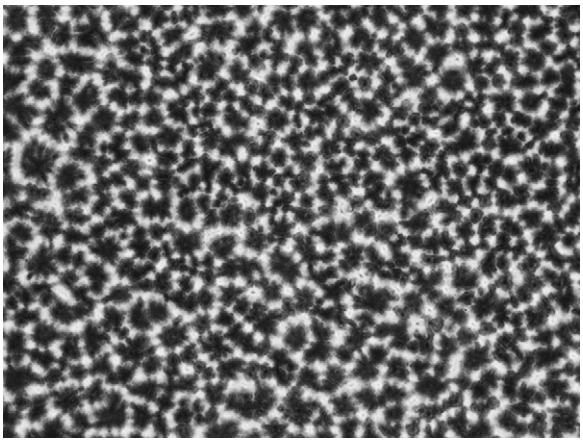

Fig. 3. Optical microscopic view on a typical membrane; magnification of 40 times.

The quality of the membrane is essential insofar as a rather homogeneous distribution of the catalyst is concerned. Small crystals of cobalt chloride are finely distributed over the whole membrane and fixed by the polymer to the support. Membrane criterions, such as stability or solubility in the analyte solution are not important because the sensor is used for one measurement only and then discarded.

The concentration of the polymer, the catalyst, and the surfactant in the polymer solution as well as the concentrations of sodium phosphate and luminol in the test solutions were optimized. The concentration of the polymer was tested in the concentration range of 0.5–1.9% (m/v) (Fig. 4).

The signal is increasing up to a polymer concentration of 1.7% (m/v) in the solution, and then starts to level off. The reason for the decrease of the signal could be that the chemiluminescent light is scattered more in a membrane with a higher content of the polymer, or that the accessibility of the catalyst gets worse with increased amounts of the matrix. In order to be in a range where small variations in concentration of the polymer cause only slight changes of the signal, 1.5% (m/v) was chosen as an acceptible value for the polymer concentration in the casting solution.

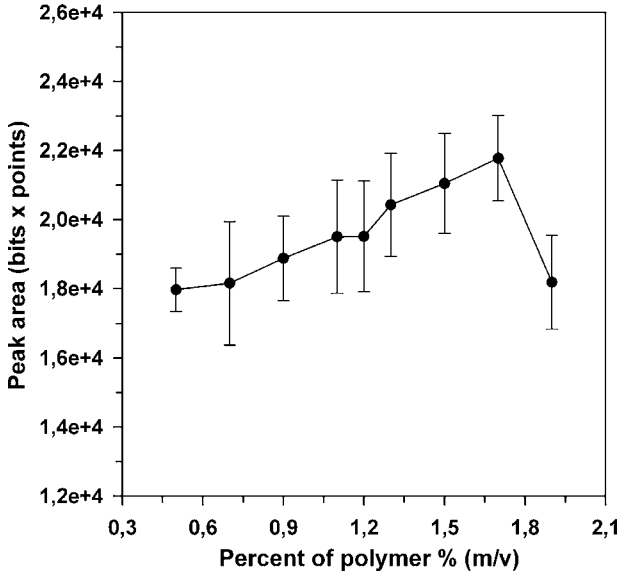

Fig. 4. Effect of the concentration of the polymer in the casting solution on the chemiluminescence signal. Casting solution: hydroxyethyl cellulose (0.5–1.9% (m/v)), cobalt chloride (2 mmol/L), sodium lauryl sulphate (400 mg/L); test solution: sodium phosphate (53 mmol/L), luminol (1.13 mmol/L), H_2O_2 (100 μg/L); casting volume (10 μL); sample volume (10 μL).

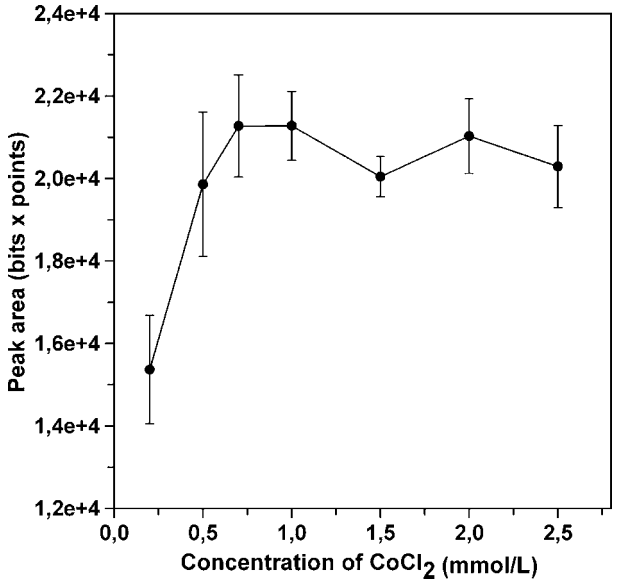

Fig. 5. Effect of the concentration of cobalt chloride in the casting solution on the chemiluminescence signal. Casting solution: hydroxyethyl cellulose (1.5% (m/v)), cobalt chloride (0.2–2.5 mmol/L), sodium lauryl sulphate (400 mg/L); test solution: sodium phosphate (53 mmol/L), luminol (1.13 mmol/L), H_2O_2 (100 μg/L); casting volume (10 μL); sample volume (10 μL).

The concentration of $CoCl_2$ was varied from 0.2 mmol/L to 2.5 mmol/L (Fig. 5). The CL signals increased up to a concentration of 0.7 mmol/L. After that it reached a plateau so that higher amounts of the catalyst did not show any improvement of the response. In fact, a slight decrease of the signal could be observed beyond 1 mmol/L. A concentration of 1 mmol/L Co(II) was therefore taken as an optimum for the casting solution (Fig. 5).

The efficiency of the chemiluminescence reaction of luminol is dependent on the pH of the reaction medium. In the solution the pH can be basically adjusted with NaOH. It was found that in the membrane sodium hydroxide exerts a rather negative effect with a quick decrease of the signal by storage time of the sensors. Applicable in the membrane was trisodium phosphate, which yielded more stable and reproducible signals, but when comparing data with its presence and its absence in the membrane, phosphate free polymer matrices yielded significantly higher signals; thus, sodium phosphate was added to the sample solution. Its concentration influence was investigated in the range of 13–79 mmol/L. The CL signal was slightly increasing up to a concentration of around 50 mmol/L with rather a constant response from 50 mmol/L to 65 mmol/L, but increasing standard deviations occur with increasing concentrations. Beyond 65 mmol/L the signal starts to level off. One of the main reasons for this kind of behaviour could be the increased precipitation of the catalyst (Co^{2+}). In order to avoid too high concentrations of a strongly alkaline compound which can also influence the stabil-

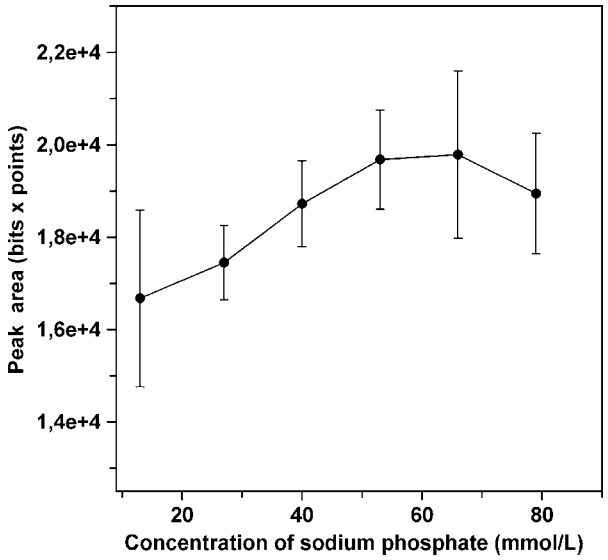

Fig. 6. Effect of different concentrations of sodium phosphate in the sample solution on the chemiluminescence signal. Casting solution: hydroxyethyl cellulose (1.5% (m/v)), cobalt chloride (1 mmol/L), sodium lauryl sulphate (400 mg/L); test solution: sodium phosphate (13–79 mmol/L), luminol (1.13 mmol/L), H_2O_2 (100 μg/L); casting volume (10 μL); sample volume (10 μL).

ity of target analyte, 53 mmol/L sodium phosphate was chosen as the optimum value (Fig. 6).

The amount of sodium phosphate added was high enough to compensate pH variations of the samples or test solutions (pH 4–8), so that the resulting solutions did not produce any significant deviations of the signals.

The concentration of luminol as the main reagent influences strongly the signal (Fig. 7). The dependence of the signal on the luminol concentration in the sample was investigated in the range of 0.28–1.69 mmol/L. The results showed an increase of the signal up to a concentration of 1.4 mmol/L luminol in the test solution, and after that the signals starts to level off. The cause for decrease of the signal at the concentrations higher than 1.4 mmol/L could be probably a reaction of luminol via its amino group and one of the hydrazide carbonyls as a chelating agent for cobalt to form a six-membered ring, thus reducing the concentration of free Co^{2+} ions [36]. Therefore, 1.4 mmol/L was taken as an optimum value. When luminol was added to the membrane rather than to the sample solution, generally no signals or very small signals appeared depending on the composition of casting or test solution. The intensity of the signals was much higher when luminol was applied in the test solution together with sodium phosphate.

Addition of the surfactant to the membranes was found necessary because it provides a quick and uniform spreading of the sample drop on the entire area of the membrane. The surfactant also influences the wettability of the membranes which is crucial for the reproducibility and the sensitivity. Various surfactants (Triton X 100, cetyl trimethylammonium bromide, sodium lauryl sulphate) were tested for their ability to improve the CL signals and the reproducibility. Among the investigated surfactants, sodium lauryl sulphate was chosen because it gave best results with respect to the intensity of the signals and their reproducibility. Other investigated surfactants showed worse reproducibility and the obtained signals were two to three times lower as compared to signals obtained with SLS. The effect of the sodium lauryl sulphate concentration was investigated in the range between 100 mg/L and 800 mg/L in the casting solution (Fig. 8).

The maximum value was obtained with a concentration of 400 mg/L whereas signals were decreased at higher concentra-

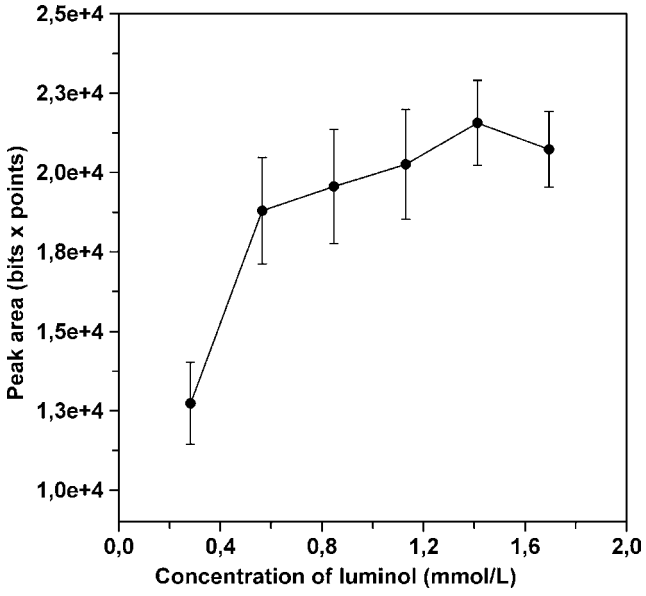

Fig. 7. Effect of the concentration of luminol in the sample solution on the chemiluminescence signal. Casting solution: hydroxyethyl cellulose (1.5% (m/v)), cobalt chloride (1 mmol/L), sodium lauryl sulphate (400 mg/L); test solution: sodium phosphate (53 mmol/L), luminol (0.28–1.69 mmol/L), H_2O_2 (100 μg/L); casting volume (10 μL); sample volume (10 μL).

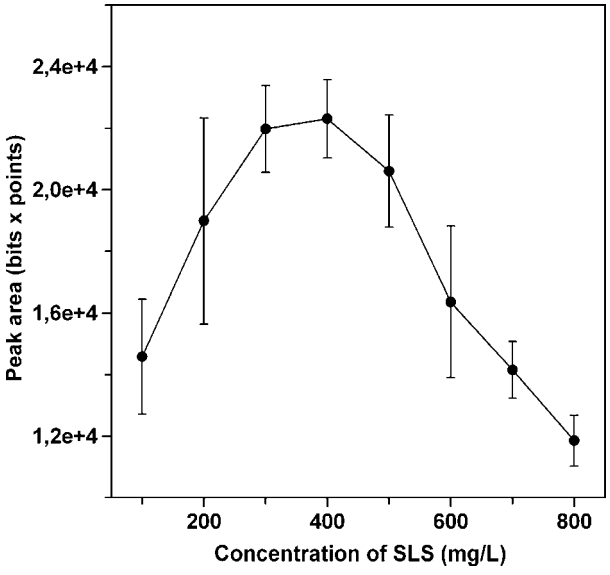

Fig. 8. Effect of the concentration of sodium lauryl sulphate in the casting solution on the chemiluminescence signal. Casting solution: hydroxyethyl cellulose (1.5% (m/v)), cobalt chloride (1 mmol/L), sodium lauryl sulphate (100–800 mg/L); test solution: sodium phosphate (53 mmol/L), luminol (1.4 mmol/L), H_2O_2 (100 μg/L); casting volume (10 μL); sample volume (10 μL).

tions probably due to quenching effects and micelle formation of sodium lauryl sulphate as the dominant factors.

The long-term stability of the sensors stored in a desiccator over sodium hydroxide during 13 days was investigated. A decrease of the chemiluminescence signal during whole storage time was noticed which summed to about 25% at the end of monitoring period. The reason for the deterioration of the signal could be physical and chemical changes in the membrane such as aging processes and also increasing turbidity of the polymeric matrix. Also the catalytic activity of Co(II) ions could be changed during the time, which can lead to a lowering of measured signals. Investigations are now in progress to increase the storage time of the sensors.

3.3. Calibration curve

Under optimum conditions, the chemiluminescence response of the sensor was linearly dependent on the concentration of hydrogen peroxide in the range 20–1600 μg/L with a detection limit of 9 μg/L (3σ). The regression equation for the signal I (integrated peak area) was I [bits × points] = 176.4 + 2293.3c(H_2O_2) [μg/L], with a correlation coefficient 0.9991 (n = 5). The relative standard deviation was 4.5% for 100 μg/L H_2O_2 (n = 11) (Fig. 9).

The calibration curve was also recorded in the presence of ethylenediaminetetraacetic acid, EDTA (1×10^{-5} mol/L), in the test solution. At this concentration EDTA does not influence significantly the signal of the analyte up to 1200 μg/L H_2O_2. The change of the signal was below ±5% compared with the signals obtained in the absence of the complexant.

The detection limit is higher as for some other chemiluminescence sensors reported so far [30], but it seems very convenient for a majority of rainwater samples, which have concentrations of hydrogen peroxide significantly above the detection limit imposed by this sensor. On the other hand this disadvantage is overcompensated by the simplicity of the measurement method allowing simple field determinations.

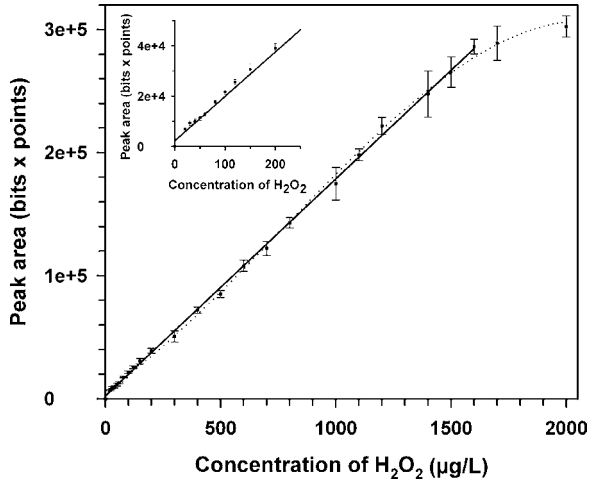

Fig. 9. Calibration graph of hydrogen peroxide with CL sensors; casting solution: hydroxyethyl cellulose (1.5% (m/v)), cobalt chloride (1 mmol/L), sodium lauryl sulphate (400 mg/L); test solution: luminol (1.4 mmol/L), sodium phosphate (53 mmol/L), hydrogen peroxide (20–2000 μg/L); casting volume (10 μL); sample volume (10 μL); straight line, linear concentration range; dotted line, investigated concentration range.

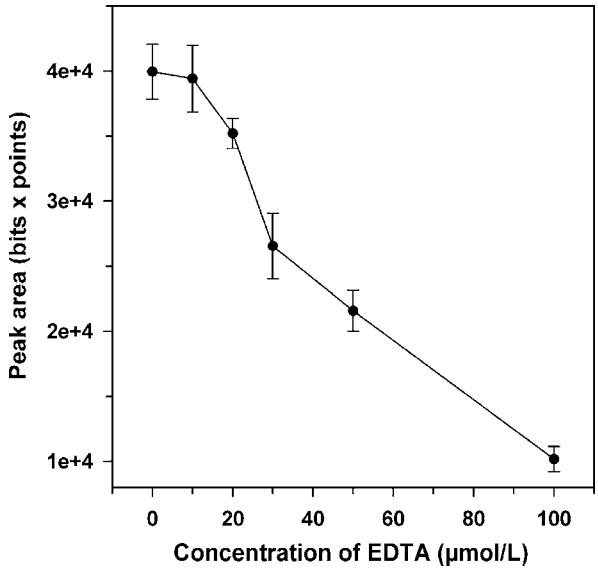

Fig. 10. Influence of EDTA on the CL signal of H_2O_2 (200 μg/L). Casting solution: hydroxyethyl cellulose (1.5% (m/v)), cobalt chloride (1 mmol/L), sodium lauryl sulphate (400 mg/L); test solution: luminol (1.4 mmol/L), sodium phosphate (53 mmol/L), EDTA (1×10^{-4} mol/L to 1×10^{-5} mol/L); casting solution (10 μL); test solution (10 μL).

3.4. Influence of EDTA on the CL signal

It has been reported by some authors that Mn(II), Fe(III), and other transition metal ions present in rainwater interfere with the hydrogen peroxide, and reduce the CL signal of luminol in the presence of a catalyst, either by decomposing the analyte or by interfering with the catalyst. One of the possible ways to reduce or eliminate these interferences is the addition of a chelating agent in order to decrease their free ionic concentration in the sample solution by complexation.

As ethylenediaminetetraacetic acid (EDTA) can complex Co^{2+} ions (catalyst) as well, the effect of EDTA on the determination of H_2O_2 was studied. EDTA or its sodium salt is the most commonly used chelator because of its ability to complex a large number of ions over a wide pH range. Standard solutions containing 200 μg/L H_2O_2 and EDTA in the range of 1×10^{-4} mol/L to 1×10^{-5} mol/L were investigated (Fig. 10).

A concentration of 10^{-5} mol/L EDTA was used for subsequent interference studies because of its negligible influence on the CL response while higher concentrations decrease the signal significantly. The decrease of the signal is probably a results of complexation of Co(II) ions in the membrane by EDTA at concentrations higher than 1×10^{-5} mol/L.

3.5. Interferences

The influence of interfering ions was investigated by analyzing a standard of 200 μg/L H_2O_2 to which increasing amounts of interfering species were added (Table 1). Interfering ions

Table 1
Investigation of the influence of interfering ions on CL signal

Intereferent (μg/L)	Signal change (%)	
	200 μg/L H_2O_2	200 μg/L H_2O_2 + 1 × 10^{-5} mol/L EDTA
Manganase(II)		
100	−15	+5
200	−20	+7
1000	−36	−3
2000	−39	−35
Iron(III)		
100	−5	−3
200	+3	−9
1000	−17	−15
2000	−19	−19
Copper(II)		
100	−43	+2
200	−88	−2
1000	−97	−24
2000	−100	−100
Zinc(II)		
100	+3	−5
200	+2	−4
1000	+13	−6
2000	−14	−13
Cobalt(II)		
100	−27	+1
200	−37	+6
1000	−49	−31
2000	−44	−42
Nickel(II)		
100	+5	+8
200	−15	+3
1000	−19	−3
2000	−18	−13
Lead(II)		
100	+1	+3
200	+7	+5
1000	+10	+2
2000	−19	−10

were used in following concentrations: 100 μg/L, 200 μg/L, 1000 μg/L and 2000 μg/L.

The influence of ions to 200 μg/L H_2O_2 was first evaluated in the absence of EDTA.

The most serious interferences were observed with Cu(II), followed by Co(II), Mn(II), at all investigated concentrations. Results obtained for the influence of Co(II) ions show that the reason for the decrease of the chemiluminescence signal is not an involvement in the reaction of luminol, but simply the fast decomposition of the analyte in the presence of the metal ion, because it is added to the sample solution prior to its application onto the sensor. This is also in agreement with investigations of some researches in respect to the influence of some metal ions on the decomposition of hydrogen peroxide in aqueous solutions through the radical chain reaction [37]. Interferences caused by the presence of Ni(II) and Fe(III) were significant and not neglible for precise determinations. Interferences were more pronounced at higher concentrations of the investigated ions (1000 μg/L and 2000 μg/L). Co(II), Cu(II), Mn(II) interfered at a mass ratio 1:1 with respect to the analyte. Zn(II) and Pb(II) showed no interferences up to a concentration of 1000 μg/L.

The influence of most transition ions is highly diminished by the addition of 1 × 10^{-5} mol/L EDTA. All investigated ions do not interfere in a mass concentration ratio of 1:1. For Mn(II), Zn(II), Ni(II), Pb(II) interferences are negligible at a ratio 5:1 but they are still present at a ratio 1:10 for all investigated ions (exhaust of the complexing capacity of EDTA). The results indicate that the addition of EDTA to rainwater samples should be advantageous.

Table 2
Determination of hydrogen peroxide in rainwater samples with the proposed method and spectrophotometric reference method

Samples #	Total concentration H_2O_2 (μg/L)[a]		Recovery (%)
	Chemiluminescence method	Spectrophotometric method	
1	165 ± 11	170 ± 27	97.0
2	118 ± 9	128 ± 14	92.0
3	174 ± 16	176 ± 15	98.8
4	104 ± 18	108 ± 14	96.0
5	109 ± 4	114 ± 18	95.0
6	575 ± 34	586 ± 18	98.0
7	627 ± 32	630 ± 14	99.8
8	100 ± 7	107 ± 14	93.4
9	105 ± 9	114 ± 18	92.1
10	472 ± 46	481 ± 15	98.1

[a] Average of five determinations ± S.D.

3.6. Sample analysis

The chemiluminescence method using the sensors designed in this work was used for the determination of hydrogen peroxide in rainwater samples (Table 2). A validation of the method and of the results was carried out by spectrophotometric reference determinations. Each sample was analyzed at the same time with both methods in order to avoid possible differences caused by degradation of the analyte in the sample. As can be seen there is a good agreement between the chemiluminescence and the spectrophotometric method. The recovery rates referred to the reference determinations were between 91.2% and 99.8% which is sufficiently good for practical applications of the simple CL device.

4. Conclusion

Low cost one-shot chemical sensors containing hydroxyethyl cellulose as a carrier, cobalt chloride and a surfactant were constructed for the determination of hydrogen peroxide in rainwater. Luminol and sodium phosphate were mixed to the analyte solution prior to analysis.

The proposed sensor is selective and sensitive for determination of hydrogen peroxide in rainwater with low detection limit and wide linear concentration range from 20 ppb to 1600 ppb H_2O_2. In comparison with previously reported flow CL sen-

sors, this sensor has a higher detection limit, and the addition of EDTA to the sample solutions is necessary to prevent influences from interfering ions. The long-term stability of the sensor is still rather short in comparison with other reported CL sensors, and it should be improved in further work for consideration of mass production.

Some of the advantages of this sensor are use of very simple instrumentation which does not need use of pumps for reagents or sample introduction. In case that a larger quantity of sensors is prepared in a single batch, the surplus of time required for the production is over compensated by the short analysis time, which is significantly shorter than in most flow injection analytical systems. The sensor operates with small consumption of sample and reagents only. Due to the nature of the designed sensor to act for single use only, there are no such problems as leaching of reagents from the immobilization supports as in flow systems.

The developed sensors are inexpensive and simple to produce with possible field application. A response time of the signal is approximately 35 s, so that the total time to perform complete analysis of the sample is about couple minutes.

Acknowledgements

This study was supported by Ministry of Education and Science of Austria, World University Service, Austria and Austrian Academic Exchange Service as well as by the Bosnian Ministry of Science and Education (project 11-14-31575-4) which we gratefully acknowledge.

References

[1] B.A. Watkins, D.D. Parrish, M. Trainer, R.B. Norton, J.E. Yee, F.C. Fehsenfeld, B.G. Heikes, J. Geophys. Res. 100 (1995) 22831.
[2] H. Sakugawa, W. Tsai, I.R. Kaplan, Y. Cohen, Environ. Sci. Technol. 24 (1990) 1452.
[3] D.W. Gunz, M.R. Hoffmann, Atmos. Environ. A 24 (1990) 1601.
[4] C. Brandt, R. van Eldik, Chem. Rev. 95 (1995) 119.
[5] Y. Deng, Y. Zuo, Atmos. Environ. 33 (1999) 1469.
[6] R.M. Pena, S. Garcia, C. Herrero, T. Lucas, Atmos. Environ. 35 (2001) 209.
[7] T.E. Graedel, M.L. Mandich, C.J. Weschler, J. Geophys. Res. 91 (1986) 5205.
[8] T.J. Kelly, P.H. Daum, S.E. Schwartz, J. Geophys. Res. 90 (1985) 7861.
[9] Y. Zuo, J. Hoigne, Environ. Sci. Technol. 26 (1992) 1014.
[10] K. Yoshizumi, K. Aoki, I. Nouchi, T. Kobayashi, S. Kamakura, Atmos. Environ. 18 (1984) 395.
[11] F.G. Römer, J.W. Viljer, L. Van Den Beld, Atmos. Environ. 19 (1985) 1847.
[12] Y.N. Lee, J. Shen, P.J. Klotz, Water Air Soil Pollut. 30 (1986) 143.
[13] P. Jacob, T.M. Tavares, V.C. Rocha, D. Klockow, Atmos. Environ. A 24 (1990) 377.
[14] R.G. Zika, E.S. Saltzman, W.L. Chameides, D.D. Davis, J. Geophys. Res. 87 (1982) 5015.
[15] B. Tang, Y. Wang, Y. Sun, H.X. Shen, Spectrochim. Acta A 58 (2002) 141.
[16] F. Sauer, S. Limbach, G.K. Moortgat, Atmos. Environ. 31 (1997) 1173.
[17] P.A. Tanner, A.Y.S. Wong, Anal. Chim. Acta 370 (1998) 279.
[18] A.L. Lazrus, G.L. Kok, S.N. Gitlin, J.A. Lind, S.E. McLaren, Anal. Chem. 57 (1985) 917.
[19] T. Taniai, A. Sakuragawa, T. Okutani, Anal. Sci. 15 (1999) 1077.
[20] K. Schachl, H. Alemu, K. Kalcher, H. Moderegger, I. Svancera, K. Vytras, Fresenius J. Anal. Chem. 362 (1998) 194.
[21] K. Schachl, H. Alemu, K. Kalcher, J. Jezkova, I. Svancera, K. Vytras, Analyst 122 (1997) 985.
[22] G.L. Kok, Atmos. Environ. 14 (1980) 653.
[23] T. Ibusuki, Atmos. Environ. 17 (1983) 393.
[24] J. Yuan, A.M. Shiller, Anal. Chem. 71 (1999) 1975.
[25] K. Hool, T.A. Nieman, Anal. Chem. 59 (1987) 869.
[26] P. van Zoonen, D.A. Kamminga, C. Gooijer, N.H. Velthorst, R.W. Frei, G. Gübitz, Anal. Chim. Acta 174 (1985) 151.
[27] W. Qin, Z.J. Zhang, H.H. Chen, Int. J. Environ. Anal. Chem. 66 (1997) 191.
[28] J. Li, P.K. Dasgupta, Anal. Chim. Acta 442 (2001) 63.
[29] D. Price, P.J. Worsfold, R. Fauzi, C. Mantoura, Anal. Chim. Acta 298 (1994) 121.
[30] L. Marle, G.M. Greenway, Anal. Chim. Acta 548 (2005) 20.
[31] W. Qin, Z.J. Zhang, B.X. Li, S.N. Liu, Anal. Chim. Acta 372 (1998) 357.
[32] S. Hanaoka, J.M. Lin, M. Yamada, Anal. Chim. Acta 426 (2001) 57.
[33] J.M. Lin, K. Sato, M. Yamada, Microchem. J. 69 (2001) 73.
[34] H. Moderegger, Development of One-shot Sensors based on Chemiluminescence, PhD Thesis, Karl-Franzens University, Graz, Austria, 2003.
[35] A. Tahirovic, Development of Chemiluminescence Sensors for the Determination of Hydrogen Peroxide in Rainwater, PhD Thesis, Karl-Franzens University, Graz, Austria, 2006.
[36] G.T. Burdo, R.W. Seitz, Anal. Chem. 47 (1975) 1639.
[37] I. Mochida, K. Takeshita, J. Phys. Chem. 78 (1974) 1653.

Available online at www.sciencedirect.com
ScienceDirect
Talanta 72 (2007) 1593–1597
Talanta
www.elsevier.com/locate/talanta

Short communication

An ethanol sensor based on cataluminescence on ZnO nanoparticles

Huarong Tang [a], Yaming Li [a], Chengbin Zheng [a], Jun Ye [a], Xiandeng Hou [a,b], Yi Lv [a,*]

[a] *Key Laboratory of Green Chemistry & Technology of MOE, College of Chemistry, Sichuan University, Chengdu, Sichuan 610064, China*
[b] *Analytical & Testing Center, Sichuan University, Chengdu, Sichuan 610064, China*

Received 20 September 2006; received in revised form 12 January 2007; accepted 14 January 2007
Available online 20 January 2007

Abstract

A novel gas sensor for the determination of ethanol was proposed in the present work, which was based on the generated cataluminescence emission from catalytic oxidation of ethanol on the surface of ZnO nanoparticles. The cataluminescence characteristics and the effect of different parameters on the signal intensity, such as morphology of synthesized ZnO, temperature and flow rate, were discussed in detail. Under the optimized experimental conditions, the calibration curve of cataluminescence intensity versus ethanol vapor concentration was linear in the range 1.0–100 ppm, and with a detection limit of 0.7 ppm (S/N = 3). Compared with the traditional electrical conductivity-based ZnO gas sensor for the determination of ethanol, the proposed ethanol sensor showed the advantages of high sensitivity, high selectivity and low working temperature.

Keywords: Cataluminescence; ZnO; Nanomaterials; Ethanol; Sensor

1. Introduction

In the field of gas sensors, it is well known that ethanol vapor is one of the most exhaustively studied gases, particularly due to the great demand in the biomedical, chemical, and food industries, especially in wine-quality monitoring and breath analysis [1–7]. Metal oxide semiconductor, usually representing a property that the electrical conductivity varies with the composition of the gas atmosphere surrounding it, is a popular and useful sensing material for ethanol vapor sensing. Many researchers have devoted themselves to develop ethanol vapor sensors based on semiconductor metal oxides, such as ZnO, SnO_2, TiO_2, WO_3, Fe_2O_3 and In_2O_3 [8–15]. However, most of the traditional semiconductor sensors usually suffer from high working temperature (usually above 400 °C), poor selectivity, low long-term stability, and/or limited applications [16].

Recently, nanomaterials have attracted widespread attention in the field of gas sensors because of their specific features that differ from bulk materials [17–19]. The application of nanomaterials to the design of ethanol gas sensors is nowadays one of the most active research fields, due to their high activity, high surface-to-bulk ratio, good adsorption characteristics and high selectivity. For example, Li's research group [20], recently, has developed a highly selective and stable ethanol sensor based on single-crystalline V_2O_5 nanobelts, which was prepared by a simple mild hydrothermal method. It is also worth mentioning that nanosized ZnO as a wide-band-gap semiconductor has attracted more and more attention over the past few years [21,22], and it has been investigated widely as a gas sensor [23–28] mostly based on electrochemical response to ethanol vapor.

Chemiluminescence (CL) resulting from the interaction between gases and solid surfaces has been studied for decades. The phenomenon was observed during the catalytic oxidation of carbon monoxide on a thoria surface by Breysse et al. in 1976 [29], and was called "cataluminescence". In recent years, cataluminescence on the surface of nanosized materials has shown its great prospect in chemical sensing. Zhang and co-workers [30–36] have observed CL phenomena during the catalytic oxidation of organic/inorganic vapor on the surface of several nanomaterials, such as titanium dioxide, strontium carbonate, yttrium oxide, ferric oxide and zirconium dioxide, and constructed a series of gas sensors for the determination of volatile or gaseous substances, such as ethanol, hydrogen sulfide, trimethylamine and acetaldehyde.

In this work, we have proposed a novel ethanol sensor based on cataluminescence on nanosized ZnO. When the ethanol vapor passes through the surface of nanosized ZnO, strong catalu-

* Corresponding author. Tel.: +86 28 85412798; fax: +86 28 85412798.
E-mail address: lvy@scu.edu.cn (Y. Lv).

0039-9140/$ – see front matter © 2007 Elsevier B.V. All rights reserved.
doi:10.1016/j.talanta.2007.01.035

minescence could be observed from the catalytic oxidation of ethanol. Compared to the former cataluminescence-based [30–32] and the conventional semiconductor-based ethanol gas sensor [10,12,15,27], the proposed gas sensor showed high sensitivity with a detection limit (S/N = 3) of 0.7 ppm. The present gas sensor has been also used for the determination of ethanol in the artificial samples, and the results showed the advantages of high stability and the satisfying possibility of routine measurements.

2. Experimental

2.1. Chemicals and preparation of ZnO nanoparticles

All chemicals used in the experiment were of analytical grade or better. The following was the abbreviation of the chemicals and the corresponding manufacturers: $ZnSO_4 \cdot 7H_2O$ (A.R., Shengyang Chemical Reagent Factory, China), NH_4HCO_3 (A.R., Shantou Xilong Chemical Co. Ltd, China), Triton X-100 ($C_{34}H_{62}O_{11}$, CP, Shantou Xilong Chemical Co. Ltd, China), and ethanol (AR, Changzheng Chemical Company of Chengdu, China).

Nanosized ZnO was synthesized by a wet chemical method described as following: 4.3 g $ZnSO_4 \cdot 7H_2O$ was dissolved in 0.2% (v/v) Triton X-100 solution, then a certain volume NH_4HCO_3 solution (0.15 mol L^{-1}) was added drop-wise with vigorously stirring. The resulting product, a gelatinized precipitate, was transferred into a beaker for ultrasonication for 1 h, then filtrated and washed with distilled water three times to remove residual SO_4^{2-}. After these treatments, the precipitate was dried in a vacuum chamber for 2 h at 90 °C, and then calcined in a muffle furnace for 2 h at a certain temperature to obtain pure ZnO nanoparticles with different size. It should be mentioned here that by changing the mol ratio of $ZnSO_4$ to the NH_4HCO_3 (1:1.25 for a and c, 1:3.75 for b) and calcining temperatures (300 °C for a, 600 °C for b and c), the ZnO particles with different size could be obtained.

The morphology of the synthesized ZnO was characterized with a transmission electron microscope (TEM-100CX) at an accelerating voltage of 80 kV. Fig. 1 showed that the grain sizes of the nanosized ZnO varies with different experimental conditions. The prepared material (a) was eventually selected for use, with the grain size in the range of 20–50 nm.

An X-ray powder diffraction (XRD) experiment was carried out with an X'pert PROMPD diffractometer (Philips, The Nethertands) equipped with a plumbaginous-monochromated Cu Kα radiation source. It can be seen from Fig. 2 that the XRD patterns of all the ZnO nanoparticles were attributed to the wurtzite structure according to the XRD standard spectrum of ZnO.

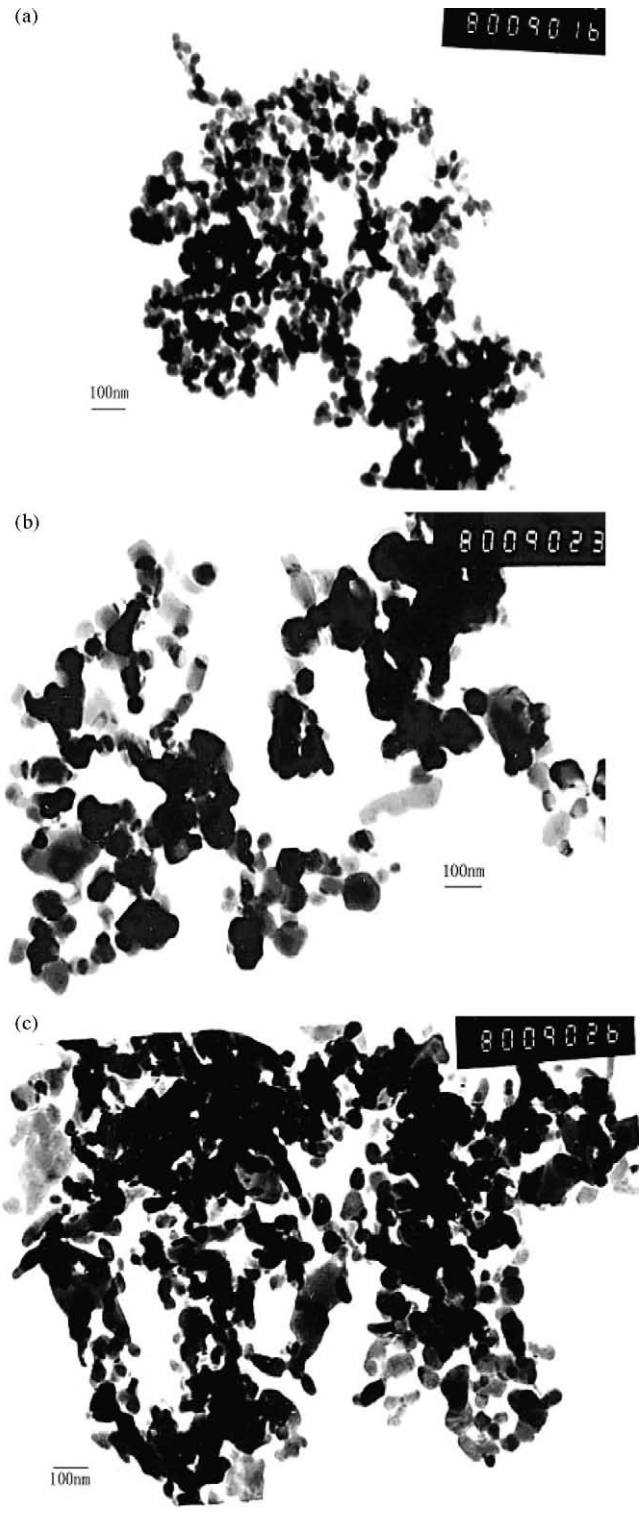

Fig. 1. TEM image of the nanosized ZnO. The image was obtained from a TEM-100CX operated at an accelerating voltage of 80 kV.

2.2. Apparatus

The schematic diagram of the detection system was shown in Fig. 3. According to the procedure in reference [30], about 0.03 g nanosized ZnO was coated as a layer on a ceramic heating tube which was put into a quartz tube with an inner-diameter of 15 mm. The air from the pump was mixed with ethanol and flowed through the quartz tube, in which ethanol was oxidized on the surface of the catalyst by the oxygen in the air. The producing CL intensity was directly measured with a BPCL Ultra Weak Chemiluminescence analyzer (Biophysics Institute of Chinese Academy of Science, China). By changing the optical filters, the

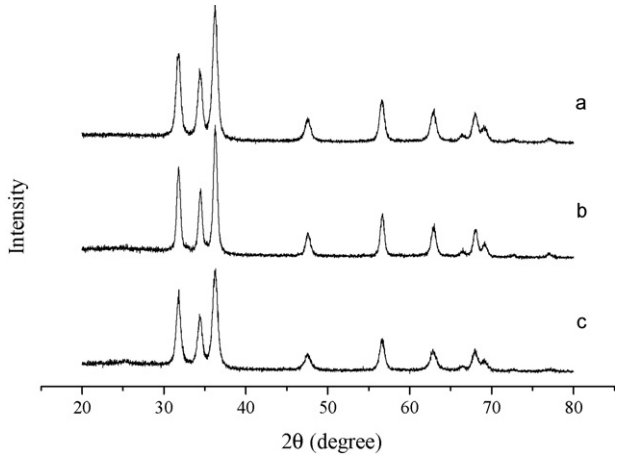

Fig. 2. X-ray powder diffraction pattern of the nanosized ZnO. The diffraction data were collected on an X'pert PROMPD diffractometer using Cu Kα radiation. The sample was scanned from 20° to 70° (2θ) with a step size of 0.02°.

wavelengths used for detection could be selected over the range of 400–600 nm.

3. Results and discussion

3.1. Effect of the nanosized ZnO morphology

To explore the effect of the ZnO morphology on the cataluminescence, the three prepared nanosized ZnO with different size were used for constructing the gas sensor, respectively. The cataluminescence emission on the nanosized ZnO surface was investigated by a 25.0 ppm ethanol vapor sample with a flow rate of 80 mL min^{-1} through a series of interference (band-pass) filters in the region of 400–555 nm (400, 425, 440, 460, 490, 525, 555 nm). The results were shown in Fig. 4. It can be seen that the cataluminescence intensity on the surface of the nanosized ZnO (a) was the strongest, on the other hand, the profile of curves for ethanol vapor on different nanosized ZnO were similar, and each curve had the same maximum of cataluminescence emission at about 490 nm. This also implied that the nanosized ZnO materials with higher surface-to-bulk ratio would have a higher catalytic ability for producing cataluminescence emission. Therefore, the prepared nanosized ZnO (a) was the best one for the detection of ethanol vapor in the present work.

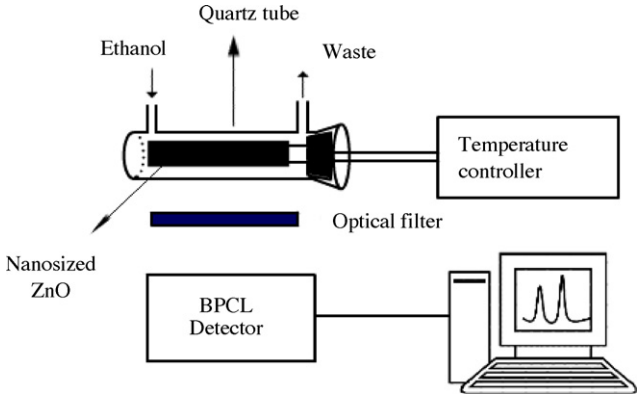

Fig. 3. Schematic diagram of the cataluminescence sensor system for determination of ethanol.

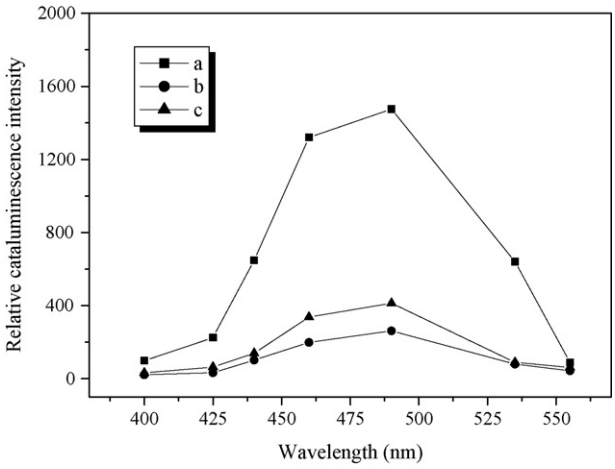

Fig. 4. The cataluminescence emission spectra of ethanol on three prepared nanosized ZnO. Temperature: 358 °C; ethanol vapor concentration: 25.0 ppm; sampling volume: 50 mL; and gas flow rate: 80 mL min^{-1}.

3.2. Cataluminescence responses of ethanol vapor on the surface of ZnO

Although the preliminary experimental showed that the maximum wavelength of cataluminescence emission resulting from the oxidation of ethanol vapor on the surface of different nanosized ZnO particles was similarly about 490 nm (Fig. 4), the influence from the heat radiation that usually increased with the increase of wavelength in the range of 400–555 nm in the current detection system, should not be ignored. The experimental result of the influence of the cataluminescence detection wavelength on the signal to noise ratio (S/N) showed that the maximum S/N was at about 460 nm. Therefore, the 460 nm was the optimal detection wavelength for the current ethanol vapor sensor.

Furthermore, the cataluminescence response profiles of ethanol vapor on the surface of nanosized ZnO were studied by injecting ethanol vapor sample with different concentration into detection system with a flow rate of 80 mL min^{-1}. Fig. 5 shows the CL response profiles of ethanol with different concentrations at 358 °C. Curves a, b and c denote the results for different concentrations of 5.0, 10.0 and 30.0 ppm, respectively. It can be seen that the profiles of cataluminescence emission are similar to each other, and each signal sharply increased after ethanol vapor was introduced, which indicated that the ethanol sensing was a fast process. The response time (which is usually defined as the time needed to reach the maximum of cataluminescence emission signal) and the recovery time (usually defined as the time needed to recover to the baseline) were less than 3 and 60 s, respectively. This also indicated that the present sensor has an advantage of high throughput in the measurement of ethanol vapor.

It was noteworthy that the cataluminescence spectra of ethanol vapor on the surface of ZnO were very similar to the one on the surface of $SrCO_3$ reported in the previous work [32], which suggested that the CL emission was associated

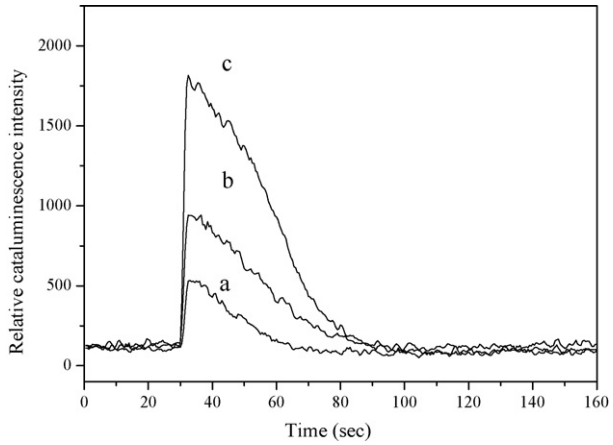

Fig. 5. Typical cataluminescence temporal profiles. Ethanol vapor concentration is (a) 5.0 ppm, (b) 10.0 ppm, and (c) 30.0 ppm, respectively.

with a common chemiluminescent species in the two catalytic CL reactions. The cataluminescence response of ethylene and acetaldehyde, which were taken as possible intermediates in the $SrCO_3$-based catalytic reaction, also showed similar emission spectra on the surface of ZnO. For this point of view, it could be supposed that the mechanism of this cataluminescence on nanosized ZnO is similar to the one on $SrCO_3$, and ethylene and acetaldehyde could be considered as the possible intermediates in the process of ethanol oxidation on nanosized ZnO. According to the Shi's suggestion, the possible mechanism might be expressed as

$$C_2H_5OH \xrightarrow{[O]} C_2H_4 \quad \text{or} \quad CH_3CHO \xrightarrow{[O]} CO_2 + H_2O + h\nu$$

However, further work is needed to confirm the mechanism in the future.

3.3. Optimization of flow rate of carrier gas

The effect of carrier gas flow rate on cataluminescence intensity was investigated in range of 25–250 mL min^{-1} at 358 °C with a band-pass filter of 460 nm. The ethanol vapor concentration was 30.0 ppm. The results indicated that the cataluminescence intensity increases gradually with the increase of flow rate, ranging from 25–100 mL min^{-1}, and it was relatively stable at above 100 mL min^{-1}. Therefore, the optimal flow rate was 100 mL min^{-1}.

3.4. Optimization of the working temperature

The effect of working temperature on cataluminescence was also explored by introducing 5.0 ppm ethanol vapor into the chamber at the carrier gas flow rate of 100 mL min^{-1} and wavelength of 460 nm. The results showed that the cataluminescence intensity increased with the increase of working temperature from 276 to 410 °C. This may be attributed to the higher catalytic activity of nanosized ZnO at higher temperature. However, the experimental also indicated that the background signal, which mainly arose from the heat radiation, also increased with the increase of temperature and even increased faster than the CL intensity at higher temperature. The results showed that the maximum value of S/N versus temperature could be obtained at 358 °C. Under or above this temperature, the values of S/N decreased. Therefore, the temperature of 358 °C was chosen for the further study.

3.5. Analytical characteristics

Under the optimal experimental conditions, the calibration curve of cataluminescence intensity versus ethanol vapor concentration was linear in the range of 1.0–100.0 ppm with a detection limit of 0.7 ppm (based on S/N = 3). The linear regression equation for the present ethanol vapor sensor was $Y = 65.18X + 69.19$ ($r = 0.996$, $n = 6$, where r was the correlation coefficient and n represents the six ethanol samples tested in the experiment), where Y was the cataluminescence intensity and X was the concentration of ethanol vapor (ppm).

3.6. Selectivity

Gas-selective properties of the nanosized ZnO sensor were measured under the optimum conditions. Some possible coexistence substances, such as ammonia, methanol and hydrogen, usually had an obviously interference on the determination of ethanol vapor in the traditional semiconductor oxide sensors [15], which would seriously limit the extensive utilization. To explore the selectivity of the cataluminescence sensor for ethanol vapor, the responses to some common gases with a same concentration of 50.0 ppm were investigated. The result was shown in Fig. 6. It can be seen that the present sensor has a significantly high selectivity to ethanol vapor. No significant cataluminescence emission could be detected for ammonia, nitrogen, carbon dioxide, sulfur dioxide, dichloromethane and carbon tetrachloride. The cataluminescence emission was also detected for benzene, toluene, xylene and methanol, however, compared with ethanol, it was too weak to cause an obvious interference.

3.7. Lifetime of the sensor

The experiment about stability and durability of this sensor was carried out by sampling of 10.5 ppm ethanol vapor into the sensor everyday for 10 times at 358 °C at the flow rate of

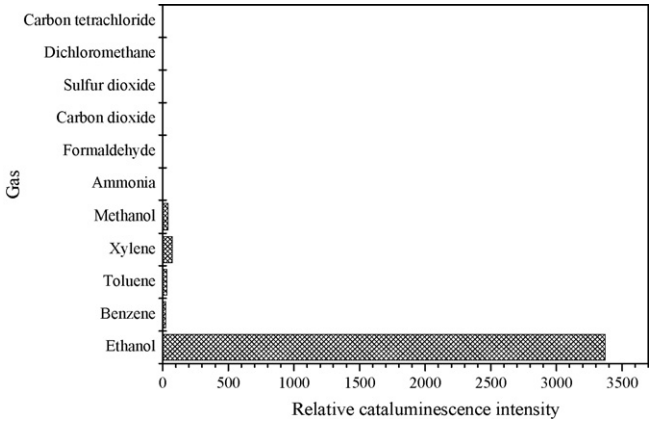

Fig. 6. Selectivity of the cataluminescence ethanol sensor.

Table 1
Determination of ethanol in the artificial samples with the proposed gas sensor

Sample no.	Labeled value[a] (ppm)	Detected value (ppm)	Recovery experimental		
			Added value (ppm)	Founded value (ppm)	Recovery[b] (%)
1	6.0	6.3	15.8	22.8	104.4
2	7.4	7.6	19.0	26.0	96.8
3	8.8	9.2	12.6	22.8	107.9

[a] Labeled value is referred to the calculated concentration in the artificial gas samples.
[b] Recovery (%) is defined as: (founded value − detected value)/added value.

100 mL min^{-1}. The cataluminescence intensity was measured at the wavelength band-pass of 460 nm. After a week, no obvious change could be found. The RSD ($n = 7$) was about 3.5% in a successive experiments, which implied that the sensor had good stability and durability.

4. Sample analysis

In order to estimate the validation of the present gas sensor, a series of artificial gas samples with different concentrations of ethanol were analyzed. The artificial gas samples were prepared by the following procedures: a certain volume wine sample (56%, v/v) was injected into a 25-mL airtight bottle which was placed in a thermostatic water bath (95 °C). After an incubation of five minutes for ethanol evaporation, the vapor sample was carried into the cataluminescence chamber for measurement. The results are shown in Table 1. From the results, we can conclude that the present ethanol gas sensor is capable for the determination of ethanol in air samples with satisfactory recoveries.

5. Conclusions

An ethanol vapor sensor has been developed based on the cataluminescence on the surface of nanosized ZnO. Under the optimized conditions, it is sensitive to a concentration range up to 100 ppm, with a best detection limit of 0.7 ppm. Rapid response, satisfactory stability and high selectivity show the prospect of this sensor for ethanol determination in industry and other fields. Also, the work may be useful for the development of miniaturize equipment for the determination of breath alcohol concentration of a drunk driver.

Acknowledgements

The authors gratefully acknowledge the financial support for this project from the National Natural Science Foundation of China (no. 20605013) and Young Scholar Foundation of Sichuan University (no. 200548).

References

[1] B. Kieser, F. Dieterle, G. Gauglitz, Anal. Chem. 74 (2002) 4781.
[2] T. Qin, X.B. Xu, T. Polák, V. Pacáková, K. ŠtulÍk, Talanta 44 (1997) 1683.
[3] J.K. Park, H.J. Yee, S.T. Kim, Biosens. Bioelectron. 10 (1995) 587.
[4] C.X. Cai, K.H. Xue, Y.M. Zhou, H. Yang, Talanta 44 (1997) 339.
[5] P.A.D.P. Pereira, E.T.S. Santos, T.D.F. Ferreira, J.B.D. Andrade, Talanta 49 (1999) 245.
[6] J. Keith, S. Puckett, G.E. Pacey, Talanta 61 (2003) 417.
[7] E.T. Hayes, A. Galal, H.B. Mark, Talanta 42 (1995) 873.
[8] O.K. Tan, W. Cao, W. Zhu, J.W. Chai, J.S. Pan, Sens. Actuators B 93 (2003) 396.
[9] R. Ionescu, A. Hoel, C.G. Granqvist, E. Llobet, P. Heszler, Sens. Actuators B 104 (2005) 132.
[10] C. Garzella, E. Bontempi, L.E. Depero, A. Vomiero, G. Della Mea, G. Sberveglieri, Sens. Actuators B 93 (2003) 495.
[11] X.F. Chu, C.H. Wang, J.D. Jiang, C.M. Zheng, Chem. Phys. Lett. 399 (2004) 461.
[12] V.S. Vaishnav, P.D. Patel, N.G. Patel, Thin Solid Films 490 (2005) 94.
[13] Y. Chen, K.Y. Chen, A.C.C. Tseung, J. Electroanal. Chem. 471 (1999) 151.
[14] T. Brousse, D.M. Schleich, Sens. Actuators B 31 (1996) 77.
[15] C. Garzellaa, E. Cominia, E. Tempestia, C. Frigerib, G. Sberveglieria, Sens. Actuators B 68 (2000) 189.
[16] E. Comini, Anal. Chim. Acta 568 (2006) 28.
[17] J. Riu, A. Maroto, F.X. Rius, Talanta 69 (2006) 288.
[18] G.N. Chaudhari, A.M. Bende, A.B. Bodade, S.S. Patil, S.V. Manorama, Talanta 69 (2006) 187.
[19] P.G. Su, Y.L. Sun, C.C. Lin, Talanta 69 (2006) 946.
[20] J.F. Liu, X. Wang, Q. Peng, Y.D. Li, Adv. Mater. 17 (2005) 764.
[21] Y. Cui, Q. Wei, H. Park, C.M. Lieber, Science 293 (2001) 1289.
[22] M.H. Huang, S. Mao, H. Feick, J.Q. Yan, Y.Y. Wu, H. Kind, E. Weber, R. Russo, P.D. Yang, Science 292 (2001) 1897.
[23] J.G. Zhou, Y.L. Wang, F.Y. Zhao, Y.L. Wang, Y. Zhang, L. Yang, J. Lumines. 119–120 (2006) 248.
[24] C.S. Rout, S.H. Krishna, S.R.C. Vivekchand, A. Govindaraj, C.N.R. Rao, Chem. Phys. Lett. 418 (2006) 586.
[25] P.P. Sahay, S. Tewari, S. Jha, M. Shamsuddin, J. Mater. Sci. 40 (2005) 4791.
[26] Q. Wan, Q.H. Li, Y.J. Chen, T.H. Wang, X.L. He, J.P. Li, C.L. Lin, Appl. Phys. Lett. 84 (2004) 3654.
[27] D.F. Paraguay, M. Miki-Yoshida, J. Morales, J. Solis, L.W. Estrada, Thin Solid Films 373 (2000) 137.
[28] B. Bhooloka Rao, Mater. Chem. Phys. 64 (2000) 62.
[29] M. Breysse, B. Claudel, L. Faure, M. Guenin, R.J.J. Williams, J. Catal. 45 (1976) 137.
[30] Y.F. Zhu, J.J. Shi, Z.Y. Zhang, X.R. Zhang, Anal. Chem. 74 (2002) 120.
[31] Z.Y. Zhang, C. Zhang, X.R. Zhang, Analyst 127 (2002) 792.
[32] J.J. Shi, J.J. Li, Y.F. Zhu, F. Wei, X.R. Zhang, Anal. Chim. Acta 466 (2002) 69.
[33] Y. LV, S.C. Zhang, G.H. Liu, M.W. Huang, X.R. Zhang, Anal. Chem. 77 (2005) 1518.
[34] G.M. Huang, Y. Lv, S.C. Zhang, C.D. Yang, X.R. Zhang, Anal. Chem. 77 (2005) 7356.
[35] Z.Y. Zhang, K. Xu, Z. Xing, X.R. Zhang, Talanta 65 (2005) 913.
[36] Z.Y. Sun, X.R. Zhang, N. Na, Z.M. Liu, B.X. Han, G.M. An, J. Phys. Chem. B 110 (2006) 13410.

Available online at www.sciencedirect.com
ScienceDirect
Talanta 72 (2007) 1573–1580
Talanta
www.elsevier.com/locate/talanta

Classification and pattern recognition of acyclic octenes based on mass spectra

J.I. Villegas [a,*], D. Kubička [b], S.-P. Reinikainen [c], G. Addová [d], R. Kubinec [d], T. Salmi [a], D. Yu. Murzin [a,**]

[a] *Laboratory of Industrial Chemistry, Process Chemistry Centre, Åbo Akademi University, Biskopsgatan 8, FIN-20500, Åbo/Turku, Finland*
[b] *VÚAnCh, Department of Refinery and Petrochemical Research, 43670 Litvínov, Czech Republic*
[c] *Laboratory of Inorganic and Analytical Chemistry, Department of Chemical Technology, Lappeenranta University of Technology, P.O. Box 20, FIN-53851 Lappeenranta, Finland*
[d] *Institute of Chemistry, Faculty of Natural Sciences, Comenius University, Mlynská Dolina, Bratislava 84215, Slovak Republic*

Received 27 September 2006; received in revised form 25 January 2007; accepted 5 February 2007
Available online 16 February 2007

Abstract

Two SIMCA models were developed for the classification of acyclic octene isomers, which only form a fraction of a very complex product mixture obtained, for example, from the transformation of 1-butene. The effects of spectral transformation, namely autocorrelation and logarithmic intensity ratios transforms, and (square-root) scaling of the octane isomers mass-spectral data were investigated. Both the spectral-features preprocessing methods and scaling were found to be vital for an adequate development and improvement of the classification models. The best SIMCA models were successfully applied on gas-chromatography–mass spectroscopy (GC–MS) analysis collected from the dimerization of 1-butene over heterogeneous catalysts in the liquid phase.

Keywords: SIMCA; Pattern recognition; Spectral features; Classification; Acyclic octenes

1. Introduction

In order to correctly analyze kinetic data and, most importantly, unveil the reaction mechanism, an exhaustive analysis of the product distribution of a specific reaction mixture is critical. However, such analysis becomes more demanding as the complexity of the product mixture increases. In general, hydrocarbon transformation reactions, *e.g.* dimerization of 1-butene or isobutene, comprise a large number of molecules ranging from propene up to tetradecene [1,2]. In the particular case of the dimerization of butene over acid catalysts in the liquid phase, acyclic C_8-olefin isomers (molecular weight (MW) = 112 g/mol), both skeletal and stereoisomers, are the most important reaction products and its main objective is to produce isooctenes for "green" gasolines. Often, acyclic octene isomers are regarded as top octane-number contributors for the gasoline pool that seem to follow new environmental restrictions due to their low volatility, reactivity and toxicity. The C_8 fraction mainly consists of dimethylhexenes (DMH), trimethylpentenes (TMP) and methylheptenes (MH) where the rule of thumb is that the more alkyl-substituted molecules possess higher octane numbers (ON), thus assigning the highest ON to the TMP, also known as isooctenes. However, linear octenes (LO) may also coexist. Isomers with the double bond located in position 2 predominated. In addition to all this, Froment and coworkers demonstrated in the alkylation of isobutane with *n*-butene that the distribution of these species within the same carbon fraction was far from the equilibrium composition [2]. An overall product distribution with such large variety of species clearly illustrates the complexity of the reaction mixture and poses a huge challenge for their separation and identification. Firstly, due to their similar vapor pressures, full separation of these isomers by means of capillary gas-chromatographic techniques (GC) is rarely accomplished and secondly, the spectra obtained for separate compounds by mass spectroscopy (MS) usually lack a standardized spectral library to be used as reference. Fortunately, in order to deal with these problems and hence classifying

* Corresponding author. Fax: +358 2 215 4479.
** Co-corresponding author.
E-mail address: dmurzin@abo.fi (D.Yu. Murzin).

0039-9140/$ – see front matter © 2007 Elsevier B.V. All rights reserved.
doi:10.1016/j.talanta.2007.02.009

and identifying the product mixture, it is possible to group them into classes based on structural similarities (*e.g.* branching degree and double-bond positioning), which can be extracted from MS spectra, bringing extra advantages for kinetics analysis. Also, there are several multivariate deconvulation techniques and commercial software available for extracting "pure" spectra for a specific analyte, *i.e.* chemical component contributing to measured signal, from the acquired GC–MS spectra. The basic idea behind these methods is to decompose the raw data matrix into matrices containing pure spectra in row vectors and pure chromatographic profiles in column vector [3]. However, further investigation of the impact of these techniques falls outside the scope of this work.

Multivariate statistical techniques offer powerful tools in interpreting complex data. Soft Independent Modeling of Class Analogy (SIMCA) and Principal Component Analysis (PCA) are the two major techniques dealing with this sort of problems. On the one hand, PCA relies on the linear transformation of a training set of samples (objects) into smaller sets of uncorrelated variables while retaining as much information present in the original data set as possible. SIMCA, on the other hand, is a class modeling method that provides a chemical class assignment to an unknown by first conducting PCA on each defined class [4,5]. New (unknown) objects can be projected onto the model and the distances to each class can be calculated. If such distances lie between the defined limits for a certain class then the objects belong to the class. In addition, it is possible to identify by the SIMCA model whether new objects are outliers or belong to a class. Previously, PCA and SIMCA have been successfully applied to interpret and classify complex data in different areas, such as environmental chemistry [6,7], organic chemistry [8–11], fire investigation [12] and even doping analysis [13]. Recently, a similar work has been performed at our Laboratory in the ring opening reaction of decalin [11], nonetheless the novelty of this specific work is the real application of the models since the correct classification of all octene products could be used in the prediction of important gasoline properties, such as the octane number, which is still accomplished by heavy-duty, single-cylinder engines (knock engine method); a expensive and troublesome method.

Herein, the classification of acyclic octene isomers is stressed due to their importance in the dimerization of 1-butene. Four classes of acyclic octenes are proposed based on mass spectra featuring branching degree in acyclic octenes. Particular attention is paid to the transformation of raw mass spectra, scaled or not, and its effects on the resulting SIMCA models. Finally, the best models were tested with real GC–MS data from the liquid phase dimerization of 1-butene over heterogeneous catalysts.

2. Experimental

2.1. Data

The mass spectral data of all acyclic octene isomers were gathered as described by Kubinec and coworkers [14] and from a MS library [15]. In total, 93 spectra for all the acyclic octenes were collected, however 21 spectra from ethyl-substituted molecules were directly dismissed due to the unlikeness of these molecules to be formed in the transformation of 1-butene inside the catalyst pores. Hence, only 72 mass spectra were used for the modeling, from which 40 originated from the MS library and the rest were synthesized and analyzed as mentioned in Ref. [14]. The octene model mixtures were prepared from standard reference materials of octenes, products of methylene insertion reaction and octenes from FCC gasoline. These model mixtures were separated by GC in a laboratory-prepared glass capillary column (93 m × 250 μm i.d. dynamically coated with equalane as a stationary phase). More detailed information on the GC–MS measurements is outside of the scope of this paper and was addressed in Ref. [14].

For modeling purposes, the number of relevant mass-spectra fragments (variables) kept for the data sets was 24 since it is well-known that the information in a complete mass spectrum is highly redundant; therefore it is not necessary to use the full spectrum for pattern recognition studies. The ultimate goal for the final model was to identify and classify real GC–MS spectral data from catalytic experiments, which was successfully performed. Such analysis was carried out in an HP 6890–5973 instrument equipped with a capillary column (DB-Petro 50 m × 0.2 μm × 0.5 μm) and a FI detector. Helium was used as carrier gas. The following temperature program was applied: dwelling for 2 min at 323 K, heating 1.2 K/min to 393 K followed by heating 2 K/min to 473 °C and dwelling at the same temperature for 20 min. No internal standards were used for such purpose.

Evaluation of the collected data revealed that four classes could be defined for acyclic octenes based principally on the branching degree of the molecule, *i.e.* number of methyl-substituents that the molecule backbone possess. Consequently, four classes were established according to this criterion, *i.e.* dimethylhexenes, trimethylpentenes, methylheptenes and linear octenes. Fig. 1 shows representative structures for each of these classes. However, it was observed on the score plots that some spectra from the DMH and MH classes behaved differently than the majority of their corresponding class, overlapping with each other. These mass spectra (19 in total) corresponded to octene molecules with the double bond in position 3, *e.g.* dimethylhep-3-enes, thus they were extracted from the original data set and a sub-model with two classes was built with both criteria, *i.e.* 3-DMH and 3-MH.

2.2. Data preprocessing

MS data required initial preprocessing for the creation of a data matrix suitable for subsequent analysis. All spectra were normalized to a base peak and the 24 most representative fragments for acyclic octenes were chosen for modeling the individual classes. Nonetheless, the data were preprocessed before any modeling was performed. Class modeling and object classification were carried out by Matlab. This Matlab non-commercial tool was programmed by the chemometrics group at Lappeenranta University of Technology with the participation of one of the authors. The tool is based on SIMCA algorithm presented in [16] and updated with Multivariate Control Charts (Q and T2).

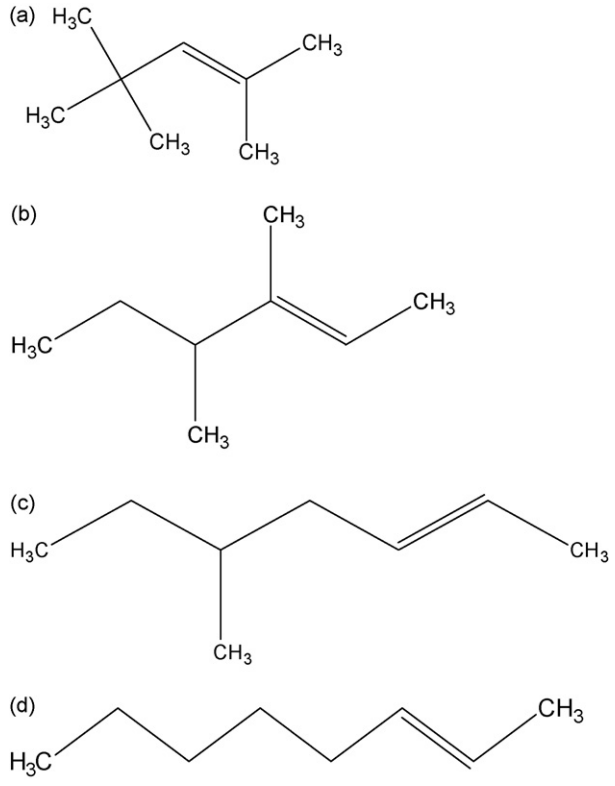

Fig. 1. Representative structures of acyclic octene isomers as identified from literature and MS-library data. (a) Trimethylpentenes (TMP), (b) dimethylhexenes (DMH), (c) methylheptene (MH) and (d) linear octene (LO).

Mathematical transformation of mass spectra before applying interpretation methods dates back to early applications of multivariate methods for pattern recognition. The main purpose of spectral transformation is to obtain a set of spectral features that are closely related to molecular structures [17], while a spectral feature x_j is a number that can be automatically computed from a spectrum. Different mathematical transformations have been proposed such as autoscale [11,17], Hadamard and Fourier transform [17], logarithmic intensity ratio [8,11], intensity sums [8] and autocorrelation [7,8,11,17]. In this particular study, the autocorrelation transform and logarithmic intensity ratio were used before modeling but also the raw data were modeled for comparison sake. The main reason for choosing these feature groups is that they have been effectively applied on hydrocarbon systems with similar complexity [7,8,11]. Obviously, it is believed that each preprocessing technique is data-structure sensitive, thus preprocessors perform optimally in different systems. Nevertheless, the other mathematical transformation has been tried but not presented due to their poor performance. Definitions of mass spectral features have already been published elsewhere [9,18], thus only a short description is given below.

2.2.1. Feature group: logarithmic intensity ratios [8,11]

Logarithmic intensity ratios are more suitable for reproducing intensity ratios in comparison to absolute intensities.

$$x_j = \ln \frac{I_j}{I_{j+k}} \tag{1}$$

with $1 \leq k \leq 14$, where k is mass difference, while masses j vary between 41 and 112, which are, respectively, the minimum and maximum mass number in the data set. I_j and I_{j+k} are the intensities of mass fragments j and $j+k$, respectively. The variables containing only zeros for all objects were removed.

2.2.2. Feature group: autocorrelation [7,8,11]

These features reflect mass differences between peaks. In fact, the new data set may account for losses of particular fragments, such as CH_2^+, from the parent molecule. Thus, the information can be easily interpreted from a chemical point of view. The autocorrelation transform can be computed by the following equation:

$$x_j = \frac{\sum I_k I_{j+k}}{\sum I_k^2} \tag{2}$$

where I_k and I_{j+k} are the intensities of mass fragments j and $j+k$, respectively. Mass difference (k) varied between 1 and 54, *i.e.* lowest and highest mass number in the dataset, respectively. Variables containing only zeros for all objects were also excluded.

2.2.3. Scaling and modeling

As mentioned before, prior to spectral (features) transformation, spectral data were also scaled since the high-intensity ions might have gained too much weight in comparison to the ones with low intensity due to their normalization to a base peak. In this way, the distortion of the results by unconsidered variables may be avoided. The square-root was used as scaling procedure to study the effect of intensity scaling. Nonetheless, the data were also modeled with no scaling in order to prove that the effect of the data preprocessing is not annulled by the autoscaling procedure performed before.

Each class was autoscaled separately after preprocessing, *i.e.* first the column means were subtracted from all values in the corresponding columns and then the mean centered data were divided by standard deviations of the samples from the same column as it has been effectively done in prior studies [11,19]. It is important to note that in absence of autoscaling, only the ions with high intensities are considered by the SIMCA model. Then, independent PCA models using the preprocessed and autoscaled data were calculated according to Eq. (3) [4]:

$$x_{ij}^q = \sum_{a=1}^{\mathrm{Aq}} t_{ia}^q p_{aj}^q + e_{ij}^q \tag{3}$$

where i and j are, respectively, variable and component index. Aq is the number of significant principal components (PC) in class q, while t, p and e are the model scores, loadings and residuals, correspondingly. The score plots for all classes were visually inspected in order to detect outliers. Often, it is commonly believed that autoscaling may add noise to the models by giving more significance to meaningless variables with small random variation. However, this is not the case since such variation would not enter the PCA model if it is random and not dominating, staying instead in the residual matrix.

Due to the lack of a completely independent data set for testing, the validation of the class models had to be carried out by a leave-one-out cross-validation procedure (LOO CV). As the name suggests, LOO CV involves using a single component from the original set as the validation data and the remaining ones as the training data. This is repeated such that component in the data set is used once as the validation data. This is the same as K-fold cross-validation, where K is equal to the number of observations in the data set. In order to assign new objects in the data set to the classes, each of these objects is fitted to each class model and the distance between them is related to their residual standard deviation (Eq. (4)) and the total residual standard deviation of the class (Eq. (5)):

$$(s_k^q)^2 = \frac{\sum_{i=1}^{N_i}(e_{ki}^q)^2}{(N_i - \mathrm{Aq})} \tag{4}$$

$$(s_o^q)^2 = \frac{\sum_{j=1}^{N_j}\sum_{i=1}^{N_i}(e_{ji}^q)^2}{((N_j - \mathrm{Aq} - 1)(N_i - \mathrm{Aq}))} \tag{5}$$

N_i and N_j are, respectively, the number of variables and objects of class q. The subscript k is the object index in the data set and s^2 is the residual variance, while the rest of symbols are in accordance with Eq. (3).

From the class-model standard deviation, an interval around each model (99% confidence limit) can be defined in which there is a high probability of finding a new member of that class. Hence, if the calculated distance is smaller than the limiting one, the unknown is considered to belong to the class. In other words, the classification criterion is that an unknown sample belongs to the class to which is the closest.

In addition to Eq. (4), also referred to as Euclidean distance, the Hotelling T^2 and Q (SPE_x) measure were used [20,21]. Based on the first A PCs in Eq. (3), T^2 can be calculated, providing a test for the deviations in the set of the most important variables (Eq. (6)). Nonetheless, monitoring the model calibration only by T^2 is just not adequate [21], since it will only detect whether or not the variation in the variables in the A PCs plane is larger than can be explained by random noise. Fortunately, Q statistics or distance to the model is capable of, for example, detecting new samples foreign to the calibration data by computing the squared prediction error (SPE_x) of the residuals of a new observation (Eq. (7)) by projecting the squared perpendicular distance of a new multivariate observation into the space. Both Q statistics and T^2 criteria can mask outliers in the data and therefore a more robust approach has been recommended by Hubert et al. [22,23]. Since no problem caused by outliers were observed, the classification result sems to justify the use of Q statistics and T^2 criteria in the present study:

$$T_A^2 = \sum_{i=1}^{A}\frac{t_i^2}{s_{t_i}^2} \tag{6}$$

where $s_{t_i}^2$ is the estimated variance of t_i.

$$\mathrm{SPE}_x = \sum_{i=1}^{k}(x_{\mathrm{new},i} - \hat{x}_{\mathrm{new},i})^2 \tag{7}$$

where k is the number of variables, x_{new} the vector of the new variables and $\hat{x}_{\mathrm{new}}$ into the model (Eq. (3)) using the A first PCs.

3. Results and discussion

Matlab was used to create a PCA model for each of the defined classes with which unknowns could be predicted. Regardless of the preprocessing method or scaling method applied to the spectral data before modeling, nine principal components were able to explain typically at least 70% of the variation in the DMH data while from two to four PCs captured the same variance in TMP data. Meanwhile, the number of PCs for MH class was between five and seven, depending on the spectral transformation and/or scaling, in order to capture at least 70% of the cumulative variation. Interestingly, only one PC was needed for the linear octenes class. As for model 2, two to four PCs were able to capture 85% of the variance in data. It is worth mentioning that such captured values of the variation in the different models have not been taken as cut-off criterion for PCs utilized. Both the eigenvalue criterion [24] and cross-validation were employed to determine the adequate number of PCs for each class, which was substantiated by the successful classification of real GC–MS data. Visual inspection of the score plots did not show any obvious outliers; however, it was observed that objects of the DMH and MH class were overlapping with each other, reducing the distance between both classes. By thoroughly scrutinizing the spectral data, such objects were identified as dimethylhex-3-ene (11) and methylhept-3-ene (8). It was decided that instead of completely excluding these 19 spectra from the current study, a new SIMCA (sub-) model (model 2) with only two classes, *i.e.* 3-DMH and 3-MH, would be built and studied as mentioned before. The remaining spectral data were modeled, as stated, with four classes (model 1). Figs. 2 and 3 exhibit the best calibration models for each class obtained correspondingly in model 1 and 2. The best results with model 1 were obtained after the mass spectra were transformed into autocorrelation features scaled by square-root, while model 2 performed the best after data was transformed into the logarithmic ratio intensities with no previous scaling. It is clear that the classes are mainly separated due to the distance of alien objects to the certain class (Q) and less due to variation in their scores (T^2) (Figs. 2 and 3). In fact, the value of Q may be so small that some objects fall into the space of other classes, particularly visible in the DH class but also in DMH class to some extent in model 1. Similarly, such overlapping of class spaces is self-evident in the 3-DMH (model 2). The results summarized in Tables 1 and 2 corroborate these observations. Table 1 shows that most of the misclassified objects after the LOO CV are placed into the DMH and MH classes despite of the preprocessing method or scaling. The transformation of the original spectral data into spectral features did not seem to reduce the number of misclassified objects. In fact, it seemed to worsen the models and the classification. While the original data spectral data have a span of mass fragment intensities from 0 to 100 due to their normalization to a base peak and scaling such span is reduced in the course of their transformation into spectral features. Consequently, the need for scaling of transformed data is less as can

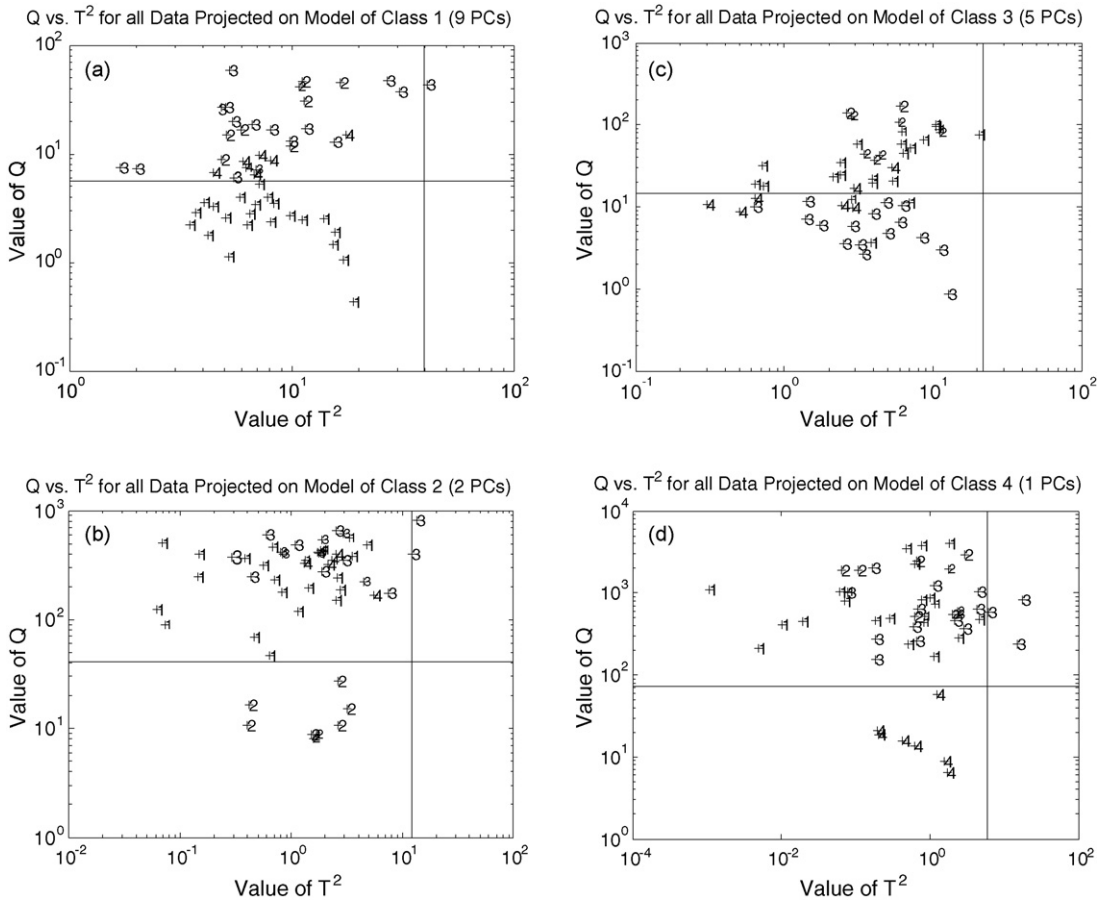

Fig. 2. Calibration model for four classes of octene isomers (model 1). The mass spectral data were transformed into spectral features and scaled (square-rooted). (a) Class 1 refers to DMH; (b) class 2 refers to TMP; (c) class 3 refers to MH and (d) class 4 refers to LO.

Table 1
Cross-validation results of the SIMCA models for the original spectral data and different preprocessing methods including scaling (model 1)

	Class (no. of objects)			
	DMH (22)	TMP (8)	MH (16)	LO (7)
No preprocessing				
Principal components	9	2	5	1
Correctly-classified objects	11	4	8	4
Misclassified objects into another class	5	4	5	2
Misclassified objects into this class	9	1	6	0
Logarithmic intensity ratios transform				
Principal components	9	3	7	1
Correctly-classified objects	9	3	9	2
Misclassified objects into another class	9	4	3	5
Misclassified objects into this class	7	1	13	0
Autocorrelation transform				
Principal components	9	4	7	1
Correctly-classified objects	9	2	7	4
Misclassified objects into another class	9	4	4	2
Misclassified objects into this class	10	1	8	0
Autocorrelation transform + square-root scaling				
Principal components	9	2	5	1
Correctly-classified objects	15	5	8	5
Misclassified objects into another class	4	0	2	0
Misclassified objects into this class	1	2	2	1

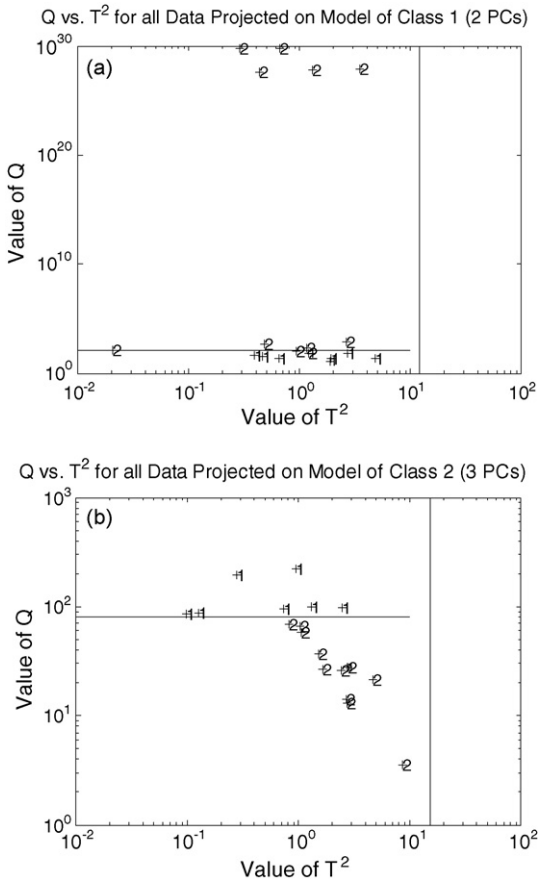

Fig. 3. Calibration model for two classes of octene isomers (model 2). The mass spectral data were transformed into spectral features. (a) Class 1 refers to 3-DMH and (b) class 2 refers to 3-MH.

Table 2
Cross-validation results of the SIMCA models for the original spectral data and different preprocessing methods including scaling (model 2)

	Class (no. of objects)	
	3-DMH (8)	3-MH (11)
No preprocessing		
Principal components	3	4
Correctly-classified objects	3	7
Misclassified objects into another class	4	1
Unclassified objects	1	3
Logarithmic intensity ratios transform		
Principal components	2	3
Correctly-classified objects	4	10
Misclassified objects into another class	0	1
Unclassified objects	4	0
Autocorrelation transform		
Principal components	2	3
Correctly-classified objects	4	6
Misclassified objects into another class	3	2
Unclassified objects	1	3
Logarithmic intensity ratio + square-root scaling		
Principal components	2	3
Correctly-classified objects	4	9
Misclassified objects into another class	2	0
Unclassified objects	2	2

be seen from the LOO CV results in Table 2. Fortunately, the separation between the classes improved dramatically when the spectral data was scaled (square-rooted) prior to the autocorrelation transformation. The beneficial effect of (square-root) scaling for this kind of application has been already mentioned in a previous study [19]. Table 2 demonstrates that on this particular training data set (model 2), cross-validation results are improved by any of the different preprocessing method. Once again, the beneficial effect of data preprocessing is observed. In contrast to the cross-validation results with model 1, the logarithmic intensity ratios transform brought the best results for this data set. Clearly, it is confirmed that preprocessors that concentrate and emphasize frequency information are the most effective for mass spectral data as it has been already reported by McGrill and Kowalski [17]. Four objects in the 3-DMH class were not possible to classify whether the data were transformed or not. After a detailed examination, these components have been identified as *cis*- and *trans*-2,2-dimethylhex-3-ene and 2,3-dimethylhex-3-ene. These components account for less than 3% of the total concentration of octene isomers, so it will not significantly affect the performance of the models while testing "real" GC–MS data. In general, cross-validation results are not affected much by the scaling methods since the span of the mass fragment intensities has been reduced in the course of their spectral (features) transformation [11]. Even though the training models may seem to have low classification capabilities, the truth is that both models perform adequately when it comes to classify data originated in the dimerization of 1-butene, which is discussed posteriorly.

The ultimate goal of any pattern recognition technique is to be applied on real data, therefore the components can be grouped according to the characteristics of each class, since otherwise it had been impossible to obtain an accurate identification of these products by regular analytical means. In this study, real GC–MS data collected from the dimerization of 1-butene over heterogeneous catalysts in the liquid phase was classified using the best models and data preprocessing techniques in order to understand the product distribution and the mechanism of this reaction. All spectra recorded in the octene region were used to obtain spectra of pure components for each chromatographic peak. The "real" test set was preprocessed accordingly to the model that showed the best results for model 1, *i.e.* autocorrelation transform plus square-root scaling (model 1) and logarithmic intensity ratios (model 2), and projected into the models. The results of the GC analysis and interpretation by both SIMCA models have been gathered in Fig. 4, where class 1 refers to DMH and 3-DMH, class 2 to TMP, class 3 to MH and 3-MH and finally class 4 to LO. It was expected that no linear octenes would be detected since it is very unlikely that such molecules are formed due to mechanistic constrains [2]. Most of the peaks have been identified as DMH, followed by TMP and MH in that order. Unidentified objects in the real GC–MS spectra were still present after classification. A reason could be the difficulty of retrieving pure mass spectra for a particular compound from strongly overlapped peaks. The total concentration of these unknown components is negligible; hence it does not affect the overall quality or performance of the SIMCA models. Although Fig. 4 is just a representative

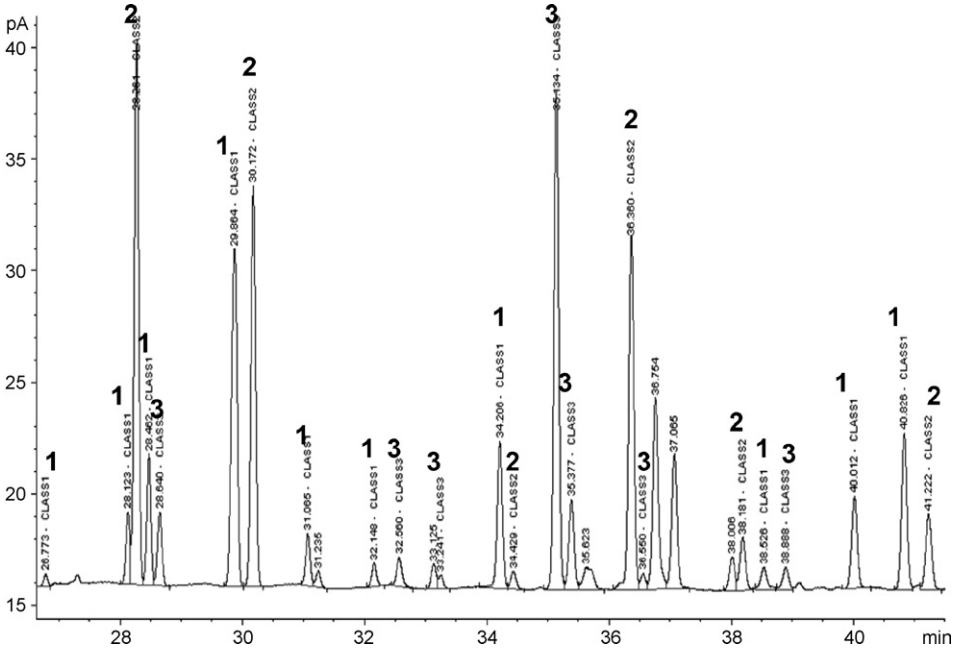

Fig. 4. GC–MS analysis and classification of a fraction of the acyclic-octene region. Class 1 refers to DMH and 3-DMH, class 2 to TMP, class 3 to MH and 3-MH and class 4 to LO.

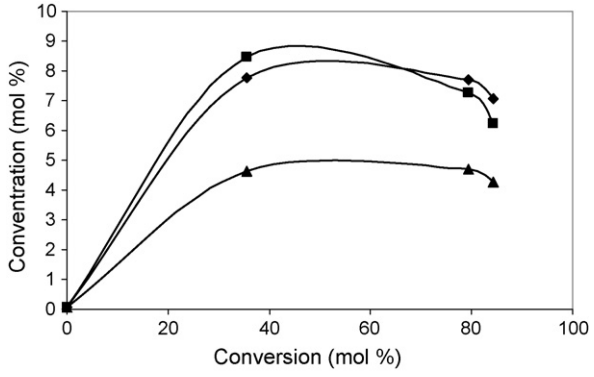

Fig. 5. Concentration profile of octene isomers as a function of butene conversion. Isomer class: DMH (■); TMP (♦) and MH (▲).

section of the GC chromatograph in the octene region; nevertheless, the conclusions presented are further confirmed by Fig. 5 where classification results were combined with experimental results. Butene isomers in the dimerization/oligomerization over zeolitic catalysts are found to undergo several consecutive reactions, *i.e.* oligomerization and cracking, forming a wide range of molecules from propene up to dodecenes; thus, the concentration of the octene isomers decrease, while the oligomer products, *i.e.* molecules greater than nonenes, increase in concentration. Ultimately, it means that this specific reaction is not primarily yielding octenes but oligomers.

It is worth noting that prior to using "real" data, a model mixture with the most characteristic commercially-available compounds, *i.e.* 2,4,4 trimethyl-1-pentene; 2,3 dimthyl-2-hexene; 2-methyl-1-heptene and 1-octene, from each class was analyzed by GC and the developed SIMCA models was able to classify them accurately.

4. Conclusions

Soft Independent Modeling of Class Analogy (SIMCA) pattern recognition has effectively led to a novel strategy of classifying original and preprocessed mass spectra of acyclic octene isomers into four main classes. These detailed classes are principally defined according to the branching degree of the molecule but also to the position of the double bond, thus the classes have been tagged as DMH (including 3-DMH), TMP, MH (including 3-MH) and LO. It was observed that the transformation of spectral data into spectral features with or without scaling is essential for the development of models for octenes mass spectra mainly due to their diversity. In model 1, the autocorrelation transform of (square-rooted) scaled data showed the overall best performance. On the other hand, the logarithmic intensity ratios transform with no prior scaling of the data brought the most improvements to model 2.

The developed SIMCA models have contributed to detailed identification of acyclic octene isomers by using real GC–MS data from the dimerization of 1-butene, which, after further analysis of other products, will be used for elucidation of the reaction mechanism.

Acknowledgements

This work is part of the activities at Åbo Akademi Process Chemistry Centre within the Finnish Centre of Excellence Program (2000–2011) by the Academy of Finland. Financial support from the Graduate School of Materials Research for José Ignacio Villegas is also gratefully acknowledged.

References

[1] M.L. Honkela, O.I. Krause, Ind. Eng. Chem. Res. 44 (2005) 5291.
[2] J.M. Martinis, G.F. Froment, Ind. Eng. Chem. Res. 45 (2006) 940.
[3] S.A. Mjøs, Anal. Chim. Acta 488 (2003) 231.
[4] S. Wold, Patterns Recog. 8 (1976) 127.
[5] S. Wold, M. Sjöström, in: B.R. Kowalski (Ed.), Chemometric: Theory and Application, ACS Symposium Series, No. 52, Am. Chem. Soc., 1977, p. 243.
[6] W.J. Dunn III, Anal. Chem. 56 (1984) 1308.
[7] W.J. Dunn III, S.L. Emery, W.G. Glen, Environ. Sci. Technol. 23 (1989) 1499.
[8] K. Vermuza, W. Werther, J. Chem. Inf. Comput. Sci. 36 (1996) 323.
[9] H. Lohninger, K. Vermuza, Anal. Chem. 59 (1987) 236.
[10] D.R. Scott, Anal. Chem. 58 (1996) 881.
[11] D. Kubička, M. Rönnholm, S.-P. Reinikainen, T. Salmi, D. Yu. Murzin, Anal. Chim. Acta 537 (2005) 339.
[12] B. Tan, J.K. Hardy, R.E. Snavely, Anal. Chim. Acta 422 (2000) 37.
[13] M. Praisler, J. Van Bocxlaer, A. De Leenheer, D.L. Massart, Turk. J. Chem. 26 (2002) 45.
[14] L. Soják, G. Addová, R. Kubinec, A. Kraus, A. Boháč, J. Chromatogr. A 1025 (2004) 237.
[15] NIST05 Mass spectral database.
[16] (a) S.-P. Reinikainen, SIMCA Tool Ver. 0. 5, Lappeenranta University of Technology, 2004;
(b) M.A. Sharaf, D.L. Illman, B.R. Kowalski, Chemometrics, Wiley, New York, 1986.
[17] J.R. McGill, B.R. Kowalski, J. Chem. Inf. Comput. Sci. 18 (1978) 1.
[18] B. Curry, D.E. Rumelhart, Tethahedron Comput. Methodol. 3 (1990) 213.
[19] D. Kubička, S.-P. Reinikainen, D. Yu. Murzin, in: A.L. Pomerantsev (Ed.), Modern Methods of Multivariate Data Analysis, Nova Science Publishers, NY, 2005, pp. 95–101.
[20] H. Hotelling, in: C. Eisenhart, M.W. Hastay, W.A. Wallis (Eds.), Techniques of Statistical Analysis, McGraw-Hill, New York, 1947, pp. 113–184.
[21] F.B. Alt, N.D. Smith, Multivariate process control, in: P.R. Kishnaiah, C.R. Rao (Eds.), Handbook of Statistics, vol. 7, North-Holland, Amsterdam, 1998, pp. 333–351.
[22] M. Hubert, P.J. Rousseeuw, K. Vanden Branden, Technometrics 47 (2005) 64.
[23] K. Vanden Branden, M. Hubert, in: J. Antoch (Ed.), Proceedings in Computational Statistics, Compstat 2004, Springer-Verlag, Heidelberg, 2004, pp. 1925–1932.
[24] D.L. Massart, B.G.M. Vandeginste, L.M.C. Buydens, S. de Jong, P.J. Lewi, J. Smeyers-Verbeke, C.K. Mann, Appl. Spectrosc. 52 (1998) 302.

Available online at www.sciencedirect.com
ScienceDirect
Talanta 72 (2007) 1342–1347
Talanta
www.elsevier.com/locate/talanta

Running buffers for determination of chromium(VI)/(III), cobalt(II) and zinc(II) in complex matrices by capillary electrophoresis with contactless conductivity detection

Li-Shi Wang [a,*], Shui-Feng Zhang [a], Zhi Dang [a], Xiao-Xiao Liu [a], Xin-Jian Huang [a], Ming-Wei Xiao [a], Zuan-Guang Chen [b]

[a] *College of Environmental Science and Engineering, South China University of Technology, Guangzhou 510640, PR China*
[b] *School of Pharmaceutical Science, Sun Yat-Sen University, Guangzhou 510275, PR China*

Received 25 November 2006; received in revised form 17 January 2007; accepted 17 January 2007
Available online 30 January 2007

Abstract

Complex matrices and rather high acidity in environmental samples are often the impelling challenges for the used running buffers of capillary electrophoresis. Twelve binary acid–base buffers were evaluated for separation of Cr(VI)/Cr(III), Co^{2+} and Zn^{2+} in a sample containing various salts by capillary electrophoresis with contactless conductivity detector. The malic acid (MA) systems including MA–His (histidine), MA–Arg (arginine) and MA–Tris (tris(hydroxymethyl)aminomethane) were selected as the candidates with powerful separation efficiency and good response sensitivity. In the MA–Tris buffer, optimization were further carried out in terms of the pH value and the concentration of MA, and the optimal conditions were obtained as 6 mM MA–Tris and 2 mM 18-crown-6 at pH 3.5. Furthermore, a real application was demonstrated by analyzing the plating rinse water (pH 0.8), in which the Ca^{2+}, Na^{+}, Cr(VI)/Cr(III), Co^{2+} and Zn^{2+} were all detected by adjusting at pH 3.5 with 5% (v/v) diluent ammonia. Both the cations, e.g., K^{+}, Ca^{2+}, Na^{+}, Mg^{2+}, and the common high concentration anions in the sample, e.g., Cl^{-}, SO_4^{2-} and NO_3^{-} did not cause any disturbance to the concerned analytes.

Keywords: Capillary electrophoresis; Contactless conductivity detection; Chromium(VI)/(III); Cobalt(II); Zinc(II); Speciation

1. Introduction

The speciation analysis of chromium [1–4] attracted lots of interests because of its important role in life science and environmental analysis. Cr(III) is an essential and necessary trace element for humans, however, Cr(VI) is very noxious, which hurts cardiovascular system, kidney, liver and hematogenic function. In environmental analysis, thus, the speciation of chromium shows more significant than the determination of total chromium [5,6].

Capillary electrophoresis is a very powerful instrument for speciation analysis. Many methods of determination had been developed for capillary electrophoresis to analysis the speciation of chromium including UV–vis detector [3,7], graphite furnace atomic absorption spectrometry (GFAAS) [8], inductively coupled plasma mass spectrometry (ICP-MS) [9], flame atomic absorption spectrometry [10], and chemiluminescence determination [11], etc. A procedure of derivatization by pre-capillary [12] or in-capillary [13] complexation was commonly used in most of the reported methods, by which some complexing reagents, such as iminodiacetic acid, nitrilotriacetic acid, *N*-(2-hydroxyethyl)ethylenediaminetriacetic acid, trimethylenediaminetetraacetic acid, and ethylenediaminetetraacetic acid [3], diethylenetriaminepentaacetic acid [9], 2,6-pyridinedicarboxylic acid [12], 1,5-diphenylcarbazide [13], *trans*-1,2-cyclohexanediaminetetracetic acid [3,14,15], etc. were added into the running buffers to form complex compound with the analytes, e.g., Cr(III). However, the whole analysis procedure commonly required of expensive instruments and complicated manipulation.

An alternative technology has been developed for CE with a simple detection configuration, namely, the contactless conduc-

* Corresponding author. Tel.: +86 20 88586766.
E-mail address: wanglsh@scut.edu.cn (L.-S. Wang).

0039-9140/$ – see front matter © 2007 Elsevier B.V. All rights reserved.
doi:10.1016/j.talanta.2007.01.041

tivity detector (CCD) based on two tubular detective electrodes [16,17]. The electrodes of the CCD did not contact with the solution inside the capillary directly, thus, electrode contamination, which was common in the electrochemical detector, e.g., amperometric detector, could be avoided effectively. Also, no special and troublesome interface was required, so the installation was very easy and convenient, and it was only needed to push the capillary through both the tubular electrodes. Besides, a detective window formed by a burning procedure required by UV detection was abolished, and the detective position can be placed at any desired place of the capillary by moving the CCD. CCD has been employed to analysis of inorganic anions and cations [18,19], as well as some organic compounds, such as aliphatic ammonium compounds [20], mono- and disaccharides [21], herbicides and its metabolites [22], chemical warfare agent degradation products [23], and amino acids [24–26], etc. CCD has also been employed for Cr(III) analysis [27], and for simultaneous analysis of Cr(III) and Cr(VI) [28].

The basic principle of CCD is based on the difference between the sample zone and the background electrolyte (BGE). Therefore, the characteristic of the selected buffers will greatly affect the response sensitivity of CCD. Katzmayr et al. [29] gave a theoretical calculation for selection of suitable co- and counterion to construct desired buffers for conductivity detection (CD) of low-molecular-mass anions, and an optimal signal-to-noise (S/N) ratio was demonstrated to be the BGE with low-mobility co- and counterion by an actual example. Zemann [30,31] also suggested that, to balance the separation efficiency and detection sensitivity, some ampholytes with low conductivity (i.e., mobility) and high ion strength can be considered firstly.

For common inorganic ions, therefore, it is better to employ the buffer consisting of organic acids (e.g., MA, MES) and/or ampholytes (e.g., His), which are both characterized as low conductivity and high ion strength. However, a complexing reaction often happened between the transition metal ions and the organic electrolytes (e.g., MES–His system) unavoidably, which frequently led to deterioration of response [18], despite the improvement of separation which could be expected. Besides, in some real samples, high salt concentration and/or high acidity are encountered [32,33], which is an impelling challenge for the used running buffers of capillary electrophoresis. And their analysis often requires a minimum pretreatment consisting of a dilution.

In this work, we focused on evaluating both the separation and response sensitivity of the running buffers for analyzing Cr(VI)/Cr(III), Co(II), and Zn(II) in the complex matrix. Some electrolytes, which met the demand for separation of the speciation of chromium by capillary electrophoresis with CCD according to Katzmayr's discussion [29], were selected to construct 12 binary acid–base buffers; and those electrolytes included four organic acids: the monocarboxylic acid α-hydroxyisobutyric acid (HIBA), two dicarboxylic acids malic acid (MA) and tartaric acid (TA), and the tricarboxylic acid citric acid (CA); as well as three organic bases: histidine (His), arginine (Arg) and tris(hydroxymethyl)aminomethane (Tris). Some comparison among such buffers were carried out, and the obtained results offers us an insight into the selection of a suitable buffer for separation of the chromium speciation Cr(VI)/Cr(III), as well as Co(II), Zn(II) in the complex environmental samples.

2. Experimental

2.1. Reagents and samples

All reagents were of analytical grade purity. The cations of sodium, potassium, zinc, cobalt, chromium(III), ammonium, calcium and magnesium were all prepared from the relevant chloric salts except that chromium(VI) was prepared from potassium dichromate, and they, as well as acetic acid, ammonia, were all the products of Guangzhou Chemical Reagents Co. (Guangzhou, China). All of the standard samples were prepared from relevant stock solutions of 20 mM in terms of expected proportion. The reagents used to prepare the running buffers included MA, Tris, 18-crown-6, His, TA, CA, Arg which were all from Sigma (St. Louis, MO) except that the HIBA was the product of Aldrich. MA of 40 mM was freshly prepared daily and stored in an icebox at a constant temperature of 4 °C in order to avoid its degeneration.

2.2. Electrophoresis system

A home-made compact CCD excited by a square wave signal of 9 V (peak-to-peak) and 198 kHz was used [34]. The function generator, mainly consisting of a component (model NE555P, Texas Instruments, TX, USA), provides a square wave excitation signal with a peak-to-peak amplitude of 9 V. The operational amplifier (model TL081, Texas Instruments, TX, USA) was fitted with a feedback resistor of 100 kΩ, thus, transformed the cell current to the cell output voltage, then rectified and amplified. At last the signal was registered by an A/D converter in a C8051F020 chip obtained from Cygnal, USA, and then was transmitted to a PC through Rs232 interface. The data display and disposal were performed with a software written with C++ Builder. The excitation frequency and output voltage of this detector was monitored by a dual-channel oscilloscope (Model ST4328, Ningbo Zhongce Electron Ltd., Ningbo, China).

A purpose-made electrophoretic instrument was used for all measurements. The High-voltage power supply was easy to be adjusted in the range of 0–30 kV consecutively. Fused-silica capillaries coated with polyimide of 150 μm i.d. and 300 μm o.d. were obtained from Yongnian Fiber Co. (Yongnian, Hebei, China).

The electrophoresis was carried out by applying a desired voltage (related to earth ground) between the running buffer reservoir and the grounded reservoir. Each new capillary was activated by sequentially flowing (pressure-driven by a medicine syringe) 0.5 M solution of sodium hydroxide, deionized water, and running buffer for 20 min, respectively. The capillary was then equilibrated in the buffer under a voltage of 20 kV for about 20 min prior to sample injection. Otherwise, pretreatment was carried out daily by washing with 0.1 M sodium hydroxide for 5 min. The capillary was rinsed with 3 mL running buffer between runs to improve reproducibility. Gravity injection was

Table 1
Evaluation of separation between K^+ and NH_4^+ (R_{s1}), Cr^{3+} and Mg^{2+} (R_{s2}), Cr^{3+} and Co^{2+} (R_{s3}), Co^{2+} and Zn^{2+} (R_{s4}) in different running buffers

Evaluation	HIBA-based			His [b]	MA-based			TA-based			CA-based		
	Arg	Tris	His [a]		Arg	Tris	His	Arg	Tris	His	Arg	Tris	His
R_{s1}	1.64	1.78	- [c]	- [c]	1.72	1.84	- [c]	2.03	1.96	- [c]	2.05	2.30	- [c]
R_{s2}	0.95	1.25	1.35	- [c]	2.12	2.08	2.62	2.14	3.72	3.4	2.58	2.93	3.71
R_{s3}	- [c]	- [c]	- [c]	0.18	2.65	2.75	3.09	2.32	2.97	3.67	- [c]	∅ [d]	∅ [d]
R_{s4}	0.78	0.84	0.47	0.31	1.71	1.80	2.17	3.67	4.15	∅ [d]	∅ [d]	∅ [d]	∅ [d]
$R_{s,t}$ [e]	<0.95	<1.25	<1.35	<0.31	>1.71	>1.80	>2.17	>2.14	>2.97				
S_a/N [f]					118	123	127	86	85				

[a,b] See the literature [28]. [c] $R_s < 0.10$. [d] The peak is not present in the time scale observed (90 min). [e] General evaluation for the separation of Cr^{3+}, Co^{2+} and Zn^{2+}. [f] Average of the S/N ratios of Cr^{3+}, Co^{2+} and Zn^{2+}.

performed by elevating the sample vials to a height of 10 cm for a specified time interval.

All of the tested buffers were evaluated according to the separation resolution (R_s) value of each two adjacent peaks in the obtained electropherograms. The R_s value was defined as: $R_s = (t_2 - t_1)/[(1/2)(t_{w2} + t_{w2})]$, where t_2 and t_1 values are the migration time for the second and first peaks of the analytes, respectively, and t_{w1} and t_{w2} are the peak width values for the first and second peaks of the analytes, respectively [35].

3. Results and discussion

3.1. Evaluation of buffers

A series of buffers were assembled in pairs based on four organic acids: the monocarboxylic acid HIBA, two dicarboxylic acids MA and TA, and the tricarboxylic acid CA, as well as the organic bases: His, Arg and Tris, respectively. Thus 12 groups were obtained as HIBA–Arg, HIBA–Tris, HIBA–His, MA–Arg, MA–Tris, MA–His, TA–Arg, TA–Tris, TA–His, CA–Arg, CA–Tris and CA–His. Such groups all consisting of 6 mM acid and 6 mM base were each adjusted at pH 3.4 with 10% (v/v) acetic acid (leading to about 85 mM acetic acid) except that the buffer of 5 mM HIBA and 5 mM His at pH 3.75 and the buffer of 4 mM His at pH 3.4 were prepared according to the literature [28], and 2 mM 18-crown-6 was added into each buffer as a complexing reagent for separation of K^+ and NH_4^+. Electrophoresis was carried out in each buffer mentioned above by imposing a high voltage of 7.8 kV. To examine the separation capacity of the tested buffers, a standard sample containing 250 μM NH_4^+, Cr^{3+} and 400 μM K^+, Co^{2+}, Zn^{2+}, Ca^{2+}, Na^+, Mg^{2+} was purposely injected for 5 s. The evaluation of separation was mainly carried out for cations, including K^+ and NH_4^+ (R_{s1}), Mg^{2+} and Cr^{3+} (R_{s2}), Cr^{3+} and Co^{2+} (R_{s3}), Co^{2+} and Zn^{2+} (R_{s4}), while the evaluation of S/N ratio was only for the heavy metal cations; and the common cations, such as Ca^{2+}, Na^+ and Mg^{2+} were not the preferential consideration in our present work. The obtained results were listed in Table 1.

As the results shown in Table 1, in the HIBA-based systems, the peaks of Co^{2+} and Cr^{3+} nearly overlapped completely ($R_{s3} < 0.1$), and the separation resolution between Co^{2+} and Zn^{2+} (R_{s4}) was also less than 1, which means that the HIBA-based buffers could not make the components separated completely. It was also observed that the buffer systems of 5 mM HIBA–His (pH 3.75) and 4 mM His (pH 3.4) [28] showed poor separation capacitance, which could be ascribed to the use of a broader capillary and higher concentration sample under our experimental conditions. Instead, in the dicarboxylic acid MA or TA or tricarboxylic acid CA buffer systems, an evident enhancement in the separation efficiency was reached (Table 1). In the MA-based systems, Cr^{3+}, Co^{2+}, Zn^{2+} were all separated completely and the R_s values were all greater than 1.7. Best separation was obtained in the MA–His buffer giving $R_{s3} = 3.09$, between Cr^{3+} and Co^{2+}. In the TA-based buffers, the results showed a better separation for Cr^{3+}, Co^{2+}, Zn^{2+}, as well as Na^+, Ca^{2+} and Mg^{2+}. The three CA-based buffers showed the most excellent separation between Cr^{3+} and Mg^{2+}. However, it was observed that the signal-to-noise ratios for Cr^{3+}, Co^{2+}, especially for Zn^{2+} in the TA-based systems decreased greatly at pH 3.4 compared with that in the MA-based systems. Even, at pH 3.5, the peak of Zn^{2+} was not presented in the observed time scale (90 min). Similarly, in the CA-based systems both the peaks of Co^{2+} and Zn^{2+} were also not observed. So it was obvious that a strong complexation reaction occurred between the CA anions and the metal cations, as well as between the TA anions and the metal cations. In summary, in despite of the challenges from the broad

capillary of 150 μm i.d. and the analytes in the complex matrix, the MA-based buffers still showed a best compromise between the powerful separation efficiency and the sensitive response.

Electrophoretic separation of Cr(VI) (refer to Fig. 4) were carried out by cathodic end injection, where the Cr(VI) peak was completely separated from a very big co-migrating peak of Cl^-, SO_4^{2-} and NO_3^- ascribed to their very high concentration under the used experimental conditions. Consequently, considering the relative slower migration rate of Cr(VI), this co-migrating peak would not bring any interference with the concerned peaks of $HCrO_4^-$.

The 18-crown-6 was known as an inclusive complexing agent for K^+, which was frequently employed to form a complex with K^+, thus, different electromigration rates could be reached between the NH_4^+ and K^+ complex [27,36]. Another advantage of 18-crown-6 was that it did not increase the electrolyte conductivity [27]. Under the tested experimental conditions (pH 3.5), however, an interesting phenomenon (Table 1) was observed that the NH_4^+ and K^+ could not be separated completely by adding 2 mM 18-crown-6 into the His-based buffers. On the contrary, such two cations were completely separated in any other tested buffer without His under the same electrophoretic conditions. Consequently, it was very evident that some molecular interaction happened between His and 18-crown-6. As far as the configurations were concerned, it can be concluded that, under the used experimental conditions, an interaction happened between the imidazolium group of His and the cavum structure of the 18-crown-6, which was a hindrance to forming a complex compound between the crown ether and K^+, thereby, the separation of K^+ and NH_4^+ was weaken.

The experimental results listed in Table 1 showed that these three organic bases, i.e., Arg, Tris and His, exhibited as an important modifier for separation as well as a similar influence on the separation tendency of the concerned analytes (as marked by the arrows in Table 1), respectively.

By intercomparsion, three excellent buffers for separation of Cr^{3+}, Co^{2+} and Zn^{2+} with CCD were picked out as MA–His, MA–Tris and MA–Arg, respectively. Under the given conditions, the buffer of 6 mM MA–His showed the optimal separation for the tested components, however, which could not make the K^+ and NH_4^+ separated completely by adding 2 mM 18-crown-6. The buffer of 6 mM MA–Tris system demonstrated to be a little better than the buffer of 6 mM MA–Arg. Here we mainly continued to optimize the MA–Tris system for the separation of Cr^{3+}, Co^{2+} and Zn^{2+}.

3.2. Effects of pH on the separation

In the initial experiments, in each tested buffer, we found that the pH in the range 3.2–3.8 showed little effects on the separation of Cr(VI) from the other anions, e.g., Cl^-, SO_4^{2-} and NO_3^-. So our efforts were mainly focused on optimizing the separation of cations. Both the migration time and peak height as functions of pH of the buffer were plotted in Fig. 1. Increasing the pH value resulted in an evident enhancement of the separation among Cr(III), Zn(II) and Co(II). For example, by increasing the pH from 3.2 to 3.6, the R_{s3} value between Cr^{3+} and Co^{2+} increased from 1.6 to 3.1. It was apparent that a better separation among Na^+, Ca^{2+}, Mg^{2+} was achieved in the range of pH 3.5–3.6. As shown in the peak height evolvement (Fig. 1), it can be noticed that at pH 3.8 the responses of Co^{2+}, Zn^{2+} decreased significantly, and the Zn^{2+} even presented as a weak negative peak ascribed to its strong complexing reaction with MA. Despite the uncertain evolvement trend shown by the measured baseline noise, a relative smooth baseline was certain to be observed at about pH 3.5. As a result, in the buffer of 6 mM MA–Tris, the optimal pH was at 3.5 for the separation of Cr^{3+}, Co^{2+} and Zn^{2+}. Similar results were observed in the buffer of 6 mM MA–His system, where the electromigration showed a more sensitive dependence on the pH value (the data was not shown).

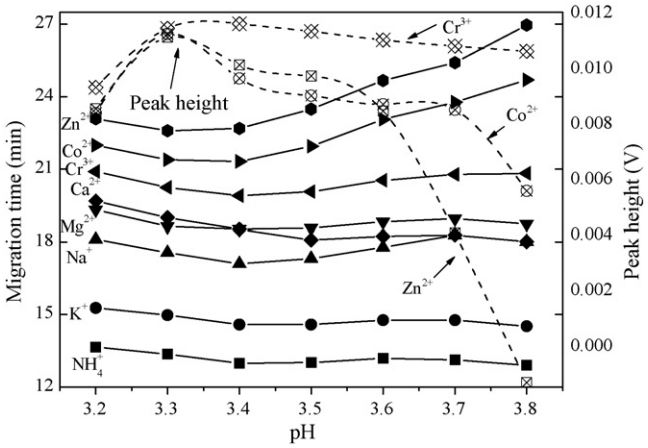

Fig. 1. Migration time and peak height as functions of pH in the MA–Tris buffer. Conditions—capillary: 90 cm (effective length 60 cm); gravity injection: anodic end, 10 cm for 3 s; buffer: 6 mM MA–Tris, 2 mM 18-crown-6; separation: 8.2 kV; sample: NH_4^+, 100; K^+, 500; Na^+, Ca^{2+}, Mg^{2+}, Zn^{2+}, Co^{2+}, Cr^{3+}, 400 μM.

3.3. Effects of the MA concentration on separation

The dependence of migration time on MA concentrations was showed in Fig. 2. By increasing the concentration of MA from 2 mM to 8 mM, the best separation was obtained at 6 mM MA by immobilizing Tris at 6 mM. The separation among Cr^{3+}, Co^{2+} and Zn^{2+} was improved by increasing the concentration of MA. However overlap happened between Cr^{3+} and Co^{2+} when the concentration of MA was less than 3 mM.

In the MA–His buffer, a similar dependence of MA was also observed and the best compromise between separation and sensitivity was obtained as MA in the range from 5 mM to 6 mM by immobilizing the concentration of His at 6 mM.

3.4. Pretreatment and analysis of real sample

The above results demonstrated that electromigration rates of the analytes showed a sensitive dependence on the pH value of the running buffer. Thus, a procedure of pretreatment of the real samples was necessary to improve the separation. Fig. 3a shows the electropherograms of a standard sample in the buffer of 6 mM MA–Tris and 2 mM 18-crown-6 at pH 3.5. In the exam-

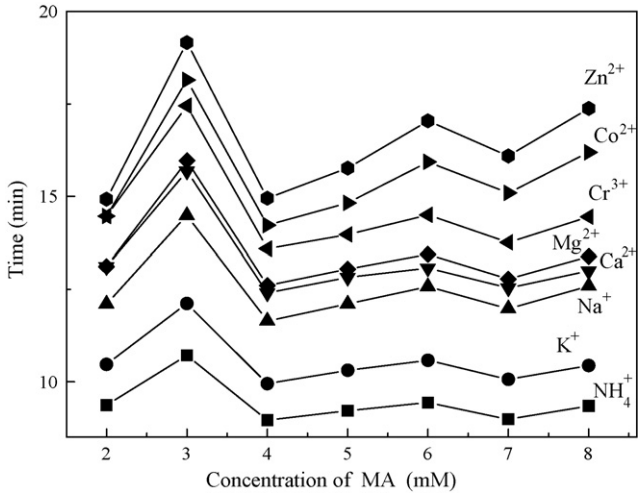

Fig. 2. Migration time vs. the concentration of MA for the cations. Conditions as in Fig. 1 except immobilizing 6 mM Tris and 2 mM 18-crown-6, pH 3.5; separation, 12.2 kV.

ined concentration range of 5.0–400 μM (conditions—capillary: 90 cm; detective position: 65 cm from the anodic end; injection time: 10 s; separation: 9.0 kV), the correlation coefficients (r) for the peak areas were all over 0.9993 ($n = 5$), and a higher concentration range over than 400 μM for each ion was not examined. The relative standard deviations (R.S.D., %, $n = 5$) for the intraday reproducibility of peak areas and migration times were less than 4.90% and 3.72%, respectively. The limits of detection (LODs) for Cr(VI)/Cr(III), Co^{2+} and Zn^{2+} (the electropherogram of Cr(VI) can refer to Fig. 4) were obtained as 3.5 μM, 3.9 μM, 4.4 μM and 4.3 μM, respectively, in terms of three times noise in a standard solution of 50 μM solutes. Compared with the reported results [28] using CCD, our LODs were about one order of magnitude higher, which could be ascribed to some factors from the hardware, e.g., the inexpensive components employed. Further evaluations were carried out in the buffers, 6 mM MA–Tris (pH 3.5) and 4.5 mM His (pH 3.4) [28], respectively, and two LODs with same magnitude were obtained, which indicated that our buffer matched the CCD very well. Fig. 3b is the electropherograms of the real wastewater from the plating factory, and it was diluted with deionized water, adjusted using 5% (v/v) ammonia, and the resulting sample was 300 times dilution at pH 3.5. The results showed that the baseline was smoother and more stable, and the peaks were sharp without overlapping. The disadvantageous aspect was that the pretreatment procedure led to existence of lots of NH_4^+ in the sample solution, thereby, made the peaks of NH_4^+ and K^+ overlapped completely. As a contrast, a real sample of 250 times (pH 0.9) dilution with deionized water was injected in the same buffer system (Fig. 3c). Despite complete separation reached, somewhere the baseline was instable. Besides, the peak response was weaker than that in Fig. 3b ascribed to that the original components in the plating wastewater were very complex with a rather lower pH value around 0.8. As a result, for a rather acidic water sample, e.g., plating wastewater, it is feasible and necessary to adjust the pH to an appropriate value using the suitable basic solution, e.g., diluted ammonia.

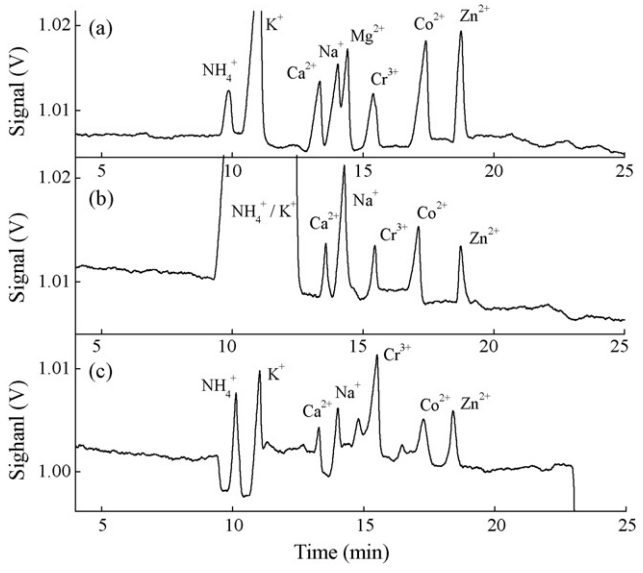

Fig. 3. Electropherograms of the samples: (a) standard sample; (b) real sample diluted to 300 times, pH 3.5 and (c) diluted to 250 times, pH 0.9. Conditions—capillary: 82 cm (effective length 47 cm); gravity injection: anodic end, 10 cm for (a) 3 s, (b) 5 s and (c) 5 s, respectively; buffer: 6 mM MA–Tris, 2 mM at pH 3.5 18-crown-6; separation: 7.8 kV; standard sample: NH_4^+, 100; K^+, 500; Na^+, Ca^{2+}, Mg^{2+}, Zn^{2+}, Co^{2+}, 400 μM; Cr^{3+}, 200 μM.

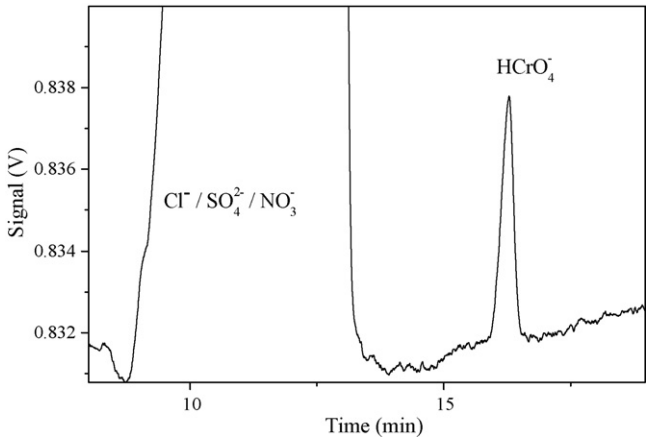

Fig. 4. Electropherogram of Cr(VI) in the plating wastewater. Conditions—capillary: 90 cm (effective length 40 cm); gravity injection: cathodic end, 10 cm for 5 s; and the other conditions as in Fig. 3.

Dual opposite end injection [19,28] provides an approach for simultaneous determination of anions and cations by capillary electrophoresis with CCD. In our initial experiments, simultaneous determinations of Cr(III) and Cr(VI) in standard solutions were also successfully carried out by dual opposite end injection. However, when it related to the real sample, an unavoidable interference was observed from the rather broad co-migrating peak of SO_4^{2-}, Cl^-, NO_3^- (Fig. 4), as well as the high concentration of NH_4^+ (Fig. 3b). Consequently, the determinations of Cr(III) and Cr(VI) were only carried out by anodic end injection and cathodic end injection, respectively.

The results for determination of the Cr(VI), Cr(III), Co^{2+} and Zn^{2+} in a plating wastewater sample were obtained as 17.24 mM, 30.31 mM, 31.52 mM and 24.34 mM, respectively,

and the R.S.D.% of three determinations were all less than 5.30%.

4. Conclusions

In this work, we demonstrated that 12 similar electrolyte systems showed different separation capacitances for chromium(VI)/(III), cobalt(II) and zinc(II) by capillary electrophoresis with CCD, and three MA-based buffers, i.e., MA–Tris, MA–His and MA–Arg were demonstrated to be the most feasible buffers by balancing the separation efficiency and response sensitivity. An example for analysis of a complex wastewater sample from plating factory was demonstrated in the buffer of 6 mM MA–Tris, 2 mM 18-crown-6, pH 3.5.

Acknowledgements

Financial support from the National Natural Science Foundation of China (Nos. 20475018, 40502031), the Key Program of Guangdong Nature Science Foundation (No. 05103552) and the Science and Technology Program of Guangdong Province (No. 2004B20501006), are gratefully acknowledged.

References

[1] J. Chwastowska, W. Skwara, E. Sterlińska, L. Pszonicki, Talanta 66 (2005) 1345.
[2] H. Cui, R. He, J. Wang, Talanta 70 (2006) 139.
[3] R.F. Carbonaro, A.T. Stone, Anal. Chem. 77 (2005) 155.
[4] A.A. Mohamed, A.T. Mubarak, Z.M.H. Marstani, K.F. Fawy, Talanta 70 (2006) 460.
[5] D.G. Themelis, F.S. Kika, A. Economou, Talanta 69 (2006) 615.
[6] D.L. Rodman, N.A. Carrington, Z.-L. Xue, Talanta 70 (2006) 668.
[7] J.I. Friese, B. Ritherdon, S.B. Clark, Z. Zhang, L. Rao, D. Rai, Anal. Chem. 74 (2002) 2977.
[8] L. Yang, Y. He, W. Gan, M. Li, Q. Qu, X. Lin, Talanta 55 (2001) 271.
[9] M.F. Giné, A.P.G. Gervasio, A.F. Lavorante, G.E.S. Miranda, E. Carrilho, J. Anal. Atom. Spectrom. 17 (2002) 736.
[10] Y. He, M.L. Cervera, M.I. Garrido-Ecija, M. de la Guardia, Anal. Chim. Acta 421 (2000) 57.
[11] W.-P. Yang, Z.-J. Zhang, W. Deng, Anal. Chim. Acta 485 (2003) 169.
[12] Z. Chen, R. Naidu, A. Subramanian, J. Chromatogr. A 927 (2001) 219.
[13] F. Priego-Capote, M.D.L. de Castro, J. Chromatogr. A 1113 (2006) 244.
[14] O.P. Semenova, A.R. Timerbaev, R. Gagstädter, G.K. Bonn, J. High Resolut. Chromatogr. 19 (1996) 177.
[15] A.R. Timerbaev, O.P. Semenova, W. Buchberger, G.K. Bonn, Fresen. J. Anal. Chem. 354 (1996) 414.
[16] A.J. Zemann, E. Schnell, D. Volgger, G. Bonn, Anal. Chem. 70 (1998) 563.
[17] J.A.F. da Silva, C.L. do Lago, Anal. Chem. 70 (1998) 4339.
[18] J. Tanyanyiwa, P.C. Hauser, Electrophoresis 23 (2002) 3781.
[19] P. Kubáň, B. Karlberg, P. Kubáň, V. Kubáň, J. Chromatogr. A 964 (2002) 227.
[20] J. Muzikár, T. van de Goor, B. Gas, E. Kenndler, J. Chromatogr. A 924 (2001) 147.
[21] A.Z. Carvalho, J.A.F. da Silva, C.L. do Lago, Electrophoresis 24 (2003) 2138.
[22] L. Goodwin, M. Hanna, J.R. Startin, B.J. Keely, D.M. Goodall, The Analyst 127 (2002) 204.
[23] J. Wang, M. Pumera, G.E. Collins, A. Mulchandani, Anal. Chem. 74 (2002) 6121.
[24] J. Tanyanyiwa, K. Schweizer, P.C. Hauser, Electrophoresis 24 (2003) 2119.
[25] P. Coufal, J. Zuska, T. van de Goor, V. Smith, B. Gaš, Electrophoresis 24 (2003) 671.
[26] Z. Chen, Q. Li, O. Li, X. Zhou, Y. Lan, Y. Wei, J. Mo, Talanta 71 (2007) 1944.
[27] P. Kubáň, P. Kubáň, V. Kubáň, Electrophoresis 23 (2002) 3725.
[28] P. Kubáň, P. Kubáň, V. Kubáň, Electrophoresis 24 (2003) 1397.
[29] M.U. Katzmayr, C.W. Klampfl, W. Buchberger, J. Chromatogr. A 850 (1999) 355.
[30] A.J. Zemann, Electrophoresis 24 (2003) 2125.
[31] A.J. Zemann, Tr. Anal. Chem. 20 (2001) 346.
[32] C. Rivasseau, L. Lando, F. Rey-Gaurez, I. Bisel, D. Sans, M. Faucon, J.M. Adnet, J. Chromatogr. A 1015 (2003) 219.
[33] S.M. Valsecchi, S. Polesello, J. Chromatogr. A 834 (1999) 363.
[34] S.F. Zhang, L.S. Wang, Z. Dang, Chin. Chem. Lett. 17 (2006) 1229.
[35] L.R. Snyder, J.J. Kirkland, Introduction to Modern Liquid Chromatography, 2nd ed., Wiley–Interscience, New York, 1979, pp. 31–34.
[36] K. Mayrhofer, A.J. Zemann, E. Schnell, G.K. Bonn, Anal. Chem. 71 (1999) 3828.

Available online at www.sciencedirect.com
ScienceDirect
Talanta 72 (2007) 1269–1274
Talanta
www.elsevier.com/locate/talanta

Determination of polycyclic aromatic hydrocarbons in aqueous samples by microwave assisted headspace solid-phase microextraction and gas chromatography/flame ionization detection

Ming-Chi Wei [a], Jen-Fon Jen [b,*]

[a] *Department of Food Science, Central Taiwan University of Science and Technology, Taichung, Taiwan*
[b] *Department of Chemistry, National Chung Hsing University, Taichung 402, Taiwan*

Received 17 October 2006; received in revised form 9 January 2007; accepted 9 January 2007
Available online 16 January 2007

Abstract

The novel pretreatment technique, microwave-assisted heating coupled to headspace solid-phase microextraction (MA-HS-SPME) has been studied for one-step in situ sample preparation for polycyclic aromatic hydrocarbons (PAHs) in aqueous samples before gas chromatography/flame ionization detection (GC/FID). The PAHs evaporated into headspace with the water by microwave irradiation, and absorbed directly on a SPME fiber in the headspace. After being desorbed from the SPME fiber in the GC injection port, PAHs were analyzed by GC/FID. Parameters affecting extraction efficiency, such as SPME fiber coating, adsorption temperature, microwave power and irradiation time, and desorption conditions were investigated.

Experimental results indicated that extraction of 20 mL aqueous sample containing PAHs at optional pH, by microwave irradiation with effective power 145 W for 30 min (the same as the extraction time), and collection with a 65 μm PDMS/DVB fiber at 20 °C circular cooling water to control sampling temperature, resulted in the best extraction efficiency. Optimum desorption of PAHs from the SPME fiber in the GC hot injection port was achieved at 290 °C for 5 min. The method was developed using spiked water sample such as field water with a range of 0.1–200 μg/L PAHs. Detection limits varied from 0.03 to 1.0 μg/L for different PAHs based on S/N = 3 and the relative standard deviations for repeatability were <13%. A real sample was collected from the scrubber water of an incineration system. PAHs of two to three rings were measured with concentrations varied from 0.35 to 7.53 μg/L. Recovery was more than 88% and R.S.D. was less than 17%. The proposed method is a simple, rapid, and organic solvent-free procedure for determination of PAHs in wastewater.

Keywords: PAHs; Microwave-assisted; Headspace; SPME; GC/FID; Incineration system

1. Introduction

Polycyclic aromatics hydrocarbons (PAHs) are chemical species with two to six fused benzene rings and are well known toxic hazardous pollutants and highly potent carcinogens that can cause tumors in some organisms. They have recently been concerned about interference of PAHs with hormone systems, their potential effect on reproduction, and their ability to depress immune function [1]. PAHs are produced by incomplete combustion of fuels or incineration process, and also present in coal tars, crude oil and petroleum products such as creosote and asphalt. In addition to contaminate in land, the widespread contamination of PAHs in aquatic systems has led to concern about effects of PAHs on aquatic life [2]. Therefore, monitoring the levels of PAHs contents in aqueous systems are required.

The analyses of trace PAHs in aqueous media have been accomplished by many different procedures such as liquid chromatography [3–5], gas chromatography [6–8], capillary electrophoresis [9,10] and hyphenated techniques but many require preliminary extraction and enrichment of the analytes. Traditionally, this process was performed by liquid–liquid [11,12] or solid phase extraction [3–5,7,8]. In both cases the analytes were extracted from the water and dissolved in an organic solvent. The solvent was then evaporated to a small volume to concentrate the analytes and suppress the detection limits for the

* Corresponding author. Tel.: +886 4 22853148; fax: +886 4 22862547.
E-mail addresses: mcwei@ctust.edu.tw (M.-C. Wei), JFJen@dragon.nchu.edu.tw (J.-F. Jen).

0039-9140/$ – see front matter © 2007 Elsevier B.V. All rights reserved.
doi:10.1016/j.talanta.2007.01.017

method. Although these pretreatments efficiently yield precise results, they are tedious, time consuming, highly expensive and hazardous to health due to the usage of organic solvents, and lead to errors of contamination. Therefore, methods of pretreatments that take a short time with little or no use of organic solvents have recently been developed.

Solid-phase microextraction (SPME) was developed to overcome disadvantages of the LLE and SPE, and has been used for successful extraction in a variety of compounds, including PAHs, from different matrixes [6,13–16]. Headspace SPME (HS-SPME) was developed later and has been successfully applied to eliminate interference problems [17–19]. However, HS-SPME has been reported to be efficient only for analytes with high and medium Henry coefficients [20]. Although HS-SPME has been applied to extract PAHs, with preheating of the samples to enhance extraction of PAH [21–24], however it was still time-consuming, and it was unfavor to SPME sampling due to adsorption is an exothermic process. Herbert et al. [25] recently used microwave-assisted HS-SPME to enhance the extraction efficiency in the determination of PAHs and PCBs in landfill leachates. Ghiasvand et al. [26] also applied a new cold-fiber HS-SPME device to decrease fiber temperature and increase extraction quantity of PAHs from sediment. Both methods offered efficient and precise results.

We have recently investigated use of microwave heating to enhance the evaporation of semi-volatile analytes for one-step in situ HS-SPME sampling before GC analysis within a short time [27–31]. It depicts MA-HS-SPME technique has potential to improve the HS-SPME sampling of PAHs in aqueous samples. Because the optimum conditions for MA-HS-SPME depend on the boiling point and polarity of analyte, it is necessary to investigate the MA-HS-SPME technique for a wide range of high-boiling-point PAHs.

In this report we have systematically investigated the applicability of microwave-assisted (MA) heating in situ on-line HS-SPME (MA-HS-SPME) coupled to GC/FID for simple, rapid, sensitive, and solvent-free analysis of PAHs in wastewater.

2. Experimental

2.1. Chemicals and reagents

Deionized water for all aqueous solutions was produced by use of a Barnstead (New York, USA) Nanopure water system. All chemicals and solvents were of ACS reagent grade. The standard mixtures of 16 PAHs dissolved in a mixture of methylene chloride/benzene (1:1), containing naphthalene (NaP), acenaphthene (AcP), acenaphthylene (AcPy), fluorene (Flu), phenanthrene (PhA), anthracene (AnT), fluoranthene (FluA), pyrene (Pyr), benz(a)anthracene (B(a)A), chrysene (Chr), benzo(b)fluoranthene(B(b)F), benzo(k)fluoranthene (B(k)F), benzo(a)pyrene (B(a)P), indeno(1,2,3-cd)pyrene (InP), dibenz(a,h)anthracene (DbA), and benzo(-ghi)perylene (B(ghi)P) in concentrations of 2000 μg/L, purchased from Supleco (Bellefonte, PA, USA), were used for preparing working standard solutions. Commercial individual of 16 PAHs was purchased from Dr Ehrenstorfer GmbH (Augsburg, Germany). Working solutions (10 μg/mL in acetone) were prepared weekly by appropriately dilution of the stock solutions with acetone (Mallinckrodt, Paris, Kentucky, USA). All standards and working solutions were stored at 4 °C in silanized brown glass bottles with Teflon-lined caps. Highly pure nitrogen (99.9995%) and hydrogen (99.9995%) were obtained from Lien-Hwa Co. (Taichung, Taiwan).

2.2. GC/FID System

GC/FID used in this work was a Hewlett-Packard 5890 system (Pennsylvania, USA) equipped with a flame ionization detector (FID), and a split/splitless injector. Compounds were separated on a fused silica DB-5 capillary column (30 m × 0.25 mm i.d., 1.0 μm film thickness) (J&W Scientific, Folsom, CA, USA). Nitrogen was used as carrier gas, make-up gas, and purge gas at flow rates of 1.0, 35 and 5.0 mL/min, respectively. The flow rates for FID were 400 and 45 mL/min for air and hydrogen, respectively. The gas chromatograph was operated in splitless mode with a desorption time of 5 min. Separation was conducted with temperature programming as follows: oven temperature was set initially at 50 °C (1 min hold), increased to 140 °C at 20 °C/min (1 min hold), again increased to 250 °C at 3.5 °C/min (1 min hold), and finally increased to 320 °C at 8 °C/min (10 min hold). The injector was held between 270 and 300 °C to desorb PAHs from SPME fiber. The FID was maintained at 320 °C. A Chem-Lab Data system (Chem-Lab., Taipei, Taiwan) was used to obtain the chromatogram and perform data calculations.

2.3. MA-HS-SPME system

The microwave oven used in this work was a modified version of the domestic NN-L520 inverter system (2450 MHz, Panasonic, Canada) with a maximum power of 1100 W, equipped with a temperature-control cooling system (YIH DER BL-720, Taiwan). A microwave stirrer (Scienceware, Bel-Art Products, NJ, USA) was used for stirring the samples at 300 rpm during extraction. After modification, microwave with effective powers of 75, 100, 145, 160 and 200 W were used in this study. The set up of MA-HS-SPME system was similar to our previous study [32]. Aluminium foil was attached to the inner wall and the outer wall of the microwave at the interface between the microwave body and the headspace sampling apparatus to prevent leakage of irradiation. A microwave leak detector (MD-2000, Less EMF, NY, USA) was used to check the safety aspects of the equipment during the experiment.

The SPME device, consisting of the holder and fiber assembly for manual sampling, was obtained from Supelco (Bellefonte, PA, USA) and was used without modification. The fibers selected in this study were 1 cm in length and coated with different materials and thickness (75 μm CAR/PDMS, 65 μm CW/DVB, 65 μm PDMS/DVB, 85 μm PA, 50 μm DVB/CAR/PDMS and 7, 30 and 100 μm PDMS). Before use the fibers were conditioned under nitrogen in the hot injection port, as recommended by the manufacturer according to the type of fiber. The needle on the SPME holder was set at its maximum

length of 4 cm in the GC injector port. Desorption condition was investigated in the temperature of 270–300 °C for 2–5 min. All tests were performed with a 50-mL flask with ground-glass joints containing 20 mL aqueous solution (10 μg/L PAHs).

3. Results and discussion

3.1. Selection of SPME fiber

Due to the different physiochemical properties, PAHs have different sorption behaviors in the polymeric organic phases as well as in the environmental media. Although polyacrylate (85 μm) and polydimethylsiloxane (100 μm) were recommended as the most appropriate fiber coatings for the study of PAH in various matrices [21–24,33], however, some new complex-polymer SPME fibers have been developed and commercial available. Therefore, eight commercial available SPME fibers (75 μm CAR/PDMS, 65 μm CW/DVB, 65 μm PDMS/DVB, 85 μm PA, 100 μm PDMS, 30 μm PDMS, 7 μm PDMS and 50 μm DVB/CAR/PDMS) were evaluated for the PAHs sampling. A fortified aqueous sample (20 mL water containing 10 μg/L PAHs) was analyzed in triplicate by use of each fiber to sampling. The MA-HS-SPME sampling was performed at the circumstance of 20 °C circulating water system under 145 W irradiation for 30 min (same with the extraction time). After the MA-HS-SPME sampling and GC-FID determination, the results by use of different fibers are illustrated in Fig. 1, which indicated that the extraction efficiency of fiber for PAHs depended on the relative polarity of coating polymer and fused-benzene rings. The relatively polar fibers (PA, CAR/PDMS, DVB/CAR/PDMS and CW/DVB) were shown to have higher affinities for low-ring PAHs, not for high-ring PAHs, which met the result in literature [23]. As expected, high molecular weight PAHs were partitioned into more non-polar coating fibers (PDMS) rather than polar fibers, and the higher film thickness of PDMS fiber (100 μm) showed a better sorption than other two PDMS fibers (30 and 7 μm). In our study, among all fibers, the bipolar PDMS/DVB fiber not only had almost the same adsorption amounts with 100 μm PDMS fiber, but higher adsorption efficiency for two to three ring PAHs. It may due to the π–π interaction of PAHs with the phenyl group of PDMS/DVB coating. Considering the detection sensitivity of all PAHs, the PDMS/DVB fiber was therefore chosen herein.

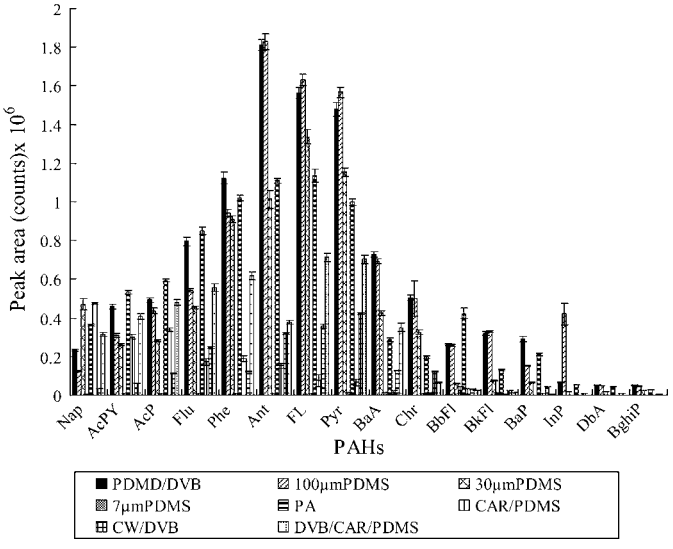

Fig. 1. Extraction efficiency of PAHs on different SPME fibers. Conditions: microwave irradiation at 145 W effective power for 30 min, circulating water temperature at 20 °C.

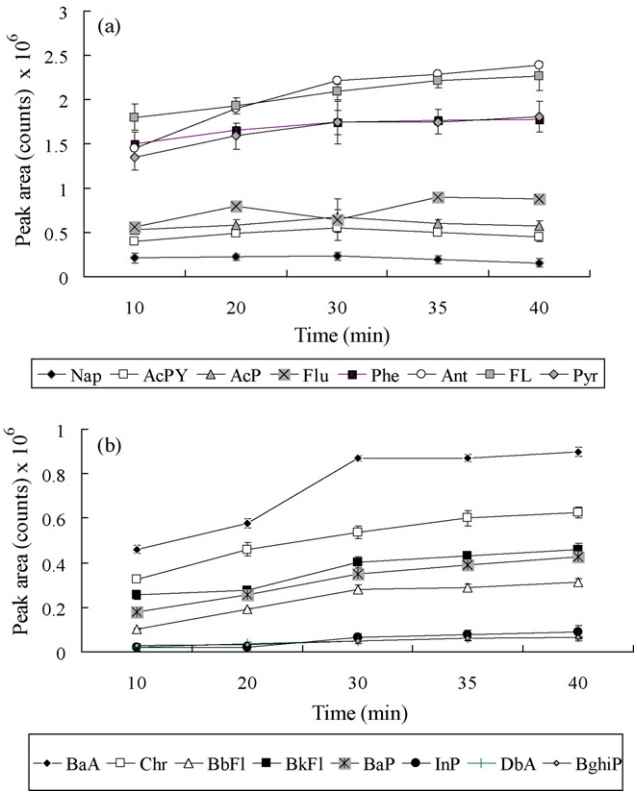

Fig. 2. (a) Extraction efficiency of PAHs on different microwave irradiation time. At 145 W effective power irradiation. (b) Extraction efficiency of PAHs on different microwave irradiation time. At 145 W effective power irradiation.

3.2. Optimization of microwave irradiation conditions

In the proposed method, microwave irradiation was used to promote vaporization of the PAHs from water sample into headspace for SPME sampling. Microwave irradiation was optimized at effective powers of 75, 100, 145, 160 and 200 W for 10–40 min. Fig. 2(a) and (b) showed extraction quantities (related to peak areas) of PAHs onto the PDMS/DVB fiber during different irradiation times under 145 W irradiation. During the sampling, the low-ring PAHs increased significantly at the first 20 min, reached to the maximum at 20 min, declined slightly after that. As for higher-ring PAHs, the extraction quantities increased with the irradiating time, and turned to constant slowly after 35 min. It depicted that the competition among PAHs for adsorption sites on fiber occurred during adsorption. At low temperature (short irradiation time), the high-ring PAHs were insignificant to compete with low-ring PAHs for adsorption onto fiber due to their extremely low vapor pressures. However, the competency of high-ring PAHs was enhanced by long-time irra-

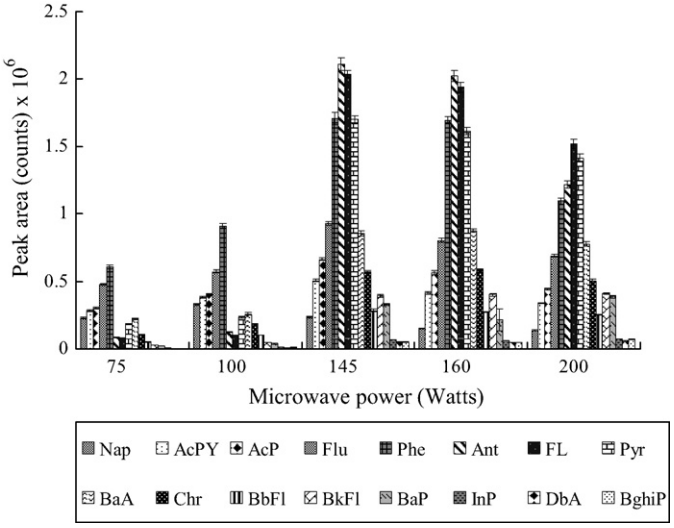

Fig. 3. Extraction efficiency of PAHs under different effective powers of microwave irradiation. For 30-min irradiation time.

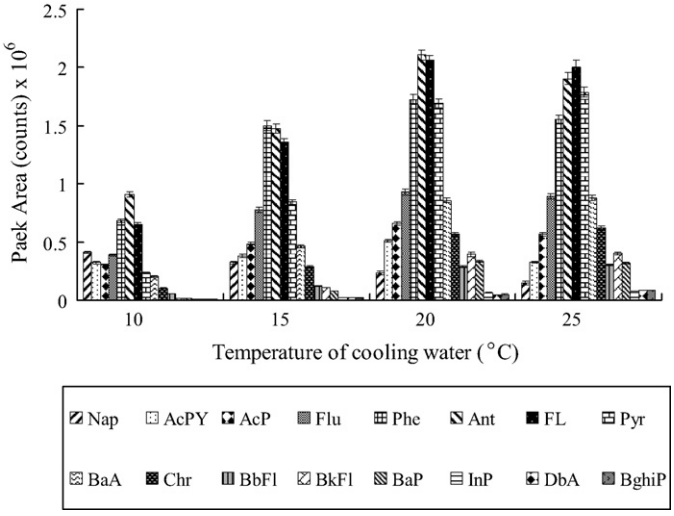

Fig. 4. Extraction efficiency under different temperatures of circulating water.

diation. Same as in irradiation power level, a high irradiating power favored high-ring PAHs adsorption, and a low irradiating power favored low ring PAHs adsorption. Fig. 3 illustrated the optimal irradiation power is at 145 W effective power. Compromise the extracted quantities of PAHs and sampling times, the microwave irradiation at 145 W effective power for 30 min was recommended to assist the HS-SPME sampling.

3.3. Effect of temperature of the circulating water system

Microwave heating accelerates vaporization of the PAHs and water from aqueous sample into headspace for SPME sampling. However, adsorption of PAHs on to the fiber was not favored by high temperature due to adsorption is an exothermic process. During this study, a circulating water system was therefore used to control the temperature around the sampling zone. Although use of a low temperature was thermodynamically helpful for adsorption of the PAHs, but it was not for the vapors of PAHs reaching to the sampling zone. Therefore, the optimal temperature of the circulating water was investigated to build up an appropriate circumstance for HS-SPME sampling. Fig. 4 demonstrated the extraction quantities (related to peak area) of PAHs being maximized at 20 °C. The temperature of the circulating water (20 °C) was used herein.

3.4. Thermal desorption conditions for PAHs

Because of the wide boiling-points range of PAHs (naphthalene (2-ring) at 218 °C and benzo(a)pyrene (5-ring) at 493 °C), the temperature of thermal desorption in the GC injection port should be optimized. After a series of tests, results demonstrated that the maximum peak area (related to the efficiency of desorption) of the PAHs was obtained when the fiber was heated at 290 °C for 5 min. After desorption at this condition, no significant PAHs signals were observed in the chromatogram after re-injection. Thus, further regeneration of fiber was not required between runs. Although the manufacture suggested the operating temperature of the PDMS/DVB fiber should not be higher than 270 °C, the fiber was used more than 100 times in our studies.

3.5. Validation of the methods

In order to test the suitability of the method for quantitative determination of PAHs in water samples, different concentrations of standard PAHs spiked in water were used for calibration after being subjected to the complete overall treatment procedure, i.e. MA-HS-SPME and thermal desorption from the fiber into the chromatographic system. The linearity of the method was tested by GC-FID by extracting aqueous standards, with increasing concentrations, over a range of 0.1–200 μg/L of PAHs. Table 1 illustrated the calibration range, linearity, precisions and detection limits of PAHs with PDMS/DVB fiber. The amount of analyte extracted by the fiber compared to the initial amount of analyte in the aqueous samples was around 1.0–23% depending on the volatility of species. The detection limits were calculated on the base of three times the average background noise divided by the detection sensitivity (slope of the calibration plot) and varied from 0.03 to 1 μg/L. Precision of this method was estimated by performing seven extractions and determinations of sample solutions spiked with all the studied PAHs at the concentration of 10 μg/L. Precisions ranged from 5 to 13% R.S.D., which should be satisfactory for determining the PAHs in water matrix.

3.6. Application to real sample

In order to examine the suitability of the method for quantitative determination of PAHs in real sample, a wastewater from the scrubber of a pilot-scale fluidized bed incinerator system was collected and analyzed by the proposed method. The chromatogram obtained from the PAHs in the sample is shown in Fig. 5. Peaks appeared in chromatogram were also confirmed by GC–MS, which are listed in Table 2. It can be seen only two to three rings of PAHs were found in the scrubber water.

Table 1
Calibration parameters of 16 PAHs with the proposed method

PAHs	Calibration range (μg/L)	Linearity (R^2)	R.S.D.[a] (%, $n=7$)	LOD (μg/L)	PE[b] (%)
NaP	0.5–100	0.9950	7	0.1	3.9
AcPy	0.5–100	0.9985	9	0.1	7.2
AcP	0.5–100	0.9978	5	0.07	7.1
Flu	0.5–100	0.9988	6	0.08	12
PhA	0.1–20	0.9975	8	0.04	15
AnT	0.1–20	0.9989	9	0.03	17
FluA	0.1–20	0.9992	8	0.03	23
Pyr	0.1–20	0.9989	6	0.03	18
B(a)A	0.5–100	0.9970	9	0.1	12
Chr	0.5–100	0.9974	8	0.1	9.8
B(b)F	1–100	0.9865	12	0.5	4.7
B(k)F	1–100	0.9888	13	0.5	4.5
B(a)P	1–100	0.9890	7	0.5	3.2
InP	2–200	0.9826	9	1.0	1.0
DbA	2–200	0.9813	5	1.0	1.2
B(ghi)P	2–200	0.9858	7	1.0	1.1

[a] Estimated by seven determinations of sample solutions spiked with 10 μg/L.
[b] The percentage of PAHs extracted from the water sample to the fiber.

It depicts that in the fluidized bed incinerator, the low-ring PAHs with relatively volatile can be diffusive into scrubber, whereas the less-volatile high-ring PAHs are thus adsorbed on bottom ash or fly ash (particle) of cyclone. Besides, the two to three ring PAHs also exhibits higher solubility than high-ring PAHs. Recovery was tested to investigate the effect of the real sample matrix by spiking scrubber water sample with PAHs at 10 μg/L and analyzed with the MA-HS-SPME sampling/thermal desorption/GC-FID determination. Recoveries of the PAHs varied from 88 to 103% as listed in Table 2. The accuracy and precision are acceptable in environmental analysis of complicated matrix samples. Because the scrubber water was too cloudy, serious interferences occurred when using direct immersion SPME method to sampling PAHs, and the fiber was worsen and easily broken. Therefore, it is inappropriate to use direct immersion SPME method to collect analytes.

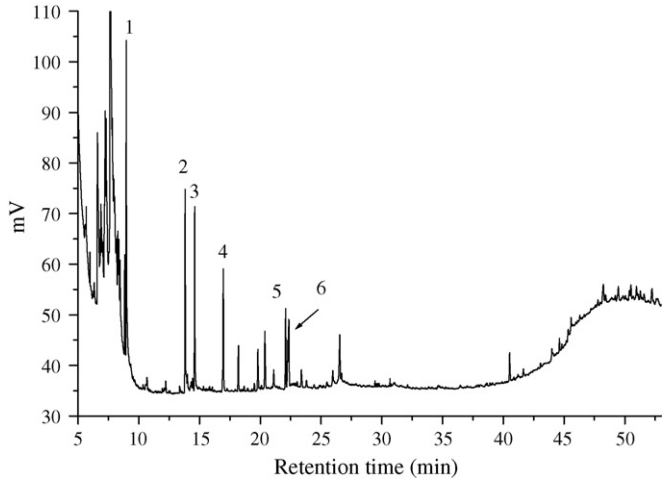

Fig. 5. Chromatogram obtained from PAHs in a real sample collected from scrubber water of incineration system Peak 1: NaP; 2: AcPy; 3: AcP; 4: Flu; 5: PhA; 6: AnT.

3.7. Comparison of the proposed MA-HS-SPME method with other SPME methods

All the SPME methods have the advantages of being fast, low-cost and solving the organic solvent problems in sample pretreatment. The conventional immersed SPME has been solvent-less and usually takes 30–60 min to achieve a sampling for PAHs in water sample [34–36], but it suffers the matrix effect in complicate samples. Although the HS-SPME method is free to matrix effect, it takes more than 1 h to collect most PAHs, but still cannot determine the high-ring PAHs (more than five ring) [23,37,38]. As described previously, the MA-HS-SPME is proposed to shorten the sampling time. It takes only 30 min to complete the sample pretreatment for PAHs.

Table 2
Concentration of PAHs in a real sample and recovery

PAHs	Concentration detected in real sample (μg/L)	Recovery[a] (%)	R.S.D.[a] (%)
NaP	7.53	94	12
AcPy	6.41	95	8
AcP	4.35	93	9
Flu	3.57	92	6
PhA	0.83	103	10
AnT	0.35	94	7
FluA	ND[b]	85	8
Pyr	ND	90	7
B(a)A	ND	94	10
Chr	ND	90	9
B(b)F	ND	88	12
B(k)F	ND	93	13
B(a)P	ND	91	8
InP	ND	89	11
DbA	ND	89	15
B(ghi)P	ND	92	17

[a] For three determinations of spiking scrubber water sample with PAHs at 10 μg/L.
[b] Non-detectable.

4. Conclusion

In this study, determination of PAHs in water matrix by the MA-HS-SPME with GC/FID system has been described. The optimum conditions have been established. Results from suitability tests indicate the proposed method is a simple, rapid, convenient, and free from toxic organic solvent procedure for isolation of PAHs from complicated water matrix before GC-FID determination.

Acknowledgement

The authors thank the National Science Council of Taiwan for financial support under the grant number NSC93-2113-M-005-026.

References

[1] K. Chaloupka, N. Harper, V. Krishnan, M. Santostefano, L.V. Rodriguez, S. Safe, Chem. Biol. Interact. 89 (1993) 141.
[2] D.M. Wassenberg, R.T. Di Giulio, Environ. Health Perspect. 17 (2004) 112.
[3] H.D. Liang, D.M. Han, X.P. Yan, J. Chromatogr. A 1103 (2006) 9.
[4] Y.Y. Zhou, X.P. Yan, K.N. Kim, S.W. Wang, M.G. Liu, J. Chromatogr. A 1116 (2006) 172.
[5] E. Martinez, M. Gros, S. Lacorte, D. Barcelo, J. Chromatogr. A 1047 (2004) 181.
[6] S.B. Hawthorne, C.B. Grabanski, D.J. Miller, J.P. Kreitinger, Environ. Sci. Technol. 39 (2005) 2795.
[7] P.W. Crozier, J.B. Plomley, L. Matchuk, Analyst 126 (2001) 1974.
[8] H. Bagheri, A. Mohammadi, J. Chromatogr. A 1015 (2003) 23.
[9] G. Kavran, F.B. Erim, J. Chromatogr. A 949 (2002) 301.
[10] M.M. Hsieh, Y.C. Kuo, P.L. Tsai, H.T. Chang, J. Chromatogr. A 924 (2001) 397.
[11] ISO 7981-2, International Organization for Standardization, 2005.
[12] Y. Takagai, S. Igarashi, Anal. Bioanal. Chem. 373 (2002) 87.
[13] J. Koziel, M. Jia, A. Khaled, J. Noah, J. Pawliszyn, Anal. Chim. Acta 400 (1999) 153.
[14] L.M. Diaz-Vazquez, O. Garcia, Z. Velazquez, I. Marrero, O. Rosario, J. Chromatogr. B 825 (2005) 11.
[15] A.J. King, J.W. Readman, J.L. Zhou, Environ. Geochem. Health 25 (2003) 69.
[16] H.W. Chen, Anal. Sci. 20 (2004) 1383.
[17] M. Chai, J. Pawliszyn, Environ. Sci. Technol. 29 (1995) 693.
[18] F. Guan, K. Watanabe, A. Ishii, H. Seno, T. Kumazawa, H. Hattori, O. Suzuki, J. Chromatogr. B 714 (1998) 205.
[19] J. Czerwinsky, B. Zygmunt, J. Namiesnik, J. Anal. Chem. 356 (1996) 80.
[20] M. Llompart, L. Li., M. Fingas, Anal. Chem. 70 (1998) 2510.
[21] D. Djozan, Y. Assadi, J. Microchem. 63 (1999) 276.
[22] R.-A. Doong, S.-M. Chang, Y.-C. Sun, J. Chromatogr. Sci. 38 (2000) 528.
[23] R.-A. Doong, S.-M. Chang, Y.-C. Sun, J. Chromatogr. A 879 (2000) 177.
[24] S. Waidyanatha, Y. Zheng, S.M. Rappaport, Chem. Biol. Interact. 145 (2003) 165.
[25] P. Herbert, A.L. Silva, M.J. Joas, L. Santos, A. Alves, Anal. Bioanal. Chem. 386 (2006) 324.
[26] A.R. Ghiasvand, S. Hosseinzadeh, J. Pawliszyn, J. Chromatogr. A 1124 (2006) 35.
[27] M.-C. Wei, J.-F. Jen, Chromatographia 55 (2002) 701.
[28] J.-F. Jen, Y.-S. Su, Y.-I. Chen, J. Chromatogr. A 976 (2002) 349.
[29] M.-C. Wei, J.-F. Jen, J. Chromatogr. A 1012 (2003) 111.
[30] H.-P. Li, G.-C. Li, J.-F. Jen, J. Chromatogr. A 1012 (2003) 129.
[31] C.-T. Yan, J.-F. Jen, Chromatographia 59 (2004) 517.
[32] M.-C. Wei, W.-T. Chang, J.-F. Jen, Anal. Bioanal. Chem. 387 (3) (2007) 999–1005.
[33] M.D. Guillén, P. Sopelana, J. Dairy Sci. 88 (2005) 13–20.
[34] A.J. King, J.W. Readman, J.L. Zhou, Anal. Chim. Acta 523 (2004) 259.
[35] G. Grimmer, Environmental Carcinogens: Polycyclic Aromatic Hydrocarbons, CRC Press, 1983.
[36] National Institute for Occupational Safety and Health, NIOSH Manual of Analytical Methods, 4th ed., vol. 3, Method, 5506, Issue 12, 1994.
[37] M. Llompart, K. Li, M. Fingas, Talanta 48 (1999) 451.
[38] M.R. Negrao, M.F. Alpendurada, J. Chromatogr. A 823 (1998) 211.

Available online at www.sciencedirect.com
ScienceDirect
Talanta 72 (2007) 1336–1341
Talanta
www.elsevier.com/locate/talanta

Microwave plasma treated carbon nanotubes and their electrochemical biosensing application

Zhaoyang Wu *, Yinyu Xu, Xiaolei Zhang, Guoli Shen, Ruqin Yu

State Key Laboratory for Chemo/Biosensing and Chemometrics, College of Chemistry and Chemical Engineering, Hunan University, Changsha 410082, China

Received 8 August 2006; received in revised form 16 January 2007; accepted 17 January 2007
Available online 1 February 2007

Abstract

A convenient microwave plasma treatment method with ammonia precursor was proposed to enhance the solubility of carbon nanotubes (CNTs). The SEM, XRD and FTIR spectra clearly demonstrated that the carbon skeleton structure of the resultant ammonia plasma-treated CNTs (ammonia PT-CNTs) was not destroyed and amine groups of different forms were successfully coupled to CNTs in the MWP treatment process. The ammonia PT-CNTs have excellent solubility in water and are insoluble in nonpolar tetrahydrofuran, and the cyclic voltammograms suggest that the enhanced wetting properties clearly favor faster electron transfer kinetics on the ammonia PT-CNT electrodes. By choosing glucose oxidase as a model enzyme, the application of the ammonia PT-CNTs in construction of biosensors was further investigated. Due to the biocompatibility and electron transfer capability of the ammonia PT-CNTs, the resultant GOD biosensor displayed a good sensing performance. The biosensor has a fast response of less than 10 s, and the response current linearly increases with the glucose concentration in the range of 1.2×10^{-4} to 7.5×10^{-3} M with a detection limit of 1.0×10^{-5} M.

Keywords: Microwave plasma; Carbon nanotubes; Biosensor

1. Introduction

Electrochemical biosensors have gained increasing attention due to their potential application in the areas of food industry [1,2], clinical analysis [3,4], and environmental monitoring [5,6]. They are generally constructed by immobilizing biomaterials with recognizing and/or catalyzing abilities to sensing matrices and combining these with electrochemical sensing devices, which can convert analyte concentrations into electrical signals. For electrochemical biosensors, the electrochemical performance is directly related to the sensing matrix materials, and thus many efforts have still been directed to the development of new sensing materials with outstanding physicochemical properties.

Since Lijima [7] discovered carbon nanotubes (CNTs), they have led to many new technical developments and applications due to their high chemical stability, large surface area, unique electrochemical properties, and excellent mechanical strength [8]. In particular, their applications in electrochemical sensors and nanoscale electronic devices have attracted increasing attention [9–13]. It has been found that CNTs have a high electrocatalytic effect and a fast electron-transfer rate, and thus they have great potential to be applied to biosensors, especially amperometric biosensors, to enhance their sensing performances. However, one of major obstacles for developing the CNT-based devices is their insolubility nearly in all solvents [14,15], which is unfavorable to the immobilization of biomolecules in aqueous solutions and to the preservation of their bioactivities. At present, the challenge has somewhat been addressed through various chemical modifications. For instance, CNTs can be treated by refluxing in HNO_3 and/or H_2SO_4 to introduce –COOH and –OH groups and increase their aqueous solubility [15,16]. However, the treatment in such harsh conditions clearly deviates from principles of green chemistry, and it is also possible to damage their sidewalls [17], to decrease their stability [18], and even to cut them into short pieces [19].

Plasma treatment is an attractive technique as it is a rapid, versatile and contaminant-free procedure for the introduction of

* Corresponding author. Tel.: +86 731 8821916; fax: +86 731 8821916.
E-mail address: zywu@hnu.cn (Z. Wu).

0039-9140/$ – see front matter © 2007 Elsevier B.V. All rights reserved.
doi:10.1016/j.talanta.2007.01.052

various functional groups. In a plasma treatment process, particle energies of plasmas are usually comparable with chemical bond energies, and the particle densities and energies can be controlled by the external plasma parameters (e.g. power, pressure, frequency, etc.). Accordingly, the plasma treatment technique enables various kinds of precursor monomers to be activated into reactive radicals, and thus the surface functionalization even of the most inert materials can also be conveniently tailored. Many reports have well demonstrated its applications in polymerization depositions, and the surface modifications of polymeric materials and fine powders [20–22]. Furthermore, plasma treatments to biosensor substrates have also been verified to be quite effective for the immobilization of enzymes [23,24], antibodies [25–27] or DNAs [28].

Recently, some efforts have been directed to the plasma modifications of CNTs [29,30]. Dai group [29] studied the acetaldehyde or ethylenediamine plasma activation of carbon nanotubes for chemical modification, and the resulting polysaccharide-grafted carbon nanotubes show good hydrophilicity. Khare et al. [30] successfully functionalized single-walled carbon nanotubes (SWCNTs) through a microwave discharge of ammonia. However, the effects of plasma modifications on the electrochemical properties and sensing applications of CNTs have not yet been addressed.

In this study, we used a microwave plasma (MWP) with an ammonia source to treat carbon nanotubes. This is primarily aimed at introducing hydrophilic groups on the surface of CNTs to enhance their aqueous dispersion. The electrochemical behavior of the modified CNTs was studied using glucose oxidase as a model enzyme for the construction and development of a working biosensor. Due to the good hydrophilicity and electrochemical performance of the modified CNTs, the CNT matrix can effectively entrap glucose oxidases and preserves their bioactivity giving excellent sensing response.

2. Experimental

2.1. Reagents

Glucose oxidase (GOD; EC 1.1.3.4. 196 U mg^{-1}) and vinylferrocene (VF, 98%) were supplied by Sigma. Nafion was purchased from Aldrich. β-D-glucose was obtained from ICN. The single-walled carbon nanotubes (SWCNTs) with a diameter of 1–2 nm and with a length of up to 0.5–1 μm were purchased from Organic Chemistry Engineering Technology Center (Chengdou, China) and were used without any further pretreatment. Glucose stock solution was allowed to mutarotate at room temperature overnight before use. All other chemicals were of analytical grade or higher commercially available purity and were used as received. Doubly distilled water was used throughout.

The supporting electrolyte was 0.067 M phosphate buffer (PB), which was prepared with KH_2PO_4 and Na_2HPO_4.

2.2. MWP treatment of CNTs

The plasma treatment of CNTs was completed in a stainless reactor with a MWP system (Guowei Limited Corporation, Hubei Province, China). Ammonia (30%) was used as a precursor, and pure hydrogen (99.99%) as a carrying gas. During the deposition process, the flowing rate of carrying gas was kept at 1.0 mL min^{-1}, the pressure of the reactor chamber at 266 Pa, and the MW power being 30 W. The resultant ammonia plasma-treated CNTs (ammonia PT-CNTs, 2 mg) was added into 0.5 mL water, and the mixture was then sonicated for 20 min in ultrasonic bath, a dispersed solution of carbon nanotubes was formed finally.

2.3. Fabrication of the GOD electrodes

A GOD solution of 10 mg mL^{-1} was prepared with 0.067 M PB at pH 6.9. Prior to use, the platinum disk (0.2 mm diameter) electrode was polished successively with 1, 0.3 and 0.05 μm of α-alumina powders in each experiment. After thoroughly rinsed in ultrasonic bath, the electrode was immersed in 50 μL of 0.15 M VF solution in methanol and air-dried. Subsequently, a mixture solution was prepared by mixing 3 μL of ammonia PT-CNTs solution, 2 μL of GOD solution, 5 μL of 1.0 mg mL^{-1} BSA (bovine serum albumen) and 2 μL of 2.5% GLU (glutaraldehyde), and 5 μL of the mixture solution was then pipetted onto the electrode surface and dried at 4 °C overnight. Finally, the electrode was rinsed with PB to remove the non-covalently bound enzymes, and the GOD electrode was then obtained. As a comparison, the GOD electrode without the ammonia PT-CNTs was prepared by the same procedure described above. When not in use, the electrodes were stored at 4 °C in a refrigerator.

2.4. Electrochemical measurements

Electrochemical measurements were performed using an electrochemical analyzer (Shanghai Chenhua Instrument Company, China). The three-electrode system consisted of a GOD electrode as working electrode, a saturated calomel reference electrode (SCE) and a platinum foil counter electrode. All electrochemical experiments were carried out in 10 mL phosphate buffer (pH 6.9) at room temperature (20 ± 2 °C) in an air-saturated condition unless otherwise stated. All potentials were measured versus a saturated calomel reference electrode under stirring conditions. Alternating current (ac) impedance experiments were performed in a laboratory-made measuring cell using a Model VMP2 Multichannel Potentiostat with Ec-Lab V6.70 and ZsimpWin Version 2.00 software (EG&G Princeton Applied Research, Princeton, NJ). Impedance spectra were recorded over a frequency range of 0.1–100,000 Hz at zero dc potential with the ac potential amplitude of ±20 mV.

3. Results and discussion

3.1. Characterization of ammonia PT-CNTs

Ammonia has been considered to be an effective precursor to introduce amine functionalities to the carbon nanotubes [30] and other materials [31,32], enhancing their hydrophilicity and biocompatibility. Fig. 1 shows the SEM images of the CNTs before and after the ammonia plasma treatment. It can

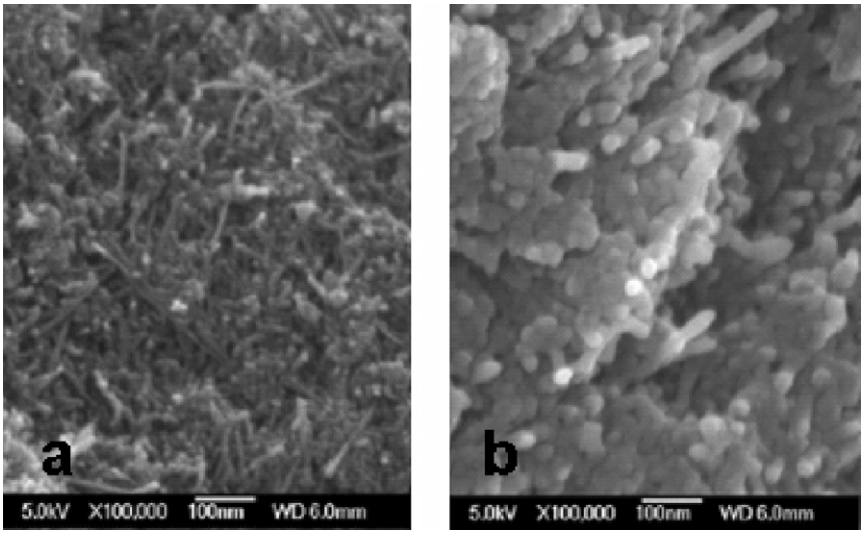

Fig. 1. SEM images of the CNTs (a) before and (b) after the ammonia plasma treatment.

be shown that after the ammonia plasma treatment, the tubular diameter of the ammonia PT-CNTs was about two times larger than that of the pristine CNTs, clearly indicating a homogeneous ammonia plasma deposition coating on the carbon nanotube sidewall. However, the MWP modification reactions are somewhat complex because the ammonia precursor can produce multiple reactive radicals, such as N, NH, NH_2, etc., under microwave radiation [33]. Fig. 2 shows the typical FTIR transmittance spectrum of the ammonia PT-CNTs. Compared to the absorption curve of the pristine CNTs (curve a), a peak at 3319 cm^{-1} can be observed from that of the ammonia PT-CNTs (curve b), indicating the presence of N–H stretching mode. And the absorption peaks at 1650–1458 cm^{-1} can be assigned to the deformation vibrations of N–H bonding. These absorption peaks clearly demonstrated that some hydrophilic amine groups were introduced in the ammonia PT-CNTs. Moreover, it can also be noticed that the peak at 3319 cm^{-1} is relatively wide and the peaks at 1650–1458 cm^{-1} are relatively complex. These phenomena seem to be related to the fact that amine groups of different forms and even some groups containing oxygen are coupled to CNTs in the MWP treatment process.

To investigate the effect of MWP treatment on the structure of CNTs, the XRD spectra of the CNTs before and after treated by MWP were compared (see Fig. 3). Fig. 3a displays the XRD spectrum of the pristine CNTs, and Fig. 3b displays the XRD spectrum of the ammonia PT-CNTs. It can be seen that the ammonia PT-CNTs have the same characteristic diffraction peaks at thetal 25.8 (assigned as a peak arising from the 002 lattice face) and thetal 43.4 (assigned as a peak arising from the 100 lattice face) as the pristine CNTs and the intensity of carbon peaks are not clearly changed, implying that the carbon skeleton structure of ammonia PT-CNTs is not destroyed in the MWP treatment process. On the other hand, we also notice that there are two small peaks in thetal 15 and thetal 35 in Fig. 3b, suggesting that CNTs is successfully modified and some new substances are formed in the MWP process. These results further demonstrate that the MWP treatment is a reliable and effective approach, which can conveniently endow CNTs with various new functional groups while maintaining their original physicochemical properties.

3.2. Solubility of the ammonia PT-CNTs

The photographs in Fig. 4 were used to describe the solubility of the ammonia PT-CNTs in different solvents. The

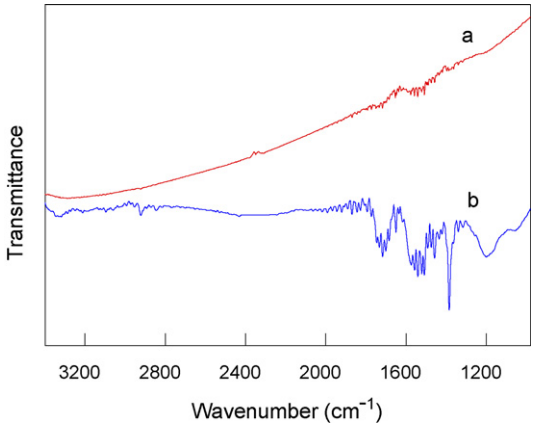

Fig. 2. FTIR spectra of the pristine CNTs (a) and the ammonia PT-CNTs (b).

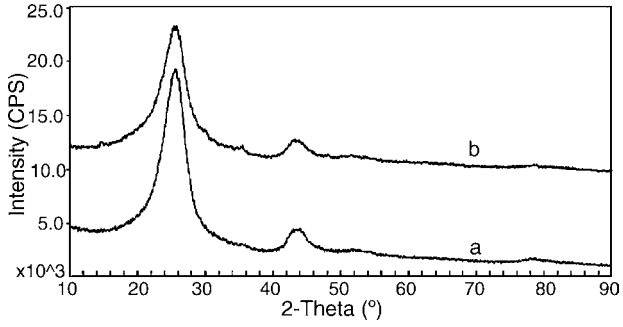

Fig. 3. XRD spectra of the pristine CNTs (a) and the ammonia PT-CNTs (b).

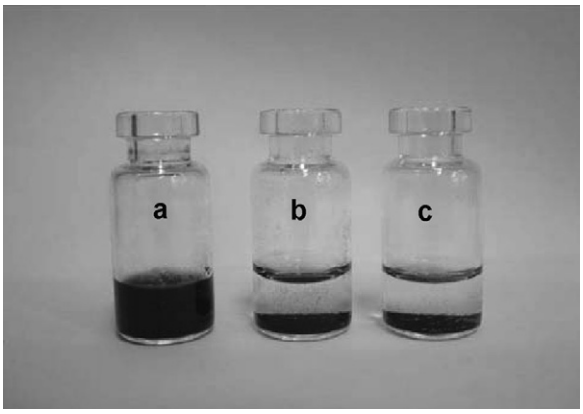

Fig. 4. Photographs of the ammonia PT-CNTs in water (a) and in THF (b) and the pristine CNTs in water (c).

ammonia PT-CNTs were uniformly dispersed in water even after 10 days (Fig. 4a), whereas the untreated pristine CNTs rapidly settled in water in about 1 h (Fig. 4c). Moreover, the solubility of the ammonia PT-CNTs in tetrahydrofuran (THF) was also investigated (Fig. 4b), and the result showed that the ammonia PT-CNTs also settled in a nonpolar solvent in about 1 h. These phenomena suggest that the introduction of polar amino groups in the MWP treatment process greatly increase the hydrophilicity of CNTs, and consequently the ammonia PT-CNTs are soluble in water and insoluble in nonpolar solvent. The improvement in hydrophilicity of CNTs will not only benefit their biocompatibility to a certain degree but also make the applications of CNTs in biomolecular immobilizations and biosensor constructions more convenient. For instance, the couple between biomolecules and CNTs can be completed at an aqueous environment, and thus the activity of biomolecules can be better maintained.

3.3. Electrochemical performance of the ammonia PT-CNTs

It has been recognized that the electron transfer capacity of electrodes in electrochemical processes is directly associated to the surface conditions of electrode materials. The plasma treatment of electrodes has also been demonstrated to be an effective approach to drive the electron transfer faster [34]. For the ammonia PT-CNTs, the introduction of the hydrophilic groups greatly enhances the wetting properties of CNTs interface, as well as improving the electron transfer properties of CNTs. In this study, the oxidation of potassium ferrocyanide served as a benchmark to compare the electrochemical properties of the ammonia PT-CNTs and the pristine CNTs. In view of the bad dispersibility of the pristine CNTs in water, both the CNTs were dispersed in 0.5% Nafion solution in an ultrasonic bath for 2 h. The two kinds of CNTs (10 μL of 3 mg mL^{-1} solutions) were then coated onto the rinsed electrodes, respectively, to form the CNT-modified electrodes. Fig. 5 shows the current-normalised cyclic voltammograms of 5 mM potassium ferrocyanide at the two electrodes. It can be seen that for the ammonia PT-CNTs modified electrode, the peak potential separation (ΔE_p) of the cyclic voltammetric

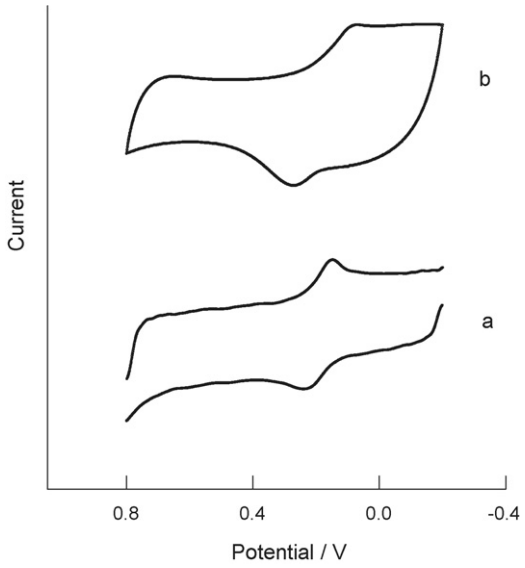

Fig. 5. Cyclic voltammograms of 5 mM potassium ferrocyanide at the two Nafion membrane electrodes consisting of the ammonia PT-CNTs (a) or the pristine CNTs (b).

curve (curve a) at a sweep rate of 150 mV s^{-1} is 80 mV, while the ΔE_p value for the pristine CNTs modified electrode is 200 mV. The clear decrease in the ΔE_p value indicates that the ammonia PT-CNTs has a faster electron transfer capability than the pristine CNTs, and the electron transfer rate constant (k_0) values of potassium ferrocyanide at the two electrodes were estimated to be 0.5 and 0.06 cm s^{-1}, respectively [35]. These results demonstrate that the enhanced wetting properties can favour faster ET kinetics on the ammonia PT-CNTs electrodes as well as this convenient MW plasma treatment has little effect on the carbon skeleton structure of CNTs, retaining conducting properties of the ammonia PT-CNTs.

3.4. Performance of the ammonia PT-CNTs in biosensor construction

To further study the electrochemical properties and biosensing applications, we applied the ammonia PT-CNTs to construct an electrochemical GOD biosensor and investigated the influences of the ammonia PT-CNTs on the electrochemical behaviors and sensing characteristics of the biosensor in detail. Fig. 6 is the Faradaic impedance spectra corresponding to the GOD electrodes with the ammonia PT-CNTs or without the ammonia PT-CNTs. It can be seen that the Faradaic resistance of the electrode only with a VF layer is 400 Ω (curve a), whereas a linear Faradaic impedance curve is observed and the Faradaic resistance almost reaches zero when 5 μL of ammonia PT-CNTs (1.0 mg mL^{-1}) is added on the electrode (curve b). Moreover, curve c and d reveal that the Faradaic resistances of the GOD electrode consisting of VF, GOD, GLU, and BSA with or without the ammonia PT-CNTs are 450 and 4000 Ω, respectively. It is thus obvious that the presence of the ammonia PT-CNTs can clearly increase the Faradaic resistance of enzyme membrane and enhance the electron transfer kinetics of GOD biosensor.

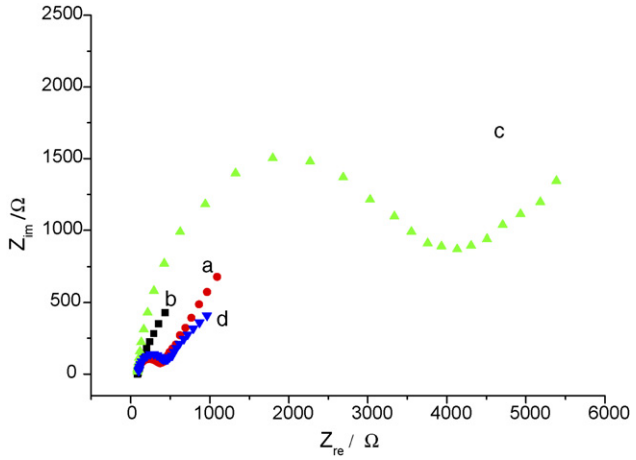

Fig. 6. Nyquist plots (Z_{im} vs. Z_{re}) corresponding to the Faradaic impedance analyses of the electrodes. (a) With only a VF layer; (b) with a mixture layer of the ammonia PT-CNTs and VF; (c) with a mixture layer of GOD, GLU and BSA on the VF layer; (d) with a mixture layer of GOD, GLU, BSA and ammonia PT-CNTs on the VF layer. All impedance spectra are recorded in 0.1 M phosphate buffer in the presence of 5 mM $[Fe(CN)_6]^{3-/4-}$.

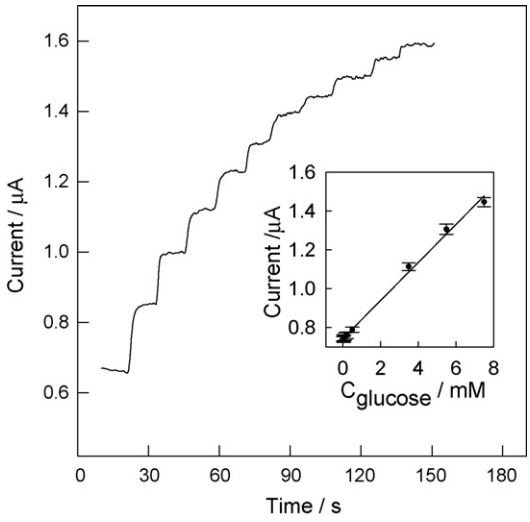

Fig. 7. Dynamic response of the GOD electrode to successive addition of 0.3 mM glucose in 0.067 M phosphate buffer (pH 6.9) at the applied potential of +400 mV vs. SCE. The insert figure shows the calibration curve.

To investigate the influence of the ammonia PT-CNTs on the sensing performance of GOD electrodes, we compared the current responses of the GOD electrodes with and without the ammonia PT-CNTs to glucose at the applied potential of +400 mV versus SCE. The result showed that the response current values of the GOD electrode with the ammonia PT-CNTs in glucose solutions of different concentrations were much larger than those obtained from the GOD electrode without the ammonia PT-CNTs. For example, the response current of the GOD electrode with the ammonia PT-CNTs in 12 mM glucose solution is 1.48 μA while that of the GOD electrode without the ammonia PT-CNTs is only 0.32 μA. The result suggests that the ammonia PT-CNTs can play a similar role as the common CNTs in enhancing the electron transfer of enzymatic electrodes as well as making the immobilization of biomolecules and the construction of biosensors more convenient. On the other hand, the amount of the ammonia PT-CNTs in the GOD matrix membrane also affects the sensing characteristics of the biosensor. The ammonia PT-CNTs of different concentrations is used for the construction of the GOD electrodes. The experiment result shows that the addition of the ammonia PT-CNTs distinctly increases the response current. When the concentrations of the ammonia PT-CNTs are 0.5, 1, 2 and 4 mg mL^{-1}, the response currents of the prepared GOD electrodes in 6 mM glucose solution were 0.46, 0.90, 1.65 and 2.23 μA, respectively. However, the increasing ammonia PT-CNTs make the stability of the GOD matrix membrane somewhat deteriorated. In this experiment, 1 mg mL^{-1} CNTs is preferably used for the remainder of experiments.

3.5. Response characteristics of the GOD electrodes

The applied experimental potential could affect the amperometric determination of glucose, and thus we investigated the electrode responses at different potentials. With the increasing potential from 400 mV to 700 mV, the response current of the GOD electrode reached a plateau. To avoid interference at higher applied potential, a potential of 400 mV (versus SCE) was selected as the applied potential for amperometric measurements. Fig. 7 displayed typical amperometric i–t curve of the GOD electrode for successive additions of the same amounts of glucose (0.3 mM) under the optimized experimental conditions. The GOD electrode exhibited a rapid and sensitive response to glucose solution, and the response time was less than 10 s. As shown in the inset figure in Fig. 7. The response current linearly increased with the glucose concentration in the range of 1.2×10^{-4}–7.5×10^{-3} M, and the detection limit was 1.0×10^{-5} M (S/N > 3).

The repeatability of response current of the GOD electrodes was studied at a glucose concentration of 0.12 mM. The variation coefficient (VC) was 2.5% for five successive assays. Three GOD electrodes prepared independently in the same batch showed an acceptable reproducibility with a VC of 4.76% ($n = 4$) for the current determinations in 0.3 mM glucose solution.

Moreover, the GOD electrodes also displayed good storage stability. We measured the sensing response of the GOD electrode to 0.1 mM glucose. The response current of the GOD electrode decreased to 97.3% after storing for 10 days, and it maintained about 85.7 and 70.4% of its original response after 20 and 30 days, respectively.

4. Conclusion

A microwave plasma treatment method has been developed to enhance the solubility of carbon nanotubes. By using ammonia as precursor monomer, the resultant ammonia PT-CNTs maintained the carbon skeleton structure, while grafting new functional groups. The introduction of polar functional groups in the MWP treatment process greatly increased the hydrophilicity of CNTs, making the applications of CNTs in immobilizations of biomolecules and construction of biosensors more convenient.

Moreover, the ammonia PT-CNTs had a faster electron transfer capability than the pristine CNTs. It is thus evident that this microwave plasma treatment is a quite effective and reliable method for the functionalization of CNTs.

Acknowledgements

This work was supported by the National Natural Science Foundation of China (No. 20205004) and the Key Project of Chinese Ministry of Education (No. 106122).

References

[1] R.W. Keay, C.J. McNeil, Biosens. Bioelectron. 13 (1998) 963–970.
[2] K. Rekha, M.D. Gouda, M.S. Thakur, N.G. Karanth, Biosens. Bioelectron. 15 (2000) 499–502.
[3] S.J. Updike, B.J. Gilligan, M.C. Shults, R.K. Rhodes, Diabetes Care 23 (2000) 208–214.
[4] B. Aussedat, V. Thomé-Duret, G. Reach, F. Lemmonier, J.-C. Klein, Y. Hu, G.S. Wilson, Biosens. Bioelectron. 12 (1997) 1061–1071.
[5] L. Campanella, F. Pacifici, M.P. Sammartino, M. Tomassetti, Bioelectrochem. Bioenerg. 47 (1998) 25–38.
[6] K. Kriz, M. Anderlund, D. Kriz, Biosens. Bioelectron. 16 (2001) 363–369.
[7] S. Lijima, Nature 354 (1991) 56–58.
[8] P.M. Ajayan, Chem. Rev. 99 (1999) 1787–1799.
[9] Y.-D. Zhao, W.-D. Zhang, H. Chen, Q.-M. Luo, Talanta 58 (2002) 529–534.
[10] J. Wang, N. Li, Z. Gu, Anal. Chem. 74 (2002) 1993–1997.
[11] Y. Tu, Y. Lin, Z.F. Ren, Nano Lett. 3 (2003) 107–109.
[12] C.V. Nguyen, J. Delzeit, J. Han, M. Meyyappan, Nano Lett. 2 (2002) 1079–1081.
[13] M. Shim, N.W.S. Kam, R.J. Chen, Y.M. Li, H.J. Dai, Nano Lett. 2 (2002) 285–288.
[14] J. Li, H.T. Ng, A. Cassell, W. Fan, H. Chen, Q. Ye, J. Koehne, J. Han, M. Meyyappan, Nano Lett. 3 (2003) 597–602.
[15] X. Yu, D. Chattopadhyay, I. Galeska, F. Papadimitrakopoulos, J.F. Rusling, Electrochem. Commun. 5 (2003) 408–411.
[16] P.J. Poul, E.T. Mickelson, C.B. Huffman, L.M. Ericson, I.W. Chiang, K.A. Smith, D.T. Colbert, R.H. Hauge, J. Margrave, R.E. Smalley, Chem. Phys. Lett. 310 (1999) 367–372.
[17] A.R. Harutyunyan, B.K. Pradhan, J. Chang, G. Chen, P.C. Eklund, J. Phys. Chem. B 106 (2002) 8671–8675.
[18] M. Zhang, M. Yudasaka, S. Iijima, J. Phys. Chem. B 108 (2004) 149–153.
[19] J. Liu, A.G. Rinzler, H. Dai, J.H. Hafner, R.K. Bradley, P.J. Boul, A. Lu, T. Iverson, K. Shelimov, C.B. Huffman, F. Rodriguez-Macias, Y.-S. Shon, T.R. Lee, D.T. Colbert, R.E. Smalley, Science 280 (1998) 1253–1255.
[20] R.-Q. Kou, Z.-K. Xu, H.-T. Deng, Z.-M. Liu, P. Seta, Y. Xu, Langmuir 19 (2003) 6869–6875.
[21] D. Liming, J.G. Hans, W.H.M. Albert, J. Phys. Chem. B. 101 (1997) 9548–9554.
[22] Y. Iriyama, S. Ikeda, Polym. J. 26 (1994) 109–111.
[23] G. Kampfrath, R. Hinsche, Anal. Lett. 22 (1989) 2423–2431.
[24] B. Liu, Y.-H. Yang, Z.-Y. Wu, H. Wang, G.-L. Shen, R.-Q. Yu, Sens. Actuators B 104 (2005) 186–190.
[25] M. Muratsugu, S. Kurosawa, Y. Mori, N. Kamo, Chem. Pharm. Bull. 40 (1992) 501–503.
[26] K. Nakanishi, H. Muguruma, I. Karube, Anal. Chem. 68 (1996) 1695–1700.
[27] Z.-Y. Wu, Y.-H. Yang, G.-L. Shen, R.-Q. Yu, Anal. Chim. Acta 412 (2000) 29–35.
[28] H. Miyachi, A. Hiratsuka, K. Ikebukuro, K. Yano, H. Muguruma, I. Karube, Biotechnol. Bioeng. 3 (2000) 323–329.
[29] Q. Chen, L. Dai, M. Gao, S. Huang, A. Mau, J. Phys. Chem. B 105 (2001) 618–622.
[30] B.N. Khare, P. Wilhite, R.C. Quinn, B. Chen, R.H. Schingler, B. Tran, H. Imanaka, C.R. So, C.W. Bauschlicher, M. Meyyappan, J. Phys. Chem. B 108 (2004) 8166–8172.
[31] P. Chevallier, M. Castonguay, S. Turgeon, N. Dubrulle, D. Mantovani, P.H. McBreen, J.C. Wittmann, G. Laroche, J. Phys. Chem. B 105 (2001) 12490–12497.
[32] B.R. Samy, T. Michael, A.K. Farzaneh, F.D. Nathalie, M. Annie, F.L. James, A. Jacques, L.G. Francois, Anal. Chim. Acta 376 (1998) 133–138.
[33] M.A. Wójtowicz, F.P. Miknis, R.W. Grimes, W.W. Smith, M.A. Serio, J. Hazard. Mater. 74 (2000) 81–89.
[34] J.F. Evans, T. Kuwana, Anal. Chem. 49 (1977) 1632–1635.
[35] R.S. Nicholson, Anal. Chem. 37 (1965) 1351–1355.

Available online at www.sciencedirect.com
ScienceDirect
Talanta 72 (2007) 1288–1292
Talanta
www.elsevier.com/locate/talanta

Aminopyrene functionalized mesoporous silica for the selective determination of resorcinol

Wenxiang Xiao [a,b], Dan Xiao [a,*]

[a] College of Chemical Engineering, Sichuan University, Chengdu 610065, China
[b] Department of Electronic Engineering, Guilin University of Electronic Technology, Guilin 541004, China

Received 21 August 2006; received in revised form 30 December 2006; accepted 14 January 2007
Available online 20 January 2007

Abstract

Aminopyrene was convalently anchored onto the surface of mesoporous MCM-41 silica by post-grafting. This organic–inorganic hybrid has been applied as sensing material to phenols determination. Experimental results reveal that the functionalized material presents good sensitivity and selectivity towards resorcinol and can be used for resorcinol determination in water at pH 6.0. The fluorescence intensity of aminopyrene functionalized mesoporous silica decreases proportionally to the logarithm of resorcinol concentration in water. The linear range for resorcinol detection lies in 4.79–163 μM with a detection limit of 2.86 μM (S/N = 3).

Keywords: Mesoporous silica; Aminopyrene; Functionalization; Resorcinol

1. Introduction

Phenolic compounds are widely used chemicals and released into the environment by a large number of industries including resins and plastics, wood preservation, petroleum refining, dyes, chemicals and textiles [1]. However, most phenols are also major environmental pollutants with toxicity that pose a great threat to human health [2]. Thus the presence and concentration of these contaminants must be detected and monitored not only in aqueous effluents from industrial processes but also in beverages, juice and bottled drinking water. Many techniques have been used for monitoring phenols, such as spectrophotometric [3], high-performance liquid chromatography with diode array detection [4], microchip capillary electrophoresis with end-channel amperometric detection [5], quartz crystal microbalance [6], flow injection chemiluminescence [7] and surface plasmon resonance [8], fluorescence [9,10]. Biosensors based on immobilized enzymes for the detection of phenols have been recently reported in the literatures, involving tyrosinase [11–14], recombinant fungal laccase [15] and immobilized bacteria [16].

Herein, we report on the synthesis and characterization of aminopyrene functionalized MCM-41 type mesoporous silica material that serves as fluorescence probe for the selective determination of phenols in water. By post-grafting, mesoporous silica was first functionalized with 3-aminopropyltriethoxysilane and then 1-pyrenecarboxaldehyde was anchored onto the matrix through a Schiff base condensation. This aminopyrene functionalized material shows different response behaviors to phenols and possesses good selectivity and sensitivity towards resorcinol.

Since the discovery of periodic mesoporous materials in 1992, various routes of functionalizing their pore surface have been reported to yield hybrid materials with improved adsorption, extraction, ion exchanges, or catalytic abilities [17]. The optical organic–inorganic hybrids are excellent materials in the development of optical sensors because microscopic mesoporous siliceous hosts possess the advantages of optical transparency in the visible region while guaranteeing fastness toward UV radiation. Based on mesoporous silica monolith containing functional groups, an optical metal ion sensor has been developed by converting the conventional fast metal-ligand complexation into slow diffusion-controlled binding, which is suitable for metal ion quantitative analysis [18]. Metal ions sensing materials could also be obtained by incorporating fluorescent chelate ligands into the mesopores of MCM-41 through

* Corresponding author. Tel.: +86 28 85407958; fax: +86 28 85407859.
E-mail address: xiaodan99@sohu.com (D. Xiao).

0039-9140/$ – see front matter © 2007 Elsevier B.V. All rights reserved.
doi:10.1016/j.talanta.2007.01.032

simple assembling [19]. Attaching pH sensitive dyes, fluorescein isothiocyanate, covalently to mesoporous silica matrix, pH-sensor with mesoporous thin films was developed [20]. Nicole et al. reported a dibenzoylmethane-silica mesostructured optical sensor for uranyl cations determination [21]. Functionalized mesopores can even be used as receptor for the selective determination of anions [22,23]. Selective functionalization of the exterior and interior surface of the structurally uniform mesoporous materials, such as MCM-41 or SBA-type of silica, with different organic moieties allows for precise regulating the penetration of molecules with certain sizes and chemical properties into the nanoscale pores [24–26]. Basing on the gatekeeping effect of poly(lactic acid), fluorescence probe based on mesoporous silica nanospheres has been developed for distinguishing neurotransmitters containing amino according to their different penetrating rates through the gatekeeping layer [27].

2. Experimental

2.1. Instrumentations

Fluorescence spectra were obtained on a Perkin-Elmer LS-55 spectrofluorimeter equipped with a 10 mm quartz cuvette. The excitation and emission slit widths were set at 10 and 7.5 nm, respectively. The scanning rate of monochromators was maintained at 240 nm min^{-1}. Mesoporous silica was characterized by transmission electron microscope (TEM, Hitachi H-800) operating at an accelerating voltage of 200 kV. Powder X-ray diffraction (XRD) data were recorded using a Philip X'pert pro diffractometer with Cu Kα radiation (λ = 1.5406 Å). And Fourier transform infra-red (FT-IR) spectra were obtained on a Thermo Nicolet NEXUS 670 FT-IR spectrophotometer.

2.2. Reagents

All reagents were of analytical reagent grade unless stated otherwise. Reagents such as 1-pyrenecarboxaldehyde (Lancaster, A Johnson Matthey Company), tetraethyl orthosilicate (TEOS), phenol, resorcinol, catechol, hydroquinone, phlorglucinol, and pyrogallol were used as received except that 3-aminopropyltriethoxysilane (APTSi) was purified by under-pressure distillation before use. Phenols stock solutions (0.1 mol L^{-1}) were prepared with doubly distilled water and kept in dark glass at 4 °C. Doubly distilled water was used throughout the experiment.

2.3. Preparation of aminopyrene functionalized mesoporous silica (solid 1)

Mesoporous silica MCM-41 was synthesized according to the reported method [28]. Mesoporous silica was dispersed in dry toluene (1 g solid in 30 mL), and then excess of 3-aminopropyltriethoxysilane (3.0 mL) was added. The mixture was refluxed for 24 h. The amino-functionalized solid was filtered and washed first with dichloromethane and then with ethanol. One gram of the resulting solid was redispersed in dry toluene and reacted with 0.5 g 1-pyrenecarboxaldehyde under refluxing for 24 h. After that, excessive $NaBH_4$ (110 mg) was added and stirred at room temperature for 10 h. The resulting solid was washed with 0.01 M HCl and then with water until pH was 5–6. Any residual reactants were removed by Soxhelt extraction over ethanol for two days. Finally, yellow powder was obtained and dried for use. This organic–inorganic hybrid material is denoted as *solid 1* in the context.

2.4. Phenols determination

Solid 1 floats on aqueous solution and does not disperse well direct in water, while a stable suspension can form in ethanol and DMSO. Solid 1 (0.2500 g) was first wetted with ethanol and then diluted with water to 250 mL to obtain a solution with concentration of 1.0 mg mL^{-1}. For phenols determination, 2.50 mL of solid 1 solution and appropriate volume of phenols stock solution were added into a 10 mL flask and diluted to the mark with water. After 10 min, fluorescence emission was recorded at 471 nm with excitation wavelength at 403 nm in a 10 mm cuvette. Based on the fluorescence quenching of solid 1 caused by phenols addition, a method for phenols determination in water can be established.

3. Results and discussion

3.1. Synthesis of solid 1 as sensing material

Mesoporous materials especially siliceous MCM-41 have increasingly gained popularity in chemical sensing due to their narrow and controlled pore size distribution in ordered hexagonal channels with comparatively large pore opening. In this research, the MCM-41 solid was converted to a suitable receptor by a straight reaction with 3-aminopropyltriethoxylsilane and then further reaction with 1-pyrenecarboxaldehyde to obtain the sensing material, solid 1, for the detection of phenols (Scheme 1). In this functionalized hybrid, aminopyrene groups

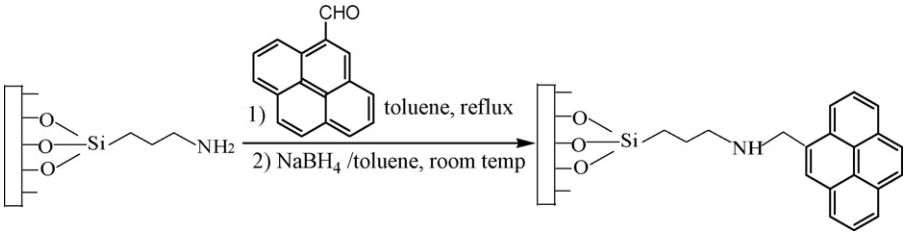

Scheme 1. Synthesis of the functionalized MCM-41 solid 1.

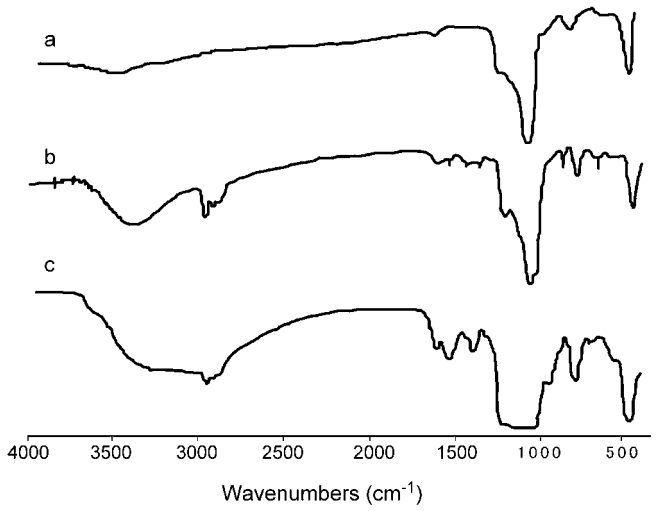

Fig. 1. FT-IR spectra of three solids: curve a, MS; curve b, amine functionalized MS; curve c, aminopyrene modified MS.

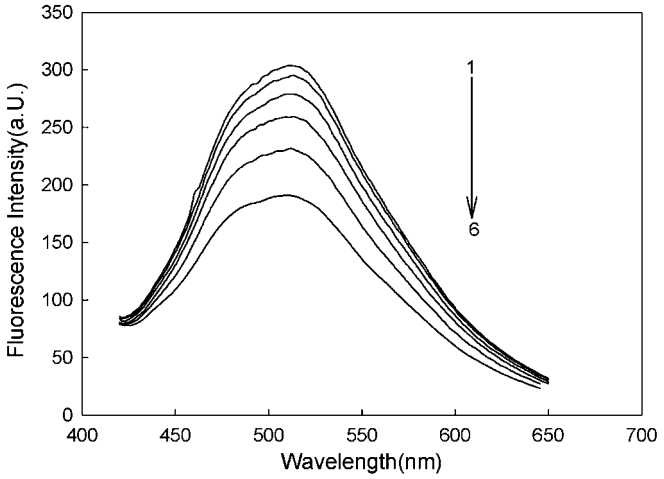

Fig. 2. Fluorescence emission quenching of solid 1 caused by increasing resorcinol additions. And the resorcinol concentration of curves 1–6 is 0, 4.79×10^{-6}, 9.58×10^{-6}, 1.92×10^{-5}, 2.87×10^{-5}, 4.79×10^{-5} mol L^{-1}, respectively.

were convalently grafted onto mesoporous silica materials. Amino groups are good coordination sites, whereas pyrene moiety has been included as signaling subunit to detect phenol-solid interaction. X-ray diffraction (XRD) analysis (not shown) reveals that the modified solid only has a slight decrease in *d*-spacing for the (1 0 0) diffraction peak (from 4.40 to 4.10 nm) and the typical features of MCM-41 phase are retained after aminopyrene functionalization. As shown in Fig. 1, upon amine functionalization the infrared spectrum shows the typical N–H and C–H stretching vibrations in the region of 3400–3000 and 2974 cm^{-1}, respectively. After pyrene was anchored, new bands are observed at 1400 cm^{-1}, which may be ascribed to C–N stretching vibration. These results indicate that aminopyrene was convalently anchored on the mesoporous silica through a Schiff condensation between the free amine groups on the surface of the material and C=O of 1-pyrenecarboxaldehyde, just as depicted in Scheme 1.

3.2. Fluorescence characteristics of solid 1

The fluorescence intensity and emission wavelength of solid 1 are dependent on the polarity of solvent. The maximal fluorescence excitation and emission occur at 405 nm/511 nm in DMSO and 405 nm/455 nm in ethanol while 403 nm/471 nm in aqueous solution. The fluorescence intensity is water > ethanol > DMSO. Phenols, especially resorcinol, can remarkably quench the fluorescence emission of aminopyrene functionalized mesoporous silica. Upon phenol additions, fluorescence intensity at 471 nm decreases as the phenol concentration increases (Fig. 2).

3.3. Effect of pH on the fluorescence intensity of solid 1

Using HCl and NaOH as pH adjusting reagents, the effect of pH on the fluorescence intensity of solid 1 was investigated. Fluorescence intensity of solid 1 is significantly affected by the acidity of the media, as shown in Fig. 3. In basic media, fluorescence intensity maintains almost the same level. However, emission decreases apparently and the pale yellow particles turn orange immediately when exposing to acid media. Maximal fluorescence emission was obtained when pH was around 6.0. Thus pH was kept at 6.0 in the following experiments.

3.4. Responses of solid 1 to different phenols

Phenols can cause fluorescence quenching of solid 1. Fig. 4 shows the relative fluorescence quenching I_0/I (I_0 and I are the fluorescence intensity of solid 1 in the absence and presence of phenols, respectively) of the pyrene signaling subunit of solid 1 versus the phenols concentration in water. Phenol, resorcinol and phloroglucinol with one, two and three hydroxyl groups, respectively, have been investigated as target analytes. Resorcinol addition to the functionalized MCM-41 particle suspension results in a remarkable fluorescence quenching. At the same concentration as resorcinol (for example,

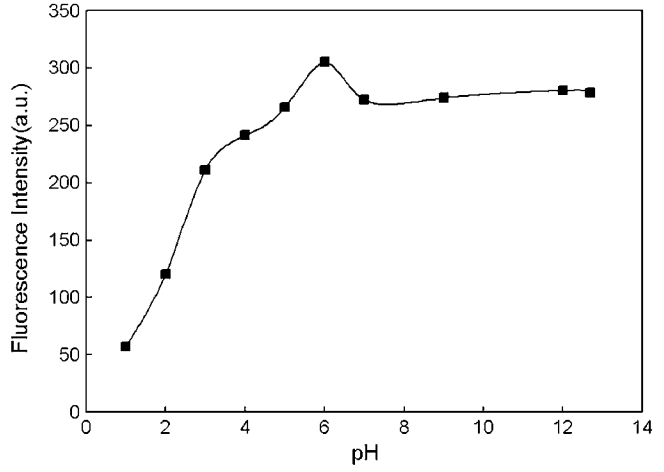

Fig. 3. Effect of pH on the fluorescence intensity of solid 1.

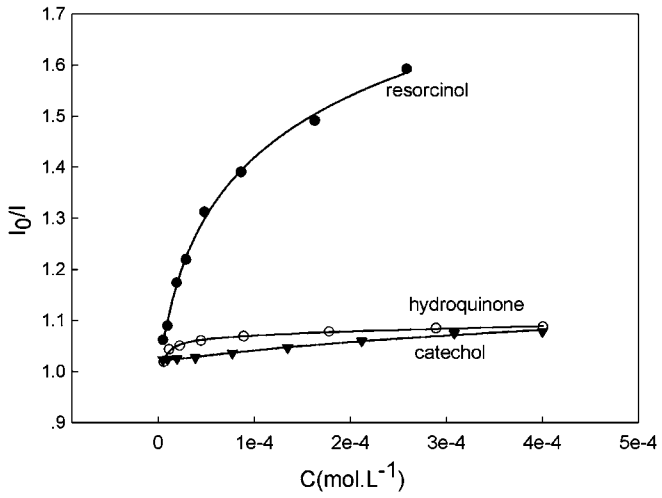

Fig. 4. Fluorescence titration curve of solid 1 for bi-hydroxy phenols.

1.00×10^{-4} mol L^{-1}), the addition of phenol caused about 30% fluorescence quenching and phloroglucinol induced 5% quenching comparing to resorcinol addition. It seems that the different response behaviors of solid 1 to phenols may be related to the number of hydroxyl. Bi-hydroxyl phenols, hydroquinone and catechol, were also investigated on the fluorescence quenching of solid 1 and the results are shown in Fig. 4. Resorcinol shows the largest response once again. Solid 1 presents insensitive and indistinctive response to tri-hydroxyl phenols—phloroglucinol and pyrogallol. Among the phenol and poly-phenols investigated, it can be concluded that solid 1 possesses good selectivity and sensitivity towards resorcinol.

Why solid 1 shows determining selectivity towards resorcinol among the similar bi-hydroxyl phenols? On the one hand, changes in the fluorescence of solid 1 caused by the presence of resorcinol can probably be attributed to the formation of hydrogen bonds between –OH and the amino groups, and/or to a π-stacking interaction between resorcinol and pyrene moieties. On the other hand, anchoring functional groups onto mesoporous MCM-41 as sensing materials can usually improve sensitivity and selectivity due to its characteristic periodicity of mesoporosity. Functional groups were usually combined with mesoporous silica through silanol condensation. In the most of synthetic methods of functionalized mesoporous silica, functional groups are not aligned in similar or parallel orientation but in intersectional style because of the not so highly ordered mesostructure [29,30]. Thus the neighboring two functional groups and the mesopore wall would constitute a nanoscale cavity. These nanosized cavities could act as binding pockets and be used as hosts for the target guest to be coordinated and sensed. In order to test the effect of the nanoscale pores, research group of R. Martínez-Máñez prepared materials from fumed silica, which lacks the homogeneous porosity characteristic of mesoporous solids, with similar functionalization [22,25]. Their studies indicated that fumed silica showed a very poor response to the same analyte compared to that of mesoporous one. This suggests that the presence of pores in mesoporous silica could favor spatial proximity between coordination subunits and thus enhance the coordinating ability of the binding groups in the nanoscale pockets towards analyte. Though after aminopyrene functionalization the mesopore size of the solid will decrease and even may be blocked, the surface of the solid must still retain its periodicity: a periodicity that, conveniently modulated by the bonded ligand molecules, fits with analyte's size, charge and geometry. The nanosized cavities lined with binding sites from the surface of mesoporous solid act as spatial selector in sensing. If resorcinol's shape fits the cavities, there must be a larger number of amino-resorcinol contact occurring than other phenols. In the case of hydroquinone and catechol, their structures may not be so suitable for enclosing in the cavity host comparing to that of resorcinol. Hence a weak interaction occurs between solid 1 and hydroquinone and catechol. Using its solid surface and nanosized cavities as an additional sensing factor, solid 1 remarkably enhances its response to resorcinol. However, the real mechanism for the selective response of solid 1 to resorcinol is still under investigation.

3.5. Analytical parameters for resorcinol detection

For resorcinol determination, calibration curve can be established based on the linear relationship of fluorescence quenching (I_0/I) of solid 1 versus the logarithm of the resorcinol concentration in water. In the range of 4.79–163 μM, the calibration curve equation can be expressed as: $I_0/I = 2.6806 + 0.3165 \log C$ (mol L^{-1}) with a correlation coefficient $r^2 = 0.997$ (Fig. 5). The detection limit (LOD) is 2.86 μmol L^{-1} of resorcinol calculated from three times of standard deviation (S/N = 3). The relative standard deviation for five replicate measurements is 2.2%.

3.6. Interferences

The influence of some common substances on the determination of resorcinol was investigated by preparing solutions containing 5×10^{-5} mol L^{-1} resorcinol. Within an error less

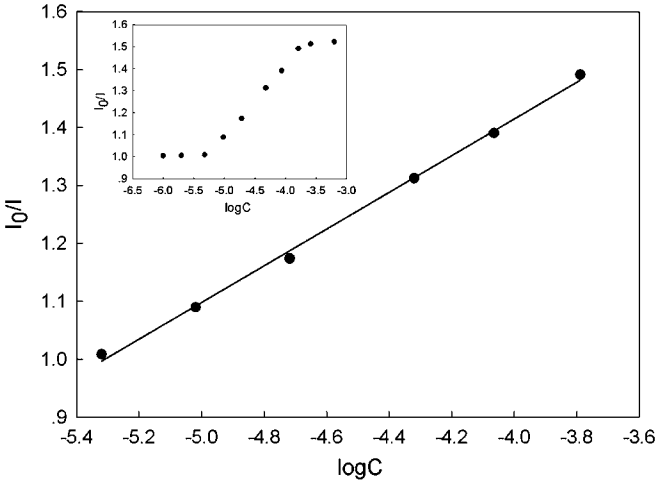

Fig. 5. The calibration curve for resorcinol determination.

Table 1
Determination of resorcinol in pharmaceutical samples

Pharmaceutical samples	Determined[a] (μmol L^{-1})	Added (μmol L^{-1})	Found (μmol L^{-1})	Recovery (%)
Sample 1	18.16	10.00	10.35	103.50
		40.00	40.44	101.10
Sample 2	41.37	40.00	39.92	99.80
		80.00	83.92	104.90
Sample 3	90.82	20.00	19.72	98.60
		50.00	47.86	95.73

[a] The results listed are the 10 000, 1000, 10 000 times diluted solution of samples 1, 2 and 3, respectively.

than 5% on the fluorescence intensity, no interference was observed when including up to 200-fold Cl^-, NO_3^-, CO_3^{2-}, PO_4^{3-}, SO_4^{2-}, AcO^-, Na^+, K^+, Ca^{2+}, Mg^{2+}, Cu^{2+}, Co^{2+}, Mn^{2+}, Hg^{2+}, Pb^{2+}, Ni^{2+}, Sr^{2+}, Cr^{3+}, Ba^{2+}, Cd^{2+}, Fe^{2+}, Al^{3+}, Tb^{3+}, Ag^+, SCN^-, NO_2^-, $C_2O_4^{2-}$, H_2O_2, ascorbic acid, salicylate, citrate, aniline, *o*-nitroaniline and 50-fold Fe^{3+}, Zn^{2+}, Nd^{2+}, $Cr_2O_7^{2-}$. However, *o*-nitrophenol, *m*-nitrophenol, *p*-nitrophenol, 2,4-binitrophenol, picric acid would interfere the detection of resorcinol.

3.7. Applications

The proposed method was applied to the determination of resorcinol in several pharmaceutical samples. Compound salicylic acid liniment (sample 1, San Yi Pharmaceutical Ltd., Wuhu China), Piyanning tincture (sample 2, Zheng Dong Pharmaceutical Co., Sichuan China) and compound resorcinol lotion (sample 3, Huaxi Hospital, Chengdu China) were commercial products and filtered through a cellulose acetate membrane (0.45 μm pore size) before measurements. Fluorescence measurement and calculation were performed following the analytical procedure described above. Samples 1, 2 and 3 were 10 000, 1000 and 10 000 times diluted respectively to ensure that the response lies in the linear range of the calibrated curve. The results are summarized in Table 1 (data based on the average of three determinations). Recovery tests were also carried out based on the commercial formulations and results show that the recoveries are acceptable.

4. Conclusion

Mesoporous silica was functionalized with aminopyrene and applied to the selective determination of resorcinol in water. Combining the binding properties of molecular receptors with the structure characteristic of mesoporous material opens possibilities in developing new sensing system. This work presents another example for the potential use of the organic–inorganic hybrid materials in optical sensing applications.

Acknowledgements

This work was financially supported by National Natural Science Foundation of China (no. 20575042) and the Key Project of Chinese Ministry of Education (no. 105141).

References

[1] G.W. Ware (Ed.), Reviews of Environmental Contamination and Toxicology, vol. 126, Springer, New York, 1992, p. 100.
[2] A.M. Klibanov, T.M. Tu, K.P. Scott, Science 221 (1983) 259.
[3] C. Kang, Y. Wang, R. Li, Y. Du, J. Li, B. Zhang, L. Zhou, Y. Du, Microchem. J. 64 (2000) 161.
[4] L. Yang, Z. Wang, L. Xu, J. Chromatogr. A 1104 (2006) 230.
[5] Y. Wu, J.-M. Lin, J. Sep. Sci. 29 (2006) 137.
[6] A. Mirmohseni, A. Oladegaragoze, Sens. Actuators B 98 (2004) 28.
[7] J. Du, Y. Li, J. Lu, Talanta 55 (2001) 1055.
[8] J.D. Wright, J.V. Oliver, R.J.M. Nolte, S.J. Holder, N.A.J.M. Sommerdijk, P.I. Nikitin, Sens. Actuators B 51 (1998) 305.
[9] M. del Olmo, A. Zafra, A.B. Jurado, J.L. Vilchez, Talanta 50 (2000) 1141.
[10] M.F. Pistonesi, M.S. Di Nezio, M.E. Centurión, M.E. Palomeque, A.G. Lista, B.S. Fernández Band, Talanta 69 (2006) 1265.
[11] Z. Dai, X. Xu, L. Wu, H. Ju, Electroanalysis 17 (2005) 1571.
[12] T. Mai Anh, S.V. Dzyadevych, A.P. Soldatkin, N. Duc Chien, N. Jaffrezic-Renault, J.-M. Chovelon, Talanta 56 (2002) 627.
[13] R. Solná, S. Sapelnikova, P. Skládal, M. Winther-Nielsen, C. Carlsson, J. Emnéus, T. Ruzgas, Talanta 65 (2005) 349.
[14] J. Abdullah, M. Ahmad, L.Y. Heng, N. Karuppiah, H. Sidek, Talanta 70 (2006) 527.
[15] J. Kulys, R. Vidziunaite, Biosens. Bioelectron. 18 (2003) 319.
[16] P. Skláda, N.O. Morozova, A.N. Reshetilov, Biosens. Bioelectron. 17 (2002) 867.
[17] K. Moller, T. Bein, Chem. Mater. 10 (1998) 2950.
[18] R.L. Rodman, H. Pan, C.W. Clavier, X. Feng, Z.-L. Xue, Anal. Chem. 77 (2005) 3231.
[19] H.-D. Zhang, P. Zhang, Y.-H. Sun, K.-Q. Ye, J.-Y. Zhang, Y. Wang, Chem. J. Chin. Univ. 27 (2006) 506.
[20] G. Wirnsberger, B.J. Scott, G.D. Stucky, Chem. Commun. (2001) 119.
[21] L. Nicole, C. Boissière, D. Grosso, P. Hesemann, J. Moreau, C. Sanchez, Chem. Commun. (2004) 2312.
[22] A.B. Descalzo, D. Jimenez, M.D. Macros, R. Martínez-Máñez, J.E. Haskouri, C. Guillém, D. Beltrán, P. Amorós, M.V. Borrachero, Adv. Mater. 14 (2002) 966.
[23] A.B. Descalzo, K. Rurack, H. Weisshoff, R. Martínez-Máñez, M.D. Macros, P. Amorós, K. Hoffman, J. Soto, J. Am. Chem. Soc. 127 (2005) 184.
[24] V.S.-Y. Lin, C.-Y. Lai, J. Huang, S.-A. Song, S. Xu, J. Am. Chem. Soc. 123 (2001) 11510.
[25] M. Comes, G. Rodríguez-López, M.D. Marcos, R. Martínez-Máñez, P. Amoró, J. Soto, L.A. Villaescusa, P. Amorós, D. Beltrán, Angew. Chem. 117 (2005) 2978.
[26] M. Comes, M.D. Marcos, R. Martínez-Máñez, F. Sancenón, J. Soto, L.A. Villaescusa, P. Amorós, D. Beltrán, Adv. Mater. 16 (2004) 1783.
[27] D.R. Radu, C.-Y. Lai, J.W. Wiench, M. Pruski, V.S.-Y. Lin, J. Am. Chem. Soc. 126 (2004) 1640.
[28] Q. Cai, W.-Y. Lin, F.-S. Xiao, W.-Q. Pang, X.-H. Chen, B.-S. Zou, Micropor. Mesopor. Mater. 117 (1999) 1.
[29] X. Feng, G.E. Fryxell, L.Q. Wang, A.Y. Kim, J. Liu, K.M. Kemner, Science 276 (1997) 923.
[30] Q. Yang, M.P. Kapoor, S. Inagaki, J. Am. Chem. Soc. 124 (2002) 9694.

Available online at www.sciencedirect.com
ScienceDirect
Talanta 72 (2007) 1316–1321
Talanta
www.elsevier.com/locate/talanta

Separation of aminophenol isomers in polyelectrolyte multilayers modified PDMS microchip

Yan Xiao, Kai Wang, Xiao-Dong Yu, Jing-Juan Xu, Hong-Yuan Chen *

The Key Lab of Analytical Chemistry for Life Science, School of Chemistry and Chemical Engineering, Nanjing University, Nanjing 210093, China

Received 6 November 2006; received in revised form 11 January 2007; accepted 14 January 2007
Available online 19 January 2007

Abstract

The separation of three kinds of aminophenol isomers were achieved within 1 min in polyelectrolytes multilayers modified PDMS microchips by layer-by-layer assembly with electrochemical detection (EC). Two polyelectrolytes, poly(dially dimethyl ammonium chloride) (PDDA) and poly(sodium-4-styrene-sulfonate) (PSS) were used to form polyelectrolyte multilayers (PEMs). The surface characteristic of the modified microchip was studied by XPS. The electroosmotic flow (EOF) on PEMs modified PDMS microchips was more stable than that of the native PDMS microchips and the adsorption of samples was greatly reduced on PEMs modified PDMS microchips during the electrophoretic process. The column efficiencies on PEMs modified microchip were increased by 100 times and the signals enhanced by 2 times compared with those of native microchips. The separation conditions such as running buffer pH, running buffer concentration and separation voltage were also optimized.

Keywords: Aminophenol isomer; Modified PDMS microchips; Polyelectrolyte multilayers; Poly(dially dimethyl ammonium chloride); Poly(sodium-4-styrene-sulfonate); Electrochemical detection

1. Introduction

Aminophenol isomers with similar characteristics belong to one kind of positional isomers. They are the important synthetic intermediates of many compounds in chemical engineering. Therefore, it is important to establish the separation method of aminophenol isomers. Thin-layer chromatrography [1], capillary electrophoresis (CE) [2] and high performance liquid chromatography [3,4] have been widely used to separate aminophenol isomers. Recently, microfluidic devices as potential powerful tools for chemical and biological assays, which offer rapid analysis and low sample consumption and cost, are paid great attention [5–8]. However, to the best of our knowledge, there is only one report related to separation of aminophenol isomers, in which gold-nanoparticle modified glass microchips with the total separation length of 77 mm were used to successfully separate aminophenol isomers within 160 s [9].

Because the microfluidic devices made of glass and quartz are expensive and time-consuming, and the microchannels are easy to be blocked up, polymer substrates, such as poly (dimethylsiloxane) (PDMS), poly(methylmethacrylate) (PMMA), polystyrene, polycarbonate and others have been used to fabricate microfluidic devices [10–12] recently. These polymer substrates are less fragile and more suitable for mass production, thus the polymeric microfluidic devices are more cost effective. Among them, PDMS has been the most popular soft plastic substrate because of its optical transparency, elasticity, easy handling, and good sealing properties. However, PDMS microfluidic devices exhibited poor separation efficiency that must be overcome. The peak broadening was believed to be due to the adsorption of hydrophobic analytes or species containing hydrophobic domains to the polymer surface. Also, the electroosmotic flow (EOF) in PDMS channels is unstable.

The layer-by-layer (LbL) assembly method which was first introduced by Decher in 1991 [13] is a rich, versatile, and significantly inexpensive approach to the formation of thin films via alternating adsorption of positively and negatively charged species from aqueous solutions and this method has been applied in many fields such as biosensors [14–18], nonlinear optical devices [19–21] and surface modification [22–24]. Recently, polyelectrolyte multilayers (PEMs) method has been introduced as more permanent and stable modification method in capillary electrophoresis (CE). The alternate adsorption of a cationic and

* Corresponding author. Tel.: +86 25 83594862; fax: +86 25 83594862.
E-mail address: hychen@nju.edu.cn (H.-Y. Chen).

0039-9140/$ – see front matter © 2007 Elsevier B.V. All rights reserved.
doi:10.1016/j.talanta.2007.01.037

anionic polyelectrolyte leads to the formation of a stable coating, which can greatly reduce the adsorption of solutes and improve the separation efficiencies. Some PEMs such as PDDA/PSS [25] and dextran sulfate (DS)/polybrene [26,27] were used to modify the capillaries for the separation of protein. The successful application of PEMs in CE suggested that it is a good idea to use PEMs to dynamically coat microfluidic devices [28,29]. For example, a DS/polybrene modified PDMS microchip has been used to separation dopamine and hydroquinone by EC detection [28]. The achievements of using PEMs to modify microchips indicate that PEMs modification method can be employed to suppress the analytes adsorption and to control EOF of PDMS microchips effectively.

In this paper, the multilayer film of PDDA/PSS was applied to modify PDMS microchips successfully. Separation of aminophenol isomers was performed within 1 min on the PEMs modified PDMS microchip. The results showed that samples adsorption was greatly reduced on the PEMs modified PDMS microchips during the electrophoresis process. The column efficiencies on PEMs modified microchips were increased by 100 times than those of native microchips.

2. Experimental section

2.1. Chemicals and solutions

Sylgard 184 (PDMS) was purchased from Dow Corning (Midland, MI, USA). The carbon fiber ($d = 8\ \mu m$) was purchased from Goodfollow Corporation (Oxford, UK). PDDA (20% in water, $d = 1.04$, $M_w = 200{,}000$–$350{,}000$) and PSS (30% in water, $d = 1.147$, $M_w = 200{,}000$) were purchased from Sigma–Aldrich (St. Louis, MO, USA). Aminophenol isomers, acetic acid, potassium dihydrogen phosphate and sodium hydroxide were obtained from Shanghai Chemical Reagents Corporation (Shanghai, China). Sodium acetate trihydrate, sodium phosphate dibasic and phosphorous acid were obtained from Nanjing Chemical Reagents No. 1 Factory (Nanjing, China). All reagents were of analytical grade and used without further purification. The phosphate-buffered salines (PBS) in different pH were prepared with 20 mM KH_2PO_4 and Na_2HPO_4 solutions. The running buffer used for electrophoresis separation was prepared by mixing 0.10 M sodium acetate solution and 0.10 M acetic acid at different volume ratio diluted to proper concentration with distilled water. One millimolar stock solutions of aminophenol isomers were prepared with doubly distilled water before each experiment. Before use, they were diluted with corresponding running buffer to proper concentration. PDDA and PSS solutions were prepared with 1:10,000 dilution of original material with distilled water, respectively. All the solutions were filtered through a 0.22 μm cellulose acetate filter (Xinya Purification Factory, Shanghai, China) before use.

2.2. Fabrication of PDMS microchips

A straight separation PDMS microchannel with cross-sampling channel was made based on a master composed of a positive relief structure of GaAs for the channels microfabricated in No. 55 Electronic Institution (Nanjing, China) by using standard microphotolithographic technology. The PDMS was weighed, degassed, and poured over the channel master. After curing at 80 °C for 2 h and cooling at room temperature, the PDMS was stripped from the master, producing a pattern of negative relief channels and reservoirs in the PDMS. Then it was cut into suitable size and punched holes of 4 mm in diameter. A thin piece of PDMS substrate was obtained by casting the polymer mixture in a glass box. The sampling channel was 30 μm in width, 18 μm in depth and the separation channel was 50 μm in width and 18 μm in depth, respectively. The structured PDMS piece and PDMS substrate were ultrasonically cleaned with acetone, methanol and water for 20 min, respectively. Then they were dried under an infrared lamp and adhered with each other reversibly by finger pressure. The total length of the separation channel was 40 mm and the effective separation length was 35 mm. The electrochemical detection was carried out with in-column detection mode.

2.3. Dynamic coating of microchannel

PDMS microchannels were coated with PDDA and PSS according to the conventional procedures described in literature [25]. Briefly, the PDDA solution was first syringed into buffer reservoir, sample reservoir and sample waste reservoir, respectively. Then the solution was forced into the PDMS microchannels by a vacuum pump and allowed to stand for 15 min to form a PDDA covered surface. Then the PDDA solution was pumped out of the microchannels. After that the doubly distilled water was forced into the microchannels to rinse them completely and pumped out. With the same procedure, the PSS layer was adhered to PDDA layer by electrostatic interaction. Repeating the above procedures, a $(PDDA/PSS)_2$ film were obtained. These kind of modified microchips have a negatively charged surface. The structures of PDDA and PSS were shown in Fig. 1.

2.4. Microanalysis system

PDMS microchip was horizontally fixed on a plexiglass holder with a precisely three-dimensional system (Shanghai Lian Yi Instrument Factory of Optical Fibre and Laser, China) as we reported previously [30]. At the end of the channel was a solution reservoir with silicone grease providing a proper sealing. This reservoir served as both the cathodic buffer waste reservoir

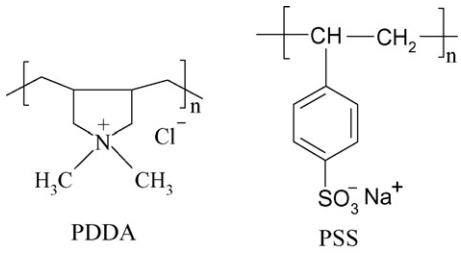

Fig. 1. The structures of PDDA and PSS.

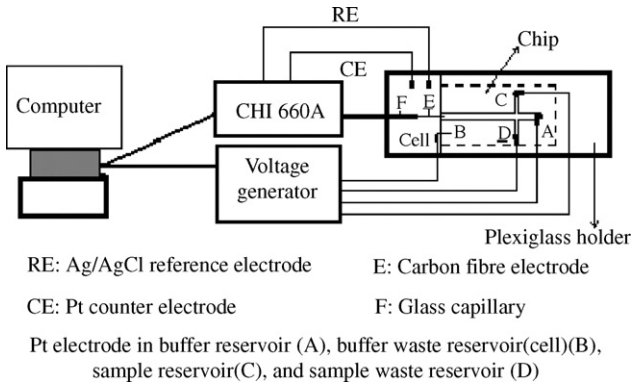

Fig. 2. Schematic diagram of the microanalysis system.

for the electrophoresis and the electrochemical detection cell. The working electrode placed in a plexiglass screw was inserted into the electrode hole on the platform with silicon grease to prevent leaking of the detection cell. The location of working electrode in channel was adjusted under the stereoscopic microscope (XTB-1, Jiangnan Optical Instrument Factory, Nanjing, China). A carbon fiber cylindrical electrode with a diameter of 8 μm served as working electrode, and the electrode was placed in the end of the separation channel with a distance of 40 μm from the tip of the working electrode to the channel exit. An Ag/AgCl reference electrode, a platinum wire counter electrode and a grounding platinum electrode were placed into the detection cell. This microanalysis system was shown in Fig. 2. Electrochemical detection based on "amperometric *i–t* curve" mode was carried out at a detection potential of 1.0 V with a three-electrode system and performed on Electrochemical Analyzer CHI 660A (CHI Instrument, USA). A homemade voltage supply provides the separation voltage ranging from 0 to 5000 V. All parameters can be set up and automatically switched via RS232 communication port of personnel computer with homemade software. The separation current can be monitored graphically in real time automatically. Four platinum electrodes were used to connect the reservoirs and the voltage supply in the injection and separation procedures.

2.5. X-ray photoelectron spectroscopy (XPS) measurement

A $(PDDA/PSS)_2$ coated PDMS slide was analyzed by XPS. The spectra were recorded with ESCALAB MK2 spectrometer (VG Corporation, UK) with an Mg K-alpha X-ray radiation as the source for excitation.

2.6. Electrophoresis procedure

Before separation, a running buffer was directly syringed into the reservoirs, flushed through channels under vacuum. Then the device was flushed for 15 min with the running buffer at high voltage of 1000 V. A sample was injected into the separation channel using a simple crossing injection mode. The injection was carried out by applying high voltage to the sample reservoir for a suitable time through Pt electrode connected to the power supply, with the sample waste reservoir grounded and the other reservoirs floating. During the separation procedure, the sample reservoir and sample waste reservoir were kept floating.

3. Results and discussion

3.1. Electrochemical detection

Electrochemical detection would be a good candidate coupled with micro total analysis systems (μ-TAS) for its inherent miniaturization and high sensitivity [31]. Here we use an in-channel amperometric detection mode for microchip with a single carbon fibre cylindrical electrode directly mounted in the end of separation channel. The detection potentials of the analytes were investigated and the hydrodynamic voltammograms of analytes on PEMs modified PDMS microchips obtained (Fig. 3). As can be seen from Fig. 3, all compounds displayed similar curves. The peak current of *p*-aminophenol increased rapidly with the increase of detection potential until +1.0 V. From +0.2 to +1.0 V the peak current of *o*-aminophenol increased, and the same trend was observed with *m*-aminophenol from +0.6 to +1.0 V. When the applied potential was over +1.0 V (*versus* Ag/AgCl), the carbon fibre electrode could be oxidized with the result that baseline currents greatly increased, accompanied with the decrease of peaks currents. Therefore, +1.0 V (*versus* Ag/AgCl) was selected as the detection potential in this case, where the background current was relatively lower and the S/N ratio was the highest.

3.2. Properties of the modified microchips

3.2.1. XPS

XPS analysis was employed to confirm the presence of PDDA and PSS on the PDMS surface. Fig. 4(A) and (B) showed N 1s region and S 2p region of the native PDMS and PEMs coated PDMS, respectively. The peaks at 405–407.5 and 173 eV were ascribed to the characteristic peaks of N and S, respectively, suggesting that the PEMs had been successfully coated on PDMS. The presence of double peaks of N 1s was likely due to the X-ray-induced decomposition of sample during the experiment.

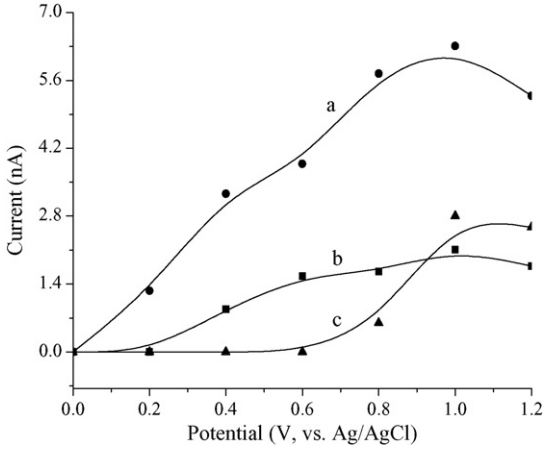

Fig. 3. Hydrodynamic voltammograms for 40 μM *p*-aminophenol (a), 60 μM *o*-aminophenol (b), and 100 μM *m*-aminophenol (c). Condition: 20 mM acetate buffer, pH 5.0; sample injection at +600 V for 3 s; separation voltage +1000 V.

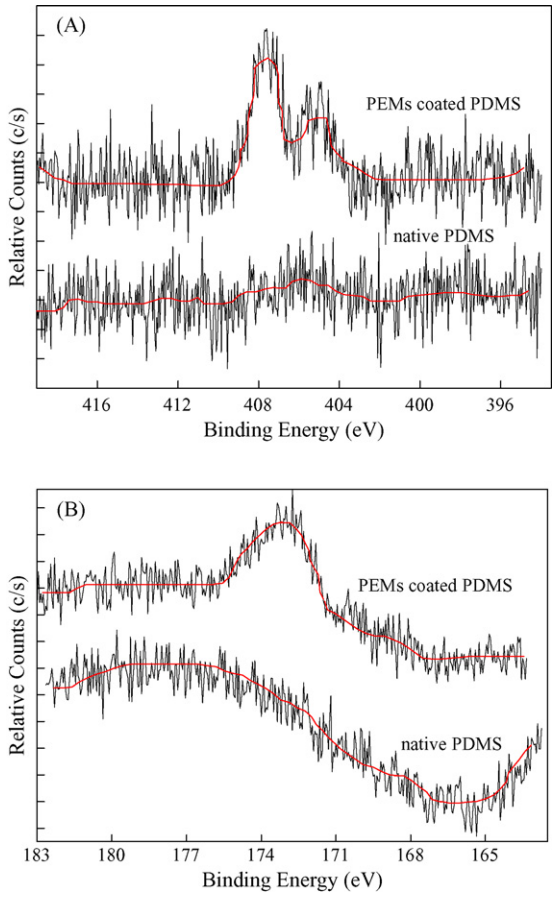

Fig. 4. XPS analysis of N 1s (A) and S 2p (B) of the PEMs coated PDMS.

3.2.2. EOF

EOF is a useful parameter to investigate surface modification and the stability of modified layers. Migration time of EOF was rapidly obtained via taking a diluted buffer as a sample. The electropherogram was monitored at 0 V (*versus* Ag/AgCl wire) [30]. The value of EOF was estimated according to the equation of $\mu_{eof} = (L/t)E^{-1}$, where L is the effective channel length, E the electric field strength, and t is the time required for the diluted buffer. Fig. 5 showed the relationship between EOF and pH of 20 mM PBS (ranged from 3.0 to 11.0) on the PEMs modified microchip and native PDMS microchip, respectively. The pH greatly influenced the EOF of native PDMS microchip. The EOF of native PDMS microchip increased with the increase of pH as a whole while the EOF of the modified microchip was more stable in tested pH range. The EOF of PEMs modified PDMS microchip in acetate buffer used for separation with pH ranged from 3.5 to 7.0 was also measured. The phenomenon is similar to that in PBS. The relative standard deviation (R.S.D.) of EOF for native PDMS chip was 4.55% ($n = 6$), and 0.81% ($n = 6$) for PDDA/PSS microchip in pH 5.0 of acetate buffer, respectively. R.S.D. of EOF in PEMs modified microchip was 1.2% ($n = 3$) for day-to-day and 0.56% ($n = 3$) for chip-to-chip, respectively.

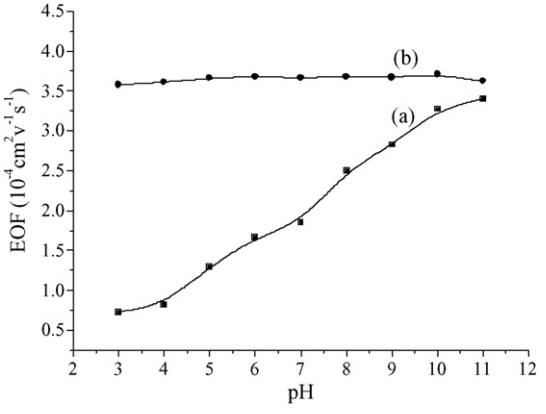

Fig. 5. Influence of the pH of the PBS buffer on EOF of (a) the native PDMS microchip; (b) the $(PDDA/PSS)_2$ modified PDMS microchips.

Fig. 6 showed the electropherograms of the separation of aminophenol isomers on a native PDMS microchip and the modified PDMS microchip, respectively. In the native PDMS microchip, the adsorption of aminophenol isomers which results in the peak broadenings was obvious. While in the $(PDDA/PSS)_2$ modified microchip, base-line separation of the analytes was successfully obtained and the adsorption of analytes was greatly suppressed. The *p*-, *o*-, and *m*-aminophenol isomers were eluted in sequence. The total separation time was within 1 min.

3.3. Optimization of electrophoresis conditions

3.3.1. Effects of buffer pH and concentration

The pH value and concentration of running buffer, which can influence the mobility of analytes by adjusting the velocity of EOF and the charge of the analyte molecule, have been acknowledged as one of the most important parameters for electrophoretic separation. Under the same conditions (pH and ion strength), the current of acetate buffer was lower than that of PBS buffer. In order to decrease the Joule heat, suppress bubbles in microchannel and to obtain better separation, the acetate

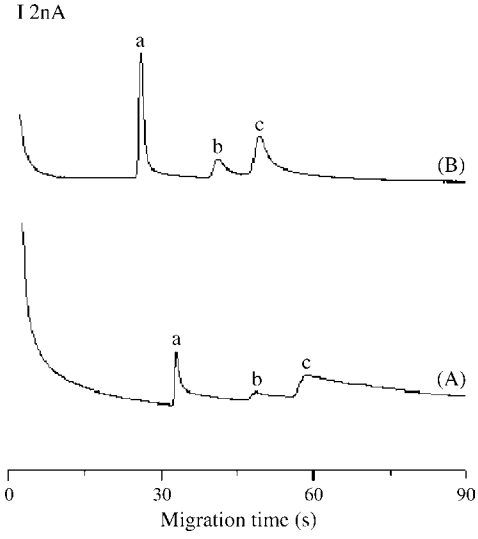

Fig. 6. Electropherograms of aminophenols on the native PDMS microchips (line A) and the $(PDDA/PSS)_2$ modified PDMS microchips (line B). Peaks: (a) *p*-aminophenol, (b) *o*-aminophenol, and (c) *m*-aminophenol. Condition: 40 μM *p*-aminophenol, 60 μM *o*-aminophenol, 80 μM *m*-aminophenol; 20 mM acetate buffer, pH 5.0; sample injection at +600 V for 3 s; separation voltage +1000 V; detection at +1.0 V (*vs.* Ag/AgCl).

Table 1
The resolutions of aminophenol in different buffer pH and buffer concentration (pH 5.0) on modified microchips

Buffer pH	$R_{p,o}$	$R_{o,m}$	Buffer concentration (mM)	$R_{p,o}$	$R_{\alpha,m}$
4.0	1.37	1.09	10	2.70	1.40
5.0	2.28	1.40	20	4.78	2.12
6.0	2.47	1.11	35	3.76	1.51
7.0	1.79	0	40	3.58	1.50

buffer (10 mM) with pH ranged from 4.0 to 7.0 was selected to test the separation of analytes. The different buffer concentration in pH 5.0 was also studied. The separation voltage of 1000 V was used in this test. Table 1 showed the effect of buffer pH and concentration on the resolution (based on equation: $R = 1.18((t_2 - t_1)/(w_{1/2(2)} + w_{1/2(1)}))$) of the analytes. As can be seen in Table 1, the buffer pH greatly influenced the resolution of *o*- and *m*-aminophenol. At pH 5.0 the resolution was higher than that at other test pH; therefore the pH 5.0 was selected as separation buffer pH. The buffer concentration was then optimized at pH 5.0. The resolution increased with the buffer concentration; but further increasing buffer concentration the resolution decreased on the contrary, which probably attributed to more joule heat produced in the channels. The optimal separation can be obtained when 20 mM acetate buffer was used.

3.3.2. Effect of applied voltage

When buffer pH 5.0 and buffer concentration 20 mM were selected, the effect of applied voltage on separation was investigated in the range of 600–1200 V on PDDA/PSS modified microchip. In the experiment, we found that at lower voltages the detection current signals were low; at higher voltage the base line current increased and the detection current signals decreased accordingly; the migration time decreased with the increase of voltage; while the separation voltage had little influence on the resolution. When 1000 V was used, the higher detection current signals were obtained. So, a voltage of 1000 V was applied for the separation of aminophenol isomers on the $(PDDA/PSS)_2$ modified microchip.

3.4. The separation reproducibility

Under the optimal separation condition, the separation reproducibility on the modified microchips was tested based on the R.S.D. of the migration time and the peak height of the analytes for continuous detections. The results were shown in Table 2. The results showed good reproducibility achieved on the $(PDDA/PSS)_2$ modified microchip. In addition, more than 50 runs with good resolution were performed continuously.

3.5. The linear range and detection limit

Under the selected conditions, a linear relationship was obtained between the height of detection signal with electrochemical detection and the concentration of analyte. The linear range and detection limit in the modified microchips were shown in Table 3. The detection limit was in the order of μmol/L. The column efficiencies (based on equation: $N = 5.54(t_R/w_{1/2})^2$) were also calculated based on Fig. 5. The column efficiencies for *o*, *m*, *p*-aminophenol isomers were 4.3×10^2, 1.0×10^2, 2.6×10^3 plate/m in the native microchip, and 3.7×10^4, 7.6×10^4, 1.6×10^5 plate/m in the modified microchip, respectively. The column efficiencies on PEMs modified microchips were increased by 100 times than those of the native microchips. The enhancement of column efficiencies of aminophenol isomers was attributed to the effective suppression of the analytes adsorption; meanwhile the increase of EOF of modified PDMS microchips also reduced the peak broadenings. The detection signal of *o*-, *m*-, *p*-aminophenol isomers were 0.6, 1.5, and 3.6 nA in the native microchip and 1.3, 2.8, and 8.4 nA, in the modified microchip, respectively.

Table 2
The reproducibility of migration time and peak height on the modified microchips

	R.S.D. (%) of the migration time ($n = 5$)	R.S.D. (%) of the peak height ($n = 5$)
p-Aminophenol	0.15	3.0
o-Aminophenol	0.21	4.4
m-Aminophenol	0.54	5.0

Table 3
The linear range and detection limit on modified microchips

	Linear range (μM)	Detection limit (μM, S/N = 3)	Correlation coefficients
p-Aminophenol	10.0–400	3.80	0.9974
o-Aminophenol	50.0–400	10.0	0.9936
m-Aminophenol	30.0–150	8.0	0.9972

4. Conclusions

In this work, polyelectrolyte multilayers modified method has been successfully applied to modify PDMS microchip through layer-by-layer assembly technique. In the coated PDMS microchip, aminophenol isomers were successfully separated within 1 min.

Acknowledgements

We gratefully thank the National Natural Science Foundation of China for financial support of this research (20305009, 20475025, 20435010, 20575029 and 90206037) and the National Natural Science Funds for Creative Research Groups (20521503).

References

[1] A. Mohammad, Y.H. Sirwal, J. Anal. Chem. 58 (2003) 731.
[2] W.C. Yang, X.D. Yu, A.M. Yu, H.Y. Chen, J. Chromatogr. A 910 (2001) 311.
[3] S.C. Rastogi, J. Sep. Sci. 24 (2001) 173.

[4] S.P. Wang, T.H. Huang, Anal. Chim. Acta 534 (2005) 207.
[5] D.J. Harrison, A. Manz, Z. Fan, H. Luedi, H.M. Widmer, Anal. Chem. 64 (1992) 1926.
[6] D.J. Harrison, K. Fluri, K. Seiler, Z. Fan, C.S. Effenhauser, A. Manz, Science 267 (1993) 895.
[7] R.M. McCormick, R.J. Nelson, M.G. Alonso-Amigo, D.J. Benvegnu, H.H. Hooper, Anal. Chem. 69 (1997) 2626.
[8] C.S. Effenhauser, A. Manz, H.M. Widmer, Anal. Chem. 65 (1993) 2637.
[9] M. Pumera, J. Wang, E. Grushka, R. Polsky, Anal. Chem. 73 (2001) 5625.
[10] J.C. McDonald, D.C. Duffy, J.R. Anderson, D.T. Chiu, H. Wu, O.J. Schueller, G.M. Whitesides, Electrophoresis 21 (2000) 27.
[11] R.S. Martin, A.J. Gawron, S.M. Lunte, C.S. Henry, Anal. Chem. 72 (2000) 3196.
[12] D.C. Duffy, J.C. McDonald, O.J. Schueller, G.M. Whitesides, Anal. Chem. 70 (1998) 4974.
[13] G. Decher, J.D. Hong, Macromol. Chem., Macromol. Symp. 46 (1991) 321.
[14] J. Wang, G.D. Liu, Y.H. Lin, Analyst 131 (2006) 477.
[15] G.D. Liu, Y.H. Lin, Anal. Chem. 78 (2006) 835.
[16] M. Chirea, V.G. Morales, J.A. Manzanares, C. Pereira, R. Gulaboski, F. Silva, J. Phys. Chem. B 109 (2005) 21808.
[17] S.A. Miscoria, J. Desbrieres, G.D. Barrera, P. Labbe, G.A. Rivas, Anal. Chim. Acta 578 (2006) 137.
[18] M. Germain, P. Balaguer, J.C. Nicolas, F. Lopez, J.P. Esteve, G.B. Sukhorukov, M. Winterhalter, H.R. Foy, D. Fournier, Biosens. Bioelectron. 21 (2006) 1566.
[19] L. Jiang, F.S. Lu, Y.C. Gao, Y.L. Song, H.B. Liu, H.Y. Gan, T.G. Jiu, Y.J. Li, S. Wang, D.B. Zhu, Thin Solid Films 496 (2006) 311.
[20] N.G. Caculitan, P.H.S. cudder, A. Rodriguez, J.L. Casson, H.L. Wang, J.M. Robinson, M.S. Johal, Langmuir 20 (2004) 8735.
[21] S.H. Lee, S. Balasubramanian, D.Y. Kim, N.K. Viswanathan, S. Bian, J. Kumar, S.K. Tripathy, Macromolecules 33 (2000) 6534.
[22] L.Y. Huang, M.C. Yang, J. Nanosci. Nanotechnol. 6 (2006) 3163.
[23] N. Li, D.S. Kommireddy, Y. Lvov, W. Liebenberg, L.R. Tiedt, M.M. De Villiers, J. Nanosci. Nanotechnol. 6 (2006) 3252.
[24] J.H. Fu, J. Ji, D.Z. Fan, J.C. Shen, J. Biomed. Mater. Res. A 79 (2006) 665.
[25] T.W. Graul, J.B. Schlenoff, Anal. Chem. 71 (1999) 4007.
[26] H. Katayama, Y. Ishihama, N. Asakawa, Anal. Chem. 70 (1998) 2254.
[27] H. Katayama, Y. Ishihama, N. Asakawa, Anal. Chem. 70 (1998) 5272.
[28] Y. Liu, J.C. Fanguy, J.M. Bledsoe, C.S. Henry, Anal. Chem. 72 (2000) 5939.
[29] S.L.R. Barker, M.J. Tarlov, H. Canavan, J.J. Hickman, L.E. Locascio, Anal. Chem. 72 (2000) 4899.
[30] N. Bao, J.J. Xu, Y.H. Dou, H.Y. Chen, J. Chromatogr. A 1041 (2004) 245.
[31] A.T. Woolley, K. Lao, A.N. Glazer, R.A. Mathies, Anal. Chem. 70 (1998) 684.

Available online at www.sciencedirect.com
ScienceDirect
Talanta 72 (2007) 1416–1422
Talanta
www.elsevier.com/locate/talanta

Simultaneous determination of rosiglitazone and metformin in plasma by gradient liquid chromatography with UV detection

Ceren Yardımcı [a], Nuran Özaltın [a,*], Alper Gürlek [b]

[a] *Department of Analytical Chemistry, Faculty of Pharmacy, Hacettepe University, 06100 Sıhhıye, Ankara, Turkey*
[b] *Division of Endocrinology, Department of Internal Medicine, Faculty of Medicine, Hacettepe University, 06100 Sıhhıye, Ankara, Turkey*

Received 19 September 2006; received in revised form 19 January 2007; accepted 22 January 2007
Available online 30 January 2007

Abstract

A novel, fast and simple liquid chromatographic method was developed and validated for the simultaneous determination of rosiglitazone and metformin in human plasma. The analysis was performed on a phenyl column (250 mm × 4.6 mm i.d., 5 μm) using a gradient method starting with mobile phase composed of acetonitrile:5 mM acetate buffer pH 5.5 (75:25, v/v). The flow rate was 1 mL min^{-1}. UV detection was performed at 245 nm and verapamil was used as internal standard. The total run time was less than 10 min. Sample preparation included a simple protein precipitation step with acetonitrile. Validation experiments were performed to demonstrate stability, specificity, sensitivity, linearity, accuracy, precision and robustness. The limit of quantification was 100 ng mL^{-1} for rosiglitazone and 250 ng mL^{-1} for metformin. The extraction recoveries were 100.02–105.0% for rosiglitazone and 105.64–103.88% for metformin. The method was applied with success to plasma samples obtained from diabetic patients undergoing treatment with rosiglitazone and metformin.

Keywords: Rosiglitazone; Metformin; Simultaneous determination; Gradient liquid chromatography; Validation; Human plasma

1. Introduction

Many patients with type 2 diabetes require treatment with more than one antihyperglycaemic drugs to achieve optimal glycaemic control. The thiazolidinediones are novel oral antihyperglycaemic drugs that improve glycaemic control primarily by decreasing insulin resistance by sensitizing the skeletal muscle, liver and adipose tissue to the actions of insulin. They also improve beta-cell function. The combination of metformin hydrochloride (M) (Fig. 1a), a biguanide that enhances glucose uptake in peripheral tissues and reduces hepatic gluconeogenesis, with rosiglitazone maleate (R) (Fig. 1b), one of the newly available members of the thiazolidinedione family, offers a rational therapeutic approach for the treatment of type 2 diabetes [1]. The two agents can be used in combination to achieve additive glucose-lowering efficacy in the treatment of type 2 diabetes, without stimulating insulin secretion and without causing hypoglycaemia [2]. A fixed-dose formulation of R/M was recently approved in the EU and the US for the treatment of type 2 diabetes mellitus in patients inadequately controlled on M monotherapy.

Following oral administration, R is rapidly absorbed and has an absolute oral bioavailability of 99%. It is extensively metabolised in the liver, giving two main metabolites with very little biological activity. Gastrointestinal absorption of M is incomplete with an absolute bioavailability of 50–60% and is not metabolised. Co-administration of the two agents does not significantly alter the pharmacokinetic properties of each agent [2].

Literature survey reveals several methods for the determination of R in biological fluids including liquid chromatography (LC) [3–8] and liquid chromatography–tandem mass spectrometry (LC/MS/MS) [9–11]. Several methods have also been described for the determination of M either alone or in combination with various drugs, such as LC [12–26], LC/MS/MS [27–31], capillary electrophoresis (CE) [32], chemiluminescence [33] and gas chromatography (GC) [34–35].

To our knowledge, there have been no reports for the simultaneous determination of both drugs in biological fluids. Measuring the plasma concentrations of R and M are important

* Corresponding author. Tel.: +90 312 305 26 03.
E-mail address: nozaltin@hacettepe.edu.tr (N. Özaltın).

0039-9140/$ – see front matter © 2007 Elsevier B.V. All rights reserved.
doi:10.1016/j.talanta.2007.01.042

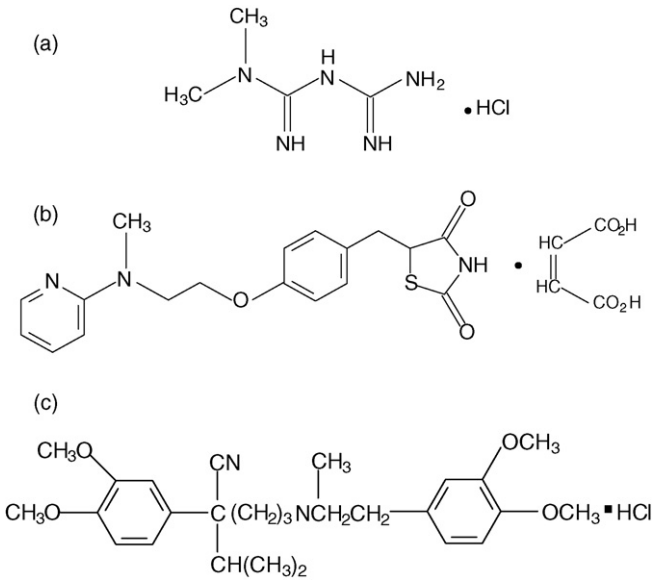

Fig. 1. Chemical structures of (a) metformin hydrochloride; (b) rosiglitazone maleate; (c) verapamil hydrochloride (internal standard).

for studying the pharmacokinetics of these drugs, for determination of patient adherence with prescribed therapy in diabetic patients and for general drug monitoring. Therefore, it is necessary to establish a new analytical method for their simultaneous determination in human plasma.

The aim of this study was to develop and validate a simple, rapid and reliable liquid chromatographic method for the simultaneous determination of R and M in human plasma. The validated method was successfully applied to the analysis of clinical samples from diabetic patients.

2. Experimental

2.1. Chemicals and reagents

Rosiglitazone maleate reference standard was kindly supplied by Glaxo SmithKline (İstanbul, Turkey). Metformin hydrochloride and verapamil (V) used as internal standard (IS) (Fig. 1c) were purchased from Sigma (St. Louis, MO, USA) and Acros (New Jersey, USA), respectively. Acetonitrile and methanol were LC grade (Merck, Germany). All other chemicals were analytical reagent grade. Deionized water was prepared using a Barnstead Nanopure Diamond Analytical (USA) ultrapure water system.

Drug free human plasma was obtained from the Hacettepe University Faculty of Medicine Hospital Blood Bank (Ankara, Turkey) and stored at −20 °C.

2.2. Instrumentation and chromatographic conditions

The LC system consisted of a SpectraSYSTEM P2000 gradient pump, a SpectraSYSTEM SCM 1000 degasser, a Rheodyne manual injector with a 20 μL injection loop and a SpectraSYSTEM UV2000 detector (Thermo Separation Products, Inc., USA). The analytical column was a Ace 5 phenyl column (250 mm × 4.6 mm i.d., 5 μm, Advanced Chromatography Technologies, Scotland) protected by a phenyl guard column (4.0 mm × 3.0 mm i.d., Phenomenex, USA). A gradient consisting of acetonitrile and 5 mM pH 5.5 sodium acetate (adjusted with 1 M glacial acetic acid) was used as shown in Table 1. The flow rate was 1 mL min^{-1}. The detection wavelength was set to 245 nm. Operation, data acquisition and analysis were performed using ChromQuest software.

Table 1
Gradient elution conditions of the developed LC method

Time (min)	Acetonitrile (%)	Buffer A[a] (%)	Flow rate (mL min^{-1})
0.0	75.0	25.0	1.0
0.7	70.0	30.0	1.0
1.0	65.0	35.0	1.0
4.5	70.0	30.0	1.0
4.7	75.0	25.0	1.0

[a] Buffer A: 5 mM acetate buffer (adjusted to pH 5.5 with 1 M glacial acetic acid).

For pH measurements, a pH meter (Mettler Toledo MA 235, Switzerland) was employed.

Mobile phase was filtered through a 0.45 μm nylon membrane filter (Advantec MFS, Inc., CA, USA) under vacuum and degassed by ultrasonication (Sonorex, Bandelin, Germany).

2.3. Preparation of standard solutions and calibration curves

Standard stock solutions (1000 μg mL^{-1}) of M and V were prepared in water, R (1000 μg mL^{-1}) in methanol. These solutions were kept at +4 °C.

Working standard solutions for the calibration curves were prepared in the concentration range of 100–2500 ng mL^{-1} for R and 250–2500 ng mL^{-1} for M by spiking stock solutions into 500 μL blank human plasma. The 20 μL of a 200 μg mL^{-1} solution of V (IS) was added to each of them.

Calibration curves were represented by plotting the peak area ratios of R and M to V (IS) versus the concentrations of the calibration standards.

2.4. Sample preparation

According to protocol previously approved by the Ethics Committee of the Hacettepe University Faculty of Medicine (Ankara, Turkey) and with the written informed consent of the patients, blood samples were taken from diabetic patients who were subjected to therapy with R and M. Blood samples (3 mL) were collected in EDTA vacutainer tubes and centrifuged at 5000 rpm for 10 min. Each supernatant plasma sample was aliquoted (500 μL) into Eppendorf tubes, IS (V, 20 μL of a 200 μg mL^{-1} solution) was added and analyzed on the same day.

2.5. Extraction procedure

To 500 μL of plasma in an Eppendorf tube, IS (V, 20 μL of a 200 μg mL^{-1} solution) was added. After briefly mixing,

plasma proteins were precipitated by the addition of 1000 μL acetonitrile, the mixture was vortexed for 30 s and separated by centrifugation at 6000 rpm for 10 min. Finally, 20 μL of the clear supernatant was injected directly into the LC system for analysis.

3. Results and discussion

3.1. Optimization of chromatographic conditions and extraction procedure

Since M is a highly polar and strongly basic compound ($pK_a = 12.4$), it is poorly retained in reverse-phase LC mode. Preliminary experiments indicated that using different concentrations of acetonitrile or methanol with different pHs of the buffers, did not produce a suitable retention and peak shape of M on a C_{18} column.

Higher polarity of phenyl columns with respect to alkyl-bonded columns can provide alternative retention mechanism in addition to hydrophobic interaction. This retention mechanism is based upon π–π interactions occurring between the analyte molecules and the phenyl-bonded phase [36]. As expected, the use of a phenyl column improved the retention and the peak shape of M. Various mobile phases with different compositions were tried on a phenyl column and the best chromatographic conditions for the simultaneous separation of R and M in human plasma were achieved using a gradient elution method starting with a mobile phase composed of acetonitrile:5 mM pH 5.5 acetate buffer (75:25, v/v). Complete separation of R and M among interference peaks in human plasma could not be achieved under isocratic conditions. Hence, gradient elution conditions were optimized to get the best separation of R and M in human plasma (Table 1).

It was found that further increase in acetonitrile composition caused a decrease in the retention time of R, but an increase in the retention time of M. Acetate buffer was chosen as a mobile phase additive rather than the other buffers since it provided a significant increase in retention of M. This phenomenon may be explained by the ion-pairing effect of acetate, which affected the retention and the peak shape of M. It was stated in the literature that mobile phase additives profoundly influences the retention of basic drugs by ion-pair mechanism [37]. Large differences in retention with acetate ion rather than the others can be rationalized via both ion-pairing model and the Hofmeister effect [38].

Several extraction procedures were tested including protein precipitation, liquid–liquid and solid phase extraction for the simultaneous analysis of R and M in human plasma. Since M has a very high polarity, it was not possible to extract it from plasma using organic solvents or conventional solid phase extraction techniques. Ethyl acetate, dichloromethane and *n*-hexane were used for liquid–liquid extraction, but M could not be extracted. The use of solid phase extraction cartridges, such as Chromabond C_{18}, Oasis HLB and Chromabond $C_{8,}$ did not give good results. It was found that only protein precipitation with acetonitrile could remove proteins and other interfering components in human plasma with satisfactory drug recovery.

3.2. Method validation

Validation of the proposed method was performed with respect to stability, specificity, linearity, limit of detection (LOD), limit of quantification (LOQ), accuracy, precision, and robustness according to the ICH [39] and FDA [40] guidelines.

3.2.1. Stability

Stability of R and M in plasma was evaluated under different storage conditions by spiking stock solutions into blank plasma at two concentrations (250 and 500 ng mL^{-1} for R, 1000 and 2000 ng mL^{-1} for M). For short-term stability, spiked plasma samples were kept in room temperature for 24 h. The long-term stability was assessed after storage of spiked plasma samples in freezer at −20 °C for 20 days. To test for freeze and thaw stability, the spiked plasma samples were stored at −20 °C for 24 h and thawed to room temperature three times and then analyzed. The stability results were evaluated by comparing peak area ratios of R and M to IS with those of freshly prepared spiked plasma samples. The results presented in Table 2 indicate that R and M can be considered stable under the various conditions investigated.

3.2.2. Specificity

Specificity, described as the ability of a method to discriminate the analyte from all potential interfering substances and it was confirmed that the signals measured was caused only by the analytes. The chromatograms of a blank plasma (Fig. 2a),

Table 2
Stability of R and M in human plasma (mean ± standard error, $n = 3$)

	Short-term stability (24 h, room temperature)		Long-term stability (20 days, −20 °C)		Freeze–thaw stability (3 cycles)	
	Remained %[a]	R.S.D. (%)	Remained %	R.S.D. (%)	Remained %	R.S.D. (%)
Added R (ng mL^{-1})						
250	96.34 ± 1.43	2.57	112.90 ± 1.15	1.76	107.35 ± 1.12	1.81
500	99.56 ± 1.67	2.91	113.29 ± 1.02	1.56	99.20 ± 0.98	1.71
Added M (ng mL^{-1})						
1000	100.02 ± 1.60	2.77	104.91 ± 1.37	2.26	96.10 ± 1.28	2.31
2000	103.43 ± 0.85	1.42	108.52 ± 0.65	1.04	100.86 ± 0.88	1.51

R.S.D.: relative standard deviation.
[a] Remained % = (peak area of R or M after the mentioned storage conditions/peak area of fresh R or M) × 100.

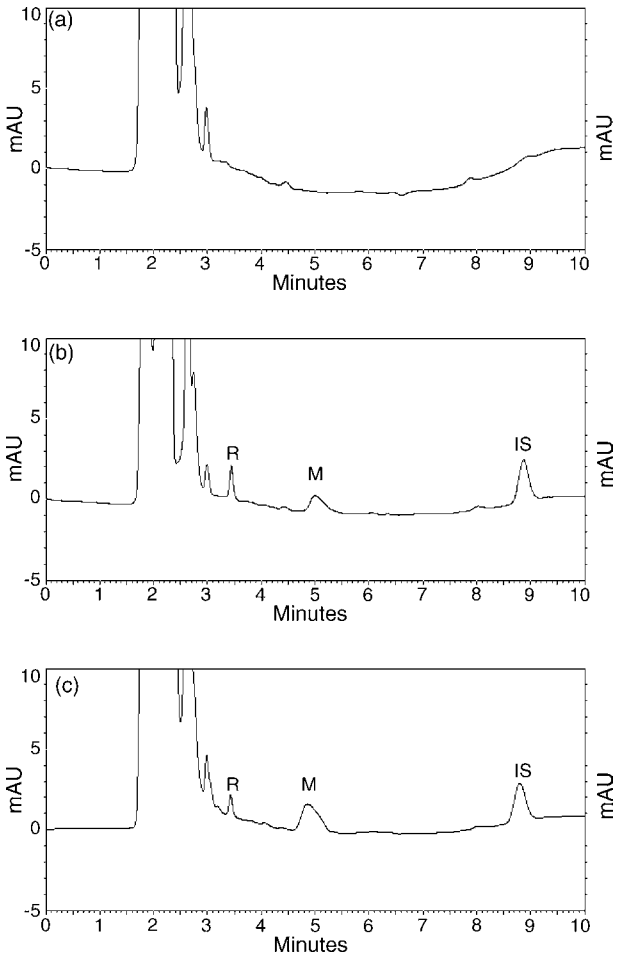

Fig. 2. Representative chromatograms of (a) blank human plasma; (b) human plasma sample spiked with R (500 ng mL^{-1}), M (500 ng mL^{-1}) and V (7.7 μg mL^{-1}); (c) plasma sample obtained from a diabetic patient subjected to treatment with R and M.

plasma sample spiked with R, M and V (IS) (Fig. 2b) and real plasma sample obtained from a diabetic patient subjected to treatment with R and M (Fig. 2c), were compared to confirm the specificity of the method developed. The peaks of the R, M and IS were well separated, no interfering peaks were observed and no significant peaks were found at the retention times of the analytes in plasma.

3.2.3. Linearity

Under the optimum analysis conditions, linearity was studied simultaneously in the concentration range of 100.0–2500.0 ng mL^{-1} for R and 250.0–2500.0 ng mL^{-1} for M in spiked plasma samples. In all cases 20.0 μL of 200 ng mL^{-1} of V was added as IS. The peak area ratios of R and M to the IS were plotted versus the nominal concentrations of the calibration standards. The linearity curves were defined by the following equations: $y = (0.0004 \pm 0.00003)x - (0.0063 \pm 0.0004)$, $r = 0.9986$ for R and $y = (0.0004 \pm 0.00001)x - (0.0071 \pm 0.0002)$, $r = 0.9994$ for M, where y is the ratio of peak areas and x is the concentration expressed in ng mL^{-1} ($n = 10$).

Table 3
System precision data for R and M

	R	M
Retention time (min)	$\bar{x} = 3.46 \pm 0.003$ S.D. = 0.009 R.S.D. = 0.27%	$\bar{x} = 5.26 \pm 0.004$ S.D. = 0.014 R.S.D. = 0.26%
Peak area	$\bar{x} = 7358.6 \pm 48.37$ S.D. = 145.11 R.S.D. = 1.97%	$\bar{x} = 24723.0 \pm 152.29$ S.D. = 430.75 R.S.D. = 1.74%
Capacity factor[a]	$\bar{x} = 0.65 \pm 0.002$ S.D. = 0.005 R.S.D. = 0.75%	$\bar{x} = 1.50 \pm 0.002$ S.D. = 0.005 R.S.D. = 0.34%
Peak asymmetry	$\bar{x} = 1.20 \pm 0.005$ S.D. = 0.017 R.S.D. = 1.44%	$\bar{x} = 1.30 \pm 0.011$ S.D. = 0.026 R.S.D. = 2.00%

$\bar{x}$ = mean ± standard error; S.D. = standard deviation; R.S.D.: relative standard deviation.
[a] Methanol was used for the determination of dead volume.

3.2.4. LOD and LOQ

The limits of detection defined as signal-to-noise ratio of 3:1 were about 50 ng mL^{-1} for R and 100 ng mL^{-1} for M. The limits of quantification were determined as 100 ng mL^{-1} for R and 250 ng mL^{-1} for M with acceptable precision (R.S.D. ≤ 10%, $n = 6$) and accuracy (bias % ≤ 20 $n = 6$) under the stated conditions.

3.2.5. Precision

The assay was investigated with respect to repeatability and intermediate precision. In order to measure system precision (injection repeatability), 10 consecutive injections were made with a spiked plasma sample containing 250 ng mL^{-1} of R and 1000 ng mL^{-1} M. The results were evaluated by considering retention time, peak area, capacity factor and peak asymmetry values of R and M. The data show good precision of the system with a R.S.D. ≤ 2% (Table 3).

Three different concentrations of R and M (in the linear range) were spiked into blank plasma and analyzed in six independent series in the same day (intra-day precision) and six consecutive days (inter-day precision) within each series every sample was injected three times. The R.S.D. values of intra- and inter-day studies varied from 0.54 to 5.65% showed that the intermediate precision of the method was satisfactory (Table 4).

3.2.6. Accuracy and recovery studies

The accuracy of a method is expressed as the closeness of agreement between the value found and the value that is accepted as a reference value. It is determined by calculating the percent difference (bias %) between the measured mean concentrations and the corresponding nominal concentrations. Table 4 shows the results obtained for intra- and inter-day accuracy.

The accuracy of the proposed method was also tested by recovery experiments. Recovery experiments were performed by adding known amounts of R, M and IS to the water and blank plasma at three different concentrations (low, medium and high) by triplicate analysis. Spiked plasma and water samples were

Table 4
Intra-day and inter-day accuracy and precision data of R and M in human plasma ($n = 6$)

	Intra-day			Inter-day		
	Found[a] (ng mL^{-1})	Precision[b] R.S.D. (%)	Accuracy[c] (bias %)	Found[a] (ng mL^{-1})	Precision[b] R.S.D. (%)	Accuracy[c] (bias %)
Added R (ng mL^{-1})						
100	94.91 ± 1.45	3.74	−5.09	100.61 ± 2.32	5.65	0.61
250	257.91 ± 2.94	2.79	3.16	249.09 ± 3.23	3.18	−0.36
500	527.73 ± 2.96	1.37	5.55	502.90 ± 5.49	2.67	0.58
Added M (ng mL^{-1})						
500	498.30 ± 2.75	1.35	−0.34	499.52 ± 4.06	1.99	−0.09
1000	989.24 ± 4.58	1.13	−1.08	994.43 ± 2.17	0.54	−0.56
2000	1959.86 ± 7.89	0.99	−2.01	1976.09 ± 20.79	2.58	−1.20

[a] Mean ± standard error.
[b] R.S.D.: relative standard deviation.
[c] Bias %: [(Found − Added)/Added] × 100.

Table 5
Recovery data for R and M ($n = 3$).

	Relative recovery* (%)	R.S.D. (%)	Absolute recovery* (%)	R.S.D. (%)
Added R (ng mL^{-1})				
100	100.95 ± 0.95	1.64	98.25 ± 1.75	3.09
250	100.02 ± 1.07	1.86	98.64 ± 1.26	2.21
500	105.00 ± 0.34	0.56	101.33 ± 1.98	3.39
Added M (ng mL^{-1})				
500	103.88 ± 1.32	2.20	94.19 ± 0.41	0.76
1000	104.13 ± 2.24	3.73	91.48 ± 0.66	1.26
2000	105.64 ± 2.28	3.74	97.62 ± 0.61	1.08

* Mean ± standard error; R.S.D.: relative standard deviation.

treated as described in the procedure for sample preparation. The relative recoveries of the analytes were measured by comparison of the peak area ratios obtained from extracted spiked plasma samples with those obtained from extracted equivalent amounts of R, M and IS spiked in water. Absolute recoveries were determined by comparison of the peak area ratios of R and M to IS obtained from extracted spiked plasma samples with those obtained from equivalent standard solutions. The results obtained are shown in Table 5, from which is clear that both the recoveries and repeatabilities are good.

3.2.7. Robustness

Robustness relates to the capacity of the method to remain unaffected by small but deliberate variations introduced into the method parameters. Several experimental parameters, like initial and final acetonitrile ratio in gradient elution, buffer pH, buffer concentration and flow rate, were varied around the value set in the method to reflect changes likely to arise in different test environments. Analyses were carried out in triplicate and only one parameter was changed in the experiments at a time. The determination of 250 ng mL^{-1} R and 1000 ng mL^{-1} M in spiked plasma samples under the various conditions was performed (Table 6). The statistically comparison was done with *t*-test [41] and no difference was found between results ($p = 0.05$). Therefore, the method is robust to the small changes in experimental conditions.

3.3. Application to plasma samples of diabetic patients

To demonstrate the suitability of the developed method for use in clinical studies, this assay was used to determine the R and M concentrations of plasma samples obtained from a group of diabetic patients. The blood samples were collected from 14 diabetic patients (11 females, 3 males, age: 37–63 years) of the Hacettepe University Faculty of Medicine Hospital (Ankara, Turkey) who were subjected to therapy with

Table 6
The robustness data of the developed LC method (R = 250 ng mL^{-1}, M = 1000 ng mL^{-1}, $n = 3$)

	R		M	
	Found (ng mL^{-1})*	R.S.D. (%)	Found (ng mL^{-1})*	R.S.D. (%)
Standard conditions	248.84 ± 3.53	2.46	1007.92 ± 6.64	1.14
Initial ACN ratio 77%	251.60 ± 5.50	3.79	991.09 ± 5.30	0.93
Final ACN ratio 73%	253.40 ± 0.85	0.58	985.99 ± 4.26	1.72
Buffer pH 5.3	246.81 ± 2.79	1.96	987.69 ± 4.63	0.81
Buffer pH 5.7	254.46 ± 5.49	3.73	993.86 ± 8.02	1.40
Buffer concentration 4 mM	246.54 ± 4.11	2.89	1008.30 ± 3.57	0.61
Buffer concentration 6 mM	252.12 ± 2.91	2.00	987.04 ± 6.71	1.78
Flow rate 0.9 mL min^{-1}	242.13 ± 1.80	1.29	1014.30 ± 7.38	1.26
Flow rate 1.1 mL min^{-1}	248.66 ± 4.89	3.41	992.11 ± 6.47	0.92

Statistical test results: small changes in experimental conditions have no effect on the determination of R and M (*t*-test, $p > 0.05$). Each mean value was compared with the mean value obtained by standard conditions.
* Mean ± standard error; R.S.D.: relative standard deviation.

Table 7
Patient plasma concentrations of R and M obtained by developed LC method ($n = 3$) (1 h after a single oral dose administration of 4 mg of Avandia® and 850 mg of Glucophage®)

Patient no.	R concentration* (ng mL^{-1})	M concentration* (ng mL^{-1})
1	293.53 ± 2.58	1410.95 ± 14.83
2	121.99 ± 2.14	2000.91 ± 22.98
3	281.24 ± 0.54	2082.46 ± 36.73
4	137.68 ± 6.87	1446.60 ± 48.79
5	251.84 ± 3.63	1407.49 ± 0.31
6	228.30 ± 5.74	1195.75 ± 22.71
7	144.09 ± 11.36	1878.37 ± 92.69
8	302.34 ± 9.70	2367.55 ± 79.90
9	214.88 ± 3.48	1048.27 ± 17.03
10	227.22 ± 2.85	2296.78 ± 29.38
11	295.78 ± 11.10	1605.38 ± 106.67
12	253.84 ± 11.37	1719.59 ± 50.36
13	191.10 ± 7.34	1886.13 ± 83.75
14	227.15 ± 2.79	2078.00 ± 77.28

* Mean ± standard error.

R (4 mg of Avandia®) and M (850 mg of Glucophage®) for at least 2 months three times daily. Blood samples were drawn 1 h after a single oral dose of 4 mg of Avandia® and 850 mg of Glucophage® administration and analyzed immediately by the developed method after the treatment as described in sample preparation part. The patient plasma concentrations of R and M in the 14 patients were within the range 121.99–302.34 ng mL^{-1} and 1048.27–2367.55 ng mL^{-1}, respectively (Table 7).

4. Conclusion

This is the first report for the simultaneous analysis of R and M in human plasma. The developed LC method was validated and was successfully applied to the analysis of clinical samples from diabetic patients. The method showed a good performance with respect to stability, specificity, sensitivity, linearity, precision, accuracy, recovery and robustness. The reported method was fast and efficient, with simple protein precipitation procedure and total running time of analytes and IS less than 10 min. The sensitivity of the method was found to be sufficient for accurately monitoring the plasma concentrations of R and M in diabetic patients. The use of this method can save time and effort when monitoring diabetic patients who take these drugs; there is no need to have more than one LC system or to change the LC column to measure plasma from patients on different medication regimes. It can be concluded that the proposed method is suitable for a reliable therapeutic drug monitoring of patients undergoing therapy with R and M.

Acknowledgements

This work is a part of the project (04D05301001) supported by Hacettepe University, Scientific Research Unit. The authors are also grateful to Dr. M. Işıldak and Dr. A. Harmancı for their help providing patient plasma samples.

References

[1] S.L. Cox, Drugs Today (Barc.) 40 (7) (2004) 633.
[2] C.J. Bailey, C. Day, Int. J. Clin. Pract. 58 (9) (2004) 867.
[3] R.S. Pedersen, K. Broesen, F. Nielsen, Chromatographia 62 (3–4) (2005) 197.
[4] M.W. Hruska, R.F. Frye, J. Chromatogr. B 803 (2) (2004) 317.
[5] K.A. Kim, J.Y. Park, Biomed. Chromatogr. 18 (8) (2004) 613.
[6] B.L. Kolte, B.B. Raut, A.A. Deo, M.A. Bagool, D.B. Shinde, J. Chromatogr. B 788 (1) (2003) 37.
[7] R.N.V.S. Mamidi, B. Benjamin, M. Ramesh, N.R. Srinivas, Biomed. Chromatogr. 17 (6) (2003) 417.
[8] A.M. Muxlow, S. Fowles, P. Russell, J. Chromatogr. B: Biomed. Sci. Appl. 752 (1) (2001) 77.
[9] C.C. Chou, M.R. Lee, F.C. Cheng, D.Y. Yang, J. Chromatogr. A 1097 (1–2) (2005) 74.
[10] E.N.M. Ho, K.C.H. Yiu, T.S.M. Wan, B.D. Stewart, K.L. Watkins, J. Chromatogr. B 811 (1) (2004) 65.
[11] Z.J. Lin, D. Desai-Krieger, L. Shum, J. Chromatogr. B 801 (2) (2004) 265.
[12] J.J. Juan, F. Fang, M. Ma, X.Z. Zhang, J. Chromatogr. Sci. 44 (4) (2006) 193.
[13] S. AbuRuz, J. Millership, J. McElnay, J. Chromatogr. B: Anal. Technol. Biomed. Life Sci. 832 (2) (2006) 202.
[14] H. Amini, A. Ahmadiani, P. Gazerani, J. Chromatogr. B: Anal. Technol. Biomed. Life Sci. 824 (1–2) (2005) 319.
[15] S. AbuRuz, J. Millership, J. McElnay, J. Chromatogr. B 817 (2) (2005) 277.
[16] S. AbuRuz, J. Millership, J. McElnay, J. Chromatogr. B 798 (2) (2003) 203.
[17] A. Zarghi, S.M. Foroutan, A. Shafaati, A. Khoddam, J. Pharm. Biomed. Anal. 31 (1) (2003) 197.
[18] M. Zhang, G.A. Moore, M. Lever, S.J. Gardiner, C.M.J. Kirkpatrick, E.J. Begg, J. Chromatogr. B: Anal. Technol. Biomed. Life Sci. 766 (1) (2002) 175.
[19] C.L. Cheng, C.H. Chou, J. Chromatogr. B: Biomed. Sci. Appl. 762 (1) (2001) 51.
[20] F. Tache, V. David, A. Farca, A. Medvedovici, Microchem. J. 68 (1) (2001) 13.
[21] O. Vesterqvist, F. Nabbie, B. Swanson, J. Chromatogr. B: Biomed. Sci. Appl. 716 (1–2) (1998) 299.
[22] K.H. Yuen, K.K. Peh, J. Chromatogr. B: Biomed. Sci. Appl. 710 (1–2) (1998) 243.
[23] R. Huupponen, P. Ojala-Karlsson, J. Rouru, M. Koulu, J. Chromatogr.: Biomed. Appl. 583 (2) (1992) 270.
[24] L. Benzi, P. Marchetti, P. Cecchetti, R. Navalesi, J. Chromatogr. B: Biomed. Sci. Appl. 375 (1986) 184.
[25] J. Keal, A. Somogyi, J. Chromatogr. B: Biomed. Sci. Appl. 378 (1986) 503.
[26] B.G. Charles, N.W. Jacobsen, P.J. Ravenscroft, Clin. Chem. 27 (3) (1981) 434.
[27] G. Zhong, H. Bi, S. Zhou, X. Chen, M. Huang, J. Mass Spectrom. 40 (11) (2005) 1462.
[28] N. Koseki, H. Kawashita, M. Niina, Y. Nagae, N. Masuda, J. Pharm. Biomed. Anal. 36 (5) (2005) 1063.
[29] Y. Wang, Y. Tang, J. Gu, J.P. Fawcett, X. Bai, J. Chromatogr. B 808 (2) (2004) 215.
[30] X. Chen, Q. Gu, F. Qiu, D. Zhong, J. Chromatogr. B 802 (2) (2004) 377.
[31] K. Heinig, F. Bucheli, J. Pharm. Biomed. Anal. 34 (5) (2004) 1005.
[32] J.Z. Song, H.F. Chen, S.J. Tian, Z.P. Sun, J. Chromatogr. B: Biomed. Sci. Appl. 708 (1–2) (1998) 277.
[33] C. He, Z. Zhang, D. He, Y. Xiong, Anal. Bioanal. Chem. 385 (1) (2006) 128.
[34] M.S. Lennard, C. Casey, G.T. Tucker, H.F. Woods, Br. J. Clin. Pharmacol. 6 (2) (1978) 183.
[35] J. Brohon, M. Noël, J. Chromatogr. B: Biomed. Sci. Appl. 146 (1) (1978) 148.
[36] K. Croes, A. Steffens, D.H. Marchand, L.R. Snyder, J. Chromatogr. A 1098 (1–2) (2005) 123.
[37] J. Dai, P.W. Carr, J. Chromatogr. A 1072 (2005) 169.
[38] J.M. Roberts, A.R. Diaz, D.T. Fortin, J.M. Friedle, S.D. Piper, Anal. Chem. 74 (2002) 4927.

[39] ICH Harmonised Tripartite Guideline, International Conference on Harmonisation of Technical Requirements for Registration of Pharmaceuticals for Human Use, "Validation of Analytical Procedure: Methodology", 1996.
[40] Guidance for industry: Bioanalytical Method Validation, US Department of Health and Human Services, Food and Drug Administration, Center for Drug Evaluation and Reserch (CDER), Center for Biologics Evaluation and Research (CBER), May 2001.
[41] J.C. Miller, J.N. Miller, Statistics for Analytical Chemistry, third ed., Ellis Horwood Limited, Chichester, England, 1993, p. 55.

Available online at www.sciencedirect.com
ScienceDirect
Talanta 72 (2007) 1527–1532
Talanta
www.elsevier.com/locate/talanta

Microwave-assisted acid hydrolysis of toluene diamine conjugates in urine samples for biomarkers in toluene diisocyanate analysis

Hui-Jung Yeh [a,b,c], Wei-Chao Lin [d], Shiann-Cherng Sheu [e], Tung-Sheng Shih [f], Lien-Huei Chen [g], Ho-Yuan Chang [a,*]

[a] *Department of Environmental and Occupational Health, College of Medicine, National Cheng Kung University, Tainan, Taiwan, ROC*
[b] *Institute of Basic Medical Sciences, College of Medicine, National Cheng Kung University, Tainan, Taiwan, ROC*
[c] *Department of Childhood Education and Nursery, Chia Nan University of Pharmacy and Science, Tainan, Taiwan, ROC*
[d] *Department of Cosmetic Science, Chia Nan University of Pharmacy and Science, Tainan, Taiwan, ROC*
[e] *Department of Occupational Safety and Health, Chang Jung Christian University, Tainan, Taiwan, ROC*
[f] *Institute of Occupational Safety and Health, Council of Labor Affairs, Taipei, Taiwan, ROC*
[g] *Department of Occupational Safety and Health, Chia Nan University of Pharmacy and Science, Tainan, Taiwan, ROC*

Received 20 October 2006; received in revised form 1 February 2007; accepted 1 February 2007
Available online 9 February 2007

Abstract

Toluene diamines (TDAs) in urine have been used widely to determine the amount of toluene diisocyanate (TDI) absorbed by humans. Conventional hydrolysis to prepare a sample of urine takes approximately 16 h. An attempt is made to apply microwave-assisted heating (MAH) to reduce the duration of analysis. Urine collected from rats exposed to a mixture of 2,4- and 2,6-TDI was diluted with non-exposed human urine 1/1250-, 1/500- and 1/250-fold. The urine samples were hydrolyzed by both conventional heating and MAH. The hydrolysis efficiency obtained using MAH significantly exceeded that obtained using conventional heating. Hydrolysis by MAH required only 20 min, 48 times faster than with conventional heating. The use of the MAH method in hydrolysis was demonstrated to be reproducible, timesaving and efficient technique in measuring the concentration of urinary TDAs.

Keywords: Toluene diisocyanate; Toluene diamine; Microwave-assisted heating; Hydrolysis

1. Introduction

Toluene diisocynates (TDI) are widely used in polyurethane (PU) products, such as PU foam, elastomers, coatings, paints and adhesives. The commercial form of the raw material utilized in industry is a mixture of two TDI congeners – the 2,4- and 2,6-forms [1]. TDIs have been documented to be one of the leading causes of occupational asthma (OA). Five to 10% of workers exposed to TDI suffer from OA [2–6]. Overexposure to TDI is also reportedly associated with the elevated prevalence of hypersensitivity pneumonitis and contact dermatitis [2–7].

Toluene diamine (TDAs), one of the hydrolytic metabolites of TDIs, in urine has been extensively used as a dose indicator of TDI-exposed workers [8–17]. Studies have shown satisfactory linear relations between urinary TDA levels and measured exposure to TDI in air ($r = 0.86$–0.99) [8–12,15–17]. TDA in urine (U-TDA), however, is present mostly in a conjugated form rather than a free-form in rats [18]. No detectable amount of free TDA was present in the urine of TDI-exposed workers [19]. In the analysis of U-TDA, hydrolysis is necessary to decompose conjugated TDA into free TDA. Conventionally, strong acids and heating were applied to break the covalent bonds of the conjugated TDA and then to convert them into free-form TDAs prior to instrumental analysis [8–17]. Several studies have utilized strong alkali in place of acid before heating [20]. However, more free amines in urine were lost than in the acidic preparation process [20]. Sixteen-hour heating in 3 M of H_2SO_4, recommended by Skarping et al. [9,10,15,16,20] has been extensively adopted as the standard hydrolysis procedure for determining the U-TDA concentration before analysis using GC/MS instruments. Therefore, the hydrolysis procedure in this method took more than 90% of the total analytical time.

* Corresponding author. Tel.: +886 6 235 3535x5597; fax: +886 6 274 3748.
E-mail address: h7154@mail.ncku.edu.tw (H.-Y. Chang).

0039-9140/$ – see front matter © 2007 Elsevier B.V. All rights reserved.
doi:10.1016/j.talanta.2007.02.001

Additionally, the long heating process tended to increase the risk of laboratory fire and/or explosion. Hence, the sample pretreatment procedure must be improved to effectively reduce the heating duration.

The use of microwave energy to provide heat to drive the decomposition of acid was first proposed in 1975 by Abu-Samra et al. who reported its application in the analysis of Cu, Zn and Pb by the wet digestion of orchard leaves and bovine liver biological samples [21]. Over recent decades, microwave-assisted heating (MAH) has been improved and is now widely applied in analytical chemistry, such as in accelerating the digestion and/or extraction of samples [22–24]. Biological specimens and various environmental media exhibit electronic disequilibrium (dipolar charge). Dipolar charged chemicals are sensitive to microwaves and can efficiently absorb energy during microwave irradiation. Therefore, heating may be accelerated using microwaves. To our knowledge, however, no MAH has been applied to analyze U-TDA.

The objectives of this study were to develop a sample pretreatment method using MAH in the analysis of U-TDA and to compare the effectiveness (recovery) and efficiency (time expenditure) of MAH with those of the conventional heating method.

2. Experimental

2.1. Reagents

2,4-TDI (98%) was obtained from Sigma (St. Louis, MO, USA), 2,6-TDI (97%), 2,4-TDA (98%) and heptafuorobutyric anhydride (HFBA, 98%) from Aldrich Chemical (St. Louis, MO, USA), 2,6-TDA (97%) from Lancaster (Morecambe, England), H_2SO_4, NaOH, HCl and K_2HPO_4 from Merck (GR grade, Darmstadt, Germany) and GC-grade toluene from Tedia (Fairfield, OH, USA).

2.2. Equipment

A pH meter (Suntex SP-701, Taipei) was utilized to adjust the pH of the buffers. All GC analyses were performed using Agilent Model 6890 GCs equipped with μ-electron capture detectors (μ-ECD, Agilent G2397A). A DB-5MS (J&W Scientific, Folsom, CA, USA) (60 m × 0.25 mm i.d.) with a film thickness of 0.25 μm fused silica capillary column was used to perform the separation. The carrier gas was ultra high-purity nitrogen (purity ≥ 99.99%) at a flow rate of 0.8 ml min^{-1} and the make-up gas was nitrogen at 30 ml min^{-1}. The column temperature program was initially 150 °C for 1 min, followed by an increase at 10 °C min^{-1} to 250 °C, at which temperature the column was held for 5 min. The injector and detector temperatures were 250 and 290 °C, respectively. The injection volume was 1 μl in split mode with the split ratio was 30:1.

2.3. Collection and storage biological samples

Due to the complexity of the composition and heterogeneity of conjugated form of urinary TDAs in organisms as well as no any commercially available conjugated TDA standard reagents, an animal experiment was conducted to obtain the actual TDI exposed urine samples following by oral administration of a known TDI dose. A Wistar rat (male, 9 weeks old, 480 g) obtained from the National Cheng Kung University Animal Facility Center was orally given 206.5 mg kg^{-1} (equivalent to 1/20 LD_{50}) [25] of the mixture of 2,4- and 2,6-TDI prepared in 2 ml dried corn oil (MP, USA) [18]. The rat was then housed in metabolism cages (2100R, Biomedic, USA), which had been designed for the separate collection of urine and feces. Urine samples were collected 24 h before and after exposure in 50 ml polyethylene conical tubes. The rat urine samples were then diluted 1/1250-, 1/500- and 1/250-fold with non-TDI-exposed human urine, to be comparable to the urine concentrations from occupational settings in the literature [20]. The urine samples were stored in a freezer at −20 °C until analysis.

2.4. Preparation and analysis of sample

2.4.1. Preparation of standards

Low and high calibration curves of both 2,4- and 2,6-TDA were obtained separately by preparing concentrations from 1 to 50 and from 50 to 500 ng ml^{-1}, respectively, in 0.1 M HCl solution. Then, the TDA derivatization procedure was implemented. The retention times of 2,6- and 2,4-TDA derivatives were 10.796 and 11.057 min, respectively (Fig. 1a) in the GC chromatogram. 2,4- and 2,6-TDA calibration curves both yielded linear relationships between peak areas and the TDA concentrations. The correlation coefficient (r) exceeded 0.995 for both TDAs at high and low concentrations.

2.4.2. Hydrolysis

2.4.2.1. Reference procedure: conventional heating procedure. One milliliter of urine sample was hydrolyzed with 1.5 ml of 3 M H_2SO_4 for 16 h at 100 °C, as recommended by Skarping et al. [20], using a Firefox Dry Bath 6100 (Panttech, Taiwan) in 15 ml test tubes with Teflon screw caps.

2.4.2.2. Microwave-assisted heating (MAH) procedure. One milliliter of urine sample and 1.5 ml of 3 M H_2SO_4 in 15 ml test tubes with Teflon screw caps was placed in a 120 ml microwave vessel. In each hydrolysis cycle, four vessels were used simultaneously. MAH was performed with a microwave digestion system (MDS 2000, CEM, USA) with a maximum output power of 650 W. The MAH operational parameters including power, pressure and time were finalized and shown in Table 1 after a series of optimization experiments for the hydrolysis process (as described in Section 3.2).

The optimization of the MAH was evaluated at each stage of four stages in the heating program using the rat urine samples, diluted 1/200-fold with non-TDI exposed human urine, as described in Section 2.3. Various powers, pressures and times (Table 1) were examined to maximize the efficiency of the hydrolysis process.

After the MAH process was completed, the vessels were further cooled down at room temperature, and took out the test tubes

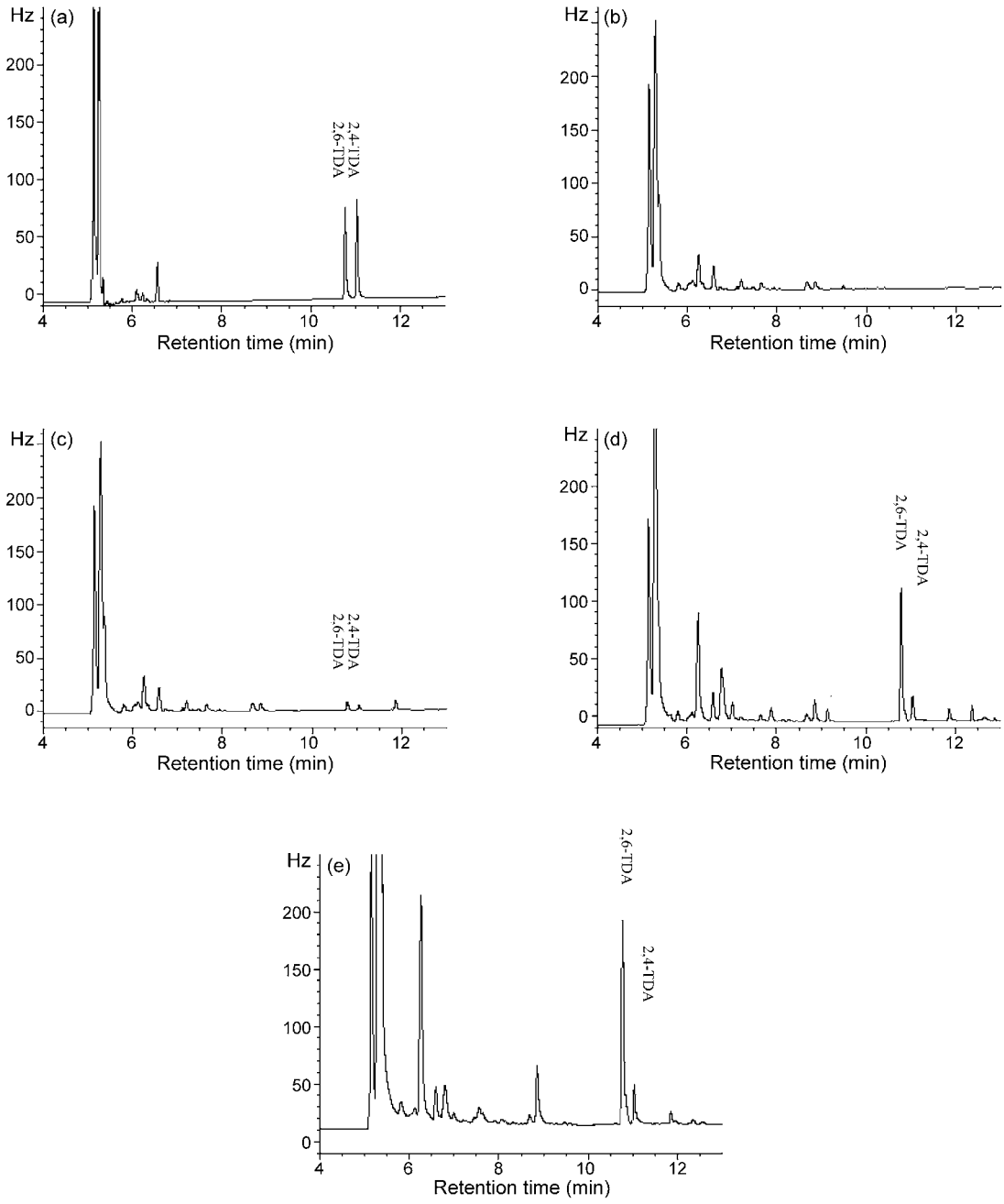

Fig. 1. Chromatograms: (a) spiked at 200 ng ml^{-1} of 2,6- and 2,4-TDA in the deioned water; (b) blank urine; (c) urine specimen from a TDI-exposed rat without undergoing any hydrolysis process; (d) after hydrolysis by conventional heating method for urine specimen from a TDI-exposed rat (dilution at 1/250-fold). The concentrations of two peaks refer to 480.2 ng ml^{-1} of 2,6-TDA and 65.6 ng ml^{-1} of 2,4-TDA, respectively; (e) after hydrolysis by MAH method for urine specimens from a TDI-exposed rat (dilution at 1/250-fold). The concentrations of two peaks refer to 457.1 ng/ml of 2,6-TDA and 89.5 ng ml^{-1} of 2,4-TDA, respectively.

via the analytical procedure that was described in the section on TDA derivatization.

2.4.3. TDA derivatization

After hydrolysis, 5 ml of saturated NaOH solution and 2 ml of toluene were added into the samples. The mixtures were shaken for 2 min and then centrifuged for 10 min at 1500 rpm. 1.5 ml of the organic supernatant was transferred to a new test tube and 25 μl HFBA was added [26]. The samples were immediately shaken vigorously for 2 min and allowed to stand for 10 min. Excess reagent was removed by extraction with 1 ml of 1 M phosphate buffer solution (pH 7.2). The toluene layer, containing the amide derivatives, was transferred into 1.5 ml auto sampler vials with Teflon seals for further GC analysis.

2.5. Comparison of recoveries of TDAs in blank urine obtained using conventional heating and MAH

Blank urine samples were spiked with 2,6- and 2,4-TDA standard reagents at levels of 100–500 and 20–100 ng ml^{-1}, respectively. Conventional heating and MAH hydrolysis meth-

Table 1
Different test programs for optimization

Program	I	II	III	IV	V	VI
Stage 1						
Power (W) (%)	126 (20)	126 (20)	126 (20)	126 (20)	126 (20)	120 (20)
Pressure (psi)	20	20	20	20	20	20
Time (min)	10	10	10	10	10	10
Stage 2						
Power (W) (%)	252 (40)	252 (40)	252 (40)	252 (40)	252 (40)	
Pressure (psi)	60	60	60	60	60	
Time (min)	10	10	10	10	10	
Stage 3						
Power (W) (%)	378 (60)	378 (60)	378 (60)	378 (60)		
Pressure (psi)	80	80	80	80		
Time (min)	10	10	10	10		
Stage 4						
Power (W) (%)	378 (60)	378 (60)	378 (60)			
Pressure (psi)	100	100	100			
Time (min)	15	10	5			

ods were implemented, according to the described TDA derivatization procedure ($n = 4$ for each test).

3. Results and discussion

3.1. Chromatograms

Fig. 1a shows the chromatogram of 2,6- and 2,4-TDA derivatives, which was obtained from 2,6 and 2,4-TDA spiked in deionized water following extraction and derivatization. Two peaks were well separated without any notable interference peaks.

The chromatogram showed no endogenous peak from the blank urine samples (Fig. 1b). Very small amounts of 2,4- and 2,6-TDA in the urine collected from a TDI-exposed rat without heating hydrolysis process was observed in Fig. 1c, inconsistent with the findings for humans in literature, which no free TDA was detected for the TDI-exposed workers [19]. The trace amount of free TDA might be present as a result that TDI was hydrolyzed to TDA in the acidic environment of the stomach, following oral administration of TDI [18]. The stability of the TDI-corn oil mixture should be acceptable because dried corn oil was used before it was administered to rats. However, the GC chromatogram in Fig. 1c showed that the urine samples still underwent minor hydrolysis and yielded less peaks (4.2% for 2,6-TDA and 14.3% for 2,4-TDA) than those obtained in the hydrolysis of urine specimens by either the conventional heating method (Fig. 1d) or by the MAH method (Fig. 1e).

3.2. MAH optimization

The power and pressure were maintained below 450 W (=75%) and 50 psi, respectively, to avoid abrupt gas generation and explosion in the initial stage throughout MAH. Table 1 presents various heating parameters—microwave powers, pressures and times.

For 2,6-TDA, program I yielded the lowest concentration of 113.5 ng ml^{-1}, and programs II–IV yielded similar concentrations of 320.8, 289.2 and 314.3 ng ml^{-1}. These values were superior to those in program I but inferior to that, 484.5 ng ml^{-1} in program V. Program VI yielded a lower concentration of 226.4 ng ml^{-1} (Fig. 2). For 2,4-TDA, programs I–VI yielded concentrations of 30.4, 60.5, 52.1, 56.3, 63.1 and 35.7 ng ml^{-1}, respectively. 2,4-TDA and 2,6-TDA yielded exactly the same order of concentrations. Programs I to IV incorporated longer periods of heating but yielded lower concentrations than program V, perhaps because carbonization occurred during over-heating process. However, incomplete hydrolysis, due to insufficient MAH, could explain why the concentration obtained using program VI was much less than that obtained using program V. The effect of the hydrolysis duration was investigated in the range 10–45 min. The hydrolysis yield was very close in the range 30–40 min (programs II–IV), however, the hydrolysis yield decreased while the heating duration was over 40 min or under 10 min. Therefore 20 min for the hydrolysis duration was selected. The above results showed that program V with two-stage heating yielded the best efficiency and was therefore adopted as the MAH process thereafter.

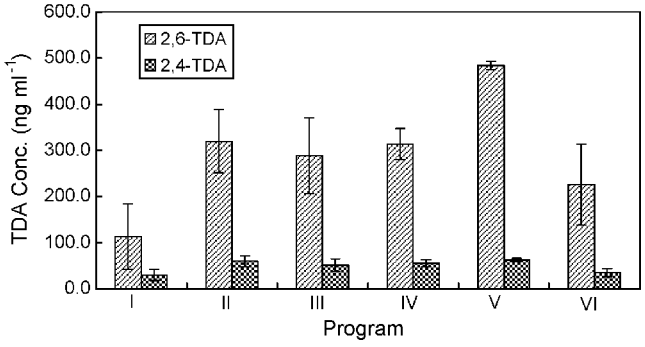

Fig. 2. Comparisons on the yielding concentrations of 2,6- and 2,4-TDA among six MAH programs during optimization experiment. The details of the program for each experimental setting please refer to Table 1.

Table 2
Comparisons on recoveries[a] of blank urine spiked with free-form TDAs at three concentrations between the methods of conventional heating (CH) and microwave-assisted heating (MAH)

Addition (ng ml^{-1})	n[b]	CH		MAH[c]	
		Mean (S.D.) (%)	R.S.D. (%)	Mean (S.D.) (%)	R.S.D. (%)
2,6-TDA					
100	4	90.2 (0.4)	0.4	94.3 (3.8)	4.0
250	4	95.0 (2.6)	2.7	101.5 (4.7)	4.6
500	4	101.8 (5.8)	5.7	99.8 (4.3)	4.3
Mean		95.7 (2.9)	3.0	98.5 (4.3)	4.3
2,4-TDA					
20	4	95.4 (6.1)	6.4	103.1 (1.3)	1.2
50	4	96.1 (3.9)	4.1	102.5 (5.0)	4.9
100	4	99.4 (6.4)	6.4	99.8 (4.9)	4.9
Mean		97.0 (5.5)	5.6	101.8 (3.7)	3.7

[a] The recovery was defined as the amount quantified vs. the amount spiked.
[b] Number of replicates.
[c] Program V.

3.3. Comparison of MAH with conventional heating method

3.3.1. Recovery

Table 2 showed the mean recoveries obtained using conventional heating and MAH hydrolysis for 2,6-TDA in the range 100–500 ng ml^{-1}, which were 95.7 ± 2.9% (R.S.D. 3.0%) and 98.5 ± 4.3% (R.S.D. 4.3%), respectively. The mean recoveries of conventional heating and MAH hydrolysis for 2,4-TDA in the range 20-100 ng ml^{-1} were 97.0 ± 5.5% (R.S.D. 5.6%) and 101.8 ± 3.7% (R.S.D. 3.7%), respectively. The mean recoveries were both considered to be satisfactory and the precisions with R.S.D. values of between 0.4% and 6.4% were also favorable. The recoveries of the MAH method slightly exceeded those of the conventional heating method, none of the differences was statistically significant ($p > 0.05$, Student's t-test). Over 95% recoveries and under 7% R.S.D., indicated that both heating methods provided satisfactory accuracy and precision in the determination of U-TDAs.

3.3.2. Hydrolysis efficiency

The MAH method consistently yielded higher efficiencies than the conventional heating method at three TDA levels, in hydrolysis efficiency tests of urine specimens obtained following TDI exposure (Table 3). Comparing the hydrolysis efficiency of conventional heating with that of MAH method at different

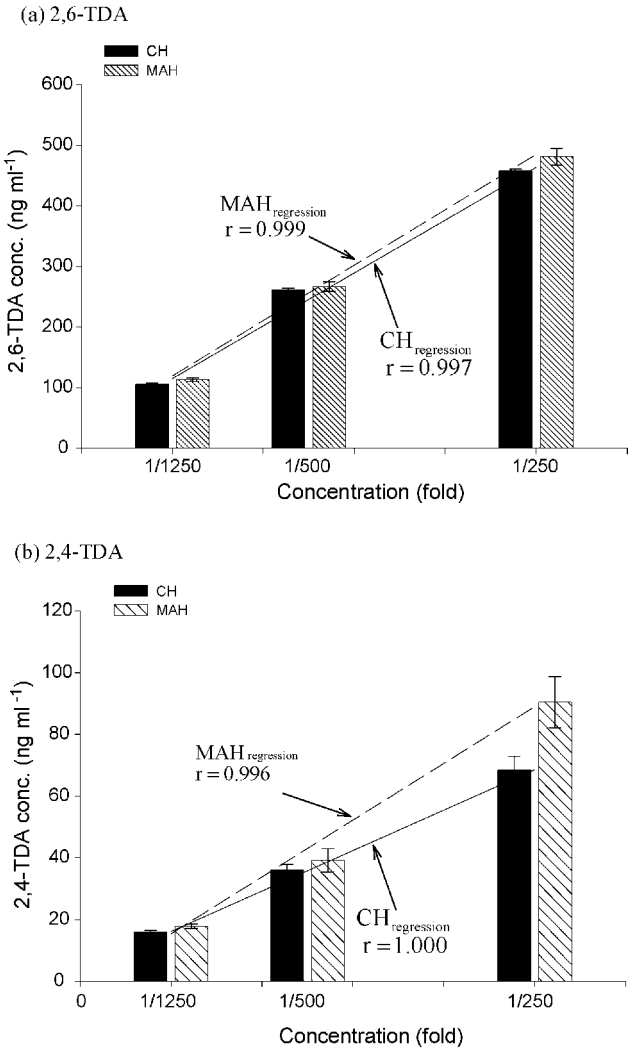

Fig. 3. Comparisons on the linearity of measured concentration at three diluted concentration (fold) between CH and MAH for 2,6-TDA (upper) and 2,4-TDA (lower).

U-TDAs levels revealed no significant difference between the 1/500 groups of both TDAs ($p > 0.05$). However, the hydrolysis efficiency of MAH was significantly higher than that of conventional heating for the 1/1250 ($p < 0.01$ for 2,6- and 2,4-TDA) and 1/250 ($p < 0.05$ for 2,6-TDA, $p < 0.01$ for 2,4-TDA) groups. Moreover, the measured concentrations increased in proportion to the concentrations in urine for both conventional heating and MAH (Fig. 3). The coefficients of correlation (r) for 2,6-TDA for conventional heating and MAH were 0.997 and

Table 3
Comparisons on the concentrations of 2,6- and 2,4-TDA (ng ml^{-1}) in hydrolysis efficiency tests determined by CH and MAH methods from urine specimen ($n = 4$)

Dilution factor	2,6-TDA, mean (R.S.D.%)			2,4-TDA, mean (R.S.D.%)		
	1/1250**	1/500	1/250*	1/1250**	1/500	1/250**
CH	105.2 (2.4)	261.2 (1.0)	457.6 (0.7)	15.9 (3.3)	36.2 (4.5)	68.4 (6.5)
MAH	113.0 (2.6)	266.7 (3.1)	481.1 (2.9)	17.8 (3.8)	39.2 (9.5)	90.4 (9.2)

n: number of replicates.
* $p < 0.05$ by Student's t-test.
** $p < 0.01$ by Student's t-test.

0.999, respectively (Fig. 3a). For 2,4-TDA, they were 1.000 and 0.996, respectively (Fig. 3b), indicating satisfactory linearity of the measured concentrations for both conventional heating and MAH. However, the slopes for conventional heating and MAH for 2,6-TDA were quite close to each other, indicating that the measured outcomes were only slightly discrepant. For 2,4-TDA, however, the yield of MAH increased with concentrations (1/250 and 1/500 groups), suggesting that the higher hydrolysis efficiency of MAH exceeded that of conventional heating in the analysis of high concentrations of 2,4-TDA.

The application of microwave heating to accelerate the chemical synthesis reactions began with the work of the teams of Giguere et al. [27] and Gedye et al. [28] at the end of 1980s. Because microwave heating is able to improve reaction rates, enhance selectivity, and provide cleaner products with higher yields and shorter reaction duration, quite a few microwave-assisted reactions have been investigated in organic chemistry [29]. Particularly, microwave-assisted method is very promising to implement the hydrolysis of organic compounds in acid and alkaline media, reactions involving the hydrolysis derivatization since 1993 [30]. In our study, while hydrolysis by the conventional heating method required 16 h, MAH took only 20 min to yield similar recoveries and precision, perhaps because of its ability to rapidly increase the temperature of a reaction. Heating by microwave is a highly efficient process and saves considerable energy, primarily because the fundamental mechanism of microwave involves an agitation of dipolar molecules or ions that could oscillate under the effect of an oscillating electric or magnetic field [31]. Microwave heating, unlike conventional heating, provides uniform heating to drive a reaction throughout a reaction mixture. In conventional heating, temperature differences always exist between the container wall and the solvent. Therefore, heating by MAH is a highly efficient process and saves significant time.

4. Conclusions

Hydrolysis by MAH took 48 times faster than that by the conventional heating method with comparable analytical recoveries and precision for both U-TDAs samples at various concentrations. This study demonstrated that the application of the MAH method in hydrolysis was a reproducible, timesaving and efficient measure during the preparation of samples for determining urinary TDA concentrations.

References

[1] H.J. Yeh, T.S. Shih, P.J. Tsai, H.Y. Chang, J. Exp. Anal. Environ. Epidemiol. 12 (2002) 157.
[2] X. Baur, Lung 174 (1996) 23.
[3] J.A. Bernstein, Toxicology 111 (1996) 181.
[4] F. Deschamps, A. Prevost, F. Lavaud, S. Kochman, Ann. Occup. Hyg. 42 (1998) 33.
[5] C.E. Mapp, P.C. Corona, N. De Marzo, L. Fabbri, Am. Rev. Respir. Dis. 137 (1988) 1326.
[6] M.G. Ott, W.F. Diller, A.T. Jolly, Crit. Rev. Toxicol. 33 (2003) 1.
[7] J.D. Wang, P.H. Huang, J.M. Lin, Am. J. Ind. Med. 4 (1998) 73.
[8] C. Rosenberg, H. Savolainene, J. Chromatogr. 367 (1986) 385.
[9] G. Skarping, T. Brorson, C. Sangö, Int. Arch. Occup. Environ. Health 63 (1991) 83.
[10] T. Brorson, G. Skarping, C. Sangö, Int. Arch. Occup. Environ. Health 63 (1991) 253.
[11] P. Persson, M. Dalene, G. Skarping, M. Adamsson, L. Hagmar, Br. J. Ind. Med. 50 (1993) 1111.
[12] A. Maitre, M. Berode, A. Perdrix, S. Romazini, H. Savolarinen, Int. Arch. Occup. Environ. Health 65 (1993) 97.
[13] P. Lind, M. Dalene, G. Skarping, L. Hagmar, Occup. Environ. Med. 53 (1996) 94.
[14] P. Carbonnelle, S. Boukortt, D. Lison, Analyst 121 (1996) 663.
[15] H. Tinnerberg, M. Dalene, G. Skarping, Am. Ind. Hyg. Assoc. J. 58 (1997) 229.
[16] M. Dalene, G. Skarping, P. Lind, Am. Ind. Hyg. Assoc. J. 58 (1997) 587.
[17] K. Kääriä, A. Hirvonen, H. Norppa, Analyst 126 (2001) 1025.
[18] C. Timchalk, F.A. Smith, M.J. Bartel, Toxicol. Appl. Pharmacol. 124 (1994) 181.
[19] C.J. Sennbro, C.H. Lindh, H. Tinnerberg, C. Gustavsson, M. Littorin, H. Welinder, B.A. Jonsson, Biomarkers 8 (2003) 204.
[20] P. Lind, G. Skarping, M. Dalene, Anal. Chim. Acta 333 (1996) 277.
[21] A. Abu-Samra, J.S. Morris, S.R. Koirtyohann, Anal. Chem. 47 (1975) 1475.
[22] A. Zlotorzynski, Crit. Rev. Anal. Chem. 25 (1995) 43.
[23] H.M. Kingston, S.T. Haswell, J. Am. Chem. Soc. 119 (1997) 772.
[24] F.O. Silva, V. Ferraz, Talanta 68 (2006) 643.
[25] P.F. Woolrich, Am. Ind. Hyg. Assoc. J. 43 (1982) 89.
[26] C. Rosenberg, H. Savolainene, J. Chromatogr. 323 (1985) 429.
[27] R.J. Giguere, T.L. Bray, S.M. Duncan, G. Majetich, Tetrahedron Lett. 27 (1986) 4945.
[28] R. Gedye, F. Smith, K. Weataway, H. Ali, L. Baldisera, L. Laberge, Tetrahedron Lett. 27 (1986) 279.
[29] J. Warrand, H.G. Janssen, Carbohydr. Polym. 69 (2007) 353.
[30] K.D. Khalaf, A. Morales-Rubio, M. de la Guardia, Anal. Chim. Acta. 284 (1993) 249.
[31] Developments in Microwave Chemistry, Evalueserve, 2005.

Available online at www.sciencedirect.com
ScienceDirect
Talanta 72 (2007) 1500–1506
Talanta
www.elsevier.com/locate/talanta

Determination of vitexin-2″-*O*-rhamnoside in rat plasma by ultra-performance liquid chromatography electrospray ionization tandem mass spectrometry and its application to pharmacokinetic study

Xixiang Ying [a,b], Xiumei Lu [a], Xiaohong Sun [a], Xiaoqin Li [a], Famei Li [a,*]

[a] *School of Pharmacy, Shenyang Pharmaceutical University, 103 Wenhua Road, Shenyang, Liaoning Province 110016, PR China*
[b] *School of Pharmacy, Liaoning University of TCM, 79 Chongshan East Road, Shenyang, Liaoning Province 110032, PR China*

Received 24 August 2006; received in revised form 23 January 2007; accepted 27 January 2007
Available online 9 February 2007

Abstract

A rapid, sensitive and selective ultra-performance liquid chromatography electrospray ionization tandem mass spectrometry (UPLC-ESI-MS/MS) method was developed for the determination and pharmacokinetic study of vitexin-2″-*O*-rhamnoside (VOR) in rat plasma. The method involved a simple protein precipitation with methanol. The separation was performed on an ACQUITY UPLC™ BEH C_{18} column (50 mm × 2.1 mm, i.d., 1.7 μm) with gradient elution using a mobile phase composed of acetonitrile and water (containing 0.1% formic acid) at a flow rate of 0.25 mL min^{-1}. Electrospray ionization (ESI) in positive ion mode and multiple reaction monitoring (MRM) was used for the quantification of VOR with a monitored transitions *m/z* 579 → 433 for VOR and *m/z* 611 → 303 for internal standard (I.S., hesperidin). Linear calibration curves were obtained over the concentration range of 10–2500 ng mL^{-1} with lower limit of quantification (LLOQ) of 10 ng mL^{-1}. The intra- and inter-day precisions (R.S.D. %) were less than 11% and 2.4%, and accuracy (RE %) between −9.3% and 1.0% ($n = 5$). The average extraction recovery of VOR was 97.2 ± 2.6%. The developed method was applied for the first time to the pharmacokinetic study of VOR in rats following a single oral dose.

Keywords: Vitexin-2″-*O*-rhamnoside; UPLC-ESI-MS/MS; Pharmacokinetics; Rat plasma

1. Introduction

Vitexin-2″-*O*-rhamnoside (VOR) is one of the main components of flavonoid of the leaves of *Crataegus pinnatifida* Bge. var *major* N. E. Br. [1], which has been demonstrated to strongly inhibit DNA synthesis in MCF-7 human breast cancer cells [2], and it belongs to polyphenolic compound, which has shown many other biological and pharmacological activities, such as antioxidation and treating heart disease [3,4] Many methods have been reported for quantification of VOR in pharmaceuticals or plants using high-performance liquid chromatography (HPLC) [5,6] and capillary zone electrophoresis (CZE) with UV detector [7,8]. Because flavonoid glycosides have been considered that were hydrolyzed firstly by the microflora before being absorbed [9,10], little attention has been devoted to the pharmacokinetic study of VOR in vivo. Hence, it is necessary to develop an assay to fully evaluate the pharmacokinetics of VOR. Recently, the high sensitive and selective LC–MS method has been employed to the analysis of flavonoid glycoside in biological fluids [11]. In this paper, a rapid, sensitive and selective approach using UPLC-ESI-MS/MS method is described to investigate the pharmacokinetics of VOR in rat after oral administration. The LLOQ of this method is 10 ng mL^{-1}. The total run time of each sample was 3.0 min which met the requirement for a high-throughput determination of biosamples. To the best of our knowledge, this is the first report on the development, validation and application of UPLC-ESI-MS/MS method for the determination of VOR in rat plasma and its pharmacokinetic study after oral administration.

2. Experimental

2.1. Chemicals and reagents

The leaves of *C. pinnatifida* Bge. var *major* N. E. Br. (collected in Shenyang, Liaoning Province, China) were

* Corresponding author.
E-mail address: fameili@163.com (F. Li).

0039-9140/$ – see front matter © 2007 Elsevier B.V. All rights reserved.
doi:10.1016/j.talanta.2007.01.059

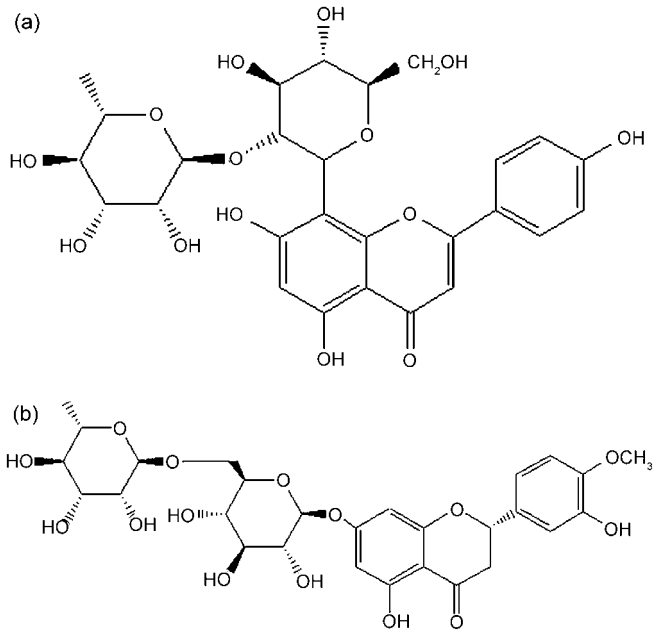

Fig. 1. The structures of vitexin-2″-*O*-rhamnoside (a) and hesperidin (b).

extracted with 70% aqueous EtOH, the crude extract was then concentrated and passed through a porous-polymer resin (AB-8, Tianjin, China) eluted with 60% EtOH. The solvent was evaporated under reduced pressure to obtain a mixture which was partitioned with chloroform and *n*-butanol. The *n*-butanol layer (100 g) was chromatographed on silica gel with chloroform–methanol as the eluent in gradient to afford 10 fractions. Fraction 7 [10 g, chloroform–methanol (4:1)] were subjected to silica gel column chromatography eluted with an ester acetic acid–butanone–formic acid–water (4:3:1:1) to give VOR of 0.8 g (99.0% purity checked by HPLC) which was fully characterized by comparison of ^{1}H NMR and MS data with those in literature [12]. Hesperidin (internal standard, I.S.) was purchased from National institute for the Control of Pharmaceutical and Biological Products (Beijing, China). The structures of VOR and I.S. are shown in Fig. 1. Acetonitrile and methanol of HPLC grade were purchased from Tedia Company, Inc (Fairfield, OH, USA). Water was purified in a Milli-Q® Biocel Ultrapure Water System (Millipore, MA, USA) in all the study. Other chemicals were of analytical grade.

2.2. Instrumentation and conditions

2.2.1. Ultra-performance liquid chromatography

Liquid chromatography was performed on an ACQUITY^{TM} UPLC system (Waters Corp., Milford, MA, USA) with conditioned autosampler at 4 °C. The separation was carried out on an ACQUITY UPLC^{TM} BEH C_{18} column (50 mm × 2.1 mm, i.d., 1.7 μm; Waters Corp., Milford, MA, USA). The column temperature was set at 40 °C. The analysis was achieved with gradient elution using (A) acetonitrile and (B) water (containing 0.1% formic acid) as the mobile phase at a flow rate of 0.25 mL min^{-1}. Gradient condition of the mobile phase was as follows: A was linear from 30% to 40% during the first 1.0 min, linearly increased to 90% for 0.5 min and returned to initial condition for 1.5 min re-equilibration. The injection volume was 5 μL using partial loop mode for sample injection.

2.2.2. Mass spectrometry

Mass spectrometric detection was carried out on a Micromass® Quattro micro^{TM} API mass spectrometer (Waters Corp., Manchester, UK) with an electrospray ionization (ESI) interface. The ESI source was set in positive ionization mode. Quantification was performed using multiple reaction monitoring (MRM) of the transitions of *m/z* 579 → 433 for VOR and *m/z* 611 → 303 for I.S., respectively, with a dwell time of 100 ms per transition. The optimized ionization parameters were as follows: capillary 3.1 kV, cone 40 kV, source temperature 110 °C and desolvation temperature 300 °C. Nitrogen was used as desolvation and cone gas with the flow rate of 300 and 40 L h^{-1}, respectively. Argon was used as collision gas and the collision energy was 20 eV for both VOR and I.S. Multipliers were set at 650 V. All data were acquired and processed using MassLynx^{TM} NT 4.0 software with a QuanLynx^{TM} program (Waters Corp., Milford, MA, USA).

2.3. Animals and blood sampling

All animal studies were performed according to the Guidelines for the Care and Use of Laboratory Animals that was approved by the Committee of Ethics of Animal Experimentation of Liaoning University of TCM.

Male Wistar rats, weighing 250–300 g, were obtained from the Laboratory of Animal Center, Liaoning University of TCM (Shenyang, China). They were kept in environmentally controlled breeding room for 1 week before the experiments, fed with standard laboratory food as well as water ad libitum and fasted overnight before the test. VOR (120 mg kg^{-1}) was administered to the rats via gastric gavage. A blood sample of 0.5 mL was withdrawn from vena orbitalis at times of 0, 5, 10, 15, 30, 45, 60, 90, 150, 240 and 360 min to heparinized polythene tubes and centrifuged at 1300 × *g* for 15 min to obtain plasma samples. Samples were stored at −20 °C until analysis.

2.4. Calibration standards and quality control samples

Stock solutions of VOR and I.S. were prepared in methanol at 100 and 400 μg mL^{-1}, respectively, and were stored at 4 °C. Working solutions were obtained by serial dilution of stock solution with methanol. The calibration samples for VOR were prepared by spiking blank rat plasma at 10, 25, 50, 100, 250, 500 and 2500 ng mL^{-1}. The quality control (QC) plasma samples of VOR (25, 250 and 2000 ng mL^{-1}) were similarly prepared.

2.5. Plasma sample preparation

Aliquots of 200 μL of plasma sample were spiked with 20 μL of acetic acid, 50 μL of I.S. (40 μg mL^{-1}) and 1 mL of methanol followed by vortex mixing for 1 min and centrifuging at 1300 × *g* for 15 min, and the supernatant was transferred into 1.5 mL tubes and evaporated to dryness under

a stream of nitrogen (50 °C). The residue was dissolved with 100 μL initial mobile phase, vortexed for 1 min and centrifuged at 12,700 × *g* for 10 min. An aliquot of 5 μL of the supernatant was injected into the UPLC-ESI-MS/MS system for analysis.

2.6. Method validation

Validation runs were conducted on three consecutive days. Each validation run consisted of a minimum of one set of calibration standards and six sets of QC plasma samples at three concentrations. The results from QC plasma samples in three runs were used to evaluate the precision and accuracy of the method developed. The peak area ratios of VOR/I.S. of unknown samples were then interpolated from the calibration curve to give the concentrations of VOR. During routine analysis, each analytical run included a set of calibration standards, a set of QC plasma samples in duplicate and plasma samples to be determined.

Selectivity was investigated by comparing chromatograms of blank plasma obtained from six rats with those of corresponding standard plasma sample spiked with VOR and I.S. (40 μg mL^{-1}) and plasma sample after oral determination of VOR in rat.

The matrix effects on the ionization efficiency of VOR and I.S. were evaluated by spiking blank plasma extracts at three different concentration levels of VOR (25, 250 and 2000 ng mL^{-1}). The resulting peak areas of VOR (A) were compared with those obtained from corresponding standard solutions dried and dissolved with mobile phase (B). The ratio (A/B × 100%) was used to evaluate the matrix effect, if it is between 85% and 115%, there is no significant matrix effect. The matrix effect of I.S. was evaluated using the same procedure.

The calibration curves over the concentration range of 10–2500 ng mL^{-1} for VOR were constructed by plotting the peak area ratios of VOR to I.S. versus VOR nominal concentrations in the standard plasma samples by the weighted ($1/x^2$) least-square linear regression. The limit of detection (LOD) was determined in signal to noise ratio of 3 (S/N) and the lower limit of quantification (LLOQ) determined in signal to noise ratio of >10 (S/N). The acceptable accuracy (RE) within ±20% and a precision (R.S.D.) not exceed 20% should be obtained.

Precision and accuracy were evaluated by analyzing the QC samples at three concentration levels of VOR (25, 250 and 2000 ng mL^{-1}). Precision was expressed as relative standard deviation (R.S.D. %) and accuracy as (mean found concentration − nominal concentration)/(nominal concentration) × 100%. Intra-day precision and accuracy were determined by repeated analysis of a set of standards on 1 day ($n = 5$), while inter-day precision and accuracy by repeated analysis on three consecutive days ($n = 5$ series per day). The R.S.D. and RE should be less than 15%, except at the LLOQ where it should not exceed 20%.

The extraction recovery was determined by comparing the peak areas of VOR obtained from QC samples that were subjected to the extraction procedure with those obtained from blank plasma extracts that were spiked post-extraction with the same nominal concentrations. The extraction recovery of I.S. was determined similarly. This procedure was repeated for QC samples at the concentration of 25, 250 and 2000 ng mL^{-1}.

The stability of VOR and I.S. stock solutions was evaluated after storage at room temperature for 6 h and at 4 °C for 15 days. The stability of VOR and I.S. working solutions was investigated at room temperature for 6 h.

Short-term stability was assessed by analyzing QC plasma samples kept at room temperature for 6 h that exceeded the routine preparation time of samples. Long-term stability was determined by assaying QC plasma samples after storage at −20 °C for 15 days. Freeze–thaw stability was investigated after three freeze (−20 °C at least 24 h)–thaw (room temperature for 2–3 h) cycles. Post-preparative stability was assessed by analyzing the extracted QC plasma samples kept in the autosampler at 4 °C for 24 h.

3. Results and discussion

3.1. ESI-MS/MS optimization

To determine VOR, electrospray ionization was used to obtain good sensitivity and fragmentation. The instrument setting was adjusted to maximize the responses for VOR and I.S. by direct injection of their standard solutions into the mass spectrometry. Positive ion mode was chosen for the quantification because of better sensitivity. MRM was used for the quantification of VOR on account of great advantage in selectivity. In MS scan mode we optimized the parameters which generated most intensive responses of precursor ions $[M+H]^+$ of VOR and I.S. Then the analyzer parameters were optimized in daughter scan mode with collision energy 20 eV for both VOR and I.S. to yield the most intensive product ions *m/z* 433 and *m/z* 303, respectively. The product ion mass spectra of $[M+H]^+$ ions of VOR and I.S. are shown in Fig. 2. The mass transitions chosen for quantification were *m/z* 579 → 433 for VOR and *m/z* 611 → 303 for I.S.

3.2. Chromatography optimization

Different mobile phases were evaluated to improve UPLC separation and enhance sensitivity in MS detection. Gradient elution using a mobile phase composed of acetonitrile–water (containing 0.1% formic acid) was finally chosen for separation with excellent peak shape and mass spectral response. A small amount of formic acid in the mobile phase was used to provide better ionization and higher sensitivity. Two channels were used for recording, channel 1 for VOR with the retention time of 0.69 min and channel 2 for I.S. with the retention time of 0.86 min. Both VOR and I.S. were rapidly eluted with retention times less than 1 min, and the total run time of each sample was 3.0 min which met the requirement for high-throughput determination of biosamples. Typical MRM chromatograms of a blank sample spiked with VOR of 500 ng mL^{-1} and I.S. (40 μg mL^{-1}) are depicted in Fig. 3. The very narrow chromatographic peaks generated by UPLC resulted in an increase in the chromatographic sensitivity and selectivity.

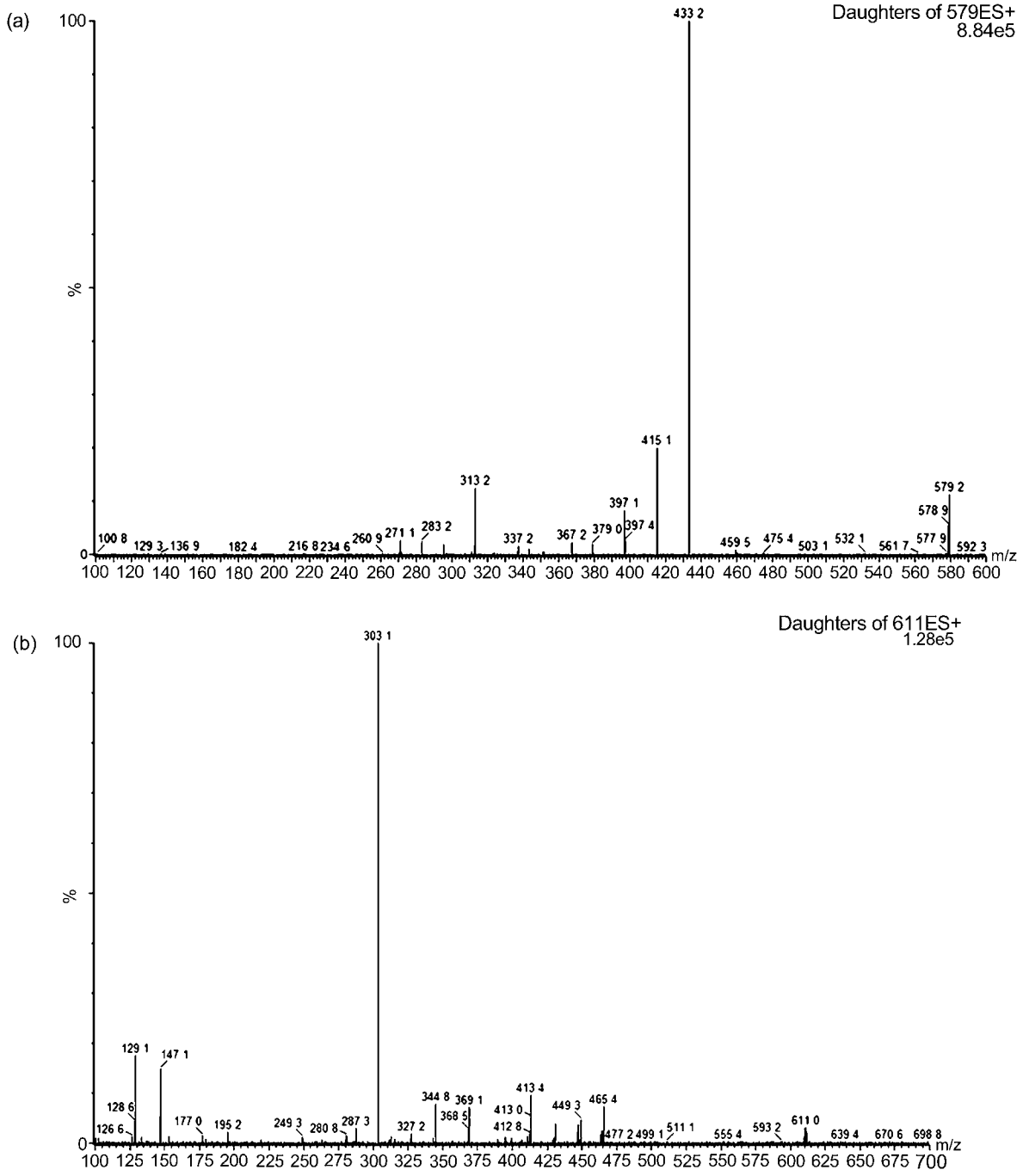

Fig. 2. Product ion mass spectra (ESI^+) of vitexin-2″-*O*-rhamnoside (a) and hesperidin (b).

3.3. Method validation

3.3.1. Selectivity and matrix effect

Representative chromatograms of an extracted blank rat plasma (a), a blank rat plasma spiked with VOR (500 ng mL^{-1}) and I.S. (b), and a rat plasma sample 10 min after oral administration of 120 mg kg^{-1} of VOR (c) are shown in Fig. 3. No interferences were observed at the retention times of the analytes.

To evaluate the matrix effect, the peak areas of blank plasma extracts spiked with analyte post-extraction (A) were compared with those of the standard solutions dried directly and reconstituted with mobile phase (B). The ratios (A/B × 100%) were 97.6 ± 2.2%, 102.9 ± 2.6% and 105.2 ± 6.7% at three concentration levels of VOR (25, 250 and 2000 ng mL^{-1}), respectively, while the I.S. was result 98.2 ± 4.6%, in the concentration levels of VOR, which means no significant matrix effect for VOR and I.S. in this method.

3.3.2. Calibration curve

Seven calibration standards were prepared by spiking blank plasma with 50 μL of VOR and I.S., and pre-treated with the same procedure as described under Section 2.5. The seven points

(10, 25, 50, 100, 250, 500 and 2500 ng mL^{-1}) calibration curves were linear over the concentration range. The regression equations were obtained using weighted ($1/x^2$) least squares linear regression: typically $y = 2.92 \times 10^3 x + 47.4$ with a correlation coefficient (r) of 0.9946, where y is the peak area ratio of VOR to I.S. and x is the spiked concentration of VOR.

3.3.3. Limit of detection and quantification

The limit of detection (LOD) was determined in signal to noise ratio of 3 (S/N), which was 2 ng mL^{-1} for VOR. The lower limit of quantification (LLOQ) was defined as the lowest concentration on calibration curve with acceptable precision and accuracy. The LLOQ of the assay was of 10 ng mL^{-1} (S/N = 14.7) with R.S.D. % of the intra- and inter-day precisions below 7.6% and 11.4%, accuracies (RE %) between −5.3% and 12.0%, respectively.

3.3.4. Precision and accuracy

The intra- and inter-day precisions and accuracies were determined by analyzing five replicates of QC samples at three concentrations (25, 250 and 2000 ng mL^{-1}) on the same day and on three consecutive days. The R.S.D. % of the intra- and inter-day precisions were below 11% and 2.4% and the accuracies (RE %) were between −9.3% and 1.0%, respectively. The R.S.D. and RE of the precision and accuracy of VOR were less than 15%, and that of LLOQ were not exceed 20%, which

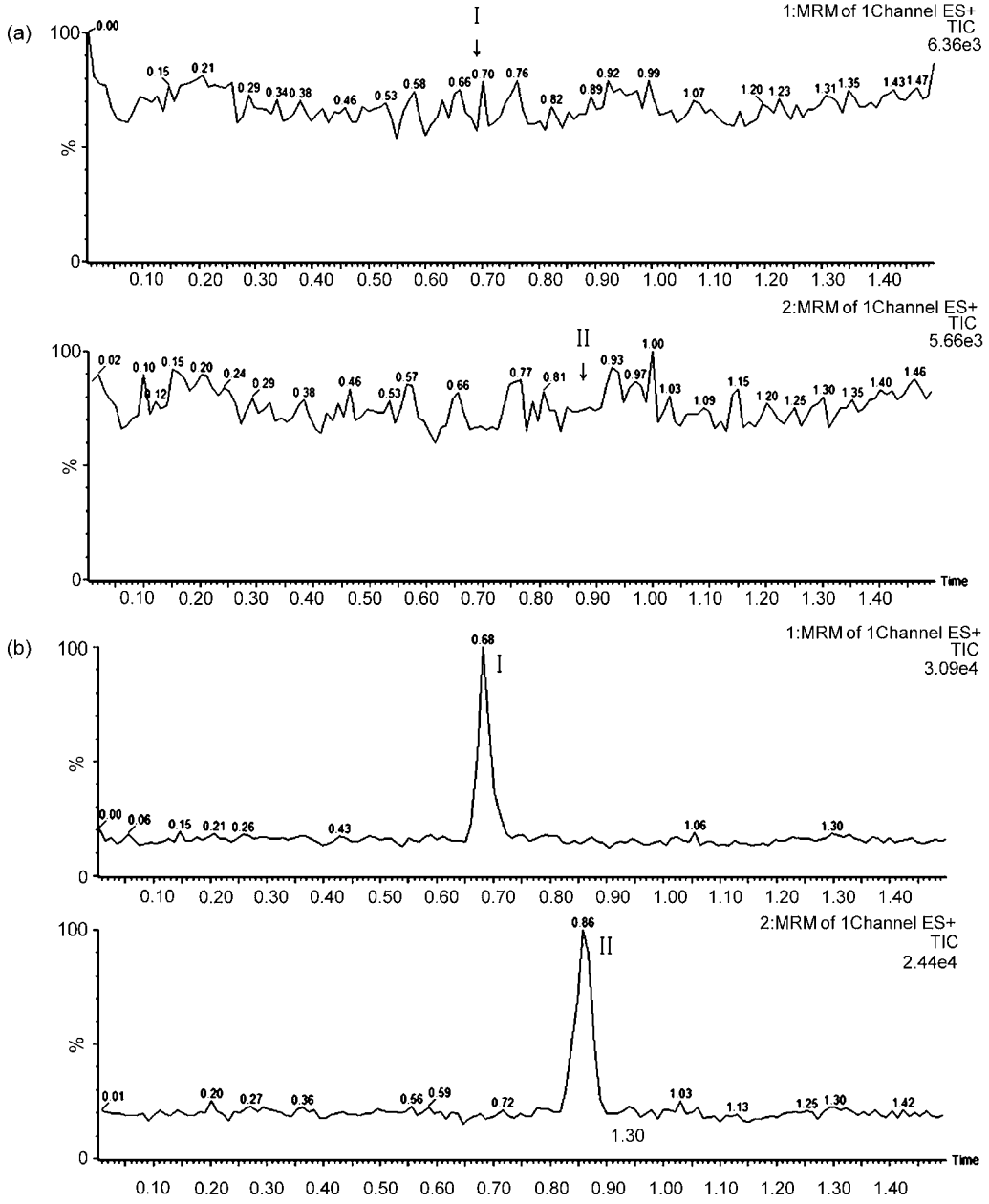

Fig. 3. Typical MRM chromatograms of (a) blank plasma; (b) blank plasma spiked with vitexin-2″-*O*-rhamnoside (500 ng mL^{-1}) and hesperidin; (c) plasma sample at 10 min after oral administration of 120 mg kg^{-1} vitexin-2″-*O*-rhamnoside. Peak: vitexin-2″-*O*-rhamnoside and peak: hesperidin.

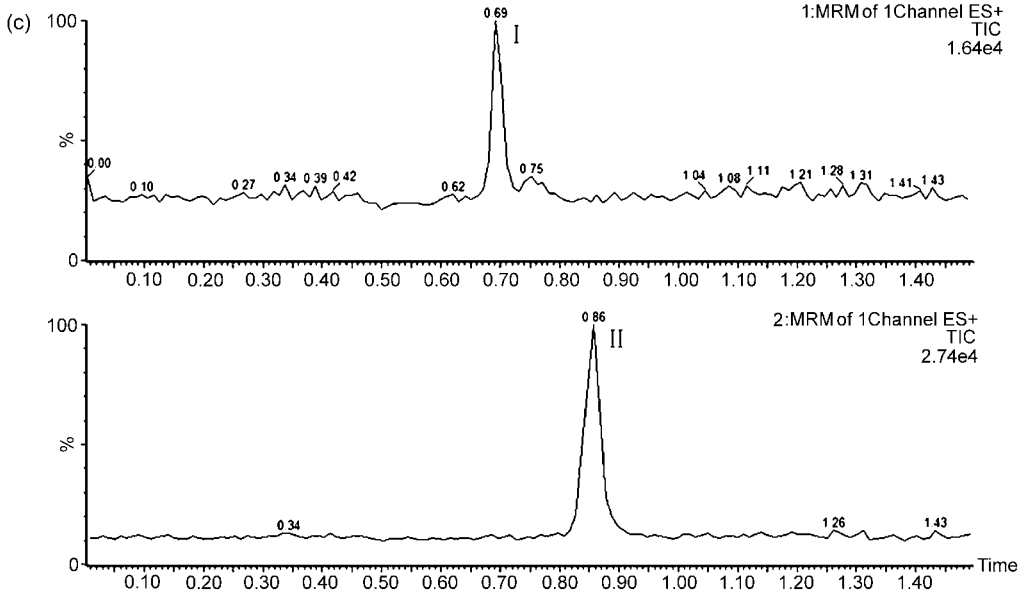

Fig. 3. (*Continued*).

were acceptable and meant that the method was precise and accurate.

3.3.5. Recovery

The extraction recoveries of VOR at concentration levels of 25, 250 and 2000 ng mL^{-1} were 94.6 ± 8.8%, 97.3 ± 5.6% and 99.7 ± 3.2%, respectively. The average extraction recovery of VOR and I.S. were 97.2 ± 2.6% and 96.9 ± 5.4%, respectively. The high extraction recoveries of VOR may be attributed to the one-step protein precipitation with methanol. With the consistency in the recoveries of the analyte and the I.S., the assay has proved to be robust in high-throughput analysis.

3.3.6. Stability

The stock solutions of VOR and I.S. were found to be stable at room temperature for 6 h and at 4 °C for 15 days. Both working solutions were stable at room temperature for 6 h. The results for short-term, long-term, freeze–thaw and post-preparative stability of QC plasma sample (250 ng mL^{-1}) expressed as accuracy (mean ± S.D., %) were 104.1 ± 8.7%, 102.6 ± 8.9%, 100.8 ± 5.4% and 98.2 ± 9.4%, respectively. These results indicate reliable stability behavior of VOR under the experimental conditions of the regular analytical procedure.

3.4. Application

The present method was successfully applied to determine VOR in rat plasma, following oral administration of VOR aqueous solution at a dose of 120 mg kg^{-1}. The pharmacokinetic parameters were analyzed using the 3P97 computer program (The Chinese Society of Mathematical Pharmacology, Beijing, China). The concentration–time curve of VOR in rat plasma was fitted to a two-compartment model with first order absorption (with a weighting factor of 1/x). The pharmacokinetic profile obtained following single dose administration of VOR

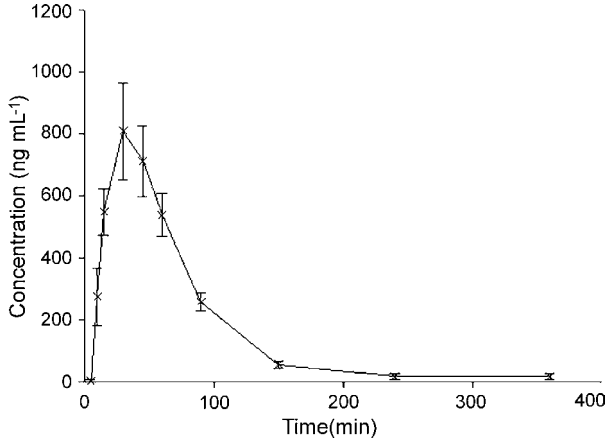

Fig. 4. Mean concentration–time profile of vitexin-2″-*O*-rhamnoside in rats (mean ± S.D., n = 5) after single oral administration of vitexin-2″-*O*-rhamnoside (120 mg kg^{-1}).

(120 mg kg^{-1}) in rats within 360 min is shown in Fig. 4, and the pharmacokinetic parameters of VOR in rats are summarized in Table 1. According to the literature [9], flavonoids are poorly absorbed from the gut and are subjected to degradation by intestinal micro-organisms. Although VOR is one of the flavonoids, it was determined in rats up to 360 min after dosing by our method for the first time. The result suggests that VOR can

Table 1
Mean pharmacokinetic parameters of VOR (120 mg kg^{-1}) in rats (mean ± S.D., n = 5) after an oral administration

Parameter	VOR
AUC_{0-t} (μg min mL^{-1})	78,556 ± 9900
$AUC_{0-\infty}$ (μg min mL^{-1})	82,010 ± 10,155
C_{max} (μg mL^{-1})	807.5 ± 173.6
T_{max} (min)	30.8 ± 1.4
$T_{1/2}$ (min)	20.1 ± 1.3

be absorbed into circulation after oral administration and the method established in this paper might be of some value.

4. Conclusion

A rapid, sensitive and selective UPLC-ESI-MS/MS method was developed and validated for the determination of VOR in rat plasma, which showed great advantages of not only the simple sample preparation but also satisfactory selectivity and short run time of 3.0 min. The method was successively applied to the pharmacokinetics of VOR in rat plasma after oral administration at a single dose of 120 mg kg^{-1} for the first time. The investigation contributes to the determination method of VOR as well as the understanding of the pharmacokinetics of VOR in rat.

Acknowledgement

This study was supported by the funds of Scientific Research Planning of the Educational Department of Liaoning Province (2004D264), China.

References

[1] X.B. Ding, Y.Q. Jiang, Y. Zhong, C.X. Zuo, Zhongguo Zhongyao Zazhi 15 (1990) 295.
[2] P. Ninfali, M. Bacchiocca, A. Antonelli, E. Biagiotti, A.M. Di Gioacchino, G. Piccoli, V. Stocchi, G. Brandi, Phytomedicine 14 (2007) 216.
[3] W. Ren, Z. Qiao, H. Wang, L. Zhu, L. Zhang, Med. Res. Rev. 23 (2003) 519.
[4] A. Kirakosyan, P. Kaufman, S. Warber, S. Zick, K. Aaronson, S. Bolling, S. Chul Chang, Physiol. Plant 121 (2004) 182.
[5] J. Su, W.D. Zhang, Y. Zhou, J. Zhou, Z.B. Gu, Zhongguo Zhongyao Zazhi 29 (2004) 525.
[6] V. Jakstas, V. Janulis, J. Labokas, Medicina (Kaunas) 40 (2004) 750.
[7] W. Liu, G. Chen, T. Cui, J. Chromatogr. Sci. 41 (2003) 87.
[8] M. Urbanek, M. Pospisilova, M. Polasek, Electrophoresis 23 (2002) 1045.
[9] J.V. Formica, W. Regelson, Food Chem. Toxicol. 33 (1995) 1061.
[10] C. Felgines, O. Texier, C. Morand, C. Manach, A. Scalbert, F. Regerat, C. Remesy, Am. J. Physiol. Gastrointest. Liver Physiol. 279 (2000) G1148.
[11] Y.H. Yang, Talanta 71 (2007) 596.
[12] J.Y. Sun, S.B. Yang, H.X. Xie, G.H. Li, H.X. Qiu, Zhong Cao Yao 6 (2002) 483.

Available online at www.sciencedirect.com
ScienceDirect
Talanta 72 (2007) 1487–1493
Talanta
www.elsevier.com/locate/talanta

Detection of prostate specific antigen with 3,4-diaminobenzoic acid (DBA)–H_2O_2–HRP voltammetric enzyme-linked immunoassay system

Shusheng Zhang *, Ping Du, Feng Li

College of Chemistry and Molecular Engineering, Qingdao University of Science and Technology, Qingdao 266042, China

Received 30 October 2006; received in revised form 24 January 2007; accepted 26 January 2007
Available online 9 February 2007

Abstract

A new voltammetric enzyme-linked immunoassay system of 3,4-diaminobenzoic acid (DBA)–H_2O_2–horseradish peroxidase (HRP) for sensitive detection of prostate specific antigen (PSA) in human serum was present. In the proposed procedure, labelled HRP efficiently catalyzed the oxidation reaction of DBA by H_2O_2 and generated the electroactive product, 2,2′-biamino-4,4′-bicarboxyl azobiphenyl, which produced a sensitive second-order derivative linear sweep voltammetric peak at potential of −0.62 V (versus SCE) in Britton–Robinson (BR) buffer solution. The linear range for detection free HRP was from 4.0×10^{-12} to 4.0×10^{-9} g ml^{-1} and the detection limit was about 6.0×10^{-13} g ml^{-1}. The proposed new system could be used for detection of PSA ranging from 0.20 to 16.0 ng ml^{-1} with a detection limit of 0.10 ng ml^{-1}, which was five times lower than that of the traditional *o*-phenylendiamine spectrophotometric enzyme-linked immunosorbent assay (ELISA) method. The proposed electrochemical ELISA method is simple, inexpensive, reproducible and sensitive, which shows potential for detecting PSA in clinical diagnosis.

Keywords: Electrochemical immunoassay; Prostate specific antigen; Horseradish peroxidase; 3,4-Diaminobenzoic acid

1. Introduction

Prostate cancer is a deadly malignancy and major cause of death in the male population aged over 50 years. No curative therapy is now available once the disease spreads the limits of the organ. To combat against the disease and control the mortality rate, therefore, accurate detection of prostate cancer at early stage while it is localised in the prostate gland offers the best hope. Prostate specific antigen (PSA), a glycoprotein in human serum, has been proved to be the most reliable and specific clinical tool for preoperative diagnosing and monitoring prostate cancer. Normally, prostate cancer is suspected if the total PSA level is higher than 10 ng ml^{-1} [1–4]. Therefore, sensitive and specific detection of PSA for early prostate cancer detection is of great significance.

As one of the most selective analytical methodologies, immunoassay is developed in the last 30 years and has been successfully applied for the assay of PSA. Different immunoassay readout techniques, e.g., fluorescence, chemiluminescence, enzyme, surface plasmon resonance (SPR), have been developed in past years. Amongst them, enzyme-linked immunosorbent assays (ELISA) are currently the predominant analytical technique for quantitative determination of broad variety of analytes in fields of clinic, medicine, biotechnology and environment [5–9]. Compared with spectrophotometric detection, the most used readout modality for ELISA, electrochemical technique emerges as the very attractive alternative to carry out detection in ELISA. The reason lies in the prominent characteristics of electrochemical methods including simple and low cost fabrication, high sensitivity and selectivity, and conveniently practical application [10–16]. Sarker et al. have described the detection of PSA using amperometric immunosensor [12]. In the three electrode system used, working electrode (WE) was made of hydroxyethyl cellulose (HEC) and rhodinised carbon. Monoclonal capture antibody (Mab) to PSA was immobilized on the WE and the other Mab was labelled by the tracer enzyme, horseradish peroxidase (HRP). Due to enzymatic reaction via a sandwich immunoassay on the WE, the electrochemical response was directly observed and the limit of detection was 0.25 ng ml^{-1}. Ip et al. have reported the enzyme immunoassay for PSA by flow-injection electrochemical detection [13]. The alkaline phosphatase was used as the labelled enzyme, which converted

* Corresponding author. Tel.: +86 532 84022750; fax: +86 532 84022750.
E-mail address: shushzhang@qust.edu.cn (S. Zhang).

0039-9140/$ – see front matter © 2007 Elsevier B.V. All rights reserved.
doi:10.1016/j.talanta.2007.01.063

p-aminophenyl phosphate to *p*-aminophenol. The concentration of *p*-aminophenol was then determined amperometrically in the flow-injection system.

Microtiter plates (96-well) are the most commonly and commercially available solid supports used in heterogeneous ELISA. They show potential in high throughout detection because many samples can be measured in parallel [17]. Our group has coupled the application of electrochemical methods and ELISA by incorporating microtiter plates with electrochemical detection. Compared with spectrophotometric detection by expensive microtiter plate reader, ELISA analysis with electrochemical detection is relatively inexpensive and free from color and turbid interferences. Moreover, more sensitive detection than the spectrophotometric analysis could be obtained [18–22]. With horseradish peroxidase (HRP), the most widely used enzyme in immunoassays being the label, we developed a variety of voltammetric enzyme-linked immunoassay systems using substrates such as *o*-dianisidine, *m*-aminophenol, *o*-phenylenediamine, 3,3′-5,5′-tetramethylbenzidine and so on.

In this paper, sensitive detection of PSA in human serum based on a new electrochemical enzyme-linked immunoassay system was proposed. With HRP being the labelled enzyme, the usage of a novel substrate, 3,4-diaminobenzoic acid (DBA), was first reported. Resulting from the oxidation reaction of DBA in HRP–H_2O_2 system, the electroactive product, 2,2′-biamino-4,4′-bicarboxyl azobiphenyl, was formed and could be voltammetrically measured. In comparison with the *o*-phenylenediamine spectrophotometric ELISA, this electrochemical method improves the sensitivity of PSA detection by about five times. As a promising alternative approach for detecting PSA in the clinical diagnosis, the proposed assay is simple, inexpensive, rapid, reproducible and sensitive.

2. Experimental

2.1. Instrumentation

The electrochemical measurement was carried out with a MP-2 voltammetric analyzer (Shangdong No. 7 Electric Communication Corp., China). A three-electrode system was employed using a dropping mercury electrode or a hanging mercury drop electrode as working electrode, a platinum electrode as auxiliary electrode and a saturated calomel electrode (SCE) as reference electrode. OG3022A enzyme-linked immunity measure implement (Huadong Electronal Group Medical Treatment Instrument Ltd., China) was used for the spectrophotometric ELISA.

2.2. Chemicals

3,4-Diaminobenzoic acid (DBA, ABCR GmBH & Co.) solution was prepared by dissolving 0.0570 g DBA in water and diluted to 50.00 ml (7.5×10^{-3} mol l^{-1}). The solution of HRP (250 units per mg enzyme, Xueman Biochemical Technique Corp., China) was prepared by dissolving 10.00 mg HRP in 10.00 ml water (1.0×10^{-3} g ml^{-1}). It was stored in a refrigerator at 4 °C. H_2O_2 solution at a concentration of 4.0×10^{-4} mol l^{-1} was prepared freshly. 0.2 mol l^{-1} Britton–Robinson (BR) buffer solutions at pH 4.5 or 8.0 were used in the study. The substrate solution in the enzyme-linked immunoassay system was prepared by adding the following solutions in sequence: 1.0 ml of 7.5×10^{-3} mol l^{-1} DBA solution, 3.0 ml of 4.0×10^{-4} mol l^{-1} H_2O_2 solution and 2.0 ml of BR buffer solution at pH 4.5. Afterwards, the resulting mixture was diluted to 10.0 ml and shaken to obtain a uniform solution. The PSA ELISA kit was purchased from Peking Northward Biology Technique Graduate School and stored at 2–8 °C. The kit included immunoplate precoated by anti-PSA serum, HRP-linked anti-PSA, standard PSA sample, substrate solution (*o*-phenylendiamine solution), rinsing solution (PBS) and stop solution (H_2SO_4). Other chemicals employed were of analytical grade and doubly deionized water (DDW) was used throughout.

2.3. Electrochemical measurement of free or labelled HRP

The 1.0 ml DBA (7.5×10^{-3} mol l^{-1}), 3.0 ml H_2O_2 (4.0×10^{-4} mol l^{-1}), 2.0 ml BR buffer solution (0.2 mol l^{-1}, pH 4.5) and 1.0 ml HRP solution (1.0×10^{-8} g ml^{-1}) was mixed and diluted to 10.0 ml with DDW. Then, the mixture was sat at 37 °C for 50 min in a constant temperature water bath. 3.0 ml of the above solution was transferred into a 10.0 ml colorimetric tube and 7.0 ml of BR buffer solution (0.2 mol l^{-1}, pH 8.0) was subsequently added. The resulting solution was then transferred into a 10 ml electrolyte cell. The second-order derivative linear-sweep voltammogram was recorded with the MP-2 voltammetric analyzer. The instrumental conditions were as follows: initial potential, −0.20 V; mercury drop standing time, 7 s; potential scanning rate, 300 mV s^{-1}.

2.4. Detection of PSA

The detection of PSA was carried out with double-antibody-sandwich immunoassay method. In the assay, the commercial PSA Kit was directly used. The conditions of the immunoreaction were controlled according to the procedure recommended. In brief, all regents were equilibrated at room temperature before measurement. The 100 μl of control serum with different concentrations of PSA or real serum sample were added to each well of the polystyrene immunoplate, which was precoated with anti-PSA. Then, 100 μl of HRP-linked anti-PSA was added to each well. The incubation reaction was controlled at 37 °C for 60 min. After rinsed with PBS buffer (300 μl) three times followed by DDW for three or four times, 300 μl of the substrate solution was added to each well and incubated at 37 °C for 50 min. The enzymatic product generated in the plate was transferred to a 5 ml electrochemical measuring cell. After 700 μl of BR buffer (pH 8.0) were added into the cell, the second-order derivative linear-sweep voltammogram was recorded.

For comparison, spectrophotometric detection of ELISA was also preformed in parallel using OG3022A enzyme-linked immunity measure implement.

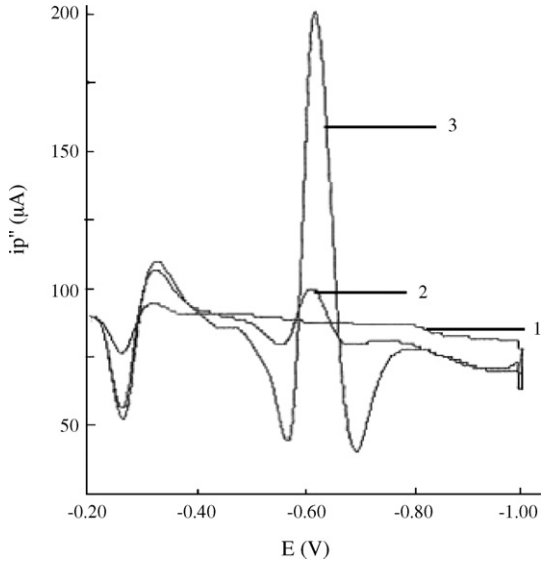

Fig. 1. Second-order derivative linear-sweep voltammogram of BR buffer (1), BR + DBA + H_2O_2 (2) and BR + DBA + H_2O_2 + HRP (3).

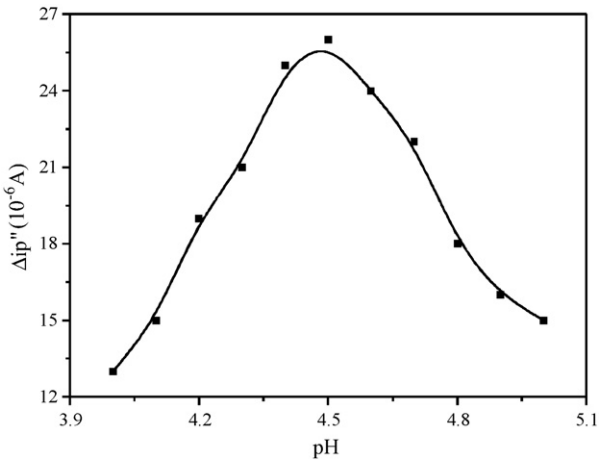

Fig. 3. Effect of pH of BR buffer solution on the HRP-catalyzed oxidation reaction.

3. Results and discussion

3.1. The second-order derivative linear-sweep voltammograms

Linear sweep second-order derivative polarography has advantages, such as the highest sensitivity, the lowest detection limit, short experimental time, fast electrochemical procedure and simple manipulation. With the catalysis of HRP, DBA could be oxidized by H_2O_2 in BR buffer solution at pH 4.5. The resulting enzymatic product generated excellent voltammetric peaks or polarographic waves in linear sweep second-order derivative polarography, as shown in Fig. 1 (curve 3). However, no voltammetric peak was observed in the voltammogram of BR buffer solution (curve 1). Curve 2 represented the voltammogram of BR solution containing DBA and H_2O_2. A small voltammetric peak at −0.62 V was observed. Such small peak was due to the product formed by slow oxidation of DBA by H_2O_2. By addition of HRP in mixture of DBA and H_2O_2 in BR solution, oxidation of DBA by H_2O_2 was greatly quickened. As a result, the reaction product produced a large and well-defined voltammetric peak at −0.62 V (curve 3). When the HRP content was controlled as low as 1.0×10^{-9} g ml^{-1}, a distinctive increase of this voltammetric peak can still be observed.

3.2. Conditions for enzyme-catalyzed reaction

As seen from the voltammogram, HRP intensely catalyzed the oxidation reaction of DBA by H_2O_2. Considering the structure of the product and catalysis cycle of HRP in reaction, HRP-catalyzed DBA oxidation process was demonstrated in Fig. 2. The enzymatic oxidation of DBA generated a stable product, 2,2′-biamino-4,4′-bicarboxyl azobiphenyl in BR buffer solution at pH 4.5.

The effect of pH on enzyme-catalyzed reaction was studied by varying the pH of BR buffer solution between 2.0 and 12.0. The electrochemical respond of the enzymatic product in different conditions was shown in Fig. 3. When pH was in the range of 4.0–5.0, a sensitive and stable voltammetric peak could be obtained. Therefore, BR buffer solution at 4.5 was chosen for enzyme-catalyzed reaction. Additionally, the concentrations of each component in substrate solution, including BR buffer solution, DBA and H_2O_2, were also optimized. When the final 10 ml substrate solution consisted of 2.0 ml of BR buffer solution (0.2 mol l^{-1}, pH 4.5), 1.0 ml DBA solution (7.5×10^{-3} mol l^{-1}) and 3.0 ml H_2O_2 solution (4.0×10^{-4} mol l^{-1}), the electrochemical peak was the highest and stable. Under such enzyme-catalyzed reaction conditions, the electrochemical peak of the product had no change after reaction last 50 min at 37 °C, indicating the equilibrium of the reaction. Thus, 50 min was selected as the time for the enzyme-catalyzed reaction.

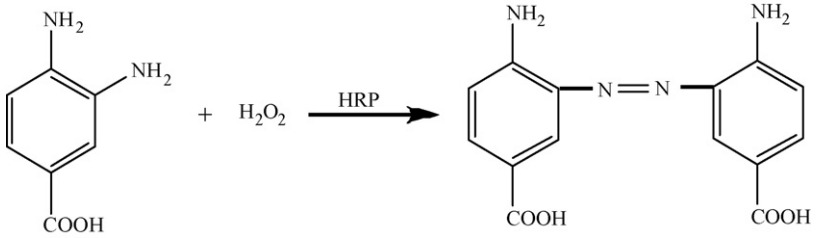

Fig. 2. The process of the HRP-catalyzed oxidation reaction of DBA by H_2O_2.

3.3. Detection conditions

The fine second-order derivative linear-sweep voltammetric peak for the enzyme-catalyzed product could be obtained in certain buffer solutions, such as BR, or NaAc–HAc. In this work, BR buffer solution was selected as the supporting electrolyte for the measurement. After enzyme-catalyzed reaction finished, the effect of pH of the supporting electrolyte (BR buffer solution) on the second-order derivative linear-sweep voltammetric peak of enzymatic product was investigated. Results showed that the peak potential shifted negatively with the increase of pH. In BR buffer solution at pH 8.0, the peak height was the highest and stable. In addition, the optimized amount of BR buffer solution (pH 8.0) was 7.0 ml for 10 ml of the overall electrolyte solution.

3.4. The electrode procedure of the enzymatic product

The relation between the reduction peak height of the enzymatic product and the static period τ was investigated using the

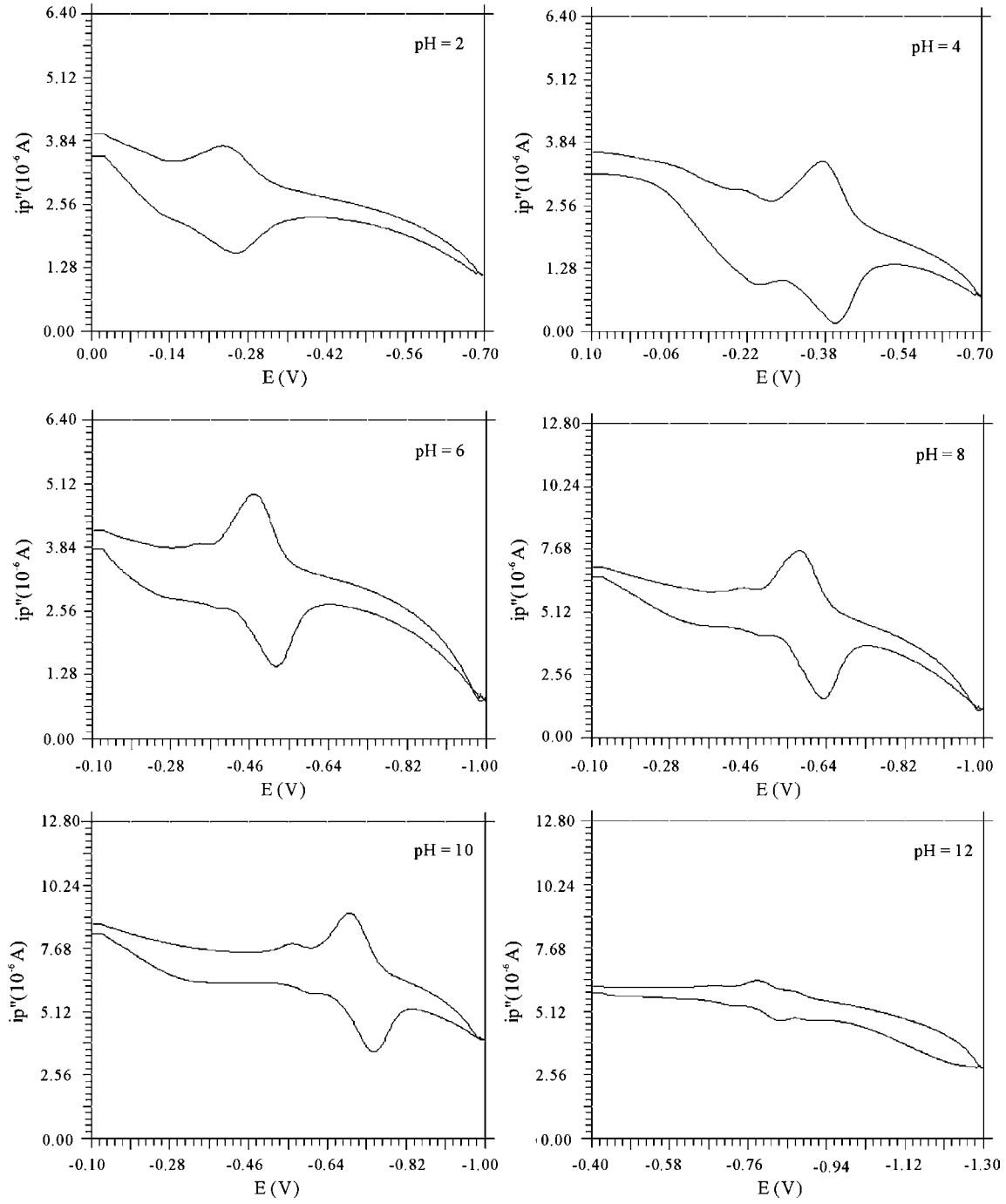

Fig. 4. Cyclic voltammograms of enzymatic product in BR buffer solution at different pH. The enzymatic product was generated by oxidation reaction of DBA in BR buffer solution at pH 4.5.

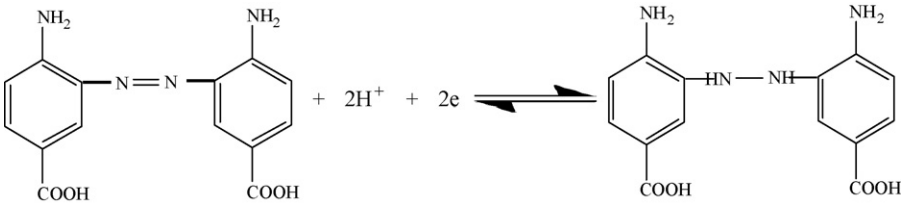

Fig. 5. A two-electron reversible redox process of azo-nitrification in BR buffer solution at pH 6.0–8.0.

hanging mercury drop electrode. We found that the peak height did not change when τ changed between 0 and 18 s, indicating the diffusion of the product.

The plot of the peak current versus the square root of the scanning rate was linear in the range of 150–935 mV s^{-1}. It indicated that the reduction of the enzymatic product on the mercury electrode was diffusion-controlled.

The cyclic voltammetric experiment was also performed for solution containing enzymatic product. After enzyme-catalyzed oxidization reaction in BR buffer solution at pH 4.5, the cyclic voltammograms were recorded at different pH from 2.0 to 12.0. The results were shown in Fig. 4. The peak potential has a good linear relation with the pH value. The regression equation was $E_p = -0.126–0.061$ pH ($\gamma = -0.9905$). The formula was provided by the literature [23], $-0.059\,x/n = -0.061$, where n was the number of the electron transfer, x was the hydrogen ion number participating the reaction, $x \approx n$. As we could see, both anodic peak and cathodic peak appeared in the buffer solution with pH range of 2.0–8.0. The heights of these two peaks increased with the increase of pH. When pH was in the range of 6.0–8.0, the peak height distinctly increased and the height of the two peaks was almost equal. The phenomenon indicated the appearance of one pair of reversible redox peaks. In the pH range of 10.0–12.0, the two peaks decreased with the increase of pH. Based on the theory developed by Nicholson [24], the voltammogram at pH 8.0 showed a two electron reversible electrode process. As reported in the literatures [25,26], the electrochemical reaction on electrode was a two-electron reversible redox process of azo-nitrification in BR buffer solution at pH 6.0–8.0. Such electrode process could be demonstrated in Fig. 5.

In summary, the oxidation of DBA by H_2O_2 yielded a stable product, 2,2′-biamino-4,4′-bicarboxyl azobiphenyl, when the enzyme-catalyzed reaction occurred in BR buffer solution at pH 4.5. In BR buffer solution at pH 8.0, such enzyme-oxidized product could be reduced on electrode through a two-electron transfer process. Based on such electro-reduction peak, free HRP and labelled HRP can be determined. Additionally, different antibodies and antigens can also be identified through HRP-linked immunoassay.

In BR buffer solution at pH 8.0, multiple-sweep voltammograms were recorded. There were good cathodic and anodic peaks and those two peaks were similar in height. Moreover, the peaks almost did not change with the increasing of the scanning cycle. This was the diffusive behavior of the products and reactants.

3.5. Electrochemical detection of free HRP

Different quantities of free HRP were used to catalyze the oxidation reaction of DBA by H_2O_2. The second-order derivative linear-sweep voltammograms of the following enzymatic products were recorded. The peak height exhibited a good linear relation with free HRP concentration in solution in the range of 4.0×10^{-12} to 4.0×10^{-9} g ml^{-1}. The detection limit was about 6.0×10^{-13} g ml^{-1}. The relative standard derivative (R.S.D., $n = 11$) for detection of 4.0×10^{-11} g ml^{-1} free HRP was 2.1%.

3.6. Detection of labelled HRP

Similar with free HRP, labelled HRP could also be determined. We compared the sensitivity for determining free HRP (1) and labelled HRP. Five HRP-conjugated antibodies were α-fetoprotein (αFP-Ab-HRP, 2), ferritin-Ab-HRP (3), carcinoma embryo (CEA-Ab-HRP, 4), PSA (PSA-Ab-HRP, 5), and full-mouthed disease (FMD-Ab-HRP, 6). In comparison with the *o*-phenylenediamine spectrophotometric ELISA, the newly developed method showed higher sensitivity for detection of labeled HRP. The dilution curves for both electrochemical and spectrophotometric assay were shown in Fig. 6. The highest dilution ratios for detection of labelled HRP using PSA-Ab-HRP through the two methods were shown in Table 1. The highest dilution ratio of our electrochemical method was 1:5000, whereas, that of the *o*-phenylendiamine spectrophotometric ELISA method was 1:1000. Thus, our electrochemical enzyme-linked immunoassay system could detect five times lower concentration of labelled HRP than that of the *o*-phenylendiamine spectrophotometric ELISA.

3.7. The linear range, detection limit and precision of PSA detection

Under the optimum conditions, the proposed new DBA–H_2O_2–HRP system could be used for quantitative detection

Table 1
The comparisons of electrochemical ELISA ($\Delta i_p''$) with spectrophotometric ELISA (A_{450}) for the detection of labelled HRP using PSA-Ab-HRP

	Dilution ratio				
	1:10	$1:10^2$	$1:10^3$	$1:10^4$	$1:10^5$
$\Delta i_p''$ (μA)	103	23	18	14	0
A_{450}	0.85	0.29	0.10	0.01	0.00

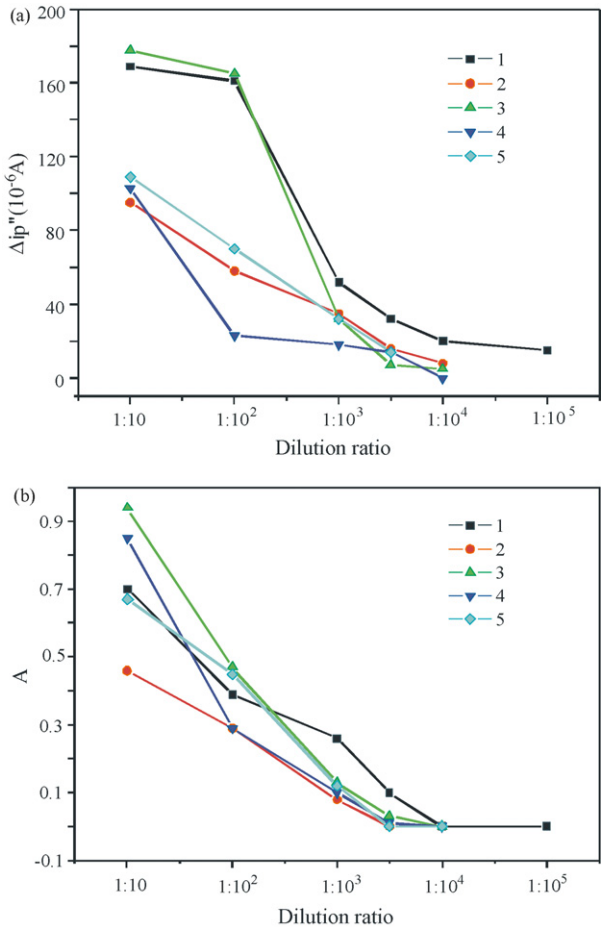

Fig. 6. Dilution curves for detection of labelled HRP using both electrochemical (a) and spectrophotometric ELISA (b). Labelled HRP was αFPAb-HRP (1), ferritin-Ab-HRP (2), CEA-Ab-HRP (3), PSA-Ab-HRP (4), and FMD-Ab-HRP (5), respectively.

of PSA by second-order derivative linear-sweep voltammogram. The linear range was from 0.20 to 16.0 ng ml^{-1} with a detection limit of 0.10 ng ml^{-1} at a signal-to-noise ratio of 3. The linear regression was $y = -0.7471 + 5.4259x$ ($\gamma = 0.9972$), where y represented $\Delta i''_p$, i''_p was the peak current (μA), x was the concentration of PSA. The reproducibility of assay has also been studied. The relative standard deviation (R.S.D., $n = 11$) for the detection of 6.0 ng ml^{-1} of PSA was 3.1%.

For *o*-phenylendiamine spectrophotometric ELISA method, the linear range of PSA was 1.0–32 ng ml^{-1}. The equation of linear regression was $A = 0.0823 + 0.0467C$ ($\gamma = 0.9974$), where A was the absorbency, C was the concentration of PSA. The detection limit was 0.5 ng ml^{-1}. Therefore, the detection limit of our electrochemical enzyme-linked immunoassay method was five times lower than that of the *o*-phenylenediamine spectrophotometric ELISA method.

3.8. Detection of human serum samples

The human serum samples were detected using both electrochemical enzyme-linked immunoassay method and spectrophotometric ELISA method. The comparison results were listed in Table 2. We could find that the two methods showed good agreement. The results of electrochemical method were linear proportional to that of spectrophotometric method. The regression was $y = -0.0833 + 1.0136x$ ($\gamma = 0.9996$), where x was the results of electrochemical method, y was results of spectrophotometric method.

Table 2
The comparisons of electrochemical ELISA with spectrophotometric ELISA for the detection of PSA in human serum

Sample	Electrochemical ELISA (ng ml^{-1})	R.S.D. (%)	Spectrophotometric ELISA (ng ml^{-1})	R.S.D. (%)
1	0.23	4.5	–	
2	0.46	4.2	–	
3	0.82	3.9	–	
4	3.75	3.4	4.23	3.3
5	8.65	2.7	7.92	2.9
6	42.63	2.3	43.24	3.6
7	–		–	
8	62.81	2.1	63.25	2.2
9	12.0	2.7	11.62	2.8
10	25	2.5	26.30	2.5

3.9. Specificity for detection of PSA

The specificity for detecting PSA was investigated using dilutions of PSA, α-fetoprotein (αFP), carcinoma embryo antigen (CEA), ferritin, and full-mouthed disease (FMD). 0.2 ng ml^{-1} PSA could be readily detected. However, there were no significant reactions with the αFP, CEA, ferritin and FMD samples in the concentration of 10.0–1.0 μg ml^{-1}. In addition, uninfected human serum and human serum infected with αFP, CEA, ferritin and FMD, respectively, gave no detectable reactions.

4. Conclusions

Based on the new system of 3,4-diaminobenzoic acid–H_2O_2–HRP, the developed electrochemical enzyme-linked immunoassay showed potential performance for detection of prostate specific antigen (PSA) in human serum. The processes of the enzyme-catalyzed reaction and electro-reduction of the product on the electrode was investigated. The detection limit for PSA was five times lower than that of the traditional spectrophotometric ELISA method. The simple, inexpensive, reproducible and sensitive assay showed a promising alternative approach in clinical diagnosis.

Acknowledgements

This research was supported by the National Natural Science Foundation of China (No. 20475030), the Program for New Century Excellent Talents in Universities (No. NCET-04-0649) and the Natural Science Foundation of Shandong Province (No. Z2006B01).

References

[1] C. Cao, J.P. Kim, B.W. Kim, H. Chae, H.C. Yoon, S.S. Yang, S.J. Sim, Biosens. Bioelectron. 21 (2006) 2106.
[2] C. Li, M. Curreli, H. Lin, B. Lei, F.N. Ishikawa, R. Datar, R.J. Cote, M.E. Thompson, C.W. Zhou, J. Am. Chem. Soc. 127 (2005) 12484.
[3] D.S. Grubisha, R.J. Lipert,.H.Y. Park, J. Driskell, M.D. Porter, Anal. Chem. 75 (2003) 5936.
[4] G.A.J. Besselink, R.P.H. Kooyman, P.J.H.J. van Os, G.H.M. Engbers, R.B.M. Schasfoort, Anal. Biochem. 333 (2004) 165.
[5] J.C. Chuang, J.M. Van Emon, J. Durnford, K. Thomas, Talanta 67 (2005) 658.
[6] F. Yu, B. Persson, S. Lofas, Anal. Chem. 76 (2004) 6765.
[7] S. Rodriguez-Mozaz, M.J.L. de Alda, M.P. Marco, D. Barcelo, Talanta 65 (2005) 291.
[8] M. Bach, K. Jung, B. Ivankovic, Clin. Chem. 46 (2000) 618.
[9] H. Nakajima, M. Yagi, Y. Kudo, T. Nakagama, T. Shimosaka, K. Uchiyama, Talanta 70 (2006) 122.
[10] W. Vastarella, R. Nicastri, Talanta 66 (2005) 627.
[11] M. Antonini, P. Ghisellini, C. Paternolli, C. Nicolini, Talanta 62 (2004) 945.
[12] P. Sarker, P.S. Pal, D. Ghosh, S.J. Steford, I.E. Tothill, Int. J. Pharm. 238 (2002) 1.
[13] S.F. Chen, Y. Xu, M.P.C. Ip, Clin. Chem. 43 (1997) 1459.
[14] S.H. Alarcon, G. Palleschi, D. Compagnone, M. Pascale, A. Visconti, I. Barna-Vetro, Talanta 69 (2006) 1031.
[15] A. Salimi, H. MamKhezri, R. Hallaj, Talanta 70 (2006) 823.
[16] R. Jain, N. Jadon, K. Radhapyari, Talanta 70 (2006) 383.
[17] M. Díaz-González, M.B. González-García, A. Costa-García, Electroanalysis 17 (2005) 1901.
[18] W. Sun, K. Jiao, S.S. Zhang, Talanta 55 (2001) 1211.
[19] W. Sun, K. Jiao, S.S. Zhang, Anal. Chim. Acta 434 (2001) 43.
[20] K. Jiao, W. Sun, S.S. Zhang, Anal. Chim. Acta 413 (2000) 71.
[21] S.S. Zhang, K. Jiao, H.Y. Chen, Talanta 50 (1999) 95.
[22] K. Jiao, S.S. Zhang, L. Wei, Talanta 47 (1998) 1129.
[23] I.M. Kolthoff, J.J. Lingane, Polarography, Interscience Publisher, New York, 1952, p. 247.
[24] R.S. Nicholson, Anal. Chem. 37 (1968) 1351.
[25] T.M. Florence, J. Electroanal. Chem. 52 (1974) 115.
[26] K. Jiao, X.X. Gao, Sci. Sin. (Ser. B) 28 (1985) 1121.